Lecture Notes in Civil Engineering

Ranjith Dissanayake ·
Priyan Mendis · Kolita Weerasekera ·
Sudhira De Silva · Shiromal Fernando ·
Chaminda Konthesingha ·
Pradeep Gajanayake *Editors*

ICSBE 2022

Proceedings of the 13th International Conference on Sustainable Built Environment

Springer

Lecture Notes in Civil Engineering

Volume 362

Series Editors

Marco di Prisco, Politecnico di Milano, Milano, Italy

Sheng-Hong Chen, School of Water Resources and Hydropower Engineering, Wuhan University, Wuhan, China

Ioannis Vayas, Institute of Steel Structures, National Technical University of Athens, Athens, Greece

Sanjay Kumar Shukla, School of Engineering, Edith Cowan University, Joondalup, WA, Australia

Anuj Sharma, Iowa State University, Ames, IA, USA

Nagesh Kumar, Department of Civil Engineering, Indian Institute of Science Bangalore, Bengaluru, Karnataka, India

Chien Ming Wang, School of Civil Engineering, The University of Queensland, Brisbane, QLD, Australia

Lecture Notes in Civil Engineering (LNCE) publishes the latest developments in Civil Engineering—quickly, informally and in top quality. Though original research reported in proceedings and post-proceedings represents the core of LNCE, edited volumes of exceptionally high quality and interest may also be considered for publication. Volumes published in LNCE embrace all aspects and subfields of, as well as new challenges in, Civil Engineering. Topics in the series include:

- Construction and Structural Mechanics
- Building Materials
- Concrete, Steel and Timber Structures
- Geotechnical Engineering
- Earthquake Engineering
- Coastal Engineering
- Ocean and Offshore Engineering; Ships and Floating Structures
- Hydraulics, Hydrology and Water Resources Engineering
- Environmental Engineering and Sustainability
- Structural Health and Monitoring
- Surveying and Geographical Information Systems
- Indoor Environments
- Transportation and Traffic
- Risk Analysis
- Safety and Security

To submit a proposal or request further information, please contact the appropriate Springer Editor:

– Pierpaolo Riva at pierpaolo.riva@springer.com (Europe and Americas);
– Swati Meherishi at swati.meherishi@springer.com (Asia—except China, Australia, and New Zealand);
– Wayne Hu at wayne.hu@springer.com (China).

All books in the series now indexed by Scopus and EI Compendex database!

Ranjith Dissanayake · Priyan Mendis ·
Kolita Weerasekera · Sudhira De Silva ·
Shiromal Fernando · Chaminda Konthesingha ·
Pradeep Gajanayake
Editors

ICSBE 2022

Proceedings of the 13th International Conference on Sustainable Built Environment

Springer

Editors
Ranjith Dissanayake
Department of Civil Engineering
University of Peradeniya
Kandy, Sri Lanka

Kolita Weerasekera
Department of Civil Engineering
The Open University of Sri Lanka
Nugegoda, Sri Lanka

Shiromal Fernando
Civil and Structural Engineering
Consultants (Pvt) Ltd.
Rajagiriya, Colombo, Sri Lanka

Pradeep Gajanayake
Department of Biosystems Technology
University of Sri Jayawardanepura
Homagama, Sri Lanka

Priyan Mendis
Department of Infrastructure Engineering
University of Melbourne
Parkville, VIC, Australia

Sudhira De Silva
Department of Civil and Environmental
Engineering
University of Ruhuna
Galle, Sri Lanka

Chaminda Konthesingha
Department of Civil Engineering
University of Sri Jayawardanepura
Jayawardanepura, Sri Lanka

ISSN 2366-2557 ISSN 2366-2565 (electronic)
Lecture Notes in Civil Engineering
ISBN 978-981-99-3470-6 ISBN 978-981-99-3471-3 (eBook)
https://doi.org/10.1007/978-981-99-3471-3

© The Editor(s) (if applicable) and The Author(s), under exclusive license to Springer Nature Singapore Pte Ltd. 2023

This work is subject to copyright. All rights are solely and exclusively licensed by the Publisher, whether the whole or part of the material is concerned, specifically the rights of translation, reprinting, reuse of illustrations, recitation, broadcasting, reproduction on microfilms or in any other physical way, and transmission or information storage and retrieval, electronic adaptation, computer software, or by similar or dissimilar methodology now known or hereafter developed.
The use of general descriptive names, registered names, trademarks, service marks, etc. in this publication does not imply, even in the absence of a specific statement, that such names are exempt from the relevant protective laws and regulations and therefore free for general use.
The publisher, the authors, and the editors are safe to assume that the advice and information in this book are believed to be true and accurate at the date of publication. Neither the publisher nor the authors or the editors give a warranty, expressed or implied, with respect to the material contained herein or for any errors or omissions that may have been made. The publisher remains neutral with regard to jurisdictional claims in published maps and institutional affiliations.

This Springer imprint is published by the registered company Springer Nature Singapore Pte Ltd.
The registered company address is: 152 Beach Road, #21-01/04 Gateway East, Singapore 189721, Singapore

Preface

It is with great pleasure that we present the proceedings of the 13th International Conference on Sustainable Built Environment (ICSBE) 2022. This is the eleventh consecutively organized conference following a series of international conferences since 2010, keeping its tradition of adhering to engineering excellence.

Taking a step forward from the last ten events, the coverage of specialty areas in this conference has been diversified. This book contains manuscripts of research work from many different sub-specialties. All the manuscripts were presented in parallel sessions from 16 to 18 December 2022.

We would like to express our appreciation to all keynote speakers for their invaluable contribution to the development of a sustainable world. We are also very grateful to the authors for contributing research papers of high quality. The manuscripts in this proceeding book have been reviewed by a panel of academic and professional experts who have vast expertise in their respective fields. The enormous work carried out by these reviewers is gratefully appreciated as well. We are also pleased to acknowledge the advice and assistance provided by the members of the international advisory committee and members of the editorial committee along with many others who volunteered to assist to make this very significant event a success. Furthermore, we acknowledge the financial sponsorship provided by many organizations that have been extremely supportive towards the success of this international conference.

It is the earnest wish of the editors that this proceeding book would be used by the research community and practicing engineers who are directly or indirectly involved in studies related to sustainable built environments.

Editorial Committee

Kandy, Sri Lanka	Prof. Ranjith Dissanayake
Parkville, Australia	Prof. Priyan Mendis
Nugegoda, Sri Lanka	Prof. Kolita Weerasekera
Galle, Sri Lanka	Prof. Sudhira De Silva
Rajagiriya, Colombo, Sri Lanka	Eng. Shiromal Fernando
Jayawardanepura, Sri Lanka	Prof. Chaminda Konthesingha
Homagama, Sri Lanka	Prof. Pradeep Gajanayake

Contents

Bridge Design Construction and Maintenance

Effect of Live Load Increment of Old Steel Railway Bridges in Sri Lanka 3
H. S. C. Padmasiri, G. L. A. S. Punyawardhana, D. K. D. Limesha, and P. A. K. Karunananda

Use of Markov Chain Method to Predict Service Life of Reinforced Concrete Bridge Decks 17
W. G. K. Nirmal, P. Thadsanamoorthy, and G. Tharmarajah

Thin-Walled Hollow Steel Box Piers with Energy Dissipation Mechanism Under Bi-directional Cyclic Loading 29
M. Jenothan, J. A. S. C. Jayasinghe, C. S. Bandara, and A. J. Dammika

Damage Prediction by Using Nonlinearity of Damping 47
G. B. Dissanayake, A. J. Dammika, C. S. Bandara, J. A. S. C. Jayasinghe, and P. B. R. Dissanayake

Chemical Processes for a Sustainable Future

Effects of Refined Coconut Oil and Vegetable Oil on the Mechanical, Thermal, Morphological, and Biodegradable Properties of Cassava Starch-Based Thermoplastic (TPS) Films 61
N. M. L. Fernando, S. M. Amaraweera, O. H. P. Gunawardene, W. M. D. B. Wanninayaka, C. A. Gunathilake, W. A. Manamperi, A. K. Kulatunga, and A. Manipura

Batch Adsorption Study for the Removal of Textile Dyes from Aqueous Solutions Using Pandanus Amaryllifolius (Rampe) Leaves 75
S. L. G. Haththotuwa and B. M. W. P. K. Amarasinghe

Tea Waste Bio-Char as an Adsorbent for the Removal of Pb(II) in the Industrial Wastewater 89
N. B. I. M. N. Bandara and V. Edussooriya

Mechanical Recycling and Valorisation of Disposable Face Masks: A Potential Solution to the COVID-19 Waste Issue 101
D. G. K. Dissanayake, S. D. Gunawardane, Dakshitha Weerasinghe, Nadeeka Tissera, and Damith Mohotti

Assessment of Dispersion Potential of Discarded Coconut Fibres in Concrete Pavements 115
Someen Khute, Raul Zerbino, Surender Singh, and Ravindra Gettu

Concrete Technology and High-Performance Concrete

Evaluation of Thermal Conductivity of Concrete Using Finite Element Analysis 135
E. Thavarajah, K. M. C. Konthesingha, S. M. A. Nanayakkara, I. R. Upasiri, W. P. H. P. Weerasinghe, and H. M. S. C. Rathnasiri

Effect of Carbonation on Microstructure of Cement Pastes with Different Water-to-Cement Ratios 149
K. Kopitha, S. Krishnya, Y. Elakneswaran, R. Kitagaki, Y. Yoda, M. Tsujino, and A. Nishida

Development of Lightweight Aggregate Concrete with Locally Available Lightweight Materials 161
R. W. P. K. Rupasinghe, K. M. C. Konthesingha, S. M. A. Nanayakkara, H. M. S. C. Rathnasiri, I. R. Upasiri, and W. P. H. P. Weerasinghe

Assessment of Heat of Hydration of High-Strength Concrete 175
S. A. P. Madusanka and H. D. Yapa

Construction Management

Critical Selection Factors for Contractors to Make Bid/No-Bid Decision in Construction Projects in Sri Lanka 191
K. M. P. B. G. Dissanayake, P. L. Perera, and K. D. M. Gimhani

Cost Control Techniques on the Delivery of Sustainable Construction Projects in Sri Lanka 205
W. M. P. T. Andrady, C. Allis, and B. K. C. Perera

Lean and Green: How the Synergy Can Promote Sustainable Construction 219
Prangige Achini Nadeesha Peiris, Nilupa Herath, Tuan Ngo, Colin Duffield, and Felix Kin Peng Hui

Geotechnical Engineering

Influence of Recycled USP on Shear Behaviour of Railway Ballast: Experimental and Numerical Approach 231
H. G. S. Mayuranga, S. K. Navaratnarajah, C. S. Bandara, and J. A. S. C. Jayasinghe

Experimental and Numerical Study on the Shear-Strain Behavior of Ballast with Different Gradations 245
S. Venuja, S. K. Navaratnarajah, C. S. Bandara, and J. A. S. C. Jayasinghe

Sub-Structure Soil Strengthening Using "Low-Pressure Grouting" After the Subsidence Incident of a Historic Unrefined Building—a Case Study 255
Hafsha Fazal Mohamed, Athula Samarasinghe, Shiromal Fernando, and Priyan Mendis

Green Innovations and Green Building Techniques

Risk Mitigation Measures in Green Building Projects: An Investigation 277
Nilupa Herath, Paulo Vaz-Serra, Felix Kin Peng Hui, Priyan Mendis, and Lu Aye

Impacts of Selected Urban Tree Species on Outdoor Thermal Comfort in the City of Colombo 291
A. P. Sirimanne and V. M. Jayasooriya

Analysis of Passive Solar Design and Thermal Mass Optimization to Reduce Cooling Energy Demand of Existing Building 303
S. V. I. R. V. Serasinghe, I. D. Nissanka, and M. A. Wijewardane

Innovations in Building Materials

Shrink Index-Based Timber Classification and Finger Joint Production 319
C. K. Muthumala, K. K. I. U. Arunakumara, Sudhira De Silva, P. L. A. G. Alwis, and S. M. J. P. Dayawansha

Structural Performance of Welded Joints—A Numerical Study 333
K. A. D. P. Sachintha, A. C. D. Pigera, and C. S. Bandara

Effect of Ground Rice Husk on the Properties of Cement Block 341
P. L. J. Sajeevan, M. Nithurshan, and T. Thinojah

Effectiveness of Sri Lankan Bamboo as a Structural Material 353
S. V. P. Allalagoda, S. S. Bandaranayake, T. V. D. V. K. Vitharana, M. T. R. Jayasinghe, P. L. N. Fernando, and H. M. S. T. Herath

Life Cycle Assessment Perspectives in Buildings

A Study of Circular Economy Strategies for the Life Cycle of Building Construction Projects: A Systematic Review 371
H. C. Victar and K. G. A. S. Waidyasekara

A Study on the Applicability of Sustainable Features to Sri Lankan Road Construction 391
M. G. K. Hasanthika, V. Disaratna, and H. C. Victar

The Role of Landscape Characteristics on Thermal Environment of Residential Streets in Warm-Humid Colombo 405
C. Dissanayake and U. G. D. Weerasinghe

Assessment of Indoor Air Quality and Sick Building Syndrome in Apartment Buildings 421
N. R. Kumarage, C. Jayasinghe, K. P. H. Perera, K. K. G. K. D. Kariyawasam, and E. P. Wickramasinghe

Life Cycle Assessment (LCA) of a Textile Waste Thermoplastic Composite Material for Wall Partitioning Applications 441
R. M. N. Sulochani, R. A. Jayasinghe, C. Fernando, A. H. L. R. Nilmini, and G. Priyadarshana

Prefabricated Construction in Sri Lanka: From a Sustainability Perspective 451
J. Jayawardana, J. A. S. C. Jayasinghe, A. K. Kulatunga, M. Sandanayake, and G. Zhang

Resilience of Civil Infrastructure

Optical Fibre Sensing and Deep Learning-Based Disaster and Climate Change Risk Assessments of Civil Infrastructure: Current Status and Future Perspective 463
R. W. K. Anjana, H. M. C. M. Herath, U. M. N. Jayawickrema, and J. A. Epaarachchi

Numerical Investigation on the Impact of Corrosion on the Ultimate Compressive Strength of a Steel Angle Member Using the Thickness Reduction Method 477
G. R. C. R. Senevirathna, C. S. Bandara, and S. A. S. C. Siriwardane

Conservation and Management of Ancient Stupa Using Digital Twins: A Case Study of Uav-Based 3D Photogrammetric Digitization of Rankoth Wehera Stupa 493
S. Egodawela, H. A. D. S. Buddika, W. A. N. I. Harischandra, M. Mahmoodian, and M. R. S. N. M. Mathota

Use of Recycled Glass in Non-structural Building Elements for Improved Fire Performance 509
T. Thevega, J. A. S. C. Jayasinghe, C. S. Bandara, D. Robert, and S. Setunge

Fragility Prediction for Earthquake-Induced Embankment Failures Through Empirical Methods 519
S. U. Sathya, M. Mahmoodian, C. S. Bandara, N. Naderpajouh, and P. B. R. Dissanayake

Sustainable Construction

Co-Benefits of Adopting Green Concept for the Sustainable Building Construction in Sri Lanka 539
M. A. D. D. Mudannayaka and Jeeva Wijesundara

Effect of Malic Acid as a Compatibilizer in Chemically Modified Cassava Starch/Polyvinyl Alcohol Blends for Potential Packaging Applications 559
O. H. P. Gunawardene, S. M. Amaraweera, W. M. D. B. Wannikayaka, N. M. L. Fernando, C. A. Gunathilake, W. A. Manamperi, A. K. Kulatunga, and A. Manipura

Development of Cellulose Fibre-Reinforced Soil-Based Composite Wall Panels Using Selected Lignocellulosic Materials 597
M. M. H. Malshan, W. M. I. S. Jayaweera, G. I. P. De Silva, and T. N. Fernando

Application of Sustainability Concepts in the Lifecycle of Building Façade: A Review 611
Olga Pilipenets, Felix Kin Peng Hui, Tharaka Gunawardena, Priyan Mendis, and Lu Aye

Producing Sustainable Rigid Pavements with the Addition of Graphene Oxide 629
I. Fonseka, T. Ginigaddara, K. Wijesooriya, D. Mohotti, P. Mendis, and C.-K. Lee

The Role of Professionals Involved in the Built Environment in Contributing to Climate Change Adaptation in Sri Lanka 639
Deshan Pasindu, Bawantha Rathnayaka, Dilum Rajapaksha, Chandana Siriwardana, and Lalith Rajapaksse

A Systematic Literature Review on Climate Change Adaptation Measures for Coastal Built Environment 651
Dilum Rajapaksha, Bawantha Rathnayaka, Chandana Siriwardana, and Lalith Rajapakse

Tall Buildings

Achieving Net-Zero-Energy Tall Buildings in Sri Lanka 675
Lu Aye, Amitha Jayalath, and Dan Wu

Effectiveness of Various Outrigger Systems of Different Structural Materials for Lateral Load Resistance in Reinforced Concrete High-Rise Buildings 687
N. A. A. C. Nissanka, A. M. Fernando, and J. C. P. H. Gamage

Quantification of Degree of Irregularity in Mass Irregular RC Buildings Using Irregularity Index Based on Dynamic Characteristics 703
H. M. S. C. Rathnasiri, J. A. S. C. Jayasinghe, and C. S. Bandara

Effects of Spandrel Heights on Leapfrog Effect in Tall Buildings 717
R. A. D. M. Kahatapitiya, T. A. Reckerman, T. G. P. L. Weerasinghe, I. R. A. Weerasekera, W. J. B. S. Fernando, and P. Mendis

Technological Advancement for Safe Water Supply

Advances in Coagulation Technique for COD Removal of Petroleum Wastewater—A Review 733
Poornima Moremada and Senajith Kalpage

Efficiency of Emerging Low-Cost Adsorbent Materials in Removal of Colour from Stabilized Landfill Leachate 749
W. S. M. S. K. Wijerathna, L. M. L. K. B. Lindamulla, R. M. L. D. Rathnayake, K. G. N. Nanayakkara, and K. B. S. N. Jinadasa

Simulation of the Dynamic Behaviour of Pollutants Releasing from a Long Sea Outfall 759
D. P. C. Laknath, R. N. Udarika, and I. L. Abeygoonasekera

Coastal Pollution in Sri Lanka: Perspectives on the Current Status, Policy Implementation, and Institutional Mechanism 771
D. P. C. Laknath, I. G. I. K. Kumara, and T. U. S. Manamperi

Experimental Investigation of Debris Transport Due to Extreme Hydrodynamic Flows Induced by Tsunami 785
N. R. Josiah, S. Araki, and D. P. C. Laknath

Waste in the Construction Industry

Manufacturing of Paving Blocks Using Tile Waste 801
D. L. C. P. Chandrasekara and M. L. C. Surangi

Use of Waste Materials for Sustainable Pavement Industry in Australia: A Review 811
C. Gallage and S. Jayakody

Evaluation of Elemental and Chemical Compositions of Recycled Concrete Aggregates Produced from the Cowam Center, Sri Lanka 823
K. P. Arandara, S. T. Priyadarshana, G. N. Paranavithana, R. B. Mallick, and R. Dissanayake

Water Resources Planning and Pollution Control

Greywater Treatment by Vertical Subsurface Flow Constructed Wetlands Planted with *Cyperus Involucratus* 837
M. N. S. Dayarathna, G. M. P. R. Weerakoon, and M. I. M. Mowjood

Reuse Potential of Drinking Water Treatment Plant Sludge for the Manufacture of Concrete Paving Blocks 853
S. Sajitthan, E. P. Rajapakshe, I. M. W. K. Illangasinghe, and J. M. A. Manatunge

Effect of Available Topographic Maps on Flood Modeling Studies in Sri Lanka 869
P. D. P. O. Peramuna, N. G. P. B. Neluwala, K. K. Wijesundara, P. B. R. Dissanayake, S. DeSilva, and S. Venkatesan

Importance of Leaving Intermittent Rivers and Ephemeral Streams (Ires) Untouched in a Sustainably Built Environment 887
M. D. D. Perera, T. M. C. I. Madhushani, and P. I. A. Gomes

Bridge Design Construction and Maintenance

Effect of Live Load Increment of Old Steel Railway Bridges in Sri Lanka

H. S. C. Padmasiri, G. L. A. S. Punyawardhana, D. K. D. Limesha, and P. A. K. Karunananda

Abstract In Sri Lanka, most of the railway steel bridges are about 100 years old, and they were built during the British colonial period. But nowadays there are existences of various failures on bridges due to the increasing weight and speed of modern trains. At the time of the construction of the railway bridges in Sri Lanka, the speed of the trains used for transport ranged between 45 and 50 km/h and the weight of the trains was 60 tons. But at present, the weight of trains has significantly increased to 120 tons and the speed is 120 km/h. This issue is more prominent in the Northern railway line after Mahawa railway station. Most of the bridges on the Northern railway line have deteriorated, among them Malwathu Oya and Kala Oya bridges were identified as critical by the railway department. On those two bridges loosening nuts and bolts and cracking of the bridge members are visible. Using the visual condition and field visit data gathered, highly deteriorated bridge members were selected to evaluate the occurrence of the vibration effect. The modern vibration test was used to find vibration responses, and bridge material was tested to find the basic mechanical properties. The selected bridges were modelled with SAP2000 V.16, general-purpose structural analysis software, and moving load nonlinear analysis was done using the data of historical locomotives operated over the bridge. Here the locomotive loads were multiplied by a factor to simulate the dynamic effect. SAP2000 results were used to find the stresses of critical members of those two bridges. Then numerical results of the validated analytical model were verified through the experimental result. The results show that there was a significant dynamic effect due to the live load increment of these two bridges.

Keywords Steel bridges · Vibration analysis · Live load increment · Finite element analysis

H. S. C. Padmasiri (✉) · G. L. A. S. Punyawardhana · D. K. D. Limesha · P. A. K. Karunananda
Department of Civil Engineering, The Open University of Sri Lanka, Nawala, Sri Lanka
e-mail: hscp.eng@gmail.com

© The Author(s), under exclusive license to Springer Nature Singapore Pte Ltd. 2023

R. Dissanayake et al. (eds.), *ICSBE 2022*, Lecture Notes in Civil Engineering 362,
https://doi.org/10.1007/978-981-99-3471-3_1

1 Introduction

In the modern era, public transportation is highly effective than private transportation. In public transportation, the train is one of the most effective methods of transportation than any other method of transportation as it saves time and money for its users. Therefore, the development of the train system and its infrastructure play a vital role in transportation.

Metal bridges were introduced to Sri Lanka in the nineteenth century with the development of the railway network. A maximum of the metallic bridges is nevertheless in operation even after 10–15 long decades. Those aged, Annealed steel bridges are still servicing the railway network and to achieve high velocity and performance, the Sri Lanka railway has started working with heavy engines. Due to the increasing weight and speed of trains, the dynamic impact on bridges has increased. This issue is more prominent in the Northern railway line after Mahawa railway station. Railway bridges are experiencing heavy fluctuation loads because of the operation of heavy engines. Most of the metallic railway bridges have started to deform or even cracks have formed in some of the bridge components.

The dynamic performance of metallic railway bridges attracts in-intensity interest in engineering applications due to the importance and particularity of shifting trains' movements. The monitoring of railway bridges is consequently, increasingly famous because it offers a trustworthy method to help understand the train-brought approximately dynamic responses of bridges. Usually, for all railway bridges induced by train speeds over 200 km/h, a dynamic assessment is needed [1]. The magnitude, direction, position of a dynamic load, and structural response to dynamic loads vary with time. The dynamic impact of railway bridges underneath the motion of shifting trains is a complex phenomenon. Dynamic means the damper to the elastic resistance force and the addition of inertia force. Damping does oppose the motion of the structure and it tends to the capability of reducing the magnitude of vibration. This happens due to the dissipation of energy and low damping creates a high resonance and high-stress experience by structure. Due to the low damping of a bridge, various cracks and defects may occur in the bridge. The inertial forces are produced, which resist the accelerations of the structure. If a dynamic load is applied to a structure, the resultant response depends not only on the load but on the inertial forces as well. Thus, the corresponding internal response in the structure must equilibrate not only to the externally applied forces but also to the inertial forces resulting from the accelerations of the structure.

Since the British colonial era, the Sri Lanka railway consists of seven main lines with around 1350 bridges and culverts of various types. More than 90% (1180) of those bridges were constructed using steel. Table 1 shows details of the Sri Lanka railway network.

In this study, a railway bridge in a Northern railway line was visually inspected and defects were identified and recorded. Thereby, most of the bridges on the Northern railway line have deteriorated and among them, Malwathu Oya and Kala Oya bridges were critical, according to the railway engineers in the railway department (Figs. 1 and 2).

Both bridges consist of different type's members such as top chords, bottom chords, cross girders, rail bearers, vertical members, and diagonal bracing with irregular sizes and shapes. Some cracks occurred in the members, especially in the burst of the rail bearers in the "Malwathu Oya" bridge, and the Sri Lanka railway has used temporary remedies to manage some critical situations related to these bridges. There were a lot of losing nuts and bolts in joint connections and corroded members on both two bridges. A lot of members were attacked by the pitting corrosion reducing their

Table 1 Detail of main railway lines in Sri Lanka

Line no.	Line	Completed year	Line length (km)	No of bridges
01	Mainline (Colombo–Badulla)	1924	290.5	159
02	Northern line (Polgahawela–Kankasanthurai)	1905	339	352
03	Batticaloa line (MahaOya–Batticloa)	1926	212	119
04	Puttalam line (Ragama–Puttalam)	1926	133	76
05	Coastal line (Maradana–Matara)	1895	157.88	61
06	Trincomalee line (Gal Oya–Trincomlee)	1927	70	46
07	KV line (Colombo fort–Avissawella)	1902	60	42

Fig. 1 General view of Kala Oya bridge

Fig. 2 General view of Malwathu Oya bridge

effective thicknesses. The bearing condition of the main girder and supports is not properly working. As this joint is a roller joint, no maintenance work such as applying grease to smooth the surface has been done in the last 50 years (Figs. 3 and 4).

This paper aims to find the critical members of the bridges when it's under cyclic loading and validate the numerical modal through the experimental outcomes. Also, estimate the vibration effect results and possible solutions for defects of the railway steel bridges.

Fig. 3 Crack in rail bearer

Fig. 4 Corroded steel components

2 Methodology

The methodology can be summarized as follows

I. Identification of the problem through the literature survey. (technical papers, past research, journals, and books)

The reason for the selection of these is that bridges 100 years old have never been assessed based on vibration before, particularly in Sri Lanka, reported nut & bolt loosened in the last two years, and also repairs have been reported eight times in 2019,2020 alone.

II. Conduct field visits and inspections of the selected bridges

The dimensions of each component of the bridge were obtained and critical failures of both bridges were identified. Also, the number of locomotives travelling through the bridges and their cycling loads data were gathered.

III. Performing material testing and vibration-based test

The Hammer Hitting Type Brinell Hardness Tester Model was conducted to identify the material properties and the vibrational effects were identified by using single-axis and tri-axial vibrational measurement equipment. According to the data gathered, maximum vibration stress and deflection of members were identified.

IV. Develop a numerical modal of the bridges

Kala Oya and Malwathu Oya railway bridges were modelled where stresses have been analysed through the SAP 2000 V.16, a general-purpose software package.

V. Validate the finite element model to analyse the bridges

Corrected stresses are arranged according to the daily train schedule and applied in the proposed model. Then compare the value of the vibrational experimental test data and finite element method numerical data based on different train load variations.

VI. Improve dynamic characteristics of the bridges

Dynamic characteristics of bridges were identified, and possible solutions were recommended for defects.

3 Material Testing

HBC Hammer-Hitting Type Brinell Hardness Tester is designed to determine the Brinell hardness value of different metals by measuring the diameter of the indentation left on the test piece and the standard hardness test block. Indentations are obtained in such a way that a steel ball of a certain diameter is put in between the test piece and the standard hardness test block, and then an instant impact load is applied to them. The Brinell hardness value is thus obtained by first measuring the indentation and then referring to the conversion table (Fig. 5).

According to the data gathered, the yield strength of the steel used for constructing the Kala Oya Bridge is 419.57 MPa and the steel's yield strength used to construct the Malwathu Oya Bridge is 376.78 MPa.

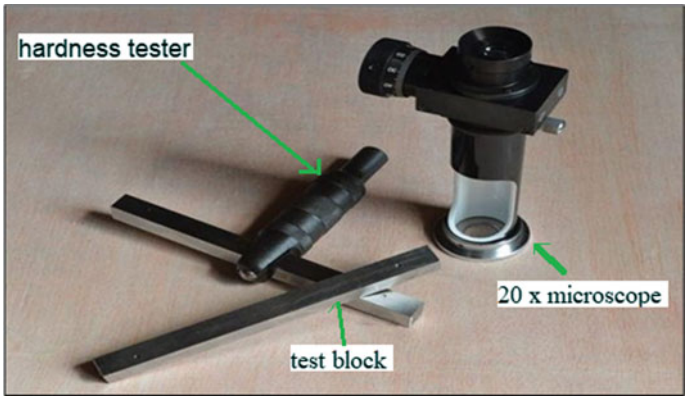

Fig. 5 HBC type Brinell hardness tester

4 Vibration Analysis

In this study, vibration responses on the bridge elements were found by using a tri-axial accelerometer and a bi-axial accelerometer. In both two bridges, when a train was travelling, member acceleration, velocity, and absolute displacement were obtained for two bridge members using single-axis and tri-axis accelerometers at the same time as follows (Figs. 6 and 7).

Tri-axial accelerometers provide simultaneous measurements in three orthogonal directions for analysis of all the vibrations being experienced by a structure. The wireless triaxial accelerometer and single-axis accelerometer were placed for different

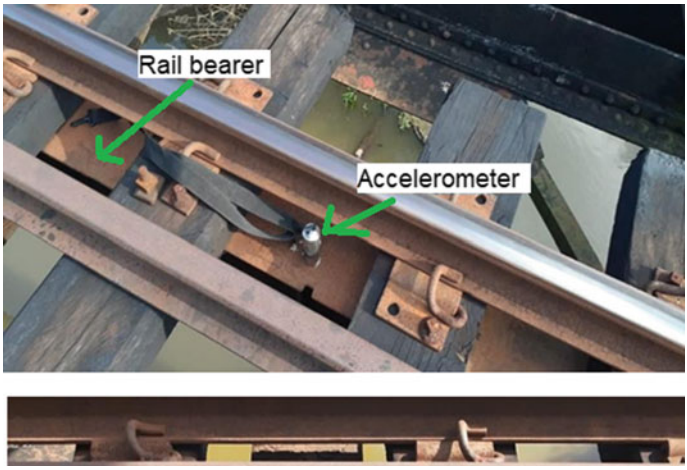

Fig. 6 Triaxle accelerometer placed in rail bearer

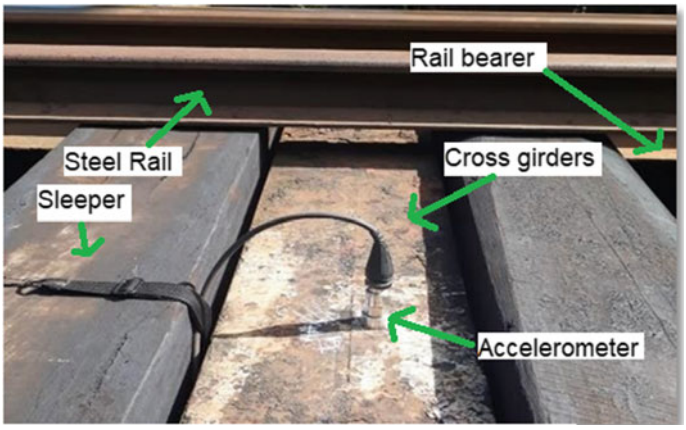

Fig. 7 Single axis accelerometer placed in cross girder

trains with different velocities in selected connection critical places to observe their vibration. Vibration speed is the parameter of the finest interest from the standpoint of damage potential. This is due to the fact the maximum stresses in a shape subjected to a dynamic load generally are due to the responses of the regular modes of the shape, this is, the responses at natural frequencies. Also, modal vibration stress is proportional to the natural frequency stress of members (Piersol and Paez 2010).

When determined by the maximum velocity, the maximum stress for any potential free vibration shape depends solely on the material's characteristics and a beam cross-sectional shape factor h /η, not on frequency [2].

$$\sigma \max = \mathrm{V}\max \frac{h}{\eta}\sqrt{E\rho} \tag{1}$$

here σ_{max} is the maximum modal stress in the structure, V_{max} is the maximum modal velocity of the structural response, E is Young's modulus, ρ is the density of the structural material, h is the maximum cross-sectional distance from the neutral axis and η is the radius of gyration.

$$\eta = \sqrt{I/A} \tag{2}$$

where "A" is a cross-sectional area, and "I" is the second moment of area about the neutral axis of the member.

The above data mainly show that the axial direction is more stressed than the horizontal and vertical directions. It is also a fact that as the speed of the train increases, the stress on its members increases. In addition, it seems that the bottom main girder receives less stress than the other members.

5 Finite Element Modeling of the Bridges

To predict the dynamic effect of the old steel bridges, critical total stresses of the bridge members should be found. It was intended to predict the dynamic and vibration effect of the identified critical bridges on the Northern railway line. Gathered data was used to analyse the process to determine the maximum total stress of each critical member by numerical modelling using SAP2000 V.16, a general-purpose software package.

The Kala Oya Railway bridge's total length is 95.097 m with two spans of truss girders, each simply supported on piers. Two spans are of similar trusses. A 3D skeletal frame finite element model was developed for a complete bridge span incorporating the double trusses, cross girders, rail bearers and bracings. The Malwathu Oya railway bridge consists of three spans of truss girders, each simply supported on piers. The bridge is a through bridge with a similar three-span having cross girders made of Annealed steel and supported on cylindrical piers. This is a Through-Warren Girder type bridge and consists of a 101.194 m overall length, with three spans. The

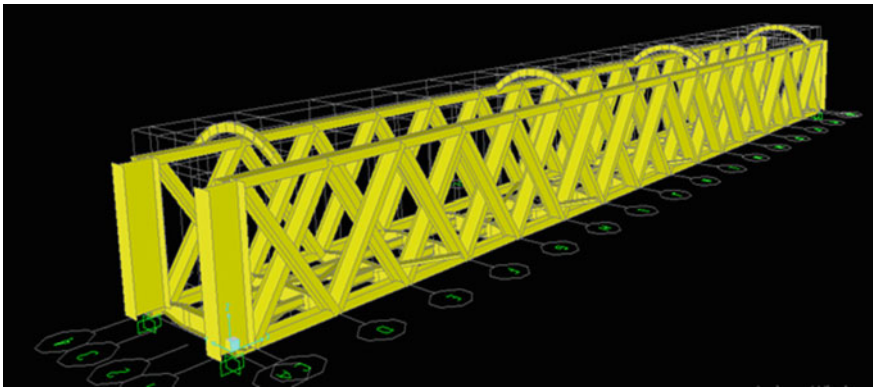

Fig. 8 3D bridge component arrangement

cross girders carry stringers, which support the two lines of the railway of gauge 1.676 m. The truss has a height of 4.140 m (Fig. 8).

5.1 Load Modal

The bridge is subjected to a combination of dead load and live load due to train traffic during the train's passage over the bridge. The identified maximum live load was the load due to the presently operative M11(130 tons) locomotive. Live loads of passenger compartments are negligible compared to the engine. To simulate the dynamic condition in this dynamic moving analysis, the live load was multiplied by a dynamic factor introduced as 1.5 [3]. Then, the stresses for other engine weights were calculated by multiplying the ratio of weights of a particular engine by the critical member's maximum and minimum stress values. According to British standard code 5400 part 2, a 1.25 factor of safety value was used for minimum stress in the 60–80 km/h speed limit and 1.5 value for the 80–100 km/h speed limit.

The load geometry here is based on transmitting the total weight through the axle to the wheels and finally to the rail bearer. Also, the power transmitted by one wheel is given as point load, and the distance between their axles is given in meters.

6 Results

From the vibration analysis, stresses on the cross girder and bridge members were determined using Eq. (1) (Tables 2 and 3) and outcomes were contrasted with the stress obtained from the numerical modal analysis. A comparison is shown in the Tables 4, 5 and 6.

Table 2 Vibration velocities and stresses on Malwathu Oya Bridge

Date	Time	Train velocity (km/h)	Locomotive	Location of member	Direction	Vibration velocity (m/s)	Stress (MPa)
21/11/21	2.42 p.m	85	S13	1st girder	Vertical	0.05	3.14
				7th girder	Vertical	0.06	3.86
				7th girder	Horizontal	0.02	1.27
				7th girder	Axial	0.05	3.14
21/11/21	4.00 p.m	90	S13	Left rail bearer	Vertical	0.06	4.00
				Right rail bearer	Vertical	0.07	4.25
				Right rail bearer	Horizontal	0.05	2.93
				Right rail bearer	Axial	0.10	6.76
21/11/21	5.20 p.m	102	S12	14th girder	Vertical	0.05	3.53
				8th girder	Vertical	0.04	2.90
				8th girder	Horizontal	0.02	1.49
				8th girder	Axial	0.13	9.35

7 Conclusions

The actual axial deflection values and the numerical axial deflection values of the rail support on the right side of the Malwathu Oya bridge are taken into account differently. Its actual deflection values are extreme compared to the numerical values. Also, axial stress and axial deflection values of some cross girders of the Kala Oya bridge are different compared to the actual and numerical values.

When the Kala Oya bridge is considered, the behaviour of its main members differs from each other. This is due to the vibration felt by the bridge due to the increase in speed and weight of the trains used. This scenario is the same for the Malwathu Oya bridge. According to the data gathered, there is no equal distribution of forces on the bridge as the properties of the material of which the bridge was made have changed. Malwathu Oya bridge is in a more critical condition than the Kala Oya bridge. The acceleration, speed and displacement due to trains on these two bridges are higher in the axial direction by comparing vertical and horizontal directions. Also, the cross girders rest on the main bottom girder which has less stress transferring and therefore more stress transfer along the rail bearing. Although the supports have a pin and roller, due to changes in their nature, their movement cannot be seen properly. Therefore, the load from the bridge is not properly transferred to the pier through the ground. Otherwise, loads on the bridges are distributed on the bridge itself.

Table 3 Vibration velocities and stresses on Kala Oya Bridge

Date	Time	Train velocity (km/h)	Locomotive	Location of member	Direction	Vibration velocity (m/s)	Stress (MPa)
21/11/21	6.45 a.m	49	M8	2nd girder	Vertical	0.05	3.20
				15th girder	Vertical	0.07	4.33
				15th girder	Horizontal	0.03	1.48
				15th girder	Axial	0.20	12.09
21/11/21	8.45 a.m	55	S12	12th girder	Vertical	0.12	6.81
				12th girder	Vertical	0.07	4.14
				12th girder	Horizontal	0.05	3.34
				12th girder	Axial	0.16	9.92
21/11/21	9.00 a.m	51	S13	8th girder	Vertical	0.07	4.38
				Rail bearer right	Vertical	0.03	1.89
				Rail bearer right	Horizontal	0.03	1.93
				Rail bearer right	Axial	0.17	11.20
21/11/21	10.00 a.m	65	S13	9th girder	Vertical	0.07	4.34
				Bottom main girder	Vertical	0.03	0.40
				Bottom main girder	Horizontal	0.03	0.42
				Bottom main girder	Axial	0.01	0.10

8 Recommendation

The following recommendations will focus on the assessment with a description of the potential for greater economic convenience and the durability of bridges.

(1) According to the analysis data, the Malwathu Oya & Kala Oya bridges are in critical condition. Among them Malwathu Oya is more critical; So the Sri Lanka railway should pay more attention to the Malwathu Oya bridge.
(2) Considering the vibrational stress felt on bridges using trains running at different speeds, the stress values for low speeds are lower and the stress values for higher speeds are higher. According to the analysis results maintaining an 80 km/h speed is recommended. Failure to do so will create further bridge damage.
(3) From the inspection data and data gathered from the railway department of Sri Lanka, it is evident that the bearings between the supports and the main girder of the bridges have not been serviced in 50 years. So, service should be done for the function of the bearing to be performed properly.

Table 4 Live load due to train traffic

No	Locomotive Type	Total Load (MT)	Load Geometry	SLS Factored Load per Wheel (kN)	ULS Factored Load per Wheel (kN)
1	M-04	91.28 MT	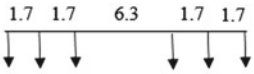	93.275	111.93
2	M-07	66.0 MT	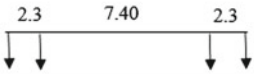	101.165	121.398
3	M-08	112.78 MT	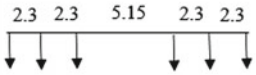	115.247	138.296
4	M-09	112.78 MT	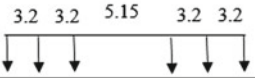	100.56	120.672
5	M-10	119.0 MT	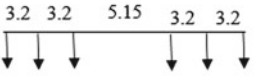	121.603	145.923
6	M- 11	130 MT	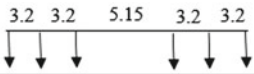	132.843	159.411
7	S-12	76 MT	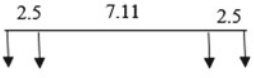	126.856	172.227
8	S-13	92 MT	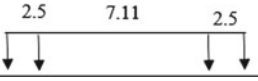	145.25	194.300

Table 5 Actual stress versus numerical stress on Kala Oya Bridge

Train	Member	Direction	Actual stress (MPa)	Numerical maximum stress (MPa)
M8	2nd cross girder	Horizontal	1.48	1.82
S12	5th cross girder	Horizontal	3.34	1.48
S13	Rail bearer	Axial	11.19	8.43
S13	Main bottom girder	Axial	0.10	1.20

Table 6 Actual stress versus numerical stress on Malwathu Oya Bridge

Train	Member	Direction	Actual stress (MPa)	Numerical maximum stress (MPa)
S13	7th cross girder	Horizontal	1.27	1.12
S13	Rail bearer right	Axial	6.76	3.48
S12	8th cross girder	Horizontal	1.49	1.68

(4) A system that properly transfers the stress felt from the cross girder to the main girder should be introduced for the two bridges. Therefore, introducing a bracing system is proposed.
(5) When the trains are running on the bridge it is recommended that running at uniform velocity without acceleration or deacceleration is advisable to prevent the hammering effect on the bridge.

Acknowledgements This work was carried out with the support of the Sri Lanka railway department.

References

1. Björklund L (2005) Dynamic analysis of a railway bridge: Subjected to high speed trains. Department of Civil and Architectural Structural Engineering the division of Structural Design and Bridges, at the Royal Institute of Technology, Stockholm
2. Gaberson HA, Chalmers RH (1969) Modal velocity as a criterion of shock severity. A Publication of The Shock and Vibration Information Center U.S Naval research laboratory, Washington, DC
3. Ranaweera MP, Aberuwan H, Maharoof ALM, Herath KRB, Dissanayake PBR, Siriwardane SASC, Adasooriya AMND (2002) Assessment of Kelani railway over Kelani River. University of Peradeniya, Sri Lanka, Engineering Design Centre
4. Frýba L (2001) A rough assessment of railway bridges for high speed trains. Eng Struct 23(5):548–556. https://doi.org/10.1016/s0141-0296(00)00057-2
5. Caglayan B, Ozakgul K, Tezer O (2012) Assessment of existing steel railway bridges. J Constr Steel Res 69:54–63. https://doi.org/10.1016/j.jcsr.2011.08.001
6. Icta (2011) History. Welome to department of railways. http://www.railway.gov.lk/web/index.php?option=com_content&view=article&id=137&Itemid=181&lang=en
7. Scribe (2022, April 12) Vibration measurement; vibration sensors; measuring vibration precisely. Lion Precision. https://www.lionprecision.com/vibration-measurement-and-sensors/

Use of Markov Chain Method to Predict Service Life of Reinforced Concrete Bridge Decks

W. G. K. Nirmal, P. Thadsanamoorthy, and G. Tharmarajah

Abstract Bridges are recognized as the most salient module in road and highway infrastructure in a country due to their unparalleled line of service to the nation's transportation framework. Therefore, the availability of a comprehensive Bridge Management System (BMS) in a country to evaluate aging bridges for long-term performance and life expectancy is highly productive and rewarding in terms of ensuring the structural reliability of commissioned bridges in that country. Currently, Sri Lanka has about 4800 bridges on National Highway Network (A & B class roads) spanning over the country. Aggressive environmental conditions, such as Chloride and CO_2 contamination in the atmosphere make reinforced concrete bridge structures corrode over time reducing their maximum designed service life (life expectancy). Therefore, the present research study was intended to develop a bridge remaining service life prediction model (bridge deterioration model) using the State-based Markov chain modelling process that involves bridge condition ratings assigned for 24 concrete bridges in Sri Lanka based on first-hand visual inspection and Non-destructive testing evaluation (NDTE) conducted on the reinforced concrete bridges.

Keywords Markov chain · Bridge management system (BMS) · Service life prediction · State-based modelling · Non-destructive testing evaluation (NDTE) · Condition rating

1 Introduction

Bridges are recognized as the most salient module in the Road and Highway infrastructure in a country due to their unparalleled line of service to the nation's transportation framework. Road Development Authority (RDA) of Sri Lanka with the deployment of Bridge Management and Assessment Unit (BM-AU) involves local bridge stock inspection, maintenance and repairing of bridges. BM-AU unit governed by

W. G. K. Nirmal · P. Thadsanamoorthy · G. Tharmarajah (✉)
Department of Civil Engineering, Sri Lanka Institute of Information Technology, Malabe, Sri Lanka
e-mail: gobithas.t@sliit.lk

© The Author(s), under exclusive license to Springer Nature Singapore Pte Ltd. 2023

R. Dissanayake et al. (eds.), *ICSBE 2022*, Lecture Notes in Civil Engineering 362,
https://doi.org/10.1007/978-981-99-3471-3_2

RDA currently manages 4,456 bridges with 3 m or greater span over the 9 provinces of the country. The bridges observed in Sri Lanka were built over the last 100 years which fall under major 4 categories of bridge types, such as Reinforced Concrete Slab (RC slab), Prestressed Concrete Beam (PSC Beam), Steel Composite and Bailey. The primary design standard incorporated in fabricating reinforced concrete bridges is BS 5400 and the construction practices have been changed and modernized with the advancement of the technology over the years. The bridge loading consists of self-weight of the bridge and truck live loads [1].

Bridge infrastructure deterioration with time is a substantially recognized threat to the national road infrastructure which can eventually lead to cause structural failure by exceeding designed moment capacities (resistance) of bridge structures. Both reinforced concrete and steel bridge elements tend to deteriorate due to natural and artificial occurrences. Depending on the various environmental conditions and the related exposure conditions throughout the island, it is necessary to pay attention about the corrosion of RC slab and beam bridges located along the coastal belt (e.g., 1–2 km from the ocean) of the island, since RC slab beam bridges tally up to a 55.5% of the total bridges of the country [2]. Potential bridge deterioration types identified in the study are chloride-induced corrosion, carbonation of concrete, alkali-silica reaction, mechanical damages resulting structural deformations, strains, cracks and superfluous vibrations mechanisms. Corrosion of reinforcement steel due to the chloride contamination in the atmosphere is significant and it may considerably impact the long-term performance of reinforced concrete bridges [1]. Corrosion of reinforcement may lead to loss of steel bar area which will ultimately cause to reduce the service life of the bridge structures. The linear correlation between the bar area loss and the bending moment capacity loss is generalized knowledge hence no thorough explanation is provided in the context [3]

Given the magnitude of the challenge to aging bridge structures in Sri Lanka, BM-AU unit of RDA has established a methodical condition rating criterion to evaluate the structural soundness of a bridge structure entirely based on data gathered over visual inspection of bridge structures. The check-listed data gathered over visual inspection are fed into a Bridge Information Database System utilizing Global Positioning System (GPS) technology to track down each evaluated bridge structure in the country. Based on the collected data, it has suggested that BM-AU possesses with sufficient information to identify potential deterioration hazards caused to the RC bridge structures. Even though BM-AU of RDA possessed with the bridge inspection records for evaluating the structural health of the aging bridges, a well-defined bridge deterioration model to predict the time-dependent performance and remaining service life of Class A and Class B Road bridges is still unavailable with local Bridge Management authorities in Sri Lanka. Presence of an efficient bridge deterioration model will benefit in making decisions related to life-cycle cost (LCC) assessment of highway bridges in terms of total cost amassed over the entire life span of the bridge from starting of the bridge inauguration until bridge replacement or demolition.

Reinforced Concrete (RC) Bridge structures have a designed life of 120 years. However, a typical bridge structure cannot be expected to survive the service life due to deteriorating nature taking place on structurally significant bridge elements such

as main girders, deck slabs, and bridge piers. Major deterioration factors influencing designed life of the concrete bridges are chloride ions and carbonation of concrete. Having relied upon above discussed exposure conditions affecting local bridge structures, it can be useful to have a tool that can predict the remaining service life of aging concrete bridge structures to make efficient decisions to replace or renew the existing bridge structures considering the structural safety.

Therefore, a research study was carried out to incorporate stochastic modelling techniques to predict the remaining service life of aging concrete bridges. Visual inspection and non-destructive testing of aging bridges were carried out as the assessment tool for feeding data to the bridge lifetime prediction model. 24 concrete bridges in Colombo and Gampaha districts had been visually inspected, and condition rated based on FHWA [4, 5] numerical bridge condition rating scheme.

2 Research Significance

Even though the local bridge management authority involves in the bridge management in terms of maintenance, repair and rehabilitation (i.e., MR&R) based on their identical way of condition rating of bridge infrastructure, no framework has been established to predict long-term performance of bridge facilities by providing reasonable estimates on bridge lifetime expectancy. Consequently, the bridges situated in the country have not been classified based on bridge deterioration governing parameters, such as annual daily traffic (ADT), climatic conditions, bridge construction type/material (i.e., Reinforced Concrete and Prestressed concrete) and construction era which are proven to be the primary bridge deterioration affecting parameters. On that account present study was intended to propose bridge remaining life prediction model by incorporating State-based Markov chain concept, the technique used by many advanced bridge management systems (BMS) like PONTIS [6] and BRIDGIT [7], etc. Since there has not been a large set of bridge inspection records employed in the research (only 24 bridges) the same consecutive generation of condition state transition probabilities was not involved when referring to Markov chain computations, rather a predefined set of condition transitioning probabilities originally derived by Jiang and Sinha [8] for bridge superstructure and substructure were employed to predict remaining service lives of selected set of concrete bridges.

This research is to propose a concrete bridge deterioration model that is capable of predicting the remaining service life of aging concrete bridges under a stochastic nature of modelling framework. Therefore, a prerequisite set of concrete bridges that are fallen under four structural soundness grades (A-Good to D-Critical) defined by BM-AU had to be selected for condition rating evaluation, which the condition rating data of each bridge will be used in State- based Markov Chain Decision Process (MDP) to compute the remaining service life of a bridge structure by considering a series of transitions between FHWA defined [4] bridge condition rating scales. When the condition of the rating reaches a certain portal value the bridge shall be repaired or replaced otherwise the bridge must be closed for the traffic. On that account,

researchers aim to contrive the most realistic service lifetime predictions for aging bridges by validating the Markov chain state-based model as there is high uncertainty and randomness involved in the bridge structure deterioration [9].

3 Stochastic Markov Chain State-Based Modelling

Markov chain in the form of typical state-based modelling was used to predict the remaining service life of the inspected bridge structures in this study. In the present study, Markov chain considered a sequence of transitions between FHWA (1995) bridge condition rating defined from 0 to 9 as 0 being the failed condition and 9 being the excellent condition. Table 1 demonstrates the FHWA (1995) condition rating scheme.

The fundamental teaching of the Markov chain concept is the future condition state of a bridge or any other infrastructure only depends on the present condition state of that structure and it doesn't depend on the past condition state of that particular infrastructure.

Table 1 FHWA defined condition rating system

FHWA defined condition rating system			
Condition index %	Number	Condition state	Physical description
91–100	9	Excellent	A new bridge
81–90	8	Very good	No problem noted
71–80	7	Good	Some minor problems
61–70	6	Satisfactory	Structural members show minor some deterioration
51–60	5	Fair	All primary structural elements are sound but may have minor section loss, deterioration, spalling or scour
41–50	4	Poor	Advanced section loss, deterioration, spalling. Scour
31–40	3	Serious	Loss of section, etc. has affected primary structural components. Local failures are possible. Fatigue cracks in steel or shear cracks in concrete may be present
21–30	2	Critical	Advanced deterioration of primary structural elements. Fatigue cracks in steel or shear cracks in concrete may be present or scour may have removed structural support. Unless closely monitored it may necessary to close the bridge until corrective action is taken
11–20	1	Imminent failure	Major deterioration or loss of section in critical structural component or obvious vertical or horizontal movement affecting structural stability. Bridge is closed for traffic but corrective action may put back in light service
0–10	0	Failed	Out of service. Beyond corrective action

3.1 Bridge Service Life

Bridge service life = Bridge Age + Time taken to reach condition state 3 (Remaining service life).

As shown by the above expression when condition rating value of a bridge structure reaches condition state 3, the bridge has to be repaired, replaced, demolished or closed for traffic. The duration between the bridge construction year and the year it will take to reach condition state rating 3 is defined as the bridge service life.

3.2 Employment of Markov Chain for the Bridges with Known Present Condition Ratings

Application of Markov chain concept in predicting remaining service life of concrete bridges involves definition of condition states in terms of bridge condition ratings and fitting of condition state transition probabilities from one condition state to another [8]. Seven bridge condition states were defined in relation to the corresponding seven condition ratings (FHWA 1995). Since there has not been any repair or bridge rehabilitation taken place within the bridge life span, condition rating is supposed to decrease along with the bridge age. In general, the probability of condition transitioning from a higher condition rating state to a lower condition rating in 1-year period can be notated as Pij. Figure 1 summarizes the predefined condition states and corresponding bridge condition ratings [8].

Bridge condition transition observed during bridge's life span is non-homogeneous since bridge deterioration rates vary in each stage of its life span. In order to overcome this difficulty bridge service life is divided into 6-year age groups. Within each of this age group Markov chain is assumed to be showing homogeneous transitioning. The transition matrix has the following form illustrated in Fig. 2.

In the above figure p(i) represents the probability of remaining at the same condition state and q(i) represents the probability of lowering the condition state. The condition state cannot be upgraded if any bridge maintenance has not been taken place. Due to the lack of previous bridge maintenance records of inspected bridge structures and the complexity of condition rating upgrading only the lowering of condition rating was considered.

3.2.1 Benchmark Example (Bridge No. 21/1 on B208)

Bridge remaining service life prediction using Markov chain process is demonstrated by the following shown numerical example:

FHWA bridge **Superstructure** condition rating is calculated as 5 (CR = 5) with a bridge age of 77 years (i.e., constructed in the year 1941).

		R=9	R=8	R=7	R=6	R=5	R=4	R=3
		S=1	S=2	S=3	S=4	S=5	S=6	S=7
R=9	S=1	$p_{1,1}$	$p_{1,2}$	$p_{1,3}$	$p_{1,4}$	$p_{1,5}$	$p_{1,6}$	$p_{1,7}$
R=8	S=2	$p_{2,1}$	$p_{2,2}$	$p_{2,3}$	$p_{2,4}$	$p_{2,5}$	$p_{2,6}$	$p_{2,7}$
R=7	S=3	$p_{3,1}$	$p_{3,2}$	$p_{3,3}$	$p_{3,4}$	$p_{3,5}$	$p_{3,6}$	$p_{3,7}$
R=6	S=4	$p_{4,1}$	$p_{4,2}$	$p_{4,3}$	$p_{4,4}$	$p_{4,5}$	$p_{4,6}$	$p_{4,7}$
R=5	S=5	$p_{5,1}$	$p_{5,2}$	$p_{5,3}$	$p_{5,4}$	$p_{5,5}$	$p_{5,6}$	$p_{5,7}$
R=4	S=6	$p_{6,1}$	$p_{6,2}$	$p_{6,3}$	$p_{6,4}$	$p_{6,5}$	$p_{6,6}$	$p_{6,7}$
R=3	S=7	$p_{7,1}$	$p_{7,2}$	$p_{7,3}$	$p_{7,4}$	$p_{7,5}$	$p_{7,6}$	$p_{7,7}$

Note: R = Condition Rating

S = State

$p_{i,j}$ = Transition Probability from State i to State j

Fig. 1 Condition ratings, states and transition probabilities [8]

$$P = \begin{vmatrix} p(1) & q(1) & 0 & 0 & 0 & 0 & 0 \\ 0 & p(2) & q(2) & 0 & 0 & 0 & 0 \\ 0 & 0 & p(3) & q(3) & 0 & 0 & 0 \\ 0 & 0 & 0 & p(4) & q(4) & 0 & 0 \\ 0 & 0 & 0 & 0 & p(5) & q(5) & 0 \\ 0 & 0 & 0 & 0 & 0 & p(6) & q(6) \\ 0 & 0 & 0 & 0 & 0 & 0 & 1 \end{vmatrix}$$

Fig. 2 Transition matrix

Initial state vector for the bridge = $Q_{(0)}$ = [0 0 0 0 1 0 0] where the condition rating value 5 is represented by a unit value in the initial state vector.

Condition rating vector, R = [9 8 7 6 5 4 3].

Estimated condition rating by Markov chain at time t can be denoted as E (t, P),

$$E(t, P) = Q_{(t)} \times R' \tag{1}$$

where,

$$Q_{(t)} = Q_{initial} \times P$$

$Q_{(t)}$ state vector at time 't'.
$Q_{initial}$ initial state vector.
P transition probability matrix.
R' transform of condition rating vector R (i.e., R = [9 8 7 6 5 4 3]).

For the benchmark bridge 21/1.

E(0, P) $Q_{(0)} \times R' = 5$ = Current condition rating (Current Bridge Age = 77).
$Q_{(1)}$ $Q_{(0)} \times P$ [P is developed based on Superstructure transition probabilities (Age > 60)].
E(1, P) $Q_{(1)} \times R'$ = Condition rating of the Bridge after 1 year of period (Bridge Age = 78).
$Q_{(2)}$ $Q_{(1)} \times P$.
E(2, P) $Q_{(2)} \times R'$ = Condition rating of the Bridge after 2 years of period (Bridge Age = 79).
$Q_{(21)}$ $Q_{(20)} \times P$.
E(21, P) $Q_{(21)} \times R' = 3$ = Condition rating of the Bridge after 21 years of period (Bridge Age = 98).

As shown in the above steps vector-matrix multiplication and vector row-column cross multiplication are executed until the condition rating value reaches 3. The time in 'years' is measured until the future condition rating state reaches 3, where the bridge should be repaired or replaced subsequently. Otherwise, the bridge should be closed for the traffic.

4 Results and Discussion

The Overall Condition Rating (OCR) of a bridge was represented by either Superstructure or Substructure condition rating as shown in the Table 2.

From Table 2, it is evident that the bridge life expectancy or long term structural performance is primarily governed by the superstructure components. Due to the structural significance, distress observed in the superstructure components was weighted over distress observed in the substructure components.

Also, the present study investigates the relationship of structural performance under various criteria, such as major types of structural components (superstructure and substructure), material type (reinforced concrete and prestressed concrete) distance to coastline, and the period of construction (construction era).

Bridge deterioration rate based on the construction period is plotted in Fig. 3. The bridges constructed since 1940 till 2017 have been divided into four groups each having around 20 years of time duration. This study encompasses the fact that the quality of construction techniques and the material has been enhanced over the years from 1940 to 2017.

As the age (i.e., total life span) of the bridge structures increases, the rate of bridge deterioration also increases proving the fact that the bridges tend to reach the end of

Table 2 Overall condition ratings of the investigated bridges

No.	Route no.	RDA bridge no.	Class	Bridge construction year	Span arrangement	Dominant distress type	Condition rating % (condition state)
1	B240	7/1	A	1982	3	None	92.1 (9)
2	B307	2/1	A	2015	3	Scalling	95.1 (9)
3	B228	1/1	B	1998	1	Cracking	75.5 (7)
4	B322	9/1	B	1945	1	Cracking	46 (4)
5	B425	1/1	C	1962	1	Rebar Exp	47.7 (4)
6	B324	2/1	D	1978	1	Erosion/ crack	74.6 (7)
7	B324	10/4	D	1945	1	Spall/crack	59.8 (5)
8	B324	14/1	D	1945	1	Spall/crack	69.3 (6)
9	B324	14/2	D	1945	1	Spall/crack	71.5(7)
10	B111	19/2	D	1950	1	Crack in Abutment	63.2 (6)
11	B208	21/1	D	1941	1	Spall/crack	58.8 (5)
12	B445	8/3	B	1970	1	Spall/crack	59.3 (5)

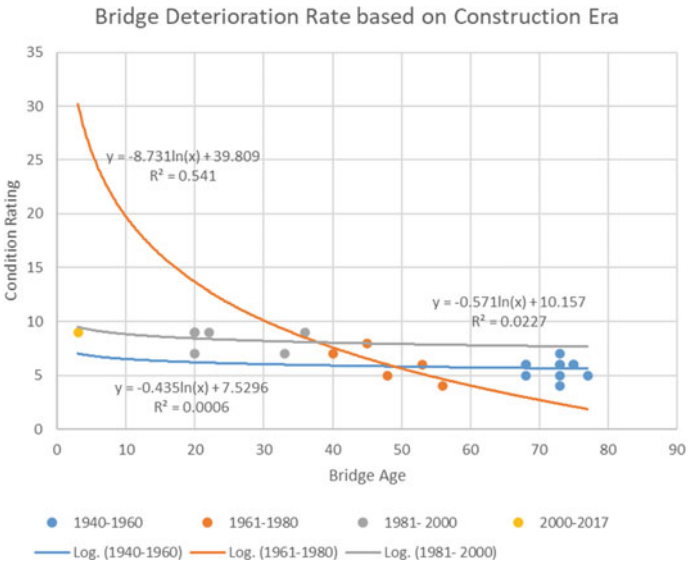

Fig. 3 Construction period vs condition rating

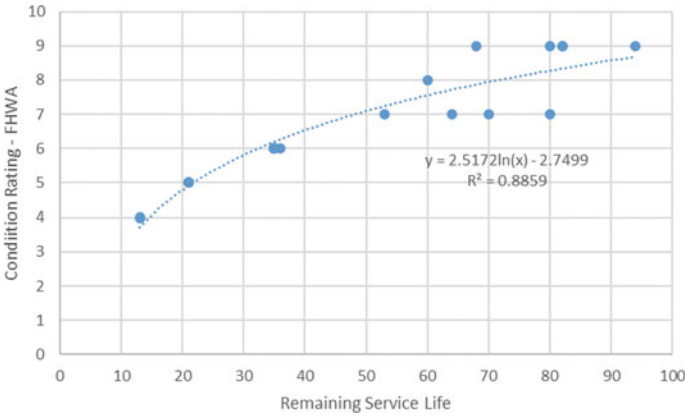

Fig. 4 FHWA condition ratings versus remaining service lives of bridges

service lives faster in the latter phase of the service life cycle. A similar observation was made by Jiang & Sinha (1990). It is evident that the recent construction era (1981–2000) is showing less deterioration rate than older constructions (1961–1980). However, it is believed, that increasing the number of data will enhance the accuracy of the results.

The FHWA Bridge condition rating plotted against remaining service life is shown in Fig. 4. The graph depicts the variation of remaining service life among bridges despite having the same condition rating.

Table 3 shows the condition ratings forecasted using the Markov Chain method. The bridges are also compared with RDA classifications. It can be observed that the authorities assigned lower condition rating for class C and D bridges than their actual structural health condition determined by the present study using weighted average technique and FHWA (1995) condition rating scheme. It shows that the rating classification used by local authorities requires improved methodology as Markov chain to predict the service life 21–35 years ahead without having any major rehabilitation while local authorities classify them as type C and D bridges that require agent attention.

5 Conclusion and Recommendations

The research study presents an integrated process (bridge deterioration model) to determine the remaining service life of the concrete bridge structures by employing a comprehensive bridge condition rating system under a stochastic and probabilistic framework. Deterioration model has two components, such as condition rating assessment based on weight averaging technique and the Markov chain state-based process for forecasting future condition state of a bridge. It is evident that the bridge

Table 3 Estimated total life span using the Markov chain method

No.	Route no.	RDA bridge no.	RDA bridge structural health classification	Bridge type	FHWA percent condition rating and the (condition state)	Remaining service life (Markov chain probabilities)	Total life span
1	B240	7/1	A (100-75)	PSC Beam	95(9)	68	104
2	B307	2/1	A	RC Slab	95.1(9)	94	97
3	B426	10/2	A	PSC Beam	81.6(8)	60	105
4	B263	1/5	A	PSC Beam	92.1(9)	80	102
5	B47	1/2	A	PSC Beam	92.1(9)	82	102
6	A0	5/1	A	PSC Beam	92.1(9)	82	102
7	B322	9/1	B (75-50)	RC Slab	46(4)	13	86
8	B445	8/3	B	RC Slab	59.3(5)	21	98
9	B095	7/3	B	RC Slab	58.8 (5)	21	89
10	B095	7/2	B	RC Slab	69.2(6)	35	103
11	B228	1/1	B	PSC Beam	75.5(7)	80	100
12	B228	2/1	B	PSC Beam	73.7(7)	70	103
13	B426	7/12	C (50–25)	RC Slab	71.8(7)	53	126
14	B435	6/1	C	RC Slab	70(6)	35	110
15	B435	4/1	C	RC Slab	70(6)	35	110
16	B435	4/2	C	RC Slab	68.6(6)	35	110
17	B425	1/1	C	RC Slab	47.7(4)	13	69
18	B367	6/3	C	RC Slab	70(6)	36	89
19	B324	2/1	D (25–0)	RC Slab	74.6(7)	64	104
20	B324	10/4	D	RC Slab	59.8 (5)	21	94
21	B324	14/1	D	RC Slab	69.3(6)	35	108
22	B324	14/2	D	RC Slab	70(6)	53	126
23	B111	19/2	D	RC Slab	70(6)	35	103
24	B208	21/1	D	RC Slab	58.8(5)	21	98

deterioration stochastic model is not familiar to the Sri Lankan bridge management authorities because no past data is available on the stochastic modelling carried out based on the climatic condition, construction technique and construction era.

Avant-garde of this study is the incorporation of predefined set of condition transitioning probabilities in order to forecast the bridge remaining life expectance which solely depends on the present condition rating and the age of the evaluated bridge structure. The life expectancy of the bridge is not mandatorily the design life. The regression analysis over the predicted remaining life manifested that the coastal bridges were supposed to have lesser life expectancy than the inland bridges. Hence maximum design life ranging from 98 to 110 years can be expected for a typical concrete bridge structure.

The Markov chain Decision Process (MDP) was used to obtain the time needed for a concrete bridge to change from a higher condition rating to a lower condition rating and the computations involving iterations were done using MATLAB which employed a set of predefined condition transition probabilities. The investigated 24 bridges provided reasonable time estimates despite challenges in local data collection. Thus, the methodology adopted in this research study can be improved by incorporating large set of bridge condition rating data collected by Bridge Management and Assessment Unit of Road Development Authority, Sri Lanka.

Acknowledgements Support provided by Bridge Management Unit of Road Development Authority (RDA), Sri Lanka to collect data and visit bridge sites is greatly acknowledged by the authors.

References

1. Stewart MG, Rosowsky DV (1998) Time-dependent reliability of deteriorating reinforced concrete bridge decks. Struct Saf 20(1). https://doi.org/10.1016/S0167-4730(97)00021-0
2. JICA (2013) Data collection survey on primary bridges on national roads and maintenance system of bridges
3. Heitner B, Obrien EJ, Schoefs F, Yalamas T, Décatoire R, Leahy C (2016) Probabilistic modelling of bridge safety based on damage indicators. Proc Eng 156. https://doi.org/10.1016/j.proeng.2016.08.279
4. FHWA (1995) Recording and coding guide for the structure inventory and appraisal of the nation's bridges. In: Federal highway administration report FHWA-PD-96-001 (Issue FHWA-PD-96-001)
5. United States Department of Transportation (US DOT) (2020) National Bridge Inventory (NBI)
6. Thompson PD, Small EP, Johnson M, Marshall AR (1998) The Pontis bridge management system. Struct Eng Int J Int Assoc Bridge Struct Eng (IABSE) 8(4). https://doi.org/10.2749/101686698780488758
7. Hawk H (1999) BRIDGIT: user-friendly approach to bridge management. Transportation Research Circular
8. Jiang Y, Sinha KC (1989) Bridge service life prediction model using the Markov chain. Transp Res Record 1223
9. Morcous G (2006) Performance prediction of bridge deck systems using Markov chains. J Perform Constr Facil 20(2). https://doi.org/10.1061/(asce)0887-3828(2006)20:2(146)

Thin-Walled Hollow Steel Box Piers with Energy Dissipation Mechanism Under Bi-directional Cyclic Loading

M. Jenothan, J. A. S. C. Jayasinghe, C. S. Bandara, and A. J. Dammika

Abstract The seismic design of bridge piers is often conducted using horizontal dynamic analysis employing several orthogonal directional seismic acceleration data. This simplistic treatment, however, does not account for the effect of complex earthquake loading as a structural response to inelastic interactions. This study explores the hysteretic behaviour of a proposed thin-walled steel square box column with an energy dissipation mechanism under constant axial force and linear and non-linear cyclic lateral loading. First, the adopted finite element model (FEM) in ABAQUS is validated with experimental results from the published research and then used for analysis. Then, several linear and non-linear idealised loading patterns are used to evaluate the strength and ductility of the proposed and standard columns. In addition, the failure mechanisms of each proposed column were explored for specified loading patterns.

Keywords Cyclic lateral loading · Ductility · Load pattern · Non-linear finite element simulation · Strength · Thin-walled steel box column

1 Introduction

Steel bridge piers with hollow box sections are commonly employed in urban locations such as elevated towers, viaducts, bridges, flyovers and transmission towers worldwide due to their faster construction than concrete piers [1, 2]. In contrast to the steel columns in buildings, these piers have a low axial force ratio (i.e., the ratio of axial force to the squash load) [3, 4]. Consequently, they are designed with relatively high width-to-thickness ratios of component plates, which make them susceptible to local buckling damage during a significant seismic event [5]. One of the most critical considerations in earthquake zones is the structural soundness of bridge piers. After experiencing catastrophic damage to bridge piers and their collapse during the 1995 Hanshin-Awaji Earthquake [magnitude (Mw) 7.1], the design code for

M. Jenothan (✉) · J. A. S. C. Jayasinghe · C. S. Bandara · A. J. Dammika
University of Peradeniya, Getambe, Sri Lanka
e-mail: makeswaranjenothan@eng.pdn.ac.lk

© The Author(s), under exclusive license to Springer Nature Singapore Pte Ltd. 2023

R. Dissanayake et al. (eds.), *ICSBE 2022*, Lecture Notes in Civil Engineering 362,
https://doi.org/10.1007/978-981-99-3471-3_3

bridges in Japan was extensively altered to account for such a massive earthquake [6]. The most recent specification for highway bridges [7, 8] recommends using reliable and well-established time-domain simulation techniques to evaluate the seismic performance of bridge piers to mitigate damage and prevent a collapse during rare significant earthquakes such as the Hanshin Earthquake. Consequently, their seismic performance is crucial for reducing disruptions to the urban transportation system.

However, the current seismic design standards for steel columns are based on several analytical and experimental studies carried out with constant axial loads and uni-directional lateral loads [9]. In reality, earthquake ground motion is complicated, with three-dimensional loading components acting concurrently instead of the presumed uni-directional loading patterns [10]. Furthermore, the hysteretic behaviour of thin-walled steel tubular columns subjected to multi-directional cyclic lateral stress is projected to be more critical and severe than uni-directional cyclic loading of the same amplitude [11]. Therefore, several scholars have studied the hysteretic behaviour of thin-walled steel tube columns under bidirectional cyclic lateral loads computationally and experimentally during the last few decades [9, 11–15]. An experimental study conducted by Dang et al. [16] demonstrated that thin-walled steel tubular columns subjected to bidirectional cyclic lateral loading suffer a significant loss in strength and ductility compared to uni-directional cyclic lateral loading and suggested to be used in seismic design. However, in recent years, seismic capacity checks have incorporated the superposition of independent action of uni-directional design seismic motion in orthogonal directions or the behaviour in the most critical direction. However, It is pretty challenging to evaluate the effect of interaction between the bidirectional non-linear behaviours of steel columns on the dynamic response [9].

Researchers have investigated conventional thin-walled steel square box columns with uniform plate thickness under multi-directional cyclic lateral loading. All these studies addressed that thin-walled steel columns suffer local buckling near the base [1, 5, 17–20]. To encounter this limitation and ensure adequate strength and ductile behaviour, a thin-walled steel stiffened square box column with energy dissipation mechanism has been recently proposed and investigated by the authors under constant axial force and uni-directional cyclic lateral loading [21]. In evaluating the proposed column, its strength and ductility improvement under uni-directional cyclic lateral loading is evident. The proposed column with an energy dissipation mechanism can be replaced after severe earthquakes without interrupting the transportation network. However, due to the complicity of the actual earthquakes, verifying the proposed column's performance under bidirectional loading is essential to ensure that the low yield point (LYP) steel plates are bucked before the L angles to fill the above-mentioned objectives of the proposed piers.

In this study, the proposed steel stiffened square box columns with an energy dissipation mechanism are to be evaluated and compared with the conventional piers with regard to the strength and ductility under uni-directional and bi-directional cyclic lateral loading with constant axial force. Further, by investigating the failure modes of the proposed piers, it was ensured that the corners of the pier can survive during

the complex bidirectional loading while the LYP plate buckle first. Initially, a reference thin-walled steel stiffened square box column (SM-B) from the reported literature was numerically analysed under constant axial force and bidirectional cyclic lateral loading to validate the accuracy of the adopted FEM. Then, the proposed column with energy dissipation mechanism is investigated under several bidirectional loading conditions. The study results show that the proposed columns are superior in terms of ultimate strength and ductility, compared to standard columns. Finally, each column's failure modes were compared extensively with each loading pattern and recommendations were made for future studies.

2 Numerical Analysis

2.1 Material Properties

In this study, a commercial finite element software ABAQUS 6.21 is employed for the FE analysis, where material and geometric non-linearities are considered during the computational process. The combined hardening material model, with the Von Mises yield criterion and associated plastic flow rule, is used in this study. This model simulates the inelastic behaviour of materials subjected to cyclic loading. Both LYP steel (LYP100) and normal strength steel (SM490) (Japanese Industrial Standard) grades are employed in this investigation. SM490 steel has a yield strength of 420 MPa, a tensile strength of 550 MPa, and Young's modulus of 206 GPa [22]. LYP100 steel has a yield strength of 100 MPa but an ultimate strength of 296 MPa and Young's modulus of 200 GPa, which is approximately three times greater [23]. Figure 1 depicts the combined hardening material model with the bi-linear material stress-strain curve utilised in this investigation.

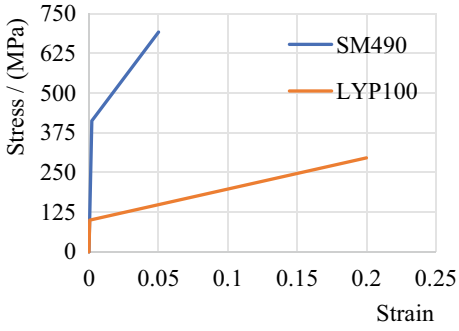

Fig. 1 Stress-strain behaviour of steel

2.2 Equivalent Thickness of LYP Steel Plate

Figure 1 shows that the yield stress of LYS steel is around 100 MPa and that strain hardening increases the tensile strength to approximately 271 MPa. The cycle loading test for steel piers necessitates extremely high strain levels exceeding the elastic limit, and the plastic limit surface of LYS steel is observed to expand significantly with cyclic loading [24]. As a result, the standard 0.2% yield stress level is no longer regarded as permissible. Therefore, the ultimate strength of the LYP steel was considered instead of its yield strength to determine the equivalent thickness of the LYP plate and the equivalent thickness of the LYP plate (t_{LY}) was calculated using Eq. (1), where (t_{SM}) is the plate thickness of SM490 steel and σ_{ySM} is the yield strength of the steel.

$$t_{LY} = \frac{\sigma_{ySM}}{\sigma_{uLY}} t_{SM} \tag{1}$$

2.3 Geometrical Details of the Columns

The 450 mm × 450 mm square cross-section gives all four columns an identical height of 2420 mm (Figs. 2 and 3). Furthermore, three columns were modelled with the energy dissipation component of the replaceable stiffened LYP steel plates welded to the L angles between the bottom diaphragm and base plate (Fig. 3).

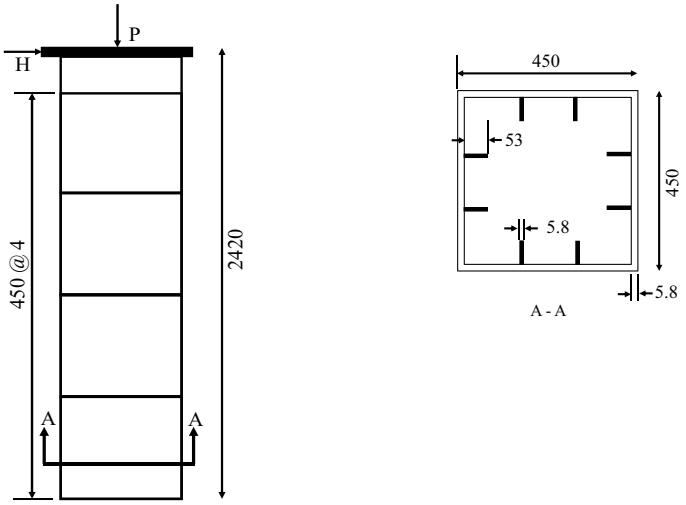

Fig. 2 Longitudinal and cross sections of standard column SM-B (Dimensions in mm)

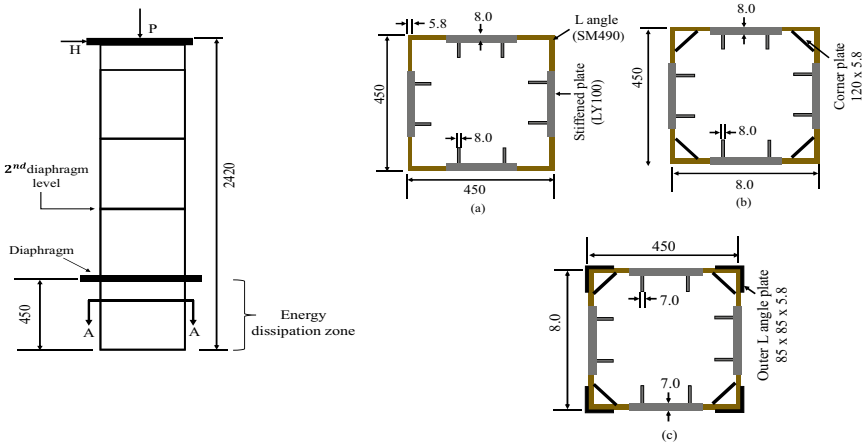

Fig. 3 Cross sections (A-A) of column arrangement: **a** LY-PL, **b** LY-PL-CO and **c** LY-PL-CO-LCO (Dimensions in mm)

The first column, SM-B, was composed of SM490 steel and served as a reference benchmark (Fig. 2). The FE model was validated using experimental results from the literature (Susantha, Aoki and Jayasinghe, 2007). The second column LY-PL is made up of four L angles welded between the bottom diaphragm and the base plate (450 mm height) and LYP steel plates welded between the L angles (Fig. 3a). The third column LY-PL-CO was designed the same way as the LY-PL specimen, with corner plates added to prevent pier corners from buckling (Fig. 3b). Finally, the last column, LY-PL-CO-LCO, was stiffened further using L corner stiffeners (Fig. 3c) to prevent corner buckling. Figures 2 and 4 show the geometrical features of the standard and columns with the energy dissipation components, with the main geometrical characteristics stated in Table 1.

Table 1 Geometrical details of the columns

Specimen	SM-B	LY-PL	LY-PL-CO	LY-PL-CO-LCO
Plate thickness/(mm)	5.8	8	8	7
L angle/(mm)	–	100 × 100 × 5.8	100 × 100 × 5.8	100 × 100 × 5.8
Longitudinal stiffener/(mm)	53 × 5.8	53 × 5.8	53 × 5.8	53 × 5.7
Corner plate stiffener/(mm)	–	–	120 × 5.8	120 × 5.8
L plate stiffener/(mm)	–	–	–	80 × 5.8
Cross section/(cm^2)	128	159	189	193

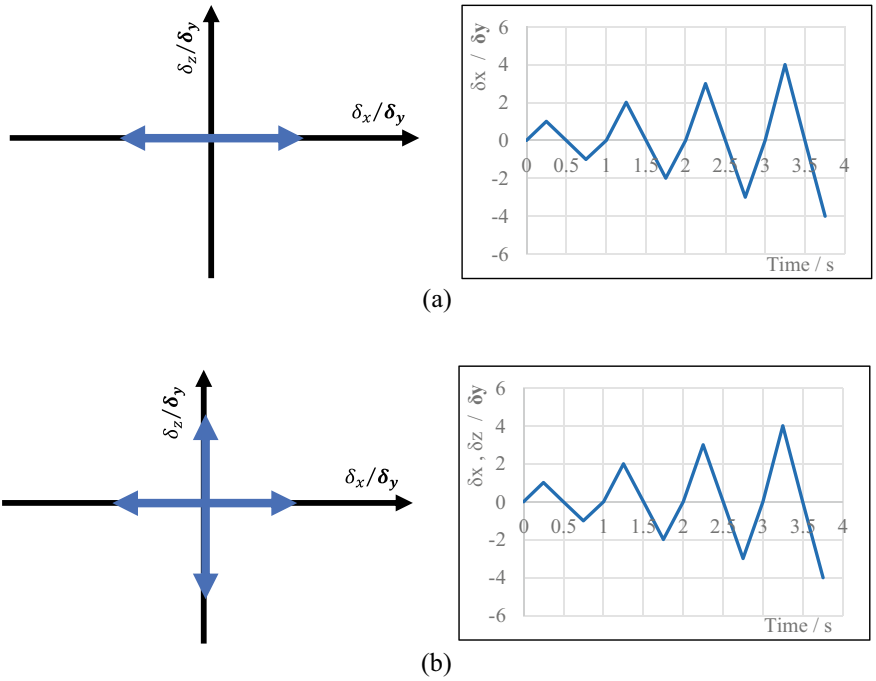

Fig. 4 Linear loading patterns: **a** UNI and **b** BI-L45

2.4 Loading Procedure

All the specimens were first loaded with 0.2 times the yield axial load (P_y) of the SM-B column, along with those two cases of lateral loading patterns (linear and non-linear). In the initial phase of this study, two forms of linear loading patterns were examined and validated using past experimental data [10]. As depicted in Fig. 4, the numerical model was subjected to (a) uni-directional loading (UNI) and (b) loading along an axis of an angle of 45° to the primary axis (BI-L45). In addition, as depicted in Fig. 5, piers were subjected to two non-linear loading patterns, BI-CI and BI-SQ, which are considered aa the most severe loading path among the many recorded earthquake ground motions [11, 25]. Throughout the loading history, the top of the column has been subjected to a combination of quasi-static cyclic lateral loading and constant axial load (P). The amplitude of the cyclic displacement was increased gradually as a multiple of the yield displacement (δ_y), which is defined by Eq. (2):

$$\delta_y = \frac{H_y h^3}{3EI} \tag{2}$$

$$H_y = \frac{M_y}{h}\left(1 - \frac{P}{P_y}\right) \tag{3}$$

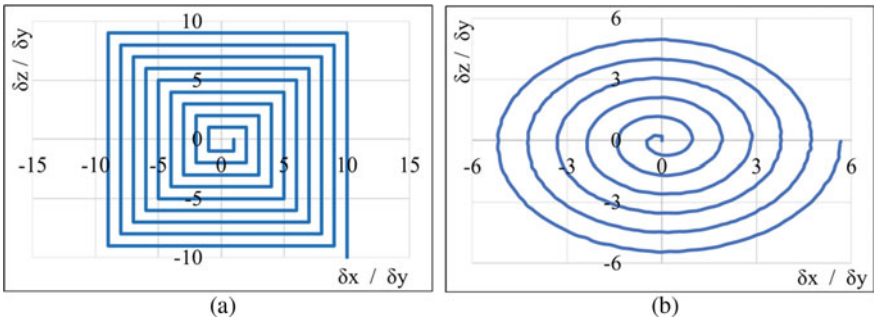

Fig. 5 Non-linear loading patterns: **a** BI-SQ and **b** BI-CI

where A, h, E, $I and M_y$ represent the cross-sectional area, height, Young's modulus, moment of inertia of the cross-section, and yield moment of the system, respectively.

2.5 Numerical Model

Subpanels, longitudinal stiffeners and diaphragms were modelled with four-node shell elements with reduced integration (S4R) and five integration points across the thickness. Then, a fixed boundary condition was applied to the base. Next, an axial and lateral cyclic load was applied using a reference point attached to the top of the column via a rigid connection. The experimental results of square box columns made of thin-walled steel indicate that local buckling occurs between the base and bottom diaphragm around the column base [5, 19, 20]. Consequently, the lower half of the pier was made up of 15 mm S4R elements. In comparison, the remaining height comprised of coarse mesh size of 20 mm S4R elements (see Fig. 6). Finally, mesh convergence tests were conducted to identify the above-illustrated mesh sizes. It was established that this mesh density produces precise results without significantly increasing processing time.

In addition, the current study does not account for initial geometrical imperfections and residual stresses because they were not quantified for the tested columns [18, 19, 26]. In addition, neither initial geometrical imperfections nor residual stresses caused by flange and web plate welding affected the entire cyclic behaviour after the first half-cycle. The impacts of early geometrical imperfection and residual stresses, according to Banno et al. [27] and Mamaghani et al. [3], reduce the initial stiffness and strength of thin-walled structures under monotonic loading. Nevertheless, they do not affect the global hysteretic response under cyclic loading.

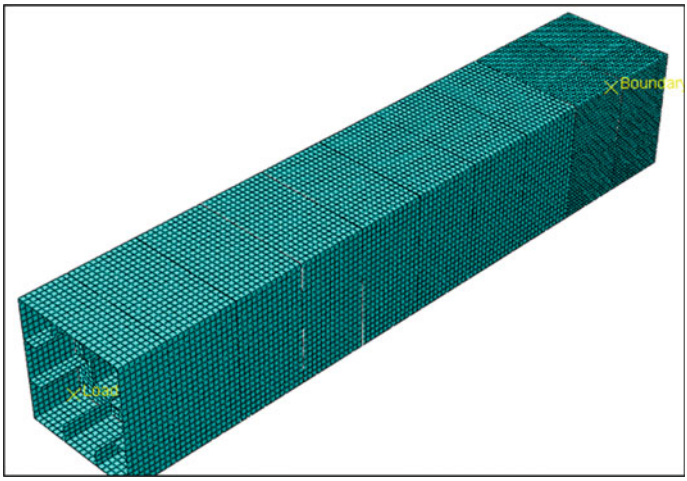

Fig. 6 Numerical model of the stiffened steel pier

3 Results and Discussion

3.1 Validation of the Numerical Model

The hysteretic and envelop curves of the finite element model were compared with experimental results from the literature [10]. As illustrated in Fig. 7, both the UNI and BI-45 loading patterns were used, with incremental cyclic lateral displacements along the X and Z directions. To ensure a valid comparison between the test and the numerical analysis, the similar loading history utilised in the test was used in the analysis. Figure 7 compares the test and the analytical results of the loading type UNI and BI-L45. Further, the hysteretic behaviour of the tested column under loading pattern BI-L45, in the lateral X direction, obtained from the analysis is compared to the experimental results in the literature [10]. The FE analytical and experimental results are comparable in both loading conditions (UNI and BI-L45). Therefore, the ultimate strength of the column is predicted with a 5% error in the UNI loading pattern (FEM: $H_{mx}/H_y = 1.2$, Experiment: $H_{mx}/H_y = 1.3$; see Fig. 7a), while the error percentage was a bit higher for the BI-L45 loading (error = 15%) in the X direction (FEM: $H_{mx}/H_y = 0.90$, Experiment: $H_{mx}/H_y = 0.78$; see Fig. 7b). In conclusion, the proposed FE model can accurately represent the structural behaviour of thin-walled steel-strengthened square box columns subjected to constant axial force and both uni and Bidirectional loading.

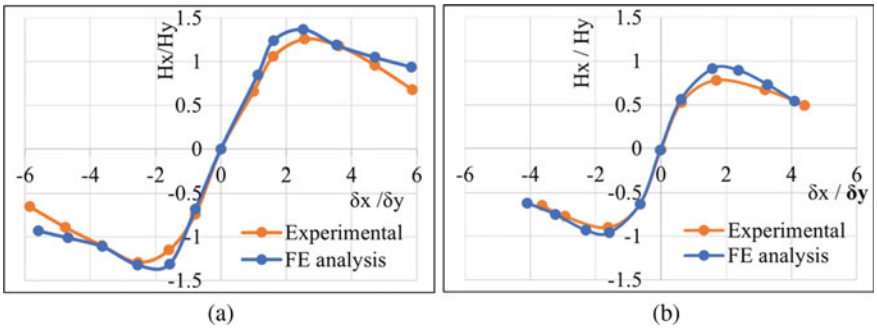

Fig. 7 Envelop curves of experimental results and finite element analysis: **a** UNI and **b** BI-L45 loading pattern

3.2 Hysteretic Behaviour and Performance of Thin-Walled Steel Hollow Piers with Energy Dissipation Mechanism

To examine the hysteretic behaviour of the column with the energy dissipation mechanism under constant axial force and bidirectional cyclic lateral loading, the validated FEM was utilised to conduct FE analyses. Figures 4b and 5 show that the displacement is applied in both X and Z directions under a bidirectional cyclic lateral loading pattern. Therefore, the columns display isotropic responses in the X and Z dimensions. In this study, the results in the X direction are only reported in the subsequent analysis to maintain clarity. For comparison, the value of the maximum load (H_m) is dimensionless using H_y of the standard pier and plotted in Fig. 9, along with ductility factors μ_m and μ_{95}, which are derived from Eqs. (4) and (5), respectively.

$$\mu_m = \delta_m/\delta_y \tag{4}$$

$$\mu_{95} = \delta_{95}/\delta_y \tag{5}$$

where δ_m = maximum displacement corresponding to the H_m and δ_m = displacement at 95% of the H_m after the peak.

Figure 8 depicts the normalised lateral load versus lateral displacement hysteresis loops for both standard and proposed columns for various loading patterns. The depicted envelop curve indicates a significant difference in strength and ductility between the bidirectional and the UNI loading pattern for the proposed columns. In addition, due to the bidirectional loading, particularly for BI-CI, the post-buckling behaviour of the column is significantly affected.

The strength and ductility versus the load pattern of all the specimens are plotted in Fig. 9 to inspect the loading pattern's sensitivity to the column's performance. A comparison between the uni-directional and bidirectional loading conditions was conducted to highlight the effect of the cyclic loading pattern on the hysteretic

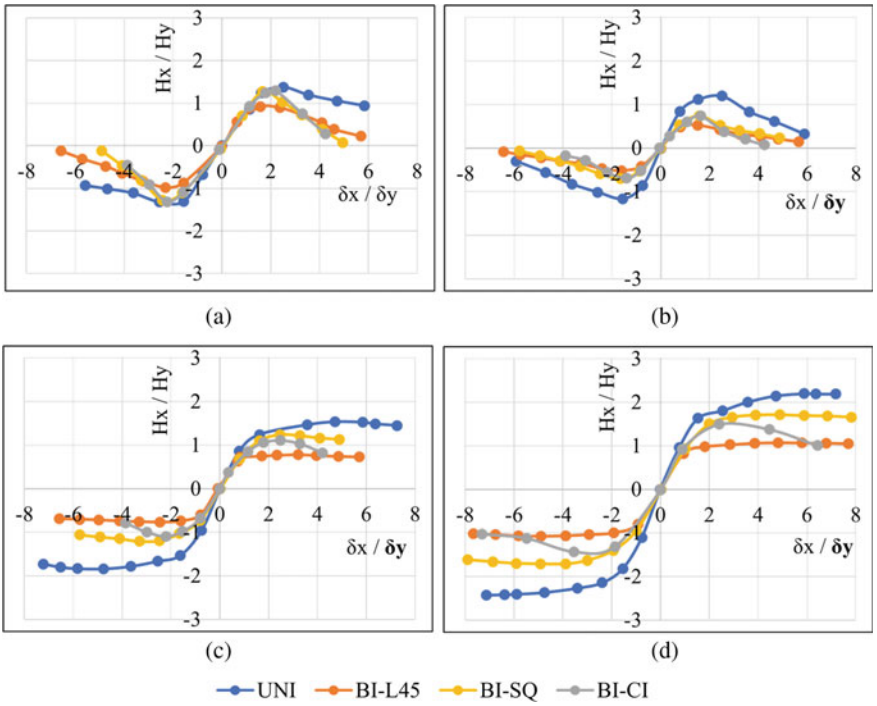

Fig. 8 Comparison of envelop curves with different load patterns: **a** SM-B, **b** LY-PL, **c** LY-PL-CO and **d** LY-PL-CO-LCO

behaviour of thin-walled steel stiffened square box columns with the energy dissipation mechanism. At the same amplitude of the applied displacement, the bidirectional loading pattern significantly caused more degradation in the strength and ductility of the column than the uni-directional loading pattern. Figures 8 and 9c indicates that the hysteresis loops under circular bidirectional cyclic lateral loading give the worst ductility parameters. On the other hand, BI-L45 gives the lowest maximum strength for all the columns, Figs. 8 and 9a. The possible reason should be the significant deterioration due to the accelerated local buckling under circular bidirectional cyclic lateral loading. However, from Fig. 9, it was understood that the inclusion of corner stiffeners is more critical in enhancing the performance of the proposed steel piers. The results of each specimen are separately discussed below, emphasising the behaviour of buckling deformation.

3.2.1 Column LY-PL (Without Corner Stiffeners)

It is evident from Figs. 8b and 9 that the LY-PL column has the lowest performance compared to the other columns, regardless of the loading pattern. Even though the μ_m and μ_{95} of the LY-PL column deviate from the SM-B column by negligible

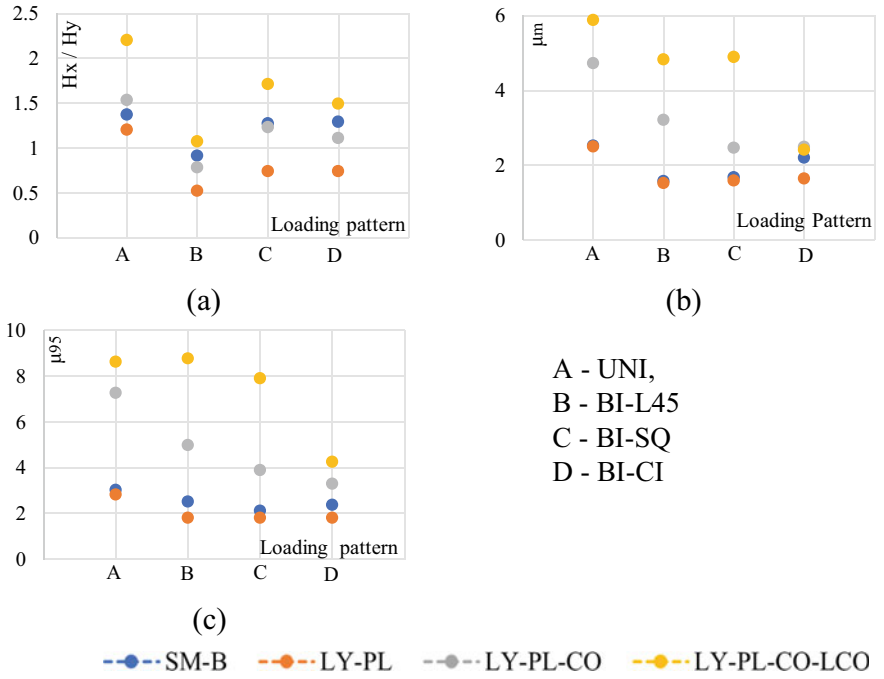

Fig. 9 Effect of loading pattern on strength and ductility: **a** LY-PL, **b** LY-PL-CO and **c** LY-PL-CO-LCO

amounts for all the loading patterns (see Fig. 9b, c), the maximum strength shows marginal deviation from the SM-B column (Fig. 9a). LY-PL has a 43% H_m/H_y value for the BI-SQ loading pattern lower than the SM-B pier. However, this difference was reduced to 22% for the UNI loading pattern (see Fig. 9a). After the maximum strength, the strength degradation rate is relatively high (particularly under Bi-CI loading), which is an unfavourable post-buckling behaviour during seismic events. The thickness of LYS steel plates is significantly more than that of SM-B. Hence it was expected that the specimen would have sufficient ultimate strength. Due to the weak tangential modulus and the absence of corner stiffeners, however, the buckling started rapidly and increased rapidly.

Furthermore, for all bidirectional loading situations, the total plate buckling of this specimen began at a displacement of the $1.5\delta_y$, and the buckling deflection proliferated with further loading, Fig. 10. Even though large deformation was seen from the UNI loading, all the other bidirectional loading caused more damage, particularly in the corners of the pier (see Fig. 10), which is a leading cause for the observation of worse post-buckling behaviour in Fig. 9c. This observation indicates that employing LYS plates without reinforcing the pier's corners is ineffective in seismic loading.

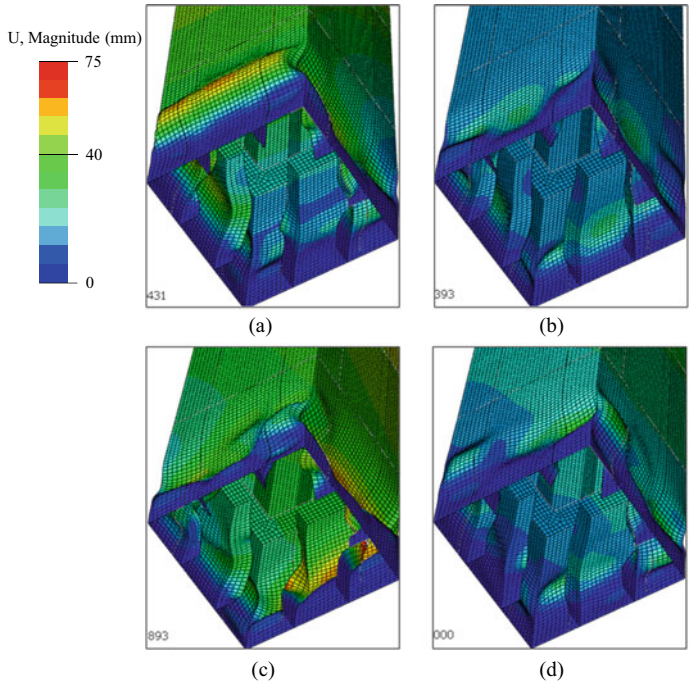

Fig. 10 Deformed shapes of LY-P type pier at the end of the loading cycle: **a** UNI, **b** BI-L45, **c** BI-SQ and **d** BI-CI

3.2.2 Column LY-PL-CO (with Corner Plate Stiffeners)

The specimen LY-PL-CO did not exhibit global buckling up to the end of the loading. However, concave-shaped local buckling waves were observed between ribs belting at the $4.5\delta_y$ displacement level for the UNI loading pattern. However, during the BI-L45, BI-SQ and BI-CL loading deltas reduced to $3.2\delta_y$, $2.4\delta_y$ and $2.48\delta_y$, respectively (see Fig. 9b). The maximum strength achieved nearly the same level as the reference specimen (SM-B), and the deformation sustained up to $3.5\delta_y$ (for the worst-case scenario of BI-CI) without a considerable load decrease, which is preferable in seismic design. On the other hand, H_m/H_y decreased below the SM-B during the BI-L45 loading (see Fig. 9a), highlighting the significance of the bidirectional loading analysis for designing piers to withstand strong earthquakes. The commencement of buckling in the L angles was observed near the end of the $3.5\delta_y > \mu_{95}$ displacement level for the UNI loading situation. However, the bidirectional load cases could initiate the buckling wave in the L angle before the μ_{95}, particularly BI-CI inducing buckling in the L angle at $3\delta_y < \mu_{95}$. As illustrated in Fig. 11, the LYP steel plate buckled before the L angles. However, buckling waves can be observed in the L angles even before the LYP steel plate during bidirectional loading. Especially, both the BI-SQ and BI-CI caused extensive damage in corners compared to the UNI

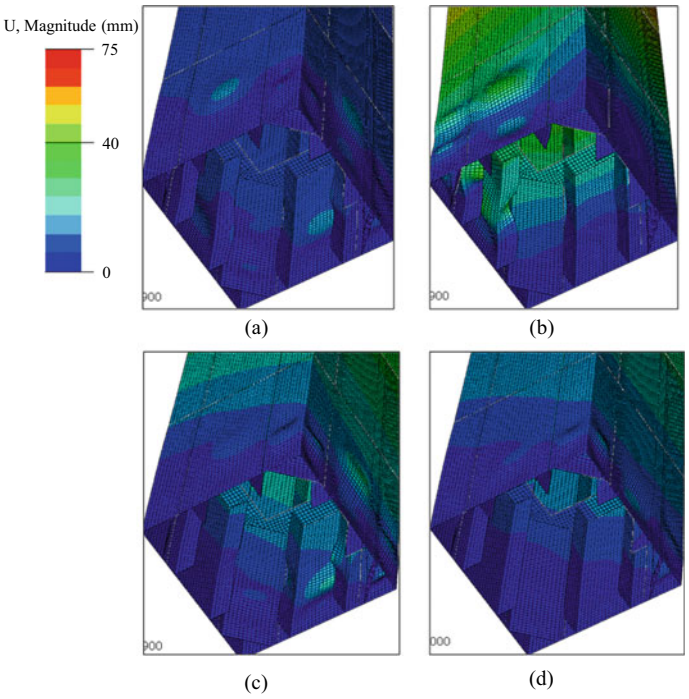

Fig. 11 Deformed shapes of LY-PL-CO type pier at the end of the loading cycle: **a** UNI, **b** BI-L45, **c** BI-SQ and **d** BI-CI

loading pattern, shown in Fig. 11. So, these observations during the bidirectional loading emphasise that further improvement in the L angle is needed to sustain the L angle during large earthquakes.

3.2.3 Column LY-PL-CO-LCO

As the L angle of column LY-CO began to distort during the later stages of loading, the LY-CO-LCO column was analysed with the L angle plate stiffener and the corner plate stiffener. Although the specimen's strength and ductility exhibit much greater values during UNI loading, a significant decrease in μ_m and μ_{95} was detected under BI-CL loading compared to the other loading scenarios. For instance, under the UNI loading, the μ_m of the LY-PL-CO-LCO was 5.88, which decreased to 4.8, 4.9 and 2.4 during the BI-L45, BI-SQ and BI-CL loading cases (see Fig. 9b), respectively. Interestingly, the SM-B and LY-CO coincide with the LY-PL-CO-LCO during the BI-CL loading (see Fig. 9b). However, as illustrated in Fig. 12, the advancement of local buckling is limited within the LYP steel plate, which can be replaced after a significant seismic event. At the same time, the L angles carry the axial stress during the repairing phase. Towards the end of the loading, minor buckling waves were

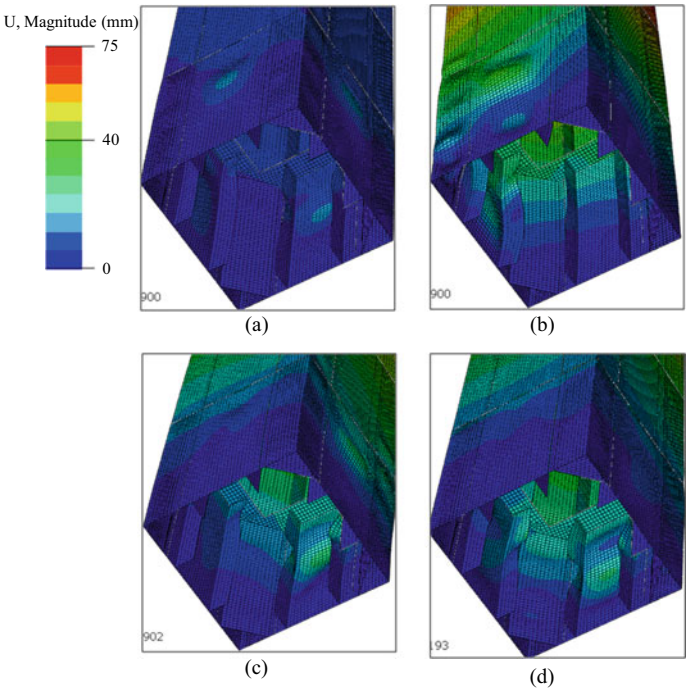

Fig. 12 Deformed shapes of LY-PL-CO-LCO type pier at the end of the loading cycle: **a** UNI, **b** BI-L45, **c** BI-SQ and **d** BI-CI

observed above the LYP plates, indicating the likelihood of buckling in the upper portion of the energy dissipation zone, which requires special attention to energy dissipation zone height, stiffening arrangement dimensions and LYP plate thickness.

4 Conclusions

The usage of LYP steel plates can improve the strength and ductility of the steel column. This work studied the seismic performance of thin-walled steel columns with replaceable energy dissipation components (LYP steel plates) coupled with the L angle at the column base under both uni and bidirectional loading. There are four column sections, three with LYP steel plates with L angles and one standard column with SM490 steel plates. The proposed method's practicality is discussed in terms

of strength, ductility, and keeping the column's corners stable where the LYP steel plates buckled first. Some significant results were drawn from this study;

1. The validity of adopted FEM in capturing the cyclic elastoplastic behaviour of the column under constant axial force and bi-directional cyclic lateral loading is verified with past experimental results, which accurately simulates the interaction between the bidirectional non-linear behaviours of the steel columns on the cyclic behaviour
2. The UNI loading pattern invariably overestimates the maximum strength of all piers compared to the bi-directional loading patterns. For example, the H_m/H_y of the LY-PL-CO-LCO column overestimated almost two times that of the BI-L45 loading pattern.
3. The UNI loading pattern estimates the H_m/H_y of the LY-PL pier higher than the standard column (SM-B). However, the BI-L45 loading pattern contradicts the previous observation, which emphasises the potential risk of using uni-directional loading alone to estimate the ultimate strength of the piers.
4. The μ_m of the SM-B and LY-PL columns showed insignificant differences for all the loading patterns. However, the BI-CI load pattern estimated the lowest μ_m value for the other types of piers (LY-PL-CO and LY-PL-CO-LCO). Therefore, for the estimation of μ_m, it is recommended to use the BI-CL loading pattern since it always predicts the minimum ductility of the specimens.
5. Two different stiffening techniques were used to delay L-angle buckling in both LY-PL-CO and LY-PL-CO-LCO columns. As a result, both columns showed significant ductility improvement concerning the standard column during the UNI loading pattern. On the other hand, both columns showed a significant reduction in μ_{95} for all the bi-directional loading. The potential reason for this phenomenon should be that the above loading cases can induce buckling in the corners of the column at a very early stage, even before the μ_{95}.
6. Seismic design criteria exclusively dependent on uni-directional loading test findings, such as displacement and force, may result in safety issues. For example, displacement changes between uni-directional and bidirectional loadings significantly depended on the column design.
7. Among the analysed linear and non-linear loading patterns, BI-CI was the most severe loading pattern in strength distortion after the peak load, since it initiates the occurrence of buckling waves in the corners of the column just after the μ_m and progressively accelerates the distortion of the column.
8. Extensive parametric studies should be carried out to investigate the effect of significant design parameters such as width-to-thickness ratio, slenderness ratio and stiffener rigidity on the lateral performance of the piers during the bidirectional loading conditions.

References

1. Yamao T, Iwatsubo K, Yamamuro T, Ogushi M, Matsumura S (2002) Steel bridge piers with inner cruciform plates under cyclic loading. Thin-Walled Struct 40:183–197. https://doi.org/10.1016/S0263-8231(01)00059-3
2. Hsu HL, Juang JL (2000) Performance of thin-walled box columns strengthened with internal braces. Thin-Walled Struct 37:241–258. https://doi.org/10.1016/S0263-8231(00)00020-3
3. Mamaghani IHP (2006) Cyclic elastoplastic analysis and seismic performance evaluation of thin-walled steel tubular bridge piers, 17th Anal. Comput Spec Conf 2006:10. https://doi.org/10.1061/40878(202)19
4. Mamaghani IHP, Khavanin M (2008) Elastoplastic analysis and ductility evaluation of steel tubular columns subjected to cyclic loading. In: Proceedings of 2008 Structural Congress, Crossing Borders, pp 566–575. https://doi.org/10.1061/41016(314)298
5. Usami T, Ge HB (1998) Cyclic behavior of thin-walled steel structures. Numer Anal. https://doi.org/10.1016/s0263-8231(98)00027-5
6. Al-Kaseasbeh Q, Mamaghani IHP (2020) Thin-walled steel stiffened square box columns with uniform and graded thickness under bidirectional cyclic loading. Eng Struct 219:110919. https://doi.org/10.1016/j.engstruct.2020.110919
7. Japan Road Association, Design specifications of highway bridges-Part IV-Substructures (2002) 92
8. Japan Road Association, Specifications for highway bridges, V Seismic design (2002)
9. Dang J, Yuan H, Igarashi A, Aoki T (2017) Multiple-spring model for square-section steel bridge columns under bidirectional seismic load. J Struct Eng 143. https://doi.org/10.1061/(asce)st.1943-541x.0001735
10. Susantha KAS, Aoki T, Jayasinghe MTR (2007) Finite element analysis of steel columns subjected to bi-directional cyclic loads. Eng J Inst Eng Sri Lanka 40:35. https://doi.org/10.4038/engineer.v40i4.7152
11. Watanabe E, Sugiura K, Oyawa WO (2000) Effects of multi-directional displacement paths on the cyclic behaviour of rectangular hollow steel columns. Struct Eng Eng 17. https://doi.org/10.2208/jscej.2000.647_79
12. Shen HX (2019) A new simple method for the strength of high-strength steel thin-walled box columns subjected to axial force and biaxial end moments. Adv Civ Eng. https://doi.org/10.1155/2019/7495890
13. Yamada S, Ishida T, Jiao Y (2018) Hysteretic behavior of RHS columns under random cyclic loading considering local buckling. Int J Steel Struct 18:1761–1771. https://doi.org/10.1007/s13296-018-0087-x
14. Hu F, Shi G (2021) Experimental study on seismic behavior of high strength steel frames: local response. Eng Struct 229. https://doi.org/10.1016/j.engstruct.2020.111620
15. P. Of, O. Under, O. For, B.C. Tang, and a Pplication of a S Imple I Nteraction F Ormula S Teel C Olumns Under F Ire C Onditions, (2001) 1206–1213
16. Dang J, Aoki T (2013) Bidirectional loading hybrid tests of square cross-sections of steel bridge piers. Earthq Eng Struct Dyn 42:1111–1130. https://doi.org/10.1002/eqe.2262
17. Usami T, Kumar S (1996) Damage evaluation in steel box columns by pseudodynamic tests. J Struct Eng 122:635–642. https://doi.org/10.1061/(asce)0733-9445(1996)122:6(635)
18. Zheng Y, Usami T, Ge H (2000) T -w s b s –c 1304–1311
19. Zheng Y, Usami T (2000) Ductility evaluation procedure for thin-walled steel structures 1312–1319
20. Usami T, Gao S, Ge H (2000) Stiffened steel box columns. Part 2: Ductility evaluation. Earthq Eng Struct Dyn 29:1707–1722. https://doi.org/10.1002/1096-9845(200011)29:11<1707::AID-EQE990>3.0.CO;2-7
21. Jenothan M, Jayasinghe JASC, Bandara CS, Dammika AJ (2023) Lateral performance of thin-walled steel box column with replaceable energy dissipation mechanism 201–214. https://doi.org/10.1007/978-981-19-2886-4_15

22. Shen C, Mamaghani IHP, Mizuno E, Usami T (1995) Cyclic behavior of structural steels. II: Theory, J Eng Mech 121:1165–1172. https://doi.org/10.1061/(asce)0733-9399(1995)121:11(1165)
23. Gao Y, Shi G, Wang X (2021) Mechanical properties of low yield point steels subjected to low-cycle structural damage. J Constr Steel Res 183:106733. https://doi.org/10.1016/j.jcsr.2021.106733
24. Susantha KAS, Aoki T, Kumano T, Yamamoto K (2005) Applicability of low-yield-strength steel for ductility improvement of steel bridge piers. Eng Struct 27:1064–1073. https://doi.org/10.1016/j.engstruct.2005.02.005
25. Aoki T, Ohnishi A, Suzuki M (2007) Experimental study on the seismic resistance performance of rectangular cross section steel bridge piers subjected to bi-directional horizontal loads. Doboku Gakkai Ronbunshuu A 63:716–726. https://doi.org/10.2208/jsceja.63.716
26. Aoki T, Susantha KAS (2005) Seismic performance of rectangular-shaped steel piers under cyclic loading. J Struct Eng 131:240–249. https://doi.org/10.1061/(asce)0733-9445(2005)131:2(240)
27. Banno Y, Kinoshita K, Barsoum Z (2021) Numerical investigation of influence of under- and over- treatment on residual stress state induced by HFMI. Weld World 65:2135–2146. https://doi.org/10.1007/s40194-021-01159-3

Damage Prediction by Using Nonlinearity of Damping

G. B. Dissanayake, A. J. Dammika, C. S. Bandara, J. A. S. C. Jayasinghe, and P. B. R. Dissanayake

Abstract The lack of rapid, simple, and reliable techniques in damage detection of large civil engineering structures has hindered the frequent application of available vibration-based structural health monitoring and damage detection methods. The basics of baseline data of undamaged structure detailed finite element models, or the need for numerous expensive sensors have further distanced the technique from practice. Thus, in this study, the application of a simple, baseline free time domain damage detection technique using acceleration data is discussed. The investigation is made using analysis of nonlinearity in damping extracted from ambient vibration data for identification of the existence of damage in a structure. It is known that the dominant mechanism of energy dissipation in the presence of structural defects such as cracks, defective connections, etc. is due to dry Coulomb friction and this type of damping is considered nonlinear. Contrary to this, in the undamaged state of structures, the dissipation of energy is mostly due to material damping which is considered a macroscopically viscous and constant type of damping. Thus, analysis of nonlinearity in damping and identification of the contribution of Coulomb friction in modal damping could reveal the existence of damage or defects in a structure. This study presents the application of the method to an experimental system at the laboratory to show the competency of the method. The experimental estimates obtained from the proposed method illustrate the effectiveness and efficiency of the method in portraying the existence of the damage and approximate quantification.

Keywords Nonlinear damping · Damage detection · Coulomb damping · Viscous damping · Ambient vibration

G. B. Dissanayake (✉) · A. J. Dammika · C. S. Bandara · J. A. S. C. Jayasinghe · P. B. R. Dissanayake
University of Peradeniya, Peradeniya, Sri Lanka

A. J. Dammika
e-mail: dammikaaj@pdn.ac.lk

© The Author(s), under exclusive license to Springer Nature Singapore Pte Ltd. 2023

R. Dissanayake et al. (eds.), *ICSBE 2022*, Lecture Notes in Civil Engineering 362,
https://doi.org/10.1007/978-981-99-3471-3_4

1 Introduction

Detection of the occurrence of damage in a structure is the initial step of every structural health monitoring (SHM) system. Such information will facilitate engineers in planning detailed inspection activities to assess the structural integrity and performance of structures such as buildings, bridges, dams, pipe networks, etc. [1, 2].

The existing structural damage detection methods can be categorized into two groups; local inspection methods and global detection methods [2]. Local inspection method includes visual inspections of the structure by an expert supplemented by localized testing based on ultrasonic or [1, 3] acoustic methods, x-ray methods, magnetic field methods, eddy-current methods, thermal field methods, etc. [4–6]. The visual inspection and testing methods are highly localized in nature and the outcome is highly dependent upon the inspectors' experience and knowledge. Further, the methods require the portion of the structure to be investigated to be readily accessible for testing [1]. Unfortunately, on most occasions, this requirement is not guaranteed, since most of the civil engineering structures especially bridges, are large and complex in nature, or their operating environment is hostile. In this situation, the development of efficient and effective methods for the detection of the occurrence of damage in structures is crucial.

The vibration-based structural damage detection method can effectively avoid the limitations of local inspection methods because it does not require that the vicinity of damage is known a priori, nor that the structural portion of interest is readily accessible for testing [7].

Methods found in the literature mostly propose damage detection, localization, and assessment using either natural frequencies or mode shapes and their derivatives [2]. It is generally acknowledged that natural frequencies have low sensitivity to damage and can usually be used to reflect damage to a moderate degree. Mode shapes and their derivatives have shown greater sensitivity to damage but capturing the mode shape and its changes requires numerous sensors distributed on the structure and proper placement. This situation has made utilizing mode shapes and their derivatives in practical applications of structural damage detection less attractive.

Compared to natural frequencies and mode shapes, damping has been proven more sensitive to damages even portraying small, visually undetectable damages (Figs. 1 and 2). More evidence of the efficiency of damping in portraying damage in structures could be found in studies of [8–10].

Generally, the damping of vibration in a large structural system is due to various forms of energy dissipation mechanisms. It is commonly identified as viscous damping and Coulomb damping. Typically, in engineering practice, a linear viscous damping model is used for the sake of simplicity as it lends to a linear equation of motion [11, 12]. It has been understood that when a structure is undamaged, most of the energy dissipation is due to material damping which is categorized as viscous, i.e., proportional to the velocity of motion. However, when the structure is damaged, the most significant energy dissipation mechanism within the cracks or in a defective connection can be represented by Coulomb friction [13].

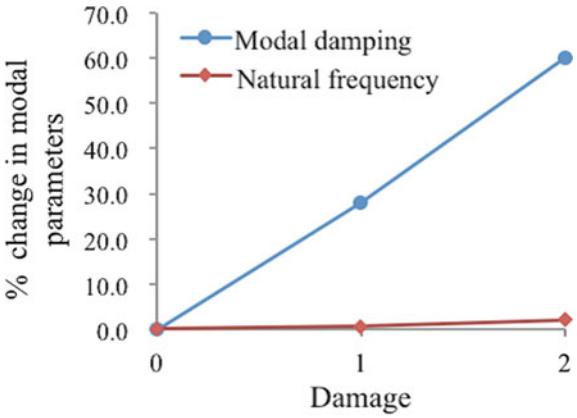

Fig. 1 Variations in modal damping and natural frequency with increased severity of corrosion damage [10]. U_0, U_1, and U_2 denote damage states 0 (undamaged), 1, and 2, respectively.

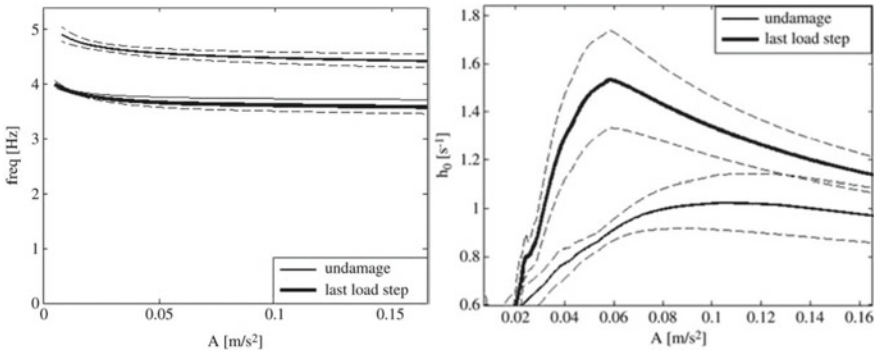

Fig. 2 Instantaneous undamped natural frequency (**a**) and instantaneous damping coefficient $h_0(t)$ (**b**) along the amplitude of vibration [8]

Bachmann and Dieterle [14] observed that energy dissipation due to excessive movements in joints, energy dissipation in opening and closing of cracks, slipping at interfaces, sliding in supports, etc. generate Coulomb type of damping with coexisting viscous type material damping.

Experiments on precast reinforced concrete slab panels [9] showed that the presence of small, visually undetectable cracks caused a considerable increase in damping. Further, they noted that the energy dissipation mechanism in a crack is mainly due to dry Coulomb friction. Further, they noted that visually undetectable cracks have very little change in natural frequencies and mode shapes, while there is a significant change in damping characteristics of the structure.

Frizzarin et al. [15] presented work on the theoretical-experimental identification technique for structural damage detection based on analysis of non-linear damping of measured structural vibration response. The experimental verifications

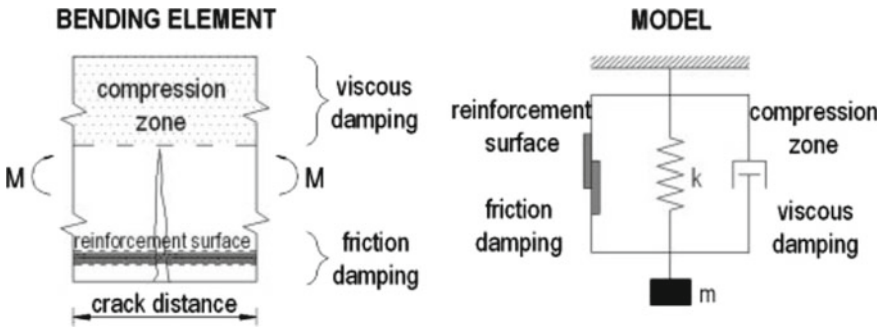

Fig. 3 Representation of cracked bending element and corresponding model [15]

were conducted using a large-scale concrete bridge model. They presented a model (Fig. 3) for a cracked bending element, where both the viscous and friction-damping phenomena co-existed at the same time. It shows that in the cracked zone where there is friction in the reinforcement surface, the most significant dissipation mechanism is friction damping. On the contrary, in the compression zone, it can be assumed that only material (viscous) damping is present. In the model, k represents the bending stiffness of the element, while m is the relevant mass.

As a result, damage to the system can be detected if the envelope of free decay of a system is examined and it is determined that dry Coulomb friction is the main source of energy dissipation.

2 Objective and Scope

The objective of this paper is the present investigation on using analysis of time-dependent damping behaviour in the prediction of damage existence of a structure based on the work by [15]. Experimental application of the method was conducted using ambient vibration data from the experimental system at the laboratory. The knowledge obtained in this investigation is useful in readily applying the vibration-based method for damage detection in real structures which will be conducted in the next stage.

3 Damping Models and Damping Estimation

Typically, in engineering practice, a linear viscous damping model is used for the sake of simplicity as it lends to a linear equation of motion. But it is important to note that in real structures the damping behaviour is more complex and often nonlinear. As mentioned by [16], commonly used damping models to describe the real damping

behaviour can generally be presented by the Equation,

$$f_d(x, \dot{x}) = a\dot{x}|\dot{x}|^{\theta-1} \tag{1}$$

where, $f_d(x, \dot{x})$ is the damping force, $\dot{x}$ is the velocity and a is the damping coefficient. The value of θ determines the damping model, e.g.

linear viscous damping ($\theta = 1$)

$$f_d(x, \dot{x}) = c\dot{x} \tag{2}$$

Coulomb (Dry friction) damping ($\theta = 0$)

$$f_d(x, \dot{x}) = \mu \frac{\dot{x}}{|\dot{x}|} = \mu \text{sign}(\dot{x}) \tag{3}$$

where, c is the viscous damping coefficient, μ is the Coulomb damping coefficient. The free decay envelope of a system under viscous damping is seen as an exponential decay and is linear for a Coulomb-damped system as shown in Fig. 4. For these ideal systems, [17] provided individual functions of coulomb, viscous and quadratic damping acting on a Single Degree of Freedom System (SDOF) as given in Table 1.

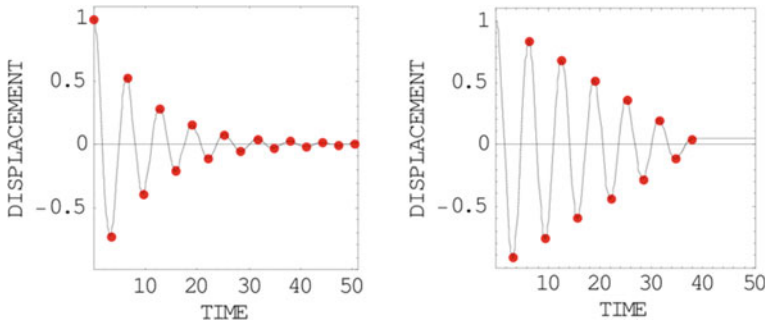

Fig. 4 Linear viscous damping and Coulomb (dry friction) damping [18]

Table 1 Coulomb, viscous and quadratic damping mechanisms [23]

Damping type	Governing equation (Homogeneous form)	Envelop signal	Equivalent viscous damping coefficient
Coulomb	$\ddot{x} + \mu \frac{\dot{x}}{\lvert\dot{x}\rvert} + \omega_n^2 x = 0$	$a_c(t) = \frac{-2\mu}{\pi\omega_n} t + y_0$	$C_{eq,c}(t) = \frac{2\widehat{\mu}}{\pi\omega_n^2 a_0 - 2\widehat{\mu}\omega_n t}$
Viscous	$\ddot{x} + 2\varsigma\omega_n\dot{x} + \omega_n^2 x = 0$	$a_v(t) = e^{-\varsigma\omega_n t}$	$C = 2\varsigma\omega_n$
Quadratic	$\ddot{x} + \varepsilon\lvert\dot{x}\rvert\dot{x} + \omega_n^2 x = 0$	$a_q(t) = \frac{3\pi a_0}{3\pi + 4\varepsilon\omega_n a_0 t}$	$C_{eq,q}(t) = \frac{4\widehat{\varepsilon} a_0}{3\pi + 4\widehat{\varepsilon}\omega_n a_0 t}$

From above, quadratic damping is mostly associated with air damping, which occurs due to the air resistance of a moving structure. In large civil engineering structures, this type of damping is not significant and is not considered in this study.

Then, the decay envelope of a system with combined viscous and coulomb types of damping should be characterized by a linear summation of the individual decay functions defined by [17]. Thus, the mass normalized equation of motion that defines a system with viscous and coulomb damping is shown in Eq. (4).

$$\ddot{x} + 2\zeta\omega\dot{x} + \mu[sign(\dot{x})] + \omega^2 x = 0 \tag{4}$$

$$(t) = x_0\left[\left(1 + \frac{\gamma}{\xi}\right)e^{-\xi.\omega.t} - \frac{\gamma}{\xi}\right] \tag{5}$$

Based on Eq. (5), it is understood that the envelope of a free decay gives information about the energy dissipation mechanisms acting on the system. This equation contains values of ξ and γ. Then, as given by [15], assuming that the total loss of energy (ΔE_{Pot}) is the simple sum of energy loss due to viscous (ΔE_{Visc}) and friction (ΔE_{Frict}) energy dissipations, the relationship for decay envelope for the combined system (shown in Eq. 4) was obtained in terms of initial amplitude x_0, the natural frequency of the system ω and the two damping ratios ξ for viscous damping and γ for friction damping as given in Eq. (5): information about the presence of each type of damping. Simultaneously, it contributes to each damping mechanism on total energy dissipation.

Value for $\gamma = 0$ suggests that there is no dry friction type of energy dissipation and the decay envelope is purely exponential, indicating only a viscous type of energy dissipation acting on the system. In contrast to this, when no viscous type of damping is present, the decay envelope is linear and $\xi = 0$. This indicates entirely the presence of coulomb friction type of damping. Values in between these extremes indicate the type of damping acting on the system, contributing to oscillation decay. Different values for γ and ξ contribute to each damping mechanism on total damping.

Therefore, identifying the presence and contribution of friction damping in a system using this method is feasible and could be directly correlated to the occurrence of damage in the system.

4 Experimental Investigation

To study the applicability of the above method, an experiment was designed at the laboratory. Experiments were conducted using flexural vibration of cantilever beams since it is recognized as one of the most favoured techniques to study different damping characteristics of structural systems by many researchers, Paimushin et al. [19–23] among others. In this method, one end of the specimen was held in place,

while the other end of the specimen was allowed to move freely to respond to manual displacement or induced vibration.

The experimental setup used in the investigation is shown in Fig. 5. The cantilever beam was a mild steel rectangular box section in which one end was clamped to a large concrete base with the dimensions of 600 mm × 600 mm × 600 mm (Appx, 550 kg weight). The length of the mild steel tube was 1790 mm. A 40 mm × 80 mm box section with a thickness of 3.0 mm was used. Dry frictional resistance was applied using a mechanism attached close to the free end of the cantilever beam. The mechanism could apply different levels of frictional resistance to the vibration oscillation.

The acceleration measurements were started with some delay which is necessary for the transition from the initial state to the first, lowest vibration mode of the specimen. The measured acceleration response was filtered and used to derive the corresponding displacement responses using a freely available signal processing tool. Based on these response measurements, decay envelopes were obtained.

Figure 6 shows a signal of the acceleration response of the free vibration of the cantilever without any dry friction damping (Force "N" absent). Then the accelerometer data were band-pass filtered from 1 to 15 Hz since it is known that the fundamental frequency of the system is lower than 15 Hz as calculated. Figure 6 also shows the overlayed acceleration response after applying the bandpass.

The Fast Fourier Transform (FFT) of the response showed the first natural frequency of the system as 11.719 Hz. Thus, it could be concluded that the system tends to vibrate in its first flexural vibration mode under the excitation and is well separated from other higher modes.

Once the acceleration response was processed, the processed signal was used to derive the displacement response using the same signal processing tool. The decay curve was then obtained using the peaks of displacement response.

The experiments were conducted with external dry frictional resistance to beam vibration. The frictional resistance was controlled by adjusting the normal force between the sliding surfaces while the coefficiency of friction was constant in this experiment setup due to no change in the mating surface. These externally applied different magnitudes of frictional forces represent the different degrees of damage

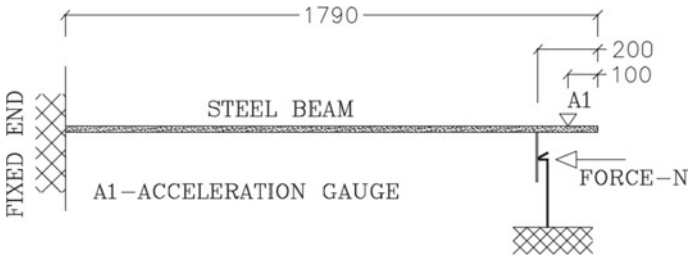

Fig. 5 Experimental cantilever beam model

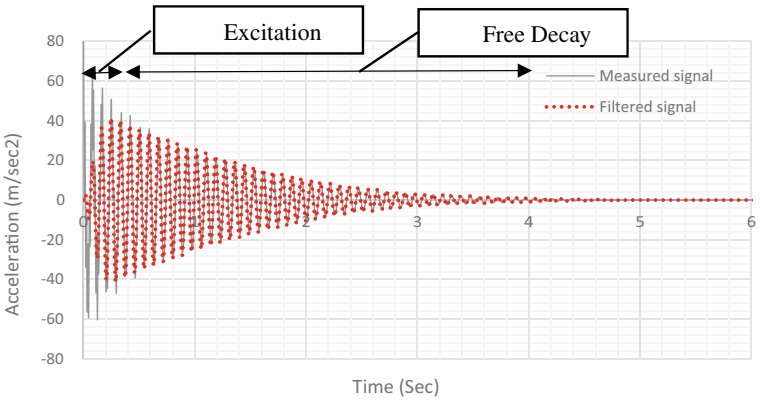

Fig. 6 Measured and filtered acceleration response

scenarios. Lower frictional resistance mimics a lower degree of damage in the system and increasing frictional resistance mimic increased damage scenarios.

Table 2 provides the details of the experiment scheme. Test 1 (T1) is without any dry coulomb friction and represents no damage scenario in the system and expected only viscous type of damping.

Other tests (T2, T3, T4) represent a system with different degrees of damage varying from low to high degrees. The displacement time history data with decay envelopes for the fundamental mode of the cantilever beam for tests T1, T2, T3, and T4 are shown in Fig. 7. The influence of an increase in dry friction force on the displacement amplitude decay envelope of free vibration is visible in the time histories.

It is known that the logarithmic decrement (δ) of the decay envelope is related to energy dissipation [23]. For an exponential decay or decay envelope of a system with only a viscous type of damping, the logarithmic decrement is considered constant over time. When dry friction damping is present, the decay envelope's logarithmic decrement (δ) becomes nonlinear [24]. To observe this with the results of the experiment, instantaneous logarithmic decrements for T1, T2, T3 and T4 are plotted against time. The variation of logarithmic decrement under different dry Coulomb friction amplitudes is presented in Fig. 8.

In Fig. 8, it is observed that the log decrement is constant when no coulomb friction is present in the test system indicating only a viscous type of damping [24].

Table 2 Experiment scheme for Coulomb damped free vibration of a cantilever

Test no.	Initial displacement (A_0) (mm)	Normal force (N)
T1	9.0	0
T2	9.0	04.6
T3	9.0	09.3
T4	9.0	13.9

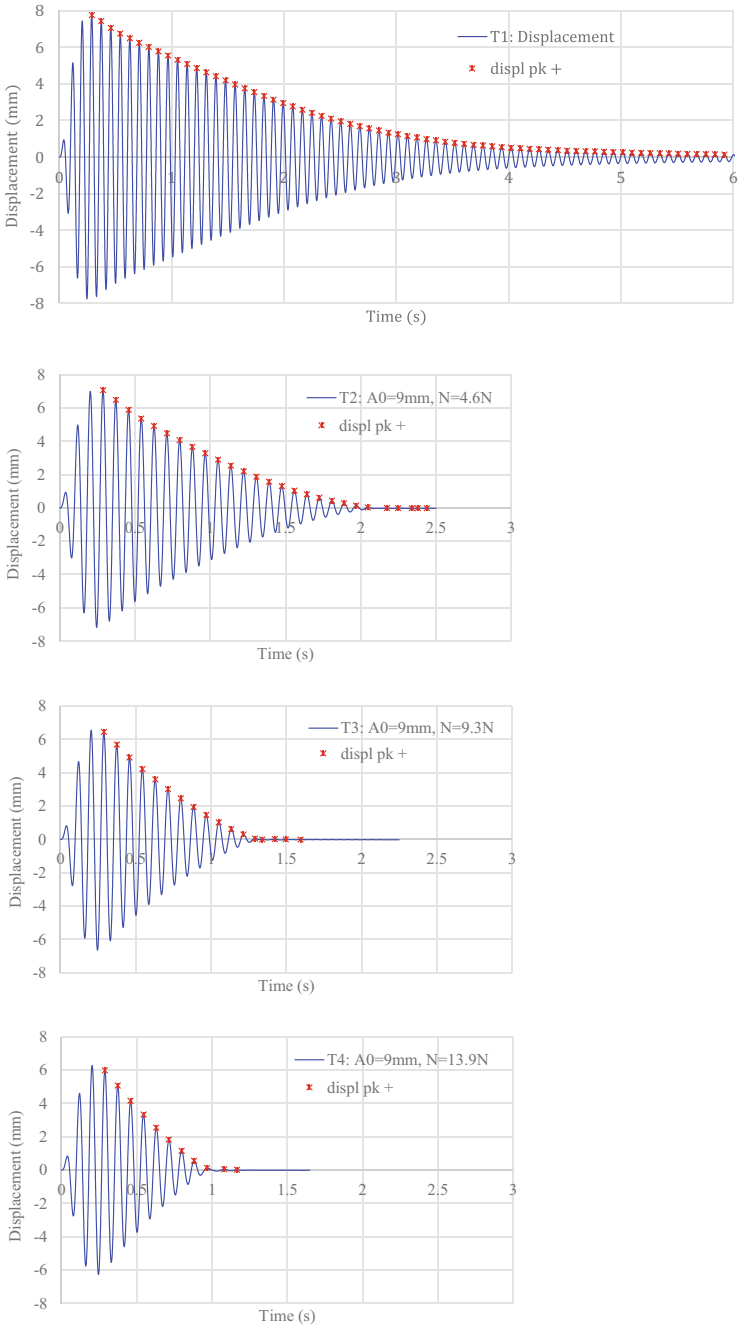

Fig. 7 Displacement—time histories under different dry Coulomb friction amplitudes and constant viscous damping

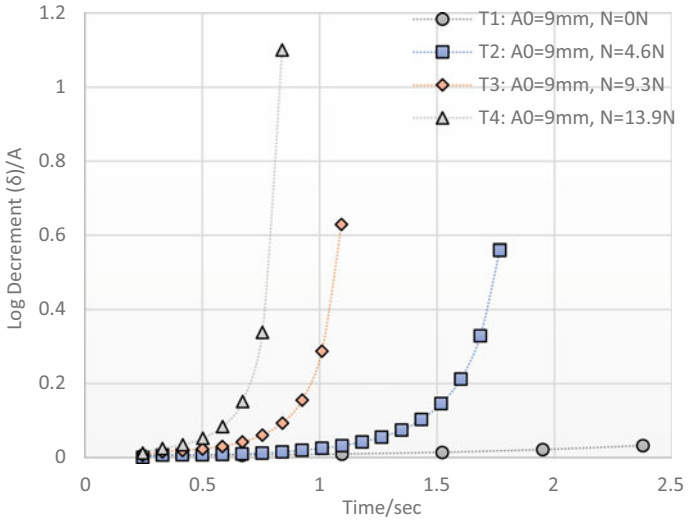

Fig. 8 Log decrement comparison for various dry friction amplitudes

When Coulomb friction is introduced to the system, the variation of log decrement becomes nonlinear. The nonlinearity is increased with an increment in the amplitude of the applied normal force.

Therefore, it is evident that the nonlinearity in the damping behavior exposes the existence of damage in the system. Nevertheless, quantification of nonlinearity provides evidence of the quantitative information of the damage in the system.

Thus, moving forward based on the analysis of decay envelopes, (based on Eq. 5), the parameters, ξ, and γ could be assessed for each test configuration using simple curve fitting techniques. Such an assessment was conducted for each test, T1, T2, T3, and T4. The result of the assessment is shown in Table 3. The same results were elaborated in Fig. 9 and represent the increase in friction damping component γ with increased friction resistance.

The numerical values in Table 2 and its graphical representation in Fig. 9 shows that the dominant damping mechanism in Test (T1) is the viscous type and it is constant over all four tests as expected due to the nature of the test setup. While, for

Table 3 Variation of friction force and observed damage percentage

Test ID	T1	T2	T3	T4
F (N)	0	4.6	9.3	13.9
ξ—visc. damping	0.042474	0.04872	0.050819	0.033814
ξ%	4.2	4.9	5.1	3.4
γ—frict. damping	0.00288	0.029573	0.062152	0.10648
γ%	0.3	3.0	6.2	10.6

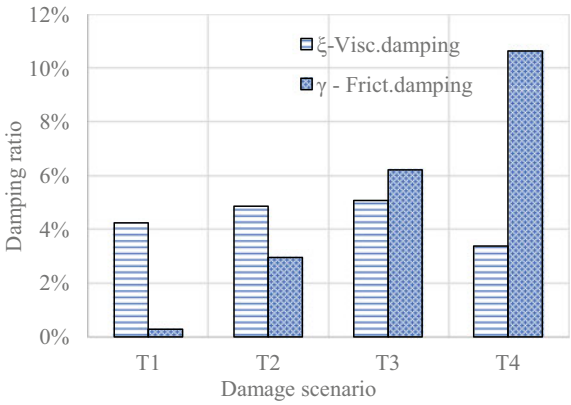

Fig. 9 Comparison of observed damage percentage

other tests T2, T3, and T4, the dominant damping mechanism gradually changed into dry friction damping consistently with the increased frictional resistance. Further, it depicts the capacity of the proposed method in portraying the quantitative information of the damage.

5 Conclusions

This study discusses the application of a simple, baseline free time domain damage detection technique using acceleration data. The investigation was made using analysis of nonlinearity in damping extracted from ambient vibration data for identification of the existence of damage in a structure. Experiments were conducted using a simple cantilever beam set up under the influence of different dry Coulomb friction magnitudes to represent different degree damage scenarios.

In the investigation, a strong correlation between the increase in the normal contact force (Coulomb friction force) and the nonlinear behaviour of damping was observed. The nonlinearity of damping behaviour was seen to increase when the dry frictional force was increasing. Thus, it is evident that nonlinearity in damping could portray the existence of damage in a structure.

Further, it was shown that the parametric identification of the decay function of the combined system could provide quantitative information on the existing damage by distinguishing the contribution of each viscous type and friction type of damping based on a controlled laboratory environment.

Further research is needed to inspect the feasibility of the method to be applied in real structures.

References

1. Doebling S, Farrar C, Prime M (1998) Summary review of vibration-based damage identification methods. The Shock and Vibration Digest, March, pp 91–105
2. Doebling S, Farrar C, Prime M, Shevitz D (1996) Damage identification and health monitoring of structural and mechanical systems from changes in their vibration characteristics: a literature review, Los Alamos, New Mexico 87545: Los Alamos National Laboratory, University of California
3. Yoon M et al (2005) Local damage detection using the two-dimensional gapped smoothing method. J Sound Vib 279(1–2):119–139
4. Chang P, Liu S (2003) Recent research in nondestructive evaluation of civil infrastructures. J Mater Civ Eng 15(3):298–304
5. Ciang C, Lee J, Bang H (2008) Structural health monitoring for a wind turbine system: a review of damage detection methods. Measur Sci Technol 19(12)
6. Diamanti K, Soutis C (2010) Structural health monitoring techniques for aircraft composite structures. Prog Aerosp Sci 46(8):342–352
7. Cao M, Sha G (2017) Structural damage identification using damping: a compendium of uses and features. Smart Mater Struct 26:14
8. Curadelli R, Riera J, Ambrosini D, Amani M (2008) Damage detection using structural damping identification. Eng Struct 30:3497–3504
9. Modena C, Sonda D, Zonta D (1999) Damage localization in reinforced concrete structures by using damping measurements. Key Eng Mater 167–168:132–141
10. Shahzad S, Yamaguchi H, Takanami R, Asamoto S (2013) Detection of corrosion-induced damage in reinforced concrete beams based on structural damping identification. Sapporo, Japan, The Thirteenth East Asia-Pacific Conference on Structural Engineering and Construction (EASEC-13)
11. Lazan B (1960) Material and structural damping for vibration control. SAE Trans 537–547
12. Lazan B (1966) Damping mechanisms and phenomenology in materials. Appl Mech 493–501
13. Lazan B, Goodman L (1956) Effect of material and slip damping on resonance behavior. In: ASME symposium on shock and vibration applied mechanics division
14. Bachmann, Dieterle R (1981) Experiments and models for the damping behaviour of vibrating reinforced concrete beams in the uncracked and cracked conditions, 1 edn. Birkhäuser
15. Frizzarin M et al (2010) Damage detection based on damping analysis of ambient vibration data. Struct Control Health Monit 17:368–385
16. Kareem A, Gurley K (1996) Damping in structures: its evaluation and treatment of uncertainty. J Wind Eng Ind Aerodyn 59:131–157
17. Smith C, Wereley NM (1999) Nonlinear damping identification from 1ansient data. California, SPIE Conference on Passive Damping and Isolation
18. Molina M (2004) Exponential versus linear amplitude decay in damped oscillators. Phys Teacher
19. Foong F, Ket T, Lee O, Aziz A (2019) Stress and damping of wide cantilever beams under free vibration. J Mech Sci Technol 33(1):21–27
20. Kume Y, Hashimoto F, Maeda S (1982) Material damping of cantilever beams. J Sound Vib 80(1):1–10
21. Paimushin V, Firsov V, Günal L, ShishkinV.M, (2015) Theoretical experimental method for determining the material damping properties based on the damped flexural vibrations of test samples. Proc Eng 106:231–239
22. Paimushin V, Firsov V, Gyunal I, Egorov A (2014) Theoretical experimental method for determining the parameters of damping based on the study of damped flexural vibrations of test specimens—experımental basıs. Mech Compos Mater 50(2):127–136
23. Stephens D, Scavullo M (1965) Investigation of air damping of circular and rectangular plates cylinder and sphere, Langley Station, Hampton: NASA, Langley Research Center
24. Chopra A (2007) Dynamics of structures. Pearson Education India

Chemical Processes for a Sustainable Future

Effects of Refined Coconut Oil and Vegetable Oil on the Mechanical, Thermal, Morphological, and Biodegradable Properties of Cassava Starch-Based Thermoplastic (TPS) Films

N. M. L. Fernando, S. M. Amaraweera, O. H. P. Gunawardene, W. M. D. B. Wanninayaka, C. A. Gunathilake, W. A. Manamperi, A. K. Kulatunga, and A. Manipura

Abstract The effect of addition of different concentrations of refined coconut oil (CO) and vegetable oil (palm olein oil) (VO) on the mechanical and thermal properties, as well as water absorption, biodegradability and morphology of cassava starch-based TPS films were investigated. Cassava starch-based TPS films were prepared by the solvent casting method using glycerol as the plasticizer incorporation with varying concentrations of CO and VO at 5,10,20, and 40 wt % based on cassava starch. The X-ray diffractometry (XRD), fourier transform infrared (FTIR) spectroscopy, thermogravimetric analysis (TGA), and scanning electron microscopy (SEM) analysis were carried out to observe the interactions between the starch matrix and oil, thermal stability, decomposition temperature and morphology of films. An increase in tensile strength was observed with the increment of both CO and VO concentration while the maximum tensile strength was observed at the oil concentration of 10 wt % for both CO and VO. However, films containing VO have higher tensile strength (4.18 MPa) than the films containing CO (3.56 MPa). Tensile strain at break decreased when increasing the oil concentration up to 10 wt % for both CO and VO. Water absorption of the films increased when increasing the oil concentration.

N. M. L. Fernando (✉) · S. M. Amaraweera · A. K. Kulatunga
Department of Manufacturing and Industrial Engineering, University of Peradeniya, Peradeniya, Sri Lanka
e-mail: nimashamf@gmail.com

O. H. P. Gunawardene · W. M. D. B. Wanninayaka · C. A. Gunathilake · A. Manipura
Department of Chemical and Process Engineering, University of Peradeniya, Peradeniya, Sri Lanka

C. A. Gunathilake
Department of Material and Nano Science Technology, Wayamba University of Sri Lanka, Kuliyapitiya, Sri Lanka

W. A. Manamperi
Materials Engineering Department, California Polytechnic State University, San Luis Obispo, CA, USA

© The Author(s), under exclusive license to Springer Nature Singapore Pte Ltd. 2023

R. Dissanayake et al. (eds.), *ICSBE 2022*, Lecture Notes in Civil Engineering 362,
https://doi.org/10.1007/978-981-99-3471-3_5

However, the value was less than the reference sample until the oil concentration was 20 wt % for both CO and VO. Moreover, all the samples are biodegradable. Cassava starch, refined coconut oil, and vegetable oil are natural resources that can be used to produce alternative materials that cause minor environmental impact.

Keywords Cassava starch · Coconut oil · Vegetable oil · Thermoplastic film

1 Introduction

Starch is a polymeric carbohydrate containing anhydroglucose units connected by glucosidic bonds. Cereal grains such as corn, wheat and rice and tubers such as potato and cassava, are the main starch sources that can be used for bio-plastics [1, 2]. Production of starch-based bio-plastics which are cheap, and fully biodegradable, could become a possible substitute to non-biodegradable synthetic plastics while creating new markets and reducing environment pollution [3, 4]. The demand for environmentally friendly biodegradable plastics is increasing day by day [5].

Cassava (Manihot esculenta) starch is more suitable to produce thermoplastic starch due to its clarity, low gelatinization temperature and good gel stability. Cassava starch has a carbohydrate content up to 99%, and 17% amylose and 83% amylopectin content [6, 7]. Cassava starch can be transformed into an amorphous thermoplastic by processing with plasticizers such as glycerol under special heat and shear conditions [8]. However, thermoplastic starch has major drawbacks such as poor mechanical properties and water resistance. The hydrophilic nature of starch and plasticizers commonly results in poor mechanical properties of thermoplastic starch [9]

The addition of hydrophobic substances, such as oils and fatty acids, may reduce the hygroscopicity of the thermoplastic starch by increasing the hydrophobic portions in the thermoplastic starch [10]. Current researchers focus on adding plant oil which exhibits admirable hydrophobic properties into thermoplastic starch to improve water resistance properties [11]. Some researchers have focused on using vegetable oil as plasticizers for biodegradable thermoplastics including palm oil [12–14], soybean oil [12, 14–16], rubber seed oil [17], corn oil [18], olive oil [18], coconut oil [19], canola oil [20], and sunflower oil [21].

Coconut oil which is obtained from the coconut tree and vegetable oil which is produced using palm kernel nuts are some abundant plant oils in the market [22]. The fatty acid content of coconut oil and palm olein oil is listed in Table 1 [22–24].

The effect of virgin coconut oil and palm oil on the properties of starch-based thermoplastic was previously studied. To the best of our knowledge, there is no study about the effect of refined coconut oil and palm olein oil (vegetable oil) on the characteristics of cassava starch-based thermoplastic. This research explored the effect of refined coconut oil and palm olein oil (vegetable oil) as hydrophobic components on the properties of cassava starch-based thermoplastics. X-ray diffraction (XRD), Fourier transform infrared spectroscopy (FTIR), thermogravimetric analysis (TGA), scanning electron microscopy (SEM), mechanical, water absorption

Table 1 The fatty acid content of coconut oil and palm olein oil

Fatty acid	Coconut oil	Palm olein oil
Caproic acid (C6:0)	0–5	–
Caprylic acid (C8:0)	8	–
Capric acid (C10:0)	6	–
Lauric acid (C12:0)	47	0–3
Myristic acid (C14:0)	18	1
Palmitic acid (C16:0)	5–8	39
Stearic acid (C18:0)	2–5	4
Oleic acid (18:1)	7	43
Linoleic acid (C18:2)	1–5	11

and biodegradability properties of the cassava starch-based thermoplastic thin films were characterized.

2 Materials and Methodology

2.1 Materials

The native cassava starch was purchased from Vilaconic joint stock company, Vietnam. Glycerol was purchased from Research Lab fine chem industry (India). Physically refined coconut oil was purchased from Marina Foods Pvt Ltd and refined palm olein vegetable cooking oil was purchased from NGO Chew Hong Edible Oil Pte Ltd. Freshly prepared distilled water was used.

2.2 Preparation of Thermoplastic Thin Film

Starch-based thin films were prepared by the solvent-casting method after the preparation of film-forming dispersions according to the method adopted by Belibi et al. [25]. Initially, native cassava starch (5 g) was dispersed in an aqueous solution, separately, with the corresponding amount of glycerol and oil at room temperature under continuous stirring for 10 min on a magnetic stirrer. Thereafter, the mixtures were stirred at 80 °C for 45 min to induce starch gelatinization. Afterwards, the films were obtained by casting the hot suspensions into petri dishes. Then, the samples were dried in an oven at 65 °C for 5 h. After that, the dishes were kept in a desiccator and finally, the dry films were carefully removed from the dishes. The sample without oils was prepared as the control sample. Different formulations of cassava starch, glycerol, water and oils are described in Table 2.

Table 2 The components of cassava starch-based thermoplastic films

Sample code	Cassava starch (g)	Glycerol (wt %)	Distilled water (mL)	Coconut oil (wt %)	Vegetable oil (wt %)
TPS	5	25	100	–	–
TPS_CO_5	5	25	100	5	–
TPS_CO_10	5	25	100	10	–
TPS_CO_20	5	25	100	20	–
TPS_CO_40	5	25	100	40	–
TPS_VO_5	5	25	100	–	5
TPS_VO_10	5	25	100	–	10
TPS_VO_20	5	25	100	–	20
TPS_VO_40	5	25	100	–	40

2.3 Thickness of the Films

The thickness of thermoplastic thin films was determined using a manual Thickness Gauge by performing at least ten random measurements for each film to the nearest 0.01 mm. The average value for each film was used to calculate the tensile properties.

2.4 Morphology

The surface morphology of thin films was observed using scanning electron microscope (SEM, 259 ZEISS EVO LS15) with accelerating voltage of 10 kV.

2.5 X-ray Diffraction (XRD)

The X-ray diffraction (XRD) patterns of thin films were obtained using a diffractometer (Rigaku Ultima IV). The XRD spectra were recorded over a range (2θ) of 5–45° with a continuous scan rate at 2.0° interval.

2.6 Fourier Transforms Infrared Spectroscopy (FTIR)

Characteristic peaks for thin films were obtained using FTIR spectrometer (PerkinElmer, USA) equipped with a universal Attenuated Total Reflectance (UATR) reflectance cell. Spectra were collected in the wavenumber range of 500–4000 cm^{-1}.

2.7 Thermogravimetric Analysis (TGA)

Thermogravimetric analyzes were performed in a thermal analyzer (PerkinElmer, model 4000) in ceramic pans. Samples (10 g) were heated up from 40 to 700 °C at a rate of 20 °C/min. Nitrogen was used as purge gas (20 mL/min) to avoid thermo-oxidative reactions.

2.8 Tensile Properties

Tensile strength and elongation at break were obtained according to ASTM D882. The tensile strength test was performed using the Universal Testing machine (Instron 3365, Buckinghamshire). The crosshead speed was fixed at 10 mm/min. The samples were prepared according to the dimensions provided by the standard. For each test, five samples were analyzed. The tensile properties were calculated as the average value from the obtained results.

2.9 Water Absorption

The water absorption test was carried according to the ASTM D570 standard. Prepared films were cut into 76.2 mm × 25.4 mm pieces, dried for 24 h in an oven at 50 °C, cooled in a desiccator, and weighed. The water absorption data of films was obtained by soaking them in water for 2 h. After that, films were dried with a cloth and immediately weighed. And after, those samples were soaked in water for another 24 h and weighed. The water absorption capacity of composites was calculated as follows.

$$\text{Water absorption, } \% = \frac{\text{wet weight} - \text{conditioned weight}}{\text{conditioned weight}} \times 100 \qquad (1)$$

2.9.1 Biodegradability

The biodegradability test was carried out according to the aerobic compost environment test [26]. Initially, the starch-based thin films were cut into pieces of 2.0 × 2.0 cm and weighed before being tested. Then, the samples were buried inside the soil at a depth of 3 cm at 25 °C and water was sprayed to maintain the moisture of the compost. The weights of the samples were measured after 15 days.

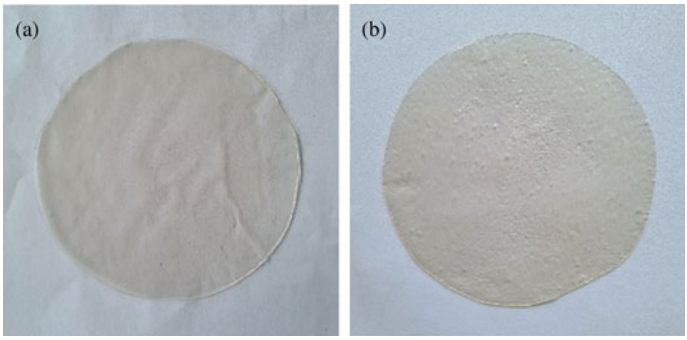

Fig. 1 Photographs of (**a**) cassava starch-based thermoplastic film without oil and (**b**) cassava starch-based thermoplastic film with oil

3 Results and Discussion

3.1 Physical Properties

According to visual examination, the obtained cassava starch-based thermoplastic films were transparent, odorless, and easy to handle. Film thickness varied from 0.32 to 0.37 mm. The prepared cassava starch-based thermoplastic films are shown in Fig. 1.

Thermoplastic starch films were visually transparent and when the oil content for both CO and VO was incresed, the transparency of the films reduced.

3.2 SEM Observation

Figure 2 shows the SEM micrographs at 1000 × magnification of surface of thermoplastic starch films with oil.

As shown in Fig. 2, the microstructures of cassava starch-based thermoplastic films with different concentrations of CO and VO were evaluated by SEM. It was

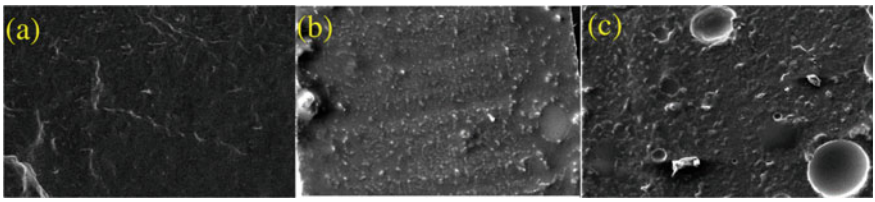

Fig. 2 SEM images of composites (×1000 magnification): (**a**) TPS, (**b**) TPS with coconut oil, and (**c**) TPS with vegetable oil

observed that the surface of the control film (TPS without oil) was homogeneous and continuous without any granules or pores (Fig. 1a). The films containing CO and VO (Fig. 1b, c) showed a discontinuous and porous structure and some oil droplets could be seen. It can be suggested that CO and VO were not dispersed homogeneously within the thermoplastic films [11].

3.3 X-ray Diffraction (XRD)

Preparation of thermoplastic film by casting method generally leads to solubilization of amylose followed by the destruction of starch crystalline structure [27]. Diffraction patterns of the control cassava starch-based thermoplastic film and cassava starch-based thermoplastic films with CO and VO oil in different contents are given in Fig. 3.

Diffraction pattern of the control film (TPS) showed a broad diffraction peak in 15–20° 2θ region. It indicates the destruction of A-type crystal structure. According to the literature, characteristic peaks (2θ) for the structure of cassava starch are at 15°, 17°, 18°, 20°, 23°, and 26° [28]. When adding the CO and VO, the shape of the peak has changed: diffraction peaks became wider. The oil-added thermoplastic films showed broad diffraction peak in 15–25° 2θ region.

3.4 Fourier Transforms Infrared Spectroscopy (FTIR)

The FTIR spectra of control cassava starch-based thermoplastic film and cassava starch-based thermoplastic films with CO and VO oil in different contents are depicted in Fig. 4.

All FTIR showed a peak which was evident at wave number 3200–3300 cm^{-1} (Fig. 4), indicates a hydrogen-bonded O-H stretching. All thermoplastic films had peaks in the range 2850–2950 cm^{-1} corresponding to a C-H functional group [29–31]. The peaks at 2920 cm^{-1} and 2850 cm^{-1} indicate the presence of long-chain alkyl groups. The peaks around 2850 cm^{-1} intensified with CO and VO contents' increasing, which confirmed the presence of oils [32]: [11]. The characteristic peak at 1750 cm^{-1} corresponds to stretching of C = O group of ester bonds. When increasing the oil contents, it displayed more intense bands at wavenumbers of 1750 cm^{-1} [11]. Another peak in the range 1620–1650 cm^{-1} corresponds to water absorption. A peak at 1320–1380 cm^{-1} in corresponding to bending vibration of a C-H group and C-O of an aromatic ring was also evident. Peaks corresponding to bending vibration of C-O, and O-H in the range of 1010–1070 cm^{-1} was also present in all samples. [29–31].

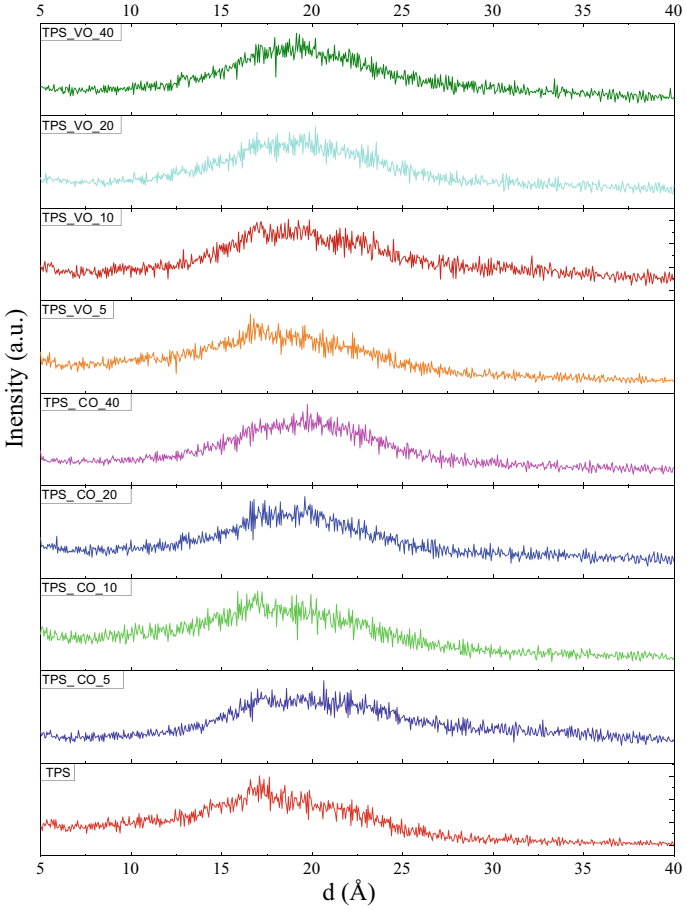

Fig. 3 XRD diffractograms for TPS films: TPS, TPS_CO_5, TPS_CO_10, TPS_CO_20, TPS_ CO_40, TPS_VO_5, TPS_VO_10, TPS_VO_20, and TPS_VO_40

3.5 Thermogravimetric Analysis (TGA)

Thermogravimetric (TG) and its derivative thermogravimetric (DTG) curves were used to evaluate the thermal stability of the cassava starch-based thermoplastic films with oils (shown in Fig. 5).

When the temperature was below 100 °C, a lower thermal weightlessness was observed. It could be due to the evaporation of water or the small molecular impurities. Films containing oil started to show different degrees of weightlessness at 180 °C. This will happen due to the thermal degradation of fatty acids in films with CO and VO. After 300 °C, thermoplastic films showed insistent weightlessness. This could be attributed to the thermal degradation of the starch components in the films [33–35]

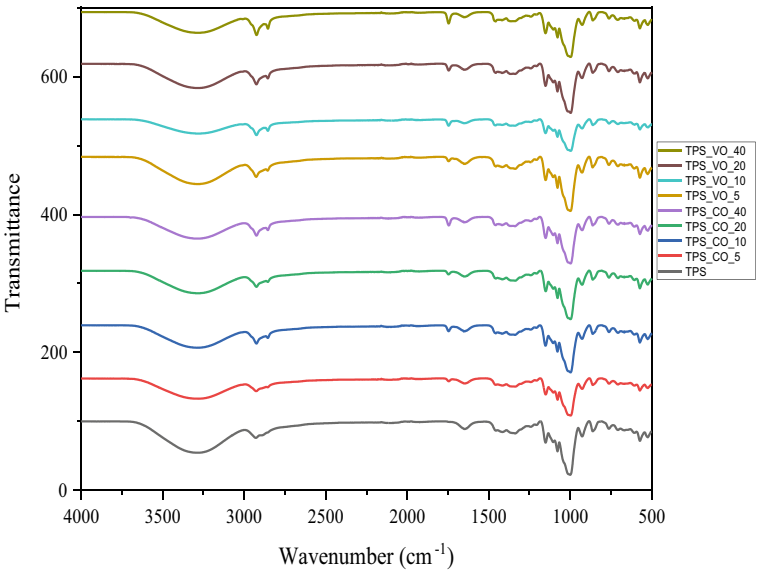

Fig. 4 FTIR spectra of TPS films: TPS, TPS_CO_5, TPS_CO_10, TPS_CO_20, TPS_CO_40, TPS_VO_5, TPS_VO_10, TPS_VO_20, and TPS_VO_40

3.6 Tensile Properties

Tensile strength and elongation at break of the thermoplastic thin films with CO ad VO are shown in Figs. 6 and 7, respectively.

As the CO content and VO content increased, the tensile strength of the thermoplastic film showed an increasing trend, followed by a decrease. When the concentration of oil was 10 wt %, the tensile strength of the film with CO reached its highest value (3.56 MPa), and the tensile strength of the film with VO reached its highest value (4.18 MPa). Moreover, the tensile strength of film containing VO is higher than the tensile strength of film containing CO for the same oil concentration. However, the addition of CO and VO in high concentration (over 20 wt%), reduced the tensile strength of the thermoplastic films by weakening the interactions between the starch molecules. This could happen due to increased discontinuity of lipid molecules in the starch matrix [34]

The elongation at break decreased with the increase in coconut oil and vegetable oil. TPS without oil shows lower elongation at break value compared with TPS with 5, 10, and 20% CO and 5 and 10% VO.

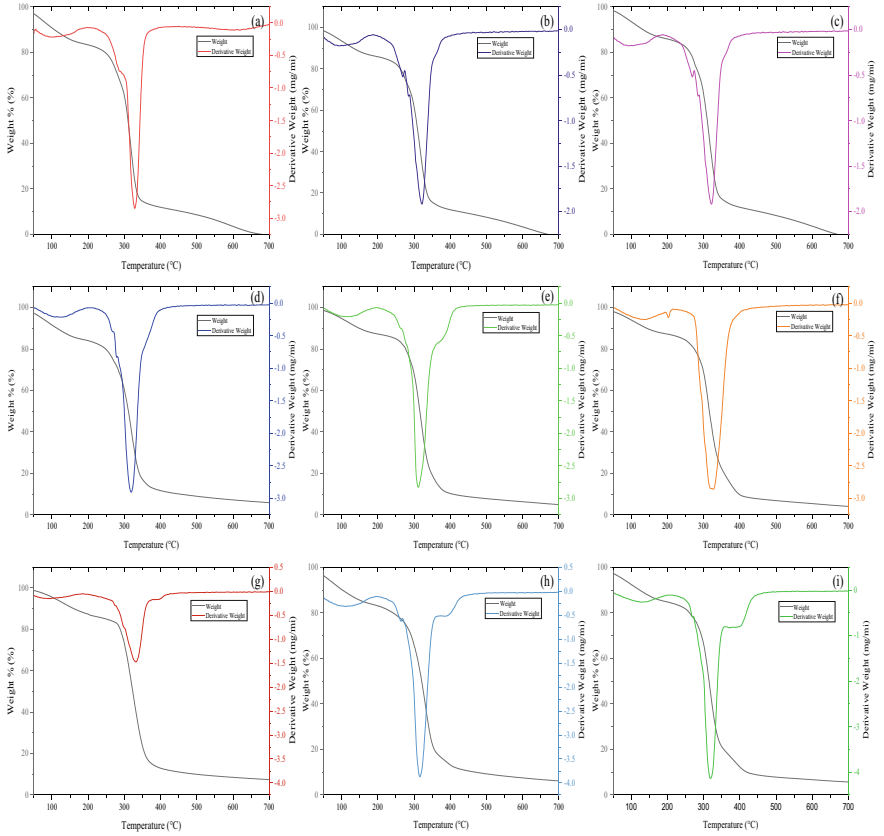

Fig. 5 Curves of TGA, and its derivative DTG of the TPS films: (**a**) TPS, (**b**) TPS_CO_5, (**c**) TPS_CO_10, (**d**) TPS_CO_20, (**e**) TPS_CO_40, (**f**) TPS_VO_5, (**g**) TPS_VO_10, (**h**) TPS_VO_20, and (**I**) TPS_VO_40

3.7 Water Absorption

Figure 8 shows the water absorption properties of cassava starch-based thermoplastic with CO and VO in different oil concentrations.

After introducing CO and VO into the composites, only a slight decrease in water absorption of the films were observed until the oil content reached 20% w/w concentration. This can be attributed to the hydrophilic character of starch and glycerol [36]. The improved water resistance properties for TPS with oil content up to 20% w/w was due to the hydrophobic characteristic of coconut oil and vegetable oil. Fatty acids improve the hydrophobic properties of the TPS films, thus increase the water resistance properties [11, 34, 37]. This behaviour is consistent with the results of previous studies [38]. However, a significant enhancement in water resistance properties were expected due to hydrophobic nature of coconut oil and vegetable oil. The

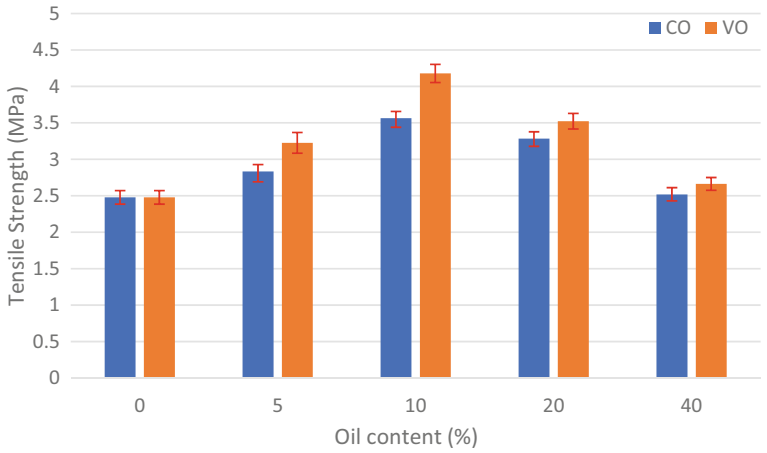

Fig. 6 Tensile strength of cassava starch-based thermoplastic thin films with different concentrations of CO and VO

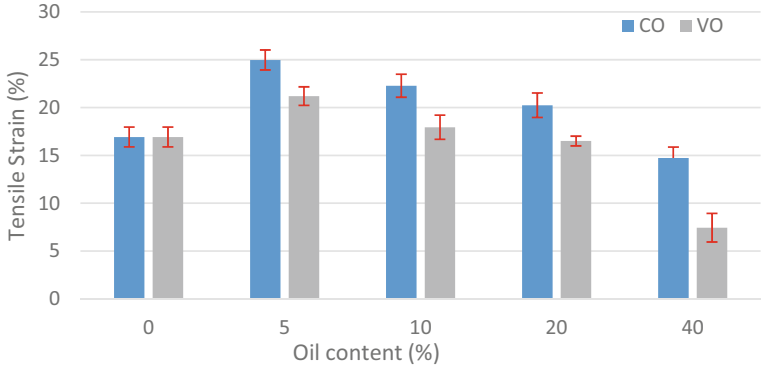

Fig. 7 Elongation at break of cassava starch-based thermoplastic thin films with different concentrations of CO and VO

addition of VO reduced the water solubility better than CO at the same oil concentration for 5% w/w and 10% w/w. The oil with 40% w/w concentration TPS film showed slightly high-water absorption when compared to the reference TPS film. This can happen due to the differences in density between oils and cassava starch leading to the movement of lipid aggregates to the material surfaces by damaging cohesive structural integrity [11].

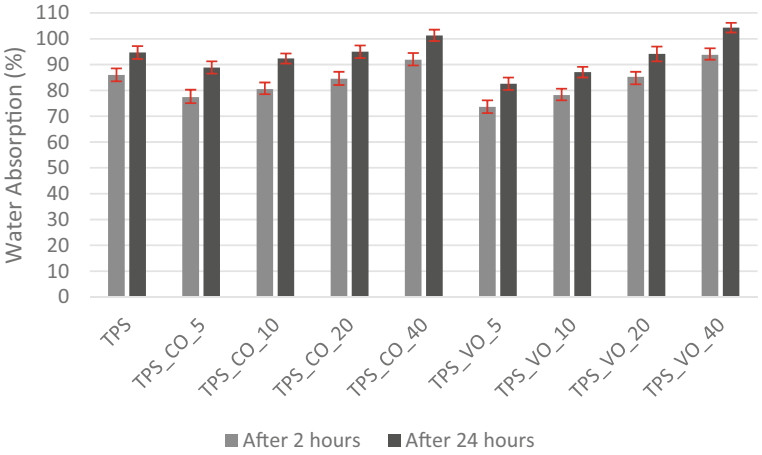

Fig. 8 The water absorption of cassava starch-based thermoplastic thin films with different concentrations of CO and VO

3.8 Biodegradability

In biodegradation test, all the thermoplastic thin films showed a significant degradation within 15 days. The percentage weight loss of all the thin films was 50–70%.

4 Conclusion

In this work, different percentages of refined coconut oil and vegetable oil (palm olein oil) were added into the cassava starch-based thermoplastic plasticized using glycerol. The prepared films were thermally and mechanically characterized. It was observed that the addition of coconut oil and vegetable oil contributes significantly to characteristics' improvement for all tested standards. Vegetable oil was more effective than coconut oil for lower oil concentration. Overall, this study recommended that CO and VO have potential to be formulated in the cassava starch-based thermoplastic for packaging since the CO and VO are non-toxic plant-based material.

Acknowledgements The authors wish to express their sincere appreciation to Accelerating Higher Education Expansion and Development (AHEAD) for the financial assistance (AHEAD/RA3/DOR/65).

References

1. Liu H, Xie F, Yu L, Chen L, Li L (2009) Thermal processing of starch-based polymers. Prog Polym Sci 34(12):1348–1368
2. Zhang Y, Rempel C, McLaren D (2014) Thermoplastic starch. In: H JH (ed) Innovations in food packaging. Elsevier, Texas, pp 391–412
3. Jiang B, Li S, Wu Y, Song J, Chen S, Li X, Sun H (2018) Preparation and characterization of natural corn starch-based composite films reinforced by eggshell powder. CyTA J Food 16(1):1045–1054
4. Tapia-Blacido D, Mauri A, Menegalli F, Sobral P, Anon M (2007) Contribution of the starch, protein, and lipid fractions to the physical, thermal, and structural properties of amaranth (amaranthus caudatus) flour films. J Food Sci 72(5):E293–E300
5. Moshood T, Nawanir G, Mahmud F, Mohamad F, Ahmad M, AbdulGhani A (2022) Sustainability of biodegradable plastics: new problem or solution to solve the global plastic pollution? Curr Res Green Sustain Chem 5:100273
6. Mali S, Grossmann M, Garcia M, Martino M, Zaritzky N (2006) Effects of controlled storage on thermal, mechanical and barrier properties of plasticized films from different starch sources. J Food Eng 75(4):453–460
7. Morgan N, Choct M (2016) Cassava: Nutrient composition and nutritive value in poultry diets. Animal Nutr 2(4):253–261
8. Lopez O, Zaritzky N, Grossmann M, Garcia M (2013) Acetylated and native corn starch blend films produced by blown extrusion. J Food Eng 116(2):286–297
9. Liu P, Sun S, Hou H, Dong H (2016) Effects of fatty acids with different degree of unsaturation on properties of sweet potato starch-based films. Food Hydrocolloids 61:351–357
10. Brandelero R, Grossmann M, Yamashita F (2012) Films of starch and poly(butylene adipate co-terephthalate) added of soybean oil (SO) and Tween 80. Carbohyd Polym 90(4):1452–1460
11. Yang J, Ching Y, Julai JS, Chuah C, Nguyen D, Lin P (2022) Comparative study on the properties of starch-based bioplastics incorporated with palm oil and epoxidized palm oil. Polym Polym Compos 30. https://doi.org/10.1177/09673911221087595
12. Chieng B, Ibrahim N, Then Y, Loo Y (2014) Epoxidized vegetable oils plasticized poly(lactic acid) biocomposites: mechanical thermal and morphology properties. Molecules 19(10):16024–16038
13. Silverajah V, Ibrahim N, Yunus W, Hassan H, Woei C (2012) A comparative study on the mechanical, thermal and morphological characterization of poly(lactic acid)/epoxidized palm oil blend. Int J Mol Sci 13(5):5878–5898
14. Tee Y, Talib R, Abdan K, Chin N, Kadir Basha R, Md Yunos K (2015) Comparative study of chemical, mechanical, thermal, and barrier properties of poly(lactic acid) plasticized with epoxidized soybean oil and epoxidized palm oil. BioResources 11(1)
15. Ali F, Chang Y, Kang S, Yoon J (2008) Thermal, mechanical and rheological properties of poly (lactic acid)/epoxidized soybean oil blends. Polym Bull 62(1):91–98
16. Xu Y, Qu J (2009) Mechanical and rheological properties of epoxidized soybean oil plasticized poly(lactic acid). J Appl Polym Sci 112(6):3185–3191
17. Thuy N, Duc V, Liem N (2018) Properties of poly(lactic acid) plasticized by epoxidized rubber seed oil. Viet J Chem 56(2):181–186
18. Liu L, Kerry J, Kerry J (2006) Effect of food ingredients and selected lipids on the physical properties of extruded edible films/casings. Int J Food Sci Technol 41(3):295–302
19. Bhasney S, Patwa R, Kumar A, Katiyar V (2017) Plasticizing effect of coconut oil on morphological, mechanical, thermal, rheological, barrier, and optical properties of poly(lactic acid): a promising candidate for food packaging. J Appl Polym Sci 134(41):45390
20. Lopera-Valle A, Caputo J, Leão R, Sauvageau D, Luz S, Elias A (2019) Influence of epoxidized canola oil (eCO) and cellulose nanocrystals (CNCs) on the mechanical and thermal properties of polyhydroxybutyrate (PHB)—poly(lactic acid) (PLA) blends. Polymers 11(6):933

21. Volpe V, De Feo G, De Marco I, Pantani R (2018) Use of sunflower seed fried oil as an ecofriendly plasticizer for starch and application of this thermoplastic starch as a filler for PLA. Ind Crops Prod 122:545–552
22. Boateng L, Ansong R, Owusu W, Steiner-Asiedu M (2016) Coconut oil and palm oil's role in nutrition, health and national development: a review. Ghana Med J 50(3):189–196
23. Fediol.eu (2022) EU vegetable oil and protein meal industry association. https://www.fediol.eu/data/fatty%20acids.pdf. Accessed 25 Aug 2022
24. Sampaio K, Ceriani R, Silva S, Taham T, Meirelles A (2011) Steam deacidification of palm oil. Food Bioprod Process 89(4):383–390
25. Belibi P, Daou J, Ndjaka J, Nsom B, Michelin L, Durand B (2014) A comparative study of some properties of cassava and tree cassava starch films. Phys Proc 55:220–226
26. Wahyuningtiyas N, Suryanto H (2017) Analysis of biodegradation of bioplastics made of cassava starch. J Mech Eng Sci Technol 1(1):24–31
27. Parker R, Ring S (2001) Aspects of the physical chemistry of starch. J Cereal Sci 34(1):1–17
28. Teixeira E, Róz A, Carvalho A, Curvelo A (2005) Preparation and characterisation of thermoplastic starches from cassava starch, cassava root and cassava bagasse. Macromol Symp 229(1):266–275
29. Almeida M, Alves R (2010) Determination of amylose content in starch using Raman spectroscopy and multivariate calibration analysis. Anal Bioanal Chem 2693–2701
30. Mendes J, Paschoalin R, Carmona V, Sena Neto A, Marques A, Marconcini J, Mattoso L, Medeiros E, Oliveira J (2016) Biodegradable polymer blends based on corn starch and thermoplastic chitosan processed by extrusion. Carbohyd Polym 137:452–458
31. Syafri E, Kasim A, Abral H, Asben A (2017) Effect of precipitated calcium carbonate on physical, mechanical and thermal properties of cassava starch bioplastic composites. Int J Adv Sci Eng Inf Technol 7(5):1950
32. Fang J, Fowler P, Tomkinson J, Hill C (2002) An investigation of the use of recovered vegetable oil for the preparation of starch thermoplastics. Carbohyd Polym 50(4):429–434
33. Edhirej A, Sapuan SM, Jawaid M, Zahari NI (2017) Preparation and characterization of cassava bagasse reinforced thermoplastic cassava starch. Fibers Polym 18:162–171
34. Fangfang Z, Xinpeng B, Wei G, Wang G, Shi Z, Jun C (2019) Effects of virgin coconut oil on the physicochemical, morphological and antibacterial properties of potato starch-based biodegradable films. Int J Food Sci Technol 55(1):192–200
35. Wang W, Wang K, Xiao J, Liu Y, Zhao Y, Liu A (2017) Performance of high amylose starch-composited gelatin films influenced by gelatinization and concentration. Int J Biol Macromol 94:258–265
36. Xiong Z, Yang Y, Feng J, Zhang X, Zhang C, Tang Z, Zhu J (2013) Preparation and characterization of poly(lactic acid)/starch composites toughened with epoxidized soybean oil. Carbohyd Polym 92(1):810–816
37. Ai Y, Hasjim J, Jane J (2013) Effects of lipids on enzymatic hydrolysis and physical properties of starch. Carbohyd Polym 92(1):120–127
38. Šuput D, Lazić V, Pezo L, Markov S, Vaštag Ž, Popović L, Radulović A, Ostojić S, Zlatanović S, Popović S (2016) Characterization of starch edible films with different essential oils addition. Polish J Food Nutr Sci 66(4):277–285

Batch Adsorption Study for the Removal of Textile Dyes from Aqueous Solutions Using Pandanus Amaryllifolius (Rampe) Leaves

S. L. G. Haththotuwa and B. M. W. P. K. Amarasinghe

Abstract The adsorption of selected textile dyes, methylene blue (MB), crystal violet (CV), Congo red (CR), reactive red 24: 1 (RR), and reactive black b (RBB) from aqueous solutions into dried leaf powder of *Pandanus amaryllifolius* (Rampe) (PALP) was studied. Batch adsorption experiments were conducted at room temperature to investigate the adsorption capacity. The experimental results showed that the adsorbent could remove MB, CV, and CR up to 95%, 90%, and 81%, respectively. However, both reactive dyes did not show significant removal. Kinetic and equilibrium studies were performed for MB, CV, and CR dyes. Kinetic data revealed that dye uptake was fast, with 90% or more of the adsorption occurring within the first 15–20 min of contact time. The kinetic data fit the pseudo-second-order model with correlation coefficients greater than 0.99. The equilibrium data were satisfactorily fitted to the Langmuir, Freundlich, and Temkin isotherms. The intra-particle diffusion model confirmed that the adsorption of dyes onto the adsorbent is controlled not only by intraparticle diffusion but also by film diffusion which plays an important role. Fourier transform infrared (FTIR) spectroscopy and Scanning electron microscopy (SEM) analysis of the adsorbent before and after adsorption revealed that MB, CV, and CR were adsorbed to PALP with chemisorption by creating hydrogen bonds. A significant amount of mass transfer has occurred through papillose cells on the surface of the PALP.

Keywords Batch adsorption · *Pandanus amaryllifolius* leaves · Textile dye

S. L. G. Haththotuwa
Department of Civil Engineering, University of Moratuwa, Moratuwa, Sri Lanka

B. M. W. P. K. Amarasinghe (✉)
Department of Chemical and Process Engineering, University of Moratuwa, Moratuwa, Sri Lanka
e-mail: padma@uom.lk

© The Author(s), under exclusive license to Springer Nature Singapore Pte Ltd. 2023

R. Dissanayake et al. (eds.), *ICSBE 2022*, Lecture Notes in Civil Engineering 362,
https://doi.org/10.1007/978-981-99-3471-3_6

1 Introduction

Contamination of textile dyes with water bodies can seriously damage the aquatic system. This can reduce the aesthetic quality of natural water resources, increase chemical oxygen demand, increase biochemical oxygen demand, create toxicity for aquatic life, create carcinogenicity, mutagenicity, bioaccumulation, and disturb photosynthesis [1].

Available chemical techniques to remove dyes from contaminated wastewater include Ozon oxidation, oxidation, Fenton oxidation, photochemical, and ultraviolet (UV) irradiation. As a result of the complex structure of many dyes, it is difficult to completely remove them using conventional biodegradation methods. Novel biological techniques are degradation using cultures of fungi and microbes and the use of algae and enzymes [2]. Biosorption is one of the best methods for dye removal because of its low cost and higher effectiveness. Examples of biomaterials such as bacteria, algae, fungi, seaweed, plant leaves, and roots are tested and evaluated for different dyes [3].

In this study, the adsorption of five textile dyes that are toxic in the natural environment was tested. *Pandanus amaryllifolius* (Rampe) leaves powder (PALP) was used as an adsorbent. The objectives of the research are as follows.

I. To determine the adsorption capacity of the *Pandanus amaryllifolius* (Rampe) leaf powder for the selected five dye types.
II. To determine the adsorption kinetics and equilibrium data for the selected dye types through batch adsorption experiments.
III. To characterize the adsorbent and determine its physical and surface properties.

2 Materials and Methods

2.1 Materials

Rampe leaves were obtained from the healthy and well-grown bush in the wetland area located in Kotavila, Matara district. Only the part of the mature leaf was selected without any dead content. The MB, CV, CR, RR, and RBB dyes were purchased from a local industrial chemical supplier named Kannan and Company.

2.2 Preparation of Biosorbent (Adsorbent)

The leaves were washed with clean well water to remove dust, mud, and debris and kept for sun drying. The dried leaves were ground into a powder and sieved using a sieve shaker to separate the particles between the 250–710 μm size range. The separated leaf powder was washed with clean flowing water to further remove

the finest particles. Then it was washed three times with 80 °C hot water and cold water to remove tannin (brown color). The cleaned leaf powder was kept in an open atmosphere for 3 h to remove excess water and then dried using a laboratory drier operating at 110 °C for 24 h. The dried PALP was stored in a sealed container [4].

2.3 Preparation of Dye Solutions (Adsorbate)

The dye powder was weighed using GIBERTINI CENT-2 4000 PT electronic precision balance. The weighed dye was dissolved in 1.0 L of distilled water in a beaker and properly mixed until all dye clusters disappeared. The prepared dye solutions were diluted proportionally to obtain the concentration required for the experiments.

2.4 Measurements with Analytical Instruments

Dye solution sample analysis was performed with the SHIMADZU UV 1800 UV-Vis Spectrophotometer with wavelengths 190–1100 nm. Distilled water was used as the reference solution. All the dye solutions were subjected to spectrum analysis and the obtained maximum absorbance values were set as each dye beam wavelength in sample analysis. A set of calibration curves were developed for all five dyes using known dye concentrations to measure the unknown dye concentration of the experimental samples.

Fourier transform infrared (FTIR) spectroscopy of raw and dye-adsorbed dry PALP was obtained using a BRUKER ALPHA FTIR scanner to observe bond formations of PALP after the adsorption of dyes. The attenuated total reflection (ATR) method was used with a wave number range of 650–4000 cm^{-1}.

Scanning electron microscope (SEM) images of raw and dye-adsorbed dry PALP samples were taken to observe the surface topography using ZEISS EVO|18 Research SEM. In SEM imaging, the applied magnification was 2500, and the beam voltage was 10 kV.

2.5 Batch Adsorption Experiments

Batch adsorption studies were performed using a variable speed IKA® RW 20 digital mechanical stirrer as an agitator. A 5.0 g of PALP was added to a beaker filled with 1.0 L of the dye solution with a known concentration when starting the timer. The agitator speed of 315 rpm, the dye solution pH of 7.00, the dye solution temperature of 25 °C, and the PALP weight of 5 g were kept unchanged for all experiments. The solution samples were withdrawn at the required time intervals and the samples were analyzed for dye concentration.

Batch experiments were conducted to determine the adsorption capacity of each selected dye. For MB, CV, and CR; batch experiments were conducted to obtain adsorption kinetics and equilibrium data.

3 Results and Discussion

3.1 Percentage Removal of Dyes

The percentage of dye removed at equilibrium was calculated for all five dyes. The percentage removal of dyes at equilibrium is given in the Fig. 1 bar chart.

The percentage removal of dyes at equilibrium for MB, CV, CR, RR, and RBB were 94.9%, 89.56%, 80.95%, 10.57%, and 3.43%, respectively, after 300 min with 5.0 g of PALP for an initial dye concentration of 0.03 g L^{-1}. According to Fig. 1, RR and RBB have a lower percentage of removal. In industrial processes, reactive dyes are applied to fibre using an alkaline solution, which means that the pH value is greater than 7.00, which is required for an effective dying process. However, the experiments were conducted at pH values of around 7.0. Therefore, pH 7.00 may not be favourable for the adsorption of reactive dyes on PALP. That may be a reason for the lesser removal of both reactive dyes.

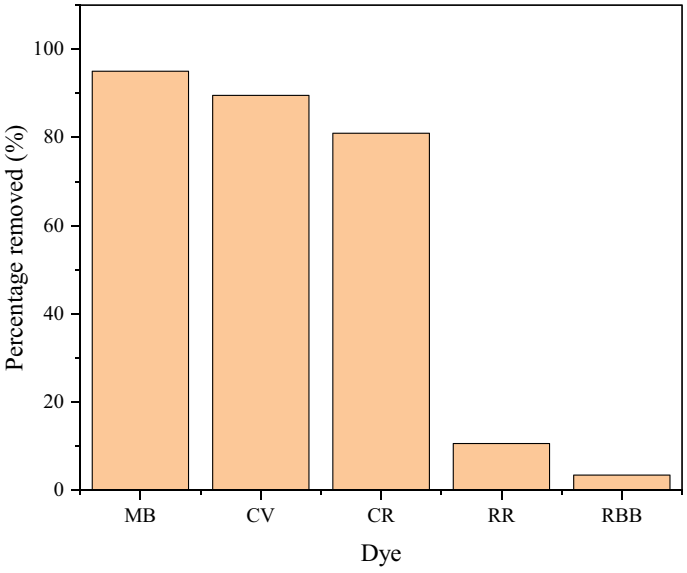

Fig. 1 Percentage removal of dyes at the equilibrium after 300 min with 5.0 g of PALP for an initial dye concentration of 0.03 g L^{-1}

Table 1 Selected dye molecular physical properties and dimensions

Dye	Molecular weight ($gmol^{-1}$)	Molecular length (nm)	Molecular width (nm)	Nature
MB	319.85	1.447[a]	0.95[a]	Cationic
CV	407.99	1.400[b]	1.40[b]	Cationic
CR	696.66	2.290[c]	0.80[c]	Anionic
RR	802.08	2.12	1.08	Anionic
RBB	991.82	3.15[d]	1.23[d]	Anionic

[a][7], [b][8], [c][9], [d] [10]

Table 1 shows the molecular properties of the selected dyes. According to the data in Table 1, with an increase in molecular weight, molecular lengths also increase significantly. Large molecular dimensions in adsorbate molecules can block access to the active pore sites in the adsorbent material [5]. The pore sizes of biosorbents are around 2.6 nm [6]. Hence, less adsorption of RBB and RR can be due to a higher molecular dimension compared to that of the PALP pore size. The good adsorption of MB, CV, and CR can be due to a lower molecular dimension compared to that of the PALP pore size. The molecular weight, molecular dimension, and nature of the molecule for all five dyes are given in Table 1.

3.2 Adsorption Isotherm Studies

Several models have been developed to describe adsorption equilibrium isotherm relationships. The Freundlich isotherm model (FIM) explains heterogeneous adsorption by sites on the adsorbent surface, and adsorption occurs in a multilayer exponential manner due to adsorbed surface repeatedly acting as an adsorbent [11]. The Langmuir isotherm model (LIM) explains homogeneous adsorption by the finite number of sites located on the adsorbent surface. Adsorption occurs as monolayer adsorption without having an interaction of adjacent ions adsorbed. The Temkin isotherm model (TIM) describes the heat of adsorption of all adsorbate molecules in the layer of the adsorbent surface which are being reduced linearly instead of logarithmically due to the interactions caused by the adsorbate molecules [12]. The linearized equations of FIM, LIM, and TIM are given by Eqs. (1)–(3), respectively.

$$logq_e = logK_f + \frac{1}{n} logc_e \tag{1}$$

$$\frac{1}{q_e} = \frac{1}{q_m K_a c_e} + \frac{1}{q_m} \tag{2}$$

$$q_e = B_T ln A_T + B_T ln c_e \tag{3}$$

where q_e is the amount of dye adsorbed at equilibrium (mg g^{-1}), and c_e is the equilibrium concentration of dye (mg L^{-1}). K_f and n are constants related to the adsorption capacity and intensity. The equilibrium constant K_a is known as the adsorption energy (Lm g^{-1}), and q_m is the maximum monolayer adsorption capacity of the adsorbent (mg g^{-1}) [13]. B_T is the TIM constant. A_T is the equilibrium binding constant of TIM related to the maximum binding energy (L g^{-1}) [12]. Figure 2 shows the equilibrium data fitted to the Langmuir isotherm.

Similarly, the data were fitted to Freundlich and Temkin isotherm equations, and the results obtained are shown in Table 2.

According to the results shown in Table 2, the MB, CV, and CR dyes were adsorbed onto PALP according to the Langmuir isotherm. However, CR shows a better fit to the Temkin isotherm equation.

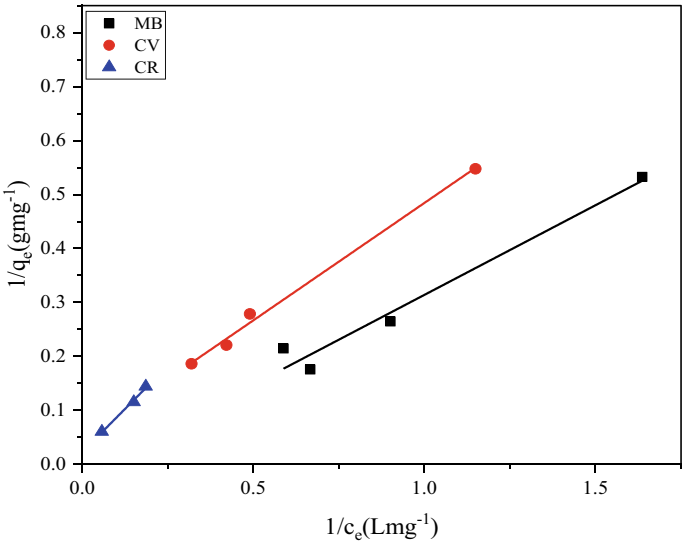

Fig. 2 Langmuir isotherm fit for MB, CV, and CR dyes at equilibrium after 300 min with 5.0 g of PALP for a different initial dye concentration of MB, CV, and CR

Table 2 Comparison of Langmuir, Freundlich, and Temkin isotherm fittings

Dye	Langmuir isotherm			Freundlich isotherm			Temkin isotherm		
	q_m (mg g^{-1})	K_a (L mg^{-1})	R^2	K_f	1/n	R^2	A_T	B_T	R^2
MB	38.46	0.080	0.9681	3.220	1.013	0.9165	2.936	3.297	0.8621
CV	20.33	0.110	0.9950	2.046	0.854	0.9918	2.158	2.708	0.9648
CR	44.05	0.035	0.9937	2.133	0.718	0.9931	0.426	8.340	1.0000

3.3 Adsorption Kinetic Studies

Lagergren's pseudo-first-order (LPFO) model explains that adsorbate's adsorption rate into the adsorbent is directly proportional to the adsorbate concentration difference between adsorbate at a given time and that at the equilibrium. The assumption is that interaction between the adsorbent and the adsorbate depends on the reaction rate. This describes the reversibility of the liquid and solid phase adsorption equilibrium. The pseudo-second-order (PSO) model explains the chemisorption kinetics of the adsorbate on the adsorbent. The linearized LPFO model is given by Eq. (4), and the PSO model is given by Eq. (5).

$$log(q_e - q_t) = logq_e - \left(\frac{K_1}{2.303}\right)t \tag{4}$$

$$\frac{t}{q_t} = \frac{1}{K_2 q_e{}^2} + \frac{1}{q_e}t \tag{5}$$

where q_e is the amount of dye adsorbed at equilibrium (mg g^{-1}), t is the contact time (min), q_t is the amount of dye adsorbed at contact time t (mg g^{-1}), K_1 is the LPFO rate constant (min^{-1}) and K_2 is the PSO rate constant (g mg^{-1} min^{-1}) [13]. The adsorption kinetic data were fitted to both the LPFO and PSO models, and the results are shown in Table 3. For all the experiments, the results show a better fit to the pseudo-second-order kinetic model. The PSO model fits of MB, CV, and CR are given in Fig. 3a–c, respectively.

Table 3 Comparison of kinetic parameters of the LPFO and PSO fit

Dye	Initial concentration (mgL^{-1})	LPFO model			PSO model		
		q_e (mgg^{-1})	K_1 (min^{-1})	R^2	q_e (mgg^{-1})	K_2 (gmg^{-1} min^{-1})	R^2
MB	30	3.148	−0.097	0.9649	5.734	0.099	1.0000
	25	2.449	−0.081	0.9240	4.711	0.109	1.0000
	20	2.080	−0.081	0.9175	3.805	0.125	1.0000
	10	1.186	−0.085	0.9333	1.895	0.199	0.9999
CV	30	3.006	−0.104	0.9331	5.406	0.107	0.9999
	25	2.399	−0.088	0.9242	4.554	0.120	1.0000
	20	1.950	−0.161	0.9651	3.606	0.251	0.9999
	10	0.671	−0.090	0.9000	1.835	0.524	1.0000
CR	50	7.889	−0.034	0.9892	9.174	0.007	0.9995
	40	6.070	−0.044	0.9754	7.194	0.013	0.9997
	30	4.952	−0.046	0.9971	5.263	0.008	0.9940
	10	1.251	−0.149	0.9974	1.326	0.250	0.9995

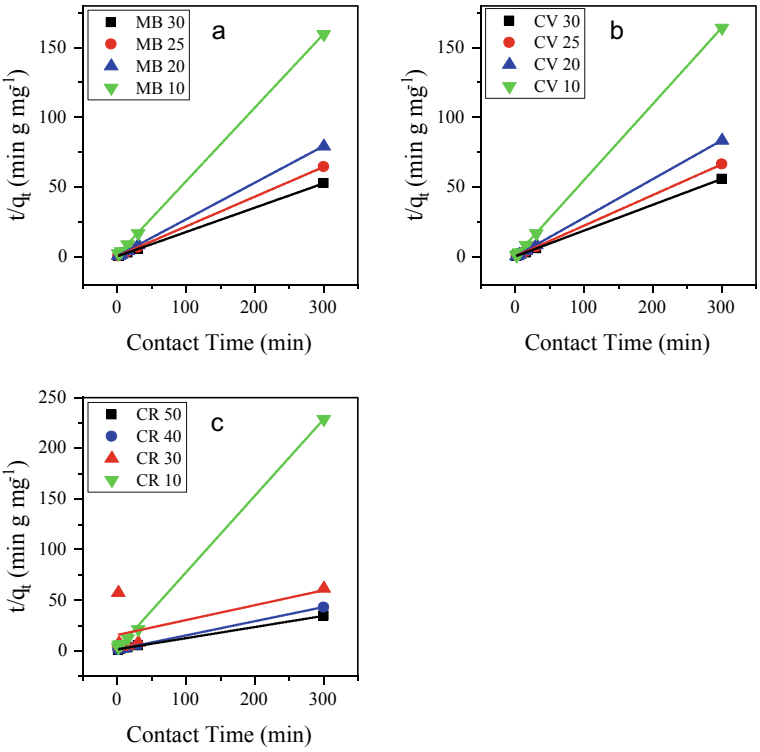

Fig. 3 PSO model fit of dyes **a** MB, **b** CV, and **c** CR at equilibrium after 300 min with 5.0 g of PALP dose for different initial dye concentrations

The dye concentrations in the adsorbent at equilibrium values (q_e) were calculated using the pseudo-second-order model, and the results are compared with the experimentally determined q_e in Table 4.

The percentage deviation values in Table 4 further confirm that the dye adsorption fits the pseudo-second-order model.

3.4 Intra-Particle Diffusion Studies

Adsorption occurs by diffusion of dye molecules into the porous interior of the PALP. Morris and Weber's model for intraparticle diffusion is given in Eq. (6).

$$q_t = k_d t^{0.5} + \delta \tag{6}$$

Table 4 Experimental q_e vs. q_c calculated with percentage deviation

Dye	Initial concentration (mg L^{-1})	q_e Experimental (mg g^{-1})	q_e Calculated (mg g^{-1})	Percentage deviation (%)
MB	30	5.70	5.73	0.53
	25	4.66	4.71	1.07
	20	3.78	3.81	0.79
	10	1.88	1.90	1.06
CV	30	5.37	5.41	0.74
	25	4.53	4.55	0.44
	20	3.59	3.61	0.56
	10	1.83	1.83	0.00
CR	50	8.67	9.17	5.77
	40	6.92	7.19	3.90
	30	4.86	6.85	40.95
	10	1.31	1.33	1.53

where q_t is the dye concentration adsorbed in contact time t (mg g^{-1}), k_d intra-particle diffusion rate constant (mg g^{-1} $min^{-0.5}$), t contact time (min), and δ is the boundary layer effect (mg g^{-1}). k_d and δ can be found by plotting q_t versus $t^{0.5}$ [14].

Figure 4a–c plots show two straight lines possible in each data set, indicating that adsorption is not limited to intra-particle diffusion. If the straight lines go through the origin, it can be concluded that only intraparticle diffusion is present as a rate-limiting step [15]. Due to the first part of the diagram being related to external mass transfer by surface adsorption and the second part related to intra-particle diffusion [16], only the second part was fitted. Figure 4a–c show that intra-particle diffusion has initiated after 16 min of adsorption. Parameters determined by analyzing Morris and Webber's model plots generated for MB, CV, and CR dyes are tabulated in Table 5.

The mass transfer resistance components are created by solute to the solid interface and solid interface to the pore sites. According to the values in Table 5 for the MB and CV boundary layer effect, the value decreases as the initial dye concentration increases.

3.5 FTIR Analysis

The FTIR spectrum obtained for raw PALP is much analogous to FTIR received from cellulose [17]. Figure 5 shows newly formed peaks after adsorption of MB, CV, and CR into PALP at 3271 and 1369 cm^{-1}. These peaks are related to O-H stretching and O-H bending, respectively. Therefore, it is sufficiently evident that the adsorption occurs by hydrogen bond formation with the dye and the PALP surface. This

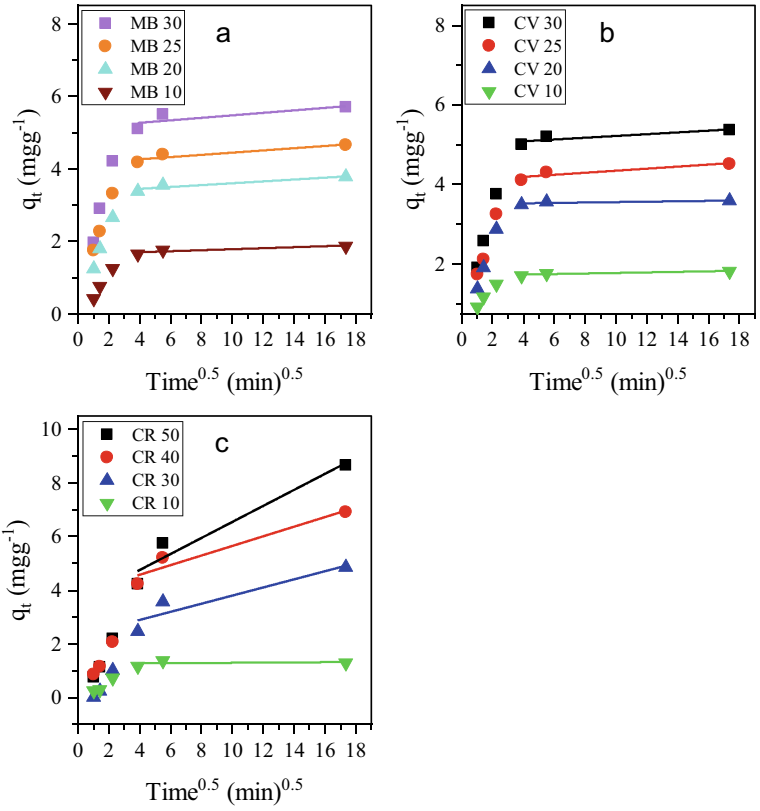

Fig. 4 Morris and Weber diagram for intra-particle diffusion of **a** CV, **b** MB, and **c** CR

Table 5 Morris and Weber model parameters of intra-particle diffusion

Dye	Initial concentration mgL^{-1}	δ (mgg^{-1})	k_d (mgg^{-1} min$^{-0.5}$)
MB	30	1.643	0.013
	25	3.342	0.025
	20	4.136	0.030
	10	5.128	0.034
CV	30	1.709	0.006
	25	3.507	0.005
	20	4.090	0.025
	10	4.997	0.022
CR	50	3.562	0.298
	40	3.863	0.179
	30	2.290	0.151
	10	1.262	0.003

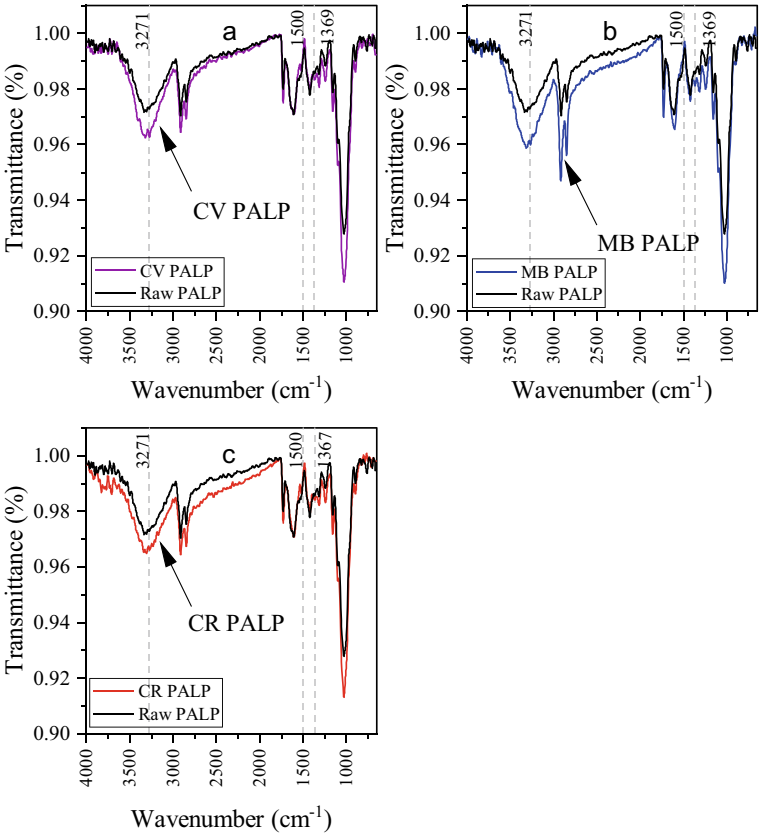

Fig. 5 FTIR spectrum of dye-adsorbed PALP and raw PALP; **a** CV, **b** MB, and **c** CR

information further confirms that surface adsorption occurred as a chemisorption. According to the FTIR spectrums for PALP after adsorption of MB, CR, and CV, it can be seen that the intensity increased in several peaks, indicating an increase in functional groups linked to the corresponding bond.

3.6 SEM Analysis

Comparison of SEM images of raw PALP and MB, CV, and CR dyes adsorbed PALP surfaces are given in Fig. 6.

Figure 6, images b and c show that the volume of the papillose cell increases. The adsorption of dye molecules on papillose cells is indicated. Papillose cells are extruded from the surface of the leaves. Therefore, these cells come into contact with water more than the surface of the PALP. The water film over the papillose

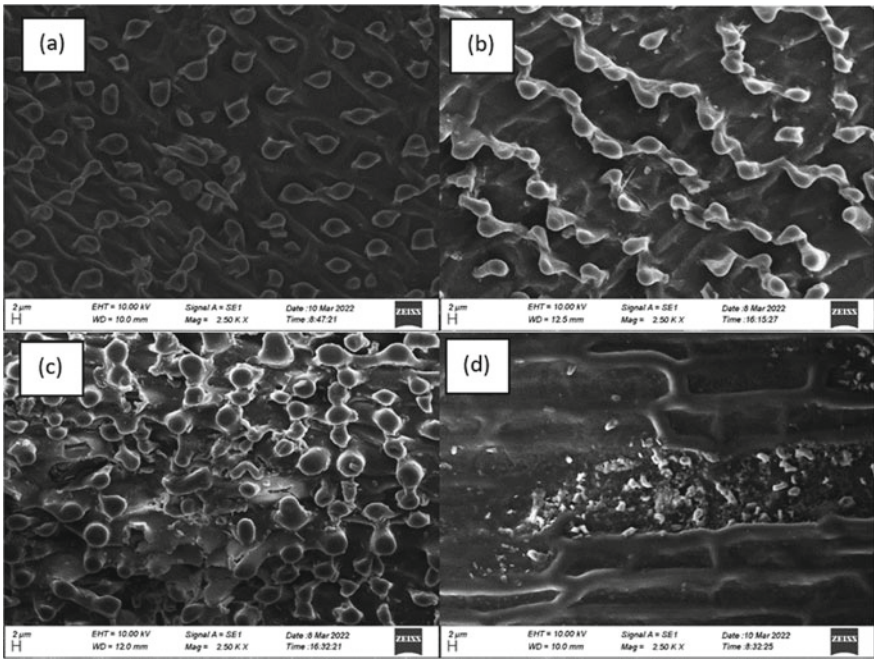

Fig. 6 **a** SEM image of raw PALP, **b** SEM image of MB adsorbed PALP, **c** SEM image of CV adsorbed PALP, **d** SEM image of CR-adsorbed PALP. Magnification 2500

cells creates a surface area for mass transfer, which is higher than other areas of the surface of the leaves. Therefore, the micropores located in papillose cells can continue the adsorption process. Image d shows the cross-sectional view of PALP, which adsorbed CR.

4 Conclusions

The removal percentages for MB, CV, and CR are 95%, 90%, and 81% respectively, under natural atmospheric conditions. The adsorption kinetics was followed by the MB, CV, and CR dyes with PALP as a pseudo second-order kinetic model. The rate-limiting factors for the adsorption of MB, CV, and CR dyes with PALP consist of intra-particle diffusion and surface adsorption. MB and CV are adsorbed into PALP according to the Langmuir isotherm model and have a maximum monolayer adsorption capacity of 38.46 mg g^{-1} and 20.33 mg g^{-1}, respectively. CR is adsorbed according to the Temkin isotherm. PALP is not suitable for the removal of RBB and RR dyes under natural atmospheric conditions. It is recommended to test PALP as an adsorbent for the removal of other polar compounds with a molecular length of 1.5 nm and a molecular mass of around 400 g mol^{-1}. Recommend testing the

performance of column adsorption trials using PALP for MB and CV. Cultivation of PALP for economic purposes as a low-cost adsorbent is encouraged.

References

1. Gita S, Hussan A, Choudhury TG (2017) Impact of textile dyes waste on aquatic environments and its treatment. Environ Ecol 35(3C):2349–2353
2. Katheresan V, Kansedo J, Lau SY (2018) Efficiency of various recent wastewater dye removal methods: a review. J Environ Chem Eng 6(4):4676–4697
3. Bouras et al (2017) Biosorption of Congo red dye by Aspergillus carbonarius M333 and Penicillium glabrum Pg1: kinetics, equilibrium, and thermodynamic studies. J Taiwan Inst Chem Eng 80:915–923
4. Amarasinghe B, Amarasinghe A (2020) Study on mass transfer, kinetic parameters, and rate determining step with statistical analysis in adsorption of pb ions onto coir pith. Int J Sci Res Innov Technol 7(9)
5. Al-Degs YS, El-Barghouthi MI, El-Sheikh AH, Walker GM (2008) Effect of solution pH, ionic strength, and temperature on adsorption behavior of reactive dyes on activated carbon. Dyes Pigments 16–23
6. Ighalo JO, Iwuozor KO, Igwegbe CA, Adeniyi AG (2021) Verification of pore size effect on aqueous-phase adsorption kinetics: A case study of methylene blue. Coll Surf A Physicochem Eng Aspects 626
7. Jia P, Tan H, Liu K, Gao W (2018) Removal of Methylene Blue from Aqueous Solution. Appl Sci 1–11
8. Wathukarage A, Herath I, Iqbal MCM, Vithanage M (2017) Mechanistic understanding of crystal violet dye sorption by woody biochar: implications for wastewater treatment. Environ Geochem Health
9. Liang H-Q et al. (2016) Hierarchically porous carbon membranes derived from PAN and their selective adsorption of organic dyes. Chin J Polym Sci 34(1):23–33
10. Yuping Q, Fang L (2006) Role of surface functionality in the adsorption of anionic dyes on modified polymeric sorbents. Chemosphere 963–971
11. Jeyavishnu K, Alagesan V (2020) Cereus sp. as potential biosorbent for removal of Congo red from aqueous solution: isotherm and kinetic investigations. Environ Monit Assess 192(4)
12. Elkady MF, Ibrahim AM, AbdEl-Latif MM (2011) Assessment of adsorption kinetics, equilibrium, and thermodynamics for the potential removal of reactive red dye using eggshell biocomposite beads. Desalination 278(1–3):412–423
13. Pimentel PM et al (2011) Adsorption of chromium ions on oil shale waste. Braz J Petrol Gas 5(2):065–073
14. Amarasinghe P, Amarasinghe K (2020) Determination of mass transfer coefficients for adsorption of Pb and Cd onto coir pith and statistical analysis. Fort J 2(3):139
15. Dahr et al (2014) Adsorption characteristics of Congo red from aqueous solution onto tea waste. Chem Eng Commun 202(2):181–193
16. Belhachemi M, Belala Z, Lahcene D, Addoun F (2009) Adsorption of phenol and dye from aqueous solution using chemically modified date pits activated carbons. Desal Water Treat 182–190
17. Abderrahim B et al (2015) Kinetic thermal degradation of cellulose, polybutylene succinate, and a green composite: comparative study. World J Environ Eng 95–110

Tea Waste Bio-Char as an Adsorbent for the Removal of Pb(II) in the Industrial Wastewater

N. B. I. M. N. Bandara and V. Edussooriya

Abstract Wastewater that contains Pb(II) creates serious health and environmental issues and this study was conducted to characterise the adsorption of Pb(II) by tea waste bio-char (TWBC) prepared by slow pyrolysis. As an adsorbent, raw tea waste has an issue of decomposing in the liquid phase. Therefore, biochar prepared from tea waste generated at a tea factory in Sri Lanka was used as the adsorbent for the laboratory experiments. Adsorption of Pb(II) at different pH, initial metal concentrations and contact times between adsorbent and adsorbate was measured. The surface characteristics of TWBC before and after the adsorption were examined by the scanning electron microscope (SEM), Energy Dispersive X-ray Spectroscopy (EDX), and Fourier transforms infrared spectroscopy (FT-IR), to explain the results. Results indicate that the adsorption of Pb(II) ions by TWBC gets an optimum value at pH 6.5. The Langmuir and Freundlich isotherm models were used in this study to analyse the data obtained, and the data were fitted to both isotherm models. The correlation coefficient is highest for the pseudo-second-order model, which suggests that chemisorption is the rate-limiting mechanism for the adsorption of Pb(II) onto TWBC. The results of SEM, EDX and FT-IR confirm that TWBC can be considered a better adsorbent and the adsorption capacity is 46.23 mg/g for Pb(II), which is comparable to some of the treated biomaterials. Therefore, biochar prepared using Sri Lankan tea waste can be considered a low-cost adsorbent for the removal of Pb(II) ions from industrial wastewater.

Keywords Tea waste biochar · Lead · Adsorption · Biomaterial · Pyrolysis

1 Introduction

Wastewater effluents, mainly from industries such as mining, fertiliser, tanneries, batteries and pesticides, contain heavy metals which result in adverse effects on human beings. Some heavy metal ions such as Pb(II), As(III), Mn(II), Ni(II) and

N. B. I. M. N. Bandara (✉) · V. Edussooriya
University of Peradeniya, Galaha Road, Peradeniya, Kandy 20400, Sri Lanka

© The Author(s), under exclusive license to Springer Nature Singapore Pte Ltd. 2023

R. Dissanayake et al. (eds.), *ICSBE 2022*, Lecture Notes in Civil Engineering 362,
https://doi.org/10.1007/978-981-99-3471-3_7

Cr(III) do not have known beneficial effects on living organisms and can also cause damage to human functions even at very low concentrations [11, 22, 33, 39].

Among the heavy metals, Pb is recorded as a strong toxin for human health as its non-biodegradability causes long-term persistence in the environment [16]. Pb would create serious threats to human health, including eye problems, seizures, constipation, anaemia, vomiting, nausea, excruciating abdominal pain, eventual muscle paralysis, and damage to the reproductive system and the nervous system [17, 28, 43].

Authorities in many countries have imposed tolerance limits for Pb(II) as a mitigating measure for polluting water with Pb [4, 39]. Furthermore, various treatment methods are practised to remove Pb(II) in wastewater, and the most widely used methods are ion exchange, solvent extraction, membrane processes, and chemical precipitation [4, 28]. Besides, limitations can be identified in these methods such as sludge production, less efficiency, high cost and operating conditions [1, 4].

Adsorption has proven to be an alternative to conventional treatment methods since it offers numerous benefits such as resource recovery, less sludge, low cost, and high efficiency [28, 42]. Fly ash, red mud, coconut shell carbon, activated phosphate, olive cake, bentonite clay, and activated carbon are the well-established adsorbents to remove Pb(II) in wastewater [17, 18, 29, 30, 37, 38]. Using agricultural waste materials for adsorption has been emerging recently since it is more economical, efficient and a renewable source of biomass [39]. The agricultural waste materials comprise hemicellulose, lignin, extractives, lipids, proteins, simple sugars, water hydrocarbons, and starch, which contain functional groups that can adsorb heavy metals [8, 19, 39]. The agricultural and forest waste products such as sawdust, tree barks, groundnut shells, coconut shells, black gram husk, hazelnut shells, walnut shells, cotton seed hulls, cassia fistula leaves, maize corn cobs, sugarcane bagasse, apple, banana, and orange peels, soybean hulls, grape stalks, and water hyacinth have proven to be potential metal adsorbents [5, 14, 19, 26, 27, 32, 36, 39, 40].

Tea waste has also been used as an adsorbent to remove metals from wastewater, including Pb(II), because the structure of tea leaves allows them to adsorb Pb(II). The cell walls of tea leaves are insoluble and made from cellulose, hemicellulose, lignin, condensed tannins and structural proteins, which consist of functional groups such as carboxylate, aromatic carboxylate, phenolic hydroxyl and oxyl groups [4, 9, 10, 40, 42, 44]. Even though tea waste has a high capability of removing heavy metals, there are some limitations in long-term use due to the decomposition of tea waste, which takes place when in contact with a liquid medium. However, this matter can be mitigated by using tea waste biochar (TWBC) instead of tea waste [41].

Interest in adsorption using biochar derived from agricultural waste has increased recently. Biochar is a cost-effective alternative since it needs less energy and can be used to remove various pollutants from wastewater [2, 24, 41].

This work investigates the potential of biochar produced by tea waste from Sri Lankan tea to remove Pb(II) from aqueous solutions. Pb adsorption into TWBC is characterised by the effect of pH, the effect of initial concentration, and adsorption kinetics to compare the adsorption capacity with other bio-sorbents.

2 Materials and Methods

2.1 Materials Preparation

The tea waste from a tea factory in Sri Lanka was obtained and the TWBC was prepared considering the methodology adopted by Amarasinghe and Williams [4]. The coloured components of tea waste were removed by washing them with distilled water. TWBC was produced through a slow pyrolysis process in a specially designed reactor. The temperature was maintained at a range of 500–600 °C throughout the pyrolysis process as the charring temperature. The temperature of TWBC was reduced to the ambient temperature once the pyrolysis process was finished to prevent the reaction between TWBC and atmospheric oxygen, which can be converted into ash. The prepared TWBC was sieved and stored in sealed polythene bags to prevent the interaction between TWBC and air. For all experiments, the fraction between 450 and 850 μm was used.

2.2 Regents Used

Synthetically prepared $Pb(NO_3)_2$ was used as the adsorbent and analytical grade $Pb(NO_3)_2$ (Sigma-Aldrich, USA) was used to prepare the solution. Initially, a 2000 mg/L concentrated Pb(II) solution was prepared, and it was used to obtain solutions with the required concentrations for each experiment.

2.3 SEM, EDS, and FT-IR Analysis

Scanning Electron Microscopy (SEM) analysis and Energy Dispersive X-ray (EDX) spectroscopy analysis were carried out to study the surface microstructures of the TWBC particles and Pb(II) adsorbed TWBC particles, using an electron microscope (TM4000, Japan) and EDS analyser. The infrared spectra of TWBC and Pb(II) adsorbed TWBC were analysed by Fourier Transform Infrared Spectroscopy (FT-IR).

2.4 Effect of pH on Adsorption

The pH range of 4–7.5 was used to examine the effect of pH on adsorption since beyond these limits the effect of precipitation on adsorption could occur. The pH of solutions was adjusted using 0.5 M HNO_3 and 0.5 M NaOH, and the applied metal concentration and the adsorbent concentration were 100 mg/L and 10 g/L, respectively. The solutions were agitated for 3.5 h, and samples of 10 mL at each

pH were withdrawn into polypropylene tubes and shaken in a water bath shaker and filtered. The filtrate was acidified for analysis by a flame atomic absorption spectrometer (AA7000), in Shimadzu, Japan.

2.5 *Effect of Initial Metal Ion Concentration on Adsorption*

TWBC was equilibrated in distilled water for 12 h to hydrate the surfaces of the material [31]. Initial Pb(II) concentrations were varied from 75 to 400 mg/L and the prepared Pb(II) solutions were added to the equilibrated TWBC solution and agitated. Samples were taken at each concentration and centrifuged for 10 min at 2,500 rpm and filtered for metal analysis. The Atomic Absorption Spectrophotometer (AA7000, Shimadzu, Japan) was used to detect Pb(II).

The adsorption data of Pb(II) was fitted to the Langmuir as shown in Eqs. (1) and (2) and Freundlich isotherm models, shown in Eqs. (3) and (4) [35] using Origin 7 software (Origin Lab Corporation, Northampton, Massachusetts).

$$q_e = \frac{QbC_e}{1 + bC_e} \tag{1}$$

A linear form of this expression is,

$$\frac{1}{q_e} = \frac{1}{Q} + \frac{1}{Qb} \cdot \frac{1}{C_e} \tag{2}$$

where q_e is the amount of adsorbate adsorbed per unit weight of adsorbent (mg/g), C_e is the equilibrium concentration of adsorbate (mg/L), Q is the significance of adsorption capacity (mg/g), and b is the energy of adsorption (mg^{-1}).

$$q_e = K_F C_e^{1/n} \tag{3}$$

where K_F and n are Freundlich constants, and a linear form of the Freundlich expression is as follows:

$$\log q_e = \log K_F + \frac{1}{n} \log C_e \tag{4}$$

where q_e is the amount of adsorbate adsorbed per unit weight of adsorbent (mg/g), C_e is the equilibrium concentration of adsorbate (mg/L), K_F is the significance of adsorption capacity, and n is the intensity of adsorption.

2.6 Effect of Contact Time on Adsorption

To investigate the effect of contact time, 1 g of air-dried TWBC was equilibrated with 95 mL of distilled water for a period of 12 h. and a Pb(II) solution with 100 mg/L concentration was prepared. At 30-s intervals, 0.5 mL (10% of the total sample volume) samples were taken from the solution. The samples were centrifuged and filtered for metal analysis. The measurements were carried out using the flame Atomic Absorption Spectrophotometer (AA7000, Shimadzu, Japan).

The data from adsorption kinetic experiments was analysed using pseudo-first-order as shown in Eq. (5) and pseudo-second-order as shown in Eq. (6) models [20].

$$\log(q_e - q_t) = \log q_e - \frac{k_1 t}{2.303} \tag{5}$$

$$\frac{dq_t}{dt} = k_2(q_e - q_t)^2 \tag{6}$$

where q_t is the amount adsorbed per g of adsorbent at time t (mg/g), q_e is the amount adsorbed per g of adsorbent at equilibrium (mg/g), k_1 is Lagergren rate constant (min^{-1}), t is time (min) and k_2 is pseudo-second order constant (g/mg/min).

3 Results and Discussion

3.1 SEM and EDS Analysis

The surface morphological characterisation of TWBC was investigated using SEM and EDS measurements. The main atomic composition of the TWBC is C with a weight of 52.31% and an atomic concentration of 65.28% and O with a weight of 27.24% and an atomic concentration of 25.52% as well as low amounts of K with a weight of 11.74% and an atomic concentration of 4.50%, Al with a weight of 5.09% and an atomic concentration of 2.83% and Mg with a weight of 1.32% and an atomic concentration of 0.81%. Additionally, the SEM–EDS spectrum confirms the adsorption of Pb(II) onto the active sites of TWBC with an absorbance of 19.97% of the weight and an atomic concentration of 1.60%.

The EDX spectrum was obtained for the TWBC sample before and after the adsorption of Pb(II) into TWBC to identify the adsorption of Pb(II) onto the TWBC. As noted from the EDX spectrum, the appearance of a lead peak in the EDX spectrum indicates the binding of lead ions to the available functional groups of TWBC. Note that 19.97% of Pb(II) ions are absorbed into the TWBC while keeping the C, Al, and Mg levels almost constant. However, O % decreased from 27.24 to 17.98 upon lead adsorption. After Pb(II) adsorption, the K on the TWBC surface disappeared.

This indicated that the Pb(II) adsorbed into the O-containing functional groups on TWBC.

3.2 FT-IR Analysis

Infrared spectra of the TWBC before and after lead adsorption are illustrated in Fig. 1, which indicates that lead ion absorbed TWBC shows a broad peak covering the entire region of 2800–3800 cm^{-1}. This broad peak indicates the OH- stretching vibrations. Note that there is no such broad peak visible in this range for TWBC samples before lead adsorption. This clearly shows that Pb(II) sorption to TWBC takes place via hydroxyl groups introduced from the aqueous medium. The TWBC sample's peak at 1600–1800 cm^{-1} can be attributed to –C=C–, –COOH, or –COO–. However, this band is difficult to distinguish due to its broadness. It is interesting to observe the increase in peak intensity of the peak observed at 1600–1800 cm^{-1} for lead-adsorbed TWBC. It can be concluded that available –C=C–, or COOH–, or –COO– in TWBC can potentially interact with Pb(II) to increase the sorption capacity.

The specific surface area calculated for TWBC was slightly small (<1 m^2/g), which indicates that physical interaction or physical sorption to the pores of TWBC

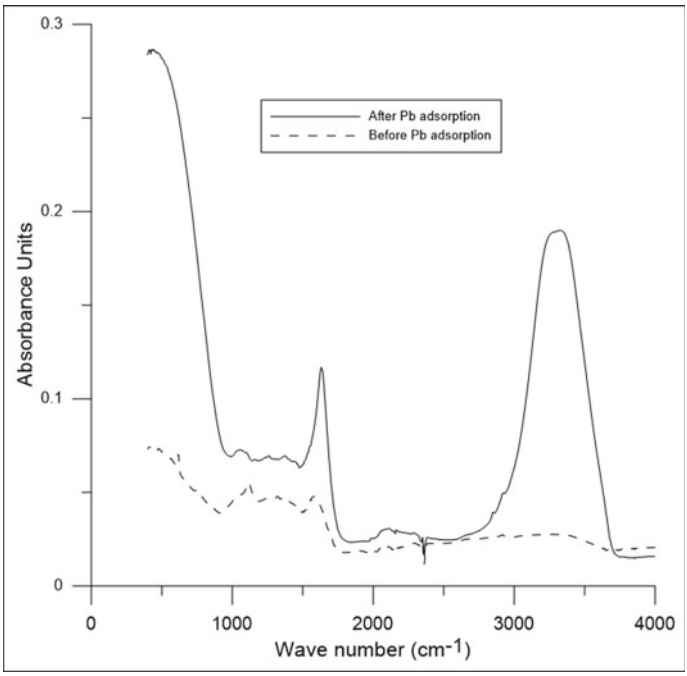

Fig. 1 FT-IR spectra of TWBC, before Pb(II) adsorption and after Pb(II) adsorption

is less significant as compared with the chemical interaction with available functional groups.

3.3 Effect of pH on Adsorption

The pH is vital in the adsorption process since it affects the solubility of the metal ions, the concentration of the ions on the functional groups of the adsorbent, and the degree of ionisation of the adsorbate during the reaction. The effect of the initial pH on Pb(II) adsorption by TWBC was examined, and initially, the Pb(II) removal per unit mass of TWBC was increased up to pH 6.5. The higher pH value is more favourable for the adsorption of Pb(II) on TWBC. However, a decrease in adsorption can be observed after pH 6.5, which may be due to the formation of insoluble hydroxyl complexes [25]. The surface of the adsorbent would be closely associated with hydroxonium ions (H_3O^+) by repulsive forces to the surface functional groups at low pH, consequently decreasing the removal percentage of metal ions [25]. When pH increases, the onset of the metal hydrolysis and the precipitation will begin, usually at pH > 7, and the onset of adsorption occurs before the beginning of the hydrolysis [7]. $Pb(OH)_2$ is formed at pH > 9 and is thermodynamically the most stable, while $Pb(OH)_3^-$ is predominantly at pH > 11. In this study, the pH was increased from 4 to 7.5, a gradual increase in de-protonation on the adsorbent surface leading to a decrease in H^+ ions on the adsorbent surface. This creates more negative charges on the adsorbent surface, creating a favourable condition for the adsorption of positively charged species [21].

3.4 Effect of Initial Metal Concentration on Adsorption

The experimental data are fitted to both Langmuir and Freundlich isotherms and isotherm constants in isotherm equations and regression coefficient (R^2) are given in Table 1. $1/n$ value for the Pb(II) lies between 0 and 1, indicating favourable adsorption [3]. Table 1 shows the Langmuir and Freundlich adsorption parameters obtained for Pb(II) adsorption. Figure 2 shows the graphical representation of experimental data fitted to Langmuir and Freundlich isotherm models.

In the Freundlich isotherm model, n is a constant related to the adsorption intensity and it indicates the degree of nonlinearity between the solution concentration and

Table 1 Langmuir and Freundlich adsorption parameters for adsorption of Pb(II)

Isotherm	Freundlich isotherm			Langmuir isotherm		
Coefficient	K (mg/g)	$1/n$	R^2	K (mg/l)	q_e (mg/g)	R^2
Value	0.2935	0.76	0.935	6.367×10^{-5}	46.23	0.9513

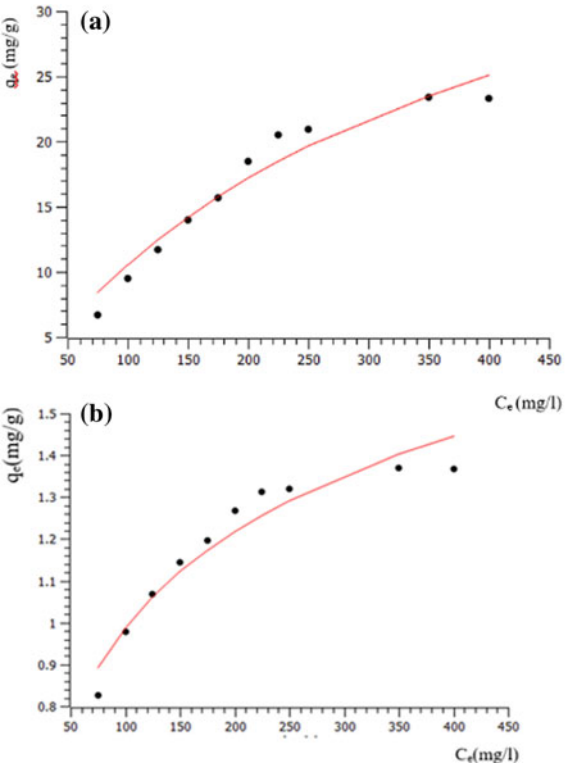

Fig. 2 Langmuir (**a**) and Freundlich (**b**) isotherm model fitted curves for Pb(II)

the adsorption as follows. As $1/n$ indicates the type of adsorption process: $1/n = 0$ is an irreversible process, $0 < 1/n < 1$ is an optimum adsorption state, and $1/n > 1$ is non-optimum adsorption or cooperative adsorption. The obtained result showed $1/n = 0.76$ for TWBC, which lies between 0 and 1, indicating favourable adsorption [12].

3.5 Effect of Contact Time on Adsorption

Adsorption efficiency and adsorbent residence time are primarily determined by the kinetics of metal ion sorption [23]. At 120 min, TWBC was approaching equilibrium. All the active sites were filled when the biochar sample was at equilibrium. In addition, the slight variation in the amount of Pb(II) ion removal by the various samples could be related to the nature and concentration of the surface groups on the active sites. The active sites are responsible for interaction with the Pb(II) ions [6] (Table 2).

Table 2 Parameters of pseudo-first-order and pseudo-second-order kinetics models for Pb(II) onto TWBC

Pseudo-first-order model			Pseudo-second-order model			
q_e (mg/g)	k_1 (min^{-1})		R^2	q_e (mg/g)	k_2 (min^{-1})	R^2
5.649	0.138	0.732	9.345	0.013	0.996	

According to the results obtained, the correlation coefficient was highest for the pseudo-second-order model, which suggests that chemisorption was the rate-limiting mechanism for the adsorption of Pb(II) onto TWBC [12, 13].

3.6 Comparison of Pb(II) Adsorption onto Biosorbents

The Pb(II) adsorption capacity of TWBC is compared with the other biosorbents. TWBC shows a higher adsorption capacity than grape bagasse and sugar beet pulp [15, 34]. However, when compared with the raw tea waste, the TWBC has less adsorption capacity [4]. Nevertheless, TWBC can be identified as a good bio-sorbent for industrial wastewater treatment.

4 Conclusions

The adsorption of Pb(II) by TWBC was investigated in this study. The adsorption of Pb(II) to TWBC increases until the pH of the solution reaches 6.5 and then decreases. The effect of initial concentrations was investigated in this study, and both Langmuir and Freundlich isotherms were fitted to the adsorption process. However, 0.760 was obtained for the $1/n$ value in the Freundlich model, which suggests that the adsorption process is favourable and optimum. An adsorption reaction constant of 0.013 min^{-1} was obtained and the correlation coefficient was highest for the pseudo-second-order model, which suggests that chemisorption was the rate-limiting mechanism for the adsorption of Pb(II) onto TWBC. The results indicated that biochar derived from tea waste can act as an effective surface sorbent, having an adsorption capacity of 46.23 mg/g, which is cost-effective and can be used in industrial wastewater treatment.

Acknowledgements The authors acknowledge Giragama Tea Factory for the supply of TW for this study and Saitama University, Japan for the support given in the sample analysis.

References

1. Ahluwalia SS, Goyal D (2005) Removal of heavy metals by waste tea leaves from aqueous solution. Eng Life Sci 5(2):158–162
2. Ahmad M, Rajapaksha AU, Lim JE, Zhang M, Bolan N, Mohan D, Vithanage M, Lee SS, Ok YS (2014) Biochar as a sorbent for contaminant management in soil and water: a review. Chemosphere 99:19–33
3. Ajenifuja E, Ajao JA, Ajayi EOB (2017) Adsorption isotherm studies of Cu (II) and Co (II) in high-concentration aqueous solutions on photo catalytically modified diatomaceous ceramic adsorbents. Appl Water Sci 7:3793–3801
4. Amarasinghe BMWPK, Williams RA (2007) Tea waste is a low-cost adsorbent for the removal of Cu and Pb from wastewater. Chem Eng J 132:299–309
5. Annadurai G, Juang RS, Lee DL (2002) Adsorption of heavy metals from water using banana and orange peels. Water Sci Technol 47:185–190
6. Augustine AA, Orike BD, Edidiong AD (2007) Adsorption kinetics and modelling of Cu (II) ion sorption from aqueous solution by mercaptoacetic acid modified cassava (manihot sculentacranz) wastes. Elec J Env Agricult Food Chem Title 6:2221–2234
7. Baes GB, Mesmer RE (1976) Hydrolysis of cations. Wiley, New York
8. Bailey SE, Olin TJ, Bricka RM, Adrian DD (1999) A review of potentially low-cost sorbents for heavy metals. Water Res 33:2469–2479
9. Brown PA, Gill SA, Allen SJ (2000) Metal removal from wastewater using peat. Water Res 34:3907–3916
10. Cay S, Uyanik A, Ozasik A (2004) Single and binary component adsorption of copper (II) and cadmium (II) from aqueous solutions using tea-industry waste. Sep Purif Technol 38:273–280
11. Celik A, Demirbas A (2005) Removal of heavy metal ions from aqueous solutions via adsorption onto modified lignin from pulping wastes. Energy Sources 27:1167–1177
12. Charoenpanich J, Cherdchoo W, Nithettham S (2019) Removal of Cr (VI) from synthetic wastewater by adsorption onto coffee grounds and mixed waste tea. Chemosphere 221:758–767
13. Chen C, Qian Y, Chen Q, Tao C, Li C, Li Y (2011) Evaluation of pesticide residues in fruits and vegetables from Xiamen, China. Food Control 22:1114–1120
14. Cimino G, Passerini A, Toscano G (2000) Removal of toxic cations and Cr (VI) from aqueous solution by hazelnut shell. Water Res 34:2955–2962
15. Farinella NV, Matos GD, Arruda MAZ (2007) Grape bagasse as a potential biosorbent of metals in effluent treatments. Bioresour Technol 98(10):1940–1946
16. Flora G, Gupta D, Tiwari A (2012) Toxicity of lead: a review with recent updates. Interdiscip Toxicol 5:47–58
17. Gupta VK, Ali I (2004) Removal of lead and chromium from wastewater using bagasse fly ash—a sugar industry waste. J Colloid Interface Sci 271:321–328
18. Gupta VK, Gupta M, Sharma S (2001) Process development for the removal of lead and chromium from aqueous solutions using red mud—an aluminium industry waste. Water Res 35:1125–1134
19. Hashem A, Akasha RA, Ghith A, Hussein DA (2005) Adsorbent based on agricultural wastes for heavy metal and dye removal: a review. Energy Educ Sci Technol 19:69–86
20. Javed MA, Bhatti HN, Hanif MA, Nadeem R (2007) Kinetic and equilibrium modelling of Pb (II) and Co (II) sorption onto rose waste biomass. Sci Technol 42(16):3641–3656
21. Kadirvelu K, Namasivayam C (2003) Activated carbon from coconut coir pith as metal adsorbent: adsorption of Cd (II) from aqueous solution. Adv Environ Res 7:471–478
22. Kjellstrom T, Shiroishi K, Erwin PE (1977) Urinary β_2-microglobulin excretion among people exposed to cadmium in the general environment. Environ Res 13:318–344
23. Krishnan KA, Anirudhan TS (2003) Removal of cadmium (II) from aqueous solutions by steam-activated sulphurised carbon prepared from sugar-cane bagasse pith: kinetics and equilibrium studies. Water SA 29:147–156
24. Lehmann J, Rillig MC, Thies J, Masiello CA, Hockaday WC, Crowley D (2011) Biochar effects on soil biota—a review. Soil Biol Biochem 43:1812–1836

25. Low KS, Lee CK, Leo AC (1995) Removal of metals from electroplating wastes using banana pith. Biores Technol 51:227–231
26. Macchi G, Marani D, Tirivanti G (1986) Uptake of mercury by exhausted coffee grounds. Environ Technol Lett 7:431–444
27. Maranon E, Sastre H (1991) Heavy metal removal in packed beds using apple wastes. Biores Technol 38:39–43
28. Mondal MK (2010) Removal of Pb (II) from aqueous solution by adsorption using activated tea waste. Korean J Chem Eng 27(1):144–151
29. Mouflih M, Aklil A, Sebti S (2005) Removal of lead from aqueous solutions by activated phosphate. J Hazard Mater 119:183–188
30. Naseem R, Tahir SS (2001) Removal of Pb (II) from aqueous/acidic solutions by using bentonite as an adsorbent. Water Res 35:3982–3986
31. OECD Guideline for the testing of chemicals: adsorption-desorption using a batch equilibrium method (2000) Organization for Economic Co-operation and Development, France
32. Orhan Y, Bujukgungor H (1993) The removal of heavy metals by using agricultural wastes. Water Sci Technol 28:247–255
33. Pastircakova K (2004) Determination of trace metal concentrations in ashes from various biomass materials. Energy Educ Sci Technol 13:97–104
34. Pehlivan E, Yanık BH, Ahmetli G, Pehlivan M (2008) Equilibrium isotherm studies for the uptake of cadmium and lead ions onto sugar beet pulp. Bioresour Technol 99(9):3520–3527
35. Purkait MK, Gusain DS, DasGupta S, De S (2005) Adsorption behavior of chrysoidine dye on activated charcoal and its regeneration characteristics by using different surfactants. Sep Sci Technol 39(10):2419–2440
36. Reddad Z, Gerente C, Andres Y, Ralet MC, Thibault JF, Cloirec PL (2002) Ni (II) and Cu (II) binding properties of native and modified sugar beet pulp. Carbohyd Polym 49:23–31
37. Sabriye D, Ali C (2006) Pb (II) and Cd (II) removal from aqueous solutions by olive cake. J Hazard Mater 138:409
38. Sekar M, Sakthi V, Rengaraj S (2004) Kinetics and equilibrium adsorption study of lead (II) onto activated carbon prepared from coconut shell. J Colloid Interface Sci 279:307–313
39. Sud D, Mahajan G, Kaur MP (2008) Agricultural waste material as potential adsorbent for sequestering heavy metal ions from aqueous solutions—a review. Bioresour Technol 99:6017–6027
40. Tee TW, Khan RM (1988) Removal of lead, cadmium and zinc by waste tea leaves. Environ Technol Lett 9:1223–1232
41. Vithanage M, Mayakaduwa SS, Herath I, Ok YS, Mohan D (2015) Kinetics, thermodynamics and mechanistic studies of carbofuran removal using biochars from tea waste and rice husks. Chemosphere. https://doi.org/10.1016/j.chemosphere.2015.11.002
42. Wasewar KL, Atif M, Prasad B, Mishra IM (2009) Batch adsorption of zinc on tea factory waste. Desalination 244:66–71
43. Weng CH, Lin YT, Hong DY, Sharma YC, Chen SC, Tripathi K (2014) Effective removal of copper ions from aqueous solution using base-treated black tea waste. Ecol Eng 67:127–133
44. Yu B, Zhang Y, Shukla A, Shukla SS, Dorris KL (2000) The removal of heavy metal from aqueous solutions by sawdust adsorption-removal of copper. J Hazard Mater 80:33–42

Mechanical Recycling and Valorisation of Disposable Face Masks: A Potential Solution to the COVID-19 Waste Issue

D. G. K. Dissanayake, S. D. Gunawardane, Dakshitha Weerasinghe, Nadeeka Tissera, and Damith Mohotti

Abstract Rapid spread of COVID-19 disease worldwide resulted in a dramatic increase in face mask consumption. Single-used surgical face masks are manufactured using plastic fibres such as polypropylene (PP) or polyester, which cause severe environmental concerns when accumulated in landfills, primarily due to their non-degradability. Furthermore, plastic fibres are derived from petroleum, a depleting resource at an alarming rate, due to which preserving is highly recommended. Massive consumption and subsequent disposal of single-use surgical face masks urge seeking alternative solutions to conserve resources and manage the ever-growing waste issue. This study investigates the feasibility of recycling surgical facemasks. Single-use surgical face masks were subjected to mechanical recycling through melt extrusion. FTIR and TGA tests were conducted to establish the raw material's chemical composition and thermolytic properties. Facemasks were initially shredded and melt-extruded to obtain filaments, which were subsequently pelletised. The pellets were hot-pressed using the compression moulding technique to make sheet-like panels. Tensile testing of the recycled sheet-like material exhibited failure stress of ~23 MPa and a failure strain of ~2.2%. While the failure stress was similar to the virgin PP material, the failure strain reduced significantly upon recycling. The material's thermal conductivity was measured to be 0.404 W m^{-1} K^{-1} using Lee's

D. G. K. Dissanayake (✉) · S. D. Gunawardane
Department of Textile and Apparel Engineering, University of Moratuwa, Katubedda, Moratuwa 10400, Sri Lanka
e-mail: kanchana.dissanayake@hb.se

D. G. K. Dissanayake
Swedish School of Textiles, University of Borås, 501 90 Borås, Sweden

S. D. Gunawardane
School of Electronic Engineering, Dublin City University, Collins Ave Ext, Whitehall, Dublin 9, Ireland

D. Weerasinghe · D. Mohotti
School of Engineering and IT, University of New South Wales, Northcott Dr, Campbell, ACT 2612, Australia
e-mail: dakshitha.weerasinghe@unsw.edu.au

N. Tissera
Institute of Technology, University of Moratuwa, Diyagama Road, Homagama 10200, Sri Lanka

© The Author(s), under exclusive license to Springer Nature Singapore Pte Ltd. 2023

R. Dissanayake et al. (eds.), *ICSBE 2022*, Lecture Notes in Civil Engineering 362,
https://doi.org/10.1007/978-981-99-3471-3_8

Disc Method. Thermal conductivity was increased significantly than the virgin PP material. The recycled material can be used in sheet form for applications such as thermal insulation and partition boards with further improved strength and thickness. Additionally, recycled pellets have the potential to be used as 3D printing feedstock, thereby enabling utilisation in bulk quantities.

Keywords Face mask waste · COVID-19 · Waste management · Recycling · Environmental pollution · Polypropylene

1 Introduction

COVID-19, the worldwide pandemic, has already caused significant changes and challenges in human lives. The disease continues to spread in a fast phase, and the world is under stringent restrictions on mobility. Lockdowns of more than 200 countries affected the global production and supply chains and revealed the adverse impacts of interdependency among countries for essential commodities [6]. In contrast to production and supply disruptions for many goods, the demand for health commodities has seen a steep rise. Most medical commodities such as masks, gloves and cringers are intended to be used only once and disposed of, thereby increasing waste generation. Daily generation of massive amounts of biomedical waste puts environmental pressure and struggles in managing such wastes. For instance, in India, Delhi alone produces 11 tons of COVID-19-related waste daily, and Mumbai produces 9 tons, whereby the total waste generation in India is increased by 10% [15]. Daily clinical waste generation in Wuhan city is 240 tons, whereas an extra 280 tons of clinical waste is generated in Manila, Philippines and 212 tons of clinical waste is created in Jakarta [15]. South Korea's generation of COVID-19-related wastes accounted for 20 tons/day [16]. It has been an extra challenge for local authorities and municipalities to handle this unexpected rise of COVID-19-related waste [22].

To control the spreading of COVID-19, it was advised that every person should wear a face mask, triggering the demand for face masks to grow at an unpredictable rate, followed by daily disposal of enormous amounts of face masks [5, 17]. Nonwoven fabrics are used for the production of both respirator masks and surgical masks. The general public prefers disposable, single-use surgical masks (facemasks) rather than FFP2-3 or N95-99 respirator masks. Facemasks are manufactured using synthetic fibres such as polypropylene, polyethylene, polyurethane and polyester and are intended to be disposed of after use. Polypropylene (PP) is the most commonly used material to produce facemasks, and it has been reported that a facemask contains approximately 4.5 g of PP [1]. The world population is about 7.8 billion, and if it were assumed that half of the world population disposed a facemask daily, the total number of facemasks disposed to the environment would

be 3.9 billion daily. Consequently, the generated PP waste globally due to disposal of facemasks daily is a minimum of 18 million tons, implying the annual PP waste generation to be approximately 6.5 billion tons.

Disposal of massive quantities of polymeric materials into waste streams not only causes health implications but also leads to serious environmental issues. Fibres such as polypropylene or polyester are derived from petroleum, a depleting resource at an alarming rate; thus, preserving is highly recommended. Using plastic-based facemasks provides an extra burden to already prevailing waste issues of growing plastic consumption and subsequent waste generation. Single-use disposable facemasks would cause severe environmental concerns if they accumulated in landfills, primarily due to their non-degradability, resulting in environmental pollution and landfill issues for decades to come [5]. Furthermore, facemasks made from plastic fibres can be a source of releasing microplastics (MPs) into the environment [3, 7]. MPs are becoming a significant global concern as an environmental pollutant due to their small particle size, ubiquity, bioavailability and adverse impacts on the ecosystem. They can be accumulated in the environment by direct release or fragmentation of larger debris as primary or secondary MPs. Due to their small size, MPs threaten a wide range of marine organisms and the terrestrial environment, which have a high probability of re-entering the food chain [8]. Recent studies indicated that a single surgical facemask might release up to 173,000 fibres/day into the environment [19].

Proper waste collection schemes for used face masks are not yet regulated in most countries, and the disposal of facemasks into the general waste stream is a common practice, especially in developing countries, where waste is often collected in mixed forms and is openly dumped. As COVID-19 has spread across the globe, waste collection schemes of some countries were impacted due to health risks and workforce reduction to meet the cost. For instance, waste collection schemes in European countries were severely affected, and France switched from separate waste collection to a mixed collection to adjust to the reduced workforce, making recycling almost impossible [11]. A separate waste collection scheme and appropriate recycling strategies must be in place to safeguard the environment.

COVID-19 is here to stay for a while; therefore, the demand for facemasks will keep rising, if not steady, for a few years, in which a similar disposal pattern can be expected. Due to health and environmental reasons, it is critical to ensure that facemasks are not entered into the general waste stream. Even though current health concerns prevent the collection and recycling of facemasks, it is recommended to explore the possibilities of cleaning them and recycling them into different applications to recover the intrinsic value of the plastic fibres and conserve resources. PP, the fibre most widely used in facemasks, is a thermoplastic fibre that exhibits various properties such as high strength and lightweight, making it suitable for a wide array of applications. It is vital to adopt the concept of the circular economy into facemasks production and consumption, where resource efficiency is increased and materials are circulated through recycling.

This paper examines the feasibility of recycling single-use facemasks through mechanical recycling. Mechanically recycled waste polymeric materials such as PP

and polyurethane have previously been used in construction and building materials [9, 12]. Such materials have been used to manufacture construction materials with attractive properties at relatively low costs [17]. Since construction activities are responsible for consuming about 40% of natural resources, using PP-based nonwoven fabrics from disposable facemasks holds promise to cater to the hefty volume of input materials required for such industries. It must be included in the research as we advance.

2 Materials and Methods

Material—Considering hygiene issues, unused surgical face masks were obtained from "safe mask" producers in Sri Lanka. According to the manufacturer, the mask consisted of 3 fabric layers; front and back spun-bonded polypropylene, while melt-blown polypropylene for the middle layer (Fig. 1a).

Material Characterisation—All three layers were separated and subjected to Fourier Transform Infrared Analysis (FTIR) using g Bruker, Vertex 80. Attenuated total reflectance (ATR) measurement mode was used with the sample mounted on a ZnSe crystal. The absorption spectra were recorded in 32 scans in the 600–4000 cm^{-1} wavenumber range with 4 cm^{-1} resolutions. Furthermore, the samples were shredded into small pieces and subjected to thermal gravimetric analysis using Q-600 TGA from TA Instruments. Finally, samples were heated from 30 to 1000 °C at a heating rate of 20 °C/min under an air purge of 100 mL/min in order to identify the thermal properties targeting the thermal recycling process.

Experimental Method

Polymer Extrusion—Four sides of the mask were removed, along with the metal stripe and the nylon ear loops. Blue colour front layer and white colour middle and back layers were carefully separated. Among those, white inner and middle layers were cut into 5 × 5 mm using scissors (Fig. 1b). 250 g of the sample was selected for the following experimental process. Targeting thermal recycling, the polymer extrusion process was carried out with KTE 20 Twin Screw Extruder developed by Nanjing KERKE extrusion equipment. The extrusion process (Fig. 1c) was carried through 5 heating zones temperature ranges of 140–160 °C (Heating Zone 1–5; 140, 145, 150, 155, 160 °C) and 170 °C maintained at the final die head. The shredded mask fabric was fed into the hopper of the extruder machine through the feeder at 4 rpm and mixed through the action of the two counter-rotating blades (21.7 mm diameter) at a rotor speed of 250 rpm. Machine pressure was maintained at 3.1 MPa. The polymer passed through the blades and was entered into a die zone which consisted of two holes that created circular cross-section filament wires as the output. The wires were subjected to rapid cooling by entering a quench tank (Fig. 1d) that contained cool water. After cooling down, the wires were processed through a palletisation process

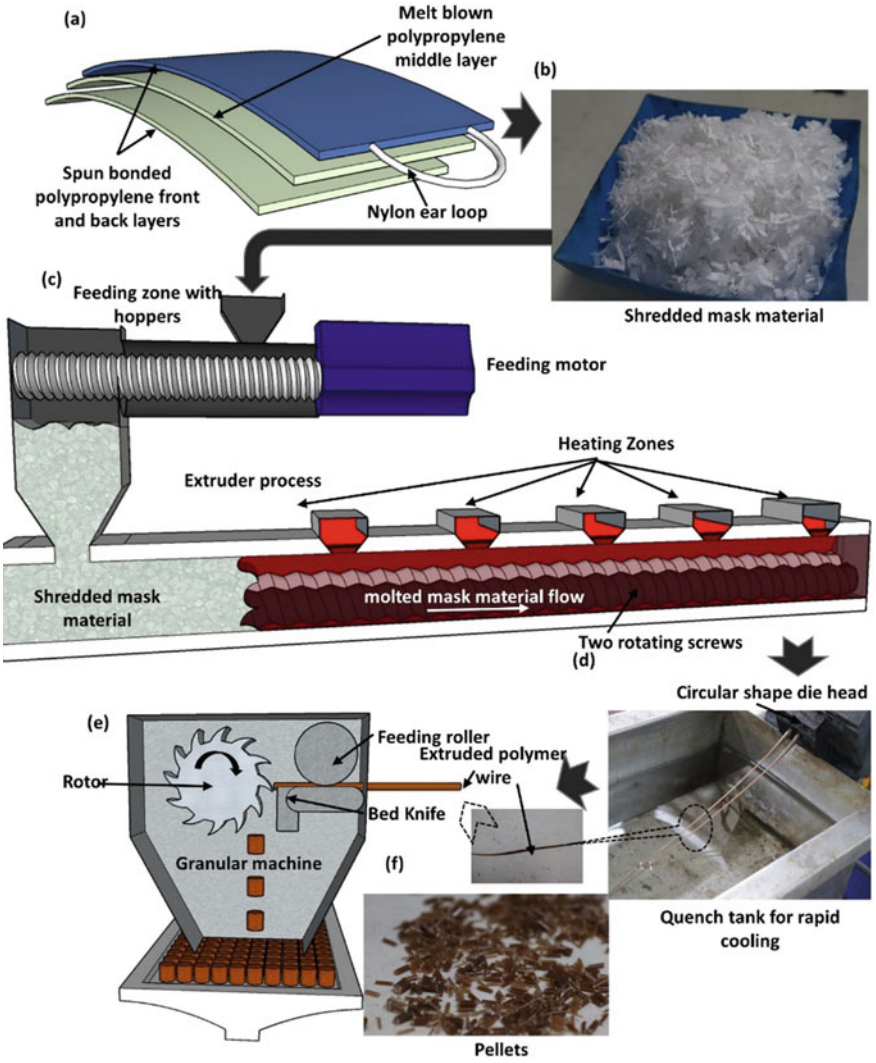

Fig. 1 Mask material extrusion process **a** Schematic of the surgical mask depicting the layers. **b** Shredded mask material as the input for the polymer extrusion process. **c** The extrusion process, **d** rapid cooling with quench tank, **e** palletisation machine and process, **f** polypropylene pellets

with Nanjing KERKE granular machine. Palletisation was carried out at the speed of 6.3 rpm and dried at room temperature (Fig. 1e, f).

Compression Moulding—Subsequently, the pellets were loaded into a mould with 10 × 10 cm dimensions (Fig. 2a) and subjected to compression moulding. Initially, the mould was kept between the compression plates (Fig. 2b), and pressure

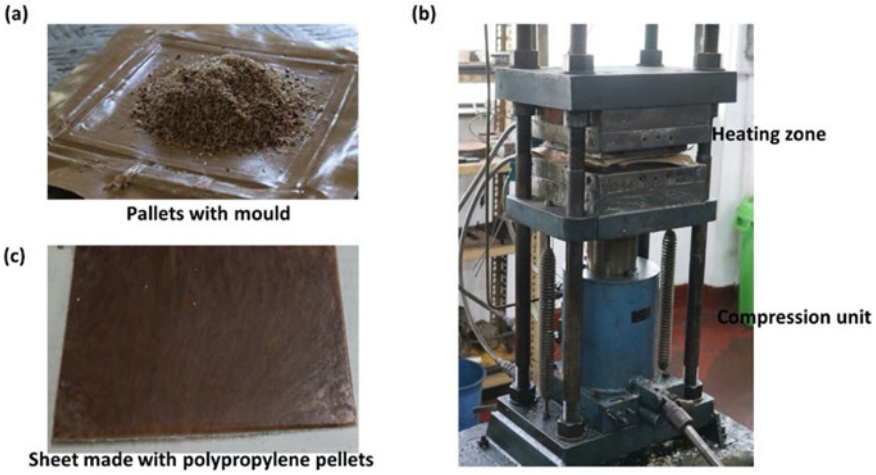

Fig. 2 Compression moulding process: **a** Polypropylene pellets loading to the 10 × 10 cm mould, **b** compression moulding machine with loaded mould, **c** final sheet

was applied in the range of ~0.5 MPa while the temperature was increased gradually from 30 to 170 °C. The machine was operated at a temperature of 0–400 °C. In the last step, the pressure increased up to 1.953 MPa; after 5 min, the whole system was cooled down.

Tensile Testing—After the mould was cooled to room temperature, the sample (Fig. 2c) was peeled off and three specimens were cut using the die used for ASTM D-412. The thickness of the specimen was measured with a 5-point average using the Sylvac μS229 thickness gauge. The specimen was loaded into an Instron Tensile tester, and testing was carried out targeting tensile properties. The ramp of the upper clamp movement was set to 25 mm/min. After the specimen was broken under the tensile stress, the results were recorded, and this was repeated three times to take the average value.

Thermal Conductivity Test—Thermal Conductivity of the sample was tested by Lee's Disc Method, a test method conducted under the Standard of American Society for Testing and Materials (ASTM) C177. A sample was prepared with a diameter of 60 mm. This was kept between the copper disc, and the test was conducted according to the method described in the ASTM standard. The thermal conductivity was calculated using Eq. 1, where; K—Thermal Conductivity, Q—Rate of heat flow, d—thickness of the sample, A—Surface area, θ_2—temperature of the top surface and θ_1—Temperature of the bottom surface.

$$K = \frac{Qd}{A(\theta_2 - \theta_1)} \tag{1}$$

3 Results and Discussion

3.1 FTIR Analysis

The FTIR spectra for all three layers were recorded in Fig. 3. Three layers showed identical spectra, which concluded that the three layers consisted of the same material. The sample spectra showed (Fig. 3) absorption bands in the range of (2850–2950) cm^{-1} and (980–1450) cm^{-1}. The absorption band at 3000–2800 cm^{-1} and the absorption bands at 2950–2890 cm^{-1} corresponds to CH_3 asymmetric and symmetric stretching, respectively [10]. The bands at 2900–2870 cm^{-1} correspond to the symmetric and asymmetric stretching vibration of CH_2 in all three layers of the mask. According to Fig. 3a, the intense absorption band at 1452 and 1375 cm^{-1} is due to the asymmetric and symmetric deformation vibrations of CH_3, respectively [14]. The absorption band at 1165 cm^{-1} could be attributed to C–C asymmetric stretching, CH_3 asymmetric rocking, and C–H wagging vibrations [21]. According to the FT-IR data obtained, the spectrum of the three layers of the mask reveals that the main material composition is polypropylene. The characteristic C=C stretching at the wave number of 1661 not present determine that all the propylene monomers are polymerised during nonwoven fabric manufacturing. Based on this result, all three layers of the surgical face mask can be subjected to a similar thermal recycling method which enables easy handling for the recycling process. Even though all three layers were produced by the same material since the first layer contains a blue colourant that layer was avoided during the recycling process.

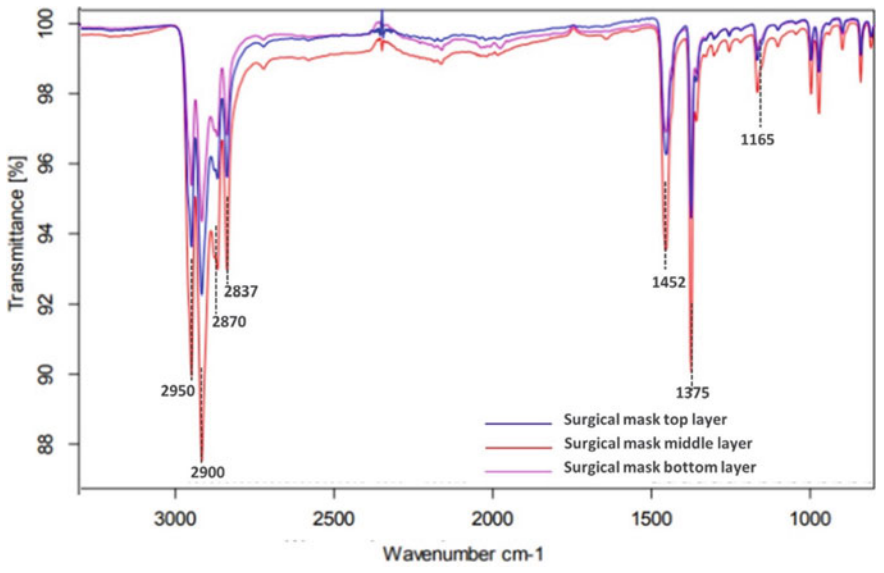

Fig. 3 FTIR spectra of the different facemask layers

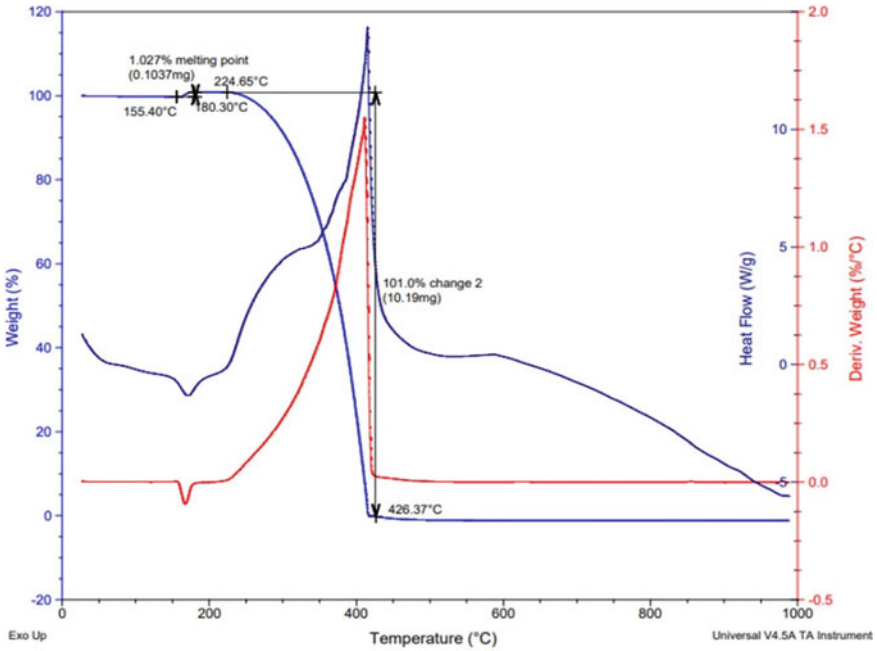

Fig. 4 TGA graph of the facemask sample

3.2 TGA Analysis

After finalising the materials, TGA analysis (Fig. 4) was carried out to understand the thermolytic profile targeting the thermal recycling method. According to the TGA graph, there is a phase change at 155.40 °C which is identical to the polypropylene material's melting point [13]. Moreover, the sample followed a one-step decomposition with an identical polypropylene decomposition curve. The temperature ranges from 224.65 to 426.37 °C resulted in complete evaporation of the material. Based on these results, to get a better recycling process, the temperature needs to increase from 155.40 °C, which should go way beyond 225 °C to prevent thermal decomposition.

3.3 Polymer Extrusion

The melt extrusion process was successfully carried out, and the filaments were drawn and cooled by passing through a water bath. Light brown colour and continuous fluid could be observed when the facemasks were extruded from the die head. It was remarkable that the fluid flowed continuously and bubble-free, facilitating a smooth draw process. The facemasks' extrusion process was very similar to a conventional polymer's melt extrusion, which did not create any unexpected difficulties. Filament

Fig. 5 Filament wires produced by extrusion

wires were successfully produced (Fig. 5), and pellets were subsequently made, showing the protentional of recycling surgical facemasks through the melt extrusion process.

3.4 Analysis of Tensile Properties

According to the tensile testing result, graph depicted in Fig. 6, 23.3 MPa maximum tensile stress has been recorded under 2.2% Tensile strain. Moreover, the recorded elastic modulus was 1685 MPa. When comparing this result with the virgin PP material, it was found that the maximum tensile stress (virgin PP—20 to 30 MPa) at break is still well within the virgin material results, but there is a drastic drop over the elongation at break. Additionally, the elastic modulus (virgin PP—800 to 1300 MPa) slightly increases over the expected value. In previous records, virgin PP has 50% elongation at the break, while the recycled material shows 2.2% elongation at the break [18].

3.5 Thermal Conductivity Test

Thermal conductivity is a factor governed by several parameters, and among those, thickness is an important inversely proportionate factor. In this experiment, the thickness of the sample was kept at 1.54 mm. The upper surface temperature at the saturation was recorded as 369 K, while the lower surface temperature was recorded as 358 K. Calculated heat flow for the process was 8.1764 J s^{-1}. Based on the experimental data, the calculated thermal conductivity for the sample is 0.404 W m^{-1} K^{-1}. Virgin polypropylene has comparatively (0.17–0.22 W m^{-1} K^{-1}) very low thermal

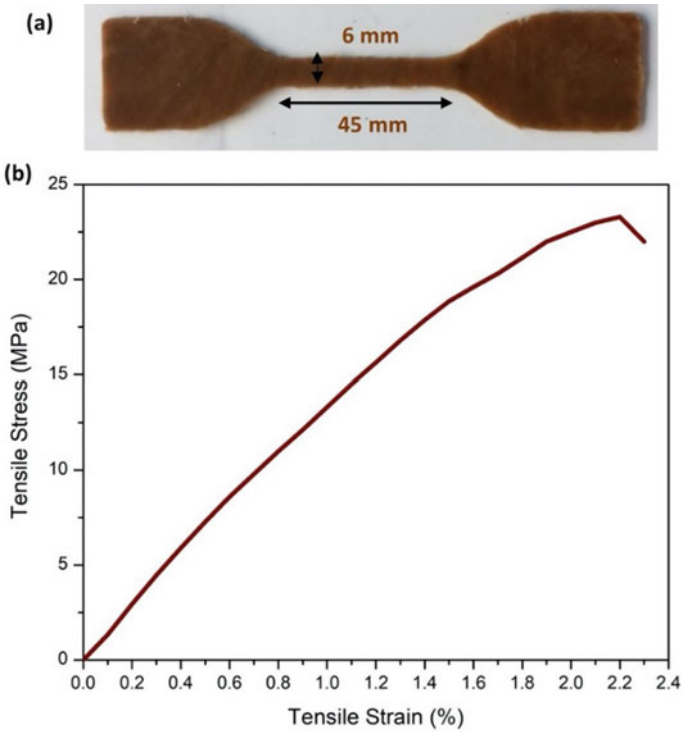

Fig. 6 **a** Tensile test specimen and **b** the stress–strain plot

conductivity compared with most of the thermoplastic materials found in the world. But due to the change of structure during the recycling process the effect of the thickness in this experiment has recorded a comparatively higher value for thermal conductivity. If this is used as a partition board or roofing material, the thickness needs to be increased by at least ten times to give better output [13].

4 Discussion

This experiment mainly focuses on the feasibility of recycling the surgical face mask with a melt extrusion process followed by compression moulding. According to the recorded results, the thermal recycling process has considerably affected the tensile properties and thermal conductivity. The fabrics used in the face mask production are melt-blown and spun-bonded. The spun bonding process used for the secondary fabric layer also affects the material's tensile properties [23]. Furthermore, melt-blown polypropylene fabrics are limited with tensile properties due to the production

process [2]. In order to produce low air permeable fabrics targeting high filtration, the extruder pressure of the melt blown process needs to be increased.

Moreover, the reduction of die air pressure and decreasing vacuum of the melt blown process targeting low air permeability are already affected to reduce the elongation at break [2]. Previous studies prove that more polypropylene recycling leads to more crystallisation over the chemical structure, thus increasing the elastic modulus and reducing the elongation at break [4]. Additionally, recycling reduces the molecular weight resulting in more chain ends to the chemical structure. That creates a close packing of the chemical structure but reduces the elongation at break [4]. According to the literature, using filler materials such as coated calcium carbonate and talc increases the mechanical properties of polypropylene [20]. It is imperative to control the use of filler materials since that can cause a significant increase in thermal conductivity properties [13].

The disposable nature of face masks has already raised challenges in hazardous waste management. While many uncertainties remain regarding the resources and waste flows of face masks, the massive generation of facemask wastes implies environmental pollution due to terrestrial and aquatic environment contamination, which ultimately affects the health of human and marine life. Improper management of used face masks can become a significant threat in terms of transmission of COVID-19. Moreover, the high usage of face masks increases the burden of plastic waste in the environment. Hence, necessary actions should be taken to remove face mask waste from the environment at the same rate they generate to eliminate long-term environmental and health consequences. It is vital to safeguard the environment by proper management of disposable face mask wastes. Recycling is one of the promising approaches to deal with such wastes in the given condition until biodegradable and reusable face masks are developed and are readily available in the market.

This study demonstrates the feasibility of mechanical recycling of face masks and the possible applications. Other than construction materials, PP is also used as feedstock for 3D printing due to its favourable mechanical properties. Since it has been reported that PP fibres can be chemically recycled into PP polymer, investigation of recycling cleaned PP fibres in facemasks to PP polymer feedstock for 3D printing is another possibility for face mask recycling.

5 Conclusion

The viability of mechanical recycling of single-use, 3-ply facemasks was studied. Based on the observations the following conclusions can be drawn.

1. The selected facemask consisted of polypropylene fibres. The proposed method is capable of recycling the facemask materials into a filament or pellets.
2. The recycled material can be easily compression moulded into sheets.

3. The recycled compression moulded material showed good mechanical properties, suitable for non-load bearing applications (23 MPa tensile strength and 2.2% strain to failure).
4. Thermal conductivity of the recycled material is 0.404 W m^{-1} K^{-1} and has potential to be used as a thermal insulating material.

Funding This work was supported by the Senate Research Grant (SRC/ST/2021/17), University of Moratuwa, Sri Lanka.

References

1. Akber Abbasi S, Khalil AB, Arslan M (2020) Extensive use of face masks during COVID-19 pandemic: (micro-)plastic pollution and potential health concerns in the Arabian Peninsula. Saudi J Biol Sci. https://doi.org/10.1016/j.sjbs.2020.09.054
2. Akber Abbasi S, Khalil AB, Arslan M (2020) Thermoplastic elastomers. Intech
3. Aragaw TA (2020) Since January 2020 Elsevier has created a COVID-19 resource centre with free information in English and Mandarin on the novel coronavirus COVID-19. The COVID-19 resource centre is hosted on Elsevier Connect, the company's public news and information. Mar Pollut Bull 159:111517
4. Aurrekoetxea J, Sarrionandia MA, Urrutibeascoa I, Maspoch ML (2001) Effects of recycling on the microstructure and the mechanical properties of isotactic polypropylene. J Mater Sci 36:2607–2613. https://doi.org/10.1023/A:1017983907260
5. Babaahmadi V, Amid H, Naeimirad M, Ramakrishna S (2021) Biodegradable and multifunctional surgical face masks: a brief review on demands during COVID-19 pandemic, recent developments, and future perspectives. Sci Total Environ 798:149233. https://doi.org/10.1016/j.scitotenv.2021.149233
6. Dente SMR, Hashimoto S (2020) COVID-19: a pandemic with positive and negative outcomes on resource and waste flows and stocks. Resour Conserv Recycl 161:104979. https://doi.org/10.1016/j.resconrec.2020.104979
7. Fadare OO, Okoffo ED (2020) Covid-19 face masks: a potential source of microplastic fibres in the environment. Sci Total Environ 737:140279
8. He D, Luo Y, Lu S, Liu M, Song Y, Lei L (2018) Microplastics in soils: analytical methods, pollution characteristics and ecological risks. TrAC - Trends Anal Chem. https://doi.org/10.1016/j.trac.2018.10.006
9. Islam MJ, Shahjalal M (2021) Effect of polypropylene plastic on concrete properties as a partial replacement of stone and brick aggregate. Case Stud Constr Mater 15:e00627. https://doi.org/10.1016/j.cscm.2021.e00627
10. Jung MR, Horgen FD, Orski SV, Rodriguez CV, Beers KL, Balazs GH, Jones TT, Work TM, Brignac KC, Royer SJ, Hyrenbach KD, Jensen BA, Lynch JM (2018) Validation of ATR FT-IR to identify polymers of plastic marine debris, including those ingested by marine organisms. Mar Pollut Bull 127:704–716. https://doi.org/10.1016/j.marpolbul.2017.12.061
11. Kahlert S, Bening CR (2020) Plastics recycling after the global pandemic: resurgence or regression? Resour Conserv Recycl 160:104948. https://doi.org/10.1016/j.resconrec.2020.104948
12. Lamba P, Kaur DP, Raj S, Sorout J (2021) Recycling/reuse of plastic waste as construction material for sustainable development: a review. Environ Sci Pollut Res. https://doi.org/10.1007/s11356-021-16980-y

13. Maier C, Calafut T (1998) Polypropylene: the definitive user's guide and databook. Choice Rev Online 36:36-1596. https://doi.org/10.5860/choice.36-1596
14. Morent R, De Geyter N, Leys C, Gengembre L, Payen E (2008) Comparison between XPS- and FTIR-analysis of plasma-treated polypropylene film surfaces. In: Surface and interface analysis. Wiley, pp 597–600. https://doi.org/10.1002/sia.2619
15. Ramteke S, Sahu BL (2020) Novel coronavirus disease 2019 (COVID-19) pandemic: considerations for the biomedical waste sector in India. Case Stud Chem Environ Eng 2019:100029. https://doi.org/10.1016/j.cscee.2020.100029
16. Rhee SW (2020) Management of used personal protective equipment and wastes related to COVID-19 in South Korea. Waste Manag Res 38:820–824. https://doi.org/10.1177/0734242X20933343
17. Saberian M, Li J, Kilmartin-Lynch S, Boroujeni M (2021) Repurposing of COVID-19 single-use face masks for pavements base/subbase. Sci Total Environ 769:145527. https://doi.org/10.1016/j.scitotenv.2021.145527
18. Saechtling H, Woebcken W, Haim J, Hyatt D (1995) International plastics handbook: for the technologist, engineer, and user. Hansen Publisher
19. Saliu F, Veronelli M, Raguso C, Barana D, Galli P, Lasagni M (2021) The release process of microfibers: from surgical face masks into the marine environment. Environ Adv 4:100042. https://doi.org/10.1016/j.envadv.2021.100042
20. Shubhra QTH, Alam AKMM, Quaiyyum MA (2011) Mechanical properties of polypropylene composites: a review. 26:362–391. https://doi.org/10.1177/0892705711428659
21. Socrates G (2001) Infrared and Raman characteristic group frequencies. Tables and charts. J Raman Spectrosc 347
22. Somani M, Srivastava AN, Gummadivalli SK, Sharma A (2020) Indirect implications of COVID-19 towards sustainable environment: an investigation in Indian context. Bioresour Technol Rep 11:100491. https://doi.org/10.1016/j.biteb.2020.100491
23. Spinnvliesen P, Leucker K (2020) Influence of the calender pattern on the mechanical properties of polypropylene spunbond nonwovens

Assessment of Dispersion Potential of Discarded Coconut Fibres in Concrete Pavements

Someen Khute, Raul Zerbino, Surender Singh, and Ravindra Gettu

Abstract Natural fibres (coir) have been preferred over their counterparts on account of lower cost, renewability, and accessibility of supply. Generally, Coir fibre, having a length greater than 50 mm is considered for various civil engineering applications and the shorter ones are typically discarded/incinerated. The use of these Discarded Coir Fibres (DCF) for concrete pavements seems to be a sustainable approach. However, their lower densities and hydrophilic nature make concrete manufacturing a challenge. To address this, a framework has been developed in the present study, primarily to uniformly distribute the DCF in concrete. The present study investigates the distribution of coir fibres in fresh concrete as well as in the hardened state. Coir fibre of lengths 10 and 50 mm with a dosage of 0.1, 0.4, and 0.7% by volume of concrete was used, considering different mixing approaches. The coefficients of variation (%) are quantified to assess the distribution of DCF in the fresh concrete and the results revealed that the dispersion of DCF in concrete decreases with an increase in length and dosage. Hardened concrete fracture surfaces were evaluated to assess fibre dispersion and orientation. The fibre density was found to be less in concrete with a low volume of fibre dosage, while more in a high volume of fibre dosage. Further, it was observed that fibre density was higher in the perpendicular direction to the casting face.

Keywords Concrete pavements · Coconut coir fibres · Orientation · Dispersion

S. Khute (✉) · R. Zerbino · S. Singh · R. Gettu
Department of Civil Engineering, Indian Institute of Technology, Madras, Chennai, India
e-mail: ce20s004@smail.iitm.ac.in

R. Zerbino
e-mail: zerbino@ing.unlp.edu.ar

S. Singh
e-mail: surender@iitm.ac.in

R. Gettu
e-mail: gettu@iitm.ac.in

R. Zerbino
Department of Civil Engineering, La Plata National University, La Plata, Argentina

© The Author(s), under exclusive license to Springer Nature Singapore Pte Ltd. 2023

R. Dissanayake et al. (eds.), *ICSBE 2022*, Lecture Notes in Civil Engineering 362,
https://doi.org/10.1007/978-981-99-3471-3_9

1 Introduction

Concrete is one of the most utilized building materials. However, it is brittle under tension, which could be improved by incorporating steel reinforcements. Although adding steel reinforcement to concrete increases its tensile strength, it does not improve the inherent tensile characteristics of concrete. One of the best ways to improve the inherent properties is by adding fibre to concrete. However, the dispersion and orientation of fibre in the concrete matrix play an important role in concrete properties. Efficient mixing is one of the keys to achieving good dispersion and consequently better performance of fibre-reinforced concrete systems [1]. Steel and synthetic fibres are two of the most popular fibres used in concrete. To mix steel and synthetic fibre in the concrete, different mixing methods have been recommended (Report of a concrete society working group—Technical report no. 65 (Macro synthetic fibres) [2], Technical report no. 63 (Steel fibres) [3], Shah et al. [4]). Various fibre parameters significantly affect the fracture behaviour of a concrete matrix. Amongst all, aspect ratio and dosage/quantity of fibre are the most dominating parameters [5]. However, the distribution of fibres in the brittle matrix offers convenient and practical means of achieving improvements in many of the engineering properties of the materials such as fracture, tensile and flexural strengths, toughness, fatigue and impact resistance [6–9]. However, the higher cost and environmental impact of steel and synthetic fibre make the researcher find alternatives for such materials. Therefore, there has been a growing interest in the fibre-reinforced concrete sector to utilize natural fibres such as Coir, Sisal, Jute, etc. due to their lower cost and low environmental impact [10–13].

India and Sri Lanka are the main producers of coconut fibre in the world. Other countries, such as Thailand, Vietnam, the Philippines, and Indonesia, produce coir, but not to the same extent as India and Sri Lanka. Amongst all, India is the highest producer of coconut fibre from coconut, *cocos nucifera*, in the world with an annual production of about 542,000 MT, which is equivalent to 55% of the total worldwide production [14]. The main advantages of coir are its toughness, durability, anti-corrosive nature, thermal insulation, resistance to fungi attack, etc. Because of these advantages, this natural material has become popular and has attracted researchers to use it as an alternative and non-conventional construction material. In addition, they can be obtained at a lesser cost and manpower with less technology [15]. Traditionally, coir-based products, such as geotextile have been used in many civil engineering applications especially for enhancing the engineering properties of subgrade/embankment soil in addition to other primary functions such as filtration, separation, reinforcement, and erosion control [16–18]. For these applications, long fibre with a length of over 50 mm is referred, to whereas shorter fibre is usually discarded [19]. Using these discarded coir fibres (DCF) for concrete pavements seems to be a viable approach. But, at higher volume fractions (4%) and higher aspect ratios (>100), mixing becomes difficult and fibre tends to cluster together resulting in an inadequate bond and reduction in strength [20]. However, before mixing fibres in the concrete, there is a need to study the dispersion of DCF in the concrete mixture.

Owing to their hydrophilic nature and lesser density, it is difficult to mix them in concrete. The existing literature on synthetic fibre indicates that low-density fibre could pose a few challenges, particularly concerning concrete mixing [1], from the existing literature, it is observed that only a few studies have been done on the dispersion of fibre in the fresh cement composites. In these studies, the dispersion of fibre is usually quantified by washing the fresh-concrete mixtures on a steel sieve, followed by the determination of standard deviation, dispersion, variation coefficients, etc. This method is easy to perform and quick in the evaluation of the dispersion of fibres in concrete mixtures compared to other methods [21].

2 Mixing Recommendations for Fibre-Reinforced Concrete

2.1 Steel and Synthetic Fibres

Different conventional mixing methods have been successfully applied in FRC, either in fixed equipment in the plant or in a concrete mixer, with variations in the sequence of material incorporation. The most important thing to keep in mind is to ensure a homogeneous distribution of the fibre. The facilities available, the type of work and/or the type of fibres can be considered in the selection of the mixing procedure.

For better distribution, it is convenient to incorporate the fibre gradually together with the aggregates. Usually, dispensers, scales, or other control elements are provided to guarantee the established dose of fibre. Fibre should never be incorporated as the first material in the mixer. Any circumstance that favours fibre segregation must be avoided. Fibre can also be gradually added to fresh concrete.

In steel FRC, incorporation speeds between 1 and 3.5 kg/s are recommended and mixing should take a few minutes (nearly 5 min) longer than the time used in conventional concrete (3–5 min) to favour its homogeneous distribution in the concrete mass [3]. It is also recommended not to overload the concrete mixer to ensure effective mixing.

To enhance the initial dispersion inside the batch there are steel fibres that are provided, grouped by a water-soluble adhesive. There are also polymeric macrofibres that are supplied in small bundles surrounded by a water-soluble film and others that are grouped in small numbers (Report of concrete society working group—Technical report No. 65-macro fibres [2]). With synthetic microfibres, the dispersion problems are usually minor. In many cases, they are usually supplied in small water-soluble bags. However, inadequate mixing time can lead to defective separation, which will result in a substantial reduction in the residual capacity provided by the fibre [22]. Overmixing, improper fibre loading or excessive dosage segregation can occur, resulting in a ball formation.

After the completion of mixing the fibre in concrete uniformly, various factors can affect the distribution of fibre during placement and compaction. Along with fibre parameters such as fibre types, lengths and dosages, other parameters such as the

dimension of structural elements, consistency of the fresh concrete, and conditions of placement and compaction can also interact with each other.

External vibration usually generates a preferential orientation of the fibres in horizontal planes, which generally coincides with the greatest tensile forces, which is the case of floors or pavement slabs [23–25]. Both excessive vibrating and the use of mixes without adequate cohesion can cause the segregation of the fibres. Kooiman [26] observed the effect of vibration and mould walls on the distribution and orientation of fibre in precast segments for tunnels. Inadequate vibration can generate a greater number of fibres in the lower central area of the segments, and the wall effect of the edges orients the fibre in their direction.

Several studies were carried out on fibre used in self-compacting concrete [27–30]. In self-compacting concrete, adequate cohesion must always be guaranteed to ensure the homogeneity of mixtures. Generally, in fluid mixtures, the main factor affecting fibre orientation is the flow of the concrete, especially in thin elements.

In the case of synthetic fibre mixing in a truck mixer, (in general, fibres were incorporated on site), it should be mixed at least five minutes at optimum speed or a minimum of 100 revolutions to ensure dispersion of fibres in the mix. While mixing the synthetic fibre in a ready-mix concrete plant, it is suggested that fibre should be added before the addition of aggregates and binders to avoid the agglomeration of fibres. Two approaches for mixing with adequate measures were suggested according to the mixing equipment used for mixing (Truck mixer or Ready-mix plant) [4]. In the case of a truck mixer, while adding the fibres in the concrete, it should not be allowed to pile up and form balls due to the landing of fibres in the mixer, one above the other (suitable for small-scale projects). But, in the case of a ready-mix plant, it is suggested that fibre should be added in the mixer with aggregates on the conveyor belt during aggregate addition and the rest of the mixing should be in the normal manner to distribute all fibre uniformly (suitable for large scale projects).

2.2 Studies on Coir Fibres in Concrete

Details of the procedures used during the elaboration of mixes with coconut fibre were given by several authors.

1. [31]—Initially, the mixing sequence consists of mixing the sand and coarse aggregate for 30 s. Then, half of the mixing water was added to the mixture and after that, the mixing was carried out for a further minute. Thereafter, the mix was covered to minimize the evaporation of water and to let the dry aggregates absorb the water. After 5 min, the cement and fly ash were added and mixed for another minute. Finally, the superplasticizer and the remaining half of the water were added and then mixed for another 3 min before the coir fibres were added gradually for an extra two minutes to formulate the self-compacting concrete mixture. The total mixing time was considered as 11 min for the homogenous mixing of fibre.

2. [32]—Firstly, aggregates and cement were mixed for 1 min and then, water was added within 2 min, followed by fibre addition with slow increments at last. Later, concrete was mixed for 3 min to avoid the balling effect of fibre.
3. [33]—Cement, fly ash, and coir fibres were added into the mixer and dry-mixed for 60 s. Then sand and coarse aggregates were added and drily mixed for another 60 s. Water and superplasticizers were added and mixed for 3 min.
4. [34]—Firstly, a layer of coarse aggregates was spread on a clean tray. Then the fibres were separated manually and spread. Fine aggregates were spread over the fibres and dry-mixed for 2 min. Then, cement was added and dry-mixed again. 50% of the total water was added first and mixed properly. After that, by adding the remaining water, the concrete was mixed and prepared**.**
5. [35]—Coir fibre reinforced concrete was prepared in such a way that a layer of coconut fibre was spread first in the pan. Then, this was followed by the spreading of aggregates, sand, and cement. The first layer of fibre was hidden under the dry concrete materials with the help of a spade. Then, another layer of coconut fibre, followed by layers of aggregates, sand and cement, was spread. This process was repeated until the rest of the materials were put into the mixing pan. Approximately three-quarters of the water was added, and the mixer was rotated for 2 min. Then the remaining water was added and mixed thoroughly for 2 min to distribute the fibre uniformly.
6. [36]—Cement and fine aggregates were manually mixed and then coir fibre was added to the mixture. After mixing in the coir fibre, coarse aggregates were introduced and followed by the addition of water.

3 Materials and Methods

3.1 Materials

53 grade Ordinary Portland Cement (OPC) conforming to IS 12269 was used [37] in this study. Crushed granite of two different sizes (20–10 mm and 10–4.75 mm) in the proportions of 54:46 was used. River sand was utilized as fine aggregate in all the considered mixes. The physical properties of ingredients include specific gravity for cement and aggregates, and water absorption for aggregates were determined according to the Indian coal provisions,the specific gravity of cement, 20–10 mm, 10–4.75 mm, and fine aggregates were found to be 3.15, 2.74, 2.68 and 2.63, respectively. Water absorption of the 20–10 mm, 10–4.75 mm and fine aggregates were 0.66, 0.70 and 0.80, respectively. Gradation of aggregates was carried out according to IRC SP-62 specifications [38]. The water used for the mixing is as per the requirements of IRC-15-2000 [39]. A polycarboxylic ether-based superplasticizer was used at a dosage of 0.8–2% by weight of cement content to attain a slump of 130–150 mm for control concrete (Unreinforced). The coconut fibre (Coir), short (nominally 10 mm in length) and long (50 mm in length), in fractions of 0.1, 0.4 and 0.7% (by volume of concrete) were incorporated in the concrete mixture. The considered fibres were

assessed for specific gravity, water absorption and tensile strength and the values found were 1.12, 100% and 87 ± 15 MPa, respectively.

3.2 Mix Proportioning and Mixing Methods

In the present study, an OPC content of 350 kg/m^3 and a water-to-cement ratio of 0.5 was considered. A granite content of 575 kg/m^3 (20–10 mm), 452 kg/m^3 (10–4.75 mm), and a sand content of 847 kg/m^3 were utilized in the unreinforced concrete mix. In reinforced mixtures of short and long fibres with three volume fractions (0.1, 0.4 and 0.7%), the OPC content considered was the same as that in un-reinforced mixtures. The aggregates used in these mixtures ranged from 567–574 kg/m^3 (20–10 mm) to 445–451 kg/m^3 (10–4.75 mm), and a sand content of 838–846 kg/m^3. The superplasticizer content was 3.25 kg/m^3 for all the mixtures. In this study, two mixing methods were adopted; End-stage mixing and Intermediate mixing. In end-stage mixing, fibres were sprinkled over the concrete after all the ingredients were thoroughly mixed, followed by 2 min of further mixing. In contrast, Intermediate stage mixing consists of fibres sprinkling in small quantities at different stages, viz. mixing with aggregates, mixing with cement and then, finally, mixing with water. Total mixing time for both mixing approaches was 12 min. There was some effect of the incorporation of fibre on the slump of the fresh concrete. However, the target range was achieved.

3.3 Measurements of Dispersion of Coir Fibres in the Concrete

3.3.1 Dispersion of Coir Fibres in the Fresh Mix

Two mixing methods were used to determine and compare the effect of the mixing approach on the dispersion of the coir fibres. For this task, fresh concrete was prepared with coir fibres to determine the fibre dispersion in the concrete mix. The methodology followed for trapping coir fibres from the concrete mixture is illustrated in Fig. 1. Initially, the fresh concrete mixture was poured into six containers of 100 × 100 × 100 mm in size. The concrete mixture in each container was w hed through a 4.75 mm sieve to separate coarse aggregate, followed by washing on a 150-μm sieve to trap the fibres. Further, the trapped fibres were dried in an oven at 105 °C for 24 h, cooled to ambient temperature, and then weighed. The recorded weight was used to calculate various dispersion parameters, such as standard deviation, variation coefficient (Ψ), and dispersion coefficient (β) using Eqs. (1–3).

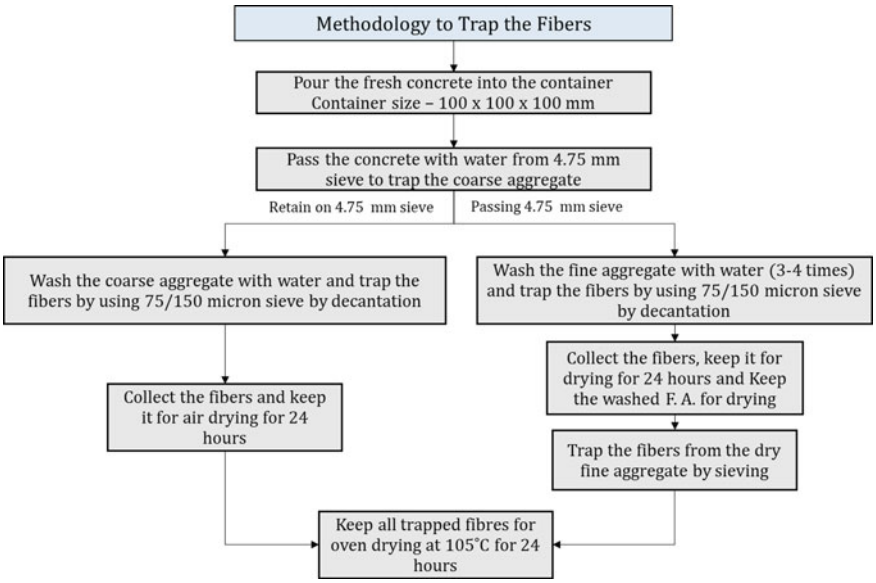

Fig. 1 The methodology adopted for trapping the fibres from the fresh concrete

$$S(X) = \sqrt{\frac{\sum_{i=1}^{n} (x_i - \overline{x})^2}{n-1}} \tag{1}$$

$$\Psi(x) = \frac{S(X)}{(\overline{x})} \times 100 \tag{2}$$

$$\beta = \mathrm{e}^{-\Psi(X)} \tag{3}$$

where $S(X)$, x_i, $\overline{x}$ are the standard deviation, trapped fibre weight of I sample, and mean of all specimens respectively.

3.3.2 Dispersion of Coir Fibre in the Hardened Concrete

Slabs of size 560 mm (l) × 355 mm (w) × 100 mm (d) were fabricated for evaluating the dispersion of coir in hardened states. These slabs were prepared, kept in an open environment, and then cut at specific distances to count the fibres. The methodology followed is explained in Fig. 2. It should be noted that these slabs were previously used for measuring the plastic shrinkage cracks. Initially, the cut was made in the longitudinal direction (X–X′), followed by splitting in the transverse (sections A–A′ and B–B′) and longitudinal directions (sections C–C′), as illustrated in Fig. 2. Following this, the fibres per unit area were counted on both fractured surfaces. The

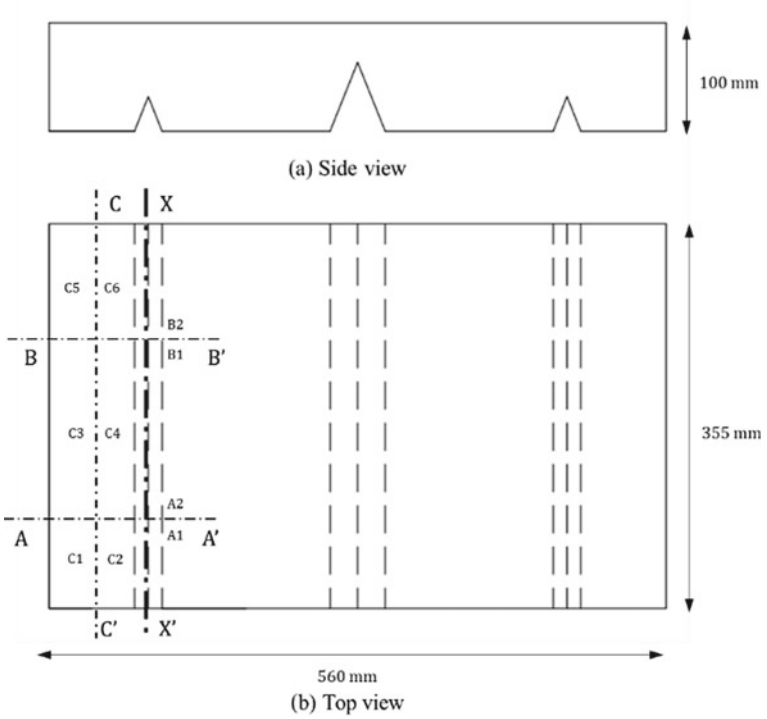

Fig. 2 Plastic shrinkage slab showing sections A–A′ and B–B′ and C–C′

ratio of fibre number to the fractured surface area was referred to as fibre density for this investigation.

4 Evaluation of Dispersion Study of Coir Fibres in Fresh and Hardened Concrete

4.1 DCF Dispersion in Fresh Concrete

The influence of mixing approaches on fibre dispersion is shown in Table 1. It was observed that the inclusion of short fibre resulted in better distribution than long fibres, irrespective of fibre dosage. For instance, slightly higher dispersion coefficients of 0.97, 0.96, and 0.95 were obtained for short fibre against the long fibre of 0.96, 0.94, and 0.93 at 0.1%, 0.4%, and 0.7% dosages, respectively. Regardless of fibre length, an increase in fibre dosage manifested a reduction in the dispersion coefficient and, consequently, increased the variation coefficients. As far as the mixing approach is concerned, the intermediate mixing approach outperformed the end-stage mixing.

For example, at higher fibre content (0.7%), the dispersion coefficient was found to be 0.95 and 0.93 for short and long-fibre concrete, respectively. The dispersion coefficient slightly improved with intermediate mixing for a similar dosage of about 0.7%; it was found to be 0.96 for concrete containing short fibre and 0.95 for concrete containing long fibre. The improved distribution of the intermediate-stage mixing could be attributed to the improved effective mixing duration of fibres in the concrete. In addition, fibre quantity addition at a time was also less, which could mitigate the piling up of fibre and consequently help to improve the dispersion of fibres. Conversely, in end-stage mixing, the effective mixing duration post introductions of total fibres were only 1 min against 9, 6, and 3 min when DCF was introduced in small quantities (1/3 fibres) (at different stages of mixing). Effective mixing duration was less. The quantity of fibre addition was high for a given time in the case of end-stage mixing. It could lead to the agglomeration of fibres and further decrease the dispersion of fibres in the matrix. These findings denote that the difference in mixing durations and the amount of fibre inclusion significantly affect the spatial distribution of fibres in the fresh concrete mixes (Figs. 3 and 4).

4.2 Dispersion and Orientation of Fibres in Hardened Concrete

Fibres from the fractured surface were evaluated to identify the distribution and analyse the agglomeration of fibres. In each concrete mixture, the fracture planes were assessed along the transverse direction (A–A′ and B–B′) as well as along the longitudinal direction (C–C′). Each fracture plane consists of two fracture surfaces; fibres from the two-fracture surfaces were identified using a high-quality camera, and then the fibre location was marked by a point using PowerPoint software. Fibres were counted on the fracture surface in the same plane, and then the average number of fibres was taken for the quantification of fibre density. The total number of fibres on each fractured surface and the area of the fractured surface were assessed for all specimens. To easily measure the area for a fractured surface, the considered fracture plane was divided into regular shapes such as rectangles and trapeziums. To determine the spatial distribution of fibre along the depth of specimens, the fracture surface was bifurcated into three parts, namely, top, middle, and bottom, as presented in Figs. 5 and 6. Tables 2 and 3 show the variation in the fibre density along the transverse and longitudinal directions for the considered fracture planes. As seen in Fig. 6, fibre density in the longitudinal direction was higher than in the transverse direction for all the considered mixtures, which confirmed that the preferential orientation of fibres was found to be perpendicular to the casting direction [24]. As anticipated, the concrete mixtures containing short fibre exhibited higher density than the mixtures with long fibres, irrespective of the fibre dosage (Tables 2 and 3). This is attributed to more numbers of short fibres than long fibres (Fig. 6).

Table 1 Trapped fibre weight from each sample in end-stage mixing

DCF length	DCF dosage (%)	End stage mixing—trapped fibre weight (g)						Intermediate stage mixing—trapped fibre weight (g)					
		Sample 1	Sample 2	Sample 3	Sample 4	Sample 5	Sample 6	Sample 1	Sample 2	Sample 3	Sample 4	Sample 5	Sample 6
10 mm (short)	0.1	0.70	0.72	0.76	0.74	0.72	0.74	Not performed					
	0.4	3.24	3.40	3.24	3.25	3.49	3.26						
	0.7	6.44	6.49	6.16	5.94	6.46	6.64	6.00	6.20	6.30	6.13	6.70	6.05
50 mm (long)	0.1	0.76	0.77	0.79	0.72	0.75	0.74	Not performed					
	0.4	3.62	3.75	3.86	3.85	3.38	4.05						
	0.7	5.84	6.88	5.79	5.81	6.22	5.94	6.04	6.32	6.34	6.55	6.10	6.85

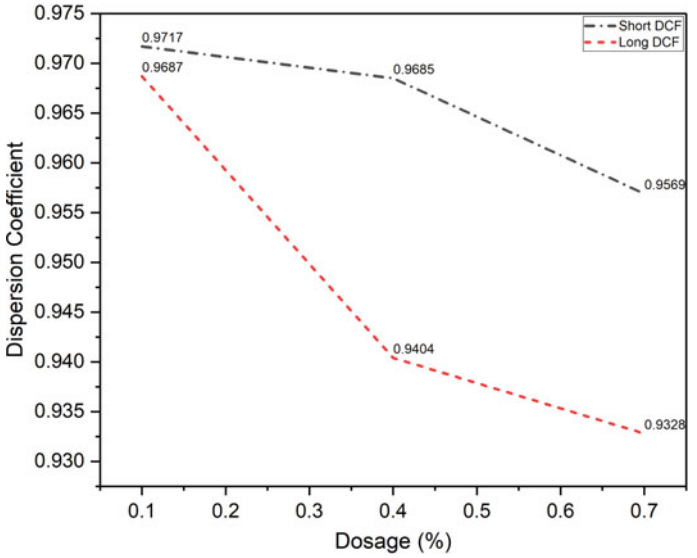

Fig. 3 Dispersion coefficient values for the considered mixes

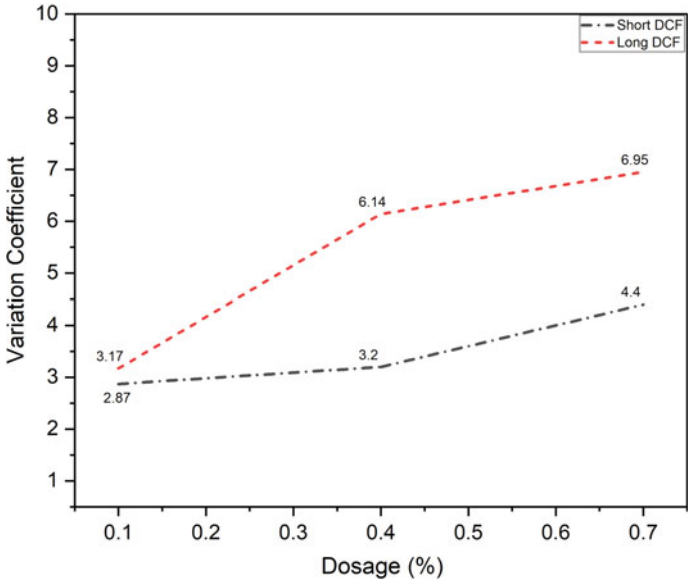

Fig. 4 Variation coefficient values for the considered mixes

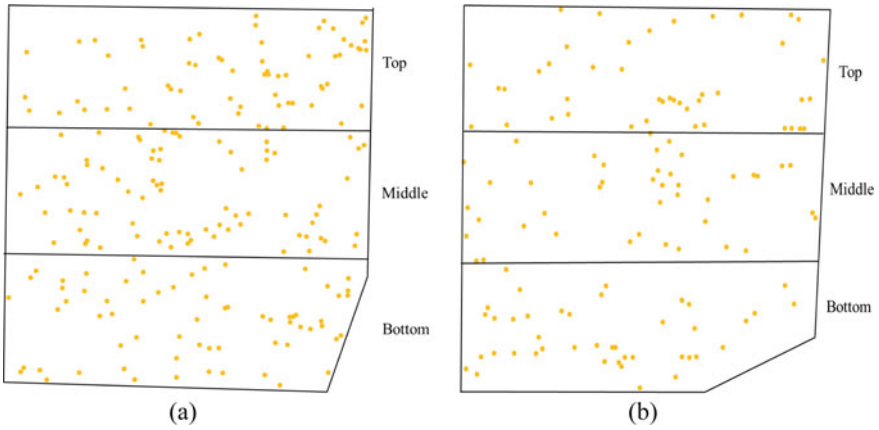

Fig. 5 Distribution of fibres over the depth of the specimen along transverse direction: **a** CM-S-0.4 and **b** CM-L-0.4

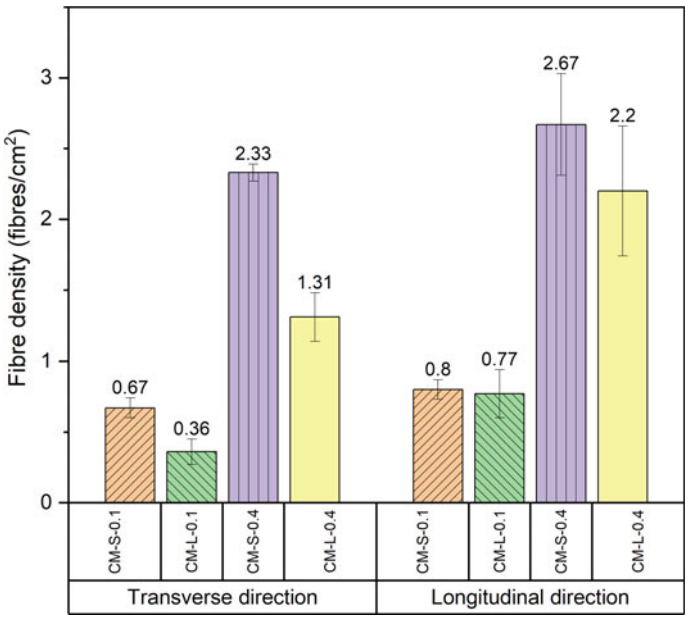

Fig. 6 Fibre densities for all the mixes along the transverse and longitudinal direction

There was an insignificant difference observed along the depth of specimens for all the mixtures. Fibre density was evaluated for fractured surfaces along longitudinal as well as transverse directions for all considered mixes (CM-S-0.1, CM-S-0.4, CM-L-0.1, CM-L-0.4) and the study revealed that fibre density (fibres/cm^2) along the transverse and longitudinal direction is less for low volume dosages. Moreover, in

Table 2 Fibre quantity (nos.) and density along transverse direction for considered mixes

Mix ID	Fracture surfaces	Position			Total no. of fibres	Fibre density (fibres/cm^2)	
		Top	Middle	Bottom		Along each fractured surface	Mean ± std. deviation
CM-S-0.1	A1	25	17	13	55	0.61	0.67 ± 0.07
	A2	20	20	21	61	0.68	
	B1	19	16	23	58	0.64	
	B2	14	29	26	69	0.76	
CM-S-0.4	A1	79	80	59	218	2.42	2.33 ± 0.06
	A2	71	71	64	206	2.28	
	B1	66	76	64	206	2.28	
	B2	89	78	45	212	2.35	
CM-L-0.1	A1	10	10	15	35	0.39	0.36 ± 0.09
	A2	18	9	15	42	0.47	
	B1	19	10	4	33	0.36	
	B2	7	10	5	22	0.24	
CM-L-0.4	A1	29	23	46	98	1.09	1.31 ± 0.17
	A2	57	24	36	117	1.30	
	B1	42	42	41	125	1.39	
	B2	43	62	29	134	1.49	

concrete containing short fibres with 0.1% the dosage was given more density than long fibre concrete with the same dosage due to the availability of more fibres present and the same trend was followed in high-volume dosages.

Concrete containing a low volume dosage of fibres and a lower aspect ratio could lead to a lesser chance of agglomeration of fibres in the mix. Moreover, concrete inclusion of longer fibre with less dosage (CM-L-0.1) shows a fibre density value of 0.32 and 0.77 fibres/cm^2. For short fibres with the same dosage (CM-S-0.1) it shows a value of 0.67 fibres/cm^2 and 0.80 fibres/cm^2 along the transverse and longitudinal direction respectively. It was due to the presence of a more number of fibres in short-fibre concrete. In the case of high-volume dosage concrete mixtures (0.4% volume fraction), fibre density along the transverse and longitudinal direction was found to be 2.33 and 2.67 fibres/cm^2 for short fibre concrete (CM-S-0.4) as well as for concrete containing long fibres (CM-L-0.4) was found to be 1.31 and 2.20 fibres/cm^2.

Table 3 Fibre quantity (nos.) and density along longitudinal direction for considered mixes

Mix ID	Fracture surfaces	Position			Total no. of fibres	Fibre density (fibres/cm^2)	
		Top	Middle	Bottom		Along each fractured surface	Mean ± std. deviation
CM-S-0.1	C1	35	36	29	100	0.91	0.80 ± 0.07
	C2	44	18	20	82	0.75	
	C3	34	25	26	85	0.71	
	C4	26	42	25	93	0.78	
	C5	44	33	22	99	0.79	
	C6	43	37	22	102	0.82	
CM-S-0.4	C1	105	85	96	286	3.01	2.67 ± 0.36
	C2	110	99	90	299	3.15	
	C3	122	98	95	315	2.63	
	C4	121	111	82	314	2.62	
	C5	92	106	89	287	2.21	
	C6	102	100	111	313	2.41	
CM-L-0.1	C1	28	25	16	69	0.58	0.77 ± 0.17
	C2	25	27	15	67	0.56	
	C3	38	18	33	89	0.77	
	C4	35	36	35	106	0.92	
	C5	51	34	19	104	0.90	
	C6	44	27	31	102	0.89	
CM-L-0.4	C1	70	63	73	206	2.01	2.20 ± 0.46
	C2	90	80	79	249	2.43	
	C3	110	89	85	284	2.77	
	C4	96	90	70	256	2.50	
	C5	59	78	80	217	1.50	
	C6	99	85	99	283	1.95	

5 Conclusions

The main objective of the present investigation was to evaluate the dispersion of the concrete mixtures containing DCF. The major findings are as follows:

- Fibre addition at intermediate stages was found to be beneficial in terms of the distribution of fibres in the concrete mix.
- Increase in fibre dosage and length tends to lower the distribution coefficient and thus, increase the coefficient of variation.
- DCF density on the fractured surfaces was found to be in line with fibre lengths and dosages.

- Orientation of DCF along the planes perpendicular to the casting direction was similar in both directions.
- Distribution of DCF on fractured surfaces over depth was found to be identical for all the mixes indicating homogenous fibre dispersion without segregation.
- Method of fibre addition and mixing time after fibre addition plays a paramount role in uniform DCF distribution; the intermediate mixing approach could be given a higher preference for the effective distribution of fibres.

Acknowledgements The authors appreciate funding received from the COIR Board, Ministry of MSME, Govt. of India, for the CoirCon project. Also, the support received from the Indian Institute of Technology Madras, Chennai, for the Institute of Eminence Research Initiative project on Technologies for Low-Carbon and Lean Construction (TLC2) is gratefully acknowledged. The authors would like to thank Mr. Shoeb Khan for helping in characterizing the coir fibres considered in this investigation. The tests were carried out in the Laboratory for the Characterization of Mechanical Properties of Civil Engineering Materials (MPCEM) partially funded through a FIST Grant SR/FST/ETII-054/2012 from DST, Govt. of India.

References

1. Stroven P, Shui Z, Cheng Y (2000) Methods for assessment of uniformity in carbon fibre dispersions in cementitious materials. In: Fifth RILEM symposium on fibre-reinforced concrete (FRC), Lyon, 13–15 Sept 2000, pp 159–168
2. Technical Report No. 65 (2007) Guidance on the use of macro-synthetic-fibre reinforced concrete. The Concrete Society, Camberley, United Kingdom
3. Technical Report No. 63 (2007) Guidance for the design of steel-fibre-reinforced concrete. The Concrete Society, Camberley, United Kingdom
4. Shah SP, Daniel JI, Ahmad SH, Arockiasamy M, Balaguru PN, Ball CG, Ball HP Jr, Banthia N, Batson GB, Bentur A, Casamatta D (1993) Guide for specifying, proportioning, mixing, placing, and finishing steel fibre reinforced concrete. ACI Mater J 90(1):94–101
5. Aziz MA, Paramasivam P, Lee SL (1981) Prospects for natural fibre reinforced concretes in construction. Int J Cem Compos Lightweight Concrete 3(2):123–132
6. Barragan B, Gettu R, Agullo L, Zerbino R (2006) Shear failure of steel fiber-reinforced concrete based on push-off tests. ACI Mater J 103(4):251–257
7. Barragán BE, Gettu R, Martín MA, Zerbino RL (2003) Uniaxial tension test for steel fibre reinforced concrete—a parametric study. Cem Concr Compos 25(7): 767–777
8. Barros JAO, Gettu R, Barragán B (2004) Material nonlinear analysis of steel fibre reinforced concrete beams failing in shear. In: 6th international RILEM symposium on fibre reinforced concrete - BEFIB 2004, vol 1. RILEM, Bagneux, pp 711–720
9. Conforti A, Zerbino R, Plizzari GA (2019) Influence of steel, glass and polymer fibres on the cracking behaviour of reinforced concrete beams under flexure. Struct Concr 20(1):133–143
10. Satyanarayana KG et al (1990) Natural fibre-polymer composites. Cement Concr Compos 12(2):117–136
11. Toledo Filho RD, Ghavami K, England GL, Scrivener K (2003) Development of vegetable fibre-mortar composites of improved durability. Cement Concr Compos 25(2):185–196
12. Munawar SS, Umemura K, Kawai S (2007) Characterization of the morphological, physical, and mechanical properties of seven nonwood plant fibre bundles. J Wood Sci 53(2):108–113
13. Shadheer Ahamed M, Ravichandran P, Krishnaraja A (2021) Natural fibres in concrete—a review. IOP Conf Ser: Mater Sci Eng 1055(1):1–8

14. IBEF (2016) India is largest producer of coir in the world. Indian Brand Equity Foundation. https://www.ibef.org/news/india-is-largestproducer-of-coir-in-the-world. Accessed 19 May 2020
15. Kore SD (2021) Sustainable production of concrete using coir fibres. IOP Conf Ser: Earth Environ Sci 795(1):1–10
16. Alobaidi I, Hoare DJ (1999) Mechanisms of pumping at the subgrade-subbase interface of highway pavements. Geosynth Int 6(4):241–259
17. Tiwari N, Satyam N (2020) An experimental study on the behaviour of lime and silica fume treated coir geotextile reinforced expansive soil subgrade. Eng Sci Technol, Int J 23(5):1214–1222
18. Zornberg JG, Mitchell JK (1994) Reinforced soil structures with poorly draining backfills. Part I: reinforcement interactions and functions. Geosynth Int 1(2):103–147
19. Desai AN, Kant R (2016) Geotextiles made from natural fibres. In: Geotextiles, pp 61–87
20. Ramaswamy HS, Ahuja BM, Krishnamoorthy S (1983) Behaviour of concrete reinforced with jute, coir and bamboo fibres. Int J Cem Compos Light Concr 5(1):3–13
21. Yang Y (2002) Methods study on dispersion of fibres in CFRC. Cem Concr Res 32(5):747–750
22. Giaccio G, Giovambattista A, Zerbino R (1986) Concrete reinforced with collated steel fibres: influence of separation. In: Journal proceedings, pp 232–235
23. Edgington J, Hannant DJ (1972) Steel fibre reinforced concrete. The effect on fibre orientation of compaction by vibration. Matériaux Constr 5(1):41–44
24. Gettu R, Gardner DR, Saldivar H, Barragán BE (2005) Study of the distribution and orientation of fibres in SFRC specimens. Mater Struct 38(1):31–37
25. Soroushian P, Lee CD (1990) Distribution and orientation of fibres in steel fibre reinforced concrete. Mater J 87(5):433–439
26. Kooiman AG (2000) Modelling steel fibre reinforced concrete for structural design. PhD thesis, Delft University of Technology, The Netherlands
27. Barragán B, Gettu R, de la Cruz C, Bravo M, Zerbino R, Dhir R, Halliday J, Csetenyi E (2004) Development and application of steel fibre reinforced self-compacting concrete. In: 6th RILEM symposium on fibre-reinforced concretes (FRC)–BEFIB, pp 457–466
28. Grünewald S (2004) Performance-based design of self-compacting fibre reinforced concrete. PhD thesis, Delft University, Holanda
29. Ferrara L, Park YD, Shah SP (2007) A method for mix-design of fibre-reinforced self-compacting concrete. Cem Concr Res 37(6):957–971
30. Torrijos MC, Barragan BE, Zerbino RL (2008) Physical–mechanical properties, and mesostructure of plain and fibre reinforced self-compacting concrete. Constr Build Mater 22(8):1780–1788
31. AL-Kadi QN, Qadi ANA, Mustapha KNB, Naganathan S, Muda ZBC (2015) Coconut fibre effect on fresh and thermo gravimetric properties to mitigate spalling of self-compacting concrete at elevated temperatures. Open J Civ Eng 5(3):328
32. Sivaraja M, Pillai MS (2010) Study on durability of natural fibre concrete composites using mechanical strength and microstructural properties. Bull Mater Sci 33(6):719–729
33. Abhishek TS, Vijaya S, Shivakumara Swamy B (2015) Study on fresh and mechanical properties of coconut fiber reinforced self compacting concrete enhanced with steel fibres. Int J Eng Res Technol 4(6):911–914
34. Shreeshail BH, Chougale J, Pimple D, Kulkarni A (2014) Effects of coconut fibres on the properties of concrete. Int J Res Eng Technol 3(12):5–11
35. Ali M, Liu A, Sou H, Chouw N (2012) Mechanical and dynamic properties of coconut fibre reinforced concrete. Constr Build Mater 30:814–825
36. Babafemi AJ, Kolawole JT, Olalusi OB (2019) Mechanical and durability properties of coir fibre reinforced concrete. J Eng Sci Technol 14(3):1482–1496
37. IS: 12269 (2013) Ordinary Portland cement-53 grade specification. Bureau of Indian Standards, New Delhi, India

38. IRC SP 62 (2002) Guidelines for design and construction of cement concrete pavements for rural roads. Indian Road Congress, New Delhi, India
39. IRC 15 (2002) Standard specifications and code of practice for construction of concrete-roads. Indian Road Congress, New Delhi, India

Concrete Technology and High-Performance Concrete

Evaluation of Thermal Conductivity of Concrete Using Finite Element Analysis

E. Thavarajah, K. M. C. Konthesingha, S. M. A. Nanayakkara, I. R. Upasiri, W. P. H. P. Weerasinghe, and H. M. S. C. Rathnasiri

Abstract The thermal conductivity of concrete is an important parameter due to the concrete's energy, thermal, and fire performance. It depends on the water–cement (w/c) ratio, coarse aggregate volume fraction, fine aggregate volume fraction, age, temperature, and concrete admixtures. Among these parameters mix proportions of cement and aggregate act as a crucial factor since concrete's mechanical properties also depend on the mix proportions. Experimental methods such as steady and transient methods are available to measure the thermal conductivity of concrete. However, conducting experiments for every mix proportion used in the construction industry is not feasible. Therefore, this study develops a Finite Element (FE) model to determine the thermal conductivity of concrete with the known thermal conductivity values of mortar, aggregates and respective mix proportions. The developed FE model considers concrete as a two-phase model with mortar and coarse aggregates in the mesoscale concept. A two-dimensional model was developed with circular shape aggregates, and then the aggregate shapes were changed into two real shape aggregates such as elliptical and polygonal and validated with the experimental results from the literatures. The average difference percentage between the experimental results and FEM results is 4.30%. Hence the developed FE model was verified to predict the concrete's thermal conductivity with known thermal conductivity values of coarse aggregates and mortar for any mix proportion.

Keywords Thermal conductivity of concrete · Finite element modelling · Mesoscale · Two-phase model · Two-dimensional analysis

E. Thavarajah (✉) · K. M. C. Konthesingha · I. R. Upasiri · W. P. H. P. Weerasinghe · H. M. S. C. Rathnasiri
University of Sri Jayewardenapura, Rathmalana, Sri Lanka
e-mail: en83103@sjp.ac.lk

S. M. A. Nanayakkara
University of Moratuwa, Katubedda, Moratuwa, Sri Lanka

© The Author(s), under exclusive license to Springer Nature Singapore Pte Ltd. 2023

R. Dissanayake et al. (eds.), *ICSBE 2022*, Lecture Notes in Civil Engineering 362,
https://doi.org/10.1007/978-981-99-3471-3_10

1 Introduction

The most frequently used construction material on the planet is concrete, with about 10 billion tons manufactured annually [1]. Concrete's key thermal parameters are specific heat capacity, conductivity, and diffusivity. However, concrete heat transmission is primarily by conduction at normal ambient temperatures. Therefore, thermal conductivity is the most critical thermal property affecting the heat transfer in conduction. Thermal conductivity is the measure of material's ability to conduct heat. Since concrete is a composite material depending on the mix proportion and constitutes used in concrete. The thermal conductivity of concrete varies in a vast range of 0.60–3.85 W m^{-1} K^{-1} for different types of concrete [1, 6].

The factors affecting the thermal conductivity of concrete are moisture condition, age, temperature, water–cement (w/c) ratio, fine aggregate fraction, type of admixtures, and the total aggregate volume fraction [1, 4, 9]. The experimental studies on thermal conductivity of concrete primarily use these factors. But Campbell-Allen et al. [3] used the two-phase concept, the concrete is considered as mortar plus coarse aggregates, which eases the study of the thermal conductivity of concrete [8]. However, the experimental analysis requires material, the cost for apparatus and time. Therefore, numerical studies can be adopted in the construction industry for planning and for material selection for infrastructure development.

This study proposes a novel finite element (FE) model development for the thermal conductivity of concrete that can be utilised for parametric changes. In this study, the concrete is considered a two-phase mesoscale with mortar and coarse aggregate phases. The two-dimensional concrete FE model was developed with mortar as a continuous element and circular shape coarse aggregate as discrete elements. Initially, the developed FE model was validated with experimental results from previous literatures, considering circular shape coarse aggregates. Then, the shape of the coarse aggregates was changed to two real shape aggregates (elliptical and polygonal), and agreement improvement of validation was checked. Hundred and fourteen (114) FE models were developed and compared with the experimental results.

2 Thermal Conductivity of Concrete

Concrete is the most widely used human-made material in the modern construction industry [10]. One-third of the energy consumption and 30% of Greenhouse gas emissions are attributed to infrastructure buildings in most countries [1]. Energy consumption of the building is correlated with the thermophysical properties. Therefore, there is a considerable requirement for research studies related to the thermal conductivity of concrete nowadays.

The thermal conductivity of concrete is the function of time, material, and mix proportion [4]. The importance of the thermal conductivity of concrete is found in determining the energy consumption of the building and is used to take measures

for global warming issues. Thermal conductivity is one of the influencing factors affecting thermal comfort, the energy required for building heating and cooling for thermal comfort depends on the thermo-physical properties of building materials [1]. Thermal conductivity is important in determining the critical points in case of fire. The thermal conductivity of concrete most influences the temperature distribution in structural elements in a fire situation [15]. Thermal conductivity is used for material selection for thermal storage, power station construction, etc. Therefore, the thermal conductivity of material used to build these should be as low as possible or in a suitable range for the respective purpose. Consequently, it is essential to know the thermal conductivity of concrete in the selection of building materials.

2.1 Experimental Studies on the Thermal Conductivity of Concrete

Several researchers studied the thermal conductivity of concrete and came up with numerical equations as follows. Campbell-Allen et al. [3] presented that, the concrete's thermal conductivity can be found by considering the concrete as two-phase material with mortar and coarse aggregates. Also, Khan [8] verified Campbell Allen's numerical model with different materials. The Campbell-Allen et al. [3] model is stated in Eqs. (1) and (2).

$$k = k_m\left(2M - M^2\right) + \frac{k_m k_a (1 - M)}{k_a M + k_m (1 - M)} \tag{1}$$

$$M = 1 - \sqrt[3]{1 - P} \tag{2}$$

where k is the conductivity of concrete, k_m is the thermal conductivity of mortar, k_a is the thermal conductivity of aggregate, P is the volume of mortar per unit volume of concrete. The core idea of this research is brought up from this literature.

Kim et al. [9] quantitatively investigated the influencing factors on the thermal conductivity of concrete such as humidity condition of the specimen, age, temperature, water–cement (w/c) ratio, fine aggregate fraction, type of admixture, and total aggregate volume fraction, moisture, and specimen's condition, and developed an equation for the thermal conductivity of concrete by analysing the factors affecting the thermal conductivity of concrete experimentally as shown in Eq. (3).

$$\begin{aligned} k_c = k_{\text{ref}}(0.293 + 1.01\text{AG})(0.8\left[1.62 - 1.54\frac{w}{c}\right] + 0.2R_h) \\ (1.05 - 0.0025T)(0.86 + 0.0036\frac{S}{A}) \end{aligned} \tag{3}$$

where, k_c is the thermal conductivity of concrete, k_{ref} is a referenced thermal conductivity measured from specimens at a condition, AG—aggregate volume fraction, $W/$

C is the water–cement ratio, T—temperature, R_h—average relative humidity, and S/A—fine aggregate fraction. Each factor is individually analysed using the linear regression analysis and the equation is combined to find the thermal conductivity of concrete.

Choktaweekarn et al. [4] investigated the thermal conductivity of fly ash concrete and the thermal conductivity of hydrated product was obtained by the use of regression analysis together with the test results of cement paste, and thermal conductivity of fly ash powder was derived from the test results of cement–fly ash pastes. The equation is derived for the thermal conductivity of concrete as stated in Eq. (4).

$$k(t) = n_g k_g + n_s k_s + n_{\text{wfree}}(t) k_w + n_{\text{uc}}(t) k_c + n_{\text{ufa}}(t) k_{\text{fa}} + n_{\text{ra}} k_{\text{ra}} + n_{\text{hp}}(t) k_{\text{hp}} \quad (4)$$

where, n_g is the volumetric ratio of coarse aggregate, n_{hp} is the volumetric ratio of hydrated product at the considered age, n_{ra} is the volumetric ratio of air, n_s is the volumetric ratio of fine aggregate, $n_{\text{uc}(t)}$ is the volumetric ratio of un-hydrated cement at the considered age, $n_{\text{ufa}(t)}$ is the volumetric ratio of unhydrated fly ash at the considered age, $n_{\text{wfree}(t)}$ are the volumetric fractions at the considered age of free water, k_c is the thermal conductivity of cement, k_g is the thermal conductivity of coarse aggregate, k_{hp} is the thermal conductivity of a hydrated product, k_{ra} is the thermal conductivity of air. K_s is the thermal conductivity of fine aggregate and K_w is the thermal conductivity of water. The model was satisfactorily verified with various experimental results for pastes, mortars and concretes. All the studies mentioned above need experimental study. However, the experimental studies need time and material cost consumption.

2.2 *Numerical Studies on Thermal Conductivity of Concrete*

The rise in computer capability has substantially supported the development of numerical simulations [10]. ABAQUS [14] is a general-purpose finite element program designed specifically for advanced structural and heat transfer analysis [2]. Abaqus FEM software was used by Borhan [2] to investigate the thermal conductivity of concrete and verified with the experimental results by three-dimensional concrete section and temperature profile. FE model development can be used for thermal conductivity of concrete analysis with reduced time and cost consumption. Therefore, this study develops the FE model to investigate the thermal conductivity of concrete with various materials. Shape analysis is receiving more attention in concrete research because of its relevance [12, 13]. Therefore, the shape of coarse aggregates was changed and validated for the developed FE model in this study.

3 Methodology

The two-dimensional FE model was developed by considering the concrete as two-phase mesoscale with continuous mortar phase and discrete coarse aggregates elements in ABAQUS CAE as shown in Fig. 1. The thermal conductivity of concrete was conculcated from heat flux results of FE model. The finite element results and experimental results of Campbell-Allen et al. [3] and Khan [8] were compared to validate the developed FE model.

ABAQUS CAE software was selected for both modeling and analysis. The development of finite element model and validation with different shapes of aggregates are discussed below.

3.1 Development of Finite Element Model

A two-dimensional (2D) concrete FE model was developed in ABAQUS CAE software. The concrete has been considered a two-phase material with mortar and coarse aggregates. Mortar is a continuous phase and coarse aggregates are discrete elements in the developed model. The concrete cross-section was selected as 150 × 150 mm square section as same as the typical cube dimension. The concrete FE model was developed according to the particle size distribution/grading of Campbell-Allen et al. [3] and Khan [8] with random distribution of coarse aggregates as shown in Fig. 2.

Materials for the mortar and coarse aggregates of concrete with their thermal conductivity were defined. One-dimensional heat flow with the steady-state heat transfer is used for the analysis to replicate the experimental method of Campbell-Allen et al. [3] and Khan [8] as shown in Fig. 3. Heat transfer was given by assigning the boundary condition of surface temperatures as the top surface temperature is 0 °C and the bottom surface temperature is 10 °C and the side ends are considered as a free end without any temperature profile assigned.

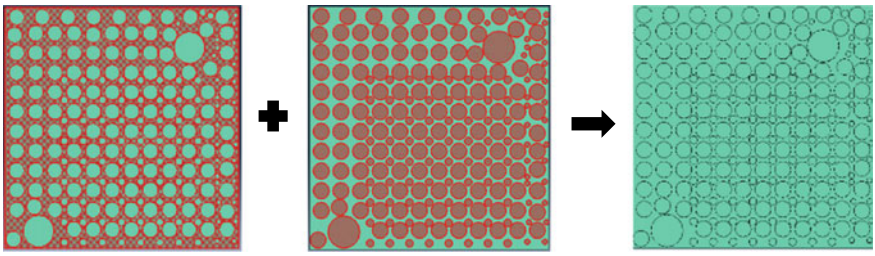

Fig. 1 **a** Mortar as continuous phase **b** coarse aggregates as discrete elements and **c** two-dimensional cross-section of concrete

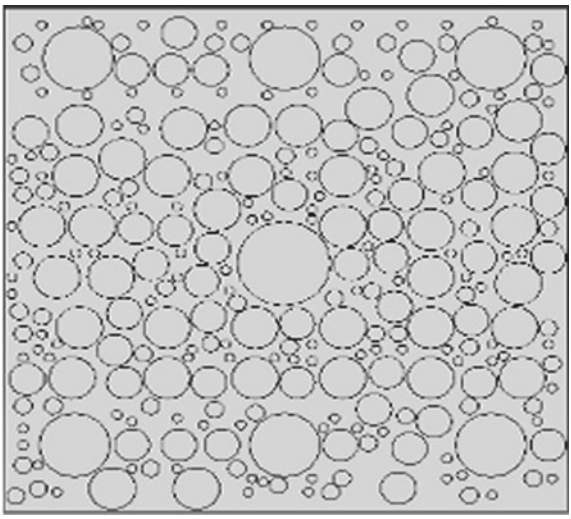

Fig. 2 Concrete as two-phase material with mortar and coarse aggregates

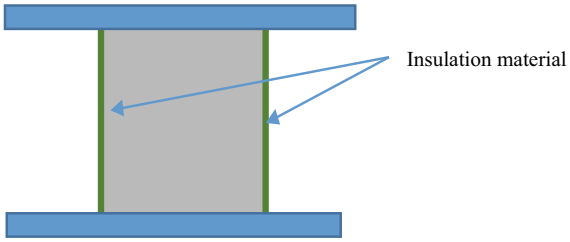

Fig. 3 Experimental setup

The model was meshed into small elements and meshing was done with the 0.001 m triangular mesh and analysed by "heat transfer" family analysis method as shown in Fig. 4. Each mesh's heat flux value received from the results of software analysis is shown in Fig. 5.

The average heat flux value of the section was used to calculate the thermal conductivity values, from top and bottom average heat flux values, with Eqs. (5) and (6).

$$\text{U value} = \frac{\text{Average heat flux}}{\text{Temperature difference}} \tag{5}$$

$$\text{Thermal conductivity of concrete} = \text{U value} \times \text{Thickness} \tag{6}$$

The visualisation of results for heat flux value per unit area leaving the surface (HFL), thermal gradient (GRADT), reference temperature value (NT11) and reaction fluxes (RFL11) was given by the software as shown in Fig. 6.

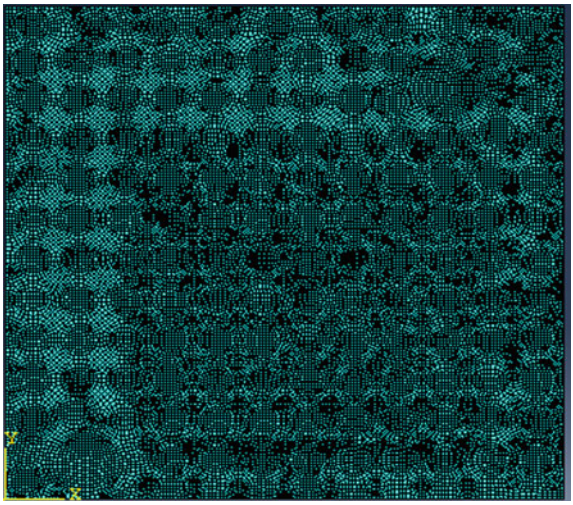

Fig. 4 Meshing the two dimenional model

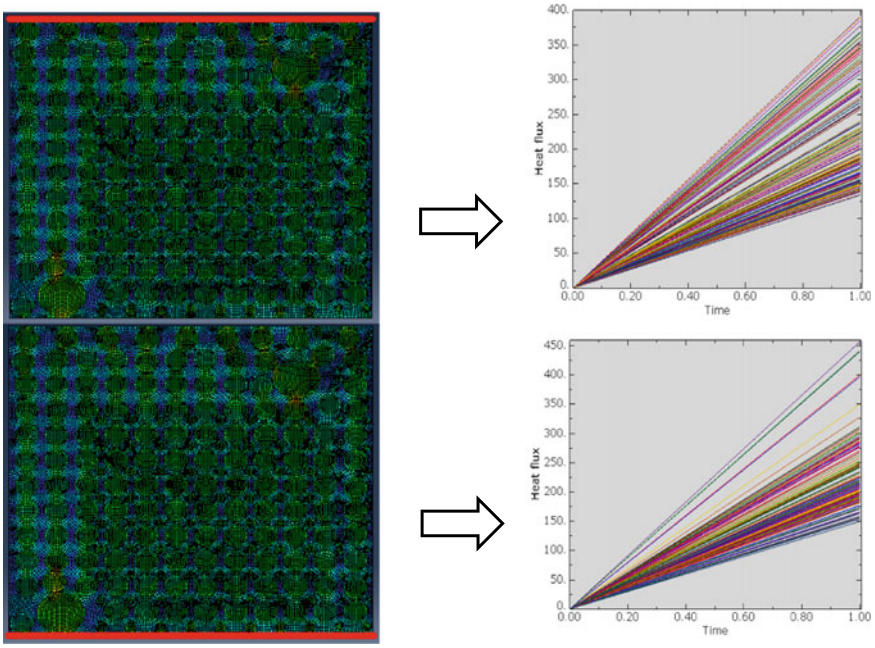

Fig. 5 Heat flux values from the analysis on top and bottom surface

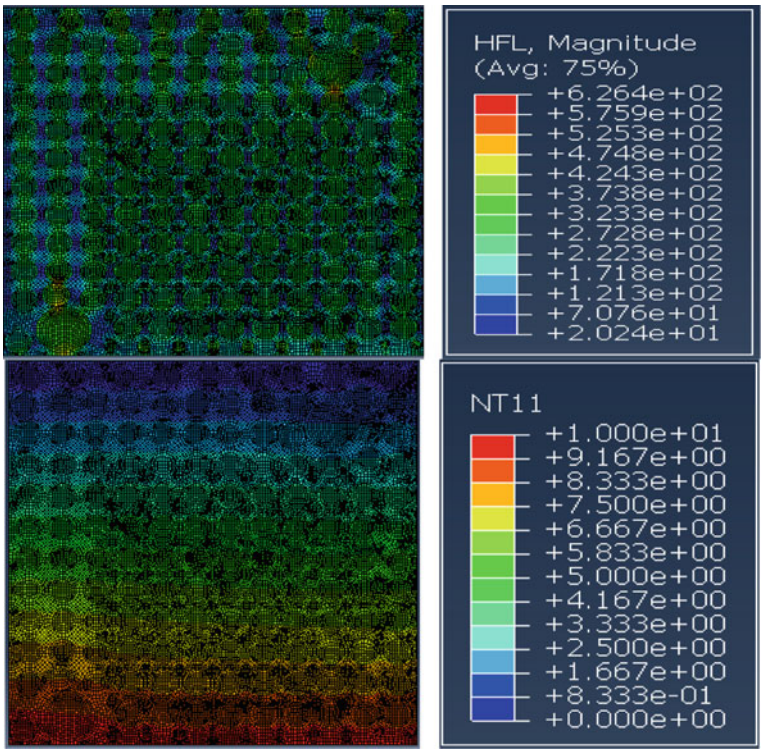

Fig. 6 Heat flux (HFL) and temperature value (NT11) visualisation after the heat application

3.2 Validation of Finite Element Model

The developed model was validated with the experimental results from literatures. Six (6) numbers of Campbell-Allen et al. [3] experimental results and thirty-two (32) numbers of Khan [8] experimental results were used for the validation of the developed model. The shape of the coarse aggregates changed as circular, elliptical and polygonal aggregates and convergence of Finite Element Modeling (FEM) results with experimental results were checked. Therefore, altogether the hundred and fourteen (114) results were used to validate the developed FE model. The developed FE model re-modeled according to the shape of coarse aggregates as shown in Figs. 7 and 8.

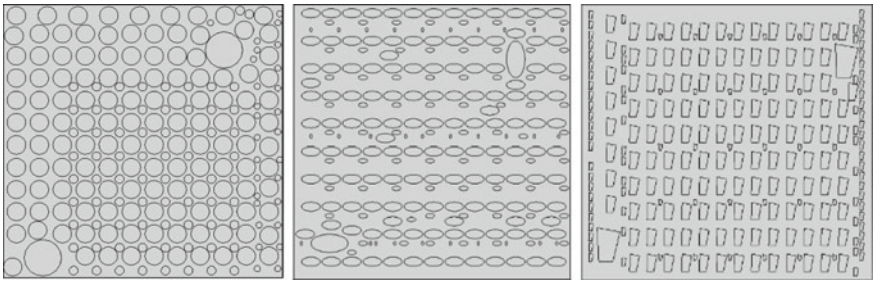

Fig. 7 Two-dimensional model with circular, ellipse and polygonal aggregates for Campbell-Allen et al. [3] model

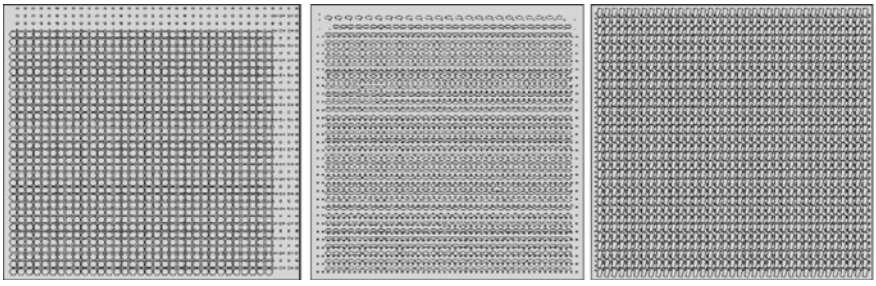

Fig. 8 Two-dimensional model with circular, ellipse and polygonal aggregates for Khan [8] model

Most of the existing studies with modeling assume that the shape of an aggregate particle is circular or spherical [7]. The critical load capacity of specimens with random circular aggregate is higher than that of specimens with arbitrary polygonal aggregate [5]. Aggregates come in a variety of shapes, although in practice, oval or crushed aggregates are also used [11].

Therefore, to increase the convergence of comparison results between experimental results and FE model results, the shapes of aggregate were changed as circular, elliptical, and polygonal to validate the results. The shape of the coarse aggregates mainly considered in this study is circular aggregates since most of the literature with modeling utilised circular shape in their studies [10]. Then the elliptical aggregates were used because the gravel aggregate's shape was assumed as an ellipse shape in previous studies. Polygonal aggregates were used because the crushed aggregate's shape was assumed as the polygonal shape in previous studies [5, 11]. It was considered as a polygon with four sides (quadrilateral) in this study.

4 Results and Discussion

The Campbell-Allen et al. [3] and Khan [8] experimental results of thermal conductivity of concrete and finite element model results of thermal conductivity of concrete from developed model were compared for each shape of coarse aggregates. The shapes of the coarse aggregates were changed as circular, elliptical and polygonal, and thermal conductivity values were compared against the Campbell-Allen model as shown in Table 1.

The thermal conductivity of concrete values from finite element modeling results was compared with the Khan [8] experimental results as shown in Table 2 and estimated the values for thermal conductivity of concrete with the correction for air voids from Khan's results using the respective thermal conductivity of mortar and thermal conductivity of coarse aggregates as shown in Table 3. The correction was done for air voids for thermal conductivity of mortar and thermal conductivity of concrete values [8].

The difference percentages between experimental results and FEM results were calculated. The overall validation results of developed FE model with different shapes of coarse aggregates are shown in Table 4.

Table 1 Validation of Campbell-Allen model with circular, elliptical and polygonal aggregates

Experimental results [3]				FEM results of thermal conductivity of concrete		
Thermal conductivity of mortar		Thermal conductivity of aggregate	Thermal conductivity of concrete	Circular	Ellipse	Crushed
Moisture content (volume %)	Thermal conductivity of mortar					
18	2.49	1.21	1.93	1.69	1.99	2.08
0	1.48	1.21	1.24	1.32	1.40	1.40
16	2.28	1.38	2.07	1.73	1.96	2.00
0	1.48	1.38	1.29	1.42	1.45	1.45
23	2.73	8.12	4.39	4.84	3.49	3.76
0	1.48	8.12	2.56	3.40	2.06	2.41

Table 2 Validation of Khan model with circular, elliptical and polygonal aggregates

Experimental results [8]			FEM results of thermal conductivity of concrete		
Thermal conductivity of mortar	Thermal conductivity of aggregate	Thermal conductivity of concrete	Circular	Ellipse	Crushed
1.9	4.03	2.26	2.77	2.26	2.98
1.9	3.15	2.03	2.46	2.15	2.55
1.9	3.52	2.21	2.60	2.20	2.74
1.9	8.58	2.77	3.86	2.54	4.80
2.65	4.3	3.52	3.39	2.98	3.52
2.65	3.49	2.92	3.05	2.84	3.10
2.65	5.22	3.61	3.73	3.11	3.97
2.65	8.63	4.18	4.71	3.39	5.45
1.37	4.03	1.97	2.33	1.72	2.64
1.37	3.15	1.6	2.08	1.65	2.26
1.37	3.52	1.91	2.19	1.69	2.42
1.37	8.58	2.29	3.11	1.89	4.22
1.95	4.3	3.24	2.90	2.34	3.13
1.95	3.49	2.71	2.62	2.24	2.75
1.95	5.22	2.9	3.18	2.42	3.54
1.95	8.63	3.49	3.93	2.60	4.86

Campbell-Allen model shows better retaliation with the polygonal shape aggregates. Therefore, the aggregates shape that is used in the experiment could be a polygonal shape aggregate. The Khan model shows better relativity with the circular shape aggregates. Therefore, the aggregates shape that is used in the experiment could be a circular shape aggregate. The average difference percentage between the experimental results and FEM results for thermal conductivity of concrete is (−4.30%). Usually, the difference percentage is below 10–15%, then it can be used as a prediction model [8]. Therefore, the developed FE model is validated and it can be used for prediction purposes.

Table 3 Validation of Khan model with air voids with circular, elliptical and polygonal aggregates

Experimental results [8]			FEM results of thermal conductivity of concrete		
Thermal conductivity of mortar	Thermal conductivity of aggregate	Thermal conductivity of concrete	Circular	Ellipse	Crushed
1.85	4.03	2.8	2.74	2.21	2.95
1.85	3.15	2.13	2.42	2.10	2.53
1.85	3.52	2.85	2.56	2.15	2.71
1.85	8.58	3.29	3.79	2.48	4.76
2.33	4.3	3.2	3.18	2.69	3.35
2.33	3.49	2.49	2.86	2.57	2.95
2.33	5.22	3.27	3.49	2.80	3.78
2.33	8.63	3.72	4.37	3.04	5.21
1.29	4.03	2.54	2.25	1.64	2.59
1.29	3.15	2.07	2.01	1.57	2.21
1.29	3.52	2.17	2.12	1.60	2.37
1.29	8.58	2.68	2.99	1.79	4.12
1.73	4.3	2.95	2.73	2.12	3.00
1.73	3.49	2.48	2.46	2.04	2.63
1.73	5.22	2.6	2.98	2.19	3.39
1.73	8.63	3.17	3.64	2.34	4.64

Table 4 Difference percentage between experimental results and FEM results

Model	Circular aggregate (%)	Ellipse aggregates (%)	Polygonal aggregates (%)
Camphell-Allen model	−5.20	2.89	−1.59
Khan model	−14.21	11.07	−28.13
Khan model with air voids consideration	−4.66	20.06	−18.86

5 Conclusion

This study developed a novel finite element model to investigate the thermal conductivity of concrete by considering the concrete as two-phase material with mortar and coarse aggregates. The two-dimensional model was modeled manually by the random distribution of coarse aggregates with the take and place method (retain merge) without overlapping aggregates in ABAQUS/CAE. Simulated heat flux values were used to calculate the thermal conductivity of concrete. Hundred and fourteen (114) FE models were developed and compared with the experimental results for

each aggregates shape such as circular, elliptical and polygonal. The difference percentage between the FEM results and experimental results is 4.30%. Therefore, it is concluded that the FEM model developed in this study can be used as a prediction model to investigate the thermal conductivity of concrete. This study can be used for a comprehensive investigation of thermal conductivity of concrete by changing shapes, grading, mix proportion and materials. The consideration of air voids in mortar and ITZ (Interfacial Transition Zone) between mortar and aggregates can be adapted in simulation for better results for future work.

Acknowledgements The authors gratefully acknowledge the support of the staffs of Department of Civil Engineering, University of Sri Jayewardenepura for their valuable support.

References

1. Asadi I et al (2018) Thermal conductivity of concrete—a review. J Build Eng 20:81–93. https://doi.org/10.1016/j.jobe.2018.07.002
2. Borhan TM (2014) Prediction of the thermal conductivity of concrete using ABAQUS model. Al-Qadisiyah J Eng Sci 7(1):127–136. https://doi.org/10.1063/1.4759317
3. Campbell-Allen D et al (1964) The thermal conductivity of concrete. Mag Concr Res 16(49):233–234. https://doi.org/10.1680/macr.1964.16.49.233
4. Choktaweekarn P, Saengsoy W, Tangtermsirikul S (2009) A model for predicting thermal conductivity of concrete. Mag Concr Res 61(4):271–280. https://doi.org/10.1680/macr.2008.00049
5. Du C et al (2013) Numerical simulation of aggregate shapes of three-dimensional concrete and its applications. J Aerosp Eng 26(3):515–527. https://doi.org/10.1061/(asce)as.1943-5525.0000181
6. Dzolev I et al (2017) Thermal analysis of concrete members subjected to fire according to EN 1991-1-2 & EN 1992-1-2, November 2015
7. Jin L et al (2018) Determination of the effect of elevated temperatures on dynamic compressive properties of heterogeneous concrete: a meso-scale numerical study. Constr Build Mater 188:685–694. https://doi.org/10.1016/j.conbuildmat.2018.08.090
8. Khan MI (2002) Factors affecting the thermal properties of concrete and applicability of its prediction models. Build Environ 37(6):607–614. https://doi.org/10.1016/S0360-1323(01)00061-0
9. Kim KH et al (2003) An experimental study on thermal conductivity of concrete. Cem Concr Res 33:363–371. https://doi.org/10.1016/j.conbuildmat.2015.10.108
10. Liu Q et al (2018) Ionic transport features in concrete composites containing various shaped aggregates: a numerical study. Compos Struct 183(1):371–380. https://doi.org/10.1016/j.compstruct.2017.03.088
11. Man HK, Mier JGM (2008) Size effect on strength and fracture energy for numerical concrete with realistic aggregate shapes. Int J Fract 154(1–2):61–72. https://doi.org/10.1007/s10704-008-9270-y
12. Moaveni M et al (2013) Evaluation of aggregate size and shape by means of segmentation techniques and aggregate image processing algorithms. Transp Res Rec 2335:50–59. https://doi.org/10.3141/2335-06
13. Ozen M, Guler M (2014) Assessment of optimum threshold and particle shape parameter for the image analysis of aggregate size distribution of concrete sections. Opt Lasers Eng 53:122–132. https://doi.org/10.1016/j.optlaseng.2013.08.020

14. Smith M (2009) Abaqus 6.11 glossary. In: ABAQUS/standard user's manual, version 6.9
15. Zehfuß J et al (2020) Evaluation of Eurocode 2 approaches for thermal conductivity of concrete in case of fire. Civ Eng Des 2(3):58–71. https://doi.org/10.1002/cend.202000001

Effect of Carbonation on Microstructure of Cement Pastes with Different Water-to-Cement Ratios

K. Kopitha, S. Krishnya, Y. Elakneswaran, R. Kitagaki, Y. Yoda, M. Tsujino, and A. Nishida

Abstract The durability of the structures is the main concern in the field of engineering. Reinforcement corrosion is the most common cause of concrete structural deterioration. Corrosion of reinforcement results primarily from chloride ingress and carbonation. Cementitious materials are prone to carbonation as carbon dioxide is present everywhere in the atmosphere. For the durability prediction of cement-based materials, it is crucial to know the effect of carbonation on the microstructure of the cement matrix. This study examines how carbonation affects the microstructure of cement paste made up of Ordinary Portland Cement (OPC) with water-to-cement ratios (w/c) of 0.3, 0.4, and 0.5 with the help of the experiments and the newly developed model predicting the hydration products and porosity of the cement paste during the CO_2 gas diffusion. As part of this study, phenolphthalein was used to determine the carbonation depth. In addition to identifying the hydrated and carbonated products using X-Ray Diffraction (XRD) and Thermal Gravimetric Analysis (TGA), changes in microstructure were detected through Scanning Electron Microscope (SEM). Furthermore, the microstructures of cement paste samples that have been exposed to 5% carbon dioxide concentration for four months were compared. Carbonation products consist predominantly of calcite type polymorph of calcium carbonate, as revealed by XRD. Portlandite and C-S-H get carbonated simultaneously and the carbonation reaction increases with the increasing w/c in accordance with XRD and TGA results. Eventually, the experimental results of calcite and portlandite were compared with the predicted results from a newly developed COMSOL-IPHREEQC interface, and a better prediction of the numerical model was observed.

K. Kopitha (✉) · S. Krishnya · Y. Elakneswaran
Laboratory of Chemical Resources, Division of Sustainable Resources Engineering, Hokkaido University, Sapporo, Japan
e-mail: kopitha.kirushnapillai.n2@elms.hokudai.ac.jp

R. Kitagaki
Laboratory of Building Materials, Division of Architecture, Hokkaido University, Sapporo, Japan

Y. Yoda · M. Tsujino · A. Nishida
Center for Construction Engineering, Shimizu Corporation, Shimizu Institute of Technology, Tokyo, Japan

© The Author(s), under exclusive license to Springer Nature Singapore Pte Ltd. 2023

R. Dissanayake et al. (eds.), *ICSBE 2022*, Lecture Notes in Civil Engineering 362,
https://doi.org/10.1007/978-981-99-3471-3_11

Keywords Durability · Carbonation · Microstructure · COMSOL-IPHREEQC

1 Introduction

It is recognized that carbonation contributes significantly to corrosion in reinforced concrete [2]. The cement paste undergoes different chemical and mechanical changes during this physicochemical process, including microstructural and chemical changes in the cementitious matrix. As the pH of the pore solution decreases when concrete is carbonated, the passive layer formed on the reinforcement becomes unstable and leads to corrosion [3]. Therefore, it is important to study the factors affecting carbonation and hence durability of cementitious materials.

Hydrated cement consists of many phases that tend to carbonate. The carbonation rate is controlled by the amount of calcium-containing phases that are capable of dissolving and reacting to form calcite. Approximately 70–80% of hydrated cement's total solid volume consists of calcium silicate hydrates (C-S-H) and calcium hydroxide (CH) which can be carbonated easily [13]. A hydrated cement paste also consists of ettringite and monosulfoaluminate, which can be subjected to dissolution and subsequent carbonation due to pH drop by carbonation [9]. The degree of hydration that decides the amount of hydrated phases depends on the water-to-cement ratios (w/c) of the cement paste. The diffusion of CO_2 and the amount of hydration products in the cement matrix are the main factors that affect the carbonation rate [11]. W/c is one of the factors that determine the amount of hydration products. Hence, it is important to study the effect of w/c on both cement hydration and carbonation.

It has been found that the diffusion rate of CO_2 has the greatest influence on cement paste carbonation [3, 15]. Cement paste matrix pore structure and liquid saturation determine the diffusion rate of CO_2 and the w/c plays a very important role in cement paste porosity and pore size distribution [10]. It has been reported that the carbonation reaction decreases as the w/c is reduced [10]. It is important to investigate the effect of w/c on carbonation and hence to develop a numerical model based on that for better prediction of durability.

In recent years, researchers have become increasingly interested in simulating the realistic changes in the hydrated matrix during carbonation by integrating diffusion and reaction processes. It is noteworthy that the previously published work did not extensively consider the thermodynamic calculations for the carbonation of cement paste; instead, portlandite and C-S-H were only considered as hydration products and calcite as a carbonate phase [12, 14, 16]. Moreover, a gas phase within the cement matrix was neglected for CO_2 diffusion [12]. Hence, a new model platform is developed herein to address the limitations identified in previous models [7] and to predict the (i) diffusion of carbon dioxide gas and (ii) phase assemblage during transportation. To fully verify the feasibility of the newly developed model, further validation is recommended for the cement paste with different w/c and different CO_2 gas concentrations. The lack of experimental data available on the carbonation of

Table 1 Chemical composition of OPC using XRD and Bogue equation

Composition	XRD	Bogue equation
C_3S	60	51
C_2S	16	23
C_3A	07	10
C_4AF	12	09
Gypsum	04	

OPC paste samples with different w/c made this research team difficult to validate the newly developed COMSOL-IPHREEQC [6, 7] interface and to investigate the carbonation effects on the microstructure of cement paste sealed-cured with different w/c.

Therefore, this study is designed to evaluate the effect of w/c on the carbonation of hardened cement paste and its microstructural characteristics to validate the numerical model developed by this research group. For this study, w/c of 0.3,0.4, and 0.5 were selected. The hydrated cement paste was exposed to carbonation for four months and mineralogical assemblage was determined as a function of depth. In addition, scanning electron microscopy (SEM) was also used to identify microstructural changes. Finally, experimental data were compared with the predicted results of the numerical model (COMSOL-IPHREEQC interface).

2 Methodology

2.1 Materials

Ordinary Portland Cement (OPC), Class (H), confirmed to the Japan Industrial Standard JIS R 5201:2015, was used as the cementitious material. Blaine of the OPC used is 339 m^2/kg and the density is 3.16 g/cm^3. The chemical composition of cement is shown based on X-ray diffraction measurements and the Bogue equation is shown in Table 1.

2.2 Sample Preparation

Using a Hobart N50 5-Quart commercial stand mixer, mixing for three minutes was performed on cement paste samples with w/c values of 0.3, 0.4, and 0.5. Casting was done with cement paste mixtures in cylindrical moulds measuring 50 mm in diameter and 100 mm in height. Three samples were cast in each w/c to take the average of three samples in each measurement. After 24 h of casting, de-moulded samples were kept under sealed curing at 20 ± 2 °C for 28 days. After sealed curing, resin was

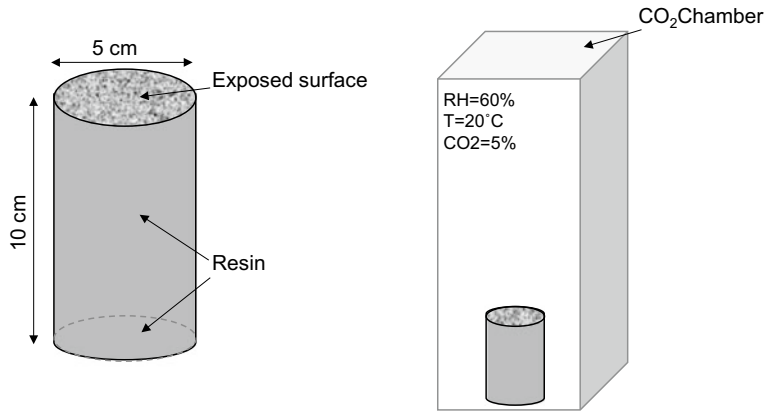

Fig. 1 Exposure of the samples to the CO_2

applied to all three faces except the bottom face of cylindrical samples and samples were exposed to carbon dioxide as shown in Fig. 1.

2.3 Exposure

The samples were exposed to CO_2 for four months in the CO_2 chamber where the concentration of CO_2 was at 5 ± 0.2%, the relative humidity at 60 ± 10%, and the temperature at 20 ± 2 °C. It was decided to use a relative humidity of 60% since this range produces the greatest carbonation rate [13]. Samples were kept in the chamber so that the face with no resin was upside. After the carbonation, samples were subjected to a phenolphthalein test, and then they were cut into discs of 2 mm as shown in Fig. 2.

2.4 Experimental Methods

2.4.1 Phenolphthalein Test

After four months of carbonation, samples were taken out from the CO_2 chamber and those cylindrical samples were split. The carbonation depth of carbonated samples was determined using phenolphthalein spray (0.4 g/L Phenolphthalein in 40 vol% ethanol). Three measurements were made of the colourless region over three samples and the average was recorded for each w/c.

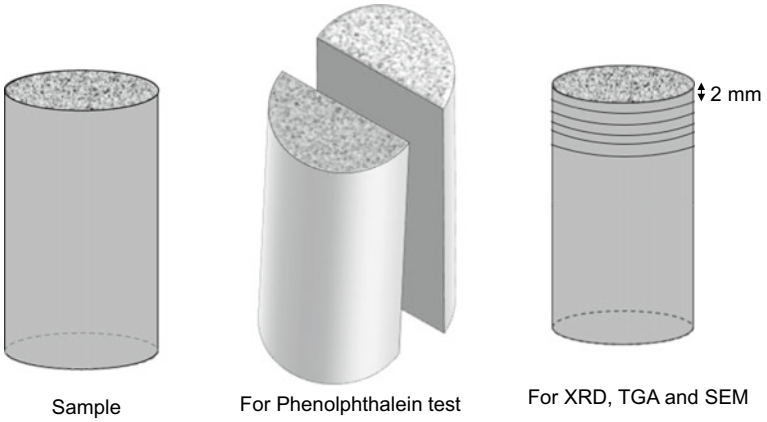

Fig. 2 Position of the cutting of samples for subsequent analysis

2.4.2 X-Ray Diffraction (XRD) Analysis

A Rigaku X-ray diffractometer with CuKα radiation was used to measure the crystalline phases in the samples of carbonated cement paste. A range of 5–70° 2θ was scanned with a step size of 0.02° and a rotating speed of 6.5°/min. Grinding the discs resulted in powder samples that were measured after four months of carbonation. For the quantitative analysis of XRD patterns, the Profex/BGMN software package was used [4]. This program permits the estimation of the weight fractions of crystalline phases using the Rietveld refinement procedure. The internal standard method was applied to obtain the absolute mass fractions of the crystalline phases. The sample was mixed with 10 wt% corundum as an internal standard.

2.4.3 Thermogravimetric Analysis (TGA)

TGA was carried out under nitrogen with a flow rate of 200 mL/min on powdered samples with a HITACHI TG/DTA 7220 and a heating rate of 10 °C/min from 20 to 950 °C. At the temperature range 400–500 °C and 540–950 °C, weight loss was used to quantify the $Ca(OH)_2$ and $CaCO_3$ respectively. The amount of $Ca(OH)_2$ and $CaCO_3$ present in the carbonated samples were calculated according to the following Eqs. (1) and (2) [1, 11, 17].

$$\%Ca(OH)_2 = \frac{(M_{400\,^\circ C} - M_{500\,^\circ C})}{M_{\text{Sample}}} \times \frac{74.09}{18.01} \times 100 \tag{1}$$

$$\%CaCO_3 = \frac{(M_{540\,^\circ C} - M_{950\,^\circ C})}{M_{\text{Sample}}} \times \frac{100.09}{44.01} \times 100 \tag{2}$$

At a given temperature, the sample mass is M. The TGA tests were performed with 15 mg (±0.2 mg) of powder derived from disc samples.

2.4.4 Scanning Electron Microscopy (SEM)

Backscattered electrons (BSE) images were obtained using SEM. BSE images can be used for phase identification based on the grey levels. Before SEM analysis, epoxy-impregnated samples were polished and coated with gold. A 15 kV accelerating voltage and 10 mm working distance were set for this analysis.

2.4.5 Thermodynamic Modelling

A new reactive transport model including the cement hydration model, thermodynamic calculation (including the kinetic model for C-S-H dissolution) and species transportation calculation is herein proposed to predict hydration products and porosity of the cement paste during the carbon dioxide gas diffusion. The elementary characteristics to determine the formation of hardened cement matrix during the hydration period such as chemical and physical properties of cement, mixture recipe and boundary conditions are the input parameters for the hydration model while the ionic concentration in the exposed environment, initiation of transport reaction relative to hydration time and duration of the transport reaction are the compulsory input data for the transport model. The cement hydration model is used to compute the dissolution rate of each clinker mineral as a function of time. Thermodynamic calculations are performed using PHREEQC open-source package and COMSOL Multiphysics is used for the transportation calculations. The implemented approach used to predict the hydration products and transport properties are detailed in our previous work [6–8]. This modelling platform is developed in MATLAB language and LiveLink™ for MATLAB® is used for data transference between MATLAB and COMSOL Multiphysics.

3 Results and Discussion

3.1 Phenolphthalein Test

Phenolphthalein-sprayed images of carbonated samples are shown in Fig. 3. The samples having w/c of 0.3 exhibited the lowest carbonation depth of 0.5 mm. This could be due to a dense microstructure that prevents CO_2 from diffusing for carbonation. The carbonation depth of samples having w/c of 0.4 and 0.5 exhibited carbonation depth of 1 mm and 4 mm respectively.

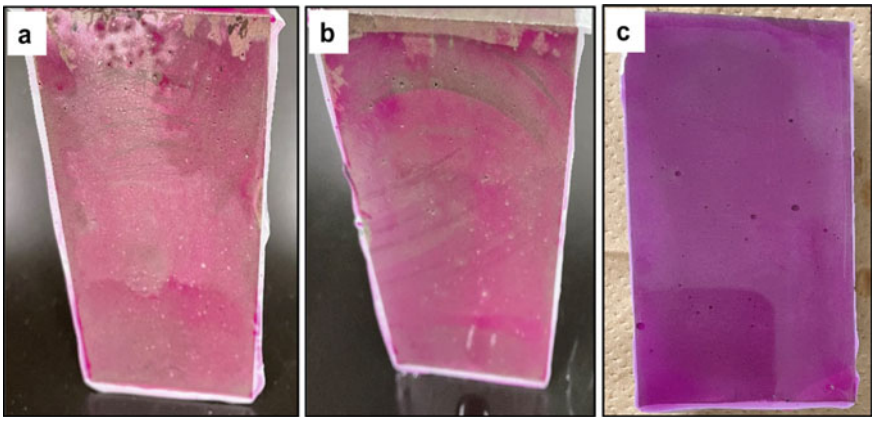

Fig. 3 Phenolphthalein-sprayed images of carbonated samples (**a**: w/c = 0.5, **b**: w/c = 0.4, **c**: w/c = 0.3)

3.2 XRD

The first layers from the surface exposed to carbonation (0–2 mm) of cement paste samples were subjected to XRD. Plots of the XRD pattern of carbonated samples having different w/c are shown in Fig. 4. Carbonated samples mainly contained calcium hydroxide and calcite. Calcite-type calcium carbonate was found to be the main carbonation product based on XRD results. Figure 5 illustrates the Rietveld quantitative analysis of the XRD scan. All non-crystalline phases such as C-S-H and silica gel belong to the amorphous part. The polymorphs of calcium carbonate such as vaterite, aragonite and calcite were described with a cumulative term called calcium carbonate. According to the results, there was simultaneous carbonation of portlandite and C-S-H. As a thermodynamic principle, it is imperative that all portlandite carbonates before C-S-H, but that is not the case in practice. Carbonated product was high in samples having w/c of 0.5. Studies [2, 5, 15] have consistently shown this result, whereby the amount of hydrated phases is high in the samples having high w/c and it enhances the rate of carbonation reaction. Figure 5 shows that amount of amorphous content in samples with w/c of 0.5 is less than that of w/c of 0.4. This is mainly due to the carbonation of amorphous phases such as C-S-H carbonated more in the samples with w/c of 0.5 as they have more diffusion rate of CO_2.

3.3 TGA

The first layers from the surface exposed to carbonation (0–2 mm) of cement paste samples were subjected to TGA. Figure 6 compares the weight loss (TG) and the

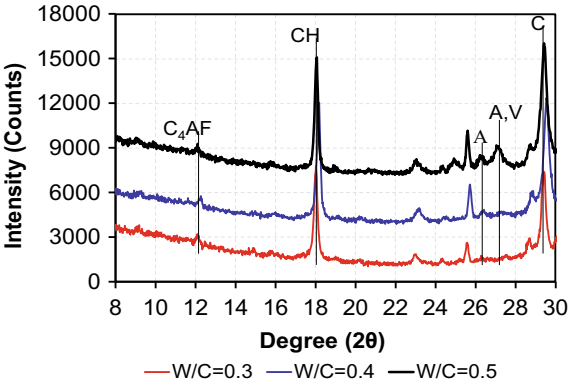

Fig. 4 XRD plots of carbonated samples having different w/c (CH: calcium hydroxide, A: aragonite, V: vaterite, C: calcite)

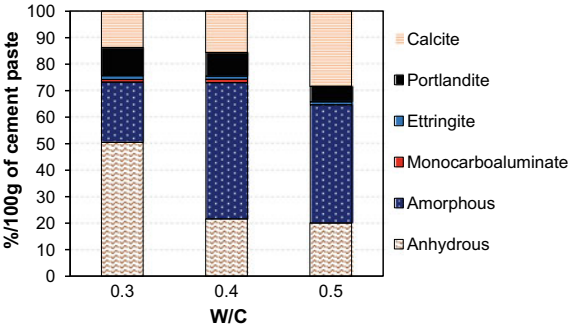

Fig. 5 Rietveld quantitative analysis of the XRD scan of carbonated samples having different w/c

differential thermal (DTG) curves of samples with varying w/c. C-S-H, Aft, and AFm phases are decomposed at temperatures of 30–300 °C, causing mass loss. From the XRD analysis, AFt and AFm phases were of small amount. Therefore, the decomposition peak corresponding to this temperature range was mainly due to the decomposition of C-S-H.

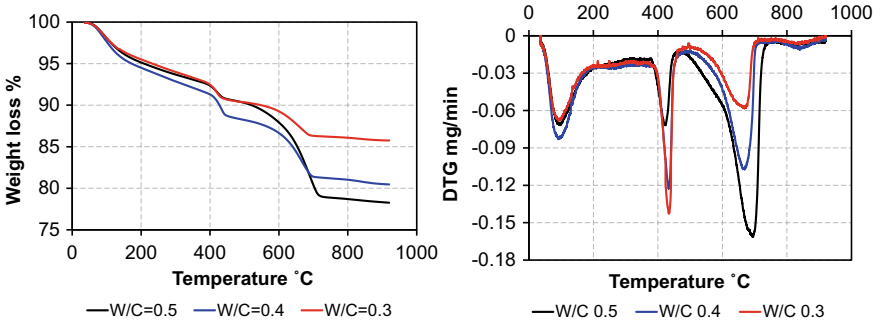

Fig. 6 TGA curves of carbonated samples having different w/c

From the DTG curve, it can be noticed that the decomposition peak of the sample with w/c of 0.5 shows a small peak compared to the sample with w/c of 0.4 in the temperature range of 30–300 °C. It shows that the amount of C-S-H is less as observed in the XRD result (Fig. 5) and confirms the carbonation of C-S-H. The samples having w/c of 0.3 shows a smaller decomposition peak in the specific temperature range compared to the other two samples as it has a low degree of hydration due to low water content.

$Ca(OH)_2$ decomposes at 400–500 °C, which results in weight loss. When the w/c was increased, the $Ca(OH)_2$ decreased significantly, mainly because $Ca(OH)_2$ was converted to $CaCO_3$. $CaCO_3$ decomposes in the temperature range of 540–950 °C. $CaCO_3$ content was higher in samples with w/c of 0.5, primarily due to active hydration products being converted to $CaCO_3$.

3.4 SEM

The first layers from the surface exposed to carbonation (0–2 mm) of cement paste samples were subjected to SEM. Figure 7 shows the BSE images of the samples having different w/c. The brightest region in the BSE image represents anhydrous cement, and black represents pores. Figure 7a depicts a sample with w/c of 0.5, with brighter products corresponding to polymorphs of $CaCO_3$ precipitated during carbonation mixed with decalcified C-S-H or silica gel appearing in the majority of areas compared to Fig. 7b, c. In contrast, Fig. 7b, c show that the samples having less w/c having the light grey products correspond to $Ca(OH)_2$ and C-S-H in the most region.

3.5 Thermodynamic Modelling

To verify the predictability of the proposed model on carbon dioxide diffusion, the computed results of the weight percentage of calcite and portlandite are compared with the XRD experimental results for the cement paste of w/c 0.4 after four months of exposure in the environment of 5% (of the air volume) CO_2 concentration. The first five layers from the surface exposed to carbonation (0–10 mm) of cement paste samples were subjected to XRD. The predicted results from the coupled model for calcite and portlandite weight percentages show an excellent agreement with experimental results as shown in Fig. 8. During the carbonation process, portlandite dissolves due to the decrease of pH, which leads to the reduction of portlandite weight percentage in the cement matrix as depicted in Fig. 8 and forms as calcite.

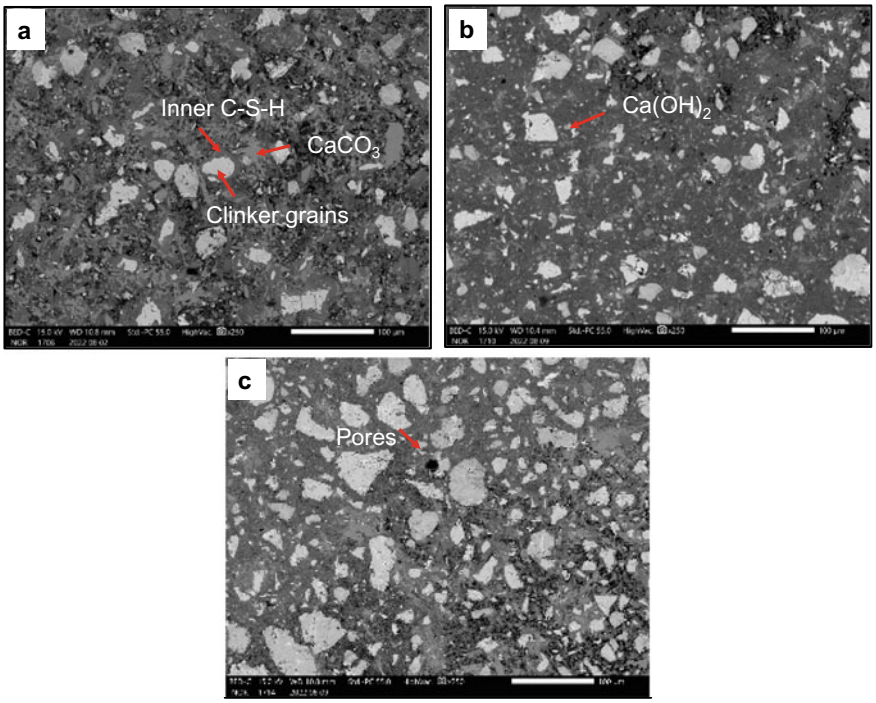

Fig. 7 BSE images of carbonated samples having different w/c (**a**: w/c = 0.5, **b**: w/c = 0.4, **c**: w/c = 0.3)

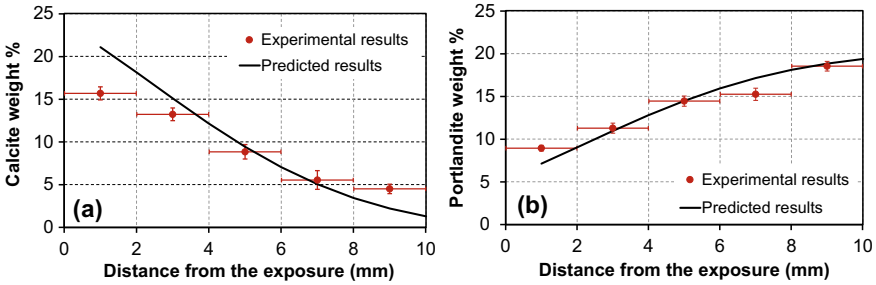

Fig. 8 Comparison of predicted calcite and portlandite weight % with experimental results

4 Conclusions

The influence of w/c of cement paste on carbonation and thus microstructural properties were studied and the results were compared with the numerical model that has been developed using the COMSOL-IPHREEQC interface. XRD, TG and SEM were

used to analyse the effect of w/c on carbonation and the changes in the microstructure due to carbonation. Based on the findings, the following conclusions can be drawn:

1. XRD results revealed that calcite-type calcium carbonate was found to be the main carbonation product.
2. From the XRD and TG results, there was simultaneous carbonation of portlandite and C-S-H.
3. Based on the phenolphthalein test, XRD, TG, and SEM analysis, carbonation increases with increasing w/c.
4. The predicted results from the coupled model for calcite and portlandite weight percentages show an excellent agreement with experimental results.

References

1. Ashraf W, Olek J (2016) Carbonation behavior of hydraulic and non-hydraulic calcium silicates: potential of utilizing low-lime calcium silicates in cement-based materials. J Mater Sci 51(13):6173–6191
2. Boumaaza M et al (2020) Influence of carbonation on the microstructure and the gas diffusivity of hardened cement pastes. Constr Build Mater 253
3. Castellote M et al (2009) Chemical changes and phase analysis of OPC pastes carbonated at different CO_2 concentrations. Mater Struct/Mater Constr 42(4):515–525
4. Doebelin N, Kleeberg R (2015) Profex: a graphical user interface for the Rietveld refinement program BGMN. J Appl Cryst
5. Kim YY et al (2014) Effect of W/C ratio on durability and porosity in cement mortar with constant cement amount. Adv Mater Sci Eng 2014
6. Krishnya S et al (2022) Coupled multi-ionic transport model with hydration model for the chloride ion ingression in cement paste. JCI 44(1):514–519. Available at: JCI
7. Krishnya S, Kopitha K et al (2022) Coupling CO_2 (g) diffusion and geochemistry for the carbonation of cement paste. In: 76th RILEM annual week 2022, pp 1–4
8. Krishnya S, Yoda Y, Elakneswaran Y (2021) A two-stage model for the prediction of mechanical properties of cement paste. Cem Concr Compos 115
9. Lagerblad B (2005) Carbon dioxide uptake during concrete life cycle: state of the art. Swedish Cement and Concrete Research Institute
10. Lo TY, Tang WC, Nadeem A (2008) Comparison of carbonation of lightweight concrete with normal weight concrete at similar strength levels. Constr Build Mater 22(8):1648–1655
11. Mehdizadeh H et al (2021) Effect of water-to-cement ratio induced hydration on the accelerated carbonation of cement pastes. Environ Pollut 280
12. Phung QT et al (2016) 'Modelling the carbonation of cement pastes under a CO_2 pressure gradient considering both diffusive and convective transport. Constr Build Mater 114:333–351
13. Shah V et al (2018) Changes in microstructure characteristics of cement paste on carbonation. Cem Concr Res 109:184–197
14. Shen X et al (2019) Numerical study of carbonation and its effect on chloride binding in concrete. Cem Concr Compos 104(September 2018):103–402
15. Wang J et al (2019) Accelerated carbonation of hardened cement pastes: influence of porosity. Constr Build Mater 225:159–169
16. Xie M, Dangla P, Li K (2021) 'Reactive transport modelling of concurrent chloride ingress and carbonation in concrete. Mater Struct/Mater Constr 54(5):1–19
17. Zajac M et al (2020) Phase assemblage and microstructure of cement paste subjected to enforced, wet carbonation. Cem Concr Res 130

Development of Lightweight Aggregate Concrete with Locally Available Lightweight Materials

R. W. P. K. Rupasinghe, K. M. C. Konthesingha, S. M. A. Nanayakkara, H. M. S. C. Rathnasiri, I. R. Upasiri, and W. P. H. P. Weerasinghe

Abstract Alternative building materials are a significant aspect of the construction industry due to the over-exploitation of natural resources and the cost increment of raw materials. Therefore, past studies have focused on the development of lightweight aggregate concrete (LWAC) using various lightweight materials such as bottom ash, waste Calicut tiles, coconut shells and fibers, wood waste, recycled plastic, expanded polystyrene, and sludge. However, most past research on the development of lightweight aggregate concrete focused on directly replacing locally accessible lightweight materials. Furthermore, no more studies were done on the development of lightweight aggregate concrete by using converted lightweight aggregates from locally accessible lightweight materials. Therefore, this study was focused on developing lightweight aggregate concrete mix designs with locally available lightweight materials. Sludge derived from the water treatment plant, Expanded Polystyrene (EPS), and waste Calicut tiles were used as lightweight materials to develop lightweight aggregate concrete. Sludge obtained from water treatment plants was fired at 1050 °C for 6–8 h to convert it into lightweight aggregate while waste Calicut tiles were mechanically crushed to convert it into lightweight aggregate. Furthermore, mineral admixtures such as fly ash and silica fume were added to improve lightweight concrete's fresh and hardened properties. It is observed that the unit weight of the developed lightweight aggregate concrete was in the range of 1130–2280 kg m^{-3}. The 28-day compressive strength of concrete ranges from 3.9 to 44.8 MPa for sludge and EPS-based lightweight concrete respectively. Due to the lower unit weight and compressive strength, sludge-based concrete mix designs can be used for non-loadbearing structural elements in multi-story, which reduces the total deadweight of the structure.

Keywords Calicut tile · Compressive strength · Concrete unit weight · Expanded polystyrene · Lightweight aggregate · Sludge

R. W. P. K. Rupasinghe (✉) · K. M. C. Konthesingha · H. M. S. C. Rathnasiri · I. R. Upasiri · W. P. H. P. Weerasinghe
Department of Civil Engineering, University of Sri Jayewardenepura, Ratmalana, Sri Lanka
e-mail: wasana.p.k.rupasinghe2021@gmail.com

S. M. A. Nanayakkara
Department of Civil Engineering, University of Moratuwa, Katubedda, Sri Lanka

© The Author(s), under exclusive license to Springer Nature Singapore Pte Ltd. 2023

R. Dissanayake et al. (eds.), *ICSBE 2022*, Lecture Notes in Civil Engineering 362,
https://doi.org/10.1007/978-981-99-3471-3_12

1 Introduction

The acceleration trends in the construction of multi-story buildings have increased during the last few centuries around the world because of the scarcity of land in urban areas [32]. However, the construction of multi-story buildings is now burdened by a major issue with changes in structural materials. Additionally, the dead load of the multi-story building has risen to be a significant factor during the design phase. Therefore, the demand for lightweight concrete in different applications in modern construction increased concerning the lower weight characteristics. The lower weight of the lightweight concrete provides a significant advantage to minimize the dead weight of structural elements and a corresponding reduction in the size of the foundation.

Lightweight concrete is available in a range of compositions, textures, and performances attributed to suit a wide range of applications [28]. It is divided into three types based on its production method: lightweight aggregate concrete, aerated concrete, and no-fine concrete. Low-specific gravity aggregates, natural or artificial, are utilized in lightweight aggregate concrete. Furthermore, volcanic activity is the source of most natural lightweight aggregates. Pumice, diatomite, scoria, and volcanic cinders are a few different lightweight aggregates with volcanic origins [25]. Alternative natural lightweight aggregates, which extended beyond the volcanic-based lightweight aggregates, were investigated in previous studies.

Alternate lightweight materials have been investigated due to the ongoing depletion of natural resources, the inaccessibility of materials produced by volcanic activity, and an unanticipated increase in the cost of raw materials. Most of the studies conducted globally focus on substitutes for lightweight aggregate concrete, including recycled plastics, PET bottles, bottom ash, rice husk, palm oil, coconut shells, sludge, brick chips, and waste ceramic tiles. Furthermore, the use of EPS in the production of lightweight concrete has piqued the interest of numerous researchers. Mandlik et al. [24], Andrea et al. [6], Tayal et al. [30], Herki et al. [15], and Daniela et al. [8] investigated the use of EPS in lightweight concrete in a variety of approaches. A combination of multiple possible aggregates was studied to compare the lightweight concrete production performance improvement. Most studies, including Zhang and Poon [36] and Kou and Poon [21], have studied the use of bottom ash as a lightweight aggregate. Mueller et al. [26] studied brick chips as a coarse aggregate to evaluate the performance of lightweight aggregate concrete and compare the performance of fiber addition variations. Water treatment sludge and sewage sludge are other alternative materials to lightweight aggregate concrete. Furthermore, Tay and Yip [29], Xie et al. [33], Yip and Tay 35, Jamshidi et al. [17], Ahmad et al. [3], and Yang et al. [34] investigated the derivation of aggregates from sludge and applicability of sludge replacement with different methods in lightweight concrete. Similarly, the goal of many investigations was to find alternative lightweight aggregates in a global context.

In contrast, Sri Lanka lacks both the resources for producing manufactured lightweight aggregates and converting naturally occurring lightweight materials to

lightweight aggregates. The majority of studies in Sri Lanka focus on replacing materials, either fully or partially, with waste products such as expanded polystyrene, recycled plastic, wood waste, waste ceramic tiles, and coconut fibers and shells. However, the development of lightweight aggregate concrete has some shortages compared to aerated concrete and no-fine concrete in Sri Lanka. Even though most of the studies focused on the production of aerated or no-fine concrete, there are plenty of naturally occurring lightweight material resources getting collected as waste to the environment without any advantage. Therefore, considerable attention should be given to developing lightweight aggregate concrete using lightweight material resources in Sri Lanka. Therefore, this study has attempted to develop a lightweight concrete mix using lightweight aggregates that are available locally, which will be a great alternative for the construction industry.

This paper is organized into six sections, with Sect. 1 providing an outline of the proposed study. The production of lightweight aggregates from selected locally available lightweight materials is described in Sects. 2 and 3. The development of lightweight concrete mixes is described in Sect. 4, and Sect. 5 describes the findings of the proposed study. Furthermore, Sect. 5 discusses the results of the developed lightweight aggregate concrete mixes in terms of workability, wet/dry densities, and compressive strength. Section 6 draws the conclusions and future directions of the present study.

2 Selection of Lightweight Materials

To develop a lightweight concrete mix using locally available lightweight aggregates, it is vital to understand past studies related to lightweight aggregate concrete. As a result, the resources of lightweight materials explored in previous studies are primarily agricultural waste, industrial by-products, and other naturally occurring resources. Ahmad et al. [2], Alsarayreh et al. [5], Gunasekaran et al. [12], and Agrawal et al. [1] are a few past studies that developed different agricultural waste as lightweight materials. Furthermore, industrial by-products such as bottom ash, water treatment plant sludge, sewage sludge, PET bottles, EPS, and waste tiles are introduced as lightweight materials by Huang and Wang [16], Lynn et al. [23], Zhang and Poon [36], Franus et al. [10], Ayati et al. [7] and Akçaözoğlu et al. [4]. In the Sri Lankan context, the appropriateness and feasibility of using different types of lightweight material resources are studied by Gamage and Tharmarajah [11], Hansika and Nanayakkara [13], Hendawitharana and Nanayakkara [14], Kumuthini [22], Pallewatta et al. [27], Costa et al. [9], and Tharshika et al. [31].

Thus, a key component of the present study is the selection of alternative lightweight materials to produce lightweight aggregate concrete. However, before selecting an alternate material for lightweight aggregate concrete, it is important to determine its appropriateness and unique characteristics. Based on their unit weight and availability, lightweight materials are selected while addressing the current prob-

Fig. 1 Selected lightweight materials: **a** water treatment sludge, **b** waste EPS, **c** waste Calicut tiles

lems along with material disposal. Sludge from a water treatment plant (Fig. 1a), EPS (Fig. 1b), and waste Calicut tile (Fig. 1c) are selected as lightweight materials in this study.

Water treatment sludge is a porous mass material with good thermal insulation and low thermal conductivity. Despite its characteristics, landfilling continues to be the most common way to dispose of sludge. Most environmental problems are a result of improper disposal practices. However, previous research has shown that sludge can be reused as a construction material. Additionally, it can be utilized in various forms as coarse or fine aggregates in the manufacturing of concrete. Calicut tiles offer possible substitutes for their use as a coarse aggregate in concrete and are water-resistant, durable, and relatively dense when compared to other clay-based waste products. However, the production of Calicut tiles generates a large amount of waste, and because of the considerable dust produced, disposing of that material poses a problem for the environment. Furthermore, EPS has a closed-cell structure with high thermal insulation and low water absorption. It is employed in a variety of fields as a packaging or insulating material, and a large volume of EPS is used and disposed of as waste. Therefore, the above-described three lightweight materials are used to produce lightweight aggregates using different techniques as discussed in Sect. 3.

3 Production of Lightweight Aggregates

Possible approaches and techniques to produce lightweight aggregates from the selected lightweight materials can be determined based on prior research, and it is essential to look into the drawbacks of these techniques. In this study, the proposed methods include mechanical crushing, heat treatment, and firing processes based on past studies.

Fig. 2 Firing process: **a** the initial state of the firing of aggregates, **b** after 2 h—start the firing process, **c** after 4 h—starting the firing process

3.1 Sludge-Based Lightweight Aggregates

The water treatment sludge collected from Biyagama and Kurunegala plants was dewatered in the air until it reached the appropriate moisture content to a workable state. The air-dried sludge was crushed into small parts before the firing process. Brick making kiln process is identified most suitable firing process for dewatered sludge according to past studies [35].

Three stages were followed in this firing process: the firing stage, the cooling stage, and the removal stage. Firing pottery was made by using bricks and clay materials. Furthermore, continuous firing for 6–8 h was supplied in the firing process (Figs. 2 and 3) and approximately 1050 °C amount of temperature was supplied.

The pottery was completely sealed using clay components during the cooling stage, which lasted from 12 to 16 h (Fig. 4). Due to the residual burned fuel inside the pottery, the cooling stage began a few hours after the firing process.

Sludge aggregates from fully opened pottery were collected at the end of the firing process. Brownish sludge aggregates were seen (in Fig. 5) and subjected to the grading and breaking down processes.

3.2 EPS-Based Lightweight Aggregates

According to prior research, there are three different ways to make waste EPS aggregates. Volume reduction by heat treatment was chosen for this study. Figure 6 depicts the modification process of waste EPS into lightweight aggregates. Different cubic samples were prepared for the EPS modification process such as 15 × 15 × 15 mm, 25 × 25 × 25 mm and 50 × 50 × 50 mm.

Fig. 3 Firing process: **a** after 6 h—start the firing process, **b** after 8 h—start the firing process, **c** after 8 h—covered pottery

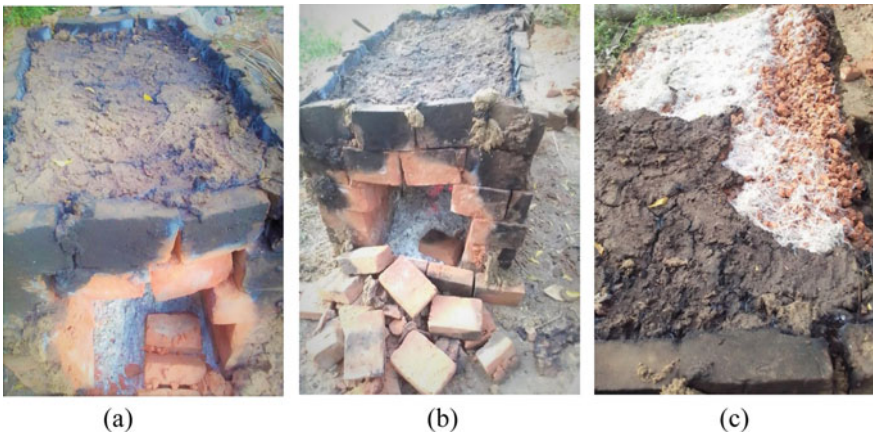

Fig. 4 Cooling process: **a** half-opened pottery after 12 h of cooling, **b** full opened pottery after 12 h of cooling, **c** removing the outside cover of clay—pottery

Fig. 5 Aggregates derived from the water treatment plant's sludge

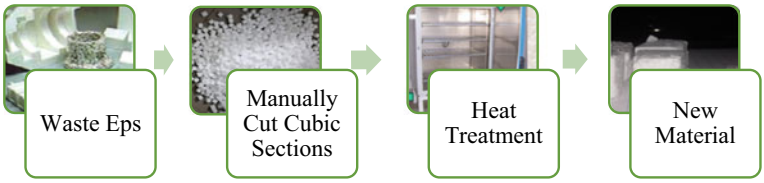

Fig. 6 Process of EPS aggregate production

All EPS samples were exposed to 130 °C temperature for 15 min in a digitally controlled oven [19]. Finally, the volume of all samples was reduced with this heat treatment. The final hard and brittle surface texture was observed in modified EPS aggregates. However, both Modified EPS aggregates (MEP) and unmodified EPS aggregates (UMEP), are used in this study.

3.3 Calicut-Based Lightweight Aggregates

To manufacture alternative lightweight aggregates from waste Calicut tiles, the mechanical crushing method was used in this study. The crushed waste Calicut tiles are shown in Fig. 7.

4 Development of Lightweight Concrete Mixes

Lightweight aggregate concrete mix designs are developed with selected water/cement ratios and fly ash content. OPC cement, 19 mm coarse aggregate, manufactured sand, fly ash, silica fume, and admixtures such as superplasticizer, stabilizer, and air entertainer are used in this study.

Fig. 7 Mechanically crushed waste Calicut tiles

Table 1 Mix proportions—sludge-based lightweight aggregate concrete

MIX DESIGN—sludge-based lightweight concrete—0.5 W/C						
Mix	Cement (kg m^{-3})	Water (kg m^{-3})	Fine (kg m^{-3})	Coarse (kg m^{-3})	Fly ash (kg m^{-3})	Total weight (kg m^{-3})
SLWC 1	270	135	469	454	30	1358
SLWC 2	270	135	497	454	30	1386

4.1 Sludge Based Lightweight Aggregate Concrete Mix Design

In this mix design, derived sludge-based lightweight aggregates are used as both coarse and fine aggregates with two different percentages. Furthermore, the coarse aggregate percentage was maintained equally in both designs and only the fine aggregate percentage varied. SLWC 1 represents the coarse fine aggregate ratio of 0.68:0.68 and SLWC 2 represents the coarse fine aggregate ratio of 0.68:0.75 as mentioned in Table 1.

4.2 EPS Based Lightweight Aggregate Concrete Mix Design

Three different concrete mixes are designed with modified EPS aggregates and unmodified EPS aggregates. Unmodified EPS-based two mixes are done with and without silica dust. Furthermore, UME is designed with unmodified EPS aggregates and UMES is designed with unmodified EPS aggregates with the addition of silica dust. Modified EPS (ME) was also considered. Mix proportions of each mix are shown in Table 2.

Table 2 Mix proportions—EPS-based lightweight aggregate concrete

MIX DESIGN-EPS-based lightweight concrete—0.45 W/C							
Mix	Cement (kg m^{-3})	Water (kg m^{-3})	M-sand (kg m^{-3})	EPS (kg m^{-3})	Silica dust (kg m^{-3})	Fly ash (kg m^{-3})	Total weight (kg m^{-3})
UME	351	158	457	10.4	0	39	1015.4
ME	351	158	457	10.4	0	39	1015.4
UMES	351	158	457	10.4	26.3	39	1041.7

Table 3 Mix proportions—Calicut tile-based lightweight aggregate concrete

MIX DESIGN—Calicut-based lightweight concrete—0.5 W/C							
Mix	Cement (kg m^{-3})	Water (kg m^{-3})	Coarse (kg m^{-3})	Calicut tiles (kg m^{-3})	Fine (kg m^{-3})	Fly ash (kg m^{-3})	Total weight (kg m^{-3})
NC-1	391.5	196	1037.5	0	662.5	43.5	2331
CTA1	391.5	196	0	503.31	662.5	43.5	1969
CT50	330	207.9	935	467.5	467.5	33	1505.9

4.3 Calicut Tile-Based Lightweight Aggregate Concrete Mix Design

Full replacement of Calicut (CTA1) and 50% replacement of Calicut (CTA50) mixtures were designed under Calicut-based LWAC. However, a control mix design (NC-1) was also developed as in Table 3.

5 Results and Discussion

Properties of the aggregate, fresh, and hardened properties of concrete were evaluated through an experimental process and the results are described below.

5.1 Suitability of Lightweight Aggregates

Grading (Fig. 8) and bulk density properties were evaluated as fundamental requirements in this study, which utilized mechanically crushed waste Calicut tiles, sludge, and manufactured sand. Compacted bulk density was identified according to ASTM 29. The bulk densities of the main aggregates are shown in Table 4.

5.2 Variation of Workability

A high slump value was observed with EPS-based lightweight aggregate concrete mix proportions compared to 8 mixes. Figure 9 shows the sludge-based LWAC's slightly lower slump values as compared to the EPS-based LWC.

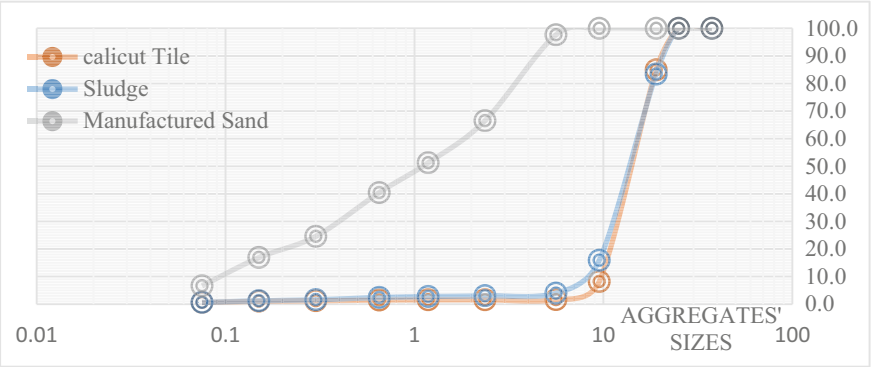

Fig. 8 Aggregate gradation

Table 4 Bulk densities of aggregates

Type of material	Bulk density (kg^{-3})
Sludge	667
Calicut tile	1043
M sand	1950

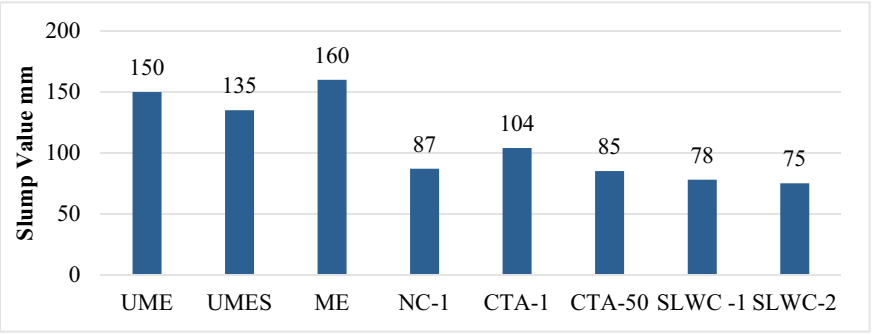

Fig. 9 Slump values variation of mixed proportions

5.3 Variation of Wet/Dry Density

Concerning the dry and wet density fluctuation of all casted mix proportions (Fig. 10), the lowest densities were exhibited with EPS-based lightweight aggregate concrete mix proportions, while the maximum densities were presented with Calicut-based lightweight aggregate concrete mix proportions.

Furthermore, added silica dust mix (UMES) showed a high-density value rather than UME lightweight concrete mix. Sludge-based lightweight aggregate mix proportions showed slightly high densities than EPS-based LWAC. Figure 10 shows

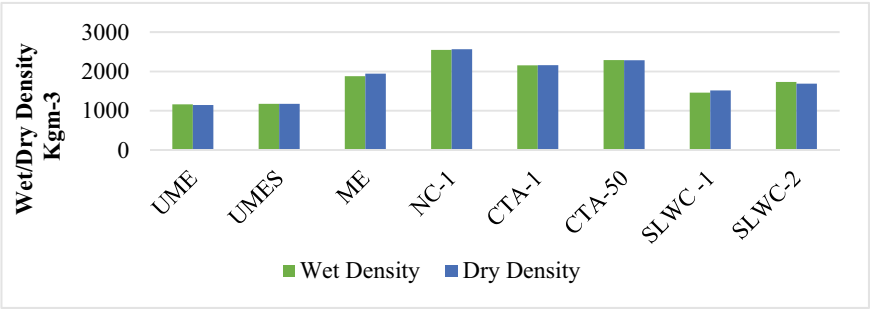

Fig. 10 Wet and dry densities variation of mixed proportions

a slight variation of dry density in the tested two types of sludge-based lightweight aggregate mix proportions.

5.4 Variation of Compressive Strength

The compressive strength of developed lightweight aggregate concrete mixes is shown in Fig. 11. Lower compressive strength values are presented for EPS-based and sludge-based LWAC mix proportions. Calicut-based lightweight mix proportions have slightly higher compressive strength.

For non-structural purposes, EPS-based LWAC and sludge-based LWAC mix proportions are suitable with the lower compressive strength, while Calicut-based LWAC is suitable for structural applications due to the higher compressive strength.

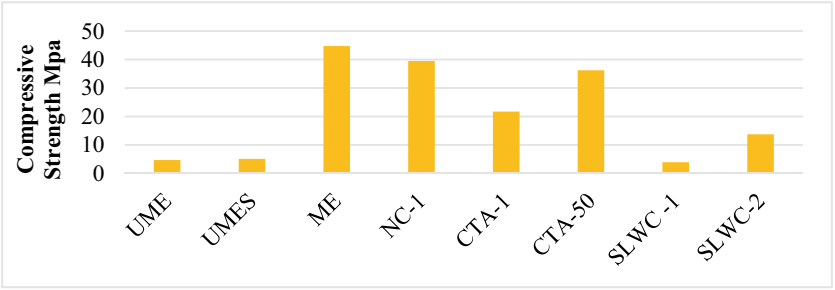

Fig. 11 Compressive strength variation of mixed proportions

6 Conclusions and Future Directions

Based on the present study, the following conclusions are drawn.

1. Sludge-based lightweight concrete mix proportions show lower compressive strength and thus, it can be used for non-structural building components.
2. Unmodified EPS-based lightweight concrete mix proportions show lower density (1100–1200 kg $m^{-3)}$ and compared to modified LWC, modified EPS-based lightweight concrete mix design shows high density with a high compressive strength value.
3. Furthermore, with the addition of supplementary cementitious material: fly ash, and silica dust to the mix design, within 28 days, an increment in the compressive strength can be observed.
4. Waste Calicut-based lightweight concrete mix proportions show high densities compared to EPS-based LWC and sludge-based LWC.

In this study, sludge-based lightweight aggregates are produced by using clay pottery. Further development can be done with furnace incineration and ball mill machine in the large-scale production process. Furnace incineration provided more facilities to develop aggregates under various temperatures and pressure values. Lightweight aggregate concrete mixes show lower compressive strength due to the porous nature of the materials. Therefore, supplementary cementitious materials can be used to develop high compressive strength values. However, in this study fly ash and silica dust are used in EPS-based lightweight concrete mixes. So, developed lightweight concrete mixes can be further developed with the addition of supplementary cementitious materials.

References

1. Agrawal AR, Dhase SS, Agrawal KS (2014) Coconut fiber in concrete to enhance its strength and making lightweight concrete. Int J Eng Res Dev 9(8):64–67
2. Ahmad R et al (2017) Feasibility study on the use of high-volume palm oil clinker waste in environmentally friendly lightweight concrete. Constr Build Mater 135:94–103. https://doi.org/10.1016/j.conbuildmat.2016.12.098
3. Ahmad T, Ahmad K, Alam M (2016) Characterization of water treatment plant's sludge and its safe disposal options. Procedia Environ Sci 35:950–955. https://doi.org/10.1016/j.proenv.2016.07.088
4. Akçaözoğlu S, Atiş CD, Akçaözoğlu K (2010) An investigation on the use of shredded waste PET bottles as aggregate in lightweight concrete. Waste Manage 30(2):285–290. https://doi.org/10.1016/j.wasman.2009.09.033
5. Alsarayreh AIM et al (2020) Experimental investigation on structural lightweight aggregate concrete using palm-oil clinker and expanded perlite aggregates. J Eng Sci Technol 15(6):3741–3756
6. Andrea P, Mundo RD, Michele N (2020) Recycled expanded polystyrene as lightweight aggregate for environmentally sustainable cement conglomerates. 13
7. Ayati B et al (2019) Manufacture and performance of lightweight aggregate from waste drill cuttings. J Clean Prod 208:252–260. https://doi.org/10.1016/j.jclepro.2018.10.134

8. Daniela GB, Edgar ARG, Gil H (2019) Characterization and evaluation of lightweight fly ash concrete modified with EPS. Int J Civ Eng Technol 10(08)
9. De Costa MBM et al (2017) Use of waste coconut shells as substitute for coarse aggregate in light-weight concrete mixes. 1–5
10. Franus M, Barnat-Hunek D, Wdowin M (2016) Utilization of sewage sludge in the manufacture of lightweight aggregate. Environ Monit Assess 188(1):1–13. https://doi.org/10.1007/s10661-015-5010-8
11. Gamage DN, Tharmarajah G (2008) Lightweight non-load bearing blocks using expanded polystyrene bead
12. Gunasekaran K, Annadurai R, Kumar PS (2013) Study on reinforced lightweight coconut shell concrete beam behavior under shear. Mater Des 50:293–301. https://doi.org/10.1016/j.matdes.2013.03.022
13. Hansika H, Nanayakkara A (2019) Investigation on properties of cellular lightweight concrete blocks with bottom ash. In: 2019 Moratuwa engineering research conference (MERCon), Moratuwa, Sri Lanka, 3–5 July 2019. IEEE, pp 424–429. https://doi.org/10.1109/MERCon.2019.8818756
14. Hendawitharana SU, Nanayakkara SMA (2018) Use of bottom ash from coal fired thermal power plants in production of cellular lightweight concrete
15. Herki BA, Khatib JM, Negim EM (2013) Lightweight concrete made from waste polystyrene and fly ash. World Appl Sci J 1356–1360. ISSN 1818-4952
16. Huang CH, Wang SY (2013) Application of water treatment sludge in the manufacturing of lightweight aggregate. Constr Build Mater 43:174–183. https://doi.org/10.1016/j.conbuildmat.2013.02.016
17. Jamshidi A, Mehrdadi N, Jamshidi M (2011) Application of sewage dry sludge as fine aggregate in concrete. J Environ Stud 37(59)
18. JiaHao L et al (2019) Study of properties and strength of no-fines concrete. IOP Conf Ser: Earth Environ Sci 357:12009. https://doi.org/10.1088/1755-1315/357/1/012009
19. Kan A, Demirbog R (2009) A new technique of processing for waste-expanded polystyrene foams as aggregates. J Mater Process Technol 209(6):2994–3000. https://doi.org/10.1016/j.jmatprotec.2008.07.017
20. Kim HM et al (2017) Overview of supplementary cementitious materials usage in lightweight aggregate concrete. Constr Build Mater 139:403–418
21. Kou S-C, Poon C-S (2009) Properties of concrete prepared with crushed fine stone, furnace bottom ash and fine recycled aggregate as fine aggregates. Constr Build Mater 23(8):2877–2886. https://doi.org/10.1016/j.conbuildmat.2009.02.009
22. Kumuthini A (2015) Management practices of water treatment sludge in Sri Lanka and reuse potential of sludge as a construction material
23. Lynn CJ et al (2015) Sewage sludge ash characteristics and potential for use in concrete. Constr Build Mater 98:767–779. https://doi.org/10.1016/j.conbuildmat.2015.08.122
24. Mandlik A et al (2015) Lightweight concrete using EPS. 4(3)
25. Mohammed JH, Hamad AJ (2014) Materials, properties and application review of lightweight concrete. 37:10–15
26. Mueller A, Schnell A, Ruebner K (2015) The manufacture of lightweight aggregates from recycled masonry rubble. Constr Build Mater 98:376–387. https://doi.org/10.1016/j.conbuildmat.2015.07.027
27. Pallewatta TM, Dissanayake WDSH, Dembatapitiya BRKC (2013) Calicut tile waste as an alternative coarse aggregate for lower grade concretes. J Eng Technol Open Univ Sri Lanka (JET- OUSL) 1:51–62
28. Singh NT (2016) Effective uses of light weight concrete. 3(3):208–211. www.researchgate.net/publication/309680177
29. Tay J-H, Yip W-K (1989) Sludge ash as lightweight concrete material. J Environ Eng 115
30. Tayal A et al (2018) Lightweight concrete using recycled expanded polystyrene beads. Int Res J Eng Technol 05(05)

31. Tharshika S, Thamboo JA, Nagaretnam S (2019) Incorporation of untreated rice husk ash and water treatment sludge in masonry unit production. Sustain Environ Res 1(1):1–10. https://doi.org/10.1186/s42834-019-0010-y
32. Wood A (2011) Trends, drivers and challenges in tall buildings and urban habitat. IABSE Congr Rep 17(29):126–133. https://doi.org/10.2749/222137908796219336
33. Xie J, Liu J, Liu F, Wang J, Huang P (2019) Investigation of a new lightweight green concrete containing sludge ceramsite and recycled fine aggregates. J Clean Prod 235:1240–1254. https://doi.org/10.1016/j.jclepro.2019.07.012
34. Yang H-C, Wang J-P, Wu J-W (2012) Mixed proportion design of lightweight concrete using the sludge kilned coarse aggregate from reservoir. 430–432:602–608
35. Yip W-K, Tay J-H (1990) Aggregate made from incinerated sludge residue. J Mater Civ Eng 02(02)
36. Zhang B, Poon CS (2015) Use of furnace bottom ash for producing lightweight aggregate concrete with thermal insulation properties. J Clean Prod 99:94–100. https://doi.org/10.1016/j.jclepro.2015.03.007

Assessment of Heat of Hydration of High-Strength Concrete

S. A. P. Madusanka and H. D. Yapa

Abstract Even though Ordinary Portland Cement (OPC) concrete has been studied for decades, the hydration process of OPC and blended cement are still a source of scientific controversy. The process of hydration is highly complicated as it is combined with various influencing factors on hydration kinetics, dissolution, and precipitation reactions. Since cement hydration is an exothermic process, the low conductivity of concrete leads to an accumulation of heat in the core of the structure. Therefore, a huge temperature gradient will propagate and cause crucial internal cracking. Even though the propagation of thermal cracks is inevitable, it is indispensable to control temperature development. Hence forecasting the heat evolution is extremely vital. One of the major predominant parameters of early temperature assessment in each concrete structure is its rate of heat of hydration. Although several experimental methods were employed towards the assessment of heat propagation, upgraded analytical approaches also provide better predictions on quantifying the temperature development and heat generation rate of the structure relevant to the given mix proportion. However, there is a dearth of existing data to expand these analytical models in the case of high-strength concrete with different SCM blends. In this light, the conduction of semi-adiabatic experiments to expand the existing databases of the heat of hydration on high-strength concrete mixes and the effect of using silica fume as a supplementary cementitious material was discussed in this context. The increase in silica fume content and carboxylic admixture concentration lengthen the period of dormancy, and the peak temperature rise is directly correlated with binder content, according to the results. Although the FEA approaches provide a good correlation with normal-strength concrete, analytic models for high-strength concrete must be amended.

Keywords Heat of hydration · Semi-adiabatic · High strength concrete · Silica Fume · Maturity

S. A. P. Madusanka (✉) · H. D. Yapa
Department of Civil Engineering, University of Peradeniya, Peradeniya 20400, Sri Lanka
e-mail: arunamadusanka1229@gmail.com

© The Author(s), under exclusive license to Springer Nature Singapore Pte Ltd. 2023

R. Dissanayake et al. (eds.), *ICSBE 2022*, Lecture Notes in Civil Engineering 362,
https://doi.org/10.1007/978-981-99-3471-3_13

Nomenclature

t_{20}	Maturity time
E	Activation energy parameter
R	Universal Gas Constant
T_i	Temperature at *i*th time interval
T	Time
FA	Fly Ash
SF	Silica Fume
C–A–S–H	Ettringite
C–S–H	Hydrated calcium silicates
T_G	Adiabatic temperature
T_V	Volumetric
T_p	Placing temperature
T_s	Surface temperature
λ	Coefficient associated with heat loss

1 Introduction

As the leading binder of concrete, cement mainly comprises C_3A(Aluminate), C_4AF(Ferrite), C_3S(Alite), and C_2S(Belite) clinker materials. The hydration of these interstitial compounds is responsible for heat development during the setting and in the initial hardening period. This exothermic behavior is incorporated with three major stages [5, 11]. Firstly the early exothermic flash is caused by aluminate which combines with water and sulfate to form a gel-like material of C–A–S–H. While C–A–S–H builds up around the grains, a gradual decrease of water infiltration and therefore, control of aluminate reaction occurs. This was followed by a period of dormancy which was responsible for a little amount of heat and physical change to the mix and lasted about 2–4 h. Meantime, the accumulation of $(OH)^-$ and Ca^{2+} can be seen in the solution due to the dissolving of C_3S and C_2S. After the super-saturation of the solution with Ca^{2+}, a coating layer of C–S–H and ettringite tends to form. In the latter, the permeability of the coating layer increases and enhances the incidence of particle collisions and moves to the second exothermic peak as stage two. Consequently, due to the continuous process of hydration, the thickness of the hydrated layer increases, and it dominates the diffusion of ions towards the un-hydrated particles. Eventually, a gradual decrease in heat propagation is apparent in stage three.

These heat propagation curves can be altered, though, by utilizing various admixtures of various SCMs. The use of supplementary cementitious material become extensively popular in concrete production to achieve sustainability, durability, and better mechanical properties. Silica Fume, Fly Ash, Blast Furnace Slag, Natural Pozzolanic material, burnt clays, and other natural pozzolanic materials are some

popular SCMs. In mass concretes the use of blended cement with Blast Furnace Slag and Fly ash is extensively popular while silica fume and fly ash are underway for decades when producing high-strength concretes. However, at normal temperatures, the reactivity of FA is at of minor level for about a week after starting off the hydration process and results in a low early strength development [6]. However, Silica contains a relatively high surface area with higher pozzolanic reactivity compared to other SCMs, This contributes to the early strength development by producing a considerable amount of C–S–H [3].

The overall heat accumulation and the heat rates can cause various consecutive damages to the existing concrete structure. When it is not produced in large masses, and at normal strength, or when it is produced in cold temperatures, this heat propagation does not significantly impact the durability of the concrete. Anyhow, in cold weather, it is necessary to trap the heat of hydration for a longer period inside the structure to avoid frosting. Nevertheless, this heat accumulation is crucial in the sense of high strength and mass concretes. Since a considerable percentage of cementitious materials is used, herein the temperature increment can be more than 80 °C in high strength. In the meantime, mass concretes are more susceptible to thermal cracking since it has a substantial heat gradient evolved between the core and the outer surface due to high thickness. These heat-induced durability issues can be lessened by using proper heat control techniques or by adjusting the mixture proportions. For that, it is extremely vital to pre-identify the heat propagation rate of a given concrete mixture that combines with different SCMs and admixtures. That heat rate can be used as an input parameter in numerical models to evaluate the temperature variation of a structure on a spatial and temporal basis [1]. Analytical methods like the multi-component model, multi-constituent model, and enhanced hydration model, which drew on the information gathered from experimental models like calorimeter methods and isothermal methods, can be used to assess the heat rate of hydration of a specific mix [4, 5, 7]. The basic difference between calorimeter methods and isothermal methods in experimental approaches is that the latter gives curing conditions that more closely resemble the realistic temperature conditions of a concrete structure.

The use of calorimeter methods, including adiabatic, semi-adiabatic, and conduction calorimeters, to measure the heat of hydration of concrete mixes under in-situ conditions with realistic curing conditions is advantageous as an alternative strategy. Although a semi-adiabatic calorimeter is accompanied by a considerable heat loss allowance of about 100 J/(hr· K), it can be used to predict the adiabatic temperature history of an adiabatic calorimeter which allows not more than 0.02 K/h heat loss by using a proper heat loss compensation technique derived mathematically by [10] as shown in Eqs. 1–3. Meanwhile, Morabito and Barberis [9] developed a concept to evaluate λ by utilizing ta temperature–time curve, when the heat generation has become negligible. At that instance, the adiabatic temperature rise ($\frac{\partial T_G}{\partial t}$) is virtually insignificant and [8] experimentally showed that this phenomenon happens after 120 h of casting (Fig. 1).

$$\frac{\partial T_G}{\partial t} = \frac{\partial T_V}{\partial t} + \lambda(T_S - T_A) \tag{1}$$

$$\lambda = -\left(\frac{\partial T_V}{\partial t}\right)/(T_S - T_A) \tag{2}$$

$$T_G = (T_V - T_P) + \lambda \sum_{i=1}^{n} (T_S - T_A)(t_i - t_{(i-1)}) \tag{3}$$

In the conversion process of semi-adiabatic temperature histories to adiabatic, it is necessary to consider the variation of curing temperature. To maintain the adiabatic state, the calorimeter maintains a negligible temperature difference between the core and surroundings while semi-adiabatic curing happens almost at a constant temperature. To adapt to this difference [2] incorporated a maturity scale instead of a time scale by considering the concrete curing at a reference temperature of 20 °C using Eqs. 4 and 5 which resulted in a contraction of the time axis as shown in Fig. 2. Using the above corrections of heat loss and maturity, it's possible to achieve almost similar adiabatic temperature variations using a semi-adiabatic calorimeter.

$$t_{20} = \sum_{i=1}^{n} \exp\left[\left(\frac{E}{R}\right)\left(\frac{1}{293} - \frac{1}{273 + 0.5(T_i + T_{i-1})}\right)\right](t_i + t_{i-1}) \tag{4}$$

$$t_i = t_{i-1} + \frac{t_{20i} - t_{20(i-1)}}{\exp\left[\left(\frac{E}{R}\right)\left(\frac{1}{293} - \frac{1}{273+0.5\left(2T_p + T_{gi} + T_{g(i-1)}\right)}\right)\right]} \tag{5}$$

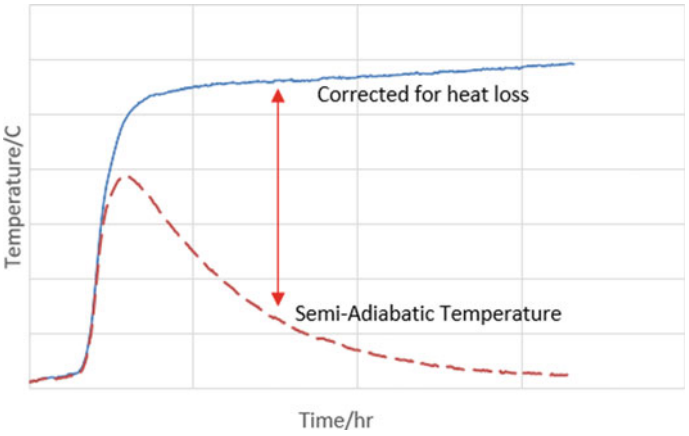

Fig. 1 Semi-adiabatic temperature variation versus time with and without heat loss correction

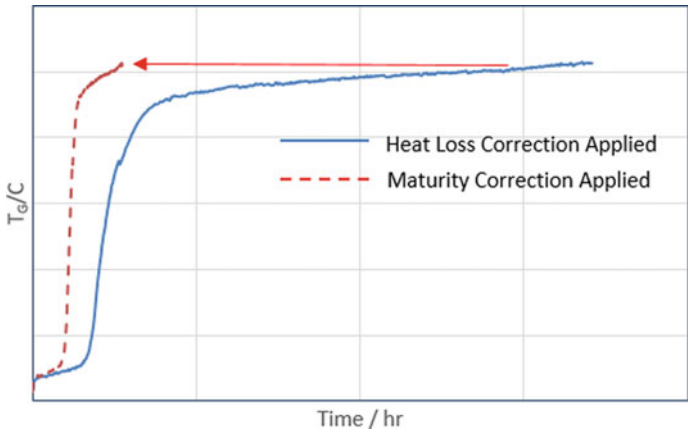

Fig. 2 Maturity correction

It is relevant in this context to conduct semi-adiabatic experiments on high-strength concrete mixtures and forecast adiabatic behavior to establish a database of the rate of the heat of hydration and test the suitability of existing analyses.

2 Selection of Material

2.1 Cement and Silica Fume

Commercially available Portland cement of CEM I confirming EN 197-1 was used in the present study with different fineness. Properties and chemical compositions extracted from X-ray fluorescence analysis are listed in Table 1. Silica fume was added as a partial replacement for cement and used in confirmation with EN 13,263 supplied by "Finco Industries". It was named micro silica 920D and replaced 10% of cement with silica fume. The mix proportions used in concrete mixtures are tabulated in Table 2.

2.2 Aggregates

Locally available natural river sand with a fineness modulus of 2.2 and crushed aggregates with a nominal maximum aggregate size of 20 mm was used as fine and coarse aggregate in the concrete mix proportions. The particle size distribution of aggregates is shown in Fig. 3a and b.

Table 1 Properties of cement and Silica Fume

Properties	Cement		Silica Fume
	Type 1	Type 2	
SiO_2 (%)	28.27	25.46	66.59
Fe_2O_3 (%)	2.42	4.2	1.00
Al_2O_3 (%)	5.94	6.14	–
CaO (%)	53.35	58.0	31.67
MgO (%)	3.0	2.21	0.7
SO_3 (%)	6.31	3.35	–
Fineness (cm^2/g)	4120	3760	–

Table 2 Mix Proportions of Concrete Mixes

Target cylinder strength (N/mm^2)	w/b	Constituent					
		Water (l/m^3)	Cement (kg/m^3)	Sand (kg/m^3)	Granite (kg/m^3)	Superplasticizer (l/m^3)	Silica Fume (kg/m^3)
30	0.54	216	400	648	1024	–	–
60	0.34	142.82	397	799	1075	10.94	44.12
70	0.33	141.82	409	788	1075	11.27	45.45
80	0.29	140.06	478	712	1075	13.74	48.39
90	0.27	140.00	491	706	1075	13.52	53.19

2.3 Water and Admixtures

The carboxylic-type water-reducing admixture was used with 40% solid content to preserve appropriate consistency at a low water-to-cement ratio.

3 Preparation of Calorimeter

Semi-Adiabatic tests were carried out with four grades of high strength and one normal-grade concrete mixture as shown in Table 2. Concretes were mixed using a pan mixer. The thermocouples were interfaced with a computer by a data acquisition system and temperature variation was measured for 150 h (Fig. 4).

The mold itself was a Polystyrene foam cubic box with a side length of 200 mm and a thickness of 20 mm. The concrete was cast into a polyethylene plastic bag which was adhered to the styrofoam mold. To reduce the conduction-type heat loss, it was covered by a 50 mm thick extruded polystyrene box. The gap between the external shell and the mold was filled with styrofoam balls and a schematic arrangement

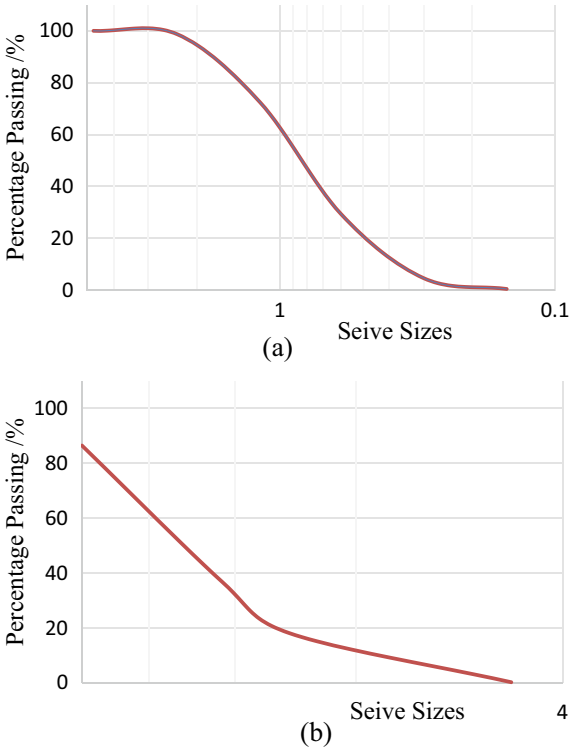

Fig. 3 Gradation curves of **a** Fine aggregate. **b** Coarse aggregate

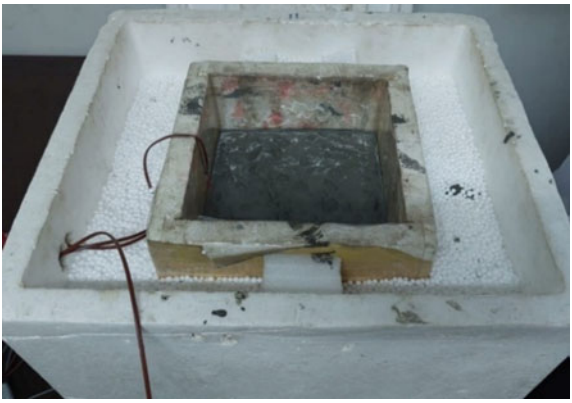

Fig. 4 Calorimeter setup

of the semi-adiabatic calorimeter and the thermo-couple arrangement used in this experimental investigation are depicted in Fig. 5.

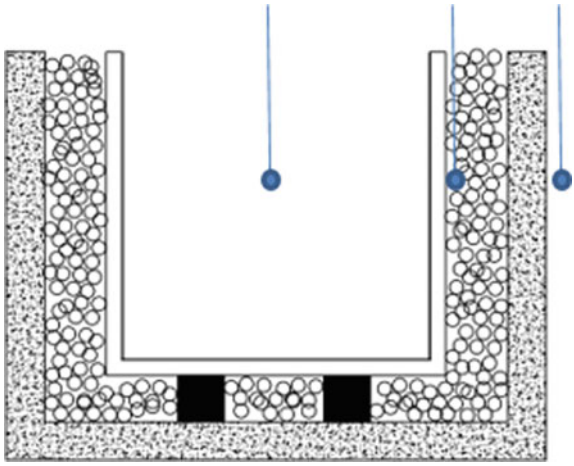

Fig. 5 Schematic Arrangements of Calorimeter Setup and thermocouple locations

4 Results and Discussion

As depicted in Fig. 6, the semi-adiabatic temperature rise is smaller than the diabatic temperature increment owing to the loss of heat with time. However, the temperature-increasing rate to reach the peak is similar for both tests. The heat loss coefficient of the system (λ) was 0.031.

As the strength increase, the ultimate temperature rise tends to move up gradually as depicted in Fig. 6. Although the cement was replaced by 10% by silica fume in all the mixtures, the increment of cementitious material content from 400 kg/m^3 to 500 kg/m^3 along with the reduction of the water-cement ratio, is leading to

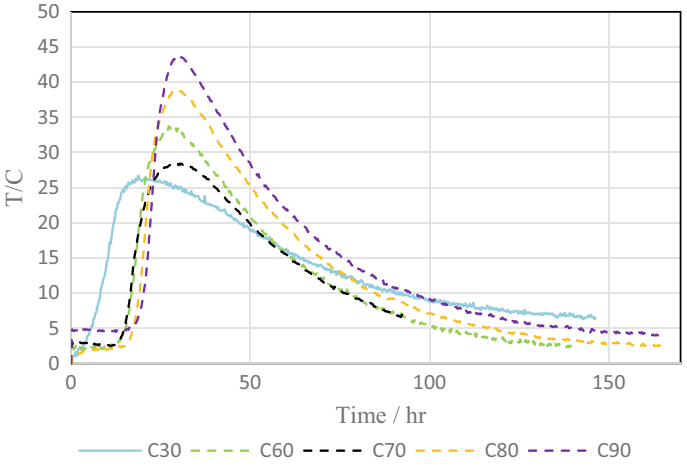

Fig. 6 Semi-adiabatic temperature variation

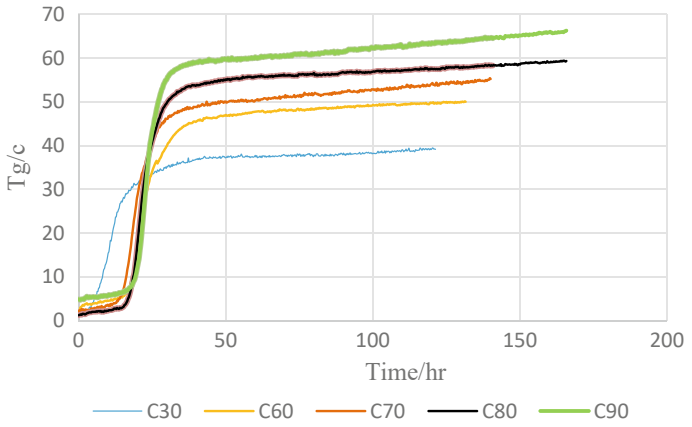

Fig. 7 Adiabatic temperature variation with heat loss compensation (Without maturity correction)

this temperature rise. However, the time taken to reach the peak is increasing with cementitious material content. As shown in the above figure, the SF does not seem to prolong the dormant period but increases the rate of heat evolution in the later stages of the acceleration period. This is similar to the findings of Kesler, (1985). Anyway, after the peak, there is a slight gradient in the temperature and that is due to the continuation of cement hydration. Although the acceleration of reactions is stretched out for high-strength mixtures, the rapid acceleration in the reaction process happens usually within a day for all the samples (Fig. 7).

As the w/c ratio increases, the curves tend to shift in the left direction. Compared to the C30 mix, C60 and higher mixes resulted in longer dormancy periods as shown in Table 3. In the period of dormancy, the dissolution of C_3S and C_2S releases Ca^{2+} and OH^- which increase the alkalinity and ultimately the pH value. As a result of this alkalinity in the Ca^{2+} supersaturated liquid phase, SF accelerated to dissolve and form a silica-rich layer by utilizing CH in the solution and it is in line with the ideas of [6]. Through the creation of extra space in the liquid phase with enhanced alkalinity, acceleration of CH dissolution occurs and consecutively reduces the period of dormancy. But as the w/c ratio decrease from 0.34 to 0.27, it prolongs the dormant period, reduces the rate of the heat of hydration during the acceleration period, and increases the rate after the acceleration period. Thus, the acceleration effect of SF begins earlier as w/c increases.

Moreover, in the hydration of SF, which is about 100 times finer than OPC particles, agglomerates around cement grains and forms a diffusive layer to CH ions in a matter of minutes after mixing. But also this effect of the formation of a substrate layer enclosed with a water lamina around the cement grain. And ultimately, this phenomenon resulted in rapid water consumption and a reduction of workability. However, this free water reduction is crucial in the sense of low w/c concretes. Further, the adsorption of SF particles will not produce water that enriches the substrate and cause a retarding effect in low w/c concretes. Nevertheless, this retarding effect is not

Table 3 Variation of dormant periode with w/c ratio

Target strength (cube)	w/c	Dormant period (hr.)
C30	0.54	3.25
C60	0.34	15
C70	0.33	17.25
C80	0.29	17.5
C90	0.28	19

much significant in the normal-strength concrete mix where the w/c ratio is higher. To mitigate the rapid loss of workability, it's important to use superplasticizers in high-strength mixtures. Nonetheless, these plasticizer molecules are also responsible for the process of hydration retardation as resulted in Table 3. Adsorption of carboxylate molecules hinders the dissolution of the clinker phase and impedes further growth of hydration products, especially C–S–H. This result ties well with previous studies of Kadri et al. (2009) wherein the complexation effect between carboxylate groups and multivalent ions causes a deficiency of ions in the aqueous phase, particularly Ca^{2+}, thus ultimately prolonging the hydration process. Other than that, the adsorption of R-COO groups on the surface of the elite alters the growth kinetics and morphology, which leads to considerable retardation. It appears that the interaction is greater when there is a higher concentration of SP present, which causes the hydration to be more retarded as stated by [8].

However, in the adiabatic temperature variations shown in Fig. 8, the maturity for the peak increases with the strength of the concrete. In this adiabatic correction, the curing temperature is adjusted as it is equal to the core temperature. This may lead to high curing temperatures for the mixes with higher cementitious material content. Ultimately the highest maturity is in the mix C80 as it reaches its peak temperature of 56 °C.

Although the peak occurring time is almost the same for both samples, the dormant period shows slight advancement in the cement type 1 concrete mixture as shown in Fig. 9. The degree of hydration and the rate of heat evolution in a particular concrete mixture are both strongly correlated with the fineness of cementitious materials. The higher specific area is known to encourage cement dispersion and speed up the process of reactions in the early hours, especially during times of initiation and growth control hydration. A similar conclusion about the effect of cement fineness for cement with the same source and mineralogy was reached by [12]. Moreover, the formation of calcium hydroxide during the first few hours of hydration is less than that in the finer cement but exceeds after 7 days. This is to be expected, as more surface area is available for reaction in finer cement. That depicts the effect of cement fineness on hydration kinetics, which dominates the reaction during the early stages of hydration.

Although the fineness measured from the air permeability apparatus is greater in type 2 cement, due to different mineralogy, particularly the higher percentage of C_3S and C_2S in cement type 1, leads to an increasing temperature rise, as depicted in Fig. 4. Even though type 1 cement concrete shows a long dormancy period, the

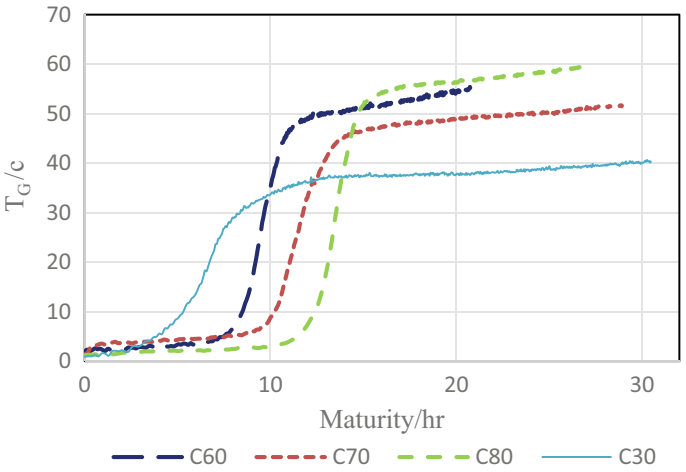

Fig. 8 Adiabatic temperature variation with maturity

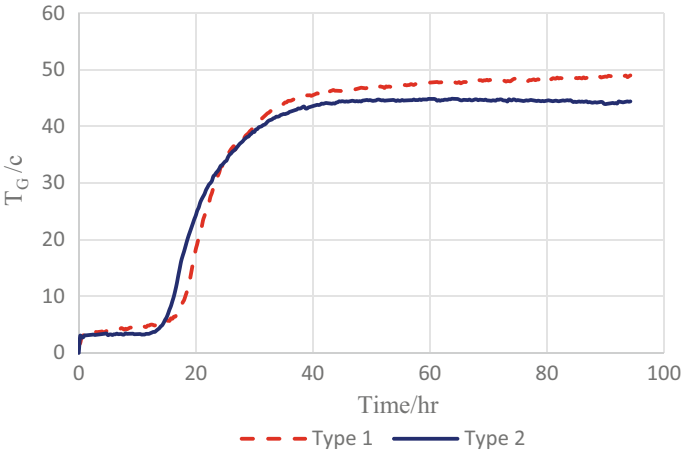

Fig. 9 Variation of temperature rise with cement types

adiabatic temperature rise surpasses type 2 cement at around the 26th hour after mixing, which might be due to a higher C_3S content with considerable fineness.

The majority of FEA programs, including ANSYS, MIDAS GEN, LUSAS, and Concrete Works, include the ability to manage the heat of hydration of the concrete structures. By differentiating the equation for adiabatic temperature rise and multiplying the specific heat and density of the concrete, MIDAS GEN allows the internal heat generation to be expressed in terms of unit time and volume. The adiabatic temperature variation used is a simple exponential function of maximum adiabatic temperature rise (K), Response speed (α), and time(t) in days as shown in

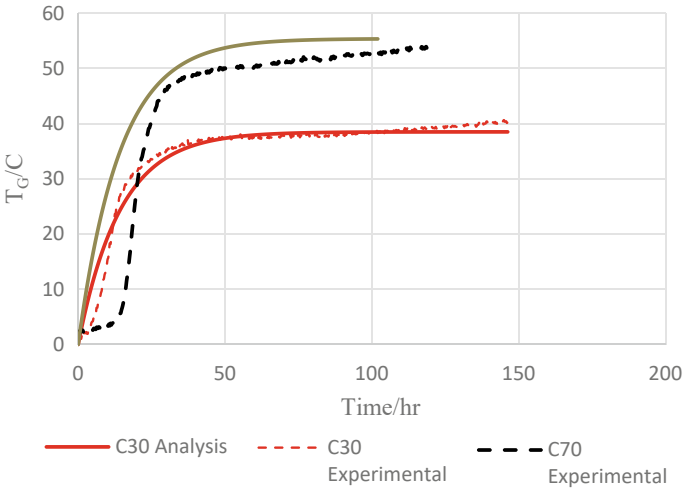

Fig. 10 Comparison of experimental data with MIDAS GEN heat source functions

the following equation. Although it shows a considerable variation in heat rate in the Grade 30 mixture due to limited inputs of interdependency parameters among reactions, it offers better correlation compared to high-strength mixtures as shown in Fig. 10.

$$F(t) = K * (1 - e^{-\alpha t}) \tag{6}$$

Modified analytical hydration models are crucial for dealing with high-strength concrete that has been mixed with multiple admixtures and supplementary cementitious materials.

5 Conclusions and Recommendations

- The addition of SF and Superplasticizers prolonged the period of dormancy and cause considerable variations in the concrete mixtures.
- Though fineness matters in heat of hydration, the mineralogy of cement and cementitious materials plays a significant role by affecting the heat rate.
- Total heat generation is a matter of the chemical composition of cement, particle fineness, SCM type, Fineness of SCM particles, Type and dosage of superplasticizer, w/c ratio, and mainly, the cement content.
- Modification in the existing analytical hydration models using these experimental data, to deal with high-strength concrete blended with silica fume is recommended via future work.

Acknowledgements Would like to acknowledge the Postgraduate Program for the financial assistance as well as the assistance provided by the University of Peradeniya Materials Laboratory staff.

References

1. Ballim Y (2004) A numerical model and associated calorimeter for predicting temperature profiles in mass concrete. Cement Concr Compos 26(6):695–703
2. Ballim Y, Graham PC (2003) A maturity approach to the rate of heat evolution in concrete. Mag Concr Res 55(3):249–256
3. Kadri EH, Duval R (2009) Hydration heat kinetics of concrete with silica fume. Constr Build Mater 23(11):3388–3392
4. Kinomura K, Ishida T (2020) Enhanced hydration model of fly ash in blended cement and application of extensive modeling for continuous hydration to pozzolanic micro-pore structures. Cement Concr Compos 114:103733
5. Kishi T, Maekawa K (1995) Multi-component model for hydration heat of Portland cement. Doboku Gakkai Ronbunshu 526:97–109
6. Langan BW, Weng K, Ward MA (2002) 'Effect of silica fume and fly ash on the heat of hydration of Portland cement. Cem Concr Res 32(7):1045–1051
7. Luan Y et al (2012) Enhanced model and simulation of hydration process of blast furnace slag in blended cement. J Adv Concr Technol 10(1):1–13
8. Marchon D, Flatt RJ (2016) Impact of chemical admixtures on cement hydration, science and technology of concrete admixtures. Elsevier Ltd.
9. Morabito P, Barberis F (1993) Measurement of adiabatic temperature rise in concrete. Concrete 2000. Economic and durable Construction through excellence, pp 749–759
10. Ng PL, Ng IYT, Kwan AKH (2008) Heat loss compensation in semi-adiabatic curing test of concrete. ACI Mater J 105(1):52–61
11. Ridi F, Chimica D, Firenze U (2010) Critical reviews hydration of cement. In: Hydration of cement, pp 110–117
12. Yang K et al (2017) Investigation of effects of Portland cement fineness and alkali content on concrete plastic shrinkage cracking. Constr Build Mater 144:279–290

Construction Management

Critical Selection Factors for Contractors to Make Bid/No-Bid Decision in Construction Projects in Sri Lanka

K. M. P. B. G. Dissanayake, P. L. Perera, and K. D. M. Gimhani

Abstract During the tender process, bidders' most crucial task is to decide whether to bid /not to bid and that has a high influence on the long-term performance and profitability of the organization. Bidding for a tender may or may not have the chance of winning the bid and a profit; besides, there is a possibility of waste of time, effect & money for the contracting firm. No bidding decision has less risk of loss of assets but there is no opportunity to grow & earn some profit. The aim of the study is to identify the most crucial variables that influence the contractors' decision for bidding on Sri Lankan construction projects. To investigate the study, a mixed-method research strategy was adopted with semi-structured interviews and a questionnaire survey. From the initial literature review, fifty- six (56) factors were identified & it was reduced to thirty-one (31) factors after conducting 10 expert interviews which aimed to confirm, modify, and amalgamate the identified selection factors. In the second stage, a questionnaire survey was conducted among one hundred twenty (120) different construction professionals to determine the most critical factors for decision-making in the bidding process from the finalized thirty-one (31) factors. Semi-structured interviews were analyzed by using the manual content analysis methods and the most significant selection factors were identified by calculating the Relative Important Index (RII) of selected factors. Size, type and duration of the contract and the project were found to be the most critical selection factors that influence the contractors. The factors which cannot be controlled by the bidders during the bidding stage or the factors that are mandatory in the bidding process for any kind of tender were ranked the lowest critical selection factors. The findings of this study will contribute to the existing knowledge gap that lies upon the contracting firms and the selection criteria for making the bid/no-bid decision. Moreover, this study can be utilized as a base study for other developing nations.

Keywords Bid · Contractors · Construction industry · Critical selection factors · Sri Lanka

K. M. P. B. G. Dissanayake · P. L. Perera · K. D. M. Gimhani (✉)
SLTC Research University, Meepe, Padukka, Sri Lanka
e-mail: malshagimhani63@gmail.com

© The Author(s), under exclusive license to Springer Nature Singapore Pte Ltd. 2023

R. Dissanayake et al. (eds.), *ICSBE 2022*, Lecture Notes in Civil Engineering 362,
https://doi.org/10.1007/978-981-99-3471-3_14

1 Introduction

Alsaedi et al. [1] have stated that contractors secure construction work under two mechanisms. Either through negotiations or by competitive bidding. Making the bidding decisions is one of the most crucial tasks done by contractors as it includes a combined effect of several critical factors [2]. Contracting companies are project-oriented businesses, and the amount of profit they make is proportional to the number of contracts they are granted. As a result, contracting companies have the incentive to bid strategically throughout the bidding process [3]. In the course of the phases of the bidding process, decision-making is an essential aspect to be concerned [4]. Even if the management team of the company is the entity that makes these choices, such decisions are heavily influenced by a variety of external variables, such as the state of the market and the level of competition, as well as the assessment criteria that the owners of the project use.

According to Hanák et al. [5], there are several considerations that contractors need to make before the selection of a project, particularly when they are preparing their bids. The choices that are crucial to the profitability, expansion, and continued existence of construction companies are the ones that are related to the project selection term criteria. The bidding procedure is extremely complicated and ad hoc, necessitating the simultaneous consideration of many factors [6]. Another restriction is having to take all of these things into account in a short period of time [7]. However, opting to bid/no-bid can have a big influence on a contractor's daily work and long-term performance.

The effective completion of the bidding procedure is extremely important given the large number of rivals in today's marketplace [8]. Moreover, according to the author in emerging nations, many medium-sized and small construction firms fail during the first five years of operation. The choice to bid and the calculation of the offer price is often the two key decisions involved in the bidding process [9]. The first choice, whether or not to submit a bid for a particular job, puts the contractor in a difficult situation [10]. In particular, choosing not to bid could result in a forgone opportunity. This opportunity loss might be in the form of failing to utilize the possibility to produce profit, strengthen the contractor's ranking in the industry, and develop a working relationship with the customer, among other chances. Given the aforementioned difficulties, the focus of this research was to identify the crucial variables influencing contractors' decisions of bidding on Sri Lankan-based construction works. To achieve the aforementioned aim of this study, these objectives have been established; (1) identify the factors of selection for making bid/no-bid decision, (2) identify the most critical selection factors when making the bidding decision for construction projects in Sri Lanka. The research community and industry will both profit from the study's outcomes. Contractors would have a better awareness of the key elements influencing the selection of a winning tender with regard to the industry. Contractors in possession of this knowledge will be in a better position to decide whether the bid is to be submitted, taking the most important factors into account.

2 Literature Review

2.1 Competitive Bidding Nature in the Construction Industry

The act of submitting a price proposal to a prospective client for the purpose of managing the construction of a project is referred to as competitive bidding [11]. According to Tan [12], the competitive environment has a significant influence on contractor performance, and successful methods assist contractors in remaining relevant in the construction industry. The presence of competition is a factor that will forever have an effect on the existence & the quality of the construction industry. Contractors need to have a successful bidding performance in order to keep the consistency of their work intact when they are putting in the hours required to complete construction projects. According to Fu [13], who conducted a quantitative study of the data obtained from 266 different Hong Kong contractors, it has been determined that experienced contractors are more competitive than beginner contractors.

2.2 The Bid/No-Bid Decision

For building contractors, choosing whether to bid or not to bid is both crucial and challenging. In order to remain competitive, contractors must look for projects for which they may submit a proposal. However, it is not good to bid on all available projects; instead, it is critical to choose just those bids that are appropriate for the organization. According to Shash [14], opting to bid or not to bid is a difficult decision to make for the reason that, if the corporation chooses not to bid, it would simply miss out on a chance. In addition, if the specific construction company chooses to submit a bid, they are responsible for bearing the direct cost, and the anticipated result of the decision will not occur within a short period. In addition, if the incorrect decision was made, there is a significant possibility that contractors may suffer a loss in their operational capability, reputation, and capital. As stated by Mohamed [15], the choice of whether or not to submit a bid is influenced by the specific qualities of the project as well as the complex situations that exist in the external environment.

Only a small number of contractors have developed methodical methods to get closer to determining unambiguous results about bid-making decisions. In addition, Lowe [16] said that a systematic model would be able to assist the contractor in accomplishing the business goals, boosting productivity, and improving the quality of decision-making. Mohamed [15] found that it is more crucial for organizations of greater sizes to take systematic consideration into account. Shash [14] discovered that, after looking through identical data, only 17.6% of the responding contractors had utilized some form of the systematic model to choose whether or not to bid on a project.

Wanous [17], has stated that the systematic approach of the bid/no-bid decision-making process is only effective for academic contexts and that it would not be of

any use for real-world industry practices. Additionally, Wanous [17] has highlighted that since this is a difficult mathematical model, the number of possible users has decreased, which is a point that was brought up by both of them. In addition, this approach prioritizes increasing the contractor's profits above achieving any of the contractor's other goals.

2.3 Factors Affecting Bid/No Bid Decision-Making in the Construction Industry

Numerous scholars have been interested in the bid/no bid decision throughout time. Few researchers have looked into and created useful bidding strategy models, but a relatively significant number of studies have concentrated on identifying the elements influencing the selection. These investigations were conducted in various geographical and cultural places throughout the world. However, a lot of the criteria that the researchers came up with are comparable.

Enshassi et al. [18] have categorized the identified factor into four (4) main groups namely, contractor's characteristics, clients' characteristics, both contract and project characteristics and external factors. Several aspects of the contractors themselves have an impact on how they decide whether bids should be submitted. These variables include things like a contractor's expertise, resources, workload, and rivals' actions. According to Mohamed [15], the need for work is the most significant issue that should be taken into consideration. Several researchers have concluded that the current amount of work is the most important aspect that must be taken into account when deciding on bid/no-bid. Moreover, they should also consider the availability of other projects as a significant factor that needed to be investigated [17].

The strength of the firm is a reflection of the success of the project, as well as the performance of smaller-sized contractors that have given a greater relevance score to the variables than the average [15]. The term "strength of firm" refers to the contractor's capacity to fulfil the tender conditions imposed by the client, the availability of cash necessary for the project, the contractor's track record of success in projects of a comparable nature, their familiarity with the site's environment, the availability of resources, the availability of subcontractors and material suppliers, and the percentage of the work that must be subcontracted [15]. In addition, Chua [6] has included the present workload in bid preparation as an additional component connected to the strength of the firm.

According to Wanous [17], the most critical factor in deciding whether or not to bid on a project is determining whether or not the contractor will be able to meet the conditions of the contract. The circumstance of the project is a factor that influences the capacity of the contractor to execute while working and attaining the profit objective. Under the project conditions terms namely project size, type, location, duration, profit made in similar projects in the past and the terms of the payment are included [15]. The capabilities of the contractor are deeply linked to the parameters of the

project, including its size, nature, location, and length. The capabilities include the amount of cash that is readily accessible, the number of competent employees that are readily available, the equipment, the plant, the management skills, and the building method knowledge [15]. According to Lowe [16], the magnitude of the project and the conditions of payment were the two most relevant elements that belonged under this category. Bageis [2] have demonstrated that the location of the project, as well as the duration of payment, are both crucial factors to consider. Many authors have also emphasized how essential it is to take into account the terms of payment [2]. Moreover, according to Mohamed [15], the direction of the future market and the availability of potentially profitable projects in the future are the two primary factors that determine the risks and opportunities that a company could face in the future. These risks and opportunities include factors such as the future market direction, the availability of potentially profitable projects in the future, and the financial situation of the company indicating the financial risks [15].

3 Methodology

This investigation is aimed at establishing critical selection factors for contractors to make bid/no-bid decision for construction projects in Sri Lanka. According to Almeida [19], mixed methods research is a strategy that integrates quantitative and qualitative techniques into a single investigation to offer a more comprehensive understanding of an issue. When a comparative analysis and thorough construction of research components are required, mixed techniques are used. Moreover, by combining quantitative and qualitative procedures, the use of mixed methods enables researchers to gain rich data that would be impossible to get using either methodology alone. Thus, a mixed research strategy that consisted of a questionnaire survey and semi-structured interviews were held for this study. The initial stage of this study consisted of a comprehensive literature survey and thereby fifty six (56) selection factors under seven (7) categories (Project Characteristics, Business Benefits, Client Characteristics, Contract Type, Project Finance, Contractor Characteristics, Market Competition) for contractors to make bid/no-bid decision for construction projects in Sri Lanka were identified through past studies. Furthermore, according to Guest [20], compared to other qualitative data-gathering techniques, semi-structured interviews provide consumers enhanced reliability and validity. As the second stage of the study the identified 56 factors were confirmed, modified, amalgamated and removed according to the comments of the ten (10) expert semi-structured interviews that have been conducted. Thereby, the identified 56 factors were reduced to 31. Then the summary of factors was subjected to a questionnaire survey that was prepared based on the five-point Likert- scale (0 to 4). The questionnaire survey was distributed among one hundred twenty (120) respondents covering a range of construction professionals including Engineers, Architects, Quantity Surveyors, and Project Managers. Experts for the semi-structured interviews and respondents for

the questionnaire survey were selected by using the purposive sampling technique due to its capability in gathering the most relevant details related to a study [21].

3.1 Semi-structured Interviews

After conducting ten (10) semi-structured interviews it was observed that data saturation was achieved and no longer the semi-structured interviews lead to new data. Hence, the data collection was stopped at the tenth (10th) semi-structured interview. Experts were selected based on the purposive sampling technique, and the profiles of the respondents are shown in Table 1.

Since manual content analysis helps to focus on the sets of data and reduces the variance between the contextual meaning of the data and the analytical method, it was used to examine the information gleaned from expert interviews. The results can be repeatedly proven, allowing one to draw a conclusion supported by reason and evidence. Face-to-face interviews have been considered a quite helpful data collecting mechanism by most researchers due to their ability to have sufficient time for understanding the research question more comprehensively. However, due to the prevailing constraints within the country, the study was done through some face-to-face interviews, some online interviews and also through telephone conversational interviews. Each interview lasted approximately 15−20 min.

Table 1 Profiles of the respondents

Code of the expert	Profile of the experts		
	Organization type	Designation	Yrs. of experience
EX-01	Public	Project Manager	25
EX-02	Private	Ch. Quantity Surveyor	22
EX-03	Private	Ch. Civil Engineer	20
EX-04	Private	Project Manager	18
EX-05	Private	Ch, Architect	16
EX-06	Public	Ch. Quantity Surveyor	15
EX-07	Private	Ch. Civil Engineer	15
EX-08	Private	Ch, Architect	13
EX-09	Public	Project Manager	13
EX-10	Private	Ch. Architect	12

3.2 Questionnaire Survey

A response rate of greater than seventy-three (73.3%), or eighty-eight (88) replies, was obtained. According to Tam & Le [22], the Relative Important Index (RII) may be used to rank and assess a collection of specified criteria in order to identify which is the most significant. Hence, for this study, RII was employed.

$$\text{Relative Importance Index(RII)} = \frac{\sum W}{A * N} \tag{1}$$

W—Weightage given by each respondent,

A—Highest Weightage,

N—Number of respondents.

4 Data Analysis

4.1 List of Factors for Contractors to Make Bid/No-Bid Decision at Construction Projects in Sri Lanka

The initially identified fifty-six (56) factors through the comprehensive literature survey were reduced to thirty-one (31) factors by the experts while providing their judgmental views on selections, alterations & combinations. The finalized thirty–one (31) factors by the experts at the end of the semi-structured interviews are demonstrated in Table 2. Following are the factors that the majority of the experts have clustered as less critical decision-making factors with a common understanding: Local climate, Site clearance of obstructions, Degree of difficulties in obtaining a bank loan, General overhead of the project, Strength in the construction industry. Further, there are augmented agreements regarding the below-mentioned factors among the experts as less critical: Expecting date of commencing, Client reputation, Availability of cash & qualified human resources. Hence, overall the above-mentioned factors were removed from the list of critical factors prior to the questionnaire survey round. Moreover, some of the factors identified through the comprehensive literature survey were combined into a single factor depending upon the similarities of each factor to the experts' suggestions and comments during the semi-structured interviews. Thereby, thirty-one (31) factors were finalized and taken into the questionnaire survey round in order to identify the significance.

The EX-02 has stated, "Most of the contractors are concerned about the contract type, size & duration of the project during the pre-bid period. This is because the firms are mostly willing to work in familiar contract types that they have performed

Table 2 Critical factors of selection for contractors to make bid/no-bid decision construction projects in Sri Lanka

Item no	Selection factor	Relative importance index (RII)	Rank
1	Size & type of contract	3.58	1
2	Duration & Type of the project	3.40	2
3	Type of resources required	2.55	12
4	Location & Site Conditions	2.28	21
5	Degree of buildability	2.45	16
6	Methods of construction	2.34	18
7	Projects' stakeholders	3.16	4
8	Design & Construction quality	3.16	4
9	Degree of technical difficulties	2.32	20
10	Health & Safety requirements that need to be followed	2.45	16
11	Completeness of drawings and specification	2.71	10
12	Type of the procurement method	2.49	14
13	The benefits expected in terms of the company's reputation	1.81	29
14	Establishing a long relationship with the client, consultant & other nominated contractors	1.70	30
15	The client: type, size & capacity requirements	3.08	7
16	Market share & market condition	2.63	11
17	Clearness & Interpretation of the work and specifications	2.89	8
18	The ability to modify the main contract & Subcontracts	2.02	25
19	Project Particular & General Conditions of Contracts	3.24	3
20	Project cash flow issues due to the possibility of delay or shortage in payment	2.15	22
21	Financial goals, Tax & third-party liability, Overhead of the company	2.1	23
22	Required insurance premium, bonds & guarantees amount, liquidated damage	1.85	28
23	Competition among the bidders	2.04	24
24	The ability to do the job	2.80	9
25	Availability & quality of resources for the project	2.49	14

(continued)

Table 2 (continued)

Item no	Selection factor	Relative importance index (RII)	Rank
26	The current workload of the company	3.12	6
27	Strength of business partners, subsidiaries & Subcontractors	1.64	31
28	Company ability of design involvement, innovation & Value management approach	1.95	27
29	Past experience in managing the similar type of projects	2.34	18
30	Risks involved in investment & price fluctuation	1.98	26
31	Pre-tender qualifications, submission period, cost & workload of tender documents	2.55	12

well. Further, contractor firms urge to having high benefits in minimum duration where they are keen on the contract duration." This statement clearly depicts that one of the major decisive sets of factors is the project characteristics of the bidding process. Further, EX-01 emphasised the contractors' concern about resource availability and quality from the local market by stating, "Every contractor should do a proper resource analysis before starting the project; specifically, labour, material and plant requirement & price variance during an economic crisis which has been encountered by our (Sri Lankan) industry(construction). They should have a proper resource management plan from commencement to the handing over stage."

Additionally, EX-04 supported that statement with more key factors such as construction method, buildable solutions with quality and many other factors. He further stated that "The bidders should concentrate on the methodology of their construction work at the initial stage for proper collaboration with other stakeholders especially with the subcontractors & suppliers to deliver a quality product. Because most of the time the project success totally depend on the process quality which paves the pathway for a lifelong relationship with all the main stakeholders". This statement clearly underlines the point that establishing a long-term relationship with other stakeholders is one of the key success factors & as a bidder, one should investigate the parties that will be involved in the project & their characteristics at the pre-tendering stage. It shows that the bidders must be concerned about their counterparts' reputation, capacity & abilities for long-term trustful relationships.

On the other hand, EX-07 explained that complexity is a must concern for the bidder at the bidding decision stage by claiming, "As per my experience majority of the contractors lack concern about the uniqueness of each project. They are simply taking that matter and trying to apply the same or similar type of process for every

project. Though, the contractors should be concerned about the technological difficulties, construction difficulties & lack of comprehensiveness in drawings & specifications at the tendering stage. This may have led to a lot of conflicts during the implantations stage that drags the project duration & increase cost while reducing the final product quality".

Additionally, EX-06 explained that most small –medium contractors are less aware of the different procurement types, and conditions of contracts. According to EX-06, Majority of SMEs lack awareness about most of the new & innovative procurement methods, different conditions of contracts—which they did not consider as critical at bidding decision stage. Hence, I strongly believe that SMEs must undergo different conditions of contracts (General & Project Particular) and procurement types. Most contractors are only aware of or practise the traditional procurement method & their mindset is only to apply the same method in other less successful procurementmethods. EX-09 mostly highlighted that the bidders believe & foresee positively financial goals they have to achieve during the pre-bid period by stating, "Contractors' financial project management is so embarrassing during the construction stage because of delays of interim payments, advance payments. Not only that, the bidders are less concerned about their initial commitments to produce bonds & guarantees upfront which can be recovered later. Most of the contractors are less concerned about the competitiveness & market share which assist them in deciding the most suitable profit margin to win a bid". Moreover, EX-08 & EX-10 have pointed out that the bidders should be concerned about their strength & ability to complete the jobs by claiming that, "Most of the SMEs overrated their abilities at the pre-tender stage. It is highly ill-effective for the entire project. As a contractor, you must evaluate your strengths along with your collaborators, value management methods, micro–macro level risk management methods, current workload and past exposure to similar projects. Additionally, in the pre-tender stage, the innovative construction approaches should be studied before the submissions".

4.2 Most Critical Selection Factors for Making Bidding Decision for Construction Projects in Sri Lanka

As illustrated in Table 2, questionnaire survey results, the highest RII score (>3.25) was gained by the size of the contract and duration & type of the project. This shows the bidders are mostly considering traditional project management factors when doing bid or no bid decisions. Further, bidders consider more conventional factors such as the condition of the contract, stakeholders' requirements & design & construction quality.

Next, the bidders must consider the internal matters of their company when they make critical decisions in the bidding process. Namely, they are Current workload, Client characteristics, Clarity & competence level of the work scope & specification & drawings, and Ability to do the job ($3.10 > RII > 2.70$). Most of the selection

factors (15) are moderately critical factors which have RII values around 2.70 to 2.00 (ranked 11 to 25). They are mostly relevant & depend on project and counterparts & less significant & depend on the contractor's perspective. Some of them are Market share & market condition, Pre tender qualifications, Type of procurement method, Health & Safety requirements & buyable solutions. The lowest RII values (2.00 > RII > 1.60) are mostly for the factors (ranked 26 to 31) that are unable to be controlled by the bidders during the bidding stage or the factors that are mandatory to bid for any kind of tender. (e.g.: Location & Site Conditions, required insurance, bonds & guarantees, liquidated damage amount, Risk involved in investment & price fluctuation, Establishing a long relationship).

5 Conclusion

Through a comprehensive literature synthesis, fifty- six (56) factors were identified under seven (7) categories that influence the decision-making process of contractors at the initial stage of the bidding process. Then, through semi-structured interviews, thirty-one (31) most critical selection factors that affect decision-making of bidding were shortlisted. According to questionnaire survey results, the most critical selection factors were related to traditional project management, such as size, type and duration of the contract. Secondly, the bidders are concerned about the internal factors of the construction company. Further, the most relevant factors for the project and other stakeholders were moderately critical factors for bidders in their bidding decisions. Least considered factors were considered to be the factors that are uncontrollable by the bidders during the bidding process or the factors that are mandatory in bidding. In any kind of tender. In conclusion, the bidders are mostly concerned about traditional project management factors & less concerned about the soft skill factors that are difficult or unable to control during the pre-bid stage. Further, as experts elaborate, the contractors should focus more on innovative construction methods and buildable solutions with a high-quality sustainable life-long process from the start of the bidding process that assists them to achieve a high amount of success in winning the tenders. The findings of this study will contribute to the existing knowledge gap that lies upon the contracting firms and the selection criteria for making the bid/no-bid decision. The Construction Industry Development Authority (CIDA/ICTAD) of Sri Lanka can use this study as a base for preparing a freely available checklist for assisting contracting organisations in Sri Lanka to make the bid/no-bid decision easier. Moreover, this study can be utilized as a base study for other developing nations. This study has been subjected to major limitations such as the data collection sample being confined to contracting organizations and large-scale contractors in construction.

References

1. Alsaedi M, Assaf S, Hassanain MA, Abdallah A (2019) Factors affecting contractors' bidding decisions for construction projects in Saudi Arabia. Buildings 9(33)
2. Bageis AS, FC (2009) Factors affecting the bid/no-bid decision in the Saudi Arabian construction contractors. Constr Manag Econ 27:53–71. s.l.:s.n.
3. Haghani Sa (2014) Modeling contractors' project selection and markup decisions influenced by eminence. s.l.:s.n.
4. Mohanty R (1992). Quality management. s.l.:s.n.
5. Hanák T, Drozdová A, Marovi´c I (2021) Bidding strategy in construction public procurement. Buildings 11(47)
6. Chua D, LD (2000) Key factors in bid reasoning model. J Constr Eng Manag 126(5):349–357. s.l.:s.n.
7. Chisala ML (2017) Quantitative bid or no-bid decision-support model for contractors. J Constr Eng Manag 143(12)
8. Aje IO, Oladinrin TO, Chibuike Nwaole AN (2016) Factors influencing success rate of contractors in competitive. J Constr Dev Ctries 21(1):19–34
9. Oyeyipo OO, Odusami KT, Ojelabi RA, Afolabi AO (2016) Factors affecting contractors' bidding decisions for construction. J Constr Dev Ctries 21(2):21–35
10. Cheaitou A, Larbib R, Al Housanic B (2019) Decision making framework for tender evaluation and contractor selection in public organizations with risk considerations. Socio-Econ Plan Sci 68
11. Waara F, BJ (2006) Price and nonprice criteria for contractor selection. J Constr Eng Manag 132:797–804. s.l.:s.n.
12. Tan YT, LySCLYL (2010) Construction project selection. s.l.:s.n.
13. Fu WKDDS, LHP (2002) Competitiveness of inexperienced and experienced contractors in bidding. J Constr Eng Manag 129:388–395. s.l.:s.n.
14. Shash (1993) Factors considered in tendering decisions by top UK contractors. Constr Manag Econ 11:111–118.. s.l.:s.n.
15. Mohamed Ea (2007). A framework for contractors to reach strategically correct bid/no bid and mark-up size decisions. Build Environ 42:1373–1385. s.l.:s.n.
16. Lowe DJ, PJ (2004) Logistic regression approach to modelling the contractor's decision to bid. Constr Manag Econ 22:643–653. s.l.:s.n.
17. Wanous MBHA, LJ (2000) o Bid or not bid: a parametric solution. J Constr Eng Manag 18:457–466. s.l.:s.n.
18. Enshassi A, Mohamed S, El Karriri A (2010) Factors affecting the bid/no bid decision in the Palestinian construction industry. J Financ Manag Prop Constr 15(2):118–142
19. Almeida F (2018) Strategies to perform a mixed methods study. Eur J Educ Stud 5(1):137–151
20. Guest G (2013) Describing mixed methods research: an alternative to typologies. J Mixed Methods Res 7(2):141–151
21. Saeed M (2020) Mediation effect of psychological contract between personality dimensions and turnover intention. J Econ, Financ Adm Sci 25(50):205–219
22. Tam V, Le K (2006) Environmental assessment by power spectrum. s.l. Br Univ Dubai
23. Abou Rizk D (1996) Utility-Theory Model for Bid Mark-Up Decisions. s.l.:s.n.
24. Ahmad I (1990) Decision-support system for modeling bid/no-bid decision problem. J Constr Eng Manag 116(4)
25. Harris, McCaffer R. (2001). Modern construction management. s.l.:s.n.
26. Hughes C (2006) Quantitative and qualitative approaches to social research. s.l.:s.n.
27. Jaselskis EJ, TA (1998) Bidding considerations in developing countries. J Constr Eng Manag 124(3):185–193. s.l.:s.n.
28. Jennings (1998) Decision making: an integrated approach. s.l.:s.n.
29. Odusote OO, FRF (1992) An examination of the importance of resource considerations when contractors make project selection decisions. Constr Manag Econ 10(2):137–151. s.l.:s.n.

30. Pinto (1992) Bidding-Building projects. s.l.:s.n.
31. Roszkowska E (2013) Rank ordering criteria weighting methods – a comparative overview. Optimum Stud Ekon 5(65):14–33
32. Skitmore Da (1997) The effect of contract type and size on competitiveness in bidding. Constr Manag Econ s.l.:s.n.
33. Vries Wad (2009) From demand driven contractor selection towards value driven contractor selection. Constr Manag Econ 27:597–604. s.l.:s.n.

Cost Control Techniques on the Delivery of Sustainable Construction Projects in Sri Lanka

W. M. P. T. Andrady, C. Allis, and B. K. C. Perera

Abstract With the progressive escalation in the development of sustainable construction projects over the period, the demand for better and greater construction has also intensified. However, the construction industry is constantly faced with various obstacles in the path to achieving these construction demands and it was noted that these issues were due to the inability to meet cost targets of the projects. Therefore, it is crucial to distinguish the possible problems along the project, with the applicable control techniques to be used in diffusing these concerns. The aim was set to identify the impact of various cost controlling tools and techniques available towards the delivery of sustainable construction projects. The study carried out a literature review, semi-structured interviews and a questionnaire survey to collect data. Among the problems that were found to be constant, cost overruns, time overruns and life cycle costing were identified as the final, end-result of all other problems along with some cost control techniques such as Performance Review, Variance Analysis, Earn Value Management, Forecasting, To-complete Performance Index, etc. After identification of the said problems, thereby, determining the most common techniques used in the mitigation of the problems, which was further illustrated through a framework were presented at the end. It has been emphasised that these techniques can be utilized not merely for cost controlling techniques but also as overall cost management tools of the sustainable construction projects. Overall outcome of the research advances the concept of cost control under the cost management within the context of Sri Lankan construction industry in delivering sustainable projects.

Keywords Cost control techniques · Project management · Sustainable construction · Sri Lanka

W. M. P. T. Andrady
DG Jones and Partners, Doha, Qatar

C. Allis · B. K. C. Perera (✉)
Sri Lanka Institute of Information Technology, Malabe, Sri Lanka
e-mail: kavinya.p@sliit.lk

© The Author(s), under exclusive license to Springer Nature Singapore Pte Ltd. 2023

R. Dissanayake et al. (eds.), *ICSBE 2022*, Lecture Notes in Civil Engineering 362,
https://doi.org/10.1007/978-981-99-3471-3_15

1 Introduction

The construction industry plays a very important role in a country's economy by accelerated feeding in national financial growth [7]. The growth and success of the industry rely on the ability of the project in achieving the aims and objectives set under the scope of the project. Thus, the scope includes the completion of the project within a predetermined budget, within the planned period of time and essentially up to the required quality [16]. A well-planned and detailed project may lead to cause various problems without an appropriate level of controlling, monitoring and scheduling. Therefore, to achieve this success, it is not only essential to plan the project, but to schedule, monitor and control the project as a whole [22]. Thus, it is common knowledge that an implementation of a construction project is habitually followed by, a complicated process, an increase in cost and a delay in time as well as owner dissatisfaction [2]. Khodeir and Ghandour [12] stated, obtaining control over the project cost has never been easy as knowledge and understanding of selecting and thereby the application of the appropriate cost-controlling techniques is required [22]. Accordingly, cost control can be defined as "the process of managing and monitoring the construction cost of the project in par with the project budget using the most suitable techniques to sustain and further increase the profitability". Cost controlling is essential to lower cost overruns as it informs the project team of the exact position of the project in terms of cost so that the team could be aware of any inconsistencies. Obtaining control over the cost is the prime factor in the matter.

Many clients/stakeholders have also been concerned with the social and environmental aspects of a construction project in conjunction with the financial aspects [19]. Although the notion of sustainability has been defined in multiple ways with various perspectives, the most applied definition for sustainability is "developments that meet the needs of the present without compromising the ability of the future generations to meet their own needs", which allows encompassing a connection between environmental, social and economic systems [30]. Moreover, the concept of sustainability in combination with construction can be used as a system that creates profit over the course of the construction project and thereafter, by using sustainable processes, resources, etc. [19]. The incorporation of economic principles in achieving value for money and acquiring maximum output with minimum input are some of the methods utilized in achieving sustainable delivery via cost control [29]. Thus, this also makes it an obligation to set environmental and social goals in addition to the financial goals, at the early stages of the planning processes. In addition, aiming more focus towards sustainability leads to improve the health and safety of the labourers, reducing environmental damage, lowering operational costs, improving productivity, etc. [19]. Although several studies have been conducted previously on the implementation of cost control techniques, there is a lack of investigations regarding the link between cost control techniques and the sustainability of the delivery of construction projects. Consequently, the aim of this research is to bridge this knowledge gap by concentrating on project cost and providing a thorough insight into various difficulties faced in managing the project cost, the various cost-controlling techniques

available to overcome such difficulties in sustainable construction and then to develop a framework for the impact that these techniques have on the delivery of sustainable construction projects. This research is essential as information acquired from this research may be beneficial in identifying the necessary improvements of cost control for future endeavours.

2 Sustainable Construction and Cost Management

The need for the notion of sustainable construction towards the betterment of climate change and reduction in project cost, has been progressively established and incorporated over time in the industry's practices [10]. According to Klotz and Horman [13], a significant portion of the concerns related to water, energy, raw materials and other resource deficiencies were essentially due to the products and processes of the construction industry. Thus, sustainable development is directed towards physical advancements which employ effective methods of material consumption and resourceful practices in assembly and disposal, which are sustained within the framework of environmental, economic and social ideals [28]. Carter and Rogers [6] stated that the implementation of sustainability within this framework, with their interconnections, leads to creating a Triple-Bottom-Line, which implies that where they interconnect "there are activities that organizations can engage in which, in addition to affecting the natural environment and society, also results in long-term economic benefits and competitive advantage for the firm". These lead in maximizing output by minimalizing the impression on the environment, socially improving the comfort and satisfaction of the occupants and upsurging the demand and profit accumulated over time [28].

2.1 Problems Encountered in Managing the Project Cost

The project cost can be described as money to be remunerated for completing the activities of the project [12]. This project cost is considered as a primary concern in meeting the quality, cost and time expectations of the project [27]. However, according to Koushki and Kartam [14], each construction project faces various challenges in managing this cost, during the implementation and throughout the construction period as a whole.

2.1.1 Delays

Time overruns are endless and inevitable in the construction industry and their causes vary between countries [1]. According to Gandhak and Sabihuddin [9], a delay is recognised as slowing the speed of work instead of discontinuing construction

entirely, which can then result in time overruns, passing the date of delivery for the project. Delays are known to have a negative influence on the execution of the project. Nonetheless, these impacts have been influencing both the construction industry and the economy [18].

Apine and Valdes [3], have identified delays to be the result of continuous reliance on the same supply provider and location. Further, time consumption was also found to be increased due to the lack of planning, which would be done towards the completion of the project where the building is being tested and commissioned as the need to comply with the standards or requirements under any sustainable project and is vital in obtaining a green certificate. They also stated that the possibility for delays is escalated with the lack of acknowledgement towards conflicts between standards. Moreover, the study revealed that the majority of the risks and thereby delays and the roots of such problems that take place in a sustainable project are much more similar to the complications at regular construction projects.

Gandhak and Sabihuddin [9], has categorised delays into four types labelled as non-excusable delays, excusable compensable delays, excusable non-compensable delays and concurrent delays, which were categorised based on the level of responsibility and the involvement of the contractor and the owner. Furthermore, they continued to state that the causes of these delays can also be classified as external and internal causes, the internal causes are said to be created by the parties involved; owner, consultants, designers and contractors, whereas suppliers, weather, government bodies etc. create the external causes. Through their questionnaire survey, conducted among industry professionals regarding the causes of delays, the results obtained indicated that design changes, financial constraints encountered by clients and contractors and thus delays in payment or funding, dissatisfaction, lack of information and poor management are the main factors leading to project delays.

2.1.2 Cost Overruns

Cost overrun is an inbuilt, foreseeable challenge faced by nearly all projects prior to their accomplishment [7]. The encounter can simply be understood as unforeseen cost escalations as a result of improper cost estimations during budgeting [11]. As per Khodeir and Ghandour [12], cost overrun is when the 'actual cost' exceeds the budget. However, it is also referred to, as 'cost escalation'. For cost overruns, there are no exceptions between developed and developing economies (Asmi Abdul [4].

As stated before, in the study conducted by Apine and Valdes [3], many of the risks and thereby the cost overruns and the cause of these difficulties in a sustainable project are comparable with the complications taking place at regular construction projects. The report also states that when it comes to establishing conflicting standards in sustainable construction, if requirements exist for the project or if the rising conflicts between standards are not acknowledged prior to instigating the project, the likeliness of the growth of cost overruns significantly increases. Further, delays are said to be a common constant factor which can cause the largest possible cost overrun in projects.

The journal article by [17], includes a study that was conducted using 80 questionnaires among Nigerian construction industry professionals and the presentation and analysis of the results have pointed out several factors such as price fluctuations, additional works, inaccurate estimates, insurance, shortening of contract periods and fraudulent practices and kickbacks caused cost overruns. Among these factors, some of the contractors, consultants and clients were found to have voted 'delays' as another factor where claims are a common variable leading to delays in many projects as mentioned above. The majority of the problems leading to cost overruns were also determined to be caused due to the lack of human and management planning and organizing along with the division of the project into different phases [17]. Asmi Abdul [4], ascertained that the use of new technologies and software and improper management at the site by contractors as the main contributors to the escalations. Through their research it was also identified that procedures for awarding the contract to the appropriate bidder considering their price and the past experience is of paramount importance to avoid higher costs due to re-tendering process if the project is abandoned for the poor performance of the contractor or the project itself. Nevertheless, Aibinu and Jagboro [2], showed that the delay and unexpected rise in prices can lead to the development of claims related to loss and expenses which can thereby have a noticeable impact on the cost overrun. About 55–80% of the cost escalation claims were found to be based on fluctuations which occurred during the period of delay. In relation to, Frimpong et al. [8], the late payments from agencies were a primary factor while owners pointed at the lack of proper contractor management to be the main concern. Koushki and Kartam [14], established that positive inflation of materials was responsible towards 13% to 14% of the cost overruns.

2.2 Cost Management

Cost management is the completion of the project within its approved budget by properly estimating, controlling, planning and budgeting [23]. Well-organized and efficient use of cost management tools has become very crucial towards achieving the expected outcome from the practice of project management. The use of these techniques also enable to centre around the elements required for the completion of the schedules and in decision making that might impact the project cost [21]. According to Premalal et al. [22], cost management is consisted of cost estimation, cost budgeting and cost controlling.

2.3 Cost Control and Techniques

Cost control is carried out to recognise and clarify modifications related to revenue and costs [19]. According to Hwang et al. [11], it can also be explained as the comparison between the baseline and the results of a project for possible nonconformities

as mitigation actions can be taken early. This process is essential for regulating the project cost successfully and this fact has been accepted by investors and lenders, globally [25]. A set of techniques have been developed and incorporated to avoid possible cost overruns, some of which are discussed below.

2.3.1 Earned Value Analysis and Earned Value Management

Earned value analysis (EVA) measures 'work in progress' to determine the conditions of impending work. This allows managers to identify risk areas which enables them to develop mitigation plans using actual cost, progress and schedules. EVA uses actual, planned and earned value limitations in evaluating the performance. It is mostly used for analysis in software like Ms. Project and Primavera [5]. On the other hand, Earned Value Management (EVM) aids in cost accounting, risk planning and guiding the management system [5] and provides contractors the ability to reply actively and swiftly to problems with good control and prominence [26]. According to Subramani et al. [7], it also helps in scheduling performances and analysing the actual cost using the return values which gives a fixed measurement unit.

EVM is common as an analysing tool in most software.

2.3.2 To-Complete Performance Index (TCPI)

To-complete performance index calculate the "projection of cost performance" [7] and Lipke [15], described it as work to be done divided by unused capita:

$$\text{Work to be done} = \text{BAC} - \text{EV (Budget at Completion} - \text{Earned Value)}$$

$$\text{Unused capital} = \text{TC} - \text{AC (Total cost Desired} - \text{Actual cost)}$$

Thus, TCPI = (BAC − EV)/(TC − AC), which detailed the cost performance required in the completion of the remaining portion of the project to reach the preferred final cost. However, TCPI can also be used for various other applications such as evaluating the realism of bottom-up derived EAC, to decide if a project cannot be improved etc. [15].

2.3.3 Forecasting

Forecasting is carried out in cost estimation of forthcoming projects and includes two types known as numerical and statistical forecasting as well as ad-hoc forecasting [11]. EVA and To-complete performance index (TCPI), etc. are all forms of forecasting techniques [24]. Table 1 presents the features of two different forecasting methods.

Table 1 Feature of forecasting. *Source* [11]

Ad-hoc forecasting	Numerical and statistical forecasting
Doesn't require details	Relies on details
Experience based	Accurate
Less accurate	Expensive
Less time consuming	Time consuming

2.3.4 Project Management Software (MS Project, Primavera Etc.)

Cost control using software is widely popular among the industry professionals today. Hwang et al. [11] have pointed out that the results of multiple investigations have concluded with more interest towards the use of software for management and control. About 97% of the participants have incorporated software for their projects. Among these, CostX, Primavera and MS Project were the most common. Olawale and Sun [20], have additionally stated MS Excel, Project costing system, WinQS, etc. would be convenient and the use of these softwares combined with improved technology is recommended. Investments in software was found to increase the success rate from about 30% to 75% [21]. The application of Building Information Modelling was recorded as a quality enhancer having an estimation of 69% of respondents in the study [27]. As stated by Bhosekar and Vyas [5], MS Project aids in assigning resources, planning, tracing progress, budgets, etc. and creates critical path schedules among others to develop cost and schedule variances. Primavera tracks cost and time through labour, plants and material to assist in controlling and managing activities.

3 Methodology

The research took on a mixed method of research approach which led to the philosophy of pragmatism. It was because the theory was developed over understanding the varied perceptions of the respondents and based on the gained experiences. Similarly, the quantitative data raised via a questionnaire survey, was empirically tested on the subject matter. Apparently, the study involved a combination of deductive and inductive perceptions to complement the design. To understand the effects of cost controlling techniques with the help of the perspectives of Quantity Surveyors, Project Managers, and the like, which cannot be obtained through a numerical study were collected first-hand via interactions with renowned industry professionals who have experience in working with and applying cost controlling techniques in sustainable projects in Sri Lanka. The 4 participants were chosen using 'selected sampling' method as only the personnel who may have experience working with or knowledge of cost control techniques were requested to take part in the interview. The questionnaire was sent up to about 100 individuals working in the construction industry with

experience and knowledge in cost control techniques and sustainable projects. After analysing both collected qualitative and quantitative data, the following arguments were derived.

4 Argument and Evidence

All the professionals who took part in the interview, had more than 6 years of experience in the field. Meanwhile the questionnaire was filled by 53 respondents and out of all, 57% had gained experience through more than 15 years. The sample of the questionnaire survey respondents consisted of both industry practitioners and academic personnel.

4.1 Problems Encountered in Managing the Project Cost

The obtained results illustrated various problems that were faced in managing the cost of the project were common to all types of construction projects, including green construction projects. Lack of materials, overlapping activities, operational costs, maintenance costs, design changes, price fluctuations, lack of planning/monitoring etc. were found to be some of the issues causing complications in the execution of the project. However, based on the results, it was identified that the final, recurring outcomes of all such problems as mentioned above, were the three main and primary problems identified as time overruns, cost overruns and life cycle cost. Furthermore, during the interviews, additional knowledge regarding the problems that can occur during project cost management, was gained. Each respondent in the interview suggested various issues that have occurred, apart from cost and time escalations, using their own experiences at project sites.

4.2 Frequently Used Cost Control Techniques in Sustainable Construction

According to the literature review, seven techniques which help to mitigate cost overrun issues in construction projects were known. They were namely EVM, Forecasting, TCPI and MS. Project, variance analysis, performance review and material and labour monitoring. The complete list of the identified cost control techniques are as follows:

- Forecasting
- Earned Value Management
- MS. Project

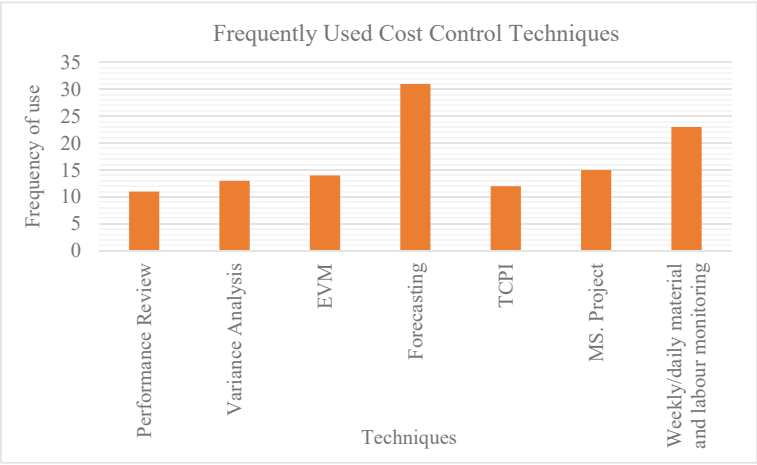

Fig. 1 Frequently used cost control techniques

- To-complete Performance Index
- Performance Review
- Variance Analysis
- Weekly/daily Material and Labour Monitoring

Using the above list, the respondents of the survey were requested to identify the most frequent techniques in-use, with their experience in the industry. The results are shown in Fig. 1. More than 58% of the participants (31 respondents) have selected forecasting as the most frequent method to be in use. Performance review was selected as the least frequent method used in professional life by the respondents with approximately 21% of the votes in comparison. Weekly/daily monitoring of material and labour has been selected as the second most prominently implemented method in the industry with 23 of the participants confirming this.

Through the survey, the participants were prompted to add any additional cost-controlling techniques that were used in sustainable projects, in which they had previously worked on, at the present projects they are working on or have knowledge of. However, prior to this, the participants were to provide relevant information on whether they had experience on working in a sustainable project. Accordingly, 28% respondents had experience in green projects and out of them, 66% used cost-controlling techniques. 35 contributors have acknowledged the use of cost control techniques in green projects. These 35 respondents were then prompted to provide the details of the particular techniques used in the said projects. Nevertheless, many contributors have also stated that the techniques used are similar to the techniques normally used in any other project. Below given are the list of techniques:

- Project budget planning
- All cost items monitored through a computer system
- Life cycle cost analysis

- Project change control
- Construction computer software (CCS) CCS buildsmart and CCS Candy
- Pre-contract cost planning in deciding systems, methods and materials
- Effective change management
- Design to budget
- Lean construction and collaborative planning
- Cost value reconciliation

Through the interview, it was suggested, the use of Enterprise Resource Planning systems and budget control. As mentioned above, there are no specific cost control techniques especially practicing for sustainable projects currently in the industry. Furthermore, it was indicated Key Performance Index and Building Management Systems are also some of the tools that are used indirectly for cost control. Ultimately, cost controlling is not merely using cheap products that don't comply with the specification of the project to complete the project but rather optimise overall value for money.

4.3 Framework on the Impact of Cost Control Techniques for the Delivery of Sustainable Construction Projects

Figure 2 shows the developed framework that can be used to learn and acknowledge the causes of some of the problems which frequently occur in the industry and the cost control techniques which are contemporarily available, successful solutions on avoiding such problems and then achieve the ultimate project goals. Thus, a proper understanding of the framework is beneficial towards the effective delivery of a successful project.

5 Conclusion

Many of the issues faced during sustainable or normal construction projects are similar and repetitive such as operational costs, price fluctuations, payment delays etc. It was also identified and concluded that all of these common problems ultimately result in three main issues known as cost overrun, time overrun and life cycle cost.

Seven main techniques were initially found for cost control techniques available to prevent any of the obstacles. Simultaneously, additional techniques used in the industry were brought to knowledge as well. Moreover, the final outcomes of the survey aided in acknowledging the techniques that are used in the industry at present and how they are used. With all the information gathered, it was found that Forecasting is the most commonly used technique.

The framework for the impact of cost control techniques on the delivery of sustainable construction projects was included along with the combination of all the findings

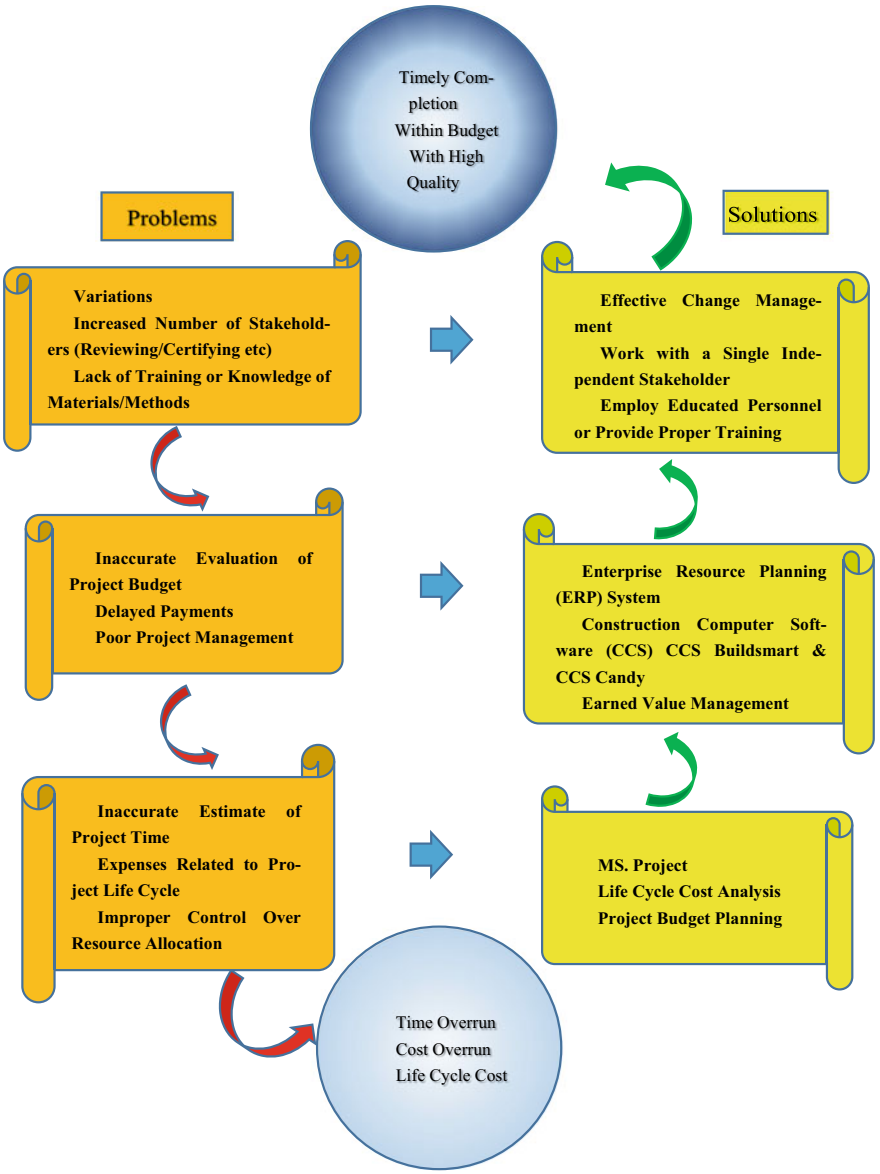

Fig. 2 Framework for better control over cost

which was obtained through the study. The framework includes some of the most constant issues that occur and the techniques which can be used in diffusing the said issues. The information provided through this framework can be utilized in gaining awareness of possible complications that can take place, aid in making the right decisions, prevent escalations in time and cost and reduce wastage of materials among others.

6 Recommendations

The provided recommendations are based on the conclusions made from the results gained from the findings in the study. Primarily, the use of the developed framework for the impact of cost control techniques on the delivery of sustainable projects is recommended to be used as a guide in determining the techniques to be used with some of the common problems. Not only the use of the proper cost control techniques by taking the scale and value of the project into consideration yet also the life cycle cost technique is highly recommended. Thus, practicing the given framework with the most effective methods of control that matches the scope/context of the organization shall improve the qualifications of the organization.

References

1. Addo JNT (2016) Delay and its effect on the delivery of construction projects In Ghana. Afr J Appl Res (AJAR) 1
2. Aibinu AA, Jagboro GO (2002) The effects of construction delays on projects delivery in nigeria construction industry. Int J Project Manage 20:593–599
3. Apine A, Valdes FJE (2017) Risk management in sustainable projects in the construction industry: cases of Swedish companies. Umea School of Business Economics
4. Asmi Abdul Azis A, Hameed Memon A, Abdul Rahman I, Tarmizi Abd Karim A (2013) Controlling cost overrun factors in construction projects in Malaysia. Res J Appl Sci Eng Technol 5:2621–2629
5. Bhosekar SK, Vyas G (2012) Cost controlling using earned value analysis in construction industries 1:10
6. Carter CR, Rogers DS (2008) A framework of sustainable supply chain management: moving toward new theory. Int Jnl Phys Dist Log Manage 38:360–387. https://doi.org/10.1108/09600030810882816
7. Cooray NHK, Somathilake HMDN, Wickramasinghe DMJ, Dissanayke TDSH, Dissanayake DMMI (2018) Analysis of cost control techniques used on building construction projects in Sri Lanka. Int J Res 5:909–923. https://doi.org/10.2139/ssrn.3311303
8. Frimpong Y, Oluwoye J, Crawford L (2003) Causes of delay and cost overruns in construction of groundwater projects in devel-oping countries; Ghana as a case study. Int J Project Manage 21:321–326
9. Gandhak P, Sabihuddin S (2014) Stakeholders' perception of the causes and effect of construction delays on project delivery-A review. J Constr Eng Proj Manag 4:41–46. https://doi.org/10.6106/JCEPM.2014.4.4.041

10. Geach I (2016) Investigating the role of sustainability in contractor selection and evaluation. Willmott Dixon.
11. Hwang B-G, Shan M, Zhu L, Lim W-C (2018) Cost control in megaprojects: efficacy, tools and techniques, key knowledge areas and project comparisons. Int J Constr Manag. https://doi.org/10.1080/15623599.2018.1484976
12. Khodeir LM, Ghandour AE (2019) Examining the role of value management in controlling cost overrun. Ain Shams Eng J 10:471–479. https://doi.org/10.1016/j.asej.2018.11.008
13. Klotz L, Horman M (2007) Transparency, process mapping and environmentally sustainable building projects. In: Proceedings of Annual Conference of the International Group for Lean Construction, East Lansing, MI, USA, pp 322–331
14. Koushki PA, Kartam N (2004) Impact of construction materials on project time and cost in Kuwait. Eng Constr Archit Manag 11:126–132. https://doi.org/10.1108/09699980410527867
15. Lipke W (2015) To Complete Performance Index 8
16. Malkanthi SN, Premalal AGD, Mudalige RKPCB (2017) Impact of cost control techniques on cost overruns in construction projects. Engineer 50:53. https://doi.org/10.4038/engineer.v50i4.7275
17. Mansfield NR, Ugwu OO, Doran T (1994) Causes of delay and cost overruns in Nigerian construction projects. Int J Project Manage 12:254–260. https://doi.org/10.1016/0263-7863(94)90050-7
18. Motaleb O, Kishk M (2010) An investigation into causes and effects of construction delays in UAE 10
19. Niţă CG, Ştefea P (2014) Cost control for business sustainability. Proc Soc Behav Sci 124:307–311. https://doi.org/10.1016/j.sbspro.2014.02.490
20. Olawale YA, Sun M (2010) Cost and time control of construction projects: inhibiting factors and mitigating measures in practice. Constr Manag Econ 28:509–526. https://doi.org/10.1080/01446191003674519
21. Owens J, Burke S, Krynovich M, Mance D (2007) Project cost control tools & techniques 26
22. Premalal AGD, Mudalige RKPCB, Malkanthi SN (2016) Study of cost control techniques used in construction industry and their impact to minimize cost overrun. Civ Environ Eng Soc 164–170
23. Project Management Institute (2017) A Guide to the Project Management Body of Knowledge (PMBOK® Guide), 6th ed
24. Pujitha KSVS, Venkatesh K (2020) Forecasting the construction cost by using unit based estimation model. Mater Today Proc. https://doi.org/10.1016/j.matpr.2020.05.546
25. Smith P (2014) Project cost management – global issues and challenges. Procedia Soc Behav Sci 119:485–494. https://doi.org/10.1016/j.sbspro.2014.03.054
26. Subramani T, Jabasingh DSS, Jayalakshmi J (2014) Analysis of cost controlling in construction industries by earned value method using Primavera. Int J Eng Res Appl 4:145–153
27. Vasista TGK (2017) Towards innovative methods of construction cost management and control. Civ Eng Urban Plan: Int J 4:15–24. https://doi.org/10.5121/civej.2017.4102
28. Zhang J, Li H, Olanipekun AO, Bai L (2019) A successful delivery process of green buildings: The project owners' view, motivation and commitment. Renew Energy 138:651e658. https://doi.org/10.1016/j.renene.2019.02.002
29. Zhou L, Lowe DJ (2003) Economic principles of sustainable construction. In: Proceedings of the 2nd International Conference on Construction in the 21st Century, Sustainability and Innovation in Management and Technology. Presented at the Second International Conference on Construction in the 21st Century, Hong Kong, pp 660–665
30. Zuofa T, Ochieng E (2016) Sustainability in construction project delivery: a study of experienced project managers in Nigeria. Proj Manag J 47:44–55. https://doi.org/10.1177/875697281604700604

Lean and Green: How the Synergy Can Promote Sustainable Construction

Prangige Achini Nadeesha Peiris, Nilupa Herath, Tuan Ngo, Colin Duffield, and Felix Kin Peng Hui

Abstract Lean construction aims to improve efficiency through the reduction of wasteful activities. These waste reduction activities also indirectly improve the sustainability approach used by organizations. Our paper examines the definition of lean construction (LC), LC activities, and green construction as understood by academics through a focused literature review. It then examines these practices considering how these activities contribute towards enhancing the sustainability of the built environment and the organization. Our findings suggest that not all waste reduction activities have the same degree of effect on sustainability improvements. Some lean tools such as standardization and just-in-time (JIT) for production scheduling can have a better effect, especially, if the key performance indicators (KPI) specifically target sustainability indicators. "Lean and Green" is not a myth and is very much achievable in the construction industry with the current efforts towards industry 4.0/5.0. Combining these two concepts remains a challenge. This paper aims to learn from what we already know and suggests ways on how "Lean and Green" can be achieved in the future. The paper includes a discussion on leveraging lean and green concepts to achieve the sustainable development goals promoted by the United Nations.

Keywords Lean construction · Green construction · Sustainability · Lean and green

1 Introduction

Lean concepts, when implemented in the context of construction, provide opportunities to identify and eliminate waste in construction processes, making them more efficient [11, 24]. Green construction, on the other hand, is perceived as sustainable development by enhancing resource efficiency, reducing operation costs, and improving

P. A. N. Peiris · N. Herath · T. Ngo · C. Duffield · F. K. P. Hui (✉)
Department of Infrastructure Engineering, The University of Melbourne, Melbourne, VIC 3010, Australia
e-mail: kin.hui@unimelb.edu.au

© The Author(s), under exclusive license to Springer Nature Singapore Pte Ltd. 2023

R. Dissanayake et al. (eds.), *ICSBE 2022*, Lecture Notes in Civil Engineering 362,
https://doi.org/10.1007/978-981-99-3471-3_16

the built environment for users [30]. Both these concepts have been around for a long time, specifically among scholars and academia. However, there is an ongoing debate on how practical these will be when implementing them on actual construction sites. There are inherent characteristics in construction that sometimes hinder the ability to apply these to all projects [11, 32]. However, recent studies attempt to understand how we can acquire the best of both these concepts by combining these practices from an early stage of construction and evaluating their usefulness. In their recent study, de Olivera et al. [6] have identified that there is potential in combining these two concepts in the search for achieving productivity and efficiency in construction [6].

Both these concepts, in their overarching view, are practices that can be implemented to improve the overall outcome of construction projects. Therefore, this study is conducted to identify the challenges of implementing lean and green concepts in construction, and how they can be overcome or minimized by combining these two practices. To achieve this aim, the following research questions are defined;

(i) What are the challenges of implementing lean construction?
(ii) What are the challenges in practicing green concepts in construction?
(iii) How do these two concepts complement each other in construction?

Upon answering these questions, this study then presents the Lean–Green wheel framework on how to incorporate lean concepts into construction, to achieve the requirements for green construction.

2 Literature Review

A focused literature review was undertaken to understand the two concepts lean and green construction, and how they complement each other. This section is divided into three sub-sections to highlight the individual strengths of the two concepts and the third section on the perceptions of how they work together, and if they have any contradictions in terms of how they can be applied to the construction context.

2.1 Lean Construction (LC)

From the findings in the literature, the most prominent and widely recognized advantage of lean is the ability to generate value by improving performance, quality, and safety and achieving low costs due to the elimination of non-value-adding activities. Tasks are most likely to be achieved when the performers' (workers) skill level and performance match the requirements of those who receive the completed task (the customers) [17]. When researching definitions of lean construction in the current body of knowledge, it was found that most of the studies refer to lean construction as a production management approach, with the perception that a construction project can be viewed as a temporary production system [13, 19, 23].

From a study conducted by Peiris et al. [24], it was evident that even during the early stage of adopting lean practices can achieve up to 50% reduction of time spent on non-value-adding activities. Lean practices that have been adopted in this case are 5S and standardization to minimize waste and improve the productivity of the work processes [24]. In addition, material waste and the number of production hours can also be reduced by the introduction of lean concepts to construction [18]. A study conducted by [36] presented the improvements obtained by lean implementation in terms of total duration and lead times [36].

Even though there are many advantages of "Lean" implementation in construction sites, there are several studies conducted to investigate the challenges of implementing lean construction in the construction industry [1]. Due to the dynamic nature of the construction industry, the implementation of lean concepts has been a challenge [26]. Lack of lean awareness, culture, and human attitudes, lack of top management commitment, and time and commercial pressure in completing the projects are some of the major issues identified in the UK construction projects [28]. Further, there are some other issues such as technicality and finance-related problems that were also identified in the UK construction industry [4].

The unwillingness of the management to adopt new systems, train their employees on lean construction and the tendency to not-change the organization and people also significantly contribute as barriers to implementing lean concepts in construction [7, 37]. Technical complexities in the design also contribute to the reluctance in implementing lean construction in the industry. Incomplete and complicated designs, the cyclic nature of the construction industry, and the less involvement of contractors and specialist design processes are among many key barriers identified in the UAE projects [12]. Further, lack of understanding and involvement in all stakeholders in a project [11] and poor communication between stakeholders [12] were also identified as barriers to implementing lean concepts in construction. Effective inventory management is a key contributor to the lean concept and the absence of such inventory management has also been identified in some countries as an obstacle to the implementation of lean construction [2]. In addition to all the above-described issues related to lean implementation in the construction industry, top–down change is one of the key drivers toward a cultural shift [16].

Having justified the advantages of lean construction, and identified the challenges for implementation, the next sections will discuss how the lean and green concepts complement each other in achieving synergistic effects.

2.2 Green Construction (GC)

Sustainability often goes together with green construction. It is a broad concept that reflects the resilience of the environment to human actions [22]. Also, green construction can be defined as the planning and implementation of the construction process to minimize the negative impacts on the environment so that there is a balance between the ability of the environment and the needs of human life for present and

future generations [8]. This can be accomplished by making sure that construction is observed from all the perspectives of a life cycle, from the conceptual stage to the construction stage, and the operational stage.

However, the use of green materials, improving technical skills in green building construction, and familiarising with green rating systems were identified as challenging topics by project partners on green construction. Lack of motivation from owners, high initial costs, and technical limitations were among the main drawbacks to implementing green construction in the construction industry [30]. High expenses on the preparation of green rating documents and the lack of training and education have incurred additional costs to the projects. The project delivery method also plays an important role in project success, and it was shown that the level of integration in the project delivery process has a significant impact on introducing green concepts into the construction industry [15]. The involvement of contractors during all-important project phases, the timing of participation, collaboration, and team characteristics are also important aspects of implementing green construction in the construction industry.

During the last few years, researchers have studied how green building construction can be better optimized using various aspects, lean construction being one of them [22]. The following section will present the Lean–Green approach and how the research in these two spectrums can come together.

2.3 Lean–Green Approach

When the fundamentals of the two concepts, 'Lean' and 'Green' are considered, there can be several synergies that highlight the strive towards a holistic improvement of the processes, specifically concerning construction. As identified by [35], nine synergies can be presented such as (i) economic advantages, (ii) competitive advantages, (iii) waste disposal, (iv) improving quality, (v) focus on people, (vi) continuous improvement, (vii) positive correlation between indicators, (viii) transparency, and (ix) long-term and holistic implementation [35].

However, it is a common notion that "Lean" emphasizes improving cost-intensive areas such as processes and people. Therefore, it is viewed as a process improvement exercise where "Green" or "Sustainability" is considered to be a life-cycle investment. In addition, the latter concentrates on eliminating environmental wastes hence preventing negative impacts on climate and the natural environment. These can be considered as different viewpoints of Lean and Green practitioners that sometimes hinder both concepts to be applied to a single scenario of a construction project [35].

With these synergies and conflicts in the Lean–Green approach, a study conducted by [6] presented an eco-efficiency assessment by using Value Stream Mapping (VSM) as a lean tool and Life-Cycle Assessment (LCA) as a green tool [6]. VSM provides the opportunity to identify and streamline all the processes that will then facilitate the recognition of non-value-adding activities. So necessary steps can be taken into

account to eliminate them [3]. LCA is a worldwide accepted systematic methodology to assess the environmental impacts of a product or process [27]. Several recent studies conducted during 2021–2022 consider this association between the two concepts, and how they can be utilized in a better way to achieve better results from a construction project. During this study, authors recognize "Green construction" as a holistic view of the entire life cycle of a construction project and look at how "Lean" principles facilitate in achieving the objectives of green construction. The following sections will identify specific lean tools and practices and discuss how they contribute to achieving sustainability in construction. Also, opportunities that will further complement this association in the future will be identified.

3 Lean–Green Wheel: How "Lean" Can Facilitate "Green"

By identifying the challenges in implementing both lean and green individually and understanding the potential for both these concepts to be combined, we can now look at how the synergies will help achieve the best in both worlds. For this, green construction is looked at from multiple phases of the project life cycle (life-cycle analysis), and the requirements to successfully achieve each phase are identified through the Lean–Green wheel presented in Fig. 1. The Lean–Green wheel identifies lean practices and tools that can be used in every stage of the green/sustainable construction life cycle. This is to facilitate the overarching goals of green construction to reduce the negative impacts of construction on the overall life cycle of the project.

Lean–Green wheel is divided into 4 main sectors such as (A) the Components of life-cycle analysis [5], (B) the Corresponding stages of lean implementation; (i) the Conceptual/Design stage, (ii) Construction/Manufacturing stage, (iii) Operational/End-of-Life stage, (C) Lean principals about each stage of implementation, and (D) Lean tools and practices that facilitate in achieving the Lean principles. These will now be discussed in detail with relevance to the respective Lean implementations.

3.1 Conceptual/Design Stage

This is the stage where resources will be identified, and materials will be processed according to the stages of LCA. In terms of a construction project, this is where the concept will be finalized, and designs will be completed to provide construction drawings for the next stage. From a Lean thinking perspective, this is the time when the customer requirements are identified and finalized to decide on a value stream. Value generation of each stage will be discussed and understood by the stakeholders at this stage enabling waste elimination workflows. The methods of project delivery will also be decided and agreed upon. Modular/prefabricated construction is one of the ways that is now commonly used to reduce time and cost, and at the same time improve the quality of the components [24]. Value stream mapping [10] is a

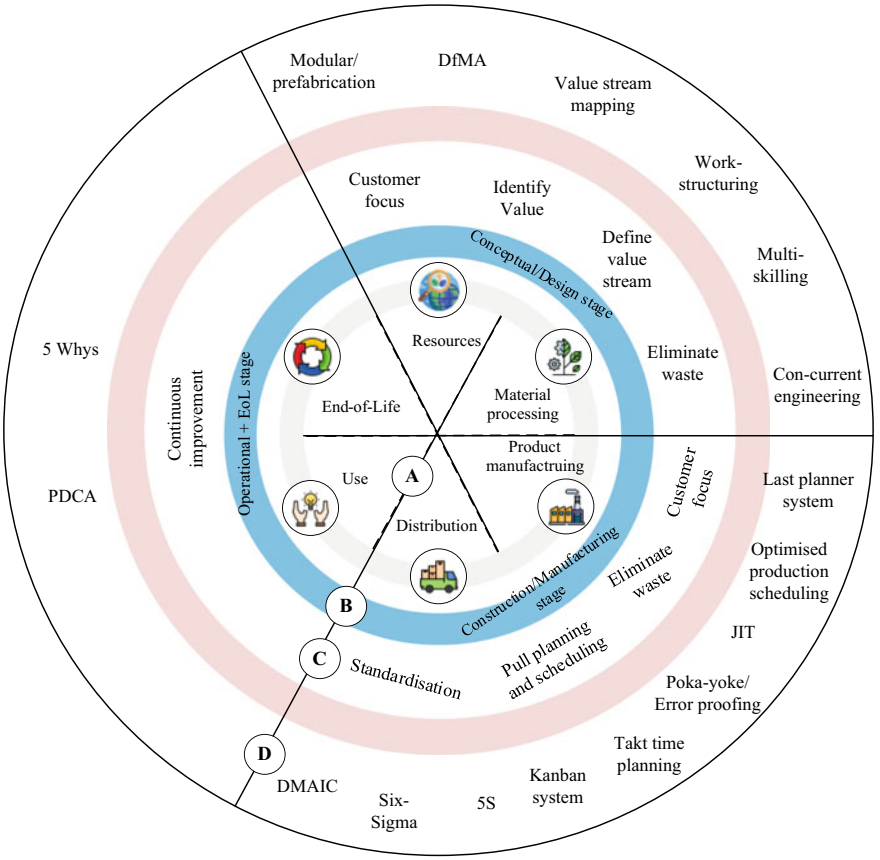

Fig. 1 Lean–Green wheel—an illustration of how lean principles, practices, and tools can be used in achieving green construction goals

technique that can be used after finalizing customer requirements and deciding upon the project delivery method, to identify the sequence of processes, while taking note of value-adding and non-value-adding activities. In addition to this, techniques such as DfMA (Design for Manufacturing and Assembly) can also play a critical role when the concept is defined and designed as per the client's requirements, to facilitate value generation. Afterward, organizational practices such as work structuring [33] and con-current engineering [3] can be used to integrate product and process design by considering all the phases of the project life cycle. These can be identified as key lean practices/tools that facilitate the conceptual/design stage of construction, ultimately facilitating the achievement of green construction goals during the resource, and material stages [3, 10, 24].

3.2 Construction/Manufacturing Stage

During this stage, the main goal is to manufacture or construct components where multiple performance objectives are achieved [9]. The main considerations during this stage are to optimize time, cost, and quality, while considering the physical/functional, environmental, economic, and social attributes of the n-bottom line [9]. When considering these attributes, synergies between Lean and Green are getting highlighted since the lean implementation is also trying to achieve similar objectives. At this stage, the application of lean principles such as customer focus, pull planning and scheduling, and standardization plays a prominent role in achieving functional and economic sustainability while eliminating waste. This facilitates achieving environmental sustainability. To implement these lean principles, tools such as optimized production scheduling, last planner system, poka-yoke error proofing methods [3], takt time planning [19], 5S [24], Just-In-Time (JIT) [25] and six-sigma (i.e. DMAIC—Design–Measure–Analyse–Improve–Control) [14, 20] can be used. Also, a study by Sepasgozer et al. [29] suggests that implementing digital technologies in construction sites can be considered an enabler for successful lean implementation, which in turn helps in achieving sustainable construction [29].

3.3 Operational/EoL Stage

The final stage of lean implementation can be identified as the operational stage or the End-of-Life stage. During this point of the construction life cycle, the project is handed over to the final users of the building. At this stage, it is essential to reflect on the experience during previous stages and come up with continuous improvement strategies to be implemented for future projects. Tools such as Plan-Do-Check-Act [31] and 5 Whys [10] can help achieve this.

4 How the Lean–Green Synergy Achieves SDGs

Sustainability Development Goals (SDGs) were introduced in the 2030 agenda for sustainable development [34]. Everyone is responsible for taking part in achieving sustainability to reach the goals. Each goal is specifically designed to address key systematic barriers to sustainable development. The construction industry can make a significant impact by achieving SDGs as the industry consumes a significant amount of energy and resources while generating a large amount of waste. Therefore, the integration of Lean and Green into construction will provide a pathway to improve the sustainability aspects of construction while achieving SDGs. The main SDGs identified to be facilitated by the synergy of Lean and Green construction are SDG 9 (Innovation and Infrastructure), 11 (Sustainable Cities and Communities), and 12 (Responsible Consumption and Production).

Each SDG has its targets and indicators, and it has been found that the construction industry considerably impacts 13 goals and 25 targets [21]. The significant negative impact created due to waste generation and disposal can be addressed through Lean and Green adoption. Greater adoption of clean and environmentally sound technologies and industrial processes is one of the targets of SDG 9. Enhanced technology to overcome some of the drawbacks in the construction industry related to sustainability can be achieved via Lean and green concepts as explained in the "Lean and Green wheel" (Fig. 1).

Sustainable construction helps to improve social well-being while reducing the number of affected people in the community due to many disasters. Reducing the per capita environmental impacts of cities due to waste management is a key target of SDG 11 (Sustainable Cities and Communities). Appropriate waste disposal and discharge of solid waste will reduce the environmental impacts while enhancing the social well-being of the community.

Reduction of waste generation through prevention, reduction, recycling, and reuse and sustainable management and efficient use of natural resources are some of the key targets of SDG 12. Synergies of Lean and Green ultimately achieve this target through different mechanisms while achieving the required productivity and efficiency through sustainable management.

5 Conclusion

This paper discussed the contribution of lean practices in achieving green construction objectives using the current know-how on "What is Lean?" and "What is Green?". From the literature review, it was found that implementing lean practices at an early stage of construction will highly benefit the organization to take the initial steps towards sustainable construction by implementing lean concepts to enhance the efficiency of construction processes. Further, this study provided a framework that can be used as a starting point for sustainable construction that was facilitated by lean implementations. Combining these two concepts and practices in the construction industry will be useful in achieving the sustainable development goals "Responsible consumption and production", "Industry, innovation, and infrastructure", and "Sustainable cities and communities". It is recommended to strategize the achievement of green construction goals from a very early stage by using lean principles as facilitators. This will be a useful reference for the practitioners who are aiming towards green construction, to consider adopting lean principles such as customer focus, identifying value, defining value stream, eliminating waste, pull planning and scheduling, standardization, and continuous improvement, as a starting point.

References

1. Ahmed S, Sobuz MHR (2020) Challenges of implementing lean construction in the construction industry in Bangladesh. Smart Sustain Built Environ 9(2):174–207. https://doi.org/10.1108/SASBE-02-2019-0018
2. Alinaitwe H (2009) Prioritizing lean construction barriers in Uganda's construction industry. J Constr Dev Ctries 14.
3. Aslam M, Gao Z, Smith G (2020) Framework for selection of lean construction tools based on lean objectives and functionalities. Int J Constr Manag: 1–12.https://doi.org/10.1080/15623599.2020.1729933
4. Bashir A, Suresh S, Oloke D, Proverbs D, Gameson R (2015) Overcoming the challenges facing Lean construction practice in the UK contracting organizations. Int J Arch, Eng, Constr 4.https://doi.org/10.7492/IJAEC.2015.002
5. Brusseau ML (2019) Sustainable development and other solutions to pollution and global change. In Brusseau ML, Pepper IL, Gerba CP (eds) Environmental and pollution science, 3rd edn. Academic Press, pp 585–603. https://doi.org/10.1016/B978-0-12-814719-1.00032-X
6. de Oliveira Rezende M, Saade MRM, Nunes AO, da Silva VG, Moris VAS, Silva DAL (2022) A Lean and Green approach for the eco-efficiency assessment on construction sites: description and case study. Clean Technol Environ Policy 24(5):1535–1552. https://doi.org/10.1007/s10098-021-02265-y
7. Dulaimi M, Tanamas C (2008) The principles and applications of lean construction in Singapore.
8. Febrianti D, Samsunan, & Mawardi, E. (2022) Study of the application of the green construction concept on the integrated college building project of Teuku Umar University. IOP Conf Ser: Earth Environ-Ment Sci 969(1):012081. https://doi.org/10.1088/1755-1315/969/1/012081
9. Foliente G, Kearns A, Shiroma M, Bai X, Barnett G (2007) Beyond triple bottom line—sustainable cities RD&D at CSIRO.
10. Gambatese JA, Pestana C, Hyun Woo L (2017) Alignment between Lean principles and practices and worker safety behavior [Article]. J Constr Eng Manag 143(1):1–10. https://doi.org/10.1061/(ASCE)CO.1943-7862.0001209
11. Ghosh S, Burghart J (2021) Lean construction: Experience of US contractors. Int J Constr Educ Res 17(2):133–153. https://doi.org/10.1080/15578771.2019.1696902
12. Kanafani JA (2015) Barriers to the implementation of lean thinking in the construction industry—the case of UAE. University of Leicester, Leicester
13. Li H, Guo HL, Li Y, Skitmore M (2012) From IKEA model to the Lean construction concept: A solution to implementation. Int J Constr Manag 12(4):47–63. https://doi.org/10.1080/15623599.2012.10773200
14. Meng X (2019) Lean management in the context of construction supply chains. Int J Prod Res 57(11):3784–3798. https://doi.org/10.1080/00207543.2019.1566659
15. Mollaoglu-Korkmaz S, Swarup L, Riley D (2013) Delivering sustainable, high-performance buildings: Influence of project delivery methods on integration and project outcomes. J Manag Eng 29(1):71–78
16. Morrey N, Pasquire C, Dainty A (2011) Developing a strategy to Enact Lean. In: 19th Annual Conference of the International Group for Lean Construction 2011, IGLC 3: pp 530–539. https://doi.org/10.32738/JEPPM.201301.0005
17. Mossman A, Ramalingam S (2021) Last planner, everyday learning, shared understanding & rework. In: Proc. 29th annual conference of the international group for Lean construction (IGLC). Lima, Peru
18. Nahmens I, Ikuma LH (2012) Effects of Lean construction on sustainability of modular homebuilding. J Archit Eng 18(2):155–163. https://doi.org/10.1061/(asce)ae.1943-5568.0000054
19. Nahmens I, Mullens MA (2011) Lean homebuilding: Lessons learned from a precast concrete panelizer. J Arch Eng. https://ascelibrary.org/doi/abs/https://doi.org/10.1061/(ASCE)AE.1943-5568.0000037

20. Nowotarski P, Paslawski J, Skwarek J (2019) Waste reduction by Lean construction-office building case study. IOP Conf Ser: Mater Sci Eng
21. Omer MAB, Noguchi T (2020) A conceptual framework for understanding the contribution of building materials in the achievement of sustainable development goals (SDGs). Sustain Cities Soc 52: 101869. https://doi.org/10.1016/j.scs.2019.101869
22. Orsi A, Guillén-Guillamón I, Pellicer E (2020) Optimization of Green building design processes: Case studies within the European union. Sustainability 12(6). https://doi.org/10.3390/su12062276
23. Pasquire C (2012) Positioning Lean within an exploration of engineering construction. Constr Manag Econ 30(8):673–685. https://doi.org/10.1080/01446193.2012.689431
24. Peiris PAN, Hui FKP, Ngo T, Duffield C, Garcia MG (2021) A case study on early stage adoption of Lean practices in prefabricated construction industry. In Dissanayake R, Mendis P, Weerasekera K, De Silva S, Fernando S (eds) Lecture notes in civil engineering, vol. ICSECM 2021, Springer, Singapore, pp 589–600
25. Peiris PAN, Hui FKP, Ngo T, Duffield C, Garcia MG (2023) Challenges in transport logistics for modular construction: A case study. In: 12th International conference on structural engineering and construction management, Singapore
26. Salem O, Solomon J, Genaidy A, Minkarah I (2006) Lean construction: From theory to implementation [Article]. J Manag Eng 22(4):168–175. https://doi.org/10.1061/(ASCE)0742-597X(2006)22:4(168)
27. Sandanayake M, Kumanayake R, Peiris A (2021) Environmental impact assessments during construction stage at different geographic levels—a cradle-to-gate analysis of using sustainable concrete materials. Eng, Constr Arch Manag (ahead-of-print). https://doi.org/10.1108/ecam-10-2020-0846
28. Sarhan S, Fox A (2013) Barriers to implementing Lean construction in the UK construction industry. Built & Hum Environ Rev 6:1–17
29. Sepasgozar SME, Hui FK, Shirowzhan S, Foroozanfar M, Yang L, Aye L (2021) Lean practices using building information modeling (BIM) and digital twinning for sustainable construction. Sustainability 13(1). https://doi.org/10.3390/su13010161
30. Shen W, Tang W, Siripanan A, Lei Z, Duffield CF, Hui FKP (2020) Understanding the Green building industry in Thailand. In Gou Z (ed) Green building in developing countries: Policy, strategy and technology. Springer International Publishing, pp 161–180. https://doi.org/10.1007/978-3-030-24650-1_9
31. Tezel A, Koskela L, Aziz Z (2018) Current condition and future directions for lean construction in highways projects: A small and medium-sized enterprises (SMEs) perspective. Int J Project Manage 36(2):267–286. https://doi.org/10.1016/j.ijproman.2017.10.004
32. Tran Q (2020) Challenges in managing green building projects from the view of the contractors: An exploratory study in Vietnam. IOP Conf Ser: Mater Sci Eng 869(6):062030. https://doi.org/10.1088/1757-899x/869/6/062030
33. Tsao CCY, Tommelein ID, Swanlund ES, Howell GA (2004) Work structuring to achieve integrated product–process design. J Constr Eng Manag 130(6):780–789. https://doi.org/10.1061/(asce)0733-9364(2004)130:6(780)
34. UN (2015) Transforming our world: The 2030 agenda for sustainable development. United Nations. https://sdgs.un.org/2030agenda
35. Weinheimer N, Schmalz S, Müller D (2017) Green building and Lean management: Synergies and conflicts. In: 25th Annual conference of the international group for Lean construction, Heraklion, Greece
36. Yu H, Tweed T, Al-Hussein M, Nasseri R (2009) Development of Lean model for house construction using value stream mapping [Article]. J Constr Eng Manag 135(8):782–790. https://doi.org/10.1061/(ASCE)0733-9364(2009)135:8(782)
37. Yu HT, Al-Hussein M, Al-Jibouri S, Telyas A (2013) Lean transformation in a modular building company: A case for implementation. J Manag Eng 29(1):103–111. https://doi.org/10.1061/(asce)me.1943-5479.0000115

Geotechnical Engineering

Influence of Recycled USP on Shear Behaviour of Railway Ballast: Experimental and Numerical Approach

H. G. S. Mayuranga, S. K. Navaratnarajah, C. S. Bandara, and J. A. S. C. Jayasinghe

Abstract The shear resistance at the sleeper–ballast interface plays a significant role in maintaining proper track stability of ballasted railway tracks. The Under Sleeper Pad (USP) application at the sleeper–ballast interface of ballasted railway tracks has become a regular practice among most of the railway authorities for reducing ballast degradation while enhancing track performance. However, the shear behaviour at the sleeper–ballast interface with and without the adoption of USP is not properly investigated. Therefore, the influence of recycled USP on shear behaviour at the sleeper–ballast interface was investigated in this study through large-scale direct shear tests and discrete element method (DEM) simulations. The large-scale direct shear tests were performed on Ballast–Ballast, Ballast–Concrete, and Ballast–USP interfaces under 60 kPa normal load. Based on the results, the Ballast–Ballast interface exhibited the highest shear stress variation, followed by the Ballast–USP and Ballast–Concrete interfaces. Also, the ballast particle breakage was quantified for each interface using experimental data. The results confirmed that the application of recycled USP has reduced particle breakage by 23% compared to the Ballast–Concrete interface. Then numerical models of large-scale direct shear tests were developed in DEM and validated using experimental data. The validated numerical models were used to evaluate the shear behaviour of different interfaces under 30, 60, 90, 120, 150, and 180 kPa normal loads. Based on the numerical results, linear and non-linear Mohr–Coulomb failure envelops were obtained for each interface and the peak friction angles were calculated. According to the findings, the Ballast–Ballast interface exhibited the highest friction angle value, followed by the Ballast–USP and Ballast–Concrete interfaces.

Keywords Ballast · DEM simulation · Large-scale direct shear test · Recycled under sleeper pad · Shear behaviour

H. G. S. Mayuranga (✉) · S. K. Navaratnarajah · C. S. Bandara · J. A. S. C. Jayasinghe
Department of Civil Engineering, University of Peradeniya, Peradeniya, Sri Lanka
e-mail: sushanm@eng.pdn.ac.lk

© The Author(s), under exclusive license to Springer Nature Singapore Pte Ltd. 2023

R. Dissanayake et al. (eds.), *ICSBE 2022*, Lecture Notes in Civil Engineering 362,
https://doi.org/10.1007/978-981-99-3471-3_17

1 Introduction

Ballasted railway tracks play a prominent role in maintaining efficient and cost-effective railway transportation facilities for passengers and freight. However, due to the current demand for faster and heavier trains, the existing ballasted rail corridors are being over-stressed [15] necessitating frequent and expensive track maintenance activities mainly due to the increased ballast degradation, track settlement, damage to track components, and poor track drainage [3, 14, 18]. Therefore, to reduce track deterioration and improve track performance under high-frequency loading, the application of Under Sleeper Pads (USPs) at the sleeper–ballast interface has become a well-known practice in many countries [1, 8, 10, 13, 17]. The USP attached to the bottom of the concrete sleeper provides a softer contact with the ballast layer where irregularly shaped ballast aggregates can embed into the USP surface and thereby improve the sleeper–ballast contact area [11, 16, 20]. This facilitates efficient and uniform transmission of load from the sleeper to the ballast layer which reduces the ballast layer stress and thereby the particle degradation.

The sleeper–ballast interface of a ballasted railway track plays a significant role in maintaining the proper connection between the track superstructure (i.e., rail and sleeper) and the substructure (i.e., ballast and underlying formation). The presence of USP attached to the concrete sleeper at the sleeper–ballast interface may alter the shear resistance compared to the concrete sleeper and that in turn, influences the track stability. Hence, a thorough understanding of shear behaviour at the sleeper–ballast interface is essential [4]. However, there is a lack of investigation on the shear behaviour of the sleeper–ballast interface when USPs are adopted. Therefore, this study explores the influence of USP made of recycled rubber on shear behaviour at the sleeper–ballast interface using large-scale experiments and Discrete Element Method (DEM) simulations.

In the laboratory investigation, three full-scale direct shear tests were conducted under 60 kPa normal stress on Ballast–Ballast, Ballast–Concrete, and Ballast–Recycled USP interfaces utilizing the large-scale direct shear facilities. The shear stress variation and the ballast breakage were obtained for each interface from experimental data. Then, three numerical models of large-scale direct shear tests representing all interfaces were developed in DEM and the parameters were calibrated using experimental data. The validated numerical models were used to evaluate the shear behaviour at each interface under different normal stresses including 30, 60, 90, 120, 150, and 180 kPa. Based on the numerical results, the Mohr–Coulomb failure envelopes were developed for each interface considering both linear and non-linear variations. Further, the apparent peak friction angle values were calculated for each interface.

2 Experimental Investigation

2.1 Large-Scale Test Apparatus

In this study, the large-scale direct shear apparatus built at the Geotechnical Engineering laboratory of the University of Peradeniya was employed. Figure 1 depicts a schematic diagram and a photograph of the apparatus, which can be used to study the shear behaviour of granular-type aggregates. The apparatus can accommodate an actual size granular aggregate specimen of 400 mm diameter and 300 mm height. To avoid the boundary effect, the ratio between the test specimen diameter and the average maximum particle diameter of ballast aggregates was maintained above 6 [6, 12]. The apparatus can separate the test sample into two equal portions under the shearing load using the upper and lower cylinders each having 400 mm diameter and 150 mm height. A lever arm system was used to apply the normal load to the top loading plate, which rests on the test sample. During the test, movement of the upper cylinder was restricted while the lower cylinder was displaced laterally at a constant rate of 4 mm/min using the manual hydraulic jack attached to the system. The reaction force on the upper cylinder during the shearing was measured using a load cell while the horizontal displacement of the lower cylinder and the vertical displacement of the top loading plate were measured using two Linear Variable Differential Transformers (LVDTs).

2.2 Test Materials and Test Procedure

The materials used in this study were fresh ballast, concrete sleeper, and recycled USP. Fresh railway ballast material was collected from a stockpile at the Gampola railway unit of the Department of Railways, Sri Lanka. The collected material was washed and air dried to remove unnecessary fine and mud particles adhered to ballast aggregates. The specific gravity and the bulk density of ballast obtained from standard laboratory tests were 2.69 and 1549 kg/m^3, respectively. The test samples were prepared following the particle size distribution shown in Fig. 2 which lies within the limits of the Indian standard gradation [7] of ballast.

The diameter and the height of the concrete sleeper used in this study were 400 mm and 150 mm, respectively. The concrete sleeper with 60 MPa compressive strength was prepared at the laboratory while the recycled USP with a thickness of 10 mm was obtained from a local manufacturer. The density, static bedding modulus (as per DIN 45673-1), and Young's modulus of the USP were 970 kg/m^3, 0.19 N/mm^3, and 6.15 MPa, respectively. Figure 3 depicts the prepared concrete sleeper as well as the recycled USP which was attached to the concrete sleeper using epoxy glue.

Three different test specimens were prepared as shown in Fig. 4 representing Ballast–Ballast, Ballast–Concrete, and Ballast–Recycled USP interfaces.

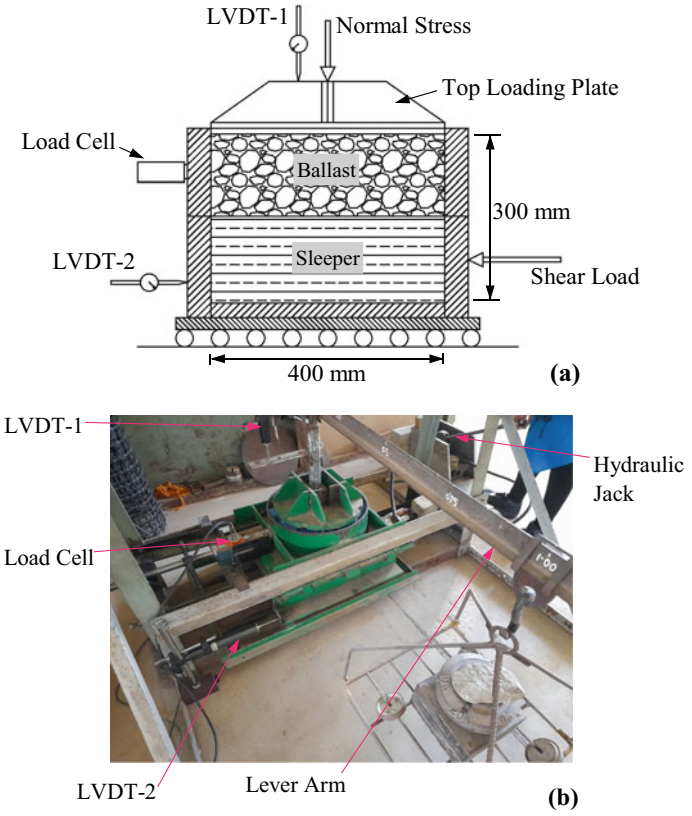

Fig. 1 Large-scale direct shear apparatus; **a** a schematic diagram and **b** a photograph

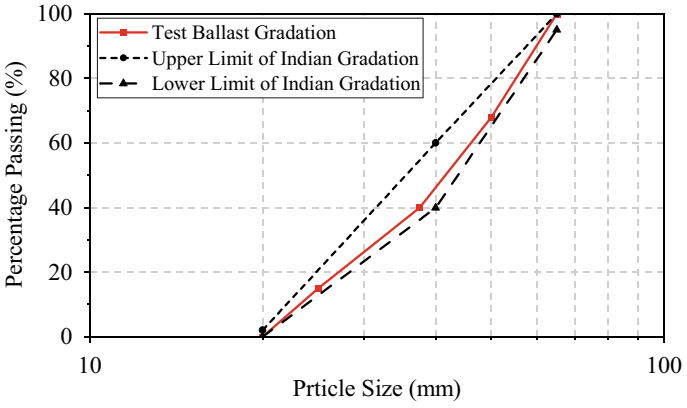

Fig. 2 Gradation of ballast and limits of Indian standard gradation

Fig. 3 Prepared concrete sleeper (left) and recycled USP attached to the concrete sleeper (right)

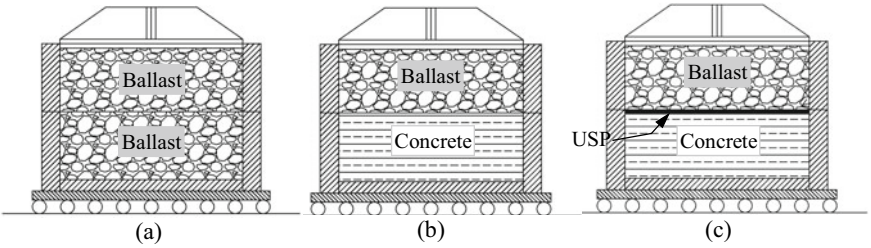

Fig. 4 Prepared test specimens; **a** Ballast–Ballast interface sample, **b** Ballast–Concrete interface sample, and **c** Ballast–Recycled USP interface sample

In the Ballast–Ballast interface sample, the test apparatus was filled with ballast aggregates in three (3) equal layers. Each layer was compacted using a rubber-padded vibratory compactor to achieve the required field density. When preparing the Ballast–Concrete interface and Ballast–Recycled USP interface samples, the lower cylinder was filled with the concrete sleeper or USP–attached concrete sleeper while the upper cylinder was filled with ballast aggregates. Here also the ballast layer was compacted in 50 and 100-mm thick layers to achieve the required field density. After filling the materials, a 60 kPa normal stress was applied on each sample through the loading plate using the lever arm system. Then the lower cylinder was displaced at a constant rate of 4 mm/min and the readings from the load cell and two LVDTs were recorded in the computer through a data logger. After each test, the ballast samples were sieved to obtain the particle size distribution after the test.

2.3 Results of Experimental Investigation

Figure 5 presents the variation of shear stress against shear strain for each interface under 60 kPa normal load. As expected, the Ballast–Ballast interface exhibited the highest shear stress variation due to the higher interlocking mechanism of highly angular ballast aggregates at the shearing plane. When considering the other two interfaces, the Ballast–Recycled USP interface showed a higher shear stress variation compared to the Ballast–Concrete interface. The recycled USP surface, as opposed to the concrete surface, allowed ballast aggregates to embed into the USP, increasing shear resistance at the Ballast–USP interface. The peak shear stresses of Ballast–Ballast, Ballast–Recycled USP, and Ballast–Concrete interfaces were 158.8, 84.4, and 43.8 kPa, respectively. According to that, the Ballast–recycled USP interface exhibited significant improvement (about 93%) in the peak shear stress compared to that of the Ballast–Concrete interface.

The variation of vertical strain against shear strain for each interface is plotted in Fig. 6. According to that, all the samples exhibited initial compression followed by dilation. Due to the higher particle rolling at the ballast–ballast interface, the Ballast–Ballast interface sample showed the highest dilatation behaviour. In addition, the dilation behaviour of the Ballast–Recycled USP interface and Ballast–Concrete interface samples was comparable, however, the initial compression of the Ballast–Recycled USP interface sample was significant.

Based on the particle size distribution data after the test, the ballast particle breakage was quantified using the Ballast Breakage Index (BBI) proposed by Indraratna et al. [5]. As depicted in Fig. 7, the Ballast–Ballast interface sample exhibited the highest BBI value followed by the Ballast–Concrete interface and Ballast–Recycled USP interface.

The presence of recycled USP reduced the BBI by about 23% compared to the concrete sleeper. Therefore, the results of this study reveal that the application of recycled USPs in ballasted railway tracks enhances the shear resistance at the sleeper–ballast interface while reducing particle breakage.

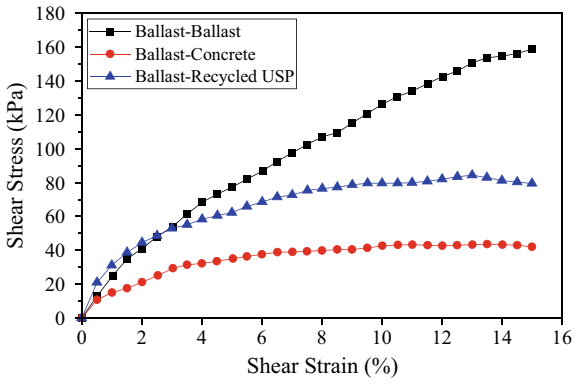

Fig. 5 Variation of shear stress against shear strain for each interface

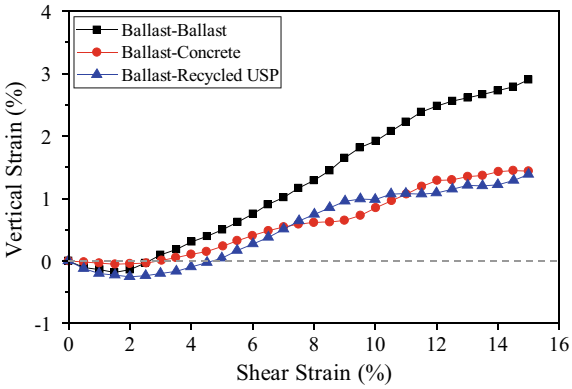

Fig. 6 Variation of vertical strain against shear strain for each interface

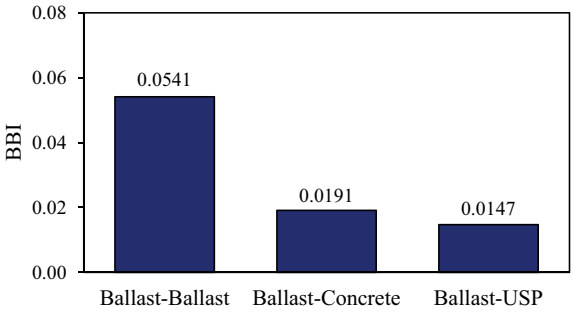

Fig. 7 BBI values for each test sample

3 Numerical Simulation

The numerical simulation was carried out using the Discrete Element Method (DEM). Three numerical models of large-scale direct shear tests representing the Ballast–Ballast interface, Ballast–Concrete interface, and Ballast–Recycled USP interface samples were developed.

3.1 Development of Numerical Models and Validation

To generate the ballast particles in DEM, four representative ballast aggregates were selected according to the particle size distribution of ballast used in the experimental study and they were scanned using a 3-D scanner to obtain the CAD templates of the particles. The CAD templates were used to generate the breakable ballast particles as shown in Fig. 8. To reduce the significantly high computational cost associated with the larger number of spheres in the simulation, only about 12 spheres were used to generate each particle without significantly damaging the shape of real ballast particles. The spheres of each particle were bonded together using finite-size glue

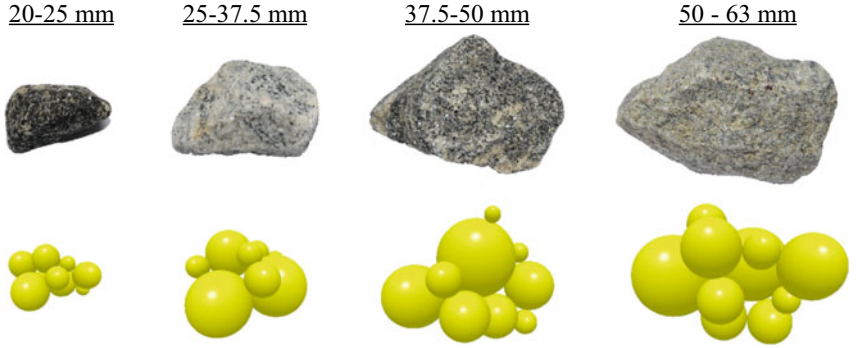

Fig. 8 Selected actual ballast particles and corresponding breakable ballast particles developed in DEM

bonds to simulate the breakage of particles which influences the shear behaviour of ballast. Also, the Hertz-Mindlin contact model was adopted in this study which provides an efficient and accurate force calculation in DEM simulation.

The upper and lower cylinders of large-scale direct shear apparatus were modelled as geometries and steel material properties were assigned to them. The concrete sleeper and USP were also modelled as geometries and corresponding material properties were assigned. Table 1 summarizes the parameter values used in DEM simulation and Fig. 9 shows the developed numerical models in DEM. After filling the ballast aggregates in each model as shown in Fig. 9, the top-loading plate was introduced with 60 kPa normal stress. Then the lower cylinder was displaced laterally at a constant rate of 4 mm/min for 900 s to achieve 15% shear strain. At the end of the simulation, the lateral displacement of the lower cylinder and the reaction force on the upper cylinder in the shearing direction were obtained for selected time steps.

Based on that, the variation of shear stress against shear strain was obtained for each interface and was compared with experimental data as shown in Fig. 10. According to that, a good agreement between experimental and numerical results was obtained. Therefore, the developed numerical models could simulate the shear behaviour of ballast with different interfaces.

3.2 Parametric Study

The validated numerical models were used to conduct the parametric study, which assessed the shear behaviour of each interface under various normal loads such as 30, 60, 90, 120, 150, and 180 kPa. In the validated numerical models, only the normal stress was changed without changing the particle configuration inside the test specimen. Based on the results, Fig. 11 presents the variation of shear stress against shear strain for each interface under different normal stresses. As expected, for each interface, shear stress increased as normal stress increased.

Table 1 The values of different parameters used in the DEM simulation

Parameter	Material			
	Ballast	*Steel*	*Concrete*	*Recycled USP*
Solid density (kg/m^3)	2950	7850	2400	970
Poisson's ratio	0.25	0.3	0.2	0.48
Shear modulus (MPa)	50	80,000	15,000	2.03
Interface	Ballast–Ballast	Ballast–Steel	Ballast–Concrete	Ballast–USP
Coefficient of static friction	0.5	0.7	0.75	1.5
Coefficient of restitution	0.2	0.7	0.6	0.3
Coefficient of rolling friction	0.01	0.05	0.01	0.08
Bond strength parameters of ballast				
Normal/shear stiffness per unit area (N/m^3)			6.84×10^9	
Normal/shear strength (MPa)			6	
Bond disc scale			0.5	

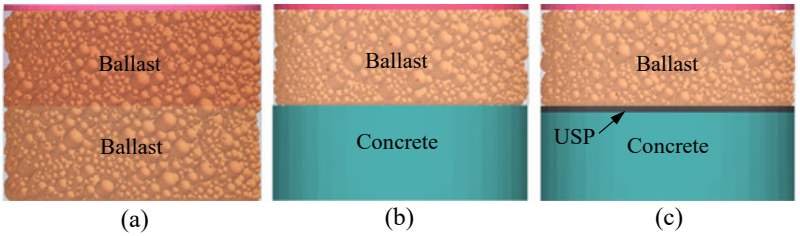

Fig. 9 Developed DEM models; **a** Ballast–Ballast interface, **b** Ballast–Concrete interface, and **c** Ballast–Recycled USP interface samples

Fig. 10 Comparison of experimental and numerical results

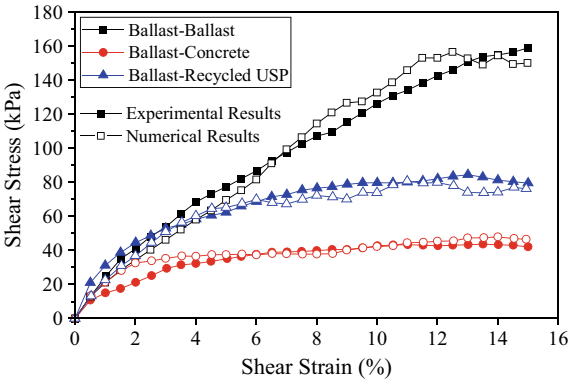

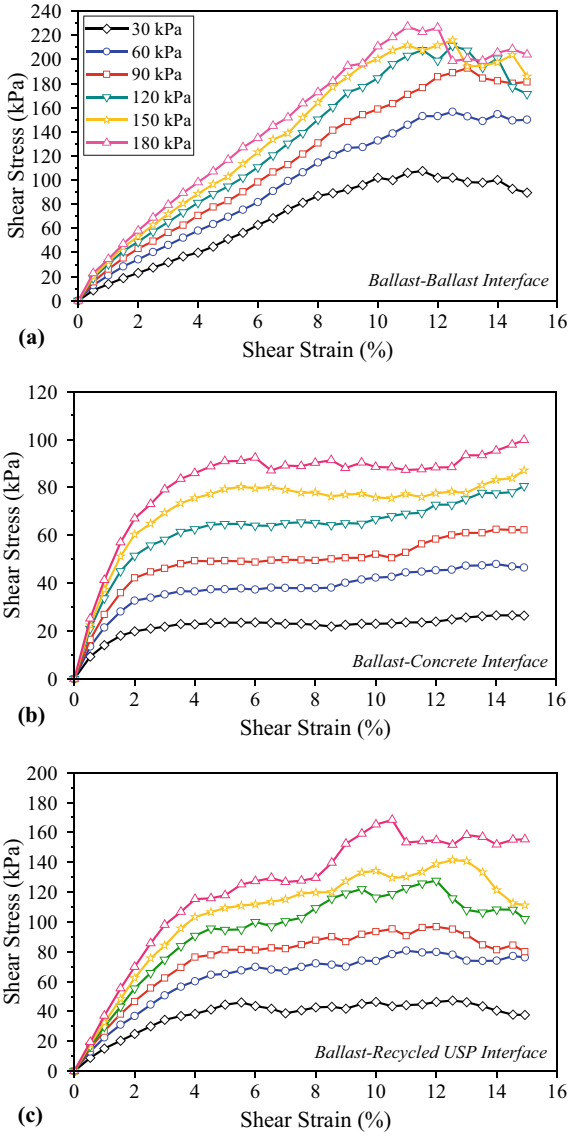

Fig. 11 Variation of shear stress with shear strain under different normal stresses for **a** Ballast–Ballast, **b** Ballast–Concrete, and **c** Ballast–Recycled USP interface samples

The peak shear stress values under different normal stresses were obtained from Fig. 11 for each interface to determine the Mohr–Coulomb (M–C) failure envelopes. Figure 12 illustrates the linear variation of M–C failure envelopes for each interface. However, linear M–C envelopes offer cohesion values for granular ballast aggregates which is not consistent [2]. Hence, previous studies have proposed the non-linear M–C failure envelope for granular materials [6, 12, 19].

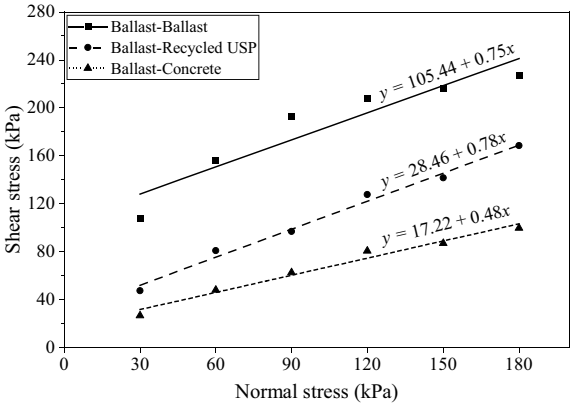

Fig. 12 Linear Mohr–Coulomb failure envelopes for each interface

Further, Indraratna et al. [6] suggested a relationship between the normalized shear stress and normalized normal stress to capture the non-linear behaviour of M–C envelope, which is given by,

$$\frac{\tau_p}{\sigma_c} = a\left(\frac{\sigma_n}{\sigma_c}\right)^b \tag{1}$$

where τ_p is the peak shear stress, σ_n is the normal stress, σ_c is the uniaxial compressive strength of the parent rock, while a and b are dimensionless constants. In this study, the uniaxial compressive strength of the ballast was considered as 120 MPa [9]. Based on that, non-linear M–C failure envelopes were developed for each interface, as illustrated in Fig. 13. The Ballast–Ballast interface sample, as expected, had the greatest variation in normalized shear stress, followed by the Ballast–Recycled USP interface and Ballast–Concrete interface samples. The apparent peak friction angle (φ_p) values for each interface under different normal stresses were then computed using:

$$\varphi_p = \tan^{-1}\left(\frac{\tau_p}{\sigma_p}\right) \tag{2}$$

where, σ_p is the normal stress. According to the computed results presented in Table 2, when the normal stress increased, the peak friction angle decreased. Additionally, the Ballast–Ballast interface exhibited the largest peak friction angle for each normal load, followed by the Ballast–Recycled USP and Ballast–Concrete interfaces. Moreover, the inclusion of recycled USP improved the average peak friction angle of the sleeper–ballast contact by 40% when compared to the concrete sleeper without USP.

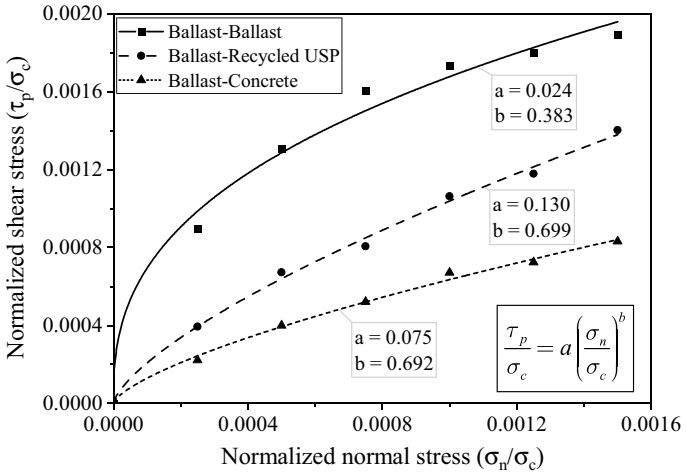

Fig. 13 Non-linear Mohr–Coulomb failure envelopes for each interface

Table 2 Apparent peak friction angle values for each interface

Normal stress (kPa)	Apparent peak friction angle (degree)		
	Ballast–Ballast	Ballast–Concrete	Ballast–Recycled USP
30	74	41	58
60	69	39	53
90	65	35	47
120	60	34	46
150	55	30	44
180	52	29	43

4 Conclusion

The shear behaviour at the sleeper–ballast interface is crucial as it influences the track stability. Therefore, this study explores the influence of recycled USP on the shear behaviour of railway ballast at the sleeper–ballast interface. According to the large-scale direct shear test results, the Ballast–Ballast interface exhibited the highest shear variation followed by Ballast–Recycled USP and Ballast–Concrete interfaces. Further, particle breakage was highest at the Ballast–Ballast interface, whereas it was lowest at the Ballast–Recycled USP interface. When compared to the Ballast–Concrete interface sample, the Ballast–Recycled USP interface sample reduced the BBI value by about 23%.

Further, a parametric study was carried out under the numerical investigation using DEM. The results revealed that the shear stress increased as the normal stress increased. Moreover, the Ballast–Ballast interface sample had the maximum peak

shear stresses for all normal loads, followed by the Ballast–Recycled USP interface and Ballast–Concrete interface samples. The highest apparent peak friction angle values were reported for the Ballast–Ballast interface for all normal loads. When compared to the Ballast–Concrete interface, the Ballast–Recycled USP interface improved the apparent peak friction angle by about 40% on average, while reducing the ballast breakage by about 23% (for 60 kPa normal stress). Therefore, based on this study, the recycled USP exhibited higher shear stress variation and lower particle breakage at the sleeper–ballast interface compared to the concrete sleeper without USP.

Acknowledgements The support provided by the Accelerating Higher Education Expansion and Development (AHEAD) Operation of the Ministry of Higher Education, Sri Lanka funded by the World Bank (Grant No: AHEAD/RA3/DOR/STEM/No.63) is gratefully appreciated.

References

1. Abadi T, Pen LL, Zervos A, Powrie W (2019) Effect of sleeper interventions on railway track performance. J Geotech Geoenvironmental Eng. https://doi.org/10.1061/(ASCE)GT.1943-5606.0002022145(4),1-17
2. Dissanayake D, Kurukulasuriya L, Dissanayake P (2016) Evaluation of shear strength parameters of rail track ballast in Sri Lanka. J Natl Sci Found. https://doi.org/10.4038/jnsfsr.v44i1.798244(1)
3. Esmaeili M, Aela P, Hosseini A (2017) Experimental assessment of cyclic behavior of sand-fouled ballast mixed with tire-derived aggregates. Soil Dyn Earthq Eng. https://doi.org/10.1016/j.soildyn.2017.03.03398,1-11
4. Guo Y, Fu H, Qian Y, Markine V, Jing G (2020) Effect of sleeper bottom texture on lateral resistance with discrete element modelling. Constr Build Mater 250:118770
5. Indraratna B, Lackenby J, Christie D (2005) Effect of confining pressure on the degradation of ballast under cyclic loading. Geotechnique. https://doi.org/10.1680/GEOT.2007.57.6.52755(4),325-328
6. Indraratna B, Wijewardena L, Balasubramaniam A (1993) Large-scale triaxial testing of grey wacke rockfill. Geotechnique. https://doi.org/10.1680/geot.1993.43.1.3743(1),37-51
7. IRS-GE-1 (2004). "Specification for track ballast." Research Designs and Standards Organisation (RDSO), Ministry of Railways—India
8. Jayasuriya C, Indraratna B, Ngo TN (2019) Experimental study to examine the role of under sleeper pads for improved performance of ballast under cyclic loading. Transp Geotech. https://doi.org/10.1016/j.trgeo.2019.01.00519,61-73
9. Jayawardena UdS (2001) "A study on the engineering properties of Sri Lankan rocks." J Inst Eng Sri Lanka XXXIV(02): 7–21
10. Kaewunruen S, Aikawa A, Remennikov AM (2017) Vibration attenuation at rail joints through under sleeper pads. Procedia Eng. https://doi.org/10.1016/j.proeng.2017.05.031189,193-198
11. Loy H (2008) Under sleeper pads: improving track quality while reducing operational costs. Eur Railw Rev 4:46–51
12. Marschi ND, Chan CK, Seed HB (1972) Evaluation of properties of rockfill materials. J Soil Mech Found Div. https://doi.org/10.1061/JSFEAQ.000173598(1),95-114
13. Mayuranga HGS, Navaratnarajah SK, Bandara CS, Jayasinghe JASC (2019) 'A state of the art review of the influence of rubber inclusions in railway tracks'. In: 10th International conference on structural engineering and construction management. Kandy, Sri Lanka, pp 367–377

14. Mayuranga HGS, Navaratnarajah SK, Gimhani MMN, Karunarathne JMMY (2022) "The effect of fouling materials on permeability behaviour of large size granular materials". In Dissanayake R, Mendis P, Weerasekera K, De Silva S, Fernando S (eds) ICSBE 2020, Lecture notes in civil engineering vol 174, Springer, Singapore, pp 33–46
15. Navaratnarajah SK (2017) Application of rubber inclusions to enhance the stability of ballasted rail track under cyclic loading. PhD thesis, School of Civil, Mining and Environmental Engineering, University of Wollongong
16. Navaratnarajah SK, Indraratna B (2020) "Application of under sleeper pads to enhance the sleeper-ballast interface behaviors", Construction in Geotechnical Engineering, Springer, pp 619–636
17. Navaratnarajah SK, Indraratna B, Ngo NT (2018) Influence of under sleeper pads on ballast behavior under cyclic loading: experimental and numerical studies. J Geotech Geoenviron-Ment Eng. https://doi.org/10.1061/(ASCE)GT.1943-5606.0001954144(9),1-16
18. Navaratnarajah SK, Indraratna B, Nimbalkar S (2015) "Performance of rail ballast stabilized with resilient rubber pads under cyclic and impact loading". In: Proceedings of the international conference on geotechnical engineering. Colombo, Sri Lanka, pp 617–620
19. Ngo NT (2012) Performance of geogrids stabilised fouled ballast in rail tracks. PhD thesis, School of Civil, Mining and Environmental Engineering, University of Wollongong
20. Sol-Sanchez M, Moreno-Navarro F, Rubio-Gámez MC (2014) Viability of using end-of-life tire pads as under sleeper pads in railway. Constr Build Mater. https://doi.org/10.1016/j.conbuildmat.2014.04.01364,150-156

Experimental and Numerical Study on the Shear-Strain Behavior of Ballast with Different Gradations

S. Venuja, S. K. Navaratnarajah, C. S. Bandara, and J. A. S. C. Jayasinghe

Abstract Rockfill materials are widely used in many infrastructure constructions including earth dams, rail tracks, retaining walls, highways, etc. The major role of these coarse granular materials is to stabilize the body of the structure and maintain the geometry. Ballast is one such material used primarily in rail track substructures. Several factors are governing the mechanical properties of the ballast layer such as particle size, shape, angularity, gradation, particle density, hardness, etc. Ballast gradations are varying from country to country based on geology, climatic condition, source of parent rock, and economics. In Sri Lanka, biotite gneiss is used as the ballast material and there is no specific gradation for ballast. Further, the shear strength behaviour of the ballast is not fully understood with different gradations. Therefore, this study was carried out to analyse the effect of gradations on the shear behaviour of ballast using experimental and numerical analysis for Sri Lanka. Shear stress increased with normal stress increase due to the improved and intensified contact between particles. About 30% increase in shear stress was obtained from the laboratory test results for gradation with a high number of larger particles. Generated numerical results showed a good acceptance of experimental results and led to carrying out a parametric study with different normal stresses. The findings of this study suggest that the presence of larger size particles causes higher friction which in turn results in an increase in shear strength.

Keywords Ballast · Contact · Gradation · Mechanical properties · Shear strength

1 Introduction

Rail transport is a popular mode of transport due to numerous benefits including safety, low cost, less time delay, and less traffic congestion. Urbanization and growing population demand faster and heavier trains on traditional ballasted tracks

S. Venuja (✉) · S. K. Navaratnarajah · C. S. Bandara · J. A. S. C. Jayasinghe
Department of Civil Engineering, Faculty of Engineering, University of Peradeniya, Peradeniya, Sri Lanka
e-mail: venujas@eng.pdn.ac.lk

© The Author(s), under exclusive license to Springer Nature Singapore Pte Ltd. 2023

R. Dissanayake et al. (eds.), *ICSBE 2022*, Lecture Notes in Civil Engineering 362,
https://doi.org/10.1007/978-981-99-3471-3_18

[2, 5, 11]. The ballast layer is the largest component in the track system. Ballast material is obtained from crushing parent rocks namely Biotite, Basalt, Granite, Gneiss, Dolomite, etc. It is placed under and around the sleepers on rail tracks. It helps to keep sleepers in position without any larger movements in longitudinal, transverse, and vertical directions. The primary function of the ballast layer is to transfer the loads from sleepers to the underlying layers at a reduced level and provide rapid drainage. With time, due to the continuous passage of trains, ballast materials undergo breakage and become fouled. This ballast deterioration affects the overall track performance and longevity [6, 9, 10]. Therefore, it is important to understand the mechanical characteristics of the ballast.

The shear strength of the ballast provides lateral confinement and resistance to maintain the geometry of the track structure. The shear behaviour of ballast varies with different factors. Ballast gradation is one such factor that affects shear strength. Particle size distribution of ballast is not the same for all the countries. It varies considering the subgrade properties, load application, climate, the strength of the parent rock, etc. [1, 8]. Gradations are selected mainly by considering the strength and drainage properties of the ballast layer. Researchers studied the shear behaviour of the ballast by conducting large-scale direct shear tests and triaxial tests [3, 4, 7, 12, 14, 16, 19–21]. Danesh et al. [3] concluded that the effect of maximum particle size (d_{max}) is having more impact on the shear behaviour than the Coefficient of Uniformity (C_u). It is found that with increasing d_{max} and C_u the shear strength increases. Sun et al. [17] considered d_{max}, C_u, median particle size (d_{50}), and initial void ratio (e_0) as controlling factors and suggested $2.3 \leq C_u \leq 2.6$ and $36 \leq d_{50} \leq 41$ mm for d_{max} of 53 mm.

In Sri Lanka, ballast particle sizes from 19 to 63 mm are used in rail tracks. There is no unique gradation used in Sri Lankan tracks. No studies have been conducted so far on the shear behaviour of ballast with various gradations in Sri Lanka. Therefore, this study mainly focuses on understanding the effect of different gradations on the shear behaviour of the ballast in Sri Lanka. A series of large-scale direct shear tests were conducted on the ballast with three different gradations and a numerical model was developed to represent the laboratory test. This paper discusses the outcome of both experimental and numerical studies.

2 Laboratory Testing Using Large-Scale Direct Shear Test Apparatus

Ballast material was collected from the Gampola stockpile. Ballast was washed, dried, and sieved using 19, 25, 37.5, 50, and 63 mm sieves to separate particles into the required size ranges. The main aim of this study is to analyse the effect of gradation on the shear behaviour of railway ballast. For that, three gradations were chosen considering Indian gradation limits as shown in Fig. 1. Indian gradation limits are considered in this study as it is adopted in the Sri Lankan rail tracks as well. Here

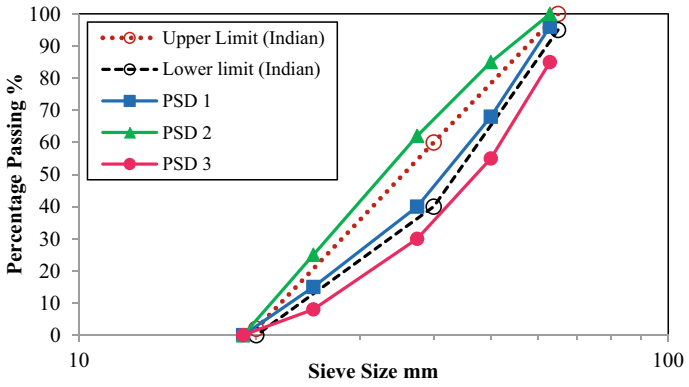

Fig. 1 Different gradations used in this study and Indian gradation limits

PSD 1 is in between the upper and lower limits of Indian standard which is normally adopted in Sri Lankan rail tracks. PSD 2 is obtained by increasing the percentage of particles between 19 mm and 37.5 mm size ranges, beyond the upper limit. On the other hand, PSD 3 is obtained by increasing the percentage of particles between 37.5 mm and 63 mm size ranges.

Large-scale direct shear apparatus with a circular shear plane was used in this study. Details of the apparatus can be found elsewhere [13, 19]. The test specimen was prepared based on the gradation by adding the required amount of ballast and thoroughly mixing using a shovel. The material was filled into the apparatus in three layers and compacted using a rubber-padded hammer to obtain field unit weight. Three different normal stresses were selected as 30, 60, and 90 kPa. Test specimen with PSD 1 was tested for all three normal stresses. Only one test under 60 kPa normal stress was conducted for specimen with PSD 2 and PSD 3 to limit the effort and laboratory testing by making use of numerical techniques.

3 Numerical Modelling Using DEM

Two major approaches in numerical analysis are (1) Finite Element Method (FEM); (2) Discrete Element Method (DEM). Considering the granular angular distinct particles of the ballast material, DEM was chosen in this study. Particle shape is an important factor that affects the mechanical behaviour of the ballast assembly. Therefore, the shape of the particle for the model was obtained as a shape file by scanning with a 3D laser scanner and creating a closed surface by connecting point cloud data. Then, particles were generated using the multi-sphere clump method as illustrated in Venuja et al. [18]. Figure 2 shows the apparatus model created along with the complete test setup. The top plate was used to apply the normal stress and shearing was applied to the lower cylinder until a 15% shear strain is obtained.

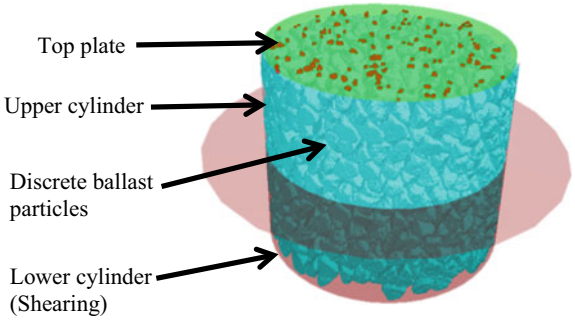

Fig. 2 Numerical model of a complete test setup

4 Results and Discussion

4.1 Effect of Gradation Experimental Results

Shear stress was calculated using the shear load and horizontal displacement data obtained from the data logger. Shear area correction factor was suggested by [15] for the circular shear plane. Figure 3 elaborates the shear stress and vertical strain variation of PSD 1 with shear strain under different normal stresses. As expected, with the normal stress increase, a growth in shear stress was observed owing to the higher particle interlocking. On the other hand, a reduction in dilation was observed with high normal stresses. This is as a result of restrictions in particle movements.

Figure 4a illustrates the shear stress vs shear strain of ballast with different gradations as explained in Sect. 2. A higher shear stress variation was obtained for PSD 3 where the percentage of particles between 37.5 mm and 63 mm is high. There is no significant improvement in shear behaviour when increasing the percentage of particles between 19 mm and 37.5 mm. When comparing with PSD 1, there are 29.7% increase and 16.5% increase for PSD 3 at 7.5% and 15% shear strains, respectively. This is mainly because of the higher contribution to the shear resistance from larger particles in comparison to smaller particles through the high contact area. As shown in Figure 4b, an initial compression followed by higher dilation was observed in PSD 2 and PSD 3. This slightly high dilation resulted from the increased void spaces.

4.2 Numerical Model Calibration and Validation

By changing the coefficients of restitution, static friction, and rolling friction at ballast-ballast contact and ballast-steel contact, an acceptable agreement between experimental shear variation and numerical shear variation was obtained for PSD 1 under 60 kPa normal stress using the trial-and-error method. Using these calibrated

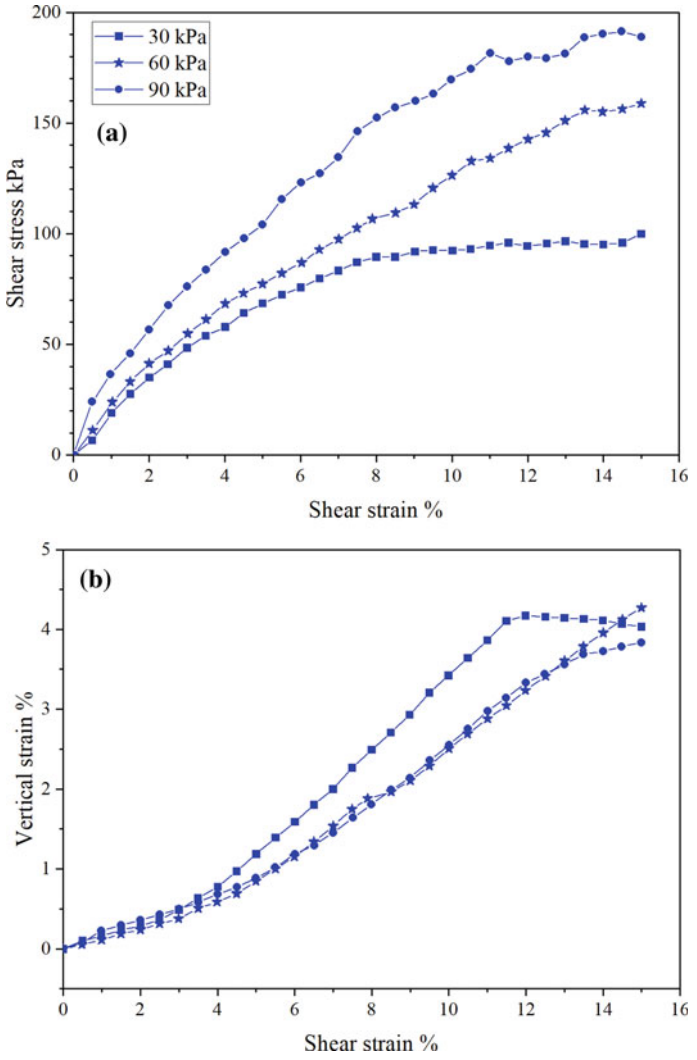

Fig. 3 **a** Shear Stress and **b** Vertical Strain variation of Ballast with PSD1 under different normal stresses

coefficients, the same model was run for the other two normal stresses of 30 and 90 kPa. Numerical results were obtained and compared with experimental results as shown in Fig. 5. An acceptable agreement was observed in this comparison and the calibrated model is validated. After that, by changing the gradations in the numerical model, the other two models for PSD 2 and PSD 3 were run and compared with the laboratory test results as illustrated in Fig. 6.

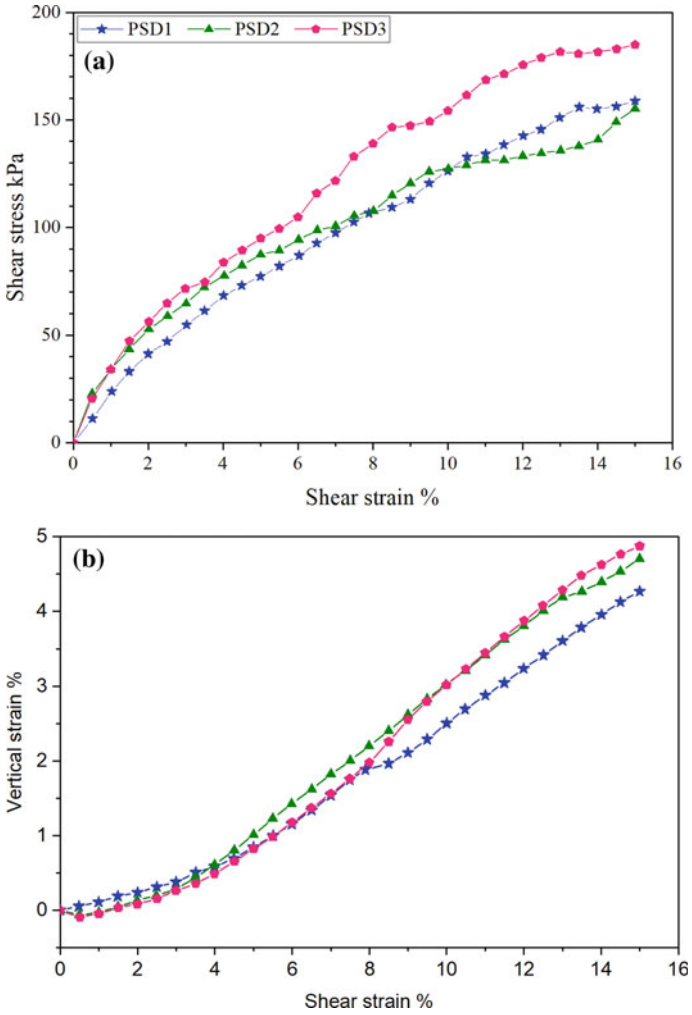

Fig. 4 **a** Shear Stress and **b** Vertical Strain variation of Ballast with different gradations under 60 kPa normal stress

4.3 Parametric Study

Using the distinct calibrated models of PSD 2 and PSD 3, models were run for 30 and 90 kPa normal stresses, and results were plotted (see Fig. 7). As observed in the laboratory test results of PSD 1, the percentage increase in shear stress is lesser for the shear stress variation from 60 to 90 kPa normal stress. In addition to this, non-linear Mohr–Coulomb failure envelopes were developed using the numerical results as shown in Fig. 8. The friction angle varied from 74° to 63° for PSD 1, from 76° to

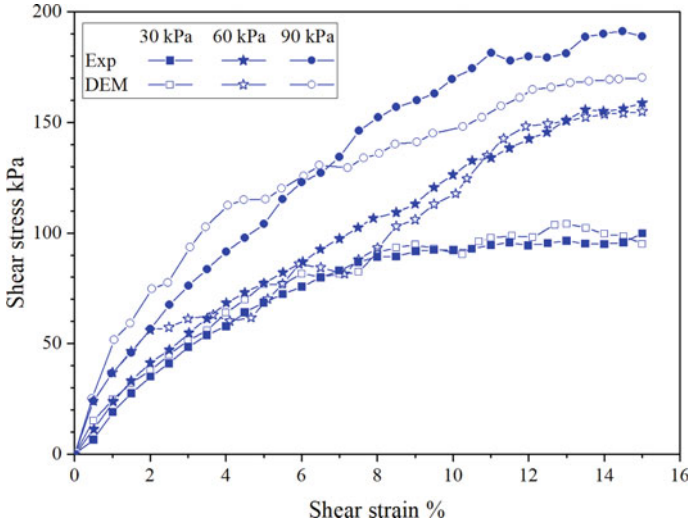

Fig. 5 Comparison of experimental and numerical shear stress variation with shear strain (For PSD 1)

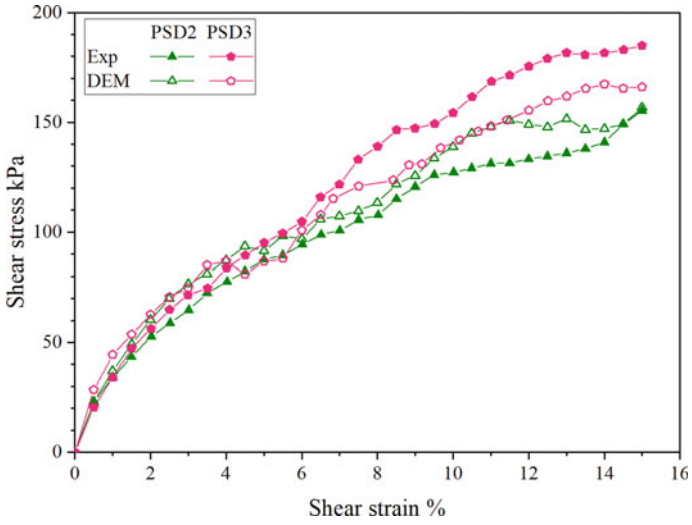

Fig. 6 Numerical model validation using experimental results for PSD 2 and PSD 3

62° for PSD 2, and from 78° to 66° for PSD 3 within the applied normal stress range. Friction angle reduced with high normal stresses due to the high particle breakage results in lesser shear resistance.

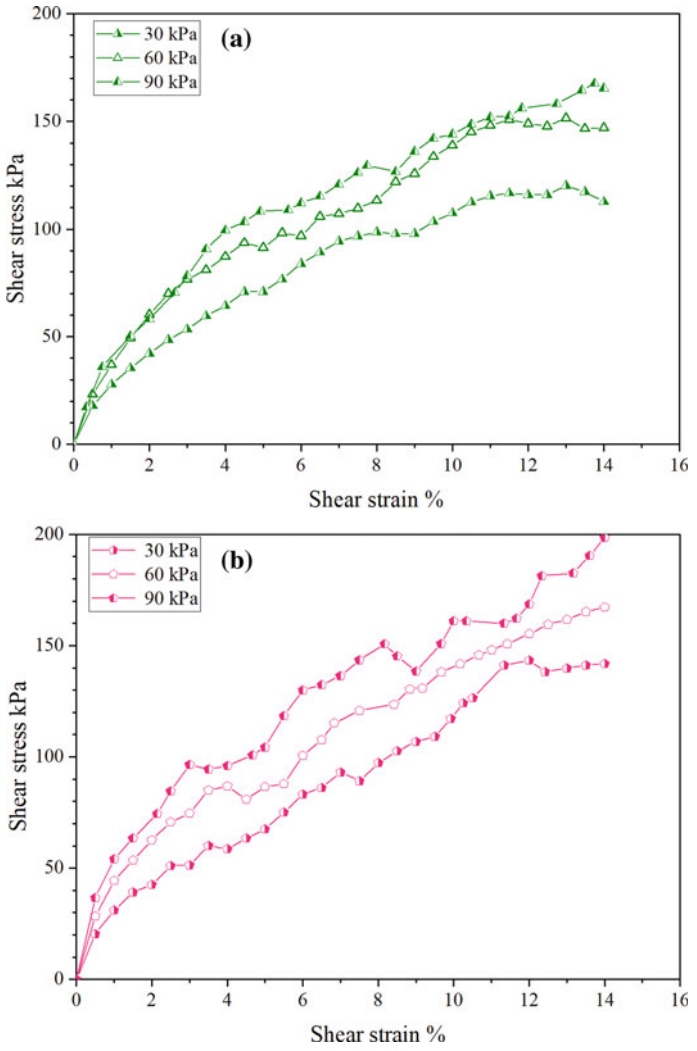

Fig. 7 Parametric study on shear stress variation using validated DEM models; **a** PSD 2; **b** PSD 3

5 Conclusions

This paper elaborates the effect of particle size distribution on the shear behaviour of ballast. For that, three different gradations were chosen, and large-scale direct shear tests were conducted. In addition to this, numerical simulation using DEM was also carried out. By increasing the normal stress, the shear stress of the ballast was observed due to the higher particle interlocking. In contrast, dilation is reduced due to the high compaction of materials. The presence of a higher number of larger particles

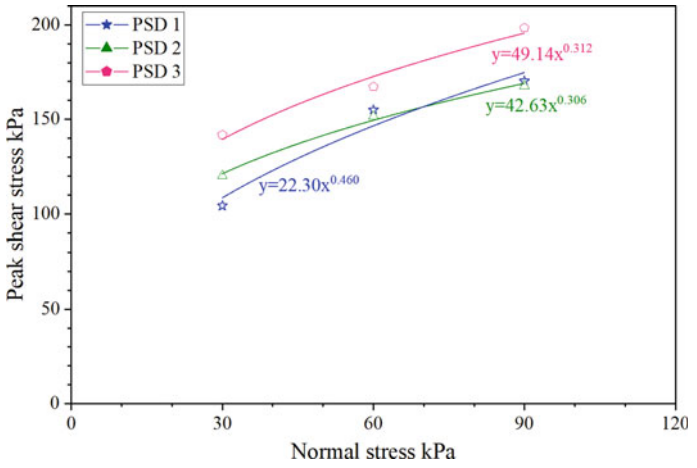

Fig. 8 Non-linear Mohr–Coulomb envelopes developed from numerical outcomes

resulted in higher shear strength. Numerical results showed acceptable agreement with the experimental results. The DEM was further extended to predict the results for normal stresses of 30 and 90 kPa, and Mohr–Coulomb envelopes were developed. As observed from experimental results of 60 kPa normal stress for all three gradations, an increase in shear stress was observed. Approximately, a 3–4-degree increase was observed in friction angle for PSD 3 than that for PSD 1.

In conclusion, the findings show that the shear behaviour of the ballast is changing with gradation and showing high shear strength for the gradation with a higher amount of larger size particles. Moreover, the validated model can be used to conduct parametric studies under higher normal stresses to find out the friction angle variation, which is always very difficult in laboratory large-scale testing.

Acknowledgements Accelerating Higher Education Expansion and Development (AHEAD) Operation of the Ministry of Higher Education funded by the World Bank (Grant No: AHEAD/RA3/DOR/STEM/No.63) is acknowledged by the authors for the financial support provided throughout this research.

References

1. Anbazhagan P, Bharatha T, Amarajeevi G (2012) Study of ballast fouling in railway track formations. Indian Geotech J 42(2):87–99
2. Chawla S, Banerjee L, Dash SK (2018) Three dimensional finite element analyses of geocell reinforced railway tracks. Indian Geotechnical Conference. Bengaluru, India, pp 1–5
3. Danesh A, Palassi M, Mirghasemi AA (2018) Effect of sand and clay fouling on the shear strength of railway ballast for different ballast gradations. Granul Matter 20(3)(51):1–14. https://doi.org/10.1007/s10035-018-0824-z

4. Dash SK, Shivadas AS (2012) "Performance improvement of railway Ballast using geocells." Indian Geotech J 42(3): 186–193. https://doi.org/10.1007/s40098-012-0017-3
5. Deshpande TS, Thakare SW, Dhatrak AI (2019) "Performance of geosynthetic reinforced ballasted rail track." Int J Innov Res Sci, Eng Technol 8(6): 6805–6813. https://doi.org/10.15680/IJIRSET.2019.0806046
6. Eller B, Fischer S (2019) "Review of the modern ballasted railway tracks substructure and further investigations." Creat Commons Attrib 4 Int 6(84): 72–85. https://doi.org/10.15802/stp2019/195831
7. Jia W, Markine V, Guo Y, Jing G (2019) "Experimental and numerical investigations on the shear behaviour of recycled railway ballast." Constr Build Mater: 310–320. https://doi.org/10.1016/j.conbuildmat.2019.05.020
8. Liu J, Sysyn M, Liu Z, Kou L, Wang P (2022) "Studying the strengthening effect of railway Ballast in the direct shear test due to insertion of middle-size Ballast particles." J Appl Comput Mech: 1–11. https://doi.org/10.22055/jacm.2022.40206.3537
9. Navaratnarajah S, Indraratna B, Nimbalkar S (2015) "Performance of rail ballast stabilized with resilient rubber pads under cyclic and impact loading". International Conference on Geotechnical Engineering, Colombo, pp 617–620
10. Navaratnarajah SK, Indraratna B. (2020a) "Application of under sleeper pads to enhance the sleeper–ballast interface behaviours." Construction in Geotechnical Engineering. Singapore, Springer, pp 619–636
11. Navaratnarajah SK, Indraratna B (2020) Stabilisation of stiffer rail track substructure using artificial inclusion. Indian Geotech J 50(2):196–203
12. Navaratnarajah SK, Mayuranga HGS (2021) "Shear and degradation behavior of rail ballast with different interfaces", In: 3rd International conference on geotechnical engineering. Colombo, Sri Lanka, pp 116–121
13. Navaratnarajah SK, Mayuranga HGS, Venuja S (2022) "Shear behavior and Permeability of rail track ballast fouled by the infiltration of finer particles". In: 1st International Conference on Engineering, University of Jaffna, Kilinochchi, Sri Lanka, pp 66–72
14. Ngo NT, Indraratna B, Rujikiatkamjorn C, Mahdi Biabani M (2016) Experimental and discrete element modeling of geocell-stabilized subballast subjected to cyclic loading. J Geotech Geoenvironmental Eng 142(4):04015100
15. Olson RE, Lai J (1989) Direct shear testing. pp 1–14
16. Sadeghi J, Tolou Kian AR, Ghiasinejad H, Fallah Moqaddam M, Motevalli S (2020) "Effectiveness of geogrid reinforcement in improvement of mechanical behavior of sand-contaminated ballast." Geotext Geomembr: 1–12. https://doi.org/10.1016/j.geotexmem.2020.05.007
17. Sun Y, Chen C, Nimbalkar S (2017) Identification of ballast grading for rail track. J Rock Mech Geotech Eng 9(5):945–954. https://doi.org/10.1016/j.jrmge.2017.04.006
18. Venuja S, Navaratnarajah SK, Jayawardhana WRR, Wijewardhana PHL, Nirmali K, Sandakelum MAM (2023) "Numerical study on the shear behaviour of railway ballast using discrete element method." ICSECM2021, Lecture Notes in Civil Engineering, Springer Nature, pp 231–240
19. Venuja S, Navaratnarajah SK, Wickramasinghe THVP, Wanigasekara DSA (2022) "A laboratory investigation on the advancement of railway ballast behavior using artificial inclusions". ICSBE2020, Lecture Notes in Civil Engineering, Springer Nature, pp 47–55
20. Wang Z, Jing G, Yu Q, Yin H (2015) "Analysis of ballast direct shear tests by discrete element method under different normal stress." Measurement. https://doi.org/10.1016/j.measurement.2014.11.01263
21. Zhao H, Chen J, Giorgio I (2020)A numerical study of railway ballast subjected to direct shearing using the discrete element methodAdv Mater Sci Eng: 1–13. https://doi.org/10.1155/2020/3404208

Sub-Structure Soil Strengthening Using "Low-Pressure Grouting" After the Subsidence Incident of a Historic Unrefined Building—a Case Study

Hafsha Fazal Mohamed, Athula Samarasinghe, Shiromal Fernando, and Priyan Mendis

Abstract This article is based on the condition assessment and substructure rectification works that were conducted after a soil subsidence incident for a historic unrefined building in the heart of Colombo. This subsidence incident was caused by poor workmanship during the construction of the secant pile soil retaining structure for its adjacent construction site, which led to continuous leakage (of soil and water) that ultimately resulted in the soil subsidence of this building. This paper discusses the immediate and long-term mitigation and rectification works that took place to control, restore, and ensure the stability of the whole structure using the low-pressure grouting method.

Keywords Sub-structure · Soil-strengthening · Subsidence · Low-pressure grouting

1 Introduction

Building A is a historical unrefined office building. The initial structure for this building was built approximately 50 years ago and comprises three separate three-storey residential buildings. These buildings were joined and extended on both the right and left sides of the building. Two floors were added to the existing structure to accommodate the lift, bathrooms, and other services required to convert it into an office building. During the initial site investigation, it was observed that the structure comprised a beam-column structure with pad footings. But several traces of strip footing with random rubble masonry were also identified. Furthermore, a security hut was constructed as a separate structure on the rear–right corner of Building A.

H. F. Mohamed (✉) · A. Samarasinghe · S. Fernando
Civil and Structural, Engineering Consultants (Pvt) Ltd, Rajagiriya, Colombo, Sri Lanka
e-mail: hafshafm@gmail.com

P. Mendis
University of Melbourne, Melbourne, Australia

© The Author(s), under exclusive license to Springer Nature Singapore Pte Ltd. 2023

R. Dissanayake et al. (eds.), *ICSBE 2022*, Lecture Notes in Civil Engineering 362,
https://doi.org/10.1007/978-981-99-3471-3_19

Building B is located adjacent to building A (Fig. 1). This building is a 31-storey building with 4 basement floors and is still in its substructure construction stage. This has a secant pile wall laterally restrained by a wailer beam-king post system to ensure water tightness. The building also has a secant pile earth retaining system restrained using a king post system, which is used as a watertight protection wall. Due to poor workmanship and bad construction practices of the secant pile wall, leakages were observed in the secant pile wall. Even though several locations were arrested by means of horizontal grouting (using Sodium Silicate) and jet grouting, it was not sufficient to arrest all soil–water leakage observed in the rear–right side of Building A.

Moreover, artificial recharging of groundwater was also conducted continuously while monitoring the groundwater table using several piezometers. Meanwhile, due to continuous water leakages and the lowering of the groundwater table around the excavated area, cavities were forming underneath Building A on the right rear side corner, which ultimately caused the failure of the shallow foundation of Building A and resulted in the formation of a sinkhole underneath the security hut.

This paper aims to explain the procedure adopted to first identify and then strengthen the vulnerable areas underneath an existing foundation using the low-pressure grouting technique.

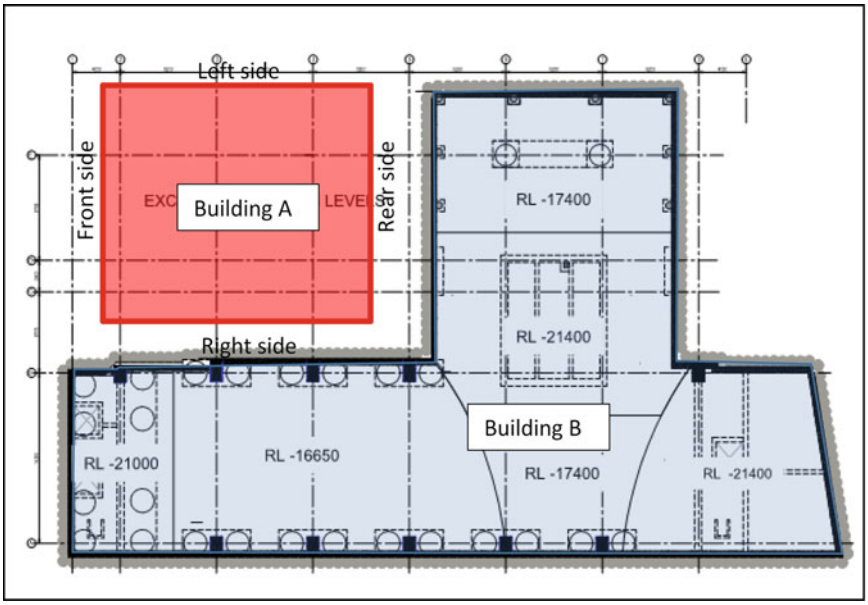

Fig. 1 Orientation of Buildings A and B

2 Literature Review

Pressure grouting is a process in which grout is forced under pressure to modify, fill, or compact the pore spaces identified in soil, rock, masonry, concrete, and similar materials to achieve a denser state [1, 2].

Due to grout's characteristics such as the availability of grout at every consistency, the ability to design for higher compressive and bond strengths, the flexibility of fresh grout, etc., it has been used for favourable adjustments of geomaterials such as blocking water flow to reduce seepage, soil or rock strengthening, filling of large sinkholes and voids, correction of settlement damages in structures, formation of bearing piles, etc. Grout is also used to repair cracks, honeycombs, splits, and other defects in concrete and masonry structures, fill cavities and provide complete support for precast or steel–concrete composite members [1].

Grouting of soils can be conducted via four main methods (as illustrated in Fig. 2):

- *Permeation grouting*—Soil is improved by filling the pores between the soil particles and gluing each particle together, hence causing an increase in its shear and bearing capacity, and a decrease in soil permeability. This method can only be used in soils with sufficient permeability for the grout to penetrate. This method has a higher risk of hydraulic fracturing of soil and losing control.
- *Fracture grouting*—Soil is reinforced by creating strong grout lenses using controlled intentional fracturing of soil using particulate suspension grout in a fluid consistency. This will reduce soil permeability based on the structure of

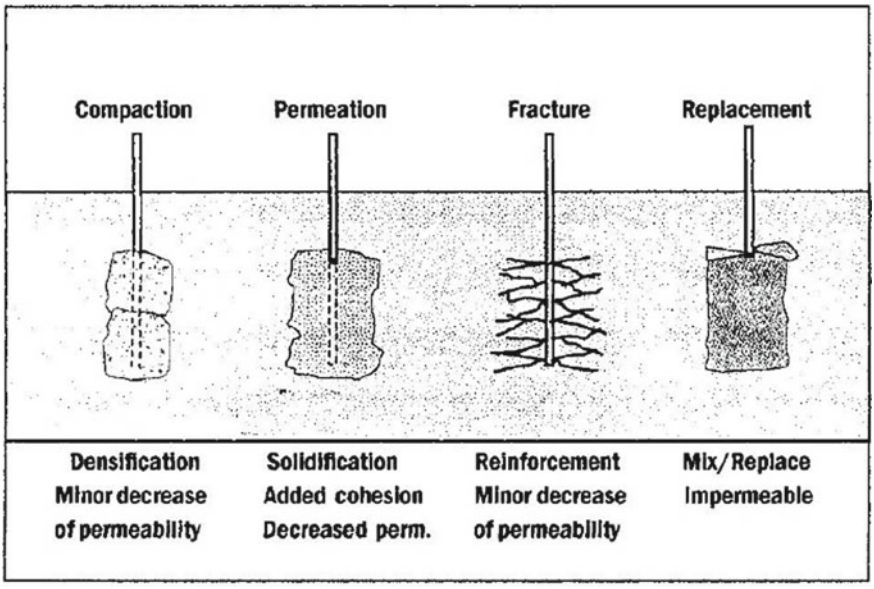

Fig. 2 Grouting methods for soil with its improvement mechanisms [1]

grout lenses. However, since grout build-up cannot be controlled, it is used only when other methods are not suitable (such as on soils with clayey formations).

- *Jet grouting*—Soil is improved by replacing the existing affected soil with "Soilcrete" which is formed during the turbulent mixing of soil with cementitious grout with a fluid consistency. Here the strength of Soilcrete will vary based on soil composition. This method can be used to create watertight walls, as Soilcrete is impermeable.
- *Compaction grouting*—Soil is densified to increase the bearing capacity by forcing individual soil grains to be tightly packed. Here the shear capacity of soil does not improve due to less additional cohesion. This method can be used for a wide range of soils, and it is the least expensive soil improvement method. As it is the least disruptive method, it can be performed in areas with poor access or other restrictions. Thus, it is the most suitable method to use around and under an existing structure.

The grouting pressure is also another important parameter that decides the degree of soil improvement. Having an exceedingly small pumping pressure may result in poor soil improvement which may result in differential settlement of structural elements of the same structure. Having an extremely high pumping rate may cause a sudden increase in pore pressure where pumping must be terminated until the relaxation of pore pressure. In worst cases, this may also result in the uplifting of the adjacent structural elements [1]. During cement hydration, since the hydration product increases by 2.4 times its initial volume, the grout mix must be at least 0.44% of the weight of water in order to achieve the optimum hydration of the grout mix, [3]. Presence of unhydrated cement when grouting above the groundwater table may cause the unreacted product to detract causing reduced strength, increased shrinkage, reduced quality, and reduced durability. The Portland Cement Association's publication "Cementitious grouts and grouting" recommends a 0.5 to 20 water-cement ratio and pressure above 1.5 to 3.0 bar for grouting to stabilize foundations under commercial and industrial buildings [2].

3 Restoration Method

On the same day as the sinkhole formation incident, C30 mass concrete was poured into the sinkhole formation location to prevent further loss of soil and mitigate further damages. The location of the sinkhole respective to Buildings A and B is shown in Fig. 3.

The strengthening of soil beneath Building A involved the following steps:

1. Conduction of a post-incident condition survey to identify and quantify the damages which occurred due to the incident.
2. Selection of the most suitable grouting method to strengthen the foundation based on the structural design report and post-incident condition survey report.
3. Strengthening of the subsoil underneath the foundation.

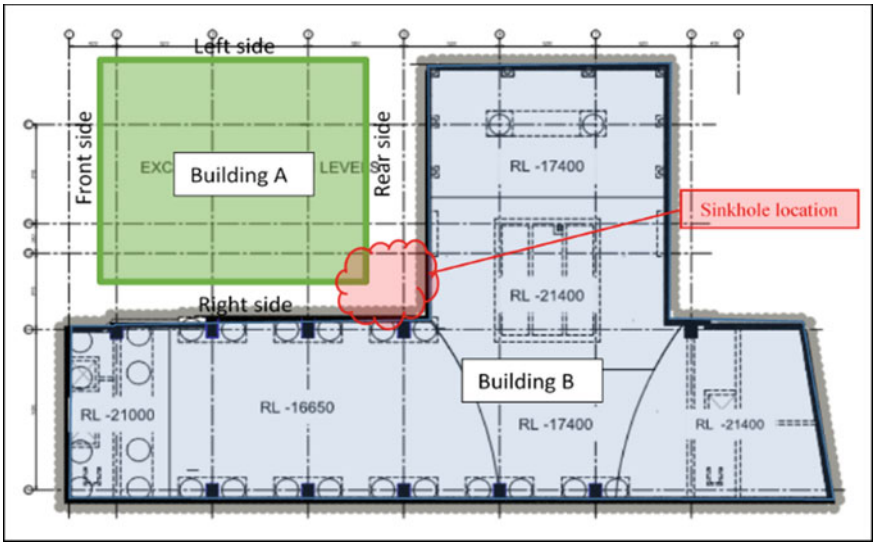

Fig. 3 Sinkhole location

4. Conduction of a Geophysical survey to ensure the grouting efficiency

4 Strengthening of the Soil Below the Foundation

4.1 Post-Incident Condition Survey

Since the commencement of construction of the Proposed Building B project, crack monitoring, building tilt, and deflection monitoring (using strain gauges) in Building-A were monitored daily. Furthermore, secant pile deflection monitoring (using Inclinometer and stain gauges in ERS system), settlement monitoring (using settlement markers and settlement pegs), and groundwater table monitoring (using piezometers) were conducted daily around the proposed Building B project. A post-incident condition survey was conducted immediately after the incident. Occupants and furniture inside Building A were removed. New cracks were identified in locations where furniture was removed and no changes in previously monitored cracks, building tilt, or deflection were observed.

A SPT test was conducted on the front and rear sides of Building A (Fig. 4) and the test results are shown in Table 1 below. Moreover, the groundwater table was found to be at a depth of 4.5 m from the existing floor level.

First, an as-built survey was conducted to identify each structural element of Building A. Then a SPT test was conducted at two borehole locations to identify the condition of soil present beneath Building A. It was concluded that the soil must

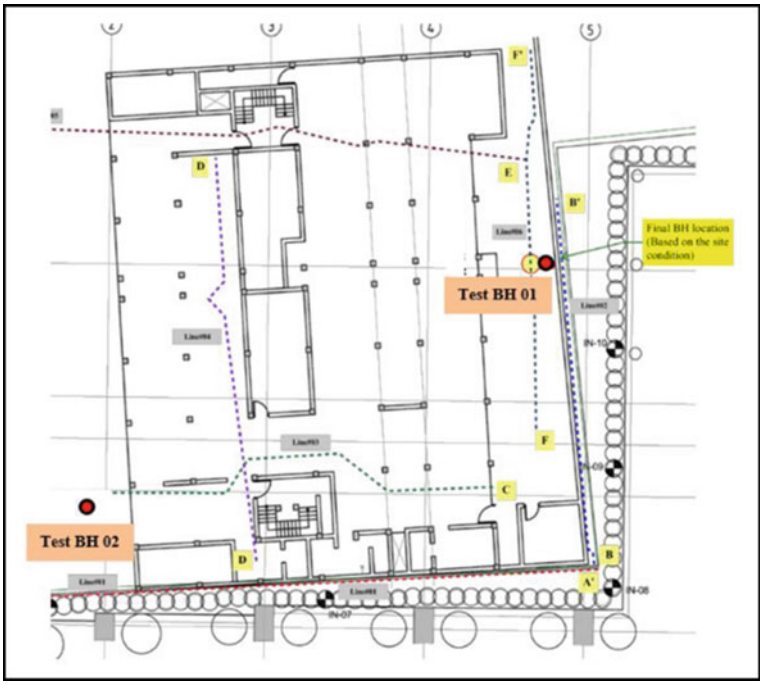

Fig. 4 SPT test locations in the Building A

Table 1 SPT test results

Depth (m)	Layer description	SPT N value
0.00–0.13	Concrete layer	–
0.13–1.30	Building material with medium dense to loosen sand	15–7
1.30–2.80	Loose to medium dense silty sand with traces of clay and building materials	6–13
2.80–4.50	Loose to medium dense silty sand with traces of clay and building materials	13–23
4.50–5.00	Medium dense sand with traces of clay	15
5.00–5.50	Dense sand with traces of clay	31
5.50–10.00	Very dense silty sand with traces of clay	>50

be improved for the building to achieve its serviceability limit state. Furthermore, a geophysical investigation (i.e., a geo-electrical resistivity survey and profiling) was conducted to investigate the formation of voids or cavities beneath the foundation of Building A. Here cavities and voids were identified at a depth of 2 to 5 m below ground level (Fig. 5). Based on these findings seventeen columns were identified to be in these vulnerable locations (Fig. 6).

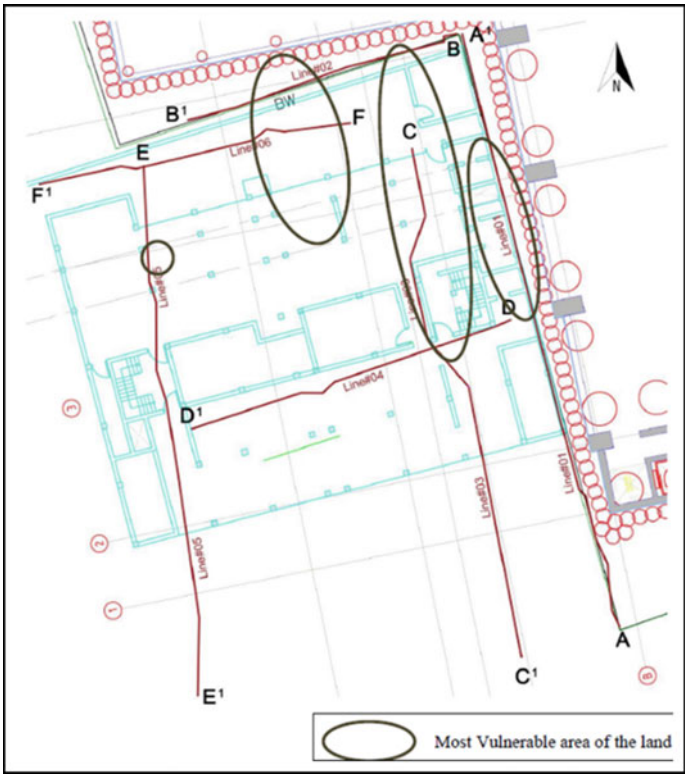

Fig. 5 Most vulnerable locations identified in the Geophysical survey

4.2 Foundation Strengthening

4.2.1 Selection of Grouting Method

Based on the literature review and the SPT test results, it was concluded that the compaction grouting technique was the most suitable method for this application.

4.2.2 Grouting Method

Since there are no records of the foundation of Building A, each footing was exposed by manual exaction (Fig. 7). Here the soil profile observed up to the top of the footing, footing sizes, and footing depth were recorded.

Based on these observations, grout holes were marked 300 mm away from the footing edge and observation holes were marked in between these grout holes (Figs. 8 and 9).

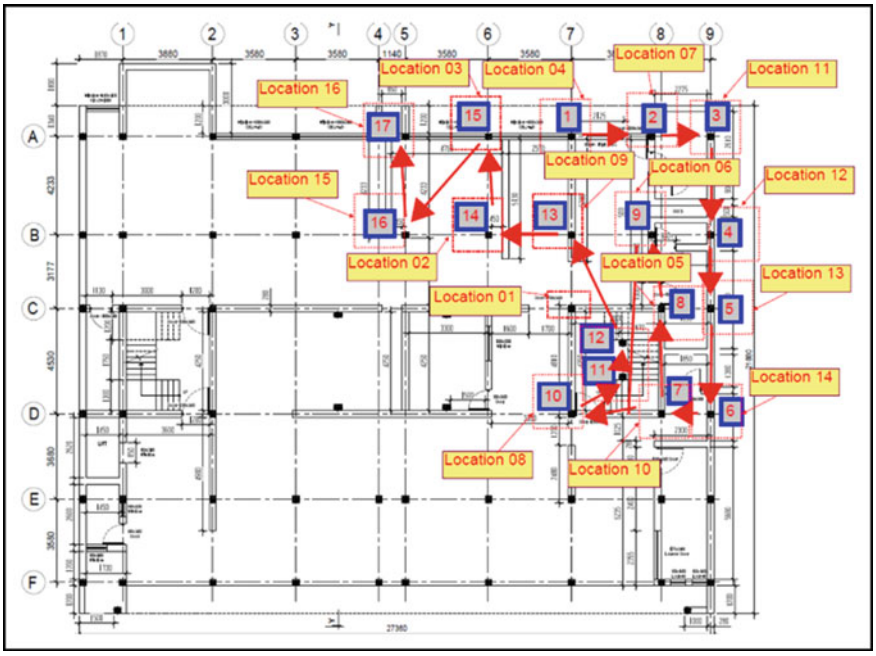

Fig. 6 Columns identified in most vulnerable locations underneath Building A

Fig. 7 Exposing column footing

First, all four observation holes were drilled using a 75 mm diameter drill bit up to a depth of 4 m using the air drilling method (Fig. 10), and perforated PVC pipes were inserted into these observation holes. Next, the grout holes were drilled using 68 mm drilling and grouting bit up to a depth of 4 m using the air drilling method.

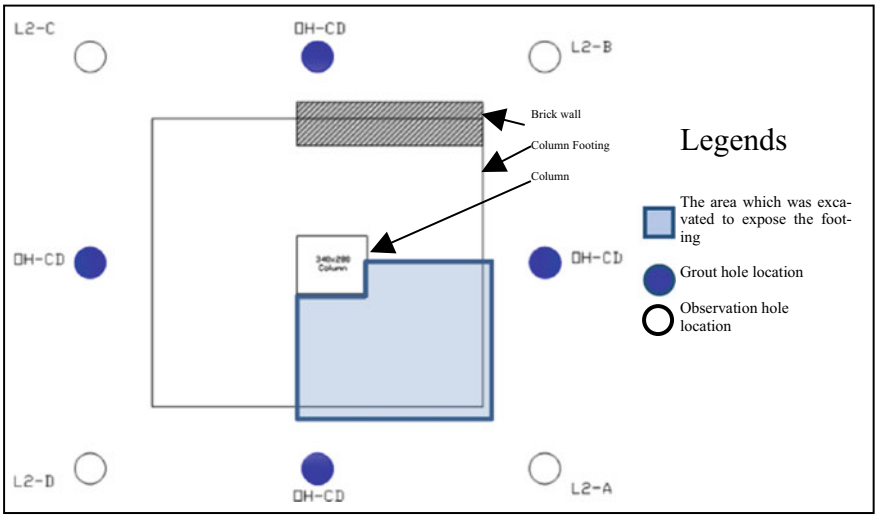

Fig. 8 Grout hole and observation hole locations of typical footings (plan view)

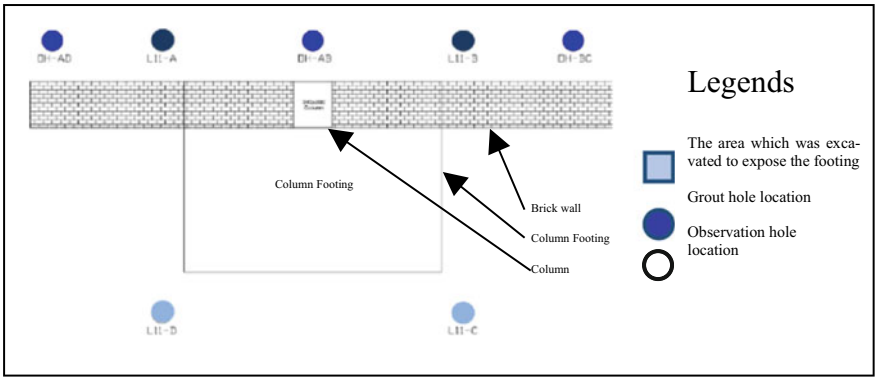

Fig. 9 Grout hole and observation hole locations of perimeter footings (plan view)

Drilling and grouting for grout holes were conducted using the same bit and steel casing. Afterwards, the grouting hose was installed for grouting.

4.2.3 Grout's Mix Design

Based on the soil type and literature review, it was concluded that the grout shall be pumped at an approximate pressure of 3 bar, and if the pumping rate reaches 5 bar, pumping of the grout shall be terminated and relaxed immediately. Furthermore, for optimum results, 0.5 was deemed the most suitable water-cement ratio and an

Fig. 10 Drilling of the observation hole

Table 2 Grout's mix design

Cement (Kg)	Water (L)	W/C ratio	Admixture flowable 50 (g)
50	25	0.5	250

expandable, plasticizing admixture was added to the grout to (a) increase the flow of grout, and (b) ensure further compaction of soil for better results. The grout's mix design is provided in Table 2 (Fig. 11).

The grout was mixed using a grout mixer with an agitator. The grout was mixed for 4 to 5 min until it achieved a homogenous consistency. The agitator was used here to prevent settling, removal of air bubbles inside the grout mixture, and ensure complete flow through the tank.

Fig. 11 Mixing of cement grout

After complete mixing of the grout, a flow cone test was conducted to ensure that the grout has sufficient ability to flow (Fig. 12). The flow was maintained between 10 and 15 s. Furthermore, three 75 mm × 75 mm × 75 mm grout cubes were cast for each grout hole to reassure the strength of the grout (Fig. 13).

The grout mix was pumped into the grout holes mechanically at low-pressure (Fig. 14). The grouting pressure and the flow rate were recorded at intervals of 2 min using a flow meter and a pressure gauge (Fig. 12).

The grout was fed into the grout hole from bottom to top. Once the pressure reached 5 bar or grout overflowed from the grout hole (Fig. 15), grouting was terminated at that level, and the grouting rod was raised to 0.5 m (half the height of one casing). If the pressure build-up did not relax or continuously overflowed, the grouting was stopped at this level and the grouting was continued after the removal of the first casing. This procedure was continued up to the depth of footing's bottom level.

Following the completion of grouting (up to foundation bottom level) the remaining height up to the ground level of the grout hole was filled with grout at zero pressure. The other 3 grout holes were grouted in a similar manner. While

Fig. 12 Flow cone test, flow Meter, and pressure gauge

Fig. 13 Casting of grout test cubes

Fig. 14 Grouting of the grout hole

Fig. 15 Grout overflowing from casing while grouting

grouting, the effectiveness of grout flow was checked by lowering a rod inside the observation hole and checking for traces of grout (Fig. 16). Furthermore, the grout consumption rate was recorded in terms of litres of grout and no of cement bags which were used for each grout hole separately.

4.3 Quality Assurance and Quality Control During the Strengthening Works

4.3.1 Hand Auguring Test

A hand auger test was carried out to obtain a continuous grout sample (Fig. 17). However, it was not successful as the apparatus could not cut through hardened

Fig. 16 Checking for traces of grout in observation holes

Fig. 17 Hand auguring test

grout that had spread during the grouting process. This was tried at a few other locations; however, it was not successful.

4.3.2 Grout Test Cube Results

The grout test cubes which were cast during the grouting process were cured and compressive strength was checked for 8 and 28 days, respectively (Fig. 18). The average compressive strength after 8 days was recorded as 27.75 MPa and the average compressive strength after 28 days was recorded as 33.17 MPa.

4.3.3 Mackintosh Probe Test

The Mackintosh probe test is a portable, lightweight dynamic penetrometer test which is used to measure the soil's bearing capacity. Here the bearing capacity of the soil at

Fig. 18 Grout test cubes samples

this footing location was calculated based on the mackintosh N value by correlating it to the relevant SPT N value based on soil type underneath the foundation. Pre- and post-grouting mackintosh tests of the footing were conducted up to a depth of 3.6 m from the footing's bottom level as shown in Fig. 19.

Based on pre-grouting and post-grouting results, the degree of improvement was measured, and it was also checked if the soil underneath the footing had reached adequate bearing capacity. If it was identified to be inadequate, the observation holes were also grouted until the footing reached its required bearing capacity.

Mackintosh test (Fig. 20) was not carried out in areas where mass concrete was poured during the sinkhole formation incident (Fig. 21) and perimeter of Building A and B (Fig. 22) due to the presence of the capping beam of the secant piles. But the overall results indicated that the soil has reached more than the required bearing capacity and that the grouting was successful (Table 3, Fig. 23).

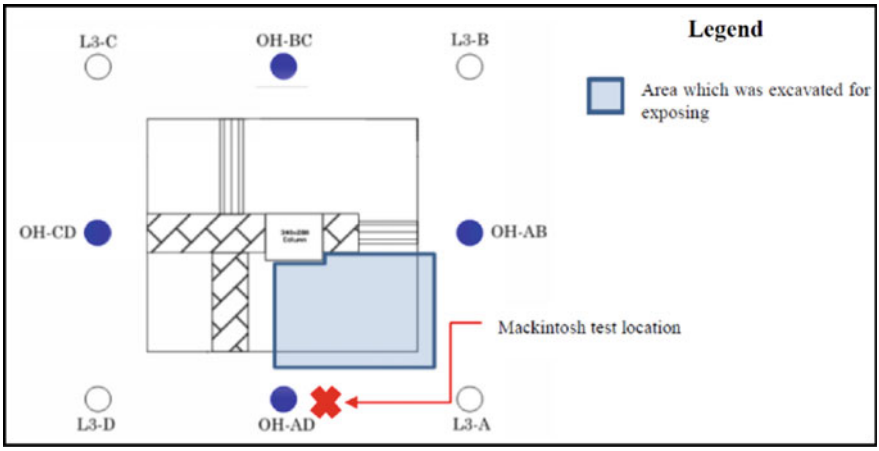

Fig. 19 Mackintosh test location

Fig. 20 Mackintosh test

Fig. 21 Mass concrete filling found near footing no. 2

Fig. 22 Capping beam located along the Building A -Building B perimeter wall

4.3.4 Geophysical Survey

A geophysical survey was conducted before and after strengthening the soil underneath Building A's foundation. This survey included a reconnaissance survey and a resistivity survey. The reconnaissance survey was carried out to check for settlement

Table 3 Mackintosh test results

Column No	Mackintosh Test Results			
	Pre-grouting		Post grouting	
	Date	Soil bearing capacity (kN/m^2)	Date	Soil bearing capacity (kN/m^2)
1	07.02.2022	130	26.02.2022	140
2	Mackintosh test wasn't carried out due to mass concrete fill			
3				
4				
6				
5	21.02.2022	30	11.03.2022	140
7	17.02.2022	75	11.03.2022	140
8	08.02.2022	125	21.02.2022	180
9	12.02.2022	125	02.03.2022	130
10	12.02.2022	130	02.03.2022	180
11	12.02.2022	125*	02.03.2022	140*
12				
13	17.02.2022	100	26.02.2022	150
14	–	–	05.02.2022	125
15	–	–	03.02.2022	125
16	21.02.2022	30	11.03.2022	140
17	21.02.2022	125	11.03.2022	140

*One common Mackintosh test was conducted for Footing no 11 &12 as it is a combined footing

features of the foundation including subsidence features, existing cracks, and continuous water seepages (groundwater losses) from the secant pile wall in Building A and B's perimeter. The resistivity survey comprised a geo-electric profiling method used to find potential zones of stagnated groundwater and cavities under Building A's foundation.

A tetrameter with an expanding electrode was used to collect a series of resistivity measurements and they were then interpreted to identify voids and cavities beneath the foundation. During the pre-grouting geophysical survey, many cavities and voids under the foundation at 2–5 m depth were identified on the right side of Building A (Fig. 5).

Following the completion of grouting works in Building A, another geophysical survey was conducted again. The resistivity survey was conducted on the same profile used for the pre-grouting resistivity survey (Figs. 24 and 25).

The locations which were previously identified as low resistive zones in the pre-grouting resistivity survey were verified to be highly resistant in the post-grouting resistivity survey. This confirms that (a) all voids and cavities identified under the

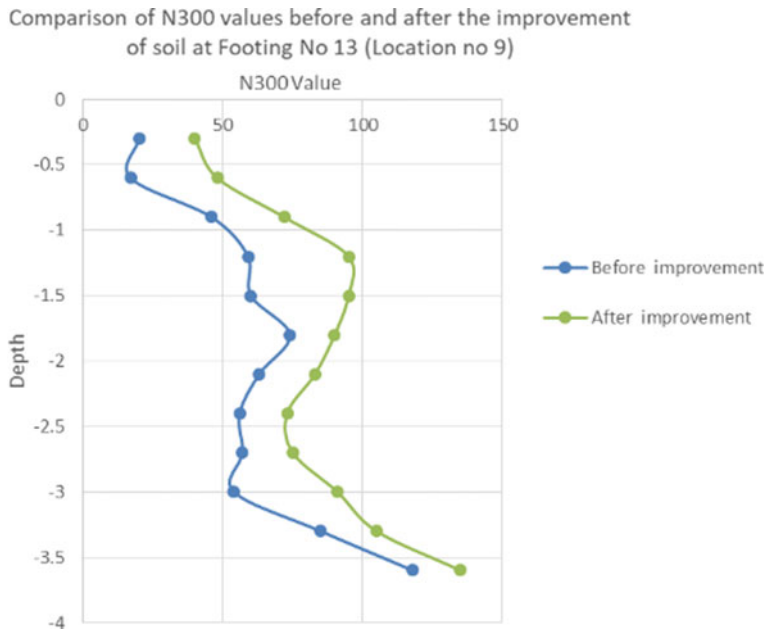

Fig. 23 Comparison of pre and post-grouting mackintosh test results for footing no. 13

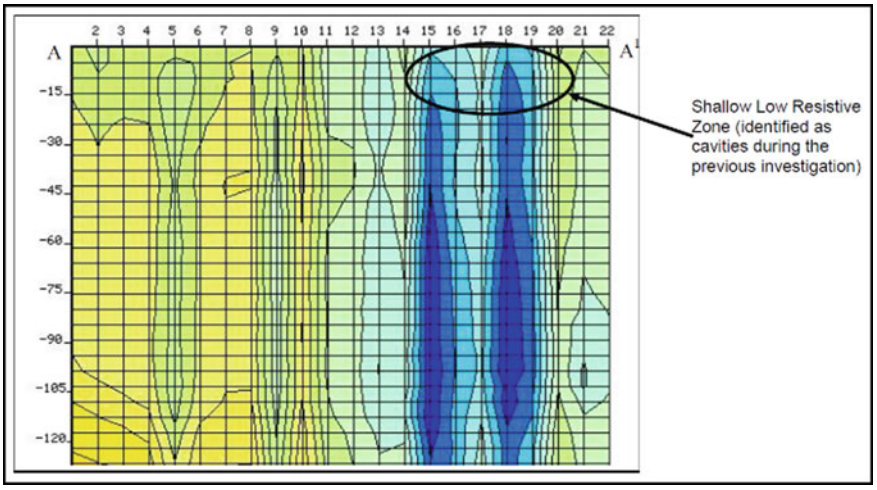

Fig. 24 Electrical Resistivity Profile Line 1 before grouting (A-A1) (Measurements are marked in meters)

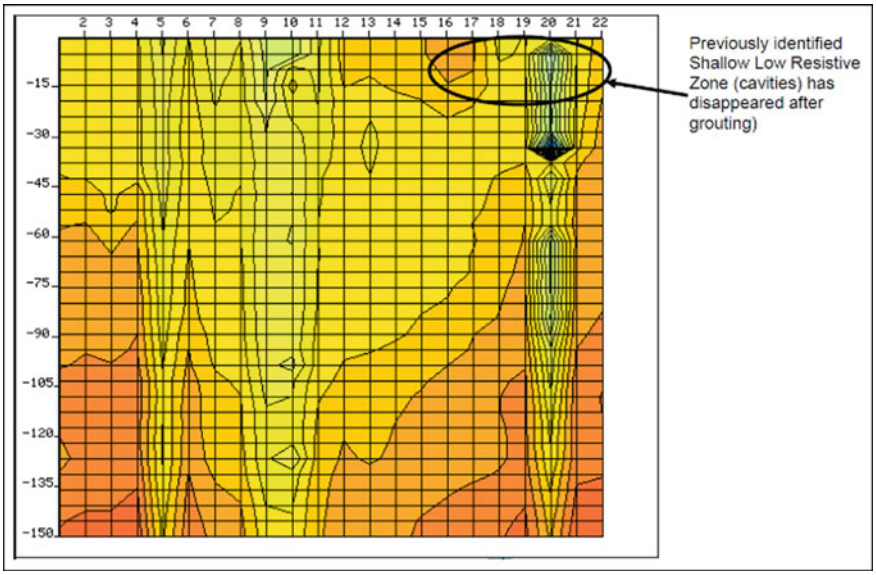

Fig. 25 Electrical Resistivity Profile Line 1 After grouting (A-A1) (Measurements are marked in meters)

foundation of building A were filled and (b) that the integrity of the soil beneath the foundation has been restored successfully.

5 Conclusion and Recommendations

In conclusion, this paper discusses the procedure adopted to identify, mitigate and restore the soil's integrity after a soil subsidence incident using a low-pressure grouting technique. Here first the sinkhole was capped by pouring a mass concrete into the sinkhole created due to the subsidence incident. Next, a post-incident condition survey was conducted to identify and quantify the damages caused due to this incident. Based on the evaluation of the structural design report and the post-incident condition survey report, low-pressure compact grouting was selected as the most suitable method to strengthen the soil beneath the foundation. This method was effectively implemented to strengthen the soil beneath the footings located in the most vulnerable areas as previously determined in the pre-grouting geo resistivity survey. The effectiveness of grouting was verified by conducting post-grouting mackintosh and geophysical survey, which confirmed the significant improvement in soil's integrity, by satisfying the bearing capacity requirement. This paper provides practical insight and outline of the procedure for successful mitigation and restoration of the soil's integrity after a subsidence and sinkhole formation incident, providing guidance for researchers and practitioners facing similar circumstances.

Acknowledgements The Authors would like to acknowledge and thank fellow site staff of the construction site, namely Kisal Jayakody, Anojan Thayanandan, and Sandaruwan Jayasundara, who supported and assisted execution of the project. Furthermore, the authors would like to acknowledge and thank all relevant Contractors and subcontractors for their support and timely delivery of this project.

References

1. James Warner P (2004) PRACTICAL HANDBOOK OF GROUTING—Soil, Rock, and Structures. John Wiley & Sons Inc., Hoboken, New Jersey
2. Portland Cement Association. (1990). Cementitious Grouts and Grouting. Portland Cement Association
3. Powers TC (1968) Properties of Fresh Concrete. John Wiley and Sons Inc., New

Green Innovations and Green Building Techniques

Risk Mitigation Measures in Green Building Projects: An Investigation

Nilupa Herath, Paulo Vaz-Serra, Felix Kin Peng Hui, Priyan Mendis, and Lu Aye

Abstract Building construction projects encounter various uncertainties in achieving their objectives because of a wide range of causes, such as finance, technology, weather. The effects of these uncertainties on the project objectives are different during each stage of its life cycle (design, construction, and operation). However, due to the high level of sustainability objectives, green building projects can face even more inaccurate cost estimation, uncertain workforce availability, and green material availability risks. Green building projects are reported to confront more risks than conventional buildings because of the need to achieve sustainability goals. This article aims to explore risk mitigation measures in green building projects. To accomplish this, we review the fundamental risk treatment strategies (avoidance, transference, mitigation, escalation, and acceptance) documented in 'The Project Management Body of Knowledge (PMBOK® Guide)'. We also review and analyse green building project case studies reported in the literature and the standard risk mitigation methods for green building projects.

Keywords Green building · Project management · Risk treatment · Review · Case study

N. Herath · F. K. P. Hui
Engineering Management Group, Department of Infrastructure Engineering, Faculty of Engineering and Information Technology, The University of Melbourne, Victoria 3010, Australia

P. Vaz-Serra
Faculty of Architecture, Building and Planning, The University of Melbourne, Victoria 3010, Australia

P. Mendis · L. Aye
ARC Centre for Advanced Manufacturing of Prefabricated Housing, The University of Melbourne, Victoria 3010, Australia

L. Aye (✉)
Renewable Energy and Energy Efficiency Group, Department of Infrastructure Engineering, Faculty of Engineering and Information Technology, The University of Melbourne, Victoria 3010, Australia
e-mail: lua@unimelb.edu.au

© The Author(s), under exclusive license to Springer Nature Singapore Pte Ltd. 2023

R. Dissanayake et al. (eds.), *ICSBE 2022*, Lecture Notes in Civil Engineering 362,
https://doi.org/10.1007/978-981-99-3471-3_20

1 Introduction

The construction industry plays a significant role in the development of a country [2]. Besides 40 and 50% of global energy consumption, 40% of the global raw materials are consumed by the construction industry [35]. There has been a steady growth in investing in green buildings around the world since 2012 [10]. With the sustainable developments around the world, green buildings were introduced to enhance the efficiency of resources, reduce operation costs, and improve the building environments [48].

Project risk is an uncertain event that can impact either positively or negatively on project objectives. Risks can impact the project scope, schedule, cost, and quality [23]. Several green rating systems were introduced to assess buildings, considering the whole life cycle. LEED (the US), BREEAM (the UK), Green Star (Australia), and Greenmark (Singapore) are some of the rating systems used in developed countries. Developing countries have also shown some increased interest in GBs in recent years [10]. Thailand has developed its own rating TREES and there is an increase in GB developments [40]. GBCSL developed the GREEN^{SL}® rating system to encourage the design of buildings with an environmentally acceptable approach in Sri Lanka.

Although sustainable construction has been developed over the last few years, there are still significant difficulties associated with the different stages of these projects [14]. Planning, identification, analysis, and controlling are the main activities involved in the risk management process [29]. The aim of this work is to investigate the risk mitigation measures in green building projects. Risks reported and risk management frameworks for green building projects are identified (Sect. 2). Risk mitigation measures reported in the current literature are reviewed (Sect. 3). Then the applications of these measures are discussed via a case study (Sect. 4).

2 Risks in Green Building Projects

Identification of risks in GB construction is important, and extensive literature reviews have been conducted to identify the risks associated with green building projects [25–30]. Planning, identification, analysis, and controlling are the main activities involved in the risk management process [29]. In most of the GB projects, there are some common risks. Complex approval processes neglected high initial costs, unclear requirements from owners, and lack of green and sustainable materials were some of the critical risks identified in residential GB projects in Singapore [35]. They have also identified other critical risks associated with commercial GB projects in Singapore. Inflation, instability of currency, and interest rates related to the import of green materials and durability and shortage of green products were among the main risks identified [35].

Commercial GB projects have more management procedures, and because of this reason, the risks related to design changes and construction quality are relatively low

compared to normal projects [25]. Different countries face different risks related to the construction of GBs. In UAE, it was identified that unreasonably tight project schedules, lack of funding from clients, and poor scope definitions are some of the major risks [11]. In Kuwait, the lack of experienced designers and contractors for GB construction was a problem [20]. Besides the risks identified during the planning, design, and construction stages, some risks are also associated with the operation stage. The lack of experienced managers during the operation stage was one of the critical risks [39].

From the literature [25, 30, 32], the main identified risks associated with GB construction were categorised according to the preliminary and planning stage, design and construction stage, and operation stage, as presented in Table 1. While there have been ongoing discussions and research into specific risks for green buildings, the development of specific risk management frameworks or risk profiles of green buildings has been quite limited. A dedicated framework to get to a set of core risk assessment techniques for green buildings was proposed by [21]. Other researchers [12] proposed an efficient process to analyse the risks of sustainable construction projects using Monte Carlo simulations to support decision-making.

3 Risk Mitigation Measures in Green Building Projects

It is clear from the literature that there are significant risks involved in the GB project. Risk mitigation is one of the key components of risk management. Due to the adoption of sustainable construction practices, it is important to identify, analyse, monitor, and control these risks. The PMI risk management processes include identification, analysis, response planning, and controlling [29]. The main aim of risk management is to provide a framework that supports the decision-making process of a GB project [1].

Early detection of risks, prioritisation and mitigation, is the key to an effective risk management plan, and a proper and systematic method is important to increase the effectiveness of the risk management plan [34]. Generally, in construction projects, the highest frequency of risks occurs during the planning and development stage, and most impact risks are determined during the design and construction stage, as shown in Fig. 1.

Risk analysis is one of the key components of risk management. Quantification of risks can be conducted using two methods: qualitative analysis and quantitative analysis. Qualitative risk analysis focuses on the probability of occurrence of the risk and the corresponding impact of the risk. Quantitative risk analysis involves numerically analysing the effect of the identified risks on overall project objectives. Data gathering and representation techniques, modelling techniques, and expert judgement are used as tools and techniques for conducting quantitative risk analysis.

Although some frameworks for risk management techniques are available, some unique risks are involved in GB construction that needs to be investigated separately. A study conducted on risk analysis of GB projects has identified that most risks

Table 1 Associated risks in Green Building project stages

	Risk	1	2	3	4	5	6	7	8	9	10	11	12	13	14	15	16	17	18
Preliminary and planning	Problems associated with importing green materials		✓			✓		✓		✓	✓						✓	✓	✓
	Lack of client interest and requirements	✓			✓	✓					✓			✓			✓	✓	
	Lack of public awareness of the benefits for sustainability				✓				✓					✓	✓	✓	✓		
	Lack of knowledge of GB costs/perception of higher GB cost	✓							✓				✓				✓		
	Change policies	✓	✓		✓		✓			✓				✓		✓	✓		✓
	Insufficient/inconsistent incentives from the government								✓					✓	✓		✓		
	Poor estimations of GBs' long-term return on investment			✓	✓	✓						✓					✓	✓	
	Lack of financial viability of the project			✓	✓						✓						✓	✓	✓
	Lengthy payback period								✓					✓	✓				
	Overlooked high initial cost									✓				✓			✓		
	Technical complexity							✓	✓										
	Improper feasibility and planning (setting expectations too high)		✓							✓	✓							✓	✓
	Insufficient site investigation not tailored to local conditions					✓										✓	✓		
	Unclear contract conditions for dispute resolution	✓	✓		✓			✓		✓								✓	
	Complex and slow planning approval and permit procedures	✓						✓					✓	✓			✓		
Design and construction	Project teams without the relevant knowledge				✓		✓	✓	✓			✓				✓			✓
	Inefficient communication and coordination				✓			✓		✓					✓		✓		
	Designers with a lack of GB design experience		✓			✓	✓		✓			✓	✓	✓	✓		✓		✓
	Risks of green design innovation					✓							✓				✓		
	Inaccurate cost estimation					✓		✓		✓				✓	✓		✓		
	Labour and materials price fluctuations	✓						✓					✓					✓	✓
	Budgeting issues due to the inexperience of green projects										✓								✓
	High cost of sustainable materials and equipment				✓	✓					✓		✓	✓		✓			✓
	Owner's unexpected cost increases					✓						✓			✓				
	Unclear contract conditions for claims and litigations		✓					✓		✓	✓								
	Unclear or poor designs/design errors		✓					✓		✓	✓	✓			✓			✓	✓
	Design changes during construction							✓			✓			✓	✓				✓
	Risk	**1**	**2**	**3**	**4**	**5**	**6**	**7**	**8**	**9**	**10**	**11**	**12**	**13**	**14**	**15**	**16**	**17**	**18**
	Unfamiliar technologies, materials and construction processes								✓	✓			✓		✓		✓		
	Improper quality control and defective work										✓	✓					✓	✓	✓
	Poor communication among projects stakeholders				✓			✓			✓				✓		✓		
	Supply chain problems	✓																	
	Difficulty in the selection of contractors	✓					✓		✓					✓			✓		✓

(continued)

Table 1 (continued)

Handover and operational	Loss of financing or losing loans for not achieving certification	✓										✓		✓					
	Not achieving the expected GB standard.					✓	✓							✓	✓	✓	✓		✓
	Green certification cost increase					✓													
	GB evaluation standard changes					✓								✓	✓				
	Energy-saving uncertainty	✓		✓	✓		✓			✓					✓	✓			
	Unstable operation performance	✓				✓										✓	✓		
	Challenges for operating renewable energy systems													✓					
	Lack of experienced managers for the building's operational phase															✓	✓		
	Unclear responsibility for Green products upgrading					✓											✓		
	Inadequate GB maintenance					✓											✓		

Zou and Couani [43], Rafindadi et al. [32], Hwang et al. [34], Zhao et al. [35], Qin et al. [30], Yang et al. [43], Zhao et al. [44], Albert et al. [4], Ming et al. [20], Shan et al. [13], Krechowicz [14], Polat et al. [17], Ismael and Shealy [14], Ranawaka and Mallawaarachchi [21], Tao and Xiang-Yuan [14], Ahmad et al. [20], Guan et al. [21], El-Sayegh et al. [13]

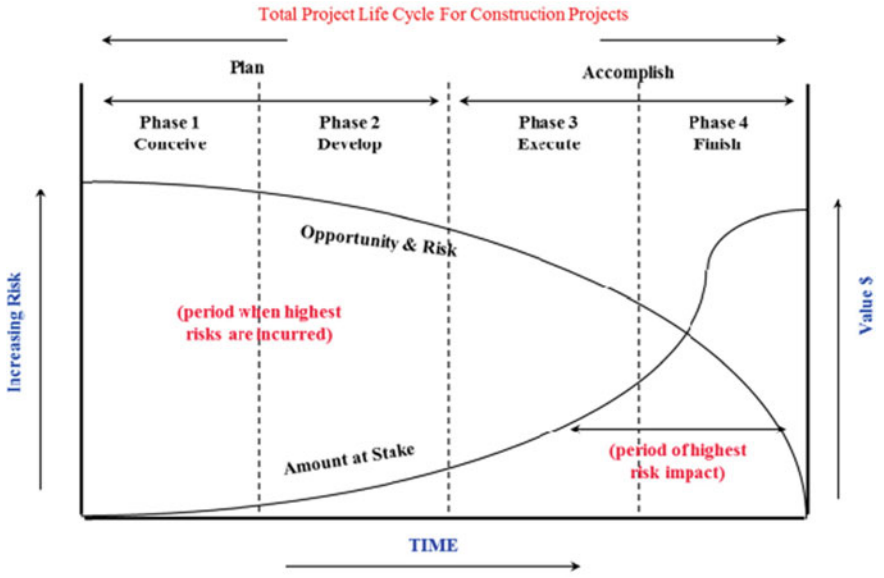

Fig. 1 Relationship between the construction project life cycle and risks [31]

were identified by brainstorming and interviewing. For the quantification of risks, many projects have used the probability and impact (PI) matrix, followed by risk probability and impact assessment and risk breakdown structure [27]. In this study, expert judgement was considered one of the most used quantitative methods in GB projects, followed by probability distributions and expected monetary value methods.

Due to the unique nature of GB projects, different projects have used different methodologies to mitigate risks. It is important to identify risk sources in GB projects to mitigate them. Most of the risks are general risks and related to stakeholders in the project. Many of these risks are interrelated and associated with internal or external stakeholders. Social Network Analysis (SNA)-based stakeholder-associated risk analysis method was introduced to analyse the risks and their interactions in complex GB projects [43]. The findings of a study conducted in China have revealed that stakeholders have different risk preferences in GB projects, which could be helpful for practitioners in creating risk management strategies for specific parties [30]. But the study conducted using stakeholders from different countries has indicated no significant difference among stakeholders [32]. Perhaps more research is needed to understand why there are contradicting findings from different regions.

In the USA, higher injury rates were found in LEED-certified buildings compared to conventional buildings [9, 13]. Higher injury rates resulted from the design strategies and construction methods implemented to earn specific LEED credits. Most of the studies considered in the literature are country-specific and conducted in developed countries. The concept of GB is still a problem in developing countries [26].

Once the risks are identified and evaluated, risk response strategies will be established to resolve the identified risks. Generally, risk avoidance, risk transfer, risk reduction, and risk retention are the main methods used to resolve risks.

Once the risks are resolved, the next step in risk management is monitoring and controlling such risks. There are three statuses of risks, namely, opened, resolved, and closed. When the risks are determined and successfully responded to with a favourable outcome, these risks are called closed risks. Continuous and consistent risk monitoring is important throughout the life cycle of the GB project. Since some risks are unique and complex compared to ordinary building projects, the risk response strategy will be varied.

Risk elimination or risk avoidance is one of the strategies used in risk mitigation. However, in GB projects, it is important to identify which risks can be avoided as not all stakeholders will be eager to avoid the specified risk. Further, sometimes, the risk avoidance related to one activity might lead to higher costs in another activity. Therefore, careful attention should be paid to identifying risks that will be avoided.

Risk transfer is another strategy that is used in risk mitigation. In risk transfer, the risks are transferred to a third party using construction contracts or insurance. The shift of responsibility to a third party reduces the impact on the project partners but incurs additional costs to the project. In general construction projects, there are three types of channels to transfer risk to other parties [41]. They are, through insurance-to-insurance firms, through contractors to sub-contractors and through editing contract terms. In mega and complex projects, public–private partnerships also help to transfer risks.

Risk reduction is also one of the strategies used in risk mitigation. Reducing the likelihood of occurrence of the risk and the impact of that risk on the project is mainly the risk mitigation method. This strategy is mainly to reduce the risk rather than eliminate it, and more precautionary measures are taken to reduce the impact of the risk. For example, in GB projects, the risk of cost increments can be reduced by considering alternative options.

The last option is risk retention, which is defined as the acceptance of the risk when it occurs. There are two risk retention method types: passive and active retentions [38]. Active retention is preparing for the risk with contingency plans and allocating additional funding for the response, whereas passive retention accepts the risk with no actions. In GB projects, these risk mitigation strategies will be used in different projects in different activities. Further, the risk mitigation strategy will also differ from country to country.

4 Case Study Green Building Project

Council House 2 (CH2) is the City of Melbourne's new green building in Melbourne [3]. This building is a 10-storey office building housing approximately 540 staff in the City of Melbourne. The gross floor area is 12,536 m^2. This building was selected as a case study since it is the first purpose-built office building to achieve a Six Green

star rating certified by the Green Building Council of Australia. Compared to other buildings, this building was designed to reduce emissions by 64%.

CH2 was designed considering sustainable and energy-efficient objectives together with improving the overall employee well-being. The rating looked at the following different aspects of the building process [42]: Building Input, Management, Indoor Environment Quality (IEQ), Energy, Transport, Water, Materials, Land Use & Ecology, Emissions, Innovation.

A team of expert designers spent approximately 8 months proposing an innovative building design. Biomimicry was a huge component in the design process, and they achieved some design outcomes.

- A vaulted precast concrete floor integrates with structure, cooling, lighting, and ventilation.
- Facades that are similar to natural systems work with external conditions.
- A healthy work environment that provides physical access to nature.

There were different sustainable systems that are used in the building. The use of solar panels to generate electricity is one of the methods, and about 60% of building domestic hot water is provided by solar panels. The operation of this building is certified carbon neutral, and all emissions associated with running the building are offset [3]. Further, the building windows are designed to assist in heating and cooling processes in the building using several features [3].

4.1 Risk Mitigation in CH2 Building

Different risk mitigation strategies were adopted to mitigate the risks in this building [6, 24]. Some of the risk mitigation strategies used in this building at various stages are discussed in this section.

4.1.1 Preliminary and Planning Stage

- Rigorous risk assessments were conducted for every innovative decision and element incorporated into the building. Extensive computational fluid dynamics (CFD) modelling was completed to determine the ceiling elements to reduce the risks associated with these concepts. Great outcomes were achieved by completing this rigorous analysis [6].
- The integration process in this building is complex. Therefore, a 2-week integrated design team intensive workshop has been conducted to ensure that innovative decisions are made with certainty in terms of cost and constructability.

4.1.2 Construction Stage

- The procurement and construction contract has a significant impact on the project. As a risk mitigation strategy, the contractor has confirmed many possible risks in the early stage of the construction process and informed the project team early in the construction stage. This has enabled the project team to reduce the impact of these risks and allow sufficient time to manage the activities. In addition, the contractor only employed a small core team as sub-contractors.
- Further, the builder has continued with their research and has advised the client about the availability of cost of innovative provisional elements of the design. For example, the builder has challenges with timber windows and rotating timber shutters that satisfy the design team's performance and cost criteria and delivery times in a timely manner.
- Substitution of materials during construction is a frequent problem in the construction industry. An environmental performance questionnaire-approved approach was developed to reduce the substitution of products on-site, and a bank guarantee was proposed.
- Sub-contractors were selected based on their previous work with the main contractor to maintain goodwill as it helps for smooth collaboration between the parties.
- Integrated team approach has benefitted not only in the design stage but also in the construction stage.
- Negotiations with contractual parties to identify solutions for unforeseeable problems arising from the novel materials were included in their communications.

Futureproofing is a term used to refer to how obsolescence can be avoided or at least delayed as long as possible. In this project, future risks were minimised, and the project team has tried to prevent the risks for 50 years.

5 Discussion and Conclusions

The risk elements for the three project stages (15 in Preliminary and planning, 17 in Design and construction, 10 in Handover and operational) identified and summarised in Table 1 could be used to develop risk mitigation measures in green building (GB) projects. The preliminary planning and concept design stage is critical and might reduce the risk exposure if done properly. In this stage, integrated design workshops and computer simulations are the effective risk mitigation measures as applied in the case study. Higher initial costs for GB lead to a different risk profile when compared with traditional buildings. Early contractor involvement (ECI) as in CH2 design workshops is needed to understand the risks. Early stakeholders' involvement and their acceptance of and willingness to actively support and participate are required to mitigate these risks.

The importance of members of project teams differs relative to certification grade [37]. Different risk mitigation mechanisms used in green buildings depend on the activities. A significant amount of resources are used in these buildings, and technologies that can minimise them could be adopted. This can lead to materials savings and accelerate the project while reducing the risks associated with material shortages. As mentioned before, some policies related to normal buildings are not relevant to green buildings, and these policies should be revised to represent the requirements of green buildings.

The transformation from normal building construction to green building construction requires some education for all the stakeholders involved in the project. The education and training will increase the construction industry to drive this transformation [16]. The transformation will require to include some change management aspects in the projects as many stakeholders are involved in the project. Early adoption and engagement of stakeholders in the change management process will provide a smooth transition to green building construction. Besides education about green construction, a skilled workforce is necessary. Technical skills in green buildings, use of green materials, and familiarisation with green building rating systems within the project team will minimise the risks in green building construction [36].

Further, the initial cost of the project is one of the main risks associated with green building construction. The introduction of government incentives and education for communities about the benefits of green buildings is necessary to support these projects to mitigate these risks [16]. The case study presented in Sect. 4 has used a number of risk mitigation measures in different activities. Appropriate risk management strategies drive towards a successful project. Therefore, it is important to identify the risks associated with green buildings and adopt the correct risk mitigation mechanisms to overcome these risks. Leveraging the demand, innovative integrated design technologies and management measures at the project and organisational levels are some of the other factors that need to be investigated in successfully completing a green building.

6 Credit Authorship Contribution Statement

Nilupa Herath: Methodology, Software, Formal Analysis, Investigation, Data curation, Writing—Original draft, Visualisation. **Paulo Vaz-Serra:** Writing—Review & Editing. **Felix Kin Peng Hui:** Validation, Writing—Original Draft, Writing—Review & Editing. **Priyan Mendis:** Supervision, Funding Acquisition. **Lu Aye:** Conceptualisation, Methodology, Validation, Resources, Data Curation, Writing—Review & Editing, Project Administration.

7 Declaration of Competing Interest

The authors have no competing interests to declare that are relevant to the content of this article.

Data Availability The datasets generated and analysed for this work are available from the corresponding author on reasonable request.

References

1. Abdul-Rahman H, Wang C, Sheik Mohamad F (2015) Implementation of risk management in Malaysian construction industry: Case studies. J Construction Eng 2015, Article 192742. https://doi.org/10.1155/2015/192742
2. Abdullah F (2004) Construction Industry and Economic Development: The Malaysian Scene. Universiti Teknologi Malaysia, Penerbit
3. Advanced Environmental Concepts. (2003). *Melbourne City Council- Passive Design Report*. City of Melbourne
4. Ahmad T, Aibinu AA, Stephan A (2019) Managing green building development – A review of current state of research and future directions. Build Environ 155:83–104. https://doi.org/10.1016/j.buildenv.2019.03.034
5. Chan Albert, P. C., Darko, A., Ameyaw Ernest, E., & Owusu-Manu, D.-G. (2017). Barriers Affecting the Adoption of Green Building Technologies. *Journal of Management in Engineering*, *33*(3), Article 04016057. https://doi.org/10.1061/(ASCE)ME.1943-5479.0000507
6. City of Melbourne. (2003). *CH2-Setting a New World Standard in Green Building Design*. City of Melbourne.
7. City of Melbourne. (2022a). *About Council House 2*. Retrieved 12 September 2022 from https://www.melbourne.vic.gov.au/building-and-development/sustainable-building/council-house-2/pages/about-council-house-2.aspx
8. City of Melbourne. (2022b). *Council House 2*. Retrieved 12 September 2022 from https://www.melbourne.vic.gov.au/building-and-development/sustainable-building/council-house-2/Pages/council-house-2.aspx
9. Dewlaney KS, Hallowell MR, Fortunato BR (2012) Safety risk quantification for high performance sustainable building construction. J Constr Eng Manag 138(8):964–971. https://doi.org/10.1061/(ASCE)CO.1943-7862.0000504
10. Dodge Data & Analytics. (2018). *World Green Building Trends 2018: Smart Market Report*. US Green Building Council.
11. El-Sayegh SM, Manjikian S, Ibrahim A, Abouelyousr A, Jabbour R (2021) Risk identification and assessment in sustainable construction projects in the UAE. Int J Constr Manag 21(4):327–336. https://doi.org/10.1080/15623599.2018.1536963
12. Erdenekhuu, N., Kocsi, B., & Máté, D. (2022). A risk-based analysis approach to sustainable construction by environmental impacts. *Energies*, *15*(18), Article 6736. https://doi.org/10.3390/en15186736
13. Fortunato BR, Hallowell MR, Behm M, Dewlaney K (2012) Identification of safety risks for high-performance sustainable construction projects. J Constr Eng Manag 138(4):499–508. https://doi.org/10.1061/(ASCE)CO.1943-7862.0000446
14. Gan X, Zuo J, Ye K, Skitmore M, Xiong B (2015) Why sustainable construction? Why not? An owner's perspective. Habitat Int 47:61–68. https://doi.org/10.1016/j.habitatint.2015.01.005
15. Guan, L., Abbasi, A., & Ryan, M. J. (2020). Analyzing green building project risk interdependencies using Interpretive Structural Modeling. *Journal of Cleaner Production*, *256*, Article 120372. https://doi.org/10.1016/j.jclepro.2020.120372

16. Hui, F. K. P., Ulya, P. F., Wilson, S., Meyliawati, A., & Aye, L. (2020). Green Buildings in Makassar, Indonesia. In Z. Gou (Ed.), *Green Building in Developing Countries: Policy, Strategy and Technology* (pp. 109–127). Springer International Publishing. https://doi.org/10.1007/978-3-030-24650-1_6
17. Hwang, B.-G., Ming, S., Helena, P., & Seokho, C. (2017). An exploratory analysis of risks in green residential building construction projects: The case of Singapore. *Sustainability*, *9*(7), Article 1116. https://doi.org/10.3390/su9071116
18. Hwang B-G, Shan M, Supa'at, N. N. B. (2017) Green commercial building projects in Singapore: Critical risk factors and mitigation measures. Sustain Cities Soc 30:237–247. https://doi.org/10.1016/j.scs.2017.01.020
19. Hwang B-G, Zhao X, See YL, Zhong Y (2015) Addressing Risks in Green Retrofit Projects: The Case of Singapore. Proj Manag J 46(4):76–89. https://doi.org/10.1002/pmj.21512
20. Ismael, D., & Shealy, T. (2018). Sustainable construction risk perceptions in the Kuwaiti construction industry. *Sustainability*, *10*(6), Article 1854. https://doi.org/10.3390/su10061854
21. Javed N, Thaheem MJ, Bakhtawar B, Nasir AR, Khan KIA, Gabriel HF (2020) Managing risk in green building projects: Toward a dedicated framework. Smart and Sustainable Built Environment 9(2):156–173. https://doi.org/10.1108/SASBE-11-2018-0060
22. Krechowicz, M. (2017). Effective Risk Management in Innovative Projects: A Case Study of the Construction of Energy-efficient, Sustainable Building of the Laboratory of Intelligent Building in Cracow. *IOP Conference Series: Materials Science and Engineering*, *245*, Article 062006. https://doi.org/10.1088/1757-899x/245/6/062006
23. Larsen, E., & Musick, R. (2008, November 16–21). *Managing project risks*. 2008 AIChE Annual Meeting, Marriott Philadelphia Downtown. https://folk.ntnu.no/skoge/prost/proceedings/aiche-2008/data/papers/P122950.pdf
24. Morison, A., Hes, D., & Bates, M. (2005). *Materials Selection in Green Buildings and the CH2 Experience*. City of Melbourne. https://www.melbourne.vic.gov.au/SiteCollectionDocuments/ch2-materials-selection-technical-paper.doc
25. Nguyen HD, Macchion L (2022) Risk management in green building: A review of the current state of research and future directions. Environ Dev Sustain. https://doi.org/10.1007/s10668-022-02168-y
26. Nguyen, H. D., Nguyen, L. D., Chih, Y.-Y., & Le-Hoai, L. (2017). Influence of participants' characteristics on sustainable building practices in emerging economies: Empirical case study. *Journal of Construction Engineering & Management*, *143*(8), Article 05017014. https://doi.org/10.1061/(ASCE)CO.1943-7862.0001321
27. Nida J, Muhammad Jamaluddin T, Beenish B, Abdur Rehman N, Ahmad KI, K., & Hamza Farooq, G. (2019) Managing risk in green building projects: Toward a dedicated framework. Smart and Sustainable Built Environment 9(2):156–173. https://doi.org/10.1108/SASBE-11-2018-0060
28. Polat G, Turkoglu H, Gurgun AP (2017) Identification of Material-related Risks in Green Buildings. Procedia Engineering 196:956–963. https://doi.org/10.1016/j.proeng.2017.08.036
29. Project Management Institute. (2021). *A Guide to the Project Management Body of Knowledge (PMBOK® Guide)* (7th ed.). Project Management Institute. https://www.pmi.org/pmbok-guide-standards/foundational/pmbok
30. Qin X, Mo Y, Jing L (2016) Risk perceptions of the life-cycle of green buildings in China. J Clean Prod 126:148–158. https://doi.org/10.1016/j.jclepro.2016.03.103
31. Rad KM, Yamini OA (2017) The importance and use of risk management in various stages of construction projects life cycle (PLC). Mod Appl Sci 11(1):48–54. https://doi.org/10.5539/mas.v11n1p48
32. Rafindadi AD, Mikić M, Kovačić I, Cekić Z (2014) Global perception of sustainable construction project risks. Procedia Soc Behav Sci 119:456–465. https://doi.org/10.1016/j.sbspro.2014.03.051
33. Ranawaka I, Mallawaarachchi H (2018) A risk-responsive framework for green retrofit projects in Sri Lanka. Built Environment Project and Asset Management 8(5):477–490. https://doi.org/10.1108/BEPAM-10-2017-0088

34. Serpell A, Ferrada X, Rubio L, Arauzo S (2015) Evaluating risk management practices in construction organizations. Procedia Soc Behav Sci 194:201–210. https://doi.org/10.1016/j.sbspro.2015.06.135
35. Shan, M., Hwang, B.-G., & Zhu, L. (2017). A global review of sustainable construction project financing: Policies, practices, and research efforts. *Sustainability*, *9*(12), Article 2347. https://doi.org/10.3390/su9122347
36. Shen, W., Tang, W., Siripanan, A., Lei, Z., Duffield, C. F., & Hui, F. K. P. (2020). Understanding the Green Building Industry in Thailand. In Z. Gou (Ed.), *Green Building in Developing Countries: Policy, Strategy and Technology* (pp. 161–180). Springer International Publishing. https://doi.org/10.1007/978-3-030-24650-1_9
37. Shen, W., Tang, W., Wang, S., Duffield, C. F., Hui, F. K. P., & You, R. (2017). Enhancing trust-based interface management in international engineering-procurement-construction projects. *Journal of Construction Engineering and Management*, *143*(9), Article 04017061. https://doi.org/10.1061/(ASCE)CO.1943-7862.0001351
38. Siew Goh, C., & Abdul-Rahman, H. (2013). The identification and management of major risks in the Malaysian construction industry. *Journal of Construction in Developing Countries*, *18*(1), 19–32. http://web.usm.my/jcdc/vol18_1_2013/art2_jcdc18-1.pdf
39. Tao, X., & Xiang-Yuan, S. (2018). Identification of risk in green building projects based on the perspective of sustainability. *IOP Conference Series: Materials Science and Engineering*, *439*, Article 032053. https://doi.org/10.1088/1757-899x/439/3/032053
40. TGBI. (2017). *TREES-EB: Thai's Rating of Energy and Environmental Sustainability for Existing Building: Operation and Maintenance.* Retrieved 6 June 2022 from https://tgbi.or.th/uploads/trees/2017_03_TREES-EB-Eng.pdf
41. Wang, M.-T., & Chou, H.-Y. (2003). Risk allocation and risk handling of highway projects in Taiwan. *Journal of Management in Engineering*, *19*(2), Article 60. https://doi.org/10.1061/(ASCE)0742-597X(2003)19:2(60)
42. Wikipedia. (2022). *Council House 2.* Retrieved 12 September 2022 from https://en.wikipedia.org/wiki/Council_House_2
43. Yang RJ, Zou PXW (2014) Stakeholder-associated risks and their interactions in complex green building projects: A social network model. Build Environ 73:208–222. https://doi.org/10.1016/j.buildenv.2013.12.014
44. Yang RJ, Zou PXW, Wang J (2016) Modelling stakeholder-associated risk networks in green building projects. Int J Project Manage 34(1):66–81. https://doi.org/10.1016/j.ijproman.2015.09.010
45. Zhao X, Hwang B-G, Gao Y (2016) A fuzzy synthetic evaluation approach for risk assessment: a case of Singapore's green projects. J Clean Prod 115:203–213. https://doi.org/10.1016/j.jclepro.2015.11.042
46. Zhao, X., Hwang, B. G., & See, Y. L. (2015, September 7–9). *Green retrofit projects: Risk assessment and mitigation.* 31st Annual ARCOM Conference, Lincoln, UK. https://www.arcom.ac.uk/-docs/proceedings/870c377f527501b54e7cf33bdb4cbadc.pdf
47. Zou PXW, Couani P (2012) Managing risks in green building supply chain. Architectural Engineering and Design Management 8(2):143–158. https://doi.org/10.1080/17452007.2012.659507
48. Zuo J, Zhao Z-Y (2014) Green building research–current status and future agenda: A review. Renew Sustain Energy Rev 30:271–281. https://doi.org/10.1016/j.rser.2013.10.021

Impacts of Selected Urban Tree Species on Outdoor Thermal Comfort in the City of Colombo

A. P. Sirimanne and V. M. Jayasooriya

Abstract Alongside rapid urbanization, the warm, humid tropical climate of Colombo exerts pressure on the city intensifying thermal discomfort. This could further create a negative influence on performing outdoor activities restricting the quality of life of urban dwellers. Therefore, creating a thermally comfortable urban space is significant. Yet, identifying the suitable tree species to provide better thermal comfort in Colombo has seldom been discussed. This study evaluates the impact on outdoor thermal comfort based on the physiologically equivalent temperature (PET) of five common species in Colombo; *Cassia fistula, Tectona grandis, Plumeria obtuse, Mangifera indica*, and *Terminalia catappa.* The field data collection was conducted on the sites of five selected species under both sunny and cloudy conditions. The parameters that contribute to assessing the urban thermal environment; sky view factor, relative humidity, air temperature, surface temperature, wind speed, solar radiation, and cloud cover were measured. The RayMan model was used to estimate thermal comfort by calculating PET values. The results indicated that the shading of trees can considerably influence outdoor thermal comfort expressed by PET. The lower PET values under the tree canopies indicated a lower level of thermal discomfort compared to an adjacent site, which was not directly shaded. Moreover, the one-way ANOVA test ($p = 0.027$) indicated that thermal comfort under *Terminalia catappa* was statistically different compared to *Plumeria obtuse* on sunny days. Additionally, among the selected species, *Terminalia catappa* was identified to be the most suitable species for improving thermal comfort in outdoor urban settings. The findings assist in the identification of species that offer greater thermal comfort in Colombo. As the use of appropriate tree species for shading is critical in alleviating heat stress, the results achieved can be employed as a measure of enhancing outdoor thermal comfort and as a vital initiative to achieve sustainability in Colombo.

Keywords Urban Microclimate · Outdoor thermal comfort · Urban greening · Sky View Factor (SVF) · Physiologically equivalent temperature (PET) · Colombo

A. P. Sirimanne · V. M. Jayasooriya (✉)
Department of Forestry and Environmental Science, Faculty of Applied Sciences, University of Sri Jayewardenepura, Sri Jayewardenepura, Sri Lanka
e-mail: varuni.jayasooriya@sjp.ac.lk

© The Author(s), under exclusive license to Springer Nature Singapore Pte Ltd. 2023

R. Dissanayake et al. (eds.), *ICSBE 2022*, Lecture Notes in Civil Engineering 362,
https://doi.org/10.1007/978-981-99-3471-3_21

1 Introduction

Over the past few decades, designing thermally comfortable outdoor spaces while maintaining beauty has been increasingly identified as a goal in sustainable urban planning and design [24]. One of the main ways of enhancing the livability in outdoor spaces is by creating thermally comfortable spaces which attract people to spend their time in open spaces [13, 17]. The term thermal comfort can be simply defined as "the condition of mind that expresses satisfaction with the thermal environment" [1]. It is a complex feeling that involves both psychological and social components. One of the most crucial elements in determining the effectiveness of outdoor spaces for pedestrians is thermal comfort [2]. It is impossible to create a suitable thermal environment in urban open areas without a proper determination and comprehension of outdoor thermal comfort [15]. The physiologically equivalent temperature (PET) is one of the most used thermal indices, which consider environmental parameters that affect thermal comfort, as well as physical activity and the clothing level of the individuals as its governing variables in evaluating thermal comfort [9]. When interpreting PET values, high PET values are often identified as thermally uncomfortable or unacceptable [32] whereas low PET values in the range between 27.0 and 33.0 °C can be identified as the thermally comfortable range for countries such as Sri Lanka [10].

Trees particularly influence the thermal environment by providing shade, reducing surface temperature, intercepting radiation with their canopy, and even heat transference through convection from warmer areas. Furthermore, by the conversion of radiation into latent heat and evapotranspiration, trees provide additional cooling [14]. Apart from reducing air temperature by increasing evapotranspiration, trees also block the Sun and reduce the mean radiant temperature in the street canyons in urban spaces. There are various studies carried out on how vegetation influences thermal comfort, which ranges from single trees to urban parks [27, 28]. Lin et al. [15] have studied the PET differences under shaded and unshaded conditions. The results of these studies indicated that during the days with high air temperatures in the hot season, the mean PET values of the unshaded areas were approximately 10 °C, higher than those of the shaded areas. Therefore, by using vegetation in urban areas such as parks, it is possible to improve the overall thermal conditions especially by decreasing air temperature and mean radiant temperature while increasing the humidity of the surrounding environment [28, 29] have identified that a greater reduction in heat stress could be achieved by shade on sunny days than on cloudy days. The canopy climate can be up to 5 °C cooler on high radiation than the ambient climate. Reference [12] studied the impact of tree types on outdoor thermal environments in Hong Kong and concluded that the trees with larger crowns, such as *Macaranga tanarius*, *Ficus microcarpa*, and *Acacia confusa* are recommended more over those with small crowns for higher thermal comfort. Moreover, [6] investigated the role of vegetation outdoors and observed that Ficus trees which have larger crowns were the most suitable.

In Sri Lanka, a country that receives abundant sunlight, trees play a significant role in providing thermal comfort in outdoor spaces. However, the specific trees have not undergone an effective selection or positioning to effectively provide thermal comfort [21]. There have been studies conducted in the global context that have proved the role of vegetation in various urban areas and the need to use vegetation to effectively provide thermal comfort [24, 25]. However, local studies have mainly focused on the influence of urban design and green influence on outdoor thermal comfort but not on the influence of tree shade on outdoor thermal comfort [5, 7, 10]. Moreover, even though tropical countries like Hong Kong [12] and Taiwan [19] have conducted studies to identify suitable tree species for the enhancement of outdoor thermal comfort, there have not been such studies conducted in Sri Lanka. Therefore, by analyzing the above-mentioned research gaps, the current study is focused on bridging the untapped areas of outdoor thermal comfort studies in Colombo, Sri Lanka.

The main objective of the present study is to understand the role of tree shade and the impact of five common trees on outdoor thermal comfort to encourage urban planners to integrate tree species as a strategy to elevate heat stress. ENVI-met and RayMan models are the most popular thermal comfort simulation tools. The present study used the RayMan model as the thermal comfort simulation tool due to its flexibility and practicality in calculating PET [24, 25]. There is a need to understand the effect of tree species on outdoor thermal comfort in hot, humid climates to develop climate-conscious urban design guidelines. The aim of this study is to demonstrate how thermal comfort is affected by tree shade and to investigate the impact of *Cassia fistula* (Ehela), *Tectona grandis* (Teak), *Plumeria obtuse* (Araliya), *Mangifera indica* (Mango), and *Terminalia catappa* (Kottamba) on outdoor thermal comfort.

2 Materials and Methods

2.1 Study Area

The selected study area for the research is Colombo (6.9271° N, 79.8612° E). It is the commercial capital and the largest city of Sri Lanka by population. The main objective of the present study is to assess the impacts of five selected common urban tree species for outdoor thermal comfort improvement in Colombo city. The local climatic conditions may highly influence thermal comfort conditions. Therefore, the sites were carefully selected by considering the roads and areas exhibiting similar microclimatic and ambient conditions.

2.2 Selection of Sites

Initially, Colombo 1–15 areas were considered as the sites for the preliminary data collection. Then, after visiting each site, six study areas were selected based on the green cover percentage of the 47 wards in Colombo 1–15. Bloemendhal (Colombo 13) and Fort (Colombo 01) areas were selected to represent the low green cover areas, and Bambalapitya (Colombo 04) and Wekanda (Colombo 02) areas were selected to represent the moderate green cover areas. Cinnamon Gardens (Colombo 07) and Thimbirigasyaya (Colombo 05) areas were selected to represent the high green cover areas [31]. The six sites were chosen to represent a different green cover percentage, ranging from low to high, to neutralize the impact of green cover on thermal comfort.

2.3 Selection of Trees

The six sites and the suitable tree species for the study were selected simultaneously. During the initial field visit, the most abundant and common tree species in Colombo 1–15 were identified. When selecting the most suitable trees, the following factors were also considered; trees with overlapping crowns and trees with trunks connected to walls should be disregarded, trees near a high-rise building or high wall or water body in proximity should be excluded, trees in an extreme microclimatic condition such as coastal areas, urban parks etc. were excluded. Moreover, the presence of all the selected tree species in the six selected sites was an essential requirement. Thereby, considering all these factors, *Terminalia catappa* (Kottamba), *Mangifera indica* (Mango), *Cassia fistula* (Ehela), *Tectona grandis* (Teak), *and Plumeria obtuse* (Araliya) were selected as the most suitable tree species out of the observed most common species. Table 1 shows the total number of each tree in each selected site.

Table 1 Total number of trees in each site

Name of the ward	Number of trees					Number of trees
	Mango	Araliya	Teak	Kottamba	Ehela	
Bloemendhal	3	2	2	2	2	11
Fort	2	2	2	2	2	10
Wekanda	2	1	2	2	1	8
Bambalapitiya	2	2	2	2	3	11
Thimbirigasyaya	2	2	2	2	2	10
Cinnamon Gardens	4	4	4	4	4	20
Total	15	13	14	14	14	70

Table 2 Specifications of instruments used for the data collection

Instrument	Parameter	Accuracy
Smart sensor humidity and temperature meter	Air temperature	±1.5
	Relative humidity	±0.1% RH
Smart sensor digital anemometer	Wind velocity	±0.1 m/s or ± 5%
Infrared radiometer	Surface temperature	±0.3 °C
Fish eye lens	Sky view factor	

2.4 Field Data Collection

In this study, data were collected between 11.00 am and 3.00 pm under both sunny and overcast conditions from August 2021 to March 2022. The data were collected both under the tree and in a near-exposed area of selected trees to compare the thermal comfort difference between the near-exposed area and under the tree canopy. Six replicate measurements were carried out for each location changing the date, time, and weather conditions. Altogether, 420 (70*6) data points were collected under the trees and 420 data points were collected in a near-exposed site of each tree. To calculate PET by RayMan model, air temperature, relative humidity, surface temperature, solar radiation, and wind velocity were measured both under the tree and in a near-exposed area at a 10 s sampling interval, then the data were averaged. Moreover, cloud cover was determined by visual inspection out of 8 Oktas and if the cloud amount reaches 6 Oktas or above, it was considered an overcast condition (Tang and Ng 2016). A fisheye image was taken 1.5 m above the root collar under the tree and 1.5 m above the ground in the near-exposed area to calculate Sky View Factor (SVF). Furthermore, as inputs for the RayMan model to calculate PET, the longitude, latitude, and altitude of the sites were measured and personal data such as age, sex, height, and weight of the observer were kept constant throughout the data collection process as a reference figure for the comparison purposes. Additionally, data related to activity level were set to 80.0W, and clothing level was set to 0.9clo since it was a prerequisite to calculate PET by RayMan model. Table 2 shows the instruments used for the field data collection.

2.5 RayMan Model

This study used the RayMan model to estimate outdoor thermal comfort. It is a micro-scale model that is one-dimensional in space, which means that all the calculations are performed for one point [22, 23]. The outdoor thermal comfort indices; PET was calculated using the RayMan model. The model inputs for the PET calculation were air temperature, relative humidity, surface temperature, solar radiation, wind velocity, cloud cover, SVF, activity level, clothing level, personal details such as age, sex, height and weight, and location details such as longitude, latitude and altitude.

Table 3 Descriptive statistics of PET under each tree

Tree	N	Mean	St. Dev	Min	Max
Araliya	78	35.96	4.490	27.2	43.3
Ehela	84	34.72	4.791	26.5	45.2
Kottamba	84	34.24	4.262	25.4	42.2
Mango	90	34.52	4.232	26.4	41.9
Teak	84	35.81	4.425	27.6	45.1

3 Results

3.1 Thermal Comfort Under Each Tree Species Under Both Sunny and Overcast Conditions

The results indicate that Araliya obtained the highest under the tree PET, which is 35.96 °C, whereas the lowest was obtained under the Kottamba tree, which is 34.24 °C. There is a 1.72 °C mean difference of PET between Araliya and Kottamba. The second lowest PET was recorded under the Mango tree while the third lowest PET was recorded under the Ehela tree. Therefore, the results suggest that out of the selected five tree species, thermal comfort is highest under the Kottamba tree followed by Mango, Ehela, Teak, and Araliya, respectively. Table 3 provides the descriptive statistics of the calculated PET values under each tree.

Figure 1 shows the distribution of PET under each tree species on both sunny and overcast days.

3.2 Comparison Between Under-The-Tree and Near-Exposed Area

The physiologically equivalent temperature (PET) index was calculated to compare the thermal comfort difference between under-the-tree and near-exposed areas of trees. Figure 2 demonstrates the graphical difference and reveals that the PET beneath a tree (denoted by PET) is lower than the PET in nearby exposed areas (denoted EX-PET), indicating that the thermal comfort under the tree was higher than in nearby exposed areas, highlighting the need to examine the impact of tree species on outdoor thermal comfort.

A parametric t-test was conducted to assess whether there is a significant difference between the PET values recorded under-the-tree and near-exposed area PET values. The results are indicated in Table 4.

The test indicated that there is a significant difference between the values of PET under-the-tree and near-exposed area obtained for each tree species ($p < 0.05$). Therefore, it is statistically proven that the thermal comfort under the tree canopy is higher

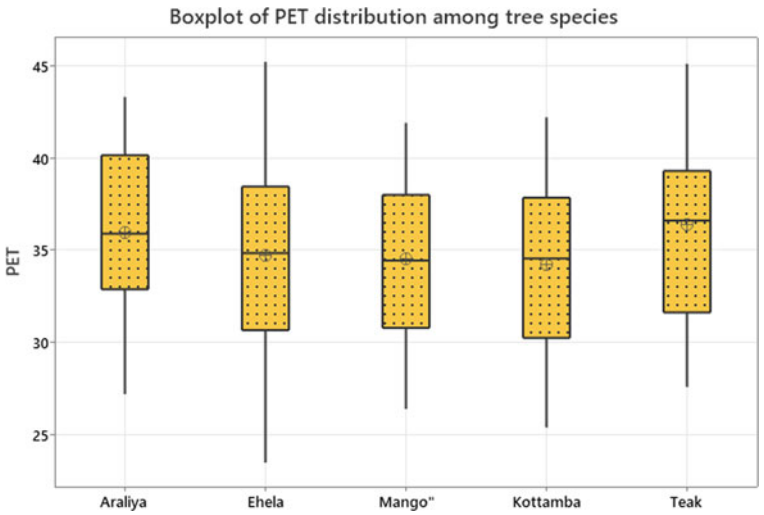

Fig. 1 Boxplot of under-the-tree PET distribution of each species under both sunny and overcast conditions

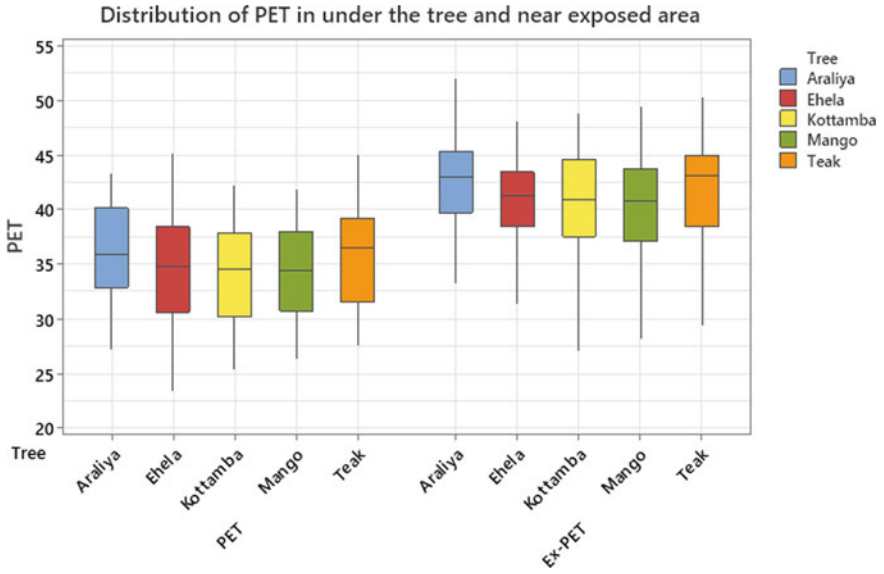

Fig. 2 Boxplot of distribution of PET under-the-tree and near-exposed area of each tree

Table 4 PET comparison between under-the-tree and near-exposed area

	t	df	Sig. (two-tailed)	Mean difference	Standard deviation
Plumeria obtuse	−6.73	144	0.000	−5.510	4.840
Cassia fistula	−7.34	165	0.000	−5.486	3.836
Mangifera indica	−7.79	170	0.000	−5.608	4.134
Terminalia catappa	−7.70	156	0.000	−5.849	4.645
Tectona grandis	−7.50	161	0.000	−5.614	3.784

compared to the thermal comfort under the near-exposed area. When comparing mean PET values of exposed areas, PET under the trees of Araliya, Ehela, Mango, Kottamba, and Teak is lower by 5.51 °C, 5.49 °C, 5.61 °C, 5.84 °C, 5.61 °C, respectively. The highest PET difference is recorded in Kottamba, which suggests that the highest thermal comfort difference between the under-the-tree and near-exposed area is a result of Kottamba.

3.3 Comparison of PET Difference Among Selected Species on Sunny Weather Conditions

The one-way ANOVA suggested a statistically significant PET difference between the selected five tree species in sunny weather conditions ($F(4,242) = 2.803$, $p = 0.027$), and the results are shown in Table 5.

A post hoc Tukey HSD (Honest Significant Difference) test was conducted to determine which of the various pairs of means difference is significant. The Tukey HSD showed that it is only the mean PET difference between *Plumeria obtuse* and *Terminalia catappa* that reaches significance. Moreover, there was no other statistically significant PET difference, thus thermal comfort difference between other tree species is statistically not different at a 0.05 significance level.

Further analysis was conducted to identify whether there is a significant difference between PET in near-exposed areas of each tree under sunny conditions. The one-way ANOVA suggested that there is no statistically significant PET difference between the near-exposed areas of each tree in sunny conditions ($F(4,242) = 1.702$, $p = 0.149$). These results indicate that the PET is the same in all of the near-exposed

Table 5 One-way ANOVA test on differences in PET between the five selected tree species on Sunny days

	Sum of Squares	df	Mean Square	F	Sig
Between groups	167.968	4	41.992	2.803	0.027
Within groups	3565.628	238	14.982		
Total	3733.596	242			

areas. However, the difference in PET under the trees of *Plumeria obtuse* (Araliya) and *Terminalia catappa* (Kottamba) suggests that there is an impact of tree species on outdoor thermal comfort.

4 Discussion

Creating a thermally comfortable outdoor environment is of paramount importance. Many studies have found that shaded spaces have less thermal stress and discomfort than open unshaded spaces [15, 20, 23, 24]. Thus, the present study was carried out to assess the role of *Cassia fistula* (Ehela), *Tectona grandis* (Teak), *Plumeria obtuse* (Araliya), *Mangifera indica* (Mango), and *Terminalia catappa* (Kottamba) for outdoor thermal comfort improvement in the Colombo city.

The PET variation with environmental parameters displays that solar radiation, air temperature, and surface temperature move in the same direction. This means that if one parameter increases, the other parameter also increases, and vice versa. Furthermore, the results suggest that the variation of air temperature and the surface temperature has a strong correlation with PET compared to solar radiation. Moreover, a low and negative correlation was found between RH and PET, which suggests that RH moves in a different direction than PET.

Results of the study reveal that the PET is significantly different between the under-the-tree and near-exposed areas where the average PET beneath a tree is 5.61 °C lower than the average PET in nearby exposed areas. Hence, it can be concluded that the thermal comfort under a tree is higher compared to unshaded locations. This highlights the conclusion that tree species have an impact on thermal comfort. The obtained results complied with the results proposed by previous studies, which stated that shaded spaces have less thermal discomfort than open unshaded spaces [14, 20, 24]. The reason behind the perceived high thermal comfort is owing to the role of tree species in regulating thermal stress. Trees are capable of providing regulatory functions to control the micrometeorological conditions, which affect outdoor thermal comfort by lowering the mean radiant temperature and air temperature by shading effect. It allows more transpiration, and wind resistance, which slows down the wind speed under a tree. Thus, urban trees can modify air temperature, increase air humidity, and reduce wind speed leading to higher thermal comfort beneath the tree [12]. SVF. This is widely employed in urban microclimate studies and has been shown to have a substantial link with the thermal environment, with a percentage of the visible sky (ranging from 0 to 1) in a hemispherical image [14, 34, 35]. A tree with a particularly dense crown will have a low SVF due to the low ratio of the visible sky under the tree. As a result, when the tree SVF is low, there is very little solar radiation reaching the ground. The thermal comfort rises as the solar radiation beneath the tree decreases. Therefore, the low SVF that is recorded under-the-tree compared to the near-exposed area also acts as a predictor for the obtained differences in thermal comfort between the trees of the near-exposed area and-under-the tree.

Out of the selected five tree species, the Kottamba tree provides the highest thermal comfort followed by Mango, Ehela, Teak, and Araliya, respectively. The thermal comfort difference between *Plumeria obtuse* (Araliya) and *Terminalia catappa* (Kottamba) was significant under sunny conditions. The thermal difference under the Araliya tree and the Kottamba tree may have resulted due to the differences in environmental parameters and the differences in tree parameters of the two species. The solar radiation under the Kottamba tree and Araliya tree is significantly different where the solar radiation under the Araliya is twice as high as the Kottamba. Moreover, the surface temperature under the Araliya tree is 2.84 °C higher compared to Kottamba. As surface temperature [11] and solar radiation [8, 33] are significant parameters that determine thermal comfort, it is evident that these three factors can act as the main predictors, which resulted in a thermal comfort difference among Araliya and Kottamba in terms of PET.

5 Conclusion

In tropical countries like Sri Lanka where the increased levels of temperature induce the risk of heat-related illnesses, thermal comfort levels are of utmost importance. To develop cities in a sustainable manner, a focal point of discussion has been the optimum utilization of outdoor spaces while providing the landscape for vegetation to elevate thermal comfort. With these benefits taken into consideration, it is paramount to build an outdoor environment that is thermally comfortable with improved urban climate conditions.

The present study analyzed the impact of five selected urban tree species on outdoor thermal comfort in Colombo. In comparison to exposed unshaded locations, there is a higher thermal comfort in locations that have tree shade, depicting a conclusion that tree species have an impact on thermal comfort. The results indicated that there is a difference in PET under the trees of Araliya and Kottamba suggesting that there is an impact of tree species on outdoor thermal comfort. Further, it was revealed that from the five tree species which were selected for this research, the *Terminalia catappa* (Kottamba) tree provides the highest degree of thermal comfort while *Mangifera indica* (Mango), *Cassia fistula* (Ehela), *Tectona grandis* (Teak), and *Plumeria obtuse* (Araliya) provide thermal comfort in the given order. The highest difference in thermal comfort between under-the-tree and near-exposed areas was recorded for *Terminalia catappa* trees, which suggests that out of the five selected tree species, Kottamba is the most capable tree species of reducing thermal stress perceived by people.

The provision of outdoor thermal comfort is crucial amidst the rapid rate of climate change, particularly in tropical countries. However, proposing tree species to an urban area is crucial as there are several different factors such as landscape architectural designs and site characteristics that need to be taken into account apart from thermal comfort. Therefore, it is crucial to promote the identification of such characteristics other than the parameters selected in the present study. Moreover, future studies

should explore more suitable tree species and novel strategies to reduce solar radiation, air temperature, and surface temperature as the present study suggested a strong positive correlation between solar radiation, air temperature, surface temperature, and PET. Thus, it can be concluded that this study provides a guide to conducting further studies to analyze the impact of different environmental parameters and tree species to achieve desired outdoor thermal comfort for the tropical city of Colombo.

References

1. ANSI/ASHRAE 2017. Standard 55–2017, Thermal environmental conditions for human occupancy. American National Standards Institute, American Society of Heating, Refrigerating and Air-Conditioning Engineers, Atlanta, GA, USA.
2. Chen L, Wen Y, Zhang L, Xiang WN (2015) Studies of thermal comfort and space use in an urban park square in cool and cold seasons in Shanghai. Build Environ 94:644–653
3. Depietri Y, Renaud FG, Kallis G (2012) Heat waves and floods in urban areas: a policy-oriented review of ecosystem services. Sustain Sci 7(1):95–107
4. Fang Z, Lin Z, Mak C, Niu J, Tse K (2018) Investigation into sensitivities of factors in outdoor thermal comfort indices. Build Environ 128:129–142
5. Galagoda RU, Jayasinghe GY, Halwatura RU, Rupasinghe HT (2018) The impact of urban green infrastructure as a sustainable approach towards tropical micro-climatic changes and human thermal comfort. Urban forestry & urban greening 34:1–9
6. Hanafi A, Alkama D (2017) Role of the urban vegetal in improving the thermal comfort of a public place of a contemporary Saharan city. Energy Procedia 119:139–152
7. Herath HMPIK, Halwatura RU, Jayasinghe GY (2018) Evaluation of green infrastructure effects on tropical Sri Lankan urban context as an urban heat island adaptation strategy. Urban Forestry & Urban Greening 29:212–222
8. Huang H, Peng M (2020) The outdoor thermal comfort of urban square: A field study in a cold season in Chongqing. IOP Conference Series: Earth and Environmental Science 467(1):012215
9. Javan K, Nasiri F (2016) Evaluating the thermal comfort of humans by RayMan model in Lake Urmia Basin, Iran. Journal of Tourism & Hospitality Research 5(1):73–89
10. Johansson E, Emmanuel R (2006) The influence of urban design on outdoor thermal comfort in the hot, humid city of Colombo, Sri Lanka. Int J Biometeorol 51(2):119–133
11. Karimi A, Sanaieian H, Farhadi H, Norouzian-Maleki S (2020) Evaluation of the thermal indices and thermal comfort improvement by different vegetation species and materials in a medium-sized urban park. Energy Rep 6:1670–1684
12. Kong L, Lau K, Yuan C, Chen Y, Xu Y, Ren C, Ng E (2017) Regulation of outdoor thermal comfort by trees in Hong Kong. Sustain Cities Soc 31:12–25
13. Lai D, Lian Z, Liu W, Guo C, Liu W, Liu K, Chen Q (2020) A comprehensive review of thermal comfort studies in urban open spaces. Sci Total Environ 742:140092
14. Lin BS, Lin YJ (2010) Cooling effect of shade trees with different characteristics in a subtropical urban park. HortScience 45(1):83–86
15. Lin T, Matzarakis A, Hwang R (2010) Shading effect on long-term outdoor thermal comfort. Build Environ 45(1):213–221
16. Lin TP, Tsai KT, Liao CC, Huang YC (2013) Effects of thermal comfort and adaptation on park attendance regarding different shading levels and activity types. Build Environ 59:599–611
17. Lin TP, Tsai KT, Hwang RL, Matzarakis A (2012) Quantification of the effect of thermal indices and sky view factor on park attendance. Landsc Urban Plan 107(2):137–146
18. Lin W, Zeng C, Lam N, Liu Z, Tao J, Zhang X, Lyu B, Li N, Li D, Chen Q (2021) Study of the relationship between the spatial structure and thermal comfort of a pure forest with four distinct seasons at the microscale level. Urban Forestry & Urban Greening 62:127168

19. Lin Y, Tsai K (2017) Screening of Tree Species for Improving Outdoor Human Thermal Comfort in a Taiwanese City. Sustainability 9(3):340
20. Makaremi N, Salleh E, Jaafar MZ, GhaffarianHoseini A (2012) Thermal comfort conditions of shaded outdoor spaces in hot and humid climate of Malaysia. Build Environ 48:7–14
21. Matzarakis A, Mayer H, Kuppe S, Holst J, Imbery F (2009) Human thermal comfort below the canopy of street trees on a typical Central European summer day. Berichte des Meteorologischen Instituts der Albert-Ludwigs-Universität Freiburg 18:211–219
22. Matzarakis A, Rutz F, Mayer H (2007) Modelling radiation fluxes in simple and complex environments—application of the RayMan model. Int J Biometeorol 51(4):323–334
23. Matzarakis A, Rutz F, Mayer H (2010) Modelling radiation fluxes in simple and complex environments: basics of the RayMan model. Int J Biometeorol 54(2):131–139
24. Nasrollahi N, Ghosouri A, Khodakarami J, Taleghani M (2020) Heat-Mitigation Strategies to Improve Pedestrian Thermal Comfort in Urban Environments: A Review. Sustainability 12(23):10000
25. Ruiz MA, Sosa MB, Correa EN, Cantón MA (2017) Design tool to improve daytime thermal comfort and nighttime cooling of urban canyons. Landsc Urban Plan 167:249–256
26. Santamouris M (2014) Cooling the cities–a review of reflective and green roof mitigation technologies to fight heat island and improve comfort in urban environments. Sol Energy 103:682–703
27. Taleghani M, Sailor DJ, Tenpierik M, van den Dobbelsteen A (2014) 'Thermal assessment of heat mitigation strategies: The case of Portland State University. Oregon, USA', Building and Environment 73:138–150
28. Tan, Z. and Ng, E. (2016) 'Enhancing Outdoor Comfort and Climate Resilience with Mitigation Strategies: Optimized Planning Methods for Tree Planting in Subtropical High-Density Cities', In: *4th International Conference on Countermeasures to Urban Heat Island*.
29. Watanabe S, Nagano K, Ishii J, Horikoshi T (2014) Evaluation of outdoor thermal comfort in sunlight, building shade, and pergola shade during summer in a humid subtropical region. Build Environ 82:556–565
30. Westreenen A, Zhang N, Douma J, Evers J, Anten N, Marcelis L (2020) Substantial differences occur between canopy and ambient climate: quantification of interactions in a greenhouse-canopy system. PLoS ONE 15(5):e0233210
31. Wickramasinghe L, Subasinghe S, Ranwala S (2016) Spatial and Temporal Changes of the Green Cover of Colombo City in Sri Lanka from 1956 to 2010. J Environ Professionals Sri Lanka 5(1):53–66
32. Yahia MW, Johansson E (2014) Landscape interventions in improving thermal comfort in the hot dry city of Damascus, Syria-The example of residential spaces with detached buildings. Landsc Urban Plan 125:1–16
33. Yin J, Zheng Y, Wu R, Tan J, Ye D, Wang W (2011) An analysis of influential factors on outdoor thermal comfort in summer. Int J Biometeorol 56(5):941–948
34. Zeng L, Lu J, Li W, Li Y (2018) A fast approach for large-scale Sky View Factor estimation using street view images. Build Environ 135:74–84
35. Zhang J, Gou Z, Shutter L (2019) Effects of internal and external planning factors on park cooling intensity: field measurement of urban parks in Gold Coast, Australia. AIMS Environ Sci 6(6):417–434

Analysis of Passive Solar Design and Thermal Mass Optimization to Reduce Cooling Energy Demand of Existing Building

S. V. I. R. V. Serasinghe, I. D. Nissanka, and M. A. Wijewardane

Abstract Half the global energy production is spent on building energy out of which, a major portion contributes to HVAC. With the projected increase in temperature under different climatic changes, the energy demand for cooling will increase significantly. If this increase in energy demand is not managed well, it can be a threat to the energy sector of a developing country like Sri Lanka, which predominantly relies on non-renewable sources for energy generation. The already hot and humid climate subjected to global warming will become an important factor for higher cooling energy demand forecasts. Hence, the prediction of energy demand and implementing cooling load-increasing mitigation tactics are important steps in building energy sustainability in Sri Lanka. Although steps have been taken to ensure energy efficiency in new buildings, the existing buildings pose a significant threat in terms of energy increase due to climatic change. There are different types of models adapted to predict the cooling load of existing buildings. This paper presents a hybrid data-driven model to calculate the air-conditioning demand predictions for several buildings in Colombo, Sri Lanka. It also uses the model to evaluate building thermal mass optimization and the usage of passive solar designs to reduce heat infiltration into buildings as cooling energy demand increases mitigation strategies. The model is used to predict the cooling load increase of eight selected zones of three different buildings for the year 2090 under two climatic change scenarios and to evaluate the energy-saving possibilities with the two countermeasures proposed. It was concluded that most zones will have a substantial reduction in cooling load: 20% on average by thermal load optimization with or without night-time ventilation, while the zones showed a significant cooling load reduction by up to 60% with optimized solar designs by 2090.

S. V. I. R. V. Serasinghe (✉) · I. D. Nissanka · M. A. Wijewardane
Department of Mechanical Engineering, University of Moratuwa, Katubedda, Sri Lanka
e-mail: serasinghesvirv.20@uom.lk

I. D. Nissanka
e-mail: nissankai@uom.lk

M. A. Wijewardane
e-mail: anusha@uom.lk

© The Author(s), under exclusive license to Springer Nature Singapore Pte Ltd. 2023

R. Dissanayake et al. (eds.), *ICSBE 2022*, Lecture Notes in Civil Engineering 362,
https://doi.org/10.1007/978-981-99-3471-3_22

Keywords Cooling energy demand prediction · Energy demand mitigation · HVAC · Global warming · Passive solar design

1 Introduction

It is a well-known fact that the world is facing an energy crisis today. Sri Lanka, being a country that relied on non-renewable energy sources such as fossil fuels and coal for its energy generation, is in dire need of either effectively managing the consumption of energy or diverging into renewable energy sources. According to a study by [3], an average of 78% of the national energy demand is supplied by non-renewable energy sources. Almost all these non-renewable fuels are being imported into the country, which is a huge burden to its economy. In a hot and humid country like Sri Lanka, amidst the threats of global warming, increased energy demand in the current infrastructure would be critical for the national power demand. The increased demand means that more energy should be produced through non-renewable sources, which in turn contributes to global warming. The building sector in Sri Lanka is consuming 46% of the total energy followed by industrial and transportation sectors consuming 29%. More than 50% of the building energy consumption in Sri Lanka is occupied by HVAC systems as calculated by the electricity bills and end-use electricity breakdown [4]. As per the rising global temperature, the HVAC energy demand is predicted to increase, which will increase greenhouse gas emissions, resulting in accelerated global warming, creating a temperature and demand increase cycle.

When predicting the future building air-conditioning energy demand patterns, localized studies are more important as the energy demand is dependent on the climate zones [5, 7, 13]. It should also be noted that from the IPCC assessment report, the frequency of hot days and hot nights is increasing throughout the globe [2, 6, 9]. These changes are dominant in the regions Southern of and South Eastern Asia, with a large increase in buildings and population [7]. A study by [11] showed that the energy demand for air-conditioning in these regions could increase up to 40 times in the year 2100, with an average annual rise of 7%. This increase in energy demand is affected by the rise in cooling energy demand of existing buildings as well as the predicted additional energy demand due to the new constructions. This research aims to develop models to predict the energy demand of several buildings in Colombo, Sri Lanka and use the models to evaluate the effectiveness of different strategies to mitigate the increasing energy demand.

In literature, most of the energy demand quantifications were carried out by statistical models. However, these models cannot identify the connection between the ambient conditions and the building's thermal properties [15]. Hence, to include the effect of global warming in energy consumption models, the relationship between ambient temperature and the building's thermal properties is a vital factor [11].

The outdoor air temperature is identified as the main controlling parameter for the cooling energy demand of a building. The sensitivity of a building to the outside air temperature will have a significant impact on the energy demand patterns of the

buildings. A study conducted by [14] suggested that an increase of 1 °C in average global temperature would cause an average increase of 10% in cooling demand. However, this sensitivity of cooling energy demand of a building is affected by factors such as the buildings' architecture, orientation, construction material, and the surrounding conditions.

There are two types of main heat gains in a building zone, namely, external heat gains and internal heat gains. Out of external heat gains, solar heat gains are usually higher in most zones with building envelope elements exposed to outdoor conditions such as external walls, windows, and roofs. Unshaded windows allow heat to enter a zone in the form of conduction as well as radiation. Passive solar designs try to reduce the number of solar gains in a zone using various methods such as external shadings to walls and windows, shaded windows, adjusting building orientation, zoning of building, external reflective coatings, and window and door area optimizations. While some of these methods should be implemented in the design stage of the building (building orientation, zoning, and door window area optimization), some of the methods can be used in existing buildings to reduce the external heat gains into the building. Thermal mass optimization is one of the methods that can be used to reduce the indoor temperature peaks. Although thermal mass optimization does not directly reduce the heat gains in a building, it helps to offset the indoor temperature peaks by delaying the heat addition to the occupied zone. Thereby, it is reducing the load off the air-conditioning system. In some cases, thermal mass optimization is used together with night-time ventilation. In dry climate areas, this is usable as the thermal mass of a zone absorbs heat during day time and when exposed to cold night-time air, the thermal mass also cools down which reduces the indoor temperature peaks during day time. This method is not effective in humid countries. When the zones are exposed to humid night-time air, the added humidity increases the latent load of the zone. Also, dew formation and high humidity can be an issue in these regions for the furniture and equipment inside the zones.

The current research uses a pre-established grey box model (Hybrid data-driven and physics-based model) to predict the cooling energy demand of eight selected zones in three buildings in Colombo, Sri Lanka by the year 2090 (Serasinghe, Nissanka and Wijewardane, 2022). The grey box models were used to evaluate the amount of energy demand, which can be reduced by introducing different passive solar designs and thermal mass optimization to the selected zones.

2 Methodology

2.1 Selected Zones and Buildings

Three buildings in urban Colombo, Sri Lanka were selected for evaluation. Several zones in the buildings were selected for the data collection and analysis, based on the number of occupants, air-conditioned/non-air-conditioned space, and west and

east facing windows, etc. The zones that are non-air-conditioned were selected as much as possible so that the data collected inside the zones are solely dependent on the natural heat additions and heat rejections. Details of the selected building zones are given below.

- Western Provincial Council Building, Battaramulla, Sri Lanka,

This building is a newer building, which started construction in 2015 and was commissioned in 2016. The building is situated in Battaramula, Sri Lanka, in an area where most government office buildings are currently situated. This newly constructed building was selected for the initial study due to the fact that heat addition due to infiltration of air caused by the aging of the building is minimal. In addition, the building has minimal disturbances by greenery, and the shadowing of the building from surrounding structures. The building has been originally designed for mechanical ventilation to provide the acoustic comfort for some zones of the building and some zones are reserved as computer laboratories and the primary use of the building is as an office space. Three zones were selected in this building,

Zone 1.1—Deck on the top floor of the building with a west-facing unshaded window, no internal loads, not air-conditioned.
Zone 1.2—Office area on first floor, air-conditioned.
Zone 1.3—Cafeteria on the first floor with large floor area, not air-conditioned.

- Sumandasa building, University of Moratuwa,

This is an older building constructed more than 40 years ago, which is situated in the University of Moratuwa, Sri Lanka. The importance of this building is that this building has been designed for natural ventilation with many passive cooling techniques to reduce the heat addition into the building zones from the external environment. However, in recent years, certain parts of the building have been mechanically ventilated. Thus, this gives an example of the existing buildings, which has been affected by the climate change impacts. Three zones were selected from this building,

Zone 2.1—Machinery laboratory on the first floor: not air-conditioned, many heat dissipating machineries are used.
Zone 2.2—Classroom on the first floor: not air-conditioned, not been in use during data collection and therefore no internal loads high furniture mass factor.
Zone 2.3—Lunchroom on the top floor: not air-conditioned, small floor area.

- Building of Department of Electronic and Telecommunication Engineering, University of Moratuwa.

An older building than the Western Provincial Council building. However, it is relatively new compared to Sumanadasa building and built for mechanical ventilation. The corridors in the building connecting the air-conditioned and non-air-conditioned areas are not air conditioned. Two zones were selected from this building:

Zone 3.1—Office area on the third floor with shaded windows, not air-conditioned.
Zone 3.2—Break room on the third floor: low exposure to outdoor conditions through external walls, not air-conditioned.

The indoor temperature, relative humidity, outdoor temperature, and relative humidity were collected for each zone at 1 min time intervals and used for the development of the grey box model. Figure 1 shows the plans and elevations of the selected zones of the buildings. The external and internal heat gains and zone envelope properties are given in Table 1.

2.2 Introduction to Model Used and Cooling Load Predictions

A hybrid grey box model was used to model the indoor temperature of each zone using outdoor conditions. The model used is given in Eq. 1.

$$T_{in}(t) = x_1\left[T_{in}(t-d) + \frac{\Delta t}{C}\left[x_3 U\left[T_{in}(t-d) - T_{out}(t-d)\right] + x_4 P(t-d) + x_5 E(t-d)\right]\right] + x_2 \tag{1}$$

where,

$T_{in}(t)$ is the indoor temperature during the current time step, d is the number of delay time steps, $T_{in}(t-d)$ is the indoor temperature in d number of previous time steps, $E(t)$ is the heat addition by solar radiation at time step t, $P(t)$ is the heat addition by the equipment and occupants inside the zone calculated through an equipment and the occupant survey conducted in the zones, U is the overall heat loss coefficient for the total zone envelope, C is the total heat capacity of the zone. x_1, x_2, x_3, x_4 and x_5 are parameters included to account for the other non-modelled parameters such as the heat addition by air infiltration. These parameters were calculated by a simulated annealing algorithm using the collected data for each zone.

Heat addition by solar radiation $(E(t))$ was calculated using a HDKR (Hay Davies Klutcher Reindall) anisotropic sky diffuse model as shown in Eqs. 2 and 3.

$$I_T = (I_b + I_d)R_b + I_d(1 - A_i)\left(\frac{1+\cos(\beta)}{2}\right)X\left[1 + f sin^3\left(\frac{\beta}{2}\right)\right] + I_{gh}\rho_g\left(\frac{1-\cos(\beta)}{2}\right) \tag{2}$$

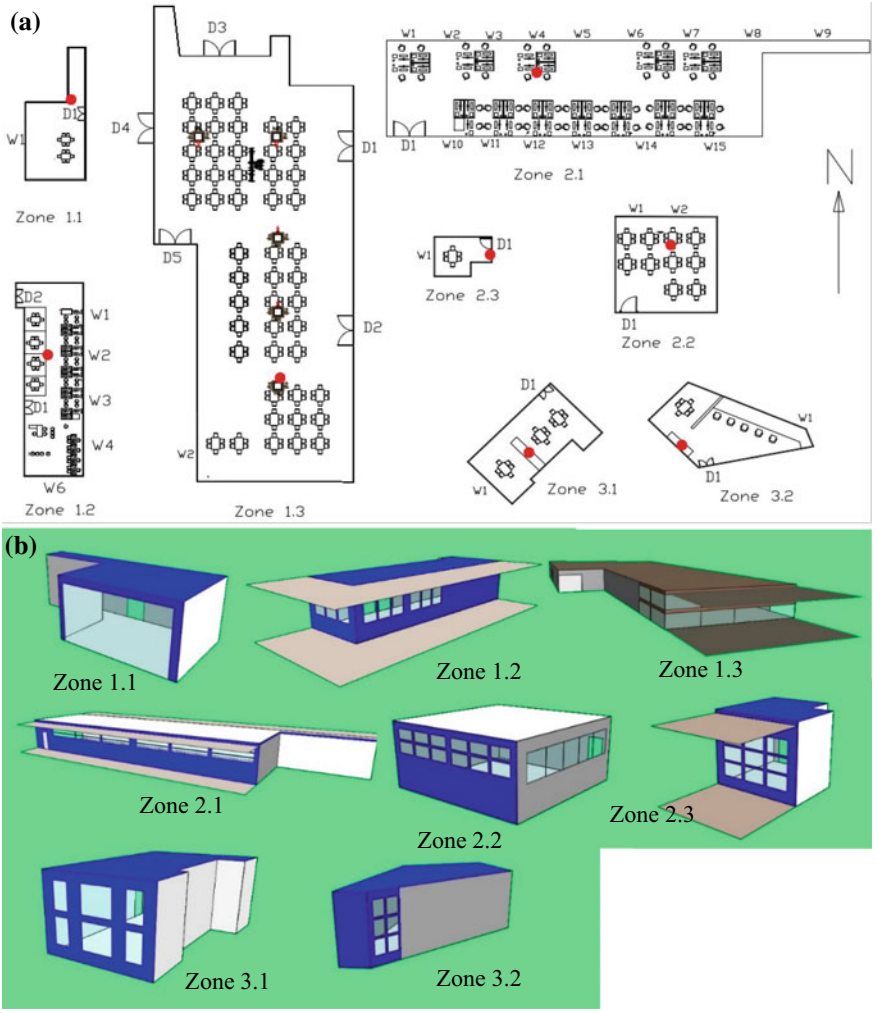

Fig. 1 Plan (**a**) and elevation (**b**) of the selected zones in three buildings

$$Q_r = I_t S_i \alpha_i \tag{3}$$

where,

I_T is the total radiation incident on the inclined plane, I_b and I_d are beam and diffuse radiation, A_i is the anisotropy index, R_b is the geometric factor, β is the angle of inclination of the plane relative to the horizontal plane, f is the cloudiness index, I_{gh} is the total radiation incident on a horizontal ground plane, ρ_g is the albedo of ground, S_i is the surface area, α_i is the index representing surface radiation absorptivity and transmittance and Q_r is the total solar radiation heat absorbed by a

Table 1 Envelope properties of the selected zones in three buildings

Property	Zones							
	1.1	1.2	1.3	2.1	2.2	2.3	3.1	3.2
Type of room	Viewing deck	Office	Cafeteria	Machinery laboratory	Lecture room	Break room	Office	Break room
Floor area (m^2)	25.49	52.39	652.62	179.47	46.23	12.14	32.57	36.36
External wall area (m^2)								
North	0	0	0	116.69	24.78	0	0	4.9 (NE)
East	0	49.38	0	0	0	0	0	0
South	0	14.45	37.62	0	0	0	15.33 (SW)	0
West	20.04	0	17.67	0	0	10.26	0	0
External window area (m^2)								
North	0	0	0	37.8	8.4	0	5.83	2.98
East	0	28.21	0	0	0	0	0	0
South	0	8.35	34.85	0	0	0	0	0
West	19.81	0	15.21	0	0	6	0	0
Internal wall area (exposed to air-conditioned space) (m^2)	0	16.46	206.18	47.18	24.64	0	32.31	0
Internal wall area (exposed to non-air-conditioned space) (m^2)	66.17	49.38	46.9	115.18	48.86	37.96	45.92	88.37
External wall area/ total wall area	0.233	0.492	0.179	0.418	0.252	0.213	0.164	0.052
External window area/total external wall area	0.99	0.573	0.905	0.324	0.339	0.585	0.380	0.608
Total door area (exposed to air-conditioned space) (m^2)	0	4.5	0	0	0	0	0	0
Total door area (exposed to non-air-conditioned space) (m^2)	4.5	18.12	4.5	1.78	3.16	1.78	4.22	2.11
West	19.81	0	15.21	0	0	6	0	0
Internal wall area (exposed to air-conditioned space) (m^2)	0	16.46	206.18	47.18	24.64	0	32.31	0

(continued)

Table 1 (continued)

Property	Zones							
	1.1	1.2	1.3	2.1	2.2	2.3	3.1	3.2
Internal wall area (exposed to non-air-conditioned space) (m^2)	66.17	49.38	46.9	115.18	48.86	37.96	45.92	88.37

Table 2 Indoor temperature and cooling load predictions by grey box model

Zone	Peak indoor temperature (°C)			Peak cooling load (kW)			Percentage increase of cooling load (%)	
	2020	2090		2020	2090			
		RCP 4.5	RCP 8.5		RCP 4.5	RCP 8.5	RCP 4.5	RCP 8.5
1.1	30.9	33.8	35.2	5.328	9.123	11.317	71.240	112.40
1.2	27.9	29.3	29.9	9.430	12.490	13.987	32.451	48.324
1.3	28.1	29.5	30.2	87.450	97.405	104.81	11.384	19.851
2.1	29.3	29.4	31.2	22.491	25.101	27.967	11.609	24.348
2.2	28.1	29.8	30.1	6.945	9.0616	10.087	30.478	45.241
2.3	30.2	31.2	32.5	1.724	2.0415	2.276	18.421	32.019
3.1	29.1	29.9	31.5	4.951	6.3601	7.797	28.461	57.483
3.2	29.4	30.8	31.5	4.881	6.5565	7.530	34.327	54.272

building envelope element. Heat addition by solar radiation *(E(t))* was calculated by adding the Q_r values for all building envelope elements in the zone.

Representative Concentration Pathway (RCP) 4.5 and RCP 8.5 emission scenarios presented by Intergovernmental Panel on climate change (IPCC) were used to calculate the indoor temperature for the eight zones by 2090. RCP 8.5 scenarios represent the global warming at an average of 8.5 W/m^2 across the planet, while RCP 4.5 scenario represents global warming at 4.5 W/m^2 due to greenhouse gas emissions. IES VE software was used with the indoor temperature values to calculate the predicted indoor cooling loads for each zone by 2090. The model calculated average peak cooling load increase by 2090 for the RCP 4.5 and 8.5 emission scenarios are given in Table 2.

2.3 Evaluation of the Passive Solar Designs and Optimized Thermal Mass

The target of passive solar designs is to modify the α_i values (Eq. 3) of different zone envelope elements using various methods. These methods include the use of reflective coatings, high radiation insulations and shading of glasses. The different emissivity

values used for different materials in the study are given in Table 3. Additionally, the use of external shadings was also considered using a shading coefficient as given in ASHRAE Fundamentals 2017 [3].

The optimization of thermal mass has two direct effects on the thermal load of a zone.

- Increase of thermal mass reduces the indoor temperature peaks. However, it increases the time the peak indoor temperature is retained.
- The time lag between the indoor and temperature increases with increasing thermal mass.

This effect can be observed in the collected data in the selected zones. Zones with high heat capacity values (Effective heat capacity) showed relatively lesser peaks and more lag between indoor and outdoor temperatures. The effect of thermal mass was evaluated by changing the C values of Eq. 1 through 1% increases and calculating the resulting change in the peak indoor temperature. The zones were simulated with an added thermal mass of -20%, -10%, +10%, and +20% for the change in peak indoor temperature and peak cooling loads. For a more elaborated result, two simulation scenarios were considered,

- Without night-time ventilation.
- Opening the windows at night (7.00 p.m. to 7.00 a.m.). MacroFlo module of IES VE was used to simulate the ventilation of the zones.

Table 3 Emissivity values for different solar designs for external surfaces of the buildings used

Design	Emissivity	Design	Emissivity	Design	Emissivity
Aluminium foil	0.04	Concrete	0.85	Lime wash	0.91
Aluminium commercial sheet	0.09	Concrete, rough	0.94	Marble White	0.95
Aluminium highly polished	0.039–0.057	Concrete tiles	0.63	Masonry plastered	0.93
Aluminium paint	0.27–0.67	Glass smooth	0.92–0.94	Mild steel	0.20–0.32
Asbestos board	0.96	Glass, Pyrex	0.85–0.95	Oil paints, all colours	0.92–0.96
Black lacquer on iron	0.875	Granite, natural surface	0.96	Plaster	0.98
Black enamel paint	0.8	Gypsum	0.85	Plaster, rough	0.91
Brick, red rough	0.93	Iron polished	0.14–0.38	Roofing paper	0.91
Cement	0.54	Iron, dark grey surface	0.31	Tile	0.97
Clay	0.91	Limestone	0.90–0.93	Wood, pine	0.95

3 Results and Discussion

3.1 Passive Solar Design

Identified methods of passive solar designs were used in Eq. 1 for all zones with RCP 4.5 and 8.5 emission scenarios. Figure 2 shows the average predicted indoor temperature variations for a sample zone (zone 2.3) under the RCP 4.5 emission scenario for 2090 with different passive cooling strategies. These figures for all zones were used to identify the suitable passive solar design elements for each zone. The selected combinations of the solar design elements for each zone are given in Table 4. The building position and geometry also limit the use of some strategies such as external shadings in some zones while in some zones, external shadings are already existing with the shade from adjacent buildings and trees. Therefore, the ability to reduce the external heat gains has been decreased due to these physical constraints. Figure 3 illustrates the unmodified cooling load increase of each zone in comparison to the predicted cooling load decrease possible by passive solar design strategies for both emission scenarios.

All zones showed benefit from the proposed passive solar designs to mitigate the predicted cooling load increase. Zone 1.1 showed the highest percentage of decrease in cooling load, with the zone managing to reduce nearly 60% of the cooling load increase through passive solar designs. Zones in building 2 did not show a significant demand increase mitigation by passive solar designs as the building already holds many passive cooling strategies such as external shadings and the building is well shaded from all sides by trees. Zone 1.3 has a very small area exposed to outdoor

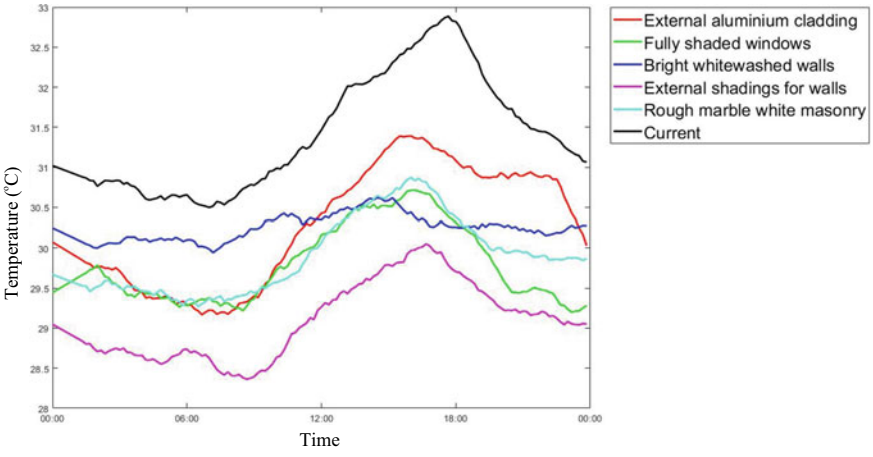

Fig. 2 Predicted indoor temperature variation under RCP 4.5 emission scenario for 2090 under different passive solar designs (zone 2.3) for an average day

Table 4 Passive solar design strategies used in different zones and the percentage decrease in cooling load in RCP 8.5 emission scenario

Zone	Used strategies	Cooling load (with solar designs for 2090) (kW)	Percentage decrease in cooling load (%)
Zone 1.1	Fully shaded glass	3.124	61.24
Zone 1.2	Fully shaded glass with aluminium cladding for walls	8.849	20.11
Zone 1.3	Fully shaded glass	84.211	3.14
Zone 2.1	Fully shaded glass with white enamel paint for external walls	20.98	4.24
Zone 2.2	Fully shaded glass with white enamel paint for external walls	5.247	2.673
Zone 2.3	Fully shaded glass, white enamel paint for external walls, roofing, or shadings for external walls/windows	0.987	6.899
Zone 3.1	Roofing or shadings for external walls/ windows	3.984	22.033
Zone 3.2	White enamel paint for external wall	4.105	11.042

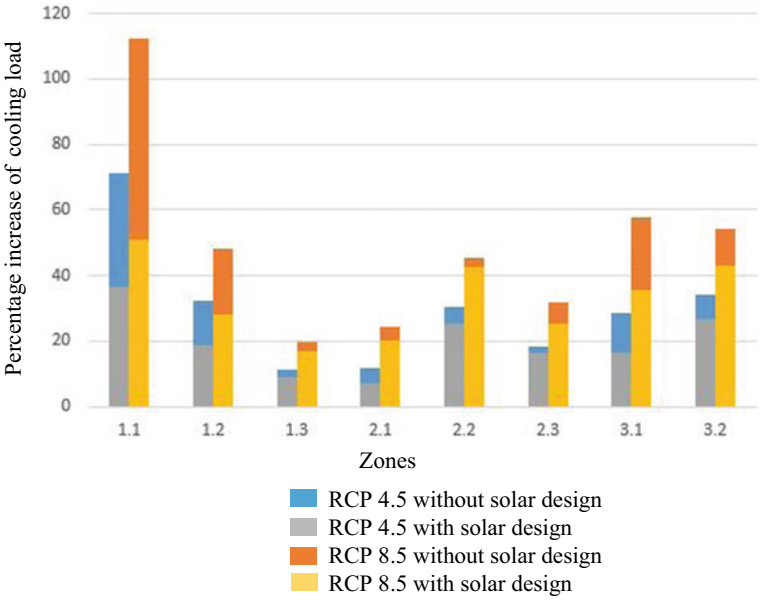

Fig. 3 Predicted cooling load increase (by 2090) with and without the suggested passive solar designs for each zone

conditions and therefore the demand mitigation through passive solar designs is minimal.

3.2 Thermal Mass Optimization

The trained grey box models were used to evaluate the variation of the indoor temperatures for the selected zones changing the thermal mass of the zones. The thermal capacity (C) values were changed for each zone to calculate the indoor temperatures. Figure 4 shows the predicted indoor temperature variation with increasing and decreasing thermal capacities by 1% increase. Zone 1.3 showed high sensitivity for indoor temperature to change in thermal mass inside the zone as it is relatively an open area while zone 2.1 showed the lowest sensitivity for indoor temperature to thermal mass inside the zone. Zone 2.1 already has a high thermal mass with many equipment, which are able to store the thermal energy.

The zones were simulated for two simulation instances (with and without night-time ventilation) for both emission scenarios for 2090 using IES VE. MacroFlo module of IES VE was used to simulate the windows of the zones. The calculated cooling loads for RCP 4.5 emission scenario for 2090 are given in Table 5. Although the peak indoor temperatures showed a reduction in both scenarios, the peak cooling load has little to no difference in the instance where night-time ventilation was not available. With night-time ventilation, the zones showed to have significant cooling load reductions.

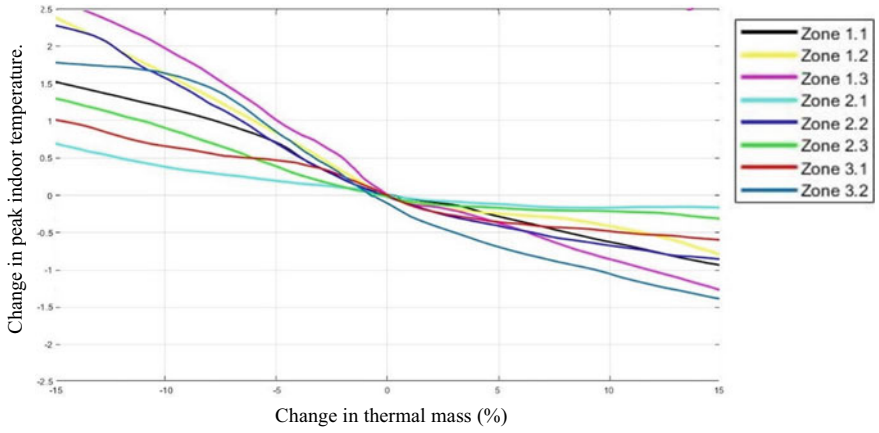

Fig. 4 Change in peak indoor temperature of each zone with the change in thermal mass

Table 5 Peak cooling loads of the zones with and without night-time ventilation for RCP 4.5 emission scenario (10% increase in thermal mass)

Zone	Without nigh time ventilation		With night-time ventilation	
	Peak indoor temperature (°C)	Peak cooling load (kW)	Peak indoor temperature	Peak cooling load (°C)
Zone 1.1	30.9	5.33	30.4	4.82
Zone 1.2	27.9	9.43	28.1	9.02
Zone 1.3	28.1	87.45	28.0	84.26
Zone 2.1	29.3	22.49	29.1	18.54
Zone 2.2	28.1	6.95	28.1	6.12
Zone 2.3	30.2	1.72	30.1	1.71
Zone 3.1	29.1	4.95	29.2	3.95
Zone 3.2	29.4	4.88	29.3	4.87

4 Conclusion

Several selected buildings in Colombo, Sri Lanka were evaluated using a pre-established grey box model by calculating the energy demand patterns. The model was also used to evaluate the effectiveness of using some passive solar designs and optimized thermal mass to reduce the predicted energy demand increase for cooling. The eight selected zones of three buildings have shown significant increase in cooling load by 2090 under RCP 4.5 and 8.5 emission scenarios. All zones have shown around 50% cooling load increase by RCP 8.5 scenario with zone 1.1 showing an increase of cooling load by a significant percentage of 112%. Furthermore, the study evaluated the use of passive solar designs to reduce this energy demand increase. Although there are some practical limitations such as lack of space in some zones in using passive solar designs, some combinations of solar designs were calculated to be effective in mitigating the predicted cooling demand increase. The 112% predicted increase of cooling load was calculated to be reduced to around 60% by using optimized solar designs. This combined with night-time ventilation and optimized thermal mass can give an additional 10%–20% reduction on cooling load. Both buildings 1 and 3 showed high capacity in mitigating demand increase through passive solar designs while building 2, with already existing passive cooling methods, have a relatively low cooling demand mitigation through new solar design strategies. The findings from this study indicate that passive solar design and optimized thermal mass are promising methods to mitigate the increasing building cooling energy demand due to climate change impacts.

Acknowledgements Authors would like to extend their gratitude to Mr. Sameera Jayarathne and Mr. L. D. Jaysuriya of Central Environment Authority (CEA), Sri Lanka for providing outdoor temperature data. Also, authors would like to acknowledge Ms. Thuthiprabha, Mr. Thalangama, and Mr. Parakrama from Western Provincial Council (WPC), Sri Lanka for granting permission to collect data in their building premises.

Funding This project was funded by Senate Research Committee (SRC) grant of University of Moratuwa, Sri Lanka (Grant number: SRC/LT/2020/09).

References

1. ANSI/ASHRAE (2017) 'ANSI/ASHRAE Standard 55–2017: Thermal Environmental Conditions for Human Occupancy', *ASHRAE Inc.*, 2017, p. 66. ISSN 1041–2336
2. Dickinson, R. and Brannon, B. (2016) 'Generating future weather files for resilience', 36 th International Conference on Passive and Low Energy Architecture. Cities, Buildings, People: Towards Regenerative Environments
3. Fernando, W., Gupta, N. and Ozveren, C. S. (2017) 'The electricity infrastructure in Sri Lanka then, now and hereafter', 2017 52nd International Universities Power Engineering Conference, UPEC 2017, 2017-Janua(April), pp. 1–6. https://doi.org/10.1109/UPEC.2017.8231986
4. Geekiyanage D, Ramachandra T (2018) A model for estimating cooling energy demand at early design stage of condominiums. Journal of Building Engineering 17(February):43–51. https://doi.org/10.1016/j.jobe.2018.01.011
5. Hamdi R et al (2014) Assessment of three dynamical urban climate downscaling methods: Brussels's future urban heat island under an A1B emission scenario', International Journal of Climatology, 34. doi: https://doi.org/10.1002/joc.3734
6. Krinner, G. *et al.* (2013) 'Long-term climate change: Projections, commitments and irreversibility', *Climate Change 2013 the Physical Science Basis: Working Group I Contribution to the Fifth Assessment Report of the Intergovernmental Panel on Climate Change*, 9781107057, pp. 1029–1136. doi: https://doi.org/10.1017/CBO9781107415324.024.
7. Li D, Yang L, Lok C (2012) Impact of climate change on energy use in the built environment in different climate zones – A review. Energy 42:103–112. https://doi.org/10.1016/j.energy.2012.03.044
8. Lundgren K, Kjellstrom T (2013) Sustainability challenges from climate change and air conditioning use in urban areas. Sustainability 5(7):3116–3128
9. Moss R et al (2008) Towards new scenarios for analysis of emissions, climate change, impacts, and response strategies : IPCC Expert Meeting report : 19–21 September, 2007, Noordwijkerhout, the Netherlands. Intergovernmental Panel on Climate Change, Geneva
10. Ortiz, L., González, J.E. and Lin, W. (2018) 'Climate change impacts on peak building cooling energy demand in a coastal megacity'.
11. Rogner, H. *et al.* (2007) 'Mitigation. Contribution of Working Group III to the Fourth Assessment Report of the Intergovernmental Panel on Climate Change', *Introduction. In Climate Change 2007*.
12. Serasinghe, S. V. I. R. V, Nissanka, I. D. and Wijewardane, M. A. (2022) 'Establishing the relationship between indoor and outdoor temperature of an existing office building using hybrid physics based and data driven models', in *2022 Moratuwa Engineering Research Conference (MERCon)*, pp. 1–6. doi: https://doi.org/10.1109/MERCon55799.2022.9906233.
13. Tewari M et al (2017) Impacts of projected urban expansion and global warming on cooling energy demand over a semiarid region. Atmospheric Science Letters 18(11):419–426. https://doi.org/10.1002/asl.784
14. Watkins R, Levermore GJ (2011) Quantifying the effects of climate change and risk level on peak load design in buildings. Build Serv Eng Res Technol 32(1):9–19. https://doi.org/10.1177/0143624409357122
15. Wonorahardjo S et al (2020) Characterising thermal behaviour of buildings and its effect on urban heat island in tropical areas. Int J Energy Environ Eng 11(1):129–142. https://doi.org/10.1007/s40095-019-00317-0

Innovations in Building Materials

Shrink Index-Based Timber Classification and Finger Joint Production

C. K. Muthumala, K. K. I. U. Arunakumara, Sudhira De Silva, P. L. A. G. Alwis, and S. M. J. P. Dayawansha

Abstract Inadequate length of sawn timber material is also reported to be a limiting factor for fully utilization of timbers. Finger joint, a method that connects two small pieces of timber together is identified as a sound technique to minimize the wastage. At the finger joint production process, different timber species have to be bonded together for making finger-jointed mixed boards. When mixing different timber species together, they should be similarly matching timber pieces based on the dimensional effects. The present study focuses on developing a classification system for 32 selected clear timber species, based on their shrinkage effect in three different environmental conditions, to assist the finger joint technique. Three climatic factors were identified through an analysis to determine the shrink index for the selected timber species. The shrink index values were grouped into five classes, as very low, low, medium, high and very high. Cluster analysis was used for grouping the species with similar shrinkage properties. Pearson correlation of Shrink Index and Density was -0.134. So, there is no significant relationship between the shrink index and density ($P > 0.05$).

Keywords Finger joint · Timber classification · Shrinkage · Shrink index · Wood

C. K. Muthumala (✉)
Research, Development and Training Division, State Timber Corporation, Sri Jayawardenepura Kotte, Sri Lanka
e-mail: ck_muthumala@yahoo.com

K. K. I. U. Arunakumara
Department of Crop Science, Faculty of Agriculture, University of Ruhuna, Mapalana, Kamburupitiya, Sri Lanka

S. De Silva
Department of Civil and Environmental Engineering, Faculty of Engineering, University of Ruhuna, Hapugala, Galle, Sri Lanka

P. L. A. G. Alwis · S. M. J. P. Dayawansha
Department of Agric. Engineering, Faculty of Agriculture, University of Ruhuna, Mapalana, Kamburupitiya, Sri Lanka

© The Author(s), under exclusive license to Springer Nature Singapore Pte Ltd. 2023

R. Dissanayake et al. (eds.), *ICSBE 2022*, Lecture Notes in Civil Engineering 362,
https://doi.org/10.1007/978-981-99-3471-3_23

1 Introduction

Timber is in high demand in the furniture and construction industry. Timber is one of the oldest building materials in Sri Lanka. It is widely used in the furniture manufacturing industry. When using timber in construction and furniture manufacturing industry, waste timber material and short length sections of timber, which are dumped by sawmills, are considered to be a matter of concern [1]. Waste sawn timber materials of Furniture factories and short length of sawn wood are common problems in the timber industry in Sri Lanka. Shorter sections of timber, which are dumped by sawmills, are considerable factors because of the scarcity of timber. However, some of this waste wood is used to fuel kiln-dried boiler [2]. Joining timber is another option for utilizing waste timber.

Finger joints are described as interlocking end joints formed by machining a number of similar tapered symmetrical fingers in the ends of timber members using a finger joint cutter and then, bonded together [3]. Finger joint is a sustainable, eco-friendly and economically valuable concept for the furniture industry. It ensures the sustainable utilization of small wood-cut pieces that are removed as waste [4]. The finger joint timber manufacturing is a viable solution for minimizing the waste generation in furniture manufacturing and construction activities. Further, it is a new concept for the Sri Lankan furniture industry [5].

Timber properties vary in different timber species. Every matured timber species has a unique density range. Shrinkage also varies with timber species. Therefore, some failures can occur due to different timber species when they are mixed to produce finger joint production. Quantitative characteristics of wood and their behavior to external influences, other than applied forces, depend on mechanical properties. These properties are important because they can significantly influence the performance and strength of wood used in structural applications [6]. The strength of a timber depends on its species and the effects of certain growth characteristics [7].

Timber species grouping based on wood properties is a common practice in many countries and is essential as well [8, 9]. There is no existing user-based timber classification system in Sri Lanka, incorporated with their strength properties and shrinkage effects. The present Sri Lankan timber classification system has been prepared according to the availability, demand and supply, and considering the plantation species. The strength properties of timber species and shrinkage behavior are not considered. When finger joint producers are producing finger joint boards, they must mix different timber species together. So, it is very important to prepare a user-based timber classification system, based on the strength index. This should consider the workability characteristics too.

The dimensional changes that accompany the shrinking and swelling of wood are major sources of both visual and structural problems in furniture. Shrinking and swelling occur as the wood changes its' moisture content in response to daily, as well as seasonal changes in the relative humidity of the atmosphere. Wood that is kiln dried to 6% moisture content and stored in a dry shed outdoors in a temperate

climate, such as that found in Indiana, will regain moisture until it eventually reaches about 12% moisture content. Under the same conditions in a tropical climate, the wood will come to a moisture content of about 16% [10]. Strength-based timber classification system was introduced by several researchers in 2019, to assist finger joint timber manufacturing industry [11].

Variations in wood density and mechanical properties have also been reported by several researchers [12, 13]. Selected timber species were classified into separate groups according to their strength values using dendrograms. Density is the single most important indicator of strength in wood and may, therefore, predict such characteristics as hardness, ease of machining and nailing resistance [14]. Wood has a relatively high strength in relation to its density when compared with other materials used in construction. The strength properties of wood depend upon its density and structure, which assist us in selecting a suitable type of wood for a particular use [15].

Main objectives of this study are to develop a user-based timber classification system by considering the shrinkage behavior for 32 timber species in Sri Lanka and to find out the relationship between the shrink index and density of selected timber species, mostly used in Sri Lanka.

2 Methodology

2.1 Timber Sample Selection

Locally available 32 timber species were selected for the study. These timber species are commonly used for structural and non-structural purposes in Sri Lanka. These timber species represent all classes; Super luxury, Luxury, Special upper, Special, Class I, Class II, Class III and below Class III in the timber classification chart of the State Timber Corporation [16].

2.2 Timber Sample Preparation

Selected timber species that are 30–40 years of age were collected from Kumbukkana and Boossa timber depots of the State Timber Corporation.

Ten specimens were prepared from timber pieces, which were taken from the heartwood of the Breast height portion with five replicates for each test. Specimens that are free from timber defects were selected. Timber samples were seasoned to reduce moisture content up to 12%. For measuring moisture content, a moisture meter was used. Specimens were prepared based on BS:373–1957.

Timber samples were prepared from each timber species according to BS standards [17]. This study was conducted in a wood laboratory at the State Timber

Corporation in Rajamalwatta road, Battaramulla, Sri Lanka and the Faculty of Material Science and Engineering, University of Moratuwa. Both laboratories consist of the facilities to measure the wood properties.

2.3 Calculation of the Shrinkage Percentage

Specimens were prepared at the State Timber Corporation timber complex in Kaldemulla. Before the experiment, the surface of each timber sample was wiped to remove sawdust or any dirty materials. Radial, tangential and longitudinal plans were marked in every sample. Every sample was approximately of the same age, maturity and samples were selected from the center part of the hardwood.

Three environmental conditions were selected to conduct the test. Critical environmental conditions were selected according to the data from the department of meteorology. Temperature and relative humidity of critical environmental conditions were,

- 35 °C & 70–80%
- 27 °C & 80–90%
- 16 °C & 90–100%

Volumetric shrinkage means how much a wood species will shrink, but it doesn't indicate the direction of the shrinkage. The two primary planes or surfaces of wood where the shrinkage takes place are across the radial plane and across the tangential plane, corresponding to radial shrinkage and tangential shrinkage. Combining these results should roughly add up to the volumetric shrinkage. Samples were kept under each environmental condition for 48 h. The dimensional data were collected before and after. Volumetric shrinkage data calculation was done according to the below equation.

$$\text{volumetricShrinkage} = \frac{(l_{tmax} \times l_{rmax} \times l_{amax}) - (l_{tmin} \times l_{rmin} \times l_{amin})}{(l_{tmax} \times l_{rmax} \times l_{amax})} \times 100 \quad (1)$$

$l_{t\,max}$—Maximum length of tangential plane
$l_{r\,max}$—Maximum length of radial plane
$l_{a\,max}$—Maximum length of longitudinal plane
$l_{t\,min}$—Minimum length of tangential plane
$l_{r\,min}$—Minimum length of radial plane
$l_{a\,min}$—Minimum length of longitudinal plane.

2.3.1 Weighting Scale

Digital balance with the accuracy of 0.01 g was used to measure the weight of the samples.

2.3.2 Vernier Caliper

Vernier caliper was used to measure dimensional values. The minimum measurement was 0.05 mm of the Vernier caliper, and the accuracy was zero before taking measurements.

2.4 Calculation of the Dry Density

Dry weight of the timber samples was taken by placing in 100–105^{0}C oven for 48 h. Density values were determined at 12% moisture content.

$$\text{Density} = \frac{\text{Weight of oven dry wood (kg)}}{\text{Volume of wood (m}^3\text{)}} \tag{2}$$

3 Results and Discussion

The factor analysis extracts maximum common variance from all variables and puts them into a common score. Principal component analysis is used to decide the number of factors from the highest Eigen values. Factor 1 and factor 2 were selected (Fig. 2).

Factor 1, factor 2 and variance values of Table 4 were used to calculate the strength index.

Fig. 1 Finger joint board prepared by using different timber species

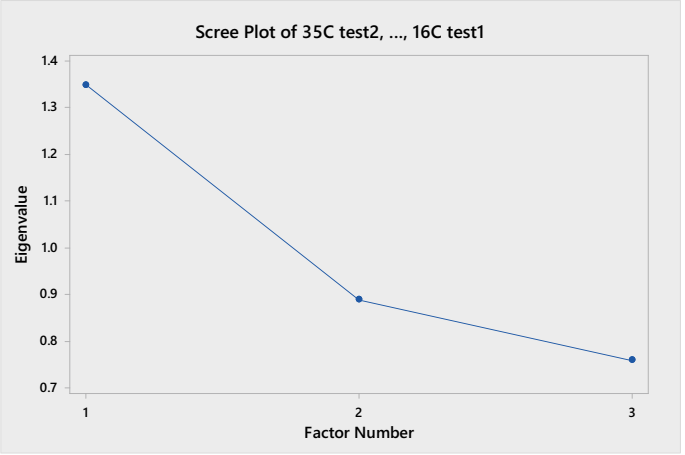

Fig. 2 Principal Component Factor Analysis—Varimax Rotation

3.1 Calculation of Shrinkage Index

Factor score was calculated by using factor loading coefficients. After that, the variance contribution rate of each factor was divided by the cumulative variance rate of all the selected factors, to determine the weights of each factor. Factor weight of each factor was multiplied by their factor scores and then added together to develop a strength index.

Shrinkage Index = Index 1 and Index 2.

where,

$$\text{Index 1} - (\text{cum. value of average shrinkage values of 3 tests} \times \text{factor coefficient}) \times \text{variance of factor 1(0.333) /Number of variables} \tag{3}$$

$$\text{Index 2} - (\text{cum. value of average shrinkage values of 3 tests} \times \text{factor coefficient}) \times \text{variance of factor 2(0.333) /Number of variables} \tag{4}$$

3.2 Classification of Timber According to Shrink Index

Figure 3 represents the dendrogram created using shrink index values of 32 timber species.

Table 1 Information of 32 selected timber species for the preparation of timber classification system, based on the shrinkage effect

No	Common name	Botanical name	Family	Origin	Floristic region
1	Albizia	Albizi a falcatari a	Fabaceae	Exotic	UC
2	Caribbean Pine	Pinus caribaea	Pinaceae	Exotic	UC/LCWZ
3	Cypress	Cypressus macrocarpa	Cupressaceae	Exotic	UC
4	Ebony	Diospyros ebenum	Ebenaceae	Indigenous	DZ/IN
5	Ehela	Cassia fistula	Leguminosae	Indigenous	DZ
6	Ginisapu	Michelia champaca	Magnoliaceae	Exotic	WL
7	Grandis(red)	Eucalyptus grandis	Myrtaceae	Exotic	UC
8	Halmilla	Berrya cordifolia	Malvaceae	Indigenous	LCDZ
9	Havarinuga	Alstonia macrophylla	Apocynaceae	Exotic	LCWZ
10	Hora	Dipterocarpus zeylanicus	Dipterocarp ac e ae	Indigenous	LCWZ
11	Jack	Artocarpus heterophyllus	Moraceae	Exotic	LCWZ
12	Khaya	Khaya senegalensis	Meliaceae	Exotic	DZ/IN
13	Kolon	Adina cordifolia	Rubiaceae	Indigenous	LCDZ
14	Kumbuk	Terminalia arjuna	Combretaceae	Indigenous	LCDZ
15	Lunumidella	Melia dubia	Meliaceae	Exotic	LCIN
16	Madan	Syzygium cumini	Myrtaceae	Indigenous	DZ
17	Mahogany	Swietenia macrophylla	Meliaceae	Exotic	IN
18	Margosa	Azadirachta indica	Meliaceae	Exotic	LCWZ
19	Mango	Mangifera indica	Anacardiaceae	Exotic	WZ/DZ
20	Mee	Madhuca longifolia	Sapotaceae	Indigenous	DZ/WZ
21	Milla	Vitex pinnata	Lamiaceae	Indigenous	IN
22	Na	Mesua ferrea	Calophyllaceae	Indigenous	LCWZ

(continued)

Table 1 (continued)

No	Common name	Botanical name	Family	Origin	Floristic region
23	Nedun	Pericopsis mooniana	Leguminosae	Indigenous	LCWZ
24	Palu	Manilkara hexandra	Sapotaceae	Indigenous	DZ
25	Paramara	Albizia saman	Leguminosae	Exotic	DZ/WZ
26	Robusta	Eucalyptus robusta	Myrtaceae	Exotic	UC
27	Rubber	Hevea brasiliensis	Euphorbiaceae	Exotic	LCWZ
28	Satin	Chloroxylon swietenia	Rutaceae	Exotic	LCDZ
29	Suriyamara	Albizia odoratissima	Leguminosae	Indigenous	DZ
30	Teak	Tectona grandis	Lamiaceae	Exotic	LCDZ
31	Tallow wood	Eucalyptus microcorys	Myrtaceae	Exotic	UC
32	Welan	Pterospermum suberifolium	Malvaceae	Indigenous	LCDZ

LCWZ-Low Country Wet Zone
UC-Up country
LCDZ-Low country Dry Zone
IN-Intermediate Zone
LCIZ-Low country Intermediate Zone
WZL-Wet Zone Lowland
DZ-Dry Zone

Table 2 Standard sizes for samples

Sample test	Standard size
Shrinkage test	2.5 × 2.5 × 10 cm
Density test	2.5 × 2.5 × 3 cm

According to the dendrogram in Fig. 3, five timber groups were prepared based on the dimensional changes of wood (see Table 5).

Previous research studies have analyzed the correlations between wood density and wood shrinkage in some wood species (see Fig. 4). Some research findings show that volumetric, tangential and radial shrinkage increased as wood density increased. Hendrigo et al. [19] showed that linear correlation between oven dry density and volumetric shrinkage was coefficient in the three species: *Cedrella sp.*, *Cassia ferruginea* and *Vataireopsis araroba* [18]. But some results indicate that there was a weak positive correlation between longitudinal shrinkage and wood density and that longitudinal shrinkage in some species tends to decrease as wood density

Table 3 Variation of shrinkage (%) of 32 timber species in three environmental conditions

No	Common name	Dendrogram No	Shrinkage (35 ^{0}C) %	Shrinkage (27 ^{0}C) %	Shrinkage (16 ^{0}C) %
1	Albizia	28	1.5122	0.3340	1.2443
2	Caribbean Pine	20	3.0621	0.7705	0.3322
3	Cypress	26	2.2511	-0.2643	0.4791
4	Ebony	30	2.1047	0.7865	0.9106
5	Ehela	1	1.8512	0.3685	0.5310
6	Ginisapu	3	3.5067	0.4566	0.4014
7	Grandis(red)	4	2.8586	1.5233	1.6915
8	Halmilla	5	1.0910	0.6208	0.4763
9	Havarinuga	6	3.5924	0.4298	1.2319
10	Hora	7	2.9596	0.2832	0.4121
11	Jack	8	2.8369	1.7288	0.3404
12	Khaya	29	2.4505	0.7010	0.4603
13	Kolon	9	2.4706	1.5780	0.4790
14	Kumbuk	10	1.9871	0.3602	0.3479
15	Lunumidella	11	2.4201	1.1770	0.4151
16	Madan	12	1.1886	1.2728	0.3424
17	Mahogany	13	1.3577	0.7614	0.9029
18	Margosa	14	2.1349	4.9679	0.9002
19	Mango	27	4.4166	0.1784	0.7504
20	Mee	15	3.0095	0.6806	0.8147
21	Milla	16	1.3423	0.1288	0.1644
22	Na	17	2.4098	-0.9707	0.6438
23	Nedun	32	1.8703	-0.8473	1.0745
24	Palu	18	2.1778	0.3453	0.4111
25	Paramara	19	0.3323	0.5681	0.6121
26	Robusta	31	2.7212	0.7212	0.1279
27	Rubber	21	2.6770	0.8653	1.4036
28	Satin	22	1.8187	0.0955	2.8885
29	Suriyamara	23	1.4561	0.2798	0.7630
30	Teak	24	1.7672	0.5297	0.2620
31	Tallow wood	2	3.0746	0.5749	0.9497
32	Welan	25	1.5833	0.8101	1.1298

Table 4 Rotated Factor Loadings and Communalities (Varimax Rotation)

Variable	Factor 1	Factor 2	Factor 3 communality	
Shrinkage 35 ^{0}C	−0.067	−0.139	0.988	1
Shrinkage 16 ^{0}C	0.012	0.99	−0.138	1
Shrinkage 27 ^{0}C	0.998	0.012	−0.065	1
Variance	1.0003	1.0002	0.9995	3
% Var	0.333	0.333	0.333	1

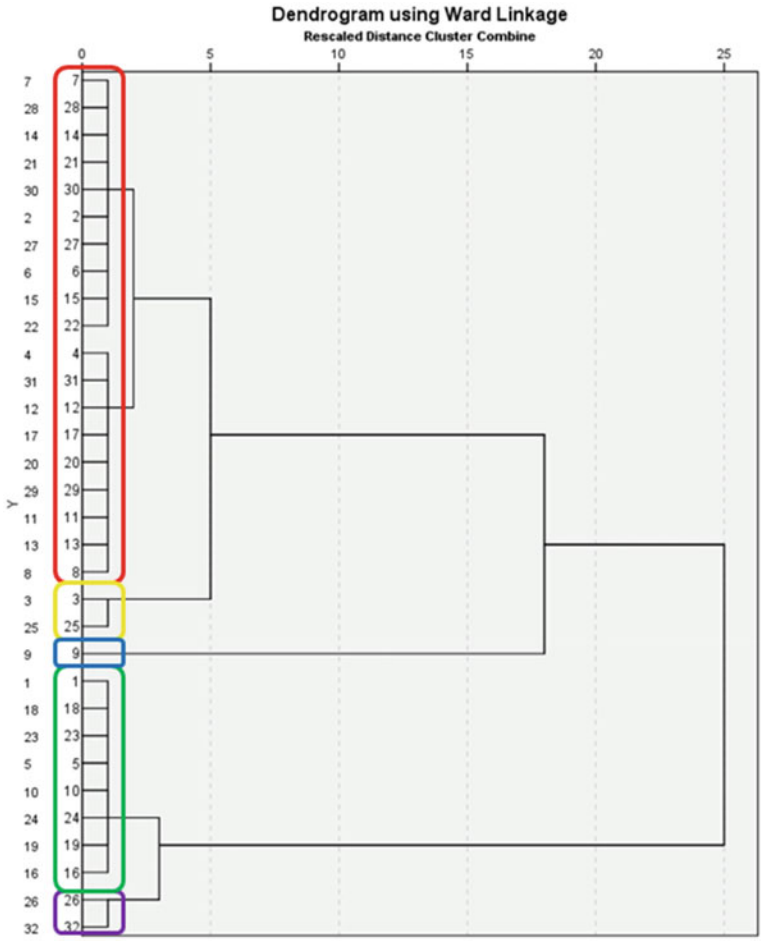

Fig. 3 Dendrogram of shrink index

Table 5 Timber classification according to shrink index

Groups	Index value		Timber Species
Group 1	<0.363	Very low	Cypress, Nedun
Group 2	0.364-0.0365	Low	Ehela, Halmilla, Kumbuk, Milla, Palu, Paramara, Suriyamara, Teak
Group 3	0.366-0.369	Medium	Eucalyptus, Havarinuga, Hora, Margosa, Mi, Pinus, Rubber, Satin, Amba, Albizia, Kaya, Ebony, Grandis, Jack, Lunumidella, Madan, Mahogany, Robusta, Na
Group 4	0.370–0.375	High	Ginisapu, Welan
Group 5	> 0.376	Very high	Kolon

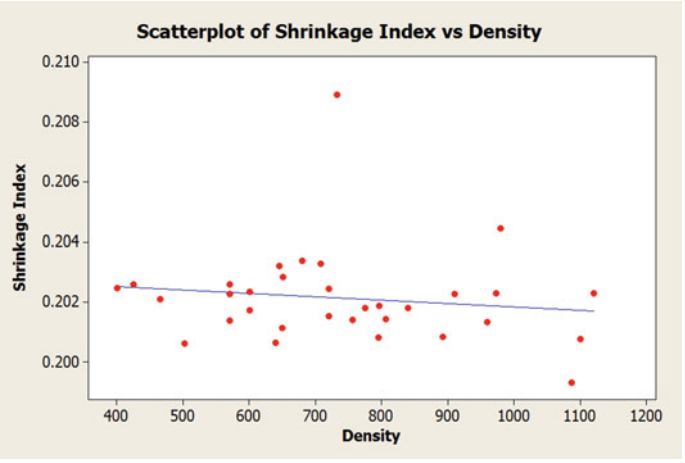

Fig. 4 Relationship between Shrink index and Density

increases [19]. Similarly, previous Sri Lankan research revealed that the mechanical properties showed positive relationship with the wood density [20]. According to Pearson correlation of Shrink Index and Density, there is no significant relationship between the shrink index and density ($P > 0.05$).

4 Conclusion

Based on the results obtained from the study conducted, the following conclusions can be drawn.

Shrink properties varied with different environmental conditions. According to three temperature level and three relative humidity level environmental conditions,

Five swell groups were created (very high, high, medium, low and very low, respectively). These groups were assisted to select timber species according to the shrink and swell properties for finger-jointed furniture manufacturing industries under different environmental conditions.

According to shrinkage-based timber class categories, they can be used for the selection of timber species in finger joint furniture manufacturing industry. When mixing different timber species to make finger joint boards, four timber groups that have been prepared according to the shrink index can be used to select the best match timber pieces. These research findings will help to reduce defects occurring in the manufacturing process.

References

1. Muthumala, C.K, De Siva Sudhira, Arunakumara KKI.U. and Alwis PLAG. (2020). Identification of joint efficiencies in 13 mm finger jointed timber species used in Sri Lanka. ICSBE 2018. LNCE 44 Springer.p.261–267 in Singapore
2. Muthumala, C.K., De Silva Sudhira, Alwis, P.L.A.G. and Arunakumara, K.K.I.U.(2018). Investigate the most suitable glue type for finger-joints production in Sri Lanka.*Research Journal of Agriculture and Forestry Sciences.*Vol. 6(11), 6–9, November (2018) ISCA. India. pp 6–9
3. British Standard Institution.(2014). BS EN 15497:2014, Structural finger jointed solid timber-Performance requirements and minimum production requirements, European Committee for Standardization. B 1000 Brussels.
4. Sandika AL, Pathirana GDPS, Muthumala CK (2017) Finger joint timber products for effective utilization of natural resources: An analysis of physical properties. International Symposium on Agriculture and Environment, University of Ruhuna, Sri Lanka, Economic factors and Consumers' perception, pp 109–111
5. Abeysinghe, L. S., Pathirana,S and Muthumala, C. K. (2016),Economic factors and physical properties of finger joint timber product to pomote effective utilization of natural resources, Proceeding of the International Forestry and Environment symposium, USJP, Sri Lanka. 60
6. Winandy JE (1994) Effects of long-term elevated temperature on CCA-treated Southern Pine lumber. For Prod J 44(6):49–55
7. Yeomans, D. (2003). Strength Grading Historic Timbers. Cathedral Communications Limited 2010 Retrieved from http://www.buildingconservation.com/articles/grading timbers /grading timbers.ht
8. Da´valos R, Ba´rcenas G (1999) Clasificacio´n de las propiedades meca´nicas de las maderas mexicanas encondicio´n '"seca."' Madera y Bosques 5:61–69
9. Ali AC, Uetimane E Jr, Lhate IA, Terziev N (2008) Anatomical characteristics, properties and use of traditionally used and lesser-known wood species from Mozambique: a literature review. Wood Sci Technol 42:453–472
10. Eckelman,C.A, (n.d). The Shrinking and Swelling of Wood and Its Effect on Furniture, Forest and natural resources, FNR 163, Purdue University, Corporative extension service, West Lafayette, IN 479071
11. Muthumala, C.K., De Silva Sudhira, Alwis, P.L.A.G. and Arunakumara, K.K.I.U.(2019). Classification of Finger Joint Timber Based on Strength Index. Vidyodaya Journal of Science, University of Sri Jayewardenepura, Vol. 22 No. 02 (2019) 32–42
12. Zhang SY (1995) Effect of growth rate on wood specific gravity and selected mechanical properties in individual species from distinct wood categories. Wood Sci Technol 29(6):451–465

13. Zobel BJ, van Buijtenen JP (1989) Wood Variation. Springer-Verlag, Berlin, Its Causes and Control
14. Hoadley RB (2000) Understanding Wood : A craftsman's guide to wood technology. The Taunton Press, Newtown, USA
15. Reinprecht L (2016) Wood Deterioration. Wiley Blackwell Publishing house, West Sussex, United Kingdom, Protection and Maintenance
16. STC, 2020. Timber classification, www.timco.lk. Accessed in 02nd April 2020
17. Institution BS, (1999).BS 373, (1957) Methods of testing small clear specimens of timber. British Standards Institution, London
18. Hendrigo, T., Almeida, Henrique, D.A., Leonardo, I, Marcolin,A., Gonçalves,D., Christoforo, L and Antonio F., (2015). Correlation between Dry Density and Volumetric Shrinkage Coefficient of Three Brazilian Tropical Wood Species, *International Journal of Materials Engineering* 2015, 5(1): 1–4. https://doi.org/10.5923/j.ijme.20150501.01
19. Ivković,M., Washington J. G., Aljoy A. and Jugo I.(2008). Prediction of wood stiffness, strength, and shrinkage in juvenile wood of radiata pine, Wood Science and Technology 43(3):237–257
20. Muthumala, C.K., De Silva Sudhira, Alwis, P.L.A.G. and Arunakumara, K.K.I.U.(2018) Investigation of the relationship between densities vs. mechanical properties of Sri Lankan timber species. International Conference on Sustainable Engineering and Construction Management. Kandy. Sri Lanka

Structural Performance of Welded Joints—A Numerical Study

K. A. D. P. Sachintha, A. C. D. Pigera, and C. S. Bandara

Abstract Welded joints in steel structures are generally considered weaker joints in the structures due to the microstructural changes that occur in the weld metal and base metal due to heat. In base metal, the zone where the grain structure is affected due to heat is called the heat-affected zone. It is important to analyse the effect of heat-affected zone on the overall strength of the welded joint. Both experimental and numerical studies have been carried out in this area but the analysis and estimation of structural effects of the heat-affected zone are rare. This study is mainly focused on the estimation of the effects of the heat-affected zone on the tensile strength of welded joints numerically. The experimental data available in the literature are used to validate the numerical model. The validated model was used to come up with important conclusions on the structural performances of welded joints. From the results of the simulations, it was found that the material properties and the thickness of the HAZ can be accurately predicted using the hardness test results and that can be used to numerically model and analyse a butt-welded joint.

Keywords Welded joints · Heat affected zone · Finite element modelling · Structural effects

1 Introduction

High-strength steel (HSS) is the most used material in various steel structures recently due to its high strength-to-weight ratio, easy prefabrication properties and attractive appearance. It is widely used in the construction of bridges, stadiums, offshore structures, and high-rise buildings. HSS is mainly available in plate form. Welds are used to manufacture built-up sections from steel for construction purposes. Butt welds and fillet welds are the most used welding types in built-up sections.

Due to the high heat input in the welding process, the fusion zone and heat-affected zone (HAZ) are formed in the welded joint of the base metal with different

K. A. D. P. Sachintha (✉) · A. C. D. Pigera · C. S. Bandara
Faculty of Engineering, University of Peradeniya, Peradeniya, Sri Lanka
e-mail: e16330@eng.pdn.ac.lk

© The Author(s), under exclusive license to Springer Nature Singapore Pte Ltd. 2023

R. Dissanayake et al. (eds.), *ICSBE 2022*, Lecture Notes in Civil Engineering 362,
https://doi.org/10.1007/978-981-99-3471-3_24

material properties [2]. Zhang et al. [13] have experimented and found that the material properties of the HAZ are heterogeneous and [14] have found that the material properties within the HAZ are highly non-uniform due to the complex welding thermal cycles and non-uniform cooling rate. Reference [12] identified that the materials in HAZ are fine-grained. This fine-grained heat-affected zone (FGHAZ) is often referred to as a 'soft layer' [11, 12] found that the tensile cracks are initiated and propagated through the HAZ region. Reference [9] investigated that if the width of the HAZ is lower than 0.33 times the specimen thickness, the loss of strength never exceeds 10%. Reference [7] experimentally found that the width of the HAZ ranged from 0.33 to 0.6 times the specimen thickness and the reduction of tensile strength of the butt joint was 3 to 8% of its original strength. They have also found that the width of the soft zone and reduction of the tensile strength increases with the cooling time. Sleczka et al. [14] numerically modelled a fillet welded joint as a 2D model, and [8] numerically modelled fillet and butt-welded joints as 3D models considering three zones of welded joint in their models. Reference [4] used temperature-dependent data in their numerically modelled butt-welded joint. Material properties of steels can be predicted using the hardness values of the respective steels [3].

When conducting a numerical simulation of the welded joints, one of the most complicated modelling parameters is the material properties of the HAZ. To numerically analyse welded joints in existing structures, it is hard to obtain temperature-dependent data and to conduct destructive material tests to obtain the tensile strength of HAZ. The main objective of this paper is to numerically analyse a butt-welded joint by simulating a tensile test using 'ABAQUS' finite element software by obtaining material properties of the HAZ using non-destructive hardness test values and to validate using experimental data from previous literature.

2 Numerical Modelling

2.1 Specimen Dimensions

Two plates of thickness 16 mm each were welded by shield metal arc welding using electrodes with a diameter of 3.2 mm. The specimen with the dimensions shown in Fig. 1 has been extracted from the welded plates [5].

2.2 Material Properties

S690Q HSS has been used as the base metal of the specimen and LB-80L has been used as the weld metal. Table 1 shows the material properties of base metal and weld metal [5].

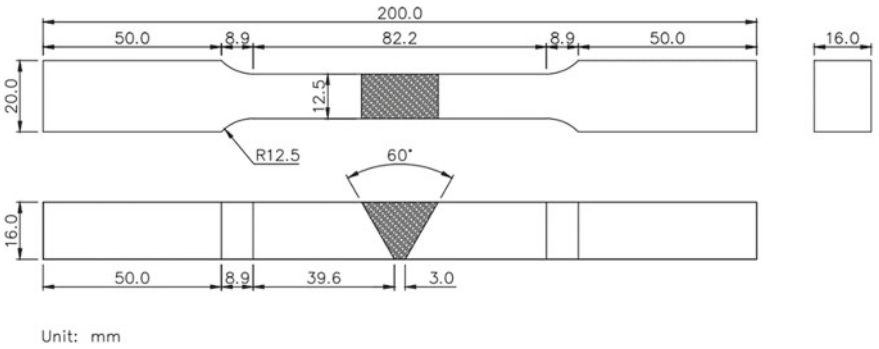

Fig. 1 Specimen dimensions [5]

Table 1 Mechanical properties of S690 HSS and weld metal [5]

Material	Elastic modulus (GPa)	Yield strength (MPa)	Ultimate strength (MPa)	Elongation (%)
S690Q HSS	208.9	745.2	837.8	14.5
LB-80L	210	767	848	22

Reference [5] obtained Vickers hardness values using 500 g force which was carried out using a micro-hardness tester, according to ISO 6507–1. From the obtained hardness values, HAZ can be differentiated from the base metal and the average width of HAZ can be determined as 6 mm. Calculated average hardness values of the base metal, HAZ and the weld metal are shown in Table 2.

According to Table 2, it can be seen that the calculated average hardness values of the base metal and the weld metal are in a close range and the hardness values of the HAZ are decreased by 22% from the hardness values of the base metal. According to [3], the tensile strength of HSS can be predicted using Eq. 1.

$$\sigma_u = 3.3Hv \tag{1}$$

$$\sigma_u - Ultimate\ tensile\ strength$$

$$Hv - Vickes\ Hardness$$

Table 2 Calculated average hardness values

Material	Hardness (HV0.5)
Base metal	275
HAZ	215
Weld metal	270

According to Eq. 1, it can be identified that the tensile strength of the HAZ is 22% less than that of the base metal and the tensile strength of the weld metal can be taken as being similar to the base metal in numerical modelling.

2.3 Numerical Model

Eight 3D models have been modelled using 'ABAQUS' finite element software for the specimen shown in Fig. 1. Models were created with four different HAZ widths as a fraction of specimen thickness and two tensile strength reductions from the base metal in the HAZ. Details of the models are shown in Table 3. HAZ was modelled with 0.3, 0.4, 0.5 and 0.6 times the thickness of the specimen and with strength reductions [7]. The finite element model created is shown in Fig. 2.

Each has been modelled considering the base metal, weld metal and HAZ as three different parts as shown in Fig. 2. HAZ was modelled as a uniform area [14]. Tie constraints were used in all base metal—HAZ and HAZ—weld metal interactions. Eight-node linear brick elements (C3D8R) were used in all models. True stress–strain values estimated as mentioned in Sect. 2.2 were given for the numerical model. Models converged to the number of elements in the mesh and the step time.

Table 3 Details of models

Model	HAZ Thickness/Specimen plate thickness	Tensile strength reduction in HAZ (%)
Model 1_a	0.3	8
Model 1_b	0.3	22
Model 2_a	0.4	8
Model 2_b	0.4	22
Model 3_a	0.5	8
Model 3_b	0.5	22
Model 4_a	0.6	8
Model 4_b	0.6	22

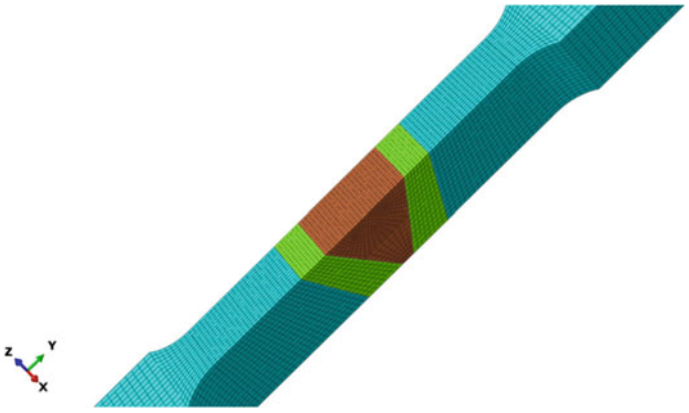

Fig. 2 Three zones of the finite element model

2.4 Results and Model Validation

The results of the numerical analysis were plotted and compared with the results of the experimental work done by [5] from Figs. 3, 4, 5 and 6.

According to the results, the stress–strain curve obtained from Model 2_b and Model 3_b shows reasonably good consistency with the corresponding experimental results of [5]. In these models, thicknesses of the HAZ were taken as 0.4 and 0.5 times the thickness of the specimen and tensile strength reduction in the HAZ was taken as 22% from the base metal. According to the Vickers hardness test results of [5] average width of HAZ can be determined as 6 mm. From both [5] and [3] the average tensile strength of the HAZ was reduced by 22% of the tensile strength of the base metal. Hence, both Models 2_b and 3_b can be validated.

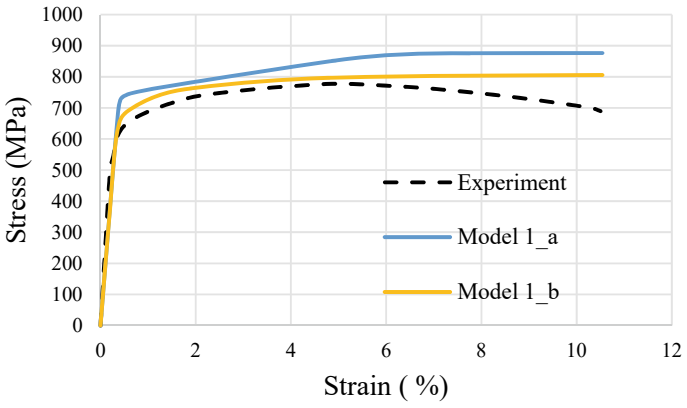

Fig. 3 Results of Model 1_a & Model 1_b

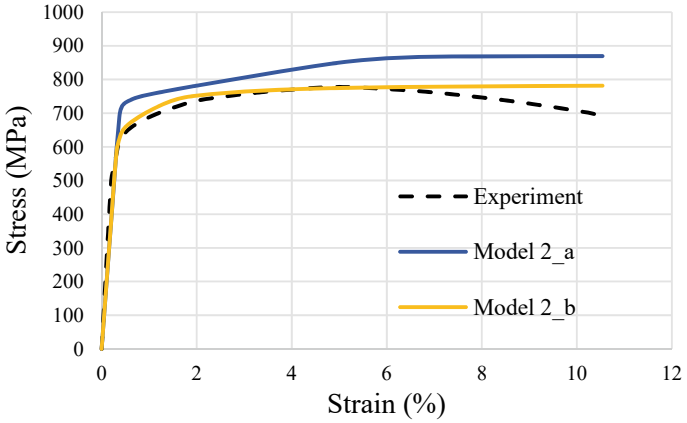

Fig. 4 Results of Model 2_a & Model 2_b

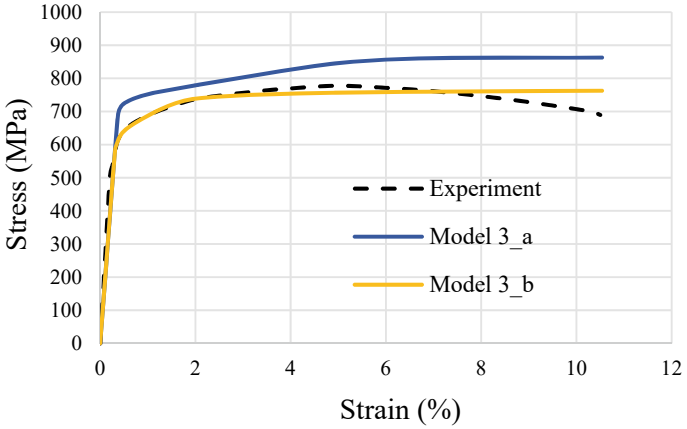

Fig. 5 Results of Model 3_a & Model 3_b

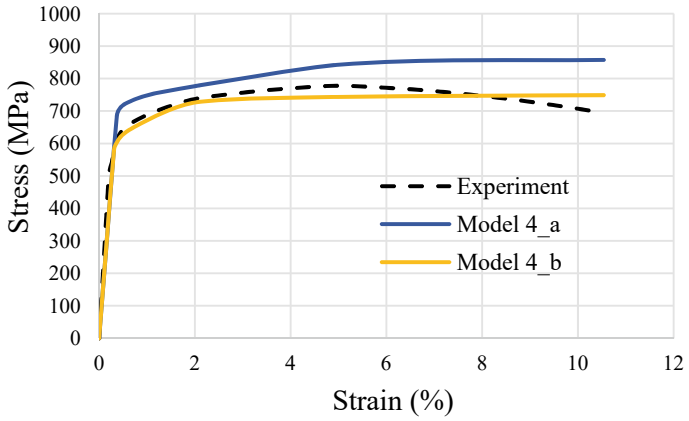

Fig. 6 Results of Model 4_a & Model 4_b

3 Conclusion

In this study, a butt-welded joint was numerically modelled, analysed and compared with experimental data from [5]. From the results, it can be concluded that.

1. A butt-welded joint can be modelled as three separate parts (Base metal, HAZ, Weld), and homogeneous material properties can be assigned to the HAZ.
2. For the numerical modelling, hardness values can be used to identify the width and the material properties of HAZ.
3. Based on the HSS used in this study, the thickness of the HAZ can be predicted as being 0.4–0.5 times the thickness of the base metal plate, and the tensile strength reduction is about 22%.

Hence, the proposed simulation method can be used to analyse a butt-welded joint with reasonable accuracy. Even though this simulation was done for a specimen, the proposed method can be used to numerically model structures with butt-welded joints. Also, it can be used to analyse existing structures with butt welds, as a hardness test is a non-destructive and portable test.

References

1. Anon (2019) ABAQUS Version 6.6 Documentation. https://classes.engineering.wustl.edu/2009/spring/mase5513/abaqus/docs/v6.6/index.html
2. Askeland, D.R., Fulay, P.P. and Wright, W.J. (2010). *The Science and Engineering of Materials 6 edition D. Askeland*. 6th ed. www.academia.edu.
3. Bandara, C. (2015). Fatigue Damage Assessment of Steel Structures and Components. 1st ed. LAP LAMBERT Academic Publishing

4. Chen, C., Chiew, S.-P., Zhao, M.-S., Lee, C.-K, Fung, T.-C. (2019) Welding effect on tensile strength of grade S690Q steel butt joint. J Const Steel Res 153, pp.153–168. https://doi.org/10.1016/j.jcsr.2018.10.009
5. Chiew, S.P., Cheng, C., Zhao, M.S., Lee, C.K., Fung, T.C. (2019). Experimental Study of Welding Effect on S690Q High Strength Steel Butt Joints. *ce/papers*, 3(3–4), pp.701–706. doi:https://doi.org/10.1002/cepa.1124
6. Garg A, Raturi M, Bhattacharya A (2019) Experimental and finite element analysis of progressive failure in friction stir welded AA6061-AA7075 joints. Procedia Structural Integrity 17:456–463. https://doi.org/10.1016/j.prostr.2019.08.060
7. Hochhauser F, Ernst W, Rauch R, Vallant R, Enzinger N (2012) Influence of the Soft Zone on The Strength of Welded Modern Hsla Steels. Welding in the World 56(5–6):77–85. https://doi.org/10.1007/bf03321352
8. Krejsa, M., Brozovsky, J., Mikolasek, D., Parenica, P., Koubova, L. and Materna, A. (2017). Numerical Modeling of Fillet and Butt Welds in Steel Structural Elements with Verification Using Experiment. *Procedia Engineering*, [online] 190, pp.318–325. doi: https://doi.org/10.1016/j.proeng.2017.05.344.
9. Rodrigues DM, Menezes LF, Loureiro A, Fernandes JV (2004) Numerical study of the plastic behaviour in the tension of welds in high-strength steels. Int J Plast 20(1):1–18. https://doi.org/10.1016/s0749-6419(02)00112-2
10. Ślęczka, L. and Kozlowski, A. (2008). *9.4 - Finite Element Modelling of Fillet Weld Connections*. [online] ScienceDirect. Available at: https://www.sciencedirect.com/science/article/pii/B9781904275282500521 [Accessed 8 Sep. 2022].
11. Su, L., Fei, Z., Davis, B., Li, H. and Bornstein, H. (2021). Digital image correlation study on tensile properties of high-strength quenched and tempered steel weld joints prepared by K-TIG and GMAW. *Materials Science and Engineering: A*, [online] 827, p.142033. doi: https://doi.org/10.1016/j.msea.2021.142033
12. Wojnowski D, Oh YK, Indacochea JE (1997) Metallurgical Assessment of the Softened HAZ Region During Multipass Welding. J Manuf Sci Eng 122(2):310–315. https://doi.org/10.1115/1.538920
13. Zhang C, Cui L, Wang D, Liu Y, Liu C, Li H (2019) The heterogeneous microstructure of heat affects zone and its effect on creep resistance for friction stir joints on 9Cr–1.5 W heat resistant steel. Scripta Mater 158:6–10. https://doi.org/10.1016/j.scriptamat.2018.08.028
14. Zhao MS, Lee CK, Fung TC, Chiew SP (2017) Impact of welding on the strength of high-performance steel T-stub joints. J Constr Steel Res 131:110–121. https://doi.org/10.1016/j.jcsr.2016.12.023

Effect of Ground Rice Husk on the Properties of Cement Block

P. L. J. Sajeevan, M. Nithurshan, and T. Thinojah

Abstract The use of solid wastes as a partial or complete replacement in the construction industry is one of the solutions for the scarcity of building materials and the conversion of natural resources. This study analyzes the feasibility of using rice husk (RH) waste, a by-product of rice milling, as secondary raw material in manufacturing cement blocks. Cement blocks were cast maintaining the cement-to-sand mix proportion of 1:3. River sand which is used in conventional cement blocks, is partially replaced with rice husk at different replacement levels (0%, 1%, 2%, 3%, 4%, 5%, 10%, 15%, 20%, and 25%) by volume. The experiments were conducted to determine the strength and physical properties, such as dry and bulk density, water absorption, and durability properties. Test results indicate that rice husk-incorporated cement blocks fulfilled the strength requirement of ASTM and SLS standards for all the replacement levels. However, cement blocks with 5% rice husk showed good results in terms of strength and durability. Hence, rice husk waste can be utilized in cement block production, resulting in economic and environmental benefits.

Keywords Building material · Cement blocks · Replacement ratio · Rice husk

1 Introduction

Rice is a staple food of Sri Lankans, and the production of paddy was estimated to be 5.1 million MT in 2020, as the Department of Census and Statistics revealed. The milling process of paddy generates about 20–25% of the husk by weight [12]. Although rice husk, an agricultural residue, is used as fertilizers, insulation materials, and fuel, massive amounts of rice husk are dumped in open land and burnt. This causes serious environmental problems such as acidification, water source contamination, and ozone depletion [15, 16]. In addition, several studies [27, 28] demonstrated that

P. L. J. Sajeevan · M. Nithurshan (✉) · T. Thinojah
Department of Engineering Technology, Faculty of Technology, University of Jaffna, Ariviyal Nagar, Killinochchi, Sri Lanka
e-mail: nithurshan@univ.jfn.ac.lk

© The Author(s), under exclusive license to Springer Nature Singapore Pte Ltd. 2023

R. Dissanayake et al. (eds.), *ICSBE 2022*, Lecture Notes in Civil Engineering 362,
https://doi.org/10.1007/978-981-99-3471-3_25

rice husk could be a construction material, such as a replacement for cement or sand, mainly because of its high silica content.

Another serious problem is the over-exploitation of river sand which has been extensively used as fine aggregates in Sri Lanka [28]. The annual sand demand for the construction industry was 9.4-million-meter cubes in 1992 [10], and it increased to 17.37 million-meter cubes in 2007. The sand demand was estimated based on cement usage for various construction purposes [28]. Currently, the Geological Survey and Mines Bureau of Sri Lanka controls the extraction of minerals, including sand, by the Mines and Minerals Act No. 33. It also maintains the information on all the issued permits for sand excavation and transportation. According to the records, the annual sand supply estimated was about a 7.99-million-meter cube, which was far lower than the estimated demand in 2007 [13]. Accordingly, the illegal excavation and overutilization of river sand cause harmful consequences to the environment such as flash flooding, drought, and the disappearance of aquatic life.

Over the last years, research has been carried out about the utilization of waste materials, especially agricultural waste, for eco masonry units. Processed tea waste [11], straw fibers adobe [23], coconut shell [14], and peanut shell [28] are among the agricultural wastes that have been used to study the compressive strength and durability properties, such as water absorption of masonry blocks. The study results revealed that the manufacture of blocks with agricultural wastes as a partial replacement for sand gives comparable compressive strength to that of control masonry blocks. Further, past studies [16, 18, 20] demonstrate that construction cost is reduced significantly with the inclusion of plant wastes that are abundantly available in rural areas while maintaining good quality construction. However, further research is required considering the strength and durability properties. Moreover, while extensive research has been carried out to study the effect of rice husk ash (RHA) on mortar and concrete properties, a minimal study has been carried out on the use of unburnt rice husk in producing mortar and concrete.

Therefore, the present study aims to study the feasibility of using rice husk waste as a partial replacement for sand in the production of masonry blocks considering the stability and durability properties.

2 Materials and Methods

2.1 Materials Used

2.1.1 Cement

Ordinary Portland Cement (OPC) with a grade of 42.5 which is specified on SLS107 (SLS 107, 2008), was used. The bulk density and specific gravity of the used cement were 1362 kg/m^3 and 3.15, respectively. The physical properties and chemical composition of the cement are outlined in Table 1.

Table 1 Physical properties and chemical composition of cement and sand

	Cement	Sand
Physical properties		
Bulk density (kg/m^3)	1362	1801
Specific gravity	3.15	2.68
Fineness	0.55	3.40
Chemical composition		
SiO_2	19.21	80.78
CaO	66.55	3.21
MgO	1.17	0.77
Al_2O_3	3.91	10.52
Fe_2O_3	3.62	1.75
SO_3	3.23	-
Na_2O	0.4	1.37
K_2O	0.39	1.23

2.1.2 Sand

Local natural river sand was used in the mortar mix. The bulk density and specific gravity of the sand were 1801 kg/m^3 and 2.68, respectively. The sand grading curve from sieve analysis that was performed per ASTM C136/ C136M(ASTM C136/ C136M, 2014) is shown in Fig. 1. The particle size distribution curve describes the uniformity of sand, and the fineness modulus was calculated to be 3.4.

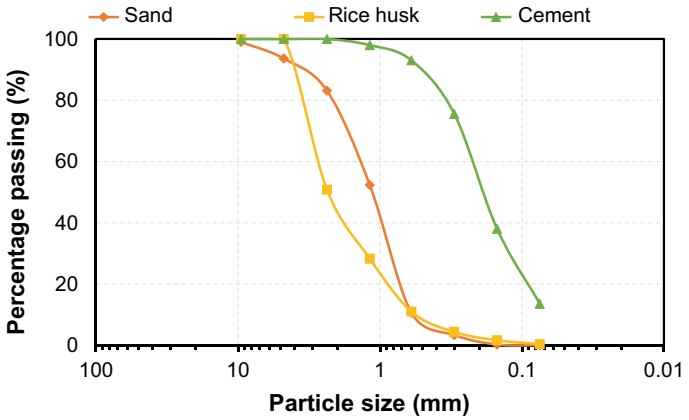

Fig. 1 Particle Size Distribution Curve of Cement, Sand and RH

2.1.3 Rice Husk

Rice husk (RH) was collected from Bala Rice Mill, Manipay, Jaffna, and dried in sunlight for 3 days. Then, the dried RH was ground using a kitchen grinder to make them finer, as shown in Fig. 2. The density of RH was found to be 537.3 kg/m^3.

2.2 Mix Design

Mix design for mortar was conducted based on the volume. Cement to sand ratio was kept at 1:3. To maintain the constant workability of mixes, water to cement ratio was maintained at 0.5 as the water requirement for the rice husk is reported to be close to the control cement sand mixture [22]. The mixes were prepared by replacing sand with different percentages (0, 1, 2, 3, 4, 5, 10, 15, 20, and 25%) of rice husk, as shown in Table 2.

Mortar mixes were prepared by manual blending and compressing. Initially, to acquire a homogenous mixture, cement, sand, and rice husk were measured and blended. Then, water was consistently added, and mixing was continued until a homogenous mixture was obtained. It took about 20–30 min for the whole mixing procedure. Cement blocks of 70.6 mm × 70.6 mm × 70.6 mm in size (Fig. 3) were cast with each mix proportion as described in Table 2. Molds were filled in three layers, and each layer was compacted using a tamping rod with 25 strokes by hand.

2.3 Testing

A total number of 240 samples were prepared. Three cement blocks were used for each mixing ratio to determine the compression strength, density, water absorption,

Fig. 2 Grained rice husk sample

Table 2 Mix design of mortar mixes

RH replacement (%)	Weight (kg)			
	Cement	***RH***	***Sand***	***Water***
0	2.533	0	6.339	1.266
1	2.533	0.018	6.275	1.266
2	2.533	0.037	6.150	1.266
3	2.533	0.054	5.965	1.266
4	2.533	0.072	5.727	1.266
5	2.533	0.090	5.440	1.266
10	2.533	0.180	4.896	1.266
15	2.533	0.270	4.162	1.266
20	2.533	0.360	3.329	1.266
25	2.533	0.450	2.497	1.266

Fig. 3 Cement blocks after removing the mold

acid attack resistance, and alkaline attack resistance. The blocks were cured under a room temperature of 30^{o} C, and a relative humidity of 90% until testing took place.

2.3.1 Compression Test

A compressive strength test was performed on the 7, 14, and 28-day-aged samples by a universal testing machine using a displacement control method at the rate of 2 mm/min according to the European standard EN 772–1 (BS EN 772–1, 2015). The ultimate load was recorded at the failure of the blocks.

2.3.2 Water Absorption Test

Weight and dimensional measurements of the cement blocks and their rice husk content were performed as per ASTM C140 (ASTM C140/C140M, 2017) to determine the density and water absorption. Cement blocks at the age of 28 days were kept at 100 °C for 24 h in an oven to remove excess moisture. Afterward, the blocks were placed in the open shed until the surface temperature of the specimen dropped to room temperature. The blocks were then completely immersed in clean water at room temperature for 24 h. The excess water on the surface was wiped off and the weight of the blocks was recorded. The water absorption was calculated using Eq. (1).

$$\text{Water absorption} = \frac{W_i - W_a}{V} \tag{1}$$

where W_a is the weight of the specimen at the fully saturated condition, W_i is the weight of the oven-dried specimen, and V is the volume of the specimen.

2.3.3 Testing for Acid and Alkaline

The cement blocks were submerged in 3% of H_2SO_4 solution for an acid test and 3% of NaOH solution for an alkaline test for 30 days according to ASTM C1152M-04 (ASTM C1152M, 2012) and ASTM C289-07 (ASTM C289, 2007), respectively. The weight of the specimen before (W_i) and after submersion (W_a) was recorded to calculate the weight loss given by Eq. (2).

$$\text{Percentage of weight loss} = \frac{W_i - W_a}{W_i} \times 100 \tag{2}$$

3 Results and Discussions

3.1 Density

Dry density and bulk density, which depend on water absorption, the specific gravity of used materials, cement–water ratio, waste material replacement, sand types, and their content, etc., were calculated for the control sample and each replacement level and plotted in Fig. 4. Based on the results, it can be understood that both dry and bulk density decreased with increasing replacement levels. This can be attributed to the relatively low specific gravity of rice husk (RH). In terms of dry density, the cement blocks with each replacement level were classified according to the ASTM

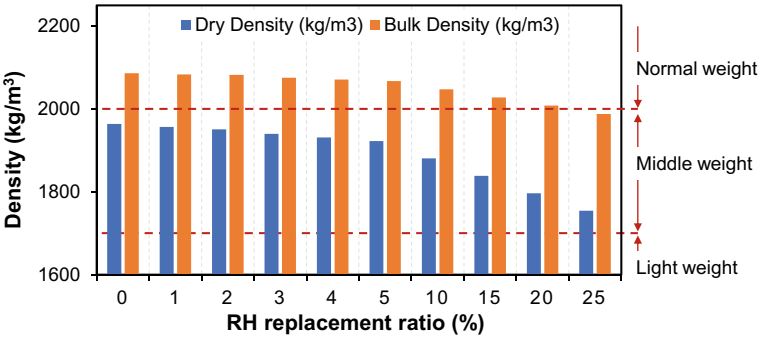

Fig. 4 Dry and bulk density variation with the different RH replacement ratio

Specifications for cement masonry units [7]. The cement blocks with RH fell under the middleweight blocks category, while the control blocks showed dry density values close to normal weight categories.

3.2 Compressive Strength

Nowadays, masonry units are used for non-load bearing structural walls, and the ASTM [2] sets the minimum value for those walls as 4.14 MPa, while Sri Lankan standards (SLS 855) set 1.2 MPa as the average of three specimens.

Compressive strength depends on the water/cement ratio, cement content, strength of the matrix, strength of aggregate, and particles. The variation of compressive strength with the replacement level of rice husk and curing age is shown in Fig. 5. From the results, it can be noticed that the compressive strength of the blocks was influenced by the addition of rice husk and its replacement percentage. In this experiment, the 5% replacement level showed the highest compressive strength (14.5 MPa) compared to other cement blocks, including the control blocks. This is because the silicious composition in rice husk promotes the formation of calcium silicate hydrates (CSH) which bind the aggregates strongly to resist compressive loads [31]. However, the compressive strength of the cement block gradually reduced with a higher replacement percentage (>5%) of rice husks. This effect could be due to the much lower mechanical resistance of rice husk compared to sand. The elevated level of replacement leads to the high porosity of the blocks, which results in lower resistance to external loads. The same trend was reported in past studies [8, 19, 21, 27], where in every experiment, compressive strength was observed to reduce with an increasing percentage of fine aggregate replacement by any kind of agricultural waste materials.

However, in this experimental program, all the cement blocks produced with different rice husk contents satisfied the minimum requirement set by ASTM C129[2] and Sri Lankan Standard (SLS 855) at the age of 28 days, as shown in Fig. 5.

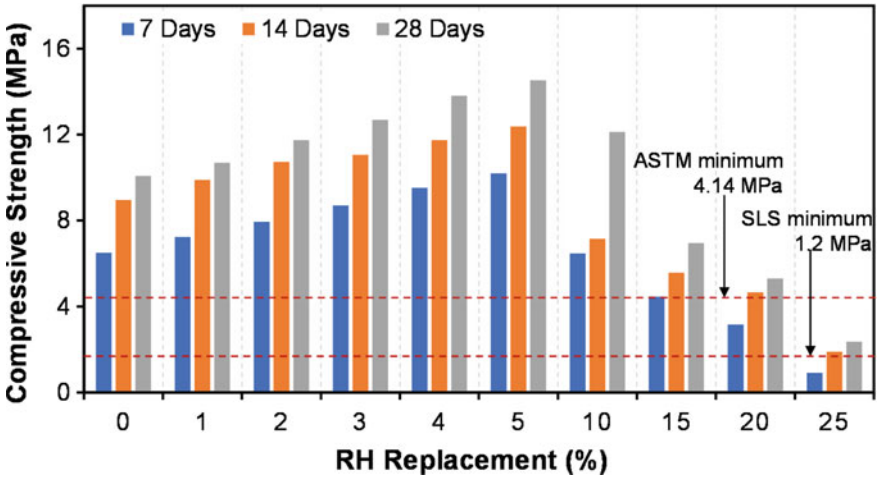

Fig. 5 Compressive strength variation with different replacement levels and curing age

Therefore, these blocks are still applicable for non-load-bearing wall construction such as low-story houses.

3.3 Durability

3.3.1 Water Absorption

The water absorption of cement blocks is mainly determined by the nature of the pore system. The high porosity of the cement block leads to more water and chemical penetration which reduces the quality of the blocks. Previous studies [17, 21] revealed that water absorption of cement blocks combined with waste materials is high when compared to that of control blocks, as the water absorption by waste materials is significantly greater. Also, the water abortion rate increases with the increase of the replacement of waste material for fine or coarse aggregates. A similar trend was observed in this study as well. The reason could be associated with the low bulk density of rice husk, which led to increased pores in the mortar mix, the high hydrophilic nature of rice husk, and the lower bond strength between rice husk and cement [28]. The allowable water absorption rates for normal-weight masonry blocks, medium-weight masonry blocks, and lightweight masonry blocks were provided as 208 kg/m^3, 240 kg/m^3, and 320 kg/m^3, respectively, by ASTM C55-11(ASTM C55, 2011). Accordingly, the water absorption rate of all the cement blocks, which were classified as medium-weight blocks in Sect. 3.1, was less than the allowable limit (240 kg/m^3), as shown in Fig. 6. Blocks made with up to 5% replacement of RH gave a remarkably close value compared to the control group.

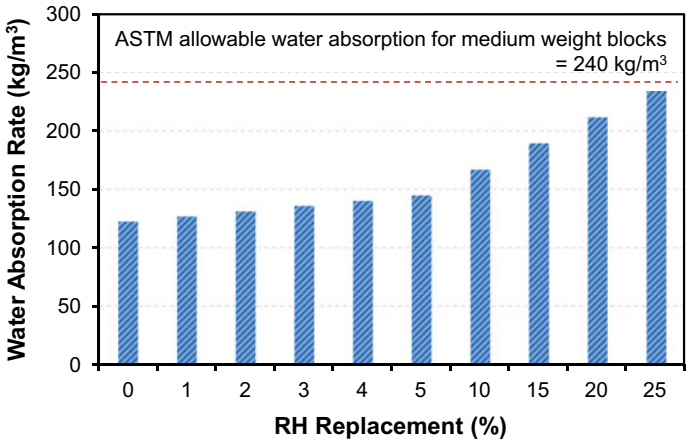

Fig. 6 Water absorption rate of cement blocks with the different replacement ratio

3.3.2 Acid and Alkaline Resistance

Weight loss of cement blocks due to acid and alkaline attacks were summarized in Fig. 7. Based on the figure, it can be observed that the weight loss of blocks that were subjected to acid and alkaline attack for 30 days gradually increased with the increment of replacement level. However, cement blocks with up to 5% rice husk replacement showed relatively lower weight loss, which is closer to control. Furthermore, weight loss due to acid attack is relatively high compared with alkaline attack for each replacement level. This can be attributed that the reaction between the rice husk (organic matter) and the acid being high compared to an alkaline attack, and thus the total weight of the block was reduced due to the weight loss of the decomposed rice husk.

Moreover, even though these blocks comply with the strength requirement set by the ASTM [2], the high content of rice husk results in an irregularly shaped surface, as shown in Fig. 8. It causes difficulty in applying joint mortar and surface plastering during construction [28].

Cement blocks with rice husk have some benefits, such as low cost, high porosity, and low density, compared to the control blocks made only using cement and sand. Moreover, construction and labor costs reduce because of their lightweight. Higher porosity lowers thermal conductivity [25, 26].

Overall, the optimum replacement level of rick husk would be 5%, as the blocks with 5% rice husk showed very close strength and durability properties compared to the control sample. However, further research regarding public education and local standardization is required to popularize the production of cement blocks incorporating rice husk.

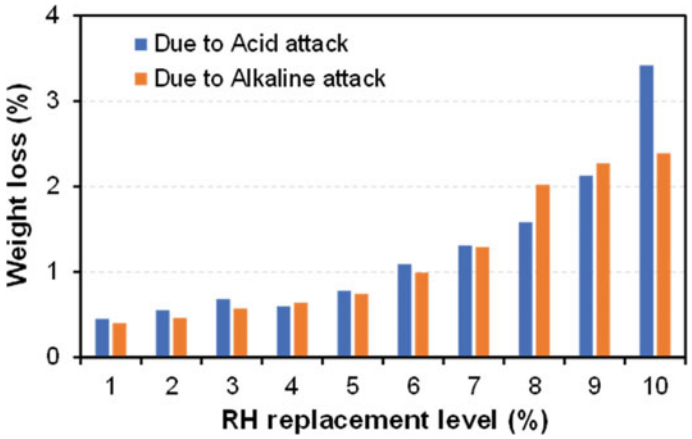

Fig. 7 Weight loss due to acid and alkaline attacks for different mix

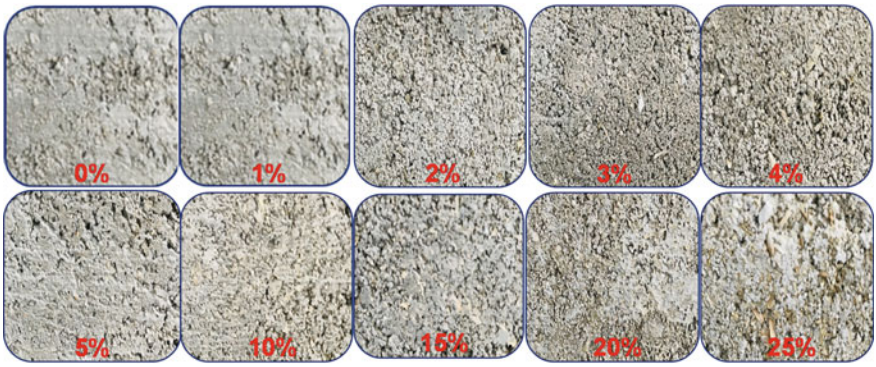

Fig. 8 Appearance of 28-day aged cement block with different replacement level

4 Conclusion

This study aims to study the feasibility of incorporating rice husk waste as a partial replacement for sand in manufacturing masonry blocks. These could be used as construction materials in houses in Sri Lanka. A series of laboratory tests were carried out to evaluate the most reasonable replacement level for sand with rice husk. The following conclusions were made based on this experimental program.

- Based on the density results, cement blocks with all replacement level were categorized as middleweight blocks according to the ASTM C90 (ASTM C90, 2011), while the density of the control sample was almost like the normal category.

- The compressive strength of cement blocks increased up to a 5% replacement level of rice husk in the mortar mix, and then it started to decrease with the high level of replacement. However, all the blocks with replacement levels up to 25% satisfied the minimum strength requirement recommended by ASTM and Sri Lankan standards.
- In terms of acid and alkaline resistance, cement blocks with up to 5% rice husk showed relatively lower weight loss, which was closer to control. But the weight loss increased with the increase of the replacement level.

Based on the above results, cement blocks with rice husk satisfied the strength and durability requirements. Thus, it can be used as a construction material where low-strength cement blocks are applicable. However, further research on long-term durability, mechanical properties such as elastic modulus, and durability properties such as carbonation, erosion, permeability, and freezing and thawing are very much needed to convince the construction industry to use these blocks in housing projects.

Acknowledgements The authors acknowledge the support given by the Construction Laboratory, Department of Engineering Technology, Faculty of Technology, University of Jaffna.

References

1. ASTM C1152M-04 (2012) Standard Test Method for Acid-soluble Chloride in Mortar and Concrete. *ASTM International, West Conshohocken, PA*
2. ASTM C129 (2006) Standard Specification for Nonloadbearing Concrete Masonry Units. *ASTM International, West Conshohocken, PA*
3. ASTM C136/C136M (2014) Standard Test Method for Sieve Analysis of Fine and Coarse Aggregates. *ASTM International, West Conshohocken, PA*
4. ASTM C140/C140M - 17a. (2017). Standard Test Methods for Sampling and Testing Concrete Masonry Units and Related Units. *ASTM International, West Conshohocken, PA*
5. ASTM C289–07. (2007). Standard Test Method for Potential Alkali-Silica Reactivity of Aggregates (Chemical Method). *ASTM International, West Conshohocken, PA*
6. ASTM C55−11. (2011). Standard Specification for Concrete Building Brick. *ASTM International, West Conshohocken, PA*
7. ASTM C90. (2011). Standard Specification for Loadbearing Concrete Masonry Units. *ASTM International, West Conshohocken, PA*
8. Brás A, Leal M, Faria P (2013) Cement-cork mortars for thermal bridge correction. Comparison with cement-EPS mortars performance. Constr Build Mater 49:315–327
9. En BS, 772–1:2011+A1 (2015) Methods of Test for Masonry Units. Determination of Compressive Strength, Comité Européen de Normalisation, Brussels
10. Delft Hydraulic and Netherlands Economic Institute. (1992). National Sand Study for Sri Lanka-Phase one
11. Demir I (2006) An investigation on the production of construction brick with processed waste tea. Build Environ 41(9):1274–1278
12. Fernando, S., Nasvi, ; M C M, Gunasekara, ; Chamila, David, ;, Law, W., Setunge, S., & Dissanayake, R. (2021). *Systematic Review on Alkali-Activated Binders Blended with Rice Husk Ash*
13. Gunaratne, L. H. P. (2015). Cost-Benefit Studies of Natural Resource Management in Southeast Asia. *Cost-Benefit Studies of Natural Resource Management in Southeast Asia*

14. Gunasekaran K, Kumar PS, Lakshmipathy M (2011) Mechanical and bond properties of coconut shell concrete. Constr Build Mater 25(1):92–98
15. Gursel AP, Maryman H, Ostertag C (2016) A life-cycle approach to environmental, mechanical, and durability properties of "green" concrete mixes with rice husk ash. J Clean Prod 112:823–836
16. Khedari J, Suttisonk B, Pratinthong N, Hirunlabh J (2001) New lightweight composite construction materials with low thermal conductivity. Cement Concr Compos 23(1):65–70
17. Kuo WT, Wang HY, Shu CY, Su DS (2013) Engineering properties of controlled low-strength materials containing waste oyster shells. Constr Build Mater 46:128–133
18. Madurwar MV, Ralegaonkar RV, Mandavgane SA (2013) Application of agro-waste for sustainable construction materials: A review. Constr Build Mater 38:872–878
19. Mannan MA, Ganapathy C (2004) Concrete from an agricultural waste-oil palm shell (OPS). Build Environ 39(4):441–448
20. Mannan MA, Ganapathy CU (2002) Engineering-properties-of-concrete-with-oil-palm-shell-as-coarseaggregate_2002_Construction-and-Building-Materials. Constr Build Mater 16:29–34
21. Olanipekun EA, Olusola KO, Ata O (2006) A comparative study of concrete properties using coconut shell and palm kernel shell as coarse aggregates. Build Environ 41(3):297–301
22. Öztürk, T., & Bayrakl, M. (2005). The Possibilities of Using Tobacco Wastes in Producing Lightweight Concrete. *Agricultural Engineering International*, *VII*, 1–9.
23. Parisi F, Asprone D, Fenu L, Prota A (2015) Experimental characterization of Italian composite adobe bricks reinforced with straw fibers. Compos Struct 122:300–307
24. Prasara-A J, Grant T (2011) Comparative life cycle assessment of uses of rice husk for energy purposes. Int J Life Cycle Assess 16(6):493–502
25. Prusty JK, Patro SK (2015) Properties of fresh and hardened concrete using agro-waste as partial replacement of coarse aggregate - A review. Constr Build Mater 82:101–113
26. Prusty JK, Patro SK, Basarkar SS (2016) Concrete using agro-waste as fine aggregate for the sustainable built environment – A review. Int J Sustain Built Environ 5(2):312–333
27. Sada BH, Amartey YD, Bako S (2013) an Investigation Into the Use of Groundnut Shell As Fine Aggregate Replacement. Nigerian Journal of Technology (NIJOTECH) 32(1):54–60
28. Sathiparan N, De Zoysa HTSM (2018) The effects of using agricultural waste as a partial substitute for sand in cement blocks. Journal of Building Engineering 19(March):216–227
29. SLS 107. (2008). *Specification for Ordinary Portland Cement Part 1: Requirements, Sri Lanka Standards Institution.*
30. SLS 855. (n.d.). Specification for Cement Blocks: part 1. *Requirements, Sri Lanka.*
31. Winarno S (2019) Comparative Strength and Cost of Rice Husk Concrete Block. MATEC Web of Conferences 280:04002

Effectiveness of Sri Lankan Bamboo as a Structural Material

S. V. P. Allalagoda, S. S. Bandaranayake, T. V. D. V. K. Vitharana, M. T. R. Jayasinghe, P. L. N. Fernando, and H. M. S. T. Herath

Abstract Bamboo is a type of woody grass from the family of *Bambusoideae* and it has been widely spread in most Asian, African, and South American countries. In Sri Lanka, 10,000 hectares of bamboo cultivation belonging to seventeen different species have been identified. Bamboo is considered highly renewable, economically feasible and fast-growing, all of which are a hallmark of a sustainable material. When used with proper treatment and comprehension of its properties under different applications, it is a durable and versatile material. The present study aims to determine the key structural properties of four species of bamboo available in Sri Lanka, namely yellow bamboo, green bamboo, giant bamboo, and hybrid bamboo. In order to identify their suitability to adopt as a load-carrying material such as bamboo reinforced concrete, its properties should be evaluated under standard conditions. As such, laboratory experiments for compressive strength, tensile strength (transverse and longitudinal) and shear strength were carried out for representative samples of the four species. All the tests have been carried out according to the standards of ISO 22157:2019 to maintain the accuracy and reliability of results. This paper presents and discusses the preparation of samples to comply with the standards. The ultimate strength, as well as the stress–strain variation for each of these loading cases, were obtained from the experimental results, and the preliminary findings are also presented. Moreover, failure patterns, especially under longitudinal tensile forces and their significance towards structural design are presented. In conclusion, the outcomes of the present research study will play a significant role in introducing bamboo as an alternative and sustainable material in the construction industry in Sri Lanka.

Keywords Sri Lankan bamboo · Sustainable materials · Sample preparation · Strength properties · Failure patterns

S. V. P. Allalagoda · S. S. Bandaranayake · T. V. D. V. K. Vitharana · M. T. R. Jayasinghe · P. L. N. Fernando (✉) · H. M. S. T. Herath
Department of Civil Engineering, Faculty of Engineering, University of Moratuwa, Moratuwa, Sri Lanka
e-mail: lakshithaf@uom.lk

© The Author(s), under exclusive license to Springer Nature Singapore Pte Ltd. 2023

R. Dissanayake et al. (eds.), *ICSBE 2022*, Lecture Notes in Civil Engineering 362,
https://doi.org/10.1007/978-981-99-3471-3_26

1 Introduction

1.1 Background

Bamboo is a woody grass from the subfamily *Bambusoideae* in the family of *Poaceae*. It is mainly spread in the regions of South Asia, Southeast Asia, East Asia, and South America with more than 1000 species. On the other hand, bamboo is considered one of the fastest growing plants in the world and a highly sustainable construction material with a minimum impact on the environment.

In Sri Lanka, a total of 10,000 ha (approx.) of bamboo cultivation which represents 17 species have been identified [2]. When considering the utilization of locally available bamboo, it is mostly used in light-duty applications such as handmade products, ornaments, covering, and fencing material. In the foreign context, bamboo is used as an alternative raw material in many industries such as the paper industry, bamboo plywood industry, and charcoal industry because it can be extracted and processed with minimum impact and carbon footprint on the environment. Currently, in Sri Lanka, bamboo is also cultivated in the riverbanks for the purpose of conservation of the natural ecosystem in the country. When considering the embodied energy and other environmental impacts related to commonly used building materials, timber produced with bamboo has been found to perform better [9].

Scaffolding can be considered a structural application where the load-bearing capabilities of bamboo are directly used. Especially in developing countries such as Sri Lanka, bamboo scaffolding and the construction of temporary structures using bamboo can be commonly observed. Moreover, the designing of structures with bamboo has been developed to a level that can challenge the conventional designs of concrete structures of low-rise buildings in some foreign regions. Standards such as ISO 22157, ISO 22156, IS 15912, and IS 6874 have been developed in those regions to use full-culm bamboo designs and to evaluate its structural properties. A potential use of bamboo in Sri Lanka is its use as a structural reinforcement material for concrete elements of low-rise light-duty structures. However, there is a lack of experimental data on the structural properties of Sri Lankan bamboo. Therefore, proper identification and the comprehension of structural properties of locally available bamboo are significant for the advancement of the use of bamboo as a structural material in Sri Lanka. This in fact will contribute to the sustainability of the construction industry.

Bamboo is a natural material, and its properties widely vary with the species, age, geological location, average climate conditions, and its geometry vary within the culm. In addition to that, different internodal distances could be observed even within the same cluster. By nature, the culm is separated into chambers by the diaphragms which are located at the nodes. Due to this special geometry of the culm (Fig. 1), it is highly possible that the strength values may also vary along the direction parallel to the fibres. Therefore, a well-organized evaluation of the structural properties of bamboo is much important to get a comprehensive understanding of its strength values when designing advanced structures using bamboo as a structural material either in full culm form or in an engineered form.

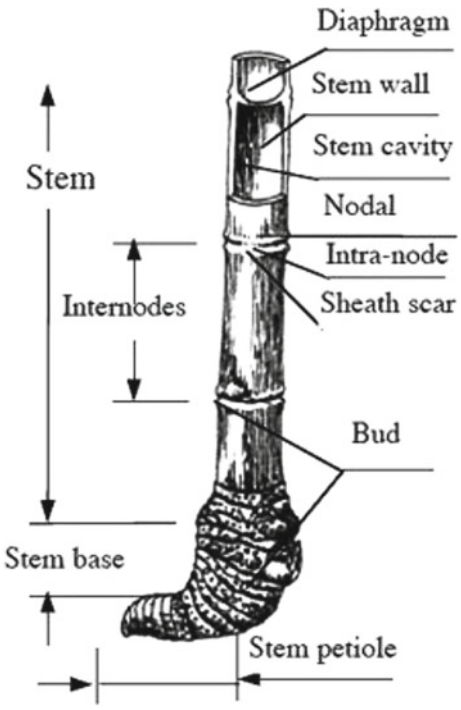

Fig. 1 Anatomy of bamboo [4]

Since fresh bamboo has a high moisture content, it is likely to get attacked by termites and fungi if a proper drying and treatment procedure is not conducted. Therefore, treatment with a suitable wood preservative is essential prior to its use in any application. Drying is also important to mitigate the effects due to shrinkage which may otherwise occur over time during the reduction of moisture content, and on the other hand, can also improve the treatment against termite attacks. Properly treated bamboo may last for more than 50 years. It can be used to build sustainable, lightweight, and durable structures.

The aim of the present study is to obtain the characteristic structural properties, namely, Compressive Strength, Shear Strength, and Tensile Strength in the parallel direction to the fibres and the Transverse Tensile Strength (or the Modulus of Rupture) of Sri Lankan bamboo. The testing methods and the parameters are based on ISO 22157:2019—*Bamboo structures—Determination of physical and mechanical properties of bamboo culms.* It must be noted that due to the lack of provisions in the standard, the Flat Ring Flexural Strength Test will be used to obtain the Modulus of Rupture [13]. Mainly, our species were selected based on current utilization and their natural variation by visual inspection. The geometric data of the culms were also considered to improve the characterization. Preliminary stress–strain graphs obtained for the above strength parameters are presented. Moreover, the potential utilization of Sri Lankan bamboo (mainly as a structural material) in both full culm

form and engineered form will be discussed since adequate data on the utilization of Sri Lankan bamboo as a structural material is yet to be investigated.

2 Summary of Literature

2.1 Bamboo in Sri Lanka

Bamboo is mainly scattered in the wet zone or the Southwestern area of the country because most of the bamboo species in the tropical regions require a high level of both humidity and moisture content in the soil. However, a considerable number of species of bamboo clumps can also be seen along the riverbanks in the dry zone of the country such as *Bambusa bambos*—in the intermediate and dry forests in the low hills, *Dendrocalamus membranaceus* and *Dendrocalamus asper*—in the intermediate zone, *Bambusa vulgaris*, and *Dendrocalamus giganteus*—in the wet zones & riverbanks [6].

2.2 Utilization of Bamboo in Sri Lanka

Past research indicates that the utilization significantly varies with the species because most of the species have their own structural and mechanical properties. For example, *Bambusa bambos, B. vulgaris, Dendrocalamus asper, D. giganteus* are used for bridges, ladders, house frames, and scaffolding, and *Thyrsostachys siamensis* is used for wattle & daub walls [6].

2.3 Use of Bamboo as a Structural Material

Since there is a lack of past research studies and data related to the use of Sri Lankan bamboo as a structural material, few research studies from foreign regions will be discussed. Their concepts, designs, and mechanisms can be implemented with the bamboo resources that are currently available in Sri Lanka.

Nowadays, bamboo has become a widely used wooden construction material all over the world. Generally, it is used for the construction of houses (or its structure), light structures with modern design concepts and for economical scaffolds. In addition to that, it is also used as a reinforcement for concrete structures and to construct small bridges in rural areas [5]. However, the utilization of bamboo in modern advanced structures can also be seen because bamboo can be used as a green building material meeting the requirements of the sustainability concepts [3]. Figure 2

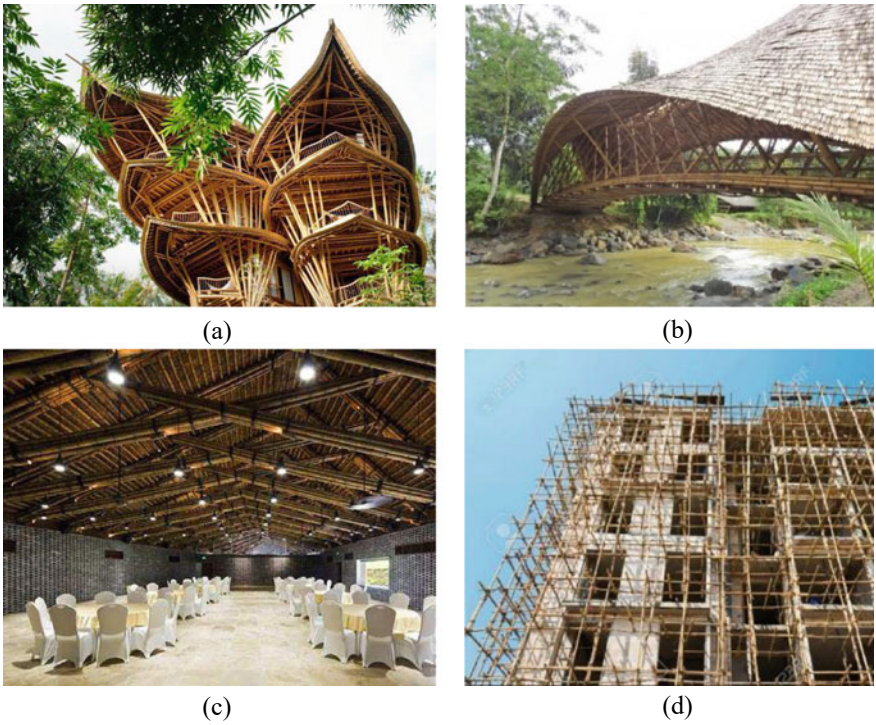

Fig. 2 **a** Full Culm Bamboo Structure, **b** Bamboo Bridge, **c** Bamboo Roof Truss and **d** Bamboo Scaffolding

illustrates some examples of the utilization of bamboo in complex architectural and structural designs.

The structure (found in Indonesia) in Fig. 2a shows the use of full culm bamboo for both architectural and structural engineering applications, where bamboo is used as the main material for both the structure and the partitions. The bridge constructed using full culm bamboo shown in Fig. 2b—located at Orangutan Haven in Indonesia—is evidence of adequate bearing capacities under different load combinations. Bamboo for roof trusses (Fig. 2c) is a structurally feasible and sustainable alternative due to the high rigidity and low weight of bamboo. Use of bamboo for scaffolding, as seen in Fig. 2(d) is commonly seen in the construction industry. The use of bamboo as reinforcement in concrete is another advanced and highly sustainable structural application of bamboo. It has been successfully implemented in many foreign regions such as Vietnam, Indonesia, Thailand, and the Philippines [11].

Apart from using bamboo in its *full culm form*, it has been used as *engineered bamboo,* which is manufactured by processing the raw bamboo into new composite material. The two basic types of engineered bamboo are *bamboo scrimber* (manufactured by compressing a resin-saturated bamboo fiber into a dense block) and

laminated bamboo (manufactured by pressing a split, planned, processed, and laminated bamboo into a form of a board). With laminated bamboo, complex structures can be built because standardized sections without variation in both dimensional and material properties are available. This in fact is a shortcoming in full culm bamboo. The sheet type is generally used for indoors, surface applications, and furniture; the bamboo scrimber is used in structural applications [10]. In this case, the tensile strength of bamboo fibers can be considered the most important property which should be evaluated during the design stage.

2.4 Harvesting

The age of bamboo, the harvesting season, and the quality of bamboo are some of the key considerations in harvesting bamboo. Since the structural properties of bamboo greatly vary with age, the harvesting age of the bamboo must be taken into consideration. For most of the species, the best harvesting age is 3–5 years, while some of them can be harvested even up to the age of 8 years. The maturity level of bamboo can be easily identified by looking at the skin of the culm. Smooth shiny skin with culm sheaths can be seen in young bamboo while the growth of fungi and moss occurs in the old bamboo. When considering the time periods for harvesting, the recommended period is at the end of the rainy season—the beginning of the dry season due to several facts. At the end of the dry season, the starch content is high, which increases the risk of attack by fungi and borer. Meanwhile, during the rainy season, the moisture content of culms is high, which causes cracks even in air drying. Moreover, as bamboo starts to dry, it tends to lose its structural properties gradually. As for the quality of bamboo, straight, mature culms with a minimum change in diameter should be selected for harvesting (Komitu Architects).

2.5 Effects of Drying Methods

The freshly harvested bamboo possesses a high moisture content, and hence is susceptible to rapid attacks by fungi and termites. Therefore, in addition to the treatment process, reducing the moisture content using a suitable method is of great significance. The current drying methods include hot air drying, kiln drying, and microwave drying. However, inappropriate drying may cause defects such as cracking, charring, change in shape and color, and loss of strength. While microwave drying increases the permeability and minimizes the drying stress, it gives a quality product in the end.

3 Methodology

The experimental program in the present study is conducted to obtain the strength properties of four selected species of Sri Lankan bamboo. In addition to these tests, the culm data such as the external diameter at nodes and the centre of internodes, internodal distance, and the geometric location of each node along the length of the culm is recorded prior to the preparation of samples.

3.1 Sample Selection & Preparation

The selection of samples has been done by visual inspection at the site of harvesting while considering the facts such as the age, diameter, thickness, and length of the usable portion of the culm for structural work. Therefore, well-grown, matured, and straight culms of the age between 3 and 5 years have been harvested and kept for indoor air drying to reduce the moisture content, as specified in the Standard for testing. The dried samples were prepared for testing, according to the geometric parameters specified in ISO 22157:2019 [1]. These parameters are summarized in Table 1.

L—length of sample, δ—thickness of the wall, D—external diameter of the culm, b—width of the sample.

For the Flat Ring Flexural Test, all the samples have been obtained from the internodal portion of the culm with a sample height between 0.25D and 0.3D to benchmark with the results of a previous test [13]. When preparing samples for all four tests, the locations of samples have been selected in a manner that represents the bottom, middle, and top of the culm because the strength varies along the length.

Table 1 Standards for sample sizing

Compressive strength parallel to fibres	Shear strength parallel to fibres	Tensile strength parallel to fibres
L = lesser of D or 10δ (If D < 20 mm, L = 2D)	L = lesser of D or 10δ (If D < 20 mm, L = 2D)	b < (δ/2) < 20 mm
50% Samples with nodes, 50% without	50% Samples with nodes, 50% without	Gauge length 50–100 mm
Node at the centre (approx.)	Node at the centre (approx.)	Node should place within the gauge length

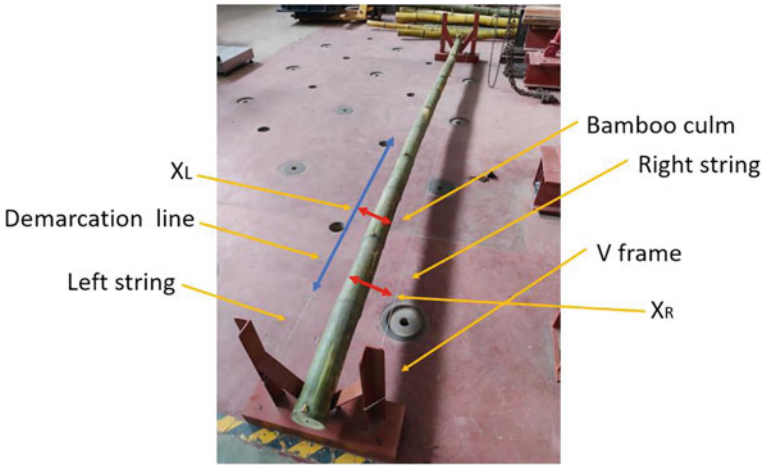

Fig. 3 Measurement of culm data

3.2 Measurements Obtained

3.2.1 Culm Data Measurement

The geometric data of the culms were recorded prior to the sample preparation using a pair of V—frames because this data is required for further analysis of the results such as the determination of the external diameter of the specimen (which is required when marking cutting lines), etc. This includes internodal distance, alignment of the nodes, and the centre of internodes in both the short span and the long span of the cross-section. Therefore, two demarcation lines were located with the V—frames as the reference lines, where X_L and X_R are the distances for node or internode from the left-side demarcation and the right-side demarcation, respectively (Fig. 3).

3.2.2 Measurements of Prepared Samples

The following measurements were taken with a precision of up to 0.1 mm using a vernier caliper.

d—External Diameter (in both short span & long span)
t—Thickness of the wall (at four locations, for circular samples)
h—Height of the sample
l—Length of the sample (for tensile test samples)
δ—Thickness of the sample (for tensile test samples)
b—Width of the sample (for tensile test samples)
m_0—Mass after oven drying (24 h @ 105^0C)
m_1—Mass before oven drying.

3.3 Testing

When obtaining samples for testing, six culms per each species of bamboo were used. The arrangement and the number of samples per culm are illustrated in Fig. 4.

3.3.1 Compressive Strength Test

The compressive strength parallel to the fibres was evaluated using the Universal Testing Machine, according to the ISO 22157:2019 Standards. In this test, the sample was kept between the loading plates (Fig. 5a), and an axial compression load was provided. The ultimate strength (load per unit area) and the density were calculated by assuming that the samples are uniformly cylindrical.

3.3.2 Tensile Strength Test

The tensile strength parallel to the fibres was evaluated using the Hounsfield Tensometer, according to the ISO 22157:2019 Standards (Fig. 5b). In this test, an axial tensile load was provided to a sample, which was prepared as a lengthwise strip. The average cross-section was considered when calculating the ultimate strength and the density.

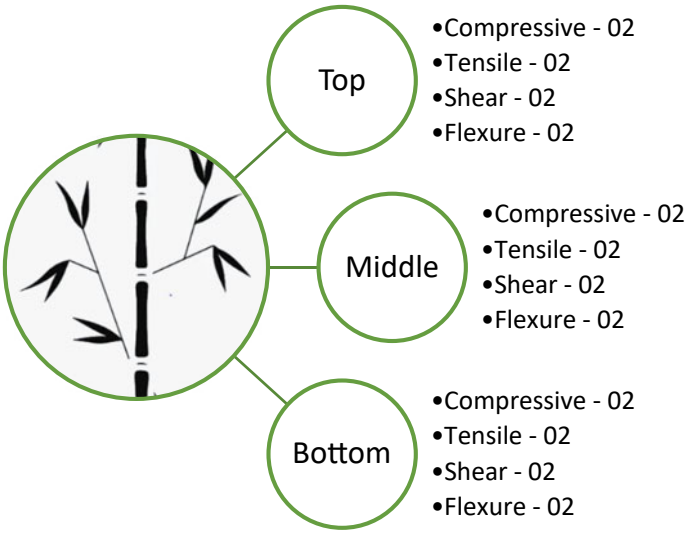

Fig. 4 Arrangement of samples

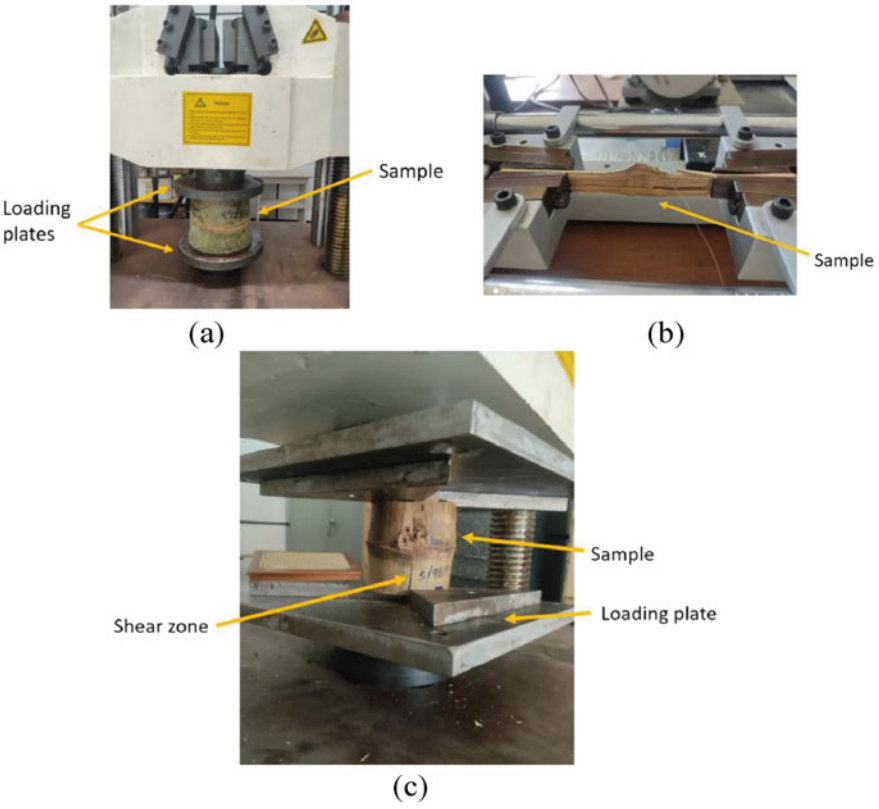

Fig. 5 Experimental setups to determine the **a** compressive strength, **b** tensile strength and **c** shear strength

3.3.3 Shear Strength Test

Using a pair of loading plates with the shape of a bow tie, the shear strength test parallel to fibres was conducted. In this test also the sample was subjected to an axial compression load provided by the Universal Testing Machine (Fig. 5c). With the special design of the loading plates—in the shape of a bow tie—the compression load was converted to a shear load which was distributed on four similar shear planes of the sample.

During the above three tests, applied load and displacement have been recorded to develop the stress–strain curves for each strength parameter.

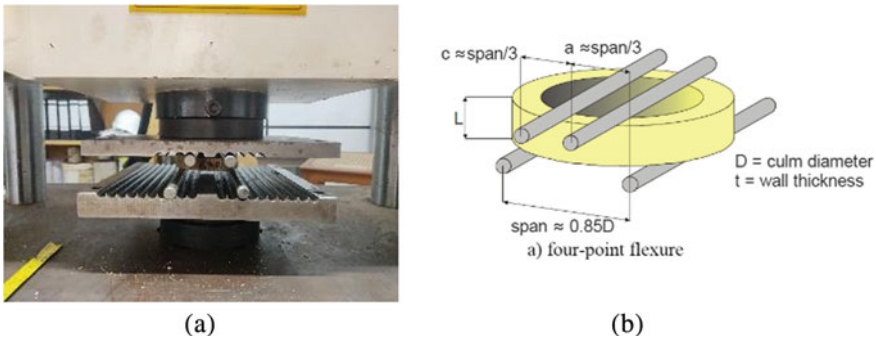

Fig. 6 **a** Experimental test setup for the Flat Ring Flexural Strength Test, **b** schematic diagram of the apparatus

3.3.4 Flat Ring Flexural Strength Test

The flat ring flexural test was also conducted with the universal testing machine as a compression test (Fig. 6a). Specially fabricated two plates with four rollers were used because the test was based on the four-point bending test as introduced by Virgo et al. [13]. The span was taken as 0.85D and the shear span was also maintained with respect to the diameter of the sample. The schematic diagram of the apparatus is shown in Fig. 6b.

4 Results

4.1 Culm Data

Table 2 shows a sample recording of culm measurement data along the long span for the species *Bambusa valgaris*. The distance between demarcation lines was 298 mm, which was a constant for all the measurements. The station of nodes or internodes stands for the distance from the "0" node or "1" internode (first node or internode on the bottom side of the pole) to each other node or internode. $Length$ indicates the length of the internode and D stands for the external diameter of the node or internode which is calculated by Eq. 1.

$$D = X_L + X_R - 298 \tag{1}$$

Table 2 Culm data measurements (all length measurements are in mm)

Node	Station	X_L	X_R	D	Internode	Station	Length	X_L	X_R	D
0	0	201	187	90	–	–	–	–	–	–
1	255	205	180	87	1	128	255	199	175	76
2	535	212	174	88	2	395	280	204	173	79
3	812	220	169	91	3	674	277	214	164	80
4	1100	230	162	94	4	956	288	218	161	81

4.2 Experimental Results

The preliminary results of the four experiments for the Giant bamboo are shown in Table 3. Furthermore, the results obtained from the middle portion of the culms (3 different culms per test) are indicated and typical stress–strain curves for each test case are also presented for a single sample. These cases are highlighted in Table 3.

Figure 7 provides typical stress–strain plots obtained from the four tests. For all the loading cases, the initial part of loading causes an approximate linear variation between stress and strain. Upon reaching the maximum stress value, the load-bearing capacity of the samples has reduced for all loading cases. However, except

Table 3 Preliminary test results for Giant bamboo

Sample ID	Test	D.avg. (mm)	T.avg. (mm)	Height (mm)	Cross sec. area (mm^2)	Failure load (KN)	Strength (MPa)	Moist. content (%)
5M2	Compressive	144.5	8.3	105.4	3551.5	142.05	39.99	14.5
6M1	Compressive	174.4	10.9	95.6	5509.5	226.40	41.1	15.1
4M2	Compressive	141.4	8.3	68.3	3470.6	173.95	50.1	13.9
6M2	Shear	174.6	10.7	97.3	4164.4	19.15	4.6	14.7
4M2	Shear	143	7.5	69.1	2073	23.55	11.36	13.8
8M1	Shear	153.5	9.2	97.3	3580.6	47.9	13.37	13.9
Sample ID	Test	D.avg. (mm)	T.avg. (mm)	Height (mm)	Shear span (mm)	Failure load (KN)	MoR (MPa)	Moist. content (%)
10M2	Flexure	147.2	10.1	31.2	35	1.95	10.41	13.9
8M1	Flexure	154.5	9.6	32.7	35	1.20	6.14	13.9
5M1	Flexure	148	8.2	39.3	35	2.35	9.74	14.7
Sample ID	Test	δ. avg. (mm)	b.avg. (mm)	Length (mm)	Cross sec. (mm)	Failure load (KN)	Strength (MPa)	Moist. content (%)
16M2	Tensile	9.1	28.3	600	257.5	40.80	158.4	14.5
8M2	Tensile	8.0	18.1	600	144.8	23.87	164.8	14.1
6M1	Tensile	9.6	20.6	600	197.7	29.02	146.8	14.9

for the compressive strength test, a sudden decrease in stress can be seen beyond the maximum stress point, which is indicative of brittle failure. This highlights the significance of using adequate margins of safety during the design stage of structures with bamboo.

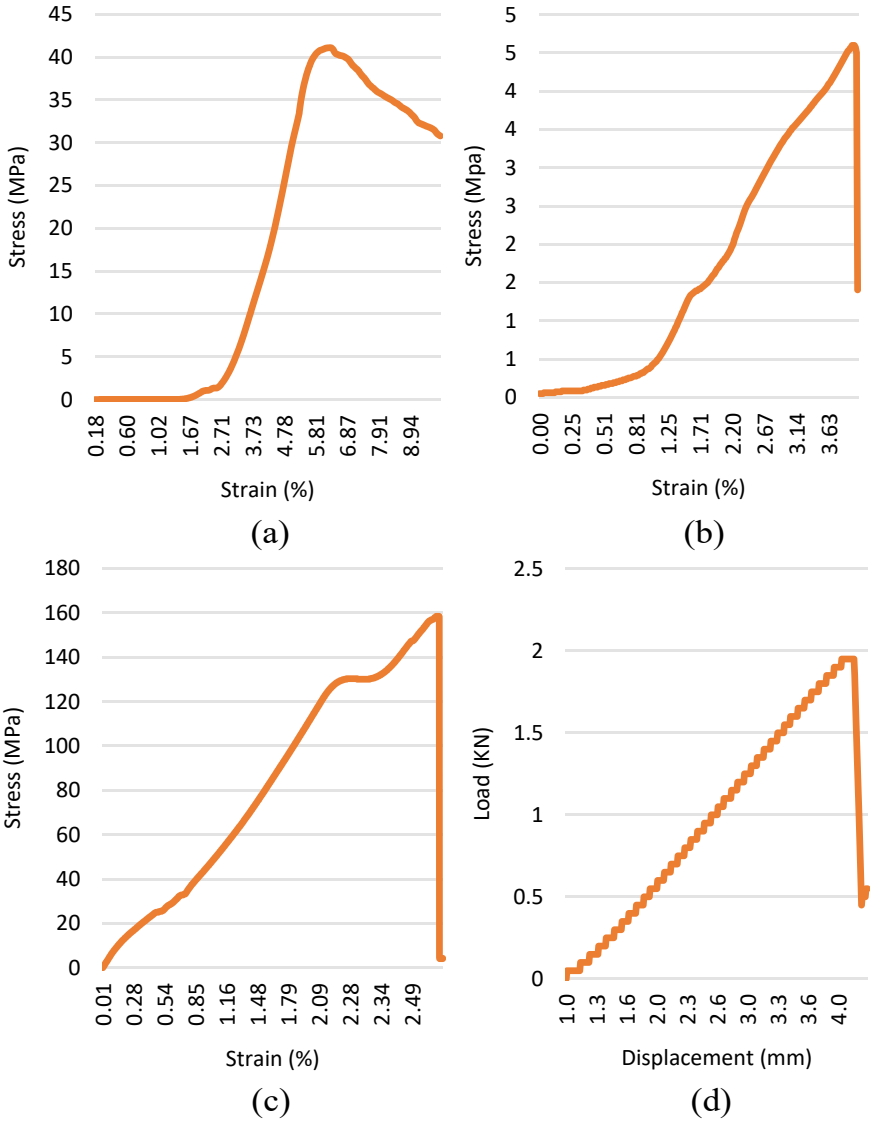

Fig. 7 Typical stress–strain graphs from **a** compressive strength test, **b** shear strength test, **c** tensile strength test and **d** flat ring flexural strength test

It must be noted that for the Flat Ring Flexural Test, the load–displacement curve is shown (Fig. 7(d)) because the result (strength) is presented as the Modulus of Rupture, where the direction of the deflection of the sample is different to that of the stress on the fibres. Calculation of the Modulus of Rupture was carried out using Eq. 2.

$$\text{MoR} = \frac{3 \times \text{Failure Load} \times \text{Shear Span}}{2 \times \text{thickness} \times \text{height}^2} \tag{2}$$

5 Discussion

The preliminary results presented in the previous section are part of a comprehensive experimental program designed towards evaluating the structural properties of Sri Lankan bamboo with the aim of improving its utilization in structural engineering-related applications. The above testing procedure and its results could be used when designing structures with bamboo either in full culm form or in engineered form. Scaffolding, elevated platforms, and ladders are the most common applications of full culm bamboo in Sri Lanka. Therefore, compressive strength, tensile strength, and shear strength parallel to fibres could efficiently ensure the accurate design of those structures. As an example, self-supporting step ladders can be manufactured using full culm bamboo instead of using Aluminium, for which all the above test parameters are necessary for its structure such as compression—acting on the main vertical members, tension—acting on the diagonal members which are used to improve the rigidity, shear, and modulus of rupture—important at the connections between members, etc.

Amongst various structural applications of bamboo, bamboo-reinforced concrete is a novel trend in the construction industry as an alternative to conventional steel-reinforced concrete. To negate the concrete's adverse behaviour under compression, steel which is a durable material in tension is embedded. Amidst all the advantages of steel including high tensile strength, durability, ductility, etc. there are several disadvantages of steel in terms of sustainability which discourages the use of steel in the construction industry. Steel consumes high energy proportions in the process of manufacturing, and it has comparatively higher coefficients of embodied carbon and energy. Additionally, the use of steel in reinforced concrete, mainly in developing countries, is costly. Due to these reasons, bamboo has been proposed as a potential candidate to replace steel in reinforced concrete. However, limited studies have been conducted on this, in the Sri Lankan context. Therefore, the results obtained from this study will be beneficial to explore the design aspects of bamboo-reinforced concrete in the Sri Lankan context.

Apart from that, it was observed that Giant Bamboo has a tensile strength of 150 MPa which is significantly higher than ABS (Acrylonitrile Butadiene Styrene)

plastic (one of the most used materials when manufacturing household and industrial tools) which is less than 50 MPa. Furthermore, the results obtained for stress–strain relationships under different parameters are significant when introducing the mechanical properties of Sri Lankan bamboo. Through this research, testing will be continued by using commonly available four bamboo species with a broad range of samples to give a reliable outcome to the industry. This will in fact provide a basis to choose the most suitable species for a given application. When focusing on the literature, the use of bamboo with structural applications is currently being practiced in many countries successfully. However, in Sri Lanka, bamboo is used only for light-duty applications, even though it is a resource that is freely available. Therefore, the outcome of this research will help to improve the utilization of Sri Lankan bamboo for more sustainable development in the country.

6 Conclusion

In conclusion, the potential of Sri Lankan bamboo to be used in structural engineering-related applications was discussed. To this end, the present research aims to fulfill an existing research gap which is the absence of reliable experimental data related to the structural strength properties of the species of bamboo found in Sri Lanka. While the preliminary results look promising, further experiments are to be conducted using the standard testing methods presented in the paper and also the obtained results will be compared with existing results for other species of bamboo, to develop a comprehensive set of reliable information, which can be used by structural engineers.

References

1. ISO 2019 ISO 22157—Bamboo structures—Determination of physical and mechanical properties of bamboo culms—Test methods. 1st ed
2. Amunugoda P 2019 "Bamboo species for specific uses, invasiveness, plantation cultivation, raw material supply chain" [PowerPoint Presentation]. Stake Holder Workshop on Bamboo Sector Road Map/Country Action/Strategic Plan Development. Colombo, Industrial Technology Institute (ITI)
3. Gatóo A, Sharma B, Bock M, Mulligan H, Ramage M 2014 Sustainable structures: Bamboo standards and building codes. Proc Inst Civ Eng—Eng Sustain 167(5): 189–196
4. Guadua Bamboo n.d. Bamboo stem anatomy. [online] Available at: <https://www.guaduabamboo.com/blog/bamboo-stem-anatomy> [Accessed 22 July 2022]
5. Kampinga C, Smit M, Bilow M 2015 Bamboo, The building material of the future. Architectural Engineering, TU Delft
6. Kariyawasam D 1998 Bamboo resources and utilization in Sri Lanka. [online] Available at: <https://www.bioversityintertional.org/fileadmin/bioversity/publications/Web_version/572/ch31.htm>

7. Komitu Architects 2022 Building with bamboo, the basics, building trust international. Available at: https://www.buildingtrustinternational.org/BTIBambooToolkit.pdf [Accessed 10 August 2022]
8. Lv H, Chen M, Ma X, Li J, Zhang B, Fang C, Fei B (2019) Effects of different drying methods on bamboo's physical and mechanical properties. For Prod J 68(04):445–451
9. Marspedia 2021 Embodied energy. [online] Available at: <https://marspedia.org/Embodied_energy> [Accessed 5 August 2022]
10. Sharma B, Gatóo A, Bock M, Ramage M (2015) Engineered bamboo for structural applications. Constr Build Mater 81:66–73
11. Syeda A, Shrujal B, Kumar J 2014 A case study on bamboo as green building material. Int J Eng Adv Technol (IJEAT) 4(2)
12. Vipushnan R 2019 Structural testing and characterization of Sri Lankan yellow bamboo—Bambusa vulgaris. Unpublished MSc thesis, University of Moratuwa
13. Virgo J, Moran R, Harries K, Garcia J, Platt S 2017 Flat ring flexure test for full-culm bamboo. In: 7th International Conference on Non-Conventional Materials and Technologies (17thNOCMAT 2017)

Life Cycle Assessment Perspectives in Buildings

A Study of Circular Economy Strategies for the Life Cycle of Building Construction Projects: A Systematic Review

H. C. Victar and K. G. A. S. Waidyasekara

Abstract The Circular Economy (CE) is a philosophy that aims to alter current consumption and output trends that are putting a tremendous strain on the earth and its environment. It has been extensively reviewed throughout the world as an alternative to the old economic model, namely, "purchase, consumption and dispose", as well as a solution to the complication of efficient use of resources and environmental pollutions. CE applies theories from environmental economics, ecological economics and industrial ecology to the business-sustainability relationship. By adopting particular CE strategies, savings may occur by creating proper systems to retain value and keep the resources flowing in a circular manner. This approach would close materials and components, energy, and water loops and minimize the associated potential environmental impacts. This has driven recent researchers to investigate the CE strategies that are applicable to the construction industry. However, those studies are limited to given local contexts, thus, the knowledge is scattered. Therefore, this paper aims to analyse CE strategies for the life cycle of building collectively, using a systematic review towards understanding the significance. Filtering the search from the period of 2015 to 2022 offered 18 out of 113 research articles suitable for the analysis. The collected data shows high variability related to different stages of building and suitable CE strategies for the building life cycle. According to the review, preconstruction, construction building renovation, use and operate, demolitions and repurpose, material recovery and production stages account for the highest portion of the life cycle of building for which CE strategies could be highly incorporated. Further, it is expected that the collective reviews regarding building stages would better guide the categorisation of CE strategies in the built environment.

Keywords Circular economy · Strategies · Life cycle of building and built environment

H. C. Victar (✉) · K. G. A. S. Waidyasekara
Department of Building Economics, University of Moratuwa, Moratuwa, Sri Lanka
e-mail: hasithchathuranga122@gmail.com

© The Author(s), under exclusive license to Springer Nature Singapore Pte Ltd. 2023

R. Dissanayake et al. (eds.), *ICSBE 2022*, Lecture Notes in Civil Engineering 362,
https://doi.org/10.1007/978-981-99-3471-3_27

1 Introduction

The concept of circular economy (CE) and the sustainability trend in the construction industry motivate conducting studies on recycling and reusing waste streams included in the reprocessed aggregate. When building materials and components are no longer needed for the intended use, they are deemed as waste, hastening destructions to the ecosystem, increasing environmental costs and generating resource scarcity [13]. Realising that, the European Union has designated building and demolition waste as a priority stream and raw materials supplies have been limited, depicting that the circular economy has gained traction in the construction industry.

Currently, most structures are demolished after 20 years on average because they no longer suit the needs of their users, lowering the service life of the facility and for the rapid emergence of new investment returns. Further, the author confirmed that the failure to remove and replace building systems and components leads to higher energy and material consumption, increased waste output, and lack of spatial and technological adaptability of the buildings. As a result, circularity sets the stage for more sustainable and resilient buildings and cities [32].

Sustainable development refers to the development that meets current demands without compromising the ability of the future generation [15]. Jones [22] confirmed that incorporating circular design into projects during the construction and planning stages of a developed asset provides an opportunity for material scarcity. Products, systems and complete building constructions are meant to survive longer with a higher residual value, and it will be easier to maintain, repair, upgrade, refurbish, remanufacture, or recycle.

Simultaneously, new materials can be produced and sourced, particularly bio-based materials that are less resource intensive or totally recyclable and designers can engage with possible partners who may be interested in post-use development [35]. Electronic information sets, that detail the properties of construction materials, and products and product systems that allow material value recovery is considered as the "Material Passport". The resources and materials utilised in a construction project can be documented and handed along from the supplier to the construction contractor, the owner and eventually the demolition contractor [33].

Furthermore, in circular building, design entails adaptability, flexibility and deconstruction at its core. Materials and components need to endure numerous life cycles, depending on the purpose of use [37]. Therefore, durability and resilience are two features that need to be taken into account when selecting materials and components to ensure there is no loss in quality or value over time and through the use cycles. The use of materials and components that are energy-intensive increases the building embodied energy and the life cycle energy consumption. In Europe, energy consumption related to building products ranges from 5 to 10% [24]. Another critical parameter to reduce energy consumption during the use phase is enhancing the building's thermal insulation. High-quality materials are needed to provide the

necessary services and thermal comfort for the users [43]. Hence, materials selection and contextual building design and layout should be considered to reduce energy consumption throughout the building's life cycle [37].

As mentioned by Esa et al. [10], buildings are built, used, adapted, repurposed and demolished with design interventions. In addition, the extraction of raw materials, material production, transportation to the construction site, construction, operation, maintenance and renovation of a building, and demolition and disposal of construction waste could all be quantified in the life cycle assessment of a building [23]. However, the building's life cycle focus must aid decision-making when selecting the best technology available and reducing the environmental effect of structures through design or refurbishment [27]. Buildings that appear to be cost-effective in the short term may have significant maintenance or WM expenses and elevated items may have extraordinarily high production costs that never get recovered [47]. Further, materials, components and products at the end of their life are processed into closed loops (of technical or biological metabolisms) and become resources for future life cycles. Instead, in the linear economy, materials, components, by products and products at the end of their life become waste and are disposed of in landfills or incinerated [3]. As a result, the chosen life cycle of building for evaluating and improving the implementation of CE principles in buildings must include all activities from the cradle to the grave [16]. The life cycle of building stages has quickly become essential to an organisation's strategy implementation. The goal of the life cycle stages in CE is to retain products, components and materials at their greatest utility and value at all times, separating technological and ecological cycles [34].

The foregoing review confirms that much work has been done on the CE strategies for construction industry. However, those studies are limited to given local contexts, thus, the knowledge is scattered in the global context over the last decade. Hence, reviewing the available literature will help to identify the global trends concerning CE strategies for life cycle of building collectively using a systematic review towards understanding the significances and whereby it can assure the stakeholders on deciding on the application of CE principles. Therefore, this paper aims to explore the analysis of CE strategies for the life cycle of building projects in the construction industry using a systematic review approach.

2 Research Methods: Systematic Review

Initially, there should be a sound research question supported by a precise aim and objective in order to develop the search strategy, the eligibility criteria and the study selection, which are very important components of the Systematic Reviews and Meta-Analyses (PRISMA) checklist [9, 25]. Accordingly, the aim of carrying out a systematic review was defined as "categorisation of CE strategies for life cycle of building in the construction industry". According to [5], the PRISMA guideline consists of a four-phased flow diagram where it passes through the phases of identification, screening, eligibility and inclusion.

2.1 Research Strategy

To derive the search terms for the systematic review, the research question was formulated using a PICO template. PICO is typically used in formulating clinical questions in medical disciplines, but recently this approach has been applied in social science studies [9]. Miller & Alvarado [30] stated that there are two types of templates when applying the PICO method: "PICO" (P-Population, I-Intervention, C-Comparison, O-Outcome) and "PICo" (P-Population, I-Interest and Co-Context)", which have slight differences considering the features of the study. Since the research question in this study is generic and there is no "Comparison" component, the research question was constructed utilising the "PICo" template. Accordingly, "How has the term 'Built environment Strategies' been established as a definition by previous scholars within the context of Circular Economy?" was formulated as the research question through PICo. Thereafter, a comprehensive logic grid as presented in Table 1 was prepared by inserting the alternative terms that can be used for each component of PICo.

Table 1 identified the key terms of the research question and indicated the synonyms, which have been used in past literature as the substitutes for each key term. Aromataris and Riitano [4] described that such a logic grid helps to build up the final search string for a study by combining each key term and synonyms. Further, the search string was developed using the terms of the logic grid (Table 1) by merging the key terms and their alternatives using "OR" along the raw and merging the terms in different rows using "AND". Moreover, truncation was used for the word "Built environment" as "Built Environ*". The initial search was based upon title, abstract and keywords. However, many of the articles did not mention the terms "Definition" and "Explanation" within the title, abstract and keywords even though they are included within the text. Therefore, in order to avoid losing the relevant important articles while conducting the initial search, the terms "Definition" and "Explanation" were eliminated from the string. Accordingly, "Circular Strategies" OR "Circular Principles" OR "Circular Practices" OR "Life Cycle of Building" AND "Built Environ*" was the search string used. A similar protocol was followed for Web of Science. Once all the search terms were identified and finalised, the final search string was developed as follows.

Table 1 Logic grid with identified keywords

Population	Interest	Context
Definition	Circular strategies	Built environment strategies
Explanation	Circular principles	
	Circular practices	
	Life cycle of building	

Table 2 Filters assigned for the literature search

Inclusion Criteria	Exclusion criteria	Rationale
Sources published in English language	Sources published other than in English	English is the international and the universal language
Publication year from 2015 to 2022	Publication year prior to 2015	Avoiding out of date results, plus the adequacy of 7 years' articles for the review
Published and u published sources		Unpublished articles also have the latest results
Research areas: Circular Economy, Environmental Science, Life Cycle Assessment, Engineering, Waste management	Research areas: Computer Science, Medicine, Business Management and Accounting, Economics and Finance	Research areas related to built environment strategies
Document type: Articles, Conference Papers, Book Chapters, Reviews, Books		

2.2 Study Selection

It is necessary to have eligibility criteria for the selection, which need to be appraised for the validity, applicability and comprehensiveness of a review [25]. These selection criteria identify the inclusion and exclusion conditions for the study. Table 2 presents the selection criteria for this study.

Finally, as per Table 2, the filtering criteria were developed through Scopus initially and the final search string was:

TITLE-ABS-KEY ("Circular Strategies" OR "Circular Principles" OR "Circular Practices" OR "Life Cycle of Building" AND "Built Environ*") AND (LIMIT-TO (PUBYEAR, 2022) OR LIMIT-TO (PUBYEAR, 2021) OR LIMIT-TO (PUBYEAR, 2020) OR LIMIT-TO (PUBYEAR, 2019) OR LIMIT-TO (PUBYEAR, 2018) OR LIMIT-TO (PUBYEAR, 2017) OR LIMIT-TO (PUBYEAR, 2016) OR LIMIT-TO (PUBYEAR, 2015)) AND (LIMIT-TO (DOCTYPE, "articles") OR LIMIT-TO (DOCTYPE, "conference papers") OR LIMIT-TO (DOCTYPE, "reviews") OR LIMIT-TO (DOCTYPE, "chapters") OR LIMIT-TO (DOCTYPE, "books")) AND (LIMIT-TO (SUBJAREA, "CIRCULAR ECONOMY") OR LIMIT-TO (SUBJAREA, "LIFE CYCLE ASSESMENT") OR LIMIT-TO (SUBJAREA, "ENVIORNMRNT SCIENCE")) AND (LIMIT-TO (LANGUAGE, "English")).

2.3 Data Extraction

The title, abstract, keywords, authors' names and affiliations, journal name and year of publication, access type and source name of the identified records were exported

to a MS Excel spreadsheet. In this stage (1) articles not relating to circular economy, (2) articles not contributing to the applicability of circular economy strategies for built environment and (3) articles that were completely irrelevant to the research area were excluded. The appropriateness of whether to include the unsure articles in the second screening process was discussed among two reviewers and, thus, the final set of articles was concluded for the second screening. In the second screening process, the full texts of all the relevant articles were reviewed and the necessary data was extracted. According to Masnoon et al. [29], a pre-defined extraction sheet should be prepared in order to ensure consistent data extraction in this exercise. As per this study, the extracted items used were the definitions of CE in built environment and its associated terms to elaborate how the distinction of the definition of disaster preparedness was made and defined. The selection of the articles is depicted in the flow diagram as illustrated in Fig. 1.

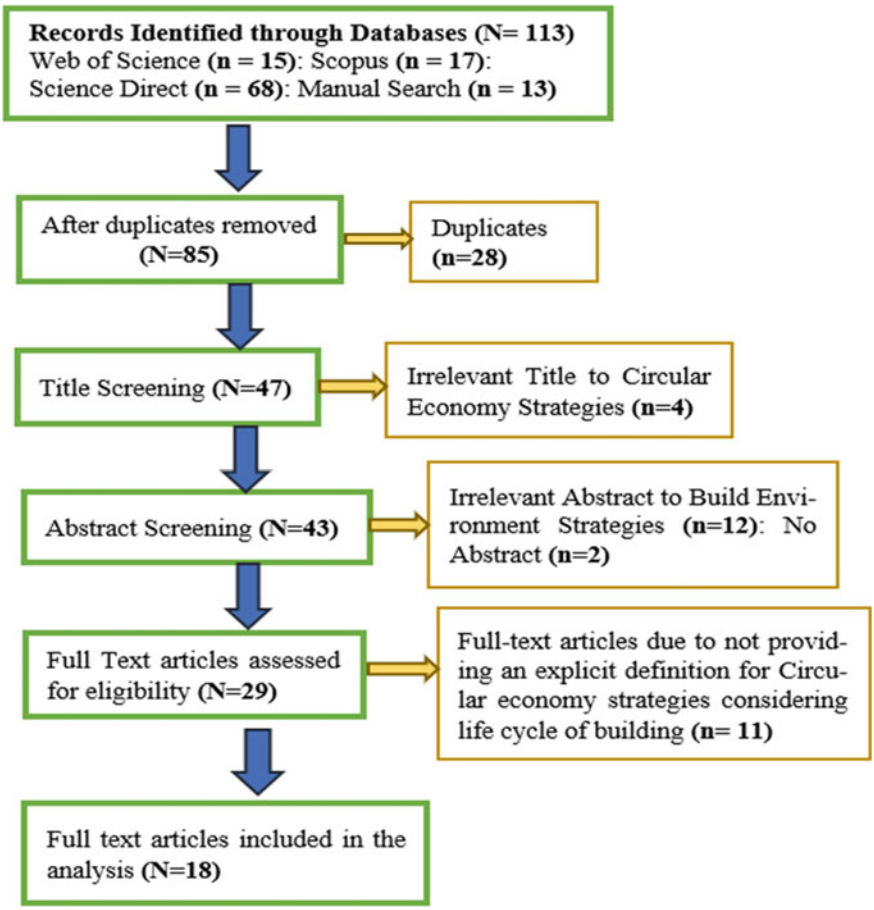

Fig. 1 Flow diagram of study selection

As per Fig. 1, 11 articles were selected for the full-text screening. Finally, 18 articles were obtained for the in-depth analysis.

3 Results and Discussions: CE Strategies for Life Cycle of Building

Buildings that appear to be cost-effective in the short term may have significant maintenance or waste management expenses and elevated items may have extraordinarily high production costs that never get recovered [47]. Further, materials, components and products at the end of their life are processed into closed loops (of technical or biological metabolisms) and become resources for future life cycles. Instead, in the linear economy materials, components, products and products at the end of their life become waste and are disposed of in landfills or incinerated [3]. As a result, the chosen life cycle of building for evaluating and improving the implementation of CE strategies in buildings must include all activities from the cradle to the grave [16].

The life cycle of building stages has quickly become essential to an organisation's strategy implementation. The goal of the life cycle stages in CE is to retain products, components and materials at their greatest utility and value at all times, separating technological and ecological cycles [34]. Akanbi et al [2] conceptualised the CE model in the construction industry in seven stages: Extraction/use of virgin raw materials, material inputs, design process, construction and production process, distribution, collection and recycling. Whereas Akanbi et al. [2], Esa et al. [10], Gálvez-Martos et al. [12], Yeheyis et al. [44] and Foster [11] have identified main five stages namely preconstruction, construction and building renovation, use and operate, demolitions and repurpose, and material recovery and production.

The main aim of these approaches is minimisation of waste and efficient use of material can be achieved by alternatives focused on optimising the planning, control and management for future construction. During the analysis, the study has adopted five main categorisations and Table 3 represents the CE strategies adaptation for the life cycle of a building in construction industry from previous authors.

Table 3 illustrates measures of strategies in CE and their adaptation for the life cycle of buildings in the construction industry. Individual strategies establish feedback loops between segments of the building life cycle. Closing material loops is a popular method for circularising a manufacturing process or supply chain. As previously stated, circularisation originates with material and extends to people in this situation. The building life cycle is depicted as a circular product supply chain in Table 3. Each segment of the circle is linked indefinitely. Strategies are categorised by the building life cycle phase and circularity zone, which indicates how well they achieve CE goals.

Table 3 CE strategies identified by authors according to life cycle stages of building

Stages of life cycle of building	CE strategies	A	B	C	D	E	F	G	H	I	J	K	L	M	N	O	P	Q	R	S	T	U	V	W	X	Y	Z	A1	B1
Preconstruction	Design for adaptability of existing buildings	●	●			●	●	●	●	●					●	●		●		●	●	●	●					●	
	Use of a simulation in a BIM model to analyse the reuse potential of the materials of different types of designs early in the project	●	●			●	●	●				●		●	●			●	●	●			●				●	●	●
	Use of Life-cycle analysis to find the benefits of reusing different types of materials in the design stage	●	●			●			●	●	●	●			●	●			●	●			●	●	●		●	●	
	Design and use of modular buildings		●		●			●		●	●				●	●				●	●		●	●				●	●
	Design for energy efficiency including passive methods	●				●	●				●			●				●	●						●	●			●
	Minimise or eliminate need for new construction materials by reducing space and multi-tasking space	●	●	●					●	●					●	●	●			●	●			●		●		●	●
	Substitute non-renewable energy supply with purchased or produced renewable energy		●			●	●								●		●	●			●		●		●	●			●

(continued)

Table 3 (continued)

Stages of life cycle of building	CE strategies	A	B	C	D	E	F	G	H	I	J	K	L	M	N	O	P	Q	R	S	T	U	V	W	X	Y	Z	A1	B1
	Use of material stock data to help reuse of materials of a new building	●	●		●				●					●	●			●			●		●		●		●		
	Design for disassembly			●	●				●		●						●	●				●	●			●	●	●	●
	Use local and culturally significant materials	●				●				●	●			●	●								●						●
	Consider environmental significant materials	●			●			●	●										●		●								
	Enhance materials durability to extend lifespan												●	●							●	●					●	●	
	Consider environmental impact scenarios in design selection	●	●	●	●										●	●	●											●	●
	Increase or maintain green space				●	●		●	●	●									●				●	●	●				
	Enhance lifespan maintainability			●												●										●	●		●
	Design achieves Green Building certificate (LEED, BREEAM, DGNB)	●			●				●			●			●		●			●			●		●		●		●
	Reduce transport by choosing local sourcing	●	●																								●		●

(continued)

Table 3 (continued)

Stages of life cycle of building	CE strategies	A	B	C	D	E	F	G	H	I	J	K	L	M	N	O	P	Q	R	S	T	U	V	W	X	Y	Z	A1	B1
	Substitute new materials with used materials wherever possible	●	●		●				●			●		●			●			●		●			●		●		●
	Substitute fossil fuel intensive materials with bio-based materials	●				●					●				●				●				●				●		●
Construction and building renovation	Limit disturbance of trees, soils and habitat	●	●				●					●						●									●		
	Change of use of materials, by giving it ownership to the manufacturers to reuse the materials after the end of life of the first building	●	●			●			●		●						●					●					●		
	Waste reduction	●			●					●				●		●			●						●				
	Off-site construction						●					●									●		●	●				●	
	Development of material passports				●						●						●										●		
	Reuse of secondary materials in the production of building materials	●		●				●						●		●			●				●		●				●
	Revive traditional construction techniques and materials		●						●								●						●						●

(continued)

Table 3 (continued)

Stages of life cycle of building	CE strategies	A	B	C	D	E	F	G	H	I	J	K	L	M	N	O	P	Q	R	S	T	U	V	W	X	Y	Z	A1	B1
	Implement brownfield developed development through hazardous waste remediation and/ or solid waste removal on site	●			●		●			●				●				●				●			●			●	
	Reuse salvaged materials from other demolitions		●			●			●				●					●			●		●					●	
	Use abandoned or neglected cultural heritage sites	●		●		●		●	●								●			●						●			
	Increase or maintain green space	●				●																							●
Use and operate	Recover water and energy with modern and historical/ cultural technology and design		●						●				●			●		●				●				●			
	Use of a tool to evaluate the state of materials during the lifespan and end of life of a building			●							●		●		●					●			●				●		●
	Minimise recuperative maintenance with preventive maintenance	●			●		●			●			●					●			●			●				●	●

(continued)

Table 3 (continued)

Stages of life cycle of building	CE strategies	A	B	C	D	E	F	G	H	I	J	K	L	M	N	O	P	Q	R	S	T	U	V	W	X	Y	Z	A1	B1
	Implement fee for services arrangements that reduce materials inputs and incentivise	●			●			●		●				●			●					●					●		●
	Improve users low carbon mobility options			●		●				●		●			●							●					●		
	Implement, incentivise and encourage users to achieve high rates of product reuse and recycling	●				●				●					●					●							●		●
	Implement use arrangements that meet needs without individual ownership			●					●			●							●			●							
	Promote and incorporate local and reginal agriculture ensure public access to greenspace and other spaces			●										●		●			●						●		●		
	Create habitats for animal and insects			●			●		●		●										●			●					
	Improve users' quality of life			●						●					●														●
	Improve land through pollutant remediations and increasing nutrients in soil	●					●										●			●					●				

(continued)

Table 3 (continued)

Stages of life cycle of building	CE strategies	A	B	C	D	E	F	G	H	I	J	K	L	M	N	O	P	Q	R	S	T	U	V	W	X	Y	Z	A1	B1
	Provide facilities for easy collection of recyclable materials and biomass for compost			●		●				●					●						●					●			●
	Strive to increase proportions of purchase and produced renewable energy whilst phasing out fossil fuels			●			●						●			●				●				●			●		
	Implement ongoing energy efficiency strategy			●			●					●	●								●			●	●				
	Measure energy efficiency continuously													●					●				●					●	
Demolitions and repurpose	Evaluation options for transformation and adaptive reuse				●							●		●				●				●				●			
	Implement materials passports to facilitate reuse	●	●					●			●			●					●					●					●
	Communicate availability of a heritage site for adaptive reuse						●		●							●				●					●	●			

(continued)

Table 3 (continued)

Stages of life cycle of building	CE strategies	A	B	C	D	E	F	G	H	I	J	K	L	M	N	O	P	Q	R	S	T	U	V	W	X	Y	Z	A1	B1
	Implement dismantling and disassembly and recovery rather than complete demolitions			●				●			●					●		●					●				●		
	Analyse the potential for reuse or recycling of existing materials and if it is feasible compared to using new materials		●			●			●		●		●					●			●					●		●	
	Create new value chains from demolition waste	●					●												●						●			●	
	Use of a circularity tool to evaluate existing buildings and give the best possible solutions to refurbishment				●						●				●								●				●		●
	Deconstruction of building structures and parts		●					●								●		●			●						●		
Material recovery and production	Using harvested materials, construction elements and building materials again to meet their original or a different function	●					●						●				●				●			●		●			

(continued)

Table 3 (continued)

Stages of life cycle of building	CE strategies	A	B	C	D	E	F	G	H	I	J	K	L	M	N	O	P	Q	R	S	T	U	V	W	X	Y	Z	A1	B1
	Returning used products to working conditions and is limited to assembly and reassembly of fixed parts			●			●				●		●						●			●				●		●	
	Improving the quality of used products by simple actions of disassembling, inspection and replacing of components		●			●		●			●		●					●					●			●			●
	Quality for used products, according to specific standards which are as rigorous as those for new products	●			●				●					●							●			●	●				
	Use of recycled content in the manufacturing of construction materials has environmental benefits over the use of raw materials		●		●					●						●				●								●	
	Possibility of applying other recovery alternatives such as energy	●				●				●				●				●			●					●			
	Substitute for natural resources for backfilling embankments			●						●					●					●				●				●	

A: [6], **B:** [11], **C:** [14], **D:** [17], **E:** [18], **F:** [19], **G:** [20], **H:** [31], **I:** [26], **J:** [28], **K:** [38], **L:** [42], **M**: [44], **N:** [45], **O:** [46], **P:** [40], **Q**: [39], **R:** [1], **S:** [41], **T:** [8], **U:** [21]; **V:** [24], **W:** [37], **X:** [36], **Y:** [7], **Z:** [10], **A1**: [15], **B1**: [21]

4 Conclusions

This paper has presented the results of the systematic review carried out on the available studies regarding the CE strategies for stages of life cycle of building. The systematic review determined CE strategies in a built environment that needs to be taken into account when selecting materials and components to ensure no loss in quality or value over time and use cycles. The use of materials and components that are energy-intensive increases the building embodied energy and therefore, the life cycle energy consumption and other effective environmental discriminations in building could be sustainable. As per the systematic review, it seems that most of the studies that discussed the practices of CE strategies considered global context in built environment. Design and use of modular buildings, Design for energy efficiency including passive methods, Minimising or eliminate need for new construction materials by reducing space and multi-tasking space, etc. are basic CE strategies that are incorporated in preconstruction stage of life cycle of building. At Construction and building renovation stage, supporting CE strategies such as Waste reduction, Off-site construction, Development of material passports, Reuse of secondary materials in the production of building materials, Review traditional construction techniques and materials were identified. Further, Evaluation options for transformation and adaptive reuse, Implementing materials passports to facilitate reuse, Communicate availability of a heritage site for adaptive reuse, etc. were strategies identified under developed Demolitions and repurpose stage of life cycle of building. Finally, using harvested materials, construction elements and building materials again to meet their original or a different function. Returning used products to working conditions and limiting to assembly and reassembly of fixed parts, etc. are main circular-built environment strategies that are applicable at Material recovery and production stage in building. It is expected that the future studies would perform a comprehensive assessment of CE strategies concerning achieving waste management and involvement of direct and indirect stakeholders in the process.

References

1. Ajayabi A, Chen H-M, Zhou K, Hopkinson P, Wang Y, Lam D (2019) REBUILD: Regenerative buildings and construction systems for a circular economy. IOP Conf Ser: Earth Environ Sci 225:012015. https://doi.org/10.1088/1755-1315/225/1/012015
2. Akanbi LA, Oyedele LO, Akinade OO, Ajayi AO, Davila Delgado M, Bilal M, Bello SA (2018) Salvaging building materials in a circular economy: A BIM-based whole-life performance estimator. Resour Conserv Recycl 129:175–186. https://doi.org/10.1016/j.resconrec.2017.10.026
3. Andrews D (2015) The circular economy, design thinking and education for sustainability. Local Econ: J Local Econ Policy Unit 30(3):305–315. https://doi.org/10.1177/0269094215578226
4. Aromataris E, Riitano D (2014) Systematic reviews: Constructing a search strategy and searching for evidence. AJN, Am J Nurs 114(5):49–56. https://doi.org/10.1097/01.NAJ.0000446779.99522.f6

5. Benachio GLF, Freitas M, do C. D., & Tavares, S. F. (2020) Circular economy in the construction industry: A systematic literature review. J Clean Prod 260:121046. https://doi.org/10.1016/j.jclepro.2020.121046
6. Charles RG, Davies ML, Douglas P 2016 Third generation photovoltaics—Early intervention for circular economy and a sustainable future. Electron Goes Green (EGG): 1–8. https://doi.org/10.1109/EGG.2016.7829820
7. Çimen Ö (2021) Construction and built environment in circular economy: A comprehensive literature review. J Clean Prod 305:127180. https://doi.org/10.1016/j.jclepro.2021.127180
8. Diaz A, Schöggl J-P, Reyes T, Baumgartner RJ (2021) Sustainable product development in a circular economy: Implications for products, actors, decision-making support and lifecycle information management. Sustain Prod Consum 26:1031–1045. https://doi.org/10.1016/j.spc.2020.12.044
9. Eriksen MB, Frandsen TF 2018 The impact of patient, intervention, comparison, outcome (PICO) as a search strategy tool on literature search quality: A systematic review. J Med Libr Assoc 106(4). https://doi.org/10.5195/jmla.2018.345
10. Esa MR, Halog A, Rigamonti L (2017) Developing strategies for managing construction and demolition wastes in Malaysia based on the concept of circular economy. J Mater Cycles Waste Manage 19(3):1144–1154. https://doi.org/10.1007/s10163-016-0516-x
11. Foster G (2020) Circular economy strategies for adaptive reuse of cultural heritage buildings to reduce environmental impacts. Resour Conserv Recycl 152:104507. https://doi.org/10.1016/j.resconrec.2019.104507
12. Gálvez-Martos J-L, Styles D, Schoenberger H, Zeschmar-Lahl B (2018) Construction and demolition waste best management practice in Europe. Resour Conserv Recycl 136:166–178. https://doi.org/10.1016/j.resconrec.2018.04.016
13. Geissdoerfer M, Savaget P, Bocken NMP, Hultink EJ (2017) The circular economy—A new sustainability paradigm? J Clean Prod 143:757–768. https://doi.org/10.1016/j.jclepro.2016.12.048
14. Geldermans RJ (2016) Design for change and circularity—Accommodating circular material & product flows in construction. Energy Procedia 96:301–311. https://doi.org/10.1016/j.egypro.2016.09.153
15. Ghaffar SH, Burman M, Braimah N (2020) Pathways to circular construction: An integrated management of construction and demolition waste for resource recovery. J Clean Prod 244:118710. https://doi.org/10.1016/j.jclepro.2019.118710
16. Ghisellini P, Ripa M, Ulgiati S (2018) Exploring environmental and economic costs and benefits of a circular economy approach to the construction and demolition sector. A literature review. J Clean Prod 178:618–643. https://doi.org/10.1016/j.jclepro.2017.11.207
17. Gorgolewski M (2006) The implications of reuse and recycling for the design of steel buildings. Can J Civ Eng 33(4):489–496. https://doi.org/10.1139/l06-006
18. Huang Y-F, Azevedo SG, Lin T-J, Cheng C-S, Lin C-T (2021) Exploring the decisive barriers to achieve circular economy: Strategies for the textile innovation in Taiwan. Sustain Prod Consum 27:1406–1423. https://doi.org/10.1016/j.spc.2021.03.007
19. Jaillon L, Poon CS (2014) Life cycle design and prefabrication in buildings: A review and case studies in Hong Kong. Autom Constr 39:195–202. https://doi.org/10.1016/j.autcon.2013.09.006
20. Jiménez-Rivero A, García-Navarro J (2017) Best practices for the management of end-of-life gypsum in a circular economy. J Clean Prod 167:1335–1344. https://doi.org/10.1016/j.jclepro.2017.05.068
21. Joensuu T, Edelman H, Saari A (2020) Circular economy practices in the built environment. J Clean Prod 276:124215. https://doi.org/10.1016/j.jclepro.2020.124215
22. Jones P 2018 The construction industry and the circular economy. 13
23. Khasreen M, Banfill PF, Menzies G (2009) Life-cycle assessment and the environmental impact of buildings: A review. Sustainability 1(3):674–701. https://doi.org/10.3390/su1030674
24. Klein N, Ramos T, Deutz P (2020) Circular economy practices and strategies in public sector organizations: An integrative review. Sustainability 12(10):4181. https://doi.org/10.3390/su12104181

25. Liberati A, Altman DG, Tetzlaff J, Mulrow C, Gøtzsche PC, Ioannidis JPA, Clarke M, Devereaux PJ, Kleijnen J, Moher D (2009) The PRISMA statement for reporting systematic reviews and meta-analyses of studies that evaluate health care interventions: Explanation and elaboration. J Clin Epidemiol 62(10):e1–e34. https://doi.org/10.1016/j.jclinepi.2009.06.006
26. Maerckx A-L, d'Otreppe Y, Scherrier N (2019) Building circular in Brussels: An overview through 14 inspiring projects. IOP Conf Ser: Earth Environ Sci 225:012059. https://doi.org/10.1088/1755-1315/225/1/012059
27. Malmqvist T, Glaumann M, Scarpellini S, Zabalza I, Aranda A, Llera E, Díaz S (2011) Life cycle assessment in buildings: The ENSLIC simplified method and guidelines. Energy 36(4):1900–1907. https://doi.org/10.1016/j.energy.2010.03.026
28. Mangialardo A, Micelli E 2018 Rethinking the construction industry under the circular economy: Principles and case studies. In Bisello A, Vettorato D, Laconte P, Costa S (eds), Smart and sustainable planning for cities and regions. Springer International Publishing, pp 333–344. https://doi.org/10.1007/978-3-319-75774-2_23
29. Masnoon N, Shakib S, Kalisch-Ellett L, Caughey GE (2017) What is polypharmacy? A systematic review of definitions. BMC Geriatr 17(1):230. https://doi.org/10.1186/s12877-017-0621-2
30. Miller FA, Alvarado K (2005) Incorporating documents into qualitative nursing research. J Nurs Scholarsh 37(4):348–353. https://doi.org/10.1111/j.1547-5069.2005.00060.x
31. Minunno R, O'Grady T, Morrison G, Gruner R, Colling M (2018) Strategies for applying the circular economy to prefabricated buildings. Buildings 8(9):125. https://doi.org/10.3390/buildings8090125
32. Murray A, Skene K, Haynes K (2017) The circular economy: An interdisciplinary exploration of the concept and application in a global context. J Bus Ethics 140(3):369–380. https://doi.org/10.1007/s10551-015-2693-2
33. Nasir MHA, Genovese A, Acquaye AA, Koh SCL, Yamoah F (2017) Comparing linear and circular supply chains: A case study from the construction industry. Int J Prod Econ 183:443–457. https://doi.org/10.1016/j.ijpe.2016.06.008
34. Norouzi M, Chàfer M, Cabeza LF, Jiménez L, Boer D (2021) Circular economy in the building and construction sector: A scientific evolution analysis. J Build Eng 44:102704. https://doi.org/10.1016/j.jobe.2021.102704
35. Peña C, Civit B, Gallego-Schmid A, Druckman A, Pires A, C.-, Weidema, B., Mieras, E., Wang, F., Fava, J., Canals, L. M. i, Cordella, M., Arbuckle, P., Valdivia, S., Fallaha, S., & Motta, W. (2021) Using life cycle assessment to achieve a circular economy. Int J Life Cycle Assess 26(2):215–220. https://doi.org/10.1007/s11367-020-01856-z
36. Pimentel-Rodrigues C, Siva-Afonso A 2019 Reuse of resources in the use phase of buildings. Water solutions. IOP Conf Ser: Earth Environ Sci 225: 012050. https://doi.org/10.1088/1755-1315/225/1/012050
37. Rahla K, Mateus R, Bragança L (2021) Implementing circular economy strategies in buildings—From theory to practice. Appl Syst Innov 4(2):26. https://doi.org/10.3390/asi4020026
38. Sanchez B, Haas C (2018) Capital project planning for a circular economy. Constr Manag Econ 36(6):303–312. https://doi.org/10.1080/01446193.2018.1435895
39. Sigrid Nordby A (2019) Barriers and opportunities to reuse of building materials in the Norwegian construction sector. IOP Conf Ser: Earth Environ Sci 225:012061. https://doi.org/10.1088/1755-1315/225/1/012061
40. Tallini A, Cedola L (2018) A review of the properties of recycled and waste materials for energy refurbishment of existing buildings towards the requirements of NZEB. Energy Procedia 148:868–875. https://doi.org/10.1016/j.egypro.2018.08.108
41. Velenturf APM, Purnell P (2021) Principles for a sustainable circular economy. Sustain Prod Consum 27:1437–1457. https://doi.org/10.1016/j.spc.2021.02.018
42. Wang J, Zhong H, Tang W, Rajagopal R, Xia Q, Kang C, Wang Y (2017) Optimal bidding strategy for microgrids in joint energy and ancillary service markets considering flexible ramping products. Appl Energy 205:294–303. https://doi.org/10.1016/j.apenergy.2017.07.047

43. Winkler H (2011) Closed-loop production systems—A sustainable supply chain approach. CIRP J Manuf Sci Technol 4(3):243–246. https://doi.org/10.1016/j.cirpj.2011.05.001
44. Yeheyis M, Hewage K, Alam MS, Eskicioglu C, Sadiq R (2013) An overview of construction and demolition waste management in Canada: A lifecycle analysis approach to sustainability. Clean Technol Environ Policy 15(1):81–91. https://doi.org/10.1007/s10098-012-0481-6
45. Yu N, Wei T, Zhu Q (2015) From passive demand response to proactive demand participation. IEEE Int Conf Autom Sci Eng (CASE) 2015:1300–1306. https://doi.org/10.1109/CoASE.2015.7294278
46. Yuan H (2013) A SWOT analysis of successful construction waste management. J Clean Prod 39:1–8. https://doi.org/10.1016/j.jclepro.2012.08.016
47. Zabalza Bribián I, Aranda Usón A, Scarpellini S (2009) Life cycle assessment in buildings: State-of-the-art and simplified LCA methodology as a complement for building certification. Build Environ 44(12):2510–2520. https://doi.org/10.1016/j.buildenv.2009.05.001

A Study on the Applicability of Sustainable Features to Sri Lankan Road Construction

M. G. K. Hasanthika, V. Disaratna, and H. C. Victar

Abstract One of the most significant contributions to environmental damage is construction activities. The main environmental challenges of Sri Lanka are soil erosion, loss of wildlife habitat, coastal degradation, water pollution, waste disposal, urban air pollution, marine pollution, and hydrological and climate changes. According to the final result of the survey of construction industries in Sri Lanka 2017–2018 (2020), roads and railways have the largest contract value out of all contract types. Sri Lanka has a road network of roughly 100,000 km, according to the Sri Lanka Road Network Assessment. The road sector creates the highest level of greenhouse gas directly, by fossil energy used in mining, transportation, and paving works, and indirectly emissions coming from vehicles. This has driven recent researchers to investigate sustainable approaches to the road construction industry. However, those studies are limited to given local contexts, thus, the knowledge is scattered. Therefore, this paper aims to analyse the applicability of sustainable features to Sri Lankan Road construction towards understanding the significance. The research apprehends a qualitative approach inclusive of expert interviews and manual content analysis for data analysis. When compared to others, energy harvesters (sun energy, thermoelectric energy, geothermal energy, piezoelectric energy and composite energy) and xanthan gum biopolymer as an alternative material had a lower application. Furthermore, as new sustainable features for Sri Lankan Road construction, solar power lights for roads, tyre retaining walls, tree planting, reducing road noise with asphalt pavement design, construction waste management, advanced dust controlling methods, sustainable excavation methods and alternative materials such as fly ash were identified.

Keywords Road construction · Sustainable features · Pollution · Alternatives

M. G. K. Hasanthika · V. Disaratna · H. C. Victar (✉)
Department of Building Economics, University of Moratuwa, Moratuwa, Sri Lanka
e-mail: hasithchathuranga122@gmail.com

© The Author(s), under exclusive license to Springer Nature Singapore Pte Ltd. 2023

R. Dissanayake et al. (eds.), *ICSBE 2022*, Lecture Notes in Civil Engineering 362,
https://doi.org/10.1007/978-981-99-3471-3_28

1 Introduction

According to estimates of global pollution, building and construction activities are responsible for 23% of air pollution in cities, 50% of climate change through gases, 40% of drinking water pollution, 50% of landfill pollution due to construction activities and 50% of ozone depletion pollution [4]. Construction activities can harm the environment by destroying natural flora, water bodies, natural sand hills, gardens and parking places, as well as causing damage to plant roots, root destruction, and dam damage. As a result, construction pollution has an impact on all humans, animals, the environment and the natural ecosystem [14]. When it comes to water pollution, heavy diesel vehicles, paints and solvents are left on site, garbage is dumped illegally and mixes with rainwater, and waste is washed away by rain and mixes with water bodies, increasing water ecotoxicity [7]. Construction waste is not properly treated and managed; one of the results is water pollution [14]. Water contamination is the main cause of death in humans all over the world. Water pollution also has an impact on our oceans, lakes, rivers and drinking water [16]. Water contamination has an impact on soil and vegetation health and quality. Some water pollution impacts can be seen right away, while some water pollution effects could not be demonstrated immediately [1]. Although, traffic is the most significant source of air pollution. Pollution caused by traffic is becoming widely available in urban areas. CO, NO_2 and PM are examples of such pollutants [15]. Polluted air contains less or more hazardous materials, pollutants, or contaminants and that create a hazard to public health [26]. Heavy dust production during construction has a significant influence on human health since it causes illnesses such as silicosis and lung cancer in those who work in this environment [14].

Road construction projects are made up of a variety of materials and parts that are manufactured using a variety of ways. Material production and construction take a lot of resources and energy [24]. Although road development generates CO_2 emissions, however additional greenhouse gases (CH_4, N_2O, hydrofluorocarbons, perfluorocarbons and SF_6) also contribute to global warming and climate change. Further, the transportation sector will contribute to 97% of worldwide greenhouse gas emissions until 2030. The environmental loads of raw material extraction, production and transportation, as well as earthmoving and final disposal, are significant during road construction and necessitate taking into account the effects of atmospheric emissions, natural resource consumption, energy demands and waste generation [25]. In earth-moving operations, a variety of types of machinery are employed. The effort to build mechanical control systems for this machinery has been rapidly rising in recent years [20]. Construction and other equivalent activities generate huge amounts of industrial waste, including petroleum combustion by-products, foundry sand, construction and demolition garbage, and steel slags [6]. Thus, investigation of the sustainable approaches to development for road construction is very important to circumvent environmental, economic and social issues relating to the Sri Lankan

Road construction industry. To attain this aim, the study had to address the following objectives:

1. To assess the applicability of sustainable features to Sri Lankan Road construction
2. Introduce new suggestions of sustainable features for Sri Lankan Road construction.

2 Literature Review

2.1 Road Construction and Environmental Pollution

According to Stripple [27], road construction differs from other production processes due to the various construction conditions, including different sites and within the same segment. Roads are one of the largest and most complex megaprojects in the construction industry, affecting millions of people at the project's conclusion [10]. Road constructions can be considered as horizontally arranged, joined and complementary activities, and complementary set of operations, each one produces boundary conditions that affect the others [23]. The last century has seen a significant rate of urbanisation, resulting in the quick construction of roads and infrastructural development [29]. Road wastes represent a major share of the 510 million tons of annual construction wastes [17], and road maintenance needs 2.7 billion tons of natural aggregate every year [3]. As a result, most governments encourage the recycling of road materials in order to conserve natural resources and reduce the amount of waste that goes to landfill [8]. If the construction material sector implements eco-friendly techniques and energy-saving or low-environmental-load construction materials are utilised on construction sites, overall environmental loads can be lowered greatly [24]. Along with economic and social development, a speedy, convenient, comfortable and sustainable transportation network should be developed immediately [18].

2.2 Sustainable Features Used in Material Usage for Road Construction

2.2.1 Recycle Material

In most countries road materials recycling rate (80–100%) is high. The majority of the time, road material is processed in a mobile recycling factory and recycled back into the same road or into a nearby project. Old road materials are sometimes blended with other comparable materials in a fixed plant and used for various projects and needs in the area [12]. Waste materials were employed as a substitute for aggregates or as an addition to standard building materials. It is possible to recycle reclaimed/recycled asphalt, Portland cement concrete pavements, bottom ash, fly ash and steel slag [5].

According to Chowdhury et al. [6], industrial by-products such as coal fly ash, coal bottom ash and recycled concrete pavement can be used in significant amounts as a whole or partial replacement for natural aggregates. Demolition trash from a variety of constructions, such as roads, bridges, buildings, and industrial waste products, is used to make mixed aggregates. It consists of a mix of unbound materials, crushed concrete, asphalt granulate [12]. Waste asphalt can also be returned to an asphalt plant and mixed into a fresh mixture [28].

If traditional natural materials are recycled, it helps to avoid possible negative environmental impact. Asphalt is the road surfacing material which is widely used in every type of road construction [21]. The majority of countries state that reclaimed asphalt should be used to make new asphalt layers [12]. Reducing resources and flotation in oil prices also made bitumen one of the most expensive materials used in the road construction; therefore, it is more important to be recycled [19].

2.2.2 Alternative Materials

Stripple [27] states according to the record data of natural aggregate has two parts such as emission from crushing, and emission from energy industry because use of energy in crushing process. It is critical to introduce substitute materials for natural aggregates in order to reduce the usage of the original materials, the requirement for resource conservation, and the lengthening of transportation distances [22]. Zoorob and Suparma [30] reported simple bituminous concrete mixtures use recovered plastics, primarily polypropylene and low-density polyethylene. Waste tyres are another commonly used recycled material in asphalt pavement construction [13]. To examine the environmental impact of several alternative materials for road construction in Finland use fly ash, steel slag and broken concrete. According to this, using industrial by-products as a substitute for natural aggregate can help to mitigate some of the environmental damage.

2.2.3 Used Local Materials (Materials Which Are Available in Construction Area)

The cost of delivering road materials to a building site is divided into two parts: the cost of the raw material at the quarry or gravel quarry and the cost of transportation. And the financial as well as the environmental expenses, which are typically the highest for those two. As a result, locally accessible materials are clearly chosen for construction [28].

3 Methodology

Fellows and Liu [9] stated that research methodology comprises the entire process ranging from theoretical underpinning to data collection and analysis. Moreover, there are three types of research approaches such as, qualitative, quantitative, and mixed approach which provide the directions to the research study [11]. In terms of this study, since it was intended to investigate the applicability of sustainable features to Sri Lankan Road construction and to identify new sustainable features to Sri Lankan Road construction that required subjective and attitudinal information, a qualitative research choice was adopted. Further, Basias & Pollalis [2] explained that qualitative approach contributes to exploring emerging concepts through in-depth investigation. The authors further explained that when the research problem is a why, what and how type questions, qualitative approach is suitable. Moreover, to the author, a small sample of respondents is adequate when undertaking qualitative approach. This study adopted qualitative data collection method, and in-depth expert interviews were carried out to investigate the applicability of sustainable features to Sri Lankan Road construction and to identify new sustainable features to Sri Lankan Road construction. The data collection was done using structured interviews in order to get faster responses and unbiased and comparable answers. The expert interviews were accomplished by interviewing fifteen respondents of various professions in the Sri Lankan Road construction industry. Table 1 reflects their disciplines, years of experience and awareness of each practice related to the research.

4 Results and Discussions

4.1 Application of Sustainable Features for Road Construction in Sri Lanka

The findings from the expert interviews were analysed with the use of content analysis form in order to compare the views of different experts on sustainable features used in the Sri Lankan construction industry. The analysis shall be thus presented as per the order of questions given in the interview. Table 2 presented all respondents' impressions about mentioned sustainable features for road construction in Sri Lanka.

4.1.1 Alternative Materials

Industrial Wastes like Fly Bottom, and Coal Ashes

Coal ash is a collection of by-products created during coal burning. Fly ash is a type of coal ash that floats up into the exhaust stacks. The heavier component of coal ash that settles on the ground in the boiler is known as bottom ash.

Table 1 Profile of the interviewees

Coding for Panel Experts	Designation	Criteria						Accessibility
		Compulsory Qualification (CQ)		Additional qualifications (Satisfy at least three of the following criteria) (AQ)				
		CQ1	**CQ2**	**AQ1**	**AQ2**	**AQ3**	**AQ4**	
R1	Civil Engineer							
R2	Quantity Surveyor				–	–		
R3	Traffic Engineer				–			
R4	Architecture				–			
R5	Project Manager							
R6	Construction Manager					–		
R7	Civil Engineer					–		
R8	Civil Engineer							
R9	Chief QS							
R10	Managing Director							
R11	Project Manager							
R12	Planning Engineer						–	
R13	Earth Resource Engineer						–	
R14	Land Surveyor				–			
R15	Planning Engineer							

CQ1: More than 10 Years of Experience in the Road Construction Industry
CQ2: Knowledge and Best Practical Understanding of Road Construction
AQ1: Graduate in Bachelor of Science Discipline
AQ2: Postgraduate Degree/Master Related to Construction Management
AQ3: Corporate Member of Chartered Professional Institution
AQ4: Research Experience Regarding Road Construction and Management

Table 2 Usage of sustainable features for road construction in Sri Lanka

Sustainable Features		Use, Not or Rarely Use used in Sri Lanka														
		R1	**R2**	**R3**	**R4**	**R5**	**R6**	**R7**	**R8**	**R9**	**R10**	**R11**	**R12**	**R13**	**R14**	**R15**
Alternative materials	Industrial wastes like fly bottom, and Coal ashes	*U*	*RU*	*U*	*U*	*RU*	*RU*	*RU*	*RU*	*U*	*RU*	*RU*	*RU*	*U*	*U*	*RU*
	Cement Stabilised Rammed Earth	*RU*	*RU*	*RU*	*RU*	*RU*	*RU*	*RU*	*RU*	*RU*	*RU*	*RU*	*RU*	*U*	*RU*	*RU*
	Cement blocks	*U*	*U*	*U*	*U*	*U*	*U*	*RU*	*RU*	*RU*	*U*	*U*	*RU*	*U*	*U*	*U*
	Xanthan gum biopolymer	*NU*	*NU*	*NU*	*NU*	*NU*	*NU*	*NU*	*NU*	*NU*	*NU*	*NU*	*NU*	*NU*	*NU*	*NU*
Recycled materials	Demolition materials such as crushed bricks	*U*	*RU*	*U*	*U*	*RU*	*RU*	*RU*	*RU*	*RU*	*RU*	*RU*	*U*	*RU*	*NU*	*U*
	Reclaimed concrete	*RU*	*RU*	*RU*	*U*	*U*	*RU*	*RU*	*RU*	*RU*	*RU*	*RU*	*RU*	*U*	*RU*	*RU*
Used local materials		*RU*	*RU*	*RU*	*RU*	*RU*	*RU*	*RU*	*RU*	*RU*	*RU*	*U*	*RU*	*RU*	*U*	*RU*
Construction waste management		*U*	*RU*	*RU*	*RU*	*RU*	*RU*	*RU*	*RU*	*RU*	*U*	*RU*	*RU*	*U*	*RU*	*U*
Dust controlling		*RU*	*RU*	*RU*	*RU*	*RU*	*RU*	*RU*	*RU*	*RU*	*RU*	*U*	*RU*	*RU*	*RU*	*U*
Renewable energy	Renewable energy collection systems	*RU*	*RU*	*RU*	*RU*	*RU*	*RU*	*RU*	*RU*	*RU*	*RU*	*RU*	*RU*	*RU*	*RU*	*RU*
	Piezoelectric energy harvesters, Sun energy harvesting, thermoelectric energy harvesting, geothermal energy harvesting and composite energy harvesting	*NU*	*NU*	*NU*	*NU*	*NU*	*NU*	*NU*	*RU*	*NU*	*RU*	*NU*	*NU*	*RU*	*NU*	*NU*

USE-(**U**); RARELY USE-(**RU**); NOT USE-(**NU**)

All of the respondents agreed upon the use of industrial wastes like fly bottom, and Coal ashes for road construction in Sri Lanka but most of the respondents mentioned that it is rarely used. **R5** mentioned that Coal Bottom Ash has been used as an aggregate substitute, cement substitute, bitumen improver and asphalt pavement filler. **R3** respondent mentioned that Coal Bottom Ash is a viable solution for cement replacement in concrete, with the potential to lower concrete carbon footprints. And also, **R3** mentioned it is more economical than cement. **R4** mentioned that natural aggregate substitution with Coal Bottom Ash has lowered construction costs and reduced the demand for natural aggregate harvesting. **R1** mentioned that "*when the asphalt mixtures incorporating bottom ash were exposed to repeat indirect tensile stiffness modulus testing under dynamic loading, they showed a greater resistance to fatigue cracking*". And also, in literature review mentioned industrial wastes like fly and bottom ashes are frequently used to reduce the amount of cement in concrete mixtures or soil stabilisation operations. And the use of coal ash in the road sector will improve not only the material shortage for road construction but will also decrease the environmental impact caused by ash disposal issues. **R5** and **R8** respondents also mentioned that using fly ash as waste material from industry is environmentally friendly.

Cement Stabilised Rammed Earth (CSRE)

The majority of respondents agreed upon the use of Cement Stabilised Rammed Earth for road construction in Sri Lanka, but they mentioned it is used rarely in Sri Lanka. Respondents **R1**, **R13** and **R15** mentioned that CSRE is a very sustainable construction approach that uses very little energy and produces very little waste during the construction process. The respondents further pointed out that Cement stabilised rammed earth technology enables for the construction of road using locally accessible materials, which is an excellent solution in less developed areas. **R7** mentioned that one of the most important aspects of rammed earth technology is determining the optimum moisture level of the soil–cement combination but there are no specific standards for creating the CSRE mixture's composition that was the issue. **R6** mentioned that "*Cement Stabilised Rammed Earth cannot be used for all types of roads construction because it is not technological advance method*". Therefore, it is only used in rural areas. **R7** mentioned that Cement Stabilised Rammed Earth is a low energy required construction method and highly economical method of road construction compared to other construction methods. And also, in literature review mentioned Cement Stabilised Rammed Earth is one such alternative construction material with a better probability of long-term sustainability.

Cement Blocks

Respondents **R1** and **R6** mentioned that cement blocks pavers require less maintenance than plain concrete or asphalt pavement. Cement block does not require

polishing on the top surface of the pavement and will not require any finishing surfaces. **R9** mentioned that cement block paving is very durable because cracking is not developed when they are properly interlocked with each other. **R8** mentioned that it is simple to install and does not necessitate the use of any large machinery or equipment and pavers can handle any type of traffic, including light, medium and heavy. **R13** mentioned that "*when compared to a solid plain surface, paver blocks are more environmentally friendly because water and chemical discharge from solid surfaces can damage natural water sources*". Concrete block pavements have long been known to let a certain%age of surface water into the bedding sand. This is called Rainwater infiltration and it is environmentally advantage. **R14** mentioned that cannot be used for all types of roads therefore limited usage. In literature review mentioned the initial cost cement blocks is higher than other types of paving materials, the overall cost is lower.

Xanthan Gum Biopolymer

Majority of the interviewers disagreed upon the use of Xanthan gum biopolymer for road construction in Sri Lanka. The literature review mentioned because of their great strengthening efficiency and low environmental impact, xanthan gum biopolymer is used as an alternative material for road construction (mostly shoulders and subbases) in Sri Lanka and other countries with similar climates and socioeconomic situations. However, in expert interviews, all the respondents said, "*It is not used in Sri Lanka*".

4.1.2 Recycled Materials

Demolition Materials Such as Crushed Bricks

All of the interviewers agreed upon the use of demolition materials such as crushed bricks for road construction in Sri Lanka but most of the respondents mentioned that it is rarely used. In literature review mentioned the road construction materials such as reclaimed concrete and demolition waste are currently not widely available in Sri Lanka. Respondents **R1**, **R3**, **R4** and **R15** mentioned that Recycling of demolition materials such as crushed bricks is solution for construction waste management and reducing environment pollution. **R9** mentioned that reduce the environmental impact of extracting and consuming virgin resources, as well as the production of new materials**. R14** mentioned that "*recycling asphalt, concrete, and rubble into aggregate or fresh asphalt and concrete products is used but not common*". Saving money while safeguarding natural resources is a benefit of recycling demolition materials. **R5** mentioned that disposal expenditures are reduced, which lowers overall construction costs. As a result, less disposal facilities will be needed, potentially lowering environmental concerns. **R10** mentioned that improve the health and safety conditions by controlling the hazardous materials. However, **R11** mentioned that sometimes those materials are not up to the required quality level and standards.

Reclaimed Concrete

Respondents **R1**, **R7**, **R8** and **R12** mentioned that reclaimed concrete is a solution for construction waste management and reducing environment pollutions. **R5** mentioned that reclaimed concrete is used as an alternative material for the aggregate requirement for roads and it gives economic benefits. However, **R4** mentioned that sometimes those materials are not up to the required quality level and standards.

Used Local Materials

Every one of the respondents agreed upon the use of used local materials for road construction in Sri Lanka without only one respondent but most of the respondents mentioned that it is rarely used. **R3** mentioned that reduce construction cost and environmental pollutions generated from the unloading activities of materials. **R5** mentioned that transportation of materials to the construction site contributes to a significant amount of construction project costs. Therefore, reducing the need for transportation is one approach to reduce those costs and using local materials we can achieve this.

Construction Waste Management

R5 mentioned that it can also include recycling facilities, which recover energy and value from waste materials. Respondents **R1**, **R2**, **R6** and **R8** mentioned construction waste management has environmental benefits such as less waste going to landfill and less usage of natural resources, lower CO_2 emissions from materials production, transportation, and use, as well as recycling and waste disposal and lower probability of environmental incidents. **R13** mentioned that "*construction waste management increase business predictions in the local community by creating jobs and economic activity in the recycling industry, especially when deconstruction and selective demolition methods are applied*". However, **R5** mentioned that waste management sector necessitates a significant investment in terms of equipment, personnel, training and regulatory compliance.

Dust Controlling

The majority of respondents agreed upon the use of dust controlling for road construction in Sri Lanka, but all of the respondents mentioned that it is rarely used. All of the respondents mentioned that dust control reduces environmental pollution generated from construction and improves the health and safety conditions in the site. **R3** mentioned that in "*Sri Lanka most of the times used wet watering as a dust controlling method, therefore, it has some disadvantages such as road become dry out fast, needs regular application and excess application makes road muddy*".

4.1.3 Renewable Energy

Renewable Energy Collection Systems

All of the interviewers agreed upon the use of renewable energy collection systems for road construction in Sri Lanka, but all of the respondents mentioned that it is rarely used. All of the respondents mentioned, "*In Sri Lankan context used only solar power*". Respondents **R1, R3, R4** and **R5** mentioned that solar power has different advantages such as energy-saving lower maintenance requirements, low life cycle cost and solar energy is pollution-free and does not emit greenhouse gases after installation. However, **R7** mentioned that "*material and installation costs of solar power system are high*". For the same quantity of power generation, the size of solar panels varies based on geographical location. It is also disadvantage of solar power system.

Piezoelectric Energy Harvesters, Sun Energy Harvesting, Thermoelectric Energy Harvesting, Geothermal Energy Harvesting and Composite Energy Harvesting

Every one of the experts disagreed upon the use of Piezoelectric energy harvesters, Sun energy harvesting, thermoelectric energy harvesting, geothermal energy harvesting and composite energy harvesting for road construction in Sri Lanka. In expert interviews, all the respondents said, "*It is not used in Sri Lanka*". In literature also not mentioned information regarding that.

4.2 Suitable Sustainable Features for Sri Lankan Road Construction

Respondents are given different kinds of sustainable features mentioning different reasons for having it. **R3** suggested solar power lights for roads considering low life cycle cost, energy saving, and easy maintenance and used tyre retaining walls as retaining wall in road construction considering the following factors: No need to use heavy retaining walls, easy to use, economical, environment friendly, and RDA carried research for use of tyre retaining walls and it has positive characteristics.

R2, **R5** and **R6** suggested tree planting considering environment friendliness, increase Oxygen%age, increase esthetic appearance, and can use for head light cut-off. **R7** suggested reducing road noise with asphalt pavement design because no need to construct noise barriers and economical. Respondents **R1**, **R7**, **R10**, **R12** and **R15** suggested construction waste management because it is reducing environment pollutions, improve the health and safety conditions. Strategic waste management strategies, including as minimising, recycling and reusing waste materials, are critical

for the long-term management of limited resources, and can thus help the environment, construction safety, and the economy. And they suggested use of alternative materials such as fly ash because it is highly economical, use of fly ash is environmentally friendly as the waste materials from industries. **R4** suggested advance dust controlling methods because reduce environment pollutions and improve the health and safety conditions. And also, he suggested sustainable excavation methods because using that can prevent natural disasters and reduce environment pollutions.

5 Conclusions

According to the findings, new biological materials and methods to improve the strength of soils, cement blocks, concrete and demolition materials as an alternative material, industrial wastes like fly and bottom ashes as an alternative materials and dust controlling methods can be considered as most applicable sustainable features to Sri Lankan Road construction. Moreover, embankment filling can be done with coal, cement stabilised rammed earth and used local materials had the high applicability to Sri Lankan Road construction. Energy harvesters (Sun energy, thermoelectric energy, geothermal energy, piezoelectric energy and composite energy) and xanthan gum biopolymer as an alternative material had the lower applicability compared to others. Further, solar power lights for roads, tyre retaining walls, tree planting, reducing road noise with asphalt pavement design, construction waste management, used advance dust controlling methods, used sustainable excavation methods and used alternative materials such as fly ash were identified as new sustainable features for Sri Lankan Road construction through literature review. Considering final outcome of this paper determined, this recommended that all the indicated sustainable features can be implemented in the Sri Lankan context excluding xanthan gum biopolymer as an alternative material without any doubt.

References

1. Ashraf MA, Maah MJ, Yusoff I, Mehmood K 2010 Effects of polluted water irrigation on environment and health of people in jamber, district Kasur, Pakistan. 10(03): 22
2. Basias N, Pollalis Y 2018 Quantitative and qualitative research in business & technology: Justifying a suitable research methodology. 7(1): 15
3. Bleischwitz R, Bahn-Walkowiak B n.d. Sustainable development in the European aggregates industry. 27
4. Brown MT, Ulgiati S 2004 Energy quality, emergy, and transformity: H.T. Odum's contributions to quantifying and understanding systems. Ecol Model 178(1–2): 201–213. https://doi.org/10.1016/j.ecolmodel.2004.03.002
5. Bryngelsson S, Dimberg LH, Kamal-Eldin A 2002 Effects of commercial processing on levels of antioxidants in oats (*Avena sativa* L.). J Agric Food Chem 50(7): 1890–1896. https://doi.org/10.1021/jf011222z

6. Chowdhury R, Apul D, Fry T (2010) A life cycle based environmental impacts assessment of construction materials used in road construction. Resour Conserv Recycl 54(4):250–255. https://doi.org/10.1016/j.resconrec.2009.08.007
7. Cole MA n.d. Air pollution and 'dirty' industries: How and why does the composition of manufacturing output change with economic development? 16
8. Ebrahimi A, Kootstra BR, Edil TB, Benson CH (2012) Practical approach for designing flexible pavements using recycled roadway materials as base course. Road Mater Pavement Des 13(4):731–748. https://doi.org/10.1080/14680629.2012.695234
9. Fellows R, Liu A (2008) Impact of participants' values on construction sustainability. Proc Inst Civ Eng—Eng Sustain 161(4):219–227. https://doi.org/10.1680/ensu.2008.161.4.219
10. Flyvbjerg B (2014) What you should know about megaprojects and why: An Overview. Proj Manag J 45(2):6–19. https://doi.org/10.1002/pmj.21409
11. Guetterman TC, Fetters MD, Creswell JW (2015) Integrating quantitative and qualitative results in health science mixed methods research through joint displays. Ann Fam Med 13(6):554–561. https://doi.org/10.1370/afm.1865
12. Ho W-J, Lee Y-Y, Lin C-H, Yeh C-W (2015) Performance enhancement of plasmonics silicon solar cells using Al_2O_3/In NPs/TiO_2 antireflective surface coating. Appl Surf Sci 354:100–105. https://doi.org/10.1016/j.apsusc.2015.03.009
13. Huang B, Mohammad LN, Graves PS, Abadie C (2002) Louisiana experience with crumb rubber-modified hot-mix asphalt pavement. Transp Res Rec: J Transp Res Board 1789(1):1–13. https://doi.org/10.3141/1789-01
14. Jain G, Gupta V, Pandey M (2016) Case study of construction pollution impact on environment. 4(6):4
15. Jung SJ, Mehta JS, Tong L (2018) Effects of environment pollution on the ocular surface. Ocul Surf 16(2):198–205. https://doi.org/10.1016/j.jtos.2018.03.001
16. Khan DMA 2011 Environmental pollution: Its effects on life and its remedies. 11
17. Ledoux L, Mertens R, Wolff P 2005 EU sustainable development indicators: An overview. Nat Resour Forum 12
18. Li Y, Zhao L, Suo J (2014) Comprehensive assessment on sustainable development of highway transportation capacity based on entropy weight and TOPSIS. Sustainability 6(7):4685–4693. https://doi.org/10.3390/su6074685
19. Liu J, Yi Y, Wang X (2020) Exploring factors influencing construction waste reduction: A structural equation modeling approach. J Clean Prod 276:123185. https://doi.org/10.1016/j.jclepro.2020.123185
20. Maas G, Van Gassel F (eds) 2003 [No title found].
21. Mampearachchi WK 2013 A sustainable road construction material for low volume roads. 13
22. Mroueh U-M, Eskola P, Laine-Ylijoki J 2001 Lifecycle impacts of the use of industrial by-products in road and earth construction. Waste Manag 7
23. Pilger JD, Machado ÊL, de Assis Lawisch-Rodriguez A, Zappe AL, Rodriguez-Lopez DA (2020) Environmental impacts and cost overrun derived from adjustments of a road construction project setting. J Clean Prod 256:120731. https://doi.org/10.1016/j.jclepro.2020.120731
24. Roh S, Kim R, Park W-J, Ban H (2020) Environmental evaluation of concrete containing recycled and by-product aggregates based on life cycle assessment. Appl Sci 10(21):7503. https://doi.org/10.3390/app10217503
25. Rosado LP, Vitale P, Penteado CSG, Arena U (2017) Life cycle assessment of natural and mixed recycled aggregate production in Brazil. J Clean Prod 151:634–642. https://doi.org/10.1016/j.jclepro.2017.03.068
26. Smith KR (2002) Indoor air pollution in developing countries: Recommendations for research †: Indoor air pollution in developing countries. Indoor Air 12(3):198–207. https://doi.org/10.1034/j.1600-0668.2002.01137.x
27. Stripple H 2001 Life cycle assessment of road. 182
28. Thom N, Dawson A 2019a Sustainable road design: Promoting recycling and non-conventional materials. 12

29. University of Moratuwa, Sri Lanaka, Liyanage KLAKT, Waidyasekara KGAS, University of Moratuwa, Sri Lanaka, Mallawaarachchi BH, University of Moratuwa, Sri Lanaka, Pandithawatta TPWSI, University of Moratuwa, Sri Lanaka 2019 Origins of Construction and demolition waste generation in the Sri Lankan construction industry. 01–08. https://doi.org/10.17501/26510251.2019.1101
30. Zoorob SE, Suparma LB (2000) Laboratory design and investigation of the properties of continuously graded Asphaltic concrete containing recycled plastics aggregate replacement (Plastiphalt). Cement Concr Compos 22(4):233–242. https://doi.org/10.1016/S0958-9465(00)00026-3

The Role of Landscape Characteristics on Thermal Environment of Residential Streets in Warm-Humid Colombo

C. Dissanayake and U. G. D. Weerasinghe

Abstract Street vegetation greatly affects the thermal comfort of pedestrians, thus creating habitable urban street landscapes. Nevertheless, the unplanned developments along streets have been a course of thermal discomfort at the pedestrian level. Therefore, the morphology of streets should be carefully considered when trees are introduced to improve outdoor thermal comfort (OTC). This research aims to assess the effects of street characteristics on the thermal comfort of residential streets in two selected local climate zones (LCZ) in Colombo. The research was conducted in five stages; (1) onsite measurements, (2) modelling the study area, (3) mapping the microclimatic and thermal comfort conditions, (4) comparing the results temporally and spatially and (5) developing recommendations. The climate parameters measured onsite were used for simulations in ENVI-met 5.0.3 Bio-met software to analyse the physiologically equivalent temperature (PET) at 1.5 m above ground level on a sunny day at 2.00 pm. Results revealed that comparatively lower Air temperature, relative humidity and higher wind speed improve OTC levels in warm-humid residential streets. Further, morning thermal discomfort conditions have resulted due to either releasing release of the stored heat in the building or high RH values and low wind speed. Streets located completely in compact low-rise LCZ thermally cause more discomfort than streets completely or partially in open low-rise LCZ. Vegetation is the most effective way to improve OTC, especially using large trees with grass. Homogenous shade coverage consistently distributes thermal comfort. However, irrespective of the street axis orientation, shade coverage is more important in terms of enhancing OTC. Planting large trees in residential land plots along narrow streets and medium trees in centre-median on wider roads is highly recommended. ENVI-met shows a strong correlation between measured and simulated Ta, yet, it is recommended to have nesting grids for more accurate results. These findings help professionals in climate-responsive policymaking for urban residential streets since local climate change is in urgent need.

C. Dissanayake (✉)
Center for Cities, University of Moratuwa, Katubedda, Sri Lanka
e-mail: dissanayakec.21@uom.lk

U. G. D. Weerasinghe
Department of Architecture, University of Moratuwa, Katubedda, Sri Lanka

© The Author(s), under exclusive license to Springer Nature Singapore Pte Ltd. 2023

R. Dissanayake et al. (eds.), *ICSBE 2022*, Lecture Notes in Civil Engineering 362,
https://doi.org/10.1007/978-981-99-3471-3_29

Keywords Outdoor thermal comfort · Microclimate · Residential streets · Colombo · ENVI-met

1 Introduction

Daytime outdoor thermal comfort (OTC) is critical due to intensive use of public places during the day, and the microclimatic conditions are affected mostly by incoming solar radiation. This has become a problem in countries with hot and moderate climatic conditions [30] creating heat stress for urbanites during daytime. The unplanned developments lead to thermal discomfort due to alteration of urban morphology, reduction of greenery and increased hard surfaces. Thermal comfort is defined as 'the condition of mind which expresses satisfaction with the thermal environment' (ISO. 7730. ISO Geneva, revised 1990; 1984). Further, as described by Franger [6], the exchange of human body heat to the surrounding urban spaces occurs by conduction, convection, radiation and evaporation. The heat transformation is determined by both the human parameters (clothing insolation and activity level) and physical parameters such as ambient temperature, humidity, thermal radiation and wind speed [10]. Moreover, the urban geometry, surfaces, vegetation and water bodies influence to alter the microclimate and human thermal environment in urban open spaces [2, 37, 33]. Therefore, outdoor thermal comfort (OTC) is a wide-ranging and complex subject matter due to its diverse spatial and temporal characteristics of outdoor environments and its conditions. Accordingly, the physiological and psychological mechanisms have been more challenging [17]. Though the OTC assessments are usually categorised into four levels, namely, physical, physiological, psychological, and social behaviour [12], only the physical and physiological levels of assessments are conducted in this study.

It is clear that the urban streets are more vulnerable to outdoor thermal discomfort due to high hard surface coverage, traffic and activity levels and lack of space for planting. Thus, the improvement of microclimate is crucial in street environments. However, residential areas are more in need of improving OTC since the impact directly affects the well-being of the urbanites. It is important to have a proper understanding on how the urban morphology and landscape design elements alter the microclimate and this provides important thoughts in improving OTC, especially in hot-humid cities [28]. Microclimate and OTC of a street is affected due to the altered duration of incoming solar radiation and the mean radiant temperature (MRT) which is created by various urban forms [27]. Street morphology is a critical factor and previous research has investigated separate parameters such as building density and height of buildings [21]. But later, combined parameters that create different urban forms such as height/width (H/W) ratio, sky view factor (SVF), and the orientation defined by the long axis of streets have been considered. These determinant factors of urban geometry [4] directly influence the transformation of incoming solar radiation into outgoing longwave radiation. This phenomenon significantly impacts the temperature variations in the surrounding environment, which is known as the urban

heat island effect [1]. Considering these microclimate variations, Stewart and Oke [25] has categorised urban or rural spaces into seventeen Local Climate Zones (LCZ). Based on this approach, initial LCZ and sub-classification has been developed for Colombo municipal area. Generally residential areas in Colombo are found under compact low-rise and open low-rise according to initial LCZ classification.

In this research, three residential roads in compact low-rise and open low-rise local climate zones are assessed in terms of understanding the effect of landscape characteristics on microclimate and thermal comfort in warm-humid Colombo. This investigation is conducted using ENVI-met micrometeorological modelling software which can be used to assess real urban contexts [5, 9, 23]. The results of this assessment provide insights for architects and landscape architects on designing road landscape and adjacent buildings in order to create comfortable outdoor environments. Further, it helps to explore the complexity of street design, and prominent components and parameters to be considered in urban design spatially and temporally.

2 Study Areas and Climate Conditions

According to the Köppen and Geiger climate classification, Colombo belongs to tropical rainforest (Af) climate zone [19]. The average annual temperature is 26.5 °C and annual rainfall is 2387 mm. Generally, Colombo is residential in terms of land coverage and 48% of the total land cover of Colombo municipal area is covered by compact-law-rise local climate zone (LCZ) and 23.7% is covered by large low-rise LCZ category refereeing to initial LCZ classification [20]. Selected site areas are situated in residential zone in Colombo 07, Sri Lanka.

- Case study A—Cambridge terrace is a one lane residential road which is situated in Colombo 07 (6.90751° N, 79.85912° E). This completely belongs to Compact low-rise LCZ and the urban/rural temperature difference (UHI effect) is 3.19 °C. The area is compacted with low-rise residential buildings and scattered vegetation (107,200 m^2). The road orientation is north-west (NW) to south-east (SE).
- Case study B—Green path is a four lane road in a residential zone which is situated in Colombo 07 (6.91167° N, 79.86162° E). This belongs to both 'open low-rise' and 'scattered trees' local climate zones (LCZ) and the urban/rural temperature difference (UHI effect) is 1.87 °C. Total area assessed is around 282,080 m^2.
- Case study C—Sir Marcus Fernando road is a two lane road in a residential zone which is situated in Colombo 07 (6.91024° N, 79.85910° E). This belongs to both 'compact low-rise' and 'open low-rise' local climate zones (LCZ) and the urban/rural temperature difference (UHI effect) are 3.19 °C 1.87 °C respectively. Total area assessed is around 190,000 m^2.

3 Methodology

The methodology of this research includes five stages as follows:

- Onsite measurements of microclimatic data at each site on a sunny day.
- Modelling the study area from site survey studies, aerial photography for three different streets.
- Mapping the microclimatic and thermal comfort conditions of the study area using ENVI-met.
- Comparing the results in the study areas in temporal and spatial manner.
- Developing recommendations according to the findings.

3.1 Onsite Measurements

A fieldwork measurement was conducted to measure climate data at site as the inputs for simulations. Fixed weather station (PCE-FWS 20N) was used to measure the climatic parameters. Air temperature (T_a), relative humidity (RH), wind speed (WS) and wind direction (WD) were measured at 1.5 m above ground level from 9.00 am to 6.00 pm on 8th Jan. 2022, 24th Dec. 2022 and 27th Feb. 2022 in Cambridge terrace (Site A), Green path (Site B) and Sir Marcus Fernando Mawatha (Site C) respectively. The weather station was fixed on the side walk in the middle of the each road stretch. The reason to fix the weather station at 1.5 m height is that this level affects the most to the human thermal comfort [34, 11, 18]. This method of conducting onsite measurement campaigns using weather stations has been frequently used in previous researches [35, 36, 31].

3.2 Modelling the Study Area and Model Input

Since real urban contexts can be assessed using ENVI-met [5, 9, 23], three real road contexts are digitised. The ENVI-met model is a reasonably reliable tool for studying plant-surface-atmosphere interaction validated by field measurements [29]. This is a three-dimensional atmospheric model which simulates the urban microclimatic conditions with time and spatial resolution of 1–10 s and 0.5–10 m, respectively. It can be used to investigate the building and vegetation impacts on different microclimatic parameters and human bio-climate [7]. Previous studies have validated the simulation output results by field measurements largely with strong correlation between simulated and measured typical hourly T_a and MRT with minimal error [16]. Therefore, ENVI-met is a reasonably reliable tool for microclimate and thermal comfort assessments [29].

The physical components are parameterized using site survey data, google earth images and onsite observations. The road and surrounding area was configured using

surface, morphology and vegetation data and microclimate and OTC conditions were simulated using ENVI-met 5.0.1 Bio-met software package. The ENVI-met model area domains were respectively 134 × 200 × 30 m, 430 × 164 × 30 m and 250 × 193 × 30 m with vertical and horizontal grid resolution at 2 m as shown in Fig. 2. Existing trees were modelled using the vegetation database in ENVI-met considering type, height, crown shape, canopy density and tree location. Since the vegetation diversity is high, the trees are roughly represented by three heights, namely, small (up to 5 m), Medium (5–15 m) and Large (15–25 m) based on field survey. Vegetation type and percentages are shown in Table 1. Building shapes, façade material, height, surface coverage and material type were configured using the site survey data and google maps. Buildings forms were approximated as regular cubic. Further, meteorological data, air temperature (T_a), relative humidity (RH), wind speed (WS), wind direction (WD), roughness length, specific humidity and cloud cover were used as input data to the simulation model. Table 2 shows the input climate data for simulation of each site.

Simulation outputs are used as inputs for 'Bio-met' software to calculate the PET value using standard human according to ISO 7730 personal human parameters; male in age of 35, weight 75 kg, height 1.75 m and surface area 1.91 m^2 with static clothing insulation (clo) 0.90 and metabolic rate 86.21 W/m^2 (standing or

Table 1 The percentage of each types of vegetation in three case studies

Vegetation type	Number of trees (%)—case study A	Number of trees (%)—case study B	Number of trees (%)—case study C
Large trees (higher than 25 m)	0	20	6
Medium trees (5–15 m)	15	42	49
Small trees (up to 5 m)	41	35	45
Palm trees	44	3	0

Table 2 Input climate data for simulations

Definition	In case study A	In case study B	In case study C
Maximum air temperature (°C)	34.1	32	33.8
Minimum air temperature (°C)	27.8	26.5	28
Maximum relative Humidity in 1.5 m (%)	81	94	74
Minimum relative Humidity in 1.5 m (%)	50	50	55
Inflow direction (0°: North; 90°: East; 180°: South; 270°: West.)	315^0	270^0	180^0
Wind speed in 10 m (m/s)	0.66	0.61	0.70
Cloud cover	0.00	0.00	0.00
Roughness length at reference point (m)	0.01	0.01	0.01

Table 3 Thermal sensation and corresponding PET values applied in Singapore [33] (Source—Yang et al.)

Thermal Sensation	PET (°C) value applied to Singapore
Very cold	N/A
Cold	N/A
Cool	N/A
Slightly cool	$20 < PET \leq 24$
Neutral	$24 < PET \leq 30$
Slightly warm	$30 < PET \leq 34$
Warm	$34 < PET \leq 38$
Hot	$38 < PET \leq 42$
Very hot	$PET > 42$

light activity). Further, the output comfort value (PET °C) distribution patterns are illustrated using 'Leonardo' illustrations to understand how the comfort levels have been varied according to spatial and temporal variations.

3.3 Thermal Comfort Index—Physiological Equivalent Temperature (PET)

PET is defined as equivalent to the air temperature in a typical indoor setting at which the heat balance of the human body is maintained [13] which is the resultant based on the human energy balance principle. PET is the most implemented [22] and advanced index yet employed in OTC assessments. According to specific climatic contexts, thermal comfort ranges definitely vary [12]. Current study employed the PET ranges used in Singapore since climate zones are similar as classified in Köppen and Geiger classification under tropical rainforest (Af) climate [19]. Table 3 shows the thermal sensation and corresponding PET values, according to which that acceptable PET range for neutral thermal sensation for tropical climates could be between 24 °C and 30 °C.

3.4 ENVI-Met Model Validation

To validate the simulation model, measured and simulated air temperature (T_a) were compared with the results of Site A using linear regression. This validation method has been widely used in previous assessments [16]. Significantly a good linear fit was observed in Site A (Cambridge terrace) as shown in Fig. 1 where the R^2 values for T_a of the 'Site A' was 0.928. However, simulation T_a results of Site B and C have shown low correlations with corresponding measured T_a at site and the R^2 values of Sites B and C are 0.025 and 0.144, respectively. Nevertheless, previous studies have

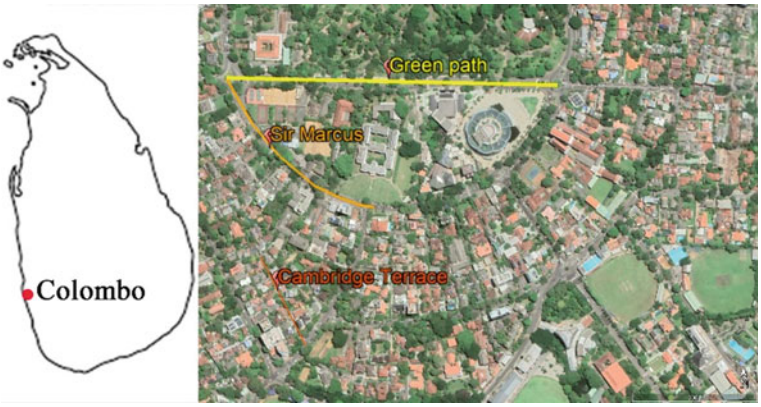

Fig. 1 Selected three residential streets in Colombo

recommended ENVI-met model as a reliable model to simulate the Atmosphere-plant-surface interactions with fairly good correlation values [26] and the boundary effect would be the reason for this deviation [8], [14]. According to Sun et al. [26], 4 nesting grids are enough to avoid the boundary effect (Fig. 3).

4 Results and Discussions

Three street environments are investigated by comparing measured microclimatic parameters at site and simulated thermal comfort conditions using ENVI-met model. The measured climatic parameters such as Air temperature (T_a), relative humidity (RH) and wind speed (WS) are compared in three residential streets in Colombo 07. Then the simulated thermal comfort conditions were compared employing physiologically equivalent temperature (PET) index for 12 h from 8.00 am to 7.00 pm to analyse comfort levels temporally. Finally, the distribution of PET values in streets is investigated spatially to understand the effect of street components and characteristics on thermal comfort. Conclusions and recommendations are made using simulated results.

4.1 Microclimate Comparison

According to the field measurement campaign, the observed microclimatic parameters are compared as shown in Figs. 4, 5 and 6. Observed T_a at Site B is the lowest during the daytime while site A and C have comparatively high air temperature recorded. The highest T_a was recorded at Site A during peak hours. The peak hours for all the sites were in between 11.30 am and 2.00 pm and T_a values of each site are

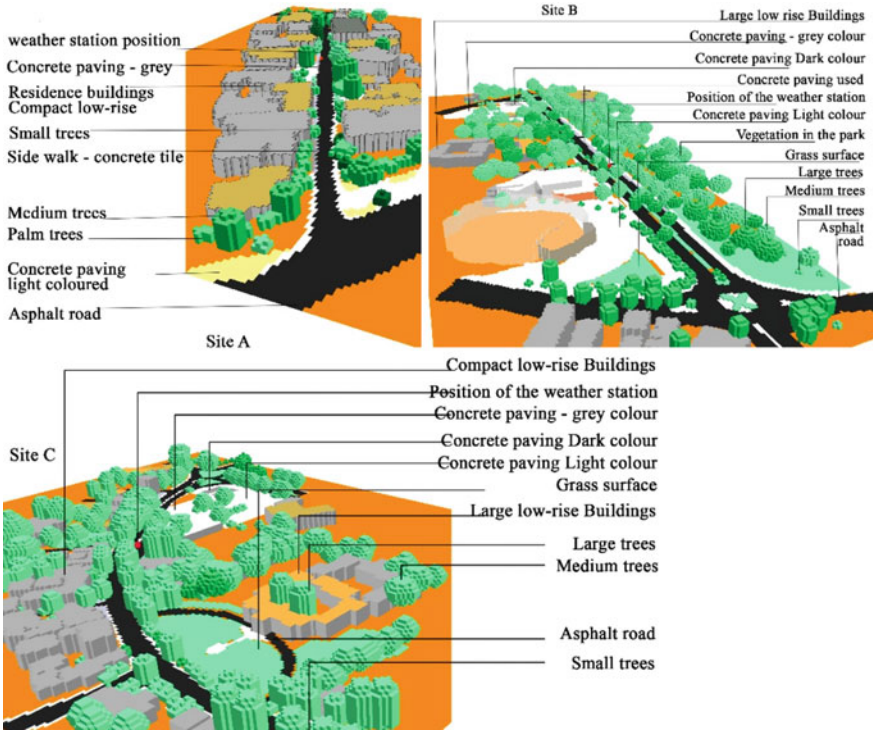

Fig. 2 ENVI-met model areas of three residential streets

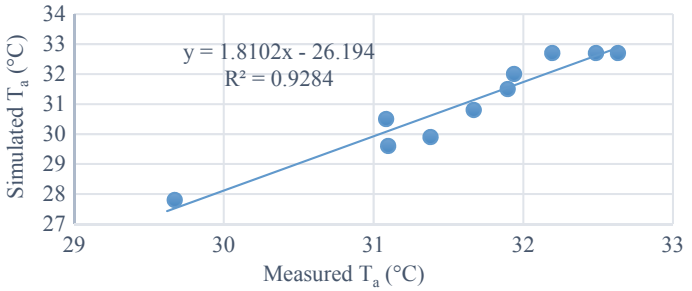

Fig. 3 Measured and simulated air temperature (T_a) values at Site A

almost same at 2.00 pm. Compared to other sites, Site C has shown high T_a values during the evening continuously. However, Sites A and B have shown less temperature in the morning and evening. In the morning, T_a in all the sites have shown similar increasing trend.

Compared to Sites A and C, Site B has shown the lowest relative humidity (RH) during the evening (from 1.00 pm to 4.30 pm) while noticeable variation has not

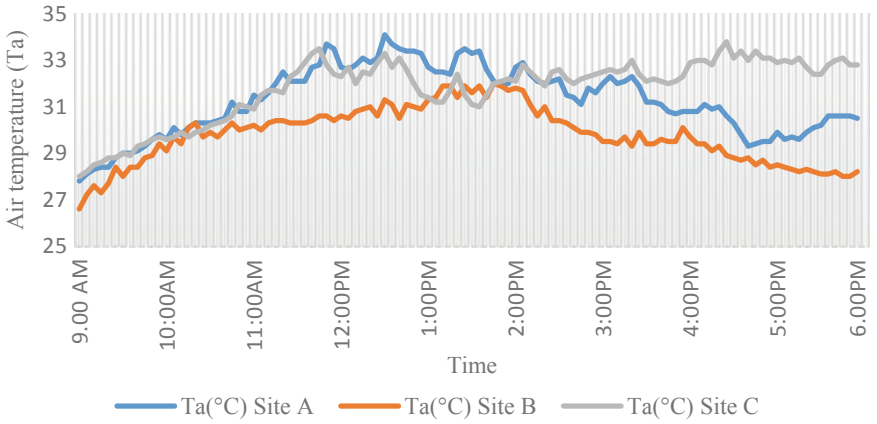

Fig. 4 Air temperature comparison of Sites A, B and C

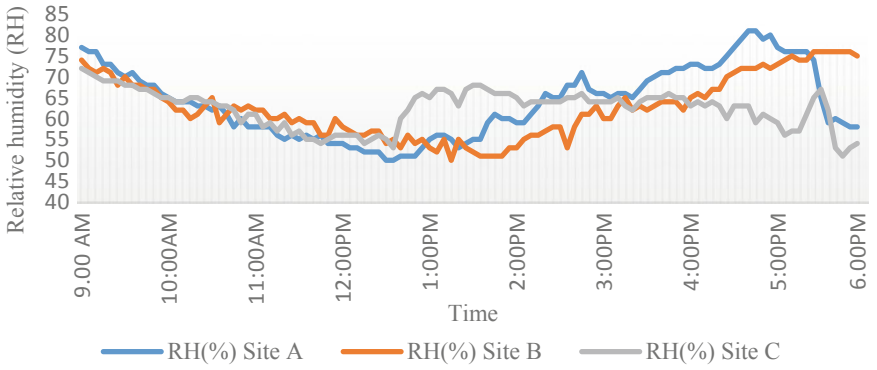

Fig. 5 Relative humidity comparison of Sites A, B and C

shown during the morning. All the sites have shown high humidity levels in the morning and evening while the lowest values have recorded from 12.00 pm to 2.00 pm. The highest RH was recorded in site A in the evening. Wind speed (WS) is significantly high in site B during the day time, especially in the evening raising it up to 4.1 m/s. This may be caused by the wind generated in the evening by high traffic conditions as the site B is a four lane road. All the sites have shown an increasing trend with fluctuated winds in WS from morning to evening. However, the heist average WS was found in site C (0.7 m/s) and 0.66, 0.61 m/s for sites A and B respectively.

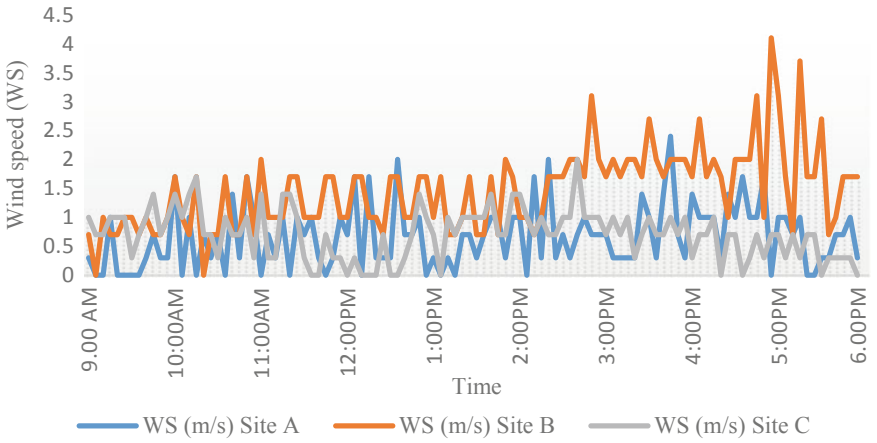

Fig. 6 Wind speed comparison of Sites A, B and C

4.2 Comparison of Thermal Comfort Conditions

Psychophysical thermal comfort assessment was conducted employing PET index in Bio-met software using simulated air temperature, mean radiant temperature (MRT), wind speed and specific humidity as input variables at each site. The simulated comfort levels (PET °C values) were compared temporally and spatially. Comparison of the simulated thermal comfort values in three residential streets is shown in Fig. 7. During daytime, Site B has shown the lowest comfort values while Sites A and C have shown comparatively high PET values. In site B, the comfort values have been transformed from 'slightly warm' ($30 < \text{PET} \leq 34$) to 'neutral' ($24 < \text{PET} \leq 30$) conditions. Irrespective of the site conditions, PET values in morning are higher than in the evening in all sites. Specially, thermal comfort levels of site A have transformed from 'hot' to 'very hot' conditions from morning to noon while in site C they have transformed from hot to warm conditions according to the thermal comfort sensation values in PET index. However, during the evening from 1.00 pm to 7.00 pm, the PET values in all the streets remain 'neutral' sensation which means the streets are comfortable.

If the average PET values are compared at 2.00 pm, the existing thermal comfort conditions have been rated as neutral (between 24 and 30 °C PET) in all tree streets while Site A, B and C have shown average of 28.14 °C, 25.7 °C and 27.11 °C PET values, respectively. Finally, the thermal comfort distribution has been investigated using 'Leonardo' illustrations in ENVI-met software package to understand the impact of street characteristics on thermal comfort. PET value distribution of three different streets at 2.00 pm is compared at pedestrian level (1.5 m from the ground). Accordingly sites A, B and C have shown comfort level distribution as illustrated in Fig. 8. Site A—Hard surface coverage is low in this site since the surrounding residence plots have enough bare soil and vegetation which positively

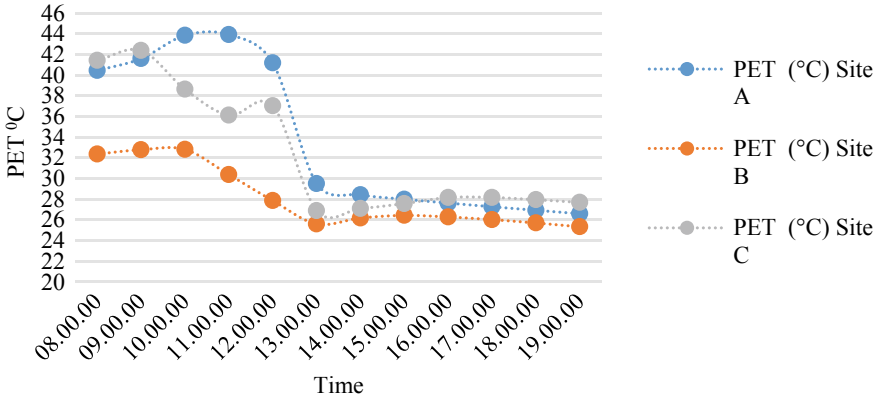

Fig. 7 Daytime thermal comfort comparison of three residential streets

affect the thermal comfort levels. There is a 3.82 °C PET increase in concrete block paved areas compared to average comfort levels showing a tendency to be slightly warm at pedestrian level, especially where the concrete surface area is expanded. Even though large trees are not found, medium and small trees available in residential lands have provided considerable shading to the road and sidewalk surfaces blocking the reflected solar radiation from the residential buildings as well. Even though the buildings are low-rise, the incoming solar radiation is relatively high, still buildings can provide enough shade to the in-between spaces due to compactness. Further, the average aspect ratio (H/W) of the road is almost 1 and the road is narrow enough to receive considerable shade both by buildings and vegetation. It is clear that the PET values are less where the buildings are taller and the street width is low agreeing to Emmanuel et al. [5] and Zakhour [35]. Therefore, the resultant average thermal comfort level is ranked as 'neutral' at 2.00 pm mainly due to amount of vegetation in house plots and narrow road.

Site B—According to comfort level distribution, the entire road stretch is comfortable as this case rated the lowest PET values at 2.00 pm even in hard paved areas. There is only a 2.42 °C difference between the average and the maximum PET values at 2.00 pm. The effect of the combination of shade trees over grass in 'Site B' has also affected to reduce the discomfort as it is the most effective landscape strategy as mentioned by Yang et al. [33]. Further, it is identified that the canopy coverage is the most important factor in reducing discomfort by providing shading and evapotranspiration cooling effects [15, 16]. As stated by Sun et al. [26], taller trees are the most influential factor on OTC, which is demonstrated by site B, which has the highest percentage of large tree (20.2%) compared to sites A and C. Moreover, almost equally distributed trees in site B have provided a covering shade thus creating a homogenous distribution of comfort in streets as proven by Zhao et al. [37].

Generally the East–West and Northwest–Southeast orientations provide the worst thermal comfort conditions [24, 34, 36]. However, sites B and A with aforementioned orientations have not resulted in higher PET values at 2.00 pm due to the high

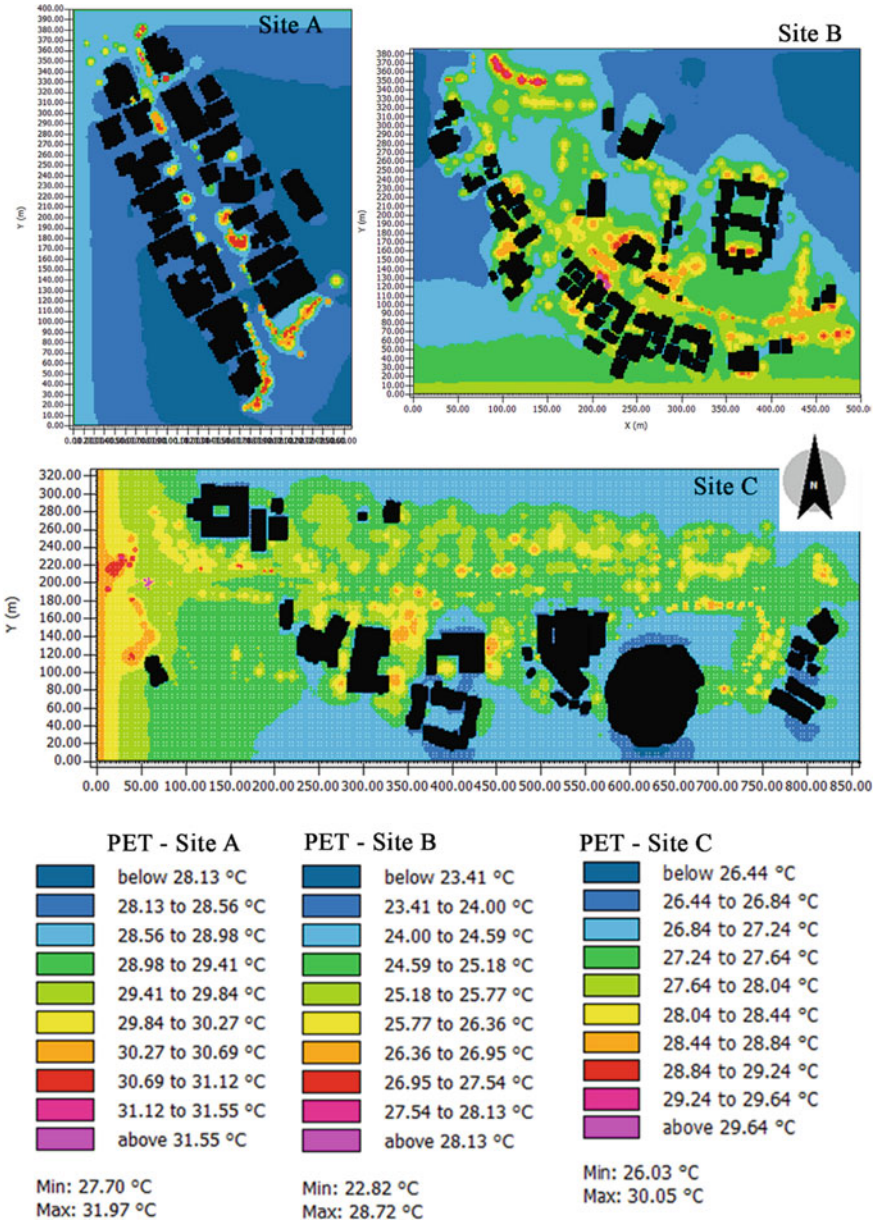

Fig. 8 PET distribution of site A, B and C at 2.00 pm at 1.5 m

vegetation coverage. Further, the average aspect ratio (H/W) of the road B is very low and always is less than 1. Therefore, the building shade is not effective in improving OTC. The wind direction is from the west side and it is parallel to the road axis which affects positively the Comfort as mentioned by Dalman et al. [3]. Therefore, the average thermal comfort is 'neutral' in Site B due to high shade coverage, and parallel wind flow with the street axis, low building density and large open spaces beside the road.

Site C—There is only a 2.95 °C difference between maximum and average PET value at 2.00 pm. Entire area can be considered as comfortable at 2.00 pm, but some areas with compact buildings which act as a wind barrier and expanded hard paved areas have slightly warm conditions. Surrounding vegetation has provided enough shading to reduce the solar access. Vast percentage of the assessed area is covered by bare soil and grass which affects positively the thermal comfort. Effective shade has been provided by medium size (49.3%) trees with sparse canopies planted near sidewalk and beyond. In this road section, trees are randomly distributed with open space in between. The average aspect ratio (H/W) is always less than 1, thus the shadow cast to the sidewalk is less. Further, the wind flow has been blocked by the compact buildings from south-west direction, thus there is a tendency of resulting 'slightly warm' conditions in the middle of the road stretch. Yahia & Johansson [32] has also mentioned the impotency of spaces between buildings.

5 Conclusion

This study assesses the microclimate and OTC in three different residential streets in Colombo using onsite measurements and numerical simulations. The thermal comfort levels were investigated temporally and spatially to understand the impact of landscape characteristics on OTC. According to the measured and climatic parameters at site and the comfort values during daytime, it is clear that lower air temperature (Ta), relative humidity (RH) and high wind speed contributed to enhance the thermal comfort levels in warm-humid residential streets, thus corroborating with the results of previous studies.

Homogenous shade coverage creates a uniform distribution of comfort levels in streets. Vegetation is the most effective and efficient way to reduce thermal discomfort of residential streets, especially large trees in adjacent lands with grass. In cases where the road is very wide, the shade to the road surface should be increased to achieve desire comfort levels in sidewalks; specially, the expanded paved areas should be shaded properly. Low building density, low hard surface coverage and high shade coverage in adjacent lands are more important in terms of improving thermal comfort in warm-humid streets. Accordingly, planting trees in residence land plots is recommended to enhance the street microclimate and OTC. Planting medium trees in centre median is highly recommended to reduce incoming solar radiation to the road surface in wider roads. Shade coverage is the most important component to be considered in street planning in terms of OTC irrespective of the

street axis orientation. These findings could be useful for landscape architects and urban designers to consider in policymaking and designing urban streets as it is an urgent need to address the global climate change issues in near future.

Acknowledgements This work is supported by the Accelerating Higher Education Expansion and Development (AHEAD)—DOR Grant affiliation with Ministry of Higher Education& University Grants Commission and funded by the World Bank. Grant NO; Credit/Grant #: 6026-LK/8743-LK (AHEAD/DOR/52).

References

1. Andreou E (2014) The effect of urban layout, street geometry and orientation on shading conditions in urban canyons in the Mediterranean. Renew Energy 63:587–596
2. Chen L, Ng E (2012Apr 1) Outdoor thermal comfort and outdoor activities: A review of research in the past decade. Cities 29(2):118–125
3. Dalman M, Salleh E, Sapian AR, Saadatian O 2013 Thermal comfort investigation in traditional and modern urban canyons in Bandar Abbas, Iran. Pertanika J Soc Sci & Human 21(4)
4. Deng JY, Wong NH (2020Feb) Impact of urban canyon geometries on outdoor thermal comfort in central business districts. Sustain Cities Soc 1(53):101966
5. Emmanuel R, Rosenlund H, Johansson E (2007Nov 30) Urban shading—a design option for the tropics? A study in Colombo, Sri Lanka. Int J Climatol: J R Meteorol Soc 27(14):1995–2004
6. Fanger PO 1970 Thermal comfort. Analysis and applications in environmental engineering. Thermal comfort. Anal Appl Environ Eng
7. Huttner S, Bruse M 2009 Numerical modeling of the urban climate–a preview on ENVI-met 4.0. In 7th international conference on urban climate ICUC-7, Yokohama, Japan, vol. 29
8. Kong F, Sun C, Liu F, Yin H, Jiang F, Pu Y, Cavan G, Skelhorn C, Middel A, Dronova I (2016) Energy saving potential of fragmented green spaces due to their temperature regulating ecosystem services in the summer. Appl Energy 183:1428–1440
9. Krüger EL, Minella FO, Rasia F (2011Mar 1) Impact of urban geometry on outdoor thermal comfort and air quality from field measurements in Curitiba. Brazil Build Environ 46(3):621–634
10. Lai D, Liu W, Gan T, Liu K, Chen Q (2019Apr) A review of mitigating strategies to improve the thermal environment and thermal comfort in urban outdoor spaces. Sci Total Environ 15(661):337–353
11. Li J, Wang Y, Ni Z, Chen S, Xia B (2020Oct) An integrated strategy to improve the micro-climate regulation of green-blue-grey infrastructures in specific urban forms. J Clean Prod 20(271):122555
12. Lucchese JR, Andreasi WA (2017) Designing thermally pleasant open areas: the influence of microclimatic conditions on comfort and adaptation in Midwest Brazil. J Sustain Dev 10(4):11
13. Matzarakis A, Mayer H, Iziomon MG (1999) Applications of a universal thermal index: physiological equivalent temperature. Int J Biometeorol 43(2):76–84
14. Morakinyo TE, Kong L, Lau KK, Yuan C, Ng E (2017Apr) A study on the impact of shadow-cast and tree species on in-canyon and neighborhood's thermal comfort. Build Environ 1(115):1–7
15. Morakinyo TE, Lam YF (2016Jul) Simulation study on the impact of tree-configuration, planting pattern and wind condition on street-canyon's micro-climate and thermal comfort. Build Environ 1(103):262–275
16. Morakinyo TE, Lau KK, Ren C, Ng E (2018Jun) Performance of Hong Kong's common trees species for outdoor temperature regulation, thermal comfort and energy saving. Build Environ 1(137):157–170

17. Nikolopoulou M (2011) Outdoor thermal comfort. Front Biosci Sch 3(4):1552–1568
18. Ouyang W, Morakinyo TE, Ren C, Ng E (2020May) The cooling efficiency of variable greenery coverage ratios in different urban densities: A study in a subtropical climate. Build Environ 1(174):106772
19. Peel MC, Finlayson BL, McMahon TA (2007) Updated world map of the Köppen-Geiger climate classification. Hydrol Earth Syst Sci 11(5):1633–1644
20. Perera NG, Emmanuel R (2018Mar) A "Local Climate Zone" based approach to urban planning in Colombo Sri Lanka. Urban Climate 1(23):188–203
21. Perini K, Magliocco A (2014Jan 1) Effects of vegetation, urban density, building height, and atmospheric conditions on local temperatures and thermal comfort. Urban For & Urban Green 13(3):495–506
22. Potchter O, Cohen P, Lin TP, Matzarakis A (2018) Outdoor human thermal perception in various climates: A comprehensive review of approaches, methods and quantification. Sci Total Environ 631:390–406
23. Raman V, Kumar M, Sharma A, Froehlich D, Matzarakis A (2021Aug) Quantification of thermal stress abatement by trees, its dependence on morphology and wind: A case study at Patna, Bihar, India. Urban For & Urban Green 1(63):127213
24. Rodríguez-Algeciras J, Tablada A, Matzarakis A (2018Aug) Effect of asymmetrical street canyons on pedestrian thermal comfort in warm-humid climate of Cuba. Theoret Appl Climatol 133(3):663–679
25. Stewart ID, Oke TR (2012) Local climate zones for urban temperature studies. Bull Am Meteorol Soc 93(12):1879–1900
26. Sun S, Xu X, Lao Z, Liu W, Li Z, García EH, He L, Zhu J (2017Oct) Evaluating the impact of urban green space and landscape design parameters on thermal comfort in hot summer by numerical simulation. Build Environ 1(123):277–288
27. Taleghani M, Kleerekoper L, Tenpierik M, Van Den Dobbelsteen A (2015Jan) Outdoor thermal comfort within five different urban forms in the Netherlands. Build Environ 1(83):65–78
28. Thani SKSO, Mohamad NHN, Abdullah SMS (2013) The influence of urban landscape morphology on the temperature distribution of hot-humid urban centre. Procedia Soc Behav Sci 85:356–367
29. Tukiran JM, Ariffin J, Ghani AN (2017) A study on the cooling effects of greening for improving the outdoor thermal environment in Penang Malaysia. GEOMATE J 12(34):62–70
30. Unal M, Uslu C, Cilek A, Altunkasa MF (2018Mar) Microclimate analysis for street tree planting in hot and humid cities. J Digit Landsc Arch 3:34–42
31. Wai KM, Xiao L, Tan TZ (2021Jan) Improvement of the outdoor thermal comfort by water spraying in a high-density urban environment under the influence of a future (2050) climate. Sustainability 13(14):7811
32. Yahia MW, Johansson E (2014May) Landscape interventions in improving thermal comfort in the hot dry city of Damascus, Syria—The example of residential spaces with detached buildings. Landsc Urban Plan 1(125):1–6
33. Yang W, Lin Y, Li CQ (2018Aug) Effects of landscape design on urban microclimate and thermal comfort in tropical climate. Adv Meteorol 29:2018
34. Yin S, Lang W, Xiao Y, Xu Z (2019Jan) Correlative impact of shading strategies and configurations design on pedestrian-level thermal comfort in traditional shophouse neighbourhoods, Southern China. Sustainability 11(5):1355
35. Zakhour S (2015Aug 25) The impact of urban geometry on outdoor thermal comfort conditions in hot-arid region. J Civ Eng Arch Res 2(8):862–875
36. Zaki SA, Toh HJ, Yakub F, Mohd Saudi AS, Ardila-Rey JA, Muhammad-Sukki F (2020Jan) Effects of roadside trees and road orientation on thermal environment in a tropical city. Sustainability 12(3):1053
37. Zhao TF, Fong KF (2017Jul) Characterization of different heat mitigation strategies in landscape to fight against heat island and improve thermal comfort in hot–humid climate (Part I): Measurement and modelling. Sustain Cities Soc 1(32):523–531

38. Zhao Q, Sailor DJ, Wentz EA (2018May) Impact of tree locations and arrangements on outdoor microclimates and human thermal comfort in an urban residential environment. Urban For & Urban Green 1(32):81–91

Assessment of Indoor Air Quality and Sick Building Syndrome in Apartment Buildings

N. R. Kumarage, C. Jayasinghe, K. P. H. Perera, K. K. G. K. D. Kariyawasam, and E. P. Wickramasinghe

Abstract Residential apartment buildings are widely implemented in Sri Lanka due to rapid urbanization and land scarcity. The confined spaces and controlled ventilation in such apartments could result in adverse health effects, including Sick Building Syndrome (SBS). Because of the usage of chemical products such as incense sticks in such compact spaces for religious activities in South Asia, SBS can occur. This study is one of the first field studies to establish a connotation between the indoor air quality of apartment buildings in Colombo, Sri Lanka, with various chemicals, including incense products and SBS. Measurements were taken from multiple locations in 50 apartments of various indoor environment parameters. Significant Total Volatile Organic Compound (TVOC) concentrations (up to 4.500 ppm) were associated with the use of chemicals, particularly cube-type incense products. Higher CO_2 concentrations were associated with migraine and headaches. The relationship between chemical and incense products with higher levels of TVOC and SBS symptoms calls for urgent attention of the key urban planning stakeholders in Sri Lanka to improve ventilation and avoid using such products indoors.

Keywords Sick Building Syndrome · Indoor air pollution · Incense products · Urban high risers · TVOC concentration

N. R. Kumarage (✉) · C. Jayasinghe · K. K. G. K. D. Kariyawasam
University of Moratuwa, Moratuwa, Sri Lanka
e-mail: nipun.kumarage@ubc.ca

K. P. H. Perera
Southern Alberta Institute of Technology, Alberta, Canada

E. P. Wickramasinghe
Estate & Urban Health Unit, Ministry of Health, Colombo, Sri Lanka

© The Author(s), under exclusive license to Springer Nature Singapore Pte Ltd. 2023

R. Dissanayake et al. (eds.), *ICSBE 2022*, Lecture Notes in Civil Engineering 362,
https://doi.org/10.1007/978-981-99-3471-3_30

1 Introduction

Residing in apartments has become popular recently since it solves the accommodation issue due to urbanization, and gives easy accessibility to basic amenities, including workplaces and schools [11, 44]. Modern working patterns, effective land-use policies, and the adoption of contemporary technology motivated many citizens to invest in apartments and use urban living styles. However, various health consequences have been noted due to the building materials' quality, ventilation standards, lighting, and air quality. One common health outcome of living in apartments is Sick Building Syndrome. The prevalence of symptoms of SBS can be due to various building defects such as poor indoor air quality [4, 41, 52], poor outdoor air quality [37], low ventilation rate [39], thermal discomfort [27], and also psychosocial factors [14, 16, 17].

Furthermore, the consumer products, household items, and chemical substances that the occupants use for their day-to-day activities may pollute the indoor environment. This in turn may eventually lead to building-related sicknesses such as Sick Building Syndrome (SBS) among residents [21, 50]. For example, using incense products for fragrance has been a common practice, especially in Asia, including Sri Lanka, since ancient times [36]. Some incense products create undesirable indoor environmental conditions by emitting many Volatile Organic Compounds (VOC) such as toluene, styrene, and formaldehyde [34].

Although several studies have been conducted worldwide on SBS, minimal research has been conducted on these uniquely created atmospheric conditions in South Asia. Therefore, the current study was carried out in the city of Colombo, Sri Lanka to explore the magnitude of SBS and associated factors for its development in these uniquely created urban apartment environment conditions.

2 Sick Building Syndrome (SBS)

Sick Building Syndrome (SBS) is a term that refers to a collection of symptoms that affect some occupants of a building during the time they spend in the building and diminish or go away during periods when they leave the building [45]. In other words, SBS is an example of a "disease that cannot be clinically identified as building-related illnesses, although that can be associated with buildings" [26]. SBS usually starts with respiratory symptoms and moves on to dermatological and even neurological symptoms [19]. Fig. 1 highlights some of the SBS symptoms identified in previous researches.

Evidence suggests that SBS symptoms were associated with unsatisfactory indoor environmental factors such as elevated concentrations of Volatile Organic Compounds (VOC), CO_2, temperature, humidity, noise, and vibration [20, 23, 32].

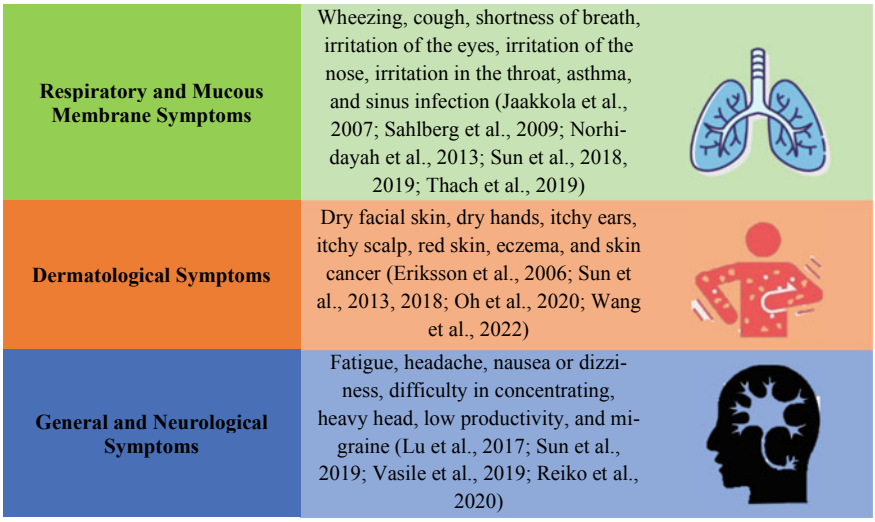

Fig. 1 SBS symptoms

In addition, low humidity levels were also found to be associated with SBS symptoms, based on past studies conducted worldwide. Table 1 summarizes several of the most prominent parameters that affect IEQ and their impact on health.

Table 1 IEQ factors and their impact on health

IEQ factor	SBS symptoms	References
Volatile Organic Compounds (VOC)	Eye irritation, Nose irritation, Throat discomfort, Skin allergies, Headache, Nausea, Fatigue, Dizziness	[3, 23, 29, 39, 42, 49, 53]
Carbon Dioxide (CO_2)	Sore throat, Blocked/Runny nose, Tight chest, Wheezing, Dry cough, Nasal congestion, Impaired work performance	[2, 23, 33, 35]
Relative Humidity	Respiratory SBS symptoms, Skin Irritation, General SBS Symptoms, Mucosal SBS Symptoms, Throat Irritation, and Impaired Work Performance	[15, 18, 31-33, 39]
Thermal Discomfort	Impaired productivity, Fatigue, and Drowsiness	[7, 43]
Noise and Vibration	Impaired Work Performance, Impaired Concentration, Fatigue	[6]

3 Methodology

A field study was conducted in selected settings in Colombo District, Sri Lanka. Data collection was carried out over three months, from June 2020 to September 2020. The field study consisted of an inspection of apartments and measurements of environmental parameters such as TVOC concentration, CO_2 concentration, temperature, relative humidity, and noise levels. In addition, an interviewer-administered questionnaire was used to gather information about the occupants' building characteristics, chemical usage, and SBS symptoms. Visits to the selected apartments were made between 10 am and 5 pm, and the sample size was limited to fifty (50) apartments.

3.1 Sampling Technique

The targeted population of the research was residents in high-rise apartment complexes in the Colombo district, Sri Lanka. The clustered sampling technique was used to list the urban areas such as Colombo Municipal Council, Kotte, Dehiwala/Mt Lavinia, Moratuwa, Maharagama, Kolonnawa, Seethawakapura, Kesbewa, Borelesgamuwa, and Kaduwela to shortlist out of the entire Colombo district. Finally, 50 apartments were selected with a simple random sampling method.

3.2 Questionnaire Survey

The questionnaire included three main sections: Building characteristics, chemical usage inside the apartment, and SBS symptoms of the occupants, as indicated in Fig. 2. Items of the questionnaire were selected based on questionnaires used in similar past epidemiological studies in workplaces, homes, schools, and day-care centers [8, 22, 40]. Serious sicknesses (Sinus infection, Asthma, Migraine, Eczema, Hay fever, and Allergy to dust) were selected and collected on a binary scale depending on a previous diagnosis by a physician. The presence of acute SBS symptoms (Irritation in eyes, runny nose, dry throat, cough, dry face/hands, lethargy/drowsiness/tiredness, and headache) were selected and collected on a 5-point Likert scale and changed to a binary scale (positive and negative) by assuming at least 3 as positive.

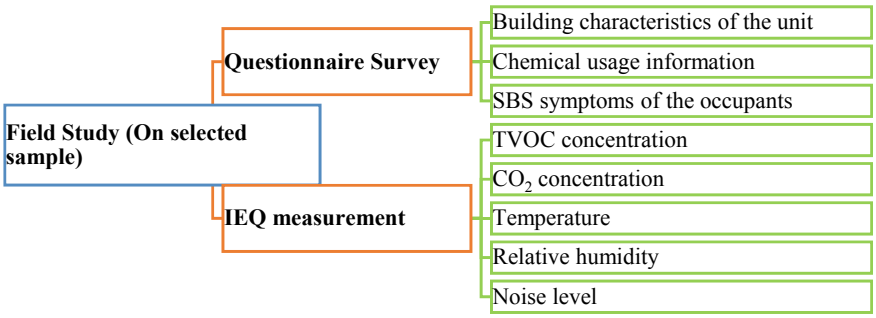

Fig. 2 Components of the field study

3.3 IEQ Measurement

A set of field measurements were taken to assess the indoor air quality of the selected apartments. The measurements included TVOC concentration, CO_2 concentration, Relative Humidity, Temperature, and Noise level. Fig. 3 illustrates the eight locations where the measurements were taken inside an apartment. These included the four corners of the living room, the center of the living room, the center of bedroom 1, the center of bedroom two, and a location on the veranda to measure the outdoor air quality. Each measurement was taken at a height of 1.2 m above floor level. The ability for cross ventilation was also noted during the measurements. The average values of the first 7 points were considered as the indoor measurement, and the final veranda reading was considered as the outdoor measurement.

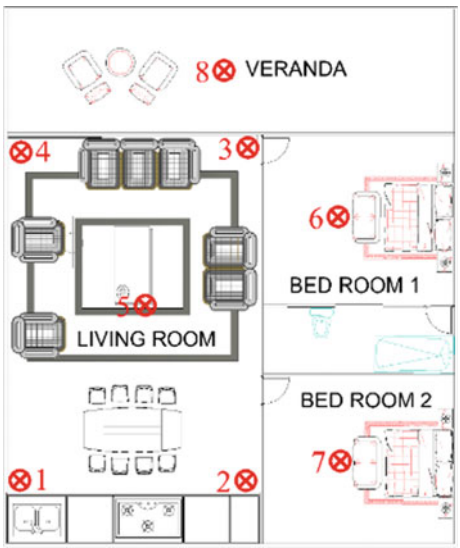

Fig. 3 Locations within an apartment where IEQ parameters were measured

3.4 Experimental Equipment

Indoor TVOC measurements were measured with a handheld Omega HHAQ-107 data logging VOC meter. Sper scientific data logging IAQ meter was used to measure the CO_2 concentration, temperature, and relative humidity. The indoor noise level was measured using an android application named Sound Meter-Decibel Meter, which was validated at a laboratory facility.

3.5 Data Analysis

Initially, the prevalence of SBS symptoms and building characteristics were analyzed with measured IEQ parameters to find magnitude, extent, and correlations. Afterward, the measured IEQ parameters were compared with indoor chemical usage to find the effect of incense products on the environment. Finally, logistic regression models were used to evaluate the associations of SBS symptoms with indoor air pollutants. The P-value < 0.05 was considered statistically significant.

4 Results and Analysis

Results of the field study, including questionnaire survey data and measurements, were analyzed and summarized according to the prevalence of SBS symptoms, chemical usage inside apartments, and IEQ measurements under Section 4.1–4.3. Possible associations were developed between data collected through the questionnaire and the measured IEQ parameters. Subsection 4.4 and 4.6 describe the possible associations between building characteristics, incense product usage, and the association of SBS with indoor air quality measurements, respectively.

4.1 Magnitude/prevalence of SBS Symptoms

The frequency distribution of the presence of SBS symptoms is indicated in Table 2. Allergy to dust and Sinus infection were found to be the most common SBS sickness prevalent in 55.8% and 46.5% of the measured apartments, respectively. Runny nose and migraine were also prevalent in 39.5% of occupants of the measured apartments. When considering at least one symptom in each category, it was visible that 86% had at least one respiratory or mucous membrane symptom, 65.1% had at least one general and neurological symptom, and 30.2% had at least one dermatological symptom.

Table 2 Frequency distribution of symptoms of SBS

	N	%
≥One respiratory or mucous membrane symptom	37	86.0
Sinus infection	20	46.5
Asthma	11	25.6
Hay fever	6	14.0
Allergy to dust	24	55.8
Irritation in eyes	15	34.9
Runny nose	17	39.5
Dry throat	9	20.9
Cough	12	27.9
≥One dermatological symptom	13	30.2
Eczema	6	14.0
Dry face/hands	8	18.6
≥One general and neurological symptom	28	65.1
Migraine	17	39.5
Lethargy/Drowsiness/Tired	12	27.9
Headache	16	37.2

N—Number of apartments corresponding out of the 43 occupied apartments
%—The percentage of apartments in the selected sample

4.2 Use of Chemicals Inside the Apartments

Since indoor TVOC concentrations can be altered since they are due to incense products and chemicals inside the apartments [34, 47], the occupants were asked to indicate relevant chemical usage information in the questionnaire. Table 3 demonstrates the summary of chemical usage inside the apartment, including the type of incense products used and the frequency.

4.3 Measurement of Indoor Air parameters

Only 43 apartments were occupied at the time of the study. Therefore, only those apartments were considered in the analysis of SBS symptoms. Hence, the descriptive analysis was carried out only for measured IEQ parameters for those 43 occupied apartments. Table 4 presents a descriptive analysis of the indoor and outdoor air quality measurements of the occupied apartments, including the mean, maximum, median, percentiles, and standard deviation.

Table 3 Summary of chemical use inside the apartments

		N	%
Incense products	Incense Sticks	17	39.5
	Spray	15	34.9
	Gels	3	7.0
	Cubes	2	4.7
	Potpourri	2	4.7
	Essential Oils	2	4.7
	Scented candles	2	4.7
	None	8	18.6
Frequency of usage of incense products	Several times a day	7	16.3
	Everyday	14	32.6
	Several times a week	15	34.9
	None	7	16.3
Cleaning products used in the living	Everyday	12	27.9
Room	Several times a week	27	62.8
	Once every few weeks	4	9.3
Cleaning products used in the	Everyday	12	27.9
Washrooms	Several times a week	27	62.8

N—Number of apartments using a particular indoor chemical/frequency of use

4.4 Potential Correlations between Building Characteristics and Indoor Air Quality Measurements

The following potential relationships have been identified between building characteristics and indoor environmental quality:

(a) The outdoor TVOC concentration was reported to be decreasing with the height of the building, as illustrated in Fig. 4. For the buildings below 4 m in height, the average TVOC was 0.36 ppm. However, when the height from ground level to the apartment increased to 4–8 m, the average dropped to 0.22 ppm. Further, when it was above 12 m, the average dropped to 0.03 ppm.

(b) The ability for cross ventilation showed a clear relationship with indoor TVOC concentration. As shown in Fig. 5, apartments with no cross ventilation had the highest average TVOC concentration of 0.76 ppm, while those with cross ventilation provided in the living room had an average of 0.56 ppm. Moreover, those with cross ventilation in both living and bedrooms had the lowest average of 0.06 ppm TVOC.

Table 4 Descriptive analysis of the IEQ measurements of the occupied apartments

	n	Minimum	Percentiles			Maximum	Mean	Median	Std. Deviation
			25	*50*	*75*				
Indoor TVOC	43	0.000	0.00000	0.00600	0.75000	4.500	0.58242	0.00600	0.946364
Outdoor TVOC	43	0.00	0.0000	0.0000	0.0000	1.87	0.1372	0.0000	0.41887
Indoor CO_2	43	386	480	525	568	883	536.60	524.80	83.48
Outdoor CO_2	43	400	461.00	490.00	535.00	772	505.67	490.00	69.078
Indoor RH	43	48.5	70.3	71.9	74.0	77.8	71.30	71.88	4.65
Outdoor RH	43	58.3	69.800	71.900	73.600	76.1	71.400	71.900	3.4442
Indoor Temperature	43	27.1	30.1	30.6	31.2	33.0	30.61	30.59	1.03
Outdoor Temperature	43	28.3	30.500	30.900	31.200	35.7	30.7537	30.900	1.0691
Indoor Noise level	43	45	56	60	62	70	59.58	60.00	4.97
Outdoor Noise level	43	50	62.00	64.00	68.00	77	63.84	64.00	5.944

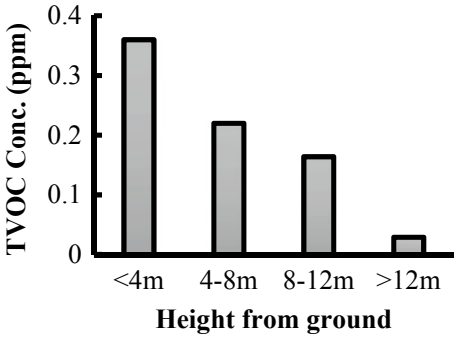

Fig. 4 Average outdoor TVOC concentration with apartment height

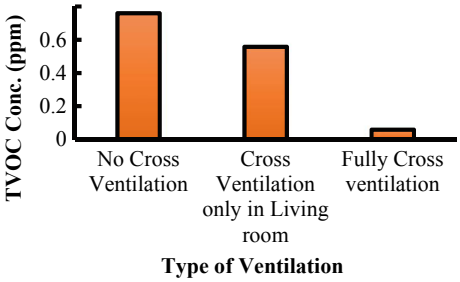

Fig. 5 Average TVOC concentration with and without cross ventilation

4.5 Correlations Between Indoor Chemical and Incense Product Use With Concentrations of Air Quality Parameters

In the present study, indoor TVOC concentrations were compared using different types of incense and chemical products. Fig. 6 represents the variation of average TVOC concentration with various incense products used in the selected sample of apartments. Cube types resulted in the highest average TVOC concentration of 3.55 ppm. Gel type, spray type, incense sticks, and scented candles had an average TVOC concentration of 0.70 ppm, 0.59 ppm, 0.45 ppm, and 0.36 ppm, respectively. However, with the essential oils and potpourris, the TVOC concentration turned out to be zero. Therefore, the sample of surveyed apartments was categorized into three levels of indoor pollutants based on the TVOC concentration. Fig. 7 indicates the probability level with different types of incense products. The categorization of TVOC concentration is as follows:

- TVOC Concentration > 0.75 ppm: red color with a patch
- 0 < TVOC concentration < 0.75 ppm: yellow color with a patch
- TVOC concentration = 0: green color with a patch

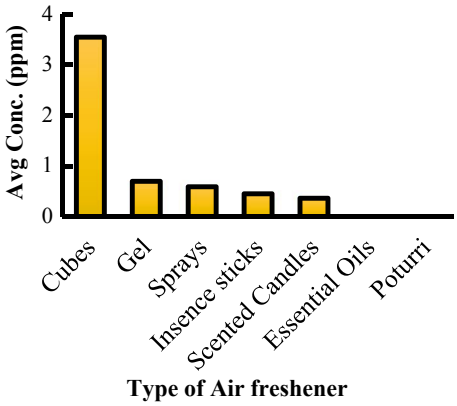

Fig. 6 Variation of average TVOC concentration with different types of air

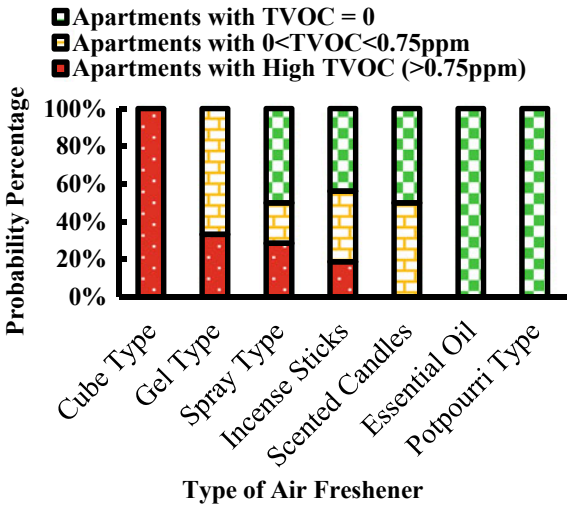

Fig. 7 TVOC concentration distribution with different types of incense products

Figure 7 reveals the following findings:

- Almost 100% of the apartments using cube-type incense products fall into the category of high TVOC emitting scenario (>0.75 ppm).
- There were about 33% of apartments using gel-type incense products that indicated a high TVOC concentration (>0.75 ppm), while the rest indicated a low TVOC concentration (<0.75 ppm).
- 27% of the apartments used Spray type incense products, indicating a high TVOC concentration (>0.75 ppm), while 23% indicated a low TVOC concentration, and the remainder indicated zero VOC concentration.
- Out of the apartments using incense sticks, 19% indicated a high TVOC concentration (>0.75 ppm), 36% indicated a low TVOC concentration, and the remaining 45% indicated Zero TVOC concentration.

4.6 Correlations Between SBS Symptoms and Associated IEQ Parameter Factors

Odds ratios were calculated for each measured physical IEQ parameter (TVOC concentration, CO_2 concentration, relative humidity, temperature, and noise level) for SBS symptoms, using multiple logistic regression models, as shown in Table 5. In order to calculate odds ratios, thresholds were determined for all IEQ parameters, i.e., 0.75 ppm for TVOC as per [25], for CO_2, although the threshold was defined as 1000 ppm [51]. Since the results indicated lower CO_2 values with a mean of 524 ppm, a threshold of 650 ppm was selected. Similarly, in the literature, thermal comfort is achieved at 27 °C [27]. Since many apartments indicated higher temperatures with an average of 30.6 °C, the threshold was selected at 31.5 °C for temperature. Also, relative humidity and noise level thresholds were taken as 70% and 60 dB, respectively. The units exceeding the thresholds were considered positive. Since literature revealed that noise is related to general SBS symptoms, it is unlikely that respiratory and dermatological symptoms occur due to noise [6]. Hence, the noise was removed when calculating multiple logistic regression models for other SBS symptoms.

High TVOC concentration and high CO_2 concentration resulted in higher odds for most of the short-listed SBS symptoms. However, for TVOC, none of the symptoms was significantly associated with a *P*-value less than 0.05 when the TVOC concentration was higher than 0.75 ppm. For CO_2, migraine and headache became significantly associated with a *P*-value less than 0.05 when CO_2 concentrations were above 650 ppm. Relative humidity, temperature, and noise level also increased the odds for some SBS symptoms, which were insignificant at a 95% confidence interval.

A forest plot was also developed to easily determine the correlations with higher odds, as shown in Fig. 8. The following symptoms resulted in greater odds than 1 when the IEQ parameters exceeded their thresholds.

- TVOC—headache, runny nose, and hay fever
- CO_2—headache, migraine, eczema, cough, dry throat, runny nose, irritation in eyes, Sinus infection
- Relative humidity—dry hands, runny nose
- Temperature—headache, migraine, cough
- Noise—migraine

5 Discussion

The present study was one of the pioneer studies conducted across apartments in Sri Lanka, which resulted in many significant findings concerning future urban planning and apartment occupancy. Allergy to dust and Sinus infection was found to be the most common SBS sickness prevalent in around 50% of the measured apartments. Runny nose and migraine were prevalent in almost 40% of the measured apartments. More than 85% of the occupants indicated at least one respiratory and

Table 5 Adjusted odds ratios of measured IEQ parameters for SBS symptoms

SBS Symptoms	Measures IEQ parameters				
	TVOC > 0.75 ppm	CO_2 > 650 ppm	RH < 70%	Temp > 31.5 °C	Noise > 60 dB
≥One symptom[a]	CBD	0.21(0.02,2.20)	0.19(0.02,1.65)	0.14(0.01,1.97)	
Sinus infection	0.43(0.06,2.99)	2.13(0.43,10.67)	0.60(0.11,3.37)	CBD	
Asthma	0.62(0.09,4.11)	0.29(0.06,1.41)	0.42(0.08,2.15)	0.91(0.12,6.74)	
Hay fever	1.01(0.09,11.63)	0.49(0.05,4.96)	0.60(0.05,6.68)	CBD	
Allergy to dust	0.36(0.07,1.94)	0.79(0.18,3.45)	0.52(0.12,2.29)	0.31(0.05,1.89)	
Irritation in eyes	0.04(0.08,2.02)	1.73(0.39,7.72)	0.55(0.11,2.79)	0.51(0.07,3.50)	
Runny nose	2.31(0.39,13.76)	1.11(0.25,4.99)	2.69(0.53,13.61)	0.15(0.01,1.60)	
Dry throat	0.63(0.08,5.35)	4.99(0.751,30.77)	0.11(0.01,1.74)	0.752(0.07,9.99)	
Cough	0.76(0.15,3.94)	1.13(0.21,5.98)	0.758(0.18,4.41)	3.29(0.58,18.64)	
≥One symptom[b]	0.27(0.04,1.83)	3.32(0.63,17.64)	0.14(0.01,1.32)	0.26(0.02,3.23)	
Eczema	0.12(0.01,1.16)	2.48 (0.27,23.09)	0.12(0.01,2.48)	0.58(0.04,8.81)	
Dry face/hands	0.70(0.06,8.46)	0.46(0.08,2.66)	3.14(0.26,38.04)	CBD	
≥One symptom[c]	1.28(0.25,6.71)	4.94(0.69,35.23)	0.30(0.06,1.46)	3.15(0.43,22.81)	0.74(0.19,2.93)
Migraine	0.56(0.10,3.06)	13.44(2.14,84.44)	0.30(0.48,1.92)	7.33(1.03,52.31)	1.23(0.28,5.45)
Lethargy/Drowsy/Tired	0.61(0.10,3.87)	0.22(0.02,2.17)	0.16(0.02,1.53)	0.79(0.10,6.31)	0.78(0.18,3.35)
Headache	6.85(0.78,60.10)	6.37(1.05,38.82)	0.25(0.04,1.66)	7.06(0.91,54.74)	0.65(0.15,2.85)

Bold means *P*-value less than 0.05

The odds ratio for SBS is calculated with Adjustment for each variable, e.g., TVOC, CO_2, RH, temperature, and noise, respectively

[a]At least one respiratory and mucous membrane SBS symptom, e.g., sinus infection, asthma, hay fever, allergy to dust, irritation in eyes, runny nose, dry throat, and cough

[b]At least one dermatological SBS symptom, e.g., eczema and dry face/hands

[c]At least one general and neurological SBS symptom, e.g., migraine, lethargy/drowsiness/tiredness, and headache

CBD—cannot be determined

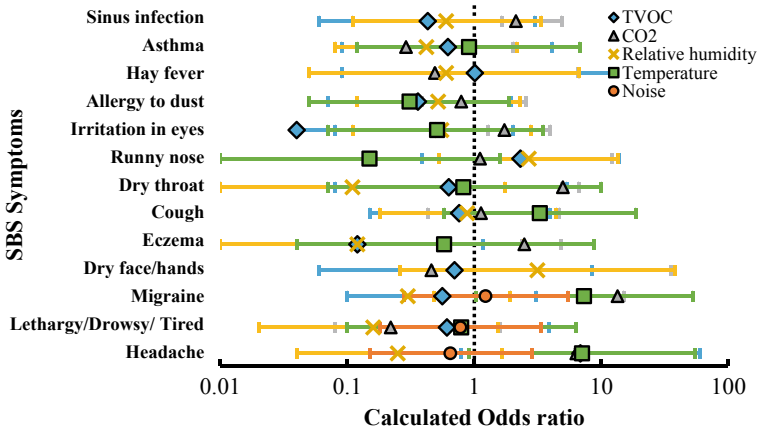

Fig. 8 Forest plot for IEQ measurements and SBS symptoms

mucous membrane symptom, 65% indicated at least one general and neurological symptom, and 30% indicated at least one dermatological symptom.

When considering the indoor and outdoor TVOC concentrations, it was clear that the indoor TVOC concentrations were higher than the outdoor TVOC concentrations. Similarly, indoor CO_2 concentrations were higher than outdoor CO_2 concentrations. However, several indicated otherwise. After further consideration, it was visible that these were either unoccupied apartments or apartments under construction during the visit.

According to the obtained results of this study, outdoor TVOC concentrations reduced rapidly with the apartment height. This can be due to two reasons. Firstly, the reduction of outdoor air pollution at higher elevations due to less activity and the quick flush out of air pollutants due to heavy cross breeze at higher elevations [12]. Eventually, they may create better indoor environments at higher elevations. Cross ventilation also greatly influenced indoor air in naturally ventilated apartments as it was associated with reduced indoor TVOC concentrations. This could be because fresh crosswinds flowing through the apartment might flush out the indoor pollutants.

Cube-type, gel-type, and incense-stick-type incense products were associated with high levels of indoor TVOC concentrations, out of which cube type indicated the worst scenario having 100% of the apartments over the threshold of 0.75 ppm [25]. Also, the results showed that potpourris and essential oil types indicated zero TVOC concentration indoors. Therefore, making it comparatively better incense products to be used in the long run.

Several associations between indoor air parameters and SBS symptoms resulted in higher odds, as per Fig. 8. However, only Headache and Migraine became significant at a 95% confidence interval with *P*-value less than 0.05. This can be due to the lower sample size [28]. Hence, further research should be carried out with a larger sample. Furthermore, for some SBS symptoms (Sinus infection, Hay fever, Dry face, and hands), the odds could not be calculated due to the limitation of sample size. The

study was conducted in 50 apartments, and some of the values required to calculate odds resulted in null and those odds were denoted by CBD in Table 5. Hence, it is advised to conduct the study with an adequate sample of apartments for future research to obtain at least several sample units from each category to overcome these situations.

6 Strengths and Limitations

In this study, the occupants self-reported their SBS symptoms in the questionnaire. This may incur recall bias due to inherent defects of the questionnaire survey. However, the questionnaire-based survey is a reliable source of information from occupants [1, 9]. Since this was a field study, controlling all the variable parameters was not feasible. However, the effect of each parameter can be tested if the study could be conducted in a laboratory environment by altering one variable at a time.

The study focused on the SBS symptoms due to the apartment environment. However, the workplaces of the occupants were not considered. Therefore, associations between SBS symptoms and apartment environments would become more apparent if all other environments were characterized.

The sample contained apartments of middle to high-income people, which can be considered a limitation of this study. However, different results could be expected if the study is expanded to slums and apartments of low-income people. The study was also based on 50 apartment units, which could be considered a low sample size and a limitation. Hence, carrying out this study with larger sample size is recommended to reduce the sampling bias and confirm whether the significant results have been masked.

However, the study is based on one region, so further field studies and controlled laboratory experiments are needed to validate these findings. Nevertheless, these new insights on the potential relationships between IAQ parameters, incense products, and SBS symptoms encourage the importance of ventilation and other means to IAQ.

7 Conclusion

This research conducted a field study on apartments in the Colombo district, focusing on IAQ parameters and SBS symptoms. It analyzed chemical usage, such as incense products' influence on indoor environmental factors. Allergy to dust and Sinus infection were found to be the most common SBS sicknesses prevalent in around 50% of the measured apartments. Runny nose and migraine were prevalent in almost 40% of the measured apartments. Indoor TVOC concentrations varied from 0 ppm to 4.5 ppm, with an average of 0.58 ppm inside occupied apartments. Indoor CO_2 concentrations ranged from 386 to 883 ppm, with a mean of 536 ppm. It was shown

that the outdoor pollutant concentrations were reduced with height and cross ventilation was one of the best ways to reduce indoor pollutant concentration. It was found that indoor chemical usage and incense products, especially the cube type and gel type, led to higher indoor TVOC concentrations. Natural incense products such as potpourris and essential oils were the relatively better incense products to be used in indoor environments concerning indoor TVOC concentrations. Migraine and headache became significant with higher CO_2 concentrations.

Finally, it can be concluded that increased ventilation and minimized usage of indoor chemicals can lead to a better indoor environment inside apartments and safeguard its occupants from Sick Building Syndrome; hence, Policymakers should provide necessary guidelines.

References

1. Andersson K 1998 'Epidemiological approach to indoor air problems*'. Indoor Air 8(S4): 32–39. Available at: https://doi.org/10.1111/J.1600-0668.1998.TB00005.X
2. Apte MG, William JF, Daisey JM 2000 'Associations between indoor CO_2 concentrations and sick building syndrome symptoms in U.S. office buildings: An Analysis of the 1994-1996'. Indoor Air 10(4): 246–257. Available at: https://doi.org/10.1034/j.1600-0668.2000.010004246.x
3. Assimakopoulos VD, Helmis CG 2004 'On the study of a sick building: The case of Athens air traffic control tower'. Energy Build 36(1): 15–22. Available at: https://doi.org/10.1016/S0378-7788(03)00043-4
4. Bakke JV et al. 2008 'Symptoms, complaints, ocular and nasal physiological signs in university staff in relation to indoor environment—temperature and gender interactions'. Indoor Air 18(2): 131–143. Available at: https://doi.org/10.1111/j.1600-0668.2007.00515.x
5. Banbury S, Berry DC 1998 'Disruption of office-related tasks by speech and office noise'. Br J Psychol 89(3): 499–517. Available at: https://doi.org/10.1111/j.2044-8295.1998.tb02699.x
6. Banbury SP, Berry DC 2005 'Office noise and employee concentration: Identifying causes of disruption and potential improvements'. Ergonomics 48(1): 25–37. Available at: https://doi.org/10.1080/00140130412331311390
7. Cao SJ, Deng HY 2019 'Investigation of temperature regulation effects on indoor thermal comfort, air quality, and energy savings toward green residential buildings'. Sci Technol Built Environ 25(3): 309–321. Available at: https://doi.org/10.1080/23744731.2018.1526016
8. Engvall K, Norrby C, Sandstedt E 2004a 'The Stockholm indoor environment questionnaire: A sociologically based tool for the assessment of indoor environment and health in dwellings'. Indoor Air 14(1): 24–33. Available at: https://doi.org/10.1111/J.1600-0668.2004.00204.X
9. Engvall K, Norrby C, Sandstedt E 2004b 'The Stockholm indoor environment questionnaire: A sociologically based tool for the assessment of indoor environment and health in dwellings'. Indoor Air 14(1): 24–33. Available at: https://doi.org/10.1111/J.1600-0668.2004.00204.X
10. Eriksson NM, Stenberg BGT 2006 'Baseline prevalence of symptoms related to indoor environment'. Scand J Public Health 34(4): 387–396. Available at: https://doi.org/10.1080/14034940500228281
11. Husein AH 2021 'Multifunctional furniture as a smart solution for small spaces for the case of Zaniary towers apartments in Erbil City, Iraq'. Researchgate.net 12(1): 1–11. Available at: https://doi.org/10.14456/ITJEMAST.2021.8
12. Irwin P, Kilpatrick J, Robinson J, and Frisque A 2008 'Wind and tall buildings: negatives and positives'. The Structural Design of Tall and Special Buildings, 17(5): 915–928. https://doi.org/10.1002/TAL.482

13. Jaakkola MS et al. 2007 'Office work exposures and respiratory and sick building syndrome symptoms'. Occup Environ Med 64(3): 178–184. Available at: https://doi.org/10.1136/OEM.2005.024596
14. Kinman G, Griffin M 2008 'Psychosocial factors and gender as predictors of symptoms associated with sick building syndrome'. Stress Health 24(2): 165–171. Available at: https://doi.org/10.1002/smi.1175
15. Lu C et al. 2016 'Outdoor air pollution, meteorological conditions and indoor factors in dwellings in relation to sick building syndrome (SBS) among adults in China'. Sci Total Environ 560–561: 186–196. Available at: https://doi.org/10.1016/j.scitotenv.2016.04.033
16. Lu CY et al. 2017a 'Personal, psychosocial and environmental factors related to sick building syndrome in official employees of Taiwan'. Int J Environ Res Public Health 15(1): 7. Available at: https://doi.org/10.3390/IJERPH15010007
17. Lu CY et al. 2017b 'Personal, psychosocial and environmental factors related to sick building syndrome in official employees of Taiwan'. Int J Environ Res Public Health 15(1): 7. Available at: https://doi.org/10.3390/IJERPH15010007
18. Mendell MJ, Kumagai K 2017 'Observation-based metrics for residential dampness and mold with dose–response relationships to health: A review'. Indoor Air. Blackwell Munksgaard: 506–517. Available at: https://doi.org/10.1111/ina.12342
19. Mendes A, Teixeira JP 2014 'Sick building syndrome'. Encyclopedia of Toxicology, 3rd edn. pp. 256–260. Available at: https://doi.org/10.1016/B978-0-12-386454-3.00432-2
20. Murniati N 2020 'Sick building syndrome in Indonesia and Singapore: A comparative study'. In: Proceedings of the 3rd International Conference on Vocational Higher Education (ICVHE 2018). Paris, France: Atlantis Press, pp. 278–283. Available at: https://doi.org/10.2991/assehr.k.200331.153
21. Nielsen GD et al. 2007 'Do indoor chemicals promote development of airway allergy?'. Indoor Air 17(3): 236–255. Available at: https://doi.org/10.1111/J.1600-0668.2006.00468.X
22. Norback D, Edling C 1991 'Environmental, occupational, and personal factors related to the prevalence of sick building syndrome in the general population.' Occup Environ Med 48(7): 451–462. Available at: https://doi.org/10.1136/OEM.48.7.451
23. Norhidayah A et al. 2013 'Indoor air quality and sick building syndrome in three selected buildings'. In: Procedia Engineering. Elsevier Ltd, pp. 93–98. Available at: https://doi.org/10.1016/j.proeng.2013.02.014
24. Oh HJ et al. 2020 'Exposure to respirable particles and TVOC in underground parking garages under different types of ventilation and their associated health effects'. Air Qual, Atmos & Health 13(3): 297–308. Available at: https://doi.org/10.1007/S11869-020-00791-0
25. OSHA 2011 OSHA Fact Sheet: Formaldehyde | Occupational safety and health administration. Available at: https://www.osha.gov/OshDoc/data_General_Facts/formaldehyde-factsheet.html (Accessed: 9 March 2021)
26. Reiko K, Norbäck D,Araki A 2020 'Indoor environmental quality and health risk toward healthier environment for all. Singapore: Springer Link. https://doi.org/10.1007/978-981-32-9182-9
27. Rodrigo GA, Perera BAKS, Ekanayake BJ 2019 'Occupant perceptions on the thermal comfort guidelines in air-conditioned offices in Colombo, Sri Lanka'. Int J Constr Manag: 1–9. Available at: https://doi.org/10.1080/15623599.2019.1639125
28. Royall RM 1986 'The effect of sample size on the meaning of significance tests'. Am Stat 40(4): 313–315. Available at: https://doi.org/10.1080/00031305.1986.10475424
29. Sahlberg B et al. 2013 'Airborne molds and bacteria, microbial volatile organic compounds (MVOC), plasticizers and formaldehyde in dwellings in three North European cities in relation to sick building syndrome (SBS)'. Sci Total Environ 444: 433–440. Available at: https://doi.org/10.1016/j.scitotenv.2012.10.114
30. Sahlberg B, Mi YH, Norbäck D 2009 'Indoor environment in dwellings, asthma, allergies, and sick building syndrome in the Swedish population: a longitudinal cohort study from 1989 to 1997'. Int Arch Occup Environ Health 82(10): 1211–1218. Available at: https://doi.org/10.1007/S00420-009-0444-3

31. Sahlberg B, Wieslander G Norbäck D 2010 'Sick building syndrome in relation to domestic exposure in Sweden—A cohort study from 1991 to 2001'. Scand J Public Health 38(3): 232–238. Available at: https://doi.org/10.1177/1403494809350517
32. Saijo Y et al. 2009 'Relation of dampness to sick building syndrome in Japanese public apartment houses'. Environ Health Prev Med 14(1): 26–35. Available at: https://doi.org/10.1007/s12199-008-0052-y
33. Shan X et al. 2016 'Comparing mixing and displacement ventilation in tutorial rooms: Students' thermal comfort, sick building syndromes, and short-term performance'. Build Environ 102: 128–137. Available at: https://doi.org/10.1016/j.buildenv.2016.03.025
34. Silva GV, Martins AO, Martins SDS 2021 'Indoor air quality: Assessment of dangerous substances in incense products'. Int J Environ Res Public Health 18(15): 8086. Available at: https://doi.org/10.3390/IJERPH18158086
35. Simoni M et al. 2010 'School air quality related to dry cough, rhinitis and nasal patency in children'. Eur Respir J 35(4): 742–749. Available at: https://doi.org/10.1183/09031936.00016309
36. Staub PO, Geck MS, Weckerle CS 2011 'Incense and ritual plant use in Southwest China: A case study among the Bai in Shaxi'. J Ethnobiol Ethnomedicine 7(1): 1–16. Available at: https://doi.org/10.1186/1746-4269-7-43/FIGURES/7
37. Sun C et al. 2018 'Outdoor air pollution in relation to sick building syndrome (SBS) symptoms among residents in Shanghai, China'. Energy Build 174: 68–76. Available at: https://doi.org/10.1016/j.enbuild.2018.06.005
38. Sun Y et al. 2013 'Effects of gender and dormitory environment on sick building syndrome symptoms among college students in Tianjin, China'. Build Environ 68: 134–139. Available at: https://doi.org/10.1016/j.buildenv.2013.06.010
39. Sun Y et al. 2019 'Indoor air quality, ventilation and their associations with sick building syndrome in Chinese homes'. Energy Build 197: 112–119. Available at: https://doi.org/10.1016/j.enbuild.2019.05.046
40. Sundell J 1994 'On the association between building ventilation characteristics, some indoor environmental exposures, some allergic manifestations and subjective symptom reports'. Indoor Air 4(S2): 7–49. Available at: https://doi.org/10.1111/J.1600-0668.1994.TB00031.X
41. Sundell J 2004 'On the history of indoor air quality and health'. Indoor Air, Suppl: 51–58. Available at: https://doi.org/10.1111/j.1600-0668.2004.00273.x
42. Surahman U, Ray HRD (2020) IOP Conference series: Earth and environmental science sick building syndrome and its effect on health of students and teachers in selected educational buildings in Bandung Sick building syndrome and its effect on health of students and teachers in selected educational buildings in Bandung. Available at: https://doi.org/10.1088/1755-1315/447/1/012049
43. Thach TQ et al. 2019 'Prevalence of sick building syndrome and its association with perceived indoor environmental quality in an Asian multi-ethnic working population'. Build Environ 166: 106420. Available at: https://doi.org/10.1016/j.buildenv.2019.106420
44. Tong XW, Lee LN, Kim MJ 2021 'Smart management services for high-rise apartments in Beijing, China'. 21(5): 1792–1800. Available at: https://doi.org/10.1080/13467581.2021.1964974
45. US EPA 2012 Indoor air quality glossary|US EPA. Available at: https://sor.epa.gov/sor_internet/registry/termreg/searchandretrieve/glossariesandkeywordlists/search.do?details=&glossaryName=IAQ%20Glossary#formTop (Accessed: 16 March 2022)
46. Vasile V, Petcu C, Iordache V 2019 Experimental studies on TVOC concentrations and their relationships with indoor comfort parameters. REV.CHIM.(Bucharest) ♦. Available at: http://www.revistadechimie.ro (Accessed: 12 April 2020)
47. Virji MA et al. 2019 'Peaks, means, and determinants of real-time TVOC exposures associated with cleaning and disinfecting tasks in healthcare settings'. Ann Work Expo Health 63(7): 759–772. Available at: https://doi.org/10.1093/ANNWEH/WXZ043
48. Wang J et al. 2022 'Eczema, facial erythema, and seborrheic dermatitis symptoms among young adults in China in relation to ambient air pollution, climate, and home environment'. Indoor Air 32(1): e12918. Available at: https://doi.org/10.1111/INA.12918

49. Wargocki P 2000 'The effects of outdoor air supply rate in an office on perceived air quality, sick building syndrome (SBS) symptoms and productivity'. Indoor Air 10(4): 222–236. Available at: https://doi.org/10.1034/j.1600-0668.2000.010004222.x
50. Wei W et al. 2022 'Predicting chemical emissions from household cleaning and personal care products: A review'. Build Environ 207: 108483. Available at: https://doi.org/10.1016/J.BUILDENV.2021.108483
51. WHO 2015 Sri Lanka HEALTH ESTIMATES. Available at: www.who.int (Accessed: 22 June 2021)
52. WHO 2018 'Health effects of Indoor air pollution in developing countries'. WHO [Preprint]
53. Zhang X et al. 2019 'Dampness and mold in homes across China: Associations with rhinitis, ocular, throat and dermal symptoms, headache and fatigue among adults'. Indoor Air 29(1): 30–42. Available at: https://doi.org/10.1111/ina.12517

Life Cycle Assessment (LCA) of a Textile Waste Thermoplastic Composite Material for Wall Partitioning Applications

R. M. N. Sulochani, R. A. Jayasinghe, C. Fernando, A. H. L. R. Nilmini, and G. Priyadarshana

Abstract As one of the most pollution-generating industries in the world, the textile industry generates large volumes of waste at the end of its manufacturing process. This waste is frequently dumped in open areas or is openly burned, contributing to GHG emissions. In recent years, emphasis has been placed on developing new materials from textile waste to promote a circular textile economy. The construction industry is one application for these novel materials. The construction industry consumes a lot of resources and energy. As a result, recycled and upcycled building materials are gaining popularity in the construction industry. The research team developed a new composite material for non-structural applications using polyester textile waste and thermoplastic packaging waste. This study aimed to conduct a Life Cycle Assessment (LCA) to determine the sustainability of this new material as a substitute for partitioning wall materials available in the market. The goal of the LCA study was to compare the Global Warming Potential (including biogenic CO_2) of the production phase of the composite material against the gypsum partitioning board. The scope of the study focused on the Sri Lankan context. The functional unit for this study was considered as 1 m^2 of each type of material. The modeling was carried out using GaBi LCA modeling software (V8.7.1.3). The LCI inputs for the production phase of the composite were based on literature data, the GaBi database (V8.7.1.3), and the Ecoinvent 3.8 database. According to the analysis, the production of 1 m^2 of the new composite board as an alternative material saves GHG 8.4617 kg CO_2 eq compared to virgin gypsum boards. These findings suggest that using waste resources to create new construction materials aids the sustainability efforts of both industries. The findings are also useful in making decisions on using waste-based composites in specific applications.

R. M. N. Sulochani (✉) · R. A. Jayasinghe · A. H. L. R. Nilmini · G. Priyadarshana
University of Sri Jayewardenepura, Homagama 10206, Sri Lanka
e-mail: sulochanirathnayaka@sjp.ac.lk

C. Fernando
The Australian National University, Canberra, Canberra ACT 2601, Australia

© The Author(s), under exclusive license to Springer Nature Singapore Pte Ltd. 2023

R. Dissanayake et al. (eds.), *ICSBE 2022*, Lecture Notes in Civil Engineering 362,
https://doi.org/10.1007/978-981-99-3471-3_31

Keywords GHG · Global Warming Potential · LCA · Wall partitioning material · Textile waste · Thermoplastic composite

1 Introduction

The textile industry is one of the largest manufacturing sectors, playing an essential role in the global economy. Despite the positive effects on the economy, the generation of large volumes of textile waste is a critical industrial and operational challenge the textile industry faces. Currently, they operate almost entirely linearly—extracting resources for production, manufacturing, consuming items, and finally disposing of waste. As such, it is also one of the world's most pollution-generating industries [12].

The textile industry is one of the largest manufacturing industries in Sri Lanka. The sector plays a critical role in the country's economy, with the largest contribution to the country's exports. It is the highest foreign exchange earner in the industrial sector, accounting for 40 percent of total exports and 52 percent of industrial exports [25]. However, improper management of textile waste and its harmful effects are some of the significant challenges the textile sector faces. In 2014, 294,000 tons of textiles were imported to Sri Lanka for garment manufacturing, leaving a minimum of 44,100 tons of pre-consumer textile waste [22]. Most of this generated textile waste usually goes to open dumpsites or is disposed of through open burning [15].

According to Mishra et al. [21], a considerable percentage of textile waste consists of polyester and polyester/cotton blends. Since synthetic textile waste is non-biodegradable, environmental concerns have increased with the increasing volumes of textile waste [6]. More than 150 million tons of textile waste will be landfilled or openly burned in 2050 [18].

Textile waste landfilling contaminates the groundwater and generates toxic greenhouse gases during decomposition [10]. Therefore, landfilling and open dumping has become serious problems. When considering the life cycle of textile products from production to disposal, the sector contributes to 10% of the world's carbon emissions [4]. Accordingly, the report "A new textile economy" by the Ellen MacArthur Foundation highlights the importance of moving away from this wasteful linear textile economy to a new circular textile economy [12].

In recent years, increased emphasis has been given to developing new materials from industrial waste products to reduce waste and protect the environment [27]. Using recycled materials in the building and construction sector has gained widespread interest because the building and construction sectors use large amounts of materials and energy. There is also a growing demand for low-cost non-structural building materials such as partition boards and wall claddings in the building and construction sector.

Using textile waste in construction sector materials has multiple advantages, including reducing fiber production for new building materials through extraction or agricultural methods while reducing pollution from landfilling or incineration of

textile waste. Accordingly, the research team developed a textile waste fiber reinforced polymer composite material using pre-consumer polyester textile waste and thermoplastic packaging material waste used in the textile industry in Sri Lanka. This study aimed to conduct a Life Cycle Assessment (LCA) to determine the sustainability of this new material in terms of Global Warming Potential (GWP), as a substitute for partitioning wall materials available in the market.

Life cycle assessment (LCA) is a systematic tool used to assess the total life cycle of a product or service from the cradle to the grave: i.e., from raw materials extraction to the end of life of the product [9]. LCA is built on a set of environmental management standards: ISO 14040, presented by the International Standards Organization [17]. Mainly, there are four phases of LCA [17]: Goal and scope definition, Lifecycle Inventory (LCI) analysis, Lifecycle impact assessment (LCIA), and Interpretation.

The results obtained from the LCA are a compilation of inflows and outflows of the product system concerning the functional unit [13]. The system boundary of LCA describes the boundaries (or margins) for which processes in the lifecycle of the product are comprised in the LCA: Which inputs and outputs decide to include or exclude [26]. Establishing system boundaries is important to determine the start and the end of a single LCA study. By establishing a system boundary, the inflows and outflows related to the functional unit within the boundary are assessed.

Although LCA is simple as it seems, it is complex because of the difficulties in establishing system boundaries, finding accurate data, and evaluating the results [26]. Despite these several limitations, LCA offers a great perception of a lifecycle of a product that no other tool can offer. Furthermore, LCA can be used to compare two or more products to find more preferred products from an environmental point of view. The interest has grown in comparing the environmental impacts of different products. Some studies have conducted comparative life cycle assessments of composites with existing conventional materials. LCA allows using a functional unit of a specific product or service which easily facilitates comparative analysis [8]. A fair comparison can be conducted by using the same functional unit of the compared products.

Few studies have conducted comparative LCA studies for applications in the building or construction industry [3, 23, 24, 29]. Some studies have shown that replacing conventional plasterboards with composites significantly reduces environmental impacts [23, 24]. Moreover, Global Warming Potential (GWP) has been used as the primary life cycle impact assessment indicator in many different fields, including the construction sector [16, 23, 24, 29]. Global Warming Potential primarily concentrates on quantifying the emissions of greenhouse gases (GHG) in the atmosphere and their influence on global warming and climate change [14].

2 Methodology

2.1 Goal and Scope Definition of the Study

An LCA study has four stages, beginning with the goal and scope definition. This defines the goals of an LCA and explains the boundaries of the study. Without identifying the boundaries, the single LCA study may include a limitless amount of data. The goal of the LCA study is to evaluate the Global Warming Potential (GWP), including biogenic CO_2 in the production phase of the polyester textile waste-based thermoplastic composites, against the gypsum partitioning board developed using virgin raw materials. The scope of the case study focused on the Sri Lankan context.

The motivation for this study comes from a recent composite material developed using industrial waste, intending to use them in non-structural building applications. The polyester textile waste fiber reinforced polymer composite materials focused on in this study were developed using pre-consumer polyester textile waste and the waste thermoplastic packaging materials discarded from the Sri Lankan textile industry. The composite manufacturing technique was compression molding.

From a series of composite materials developed by varying textile waste and packaging waste ratios, the 7.5 wt% waste polyester textile fiber reinforced thermoplastic composite showed better mechanical properties. Accordingly, the production phase of that specific composite was chosen as the scope of this study. This study excludes waste material collection for the production of the composites, use phases, and end-of-life (EoL) management. Since the material can be used for different purposes, the use phase is uncertain. Since there is no proper waste management system, the end-of-life phase also depends on the practice used to dispose of the waste materials. Waste materials collection for the production of the composites may also depend on the distance to the collection site, mode of transportation, etc. Due to these uncertainties, the data is difficult to obtain for the use phase and end-of-life phases.

The findings were compared with gypsum plasterboards made from virgin materials available in the GaBi professional database (V8.7.1.3). Secondary polypropylene was used as a proxy for the matrix because it was the most suitable material with environmental data documented in available databases.

2.2 Functional Unit

The functional unit for this study is considered to be 1 m^2 of each type of material. This is the most suitable functional unit that can be used to assess the environmental impacts of partition boards [24].

2.3 Inventory Analysis

2.3.1 Data Collection

One of the most prominent strengths of LCA is the inclusion of all inputs and outputs related to a product's entire life cycle. However, it also becomes a limitation because LCAs need a lot of time and resources to collect data. Although this issue has been addressed by establishing commercial databases, these databases cannot be detailed enough to evaluate every situation.

Therefore, this lack of data can be solved by carefully using similar processes or leaving the least essential steps out of the boundary [7]. For example, in this study, due to the lack of data related to the waste low-density polyethylene/linear-low-density polyethylene blend (matrix), the study used secondary polypropylene, which is also a polyolefin.

2.3.2 Life Cycle Inventory (LCI) Inputs

The LCI inputs for the production phase of waste polyester textile fiber reinforced thermoplastic composites were based on literature data, the GaBi professional database (V8.7.1.3), and the Ecoinvent 3.8 database. The energy requirements for different activities involved in the production of the composites are shown in Table 1.

In addition to the energy inputs and raw material inputs (textile waste and packaging material waste) required for waste polyester textile fiber reinforced thermoplastic composite development, water (3 L) required for cold pressing was considered as a material input.

The production phase, including energy and raw material inputs, is displayed in Fig. 1.

Table 1 Energy requirements of different activities involved in the production of the waste polyester textile fiber reinforced thermoplastic composites

Activity	Energy requirement (MJ/kg)	Type of energy	Reference
Shredding	2.14	Electrical energy	[5]
Pre-pressing	3.6	Electrical energy	[1]
Cold-pressing	0.9	Electrical energy	[20]
Compression molding	9.12	Electrical energy	[19]

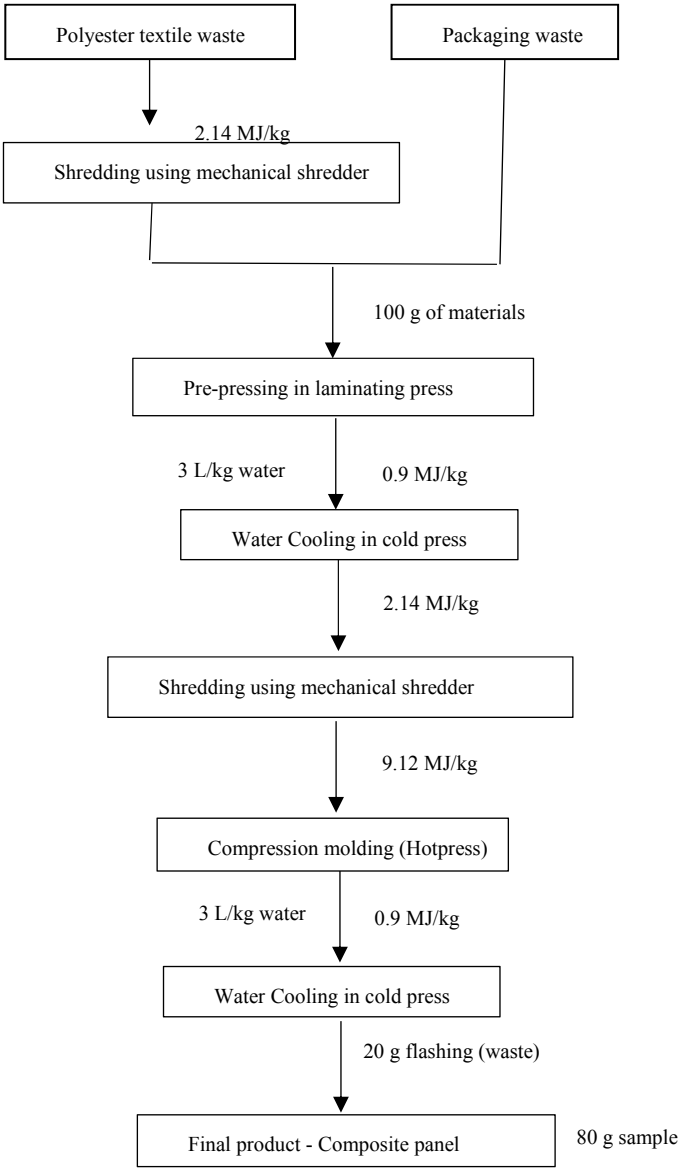

Fig. 1 The system boundary or the scope of the LCA study

2.3.3 Life Cycle Impact Assessment (LCIA)

The LCIA translates the contribution of the emissions determined in inventory analysis into potential environmental impact. The LCIA was performed according to the ILCD PEF (V1.06) recommendations.

3 Results and Discussions

The results obtained for Global Warming Potential (GWP) are shown in Fig. 2.

By producing 1 m^2 (3.5552 kg) of the completely waste-based thermoplastic composite board as an alternative material, it can save GHG 8.4617 kg CO_2 eq totally against using the gypsum plasterboards developed using virgin materials for the same application. The data available in the GaBi database (V8.7.1.3) was used for gypsum plasterboards.

Although the waste packaging material is made with a Low-density polyethylene/Linear-low density polyethylene blend, the "market for secondary Polypropylene

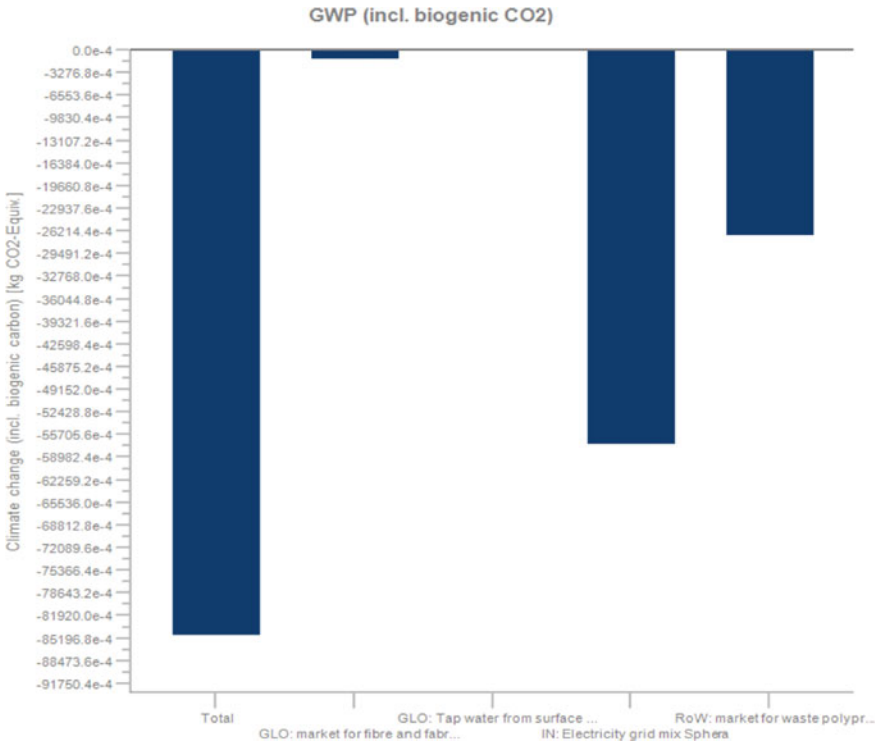

Fig. 2 GHG emissions results ($kgCO_2/m^2$)

(market to waste)" was used as a proxy from Ecoinvent 3.8 database. The matrix used in this study is a waste of predefined process. In such a situation, polypropylene, which is generated as a by-product in processes was the only option available. GWP of virgin low-density polyethylene is slightly higher than virgin polypropylene, but it is not a significant gap [2]. Hence, using polypropylene as a proxy for the packaging materials does not affect the final result of LCA.

For the polyester textile waste, the material category "market for fiber, and fabric waste, polyester (market to waste)" was used as a proxy from Ecoinvent 3.8 database [11]. This fiber and fabric waste, polyester, is also generated as a by-product in undefined processes.

Data based on a Global data set (GLO) was used for waste polyester fibers, polypropylene matrix, and tap water from surface water due to the data availability constraint in the Sri Lankan context. For the electrical grid mixed GHG factor, the Indian grid was used as a proxy from the GaBi database (V8.7.1.3).

In the meantime, there is a limitation for local data availability for the manufacturing technology used for this composite material development because, still, this is not an established industry. Moreover, the exact data related to the inputs are not available in the global databases. As there is a gap in such data availability, these limitations are identified as uncertainties for the conducted LCA study.

The environmental impact of composite materials made with recycled materials can be lower than that of composite materials made with virgin materials, which is confirmed by the results. This is attributed to the fact that the raw material extraction and processing steps are omitted since the secondary materials or by-products are used as raw materials for composite materials made with recycled materials [28].

4 Conclusion and Future Work

There is a demand for building materials made from waste as environmentally friendly materials in green buildings. The polyester textile fiber reinforced thermoplastic composite was made entirely from waste materials. This provides an excellent case study for a Life Cycle Assessment. The Life Cycle Assessment shows that the completely waste-based 7.5 wt% waste polyester textile fiber reinforced thermoplastic composite can be employed as a sustainable option in terms of global warming potential compared to the gypsum plasterboards used in partitioning applications. These findings suggest that using waste resources to create new construction materials aids the sustainability efforts of both textile and construction industries. The findings are also useful in making decisions on using waste-based composites in specific applications.

In this study, the life cycle assessment of thermoplastic composites was conducted only for Global Warming Potential (GWP). In future work, life cycle assessments can be conducted using various impact categories such as depletion of abiotic resources—fossil fuels, ozone layer depletion, and human toxicity potential—cancerous and non-cancerous.

Acknowledgements Financial assistance by the University of Sri Jayewardenepura research grant: ASP/01/RE/FOT/2017/84.

References

1. A.Buisine Sas 2021 Heat press Secabo TC_2, A.Buisine Sas. Available at: https://www.serigraphie-boutique.fr/epages/54456119.sf/en_GB/?ObjectPath=/Shops/54456119/Products/12512 (Accessed: 20 December 2021)
2. AlMa'adeed M et al (2011) Life cycle assessment of particulate recycled low-density polyethylene and recycled polypropylene reinforced with talc and fiberglass. Key Eng Mater. https://doi.org/10.4028/www.scientific.net/KEM.471-472.999
3. Asdrubali F, Schiavoni S, Horoshenkov KV (2012) A review of sustainable materials for acoustic applications. Build Acoust 19(4):283–312
4. Bell NC et al. 2018 Tackling problematic textile waste streams. Oakdene Hollins Ltd, Aylesbury, UK. Available at: http://www.resyntex.eu (Accessed: 6 May 2021)
5. Briassoulis D, Hiskakis M, Babou E (2013) Technical specifications for mechanical recycling of agricultural plastic waste. Waste Manag, Elsevier Ltd 33(6):1516–1530. https://doi.org/10.1016/j.wasman.2013.03.004
6. Briga-Sá A et al (2013) Textile waste as an alternative thermal insulation building material solution. Constr Build Mater 38:155–160. https://doi.org/10.1016/j.conbuildmat.2012.08.037
7. Corbiere-Nicollier T et al (2001) Life cycle assessment of bio fibers replacing glass fibers as reinforcement in plastics. Resour Conserv Recycl 33:267–287
8. Dassisti M et al (2016) Thermography-enhanced LCA (Life Cycle Assessment) for manufacturing sustainability assessment: The case study of an HDPE (High-Density Polyethylene) net company in Italy. Energy 108:7–18
9. David G et al (2021) Using life cycle assessment to quantify the environmental benefit of upcycling vine shoots as fillers in biocomposite packaging materials. Int J Life Cycle Assess 26:738–752. https://doi.org/10.1007/s11367-020-01824-7
10. Dissanayake DGK et al (2018) Developing a compression molded thermal insulation panel using post-industrial textile waste. Waste Manage 79:356–361. https://doi.org/10.1016/j.wasman.2018.08.001
11. Ecoinvent association 2021 Eco-invent 3.8 Dataset Documentation 'market for fiber and fabric waste, polyester—GLO'
12. Ellen MacArthur Foundation 2017 A new textiles economy: Redesigning fashion's future. Available at: http://www.ellenmacarthurfoundation.org/publications.
13. Finnveden G et al (2009) Recent developments in Life Cycle Assessment. J Environ Manag, Elsevier Ltd 91(1):1–21. https://doi.org/10.1016/j.jenvman.2009.06.018
14. Forcellese A et al. 2020 'Life cycle impact assessment of different manufacturing technologies for automotive CFRP components'. J Clean Prod, Elsevier Ltd. https://doi.org/10.1016/j.jclepro.2020.122677
15. Gannoruwa GKBM, Nanayakkara SMA, Muthurathna SSK 2019 'Utilization of textile waste in development of interlocking paving blocks for foot paths'. In Dissanayake R et al. (eds) Proceedings of the 10th International Conference on Structural Engineering and Construction Management. Moratuwa, Katubadda: Springer Nature Singapore Pte Ltd., pp 543–554. https://doi.org/10.1007/978-981-15-7222-7_44
16. Gonçalves M, Monteiro H, Iten M (2022) 'Life Cycle Assessment studies on lightweight materials for automotive applications—an overview.' Energy Rep, Elsevier Ltd 8:338–345. https://doi.org/10.1016/j.egyr.2022.01.067
17. ISO 14040 2006 Environmental management—Life cycle assessment—Principles and framework, international organization for standardization. Available at: https://www.iso.org/obp/ui/#iso:std:iso:14040:ed-2:v1:en (Accessed: 17 June 2021)

18. Kamble Z. et al. 2020 'Development and characterization of thermoset nanocomposites reinforced with cotton fibers recovered from textile waste'. J Ind Textile: 1–27. https://doi.org/10.1177/1528083720913535
19. Liddell HPH et al. 2016 'Manufacturing energy intensity and opportunity analysis for fiber-reinforced polymer composites and other lightweight materials'
20. Meng F et al (2017) 'Energy and environmental assessment and reuse of fluidized bed recycled carbon fibers.' Composites Part A, Elsevier Ltd 100:206–214. https://doi.org/10.1016/j.compositesa.2017.05.008
21. Mishra R, Behera BK, Militky J (2013) 3D woven green composites from textile waste: Mechanical performance. J Text Inst. https://doi.org/10.1080/00405000.2013.820865
22. Park C 2017 Transtextile project: High-value innovation for industrial textile waste in Sri Lanka". The UK
23. Quintana-Gallardo A et al (2020) Life-Cycle assessment and acoustic simulation of drywall building partitions with bio-based materials. Polymers 12(1965):1–16. https://doi.org/10.3390/polym12091965
24. Quintana A et al (2018) Comparative Life Cycle Assessment of gypsum plasterboard and a new kind of bio-based epoxy composite containing different natural fibers. J Clean Prod 185:408–420. https://doi.org/10.1016/j.jclepro.2018.03.042
25. Shiwanthi S, Lokupitiya E, Peiris S (2018) 'Evaluation of the environmental and economic performances of three selected textile factories in Biyagama export processing zone.' Environ Dev, Elsevier Ltd 27:70–82. https://doi.org/10.1016/j.envdev.2018.07.006
26. Song YS, Youn JR, Gutowski TG (2009) Life cycle energy analysis of fiber-reinforced composites. Composites Part A, Elsevier Ltd 40(8):1257–1265. https://doi.org/10.1016/j.compositesa.2009.05.020
27. Vadiwala K, Vaghani M 2015 'An overview reuse of solid waste for constructing building materials'. Int J Sci Res & Dev 3
28. Vidal R, Martínez P, Garraín D (2009) Life cycle assessment of composite materials made of recycled thermoplastics combined with rice husks and cotton linters. Int J Life Cycle Assess 14:73–82. https://doi.org/10.1007/s11367-008-0043-7
29. Zhenguo P, Lili MA, Xianzheng G (2014) Comparison of Life Cycle Environmental impacts between natural gypsum board and FGD gypsum board. Key Eng Mater 599:15–18. https://doi.org/10.4028/www.scientific.net/KEM.599.15

Prefabricated Construction in Sri Lanka: From a Sustainability Perspective

J. Jayawardana, J. A. S. C. Jayasinghe, A. K. Kulatunga, M. Sandanayake, and G. Zhang

Abstract Prefabricated construction is increasingly applied in the global construction sector because it offers a range of advantages compared to traditional construction. Improved product quality, enhanced productivity, reduced overall construction times, and environmental benefits such as reduced waste generation and energy savings are some advantages highlighted by recent research publications. However, the prefabricated construction adoption in Sri Lanka is comparatively less compared to developed and industrialized economies. More research is required in the Sri Lankan context to evaluate, compare, and promote these prefabrication practices. Hence, the current study aims to explore the sustainability of construction practices in Sri Lanka that accompany prefabrication. Relevant information is collected through site visits and questionnaires, and digital communications. The potential sustainability aspects of the ongoing construction of a three-storey family house using prefabricated components and selected wall panel prefabrication processes in Sri Lanka are explored. Moreover, a life cycle assessment is conducted to assess the environmental sustainability of prefabricated wall panels in Sri Lanka. LCA outcomes show that wall panels produced using paddy straw fibres have greater savings than cellular lightweight concrete wall panels manufactured using concrete foaming and precast concrete wall panels. However, decisions should be based on specific applications and conditions, such as non-load-bearing applications and temporary housing implementations. The current study aims to increase the awareness of prefabricated practices in Sri Lanka and to give some insights into the sustainability perspective of these prefabrication methods focusing on construction stakeholders.

Keywords Life cycle assessment (LCA) · Prefabricated construction · Sri Lanka · Prefabricated wall panels · Sustainability

J. Jayawardana (✉) · J. A. S. C. Jayasinghe · A. K. Kulatunga
Faculty of Engineering, University of Peradeniya, Peradeniya 20400, Sri Lanka
e-mail: s3884217@student.rmit.edu.au

J. Jayawardana · G. Zhang
School of Engineering, RMIT University, Melbourne, VIC 3001, Australia

M. Sandanayake
College of Engineering and Science, Victoria University, Melbourne, VIC 3001, Australia

© The Author(s), under exclusive license to Springer Nature Singapore Pte Ltd. 2023

R. Dissanayake et al. (eds.), *ICSBE 2022*, Lecture Notes in Civil Engineering 362,
https://doi.org/10.1007/978-981-99-3471-3_32

1 Introduction

Construction, a mega industry, has an unceasing demand over the timeline caused by the human population, economic expansion, and rapid globalization. For example, the Sri Lankan construction industry has shown accelerated growth in developing high-end residential, commercial space, hotel and resort construction, and infrastructure since 2010 (post-Sri Lankan civil war era). On top of that, multiple local and international construction organizations are active in the industry. Moreover, the construction sector contributed 6.2% of the GDP in 2020 and employed about 600,000 workers [16]. The traditional way of construction has its own sustainability issues in environmental, economic, and social domains [1, 8, 12, 14]. Hence, the increasing magnitude of the construction industry will affect more negatively on the sustainability unless the world moves into more innovative construction methods.

Prefabricated construction, a modern method of construction, manufactures prefabricated/modular components in an off-site manufacturing factory, then transports and assembles them on the final construction site [4]. Prefabricated construction initially got the attraction due to some unique benefits, such as increased product quality and process productivity. Moreover, the research has shown the potential savings in energy consumption, reduced greenhouse gas (GHG) emissions and waste generation [2, 3, 9–11, 13]. However, despite the well-documented merits, the level of application in the Sri Lankan construction industry is lesser than in other developed and industrialized economies [6, 7].

The current economic crisis has dramatically affected the Sri Lankan construction sector. Spiked material, fuel, and logistic costs directly influenced the standstill of construction projects. Thus, a novel approach to construction is required now more than ever. The use of prefabrication practices in construction has the potential to improve process efficiencies in the long term, consequently enhancing sustainability. Hence, the current study aims to explore sustainable construction practices in Sri Lanka which accompany prefabrication. The sustainability aspects of the ongoing construction of a three-storey family house using prefabricated components are presented in this paper. Furthermore, the sustainability perspective of three wall panel production processes in Sri Lanka is explored. Finally, the environmental impacts of selected prefabricated components are evaluated using the life cycle assessment (LCA) methodology.

2 Methodology

2.1 Information Collection

Prefabrication manufacturing plants were visited to identify and understand the relevant processes to produce prefabricated building elements. The case study family house building construction site was also visited to understand the way forward

in constructing the building and to see the progress from the initial plan. The required information for this study was collected through site visits and unstructured questionnaires through digital communication methods.

2.2 Life Cycle Assessment Methodology

Life cycle assessment methodology assesses the environmental performance of a product system throughout its life cycle, from the raw material extraction and processing stage to the end-of-life stage [5]. ISO 14040:2006 presents the principles and framework for LCA. LCA is elaborated under four main steps (definition of the goal and scope of the LCA, the life cycle inventory phase, the life cycle impact assessment phase, and the life cycle interpretation phase) in this standard.

The main goal of the LCA is to quantify the environmental impacts of prefabricated wall panels produced in Sri Lanka. Process-based LCA is selected for the assessment. Moreover, the system boundary of the wall panel production is selected as cradle-to-gate. In terms of life cycle inventory, the necessary data was collected as described in Sect. 2.1. Furthermore, the Ecoinvent 3.3 database is used as the main secondary data reference in this LCA study. The life cycle impact assessment was conducted in SimaPro 8.3.0.0 Ph.D. Version. ReCiPe Midpoint (H) V1.13 is selected as the primary method for the LCIA. The midpoint impacts are chosen based on a cumulative cut-off percentage of 90%.

3 Ongoing Construction of a Family House Using Prefabricated Components in Sri Lanka

The three-storey family house construction is situated in Siyambalagasthenna, Kandy, Sri Lanka. The location can be found outside the heart of the Central district (Kandy city). The building construction area has light traffic compared to the Kandy city area. The ground floor plan of the ongoing building is shown in Fig. 1. The building consists of one storey (Ground floor) above the ground level and two basement floors below the earth level. The construction floor area (CFA) of the Ground floor is 1874.57 ft^2. Lower ground floors 1 and 2 have 954.93 ft^2 and 422.91 ft^2 CFA, respectively.

The initial and current progress of the building is depicted in Fig. 2. Prefabricated components are transported to the construction site using 15–20 ton twenty feet bed trucks. The building employs slabs, beams, columns, and wall panels as the prefabricated components (Fig. 3).

The height of the wall panels is 7–12 ft., depending on the wall height denoted in the building designs. The width is around 2 ft, and the thickness is about 0.30 ft and

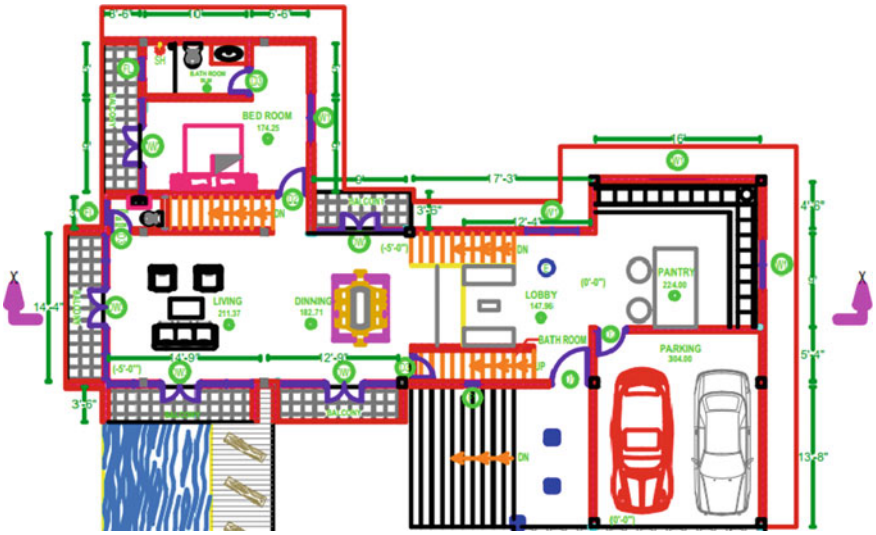

Fig. 1 Ground floor plan of the building

(a) (b)

Fig. 2 **a** Initial Stage and **b** Current Progress

0.5 ft. Columns are with two cross Sections (0.5 × 0.8 ft and 0.5 × 0.5 ft), beams are required with 0.5 × 1 ft, and slabs are designed with 2 × 0.3 ft and 1 × 0.3 ft.

(a) (b) (c)

Fig. 3 Prefabricated **a** Slabs, **b** Columns, and **c** Sample part of a Cellular Lightweight Concrete Wall panels

4 Sustainability of Prefabricated Wall Panel Manufacturing in Sri Lanka

4.1 Cellular Lightweight Concrete Wall Panel

Cellular lightweight concrete wall panels (CLCs) are manufactured by incorporating cement, fly ash, foaming agent, and water as the main constituents. Fly ash is supplied from the Norochcholai Coal Power Plant, Puttalam, Sri Lanka. Fly ash is a by-product of the power plant. Replacing a proportion of cement with fly ash favours sustainability performance due to some reasons, such as the circularity of fly ash and low cost compared to Portland Cement. Figure 4(a) shows the makeshift mould arrangement by a local manufacturer for producing CLCs. The mould is manufactured using shuttering boards and steel. Shuttering boards are made of a wood-plastic composite. The CLCs in the discussion are suitable for non-load-bearing applications. The current building is designed such that all beams and columns will bear the loading from upper structures. However, some passive loads can be applied in the CLCs. Thus, the relevant structural performance and compatibility of these CLCs were calculated and checked at the design stage. Figure 4(b) shows assembled CLCs in the building.

From a sustainability perspective, the use of fly ash and foaming agent reduced the cement quantity required and eliminated the use of sand. Thus, the environmental emissions are reduced from cement and sand processing and production. The foaming agent directly supports reducing the weight of the wall panels. When processed through a foam generator, foaming agents and water create a stiff, white foam with an increase of 20–25 times in volume and with no foam collapsing. This foam can be easily poured into the cement mix to manufacture lightweight foamed concrete [15]. Hence, overall, from an economic perspective, CLCs reduce material, machinery, logistics, and labour costs. Similarly, these savings have the potential to enhance environmental performance as well.

(a) (b)

Fig. 4 **a** Makeshift mould arrangement for producing CLCs and **b** Assembled wall panels in the case study building

4.2 Paddy Straw-Based Wall Panels

These wall panels use paddy straw fibre (the main raw material), which is a waste product of the rice production process in Sri Lanka. Paddy straw is supplied from around the region the prefabrication plant is located. The paddy straw suppliers are within a radius of 5–10 km from the location of the factory. The trucks and lorries with bed lengths of 10–20 ft. are employed to transport the main raw material. Paddy straws are compacted to a cake and glued using water-based PVA glue and covered with craft paper. These wall panels can be assembled as single-layered, double-layered, or as cavity walls.

From a sustainability perspective, the use of waste material as the main constituent of these panels directly favours environmental and economic sustainability. Material circularity in the manufacturing industry in Sri Lanka is still in the infant stage. Thus, this approach is a step forward in the Sri Lankan building material-related production industry.

4.3 Precast Concrete Wall Panels

The local manufacturer uses Elematic precast concrete technology to produce these concrete wall panels. They are mainly applied in non-load-bearing functions such as partitions and facades of residential, commercial, and office buildings. This precast solution eliminates the typical 15 mm thick plastering on both sides of the wall panel and requires only a 3–5 mm skim coat. Moreover, compared to a conventional brick wall with plaster, the precast wall panel weighs less than 2.3 times per m^2. On top of that, the use of these precast wall panels highly reduces the construction time and labour requirements. For example, estimated man hours required for completing

100 m^2 of wall area are around five times lesser in precast wall panels compared to conventional brick walls. The former advantage can be realized by shifting a part of the in-site construction work to off-site prefabrication.

From a sustainability point of view, these wall panels are made with high accuracy. The main reason is the use of a factory-based environment, which makes it possible to increase the overall efficiency of the relevant processes. Therefore, the product quality is enhanced, reducing the material and labour demands. Moreover, the bulk density of these wall panels is less compared to in-situ concrete, which makes them lightweight. Consequently, the load on machinery will be lesser. Furthermore, the non-requirement of plastering eliminates the lifting of sand and cement required for plastering. Less use of machinery reduces environmental emissions and cut-off machinery-related costs.

5 Life Cycle Assessment of Prefabricated Wall Panels

Figure 5 shows the greenhouse gas (GHG) emissions of the three wall panels selected for the LCA. WP1 is the cellular lightweight concrete wall panel presented in Sect. 4.1. WP2 is the paddy straw-based wall panel elaborated on in Sect. 4.2. WP3 is the precast concrete wall panel described in Sect. 4.3. The WP2 performs better in terms of GHG emissions (4.78 tonsCO_2-eq/m^2) than the other two wall panels. The use of paddy straw fibres in place of carbon emission-intensive cement is the main reason for this drastic reduction. However, the selection of a wall panel should be made considering the application as described in Sect. 4.

WP1 emits slightly less carbon (23.50 tonsCO_2-eq/m^2) to the atmosphere than WP3 (24.60 tonsCO_2-eq/m^2) for a square-meter area. In both wall panels, cement is the primary source of GHG emissions. The use of fly ash has positively affected the GHG emission performance of WP1. However, using a foaming agent also counts on

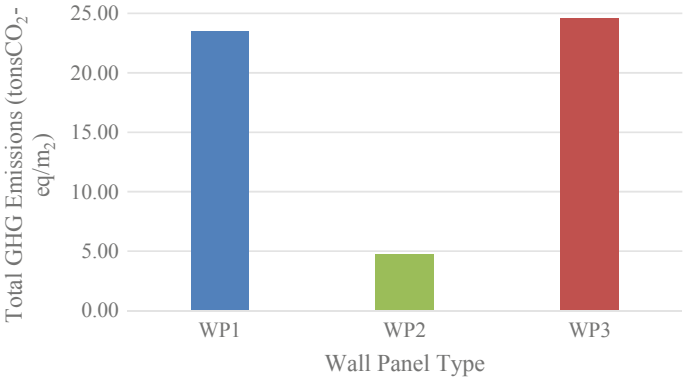

Fig. 5 GHG emissions of the prefabricated wall panels per 1 m^2 of panel area

carbon emissions compared to WP3. Moreover, the distance of the fly ash provider to the local manufacturing site has a significant effect on the transportation-GHG emissions of WP1. Both wall panels are recommended for non-load-bearing applications. Thus, though the GHG emissions can be lower than typical masonry and concrete wall systems, decisions should be taken based on the application of the construction project.

Other seven midpoint impacts are selected for the LCA based on a cumulative cut-off value of 90%. The seven impacts fallen under 90% cumulative are terrestrial acidification (TA), human toxicity (HT), particulate matter formation (PMF), terrestrial ecotoxicity (TET), freshwater ecotoxicity (FET), marine ecotoxicity (MET), and fossil depletion (FD). Figure 6 depicts the characterization results of the midpoints. WP1 and WP3 were identified as the leading contributors to all seven impact categories compared to WP2. WP3 contributes slightly more to TA, PMF, and FD compared to WP1. However, WP1 was significantly affected by TET, FET, and HT compared to WP3 and WP2. The foaming agent manufacturing process deals with several chemicals and chemical processing activities. The release of these chemicals into soil and waterbodies significantly affect terrestrial and freshwater ecosystems.

To have intercomparisons with midpoint impacts, characterization results should be normalized. Figure 7 demonstrates the normalized midpoint impacts of the prefabricated wall panels. As identified in characterization results, normalized outcomes show that WP1 has highly affected the TET and FET. Thus, WP1 is the hotspot in terms of the ecotoxicity impacts. However, WP3 is the hotspot in GWP, TA, PMF, and FD midpoint impacts. Hence, the decisions should be taken considering the specific context and the cumulative effect of these impacts.

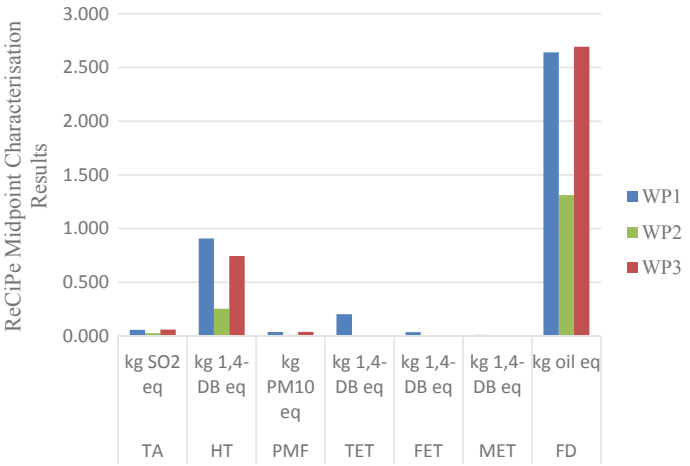

Fig. 6 Midpoint impact results of the prefabricated wall panels per 1 m^2 of panel area

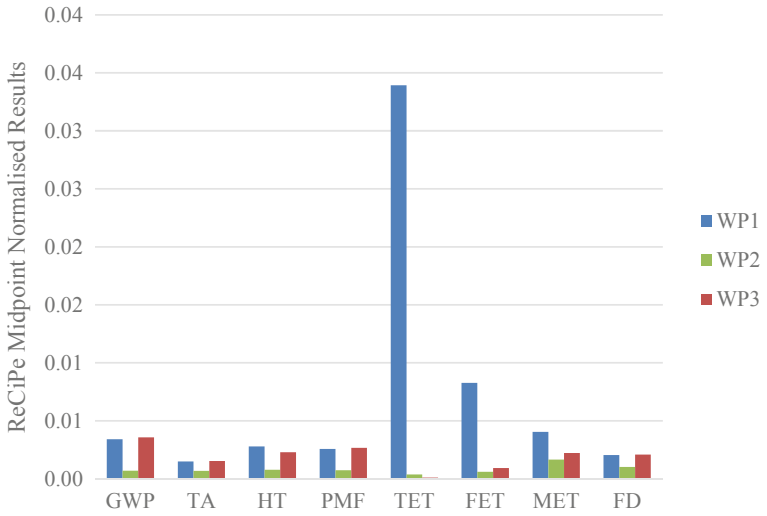

Fig. 7 Midpoint normalized impact results of the prefabricated wall panels per 1 m^2 of panel area

6 Conclusions and Future Suggestions

The current study explores the sustainability perceptions of prefabricated construction practices in Sri Lanka. An ongoing family house construction using prefabricated components is presented to identify the potential sustainability aspects. Moreover, prefabricated wall panel manufacturing practices of Sri Lanka are described highlighting the sustainability aspects. Finally, LCA methodology is applied to evaluate the selected prefabricated wall panels using cradle-to-gate system boundary to assess the environmental sustainability. The results show that paddy straw-based wall panels (WP2) perform better than cellular lightweight concrete panels (WP1) and precast concrete wall panels (WP3) in all environmental impact categories. However, the decision should be made considering the specific application of these wall panels.

Future research should focus more comprehensively on evaluating the sustainability of prefabricated construction practices in Sri Lanka. The environmental and economic aspects should be extended to the social sustainability dimension to support more holistic decision-making by construction stakeholders. The research can further focus on more prefabricated components for assessing sustainability. Moreover, circular economy and end-of-life cycle strategies could be investigated more thoroughly to promote the circularity and 6R concept implementation in Sri Lanka.

Acknowledgements The authors would like to express their sincere gratitude to Mr. Devaka Ekanayake for his support in acquiring valuable information needed for this research study.

References

1. Dong YH, Ng ST (2015) A social life cycle assessment model for building construction in Hong Kong. Int J Life Cycle Assess 20:1166–1180
2. Du Q, Bao T, Li Y, Huang Y, Shao L (2019) Impact of prefabrication technology on the cradle-to-site CO_2 emissions of residential buildings. Clean Technol Environ Policy 21:1499–1514
3. Hong J, Shen GQ, Mao C, Li Z, Li K (2016) Life-cycle energy analysis of prefabricated building components: an input–an output-based hybrid model. J Clean Prod 112:2198–2207
4. Hu X, Chong H-Y (2019) Environmental sustainability of off-site manufacturing: a literature review. Eng Constr Arch Manag
5. ISO (2006) Environmental management: life cycle assessment; Principles and Framework, ISO
6. Jayawardana J, Kulatunga A, Sandanayake M, Zhang G, Jayasinghe J (2023) Life cycle assessment for modular-constructed buildings: a proposed methodological framework. In: 12th international conference on structural engineering and construction management. Springer, pp 519–532
7. Kamali M, Hewage K (2016) Life cycle performance of modular buildings: a critical review. Renew Sustain Energy Rev 62:1171–1183
8. Liu S, Qian S (2019) Evaluation of the social life-cycle performance of buildings: theoretical framework and impact assessment approach. J Clean Prod 213:792–807
9. Minunno R, O'Grady T, Morrison GM, Gruner RL (2020) Exploring environmental benefits of reuse and recycle practices: a circular economy case study of a modular building. Resour Conserv Recycl 160:104855
10. Monahan J, Powell JC (2011) An embodied carbon and energy analysis of modern methods of construction in housing: a case study using a lifecycle assessment framework. Energy Build 43:179–188
11. Pervez H, Ali Y, Petrillo A (2021) A quantitative assessment of greenhouse gas (GHG) emissions from conventional and modular construction: a case of a developing country. J Clean Prod 294:126210
12. Sandanayake M, Zhang G, Setunge S (2016) Environmental emissions at the foundation construction stage of buildings–two case studies. Build Environ 95:189–198
13. Satola D, Kristiansen AB, Houlihan-Wiberg A, Gustavsen A, Ma T, Wang R (2020) Comparative life cycle assessment of various energy efficiency designs of a container-based housing unit in China: a case study. Build Environ 186**:**107358
14. The Economist (2017) Efficiency eludes the construction industry. https://www.economist.com/business/2017/08/19/efficiency-eludes-the-construction-industry. Accessed 31 Oct 2022
15. Tht International (2022) Foaming agent for lightweight concrete-THTFA-3. http://www.thtvietnam.com/en/products/lightweight-concrete/additives/foaming-agent/#. Accessed 06 Nov 2022
16. U.S. Department of Commerce (2021) Sri Lanka-country commercial guide-construction. International Trade Administration, U.S. Department of Commerce. https://www.trade.gov/country-commercial-guides/sri-lanka-construction. Accessed 08 Oct 2022

Resilience of Civil Infrastructure

Optical Fibre Sensing and Deep Learning-Based Disaster and Climate Change Risk Assessments of Civil Infrastructure: Current Status and Future Perspective

R. W. K. Anjana, H. M. C. M. Herath, U. M. N. Jayawickrema, and J. A. Epaarachchi

Abstract Civil infrastructures are affected by climate change including sea level rise, changes in snowfall, ice, and permafrost, and effects on hydrological systems, including precipitation floods and droughts, tropical cyclones, storms, and sea-wave heights. Also, disasters such as earthquakes, landslides, and tsunamis worldwide disrupt people's lives and cause significant property damage. This study investigates the recent advancements toward damage mitigation of civil infrastructures through early detection of natural disasters and climatic changes using the measurements of optical fibre sensing (OFS) followed by deep learning (DL) models. It was shown that pointed and distributed OFS was effective for measuring strain, temperature, and pressure to trace the changes in seismological, hydrological, and geological data at surface level, subsurface level, and submerged. OFS is a rapidly growing research area for improving inspection accuracy and performance due to its advantageous properties of being lightweight, reliable, small in size, immunity to external electromagnetic perturbations, low power, high sensitivity, multiplexing capability, and wide bandwidth. Distributed optical fibre sensing (DOFS) has gained immense interest in engineering as they offer unique advantages for spatially distributed measurements for hundreds of kilometres. DOFS could detect the damage's precise location, magnitude, and propagation over time. Climate changes and disasters triggered propagating damage to structures including buildings, bridges, highways, and dams can be identified in terms of cracks, fatigue, creep, and slip. Big data-driven methods for disaster management are developed with DL, most frequently through convolutional neural

R. W. K. Anjana · H. M. C. M. Herath (✉) · U. M. N. Jayawickrema
Department of Engineering Technology, Faculty of Technological Studies, Uva Wellassa University, Badulla, Sri Lanka
e-mail: madhubhashitha@uwu.ac.lk

R. W. K. Anjana · H. M. C. M. Herath · U. M. N. Jayawickrema · J. A. Epaarachchi
Centre for Future Materials, University of Southern Queensland, Toowoomba, Australia

J. A. Epaarachchi
School of Engineering, Faculty of Health Engineering and Sciences, University of Southern Queensland, Toowoomba, Australia

© The Author(s), under exclusive license to Springer Nature Singapore Pte Ltd. 2023

R. Dissanayake et al. (eds.), *ICSBE 2022*, Lecture Notes in Civil Engineering 362,
https://doi.org/10.1007/978-981-99-3471-3_33

networks. DL-based disaster-predicting systems that can be identified with seismological data have been developed with precision and a recall of over 90%. This review reveals that disasters due to earth movements and pore water pressure can be precisely detected through OFS followed by DL models. There is ample room for further development of combinational studies between OFS and DL for disaster and climate change risk assessment.

Keywords Disaster prediction · Fibre optic sensing · Deep learning · Structural health monitoring · Climate resilient infrastructure

1 Introduction

Natural disasters are random but differ in severity, frequency, and location. A natural disaster might be a flood, earthquake, volcano eruption, landslide, hurricane, tsunami, drought, or a consequence of climate change. With the expansion of human habitats, increased range and rate of travel immensely increased size of structures, and rapid change of climate and population growth, the impact of natural disasters has increased substantially. Climatic change adaption and disaster risk identification thus improving early warning systems through predicting natural changes, for civil infrastructure, can reduce the damage that may cause. This early warning system ranges from information that an event might occur to a forecast of its magnitude and propagation over time. In the prevailing early warning systems, remote sensing and geographical information systems have been used for the prediction of disasters [15, 19].

Due to its advantageous characteristics of being lightweight while having reliability, stability, small size, resistance to external electromagnetic disturbances, low power, high sensitivity, multiplexing capability, and wide bandwidth, fibre optic sensing is identified as one of the most fast-growing methods of improved and accurate inspection over several parameters. Fibre optic sensing has been deployed in many fields; medicine, aerospace, transportation, Structural Health Monitoring (SHM), and telecommunication [16, 28]. OFS can withstand even harsh environments so they can be employed with a proper change in the technique and a protective layer, to detect natural changes in the environment and thus predict any sudden or propagating natural disasters. The parameters, temperature, pressure, humidity, and displacement, can be measured through a change of strain in fibre optic cable. If a natural occurrence changes one or more of those parameters, OFS can be used to monitor system behaviour. Depending on the technology, the sensing range will be decided; Brillouin Optical Time-Domain Analyser (OTDA) sensing technology allows to sense temperature and strain to a maximum of 150–200 km and Brillouin Optical Time-Domain Reflectometry (OTDR) will sense to a maximum of 20–50 km [16].

The literature has revealed the deployment and the possibility of OFS in structural health monitoring during construction, repairing, and identifying any fatigue or

creep propagation after installation. This paper will review the chances of using OFS to construct climate and disaster-resilient civil infrastructures and quantitative risk assessment over natural disasters. In structural conditions monitoring the displacement of soil: vertical and horizontal, pore water pressure in sublayers and at the structure crack propagations and creep will be monitored using OFS.

Deep Learning (DL) is a subfield of Machine Learning (ML) in Artificial Intelligence (AI). When raw data is fed into a deep learning system, the system learns the representation needed for detection or classification without human interaction. Deep learning excels at discovering relationships in complex, high-dimensional data, allowing it to be used in many scientific fields where the maximum reported damage prediction accuracy for civil infrastructure was over 97%. The study is aimed to analyse the current state-of-the-art and prospective applications of deep learning with optical fibre sensors for assessing the vulnerability of civil infrastructure to disasters and climate change. The combination of FOS and DL will enable the measurement of strain and temperature variations and subsequently prediction of the magnitude and location of possible failures in buildings, roads, dams, bridges, and tunnels. In the future, the OFS and DL technology will be an unprecedented resolution for condition monitoring of civil infrastructure and early warning due to floods, earthquakes, fire, and wind [5, 15] (see Fig. 1).

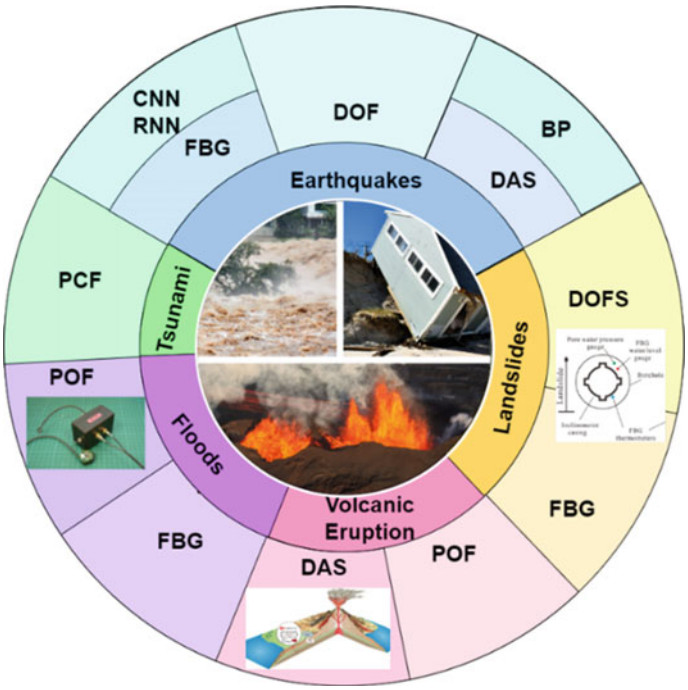

Fig. 1 Graphical representation of disaster management through OFS-based systems

This study is intended to review the existing state-of-the-art and future perspectives for applying optical fibre sensors with deep learning for disaster and climate change risk assessments of civil infrastructure. FOS and DL acting together will make it possible to quantify strain and temperature variations and, as a result, predict the size and location of potential failures in civil infrastructure. Future condition monitoring of civil infrastructure and early warning of floods, earthquakes, landslides, and tsunamis will be made possible with the help of OFS and DL technologies.

2 OFS in Climate and Disaster Management

Recently, the employment of OFS in condition monitoring has been remarkable. In OFS, the sensing component is the fibre itself, and the same cable will transmit the light and be connected to the data acquisition system [15, 36]. Continuous and real-time data extraction is made possible with OFS. Either Distributed Optical Fibre Sensor (DOFS) or Fibre Bragg Grating (FBG) can be used to monitor natural changes.

An FBG consisting of gratings gives out a set of discrete data of stain or temperature when the transmitting light characteristic changes across the gratings of the fibre. A DOFS continuously monitors strain, temperature, and vibration with exact location through backscattered light that passes in the cable where the cable itself acts as the sensing element.

When employing DOFS to identify natural disasters the employing environment is harsh, thus to increase the survivability of the sensor a protective layer must be used. According to the literature, DOFS are primarily used in structural health monitoring to measure strain: fatigue responses, temperature changes, and leakage monitoring; thus can be implemented in the natural environment also to measure the same parameters.

Natural disasters can be predicted by analysing the changes in certain variables. Hurricanes and rain storms can be predicted by atmospheric behaviour; humidity, air pressure, temperature, and wind speed [14]. Seismic waves are triggered by several natural disasters: landslides, earthquakes, snow avalanches, and debris flow. The frequency and the amplitude of the wave differentiate each wave and enable the identification of the natural hazard accordingly.

The landslide-triggering factor is soil instability. Monitoring landslides is facilitated by gathering data on the soil's surface and subsurface motion and transferring that motion to a strain in an OFS. In the literature, the employment of the FOS on different levels: the surface, underground (embedded), and retaining wall has been discussed in advance [12, 36]. The optical system has been proven to be an innovative technique for characterizing and monitoring landslides. The most viable position for detecting the landslide triggering would be just near the sliding interface,a shallower installation is better.

With the installation method, the sensor design differs. Figure 2 depicts an Optical Fibre cable attached to an inclinometer to determine landslides and Fig. 3 depicts prefabricated sensors being installed vertically underground.

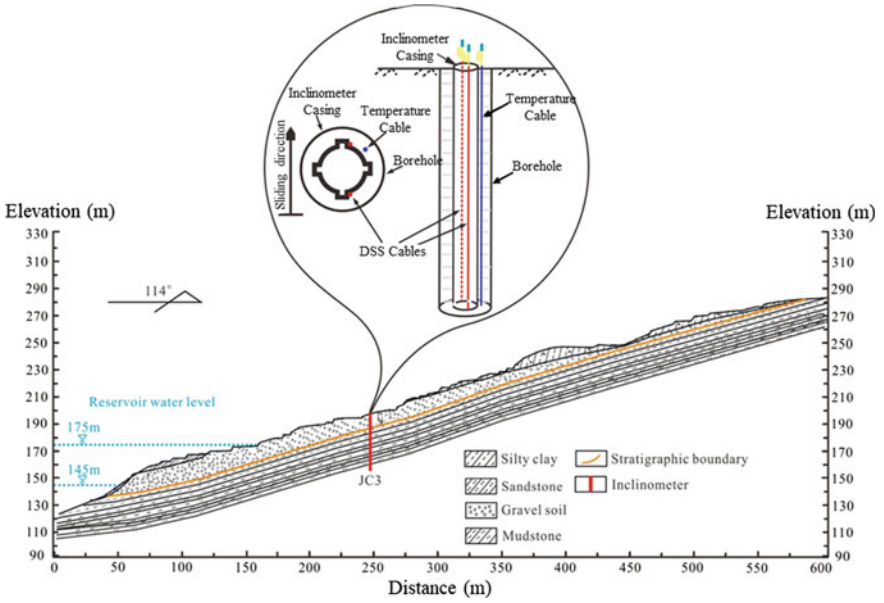

Fig. 2 The installation of the optical fibre inclinometer tube [37]. (Reused with Permission)

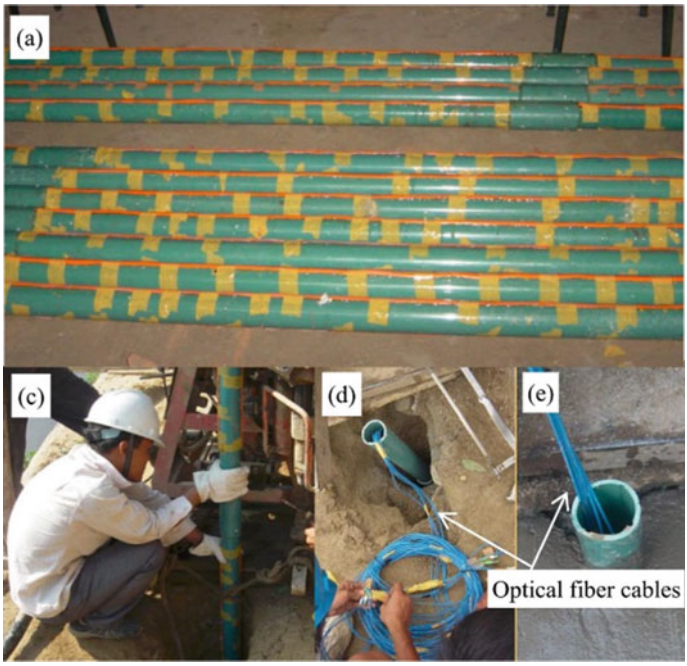

Fig. 3 **a** Prepared sensors covered in protective tubes attached to rods. **c**–**e** installing of OFS [10] (Open Access)

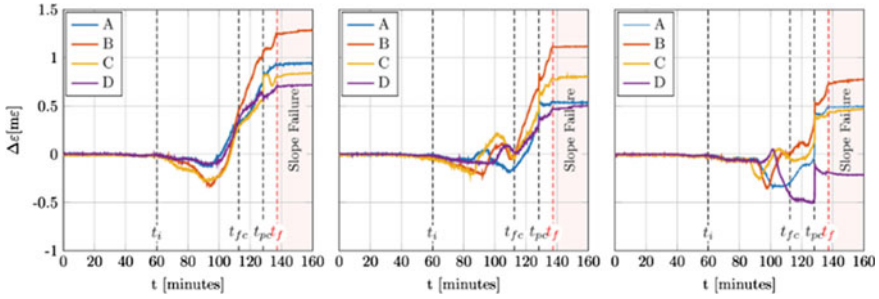

Fig. 4 Corresponding local strain measured by the FOS at the different fibre spans [30] (Open Access)

Figure 4 depicts the strain values against the time of OFS deployed at three different places: upslope, mid-slope, and downslope positions in a set of 4 cables deployed to monitor soil motion against the rainfall and subsequently detect landslides. At the time of the slope failure, the strain observed has drastically increased concluding that DOFS behaves allied with its attached environment [30].

As per the study by Schenato [30], the fibre cables for landslide monitoring which are buried in shallow ground and on the ground surface with anchors may not measure the strain in its actual value and thus will not detect the ground movement. This erroneous measurement is caused by the sensor moving with the superficial soil. He later suggested the use of an inclinometer to overcome the potential slip [30]. Wijaya et al. suggest that the surface laying of the sensor cable can face the impact of other natural changes also which might reduce the sensing accuracy [36]. A fixed-point fibre optic sensing cable (FFOSC) has been developed by Suo et al. [33] with its installation method and Fig. 5 depicts the changes identified in terms of strain.

A tsunami is described as a long wave with a wavelength of several hundred kilometres and an amplitude of a few centimetres to a few metres across the deeper ocean (open ocean), producing a dynamic pressure of a few kilopascals to hundreds of kilo Pascals. Usually, a tsunami is forecasted based on water surface changes measured by Ocean Bottom Gauges placed within the earthquake focal area [8, 31]. The hydrostatic relation between the pressure and the tsunami height (the uplifting height from the reference height) will express any pressure change in the sea bottom thus the propagation of a tsunami [23, 29]. In deep water change of temperature in several Celsius is noticeable, so necessary corrections should be implemented in the pressure measurement to compensate for the temperature effect such as using Photonic Crystal Fibre (PCF) which is capable of measuring slight pressure deviations compensating the temperature [31].

Early warning of the type of floods could be obtained by monitoring the water level in flood-prone places. Here, it is possible to utilize a fibre that is based on the optical signal's loss of total internal reflection as the sensor probe makes contact with the liquid [18]. Hydrostatic pressure relation is also applicable after a measurement

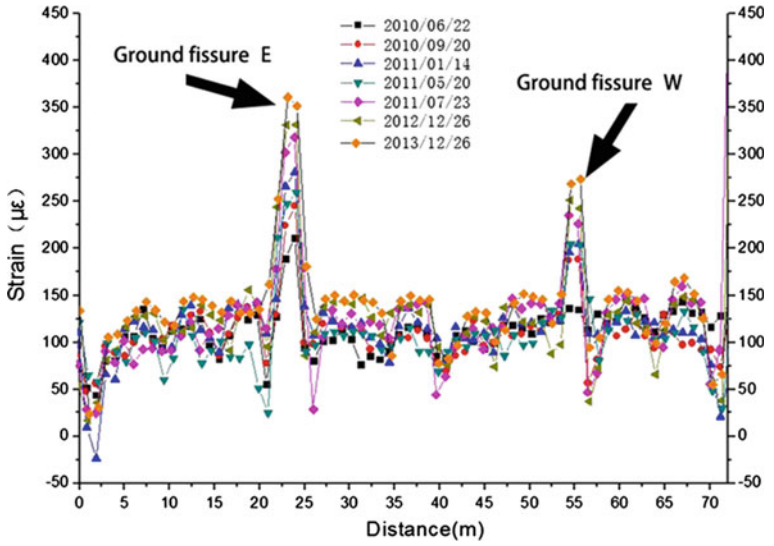

Fig. 5 The fixed-point sensor fibre experiences changes in strain. Data showing two maxima show that two earth fissures are likely to open [33]. (Reused with permission)

transformation from pressure to height. Using water level sensing the lack of water, a trend toward a flood also can be identified accurately.

There have been sensors designed to measure hydrostatic pressure using OFS. These sensors can be modified to measure the pressure underneath the soil. Figure 6 is a hybrid FBG-based earth/water pressure transducer with FBG attached over diaphragms which expand and contract according to the pressure on it. The pore water pressure triggers landslides, debris flow, and road collapse. Monitoring the pore water pressure with this sensor can forecast any changes at sublayers thus any catastrophe.

In Table 1, the data type which should be extracted to detect the relevant disaster is listed. OFS-based approaches for disaster prediction are depicted in Table 2.

A disaster caused due to a failure of civil engineering work is called a civil engineering disaster. Designing the construction for the right hazard level can also effectively mitigate civil engineering disasters and condition monitoring. Concrete, rock, and soil masses are prone to cracking under the influence of harsh environmental conditions, and porosity and high heat compromise the structural integrity of the structures: buildings, roads, dams, and tunnels. Therefore, timely monitoring is vital for sustainable construction. Francesco et al. [6] has been monitoring the bell tower of the Basilica of San Pietro, a seismic area for 2 years before the earthquake and 2 years after, and could able to detect anomalies. The substantial amount of SHM data gathered over four years made it possible to evaluate changes in the bell tower's structural behaviour under post-earthquake conditions. The study by Minardo et al. [22] describes a distributed fibre optic strain sensor connected to a tunnel wall that monitors earthflow-affected railway tunnels. The results show that the sensor can

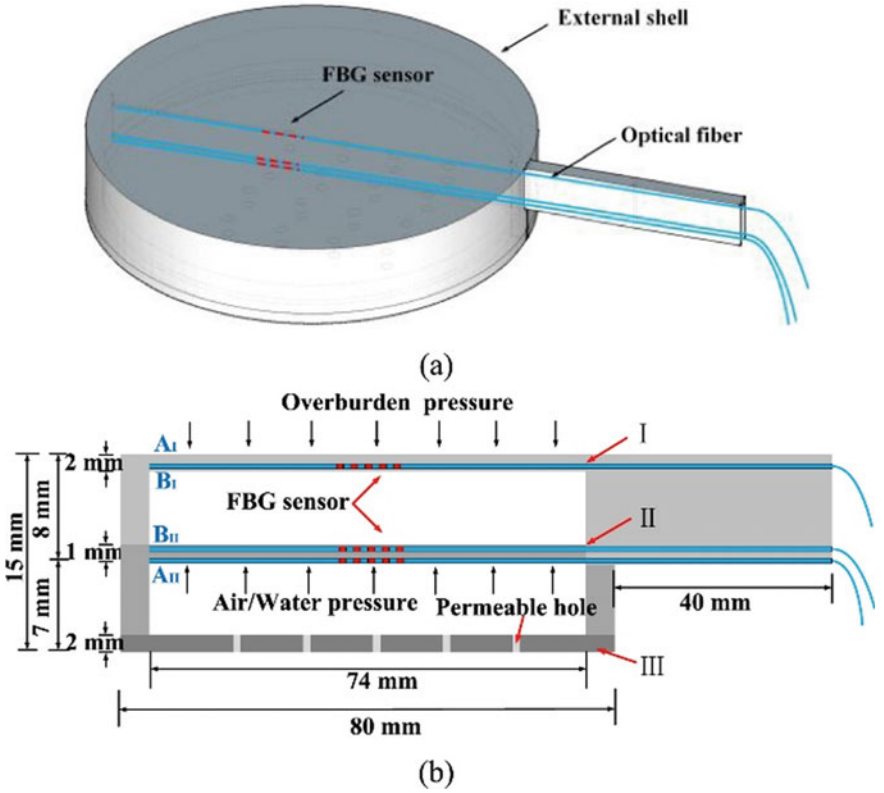

Fig. 6 Sensor design to hydrostatic pressure **a** overall geometry and **b** section view. Qin et.al. [27] (Open Access)

Table 1 Data type related to Disaster [7]

Disaster	Data	Data type
Earthquake/ tsunami	Seismological data	–
Flood/ drought	Hydrological data	Water level, pressure, density
Landslides	Geological data	Pore pressure, Tilt, vibration, water content
Volcanic eruption	Geological data and seismological data	Spatial, temporal, and thematic data

Table 2 OFS-based approaches for disaster prediction

Disaster type and reference	Location/ suggested location	Measured parameter	Technology	Sensitivity	Wavelength
Tsunami (Shinde and Jahir [31])	In ocean bottom	Dynamic pressure	Photonic Crystal fiber (PCF) Pm-1550–01	2.34×10^{-6} mpa[1]	1550 nm
Ocean-solid earth interactions (Sladen [32])	Buried for the first 2 km offshore rest on the sea floor (a 2500 m-deep oceanic plain) 41.5 km long	Strain/strain rate	Fibre optic-based distributed acoustic sensing (DAS) Electro-optic telecommunication cable	1 nstrain/s	–
Earthquake (Lindsey et al. [20])	1–2 m below ground	Strain rate	Fibre optic-based distributed acoustic sensing (DAS)	–	–
Source location for volcanic earthquakes (Nishimura et al. [25])	Embedded at a depth of approximately 50 cm	Dynamic strain	Fibre optic-based distributed acoustic sensing (DAS)	–	–
Debris flows (Huang et al. [11])	Approximately 20 cm below the surface (lab experiment) The real application-the bank of a creek	Ground vibrations	Fibre bragg grating (FBG) accelerometer (GS6500)	10 pm/g	1,510–1,590 nm
Landslides (Schenato et al. [30])	60 cm below ground (in a large-scale physical model of a slope)	–	Distributed optical fibre sensing (DOFS)	–	–
Landslides (Huntley et al. [12])	On the retaining wall block	Displacement and temperature	FBG and BOTDR	–	–
Landslides (Wei et al. [35])	On anti-slide piles	Strain and temperature	DOFS-BOTDA	–	–
Flood (Kuang et al. [18])	–	Water level	Plastic optical fibre (POF) sensors	–	–

(continued)

Table 2 (continued)

Disaster type and reference	Location/ suggested location	Measured parameter	Technology	Sensitivity	Wavelength
Volcanic eruption (Jousset et al. [17])	20 cm deep in a scoria layer on the volcano	Strain	DAS	0.1–5 Hz	–
Volcanic eruption (Beverini et al. [4])	On Mt. Etna at about 8–10 m of depth	Strain	FBG	~150 με	–
Ice and ocean temperature (Tyler et al. [34])	Within and below (800 m) the Ice Shelf	Temperature	DOFS	–	–
Climatic changes [24]	–	Strain and humidity	FBG	–	–

detect localized strains, locate them, and track their temporal progression over the monitoring period. A study explains that oil production offshore platforms in the Bohai Sea, East China, used FBG sensors for SHM against strong waves. The FBG sensors functioned for about a year without experiencing noticeable performance loss [21].

3 Deep Learning Algorithms and Optical Fibre Measurements

Deep Learning algorithms extract useful information from raw data mimicking the human brain's learning mechanism for computation. There are supposed to be several layers of artificial neurons: input, hidden, and output whereas deeper layers create high-level decisions from fundamental concepts at the first layers [3].

Different types of sensors produce large amounts of heterogeneous data. The deep learning techniques develop trainable algorithms which can learn from the collected data, thus future predictions are made. DL models discover and learn information hidden in data and predict various patterns using stacked blocks of layers of DL skeleton [3].

Practical applications of deep earning for disaster prediction with Convolutional Neural Networks (CNN) include the identification of wildfire smoke through aerial vehicle images, detection of floods and landslides using satellite images, detection

of propagation of earthquakes using social media data, and heavy snowfall and landslides through aerial images [1]. Anyhow predicting natural disasters will confront the issue of noise and severe class imbalance [1].

Recent work expresses the use of Particle swarm optimization (a population-based search algorithm), neural network, text, and regular log mining technology used to detect and predict the magnitude of an earthquake based on seismological data.

CNN technology is highly effective in computer vision tasks [2]. Hernández et al. [9] in their work, they discuss a model based on CNN, Recurrent Neural Networks (RNN), and FC-ANN (Fully Connected Artificial Neural Networks),supervised learning approaches, to detect earthquakes with seismic data recorded through DAS which obtained an accuracy of 93.86% with CNN and RNN combined model. This study has validated the CNN model to differentiate DAS seismic waveforms.

A recent study using highly scalable CNN for earthquake detection from a single waveform in Oklahoma, USA, has successfully implemented the model. The input here is three-channel waveform seismogram data and the model differentiates the data between seismic noise and an event with its geographic cluster with 94.8% preciseness of detection [26].

In a study of the early detection of landslides, anti-slide piles were monitored for strain and temperature with DOFS-BOTDA and Back Propagation (BP) neural networks used to predict the bending moment in the anti-slide piles [35]. In their study, Zhang et al. suggested a BP neural network algorithm with three layers to set the calculation mode for lateral deflection of OFS-mounted inclinometer,it was used to predict landslides. The BP model has established a function between the depth, strain, and measured displacement which can predict landslides or the tendency to slide. It says that the DFOS ML-assisted approach considerably increases the measuring range of a conventional inclinometer [37].

A set of 20 km long fibre cables underneath Stanford University recorded seismic data for three years. It was used to train two separate Machine learning models, a 2D CNN for DAS data detection and a 1D CNN for seismometer records on the DAS data; the 2D CNN obtains 92.98% accuracy and the 1D CNN accurately predicted the seismometer data with 95.54% of the time which drives to the conclusion that earthquakes can be detected through DAS-based ML model [13].

4 Conclusion

A natural disaster or a consequence of climate change can cause serious damage to lives and properties. To mitigate the seriousness and the effect on human lives and property, a proper protection system over a timely prediction is compulsory. Among the recent advances of sensing systems, fibre optic sensors: DOFS and FBG, have shown their superior capabilities in strain, temperature, and pressure measurements to detect anomalies in the attached environment and structures referring to seismic, geological, and atmospheric data. Recent studies revealed the possibility of extending Fibre Optic cable in the range of 20–40 km at surface level to identify seismic

changes. The deep learning techniques develop trainable algorithms which can learn from large amounts of heterogeneous data collected through sensors, thus future predictions are made. Early detection systems combined with OFS and DL have been developed and implemented to track earthquakes and landslides. Alternatively, CNN machine learning models are the most used model in recent studies with an accuracy exceeding 90% in identifying seismic changes. There is plenty of chances to explore the OFS-based DL system for early detection of floods, tsunamis, volcanic eruption, and snowfall.

Acknowledgements This research was supported by the 2022–2023 Fellowship of the Coalition for Disaster Resilient Infrastructure (CDRI), Application ID: 210921613, and by the Uva Wellassa University Research Grant UWU/RG/2022/39.

References

1. Aamir M et al (2021) Natural disasters intensity analysis and classification based on multispectral images using multi-layered deep convolutional neural network Sensors 21(8):2648. https://doi.org/10.3390/S21082648
2. Ahmad J, Farman H, Jan Z (2019) Deep learning methods and applications. SpringerBriefs in Computer Science, pp 31–42. https://doi.org/10.1007/978-981-13-3459-7_3/COVER
3. Azimi M, Eslamlou AD, Pekcan G (2020) Data-driven structural health monitoring and damage detection through deep learning: state-of the-art review. Sensors (Switzerland) 20(10)https://doi.org/10.3390/s20102778
4. Beverini N et al (2015) Strain sensors based on Fiber Bragg Gratings for volcano monitoring. IET Conference Publications, (CP667).https://doi.org/10.1049/CP.2015.0177
5. Flah M et al (2021) Machine learning algorithms in civil structural health monitoring: a systematic review. Arch Comput Methods Eng 28(4):2621–2643. https://doi.org/10.1007/s11831-020-09471-9
6. Francesco P et al (2020) Four years of structural health monitoring of the San Pietro bell tower in Perugia, Italy: two years before the earthquake versus two years after. Int J Mason Res Innov.https://doi.org/10.1504/IJMRI.2020.111797
7. Goswami S et al (2018) A review on application of data mining techniques to combat natural disasters, Ain Shams Engineering Journal. Ain Shams University, pp 365–378. https://doi.org/10.1016/j.asej.2016.01.012
8. Gusman AR et al (2016) Tsunami data assimilation of Cascadia seafloor pressure gauge records from the 2012 Haida Gwaii earthquake. Geophys Res Lett 43(9):4189–4196. https://doi.org/10.1002/2016GL068368
9. Hernández PD, Ramírez JA, Soto MA (2022) Deep-learning-based earthquake detection for fiber-optic distributed acoustic sensing. J Light Technol 40(8).https://doi.org/10.1109/JLT.2021.3138724
10. Hu Y et al (2018) A monitoring and warning system for expressway slopes using FBG sensing technology. Int J Distrib Sens Netw 14(5).https://doi.org/10.1177/1550147718776228
11. Huang CJ et al (2012) Calibration and deployment of a fiber-optic sensing system for monitoring debris flows. Sensors 12(5):5835–5849. https://doi.org/10.3390/S120505835
12. Huntley D et al (2014) Fiber optic strain monitoring and evaluation of a slow-moving landslide near Ashcroft, British Columbia, Canada. In: Landslide science for a safer geoenvironment, vol 1, pp 415–421. https://doi.org/10.1007/978-3-319-04999-1_58

13. Huot F, Clapp RG, Biondi BL (2022) Detecting local earthquakes via fiber-optic cables in telecommunication conduits under Stanford University campus using deep learning. https://doi.org/10.48550/arxiv.2203.05932
14. Jagany K et al (2017) Natural disaster indicators use of sensors in geotextiles. Int J Appl Environ Sci 12(6):1083–1100. http://www.ripublication.com. Accessed 15 Aug 2022
15. Jayawickrema UMN et al (2022) Fibre-optic sensor and deep learning-based structural health monitoring systems for civil structures: a review. Measurement, 111543. https://doi.org/10.1016/j.measurement.2022.111543
16. Joe HE et al (2018) A review on optical fiber sensors for environmental monitoring. Int J Precis Eng Manuf Green Technology Korean Soc Precis Eng, 173–191. https://doi.org/10.1007/s40684-018-0017-6
17. Jousset P et al (2022) Fibre optic distributed acoustic sensing of volcanic events. Nat Commun 13(1).https://doi.org/10.1038/S41467-022-29184-W
18. Kuang KSC, Quek ST, Maalej M (2008) Remote flood monitoring system based on plastic optical fibres and wireless motes. Sens Actuators A: Phys 147(2):449–455. https://doi.org/10.1016/j.sna.2008.05.030
19. Lenton TM (2011) Early warning of climate tipping points. Nat Clim Chang, 201–209. https://doi.org/10.1038/nclimate1143
20. Lindsey NJ et al (2017) Fiber-optic network observations of earthquake wavefields. Geophys Res Lett 44(23):11,792–11,799. https://doi.org/10.1002/2017GL075722
21. Min R et al (2021) Optical fiber sensing for marine environment and marine structural health monitoring: a review. Opt Laser Technol. Elsevier Ltd. https://doi.org/10.1016/j.optlastec.2021.107082
22. Minardo A et al (2018) Distributed fiber optic sensors for the monitoring of a tunnel crossing a landslide. Remote Sens 10(8):1291. https://doi.org/10.3390/RS10081291
23. Mizutani A, Yomogida K, Tanioka Y (2020) Early tsunami detection with near-fault ocean-bottom pressure gauge records based on the comparison with seismic data. J Geophys Res Ocean 125(9).https://doi.org/10.1029/2020JC016275
24. Morozov O et al (2017) Fiber-optic Bragg sensors with special spectrum shapes for climatic test systems 10342(6):357–363. https://doi.org/10.1117/12.2270750
25. Nishimura T et al (2021) Source location of volcanic earthquakes and subsurface characterization using fiber-optic cable and distributed acoustic sensing system. Sci Rep.https://doi.org/10.1038/s41598-021-85621-8
26. Perol T, Gharbi M, Denolle M (2018) Convolutional neural network for earthquake detection and location. Sci Adv 4(2).https://doi.org/10.1126/SCIADV.1700578
27. Qin Y et al (2022) A fiber Bragg grating based earth and water pressures transducer with three-dimensional fused deposition modeling for soil mass. J Rock Mech Geotech Eng 14(2):663–669. https://doi.org/10.1016/J.JRMGE.2021.07.009
28. Ramakrishnan M et al (2016) Overview of fiber optic sensor technologies for strain/temperature sensing applications in composite materials. Sensorshttps://doi.org/10.3390/s16010099
29. Saito T (2017) Tsunami generation: validity and limitations of conventional theories. Geophys J Int 210(3):1888–1900. https://doi.org/10.1093/GJI/GGX275
30. Schenato L et al (2017) Distributed optical fibre sensing for early detection of shallow landslides triggering. Sci Rep 7(1).https://doi.org/10.1038/s41598-017-12610-1
31. Shinde YS, Jahir HK (2008) Dynamic pressure sensing study using photonic crystal fiber: application to tsunami sensing. IEEE Photonics Technol Lett. https://www.academia.edu/14806459/Dynamic_Pressure_Sensing_Study_Using_Photonic_Crystal_Fiber_Application_to_Tsunami_Sensing. Accessed 8 Aug 2022
32. Sladen A et al (2019) Distributed sensing of earthquakes and ocean-solid Earth interactions on seafloor telecom cables. Nat Commun 10(1).https://doi.org/10.1038/s41467-019-13793-z
33. Suo W et al (2016) Development and application of a fixed-point fiber-optic sensing cable for ground fissure monitoring. J Civ Struct Health Monit 6(4):715–724. https://doi.org/10.1007/S13349-016-0192-5

34. Tyler SW et al (2013) Using distributed temperature sensors to monitor an Antarctic ice shelf and sub-ice-shelf cavity. J Glaciol 59(215):583–591. https://doi.org/10.3189/2013JOG12J207
35. Wei C et al (2022) A machine learning study on internal force characteristics of the anti-slide pile based on the DOFS-BOTDA monitoring technology. Sensors 22(6):2085. https://doi.org/10.3390/S22062085
36. Wijaya H, Rajeev P, Gad E (2021) Distributed optical fibre sensor for infrastructure monitoring: field applications. Opt Fiber Technol, 64.https://doi.org/10.1016/j.yofte.2021.102577
37. Zhang L et al (2020) A machine learning method for inclinometer lateral deflection calculation based on distributed strain sensing technology. Bull Eng Geol Environ 79(7):3383–3401. https://doi.org/10.1007/S10064-020-01749-3

Numerical Investigation on the Impact of Corrosion on the Ultimate Compressive Strength of a Steel Angle Member Using the Thickness Reduction Method

G. R. C. R. Senevirathna, C. S. Bandara, and S. A. S. C. Siriwardane

Abstract Steel structures are a vital component in the construction industry, but over time, their capacities are declined due to various causes such as corrosion, which causes adverse effects on the mechanical and geometrical properties of the members, when they are subjected to severe exposure conditions. Due to this reason, incidents of steel structure failures have been witnessed around the world, which has drawn the engineers' attention to preventing such failures through proper structural health monitoring and damage assessment practices. There have been several attempts by various researchers on this subject to identify the behaviour of corroded steel members under different loading conditions. This study mainly concentrates on the steel angle members, which are mostly used as axially loaded members in various applications. Since it has been identified that most of the code-based standards do not directly address the corrosion effect on the capacity of steel members, a numerical approach has been investigated to obtain reliable and exact compression capacities of steel angle members. Since enough information on experimental and numerical studies are available on this subject, they have been used to create and validate a Finite Element model to assess the residual compression capacity of the corroded steel angle members. Then, using the validated finite element model, ten different hypothetical corrosion patterns with 39 corroded members have been modelled and numerically analysed to obtain the compression capacities. In conclusion, the results obtained in the numerical approach have been evaluated to assess the amount of damage caused by different corrosion patterns and to identify the most critical scenarios.

Keywords Steel angle members · Corrosion · Structural health monitoring · Residual compression capacity · Finite element analysis

G. R. C. R. Senevirathna (✉) · C. S. Bandara
University of Peradeniya, Peradeniya, Sri Lanka
e-mail: chamath.eng@gmail.com

S. A. S. C. Siriwardane
University of Stavanger, Stavanger, Norway

© The Author(s), under exclusive license to Springer Nature Singapore Pte Ltd. 2023

R. Dissanayake et al. (eds.), *ICSBE 2022*, Lecture Notes in Civil Engineering 362,
https://doi.org/10.1007/978-981-99-3471-3_34

1 Introduction

Steel structures provide a huge contribution to the development of infrastructure in any country in the modern world. During the early 1900s, rapid industrial development occurred all around the world which resulted in the construction of steel structures for various purposes. Even though constructions are precisely completed these structures might undergo failure if they are not maintained and monitored with proper care.

During the last few decades, there has been a number of occasions where steel structures have collapsed resulting in fatal damages, which is why it has been very important to prevent such failures. To identify the possible failures, it is required to assess the damage of deterioration and evaluate the existing condition. According to Cantero and Gonzalez [4], the requirement of structural health monitoring of existing structures and assessment of the deterioration has surpassed the contributions required for the design of the structures.

According to previous studies, there are several causes for the failure of steel structures, whereas fatigue and environmental effects have been the two major factors. When the structures are exposed to severe environmental conditions, the structures are highly prone to corrosion and related consequences.

This study has concentrated on corroded steel angle members, which are largely used, in transmission towers, as bracing elements, and in many other structures mostly as axially loaded members. Therefore, this study has been further narrowed down to observe the behaviour of corroded steel angle members under compression loading, having bolted connections at one leg.

1.1 Objectives

The objectives of this study can be listed as follows:

- To investigate the applicability of the thickness reduction method in numerical models to demonstrate corrosion-equivalent properties.
- To create a Finite Element model for the damage assessment of corroded steel angle members under compression loading.
- To evaluate the impact of different corrosion patterns on the ultimate compression capacity of corroded angle members using the validated FE model.

1.2 Past Studies

Many researchers have conducted various studies on corrosion over the past years. Researchers including [11, 13] have elaborated on the different types of corrosion and

related characteristics, in their studies on corrosion. El Aghoury [5] has illustrated the various factors influencing corrosion, in his study.

Leising [7], Xiao et al. [14], and Andrade and Alonso [2] have introduced modern approaches such as 3D optical scanning, for the determination of corrosion degree which is essential for damage assessment. Even though the above methods are highly accurate, it can be identified that, in most of the previous experimental studies, the corrosion degree is calculated using the average thickness values measured with measuring tools because of the high availability and ease of use.

In regards to compressive strength determination, Ostapenko et al. [9] and Hebor and Ricles [6] have experimentally tested corroded tubular members and expressions have been developed to assess the residual compressive strengths. Nazari et al. [8] have conducted a numerical investigation into the ultimate strength and buckling behaviour of locally corroded steel tubular members, where he has used the experimental results of Hebor and Ricles [6] to validate the model. Furthermore, Ahn et al. [1], in their work, have attempted to assess the residual strength of inclined steel tubular members with local corrosion.

Since the focus of this study is the corroded angle members under compression loading, experimental and numerical studies on this scenario were referred to in detail. Shu et al. [12] and Beaulieu et al. [3] carried out experimental studies with accelerated corroded samples. But the test assemblies have been different. Shu et al. [12] have conducted a numerical analysis to assess the compressive strength of severely corroded members.

Ozvald and Dunai [10] also conducted an experimental study to investigate the effect of corrosion on the buckling of steel angle members. In this study, the cross-sectional area has been reduced by a milling process to represent different corrosion patterns.

2 Numerical Program

2.1 Finite Element Modelling

Since it was obvious that the code-based approaches are not convenient for damage assessment in locally corroded members, an experimental or numerical approach was required to achieve reliable results. It was found that sufficient experimental data is available to get a finite element model validated so that it could be used to carry out the required analyses. The model was created as done by Shu et al. [12] in estimating the damage of severely corroded members. Due to the clarity of information, his experimental results were used to validate the numerical model as well.

The model was created as a shell element extruded to the required length. Material nonlinearity was achieved by providing the bi-linear stress–strain relationship for the elastic and plastic properties of steel as shown in Fig. 1. Geometrical nonlinearity was achieved by providing second-order analysis for the model.

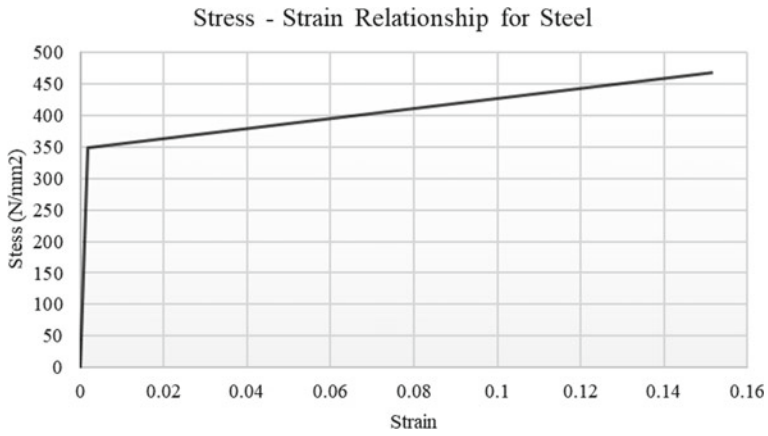

Fig. 1 Bilinear stress–strain relationship applied for material properties of steel in the FE model

Uniform and local thickness reduction strategy was used for corrosion modelling. In this method, the element was divided into several partitions depending on the proposed corrosion pattern, and reduced thickness values were provided to represent the corroded areas.

To obtain the fixed end conditions at one end of the element, the three relevant reference points were restrained for displacement and rotations in all directions. To apply an increasing load from the other end, the rotations and displacement along all the other directions except displacement along the longitudinal direction were restrained.

To estimate an appropriate mesh size, a mesh convergence study was carried out with different mesh sizes. Depending on the results, a 4 mm-sized mesh was selected as an appropriate and compatible mesh size for obtaining the results. The selected mesh size was compatible with the mesh size used in the numerical analysis by Shu et al. [12] as well. Figure 2 is an illustration of the meshed FE model.

Figure 3 is an elaboration of the deformed shape of one FE model created during the analysis. As the compression force was applied to the member, the summation

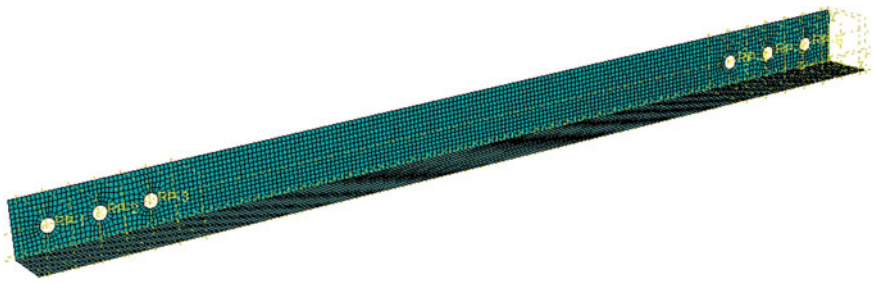

Fig. 2 Illustration of the meshed FE model

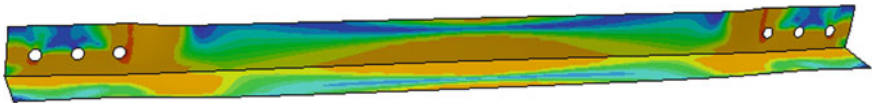

Fig. 3 Deformed shape of a sample model created in the numerical analysis

of the reactions at the three nodes of one end was taken. This compressive force was graphed with time and the maximum value of the compressive force was taken as the ultimate compression capacity.

2.2 Validation of the Model

The experimental results by Shu et al. [12] could be divided into nine sets based on their section sizes and slenderness ratios. Initially, one set of these nine was taken and five samples of that set were modelled in FE software such that the overall set is represented by the models. The experimental and numerical results of that set have been elaborated in Fig. 4, where the notations F_{EX} and F_{FEM} represent the experimental and numerical compression capacity values, respectively. As the degree of corrosion, the volume reduction percentage due to degradation of thickness has been considered.

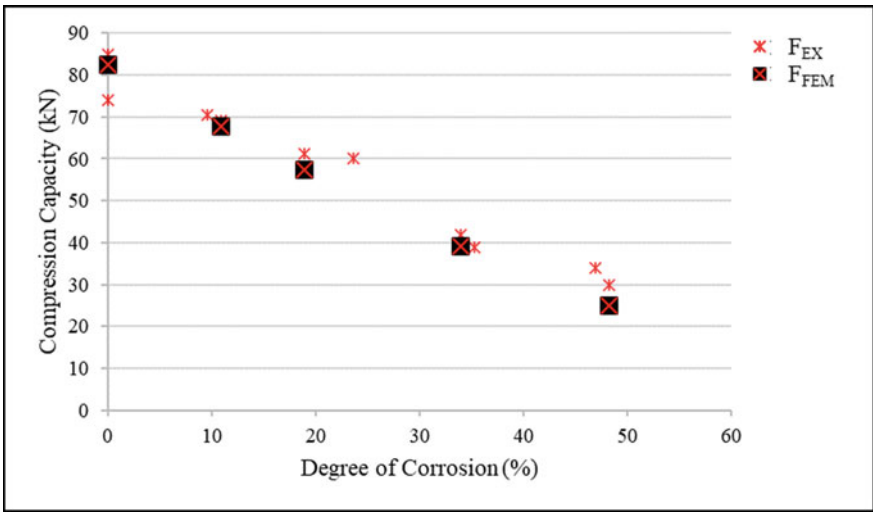

Fig. 4 Graphical representation of experimental compression capacity values and FEA results against the degree of corrosion (L50 × 50 × 4 and L/r = 120)

According to the results, it was observed that the finite element model gives very close values to the experimental values for the compression capacity, suggesting that the FE analysis is a viable evaluation method.

Then, for the other eight sets of experimental results also, one to four models were created from each set, such that the models cover the degree of corrosion range within each set. Altogether 23 models were developed, and similarly, those FEA results also gave compatible values with experimental results, confirming the validity of the model. It could also be identified that there are about three occasions where the experimental values and numerical values are considerably different. The practical errors in the experiment and in the accelerated corrosion process can be suspected as the causes of those deviations.

2.3 Numerical Evaluation of Corrosion Patterns

After validating the compatibility of the FE model to represent the effect of corrosion, the main purpose was to identify the impact of different corrosion patterns on the ultimate compression capacity of the members. For that, different thickness reduction strategies were applied to represent different corrosion patterns and developed FE models for the analysis.

The proposed corrosion patterns were divided into ten groups depending on the expected outcomes. Taking these groups into consideration, some of them, which are Groups 2, 3, 5 and 6, were based on the experimental study conducted by Ozvald and Dunai [10]. The numerical capacity values of those members could be used not only to verify the accurate experimental data but also to showcase the disputes in the previous experimental study as well. The other six groups have been designed based on different hypotheses representing different corrosion patterns to achieve the required outcomes. These hypotheses haven't been experimentally tested in previous studies.

56 × 56 × 4 angle member with a buckling length of 800 mm was taken as the reference member for the numerical analysis. The reduced thickness values were then assigned to the relevant partitions of the model to represent the corrosion patterns, as illustrated in Table 2.

In Table 1, the following abbreviations are used to represent the mentioned parameters.

L_{corr}—Corroded length, t_{corr}—Corroded thickness, D—Diameter of pits/perforations, n_{per}—number of perforations and n_{pit}—number of pits.

Table 1 Details of numerically analysed angle members

Specimen ID		Longitudinal and transverse illustration of the corrosion patterns of the members		Corrosion details
1	1A			L_{corr} = 1054 mm t_{corr} = 1 mm
	1B			L_{corr} = 1054 mm t_{corr} = 1 mm
	1C			L_{corr} = 1054 mm t_{corr} = 1 mm
	1D			L_{corr} = 1054 mm t_{corr} = 1 mm
2	2A			L_{corr} = 400 mm × 2 t_{corr} = 1 mm
	2B			L_{corr} = 200 mm × 4 t_{corr} = 1 mm
	2C			L_{corr} = 100 mm × 8 t_{corr} = 1 mm
3	3A			L_{corr} = 800 mm t_{corr} = 1 mm
	3B			L_{corr} = 800 mm t_{corr} = 1 mm
	3C			L_{corr} = 800 mm t_{corr} = 1 mm
	3D			L_{corr} = 800 mm t_{corr} = 1 mm

(continued)

Table 1 (continued)

Specimen ID		Longitudinal and transverse illustration of the corrosion patterns of the members		Corrosion details
4	4A			L_{corr} = 300 mm t_{corr} = 1 mm
	4B			L_{corr} = 150 mm × 2 t_{corr} = 1 mm
5	5A			L_{corr} = 100 mm t_{corr} = 3 mm
	5B			L_{corr} = 200 mm t_{corr} = 1.5 mm
	5C			L_{corr} = 300 mm t_{corr} = 1 mm
	5D			L_{corr} = 600 mm t_{corr} = 0.5 mm
6	6A			L_{corr} = 100 mm t_{corr} = 1 mm
	6B			L_{corr} = 100 mm t_{corr} = 1 mm
	6C			L_{corr} = 100 mm t_{corr} = 1 mm
	6D			L_{corr} = 100 mm t_{corr} = 1 mm
7	7A	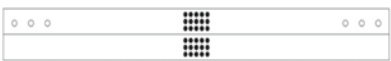		D = 10 mm n_{per} = 15
	7B			L_{corr} = 43 mm t_{corr} = 2 mm

(continued)

Table 1 (continued)

Specimen ID		Longitudinal and transverse illustration of the corrosion patterns of the members		Corrosion details
	7C			L_{corr} = 800 mm t_{corr} = 0.1053 mm
8	8A	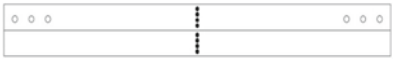		D = 8.66 mm n_{per} = 8
	8B	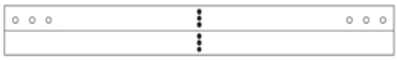		D = 10 mm n_{per} = 6
	8C			D = 12.247 mm n_{per} = 4
	8D			D = 17.32 mm n_{per} = 2
9	9A	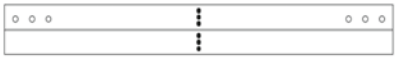		D = 8.66 mm n_{per} = 8
	9B			D = 8.66 mm n_{per} = 8
	9C			D = 8.66 mm n_{per} = 8
	9D			D = 8.66 mm n_{per} = 8
10	10A1			D = 15 mm n_{pit} = 66 t_{corr} = 1 mm
	10A2			D = 15 mm n_{pit} = 66 t_{corr} = 2 mm
	10A3			D = 15 mm n_{pit} = 66 t_{corr} = 3 mm

(continued)

Table 1 (continued)

Specimen ID		Longitudinal and transverse illustration of the corrosion patterns of the members		Corrosion details
	10B1			L_{corr} = 768.5 mm t_{corr} = 0.292 mm
	10B2			L_{corr} = 768.5 mm t_{corr} = 0.584 mm
	10B3			L_{corr} = 768.5 mm t_{corr} = 0.876 mm
	10C			L_{corr} = 768.5 mm t_{corr} = 1 mm

3 Numerical Results, Analysis and Discussion

At the validation stage, it has been emphasized that the developed model demonstrates the actual compression capacities under provided properties. Using this validated model, 39 models were created to represent the corrosion patterns described in Table 1 and analysed the results to demonstrate the impact on the compression capacity.

According to the numerical analysis, the compression capacity of the non-corroded member was 105.16kN and this value has been taken as the reference to estimate the damage caused due to corrosion.

The numerical analysis results of all members have been summarized in Table 2 with the estimated damage percentage caused by corrosion.

To calculate the residual compression capacity, the compression load to the axial deformation curve was produced using the FEA results. The maximum compressive load was taken as the compression capacity of the particular member. To calculate the damage percentage due to corrosion, the difference in compression capacity between the non-corroded member and the particular member was measured as a percentage of the compression capacity of the non-corroded member.

In Table 2, the following parameters are mentioned by each notation.

N_G—Group number, ID—Section ID, F_{RES}—Residual compression capacity and D%—Percentage of damage caused by corrosion.

The results of the Group 1 members clearly emphasize that the impact of corrosion is more severe when the corrosion occurs on the bolted leg of the member, where the compression force is applied. The corrosion damage on the compression capacity is considerably low when the leg, which is free from bolt holes, is corroded.

When the residual capacities of 1A & 1B and 1C & 1D are compared separately, there is a very low difference between each other. This behaviour emphasizes that

Table 2 Summary of the numerical analysis results

N_G	Evaluated hypothesis on compression capacity	ID	F_{RES}	D%
1	The impact of the side of corrosion (inside or outside) and the leg of corrosion (bolted or unbolted)	1A	73.50	30.11
		1B	73.87	29.75
		1C	92.45	12.09
		1D	92.73	11.82
2	The impact of the rapidity of varying the corroded leg	2A	88.77	15.59
		2B	86.18	18.05
		2C	83.84	20.27
3	To compare the criticality of corrosion to the corner of the angle and the corrosion to the edge of the width	3A	88.05	16.27
		3B	95.86	8.84
		3C	92.11	12.41
		3D	92.94	11.62
4	To investigate the criticality of the corrosion in the bolted area and the middle of the member	4A	81.80	22.21
		4B	72.02	31.51
5	The impact of thickness reduction due to corrosion when the mass reduction remains the same	5A	15.88	84.90
		5B	64.41	38.75
		5C	83.96	20.16
		5D	96.25	8.47
6	The impact of the location of local corrosion (throughout the cross-section)	6A	88.45	15.89
		6B	86.70	17.55
		6C	85.57	18.63
		6D	84.24	19.89
7	To compare the impact of perforation caused by corrosion with concentrated corrosion and distributed corrosion patterns	7A	71.58	31.93
		7B	53.16	49.45
		7C	103.91	1.19
8	The impact of different perforation patterns	8A	78.37	25.48
		8B	83.22	20.86
		8C	86.27	17.96
		8D	92.67	11.88
9	The impact of the location of perforation caused by corrosion	9A	83.22	20.86
		9B	83.91	20.21
		9C	85.66	18.54
		9D	88.73	15.62

(continued)

Table 2 (continued)

N_G	Evaluated hypothesis on compression capacity	ID	F_{RES}	D%
10	The impact of pitting corrosion compared to uniformly distributed corrosion The impact of thickness reduction due to pitting corrosion and uniformly distributed corrosion	10A1	100.83	4.12
		10A2	93.71	10.89
		10A3	87.29	16.99
		10B1	102.32	2.70
		10B2	97.95	6.86
		10B3	93.09	11.48
		10C	90.83	13.63

there is not much difference in corrosion damage, whether the corrosion happens in the inner face or outer face until the degree of corrosion remains the same. The reason behind the slight difference between these values can be the minor difference between the second moment of area values when the side of corrosion changes.

According to the results of Group 2 members, the residual capacity is decreased with the increase of rapid changing of the corroded side. Therefore, it can be suggested that even though the degree of corrosion is similar, the corrosion damage is higher, when the corroded leg rapidly changes, than having a uniformly distributed corrosion pattern in a single leg. Similar kinds of variation can also be seen in the experimental results of A9, A10 and A11 specimens in the study by Ozvald and Dunai [10] as well.

According to the obtained FEA values for Group 3 members, it can be observed that the residual compression capacity of the 3A is considerably lower than that of the 3B member, which indicates that corrosion of the corner of the member is more critical than the corrosion on the edge of the leg in the member. The members A4(I) and A5(I) in the experimental study by Ozvald and Dunai [10] also show a similar variation.

In this numerical study, 3C and 3D members, which have intermediate conditions of 3A and 3B, have shown compression capacities between the capacity values of 3A and 3B as expected. This result verifies the accuracy of the numerical analysis while confirming the suspiciousness of the experimental result of the A6 (I) specimen by Ozvald and Dunai [10].

According to the results of Group 4 members, the compression capacity of the member with corrosion surrounding the bolt holes has a considerably lower value than that of the member with corrosion in the middle, according to the results suggesting that the corrosion surrounding the connection area is more critical than the other.

As mentioned earlier, Group 5 members are designed to examine the impact of the loss of thickness due to corrosion, when the mass loss remains the same. As expected in this analysis, higher amounts of damage could be identified in the members where higher thickness losses were applied. A similar type of variation can be observed in the experimental results of L4(II) and L5(II) specimens by Ozvald and Dunai [10] as well.

When the results of Group 6 members are examined, it can be observed that the residual compression capacity decreases when the local corrosion location moves from the middle of the member to the edge. The above gradual decrease in the compression capacity of the members can also be observed in the experimental results of L1, L2 and L3 specimens in the study conducted by Ozvald and Dunai [10] as well.

According to the results of Group 7 members, the perforation has caused a damage percentage of about 32%. But for the member with similar mass loss and uniform corrosion throughout the buckling length, the capacity value is just close to that of the un-corroded member. When these two values are compared, it can be suggested that perforation creates a critical impact on the compression strength of the member. In specimen 7B, the same mass loss has been provided as local corrosion on the length of 43 mm which is considered a very low value with respect to the buckling length. In this scenario, the compression capacity has been lower than that of the perforated member. Even though the corrosion has not gone throughout the length, the existing corrosion amount has spread through the full width of the specimen to a considerable amount of depth (2 mm), which can be suggested as the reason for this low value. Therefore, it can be suggested that, if the corrosion is affected through the full width to a larger depth, the damage can be higher than perforation concentrated in a small area.

The numerical capacities of Group 8 members show the member with a greater number of perforations with lower diameters has been given a low compression capacity value than the members with a smaller number of perforations with higher diameters. This behaviour can also be justified by the area loss of the most critical cross-section. 8A member has the maximum sectional area loss at the middle of the member and has given the smallest compression capacity.

According to the results of Group 9, the members showed a different variation than local corrosion by giving a lower capacity when the perforation is in the middle and higher capacity values when the location of the perforation is close to the edge of the member.

In the results of Group 10 members, the mass loss of the members differs in the order of 10A1<10A2<10A3 and 10B1<10B2<10B3. According to the obtained residual capacities, there is a gradual reduction in the compression capacity with the mass loss either if is pitting corrosion or uniform corrosion. When the results of 10A1, 10A2 and 10A3 are compared, respectively, with 10B1, 10B2 and 10B3, it can be observed that always the member with pitting corrosion showcases the lesser value of the two, which means that even with the same mass loss pitting corrosion is more severe than uniform corrosion. In addition to that, the difference between the two values related to pitting corrosion and uniform corrosion increases with the increase of the degree of corrosion, suggesting that mass loss due to pitting corrosion more severely reduces the compression capacity than uniform corrosion.

When the compression capacity of 10A1 and 10C is compared, there is a considerably lower value in 10C than in 10A1. This difference implies that the thickness loss due to pitting corrosion is less critical than the same thickness loss within the whole cross-section throughout the member.

It can be identified that the local cross-sectional area reduction in the critical section due to pitting corrosion is higher than uniform corrosion with the same degree of corrosion. When the same uniform thickness reduction is applied as in the 10C member, the cross-sectional area reduction is more severe than in the above two occasions. The obtained variations in the compression capacity can be justified by the severity of the local effect on the critical cross-section.

4 Conclusions and Recommendations

When the thickness reduction method is applied for the numerical analysis of the corroded members, the results complied with the experimentally tested values. Therefore, it can be concluded that a thickness reduction method is a viable approach to numerically demonstrate the residual compression capacity of corroded steel angle members.

For uniformly corroded members, the corrosion behaviour, in the bolted leg, at the corner of the angle and within the bolted area is more critical than that in the unbolted leg, at the edge of the width and within the middle area. When there are rapid variations in corrosion legs, the impact on the compression capacity is higher.

In locally corroded members, the corrosion to the edge of the buckling length is more critical than the corrosion in the middle. FEA results prove that the loss of thickness governs the residual compression capacity if the mass loss due to local corrosion is similar.

When perforated conditions occur due to corrosion, the impact is much more severe than the occurrence of a similar mass loss due to uniform corrosion. The impact of perforation on the residual compression capacity increases when the perforation goes to the middle of the member and creates more cross-section loss at one location.

It can be concluded that mass loss due to pitting corrosion is more critical than mass loss due to uniform corrosion. But the thickness loss due to uniform corrosion is more critical than the thickness loss due to pitting corrosion.

The findings of this research can be used to visually observe a corrosion pattern in a real structure and predict the residual compression capacity without removing or testing the member. In addition, the trends in the reduction of compression capacity with different corrosion patterns can be identified using the results. Moreover, the findings of this work are suggested to be used as a framework for further studies and applications.

Due to the limited time periods and practical obligations, for almost all these previous experiments, specimens have been prepared to be subject to the accelerated corrosion method. But it might be interesting to observe the behaviour of the naturally corroded members under compression. There might be property changes with ageing, which can influence the ultimate compression capacity. Therefore, experimental studies with naturally corroded specimens might be worth a comparison with the currently available data.

References

1. Ahn J-H et al (2016) Residual compressive strength of inclined steel tubular members with local corrosion. Appl Ocean Res, 498–509
2. Andrade C, Alonso C (2004) Test methods for on-site corrosion rate measurement of steel reinforcement in concrete by means of the polarization resistance method. Mater Struct, 623–643
3. Beaulieu LV, Legeron F, Langlois S (2010) The compression strength of corroded steel angle members. J Constr Steel Res, 1366–1373
4. Cantero D, Gonzalez A (2017) Bridge damage detection using weigh-in-motion technology. J Bridg Eng 20(5)
5. El Aghoury IM (2012) Numerical tool for fatigue life prediction of corroded steel riveted connections using various damage models, s.l.: s.n
6. Hebor MF, Ricles JM (2002) Local buckling strength of patch corrosion damaged steel tubular bracing. Int J Steel Struct, 59–70
7. Leising C (2014) Pitting corrosion measurement using 3D profilometry. s.l.: s.n
8. Nazari M, Khedmati MR, Khalaj AF (2014) A numerical investigation into ultimate strength and buckling behaviour of locally corroded steel tubular members. Lat Am J Solids Struct, 1063–1076
9. Ostapenko A, Berger TW, Chambers SL, Hebor MF (1996) Corrosion damage effect on strength of tubular columns with patch corrosion. ATLSS, Bethlehem
10. Ozvald K, Dunai L (2012) Effect of corrosion on the buckling of steel angle members. s.l.: Periodica Polytechnica Civil Engineering
11. Safiuddin M (2006) Occurrences of corrosion: causes and prevention. BRAC Univ J III(1):71–74
12. Shu Q et al (2020) Assessing the capacity of corroded angle members in steel structures based on experiment and simulation. Constr Build Mater
13. Wang R, Guo H, Shenoi RA (2020) Experimental and numerical study of the localized pitting effect on compressive behaviour of tubular members. Mar Struct
14. Xiao L, Peng J, Zhang J (2019) Mechanical properties of corroded high-performance steel specimens based on 3d scanning. Adv Steel Constr, 129–136

Conservation and Management of Ancient Stupa Using Digital Twins: A Case Study of Uav-Based 3D Photogrammetric Digitization of Rankoth Wehera Stupa

S. Egodawela, H. A. D. S. Buddika, W. A. N. I. Harischandra, M. Mahmoodian, and M. R. S. N. M. Mathota

Abstract Stupa structures in Sri Lanka are regarded as world heritage sites with rich archaeological and artistic value, some nearing a lifetime of almost 2 millennia. Conservation and management efforts are currently hindered due to the lack of practice of modern Building Information Modelling (BIM) techniques. Recently, Digital Twins (DT) as a tool for Historic Building Information Modelling (HBIM) has gained attraction worldwide. This paper summarizes the initial work that has been carried out to apply modern HBIM techniques for Sri Lankan heritage sites, to manage and preserve these structures for the future. To this end, this article details a case study of Rankoth Wehera in Sri Lanka and the 3D photogrammetric model creation for the application of DT principles. A drone survey of the structure was done with the assistance of the Central Cultural Fund of Sri Lanka to obtain high-resolution images of the location. Following a feature detection and homography calculation step using Scale Invariant Feature Transform (SIFT), the high-fidelity features were fed to an open-source 3D point cloud generation software, Meshroom. A 3D textured mesh was generated to observe the existing structural defects in the stupa dome and the superstructure. Obtained images can be used in conjunction with processing techniques using Image processing and Deep learning fundamentals to automatically detect the defects and pinpoint the locations of the defects on the DT model. Moreover, the generated high-resolution mesh can be fed for Finite Element Modelling

S. Egodawela · M. Mahmoodian
School of Engineering, RMIT University, 124 La Trobe St., Melbourne, VIC 3000, Australia

H. A. D. S. Buddika (✉)
Department of Civil Engineering, University of Peradeniya, Peradeniya 20400, Sri Lanka
e-mail: samithbuddika@eng.pdn.ac.lk

W. A. N. I. Harischandra
Department of Electrical and Electronic Engineering, University of Peradeniya, Peradeniya 20400, Sri Lanka

M. R. S. N. M. Mathota
Central Cultural Fund, 4th Floor Sethsiripaya, Battaramulla 10120, Sri Lanka

© The Author(s), under exclusive license to Springer Nature Singapore Pte Ltd. 2023

R. Dissanayake et al. (eds.), *ICSBE 2022*, Lecture Notes in Civil Engineering 362,
https://doi.org/10.1007/978-981-99-3471-3_35

(FEM) software to carry out nonlinear analysis when required. With this premiering work, the authors intend to inspire and urge researchers and authorities to integrate intelligent HBIM techniques for the conservation and management of Sri Lankan heritage sites.

Keywords Digital twin · Photogrammetry · Drones · Image processing · Historic Building Information Modelling · Deep learning

1 Introduction

In Buddhist culture, Stupas are considered to be places of utmost reverence. Be it due to religious significance or sheer magisterial grandeur, these structures never fail to attract pilgrims and tourists from all around the world. As the influence of Buddhism grew in Sri Lanka, stupa structures were erected in the respective kingdoms where the rulers resided. Most Notably Ruwanweli Maha Seya by King Dutugemunu (161-137 BC), Abhayagiri by King Valagamba (89-77 BC), and Jetavanaramaya by King Mahasena (276-303 AD) [14]. The longevity of these structures speaks volumes of the sophisticated yet intricate engineering practices that prevailed at the time [18, 20].

Rankoth Wehera (directly translated to "golden crest stupa" from Sinhalese) was built under the rule of King Nissanka Malla and is in Polonnaruwa, Sri Lanka. The name is derived from King Nissanka Malla's offering of a golden crest for the stupa as a symbol of reverence. Having built in the period of AD 1187–1196 Rankoth Wehera is reaching almost 850 years of life span [18]. Rankoth Wehera is constructed entirely from locally sourced burnt clay made into bricks size ranging from 31.8 cm × 21.3 cm × 5.0 cm with a volume of 533.4 cm^3 [17]. The structure has a base diameter of 170 m and a current height of 33 m, however, it is said to have been reaching 60 m during the heyday of the Polonnaruwa kingdom [14]. The shape of the stupa underwent changes during the renovations by later rulers, and subsequently resulted in a drastic height decrease. Regardless of later renovations reducing the height of the structure, Rankoth Wehera remains the largest stupa in the Polonnaruwa Kingdom and the fourth largest in the country after Jethawanaramaya, Abayagiriya, and Ruwanweliseya. To support the weight of the structure four large Wahalkadas (directly translated to "entrance point" from Sinhalese) are constructed made of the same bricks reaching a height of 6.7 m and width of 3.8 m. The whole structure is inside a perimeter of a square terrace that provides both structural support to the foundation of the stupa and means of entrance to the stupa via the Weli Maluwa (directly translated to "sand terrace" from Sinhalese). The stupa is in the centre of a large square terrace, which is also supported by a brick wall. The terrace has four entrances oriented to the four cardinal points, with sand paths leading up to the stupa.

Due to the cultural and heritage significance and the artistic merit of Rankoth Wehera, efforts have been carried out by the Sri Lankan government together with the Department of Archelogy and the Central Cultural fund to preserve the structure. Work is currently being carried out on the stupa dome/relic chamber to provide

support to the cracks that occur due to weed growth from the interior. In this light, this work is funded through the Central Cultural Fund of Sri Lanka which pioneers the efforts to preserve the rich cultural heritage of Sri Lanka and improve the exposure of these ancient structures for a global audience through digitalization. To this end, the application of Historic Building Modelling (HBIM) principles and Digital Twin (DT) construction of the site is a novel initiative by the said authorities.

This work thrives to be the premiering of digital conservation of historic sites in Sri Lanka, thereby improving the effectiveness of managing and preserving these archaeological sites and global exposure.

2 Literature Review

With the rise of interdisciplinary research within the last decade, Historic Building Information modelling (HBIM) has gained immense attraction as a convenient and accurate tool for performance modelling, behaviour analysis of stuctures, deterioration modelling, and preventive maintenance of historic heritage sites. A DT is one facet of HBIM that is a convenient way to have an accurate and up-to-date mirror image of the physical structure in a digital form, which enables structural engineers to perform multiphysics and multiscale simulations, allowing decision makers to effectively understand the prevailing condition of the structure, study defects, and suggest remedial measures. DT combines the systematic application of various technical surveying methods [11] and BIM-based semantics [15]. Manual processing of archaeological information data, in the particular geometric measurement of structure magnitude, is prone to errors or omissions [12]. Furthermore, a comprehensive structural health assessment requires more than just a 3D geometric model containing archaeological data. Rather, it require further intricate details such as changes in topographical, textural, and morphological data [9] of the structure. Therefore, there is a greater need to digitize modern archaeological processes. That is, to take a step forward from manual HBIM modelling to propose a DT of the archaeological process. In this context, as modern architectural archaeologists tend to implement innovative techniques for 2D/3D documentation, the transition from HBIM models towards a DT process could be considered the next technological revolution in the archaeological analysis process [9].

UAV-based oblique photogrammetry technology and Terrestrial Laser Scanning technology (TLS) are the premier data acquisition methods in 3D-modelling in HBIM and Digital twin creation [10] in recent years. Each with unique pros and cons, both techniques are feasible for the creation of digital assets. Table 1 shows recent work done in the space of HBIM using both these techniques in conjunction and independently. A comparison of the two methods is shown in Table 2 for concise reading.

To verify the effectiveness of the HBIM and DT framework for architectural archaeological research, the authors use Rankoth Wehera as a case study in this paper. A photogrammetric survey will be done in this work together with 3D reality

Table 1 Recent work done in the space of HBIM, digital twin creation, and the data acquisition technique used in each work

Study	Venue	Country	Data collection method
Thomas et al. [21]	Bet Giorgis, a rock-hewn church	Ethiopia	Photogrammetry
Nakagura et al. [13]	Villa Foscari and Villa Pisani at Bagnolo	Veneto, Italy	Photogrammetry
Liang et al. [8]	Huanxiu Shanzhuang	Suzhou, China	TLS/ photogrammetry
Gabellone [4]	Underground oil-mill	Gallipoli (Puglia, Italy)	Photogrammetry
La Russa and Santagati [7]	Villa Zingali Tetto	Catania, Italy	TLS + Photogrammetry
De Luca [2]	Notre-Dame de Paris	Paris, France	Photogrammetry
Eloiza et al. [3]	Assisi Church	Brazil	Photogrammetry
Giuffrida et al. [5]	The Churches of San Nicola and San Basilio	Motta Sant' Agata, Italy	TLS + Photogrammetry
Parsinejad et al. [16]	Achaemenid, Persepolis	Iran	Photogrammetry
Tan et al. [20]	Xiegong	China	TLS + Photogrammetry

Table 2 Comparison of TLS and Photogrammetry as two data collection methods [10]

Parameter	Photogrammetry	TLS
Physical contact	No	No
Hardware cost	Cheaper hardware	Extremely high cost
Accuracy	±10 cm	±1 cm
Dependence on sensor localization (i.e. GPS, GNSS, RTK)	High dependence	Lower dependence
Texturing capability	Yes	No
Computational Complexity	Extremely high	Low
Processing time	Extremely high	Low

modelling, archaeological analysis, and a semantic-rich HBIM model together with a case research that validates the first step of the DT process on said structure.

3 Case Study—Rankoth Vehera Digital Twin

The focus of this study is Rankoth Wehera (latitude 7.9583° and longitude 81.0032°) which is located in Polonnaruwa, Sri Lanka. Figure 1 shows the exterior of the stupa in question and Fig. 2 shows the location on a 2D terrain plot obtained via Google Earth. The location of the structure is at an average elevation of 75 m above sea level with a study area of approximately 10,000 m^2. The area can be accessed via Maradankadawala-Habarana-Thirukkondaiadimadu Hwy/A11 and Gallambarawa Road.

Although the subordinate structures, i.e. Wahalkadas, Stone Seating, and Terrace, etc. hold a high archaeological and artistic value, this study focuses only on the main stupa structure consisting of the parts mentioned in the literature [17].

The following Methodology was followed to obtain the DT of the structure (see Fig. 3).

Fig. 1 Exterior images of Rankoth Wehera

Fig. 2 Satellite view of the Rankoth Wehera and surrounding area

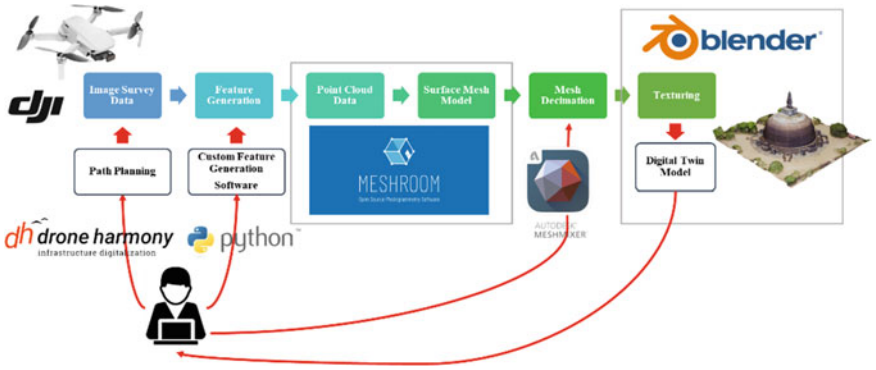

Fig. 3 Methodology of generating a texture-rich photogrammetric model of Rankoth Wehera

3.1 UAV Data Acquisition

The DJI Mavic Mini UAV was used to capture images. Manufacturer specifications of the UAV are detailed in Table 3. A proprietary application Drone Harmony® was used in this survey for automatic flight planning, waypoint navigation, and image capturing. Drone Harmony® allows the user to define and create complex 2D or 3D paths with given reference points for the UAV. Furthermore, the application allows the selection of the flight altitude, required side and forward overlap of the survey area, and adjustment of gimbal settings to obtain the desired Feild of Vision (FOV). Three flight missions were conducted with flight data mentioned below in Table 4. Figure 4 shows the flight path in a 3D setting.

Generated drone control signals are communicated to the drone in real-time and captured images are relayed back to the controller for live observation. Figure 5a, b shows samples of image data captured from the survey.

To comprehensively capture the blind spots of the intricate structure in particular the Wahalkada structures, additional images were taken using a mobile phone camera.

Table 3 Hardware and firmware specification of the UAV used for data collection

Parameter	Value
Make	DJI Mavic Mini
Type	Quad rotor
Dimensions	245 × 289 × 55 mm (L × W × H)
Weight	249 g
Max flight time	30 min
Sensor	1/2.3″ CMOS
FOV:	83°
Aperture:	f/2.8
Still image resolution	4000 × 2250

Table 4 Drone control specification of missions for data collection

Parameter	Mission 1	Mission 2	Mission 3
Type of mission	Double grid	Mapping orbits	Circle
Flight time (min)	6.9	15.6	3.8
No. of waypoints	14	10	4
Flight speed (m/s)	1.5	1	1
Image capturing type	Continuous, self-timer, 0.5 fps	Continuous, self-timer, 1 fps	Continuous, self-timer, 1 fps
Altitude (m)	60	45	20
Radius	NA	150 m	120 m
Gimbal angle Pitch/yaw	−90°/0°	−45°/0°	−20°/0°
Side overlap (%)	60	60	80
Forward overlap (%)	50	60	80

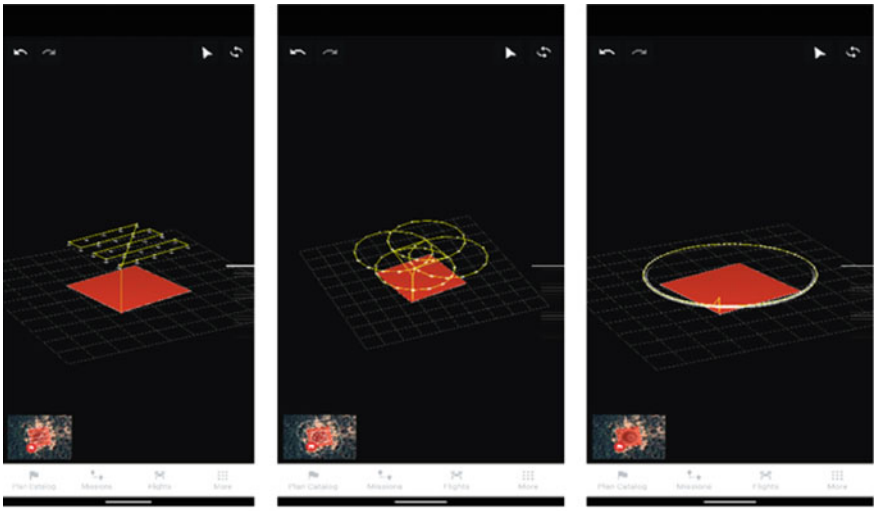

Fig. 4 Definition of Flight paths for Mission 1 (**a**), Mission 2 (**b**), Mission 3 (**c**) and path planning through the Drone Harmony® application

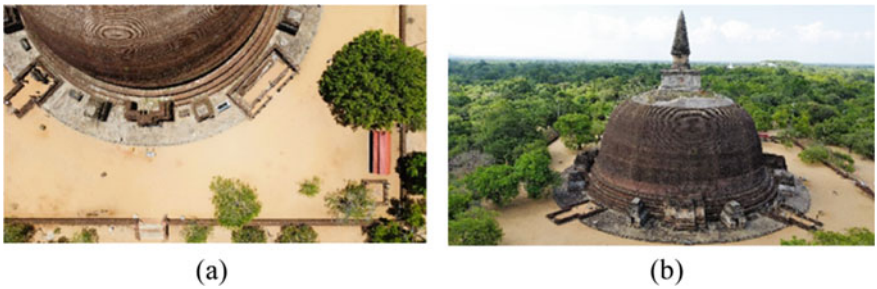

Fig. 5 Images captured during drone survey

3.2 Photogrammetric Model

3.2.1 Scale Invariant Feature Transform (SIFT)

Scale Invariant Feature Transform is an illumination, noise invariant feature selection algorithm that identifies and matches local features of interest in an image. More importantly, SIFT accounts for minor changes in the viewpoint that occurs in unstable image capturing platforms such as drones. Figure 6a, b shows SIFT features on images taken within a short time interval with the drone platform moving. Figure 6c shows the matched features from Fig. 6a, b.

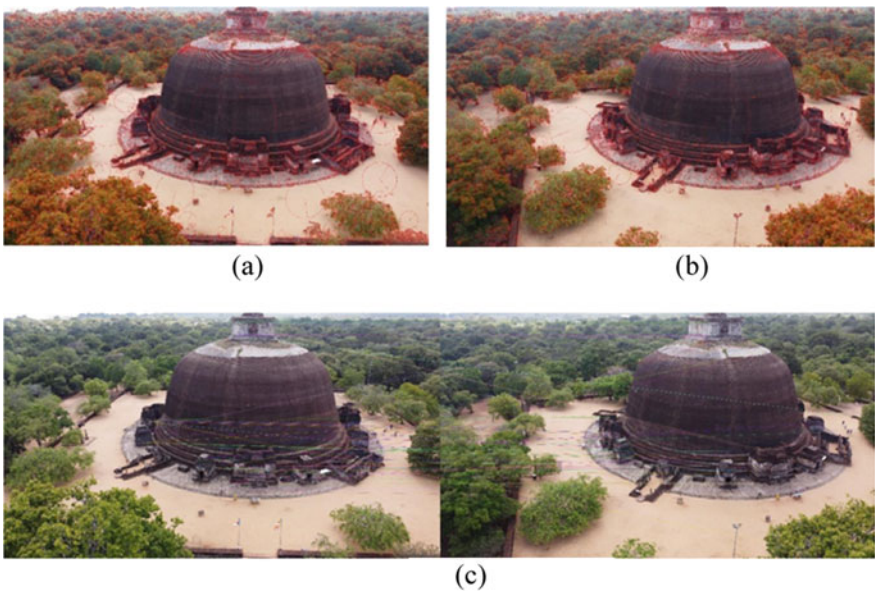

Fig. 6 SIFT features and feature matching

Fig. 7 3D point cloud of Rankoth Wehera generated using Meshroom software

3.2.2 Structure from Motion Point Cloud Generation

The matched features using SIFT of the input images are used as inputs to Meshroom (Meshroom® by Alicevision, 2022). Meshroom is a convenient open-source platform that generates structure from motion point clouds. Meshroom allows the customization of feature selection using user defined Python files paving the way to increased freedom for users. The matched features generated by SIFT are defined into tracks for each feature. Each track would ideally represent a point in space but in reality, it is a patch of pixels considered as a feature in the scene. By tracking the georeferenced SIFT features, a 3D point cloud is generated using the Meshroom. The georeferencing is done using GPS system using proprietary firmware by DJI.

A georeferenced 3D point cloud was generated as a dense point cloud of 2,484,786 points (point density 248 pt per m^2). The generated 3D point cloud data are shown in Fig. 7.

3.2.3 Mesh Generation, Decimation Texturing

Following the 3D point cloud generation, Meshroom supports mesh generation. The meshing process creates a dense geometric surface representation of the scene. The underlying algorithms used in the meshing process are 3D Delaunay tetrahedralization [1] suggested by Graph Cut Max-Flow [22] followed by Laplacian filtering to remove local artefacts (Meshroom® by Alicevision, 2022). Once the complex mesh is generated, a mesh decimation software, Meshmixer AutoCAD®, was used to select the region of interest from the surrounding. Figure 8 shows the trimmed mesh with the ROI selected.

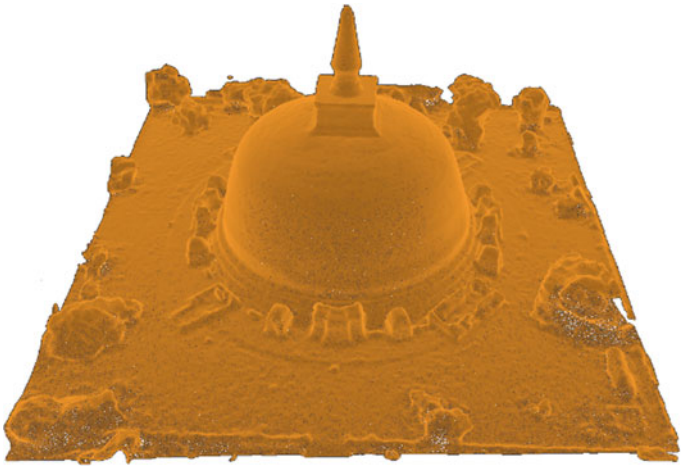

Fig. 8 3D mesh model after mesh decimation and trimming

4 Results and Discussion

4.1 3D Photogrammetric Model of Digital Twin of Rankoth Wehera

The generated textured mesh can be viewed using 3D scene visualization software Blender, commonly used for 3D applications such as virtual reality, and video game development. Blender allows the simulation of custom lighting sources for better inspection of the textured mesh. Figure 9 shows a render of the textured mesh.

4.2 Visible Structural Defects on Rankoth Wehera

Observing the photogrammetric model of Rankoth Wehera, the following existing structural defects were identified.

4.2.1 Cracks in the Dome/Relic Chamber

Diagonal cracks were observed near the base of the chamber. This may be due to vertical and hoop stresses in the Stupa that steadily increase from top to bottom [18]. States that maximum compressive stresses can be noticed at the base. Furthermore, cracks along the plastering between the brickwork were observed that may have risen due to creep induced by the thermal loading of the structure (see Fig. 10).

Fig. 9 Rendered images of the textured mesh

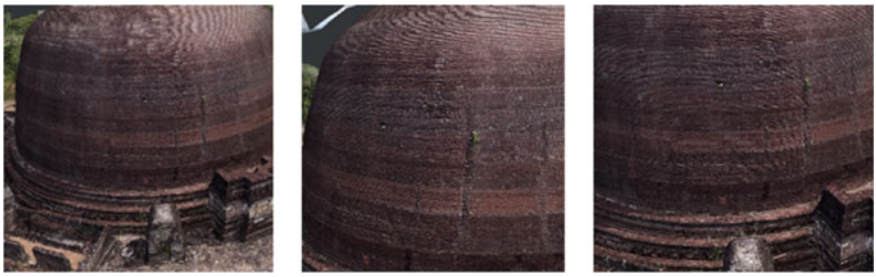

Fig. 10 Detected cracks of Rankoth Wehera dome

Fig. 11 Fresh vegetation sprouting from the dome

4.2.2 Vegetation-Induced Cracks

Vegetation sprouting from the interior of the dome might lead to cracks. Currently, vegetation that sprouts from the outside is weeded out manually however, roots existing inside the dome result in vegetation sprouting again. Cracks due to vegetation is further accelerated due to moisture contained in the clay soil used for the construction of the dome. Foundation settlement or upward thrust on a portion of the soil from roots can cause severe cracks in the dome structure (see Fig. 11).

4.2.3 Plaster Delamination

The matrix material used in the waterproof plastering is limestone slurry rather than normal stucco. Due to this the top plastering is prone to cracking from thermal expansion and moisture loss [17]. This is a severe defect on the dome and could lead to moisture ingress into the brickwork, causing plaster debonding and ultimately collapsing the dome (see Fig. 12).

4.2.4 Brick Misalignment

Local collapse in the brickwork leads to brick misalignment caused in high-stress regions in the stupa structure leading to superstructure collapse. Ranaweera et al. [18] have stated the main reason for cracking of the dome chamber in Sri Lankan stupa structures is improper keying of bricks between old and new. This leads to the ingress of water into the old brickwork subsequently causing the separation of the new brickwork from the old brickwork causing superstructure collapse (see Fig. 13).

4.2.5 Cavity Erosion and Gully Erosion

Due to water retention on the top flat surface of the Dewatha Kotuwa, cavity erosion at the base of the Dewatha Kotuwa occurs as shown in the Figure below. Additionally,

Fig. 12 Delamination of old plaster

Fig. 13 Brick misalignment and improper keying in the dome

Fig. 14 Cavity and Gully erosion in dome due to water runway

water runway paths along the stupa structure result in gully erosion on the surface (see Fig. 14).

5 Conclusions

This paper details the DT process, which connects the physical components in the real world and builds a digital mirror of the said physical entity. Drone photogrammetry was found to be an extremely capable and convenient tool for the DT process to extract 3D geometric, topological, textural, and morphological information. The semantic photogrammetric model can give information about the structural defects that exist on the structure aiding the Historic Building Information Modelling (HBIM) process.

The authors recommend the use of proportions extracted from these models to be directly used for stress analysis under self-weight and external loads resulting from thermal, cyclic wet and drying, lightning, and other environmental considerations. This will allow the predictive measure to be studied and ultimately recommend renovation work before failure.

References

1. Cignoni P, Montani C, Perego R, Scopigno R (1993) Parallel 3D delaunay triangulation. Comput Graph Forum 12:129–142
2. De Luca L (2020) Towards the semantic-aware 3D digitisation of architectural heritage. In: Proceedings of the 2nd workshop on structuring and understanding of multimedia heritage contents
3. Eloiza D-K, Mezencio DL, Miranda EDM, Sá DPD, Dias U (2020) Towards a digital twin for heritage interpretation. In: International conference of the aeation for computer-aided architectural design research in Asia (CAADRIA), pp 183–191
4. Gabellone F (2020) A digital twin for the distant visit of inaccessible contexts. In: International conference on metrology for archaeology and cultural heritage, Trento, Italy
5. Giuffrida D, Mollica Nardo V, Neri D, Cucinotta G, Calabrò IV, Pace L, Ponterio RC (2021) A multi-analytical study for the enhancement and accessibility of archaeological heritage: the Churches of San Nicola and San Basilio in Motta Sant'agata (RC, Italy). Remote Sens, 13
6. Jouan P, Hallot P (2019) Digital twin: a hbim-based methodology to support preventive conservation of historic assets through heritage significance awareness. Int Arch Photogramm Remote Sens Spat Inf Sci, XLII-2/W15, 609–615
7. La Russa FM, Santagati C (2020) Historical sentient–building information model: a digital twin for the management of museum collections in historical architectures. Int Arch Photogramm Remote Sens Spat Inf Sci, XLIII-B4-2020, 755–762
8. Liang H, Li W, Lai S, Zhu L, Jiang W, Zhang Q (2018) The integration of terrestrial laser scanning and terrestrial and unmanned aerial vehicle digital photogrammetry for the documentation of Chinese classical gardens–a case study of Huanxiu Shanzhuang, Suzhou, China. J Cult Herit 33:222–230
9. Mahmoodian M, Shahrivar F, Setunge S, Mazaheri S (2022) Development of digital twin for intelligent maintenance of civil infrastructure. Sustainability, 14
10. Marín-Buzón C, Pérez-Romero AM, León-Bonillo MJ, Martínez-Álvarez R, Mejías-García JC, Manzano-Agugliaro F (2021) Photogrammetry (SfM) vs. terrestrial laser scanning (TLS) for archaeological excavations: mosaic of cantillana (Spain) as a case study. Appl Sci, 11
11. Martínez-Carricondo P, Carvajal-Ramírez F, Yero-Paneque L, Agüera-Vega F (2019) Combination of nadiral and oblique UAV photogrammetry and HBIM for the virtual reconstruction of cultural heritage. Case study of Cortijo del Fraile in Níjar, Almería (Spain). Build Res Inf 48:140–159
12. Murphy M, Mcgovern E, Pavia S (2009) Historic building information modelling (HBIM). Struct Surv 27:311–327
13. Nakagura T, Tsai D, Pinochet D (2015) Photogrammetric models of Villa Foscari and Villa Pisani at Bagnolo
14. Paranavitana S (1952) The statue near Potgul-Vehera at Poḷonnaruva, Ceylon. Artibus Asiae, vol 15, no 3, pp 209–217
15. Parisi P, Lo Turco M, Giovannini EC (2019) The value of knowledge through H-Bim models: historic documentation with a semantic approach. Int Arch Photogramm Remote Sens Spat Inf Sci, XLII-2/W9, 581–588
16. Parsinejad H, Choi I, Yari M (2021) Production of iranian architectural assets for representation in museums: theme of museum-based digital twin. Body Space Technol 20:61–74
17. Ranaweera M, Helarisi A (2015) Materials used in the construction, conservation, and restoration of ancient stupas in Sri Lanka
18. Ranaweera M, Silva G (2006) Conservation and restoration of ancient stupas in Sri Lanka tenth East Asia-Pacific conference on structural engineering & construction–EASEC10. Bangkok, Thailand
19. Ranaweera MP (1998) Stresses in stupas of different shapes. proceedings & abstracts of the annual research sessions university of Peradeniya, Peradeniya, Sri Lanka, pp 88
20. Tan, J, Leng J, Zeng X, Feng D, Yu P (2022) Digital twin for Xiegong's architectural archaeological research: a case study of Xuanluo Hall, Sichuan, China. Buildings, 12

21. Thomas B, Zhang L, Armin G, Clive F, Heinz R (2012) Photogrammetric reconstruction and 3D visualization of Bet Giorgis, a rock-hewn church in Ethiopia. Int Arch Photogramm Remote Sens Spat Inf Sci, 34
22. Yuri B, Vladimir K (2004) An experimental comparison of min-cut/max-flow algorithms for energy minimization in vision. IEEE Trans PAMI 26:1124–1137

Use of Recycled Glass in Non-structural Building Elements for Improved Fire Performance

T. Thevega, J. A. S. C. Jayasinghe, C. S. Bandara, D. Robert, and S. Setunge

Abstract Sustainable materials always benefit the environment. In the global green concept, there are lots of materials that are recycled and reused in different forms by adapting different techniques. Among different materials, the amount of recycled glass is less than the usage, even though there are many applications with glass material in various constructions. Therefore, this study aims to promote the use of waste glass as a composite material with polymer material in non-structural applications such as interior and exterior walls in buildings. While selecting the polymer material, the thermal performance needs to be focused on since mechanical performance as polymers are weak and highly flammable under thermal loadings. The thermal performance can be evaluated by experimental or numerical analysis. In this research, numerical tools are used to investigate thermal performance. The numerical analysis is conducted using computational fluid dynamic (CFD) simulations to simulate a combustibility test for the composite material. Further, a verified simplified cone calorimeter test model is used to investigate the impact of the polymer material. From this research, it is proposed that increasing the percentage of recycled glass will help to improve the thermal performance of glass-polymer composite materials while enhancing sustainability. Moreover, it has been demonstrated that the peak heat release rate is reduced by 50% when 30% of glass fibre is added to 70% polymer in comparison to pure polymer. The results from the study will benefit Engineers to use sustainable materials in building construction rather than relying on conventional building materials.

Keywords CFD simulation · Polymer composite material · Recycled glass · Sustainable development · Thermal performance

T. Thevega (✉) · J. A. S. C. Jayasinghe · C. S. Bandara
Faculty of Engineering, University of Peradeniya, Peradeniya, Sri Lanka
e-mail: thevegat@eng.pdn.ac.lk

D. Robert · S. Setunge
School of Engineering, RMIT University, Melbourne, VIC 3001, Australia

© The Author(s), under exclusive license to Springer Nature Singapore Pte Ltd. 2023

R. Dissanayake et al. (eds.), *ICSBE 2022*, Lecture Notes in Civil Engineering 362,
https://doi.org/10.1007/978-981-99-3471-3_36

1 Introduction

Sustainability is crucial on a global scale. Most people don't think about environmental sustainability since they are focused on meeting their immediate needs rather than their long-term effects. There are many negative consequences of pollution, such as health problems and natural material and resource depletion. The importance of sustainability has grown recently. Additionally, tight laws and regulations are made, and those contribute to a greater improvement in the environmental conditions. Civil engineers, therefore, consider sustainable advancements in construction for future development. As a result of the increased scarcity of natural resources and the rapid growth of landfills, engineers work to maximize the use of waste materials and enhance the usage of recyclable materials.

In the construction business, numerous materials (concrete, glass, and plastic wastes) are recycled and repurposed using various techniques. Instead of Portland cement, recycled concrete is made from fly ash (a by-product of the industrial coal industry), and recycled aggregates are made from recycled concrete [8, 14, 16, 21, 22, 28, 34]. Plastic trash is recycled and used in many types of construction materials, such as sand, coarse aggregates, and fine aggregates in the production of tiles, bricks, and concrete, due to its huge volume and negative environmental effects [1, 11, 15, 24]. Among other materials, glass waste usage has also been increasing in recent years compared to the past.

Since glass is clear, chemically inert, environmentally friendly, sustainable, strong, accessible, and reasonably priced, it is produced in enormous quantities around the world (annually over 100 million tonnes of glass). The use of glass in buildings is encouraged by recent advancements in glass technology as well as architectural, sustainable, and environmental concerns. As a structural element (columns, beams, and floor slabs), an external glazing material, and a cladding material, glass is now used in the construction sector. Glass can be recycled; hence, it is encouraged to use recycled glass. The use of waste glass as tiles, fine and coarse aggregates in concrete, and a replacement for cement and bricks have all been the subject of extensive studies [2, 10, 17, 23, 27]. As an alternative to river sand, glass tiles, bricks, and ceramic products, cathode ray tube (CRT) funnel glass is also used as fine aggregate in mortar. However, when compared, a less amount of used glass is repurposed [3]. But currently, glass is being used more and more. The future should be taken into account when developing recycling methods and expanding uses for recycled glass in different applications.

This study focuses on the use of recycled glass in non-structural applications in buildings (external and internal walls) while enhancing the thermal performance of the building element since sustainable materials are best suited for future development in the construction sector. Additionally, it is suggested to use accurate numerical analysis instead of experimental analysis to maintain environmental sustainability. As glass is highly brittle and the polymer is highly flammable, the behaviour of the glass-polymer composite material is investigated in this case to suggest a high

performance material under mechanical and thermal loadings. However, as non-structural elements are non-load bearing elements in buildings, fire performance is a major problem than mechanical performance. Therefore, the fire performance of glass-polymer composite materials was analysed by simulating a cone calorimeter combustibility test (small-scale test). As an example, polybutylene terephthalate with glass fibre (PBT-GF) material was selected and numerically analysed. From the analysis of pure polymer and glass-polymer composite material, it was highlighted that pure polymer has a high negative impact than glass-polymer composite material when exposed to fire loadings.

2 The Performance of Glass Composite Materials

Due to its great brittleness, glass performs better when combined with other materials. Glass is typically added to polymer materials such as glass fibre or glass powder. When combined as a composite material, glass improves the tensile behaviour of the polymer and the polymer improves the ductility of glass. Few studies highlight the applications of glass fibre with different resin materials [5, 6, 25, 26]. Despite having high mechanical properties, polymer materials adversely affect the thermal properties of composite materials. Therefore, before employing a material in a building, it is important to take into account its mechanical and thermal performance because composite behaviour differs depending on the way that different materials are combined.

Numerous studies in the past have concentrated on the building's mechanical performance. However, because of the serious failures, people now recognize the severity of thermal performance. Fire testing must be conducted before construction, as fire performance of the building has lately been highlighted as a key problem [12, 32]. The combustibility test was first conducted for the building materials employed to assess the fire behaviour of the structural element. To assess the flammable behaviour of any material, vertical furnace tests and cone calorimeter tests were conducted [7, 31]. Cone calorimeter testing is still commonly used today despite its high cost since it produces accurate results.

The experimental analysis produces the genuine behaviour of a material. On the other hand, numerical analysis is produced using cutting-edge technology because experiments are expensive and have an impact on the environment's sustainability. Additionally, a variety of software is available with various functions and amenities. However, it is necessary to determine a suitable numerical approach and instrument for the simulation. Some of the parameters, such as the mass loss rate (MLR) and the heat release rate (HRR), cannot be derived from certain empirical data (For example, Abaqus and Ansys). To accurately replicate real fire, fire simulation is done using specialized Computational Fluid Dynamics (CFD) software, such as FireFOAM, COMSOL Multiphysics, XFLOW, PyroSim, and FDS. Therefore, many researchers [9, 12, 13, 33] employ the Fire Dynamic Simulator (FDS) to simulate the fire behaviour of building materials and elements.

Direct numerical simulation (DNS), Reynolds Averaged Navier–Stokes (RANS) equation simulation, and Large Eddy Simulation (LES) using Computer Fluid Dynamic (CFD) software are the three different ways that turbulent flow numerical analysis can be performed. Direct numerical simulation (DNS), Large Eddy Simulation (LES), Very Large Eddy Simulation (VLES), and Simple Very Large Eddy Simulation (SVLES) are the four different methods of simulation in FDS/Pyrosim [19, 20]. DNS method will give more accurate results and high computational resources are needed because DNS needs a very finer mesh to resolve the flow eddies. As a result, researchers employ LES to obtain a reliable solution promptly with the appropriate grid sizes. The grid resolution should be assessed before the CFD simulation. If the size of the fire is prescribed, the firing diameter is used as a tool to identify the grid size [29]. Otherwise, the resolved turbulent kinetic energy must be examined to determine the appropriate simulation grid size [18]. All CFD simulation types, including wind, fluid, and fire simulations, can be evaluated for LES quality using the energy resolution technique.

3 Numerical Analysis for the Fire Performance

LES in Pyrosim software was used to simulate and test the fire performance of polybutylene terephthalate with glass fibre (PBT-GF) composite materials. Solid phase reactions and gas phase reactions are the two categories into which thermal reactions of material degradation under fire loadings can be analysed. The software calculated the loss of mass over time while considering both reactions. For the PBT material, the experimental results of the cone calorimeter test were used to confirm the numerical model [19, 20]. Tables 1 and 2 present the PBT polymer material and PBT-GF composite material properties respectively. Following a domain convergence test, a 300 mm × 300 mm × 500 mm domain size was chosen to cover the whole fire, and a 10 mm grid size was chosen after determining that the turbulence resolution is greater than 80% (amount of resolved turbulent kinetic energy). The 100 mm × 100 mm specimen was placed with 4 mm PBT and 16 mm of wool insulation material under the cone heater. The heat loading of 50 kW/m^2 was then applied on the top surface of the specimen until it entirely decomposed, and the mass loss rate (MLR) was measured. The developed model for the cone calorimeter test and simulated fire which is developed in Pyrosim software with the domain size and the grid size is shown in Fig. 1.

The numerically developed combustibility test model for PBT composite material was validated with the experimental result. The validated variation of mass loss with time curves is shown in Fig. 2. The mass loss of material can be observed only under thermal loadings in the solid phase reaction. However, the overall mass loss under 50 kW/m^2 heat flux was compared in solid phase reaction for the glass composite material (see Fig. 2). Even though there is a shift in the time axis, it is within an acceptable range for this type of simulation.

Table 1 Properties of polybutylene terephthalate (PBT) polymer material [19]

Properties	Value
Density	1300 kg/m^3
Specific heat	2.23 kJ/kg.K
Conductivity	0.29 W/m.K
Emissivity	0.88
Absorption coefficient	2560 m^{-1}
Preexponential factor	2.49×10^{14} s^{-1}
Activation energy	2.12×10^5 kJ/kmole
Heat of reaction	507 kJ/kg
Heat of combustion	19,500 kJ/kg
Combustion efficiency	1

Table 2 Properties of polybutylene terephthalate with glass fibre (PBT-GF) composite material [19]

Properties	Value
Polymer density	1520 kg/m^3
Polymer specific heat	1.68 kJ/kg.K
Polymer conductivity	0.36 W/m.K
Polymer emissivity	0.87
Polymer absorption coefficient	2860 m^{-1}
Char density	482 kg/m^3
Char specific heat capacity	0.85 kJ/kg.K
Char conductivity	0.07 W/mK
Char emissivity	0.85
Char absorption coefficient	10,000 m^{-1}
Preexponential factor	2.49×10^{14} s^{-1}
Activation energy	2.12×10^5 kJ/kmole
Heat of reaction	355 kJ/kg
Heat of combustion	19,500 kJ/kg
Char yield	0.32
Combustion efficiency	1

However, the solid and gas phase reactions only perform the material's overall fire behaviour, and the cone calorimeter test based on AS 3837 assesses the heat release capacity to assess the range of combustibility [4]. From the validated model, the solid and gas phase reactions are performed and the combustibility behaviour with heat release rate was observed. Figure 3 shows the changes in heat release rate over time for PBT pure polymer material and PBT-GF composite material (70% of PBT with 30% of GF) with the same size and thickness.

The peak heat release rate of PBT pure polymer is higher than PBT-GF composite polymer material because of the high amount of polymer. The PBT material burns

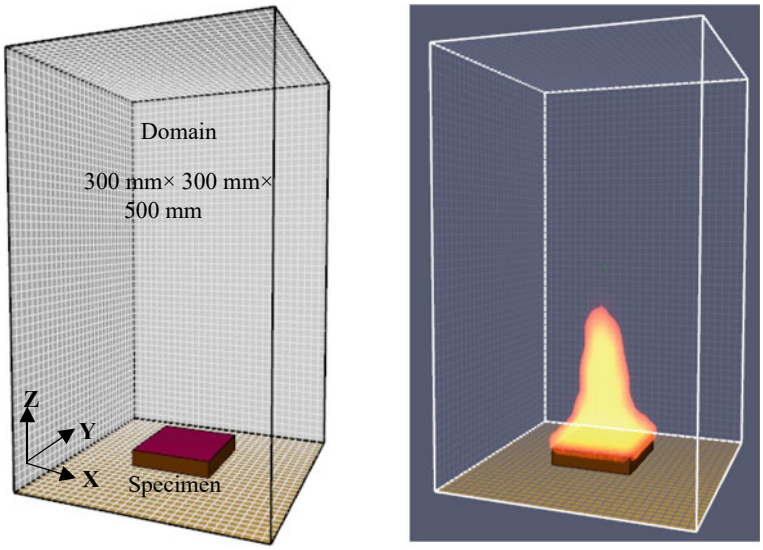

Fig. 1 Developed model for cone calorimeter test and simulated fire in Pyrosim software

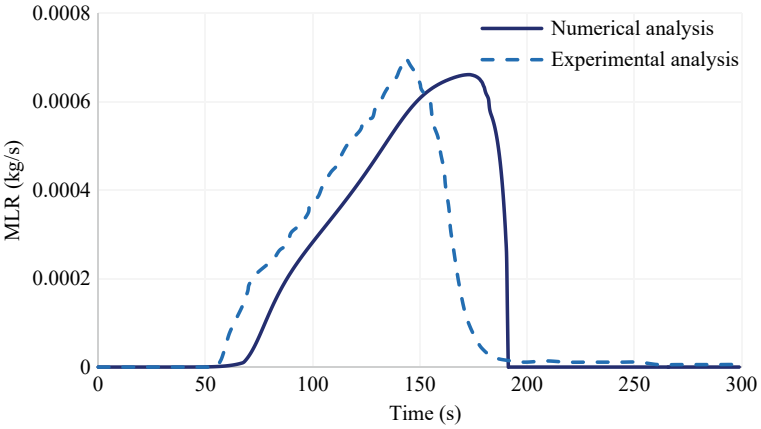

Fig. 2 The comparison of numerical and experimental analysis from the variation of mass loss rate with time for PBT polymer

completely and quickly releases a large quantity of heat; however, PBT-GF material burns more slowly and releases heat at a slower rate. While adding 30% of non-combustible glass material, the fire-related performance of the composite is enhanced by reducing about 50% of the peak heat release rate (PHRR).

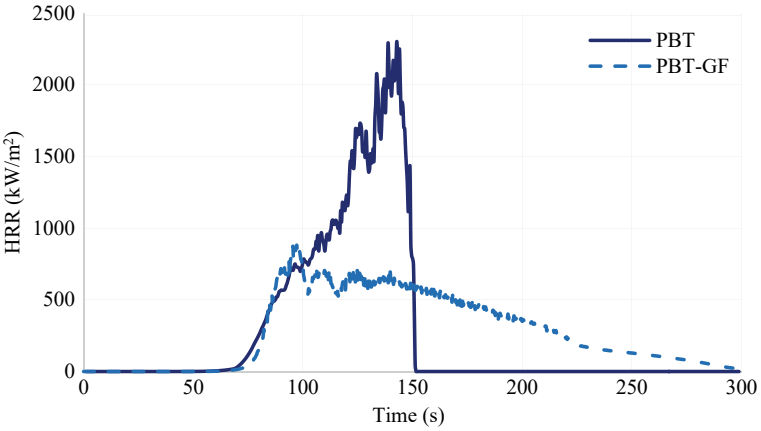

Fig. 3 The variation of Heat release rate (HRR) with time for PBT polymer material and PBT-GF composite material

4 The Fire Performance of Glass Fibre-Reinforced Polymer with Different Proportions of Glass and Polymer

Since polymer materials have a significant impact on the thermal performance of buildings, research is looking into polymer composites to lower the risk of fire and improve thermal performance. By employing less flammable or fewer polymers in composites, the fire behaviour can be improved. In this study, the polymer content of the composite is compared and suggested to increase while taking into account the material's overall suitability for various applications.

The performance of 75% and 70% of PBT polymer with glass fibre is analysed. Figure 4 illustrates the variation of heat release rate (HRR) over time for PBT-GF composite material with varying composite proportions (75% of PBT polymer with 25% glass fibre (75%PBT-25%GF) and 70% of PBT polymer and 30% of glass fibre (70%PBT-30%GF)). The 100 mm × 100 mm PBT-GF specimen with 5.6 mm is modelled for cone calorimeter simulation to compare the combustible behaviour while applying 51.5 kW/m^2 uniform heat flux [30]. The improvement in the fire performance from the increment in the amount of glass is observed based on the experimental result for 75% PBT-25%GF, and numerical results of 70% PBT-30% GF. Due to the char that forms during the decomposition, two peaks can be seen in the variation of the heat release rate of PBT-GF material. Additionally, when the amount of polymer is reduced by 5%, the overall heat release rate is not drastically reduced. But the second peak of the heat release rate is reduced. However, the glass in the composite material largely decreases the combustibility of the material.

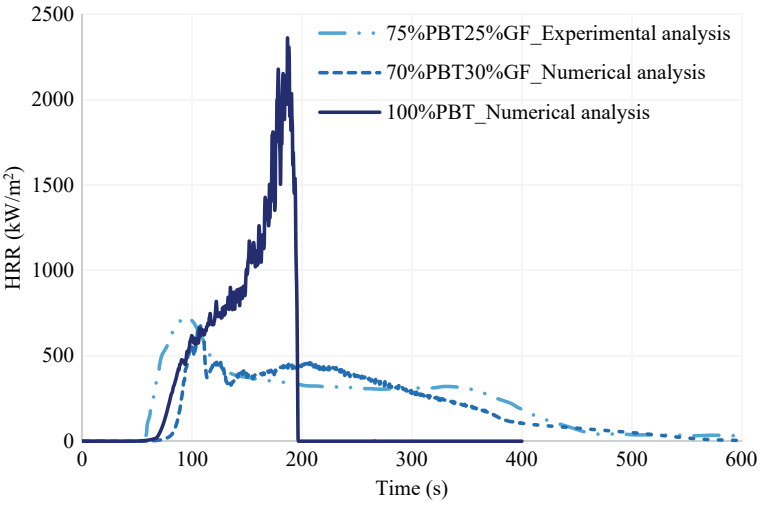

Fig. 4 The variation of heat release rate (HRR) with time for different proportions of PBT-GF composite material

5 Conclusion

In this study, the use of environmentally friendly materials is highlighted while showing the possibility of improving the fire performance of polymer composite building materials using recycled glass. Using large eddy CFD simulation, nonlinear turbulent analysis of polymer composites representing the cladding materials were conducted. The effects of pure polymers and composite polymers were examined, and the enhancements to the material's thermal and mechanical performance were discussed.

The followings are drawn as the main findings of the study:

- The addition of recycled glass to polymer composite materials reduces thermal risk while providing the building application with a sustainable alternative material to the construction industry.
- When 30% of the non-combustible glass fibre material is added, the combustibility of pure PBT polymer, which has a more ductile behaviour and high combustibility, is reduced by 50%. If the main focus is fire performance, it would be better to decrease the polymer amount by less than 50%. This will be a great achievement in the improvement of the fire performance of polymer composite material.
- Even though there is no greater difference in the total heat release rate with the addition of 25% of GF and 30% of GF with polymer in composite material, it is observed that the second peak heat release rate reduced with the increment of the amount of glass. In addition, the amount of glass materials needs to be further increased (between 30% to 70%) while considering the mechanical performance of the composite material.

- As a general conclusion, it can be mentioned that the numerical tool for predicting the fire performance will reduce the negative impacts of the experimental analysis of fire. This is because the experimental fire tests release a large volume of toxic gases that pollute the environment.

Acknowledgements This research work is funded by Cooperative Research Centre Project about Commonwealth Grant CRCPX000061. The authors also gratefully acknowledge the financial and in-kind support from Livefield Ltd. and RMIT University.

References

1. Abukhettala M (2016) Use of recycled materials in road construction. In: International conference on civil, structural and transportation engineering, pp 1–8. https://doi.org/10.14311/bit.2021.01.06
2. Akinyele JO, Igba UT, Ayorinde TO, Jimoh PO (2020) Structural effi-ciency of burnt clay bricks containing waste crushed glass and poly-propylene granules. Case Stud Constr Mater 13:e00404. https://doi.org/10.1016/j.cscm.2020.e00404
3. Andreola F, Barbieri L, Corradi A, Lancellotti I, Falcone R, Hreglich S (2005) Glass-ceramics obtained by the recycling of end of life cath-ode ray tubes glasses. Waste Manag 25:183–189. https://doi.org/10.1016/j.wasman.2004.12.007
4. A Standards Australia/New Zealand (2008) AS-NZS_3837-1998 Method of test for heat and smoke release rate for materials and products using an oxy-gen consumption calorimeter
5. Avila MB, Dempsey NA, Dore C (2008) Effect of resin type and glass content on the reaction to fire characteristics of typical FRP composites. Compos Part A: Appl Sci Manuf 39(9):1503–1511. https://doi.org/10.1016/j.compositesa.2008.05.012
6. Brown JR, Mathys Z (1997) Reinforcement and matrix effects on the combustion properties of glass reinforced polymer composites. Compos Part A: Appl Sci Manufac-Turing 28(7):675–681. https://doi.org/10.1016/S1359-835X(97)00018-3
7. Carpenter K, Janssens M, Antonio S (2005) Using heat release rate to assess combustibility of building products in the cone calorimeter. Fire Technol, 79–92.https://doi.org/10.1007/s10694-005-6390-z
8. Chen Z, Wen J, Xu B, Dembele S (2014) Extension of the eddy dissipation concept and smoke point soot model to the les frame for fire simulations. Fire Saf J 64:12–26. https://doi.org/10.1016/j.firesaf.2014.01.001
9. Dréan V, Girardin B, Guillaume E, Fateh T (2019) Numerical simulation of the fire behaviour of facade equipped with aluminium composite material-based claddings-model validation at large scale. Fire Mater 43(8):981–1002. https://doi.org/10.1002/fam.2759
10. Elaqra H, Rustom R (2018) Effect of using glass powder as cement re-placement on rheological and mechanical properties of cement paste. Constr Build Mater 179:326–335. https://doi.org/10.1016/j.conbuildmat.2018.05.263
11. Flores N, Garcia R, Hajirasouliha I, Pilakoutas K, Guadagnini M (2018) Composites with recycled rubber aggregates: properties and oppor-tunities in construction. Constr Build Mater 188:884–897. https://doi.org/10.1016/j.conbuildmat.2018.08.069
12. Guillaume E, Dréan V, Girardin B, Koohkan M, Fateh T (2020) Re-construction of grenfell tower fire. Part 2: a numerical investigation of the fire propagation and behaviour from the initial apartment to the façade. Fire Mater 44(1):15–34. https://doi.org/10.1002/fam.2765
13. Hostikka S, Bytskov G (2016) Numerical simulations of the ISO 13785-2 façade fire tests. In: MATEC web of conferences, vol 46, pp 1–11.https://doi.org/10.1051/matecconf/20164603003
14. Huda SB, Alam MS (2014) Mechanical behavior of three generations of 100% repeated recycled coarse aggregate concrete. Constr Build Mater 65:574–582. https://doi.org/10.1016/j.conbuildmat.2014.05.010

15. Lamba P, Kaur DP, Raj S, Sorout J (2021) Recycling/reuse of plastic waste as construction material for sustainable development: a review. Environ Sci Pollut Res. https://doi.org/10.1007/s11356-021-16980-y
16. Li YZ, Huang C, Anderson J, Svensson R (2017) Verification, validation and evaluation of FireFOAM as a tool for performance design. BRANDFORSK 2017:2 Report 3208 ISSN: 1402-3504
17. Lye CQ, Dhir RK, Ghataora GS (2017) Deformation of concrete made with crushed recycled glass cullet fine aggregate. Proc Inst Civ Eng Struct Build 170(5):321–335. https://doi.org/10.1680/jstbu.16.00157
18. McDermott R, Randall J, Forney GP, McGrattan K, Mell WE (2010) Fire dynamics simulator version 6: complex geometry, embedded meshes, and quality assessment. In: V European conference on compu-tational fluid dynamics: ECCOMAS CFD, pp 14–17
19. McGrattan K, Hostikka S, Floyd J, McDermott R, Vanella M (2021) Sixth edition fire dynamics simulator technical reference guide volume 3: validation
20. McGrattan K, McDermott R, Vanella M, Hostikka S, Floyd J (2021) Sixth edition fire dynamics simulator user's guide (FDS)
21. Milovanovic B, Stirmer N, Milicevic I (2012) The sustainable prefabricated wall panel system, no 1, pp 1–8
22. Mistri A, Bhattacharyya SK, Dhami N, Mukherjee A, Barai SV (2020) A review on different treatment methods for enhancing the properties of recycled aggregates for sustainable construction materials. Constr Build Mater 233:117894. https://doi.org/10.1016/j.conbuildmat.2019.117894
23. Mohajeran A, Vajna J, Ho T, Cheung H, Kurmus H, Arulrajah A (2017) Practical recycling applications of crushed waste glass in construction materials: a review. Constr Build Mater 156:443–467. https://doi.org/10.1016/j.conbuildmat.2017.09.005
24. Mohan HT, Jayanarayanan K, Mini KM (2020) Recent trends in utilization of plastics waste composites as construction materials. Constr Build Mater, 121520.https://doi.org/10.1016/j.conbuildmat.2020.121520
25. Morgan AB, Gagliardi NA, Price WA, Galaska ML (2009) Cone calorimeter testing of S2 glass reinforced polymer composites. Fire Mater 33:323–344. https://doi.org/10.1002/fam
26. Papadogianni V, Romeos A, Giannadakis A, Perrakis K, Panidis T (2020) Cone calorimeter and thermogravimetric analysis of glass phenolic composites used in aircraft applications. Fire Technol 56. https://doi.org/10.1007/s10694-019-00928-3
27. Rivera JF, Zuleny IC, Nathalie V, Ruby M (2018) Novel use of waste glass powder: production of geopolymeric tiles. Adv Powder Technol 29(12):3448–3454. https://doi.org/10.1016/j.apt.2018.09.023
28. Shi L, Chew MYL (2013) Fire behaviors of polymers under autoignition conditions in a cone calorimeter. Fire Saf J 61:243–253. https://doi.org/10.1016/j.firesaf.2013.09.021
29. Stewart JR, Herodotos NP, Gordon EA, Alan DB (2021) Evaluation of CFD simulations of transient pool fire burning rates. J Loss Prev Process Ind 71:104495. https://doi.org/10.1016/j.jlp.2021.104495
30. Tilles JL (2017) Quantification of flame heat feedback in cone calorimetry tests. Master's thesis. The University of Maryland
31. Tsai K (2009) Orientation effect on cone calorimeter test results to assess fire hazard of materials. J Hazard Mater 172:763–772. https://doi.org/10.1016/j.jhazmat.2009.07.061
32. White N, Delichatsios M (2015) Fire hazards of exterior wall assemblies containing combustible components. SpringerBriefs in Fire
33. Yasemin A, Doğan M, Bayramlı E (2016) The effect of red phosphorus on the fire properties of intumescent pine wood flour–LDPE composites Yasemin. Fire Mater 40:697–703. https://doi.org/10.1002/fam
34. Zhang W, Hamer A, Klassen M, Carpenter D, Roby R (2002) Turbulence statistics in a fire room model by large eddy simulation. Fire Saf J 37(8):721–752. https://doi.org/10.1016/S0379-7112(02)00030-9

Fragility Prediction for Earthquake-Induced Embankment Failures Through Empirical Methods

S. U. Sathya, M. Mahmoodian, C. S. Bandara, N. Naderpajouh, and P. B. R. Dissanayake

Abstract In this paper, a time-conserving fragility curve formulation methodology for extreme events is discussed. Uncertainty is a parameter that has a significant effect on the probabilistic estimations of infrastructure failures. Structural damages to civil infrastructure range from minor defects to collapse relative to serviceability or restoration measures. In this paper, earthquake-induced landslides are used as a sample case study, to study empirical methods of fragility curve formulation. Method of maximum likelihood and best-fit regression methods are applied to an extreme event, and fragility curves are derived. Monte Carlo stimulation is applied to analyse the behaviour of uncertainty parameter concerning standard sections of highway and railway embankments. Finally, the coefficient of determination was calculated to illustrate the correlation between developed curves and data points. The proposed method suggests an optimum method to quantify the failure probability from an available data sample or a real incident-based data sample, which is computationally very effective. Improvement in vulnerability estimations provides high maintenance and efficient restoration schemes for transportation networks which are prone to extreme events such as landslides.

Keywords Fragility curves · Earthquake-induced landslides · Maximum likelihood · Monte Carlo

S. U. Sathya (✉) · C. S. Bandara · P. B. R. Dissanayake
Faculty of Engineering, Department of Civil Engineering, University of Peradeniya, Peradeniya, Sri Lanka
e-mail: sathya.sathyaras@eng.pdn.ac.lk

S. U. Sathya · M. Mahmoodian
School of Engineering, RMIT University, Melbourne 3001, Australia

N. Naderpajouh
The University of Sydney, Camperdown, NSW 2006, Australia

© The Author(s), under exclusive license to Springer Nature Singapore Pte Ltd. 2023

R. Dissanayake et al. (eds.), *ICSBE 2022*, Lecture Notes in Civil Engineering 362,
https://doi.org/10.1007/978-981-99-3471-3_37

1 Introduction

Seismic events, volcanoes, and heavy rainfall are some natural causes that trigger slope or embankment failure. Any event with a massive magnitude could have a considerable effect on human lives, the serviceability of transport infrastructure, and the economy of a country. In recent years, the interest of communities in recognition of the corresponding vulnerability of infrastructures and networks has been increased. If a landslide is the secondary effect of an earthquake, it could contribute to a higher level of damage to structures, compared to the individual hazard. The Wenchuan earthquake is such a seismic event of magnitude 8.0, which triggered many landslides and directly damaged many bridges interrupting the transportation network [16].

Hazard risk zoning and quantification of landslide susceptibility have shown a substantial improvement in recent research [13, 45]. Landslide monitoring systems have improved from conventional site instruments like GPS and levelling to satellite and aerial imaginary investigation, and remote sensing applications [11]. However, the causes for the instabilities in embankments of road and rail networks, which were built decades ago, include high slope angles than the currently practised design standards, poor drainage and maintenance systems, anthropogenic activities, etc. [19, 40]. But the infrastructure managers prefer to have a comprehensive methodology to assess and minimize the vulnerability of an asset not only related to frequent events, but also extreme events. Fragility curves that distribute the failure probability of an extreme event concerning various damage states is a model frequently applied in seismic-related scenarios. The advancement of vulnerability data in the form of fragility curves is a widely appropriate approach when the documentation should account for a wide range of uncertain sources: hazard intensity, structural properties, soil properties, and operational state [10]. The threshold for initiation of damages for earthquake-induced landslides is defined by Argyroudis and Kaynia [4], in terms of permanent vertical ground displacement.

Analytical models are often used in fragility curve formulations with techniques like multiple stripe analysis [36], incremental dynamic analysis (IDA) [39, 42], response surface method [22, 26], uniform design method [28], etc. This research proposes a failure distribution model with sufficient accuracy for seismic landslides and methodology that could be applied in fragility curves formulation through data based on real incidents rather than analytical models which require high computational effort. The article presents statistical procedures for developing fragility curves under the assumption that they can be represented using two-parameter log-normal distribution functions. These procedures are subjected to the coefficient of determination test, and deviations are projected.

2 Overview of Fragility Curves

The main aim of fragility analysis is to quantify the probability of potential damage to a structure at a given intensity measure to a hazard. The data for fragility curves have several origins: Past incident data, experimental data, analytical analysis data, expert judgement, and hybrid data. The method of formulation of the fragility function also varies according to the nature of the data. ATC [7] is mainly a collection of earthquake damage evaluation data from expert surveys and past incidents and is used in fragility curve formation for HAZUS [12]. Unlike other methods, the user has more control over the results in the case of analytical data sets because the number of analyses performed at each threshold can be constrained [8]. However, vulnerability projections for many weather extremes are still performed using empirical formulations [2, 41]. The failure probability of engineering structures can be demonstrated using a lognormal cumulative probability density function, as shown below [35, 38],

$$P(C|\mathrm{IM} = x) = \varnothing\left(\frac{\ln\left(\frac{x}{\vartheta}\right)}{\beta}\right) \tag{1}$$

where $P(C|\mathrm{IM} = x)$ is the probability that an Intensity measure with $\mathrm{IM} = x$ will cause the structure to reach a limit state, $\Phi(\cdot)$ is the standard normal cumulative distribution function (CDF), ϑ is the median of the fragility function, and β is the standard deviation of ln IM. Equation 1 signifies that the IM values that cause a structure to collapse are lognormally dispersed; this is a general assumption that has been acknowledged as satisfactory across many cases [20, 37]. But there are cases where normal [18, 19], gamma [9], and beta [28] distributions are also applied. In this study, the authors discuss possible fragility curve developing methods for extreme events, concerning the mode of data collection.

The arithmetic simplicity through which two-parameter lognormal distribution functions connect actual structural strength, capacity, or resistance to design demand or load encouraged their application. Capacity is typically considered in several safety factors, each associated with a specific source of uncertainty. A fragility curve's shape describes the uncertainty in failure using probabilistic estimation. For situations with nearly zero uncertainty in capacity or demand, the fragility curve will take the form of a step function, as shown in Fig. 1a. Because failure states involve uncertainty, the fragility curves take the shape of an S curve, implying that a tendency to failure can be observed over a certain range of demand. Figure 1b, c depicts the behaviour of the fragility curve with variations in the median and standard deviation.

2.1 Definition of Damage States

The damage states can be defined quantitatively, qualitatively, or through both [25]. HAZUS-MH MR3 categorizes damage states into five damages states with

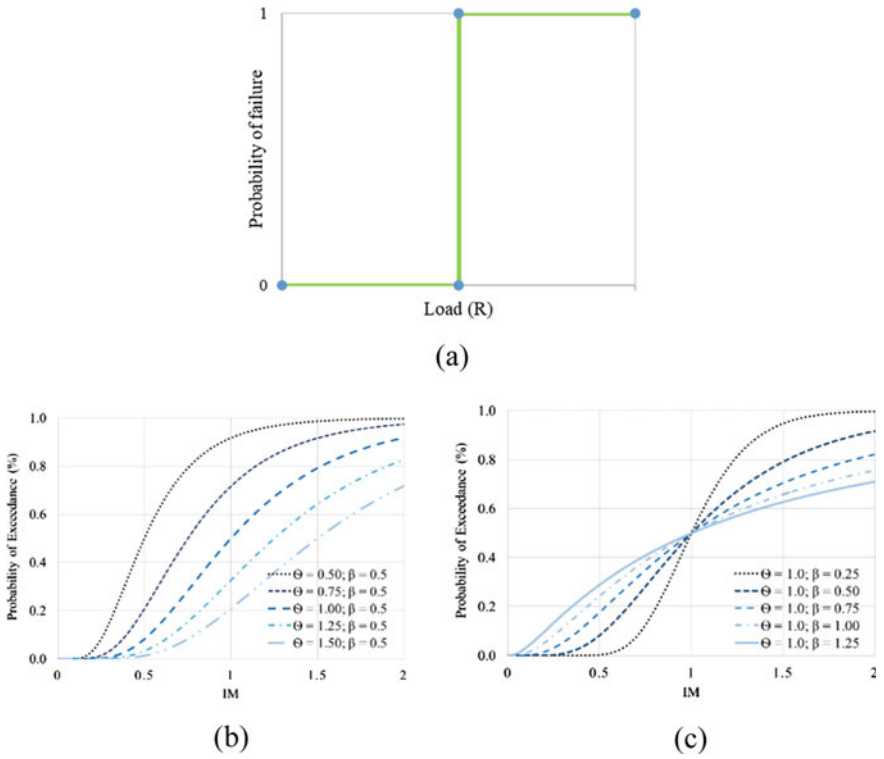

Fig. 1 Conceptual behaviour of fragility curve with median and standard deviation

four limitations; minor, moderate, extensive, and collapse [12]. For highway and railway embankments, damage states are defined using permanent vertical ground displacement as the damage parameter [4]. Table 1 provides the damage states of the embankment with the limits of serviceability.

2.2 Methods of Fragility Curve Parameters Estimation

2.2.1 Incremental Dynamic Analysis

This process requires a data set, scaling each event until it causes failure of the structure or the asset [38]. The fraction of events that fail at a level lower than x can be used to estimate the probability of failure at the given intensity measure level. Applying data to the given equations in Table 2 yields a plot that represents fragility, and it is interesting to note that the mean of lognormal IM is equal to the median, ϑ of the IM lognormally distributed data set. Other than recognizing this method as IDA, the Method of Moments (MM) or method A of Porter et al. [27] is used to refer

Table 1 Damage states with the limit states and level of serviceability [4]

Typology	Damage state	Peak ground displacement (m)			Serviceability
		Minimum	Maximum	Median	
Highway	Slight	0.02	0.08	0.05	Active, reduced speeds or trip delay
	Moderate	0.08	0.22	0.15	Inactive or partially closed during repair works
	Extreme/complete	0.22	0.58	0.4	Inactive during reconstruction works
Railway	Slight	0.01	0.05	0.03	Active, reduced speeds or train delay
	Moderate	0.05	0.1	0.08	Inactive during repair works
	Extreme/complete	0.1	0.3	0.2	Inactive during reconstruction works

to this procedure. Truncated incremental dynamic analysis is adhered to develop analytical fragility curves where some incidents are required to scale to large IM values to produce collapse. In cases where running analyses are computationally expensive to observe a failure and exceedance probability up to a certain maximum IM is known, this method can be utilized [8]. In the case of developing fragility curves for historical incidents, Maximum Likelihood Estimates can be derived, after identifying the distribution of the data set [3].

2.2.2 Multiple Stripe Analysis

Apart from Incremental dynamic analysis, by scaling a set of ground motions in seismic analysis at discrete multiple IM levels, multiple stripe analysis can be applied for the formulation of fragility curves [24]. To obtain sufficient accuracy through multiple stripe analysis, [33] recommended using 20 ground motions. However, Ground motions need to be selected covering the entire range of fragility curves, and the typical number of responses used needs to be ranged between 14 and 200 [24]. This method of fitting the fragility curve is also denoted as a method of maximum likelihood since the parameters are estimated by maximizing the logarithm of the likelihood [8, 35]. An unbiased, consistent, and sufficient estimate for the distribution is found assuming that observation of exceeding the limit or not exceeding the limit state at ground motion is independent of the observations from other ground motions. The probability of observing z_j failures out of n_j ground motions with IM $= x_j$ applying binomial distribution is provided in Table 2. Multiple stripe analysis requires incidents of the same intensity measure to apply binomial distribution. Due to the scarcity of highly intense historical events, IDA is used to develop fragility function with a maximum likelihood estimate [3, 15].

Table 2 Equations for deriving the median and standard deviation of the fragility curve

Method	Introduced by	Equations	Applications
Incremental dynamic analysis	Ang and Tang [3]	$\widehat{\vartheta} = \exp\left(\frac{1}{n}\sum_{i=1}^{n} lnIM_i\right), \widehat{\beta} = \sqrt{\frac{1}{n-1}\sum_{i=1}^{n}\left(ln\left(\frac{IM_i}{\vartheta}\right)\right)^2}$	Analytical data [8] Real data [40]
Multiple stripe analysis	Vamvatsikos and Cornell [38]	$\left\{\widehat{\vartheta}, \widehat{\beta}\right\} = \underset{\vartheta,\beta}{\text{argmax}} \sum_{j=1}^{m}\left\{ln\binom{n_j}{z_j} + z_j ln\varnothing\left(\frac{ln\left(\frac{x_j}{\vartheta}\right)}{\beta}\right) + (n_j - z_j) ln\left(1 - \varnothing\left(\frac{ln\left(\frac{x_j}{\vartheta}\right)}{\beta}\right)\right)\right\}$	
			Analytical data [8, 24, 35]

Where $\widehat{\vartheta}$ = Maximum likelihood estimate of mean

$\widehat{\beta}$ = Maximum likelihood estimate of standard deviation

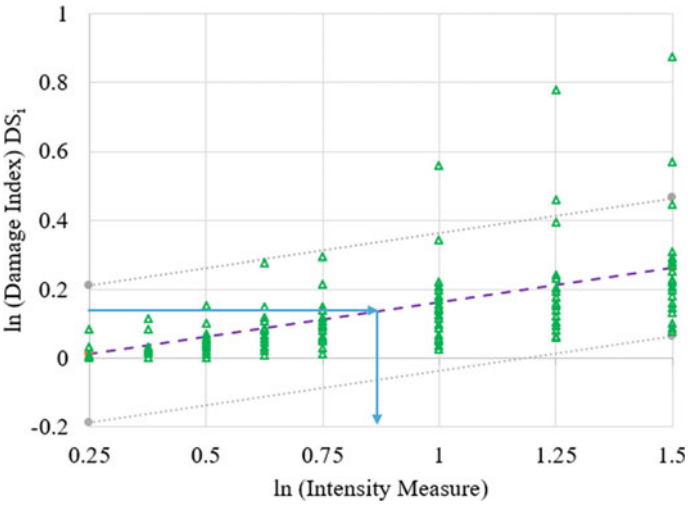

Fig. 2 Representation of evaluation of damage with an IM for a damage state, i (DS_i)

2.2.3 Through Regression

There are numerous ways of developing an equation to represent the relationship between the intensity measure and the engineering damage parameter (Fig. 2). Widely used methods are linear regression, power regression [30], and exponential and polynomial functions. To prevent the intersection of different fragility functions generated for various asset damage states, the curves are given a fixed uncertainty of 0.9 for soil type C and 0.8 for soil type D [4]. Since the intersections in fragility curves misrepresent the probabilistic representation of curves, most of the studies use constant values for standard deviation.

FEMA [12] recommended a single dispersion value of 0.6 for all ground shaking damages to avoid the intersection of any two fragility curves across damage states and multi-hazard cases. Because all fragility curves use the same standard deviation value, the median values of these curves can be compared. Lower median values indicate greater seismic vulnerability [43]. In the first two methods, the standard deviation is produced from the equations, but when following the regression method, a separate method needs to be followed to calculate the standard deviation parameter.

2.3 Methods of Standard Deviation Parameter Estimation

Generally, in analytical fragility curves, for a precise estimation of the standard deviation parameter, different approaches are followed. As explained in Sect. 2 introduction, the lesser the uncertainty would be, the higher will be the accuracy

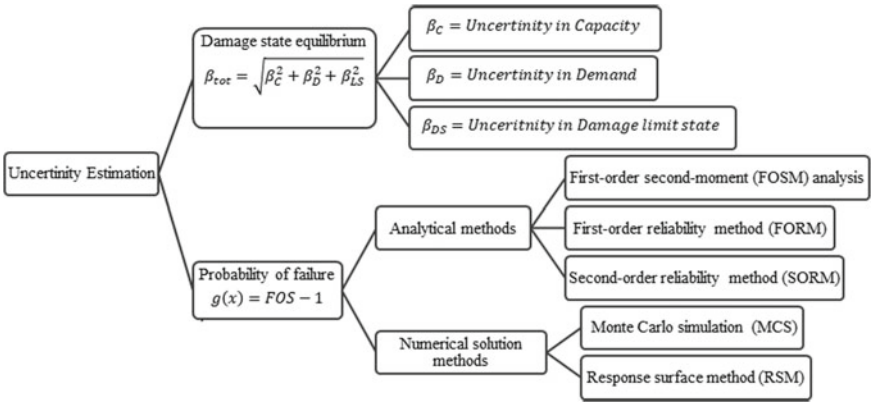

Fig. 3 Methods used in uncertainty estimation in literature

of the fragility curve. For fragility estimated with binary damage states the probability of failure method is highly adopted, while for assets with multi-damage states, the damage state equilibrium path is chosen. Time-dependent probabilistic methods or stochastic processes are available to carry out uncertainty predictions related to degradation [17]. However, this study is focused on unexpected and time-independent extreme events. The reliability method [1] is applied for data with normal distributions, and Monte Carlo stimulations would be an appropriate option for complex distributions with several variables [41]. Response surface spectrum is used to overcome the challenges faced in excessive computational work required in Monte Carlo stimulation. Figure 3 categorizes the uncertainty or randomness parameter estimation approaches available in the literature [32, 40] and Table 3 provides some constant values used in seismic-related fragility estimation for several assets.

2.4 Limit State Function

The mechanism of slope failure is connected to probabilistic studies through a limit state function. It is also referred to as performance function g(x), which defines the failure probability between the capacity (C) of a slope and the demand (D) that external load requires as in Eq. (2). This factor of safety (FOS) defined in Eq. (3) varies with the cause of failure: rainfall-induced, earthquake-induced, or slope stability [19]. According to the scope of this study, FOS function is related to the earthquake-induced slope failure. Newmark's sliding block analysis is an accepted approach to estimate the deformation in a slope or embankment during a seismic loading [23]. Over the years modified and simplified models of Newmark's sliding block analysis were developed through different research. A scaler model developed by Saygili and Rathje [29], with parameters related to slope and soil, is presented in Eq. (4),

Table 3 The parameter estimation for standard deviation

Parameter	Estimation of standard deviation	References
β_{tot}	0.60 (Ground shaking damage algorithm) 0.20 (Ground failure damage algorithm)	FEMA [12], Yilmaz et al. [43]
	0.36	Zhang et al. [44]
β_C	0.35 (Bridge piers-Underground shaking)	Argyroudis et al. [6], Argyroudis and Mitoulis [5]
	0.3–0.35 (Tunnels and bridges) 0.37 (Soil)	McKenna et al. [20]
β_D	0.5 (Bridges and related damage states)	Banerjee and Ganesh Prasad [9], FEMA [12]
	0.5 (Seismic demand)	Argyroudis et al. [6], McKenna et al. [20]
β_{LS}	0.35 (Piers) 0.20 (Bearings) 0.47 (Abutments) 0.40 (Buildings)	Argyroudis et al. [6], Argyroudis and Mitoulis [5]
	0.25 (Engineering judgement and for transport assets)	McKenna et al. [20]

$$g(x) = (C - D)\begin{cases} > 0, \text{ safe state} \\ = 0, \text{ limit state} \\ < 0, \text{ failure state} \end{cases} \tag{2}$$

$$g(x) = \text{FOS} - 1 \tag{3}$$

$$\text{FOS} = \frac{c'}{\gamma \cdot t \cdot \sin\alpha} + \frac{\tan\varphi'}{\tan\alpha} - \frac{\gamma_w \cdot m \cdot \tan\varphi'}{\gamma \cdot \tan\alpha} \tag{4}$$

where α, slope angle; c', effective cohesion; φ', effective friction angle; t, normal thickness of slope failure surface; m, saturated failure thickness as a percentage; γ, unit weight of soil; and γ_w = unit weight of water.

3 Case Study

Two data sets from analytical studies were extracted to develop fragility curves from empirical methods. Data set A collected from the research work of Hübner and Mahler [14] was based on a highway embankment, while data set B, collected from Argyroudis and Kaynia [4], was based on a railway embankment. Data set A was received through a seismic analysis carried out on a finite element software, PLAXIS 2D, and displacement of an embankment was studied during a seismic event from a nonlinear 2D ground responsive analysis. Similarly, data set B was based on the

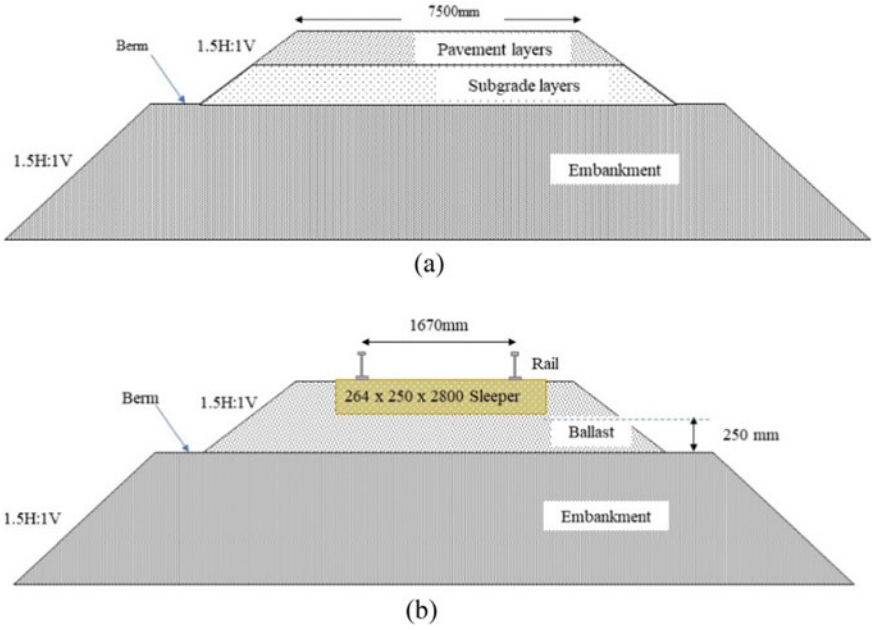

Fig. 4 Schematic figures of **a** highway and **b** railway embankments

analysis, which was performed with the 2D plane strain FE code PLAXIS. The data sets were treated with two methodologies used to develop empirical fragility curves.

3.1 Parametric Study

The schematic diagram of the selected highway embankment and railway embankment [31] with soil and shape parameters are given in Fig. 4 and Table 4, respectively. The material properties and slope stability of the embankment section are mainly considered when performing the uncertainty analysis.

3.2 Data Categorization

The selected data sets were categorized according to their permanent ground displacement in Fig. 5. Since there were very few data points available for complete damage state or damage exceeding limits of 0.58 m for highways and 0.3 m for railways, damage states: minor, moderate, and extreme were considered for fragility curve development.

Table 4 Soil parameters and shape parameters of the embankment

Parameter	Symbol	μ	σ	Distribution	Reference
A	Slope angle (°)	33.7	3.3	Normal	RTRI, (Railway Technical Research Institute) [31], Martinovic et al. [19], Xia et al. [41]
c'	Effective cohesion (kPa)	13	2.6	Normal	Hübner and Mahler [14], Martinovic et al. [19]
ϕ'	Effective friction angle (°)	20	2	Normal	Martinovic et al. [19]
T	Slope normal thickness of failure surface (m)	3	1	Normal	Rathje and Saygili [29]
m	Percentage of failure thickness that is saturated (%)	0	–	–	Rathje and Saygili [29]
γ	Unit weight of soil (kN/m^3)	18	1	Normal	Shinoda et al. [34]
γ_w	Unit weight of water (kN/m^3)	9.81	0.1	Normal	Xia et al. [41]

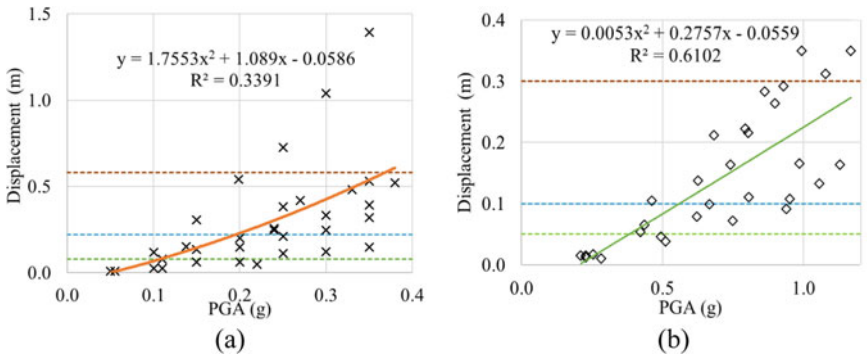

Fig. 5 **a** Data from highway embankment [14] and **b** Data from a railway embankment [4]

3.3 Maximum Likelihood Estimates

The method of maximum likelihood was applied to the categorized data to develop the fragility curves from the provided equations in Sect. 2.2.1. The two parameters relevant to curves are provided in Table 5, with plotted fragility curves in Fig. 6. Through stimulations carried out in Minitab software for the identification of individual distribution, it was estimated that the data samples fit the lognormal distribution [21].

Table 5 Derived maximum likelihood estimates for fragility function

Type	Highway embankment		Railway embankment	
Parameter	σ (g)	β	σ (g)	β
Minor	0.149	0.350	0.296	0.374
Moderate	0.190	0.422	0.614	0.312
Extreme	0.277	0.265	0.818	0.231

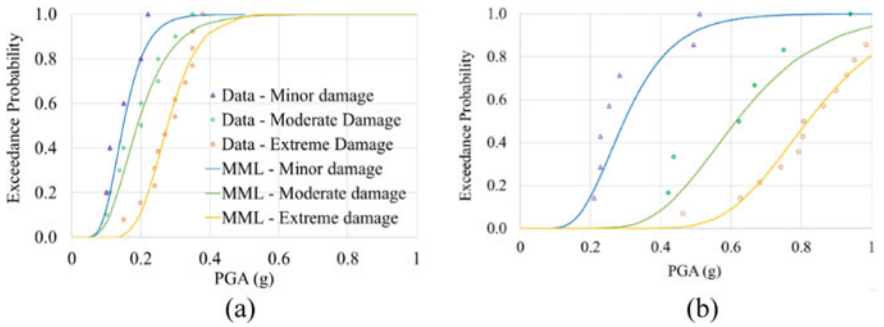

Fig. 6 Earthquake-induced **a** highway embankment and **b** railway embankment failure fragility curves derived from MML

3.4 Best-Fit Regression

The coefficient of determination, R^2, is a metric that indicates the goodness of fit of a model. From the selected data sets by calculating R^2 for each method: linear, exponential, power, and second-order polynomial, a regression equation was selected to calculate the median PGA of each damage state. In this method, to calculate the standard deviation emphasizing the features of the embankment, Monte Carlo simulations were chosen. Table 6 shows the R^2 values for each method and the selected polynomial function. For higher intensity levels, the higher order polynomial regression curves will not exhibit an increasing trend, in such situations, a regression equation with a power function can be chosen as the ideal option [4].

Table 6 Regression and COD through different techniques

Data set	A		B	
Type	Equation	R^2	Equation	R^2
Linear	$y = 1.8559x - 0.127$	0.3367	$y = 0.2827x - 0.0578$	0.6102
Exponential	$y = 0.0186e^{9.7598x}$	0.3038	$y = 0.0104e^{3.137x}$	0.5176
Power	$y = 3.3303x^{1.8637}$	0.3362	$y = 0.2216x^{1.8401}$	0.5943
Second-order polynomial	$y = 1.7553x^2 + 1.089x - 0.0586$	0.3391	$y = 0.0053x^2 + 0.2757x - 0.0559$	0.6102

Table 7 Derived values for two-parameter fragility curves from the regression method

Type	Highway embankment		Railway embankment	
Parameter	σ (g)	β	σ (g)	β
Minor	0.087	0.5	0.310	0.5
Moderate	0.154	0.5	0.488	0.5
Extreme	0.288	0.5	0.912	0.5

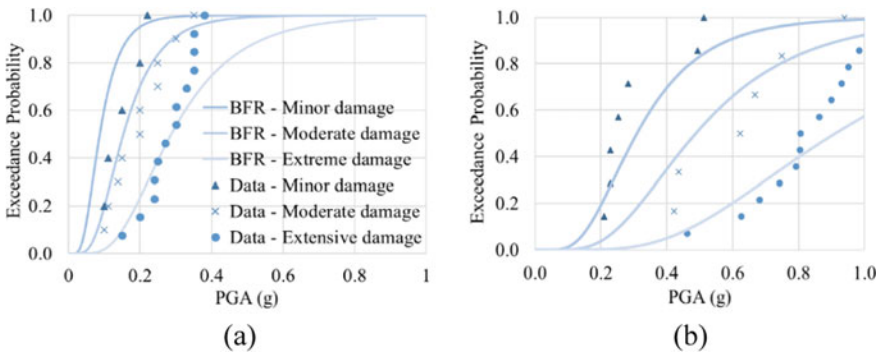

Fig. 7 Fragility curves from BFR **a** highway embankment and **b** railway embankment

3.5 Monte Carlo Stimulation

To estimate the failure probability of a standard embankment, MCS was studied with 1000 stimulations with the parameters given in Table 7 and Fig. 7. The standard deviation of the solution sample was used to calculate the seismic fragility curves of embankment failure as the uncertainty of failure in each damage state. The selected intensity measure for the fragility function is Peak Ground Acceleration and damage states were bound with peak ground displacement.

3.6 Verification for Application

The correlation between developed fragility curves and the data points is studied with the coefficient of determination. The curves developed with maximum likelihood estimates show a higher correlation compared to the curves developed from best-fit regression as represented in Table 8.

Table 8 Comparison of COD values of MML and BFR

Type	Highway embankment		Railway embankment	
Method	MML	BFR	MML	BFR
Minor	0.819	0.167	0.710	0.652
Moderate	0.944	0.869	0.872	0.791
Extreme	0.953	0.770	0.970	0.600

4 Discussion

This study is focused on developing fragility curves from a limited data set, which adopts the properties of real data. The selected data sets were from two major types of embankments: highway and railway embankments. From Table 8, it can be assured that the curves are of sufficient accuracy. For 0.2 g of PGA in the highway fragility curve (Fig. 6a), the exceedance probability of failure for minor, moderate, and extreme damage stages is 0.802, 0.551, and 0.106, respectively. Likewise, for 0.2 g of PGA in the railway fragility curve (Fig. 6b), the given exceedance probability failure for minor, moderate, and extreme stages is 0.148, 0.0, and 0.0, respectively. According to the current data set, it provides evidence for the fact vulnerability of highway to earthquake-induced embankment failures is higher compared to railway embankments. This relationship can be observed in fragility curves formulated through the other methodology as well.

Considering the data sample used in the analysis, the number of data points available varies for different damage states. From data sets of highway and railway for minor damage state, there were 5 and 7 data points, respectively. For the extreme damage state, there were 13 and 14 data points, respectively, for highway and railway embankments. COD values for the curves developed through MML and BFR for minor damage states in highways were 0.819 and 0.167. But the COD values for the extreme state of highways were 0.953 and 0.770, respectively. A reason for higher correlation values could be the reliable data sample, whereas with higher sample size COD values have been increased. Furthermore, Table 8 elaborates that COD values are lesser for the BSR method compared to IDR. So, it's advisable to select the MML for curve formulation if a satisfactory amount of reliable data points are available. Since MML is equipped with a maximization step, increasing the fitness of the curve, it produces curves with higher correlation.

The application of Monte Carlo for the determination of standard deviation also has many advantages. Research has been carried out to develop fragility curves with limited slopes and soil parameters. The ability to consider the uncertainty in several parameters with different types of distribution, with less computational effort, is an added advantage. In the case of the intersection of fragility curves, the exceedance probability of failure could be higher for a lower damage state than a higher damage state. To avoid such situations, a constant value for standard deviation can be used.

This methodology can be applied for fragility curve development with the real incident and limited data. For different cases, to estimate the uncertainty, it requires

to calculate the failure probability, with limiting equilibrium derived with an FOS. Apart from the earthquake-induced embankment or slope failures, for cases like rainfall-induced slope failures, and rock failures, fragility curves can be developed with sufficient accuracy. Fragility curve derivation from regression is of substantial importance in limited data cases, and even for different damage states. Further research can be carried out addressing other standard deviation estimating methods like the response surface method.

5 Conclusion

To accurately predict the probability of failure while considering the effect of the immediate cause, fragility curves provide a logical framework for quantifying the damage to a particular asset and damage state. This paper addresses the weaknesses and strengths of empirical fragility curve formulation methods, using some data collected through analytical means. The curves developed in this paper can be utilized for estimating the probability of failure of earthquake-induced landslides and presents a comprehensive methodology for fragility curve development for different extreme events. Methods of maximum likelihood and best-fit regression were applied to study the behaviour of slope failure and Monte Carlo simulations were used to study the randomness in the soil parameters and material parameters. The damage states can be interpreted as serviceability thresholds and can inform railways or highway authorities, in case of an early earthquake warning to reduce the speeds of vehicles or trains, with respect to the predicted damage probability.

The validation procedure conducted with the coefficient of regression agrees with the fact that, with a higher number of data points, a precise curve could be gained, while to address damage states with few or no data points, regression analysis can be used. This methodology can be used for embankment failures on highways and rail networks and can be further studied for multiple failures on a transportation network at a single extreme event.

Acknowledgements This project has received funding from the European Union's Horizon 2020 research and innovation programme under grant agreement No. 883532.

References

1. Ahamed T, Duan JG, Jo H (2021) Flood-fragility analysis of instream bridges–consideration of flow hydraulics, geotechnical uncertainties, and variable scour depth. Struct Infrastruct Eng 17:1494–1507
2. Akiyama M, Frangopol DM, Arai M, Koshimura S (2013) Reliability of bridges under tsunami hazards: emphasis on the 2011 Tohoku-oki earthquake. Earthq Spectra 29:295–314
3. Ang AHS, Tang WH (1975) Probability concepts in engineering planning and design. Basic principles vol 1. Wiley, New York

4. Argyroudis S, Kaynia AM (2015) Analytical seismic fragility functions for highway and railway embankments and cuts. Earthquake Eng Struct Dynam 44:1863–1879
5. Argyroudis SA, Mitoulis SA (2021) Vulnerability of bridges to individual and multiple hazards-floods and earthquakes. Reliab Eng Syst Saf 210:107564
6. Argyroudis SA, Mitoulis SA, Winter MG, Kaynia AM (2019) Fragility of transport assets exposed to multiple hazards: state-of-the-art review toward infrastructural resilience. Reliab Eng Syst Saf 191:106567
7. ATC-13 (1985) Earthquake damage evaluation data for California. Federal Emergency Management Agency, Washington, DC
8. Baker JW (2015) Efficient analytical fragility function fitting using dynamic structural analysis. Earthq Spectra 31:579–599
9. Banerjee S, Ganesh Prasad G (2013) Seismic risk assessment of reinforced concrete bridges in flood-prone regions. Struct Infrastruct Eng 9:952–968
10. Cho SE (2020) Failure distribution analysis of shallow landslides under rainfall infiltration based on fragility curves. Landslides 17:79–91
11. Del Soldato M, Solari L, Poggi F, Raspini F, Tomás R, Fanti R, Casagli N (2019) Landslide-induced damage probability estimation coupling insar and field survey data by fragility curves. Remote Sens, 11
12. FEMA (2012) Hazus®–MH 2.1 earthquake model-technical manual multi-hazard loss estimation methodology. Federal Emergency Management Agency, Washington, DC
13. Gameiro S, De Oliveira GG, Guasselli LA (2022) The influence of sampling on landslide susceptibility mapping using artificial neural networks. Geocarto Int, 1–23
14. Hübner B, Mahler A (2020) Analysis of seismic fragility functions of highway embankments. Period Polytech Civ Eng 64:1162–1169
15. Kammouh O, Cimellaro GP, Mahin SA (2018) Downtime estimation and analysis of lifelines after an earthquake. Eng Struct 173:393–403
16. Li J, Peng T, Xu Y (2008) Damage investigation of girder bridges under the Wenchuan earthquake and corresponding seismic design recommendations. Earthq Eng Eng Vib 7:337–344
17. Mahmoodian M (2018) Chapter 4-time-dependent reliability analysis. In: Mahmoodian M (ed) Reliability and maintainability of in-service pipelines. Gulf Professional Publishing
18. Manning LJ, Hall JW, Kilsby CG, Glendinning S, Anderson MG (2008) Spatial analysis of the reliability of transport networks subject to rainfall-induced landslides. Hydrol Process 22:3349–3360
19. Martinovic K, Reale C, Gavin K (2017) Fragility curves for rainfall-induced shallow landslides on transport networks. Can Geotech J, 55
20. Mckenna G, Argyroudis SA, Winter MG, Mitoulis SA (2021) Multiple hazard fragility analysis for granular highway embankments: Moisture ingress and scour. Transportation Geotechnics, 26
21. Minitab (2021) LLC. https://www.minitab.com
22. Misra S, Padgett JE (2019) Seismic fragility of railway bridge classes: methods, models, and comparison with the state of the art. J Bridg Eng, 24
23. Newmark NM (1965) Effects of earthquakes on dams and embankment. Géotechnique 15:139–160
24. Oblak A, Kosič M, Da Fonseca A, Logar J (2020) Fragility assessment of traffic embankments exposed to earthquake-induced liquefaction. Appl Sci, 10
25. Padgett J, Desroches R, Nielson B, Yashinsky M, Kwon OS, Burdette N, Tavera E (2008) Bridge damage and repair costs from Hurricane Katrina. J Bridg Eng 13:6–14
26. Park J, Towashiraporn P (2014) Rapid seismic damage assessment of railway bridges using the response-surface statistical model. Struct Saf 47:1–12
27. Porter K, Kennedy R, Bachman R (2007) Creating fragility functions for performance-based earthquake engineering. Earthq Spectra 23(2):471–489
28. Qiu W, Huang G, Zhou H, Xu W (2018) Seismic vulnerability analysis of rock mountain tunnel. Int J Geomech, 18

29. Rathje EM, Saygili G (2009) Probabilistic assessment of earthquake-induced sliding displacements of natural slopes. Bull N Z Soc Earthq Eng
30. Ren J, Song J, Ellingwood BR (2021) Reliability assessment framework of deteriorating reinforced concrete bridges subjected to earthquake and pier scour. Eng Struct 239:112363
31. RTRI (Railway Technical Research Institute) (2007) Design standards for railway structures and commentary (earth structures). Railway Technical Research Institute, Maruzen, Japan (in Japanese)
32. Schultz M, Gouldby B, Simm J, Wibowo JL (2010) Beyond the factor of safety: developing fragility curves to characterize system reliability. Water Resources Infrastructure Program
33. Scozzese F, Tubaldi E, Dall'asta A (2020) Assessment of the effectiveness of Multiple-Stripe Analysis by using a stochastic earthquake input model. Bull Earthq Eng 18:3167–3203
34. Shinoda M, Nakajima S, Watanabe K, Nakamura S, Yoshida I (2020) Practical seismic fragility estimation of unreinforced and reinforced embankments in Japan. Geosynth Int 28:48–64
35. Shinozuka M, Feng MQ, Lee J, Naganuma T (2000) Statistical analysis of fragility curves. J Eng Mech 126(12):1224–1231
36. Tecchio G, Donà M, da Porto F (2016) Seismic fragility curves of as-built single-span masonry arch bridges. Bull Earthq Eng 14:3099–3124
37. Tsubaki R, Bricker JD, Ichii K, Kawahara Y (2016) Development of fragility curves for railway embankment and ballast scour due to overtopping flood flow. Nat Hazard 16:2455–2472
38. Vamvatsikos D, Cornell CA (2002) Incremental dynamic analysis. Earthquake Eng Struct Dynam 31:491–514
39. Wei B, Li C, He X (2018) The applicability of different earthquake intensity measures to the seismic vulnerability of a high-speed railway continuous bridge. Int J Civ Eng 17:981–997
40. Wu XZ (2015) Development of fragility functions for slope instability analysis. Landslides 12:165–175
41. Xia Y, Mahmoodian M, Li C-Q, Zhou A (2017) Stochastic method for predicting risk of slope failure subjected to unsaturated infiltration flow. Int J Geomech, 17
42. Yilmaz MF, Ozakgul K, Caglayan BO (2021) Seismic fragility analysis of multi-span steel truss railway bridges in Turkey. Struct Infrastruct Eng, 1–18
43. Yilmaz T, Banerjee S, Johnson Peggy A (2016) Performance of two real-life california bridges under regional natural hazards. J Bridg Eng 21:04015063
44. Zhang J, Huo Y, Brandenberg SJ, Kashighandi P (2008) Effects of structural characterizations on fragility functions of bridges subject to seismic shaking and lateral spreading. Earthq Eng Eng Vib 7:369–382
45. Zhou X, Wu W, Lin Z, Zhang G, Chen R, Song Y, Wang Z, Lang T, Qin Y, Ou P, Huangfu W, Zhang Y, Xie L, Huang X, Fu X, Li J, Jiang J, Zhang M, Liu Y, Peng S, Shao C, Bai Y, Zhang X, Liu X, Liu W (2021) Zonation of landslide susceptibility in Ruijin, Jiangxi, China. Int J Environ Res Public Health 18:5906

Sustainable Construction

Co-Benefits of Adopting Green Concept for the Sustainable Building Construction in Sri Lanka

M. A. D. D. Mudannayaka and Jeeva Wijesundara

Abstract As the world moves closer to achieving sustainable development, the idea of green building has emerged as one of the most important trends in the construction sector around the world. Buildings that are environmentally friendly use less energy and less water, which saves money while preserving natural resources. As a result of growing interest in the topic on a global scale, the development of environmentally friendly buildings has recently appeared as an emerging trend in Sri Lanka. According to the findings of several studies, the initial expenditure required for the construction of environmentally friendly buildings is considerably more than that of conventional buildings. When adopting a green idea for the construction of buildings, a developing nation like Sri Lanka needs to understand the genuine advantages as well as the difficulties that may arise. Therefore, the purpose of the research was to investigate the co-benefits connected with green buildings for a country like Sri Lanka and then to examine each co-benefit in terms of the amount of time that it may expect to be realized. The primary method for collecting data was a questionnaire survey. The statistical approach of the relative importance index was utilized to analyze the collected information. According to the findings, the development of an environmentally friendly building offers various environmental, economic, and social co-benefits to the owners as well as the users of those built environments. Further, the article discusses the relative levels of the significance of each building element within the context of sustainability, green building barriers, and green building approaches in Sri Lanka. Furthermore, most co-benefits are only attainable in the long run, which takes generally more than two years following the construction of a green building.

Keywords Co-Benefits · Construction industry · Green buildings · Sustainability

M. A. D. D. Mudannayaka (✉) · J. Wijesundara
SLIIT School of Architecture, Malabe, Sri Lanka
e-mail: dulamudannayaka@gmail.com

© The Author(s), under exclusive license to Springer Nature Singapore Pte Ltd. 2023

R. Dissanayake et al. (eds.), *ICSBE 2022*, Lecture Notes in Civil Engineering 362,
https://doi.org/10.1007/978-981-99-3471-3_38

1 Introduction

The field of construction is an enormous business that has a vast impact on nature, the growth of the economy, and the development of society throughout the world. Most governments, organizations, and individuals acknowledge the importance of environmental issues in the advancement of sustainability. According to Ortiz et al. (2007), sustainable development entails improving people's lives, encouraging them to live in a safe and healthy environment while improving current and future generational social, economic, and environmental conditions. According to [1], sustainable structures in the construction industry contribute to long-term growth. Green building is a critical component when it comes to long-term sustainability [5]. According to [17], green buildings utilize essential resources such as energy, materials, water, and land more efficiently than conventional structures, resulting in improved health, comfort, and productivity [17]. Accordingly, green buildings have an impact on the long- Team financial co-benefits of structures [18].

Even though global interest in sustainable practices has grown [1], the concept of green building construction has recently emerged at the forefront of the Sri Lankan construction industry. In the present era, most building constructions are executed with a green concept in mind, and many Sri Lankan green buildings have received certification awards based on the Environmental Classification Systems for green buildings. As a developing nation, the country has several challenges guaranteeing a long-term future. According to the Holcim Foundation for Sustainable Construction, the initial cost of developing a green industrial facility in Thulhiriya was 30% more than the cost of constructing a typical manufacturing plant. At a certain final moment, questions arise as to whether it is co-beneficial to spend even more money on the construction of green buildings.

The authentic co-benefits of adopting a green concept for a developing country like Sri Lanka are numerous. When referring to the current situation in Sri Lanka (2022), it is clear that the country has several industries dedicated to this purpose as a significant exporter. However, given Sri Lanka's current crisis, energy-related issues have had a significant impact on the economy. Because of the energy crisis, Sri Lanka's economy has come to a halt, as there is insufficient energy to run these businesses properly. As a result, despite the crisis, the industries developed under the green concept in Sri Lanka continue to operate [11]. This study demonstrates how environmentally conscious industries co-benefited from the crisis. The advantages of the green concept in addressing the country's energy issues, as well as its contribution to Sri Lanka's development, will be studied [11].

Therefore, the preliminary objective of this study was to investigate the co-benefits of adopting a green concept in Sri Lanka in terms of economic, social, and environmental factors. To achieve the above objective, the study's objectives were formed as follows: to identify the concept of green buildings and the costs and co-benefits associated with green construction, to identify the green building approaches in the Sri Lankan construction industry, and to discover the most co-beneficial components in terms of economic, environmental, and social aspects, as well as the time required

to achieve each co-benefit while constructing green buildings in Sri Lanka and to investigate the barriers to Sri Lankan green building construction while gaining co-benefits, identifying green building approaches in Sri Lanka's construction industry. Finding ways to stimulate the green building industry will be easier if we understand the hurdles to green building development (as suggested in the study that follows).

1st step—To identify the prominence of Green Buildings.
2nd step—To identify Green Building development difficulties and co-benefits.
3rd step—The analyzing of the difficulties and co-benefits.
4th step—To introduce a structure to reduce difficulties and increase co-benefits.

Based on the above facts, a study will be conducted to identify the co-benefits that may be obtained from the green concept.

2 The Concept of Green Buildings

There is a concern about how to improve construction practices to reduce their negative environmental impacts [7]. According to [5], when considering Asian nations, buildings in Hong Kong use roughly 89% of the nation's electricity and approximately half of all energy. The majority of this energy is used for air conditioning, which is responsible for about 17% of the nation's total greenhouse gas emissions [5]. Green building, often known as "sustainable construction", is gaining popularity as its environmental co-benefits become more evident in construction processes. Green buildings are described as "Healthy facilities designed and built in a source of energy manner, using emerging environmental philosophies". Accordingly, Green construction investigates the influence of structures and materials on people, as well as the impact of human presence on the future of the Earth [28].

In the twenty-first century, accepting long-term economic, environmental, and social responsibility has become a symbol of long-term economic, environmental, and social well-being [25]. According to [7], the goal of green construction is to reduce the use of resources and environmental impact significantly beyond standard practice while providing adequate indoor environmental quality [7]. The idea is that the building industry may achieve environmental sustainability by lowering resource consumption and environmental loadings by continually improving the environmental implementation of individual structures [6]. According to [7], a green building maximizes environmental impact while adhering to geographic location, programmatic, governmental, and financial constraints. Green buildings, which are based on concepts and information from numerous research papers and books, make better use of assets than traditional structures. They achieve sustainable development by providing residents with co-beneficial and valued natural surroundings [6]. By assessing the concepts and data gathered from various research papers and books, it is clear that green buildings are buildings that use resources more efficiently than conventional buildings and contribute significantly to sustainable development by providing healthy and productive environments for occupants.

3 Green Building Approaches in Sri Lanka

The concept of green construction is rather concerning in Sri Lanka today. People desire to use more energy-efficient buildings. As a result, the sector is rapidly growing [21]. Sri Lanka has begun to overhaul its construction sector by incorporating green building principles. The Sri Lankan Green Building Council was formed in response to a rising trend in the built environment to utilize greener construction approaches [21]. The government of Sri Lanka announced the Haritha (Green) Lanka public effort to promote sustainable development, taking present and emerging issues into account. One of the most inventive and forward-thinking examples is the MAS Holdings Company Pvt. Ltd. Thurulie plant in Thulhiriya earned the Globe Medal for Sustainability Revolution in 2010.

Furthermore, the United States Green Building Council has conferred its LEED (Leadership in Energy and Environmental Design) Platinum certification, making it the world's first LEED Platinum new construction factory (MAS Holdings Ltd, 2010). Aside from that, there are a few buildings in Sri Lanka that have been designed as green buildings such as the Institute of Technology University of Moratuwa, Aliya Resorts and Spa in Sigiriya, Brandix eco-center in Seeduwa, and MAS Thurulie plant in Thulhiriya. The Green Building Council introduced a new construction rating system called the GREENSL® rating system, which is very similar to LEED, in 2010 to issue green certification [10]. The Sri Lankan government has introduced several national policies which indirectly drive the local green building movement as follows:

- National Energy Policy (2003)
- National Climate Change Policy (2011)
- National Air Quality Management Policy (2000)
- Cleaner Production Policy (2004)
- National Forestry Policy (1995)
- National Solid Waste Management Policy (2008)
- National Biosafety Policy (2005) (Ministry of Environment Sri Lanka, 2012). The Green Building Council of Sri Lanka (GBCSL) is the country's leading body dedicated to developing sustainable structures.

4 Costs and Benefits of Green Buildings

It is important to consider the costs and benefits of green building [7]. Green buildings are widely assumed to be much more expensive to be constructed than traditional buildings [18]. Often, it represents a 20–25% increase in the project cost of green buildings in Sri Lanka [15, 16]. The preliminary cost of construction of a green factory building in Thulhiriya, Sri Lanka, is 30% higher than the building projects of a traditional factory building. However, [24] discovered that the cost of incorporating sustainable design elements is highly dependent on a variety of factors such as

building type, project location, local climate, site conditions, and the project team's familiarity with sustainable design [24]. LEED has identified six basic principles under the characteristics of sustainable green construction, such as sustainable site, water efficiency, energy efficiency, material and infrastructure, indoor environmental quality, and designing and building, operation, and maintenance [22].

According to Richardson and Lynes (2007), green buildings have four major advantages over conventional building design and construction. They are environmental co-benefits; cost savings to the owner or occupier over the operational range of the building; and a better indoor working environment. The construction of green buildings provides co-benefits to the contractor by presenting a positive image and reputation towards that company by practically demonstrating a green approach. [27]. Keats [20] states that many of the benefits of the green approach cannot be easily expressed in dollars and cents. Furthermore, green buildings have the potential to save up to 30% on energy consumption through green features such as building envelope designs and the use of more energy-efficient air-conditioning systems and light fittings (Building and Construction Authority, 2009). Accordingly, when the building and organization are treated as an integrated system from the start, the benefits of both organizational and green building factors are more likely to occur. [12].

5 Barriers to Sri Lankan Green Building Construction

Countless researchers have highlighted various barriers to green building construction and implementation difficulties in many countries [2, 3]. One of the primary issues connected with green buildings, per, is the greater initial cost. As per [15, 16], the cost of green building construction in Sri Lanka has risen by 20–25%. The initial construction cost of the Thurulie green factory building in Sri Lanka is 30% higher than the cost of a conventional factory building in Holcim Foundation for Sustainable Construction, 2009 [15, 16]. This economic barrier to green buildings is removed by the fact that the majority of the co-benefits of green buildings can be realized over time with a short payback period [19]. On the other hand, [1] argued that government actions and guidelines may result in the compression of construction projects towards better environmental protection [1]. Even though there are sufficient environmental regulations and policies in place, there is no specific guideline or policy that focuses on green building practices in Sri Lanka. A further barrier is a failure to enforce existing government regulations and policies. Hewage and Mallika [13]. There are common misconceptions among the public that green buildings are much more expensive than traditional buildings and are rather difficult to be obtained by middle or lower-class people [4]. As a result, Djokoto et al. (2014) identified a serious barrier to green building construction as the lack of knowledge. Often, people are reluctant to change because they believe that change is always difficult [9]. A further barrier to green construction is the lack of professional knowledge. It is emphasized by the fact that the lack of professional knowledge may lengthen the time frame for green building construction. Having considered the facts presented above, the

Table 1 Scale for a period of achievement

Level of achievement		
1-no idea	2-short Term	3-long Term

No idea—The period of accomplishment is unknown to the respondents
Short Term—Period following the construction—fewer than two years
Long Term—Time after construction—more than two years

barriers to Sri Lankan green building construction can be classified as financial, regulatory, social, knowledge/skills, and industrial reasons.

6 Research Methodology

To achieve the study's objectives, a quantitative research method was used, which was identified as the most appropriate method for data collection and analysis. A questionnaire survey was used to gather information. The questionnaire findings retested the impressions of professionals about the level of co-benefit. The period of achievement of each co-benefit was discovered through the literature review. In addition, interviews with professionals in the field about the green concept and co-benefits were performed. The results of the questionnaire were used to retest experts' impressions of the rate of co-benefit and the time required to attain each co-benefit was identified in the literature review.

Site visits provided information on the steps to implement the Green Building Concept. Site visits aided in gathering information such as the technology, environmentally friendly materials, and tactics to implement the Green Concept in Sri Lanka, among other things. The Relative Importance Index (*RII*) was used to analyze the level of co-benefit, and the method was used to analyze the period of achievement. The level of co-benefit was assessed using a five-point Likert scale ranging from "not at all" (1) to "very high" (5) (Table 1).

A study was also carried out to establish how long it took to obtain the co-benefits of green-concept buildings.

7 Research Findings and Data Analysis

This section presents the research study's findings and an assessment and explanation of those findings. In addition to the data collection method, interviews were carried out with the following individuals: four architects, three engineers, and two quantity surveyors. 110 people completed the questionnaire out of 120, which is 91.6%. The number of projects completed by respondents was used to assess their knowledge and experience (Figs. 1, 2 and 3).

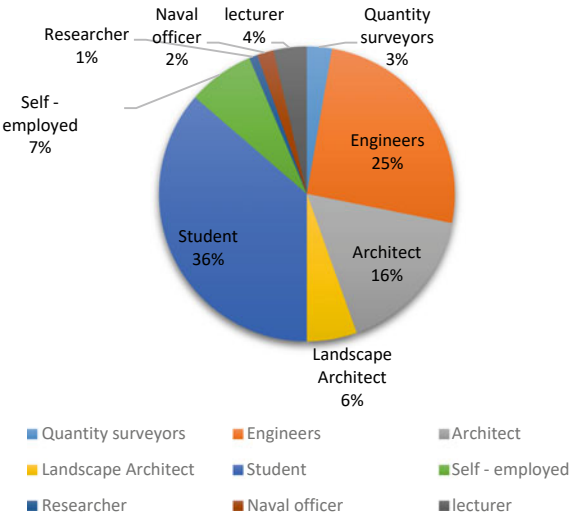

Fig. 1 Current occupation. *Source* Author

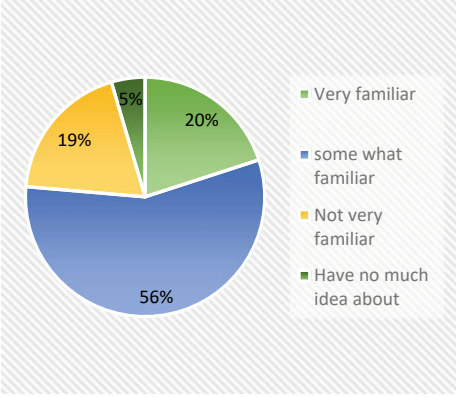

Fig. 2 The awareness of the green building concept. *Source* Author

The majority of those responding to the survey believed that the most significant co-benefit of green building projects is their environmental friendliness, with the social component receiving the least attention. The cost factor is the second most significant co-benefit. More than 76.2% agree that green building may be used in the new building and is better suited to Sri Lanka. As seen in the graph below, individuals in the building industry are highly aware of the Green Building Concept.

Many Sri Lankans have a rudimentary understanding of the "green concept". It is possible to re-propagate the green concept in Sri Lanka if one has a thorough understanding of the fundamentals of the concept. According to research data, as few as *RII* 6.66% of people have a thorough understanding of the green concept. With the help of this idea, it is feasible to discover a solution to Sri Lanka's energy

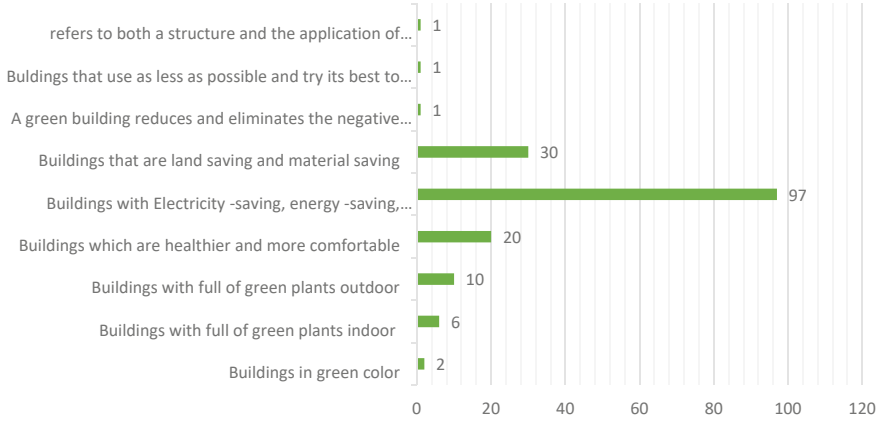

Fig. 3 Level of knowledge about the green concept. *Source* Author

predicament and further popularize it in the nation by providing people with explicit knowledge of the experiment's outcomes.

8 Analysis of Economic Co-Benefits

The RII computes the economic co-benefits, and the results are shown in the following table (Fig. 4).

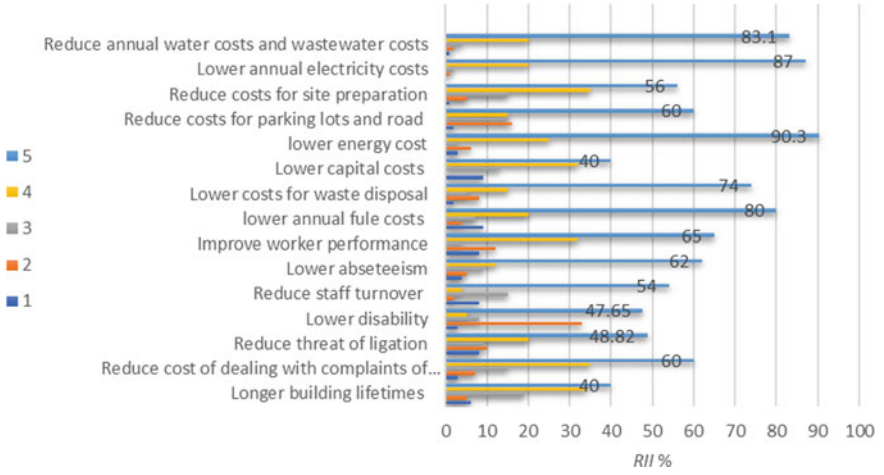

Fig. 4 Level of economic benefits. *Source* Author

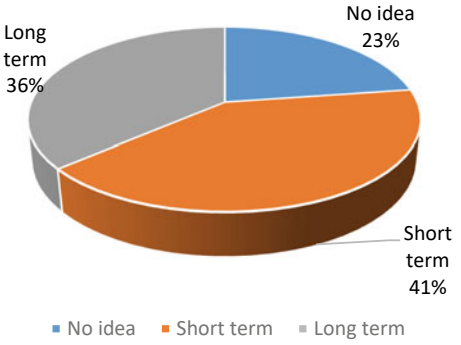

Fig. 5 Period of achievement of economic benefits. *Source* Author

The most co-beneficial economic component of implementing a green concept for building development in Sri Lanka, *RII*-90.30%, in the opinion of many respondents, results in decreased energy costs.

The research identifies lesser annual electricity costs, water and wastewater costs, fuel prices, and waste disposal costs as the five top economic co-benefits. Decreasing the cost of disability and health insurance and lowering the cost of capital were all given lower ranks, with each component's *RII* value being less than 50. The model calculated how long it would take to realize economic co-benefits. The conclusions of the expert's opinions on the time necessary to achieve economic co-benefits are revealed in Fig. 5. Most of the financial co-benefits are long term, with the majority being accessible two years after the building is built.

9 Analysis of Social Co-Benefits

The degree of social co-benefits was calculated using *RII*, and the findings are revealed in Fig. 6. The respondents highlighted the "preservation of water resources for future generations" (*RII*-86.0%) as the most valuable societal component in implementing a green concept for building development in Sri Lanka.

The top four social co-benefits are expanding the market for ethically preferred goods, reducing adverse health consequences, improving occupant contentment and comfort, and increasing worker mobility alternatives. Wastewater treatment facilities had the most negligible societal co-benefit (*RII*-50%). Figure 7 shows that many social benefits are short term, accounting for 49% of total social benefits. In other words, this is equal to half of the social co-benefits, and respondents identified 33% of the benefits as long-term achievements.

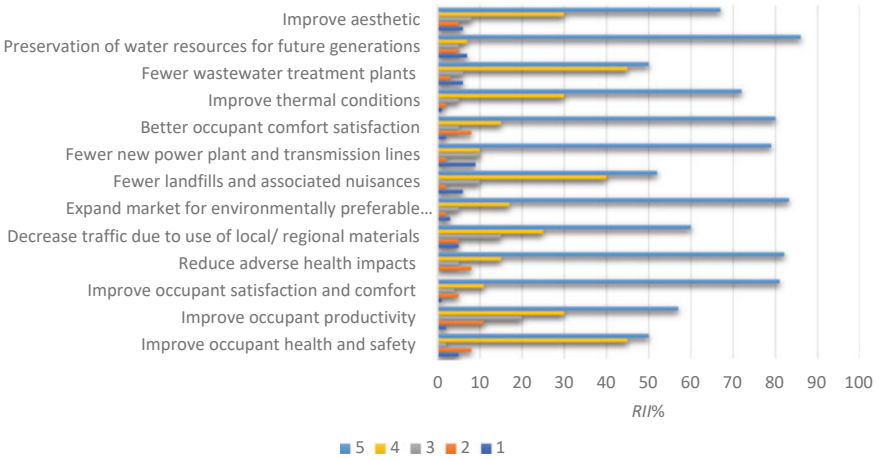

Fig. 6 Level of social benefits. *Source* Author

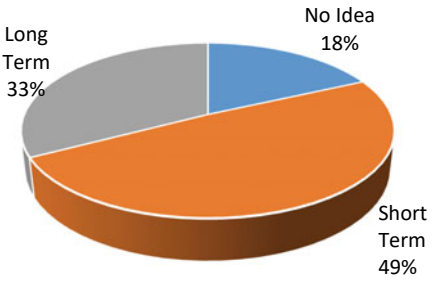

Fig. 7 Period of achievement of social benefits. *Source* Author

10 Analysis of Environmental Co-Benefit

RII was used to analyze the level of environmental co-benefits, and the findings are revealed in Fig. 8. As per survey participants, reduced potable water consumption (*RII*-90.5%) is the most favorable environmental element in applying a green concept for building construction in Sri Lanka. Out of nineteen, the top four environmental attributes were better air quality inside the factory, decreased energy usage, lower fossil fuel use, and natural resource conservation.

Figure 8 depicts the length of time it takes to reap environmental advantages.

According to Fig. 9, long-term and short-term benefits account for 50% and 37% of total co-benefits, respectively. However, 10% of those interviewed had no idea how long it takes in Sri Lanka to achieve environmental co-benefits when developing green structures.

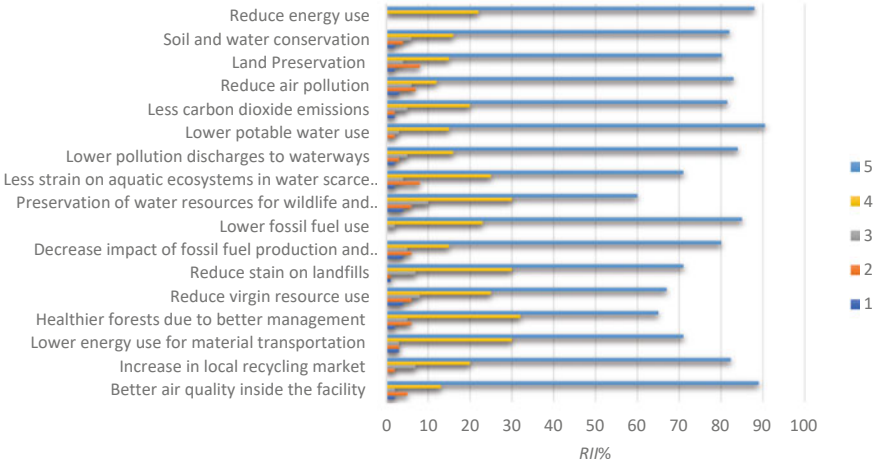

Fig. 8 Level of environmental benefits. *Source* Author

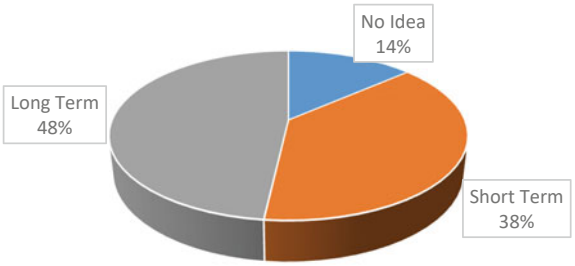

Fig. 9 Period of achievement of environmental benefits. *Source* Author

11 Comparison of Economic, Social, and Environmental Co-Benefits

An examination of the literature reveals 45 co-benefits of using green building ideas in the design of structures. These advantages are classified into economic, social, and environmental categories. Based on the information gathered throughout the research, Table 2 depicts the overall percentages of time spent acquiring co-benefits in each category. According to the opinions of experts, numerous co-benefits accrue over a lengthy period, such as more than two years. In addition, several short-term advantages were identified. According to the survey, respondents had no notion as to how long it would take to achieve a plethora of economic co-benefits compared to the social and environmental co-benefits outlined in the literature. It is possible that the answer "no notion" is related to a negative encounter with the green concept in Sri Lanka.

Table 3 lists all the co-benefits with an *RII* of more than 80% and the period for attaining each co-benefit, long term, short term, or no idea. When looking at the

Table 2 The overall percentages of time spent obtaining benefits

Professionals' perception on the period of achievement	Area		
	Economical	Social	Environmental
No idea	23	18	13
Short term	41	49	37
Long term	36	33	50

Source Author

total number of environmental co-benefits, 63% of them have outperformed the *RII* value by more than 80% in terms of co-benefits. In the review of co-benefits, 43% of the total number of environmental co-benefits surpassed the *RII* value by more than 80%.

Even though 13 economic advantages were discovered, only four of them obtained an *RII* value of more than 80%, accounting for over a quarter of the total score. If the co-benefits to the environment and society are considered, it is a great investment. Table 3 reveals that even if the RII value is greater than 80%, there is no indication of how long it will take to complete the environmental categories of soil conservation and land preservation.

The main social, environmental, and economic advantages identified, among others, are the preservation of water resources for future generations, the reduction of potable water resources, and the decrease of energy expenses. Two of the most crucial aspects of the green construction idea are water efficiency and conservation. According to the research, a building's ability to effectively manage its water usage is essential for long-term development.

12 Conclusions

A green building provides various environmental, economic, and social co-benefits to building owners and users. With the rapid growth of the construction industry, there is an important need to promote the use of green building concepts in Sri Lanka. As a result, the study's primary focus study was on identifying the co-benefits of green buildings in the local context. The study was done based on the perceptions of experts working in green construction projects, and data was collected through a questionnaire survey, site visits, and interviews. The findings revealed that the majority of the co-benefits in each category are achievable in the Sri Lankan setting. However, the magnitude of those co-benefits may fluctuate. According to the professionals' point of view, many co-benefits might be realized in the long term, which takes more than two years after construction, and a considerable number of short-term co-benefits were identified by the respondents in all three areas. Still, few structures in Sri Lanka have adopted the green concept, and many specialists have stated that they have no idea when some co-benefits listed under economic, social, and environmental

Table 3 Co-Benefits in which the *RII* is higher than 80% with their period of achievement

Area	Co-Benefits	*RII* (%)	Rank	Period of achievement
Economical	Lower energy costs	90.3	2	Short term
	Lower annual electricity costs	87	5	Long term
	Reduce annual water costs and wastewater costs	83.1	10	Long term
	Lower annual fuel costs	80		Long term
Social	Preservation of water resources for future generations	86	6	Long term
	Expand the market for environmentally preferable products	83.2	9	Long term
	Reduce adverse health impacts	82.1	13	Long term
	Improve occupant satisfaction and comfort	81	16	Short term
	Better occupant comfort satisfaction	80	19	Short term
Environmental	Lower potable water use	90.5	1	Long term
	Better air quality inside the facility	89	3	Short term
	Reduce energy use	88	4	Long term
	Lower fossil fuel use	85	7	Long term
	Lower pollution discharges to waterways	84	8	Long term
	Reduce air pollution	83	11	Short term
	Soil and water conservation	82	14	No idea
	Less carbon dioxide emissions	81.5	15	Short term
	Increase in the local recycling market	82.3	12	Long term
	Land preservation	80.2	17	No idea
	Decrease the impact of fossil fuel production and distribution	80.1	18	Long term

Source Author

aspects will be realized. The survey discovered the following significant barriers to sustainable construction: a lack of incentives (government support), a higher primary cost, a lack of credible research on the co-benefits of green building, a lack of public awareness, employee resistance to changing from conventional to green practices, and a lack of trustworthy research on the co-benefits of green building. Furthermore, the findings of this research will aid practitioners involved in green building projects in Sri Lanka in adopting the most appropriate green construction methods, resulting in increased economic, social, and environmental co-benefits. In addition, the study emphasizes the co-benefits of using a green building concept. The study

suggests that the government's engagement in this innovative notion was the most significant barrier to recognizing the green building concept. As a result, according to the recommendations, the notion of the green building might be adapted to the Sri Lankan context, boosting the country's long-term sustainability (Table 4).

Moreover, the study emphasizes the co-benefits of using a green concept for building construction. If these criteria are followed correctly when designing a green building, it is possible to reap significant co-benefits.

13 Suggestions

The government is a vital component in promoting green building in the construction industry. The government can influence the construction industry through a variety of approaches. The government must consider regulatory and incentive instruments to promote green building. Moreover, a combination of legislation entices companies and the market to promote the Green Building Concept in Sri Lanka. The government's best approach is to provide incentive packages to the construction industry to encourage them to practice sustainability in their projects. To encourage the green building concept, the government must provide necessary rebates and infrastructure facilities for contractors and investors willing to work and invest in the Sri Lankan context. Public awareness programs should be implemented to promote and spread the concept nationwide. The Green Building Council of Sri Lanka can significantly promote the Green Building Concept to the general public, schools, and universities.

Additionally, during the community awareness programs, the consultants must encourage and inform society about the co-benefits that endure and investors' gain during and after the project through Life Cycle Costing. Despite the initial cost being high, there are numerous economic, social, and environmental co-benefits to green building projects. Construction-related Senior Professionally Qualified representatives must participate in the initial and strategic planning stages of critical decisions. Due to the lack of awareness, private sector companies and individuals are unlikely to risk investing in and assisting with Green Building projects. Moreover, with the assistance of Non-Governmental Organizations and Social Networks, construction youth (fresh blood) can conduct awareness campaigns about converting traditional buildings to green buildings.

14 Recommendation

Research findings illustrate certain recommendations for achieving sustainability in the contemporary building construction environment. Therefore, it is essential to acquire full support from the government because extensive working capital is required to increase public awareness and eliminate people's reluctance to move towards green building concepts. This framework focuses on the co-benefits of using

Table 4 Checklist for implementing the green building concept in new construction in Sri Lanka

Green Building Guide Checklist				
Reference	Standard construction	Light green construction (25%)	Medium green construction (50%)	Dark green construction (90%)
1. *Developing your green team*				
An assembling the team	No green team assembled	In-Designer green team assembled	Designer professional, engineer, contractor/ supplier team assembled	Design professional, engineer, contractor/ supplier team, stakeholders assembled, plus the design process is integrated
Using green building checklists	No checklist is used	Checklist used as a general guide	A Checklist is used in conjunction with a certified green building program	Higher points/rating is sought for the project through a certified green building program
2. *Site selection criteria*				
Location	Little consideration for proximity to community services	Close to community services	Infill site, close to community services, close to alternative transportation	Infill/reclaimed/ Brownfield site, close to community services, close to alternative transportation, bicycle and pedestrian linkages
Solar Access	No consideration	Some solar access	Good solar access	Excellent solar access
Infrastructure	Cost consideration only	Cost and resources considered	Cost, resources, and infill opportunities considered	Cost, resource, infill, and density is considered
3. *Site design and landscaping*				
Site Protection	No site protection	Protect natural areas of the site	Protect natural areas of the site, save and reuse all topsoil from site	Protect natural areas of the site, save and reuse all topsoil from the site, and develop landscape and site preservation plans to address the above items

(continued)

Table 4 (continued)

Green Building Guide Checklist				
Reference	Standard construction	Light green construction (25%)	Medium green construction (50%)	Dark green construction (90%)
Water efficient landscaping	Default landscape planning using non-native plants	Intentional landscape plan using climate-appropriate plants	Intentional landscape plan using climate appropriate plants and low-water use irrigation practices	Intentional landscape plan using xeric native plants, low-water use irrigation practices, soil amendments and bedding mulch, and turf alternatives
4. *Material resource efficiency: building envelope design*				
Orientation	No solar orientation	Solar orientation within 45 degrees of due south	Solar orientation within 30 degrees of due south	Solar orientation within 20 degrees of due south
Passive solar heating	No consideration for passive solar or window placement	Proper window placement, sizing, and shading	Proper window placement, sizing and shading, introduction of low cost mass	Proper window placement, sizing and shading, introduction of higher cost mass, and increased solar glazing area
Passive solar cooling	No consideration for passive cooling	Strategic placement of vented windows, use of overhangs to reduceunwanted heat gain	Strategic placement of vented windows, use of overhangs, use of ENERGY STAR fans, and use other architectural shade structures	Strategic placement of vented windows, use of overhangs, use of ENERGY STAR and whole house fans, use of other architectural shade structures and strategic placement of landscaping for shading
Space efficiency	Default space efficiency planning	Intentional space efficiency planning	Intentional space efficiency planning, elimination of hallways	Intentional space efficiency planning, elimination of hallways, designing loft spaces, incorporation of multi-function flex space, and using built-ins
5. *Energy efficiency*				

(continued)

Table 4 (continued)

Green Building Guide Checklist				
Reference	Standard construction	Light green construction (25%)	Medium green construction (50%)	Dark green construction (90%)
Lighting	Standard lighting with incandescent bulbs, not designed for natural daylighting or southern orientation	Good daylighting, standard fixtures with 30 percent of hard-wired fixtures having compact florescent bulbs (CFLs)	Better daylighting, 60 percent of hard wired fixtures Energy Star rated with CFLs, including ceiling fans, recessed ceiling lights in unconditioned cavities only, simple lighting controls	Advanced daylighting, including the use of clearstory or tubular skylights, all fixtures Energy Star rated with 90 percent CFLs and LED bulbs, no recessed ceiling lights, advanced lighting controls, whole house fan properly insulated
6. *Waste management*				
Recycling	No recycling program	Establish a basic construction waste management plan to recycle	Establish coordinated construction waste management plan with contractors and provide bins	Establish coordinated construction waste management plan with all contractors and suppliers and provide bins and other storage areas for collection

Source Author

a green concept for building construction in Sri Lanka. It is feasible to minimize the cost and reduce waste by embracing preventive precautions, meticulous handlining, and frequent monitoring. Therefore, governmental support towards transferring the co-benefits of green building concepts to the public is an essential recommendation.

In sustainable building construction, a circular economy would be an essential strategy that is required to implement to adopt reduce, recycle, and reuse concepts in the sector. Through the adaptation of close-loop recycling approaches, it is possible to establish material recycling, reusing, and effectively reducing usage. Such approaches enhance co-benefits towards cost reduction in building construction. Green building construction improves the number of masonry components rather than employing a significant quantity of concrete in the construction phase. It also creates centralized courtyards with wind-adequate openings and space to provide natural lighting, ventilation, and air movement. Employing cost-effective and sustainable construction designs would define effective slabs, beams, and column arrangements that are beneficial to the sustainable framework.

Effective skilled labor management is an essential recommendation in sustainable building construction. By managing labor skills, the industry would be able to

acquire cost-effective and accurate construction approaches. Additionally, knowledge of sustainable building construction would result in increasing awareness of sustainable material selection and building strategies within the labor force available. It is essential to preserve the buildings in a nation like Sri Lanka in the contemporary scenario by constructing a building employing the principles uncovered through this research and the recommendations provided.

References

1. Abidin N (2010) Investigating the awareness and application of sustainable construction concept. Habitat International
2. Arif M, Egbu C, Haleem A, Kulonda D, Khalfan M (2009) State of green construction in india: drivers and challenges. J Eng Des Technol
3. Ashuri PD (2010) An overview of the benefits and risk factors of going green in existing buildings. Int J Facility Manag 1–15
4. Azizi NZ, Abidin NZ, Raofuddin A (2015) Identification of soft cost elements in green projects exploring experts' experience. Procedia - Soc Behav Sci
5. Chan EH, Qian QK, Lam PT (2009) The market for green building in developed Asian cities—the perspectives of building designers. Energy Policy 37(8):3061–3070
6. Cole (2005) Building environmental assessment methods: Redefining intentions and roles. Build Res Inf 455–467; Cole 2, Pahwa N (n.d.) [Online]
7. Cole R (2000) Cost and value in building green. Build Res Inf 304–309
8. Cole R (2005) Building environmental assessment methods. Redefining intentions and roles. Build Res Inf 35(5):455–467
9. Cooperation CFE (n.d.) Green building in North America: opportunities and challenges. [Online] Available at: : http://www3.cec.org/islandora/en/item/2335-green-building-in-north-america-opportunities-and-challenges-en.pdf. Accessed 5 May 2022
10. Council GB (n.d.) System, LEED green building rating. In: LEED green building rating. Washington DC USA, s.l.
11. Forum WE (2022) World Economic Forum. [Online] Available at: https://www.weforum.org/agenda/2022/07/economic-politics-debt-protest-crisis-sri-lanka/. Accessed 02 May 2022
12. Heerwagen (2000) Green buildings, organizational success, and occupant productivity. s.l.:s.n.
13. Hewage T, Mallika KI (2011) Current Trends in forest and environmental policies in Sri Lanka. In: International forestry and environment symposium, Colombo, Issue. University of Sri Jayewardenepura
14. IWb (2017) Green buildings market intelligence Sri Lanka country profile. World bank group, s.l.
15. Jayalath M (2010). Build green to ensure sustainability. [Online] Available at: http://www.slema.org.lk/news_events/03082010/Presentation-on-Green-Buildings.pdf. Accessed 08 May 2022
16. Jayalath MS (2010) Build green to ensure sustainability. . In Proceeding of the Sri Lanka energy managers association annual sessions, Issue 2010, Colombo 30 July 2010. Colombo
17. Kats G (2003) The costs and financial benefits of green buildings - a report to California's sustainable building task force. [Online] Available at: https://www.usgbc.org/Docs/News/News477.pdf. Accessed 23 Mar 2022
18. Kats G (2003) Green building costs and financial benefits. The USA. Massachusetts Technology Collaborative
19. Kats G (n.d.) Green building costs and financial benefits. Massachusetts Technology collaborative USA, Issue 2003

20. Keats G (2003) The costs and financial benefits of green buildings - a report to California's sustainable building task force [online]
21. Lanka GBCS (2010) Green rating system for the built environment. Sri Lanka. [Online] Available at: https://srilankagbc.org/. Accessed 09 May 2022
22. Lavy S (2011) LEED accredited professionals' perceptions affecting credit point adoption. Facilities, s.l.: s.n
23. Lavy S, Ferna´ndez-Solis JL (2009) LEED accredited professionals' perceptions affecting credit point adoption, Facilities, 27(13–14)
24. Morris P (2007) What does green cost? [Online] Available at: https://aecom.com/. Accessed 10 May 2022
25. Nsairat A (2009) Developing a green building assessment tool for developing. s.l.:s.n
26. PahwaT (n.d.) Essay on green architecture. [Online] Available at: https://www.scribd.com/doc/14198163/Essay-on-Green-Architecture. Accessed 09 May 2022
27. Richardson (n.d.) Institutional motivations and barriers to the construction of green buildings on campus. s.l.:s.n
28. Woolley T, Kimmins S, Harrison R, Harrison P (1997) Green building handbook. E & FN Spon, London

Effect of Malic Acid as a Compatibilizer in Chemically Modified Cassava Starch/ Polyvinyl Alcohol Blends for Potential Packaging Applications

O. H. P. Gunawardene, S. M. Amaraweera, W. M. D. B. Wannikayaka, N. M. L. Fernando, C. A. Gunathilake, W. A. Manamperi, A. K. Kulatunga, and A. Manipura

Abstract There has been a growing interest in developing biodegradable materials due to the continuous accumulation of non-degradable plastic wastes across the globe. Therefore, this work focuses on producing and evaluating 'green' multifunctional film materials based on a mixed eco-friendly thermoplastic starch (TPS)/polyvinyl alcohol (PVA) matrix compatibilized with malic acid. In this study, the blend films of TPS/PVA were prepared by adopting the solution casting method. Herein, a starch modification was performed under acidic conditions using tetraethyl orthosilicate (TEOS) as the chemical modifying agent. The prepared blends were characterized using Fourier transforms infrared (FTIR) spectroscopy, thermogravimetric analysis (TGA), X-ray diffraction (XRD), differential scanning calorimetry (DSC), and scanning electron microscopy (SEM). Moreover, the water absorption and tensile tests were also carried out according to ASTM standards. The biodegradability test was carried out according to the aerobic compost environment test. The results of FTIR analysis confirmed the successful preparation of modified cassava starch which exhibited enhanced thermal stability and crystallinity. Further, the compatibilized blends exhibited enhanced thermal, mechanical, and water-resistant properties with improved blend homogeneity. This suggested the possibility of occurring

O. H. P. Gunawardene (✉) · W. M. D. B. Wannikayaka · C. A. Gunathilake · A. Manipura
Department of Chemical and Process Engineering, University of Peradeniya, Peradeniya, Sri Lanka
e-mail: chamilag@pdn.ac.lk; chamila@wyb.ac.lk

S. M. Amaraweera · N. M. L. Fernando · A. K. Kulatunga
Department of Manufacturing and Industrial Engineering, University of Peradeniya, Peradeniya, Sri Lanka

C. A. Gunathilake
Department of Material and Nano Science Technology, Wayamba University of Sri Lanka, Kuliyapitiya, Sri Lanka

W. A. Manamperi
Materials Engineering Department, California Polytechnic State University, San Luis Obispo, CA, USA

© The Author(s), under exclusive license to Springer Nature Singapore Pte Ltd. 2023

R. Dissanayake et al. (eds.), *ICSBE 2022*, Lecture Notes in Civil Engineering 362,
https://doi.org/10.1007/978-981-99-3471-3_39

crosslinking reactions among starch, PVA, glycerol, and malic acid upon compatibilization while possessing a dense molecular structure. The biodegradation was slowed upon both starch modification and compatibilization whereas the least water absorption capacity was demonstrated by the TPS/PVA (40/60 w/w) blend compatibilized with 5 wt.% malic acid (M4P6-M5) valuing 28.89% and 42.17% at 2 and 24 h, respectively. Besides, improved mechanical properties could be obtained by the same blend film valuing 36.25 MPa and 162.91% for tensile strength and elongation at break, respectively. Therefore, enhanced mechanical and thermal properties, lower water absorptivity, non-toxicity, and low cost make the compatibilized cassava starch/PVA blended films beneficial for potential packaging applications.

Keywords Biodegradable TPS/PVA thin films · Compatibilization · Malic acid · Modified cassava starch · TEOS

1 Introduction

Owing to rapid industrialization and urban development across the globe, the usage of petroleum-based inert plastics has drastically increased [1, 2] due to their low cost, lightweight strength-to-weight ratio, easy processability, durability, improved barrier properties, and heat stability [3]. Currently, plastic is used in many sectors, including the biomedical field, agriculture, automotive, healthcare, packaging, and household [4]. However, the tremendous increase in the usage and production of petroleum-based plastic materials has resulted in vast amounts of plastic waste accumulation on the land sites [1, 2] since these take 100–450 years to degrade naturally [5]. Apart from the above, it is a well-known fact that non-degradable polymers are derived from petroleum and their allied components [6, 7]. Consequently, the depletion of petroleum resources can occur since the natural resources take millions of years to form and are finite in quantity [8].

Generally, single-use plastic materials used in food packaging applications, personal care products, agricultural purposes, and fishing equipment are released directly into the environment causing many environmental problems and health concerns to wildlife animals [3]. Also, it is stated that recycling is not practicable and economical for single-use plastics [9]. Nevertheless, plastic waste cannot be recycled forever. Thus, waste plastics are eventually destined to be burnt or buried in landfill sites [3]. Therefore, disposal problems, strict regulations on plastic use, new criteria for a cleaner and safer environment [10, 11], and the global shortage of petroleum resources have driven to development of biodegradable and renewable materials [5] as alternatives to replace or reduce non-degradable plastic materials.

Interestingly, starch, as a packaging material, has grabbed much attention both in academia as well as in the industry [12, 13] owing to its intriguing characteristics such as relative abundance, renewability, biodegradability [12, 13], low cost [14, 15], easy handling [4], surface functionality, non-toxicity, and the capability of dissolving

in water [16, 17]. On the contrary, starch plays a significant role as a raw material in various industries including plastics, paper, and textiles [9].

Starch was first employed as a filler material to produce eco-friendly and low-cost plastic materials [9]. The main starch sources are corn, cassava, wheat, and potato. Among different botanical origins of starch production, cassava is one of the major tuber crops which is grown in more than 80 countries due to its easy-growing nature, fertilization, and comparatively higher yield of 21.412% [18].

In recent, the blending of starch and polyvinyl alcohol (PVA) has captured greater attention since starch lowers the cost, improves the gas barrier properties, and enhances the biodegradation rate while PVA can improve mechanical, thermal, and water-resistant properties of the starch/PVA blended materials [3]. Since the 1980s, starch/PVA blends have been underway to examine primarily for preparing films utilizing solution casting [2]. Even though the combined properties of starch-PVA make them popular biodegradable blends, mechanical and water barrier properties are still poorer than those of non-degradable polymeric materials [3, 19]. Furthermore, from a cost and practical point of view, the blends should contain as much as possible. However, the properties of the blends deteriorate as the starch content in the blends increases to poor compatibility between both starch and PVA leading to phase separation during blend preparation [5].

Therefore, many techniques are currently underway to improve the compatibility between PVA and starch such as the addition of nanoparticles, plasticizers, plasma treatment, crosslinking agents, acid modification [20], fillers [19, 21], and compatibilizers [22].

In this study, we report the effect of malic acid as the compatibility agent in chemically modified cassava starch/PVA blended thin films on mechanical properties, biodegradability, water uptake, and thermal stability. Herein, the chemical modification of starch was performed using tetraethyl orthosilicate (TEOS) as the chemical modifying agent in an acidic medium. To the best of our knowledge, this is the first attempt to use malic acid as a compatibilizer in TEOS-modified starch/PVA blends films which are capable of replacing petroleum-based inert plastic packaging materials.

2 Materials and Methods

2.1 Materials

PVA (molecular weight (MW); 27,000) was purchased from Inner Mongolia Shuangxin Environment-friendly Materials Co., Ltd. Tetraethyl orthosilicate (TEOS, 98%) was purchased from Gelset Inc. Morrisville, PA, USA while HCl solution (HCl, 37%) was purchased from Techno pharm chem Haryana, India. Glycerol (not less than 99.0%) was purchased from Sigma Aldrich Co. St. Louis, MO, USA. Phthalic acid (97%) was purchased from Sisco Research Laboratories Pvt. Ltd. All

the reagents used were of analytical reagent grade and used without any further purification. Native cassava starch used in this study was purchased from Vilaconic joint-stock company, in Vietnam. The gelatinization temperature of starch used in this study was 43C7 °C.

2.2 Chemical Modification of Cassava Starch

Modified cassava starch was prepared under acidic conditions using TEOS as the chemical modifying agent according to a slightly modified method described elsewhere by Gunawardene et al. [23]. Initially, 5 g of cassava starch was dissolved in 100 ml of 0.5 M HCl under vigorous stirring at 400 rpm while maintaining the temperature at 45 °C for 1 h. Simultaneously, 22.15 cm^3 of TEOS was dissolved in 100 ml of 0.5 M HCl under stirring at 400 rpm at room temperature for 1 h. Then, the starch solution was added to the TEOS solution, and the final mixture was left under rapid stirring at 600 rpm for 2 h at 40 °C. Subsequently, the solution was hydrothermally treated in YAMATO DS 60 drier at 105 °C or 6 h until a powdered mixture was obtained. The native and modified cassava starch samples were labelled NS and MS, respectively.

2.3 Preparation of Thin Films

Biodegradable thin films were obtained using a solution casting procedure after the preparation of film-forming dispersions according to the method described by Cano et al. [10, 23], along with some modifications based on the formulations depicted in Table 1 for modified cassava starch/PVA (MS/PVA) blended thin films.

2.3.1 Preparation of Film-Forming Dispersions

For the preparation of neat TPS films, initially, native starch or MS (5% w/w) was dispersed in an aqueous solution with the corresponding amount of glycerol (25 wt.% on the dry starch basis) at room temperature under continuous stirring for 10 min at 400 rpm on a magnetic stirrer. Thereafter, the mixture was stirred at 85 °C for 30 min at 400 rpm to induce starch gelatinization.

The neat PVA thin film was prepared by dispersing PVA (5% w/w) in an aqueous solution at 85 °C for 1 h while being stirred at 600 rpm.

Pure TPS/PVA and MS/PVA film-forming dispersions were obtained as follows. Initially, the precalculated amounts of modified cassava starch and glycerol (25 wt.% on the dry starch basis) were dissolved in distilled water and stirred at 400 rpm at 85 °C for 40 min. Simultaneously, the respective amount of PVA was dispersed in another aqueous solution while being stirred at 600 rpm at 85 °C for 40 min. Afterwards,

Table 1 Composition, film thickness, density, and variation of relative crystallinity of cassava starch-based biodegradable thin films

Sample code	Starch or MS % w.r.t. total polymer weight	PVA % w.r.t. total polymer weight	Phthalic acid % w.r.t. total polymer weight	Film thickness (mm)	Density (g/cm^3)	Relative crystallinity (RC) (%)
NS powder	–	–	–	–	–	23.87
PVA crystals	–	–	–	–	–	53.11
MS powders	–	–	–	–	–	36.58
T (Native casava starch film)	100 (NS)	0	0	0.14 ± 0.02	2.76 ± 0.03	Amorphous
P (PVA film)	0	100	0	0.10 ± 0.03	2.19 ± 0.02	35.47
M (Modified starch film)	100 (MS)	0	0	0.16 ± 0.02	2.58 ± 0.03	Amorphous
TP	40 (NS)	60	0	0.21 ± 0.03	2.31 ± 0.04	19.23
MP	40 (MS)	60	0	0.23 ± 0.01	2.36 ± 0.04	20.94
MP-1	40 (MS)	60	1	0.22 ± 0.02	2.34 ± 0.03	21.88
MP-2	40 (MS)	60	2	0.20 ± 0.02	2.32 ± 0.03	22.12
MP-5	40 (MS)	60	5	0.20 ± 0.02	2.31 ± 0.02	22.83

the PVA solution and gelatinized starch solution were mixed. Subsequently, the dispersion was vigorously stirred at 85 °C for another 40 min at 600 rpm to form a homogeneous gel-like solution.

For the preparation of compatibilized MS/PVA blended thin films, malic acid was incorporated at 1, 2, and 5 wt.% w.r.t. total polymer weight. Initially, the precalculated amounts of cassava starch and glycerol (25 wt.% on the dry starch basis) were dissolved in distilled water and stirred at 400 rpm at 85 °C for 30 min. Simultaneously, the respective amount of PVA was dispersed in another aqueous solution under rapid stirring at 600 rpm at 85 °C for 30 min. Next, both the PVA and gelatinized starch solutions were mixed. Afterwards, the dispersion was continuously stirred at 85 °C for 20 min at 600 rpm. Thereafter, the respective amount of compatibility agent was incorporated, and the mixture was allowed to be homogenized at 85 °C for another 40 min at 600 rpm.

2.3.2 Film Formation

Freshly obtained hot film-forming dispersions of native cassava starch, modified cassava starch, and neat PVA were poured into Petri dishes to obtain the thin films. Subsequently, the Petri dishes were dried in an oven with air circulation at 65 °C for 5 h. Next, the dishes were conditioned in a desiccator for 12 h and finally, the dry films were carefully peeled off from the dishes.

On the contrary, the hot film-forming dispersions of pure MS/PVA and compatibilized MS/PVA blends were poured into Petri dishes. After that, the Petri dishes were dried in an oven with air circulation at 65 °C for 5 h. Then, the dishes were cured at 150 °C for 10 min to obtain complete crosslinking. Finally, the dishes were conditioned in a desiccator for 12 h, and finally, the dry films were carefully peeled off from the dishes.

2.4 Characterization of the Prepared Thin Films

2.4.1 Fourier Transforms Infrared Spectroscopy (FTIR)

FTIR spectra of the samples were obtained using FTIR Spectrum two (PerkinElmer, USA) equipped with Attenuated total (ATR). Spectra were collected in the wave number range of 400–4000 cm^1. For each sample, 4 scans were taken at a resolution of 4 cm^1. FTIR spectra were analysed using the Origin software.

2.4.2 Scanning Electron Microscope (SEM)

The morphology study was carried out at the surface of selected samples using a scanning electron microscope (SEM) (ZEISS, Germany). The morphologies were evaluated at 2500 × magnification and the samples were coated with gold and then examined at an acceleration potential of 10 kV.

2.4.3 Thermogravimetric Analysis (TGA)

The thermal weight loss (TG) curve and its derivative (DTG) of the samples were obtained using a TGA 4000 (PerkinElmer, USA) under the nitrogen atmosphere. Approximately, 10 mg of each sample was placed in platinum crucibles of 100 ml with a heating rate of 10 °C/min in the temperature range from 50 to 700 °C. The maximum degradation temperature, the difference in temperature at maximum degradation, moisture content, and residual mass at 600 °C were calculated using the TRIOS software (4.4.0 version, PerkinElmer, USA).

2.4.4 Differential Scanning Calorimetry (DSC)

The DSC parameters such as glass transition temperature (T_g) and melting temperature (T_m) were observed in the thermograms using DSC 131-evo (Setaram Instrumentation, Caluire, France). The selected samples were enclosed in a hermetically sealed aluminium pan and heated in the temperature range from 30 to 300 °C at a heating rate of 10 °C/min [16]. An empty aluminium pan was used as the reference. The calorimetry experiments were carried out in a nitrogen atmosphere.

2.4.5 Powder X-ray Diffraction (PXRD)

The X-ray diffraction patterns of the samples were obtained using a diffractometer (Rigaku Ultima IV, USA) with a Scintillation counter detector operated at 40 kV, 30 mA with a K-α FILTER. The XRD spectra were recorded over an angular range (2θ) of 3 to 50° with a continuous scanning rate of 2°/min [24, 25]. The relative crystallinity (RC) of scattering spectra was calculated as the ratio of the sharp peaks (crystalline peaks) to the total peaks (both crystalline and amorphous line) as shown in Eq. 1 according to the method adopted by Utrilla-Coello et al. [26].

$$(\%) = \frac{A_c}{A_t} \tag{1}$$

where A_c is the value of the area under the curve corresponding to the crystalline portion and A_t is the total area of the X-ray diffractograms.

2.4.6 Film Thickness

The thickness values of the prepared thin films were measured at twelve random positions using a manual Thickness Gauge (Te Clock Dial, SM—528) to the nearest 0.01 mm. The average value for each film was used to calculate the tensile properties.

2.4.7 Density of the Prepared Films

The density of the thin films was obtained directly by measuring the weight of the film and the dimension using the following Eq. 2 [27].

$$\text{Density}(\rho) = \frac{M}{A \times t} \text{g} \big/ \text{cm}^3 \tag{2}$$

where M is the weight (g), A is the area of the thin films (cm^3), and t is the film thickness (t).

2.4.8 Mechanical Test

Mechanical property measurements (tensile strength and percentage elongation at break) were conducted according to ASTM D882-02. The tensile strength test was performed using the Intron 3365 Universal Testing Machine (Intron Ltd, Buckinghamshire) with a crosshead speed fixed at 25 mm/min. All the test specimens were prepared according to the dimensions provided by the standard. Each specimen had a width of 30 mm and a length of 110 mm. For each test, five samples (five different specimens from each composition) were analysed. During the stretching, tensile strength and percentage elongation at break were calculated as the average value from the obtained results.

2.4.9 Water Absorption Test

The percentage water absorption of the cassava starch-based thin films was measured according to ASTM D570-98. Initially, all the samples were conditioned at 50 °C for 24 h and weighed (M_o) before being tested. Afterwards, the samples were soaked in distilled water. After 2 h, all the samples were removed from distilled water, blotted with a cloth, and immediately weighed (M_1). Next, those samples were soaked in water for another 22 h and weighed (M_2). The experiments were carried out in triplicates. The percentage water absorption capacities of the test specimens were calculated as follows.

$$\text{Water absorption at 2 hours} = \frac{M_1 - M_0}{M_0} \times 100\% \tag{3}$$

$$\text{Water absorption at 24 hours} = \frac{M_2 - M_0}{M_0} \times 100\% \tag{4}$$

2.4.10 Biodegradability

The degradation behaviour of the prepared thin films was explored according to the aerobic compost environment test [28, 29]. The compost soil used as the compost medium consists of 13.8% of total C and 1.07% of total N, respectively. Initially, the test specimens were cut into pieces of 20 mm × 20 mm. Thereafter, the samples were buried inside the soil medium at a depth of 3 cm at 25 °C. water was sprayed to maintain the moisture content of the compost environment. The remaining weight of the samples over the degradation period was measured according to Eq. 5

$$\text{Remaining amount of weight} = \frac{W_x}{W_0} \times 10\% \tag{5}$$

where W_0 is the initial weight of the sample before the test and W_x is the weight of the sample after a specific time duration within the degradation period. The reported results represent the average of three replicates for each sample.

2.4.11 Dynamic Mechanical Analysis (DMA)

Dynamic mechanical analysis (DMA) was carried out using the DMA Q8000 (TA Instruments, New caste, DE, USA) in tension mode at a frequency of 1 Hz for selected samples, namely neat starch film, neat PVA film, and M4P6-M0 and M4P6-P5 thin films. A standard heating rate of 5 °C/min over a temperature range of −60 to 80 °C was used.

3 Results and Discussion

3.1 Proposed Mechanism for Chemical Modification of Cassava Starch

Synthesis of the modified cassava starch involves the hydrolysis of both starch (Fig. 1a) and TEOS (Fig. 1b) and crosslinking steps (Fig. 1c), as shown in Fig. 1. Herein, the chemical modification of cassava starch was carried out in an acidic medium. During the synthesis, both cassava starch and TEOS are hydrolyzed separately under acidic conditions as illustrated in Fig. 1a, b. After mixing both hydrolyzed products, the final product is obtained via crosslinking reactions as depicted in Fig. 1c. As can be seen from Fig. 1c, the hydroxyl groups available in cassava starch are eliminated using the modification using TEOS while promoting the hydrophobicity of cassava starch. In contrast, this chemical modification process can incorporate rigid silica particles into the starch structure.

3.2 General Properties of the Films

During the drying of the thin films, all the films were not allowed to be completely dried to maintain flexibility and not to be brittle. According to visual inspection, the air-contact surface was slightly rougher compared to that of the glass-contact surface of the solution-cast film as previously reported by [1, 2]. The neat PVA film was completely transparent and the flexibility was comparatively higher and this observation is in accordance with [30]. Moreover, the neat PVA film was easily peeled off from the petri dish as mentioned by [12, 13]. Despite the fact that the neat PVA film was clear and completely transparent, the neat TPS film was somehow opaque. On the other hand, the modified starch (MS) thin film was opaquer compared

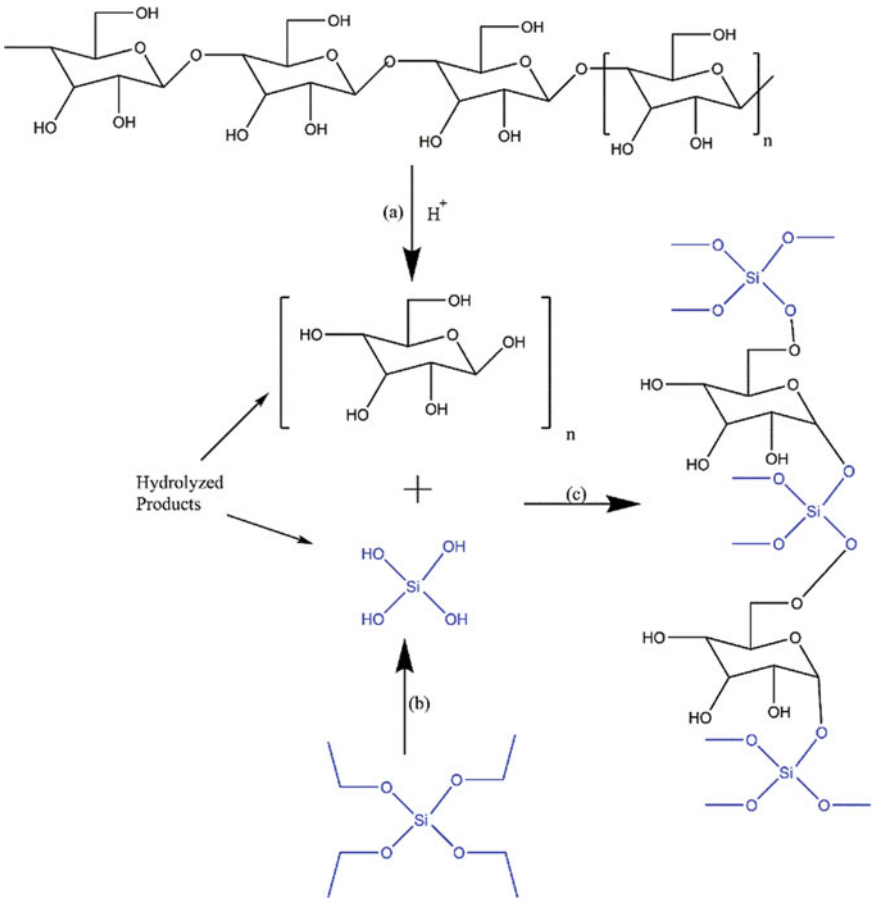

Fig. 1 Mechanism for chemical modification of cassava starch

to that of the neat native cassava starch film and the MS film was slightly white in colour. Such observation can be ascribed to the incorporation of silica into the starch structure during chemical modification. Similar results were previously noted by Lima et al. [13, 20]. Therefore, the addition of modified starch into PVA reduced the transparency to a comparable extent. Similar observations were reported by [1, 2]. Besides, all the formulations were continuous and visually homogeneous without blisters and they were opaque. However, the addition of starch into PVA made the films to be less flexible and the transparency got reduced to some extent as noted by [1, 2, 12, 13, 20, 30, 31].

3.3 Molecular Interactions Within the Prepared Blends

In this study, FTIR analyses were conducted for all the samples. Figure 2 demonstrates the FTIR spectra of NS, MS, PVA crystals, and all the prepared thin films.

The successful preparation of chemically modified cassava starch was evidenced by FTIR spectra of both modified starch powder and MS film. The modified starch sample additionally exhibited two peaks around 1106 and 1082 cm^{-1} which can be ascribed to Si–O–C asymmetric bending vibration (see Fig. 2) whereas a peak was also visible at 802 cm^{-1} which can be attributed to Si–O stretching vibration. Furthermore, the modified cassava starch sample did not show the IR bands at 1149 and 1014 cm^{-1} which were exhibited only by the native cassava starch sample. This behaviour can be ascribed to the breakdown of α-1,4 and α-1,6 glycosidic bonds upon acid hydrolysis during the synthesis of modified starch in an acidic medium [32].

Apart from the above, it is evidenced that the FTIR spectra of PVA crystals exhibit absorbance bands related to C = O group and C–O–C group vibrations and this indication is due to the residual acetate group remaining after manufacturing of PVA via hydrolysis of polyvinyl acetate or oxidation [12, 13]. On the contrary, this implies that PVA used in this study is partially hydrolyzed. In contrast, the IR spectra of the TP film show all the specific bands of cassava starch, PVA, and glycerol while the MP film demonstrates all the characteristic bands associated with modified cassava starch, PVA, and glycerol.

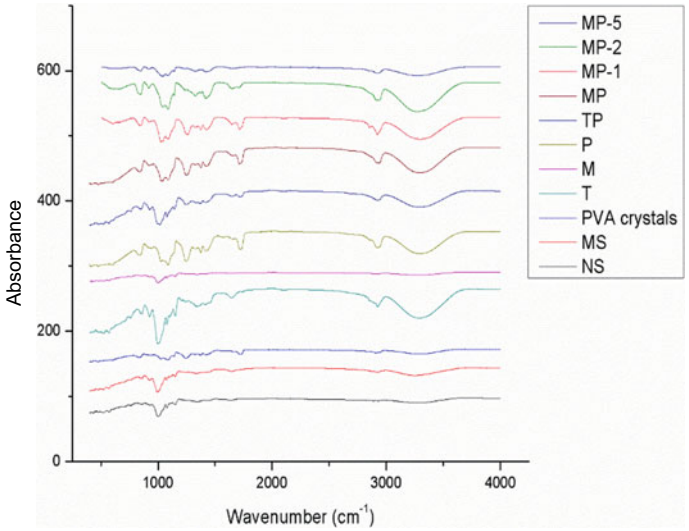

Fig. 2 FTIR-ATR spectra of PVA crystals, native cassava starch powder, modified starch, and the prepared thin films

Besides, the compatibilized MS/PVA thin films exhibit characteristic peaks associated with modified cassava starch, PVA, glycerol, and malic acid. However, the characteristic absorption bands related to malic acid are visible with lower intensities and such behaviour might be due to the comparatively lower concentration of compatibilizer incorporated in blended films compared to those of the other components.

According to Fig. 2, it can be noted that the compatibilized films exhibited a shift in the peak frequency associated with the OH group to higher wave numbers (the band in the region of 2700–3700 cm^{-1}) after the addition of malic acid compared to the non-compatibilized blend. According to the harmonic oscillatory model, this frequency shift is negatively correlated with molecular interactions as stated by [33]. Furthermore, the peak frequency gradually shifted to higher wave numbers with the increased addition of malic acid. This observation can be attributed to the random covalent links formed among starch, PVA, and plasticizers in the presence of malic acid via crosslinking reactions which consequently resulted in the decrease of hydroxyl functionality available for H-bonding where similar behaviour was reported by Sreedhar et al. [17] for TPS/PVA films crosslinked by epichlorohydrin (EPI).

However, crosslinking was not reflected in FTIR spectra with the appearance of a new peak since the significant peak which should be appeared in the range of 1700–1740 cm^{-1} due to the ester carbonyl stretching (C = O) of the ester group is originally present in PVA structure. In contrast, crosslinking modifications are effective to enhance the properties of MS/PVA films. These modifications improve the tensile strength, water resistivity, and thermal stability of a polymeric material [34].

3.4 Variation of Film Thickness

The thickness of a particular film is a variable that influences its flexibility and mechanical and barrier properties [3]. The variation of thickness values can be mainly ascribed to the casting step, and therefore, the casting step should be carried out with great care. In spite of maintaining the same solid surface density during the casting process, some differences in film thickness values could be observed. According to [12, 13], the thickness of the prepared films varies with the chemical composition, molecular organization, and interactions among the macromolecules.

Table 1 tabulates the film thickness, density, and the variation of relative crystallinity values of the prepared thin films. Among the various thin films prepared, the least thickness was exhibited by the neat PVA film as depicted in Table 1. Besides, the blended thin films showed thickness values in the range of 0.20–0.23 mm, higher compared to those of both neat PVA and TPS films. The variation of the film thickness values obtained in the present study is in agreement with the previously reported values by Cano et al. [10, 35] and Aryaphan et al. [36]. On the other hand, according to Table 1, the thickness value of neat MS film is higher compared to neat TPS film due to the presence of small particles of silica in the film as noted by Lima et al. [13,

20]. Moreover, this behaviour is also present in the MS/PVA blended thin films, that is, the film thickness of MS/PVA films is higher compared to the TP film. Besides, the gradual reduction of the film thickness values with the increased addition of malic acid confirms the formation of more compact structures within the blend matrix via crosslinking. Furthermore, these results are in accordance with water absorption and mechanical property data.

3.5 Density of the Films

The calculated density values of the prepared MS/PVA thin film samples are enumerated in Table 1. According to the data shown in Table 1, the density of the neat MS film and MS/PVA films is higher compared to those of the neat native starch film and TP films, respectively. This behaviour is due to the incorporation of silica into the film matrix via the starch modification process. Moreover, the density values gradually decreased at the elevated malic acid concentrations due to the consumption of hydroxyl groups in starch, PVA, and glycerol via esterification and/or crosslinking reactions that occurred in the presence of organic acids which reduce the hydroxyl groups per unit mass. Similar observations were previously reported by Hiremani et al. [27] for oxidized maize starch/PVA blends compatibilized with 7-Hydroxy 4-methyl coumarin (7H4MC).

3.6 Structural Characterization

3.6.1 Morphological Analysis (SEM Micrographs)

The SEM micrographs of native cassava starch granules, modified cassava starch, PVA crystals, and the prepared thin film samples are elaborated in Fig. 3. According to Fig. 3a, the average diameter of native cassava starch granules ranges from 12 to 20 μm with a spherical shape and smooth surfaces without cracks. Similar observations were previously reported by other resaerch groups [10, 13, 20, 37]. Moreover, the modified cassava starch granules (see Fig. 3b) exhibit an average diameter in the range of 5–20 μm and the spherical nature of the native starch granules has been disturbed upon acid hydrolysis and chemical modification. Apart from the above, much smaller sizes and rougher morphology are found on the surfaces of modified cassava starch. On the other hand, PVA performed irregularly shaped crystals as can be seen in Fig. 3c. According to Fig. 3d, e, f, as expected, both the neat starch, neat MS, and PVA films show homogeneous singular dispersed phases as the sole component in the films is starch, modified starch, or PVA, respectively. Besides, the native starch and modified cassava starch granules completely collapsed during gelatinization and thin film preparation. Furthermore, the surfaces of these three films were found to be clear and smooth without any cracks or pores. Their results coincide

with those obtained by several authors working on starch/PVA blended thin films obtained by casting [10–13, 27, 35].

As can be evidenced from Fig. 3g, h, both the TP and MP thin films were found to be smooth and almost homogeneous without any fractures, erupted bubbles, pores, or wrinkles while this behaviour implies that cassava starch and PVA are already miscible. Similar results were previously observed by [10, 31, 38, 39]. Moreover, this observation is in conformity with DSC and DMA studies. In pure TPS/PVA blends, the starch and PVA molecules could associate with each other via intermolecular hydrogen bonding interactions [25, 39]. Moreover, the granular structure of starch was almost completely destroyed during processing and this uniform blending of starch and PVA resulted in the single-phase morphology as in accordance with [37, 39]. This result is very important when considering the mechanical and barrier properties since a fine morphology is required for better mechanical properties [20].

In contrast, all the compatibilized MS/PVA thin films showed slightly enhanced homogeneity compared to that of the pure MP thin film due to crosslinking occurring in the presence of malic acid. On the contrary, according to Fig. 3i, j, k, a slight increase in the blend homogeneity could be observed along with the increased addition of malic acid. However, all the blended thin films demonstrated smooth, uniform, and homogeneous surfaces without any cracks or pores while positively correlating with better tensile properties as previously reported by [11, 31, 37, 39] for crosslinked TPS/PVA thin films in the presence of different organic acids as the compatibilizers.

3.6.2 Powder X-ray Diffraction (PXRD) Studies

The change in crystalline morphology significantly affects the mechanical and physical properties including stiffness, water resistivity, stretchability, and barrier properties of a polymer [2]. Therefore, measuring the variation of relative crystallinity is of great importance. Figure 4 demonstrates the XRD patterns obtained for native cassava starch, modified starch, PVA crystals, and the prepared thin films.

According to Fig. 4a, native cassava starch powder exhibits five characteristic peaks (2θ) at 15.42, 17.41, 18.43, 20.60, and 23.57° with a relative crystallinity value of 23.87% (see Table 1). According to previously reported literature, based on the characteristic x-ray diffraction patterns, the crystal structure of starch can be categorized into three forms, namely A, B, and C dependent on its provenience. The A form which is associated mainly with cereal starch gives stronger signals at around 15, 17, 18, 20, and 23° whereas the B form is usually found in tuber starch and performs stronger signals at 17 with lower signals at around 20, 22, and 24°. On the other hand, the C form is a mixture of the previous two types being found in different starches [4]. According to this classification, cassava starch in the present study exhibits an A-type crystalline structure in accordance with the previous studies [26, 40–42]. Furthermore, the relative crystallinity value of cassava starch observed in this study is in agreement with Jayasekara et al. [1]. However, the

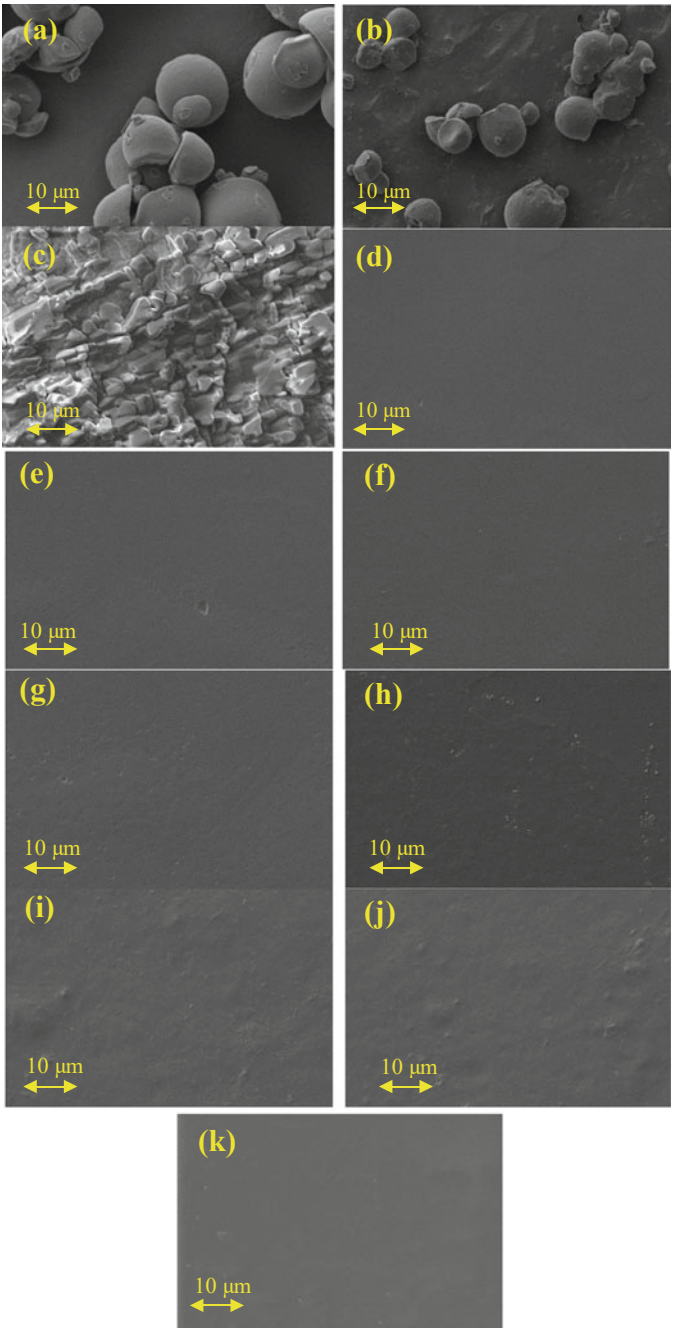

Fig. 3 Scanning electron micrographs (SEM) of **a** native cassava starch (NS), **b** modified cassava starch (MS), **c** PVA crystals, **d** neat native starch film (T), **e** neat MS film (M), **f** neat PVA film (P), **g** TP film, **h** MP film, **i** MP-1 film, **j** MP-2 film, and **k** MP-5 film

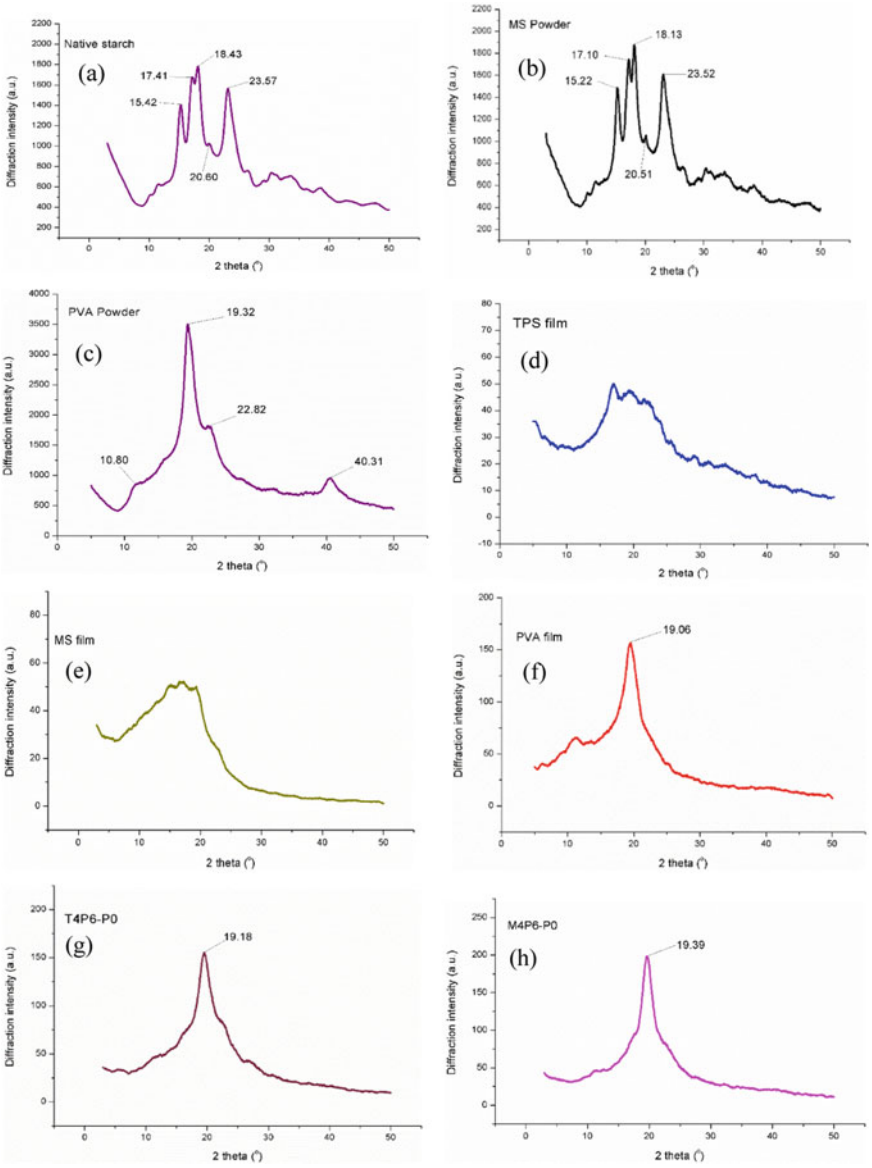

Fig. 4 XRD patterns of **a** native cassava starch (NS), **b** modified cassava starch (MS), **c** PVA crystals, **d** neat native starch film (T), **e** neat MS film (M), **f** neat PVA film (P), **g** TP film, **h** MP film, **i** MP-1 film **j** MP-2 film, and **k** MP-5 film

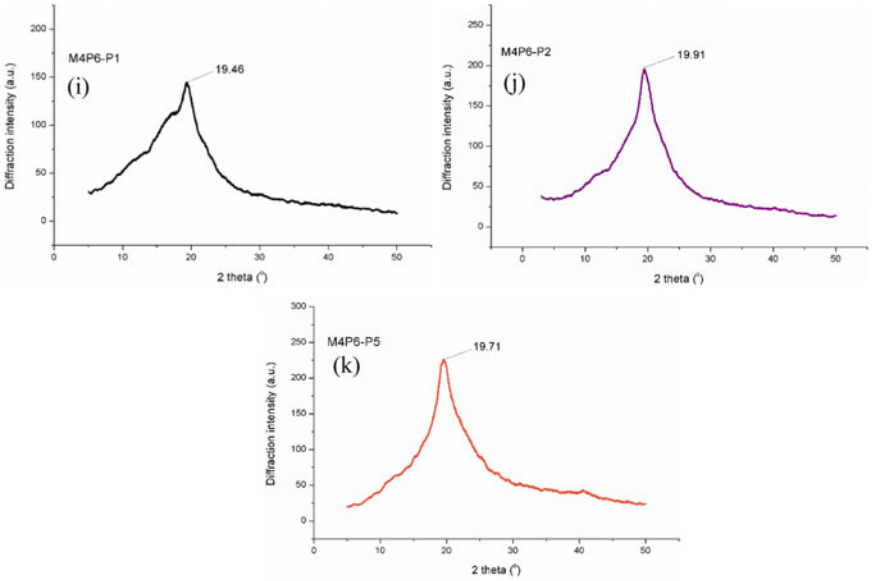

Fig. 4 (continued)

neat TPS film exhibited a fully amorphous nature (see Fig. 4d) and this behaviour is probably due to the decreased inter-molecular hydrogen bonding with water. Besides, during the gelatinization process, the starch molecules clearly loosened their ordered arrangement. This observation is in accordance with [1, 2, 13, 20]. In contrast, as can be seen from Fig. 4b, modified cassava starch powder exhibits four sharp peaks (2θ) at 15.22, 17.10, 18.13, and 23.32° while performing an RC value of 36.58% which is quite higher compared to that of native cassava starch (23.87%). This increase in RC of starch upon chemical modification can be ascribed to the selective hydrolysis of the amorphous regions by HCl during the chemical modification of cassava starch and the better orientation of crystallites into a more stable crystalline form as reported by Amaraweera et al. [37].

In the diffractogram of PVA powder (Fig. 4c), Bragg's reflection was observed at $2\theta = 19.33°$, representing the crystalline nature of PVA. Furthermore, PVA powder exhibits three other weak characteristic peaks at 10.8, 22.82, and 40.30° and our data are in agreement with the XRD patterns reported for PVA powder by [11–13, 19, 24, 25, 39, 40, 21] . The relative crystallinity (RC) value calculated for the PVA crystals was 53.11%. In contrast, neat PVA film exhibited a sharp peak only at 19.06 with an RC value of 36.40%. And the RC values for both PVA crystals and neat PVA film are in accordance with the value reported by [15]. According to the XRD spectrums, PVA crystals, native cassava starch, and modified cassava starch powder present a semi-crystalline structure due to the presence of high physical interactions (like hydrogen bonding between OH groups) existing between the polymer chains as noted by Popescu et al. [4]. The conversion of the semi-crystalline structure of starch

powder to an amorphous nature in neat starch films and the reduction of RC value in neat PVA film compared to the PVA crystals suggest that the solution casting process has reduced the overall crystallinity in the films from the values in the original powder as previously observed by [1, 2].

In the case of all the compatibilized and non-compatibilized blended thin films, though the peaks attributed to starch were absent due to the destruction of the crystalline nature of starch granules as a result of both gelatinization and plasticization during the blend preparation process, the diffraction patterns were similar to that of neat PVA film with a sharp signal around 19.8°. Such behaviour can be attributed to the higher RC of PVA while the crystal structure of PVA was not affected by the incorporation of starch into the blend matrix as stated by [13, 19, 21, 39, 40]. According to RC values shown in Table 1, it is evident that the RC decreased with the addition of starch into PVA and this observation was previously noted by [35]. Such observation is attributed to the strong interactions between starch and PVA components which could inhibit the PVA macromolecular chain arrangement and destroy the crystalline structure resulting in decreased RC values at elevated starch ratios [42].

According to RC values depicted in Table 1, the RC values for MS/PVA films are higher compared to TP thin films. This behaviour suggests that the enhanced RC of modified starch powder has also contributed to this increase in RC values for MS/PVA thin films. On the contrary, as can be evidenced from the series of blends M4P6-P0, M4P6-P1, M4P6-P2, and M4P6-P5, the RC values gradually increased with the increased addition of malic acid due to increased crosslinking ability at elevated acid concentrations. An increase in the relative crystallinity values for crosslinked starch-based films was previously observed by [11, 39] for TPS/PCL crosslinked using maleic anhydride and TPS/PVA films crosslinked using epichlorohydrin (EPI), respectively. Such behaviour can be attributed to the more ordered arrangement of the macromolecules formed via covalent bonding among the components within the blend matrix in the presence of organic acids as the compatibilizing agents.

3.7 Thermal Analysis

3.7.1 Thermal Transition of the Films (DSC Analysis)

DSC analysis is a useful technique which is used to study the thermal properties of a material such as glass transition temperature (T_g) and melting temperature (T_m) [31]. Several factors including the main-chains rigidity, moisture content, crosslinking density, and chemical structure of the crosslinking density and chemical structure of the crosslinker could influence both the T_g and T_m of crosslinked films (Sreedhar et al. 2004). Figure 5 demonstrates the DSC curves obtained for native cassava starch, modified cassava starch, PVA crystals, and the prepared thin film samples whereas Table 2 tabulates the melting and glass transition temperatures of the samples analysed.

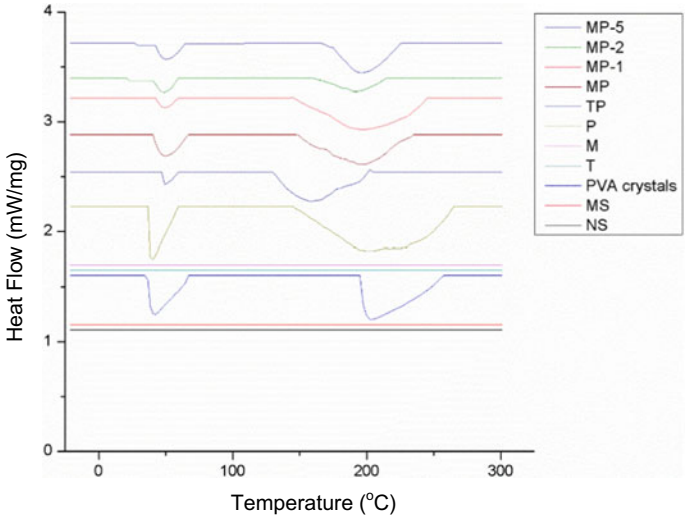

Fig. 5 DSC thermograms of PVA crystals, native cassava starch powder, modified starch, and the prepared thin films

Table 2 Variation of ΔT, T_d, char residue, and the number of degradation steps obtained through DSC analysis and T_m and T_g values obtained via DSC thermograms

Sample	T_g (°C)	T_m (°C)	Number of degradation steps	ΔT (°C)	T_d (°C)	Char residue at 600 °C
NS powder	Could not detect		2	145	318.45	6.68
MS powder	Could not detect		2	231	330.55	55.21
PVA crystals	52.75	211.33	3	240	346.11	4.23
T	Could not detect		2	229	327.34	6.91
M	Could not detect		3	269	327.56	23.19
P	52.24	207.11	3	217	343.72	4.39
TP	49.66	185.60	4	313	324.25	2.91
MP	49.81	189.58	4	342	324.67	7.18
MP-1	50.03	191.63	3	244	326.54	9.28
MP-2	50.31	195.25	3	235	328.07	11.96
MP-5	50.62	200.12	2	223	330.37	12.74

As can be evidenced from Fig. 5, no discernible changes were observed for native cassava starch and modified cassava starch and neither the T_g value nor T_m value could not be observed in this work. This behaviour can be ascribed to the following factors: rigid saccharide structure, amorphous chains surrounded by crystalline domains, physical crosslinks via strong inter and intra-hydrogen bonding which inhibit the movement of the amorphous chain segments, hygroscopic nature, and the presence

of inter-crystalline phases not showing normal thermal behaviour as reported by [24, 25]. Furthermore, no clear T_g or T_m could be identified for both the native and modified starch films and such behaviour can be ascribed to the conversion of starch into a fully amorphous nature after subjecting to both gelatinization and plasticization. This is in conformity with XRD results. Similar observations for DSC thermograms for both native cassava starch and neat TPS films were previously reported by [24, 25].

Apart from the above observations, PVA crystals exhibited a T_g value of 52.75 °C whereas the T_g value for neat PVA film was 52.24 °C and these values are closer to the values reported by Sreedhar et al. [17] (70.9 °C) and Shi et al. [43] (40 °C). Usually, the T_m of PVA ranges from 180 to 240 °C depending on its degree of hydrolysis as stated by Tang and Alavi [21]. According to Table 4, the T_m value of pure PVA is 211.33 °C whereas the T_m value of neat PVA film is 207.11 °C and these observations agree with the previous studies [27, 44].

As can be visible from Fig. 5, for TP and MS/PVA blended films, two thermal transitions were observed (i) glass transition and (ii) melting. The exhibition of only single T_g and T_m values in DSC thermograms suggests the good miscibility between native or modified cassava starch and PVA as previously noted by [31].

Further, the T_g of a polymer can be modified by blending with a small amount of additive [43]. As can be evidenced from Table 2, the T_g value slightly increased with the incorporation of malic acid as the compatibilizer in MS/PVA blended thin films while the increase was more pronounced at elevated acid concentrations. This observation might be due to the reduction of segmental mobility and free volume due to the network structure formed via crosslinking in the presence of organic acids as previously noted by [31, 45]. Also, the increase in T_g value upon compatibilization is in agreement with DMA results.

Also, a slight increase in T_m value in MS/PVA blende series could be observed with the addition of malic acid and this increase was more emphasized at higher compatibilizer concentrations. This shift of melting temperature to higher temperatures is due to the increased cohesion forces of attraction between the polymer chains via crosslinking reactions as noted by Sreedhar et al. [17] and higher RC values. As a general rule, any structural feature that reduces the segmental mobility of polymer chains will increase both the T_g and T_m [31]. In addition, the gradual increase in T_g and T_m in the presence of higher compatibilizer concentrations is due to enhanced esterification and/or crosslinking. Yoon et al. [6, 7] also reported an increase in both the T_g and T_m due to crosslinking in TPS/PVA blended thin films under higher gamma irradiations.

Interestingly, the T_g and T_m values for MS/PVA blended samples are greater than TP thin film and this observation further confirms the effectiveness of cassava starch modification this increase in T_g and T_m values for compatibilized MS/PVA films can be ascribed to the reduced chain mobility and free volume due to both incorporated silica particles into the blend matrix via starch modification. Similar observations were reported by Arayaphan et al. [36] for SiO_2-added MS/PVA films and these observations are in accordance with XRD results.

3.7.2 Thermal Stability (TGA Analysis)

The influence of malic acid on the thermal stability of the MS/PVA thin films was evaluated using the TGA analysis (The TG and DTG profiles are not shown). Herein, the loss of mass due to the volatilization of degradation products was monitored as a function of temperature. In general, the thermal stability of a polymeric material depends on the interactions between the macromolecules present in the blends and the characteristics of the sample [24, 25]. Table 2 enumerates the temperature at maximum degradation (T_d), temperature difference at maximum degradation (ΔT), number of thermal degradation steps, and the residual mass at 600 °C (char residue). Usually, according to the previous literature, the difference in temperature at maximum degradation of a sample at a particular derivative TG provides an indication for the blend homogeneity, and the reduction in ΔT may be attributed to the increase in the blend homogeneity [44].

Both the native cassava starch powder and the neat TPS film exhibit two distinct weight loss regions in the temperature range of 50–150 °C and 190–400 °C. The former event performs a weight loss of ~12.31% which corresponds to the evaporation of physically absorbed water in native cassava starch while this value represents the moisture content of the starch powder. In contrast, the former event of weight loss in neat TPS film is due to the evaporation of both physically absorbed water and glycerol [23, 32, 45]. For both samples, the latter event is attributed to the thermal degradation of the starch backbone as reported by Thessrimuang et al. [46]. The T_d values obtained for cassava starch powder and neat TPS film are in conformity with the values reported by [39, 40].

On the other hand, modified starch powder exhibits two distinct weight loss regions in the temperature range of 50–200 °C and 200–450 °C. The first thermal event is due to the evaporation of weakly physisorbed water and the latter event is ascribed to the main decomposition of starch. The moisture content of modified cassava starch is 5.03% and this value is much lower than the value obtained for native cassava starch (12.31%). This observation might be due to the consumption of hydroxyl groups in the starch structure during the chemical modification process which consequently reduced the moisture absorbance capability of modified cassava starch. In addition, the neat MS film demonstrates three weight loss regions; (i) 50–130 °C: evaporation of water, (ii) 130–180 °C: evaporation of glycerol, and (iii) 200–470 °C: starch decomposition. According to Table 2, the T_d and the char residue for both modified starch powder and neat MS film are greater compared to those of native cassava starch and neat TPS film, respectively. One of the two major reasons for enhanced thermal stability is the increased RC as the acid hydrolysis during chemical modification of starch occurs in the amorphous regions of cassava starch and the other is the incorporation of silica into the starch structure via chemical modification, which provides more rigidity. Similar results were previously reported by Gunawardene et al. [32] for TEOS-modified cassava starch in an acidic medium.

On the other hand, both the PVA crystals and neat PVA film demonstrated three distinct weight loss regions. The first thermal event in the temperature range of 50–180 °C is due to the loss of physically absorbed water in PVA crystals while the

weight loss of both water and glycerol in PVA film. The 2nd and 3rd degradation steps are due to PVA thermodegradation. Previous studies have also proved that the decomposition of PVA followed a two-step mechanism. The 2nd weight loss region in the temperature range of 200–420 °C mainly involves the dehydration of the hydroxyl groups and this is followed by the formation of volatile organic compounds which subsequently produced conjugated unsaturated polyene structures. The 3rd thermal event (430–550 °C) is attributed to the degradation of previously formed compounds during the 2nd stage [10, 24, 25, 35]. The moisture content of PVA is 8.73%.

As can be evidenced from Table 2, after scanning up to 600 °C, the ash concentration for PVA crystals was kept at 4.23% of the original weight, which was lower than native cassava starch (6.68%). This behaviour is associated with the chemical structure of starch, which is prone to form a thermal resistance layer while yielding a higher degree of residual carbon at elevated temperatures as noted by [39, 40].

Also, the TGA profile of TP exhibits four distinct weight loss regions: (i) 50–150 °C: due to evaporation of physically absorbed water, (ii) 150–250 °C: loss of volatiles such as glycerol [7, 40], (iii) 250–420 °C: the main degradation zone of both starch and PVA (predominantly due to the degradation of hydroxyl groups and the subsequent formation of low molecular weight unsaturated and aliphatic carbon spheres) [2]. Furthermore, at this stage, the breaking down of glycosidic bonds between amylose and amylopectin occurs as reported by Belleli [47]. (iv) 420–550 °C: final decomposition of the previously formed compounds [10, 11]. On the contrary, the neat MS/PVA thin film performs four distinct weight loss regions: (i) 50–200 °C: evaporation of the volatile components (both water and glycerol), (ii) 220–400 °C: main decomposition of both cassava starch and PVA, (iii) 400–440 °C: degradation of the byproducts formed during the 2nd stage, and (iv) 440–550 °C: degradation of the byproducts formed during the 2nd and 3rd stages.

In contrast, some of the MS/PVA thin films exhibit similar degradation behaviour. The TGA profiles of MP-1 and MP-2 film samples show three major decomposition steps. The 1st thermal event in the temperature range of 50–180 °C is due to the evaporation of weakly absorbed water and glycerol while the 2nd degradation zone located at the temperature range of 200–450 °C is attributed to the major decomposition of both starch and PVA chains and the 3rd thermal event is due to the final degradation of the previously formed compounds during the 2nd degradation stage. Besides, the MP-5 sample exhibits only two distinct weight loss regions. The first thermal event which occurs in the temperature range of 50–150 °C is due to the evaporation of volatiles (both water and glycerol) and the 2nd degradation zone in the temperature range of 220–430 °C is attributed to the combined degradation of the main chain of starch and PVA and the degradation of byproducts of the same time. Moreover, MP-5 did not decompose as polymers alone. The possible causes for this behaviour are the individual decomposition mechanism coupled with other ionic forces, which produced a complex mode of decomposition and the formation of crosslinking points in the presence of malic acid.

Furthermore, it is evidenced by comparing the data in Table 2 that the T_d and char residue in all the MS/PVA films are higher compared to those of TP film. This behaviour might be due to the increase in RC values and the complex molecular

structure formed due to the incorporation of silica which consequently resulted in a complex mode of decomposition as noted by Thessrimuang et al. (2018). Similar behaviours were previously reported by Aryaphan et al. [36] for SiO_2-added TPS/PVA thin films.

According to the data depicted in Table 2, the char residue and the T_d values increased in all the compatibilized samples compared to that of the pure MS/PVA film. The increase in both T_d and char residue reflects the increase in thermal stability upon compatibilization. According to [24, 25], it is stated that with the increase of amorphous fraction in a polymeric material, decomposition would more easily happen. Therefore, this enhanced thermal stability with the increased addition of malic acid can be ascribed to the increase of RC values in the blend films. Also, the increment in both T_d and char residue is due to the strongly packed complex network within the blend matrix via the presence of organic acids as the compatibilizing agents which resulted in reduced molecular mobility of the polymer chains as previously reported by [18, 48]. Also, the shift of T_d to higher temperatures upon compatibilization might be due to the strengthening of backbone chains while creating strong interactions among the macromolecules via covalent bonds as noted by Thessrimuang et al. [46]. Previous studies have also reported the increase of thermal stability and blend homogeneity in TPS/PVA blended thin films at higher loadings of carbon nanotubes (CNT), succinic acid, maleic acid, and citric acid and crosslinking via gamma irradiation [31, 41, 46].

On the contrary, according to data depicted in Table 2, during pyrolysis in an inert gas atmosphere, char formation was observed for all the samples. At 600 °C, the char formation increased with the addition of starch into the blend matrix, and this is due to the thermal resistant cycle hemiacetal in starch structure as reported by Luo et al. [2]. Similar observations were previously stated by Luo et al. [2]. Furthermore, the char formation increased along with the increased addition of malic acid.

Apart from the above observations, the ΔT values gradually decrease with the increased addition of malic acid compared to that of the neat MS/PVA film. This behaviour indicates the increase of blend homogeneity due to the compatibilization of malic acid as confirmed by SEM observations. Moreover, a reduction in the number of weight loss regions could be observed with the increased addition of malic acid (see Table 2).

As can be evidenced from Table 2, a gradual increase in blend homogeneity, $T_{d,}$ and char residue and a reduction in the number of degradation steps can be observed at elevated compatibilizer concentrations. In contrast, both the chemical modification and compatibilization have contributed to the enhanced thermal stability in compatibilized MS/PVA thin films.

3.8 Variation of Mechanical Properties

The determination of mechanical properties is of vital importance not only from scientific but also from a practical point of view since polymeric materials such as

films for packaging are required to maintain their integrity to withstand the stresses that occur during shipping, handling, and storage (Parvin et al. 2011; Pour et al. 2015). The mechanical behaviour of prepared films was analysed in terms of the tensile strength (TS) and percentage elongation at break ($\varepsilon\%$). TS represents the force per unit area required to tear the film whereas $\varepsilon\%$ is the ability of the film to stretch [10, 11, 31]. The calculated mean values of TS and $\varepsilon\%$ of the blended thin films are depicted in Table 3.

As depicted in Table 3, the poorest mechanical properties were exhibited by the neat TPS film indicating a maximum TS and $\varepsilon\%$ 4.82 MPa and 5.52%, respectively, while performing a typical mechanical behaviour of a brittle material without plastic deformation and with very low extensibility at the break. Similar observations were previously reported by [10, 11, 24, 25]. Such observations can be attributed to the strong interactions of the starch polymer via hydrogen bonding which increases the cohesion forces of the matrix, thus making it difficult for the chains to shift during the tensile test as noted by [10, 11]. In contrast, the TS is 30% higher whereas the $\varepsilon\%$ is 36% lower in neat MS film compared to that of the neat native starch film and this behaviour might be due to the incorporation of silica particles leading to a more rigid structure and hindrance of sliding of chains. Similar results were previously reported by [13, 20] for TEOS-incorporated starch films. The highest resistance towards breaking was performed by neat PVA film demonstrating a TS of 54.67 MPa and an $\varepsilon\%$ of 447.53% and better mechanical properties were observed due to the availability of hydroxyl groups and flexible nature of C–C backbone as denoted by Hiremani et al. [27]. Even though neat PVA film was very resistant and stretchable, it was not as stiff as neat TPS film as previously reported by [10, 11].

As reported in the literature, the mechanical properties of TPS/PVA blended thin films depend on the starch content and the content of crosslinkers or plasticizers [6]. According to data depicted in Table 3, it is indicative that the incorporation of starch into PVA caused a fall in tensile properties as previously noted by [12, 13, 39, 40]. However, both the TS and $\varepsilon\%$ values for all the TPS/PVA blended thin films were

Table 3 Variation of TS and $\varepsilon\%$, water absorption, and biodegradability of the prepared film materials

Sample	TS (MPa)	$\varepsilon\%$	WA at 2 h (%)	WA at 24 h (%)	Biodegradability (%) (After 4 months)
T	4.82	5.52	86.21	104.32	100.00
M	6.27	3.55	74.24	87.65	87.22
P	54.67	447.53	21.26	32.45	28.44
TP	26.91	234.85	53.11	72.34	57.06
MP	28.95	193.26	33.84	59.56	51.95
MP-1	30.17	189.67	37.31	56.18	51.02
MP-2	34.87	180.88	32.38	51.87	49.06
MP-5	37.44	162.91	28.54	42.17	47.94

Table 4 Comparison of the properties of the optimum film composition of the present study with market-available packaging materials

Plastic film	t (mm)	ρ (g/cm^3)	TS (MPa)	ε (%)	Tg (°C)	T(m °C)	T (d°C)	WA (%)	RC (%)	Char residue (%)	Biodegradability (%)
PE bags	0.15	0.88–0.96	22.95	800	−110	110–130	189.35	0.008	35–80	–	Still decaying
LDPE bags	0.15	00.88–0.96	60.9–15.9	90–650	−125	160–260	400	0.015	50–60	3.5–5	Still decaying
HDPE bags	0.15	0.941–0.965	21.4–38	50–800	−100	200–300	425	0.01	>90	~7	Still decaying
PP bags	0.15	0.926–0.940	32.9	691	−25	130	500	0.2	30–60	–	Still decaying
PVC bags	0.15	1.38	40	185	−5	100–260	270	0.4	~10	~20	Still decaying
LLDPE bags	0.15	0.91–0.94	7.93–45.5	8–1100	−100	122	400	0.01	35–60	3.5–5	Still decaying
Black trash bags	0.02	-	27	39.7	–	–	–	–	–	–	–
MS/PVA (40/60) with 5 wt.% phthalic acid	0.20	2.31	37.44	162.91	50.62	200.12	330.37	42.17	22.83	12.74	47.94 (After 4 months)

found to be lower than that of pure PVA film and higher compared to neat TPS film as can be associated with the 'rule of mixtures'.

Besides, as can be seen from Table 3, the TS increased and the $\varepsilon\%$ decreased for the compatibilized MS/PVA thin films. Furthermore, the TS values are higher and the $\varepsilon\%$ values are lower for the compatibilized MS/PVA thin films compared to TP thin film. This behaviour suggests that there is a significant ($p < 0.05$) effect of the chemical modification of cassava starch on the variation of mechanical properties. Also, this observation can be attributed to the crosslinking that occurred among the components in the presence of malic acid which built a rigid dense structure while making it difficult to break them. Furthermore, the crosslinking reactions could reduce the mobility of the polymer chains due to the formation of covalent bonds which consequently reduce the $\varepsilon\%$ as evidenced by DMA results. Another reason for the improved TS and reduced $\varepsilon\%$ in MS/PVA compatibilized blends can be ascribed to the interpenetration network structure formed which makes it difficult for segments of polymer chains to undergo motion. These observations suggest that silica has acted as a reinforcement of the mechanical properties of films. And these results are in conformity with the studies carried out by [3, 19].

In contrast, in spite of maintaining the same modified starch amount, a gradual increase in TS and a gradual reduction in $\varepsilon\%$ can be evident from Table 3 for the compatibilized MS/PVA blended thin films along with the increased addition of malic acid and such behaviour could be due to the increased degree of crosslinking at elevated acid concentration. Moreover, the compatibilization in the blend films was enhanced with the increased addition of malic acid and this is in agreement with SEM observations. Also, the increase in TS is in agreement with the variation of RC values. Interestingly, according to Table 3, it is visible that one can increase the starch content in the blend film while incorporating a small amount of compatibilizer for the purpose of cost reduction without sacrificing the tensile properties of the blend.

3.9 Water Absorption (WA) of Modified Starch/PVA Blended Thin Films

In order to prevent spoilage of food or other items, it is expected that the films must be waterproof. Therefore, the reduction of moisture sensitivity is of high importance [27]. Moisture absorption is considered to be an important factor when dealing with hydrophilic thermoplastics since high water absorption capacities worsen the mechanical properties of a polymer [14]. One of the major drawbacks associated with starch-based materials is their water sensitivity which causes poor storage stability [32, 45]. Furthermore, it is a well-known fact that water is a plasticizer for starch and water absorption leads to the reduction of T_g with increased mobility, and consequently, starch molecules tend to reorganize and aggregate themselves [29]. Therefore, improvement in reducing the water sensitivity of cassava starch-based thin

films is of paramount importance in order to enhance their usage in practical applications [36]. As reported by [47], water absorption is a measure of hydrophilicity and it highly depends on the nature and structure of the polymers, availability of hydroxyl groups, crosslinkers used, temperature, and ease of diffusion of water molecules across the thickness of the films [1, 29].

Both native cassava starch and PVA are hydrophilic polymers due to the multiple hydroxyl groups along with their backbones [1, 2, 36] . Table 3 enumerates the water absorption capacities of the prepared thin films. As can be seen from Table 3, the lowest water uptake was exhibited by neat TPS film while the highest water capture capacity was demonstrated by neat TPS film. Similar observations were previously noted by Luo et al. [2]. Such behaviour can be explained by that the density of hydroxyl groups on starch molecules is larger than that on PVA molecules causing greater hydrophilicity of starch than that of PVA [43]. On the other hand, the addition of starch into the PVA matrix caused an increase in water absorption capacity and the results are in conformity with previous studies conducted by [39, 40].

Apart from the above observations, as can be evident from Table 3, the water absorption capacity of neat MS film is lower compared to that of neat TPS thin films. Also, the water absorption capacities of MS/PVA blended films are lower compared to those of their respective TPS/PVA thin films. Such behaviour can be attributed to the consumption of hydroxyl groups in the native starch structure during the chemical modification process which consequently reduced the hydroxyl groups available to combine with water molecules in the surrounding (see Fig. 1) as confirmed by FTIR and due to the prevention of water molecules from penetrating through the films due to the rigid structure obtained by incorporating silica. Moreover, the increase in relative crystallinity in the neat MS film and the MS/PVA blends compared to TP blend might also be a reason for the increase in water resistivity owing to the reduction in amorphous areas in the film matrix which promotes lower water uptake as in accordance with XRD data.

Furthermore, the results revealed that water absorption of compatibilized MS/PVA films was lower compared to MP thin film. Interestingly, the water uptake gradually decreased along with the increased incorporation of malic acid as the compatibilizing agent. The reduction in water absorption can be explained under the following hypothesis.

(i) Crosslinking between COOH on organic acids and hydroxyl groups on cassava starch, PVA, and glycerol molecules occurred during the curing of films in the oven: The consumption of available hydroxyl groups on the macromolecular structure during crosslinking reactions reduces the probability of forming hydrogen bonds between the OH– groups available in the blend matrix and water molecules in the environment thereby reducing the water uptake [4, 19, 21, 46]. The reduction in water uptake with the increased addition of malic acid can be attributed to the enhanced crosslinking degree which further reduces the hydroxyl groups on the polymer structure.

(ii) The increase in the relative crystallinity of the compatibilized blends: Usually, the water molecules preferably permeate through the amorphous areas of a

polymer. However, according to XRD results, the RC of compatibilized blends increased compared to that of the pure blend and this reduction in amorphous areas in the compatibilized blends could decrease the water uptake. Similar observations were previously stated by [31, 45, 49]. Moreover, the reduced water capture ability of films with elevated acid concentrations might be due to the gradual increase in RC with the increased addition of compatibilizers. These results agree with Panaitescu et al. [40].

(iii) The tortuous pathway created via the esterified and/or crosslinked system which makes the diffusion of water molecules across the film matrix more difficult: A dense polymer network structure is formed via crosslinking in the presence of malic acid as the compatibilizer (see Fig. 8) Also, the spacing between the polymer chains was reduced resulting in the reduction of the free volume. As a result, water molecules were prevented from penetrating into the films, and thus, reducing the water sensitivity. Similar explanations were also reported by [12, 13, 19, 21, 31, 45] for the reduction of water uptake by starch-based blends. Furthermore, the esterification and/or crosslinking reactions restricted the mobility of the polymer chains (see DSC analysis and DMA data) which could make difficult the diffusion of water across the film matrix.

On the contrary, a remarkable decrease in the water uptake performance can be observed in all the compatibilized MS/PVA films compared to TP film. This observation suggests that this increase in water resistivity was obtained upon chemical modification of cassava starch. This reduction in water uptake in these MS/PVA films can be supported by the following reasons apart from the previously mentioned three hypotheses.

(i) Further consumption of hydroxyl groups in native cassava starch upon chemical modification using TEOS (see Fig. 1).
(ii) Further promotion of tortuous path with the incorporation of rigid silica into the blend matrix which eventually reduces the diffusion of water molecules across the film.

Reduction in water uptake in silica-incorporated starch/PVA blended thin films was also previously reported by [3, 16, 19]. Besides, the least water absorption capacity was demonstrated by MP-5 blended thin film valuing 28.89 and 42.17% at 2 and 24 h, respectively.

3.10 Degradation Behaviour

Especially, PVA and starch are biodegradable materials owing to their hydro stability that undergoes a reduction in molecular weight by hydrolysis depolymerization [3, 16]. In general, the biodegradation rate of starch-based films depends on the factors such as water absorption by the film, temperature, microbial population, and the amount of starch incorporated in the film matrix [13, 30]. Besides, the

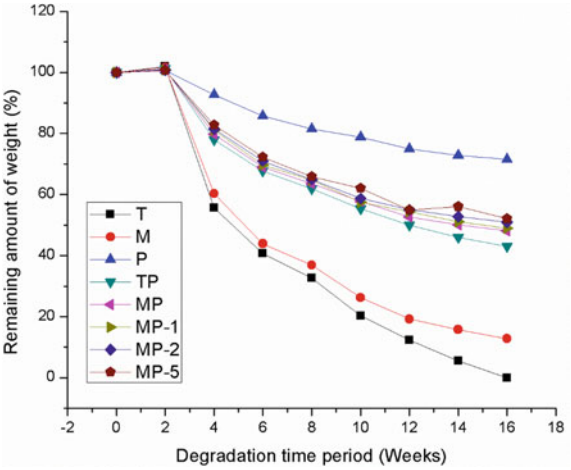

Fig. 6 Variation of the remaining amount of weight (%) of prepared films during the degradation time period

factors affecting the degradation of crosslinked films are, namely, the presence of free hydroxyl groups, relative crystallinity, and the ease of breaking the crosslinked points during the degradation process [25].

Figure 6 depicts the remaining weight of the prepared thin film samples as a function of the degradation time period, and the biodegradability after 4 months of the films is enumerated in Table 3. According to Fig. 6, it can be observed that, during the first two weeks, the weight of all the test specimens slightly increased due to the water absorption by the films owing to their hydrophilic nature of them as previously observed by [1, 2, 19, 21, 29]. Also, during this stage, the adaption of the microorganism population to the new polymeric environment occurs as reported by Parvin et al. [41].

As depicted in Fig. 6, neat TPS film degraded rapidly within the initial 4 weeks and a complete degradation was achieved after 16 weeks. Similar observations were noted by Magalhaes et al. [29]. On the contrary, the neat MS film exhibited a slower degradation behaviour compared to that of neat TPS film and such observation might be due to the reduction of infiltration velocity of microorganisms owing to the dense structure of neat MS film caused by the addition of silica during chemical modification. Similar observations were previously reported by [7, 16, 19, 35] for silica-incorporated starch-based films. Moreover, the reduction of water uptake by the neat MS film might also be due to the elimination of –OH groups in starch structure upon modification which hinders the water uptake and thereby reduces the microorganism growth. However, the neat PVA film exhibited the highest resistance against degradation as observed by [7] and such behaviour can be attributed to the chemical structure of PVA (unknown stereoregularity of OH– groups) [35] and due to the vinyl polymer in which the backbones are joined by the C–C linkages as previously noted by [1].

As demonstrated in Fig. 6, blended thin films exhibited an intermediate degradation profile between that shown by both the pre-polymeric films and this behaviour is in accordance with [35]. On the contrary, for all the film samples except for

neat PVA film, the weight loss after the first two weeks was mainly caused by the gradual breakdown of starch molecules in the presence of glycosidases and amylases which are responsible for the cleavage of glycosidic bonds and starch hydrolyzing as reported by [30, 35]. Furthermore, all the blended films exhibited a rapid degradation within the initial 60 days, followed by a slow degradation until the end of the experiment (120 days). Similar experimental results were reported by [14]. Also, the results indicate that the blends of PVA with starch enhance the biodegradability of the polymer matrix through starch degradation. These findings are in conformity with the previously published data by [30, 35].

Interestingly, according to Table 3, the degradation rates of MS/PVA films are lower compared to TP thin film sample. This behaviour could be ascribed to the increased relative crystallinity of MS/PVA films than native starch/PVA film which reduces the amorphous areas for the penetration of water molecules and the elimination of hydroxyl groups in starch structure which further reduces the moisture absorptivity resulting in lower microorganism growth. Also, the infiltration of the microorganisms through the MS/PVA films might be decreased due to the dense structure formed by the incorporation of silica into the blend matrix. On the contrary, as can be visible from Table 3, the degradation rates of compatibilized MS/PVA thin films are lower than that of the pure MS/PVA film. This is due to the increased RC and the dense structure formed via crosslinking. These findings are in conformity with the previous studies conducted by [16]. Despite the fact that the degradability slightly decreased at elevated compatibilizer, the effects were not significant.

Together with the literature, it can be proposed that a two-stage degradation has taken place in the aerobic compost environment test; (i) swelling of the samples and the growth of microorganisms due to diffusion of water into the film samples, and (ii) weight loss and the disruption of the film samples via enzymatic degradation [22, 27].

3.10.1 Determination of the Optimum Film Composition

For the preparation of a particular bioplastic, the water absorption capacity should be lower as much as possible while the tensile strength should be higher. According to Table 5, the optimum film composition was determined as MS/PVA (40/60) film compatibilized with 5 wt.% malic acids which represented the highest TS value of 36.25 MPa and the lowest water uptake at 24 h valuing 42.17% among the investigated samples. In contrast, it is important to note that the other essential properties including the thermal properties and elongation at break of the optimum film composition (MP-5) are comparable with the market-available packaging materials (see Table 4).

3.10.2 Variation of Dynamic Mechanical Properties (DMA Studies)

DMA is an analytical technique widely used to determine material properties. DMA is considered to be an intricate way of determining the interactions between different

components at molecular motion, which has a close relationship with the chain structures of polymeric materials [5, 24]. This analytical technique measures the deformation of a material in response to vibrational forces. In general, DMA measures the viscoelastic behaviour of a polymer and expresses qualitative results for the storage modulus (G') and the corresponding loss modulus (G''). Apart from the above, the loss factor (tan δ) can be expressed as the quotient of loss and storage modulus $\left(G''/G'\right)$ (Sreedhar et al. 2016). G' is a measurement of the stiffness (rigidity) of a polymer [25]. On the other hand, G' is a measure of mechanical energy stored under load (Sreedhar et al. 2016; Olivato et al. 2013). Tan δ is a damping term expressed as the ratio of energy dissipated as heat to the maximum energy stored in a particular material while it is an index of the material's viscoelasticity [25]. According to the literature, the size of the tan δ peak is related to the volumetric fraction of the material that undergoes transition [25]. Furthermore, in DMA studies, the peak temperature of the δ curve represents the glass transition temperature above which a significant chain motion takes place of a certain polymer [49].

Herein, the DMA studies were carried out only for the optimum film composition (MP-5) determined in Sect. 3.11, pure MS/PVA blended film (MP), neat TPS film, and neat PVA film. Figure 7 demonstrates the plots of storage modulus (G'), loss modulus (G''), and tan δ versus temperature for the aforementioned thin film samples. It can be evidenced from Fig. 7a that the storage modulus for all the film samples gradually decreased with the increase in temperature. This indicates that the mechanical strength gradually decreased at elevated temperatures. Also, this behaviour meant that all the film samples became softer at higher temperatures. Similar observations were previously reported by [25] for $CaCl_2$-incorporated TPS/PVA thin films. As shown in Fig. 7a, MP film exhibited higher storage modulus values within the whole temperature range compared to that of neat TPS film since both modified cassava starch and PVA are capable of forming hydrogen bonds which acted as physical crosslinks while generating stiffness to the blend material as noted by Sreedhar et al. (2016). Interestingly, the MP-5 blended thin film performs higher storage modulus values compared to that of MP film and this suggests that the incorporation of the crosslinking agent as the compatibilizer into the MS/PVA matrix helped to store a larger amount of elastic energy during dynamic loading at the whole temperature range analysed. Such behaviour can be attributed to the increase in relative crystallinity for the crosslinked films compared to those of their respective pure blend (see Sect. 3.6.2). Similar observations were previously reported by [30, 34, 46]. In contrast, higher storage modulus values reflect the difficulty of movement of the molecular chains as stated by [39], and these results are in agreement with mechanical property data and DSC studies.

Besides, as illustrated in Fig. 7b, the loss modulus values were lower for the compatibilized blend when compared to the pure blend and such observation is due to the closely packed molecules via crosslinking in the presence of phthalic acid while forming a rigid network not allowing much viscous dissipation as previously stated by [39].

According to the literature, several factors including main chain rigidity, percentage of moisture content, crosslinking density, and the chemical structure of the

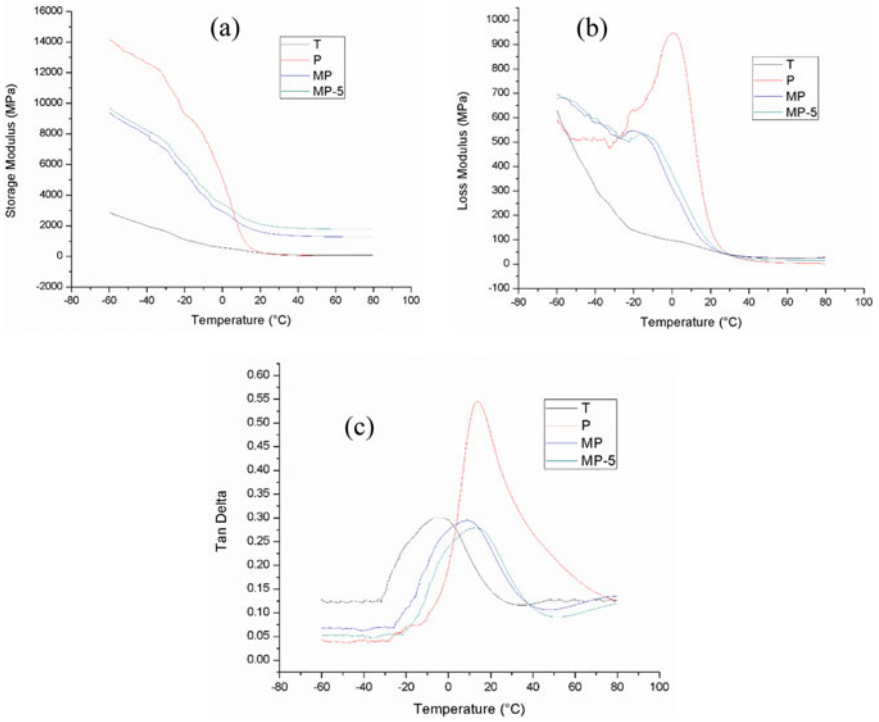

Fig. 7 Plots of **a** storage modulus, **b** loss modulus, and **c** tan δ versus temperature

crosslinkers introduced influence the T_g of crosslinked films (Sreedhar et al. 2006). As can be evidenced from Fig. 10c, the peak temperature of the tan δ curve, in other words, the T_g value increased in the compatibilized blend (15.17 °C) compared to that of the pure blend (10.77 °C). This increment in T_g showed that the chain mobility of both starch and PVA decreased in the presence of malic acid as the compatibilizer. Moreover, a single T_g value was observed for the non-compatibilized film indicating the miscibility of modified starch and PVA which is in conformity with DSC and SEM observations. Similar behaviour was previously reported by [25]. The increase in T_g suggests that the crosslinked film was more resistant to higher temperatures than the non-compatibilized counterpart. Moreover, the T_g value of neat PVA film was measured to be 22.3 °C and this value is in accordance with the previously reported value for T_g of PVA film (21.8 °C) using the DMA technique by Wang et al. (2017). However, it should be noted that the T_g values obtained using the DMA analysis for the neat PVA film, MP-0, and MP-5 blended thin films differ from the values obtained using the DSC analytical method (see Table 4). This difference in T_g values might be due to the difference between the two analytical methods as noted by [25], and the discrepancy observed in the T_g values can be ascribed to the principals involved in the methods of measurement and different constraints on sample and heating rates.

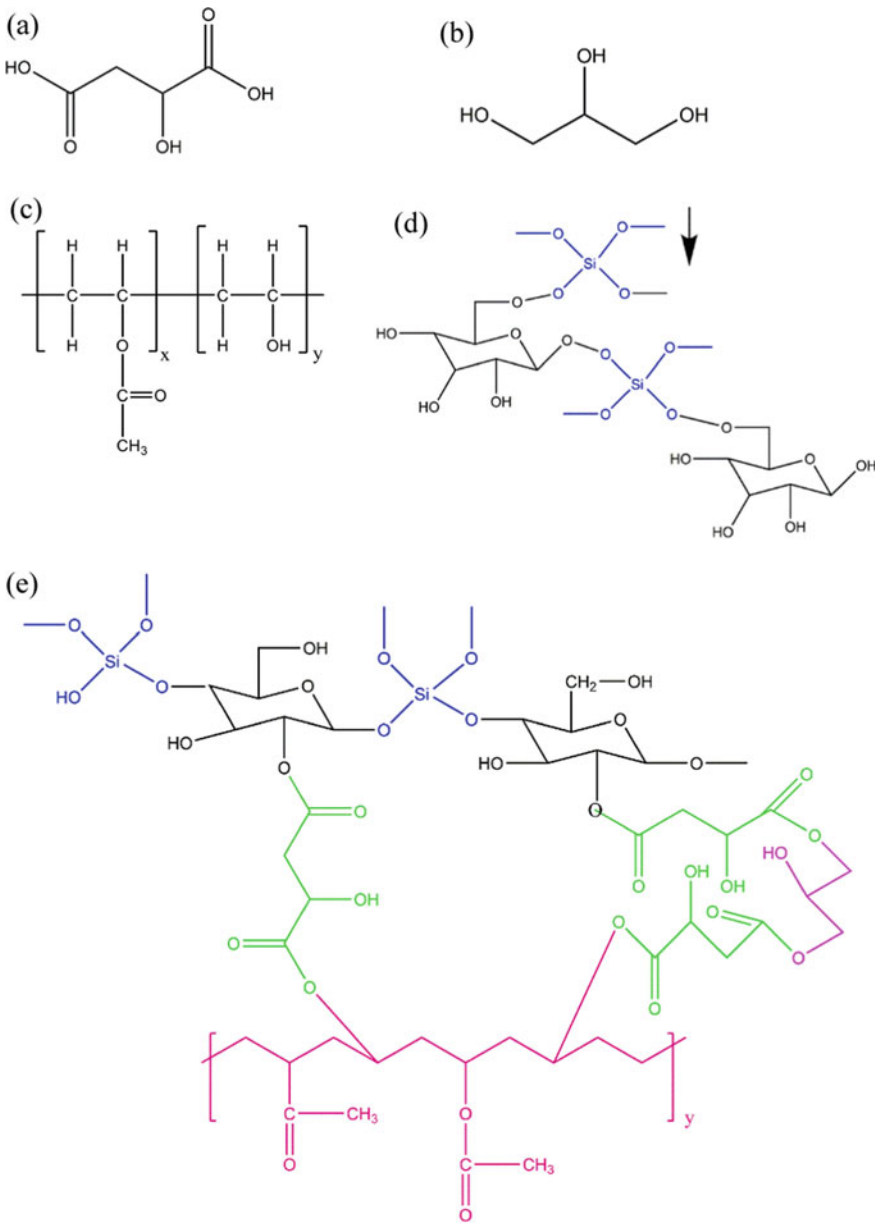

Fig. 8 Possible structure of the crosslinked system within the blend matrix

Apart from the above observations, the blends demonstrated a notable decrease in storage modulus over the glass transition temperatures and this decrease suggests that the material was becoming less elastic or conversely more permanently deformable as noted by Ren et al. (2009). On the contrary, as can be seen from Fig. 7(c), the peak volume of tan δ is smaller for the compatibilized blend compared to that of the pure blend and this reflects that a smaller portion is undergoing a transition in the compatibilized MS/PVA thin film. This behaviour can also be ascribed to the decrease in the amorphous fraction in the crosslinked film as mentioned in Sect. 3.6.2. Moreover, the reduction in tan δ peak volume exhibits the reduction in chain mobility in the compatibilized blend. In addition, the lower intensity of the tan δ peak in the MP-5 blended thin film also indicates less movement of the molecular chains as stated by [3], and this is in conformity with mechanical property and DSC data.

According to the above results, from the storage modulus, loss modulus, and tan δ curves, the compatibilized blend showed better thermo-mechanical properties compared to that of the pure counterpart. Interestingly, it can be evident that these results are similar to those of the variations of tensile strength and elongation at the break while the data positively correlated to tensile strength and elongation at break values.

3.10.3 Modelling of Preferred Interactions

In this section, a conceptual model was developed for the preferred interactions in the MS/PVA blended thin films compatibilized with malic acid. The FTIR analysis confirmed that PVA used in this study has been partially hydrolyzed during the manufacturing process and due to the reduction of hydrogen bonding interactions within the components in the blend matrix crosslinking among the molecules has taken place in the presence of malic acid as the compatibilizer. The chemical structures of modified cassava starch, partially hydrolyzed PVA, glycerol, and malic acid are illustrated in Fig. 8a, b, c, d, respectively, whereas the possible structure of crosslinked system via covalent bonds is demonstrated in Fig. 8e. Besides, according to the chemical structure of malic acid, it is a dicarboxylic acid and it is able to perform esterification and crosslinking reactions.

3.10.4 Comparison of the Essential Properties of the Optimum Film Composition with Market-Available Packaging Materials

Table 4 depicts the comparison of the essential properties of packaging materials produced using currently available non-degradable polymeric materials in the market. Interestingly, according to the data tabulated in Table 4, the thickness, density, mechanical properties (TS and $\varepsilon\%$), and thermal properties (T_g, T_m, $T_{d,}$ and char residue) in compatibilized MS/PVA thin films are comparable with those of PE, LDPE, HDPE, LLDPE, PVC packaging, and black trash bags. However, the water absorption capacity of the optimum film in the present study is still quite higher

compared to other conventional plastic materials, and hence, the improvement of water resistivity is of great importance. Therefore, these prepared films can be utilized as packaging materials that contact with materials with low moisture contents, and thus, cassava starch-based biodegradable films prepared in this study are more feasible from an industrial viewpoint for packaging applications.

4 Conclusion

In this study, chemically modified cassava starch-based thin films were fabricated successfully via solution casting technique using cassava starch, PVA, and glycerol as the plasticizer and malic acid as the compatibilizing agent. The chemical modification of cassava starch helped to reduce the hydrophobicity of starch due to the consumption of hydroxyl groups during the modification process. With the increased addition of malic acid, increased homogeneity of the blend films was attained. The conceptual model of crosslinking interactions within the blend matrix in the presence of malic acid could be used to explain the resulting mechanical, thermal, and water capture behaviours. In contrast, the biodegradation was somewhat slowed down upon both starch modification and compatibilization. The results of this study have effectively demonstrated that malic acid can be used as a successful compatibilizer for starch/PVA blends. Further, a small amount of compatibilizing agent is sufficient for a remarkable improvement in essential properties of polymeric blends. Moreover, it can also be expected that malic acid could act as a compatibilizer for other biodegradable polymers such as cellulose and polyacrylic acid that contain a lot of hydroxyl groups. The potential low-cost and easy preparation route of compatibilized starch-based thin films possessing enhanced structural, thermal, mechanical, and water-resistant properties can be seen as a low-cost 'green' substitute for packaging applications. Besides, these prepared thin film materials can be a solution to problems due to solid waste accumulation as well as to meet the demand of global requirements. Undoubtedly, the research on the compatibilization of starch/synthetic biodegradable polymer blends will continue to rise in the near future. Future research should focus on starch-based blends that possess better water barrier properties with cost competitiveness with existing non-biodegradable materials for industrial-scale applications.

Acknowledgements The authors sincerely acknowledge the encouragement and guidance provided by all the members of the academic and non-academic staff of the Department of Chemical and Process Engineering, University of Peradeniya. The authors would like to acknowledge the support from Ms. W.M.W.K. Weerasekara from the Department of Chemical & Process Engineering, Faculty of Engineering, University of Peradeniya. The authors wish to express their sincere appreciation to Accelerating Higher Education Expansion and Development (AHEAD) for the financial assistance (AHEAD/RA3/PDN/ENG/DOR/65).

References

1. Jayasekara R, Harding I, Bowater I, Christie GBY, Lonergan GT (2004) Preparation, surface modification and characterization of solution cast starch/PVA blended films. Polym Test 23:17–27
2. Luo X, Li J, Lin X (2012) Effect of gelatinization and additives on morphology and thermal behaviour of corn starch/PVA blend films. Carbohydr Polym 90:1595–1600
3. Ismail H, Zaaba NF (2011) Effect of additives on properties of polyvinyl alcohol (PVA)/tapioca starch biodegradable films. Polym-Plast Technol Eng 50:1214–1219
4. Popescu MC, Dogaru BI, Goanta M, Timpu D (2018) Structural and morphological evaluation of CNC reinforced PVA/starch biodegradable films. Biol Macromol
5. Gupta VK, Priya B, Pathania D, Singh SA (2014) Synthesis, characterization and antibacterial activity of biodegradable starch/PVA composite films reinforced with cellulosic nanofiber. Carbohydr Polym
6. Yoon SD (2013) Cross-linked potato starch-based blend films using ascorbic acid as a plasticizer. J Agricul Food Chem 62:1755–1764
7. Zanela J, Blick AP, Casagrande M, Grossmann MVE, Yamashita F (2018) Polyvinyl alcohol (PVA) molecular weight and extrusion temperature in starch/PVA biodegradable sheets. Polimeros 28(3):256–265
8. Abioye OP, Abioye AA, Afolalu SA, Ongbali SO (2018) A review of biodegradable plastics in Nigeria. Int J Mech Eng Tech 9:1172–1185
9. Ahmed J, Tiwari BK, Iman SH, Rao MA (2012) Starch-based polymeric materials and nanocomposites; chemistry, processing, and applications, CRC Press, 13, 978-1-4398-5177-3
10. Cano AI, Chafer M, Chiralt A, Martines CG (2015) Physical and microstructural properties of biodegradable films based on pea starch and PVA. J Food Eng
11. Das K, Ray D, Bandyopadhyay NR, Gupta A, Sengupta S, Sahoo S, Mohanty A, Misra M (2010) Preparation and characterization of cross-linked starch/poly (vinyl alcohol) green films with low moisture absorption. Ind Eng Chem Res 49:2176–2185
12. Jayakumar A, Heera KV, Sumi TS, Joseph M, Mathew S, Praveen G, Nair IC, Radhakrishnan EK (2019) Starch-PVA composite films with ZnO-nanoparticles and phytochemicals as intelligent pH sensing wraps for food packaging applications. Int J Biol Macromol 136:395–403
13. Lima KO, Biduski B, Silva B, Ferreira WMF, Montenegro LM, Dias ARG, Bianchini D (2017) Incorporation of tetraethylorthosilicate (TEOS) in biodegradable films based on bean starch (Phagelous Vulgaris). Europ Polym J
14. Yao K, Cai J, Liu M, Yu Y, Xiong H, Tang S, Ding S (2011) Structure and properties of starch/PVA/nano-SiO2 hybrid films. Carbohydr Polym 86:1784–1789
15. Zhou J, Ma Y, Ren L, Tong J, Liu Z, Xie L (2009) Preparation and characterization of surface crosslinked TPS/PVA blend films. Carbohydr Polym 76:632–639
16. Khan MA, Battavharia SK, Kadir MA, Bahari K (2006) Preparation and characterization of ultra violet (UV) validation cured biodegradable film of sago starch/PVA blend. Carbohydr Polym 63:500–506
17. Sreedhar B, Sairam M, Chattopadhyay DK, Rathnam PAS, Rao DVM (2005) Thermal, mechanical and surface characterization of starch-poly (vinyl alcohol) blends and borax-crosslinked films. J Appl Polym Sci 96:1313–1322
18. Aji W, Purwanto P, Suherman S (2018) Good housekeeping implementation for improving efficiency in cassava starch industry (Case study: Margoyoso District, pati Regem), E3S Web of Conference, 31, 05011
19. Kochkina NE, Butikova OA (2019) Effect of fibrous TiO_2 filler on the structural, mechanical, barrier and optical characteristics of biodegradable maize starch/PVA composite films. Int J Biol Macromol 139:431–439
20. Wang W, Zhang H, Jia R, Dai Y, Dong H, Hou H, Guo Q (2017) High performance extrusion blown starch/polyvinyl alcohol clay nanocomposite films. Food Hydrocolloids
21. Tang XZ, Alavi S (2011) Recent advances in starch, polyvinyl alcohol-based polymer blends, nanocomposites and their biodegradability. Carbohydr Polym 85:7–16

22. Guohua Z, Ya L, Cuilan F, Min Z, Caiqiong Z, Zangdao C (2006) Water resistance, mechanical properties and biodegradability of methylated-cornstarch/poly (vinyl alcohol) blend film. J Polym Degrad Stab 91:703–711
23. Gunawardene OHP, Gunathilake CA, Amaraweera APSM, Fernando NML, Manipura A, Manamperi WA, Kulatunga KMAK, Rajapaksha SM, Gamage A, Dassanayake BGND, Weerasekara PNK, Fernando CAN, Jayasinghe JASC (2021a) Removal of Pb(II) ions from aqueous solution using modified starch. J Compos Sci 5:46
24. Jiang X, Jiang T, Gan L, Zhang X, Dai H, Zhang X (2012) The plasticizing mechanism and effect of calcium chloride on starch/poly (vinyl alcohol) films. Carbohydr Polym 90:1677–1684
25. Maiti S, Ray D, Mitra D (2012) Role of crosslinking on the biodegradation behaviour of starch (polyvinyl alcohol) blend films. J Polym Environ 20:749–759
26. Utrilla-Coello RG, Hernandez-Jaimes C, Carillo-Naves H, Gonzales F, Rodriguez E, Bello-Perez LA, Vernon-Carter EJ, Alvarez-Ramirez J (2014) Acid hydrolysis of native corn starch: morphology, crystallinity, rheological and thermal properties. Carbohydr Polym 103:596–602
27. Hiremani VD, Sataraddi S, Bagannavar P, Gasti T, Masti S, Kamble R, Chougale RB (2020) Mechanical, optical and antioxidant properties of 7-Hydroxy-4-methyl coumarin doped polyvinyl alcohol/oxidized maize starch blend films. SN Appl Sci 2:1877
28. Akrami M, Ghasemi I, Azizi H, Karrabi M, Segedabadi M (2016) A new approach in compatibilization of the poly (lactic acid)/thermoplastic starch (PLA/TPS) blends. J Carbohyd Polym 144:254–262
29. Magalhaes NF, Dahmouche K, Lopes GK, Andrade CT (2013) Using an organically-modified montmorillonite to compatibilize a biodegradable blend. J Appl Clay Sci 72:1–8
30. Widiarto S (2005) Effect of Borax on mechanical properties and biodegradability of sago starch-poly (vinyl alcohol) Blend films. J Sains Tek 11:151–157
31. Pour ZS, Makvandi P, Ghaem M (2015) Performance properties and antibacterial activity of crosslinked films of quaternary ammonium modified starch and poly (vinyl alcohol). Int J Biol Macromol 80:596–604
32. Gunawardene OHP, Gunathilake C, Amaraweera SM, Fernando NML, Wanninayaka DB, Manamperi A, Kulatunga AK, Rajapaksha SM, Dassanayaka RS, Fernando CAN, Manipura A (2021b) Compatibilization of starch/synthetic biodegradable polymer blends for packaging applications: a review. J Comp Sci 5:300
33. Zhai X, Wang W, Zhang H, Dai Y, Dong H, Hou H (2020) Effects of high starch content on the physiochemical properties of starch/PBAT nanocomposite films prepared by extrusion blowing. J Carbohydr Polym 239:116231
34. Karagoz S, Ozkoz G (2013) Effects of a diisocyanate compatibilization on the properties of citric acid modified thermoplastic starch/poly (lactic acid) Blend. J Polym Eng Sci 2183–2193
35. Chiellini E, Cinelli P, Chiellini F, Imam SH (2004) Environmentally degradable bio-based polymeric blends and composites. Macromol Biosc 4:218–231
36. Aryapham J, Boonsuk P, Chantarak S (2020) Enhancement of water barrier properties of cassava starch-based biodegradable films using silica particles. Iran Polym J
37. Amaraweera SM, Gunathilake C, Gunawardene OHP, Fernando NML, Wanninayaka DB, Manamperi A, Dassanayaka RS, Rajapaksha SM, Gangoda M, Fernando CAN, Kulatunga AK, Manipura A (2021b) Preparation and characterization of biodegradable casava starch thin films for potential food packaging applications. Cellulose
38. Junlapong K, Boonsuk P, Chaibundit C, Chantarah S (2019) Highly water-resistant cassava starch/poly (vinyl alcohol) films. Int J Biol Macromol
39. Jose J, Shehzad F, Al-Harthi MA (2014) Preparation method and physical, mechanical, thermal characterization of poly (vinyl alcohol)/ poly (acrylic acid) blends. Polym Bullet 71:2787–2802
40. Panaitescu DM, Frone AN, Ghuirea M, Chiulan I (2015) Influence of storage conditions on starch/PVA films containing cellulose nanofibers. Ind Crops Prod 70:170–177
41. Parvin F, Khan MA, Saadat AHM, Khan MAH, Islam JMM, Ahmed M, Gafur MA (2011) Preparation and characterization of gamma irradiated sugar containing starch/poly (vinyl alcohol)-based blend films. J Polym Environ 19:1013–1022

42. Tian H, Yan J, Rajulu AV, Xiang A, Luo X (2017) Fabrication and properties of polyvinyl alcohol/starch blend films: effect of composition and humidity. Int J Biol Macromol 96:518–523
43. Shi R, Zhu A, Chen D, Jiang X, Xu X, Zhang L, Tian W (2010) In vitro degradation of starch/PVA films and biocompatibility evaluation. J Appl Polym Sci 115:346–357
44. Sreekumar PA, Al-Harthi MA, De SK (2012) Effect of glycerol on thermal and mechanical properties of polyvinyl alcohol/ starch blends. J Appl Polym Sci 123:135–142
45. Chen L, Zhai Z, Zhang X, Chen X, Jing X (2010) Compatibility effect of starch-grafted-poly (l-lactide) on the poly (ε – caprolactone)/starch composites. J Appl Polym Sci 117:2724–2731
46. Themissrimuang N, Prachayawarakorn J (2018) Characterization and properties of high amylose mung bean starch biodegradable films cross-linked with malic acid or succinic acid. J Polym Environ
47. Bellelli M, Licciardello F, Pulvirenti A, Fara P (2018) Properties of poly (vinyl alcohol) films as determined by thermal curing and addition of polyfunctional organic acids. Food Packag Shelf Life 18:95–100
48. Ayadi F, Mamzad S, Portella C, Dole P (2013) Synthesis of bis (pyrrolidone-4-carboxylic acid)-based polyamides derived from renewable itaconic acid— application as a compatibilizer in biopolymer blends. Soc Polym Sci 45:766–774
49. Seligra PG, Jaramillo CM, Farma L, Goyanes S (2015) Biodegradable and non-retro gradable eco-films based on starch-glycerol with citric acid as crosslinking agent. Carbohydr Polym

Development of Cellulose Fibre-Reinforced Soil-Based Composite Wall Panels Using Selected Lignocellulosic Materials

M. M. H. Malshan, W. M. I. S. Jayaweera, G. I. P. De Silva, and T. N. Fernando

Abstract The present study focuses on the preparation of composite wall panels, which are prepared by reinforcing three different pretreated lignocellulosic material fibers—bagasse (B), paddy straw (PS), and banana stem (BS). In this study, soil-based composite wall panels were prepared by mixing cement, laterite soil, and lignocellulosic materials in the weight ratios of 1: 1: 0.025 with a certain amount of water. Then, morphological characteristics, water absorption, flexural strength, and thermal conductivity were tested for the prepared wall panels by keeping moulded panels cured for 28 days. The characterization results of moulded wall panels indicate the variation of flexural strength as 1.82–4.02 MPa, percentage of water absorption as 14.9–20.5%, and thermal conductivity as 0.133–0.257 W/mk. Additionally, the characteristics of some moulded wall panels in the present study were at a satisfactory level compared to the available wall panels in the market.

Keywords Wall panel · Composite cement mixer · Lignocellulosic materials · Cellulose fibres

1 Introduction

Sustainable green building material processing is a present trend used to overcome indoor warming through thermal insulation properties of building walls [6, 7]. The clay-mixed materials of the building wall have a certain level of porosity that absorb moisture [15]. When the wall is getting warm during the daytime, the entrapped moisture will be expelled absorbing the heat. Therefore, the walls of the house act as

M. M. H. Malshan (✉) · W. M. I. S. Jayaweera · G. I. P. De Silva
Department of Materials Science and Engineering, University of Moratuwa, Katubedda, Sri Lanka
e-mail: hasinthaugc@gmail.com

T. N. Fernando
National Engineering Research and Development Center of Sri Lanka, Industrial Estate, Ekala, Ja-Ela, Sri Lanka

© The Author(s), under exclusive license to Springer Nature Singapore Pte Ltd. 2023

R. Dissanayake et al. (eds.), *ICSBE 2022*, Lecture Notes in Civil Engineering 362,
https://doi.org/10.1007/978-981-99-3471-3_40

a natural "air conditioner". But surface cracks are formed in clay-mixed walls as they are not reinforced, and this can be prevented by reinforcing with fibres. Accordingly, sustainable building materials are produced by reinforcing with natural cellulose fibers.

In recent years, the usage of natural cellulose fibres as reinforcements in composites has increased [2]. This led to the development of healthy, environmentally friendly, and commercially viable materials with natural resources. With this regard, cement mortar composites, which are reinforced with cellulose fibres are an exciting option for the construction industry. Cellulose fibres exhibit many essential advantages, such as wide availability, bio-renewability, ability to be recycled, biodegradability, nonhazardous material, zero carbon footprint, and good physical and mechanical properties. When asbestos fibres are replaced with cellulose fibres as a reinforcement in composites, some benefits such as higher bonding strength, toughness, tensile strength, compressive strength [8], and low cost can be achieved. Moreover, these fibres can increase thermal insulation, water absorption, and prevent surface cracking [13].

Thus, the indoor environment of some domestic constructions in tropical areas built with relatively lower thermal insulation materials such as cement blocks and cement-sand-based plastering affects uncomfortable living conditions. Therefore, people living in these types of houses face sick building syndromes such as anxiety, depression, and environmental discomfort [3]. However, the selection of earth soil to prepare building materials has some excellent advantages such as higher resistance to fire and lower thermal conductivity, which help to reduce warmness within the building. Further, as cement and sand prices are increasing rapidly, the production cost of cement-based blocks and cement fibre-based plastering has increased significantly. Therefore, soil-based construction materials lead to reduce the demand for sand and cement. In addition, the process of sand extraction from rivers can be minimized, which causes reducing adverse environmental impacts.

This study expects to evaluate the effects of three different lignocellulosic material fibers (bagasse, paddy straw, and banana stem) pre-treated by different concentrations of pre-treatment solutions composed of NaoH and H_2O_2 on the properties of prepared low-cost wall panels.

2 Materials and Methodology

2.1 Materials

Ordinary Portland cement (OPC), industrial grade Sodium hydroxide (NaOH), Hydrogen peroxide (H_2O_2), and Hydrochloric acid (HCl) were purchased from Glorchem Enterprise in Sri Lanka. Lignocellulosic materials—bagasse, paddy straw, and banana stem were collected from different areas in Sri Lanka. Laterite soil was collected from the Gampaha district in the Western province of Sri Lanka.

Table 1 The nine wall panels

Pretreated fibre samples	Wall panels (W)	Materials included in the composite mixer
BC1 [Bagasse (B) × 1.0 mol/L (C1)]	W1	BC1 + Cement + Laterial soil
BC2 [Bagasse (B) × 1.5 mol/L (C2)]	W2	BC2 + Cement + Laterial soil
BC3 [Bagasse (B) × 2.0 mol/L (C3)]	W3	BC3 + Cement + Laterial soil
PSC1 [Paddy straw (PS) × 1.0 mol/L (C1)]	W4	PSC1 + Cement + Laterial soil
PSC2 [Paddy straw (PS) × 1.5 mol/L (C2)]	W5	PSC2 + Cement + Laterial soil
PSC3 [Paddy straw (PS) × 2.0 mol/L (C3)]	W6	PSC3 + Cement + Laterial soil
BSC1 [Banana stem (BS) × 1.0 mol/L (C1)]	W7	BSC1 + Cement + Laterial soil
BSC2 [Banana stem (BS) × 1.5 mol/L (C2)]	W8	BSC2 + Cement + Laterial soil
BSC3 [Banana stem (BS) × 2.0 mol/L (C3)]	W9	BSC3 + Cement + Laterial soil

2.2 Methodology

2.2.1 Pre-Treating of Selected Lignocellulosic Materials

The alkaline peroxide pretreatment process practiced by [2] was used for the pre-treating of Bagasse (B), Paddy Straw (PS), and Banana Stem (BS). According to the AHP pretreatment procedure, they used 10 ml of 1.0 mol/L NaOH and 0.5 ml of 99% commercial grade H_2O_2 for pre-treating 1 g of cornhusk fibers. In the present study, three different NaOH concentrations of 1.0 mol/L (C1), 1.5 mol/L (C2), and 2.0 mol/L (C3) were used to prepare AHP pretreatment solutions for pre-treating selected lignocellulose materials. Then, the pretreated fibres of each pretreatment solution were named in Table 1.

2.2.2 Preparation of Composite Mixtures

Nine composite mixtures were prepared by mixing earth soil (laterite), cement, and nine pretreated fibre samples prepared previously. Homogeneous composite mixtures, each with a weight of 1.875 kg, were prepared by mixing laterite soil, cement, and raw fibre weights, pretreated to a ratio of 1:1:0.025, respectively. The experimental design of the present study was two-factorial. The varying factors were selected from three lignocellulosic materials and three different concentrations of pretreatment solutions. To combine these two factors, the experiment uses nine composite mixtures, which are listed in Table 1. In addition, twenty-seven wall

panels were used in the experiment, preparing three samples from each composite mixture.

After three days, prepared wall panels were removed from the mould and kept for 28 days in a shady place for curing. Then, the prepared samples were characterized to identify the best wall panel samples.

2.2.3 Characterization of Prepared Wall Panels

(a) Morphology analysis

Morphological analysis was performed using Scanning Electron Microscope (SEM)-EVO 18, Carl Zeiss AG. Pores and internal fibre arrangements were observed in all nine wall panel samples and they were compared with each other. Further, Image J software (version 2022) was used to clearly observe the porous structure of SEM images.

(b) Water absorption

Three pieces (100 × 100 mm) were used from the casted composite materials for the testing of water absorption. First, those were dried at 60 °C in an electric oven until the weight became constant. Then, they were immersed in a water tank for 48 h according to the procedure of ASTM C-1185 [12]. The difference in weight was calculated and given as a percentage of water absorbed by the composite material using Eq. (1)

$$\text{Water absorption} = \frac{\text{A} - \text{B}}{\text{B}} \times 100 \tag{1}$$

A = The weight of the specimen after 48 h of immersion, B = The weight of the dry specimen.

(c) Flexural strength

After curing the wall panels for 28 days, the flexural load was tested using an "M350-10AT Test metric universal testing machine" following the procedure of ASTM C-1185 [12]. Wall panels (305 × 152 mm) were subjected to a centerline load kept over a simply supported span of 120 mm (Fig. 1). The load was gradually applied at 5.0 mm/min until the failure of the specimen. After measuring the flexural load, the flexural strength of wall panels was calculated by using Eq. (2).

$$\text{Flexural strength} = \frac{3FL}{2bd^2} \tag{2}$$

F-flexural load, L-the width of span, b-the wall panel width , d-the thickness.

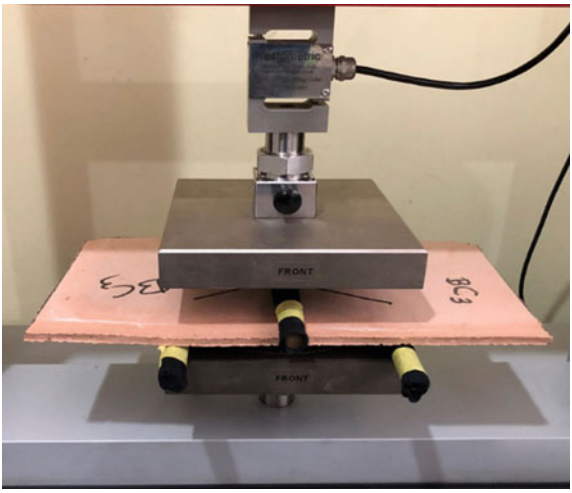

Fig. 1 Measuring the flexural load by M350-10AT Test metric universal testing machine

(d) Thermal conductivity

The Steady-state temperatures of wall panels were measured by Lee's Disc method. The heating plate was heated to 100^0C. According to Fourier's Law, the conductive heat transfer of wall panels was calculated using Eq. (3), and the heat radiated rate was calculated using Eq. (4). The thermal conductivity of wall panels was calculated using Eq. (5).

$$H = \frac{kA(T2 - T1)}{X} \tag{3}$$

$$H = ms\frac{dT}{dt} \tag{4}$$

$$k = \frac{msx}{(T2 - T1)^{\circ}A}\frac{dT}{dt} \tag{5}$$

H	the steady-state rate of heat transfer,
K	thermal conductivity of the sample,
A	the cross-sectional area,
$(T_2–T_1)$	the temperature difference across the sample thickness,
X	the sample thickness,
dT/dt	the rate of cooling at T_1,
m	the mass of the upper disc,
S	specific heat of the upper disc.

2.2.4 Comparison of Properties with the Reference Sample

The properties of the prepared wall panel samples (thermal conductivity, flexural strength, and water absorption) were compared with the reference sample of natural fibre-reinforced cement wall panels [14]. The thermal conductivity, flexural strength, and water absorption values of the reference sample were reported as 0.826 W/mk, 4.15 Mpa, and 10.7% respectively. According to the Sri Lanka standard for concrete roofing semi-sheet [11], the water absorption should be less than 28%.

3 Results and Discussion

3.1 Fibres Extracted from Bagasse, Paddy Straw, and Banana Stem

Table 2 shows the content of extracted fibres. It varies from 74.85 g to 111.48 g. When the concentration of pretreatment solutions increases, the extracted fibre content increases. Banana stem-extracted fibre content is higher than bagasse and paddy straw-extracted fibre, due to their cellulose content being higher than other materials [10].

3.2 Visual Observations of Prepared Walls Panels

Figure 2 shows a non-reinforcement wall panel composed of cement and soil, which showed surface cracking. Figure 3 shows fibers reinforced composite wall panels having a smooth surface and reddish colour.

3.3 Morphological Characteristics

The porous structure of fibre-reinforced wall panel samples was analyzed by applying the Image J software for SEM images (Fig. 4). The pores appear dark coloured and the light-coloured background is composed of a normal composite mixture.

According to the results in Table 2, extracted cellulose fibre content increases with the increasing concentration of pretreatment solutions. Generally, the porous structure of wall panels increases with a larger fibre content [10]. However, it is required to keep the porous structure at a minimum level to improve flexural strength and reduce water absorption. Results showed that samples W1, W4, and W7 have a smaller porous structure compared to the other samples.

Table 2 Pretreated fibre content

Fibre samples	BC1	BC2	BC3	PSC1	PSC2	PSC3	BSC1	BSC2	BSC3
Pretreated fibers content from 150 g of raw fibre	74.85	82.94	85.8	86.37	102.15	106.92	97.22	110.70	111.48

Fig. 2 A Non-reinforcement wall panel composed of cement and soil

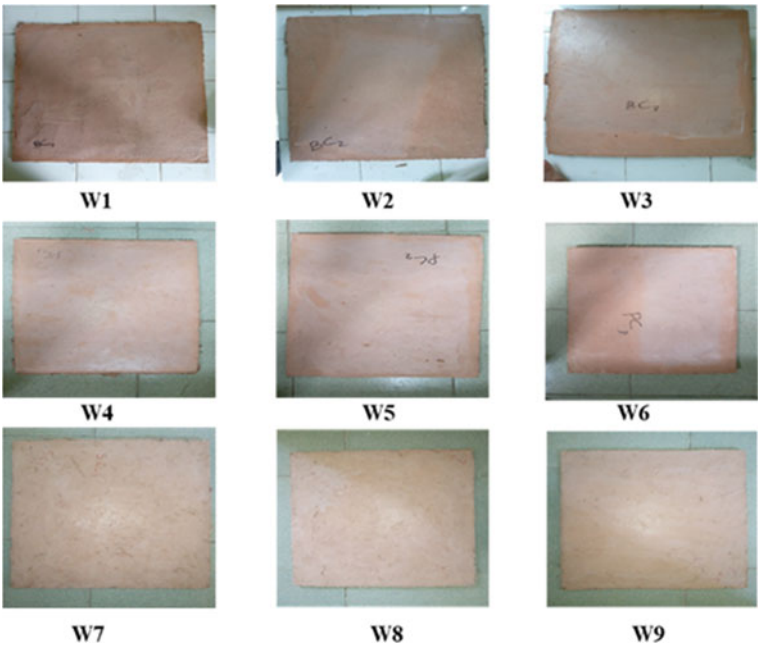

Fig. 3 Prepared fibers reinforced composite wall panels

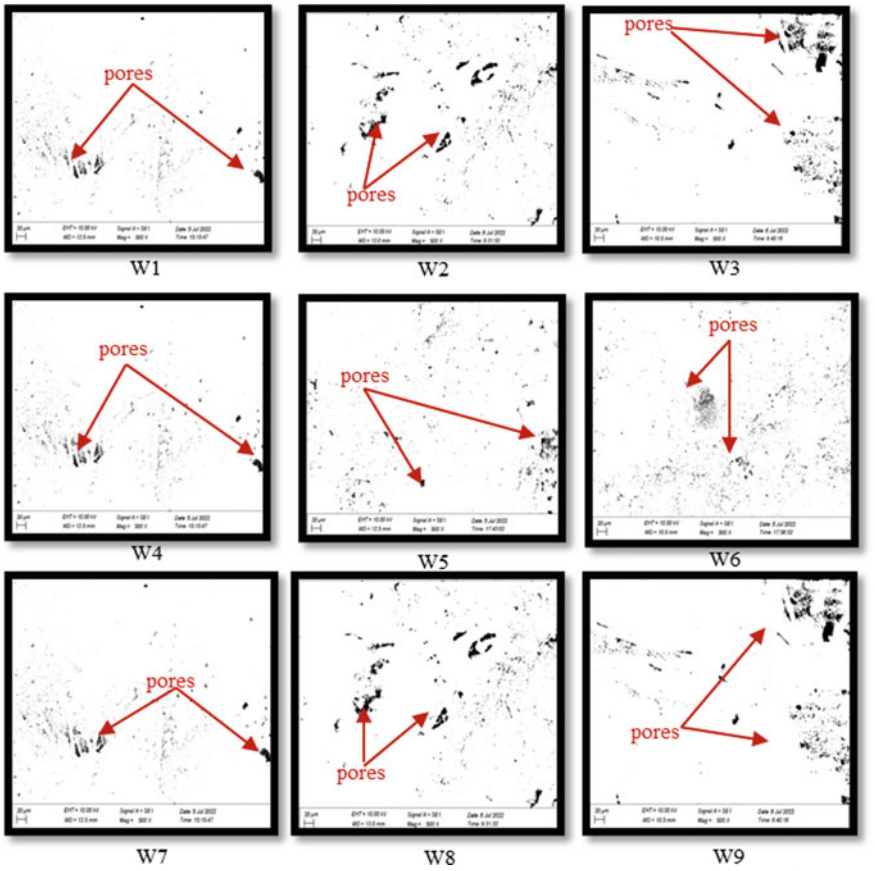

Fig. 4 Analysis of the porous structure of fibre-reinforced wall panel samples with the application of Image J software for SEM image pores

3.4 Water Absorption

The results of the percentages of water absorption are shown in Fig. 5 and it varies between 14.9% and 20.5%. When increasing the pretreatment fibre (cellulose) content in the composite, water absorption increases [9] due to the hydrophilic nature of cellulose fibres. Furthermore, cellulose fibres have a central hollow region, and it allows much water absorption through the capillary effect [1]. The present study showed that for the paddy straw fibre-reinforced composites, water absorption percentages increase to 14.9 and 17.5% with the pretreatment concentrations of C1 and C3, respectively. However, the chemical composition of the raw plant residue also affects the percentage of water absorption. Pretreated paddy straw-added wall panels show lower water absorption compared to banana stem and bagasse-added wall panels due to the high lignin and silicon content of paddy straw.

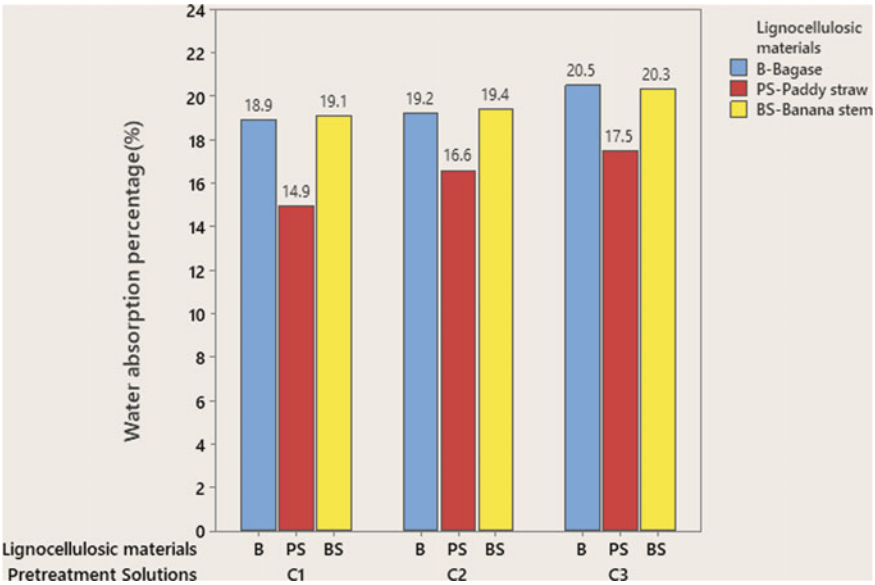

Fig. 5 Variation of percentage of water absorption

3.5 Flexural Strength

Figure 6 shows the variation of flexural strength (1.82–4.02 Mpa) of prepared wall panels with the pretreatment solution concentrations (C1, C2, and C3). The porosity, fibre surface morphology, and fibre–matrix bonding are the main factors that affect the flexural strength of fibre-reinforced composites [4]. Flexural strength reduces with higher pretreatment solution concentrations. With the increase in fibre content, fibre clusters are formed in the composite. Those clusters act as weak points and create lower bonding strength with the matrix. Therefore, wall panels composed of Paddy straw fibres, pretreated with the concentration of C1, show higher flexural strength and lower water absorption compared to other wall panels.

3.6 Thermal Conductivity

The variation of Thermal conductivities (0.133–0.257 W/mk) of prepared wall panels with the pretreatment solution concentrations (C1, C2, and C3) is shown in Fig. 7.

The thermal conductivity of fibre-reinforced composites depends on their density, homogeneity, and morphology. The increasing fibre content in the composite reduces thermal conductivity by decreasing the density of the composite [5]. The results in Fig. 7 show that there is no significant variation in thermal conductivity with different pretreatment solutions. Paddy straw fibre-reinforced composites have higher thermal

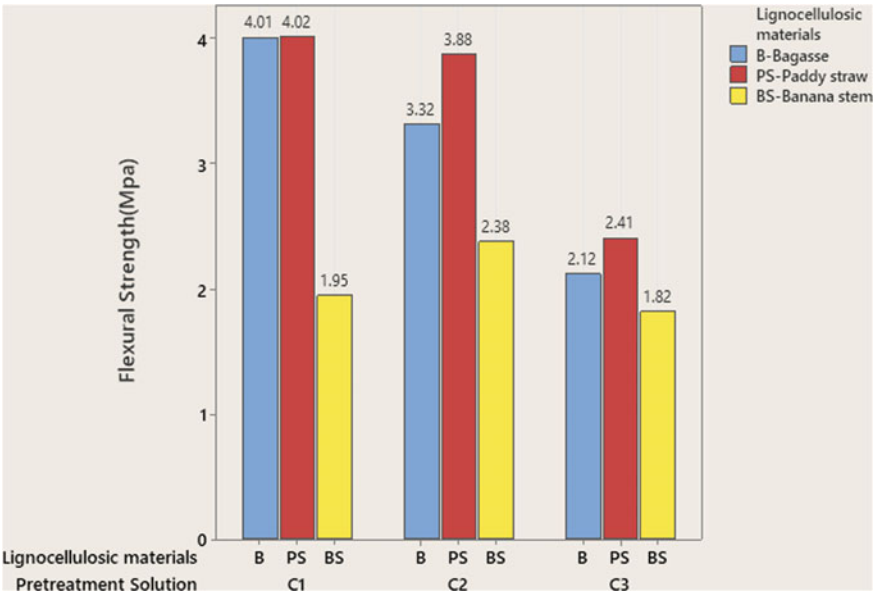

Fig. 6 Variation of flexural strength

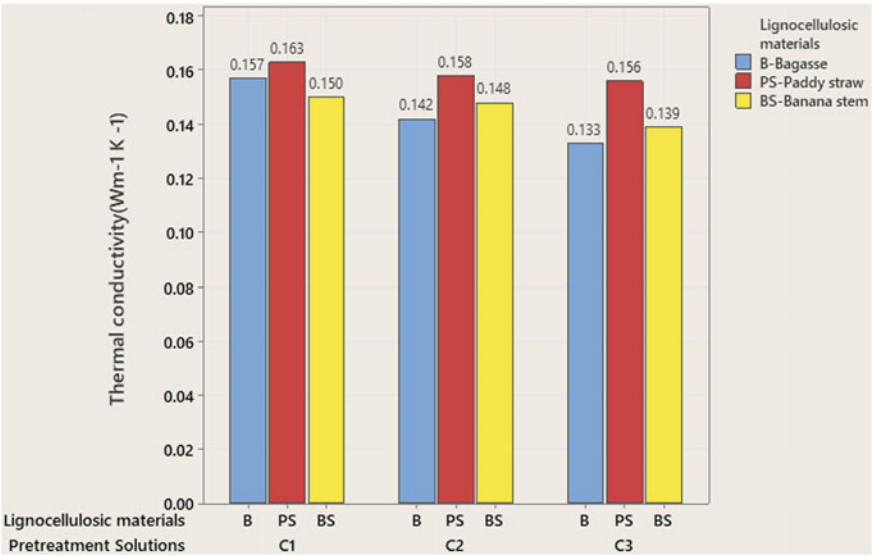

Fig. 7 Variation of thermal conductivity

Table 3 The wall panel properties compared with a reference sample

Wall panels	Flexural strength (Mpa)	Thermal conductivity (W/mk)	Water absorption percentage (%)
Reference sample	4.15	0.826	10.7
W1	4.01	0.157	18.9
W2	3.32	0.142	19.2
W3	2.12	0.133	20.5
W4	4.02	0.163	14.9
W5	3.88	0.158	16.6
W6	2.41	0.156	17.5
W7	1.95	0.150	19.1
W8	2.38	0.148	19.4
W9	1.82	0.139	20.3

conductivity than other fibre-reinforced composites. This is possibly due to the small amount of silica in paddy straw.

3.7 Comparison of Characteristics of Prepared Wall Panels with Standers

Water absorption values of all wall panels are less than the standard maximum value of 28% [11]. Table 3 shows the comparison with reference sample properties.

4 Conclusions

Low-cost green wall panels composed of cement, soil, and three different pretreated lignocellulosic material fibres (bagasse, paddy straw, and banana stem) were prepared.

The highest flexural strength of 4.02 Mpa and the lowest water absorption of 14.9% were reported in the wall panel (W4) which is reinforced with C1 solution pretreated paddy straw. Wall panel (W3) reinforced with C3 solution pretreated bagasse showed relatively higher thermal insulation, which is 0.133 W/mk.

The Wall panel samples of W1 and W4 which were reinforced with C1 solution pretreated bagasse and paddy straw fibres, respectively, have properties closer to the reference sample (flexural strength—4.15 Mpa, water absorption—10.7%, and thermal conductivity—0.826 W/mk). Therefore, these two wall panels (W1, W4) could be utilized as low-cost green wall panels with excellent thermal insulation for building constructions.

Acknowledgements The authors would like to thank Mr. V. Sivahar, head of the Department of Materials Science and Engineering, Dr. A. A. G. A. Abeygunawardana, final year project coordinator, and all the other lecturers of the department for giving us advice and helping with their professional knowledge throughout the project. Also, a special thank goes to the staff of our department and the National Engineering Research and Development Center for supporting us in several ways.

References

1. Alamri H, Low IM (2012) Mechanical properties and water absorption behaviour of recycled cellulose fibre reinforced epoxy composites. Polym Testing 31(5):620–628. https://doi.org/10.1016/j.polymertesting.2012.04.002
2. Fernando TN, Batuwita IP (2022) Reinforcing of earth soil and cement with pretreated cornhusk fibers in the development of building materials. In: 12th international conference on structural engineering and construction management. Springer, Singapore, pp 241–254
3. Ghaffarianhoseini A, AlWaer H, Omrany H, Ghaffarianhoseini A, Alalouch C, Clements-Croome D, Tookey J (2018) Sick building syndrome: are we doing enough? Architect Sci Rev 61(3):99–121
4. Hassan ML, Mathew AP, Hassan EA, El-Wakil NA, Oksman K (2012) Nanofibers from bagasse and rice straw: process optimization and properties. Wood Sci Technol 46(1):193–205
5. Ismail I, Fitri N, Mursal, Fadzullah SHS (2021) Thermal conductivity of rice straw polypropylene particleboard. IOP Conf Ser Mater Sci Eng 1087(1):012073. https://doi.org/10.1088/1757-899x/1087/1/012073
6. Kahandawa Arachchi K, Gamage J, de Silva G (2021) Modification of a bottom ash based insulation material using saw dust, EPS and aggregate chips. In: Lecture notes in civil engineering, pp 451–460
7. Kahandawa Arachchi K, Selvaratnam A, Gamage J, De Silva G (2021) Green composite plaster with modified morphology for enhanced thermal comfort in buildings. Case Stud Constr Mater 15:e00611
8. Palanisamy M, Magudeaswaran P, Professor A (2018) Development of eco brick and concrete with the partially replacement of cow dung prestressed concrete view project nano composite concrete using M-sand view project development of eco brick and concrete with the partially replacement of cow dung. Int J Sci Eng Res (IJ0SER) 6. https://www.researchgate.net/publication/325176476
9. Savastano Jr H, Warden PG, Coutts RSP (2000) Brazilian waste fibres as reinforcement for cement-based composites. Cement Concrete Compos 22(5):379–384
10. Savastano Jr H, Warden PG, Coutts RSP (2003) Mechanically pulped sisal as reinforcement in cementitious matrices. Cement Concrete Compos 25(3):311–319
11. SLSI (1999) Specification for concrete roofing semi-sheets, tiles and fittings Test Methods, SLS 1189: Part 2
12. Standards E (2022) ASTM C1185–08R16—standard test methods for sampling and testing non-asbestos fiber-cement flat sheet, roofing and siding shingles, and clapboards. [online] https://www.en-standard.eu. Available at: https://www.en-standard.eu/astm-c1185-08r16-standard-test-methods-for-sampling-and-testing-non-asbestos-fiber-cement-flat-sheet-roofing-and-siding-shingles-and-clapboards/. Accessed 11 Oct 2022

13. Shafigh P, Asadi I, Akhiani AR, Mahyuddin NB, Hashemi M (2020) Thermal properties of cement mortar with different mix proportions. Mater Constr 70(339):e224–e224
14. Shawia NB, Jabber MA, Mamouri AF (2014) Mechanical and physical properties of natural fiber cement board for building partitions. Phys Sci Res Int 2(3):49–53
15. Yu Z, Hu Y, Qin C (2021) Research on existing problems and improvement measures of fabricated composite wallboard. In: E3S Web of conferences, vol. 248. EDP Sciences, p 03057

Application of Sustainability Concepts in the Lifecycle of Building Façade: A Review

Olga Pilipenets, Felix Kin Peng Hui, Tharaka Gunawardena, Priyan Mendis, and Lu Aye

Abstract Construction companies that started to embrace the circular economy and sustainable development concepts in their organisational mission are often faced with technical and managerial challenges. The reason is that the use of sustainable building materials is not well understood. The aim of this article is to review the applications of sustainability concepts in the entire lifecycle of the building façade and to assess the alignment with universally recognised sustainable practices such as the United Nations Sustainable Development Goals. The novelty of this article is the tracing of the whole lifecycle of the most used type of façade from design and material selection to end of life, focusing particularly on the management of waste for achieving sustainability of the built environment. We review state of the art in facade waste management in Australia using published scholarly articles and industry practices. The findings show that while certain lifecycle stages, such as manufacturing and construction, are directly connected to the concept of sustainability, a few gaps within the application of sustainable core values have been revealed. The most significant knowledge gaps were identified: a lack of comparison of environmental impacts of recycled and virgin materials used, lack of consideration of transportation routes and distances, and the end-of-life waste management to divert façade waste from the landfill. This article contributes to the façade waste management domain by summarising the current knowledge.

O. Pilipenets (✉) · F. K. P. Hui
Engineering Management Group, Department of Infrastructure Engineering, Faculty of Engineering and Information Technology, The University of Melbourne, Melbourne, VIC 3010, Australia
e-mail: opilipenets@student.unimelb.edu.au

T. Gunawardena · P. Mendis · L. Aye
ARC Centre for Advanced Manufacturing of Prefabricated Housing, The University of Melbourne, Melbourne, VIC 3010, Australia

L. Aye
Renewable Energy and Energy Efficiency Group, Department of Infrastructure Engineering, Faculty of Engineering and Information Technology, The University of Melbourne, Melbourne, VIC 3010, Australia

© The Author(s), under exclusive license to Springer Nature Singapore Pte Ltd. 2023

R. Dissanayake et al. (eds.), *ICSBE 2022*, Lecture Notes in Civil Engineering 362,
https://doi.org/10.1007/978-981-99-3471-3_41

Keywords Façade materials · Waste management · Sustainable building materials · Circular economy

1 Introduction

Many organisations in the construction industry are transitioning to embrace circular economy concepts and sustainable development as part of their mission. However, implementing this appears to be technically and managerially challenging. Using sustainable building materials is a common strategy established by various stakeholders in the construction industry to achieve a circular economy, but this is not well understood or defined. Much uncertainty still exists regarding how sustainability concepts can be included in all stages of the façade lifecycle. This work aims to explore how sustainability concepts are applied in the context of building facades throughout their lifecycle: from the design and manufacturing phases to the end-of-life and waste disposal. The research question is as follows:

How are sustainable façade design, material use, material extraction, installation, transportation, operation, maintenance, and end-of-life treatment aligned with sustainable core values?

The article's novelty is that it examines the state-of-the-art knowledge on façades throughout the entire lifecycle. This work contributes to the façade design and construction waste management domain by reviewing the body of knowledge to date. The findings show the knowledge gaps that need to be addressed in future research, namely the choice of raw or recycled materials, transportation, and the end-of-life treatment for facades.

2 Facades and Sustainability

The façade is one of the key components of a building's structure, representing the outer skin protecting the building from outside weather and ambient conditions and characterising its aesthetics and appearance. Façades can be made of various materials [3], and the most common façade types based on their material composition are presented in Fig. 1. Steel and glass facades are currently dominating the business districts of contemporary cities, whereas brick and stone facades are more prevalent in suburban areas. A special type of facade included in the study is photovoltaic (PV) facades which generate electricity by converting solar radiation [17]. This innovative façade has become a research interest of many organisations in recent years due to its ability to produce low carbon electricity and help in building self-sufficiency.

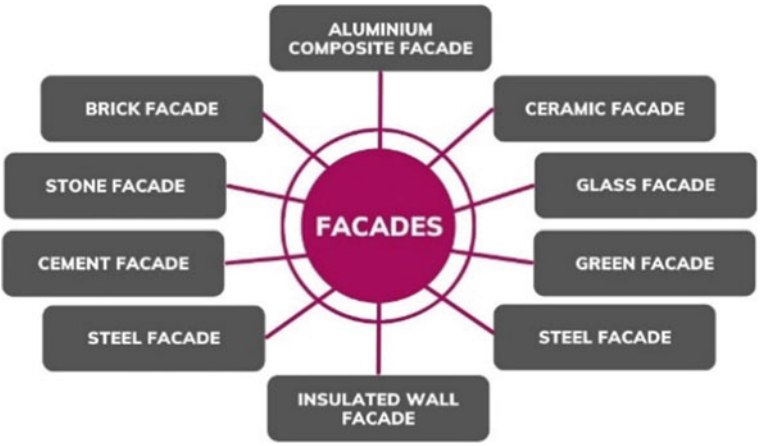

Fig. 1 Most common types of facades based on material composition (Figure by the authors)

2.1 Façade Lifecycle

The lifecycle of facades is like that of other building materials (Fig. 2). Under the lifecycle assessment framework, it includes extraction of raw materials, transportation to the factory, manufacturing, transportation to the construction site, installation/construction, operation, maintenance, and transportation to either landfill disposal or recycling [49]. Another critical stage is the design and material selection. Architects decide on what materials will be used in the new or refurbished buildings based on their characteristics and desirable performance. Therefore, it is important to include design and material selection when analysing sustainability applications throughout the lifecycle of facades.

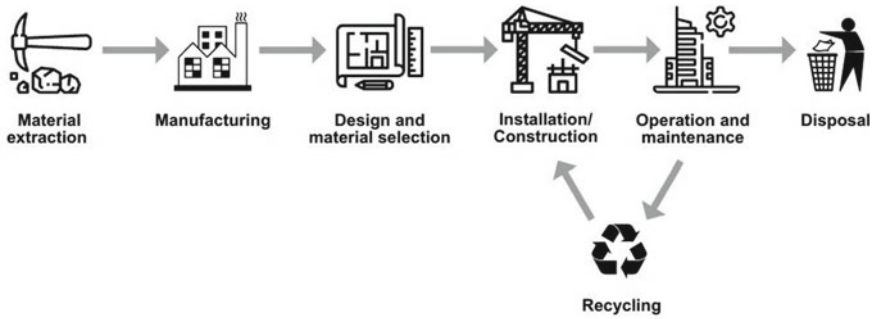

Fig. 2 Façade lifecycle (Figure by the authors)

2.2 Sustainability in Façade Management

Sustainability is usually referred to as "the balanced and systemic integration of intra and intergenerational economic, social, and environmental performance" [20]. This work mainly focuses on the technical and environmental considerations in the facades industry. However, the authors recognise the importance of the social and economic elements and incorporate them into the discussion section.

Sustainability as a concept, can be applied to all the stages of the façade lifecycle. It can be incorporated into selecting materials, improving energy efficiency, or applying innovative solutions to remove air pollutants and capture energy. Management of the end-of-life facades is also one of the critical areas aiding sustainability. It is essential to find how these materials can be diverted from conventional disposal to reduce the burden on landfills. This waste stream could essentially be brought back into manufacturing to close the loop and bring us closer to achieving a circular economy. Therefore, it is essential to explore how sustainability concepts are currently applied in the facades industry and reveal future opportunities for their applications throughout the entire façade lifecycle.

3 Method

This work presents a systematic literature review of research articles using the "Preferred Reporting Items for Systematic Reviews and Meta-Analyses (PRISMA)" statement [41]. The relevant literature search was conducted using Web of Science and Scopus databases for peer-reviewed articles published between 1 January, 2018 and 31 August, 2022 in English. The following keywords were used to create a query: "sustainable" or "sustainability", and "façade". The initial search revealed 2949 publications (Fig. 3).

Once the 1100 duplicates were removed, 66 articles that were not written in English were also excluded. Only 484 publications with the document type "article" were selected for retrieval. Based on the quick screening, 341 more articles were removed because they either did not focus on sustainability concepts (286 articles) or facades (55 articles). After all the exclusions were applied, 145 reports were left for review. The authors have shortlisted the top 50 most relevant publications for the final review. All the publications were collected and organised in EndNote 20. Lastly, bibliographic mapping was further conducted using the VOS viewer software to overview the extent of research in this area.

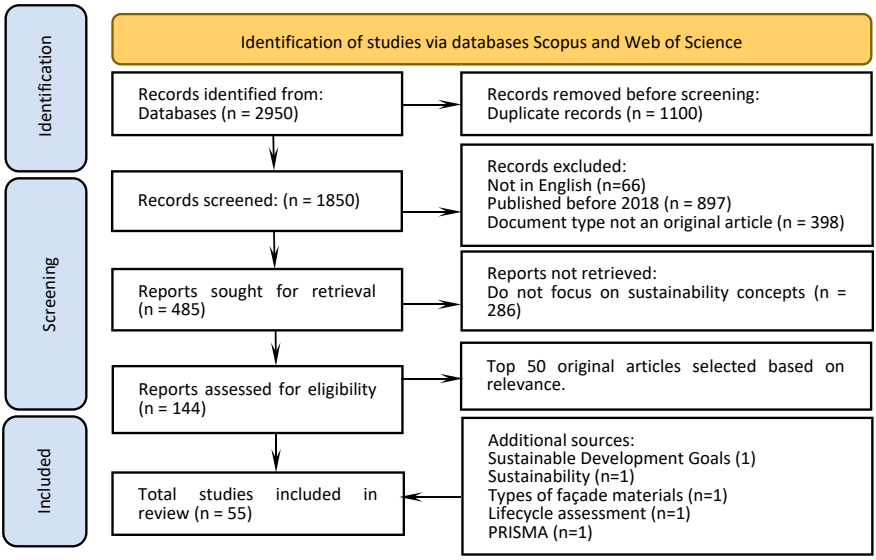

Fig. 3 PRISMA flowchart (Figure by the authors)

4 Findings

The review shows that most of the research interests regarding sustainability aspects within the façade lifecycle have focused on the design and material selection stage, covering topics such as decision-making models, design optimisation, materials recycling, use of nanomaterials, green facades, adaptive and intelligent facades, among others (see Table 1 in Appendix 1). In addition, the application of diverse methods and technologies (e.g., refurbishment, revitalisation, conservation, energy retrofitting, and green cleaning) within the maintenance stage have also been widely reported in the literature (7 articles). On the other hand, limited studies have included sustainability concepts in the stages of material extraction, transportation, and manufacturing (1 article) as part of the lifecycle assessment approach; as well as installation and construction (2 articles), operations (3 articles), and end of life (1 article). The results of the literature review show that no comprehensive investigation that covered all the façade lifecycle stages is available. The detailed literature review is presented in Table 1 of Appendix 1.

Findings from bibliometric mapping and literature review have yielded the following results. Figure 4a presents the network of collaboration between countries that have published over 5 articles. The thickness of the lines illustrates the strengths of collaboration, and the circle sizes correspond to the number of articles. For example, the highest level of collaboration occurred between Italy and the United Kingdom. Overall, Italy has the highest number of collaborations with other countries, including the Netherlands, Belgium, and Australia.

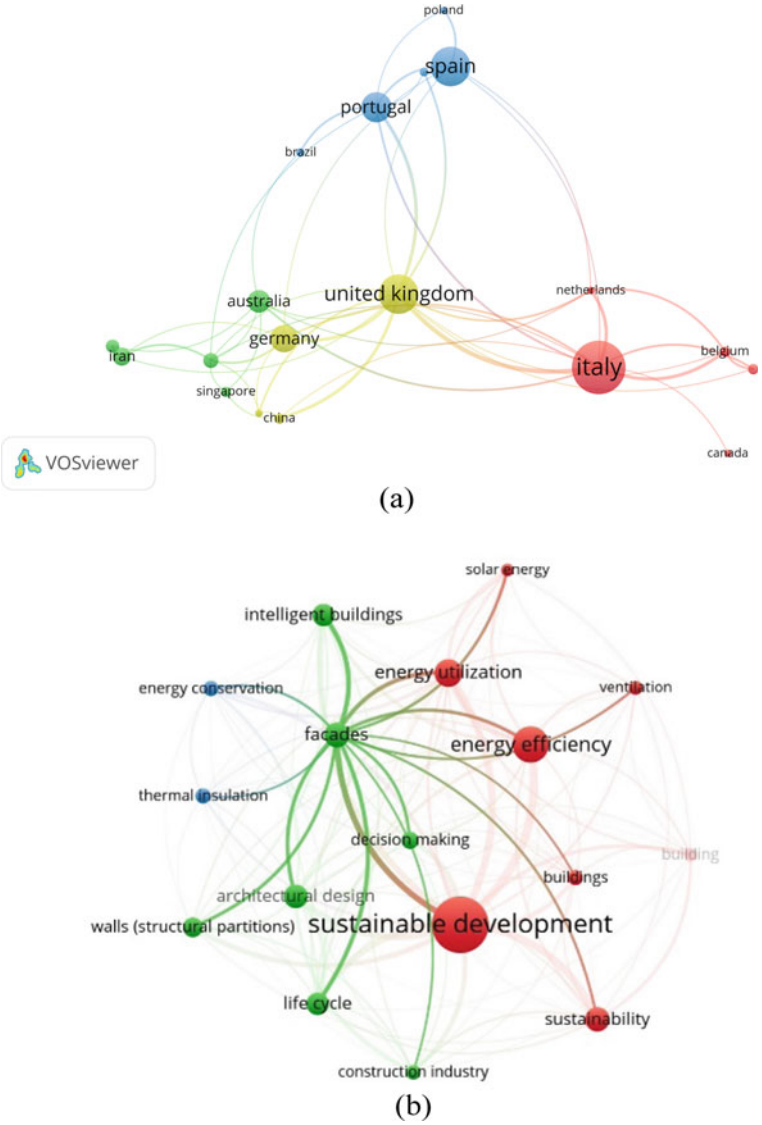

Fig. 4 Network visualisation map of **a** country co-authorship, **b** keyword co-occurrence using VOS viewer

Regarding the keyword co-occurrence, as demonstrated in Fig. 4b, facades are strongly related to sustainable development and sustainability, energy efficiency, conservation and utilisation, intelligent buildings, lifecycle, architectural design, and thermal insulation.

5 Discussion

The aim of this work is to explore how the concept of sustainability is used throughout the façade lifecycle. Although multiple studies have focused on specific phases of the lifecycle (e.g., design and material selection), this article contributes to research by examining the state of the art in façades throughout the entire lifecycle. Based on the results of the systematic literature review presented in Table 1, it can be inferred that research is not equivalent to different stages of the façade lifecycle. Some of the stages, such as design, material selection, and maintenance, have received more attention from researchers worldwide. For example, numerous articles in the design and material selection stage focus on the Mediterranean climate [11, 12, 14, 27]. However, the performance of façade materials can be substantially different if applied to a cold and dry climate. There are also noticeable knowledge gaps within the raw material extraction, transportation, and the end-of-life treatment.

5.1 Material Selection

When analysing the stage of material extraction, most studies apply the data on raw materials that are available in the databases (Table 1). However, based on their assumption, there is not much consideration of how raw materials differ from recycled materials. This is an important issue for future research because, contrary to the common misconception that recycling has a positive impact on the environment, depending on the materials and technology involved, recycled materials may be less environmentally friendly than virgin materials. For instance, certain materials would require complex disassembly that involves a significant amount of energy consumed during reprocessing, as well as manual labour used for sorting and water required to produce new products. Another significant gap identified was a lack of knowledge of transportation distances to be used in lifecycle assessment. Many studies make simple assumptions and apply rough estimations of the distances between the facilities (Table 1) that change the result of the assessment, and therefore, the impact on the environment. Hence, there is more concern about the reliability of these estimations, particularly when they are used for decision-making. The lifecycle assessment could be improved by applying live tracking of the routes used in the transportation of façade materials throughout their life cycle.

5.2 End-of-Life Treatment

Interestingly, none of the articles applying the Life Cycle Assessment used cradle-to-grave or cradle-to-cradle in their scope definition (Table 1). However, as per the Sustainable Development Goal on sustainable consumption and production (SDG

12) [55], the countries need to reduce the amount of waste generated by 2030. Since the construction industry is a significant contributor to waste generation, more opportunities, such as reuse/reduce/recycle should be considered when assessing the environmental sustainability of facades. It is essential to further investigate the options for the end-of-life treatment of facade materials at the end of their lifespan and how this waste stream could be used to produce new materials. Currently, most of the end-of-life façade materials are disposed of at landfills, which imposes significant risks to the environment in the amount of land used for landfilling [44]. Some of the end-of-life facades, for example, aluminium composite cladding, are highly combustible, which imposes a risk of fire at a landfill that could potentially cause human injuries or death, as well as many toxic emissions into the atmosphere [44].

5.3 Public Opinion: Aesthetics and Comfort

Lastly, only a limited number of studies included aesthetics and building appearance in the analysis (Table 1). Since the building façade is a determinant of the building's exterior appearance, additional research can be conducted to analyse users' perception of different façade materials and design considerations in the building envelope. However, the users' preferences might show significant variance based on the location of the building and its function. For example, office buildings in a business district are expected to have glass facades, whereas private residential housing in the suburbs would more likely be preferred to be bricked. Generational differences might also influence preferences. For instance, young people might prefer innovative solutions such as green facades, whereas an older generation might prefer concrete or stone facades.

Furthermore, the effect of the façade regarding user comfort could be further analysed to ensure contribution to the social pillar of sustainability. Facades could significantly enhance overall public comfort by contributing to the thermal comfort of building users. There are numerous studies on the thermal insulation of the facades (Table 1). However, most of them focused on the technical aspects rather than the social aspects.

There could be other factors affecting the comfort of building users. If green facades are taken as an example, while these facades might please the eyes, reducing indoor temperature and maintaining appropriate humidity, they might make occupants' lives more difficult by greenery going out of control as well as severe insect infestation.

5.4 Limitations and Further Research

Other sustainability concepts could be considered as part of future works. For example, design for disassembly, design for longevity, design for adaptability, etc.

Further research should be undertaken to analyse the effects on the environment of raw material extraction compared to the use of recycled materials. Also, it is essential to analyse transportation related to the manufacturing of facades. Most importantly, the end-of-life treatment of facades requires further research.

6 Conclusions

This article briefly reviewed the current state of knowledge on the applications of the concepts of sustainability to façade throughout their lifecycle by undertaking a systematic literature review using the PRISMA statement (Table 1). The findings reveal that while manufacturing and construction have a strong connection with the concept of sustainability, other lifecycle stages are still lacking alignment with the core principles of sustainability. The most significant knowledge gaps were identified in three areas. First, a thorough comparison of raw material extraction against the use of recycled materials is needed to identify the extent of an environmental impact, considering all the reprocessing involved with producing recycled materials. Another important area for further research is transportation at all stages of the façade lifecycle. The consideration of the actual travel distances and routes would enhance the assessment. Most importantly, the end-of-life treatment of facades was identified as a significant knowledge gap in the current research. To make the façade industry more sustainable and more circular, future research should help find ways of applying the end-of-life facade waste to bring them back to the loop and contribute to a transition to a circular economy.

Acknowledgements This work was supported by the University of Melbourne Research Scholarship and the Cooperative Research Centres Projects Round 8: CRCPEIGHT000084: Upcycling solutions for hazardous claddings and co-mingled waste. The authors thank Mr. Matt Marsh, the Managing Director of Sebastian Property Services Pty Ltd., and Dr. Omar Castrejon Campos, The University of Melbourne, for their valuable suggestions.

Credit Authorship Contribution Statement **Olga Pilipenets**: Formal analysis, Investigation, Data curation, Visualisation, Software, Writing—original draft, Writing—review and editing. **Felix Kin Peng Hui**: Methodology, Supervision, Project administration, Writing—review and editing. **Tharaka Gunawardena**: Validation, Supervision, Writing—review and editing. **Priyan Mendis**: Conceptualisation, Supervision, Funding acquisition**. Lu-Aye**: Validation, Resources, Visualisation, Supervision, Project administration, Writing—review and editing.

Declaration of Competing Interest The authors declare that they have no known competing financial interests or personal relationships that could have appeared to influence the work reported in this article.

Appendix 1

See Table 1.

Table 1 Summary of the literature review

Façade lifecycle stage	Current knowledge and knowledge gaps		
	Significant research identified	Further research directions	References
Design and material selection	Decision making models are used to identify the most sustainable combinations of façade materials. Sustainability is applied as quantification of a sustainability index based on economic, environmental, social elements, and stakeholder satisfaction. Also, durability should be included into decision- making to minimise defects and improve building performance	There is need in expanding application to other types of facades and incorporate more boundary conditions including recommendations and standards. When considering durability, all layers of the building envelope should be considered	[21, 22, 29, 35]
	Optimisation of design considerations can be implemented using multi-objective optimisation. It can be used to evaluate the impact of geometry on energy consumption Quality of projects is usually because of the lack of data, lack of definition in the design, and lack of details	Such elements as visual comfort, glare probability, external appearance should be included in the future models to enhance façade design	[8, 26]
	Recycled materials can be successfully used: recycled textile-reinforced cement façade cladding, rice straw façade panels, hemp-lime concrete and recycled-PET facades, as well as facades comprising of construction and demolition waste. Sustainability Index. Energy and carbon footprint are applied to conduct sustainability performace assessment	Future research should focus on improving aesthetics, optimising recycled material to raw material ration, fire resistance, structural integrity, durability Both green origin and green performance need to be assessed for a more holistic view	[14, 31, 34, 36, 46, 48]

(continued)

Table 1 (continued)

Façade lifecycle stage	Current knowledge and knowledge gaps		
	Significant research identified	Further research directions	References
	Nanomaterials as a new set of smart materials with responsive properties. Sustainability is applied through energy efficiency, internal environmental efficiency, resources and materials, site sustainability, and water efficiency	More research into application of nanomaterials to ensure sustainability objectives can be met. Also, what ratio of including nano particles should be used to achieve the most optimal parameters with lower costs and increased durability	[6, 15]
	Photovoltaic (PV) materials can be used to reduce energy consumption. Energy produced by these facades can cover heating/cooling of the building. These systems proved to be successful in warm and sunny climates. Sustainability is applied through technical, economic, social, environmental, and energy consumption factors using the Life Cycle Assessment (LCA) with the Friedman scores	Economic feasibility, transparency and resident comfort need to be further analysed. Time lag between the peak energy gain and the peak demand should be also calculated for different climates Optimisation to minimise emissions and energy consumption while maximising use of renewable energy is needed	[2, 4, 5, 7, 17, 18, 25, 39, 50, 51]
	Green facades can significantly improve building energy performance, increase human comfort and microclimatic conditions. Sustainability is ensured by reduscing energy use in warm and humit areas	Further research should investigate different environmental conditions More research into what plants should be used is needed	[11, 28]
	Glass facades - sustainability can be applied through energy consumption. Also, social safety and protection against terrorist attacks can be assessed. Current research also includes such innovative facades as vacuum insulated glass, Smart Water-filled glass (SWFG) to improve energy efficiency, and microalgae to reduce trnsparency of glass facades to improve comfort of muslim women	Future research should focus on acoustic insulation, resistance to blasts, coatings for SWFG, and evaluation of the entire building performance rather than a prototype	[1, 23, 30, 45, 47]

(continued)

Table 1 (continued)

Façade lifecycle stage	Current knowledge and knowledge gaps		
	Significant research identified	Further research directions	References
	Double-skin perforated facade (DSPF) with perforated screens can be used to block the sun and facilitate natural ventilation	Different orientations and different spacing of holes should be further evaluated	[53]
	Translucent concrete façade panels perform better in terms of ductility and serviceability but have large deformation	More research into its characteristics, aesthetics and human comfort is needed	[54]
	Adaptive facades and intelligent facades enahance user comfort using climatic data	Analysis of different climates, connection to weather data using internet, integration with the HVAC system is needed	[19, 27, 42]
	Expanded cork can be used as part of facades	Further research into its performance is needed	[32]
Materialextraction	Material extraction is investigated as part of the lifecycle assessment	More research comparing raw and recycled materials is needed	[38]
Transportation	Transportation is investigated as part of the lifecycle assessment. It is a large contributor to greenhouse gas emissions	Information about transport distances that can be used for assessement is needed	[38]
Manufacturing	PV panel fabrication is the largest energy consumer and emitter of greenhouse gas emissions	More research into sustainable manufacturing of facades is needed	[38]
Installation/ Construction	SDGs can be applied to improve working conditions, particularly, in extreme weather conditions by using air conditioning and faster execution time with prefabricated façades	Optimal humidity-temperature conditions for jobs carried out inside the construction site should be investigated, as well as fire resistance of facades	[13]

(continued)

Table 1 (continued)

Façade lifecycle stage	Current knowledge and knowledge gaps		
	Significant research identified	Further research directions	References
	In case of rammed earth facades, excavation takes a big part of the work and has flexible installation process by piling up	Further research can focus on optimisation of excavation and transportation to the construction site	[38]
Operation	Service line prediction models cab be used to asess durability and service life of facades. Regression models and LCA can help to reveal what facaded maintain comfortable indoor temperature	Applications for local climatic conditions should be taken into consideration	[9, 16, 52]
Maintenance	Refurbishment of the old buildings can be analysed through energy and environmental performance (LCA), and Global Sustainability Index	More studies on different façade types are needed	[24, 43]
	Revitalisation generates less emissions than demolition and new construction. It can help to decarbonise the construction by using materials with lower environmental impact	Use of different materials and their placement within the building should be further explored	[40]
	Conservation of tile facades using metakaolin-based geopolymers can be successful for filling gaps and bonding fragments	Durability, applicability to other facades, and optimisation of adhesion between ceramics and geopolymers to be investigated	[37]
	Energy retrofitting can be used to improve the original façade design	Different climate applications should be presented in the future research	[10, 12]
	Green cleaning using self-cleaning materials (e.g. TiO_2) instead of repairing can be used to increase lifespan of buildings	Further research should test self-cleaning materials in different climatic conditions	[33]
End-of-life	Materials derived from façade waste could be potentially upcycled to create new products such as packaging or pipes	End-of-life opportunities for facades should be explored	[44]

References

1. Alqalami TA (2020) Dynamic transparency in design: the revival of environmental sustainability in design elements of Iraqi buildings. Heliyon 6(11). https://doi.org/10.1016/j.heliyon.2020.e05565
2. Alrashidi H, Issa W, Sellami N, Ghosh A, Mallick TK, Sundaram S (2020) Performance assessment of cadmium telluride-based semi-transparent glazing for power saving in façade buildings. Energy Build 215. https://doi.org/10.1016/j.enbuild.2019.109585
3. ArchDaily (2022) Available at: https://www.archdaily.com/search/products/categories/construction-materials_facade-systems. Accessed 10 Aug 2022
4. Arkar C, Žižak T, Domjan S, Medved S (2020) Dynamic parametric models for the holistic evaluation of semi-transparent photovoltaic/thermal façade with latent storage inserts. Appl Energy 280. https://doi.org/10.1016/j.apenergy.2020.115994
5. Ascione F, Bianco N, de Rossi F, Iovane T, Mauro GM (2022) Are transparent double-skin facades effective for energy retrofit? Answers for an office building—with and without photovoltaic integration. Energ Source Part A 44(1):257–271. https://doi.org/10.1080/15567036.2022.2042430
6. Aziz HNA, Abdelall MI (2021) Responsive façades design using nanomaterials for optimizing buildings' energy performance. WIT Trans Ecol Environ 253:397–408. https://doi.org/10.2495/SC210331
7. Balali A, Valipour A (2020) Identification and selection of building façade's smart materials according to sustainable development goals. Sustain Mater Technol 26. https://doi.org/10.1016/j.susmat.2020.e00213
8. Carretero-Ayuso MJ, García-Sanz-Calcedo J, Rodríguez-Jiménez CE (2018) Characterization and appraisal of technical specifications in brick façade projects in Spain. J Perform Constr Facil 32(3):04018012. https://doi.org/10.1061/(ASCE)CF.1943-5509.0001149
9. Chou DC, Wu CP, Tsai JH, Lee KL, Jwo CS, Yeh SC (2019) Use of phase change materials in the thermoelectric systems of building facades. J Technol 34(1):1–16. Available at: http://ir.lib.ntust.edu.tw/bitstream/987654321/75889/2/USE%20OF%20PHASE%20CHANGE%20MATERIALS%20IN%20THE%20THERMOELECTRIC%20SYSTEMS%20OF%20BUILDING%20FACADES.pdf. Accessed 10 July 2022
10. Colombo IG, Colombo M, di Prisco M, Galzerano B, Verdolotti L (2021) Lightweight TRC sandwich panels with sustainable diatomite-based core for energy retrofitting of existing buildings. Adv Build Energy Res 15(2):231–252. https://doi.org/10.1080/17512549.2019.1697752; Convertino F (2020) Heat transfer modelling in green façades. WIT Trans Ecol Environ 243:57–68. https://doi.org/10.2495/UA200061
11. Convertino F (2020) Heat transfer modelling in green façades. WIT Trans Ecol Environ 243:57–68. https://doi.org/10.2495/UA200061
12. Corrêa D, Flores-Colen I, Silvestre JD, Pedroso M, Santos RA (2020) Old buildings' façades: Fieldwork and discussion of thermal retrofitting strategies in a mediterranean climate. Designs 4(4):1–19. https://doi.org/10.3390/designs4040045
13. Cruz Astorqui JS, Amores CP, Ramírez CP, Merino MDR, Sáez PV, Barriguete AV (2022) New execution process of a panel-based façade system that reduces project duration and improves workers' working conditions. J Build Eng 48. https://doi.org/10.1016/j.jobe.2021.103894
14. De Masi RF, Ruggiero S, Vanoli GP (2021) Hygro-thermal performance of an opaque ventilated façade with recycled materials during wintertime. Energy Build 245. https://doi.org/10.1016/j.enbuild.2021.110994
15. Desouky SK, Shanawani HSE, Arafa RI, Hamed MM (2019) Nanotechnology materials and sustainability of building facades. J Green Eng 9(3):348–359. Available at: https://www.ijert.org/using-nano-materials-and-building-sustainability. Accessed 11 July 2022
16. Feehan A, Nagpal H, Marvuglia A, Gallagher J (2021). Adopting an integrated building energy simulation and life cycle assessment framework for the optimisation of facades and fenestration in building envelopes. J Build Eng 43. https://doi.org/10.1016/j.jobe.2021.103138

17. García-Gáfaro C, Escudero-Revilla C, Flores-Abascal I, Hidalgo-Betanzos JM, Erkoreka-González A (2022) A photovoltaic forced ventilated façade (PV-FVF) as heat source for a heat pump: Assessing its energetical profit in nZEB buildings. Energy Build 261. https://doi.org/10.1016/j.enbuild.2022.111979
18. Garraín D, Herrera I, Rodríguez-Serrano I, Lechón Y, Hepbasli A, Araz M, Biyik E, Yao R, Shahrestani M, Essah E, Shao L, Rico E, Lechón JL, Oliveira AC (2020) ustainability indicators of a naturally ventilated photovoltaic façade system. J Clean Prod 266. https://doi.org/10.1016/j.jclepro.2020.121946
19. Gaspari J, Naboni E, Ponzio C, Ricci A (2019) A study on the impact of climate adaptive building shells on indoor comfort. J Facade Des Eng 7(1):27–39. https://doi.org/10.7480/jfde.2019.1.2778
20. Geissdoerfer M, Savaget P, Bocken NMP, Hultink EJ (2017) The circular economy–a new sustainability paradigm? J Clean Prod 143:757–768. https://doi.org/10.1016/j.jclepro.2016.12.048
21. Gilani G, Hosseini SMA, Pons-Valladares O, de la Fuente A (2022) An enhanced multi-criteria decision-making approach oriented to sustainability analysis of building facades: a case study of Barcelona. J Build Eng 54. https://doi.org/10.1016/j.jobe.2022.104630
22. Gilani G, Pons O, De La Fuente A (2022) "Sustainability-oriented approach to assist decision makers in building facade management. J Constr Eng Manag 148(1), 04021182. https://doi.org/10.1061/(ASCE)CO.1943-7862.0002194
23. Gutai M, Kheybari AG (2021) Energy consumption of hybrid smart water-filled glass (SWFG) building envelope. Energy Build 230. https://doi.org/10.1016/j.enbuild.2020.110508
24. Habibi S, Pons Valladares O, Peña D (2020) New sustainability assessment model for Intelligent Façade Layers when applied to refurbish school buildings skins. Sustain Energy Technol Assess 42. https://doi.org/10.1016/j.seta.2020.100839
25. Hadi E, Heidari A (2021) Development of an integrated tool based on life cycle assessment, levelized energy, and life cycle cost analysis to choose sustainable facade integrated photovoltaic systems. J Clean Prod 293. https://doi.org/10.1016/j.jclepro.2021.126117
26. Jalali Z, Noorzai E, Heidari S (2020) Design and optimization of form and facade of an office building using the genetic algorithm. Sci Technol Built Environ 26(2):128–140. https://doi.org/10.1080/23744731.2019.1624095
27. Karakoc E, Cagdas G (2021) Adaptive architecture based on environmental performance: an advanced intelligent façade (AIF) module. Gazi Univ J Sci 34(3):630–650. https://doi.org/10.35378/gujs.725902
28. Karimi K, Farrokhzad M, Roshan G, Aghdasi M (2022) Evaluation of effects of a green wall as a sustainable approach on reducing energy use in temperate and humid areas. Energy Build 262. https://doi.org/10.1016/j.enbuild.2022.112014
29. Lee JS (2018) Value engineering for defect prevention on building façade. J Constr Eng Manag 144(8), 04018069. https://doi.org/10.1061/(ASCE)CO.1943-7862.0001500
30. Lori G, Morison C, Larcher M, Belis J (2019) Sustainable facade design for glazed buildings in a blast resilient urban environment. Glass Struct Eng 4(2):145–173. https://doi.org/10.1007/s40940-018-0088-3
31. Maalouf C, Ingrao C, Scrucca F, Moussa T, Bourdot A, Tricase C, Presciutti A, Asdrubali F (2018) An energy and carbon footprint assessment upon the usage of hemp-lime concrete and recycled-PET façades for office facilities in France and Italy. J Clean Prod 170:1640–1653. https://doi.org/10.1016/j.jclepro.2016.10.111
32. Malanho S, Veiga R, Farinha CB (2021) Global performance of sustainable thermal insulating systems with cork for building facades. Buildings 11(3):1–18. https://doi.org/10.3390/buildings11030083
33. Mansour AMH, Al-Dawery SK (2018) Sustainable self-cleaning treatments for architectural facades in developing countries. Alex Eng J 57(2):867–873. https://doi.org/10.1016/j.aej.2017.01.042
34. Mayhoub MMG, El Sayad ZMT, Ali AAM, Ibrahim MG (2021) Assessment of green building materials' attributes to achieve sustainable building façades using AHP. Buildings 11(10). https://doi.org/10.3390/buildings11100474

35. Moghtadernejad S, Chouinard LE, Mirza MS (2018) Multi-criteria decision-making methods for preliminary design of sustainable facades. J Build Eng 19:181–190. https://doi.org/10.1016/j.jobe.2018.05.006
36. Moussa T, Maalouf C, Ingrao C, Scrucca F, Costantine G, Asdrubali F (2018) Bio-based and recycled-waste materials in buildings: A study of energy performance of hemp-lime concrete and recycled-polyethylene terephthalate façades for office facilities in France and Italy. Sci Technol Built Environ 24(5):492–501. https://doi.org/10.1080/23744731.2018.1438664
37. Moutinho S, Costa C, Andrejkovičová S, Mariz L, Sequeira C, Terroso D, Rocha F, Velosa A (2020) Assessment of properties of metakaolin-based geopolymers applied in the conservation of tile facades. Constr Build Mater 259. https://doi.org/10.1016/j.conbuildmat.2020.119759
38. Nanz L, Rauch M, Honermann T, Auer T (2019) Impacts on the embodied energy of rammed earth façades during production and construction stages. J Facade Des Eng 7(1):75–88. https://doi.org/10.7480/jfde.2019.1.2786
39. Noaman DS, Moneer SA, Megahed NA, El-Ghafour SA (2022) Integration of active solar cooling technology into passively designed facade in hot climates. J Build Eng 56. https://doi.org/10.1016/j.jobe.2022.104658
40. Onyszkiewicz J, Sadowski K (2022) Proposals for the revitalization of prefabricated building facades in terms of the principles of sustainable development and social participation. J Build Eng 46. https://doi.org/10.1016/j.jobe.2021.103713
41. Page MJ, McKenzie JE, Bossuyt PM, Boutron I, Hoffmann TC, Mulrow CD, Shamseer L, Tetzlaff JM, Akl EA, Brennan SE, Chou R, Glanville J, Grimshaw JM, Hróbjartsson A, Lalu MM, Li T, Loder EW, Mayo-Wilson E, McDonald S, McGuinness LA, Stewart LA, Thomas J, Tricco AC, Welch VA, Whiting P, Moher D (2021) The PRISMA 2020 statement: an updated guideline for reporting systematic reviews. BMJ. https://doi.org/10.1136/bmj.n71
42. Perez G, Sirvent P, Sanchez-Garcia JA, Guerrero A (2021) Improved methodology for the characterization of thermochromic coatings for adaptive façades. Sol Energy 230:409–420. https://doi.org/10.1016/j.solener.2021.10.062
43. Petrovski A, Petrovska-Hristovska L, Ivanović-Šekularac JA, Šekularac ND (2020) Assessment of the sustainability of facade refurbishment. Therm Sci 24, 991–1006. https://doi.org/10.2298/TSCI190218307P
44. Pilipenets O, Gunawardena T, Kin Peng Hui F, Nguyen K, Mendis P, Aye L (2022) Upcycling opportunities and potential markets for aluminium composite panels with polyethylene core (ACP-PE) cladding materials in Australia: a review. Constr Build Mater 357. https://doi.org/10.1016/j.conbuildmat.2022.129194
45. Pracucci A, Magnani S, Casadei O (2020) The integration of vacuum insulated glass in unitized façade for the development of innovative lightweight and highly insulating energy efficient building envelope—the results of Eensulate façade system design. Designs 4(4):1–15. https://doi.org/10.3390/designs4040040
46. Quintana-Gallardo A, Romero Clausell J, Guillén-Guillamón I, Mendiguchia FA (2021) Waste valorization of rice straw as a building material in Valencia and its implications for local and global ecosystems. J Clean Prod 318. https://doi.org/10.1016/j.jclepro.2021.128507
47. Rezazadeh H, Kordjamshidi M, Ahmadi F, Eskandarinejad A (2021) Use of double-glazed window as a photobioreactor for CO2 removal from air. Environ Eng Res 26(2). https://doi.org/10.4491/eer.2020.122
48. Sadrolodabaee P, Hosseini SMA, Claramunt J, Ardanuy M, Haurie L, Lacasta AM, Fuente ADL (2022) Experimental characterization of comfort performance parameters and multi-criteria sustainability assessment of recycled textile-reinforced cement facade cladding. J Clean Prod 356. https://doi.org/10.1016/j.jclepro.2022.131900
49. Saleem M, Chhipi-Shrestha G, Túlio Barbosa Andrade M, Dyck R, Ruparathna R, Hewage K, Sadiq R (2018) Life cycle thinking–based selection of building facades. J Archit Eng https://doi.org/10.1061/(asce)ae.1943-5568.0000333, 04018029
50. Simões I, Simões N, Santos I, Brett M, Tadeu S, Silva H (2019) Energy and sustainable performance of a multifunctional façade. WIT Trans Ecol Environ 237:51–61. https://doi.org/10.2495/ESUS190051

51. Sorgato MJ, Schneider K, Rüther R (2018) Technical and economic evaluation of thin-film CdTe building-integrated photovoltaics (BIPV) replacing façade and rooftop materials in office buildings in a warm and sunny climate. Renew Energy 118:84–98. https://doi.org/10.1016/j.renene.2017.10.091
52. Souza J, Silva A, de Brito J, Bauer E (2018) Analysis of the influencing factors of external wall ceramic claddings' service life using regression techniques. Eng Fail Anal 83:141–155. https://doi.org/10.1016/j.engfailanal.2017.10.005
53. Srisamranrungruang T, Hiyama K (2020) Balancing of natural ventilation, daylight, thermal effect for a building with double-skin perforated facade (DSPF). Energy Build 210. https://doi.org/10.1016/j.enbuild.2020.109765
54. Tuaum A, Shitote S, Oyawa W, Biedebrhan M (2019) Structural performance of translucent concrete façade panels. Adv Civ Eng. https://doi.org/10.1155/2019/4604132, 4604132
55. United Nations (2022) Available at: https://www.un.org/sustainabledevelopment/development-agenda/. Accessed 24 Aug 2022

Producing Sustainable Rigid Pavements with the Addition of Graphene Oxide

I. Fonseka, T. Ginigaddara, K. Wijesooriya, D. Mohotti, P. Mendis, and C.-K. Lee

Abstract Graphene has emerged as one of the most trending nanomaterials in material science since it is the strongest and thinnest material on earth, at one atom thick. Graphene oxide (GO) is a graphene derivative material, and it has gained considerable attention for possible use in the construction industry due to its good dispersity in the water because of the presence of oxygen functionalities. The current paper focuses on the sustainability aspects of GO-incorporated concrete for rigid pavement applications. In the presented experimental investigation, GO was added to the concrete mix at dosages of 0.02, 0.04, 0.06, and 0.08% by weight of cement. Compressive strength and split tensile strength tests were conducted to evaluate the mechanical properties. Abrasion tests were performed to measure the abrasion resistance of GO concrete. It was observed that the addition of GO from 0% to 0.08%, enhanced the compressive strength, split tensile strength, and abrasion resistance by 20.7, 11.8, and 22.9%, at 28 days, respectively. Based on the superior strength and abrasion properties, GO concrete directs towards reducing construction material consumption compared to conventional pavement concrete and is hence beneficial in reducing CO_2 emission. This is a preliminary test programme that has been conducted for GO-incorporated concrete. Further investigations are going on considering changing parameters like mixing techniques and functionalities of GO to achieve a compressive strength of around 30%. Finally, the research contributes to reducing the carbon footprint in the construction industry by introducing GO-incorporated concrete in rigid pavements, which will be more critical in the coming years for a sustainable solution.

Keywords Graphene oxide · Rigid pavement · Sustainable concrete · Strength · Abrasion resistance

I. Fonseka · K. Wijesooriya · D. Mohotti (✉) · C.-K. Lee
School of Engineering and IT, University of New South Wales, Canberra, ACT, Australia
e-mail: d.mohotti@unsw.edu.au

T. Ginigaddara · P. Mendis
Department of Infrastructure Engineering, University of Melbourne, Melbourne, VIC, Australia

© The Author(s), under exclusive license to Springer Nature Singapore Pte Ltd. 2023

R. Dissanayake et al. (eds.), *ICSBE 2022*, Lecture Notes in Civil Engineering 362,
https://doi.org/10.1007/978-981-99-3471-3_42

1 Introduction

Asphalt has always been the ideal type of road pavement for regional roads, while the stronger and more expensive concrete pavement has been reserved for arterial roads with high traffic flow. However, recently there has been a gradual shift towards concrete-type pavements. Life cycle analysis has shown that in the longer run, concrete pavements generally outperform asphalt in terms of initial construction costs, and maintenance costs and are less likely to be disruptive to traffic closures [8]. Similarly, it has been identified that concrete pavements throughout their lifetime have a lower overall environmental impact [7]. Whatever advantages asphalt has over concrete and or vice versa, a need for stronger and more durable pavements is essential and critical not only for the previously highlighted advantages, but also due to the ever-increasing traffic demands and constant expansion of the road networks.

In many countries, major arterial roads are often subjected to high-frequency industrial and passenger traffic, which are prone to serviceability issues, leading to costly and untimely repairs with disruptive road closures. Due to that, most countries spend huge amounts of money on transportation, primarily on roads, where a significant portion is mainly spent on maintenance. Similarly, due to their significance, airfield pavements need to be designed as high-quality and low-risk structures that, once constructed, must be monitored throughout their service life. A new airfield pavement is estimated to cost between $100–$500 million [10]. Once constructed, its life expectancy is expected to last forty years to have minimal disruptions in terms of maintenance [10]. Therefore, the advancement of concrete technology in the application of rigid pavements is a special concern in the current construction industry.

The introduction of nanomaterials presents an innovative approach to improving concrete properties. [4]. Graphene oxide (GO) is one such nanomaterial that is a derivative of graphene. Graphene is the thinnest material known to man at one atom thick, and also incredibly strong—about 200 times stronger than steel [9]. GO has gained considerable attention for possible use in the construction industry due to its good dispersity in the water because of the presence of oxygen functionalities.

The present research aims to develop an innovative approach by introducing GO as an additive for concrete in the construction of pavements. GO-incorporated concrete composites produce superior concrete that can enhance the short-term and long-term performances in rigid pavements. The performance of GO-incorporated concrete for rigid pavements was evaluated by conducting a comprehensive experimental programme. In the present research, compressive strength, split tensile strength, and abrasion resistance of concrete were investigated with the addition of different GO percentages. The paper is laid out such that Sect. 2 presents the research methodology, concrete mix design, and test methods used for GO-incorporated concrete. Sect. 3 demonstrates the test results and discussions observed for compressive strength, split tensile strength, and abrasion resistance in detail, and finally, Sect. 4 summarizes the research conclusions.

2 Experimental Investigation

2.1 Materials

A general-purpose cement conforming to Standards Australia (AS 3972–2010) was used for all concrete mixtures. The aggregates were river sand and crushed granite (maximum 20 mm). A poly-carboxylate (PCE)-based superplasticizer was used to enhance workability. The GO used in this study was procured from Ceylon Graphene Technologies, Sri Lanka, derived from Sri Lankan C99 + vein graphite. It was in the form of brown colour dry powder and has a particle size range of 63–90 μm. Attenuated Total Reflection Fourier Transform Infrared (ATR-FTIR) spectra of the used GO were recorded in the region of 800–4000 cm^{-1} at a resolution of 4 cm^{-1}.

2.2 Experimental Plan

The quantities of cement, coarse aggregate, fine aggregate, water, and superplasticizer percentage were kept constant for this experimental investigation. The dosage of GO was varied, and concrete mixes with four different percentages of GO (0.02, 0.04, 0.06, and 0.08% by weight of total cement content) were prepared. The normal conventional concrete mix was also prepared without adding GO as a control mix. Water to cement (w/c) ratio of 0.54 was maintained for all concrete mixtures. The same superplasticizer dosage of 1% (by weight of total cement content) was used for all concrete mixes to maintain the required workability. For each mix, six cylinders (100 mm diameter × 200 mm height) and two concrete blocks (350 mm × 150 mm × 80 mm) were cast. A vibrating table was used for the compaction of concrete specimens. The samples were demoulded after 24 h of casting and then placed in the laboratory fog room for curing until the date of testing.

2.3 Mix Proportions and Mixing Method

The concrete mix design was conducted according to the British method of mix design, considering 32 MPa target compressive strength at 28 days. The mix proportions used for the concrete mixing are given in Table 1.

The required amount of GO powder was mixed with water using a mechanical mixer to obtain a uniform GO aqueous solution. First, GO powder was gradually added to the water while mixing mechanically. This mixing process was conducted for 3–4 min. After adding total GO powder into the water, the mechanical mixing process was stopped and then the superplasticizer amount was directly added into that GO-water solution. The final aqueous solution containing GO and water and the superplasticizer was added to the rotating concrete mixer containing all dry

Table 1 Concrete mix proportions

Concrete Mix	CM-0	CM-1	CM-2	CM-3	CM-4
GO % by weight of cement	0.00%	0.02%	0.04%	0.06%	0.08%
Cement (kg/m^3)	315	315	315	315	315
GO (kg/m^3)	0.000	0.063	0.126	0.189	0.252
Coarse aggregates (kg/m^3)	1140	1140	1140	1140	1140
Fine aggregates (kg/m^3)	760	760	760	760	760
Water (kg/m^3)	170	170	170	170	170
Superplasticiser-ADVA® 650 (l/m^3)	3.15	3.15	3.15	3.15	3.15

aggregated and cement. The dry materials mixing process was started 2–3 min before adding the prepared aqueous solution. The mixing was continued for around 4–5 min after adding all the constituent materials into the concrete mixer to obtain a proper concrete mix.

2.4 Test Methods

2.4.1 Compressive and Split Tensile Strength Test

The concrete samples were tested to measure each concrete mix's compressive and split tensile strength as per the relevant Australian standard given below.

- Compressive strength—AS 1012.9 (2014)
- Split tensile strength—AS 1012.10 (2000)

Compressive strength and split tensile strength tests were conducted on concrete cylinders having dimensions of 100 mm diameter and 200 mm height after 28 days of casting. Three cylinders were tested for each strength test as per standards.

2.4.2 Abrasion Resistance by Sand Blasting

The standard test method for abrasion resistance of concrete was performed by the ASTM C418-20. This test method determines the abrasion resistance characteristics of concrete by subjecting it to sandblasting. Two block specimens with dimensions of 350 mm $\times$ 150 mm $\times$ 80 mm were used at 28 days.

The sandblasting apparatus consists of an injector-type gun and an angle nozzle. The walls of the nozzle have 45° of the bevels on the inside at the upper end. A suitable jig and clamps were provided to hold the test specimen in a fixed position while maintaining the constant distance of 75 $\pm$ 2.5 mm between the concrete surface the and discharge end of the nozzle. A shield made of steel and having an opening

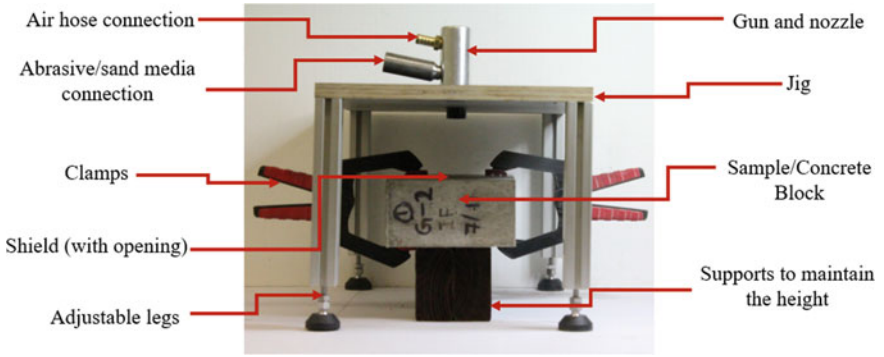

Fig. 1 Sandblasting test setup

of 28.70 ± 0.25 mm in diameter was attached to the concrete specimens using two clamps. The test setup used for sandblasting is displayed in Fig. 1.

Graded sand which passes through an 850 μm sieve and is retained in a 600 μm sieve was used as the abrasive material for sandblasting. All the test specimens were fully immersed in water for 24 h before the sandblasting and then surface dried using a damp cloth to obtain a saturated surface dry condition at the time of the sand test. After placing the block specimen in the sandblasting cabinet, the air pressure was adjusted to 410 ± 1 kPa (59.5 ± 1 psi). Finally, the concrete surface was blasted for a period of 1 min. This procedure was repeated for eight different spots on the concrete surface. The abraded volume of blasted cavities was determined by filling them with an oil base modelling clay. The clay volume in the cavity was easily measured considering the mass of clay in the cavity and the specific gravity of the used clay sample. The final abrasion test result represents an average of eight measurements. Figures 2 and 3 shows the concrete block samples before and after the abrasion test.

The abrasion coefficient is calculated on a volumetric basis by the following Eq. (1), expressed in cubic centimetres per square centimetre. The average value of abrasion coefficients was obtained considering the eight cavities per concrete sample.

Fig. 2 Block sample before abrasion test

Fig. 3 Block sample after abrasion test

$$\text{Abrasion Coefficient} = \frac{\text{Abraded Volume (cm}^3\text{)}}{\text{Area of surface abraded (cm}^2\text{)}} \quad (1)$$

3 Results and Discussion

3.1 Compressive and Split Tensile Strength

Compressive strength and split tensile strength test results are given in Table 2. Both strength values increase with the addition of GO.

The effects of the GO percentage on the compressive and split tensile strength of concrete are shown in Fig. 4 as a percentage increment compared to the control mix.

At 28 days, in comparison with the control mix the addition of 0.02, 0.04, 0.06, and 0.08% GO increased the compressive strength from 39.14 MPa to 43.65 MPa, 44.11 MPa, 45.96 MPa, and 47.26 Mpa, respectively. All the concrete mixes containing GO attained a compressive strength of more than 40 MPa, which are sufficient for the application of rigid pavements and also satisfied the minimum compressive strength requirement of 40 MPa in "Transport for NSW (TfNSW) QA Specification: R83—Concrete Pavement Base" [1].

Table 2 Compressive and split tensile strength test results

Concrete Mix/GO (%)	CM-0 (0.00)	CM-1 (0.02)	CM-2 (0.04)	CM-3 (0.06)	CM-4 (0.08)
Compressive strength (MPa)	39.14	43.65	44.11	45.96	47.26
% Increment of compressive strength	–	11.5	12.7	17.4	20.7
Split tensile strength (MPa)	4.06	4.20	4.25	4.51	4.54
% Increment of split tensile strength	–	3.4	4.7	11.1	11.8

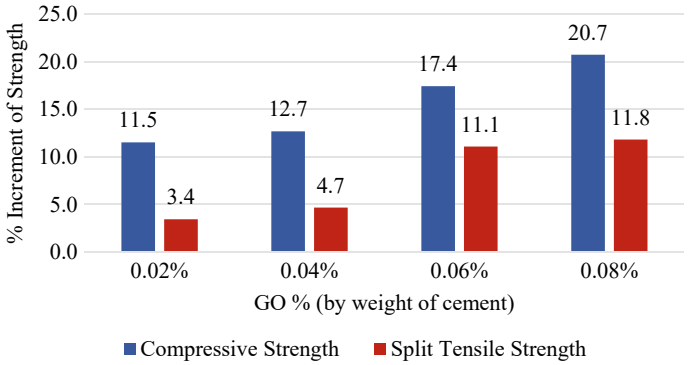

Fig. 4 % Increment of strength test results

Similarly, all GO concrete mixes show greater split tensile strength than the control mix at 28 days. The incorporation of GO in the concrete mix can increase the tensile properties of concrete. When the GO percentage was 0.08%, the split tensile strength was increased from 4.06 MPa to 4.54 MPa concerning the control mix which implies an improvement of 11.8% as a percentage.

Both compressive and split tensile strengths show a similar overall trend with increasing GO percentage in the concrete mix. The reason behind such variation is that, as curing progresses, the GO particles inside the concrete mix play the bridging role to enhance the coherence through powerful covalent bonding with C–S–H, which is the final product of the cement hydration process [5]. GO mixing and dispersion technique is also an important parameter to extract the GO-incorporated concrete's optimum properties [2].

By looking at the compressive strength test results, the concrete mix having 0.08% GO (CM-4) gives a strength of 47.26 MPa at 28 days. This implies that, instead of using a 45 MPa normal conventional concrete mix recipe for construction, it can effectively use CM-4 GO-incorporated concrete mix recipe. For this investigation, the cement amount used was 315 kg/m^3 which can be considered as 15% less cement consumption compared to the conventional concrete recipe for 32 MPa concrete. This 15% cement reduction was considered because of the advancement of current cement technology and ultimately this has contributed to the use of fewer GO amounts as well.

3.2 Abrasion Resistance

Abrasion test results are tabulated in Table 3, where the volume of clay in the cavity and the surface area of the cavity after sandblasting are recorded. The abrasion coefficient of each concrete mix is presented which has a positive relationship to the abrasion resistance of concrete.

Table 3 Abrasion test results

Concrete Mix/GO (%)	CM-0 (0.00)	CM-1 (0.02)	CM-2 (0.04)	CM-3 (0.06)	CM-4 (0.08)
Abraded volume (cm^3)	1.034	1.013	1.007	0.933	0.797
Area of surface abraded (cm^2)	706.86	706.86	706.86	706.86	706.86
Abrasion coefficient $\times 10^{-6}$ (cm^3/cm^2)	1463	1434	1425	1319	1128
Abrasion reduction as a (%)	–	2.0	2.6	9.8	22.9

The graphical view of abrasion coefficients concerning GO percentage shows in Fig. 5 and abrasion reduction as a percentage is present in Fig. 6.

Abrasion test results reveal that the abraded volume of GO-incorporated concrete was significantly reduced when increasing the GO content in the concrete mix. Concerning the control mix, an increment of 2.0, 2.6, 9.8, and 22.9% of abrasion resistance was obtained at GO percentages of 0.02, 0.04, 0.06, and 0.08% respectively at

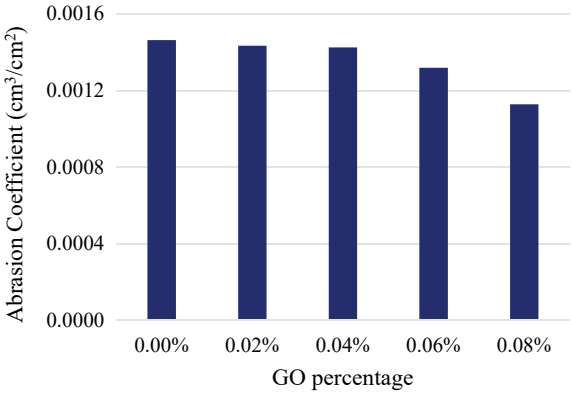

Fig. 5 Abrasion coefficient versus GO%

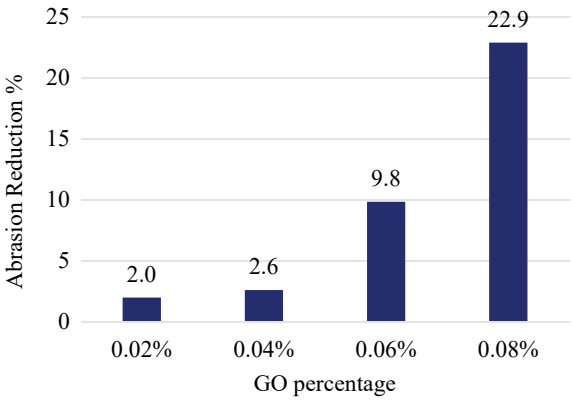

Fig. 6 Abrasion reduction percentage

the age of 28 days. Therefore, the addition of GO can drastically improve the abrasion resistance of concrete as observed. Abrasion resistance of concrete is an important parameter where the rigid pavement will be subject to heavy abrasive actions. Therefore, it is a great advantage of GO-incorporated concrete which will give 22.9% abrasion resistance enhancement by adding 0.08% GO (by weight of cement) into the concrete. An increment of 70% for abrasion resistance of GO concrete was reported by [6], with the addition of 0.3% of GO (by weight of cement) which can be considered as a high percentage of GO compared to the current investigation.

It is also a key consideration in concrete road pavements to prevent the road surface from becoming polished and losing its finish skid resistance. Due to the superior abrasion resistance of GO-incorporated concrete, it can improve the service life of rigid pavements, thus leading to less maintenance over time and saving millions of dollars in road construction and maintenance costs.

4 Conclusion

This experimental study evaluated GO-incorporated concrete's performance in applying rigid pavements from the aspects of compressive strength, split tensile strength, and abrasion resistance. Based on the experimental results and analyses reported above, the following conclusions can be drawn:

- The addition of GO in the concrete mix of about 0.08% by the weight of cement enhances the compressive strength, split tensile strength, and abrasion resistance of concrete by 20.7, 11.8, and 22.9% compared to the concrete mix without GO.
- As expected, the strength parameters and abrasion resistance were increased when increasing the GO percentage of the mixture which gives a linear increment for both strength results (compression and split tensile) and exponential type increment for abrasion test results. However, the improvement of performance was more effective on the abrasion resistance than on the strengths.
- In the application of rigid pavements, GO-incorporated concrete can be successfully utilized due to its excellent abrasion resistance and strength performance.
- The strength of concrete increases with the addition of GO thereby contributing to the reduction of overall cement and material usage and thus decreasing its carbon footprint which is an important attribute as a sustainable solution in the construction industry.

Global cement production has been significantly increasing due to the massive urbanization of countries. The concrete industry is currently the second-largest industrial emitter of CO_2 and the third-largest industrial energy user in the world [3]. On top of that, the cement manufacturing process massively affects global carbon

emissions. Therefore, adding GO into normal concrete can effectively reduce the overall concrete and cement production in the world, ultimately reducing global CO_2 emissions.

References

1. (TFNSW)-Australia TFN (2021) Transport for NSW (TfNSW) QA Specification R83—Concrete Pavement Base. Transport for NSW: Transport for NSW
2. Akarsh PK, Bhat AK (2021) Graphene oxide incorporated concrete for rigid pavement application. Trends Civ Eng ChallS Sustain
3. Chuah S, Pan Z, Sanjayan JG, Wang CM, Duan WH (2014) Nano-reinforced cement and concrete composites and new perspective from graphene oxide. Constr Build Mater 73:113–124
4. Hassani A, Fakhim B, Rashidi A, Ghoddousi P (2014) The influence of graphene oxide on mechanical properties and durability increase of concrete pavement. Int J Transp Eng 2
5. Kang D, Seo KS, Lee H, Chung W (2017) Experimental study on the mechanical strength of GO-cement composites. Constr Build Mater 131:303–308
6. Mohotti D, Mendis P, Wijesooriya K, Fonseka I, Weerasinghe D, Lee CK (2022) Abrasion and Strength of high percentage Graphene Oxide (GO) incorporated concrete. Electron J Struct Eng 22:37–43
7. Pavements ASFC (2020a) Ascp-sustainable-concrete-pavements-pavement note 002
8. Pavements ASFC (2020b) Operational and community benefits, in pavement note 001. Australian Society for Concrete Pavements
9. Sobolev K, Ferrada Gutierrez M (2014) How nanotechnology can change the concrete world. Prog Nanotechnol
10. White G (2017) Airfield pavement essentials-airport practice note 12. Australian Airports Association: Australian Airports Association

The Role of Professionals Involved in the Built Environment in Contributing to Climate Change Adaptation in Sri Lanka

Deshan Pasindu, Bawantha Rathnayaka, Dilum Rajapaksha, Chandana Siriwardana, and Lalith Rajapaskse

Abstract Climate change (CC) has turned into a global challenge, and its ramifications have continued to affect, endanger, and influence most people's livelihoods worldwide. Sri Lanka is an island vulnerable to disasters and extreme weather events. In general, urban areas are in danger due to a lack of Climate Change Adaptation (CCA) strategies in growth plans. Within this context, the built environment professional has a great responsibility in implementing CCA measures within the built environment. This study attempts to identify the roles and responsibilities of the built environment professional in adapting the built environment to climate change and building climate resilience within the built environment. A semi-structured interview series was designed and conducted inquiring about the concerns about corporate accountability, disclosure practices related to climate change, and roles, responsibilities, and challenges faced by the built environment professional in implementing the CCA strategies. Accordingly, a variety of stakeholder groups representatives from professional bodies, which include government and semi-government organizations, NGOs and intergovernmental organizations, private organizations, and independent professional organizations, were interviewed. Significant qualitative data about the roles and responsibilities of built environment stakeholders involved in climate adaptation measures, as well as details on their formal education and training, challenges they have encountered, data sharing strategies, and knowledge gaps based on climate change strategies, were obtained from the interview series. It was identified that there is a considerable knowledge gap among the built environment professionals about effective responses and adaptation mechanisms to address the climate change impacts within the built environment. Additionally, the appropriate framework for accessing climate-related data should be maintained. The findings from this study could help built environment organizations to strengthen the capabilities of the professionals within their organizations to adapt to climate change and make the climate resilient of the built environment.

D. Pasindu (✉) · B. Rathnayaka · D. Rajapaksha · C. Siriwardana · L. Rajapaskse
University of Moratuwa, Moratuwa, Sri Lanka
e-mail: 170660l@uom.lk

© The Author(s), under exclusive license to Springer Nature Singapore Pte Ltd. 2023

R. Dissanayake et al. (eds.), *ICSBE 2022*, Lecture Notes in Civil Engineering 362,
https://doi.org/10.1007/978-981-99-3471-3_43

Keywords Built environment professionals · Climate change · Climate change adaptation · Professional bodies

1 Introduction

Climate change, primarily triggered by anthropogenic activities, is currently one of the most important environmental issues [6]. The term "climate change" describes a change in the climate's condition that can be identified by changes in the mean and/or variability of its characteristics and that lasts for a long time, usually decades or longer [1] Global warming is anticipated to have far-reaching consequences on natural water resources, the built environment, agriculture, and the coastal environment, with many consequences such as causing higher temperatures, more frequent droughts, irregular rainfall, and a rise in sea level, all of which may be facing significant risks to Sri Lankan communities and livelihood of the community [13].

"The built environment mainly consists of buildings (residential and commercial) and infrastructures such as water, transportation, electricity, energy, telecommunication, health, and wastewater management"[13]. Climate change has significant negative consequences on human health, primarily manifested through heat-related deaths and illnesses, as well as the scarcity of food and water. These adverse impacts stem from the deterioration of atmospheric conditions caused by climate change. Moreover, climate change gives rise to various economic challenges, such as energy shortages, damage to infrastructure, and escalating industrial losses. These detrimental effects can hamper economic growth and stability, posing considerable obstacles for industries and societies at large. When assessing the ramifications of climate change on ecosystems, several factors come into play, including the productivity of these ecosystems, the melting of ice, heightened organic inputs impacting marine and lake productivity, as well as the occurrence of wildfires [4]. And change directly affected the transport system, buildings, and water-related infrastructures as well [2]. Therefore, adaptation of the built environment to climate change is one of the most challenging tasks in the globe, owing to the high climatic variations.

The built environment sector is comprised of several experts, including engineers, architects, surveyors, lighting specialists, landscape architects, urban designers, and planners. Furthermore, there may also be project managers, attorneys, and other administrative personnel engaged to assist projects in operating more efficiently (Built Environment Professionals—BHCPRO 2016). Engineering activities have a significant impact on the built environment since engineers must also consider the environmental system, social system, and economic system as well. One of the major roles of the engineer is to utilize the quality of the natural resources that have been left in the world [5]. This research seeks to identify the roles, responsibilities, challenges, reasons, and potential solutions in adapting the built environment to climate change with a special reference to Sri Lankan engineers. Furthermore, key roles and responsibilities of selected organizations of climate change experts as well as skills and knowledge gaps were also identified during the presented study.

2 Literature Review

2.1 Climate Variation in Sri Lanka

Sri Lanka is one of the world's hottest countries, with a mean temperature of around 27–28 °C [16]. The four main factors to consider when considering climate change are temperature, precipitation, extreme events, and sea level rise. It was determined that Sri Lanka's atmospheric temperature is rising steadily and that warming trends are accelerating using facts and evidence [12, 15]. It was found that the variability of precipitation has increased over time and that extreme weather events have become more frequent in recent years [9, 11, 12]. There has been a noticeable escalation in the occurrence of severe phenomena such as floods and droughts in recent times. In recent years, there has been a significant increase in the frequency of extreme events such as floods and drought [10]. Concerning the sea level rise, it was determined that the Asian region is somewhat greater than the world average, with a rate of 1–3 mm per year [14]. When considering the expected climatic changes in the aforementioned elements, it was also concluded that Sri Lanka should maintain an effective Climate Change Adaptation (CCA) strategy for each and every sector of the built environment [10].

2.2 Climate Change Adaptation (CCA)

Climate Change Adaptation (CCA) is a dynamic process of adjustment in response to changing conditions of climate. In recent years, adaptation to climate change has emerged as an important topic in scholarly discourse, and these studies have proposed different adaptation measures in different sectors (Adger et al. 2009; Agyekum et al. 2019; Johnson and Kulatunga n.d.; Solomon et al. 2007; Wheeler et al. 2013). In terms of climate adaptation in Sri Lanka, food security (mostly agriculture) and ecosystems are the top priority, with water resources, coastal zone management, and urban areas all being of great significance. Some literature revealed that there are five major gaps that prevent successful adaptation to climate change effects in every context: information gap, technical gap, policy and governance gap, institutional and coordination gap, and resource mobilization gap [10]. According to the "Policy challenges in climate adaptation in Sri Lanka" [8], all national and local organizations should focus on creating the conditions necessary to overcome the CCA gaps. Therefore, this study is being conducted to determine the organizations' awareness and what they are doing in the context of climate change, and it could be highly effective in identifying the gaps for each institution to overcome the climate change challenges.

2.3 Built Environment Professionals

While the term "built environment" has multiple definitions in the literature. The "built environment" can be defined as the man-made environment that consists of physical structures and supporting infrastructures such as transportation, water, electricity, etc., or a socio-ecological system [7]. A sector is defined as "a sociological, economic, or political division of society that contains similar types of agencies and organizations" [3].

The phrase "built environment professional" is used to describe a wide range of professionals from a variety of fields who work together to design, maintain, and enhance the built environment [5]. All built environmental professionals operate within a network of stakeholders and stakeholder groups that have direct and indirect effects on the quality of the built environment, individuals with unique responsibilities, and domains of influence [5].

According to the "National Adaptation Plan for Climate Change Impact in Sri Lanka," the agriculture, livestock, and fisheries sector, the water resources sector, the coastal and marine sector, the health sector, the human settlement and infrastructure sector, the ecosystems, and biodiversity sector, the industrial energy, and transportation sectors are the most critical key sectors requiring adaptation to climate change. It is also noted that the key stakeholders who can implement the CCA goals in Sri Lanka include the government sector, the private sector, civil society organizations, academics, researchers, other knowledge providers, and local community-based organizations. Moreover, the specialists who have chosen to undertake this research are drawn from the aforementioned stakeholders.

3 Methodology

A comprehensive literature review was conducted to identify climate change-related concerns associated with the built environment, including the built environment. Then it identified the built environment professionals associated with climate change adaptation.

This research utilized a qualitative approach to comprehensively address the research problems (what are the climate-related problems in Sri Lanka and what are the possible solutions to overcome them within the built environmental professionals?) and accomplish the research aim. Due to the necessity to reveal current data and identify knowledge gaps that may be applied in the industry, a qualitative technique was used. For this purpose, several questions were formulated for the interview. The responses provided in relation to the formulated questions will offer valuable insights into the context of the built environment and its association with climate change. Analyzing these responses will provide a reliable understanding of how the built environment influences and is influenced by climate change.

Figure 1 represented the methodology flow chart that has been followed. This interview guide was developed based on three sections to identify the three most important components. The first component of the questionnaire gathered respondents' background information. The second section was to identify the role of the built environment stakeholders in CCA measures, and the third section was to identify the built environment stakeholders' challenges, reasons, and proposed solutions based on the challenges related to climate change and the built environment.

A series of interviews with industry experts (All the engineers have more than four years of experience in the built environment in relation to climate change, and their current organizations' positions are connected to climate change) representing various built environment professional organizations were undertaken to clarify the research.

This study was conducted to explore the roles, responsibilities, challenges, reasons, and possible solutions associated with adapting the built environment to climate change, focusing on Sri Lankan engineers.

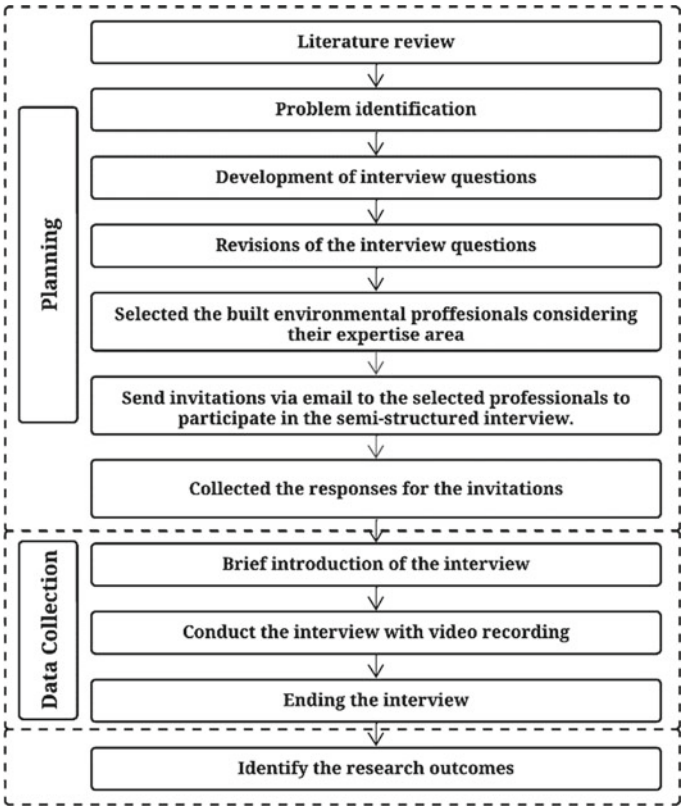

Fig. 1 Methodology flow chart

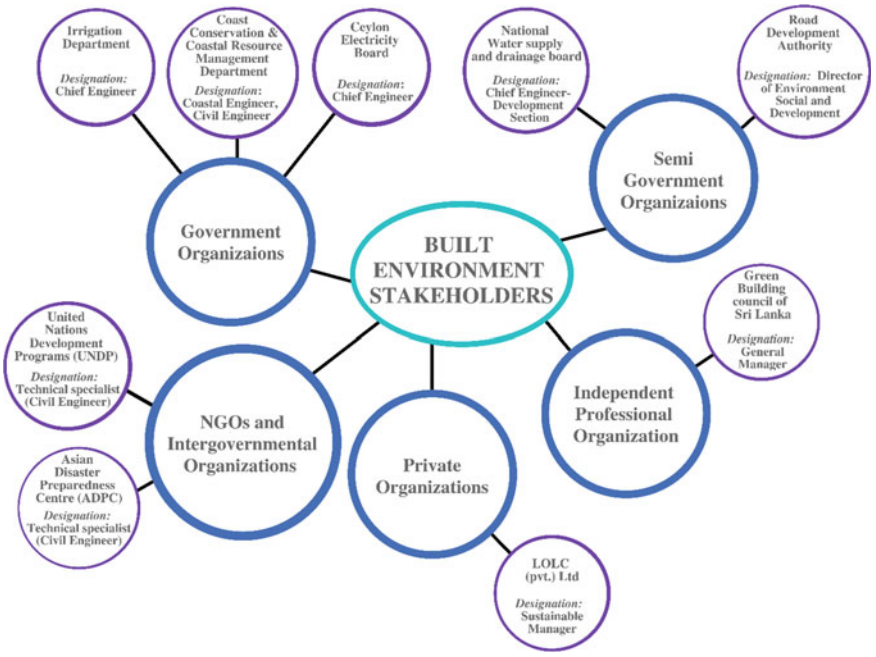

Fig. 2 Built environment stakeholders and selected organizations

According to Fig. 2, an interview series focused on the five organizations, including government, semi-government, NGOs, international, private, and independent professional organizations. Figure 2 depicts chosen institutions based on the selected organizations and the designation of the interviewee at each institution, and each interviewer has more than four years of experience in the built environment industry as well. Other than two professionals, every other professional was affiliated with a professional organization.

Based on their areas of specialization, 20 built environment specialists who are currently engaged in the industry were emailed prepared invitations for semi-structured interviews. Nine responses were received within four weeks by agreeing to participate in the interview. In order to address the specified research questions, Sri Lankan built environment professionals who agreed to participate were interviewed via an online platform between September and November 2022. Each interview was recorded and spanned around 30–45 min.

4 Discussion

Following are the summaries of the outcomes extracted from the expert interviews.

According to the perspective of selected built environment experts, the following Table 1 depicts the most significant obstacles to CCA in Sri Lanka, concerning the built environment, professionals, and the training of built environment professionals.

Table 2 contains a summary of the organizational challenges, the causes for those challenges, and the experts' recommendations for overcoming the challenges, as derived from the expert interviews. The institutions' key roles and responsibilities concerning the CCA in the built environment were identified during the interviews. Table 3 depicts these roles and responsibilities organizationally.

Figure 3 represents at which level (senior, middle management, junior, and intern) the selected organizations perceive the skills gap to be the most significant. It was identified that junior personnel, as well as interns and middle management personnel, lack a significant understanding of CCA.

Table 1 Most significant obstacles related to the Built environment, Professionals in the industry, and the training of built environment professionals

Built environment	Professionals in the industry	The training of built environment professionals
1. It should be more concerned with the proper land use patterns of the country, mainly based on climatic extremes 2. It should be constructed climate resilient structures based on landslides and floods 3. The huge disparity between the appropriate ventilation systems in local buildings to maximize energy efficiency (Lack of eco-friendly buildings measures implemented) 4. Lack of technology about climate change and the built environment, as well as the shortage of analytical tools such as supercomputers	1. The industry is involved in policy development and formulation but rarely makes use of research publications (Inter-agency collaboration issue and Industry-academia collaboration issue) 2. Lack of knowledge related to climate change and CCA measures as well	1. The sub-national and national levels lack standard capacity building and knowledge sharing secessions based on climate change and the built environment 2. More climate change awareness programs related to climate change should be undertaken 3. Some professions have adequate academic knowledge of climate change but lack sufficient exposure and practical experience to apply adaptation methods

5 Conclusion and Recommendations

Concerning the responses extracted from the expert interview, all the experts stated their team members needed appropriate knowledge and training regarding climate change. They suggested that their team members need to be engaged in Continuing Professional Development (CPD) courses based on climate change.

Table 4 represents the major skill gaps and knowledge gaps associated with built environment professionals related to CCA, and the relevant responsible authorities should take steps to overcome these knowledge and skill deficiencies.

Since Sri Lanka has a number of frameworks, acts, and guidelines pertaining to climate adaptation, it was determined that there is a significant issue with their implementation. Interviewers suggested strengthening the legal framework and enforcement to implement these because it should have an effective legal framework in the country.

In addition, it was suggested that a centralized platform for accessing climate-related data in Sri Lanka be established. Finally, this study attempts to identify the key roles and responsibilities of the built environment professionals in CCA. Eventually, several key roles and responsibilities have been identified through this study. Furthermore, challenges faced by the built environment professional and solutions to overcome the challenges were identified during the study. The findings from this

Table 2 Built environment organizational challenges, reasons, and proposed suggestions

Type of the organization	Challenges	Reasons	Suggestions
Government and semi-government organizations	1. The main issue is a lack of data. (That indicates that even while there are data available in many institutes, we require a platform for sharing them in order to use them for research or other decision-making) 2. There is a knowledge gap in government institutions concerning climate change 3. The funding available to perform climate change research is constantly limited 4. Lack of organizational members' ability to perform when it comes to climate-related challenges	1. Government officials lack awareness and education on climate change 2. Lack of a government entity to implement climate change-related legislation and regulations 3. There is a lack of training options for academics and government employees 4. Data on climate change is only available from a few sources. There is no centralized platform	1. The establishment of measures to enhance government employees' capabilities 2. Improving political leadership's understanding of the significance of funding CCA programs 3. Develop a centralized platform with climate-related data included. – Currently, the Secretariat for Climate Change is working to create an accessible national database

(continued)

Table 2 (continued)

Type of the organization	Challenges	Reasons	Suggestions
NGOs and intergovernmental organizations	1. Governmental and non-governmental organizations are provided with insufficient opportunities to engage in climate change-related initiatives 2. Lack of support extended by governmental organizations to implement CCA measures 3. Public disturbances are a result of their reluctance to modify their behavior	1. Lack of climate change awareness and education of officials 2. Lack of a government organization to carry out laws and regulations related to climate change 3. Lack of training opportunities available to professionals 4. Knowledge about climate change among the public is very limited	1. Establishment of procedures to improve the capabilities of officials 2. Develop a centralized platform with climate-related data included. – Currently, the Secretariat for Climate Change is working to create an accessible national database 3. Integration of NGOs and intergovernmental organizations into policy formulation 4. All NGOs and intergovernmental organizations should have equal access to opportunities to engage in activities related to combating climate change 5. Building capacities of agencies to independently source and apply for global funding and networking opportunities 6. Increasing the awareness of climate change among the general public
Private and independent professional organizations	1. Incapability to participate in the development of national CCA policies 2. Governmental organizations' lack of support for implementing climate change adaption measures	1. Lack of recognition of the valuable contribution private organizations can make in drafting policies 2. Officials' lack of understanding and education on climate change 3. Lack of available funding opportunities	1. Integration of private organizations into policy formulation activities 2. Introducing mechanisms to enhance the capacities of officers 3. Building capacities of agencies to independently source and apply for global funding and networking opportunities

Table 3 Key roles and responsibilities of the selected stakeholders within their respective organizations

Organization	Key Roles	Key Responsibilities
Government and Semi-government organizations	1. Implementation of CCA measures and mitigation strategies at the national level 2. Enhancing government officials' skills and improving public understanding of climate change	1. Obtaining funding from international and domestic contributors to support organizational and government projects 2. CCA policies, guidelines, and national plans are being created, updated, and implemented 3. Provide some operational and maintenance training programs integrated into the successful execution of government and other projects
NGOs and intergovernmental organizations	1. Implementation of CCA measures and mitigation strategies at the organizational level 2. Financing climate change strategies implemented by government agencies 3. Enhancing government officials' skills and improving public understanding of climate change	1. Obtaining funding from foreign and local donors to fund initiatives of organizations and government agencies 2. CCA strategies are being implemented in specific regions 3. Conducting programs in place to update existing policies, guidelines, and national plans in the context of climate change 4. Provide some operational and maintenance training programs integrated into the successful execution of government and other projects
Private and independent professional organizations	1. Provide loans and other facilities, and if the customers are affected by climate change extreme events 2. Implementation of CCA measures and mitigation strategies at the organizational level 3. Producing products and providing services to relevant organizations to be used for CCA and mitigation measures	1. Implementation of climate change mitigation measures at the organizational level, such as the use of sustainable materials while doing the construction and implementing some programs related to reforestation 2. Engaging in research and innovation activities to produce products and services to address climate change 3. Providing financial and technical support to relevant organizations to address climate change-related challenges

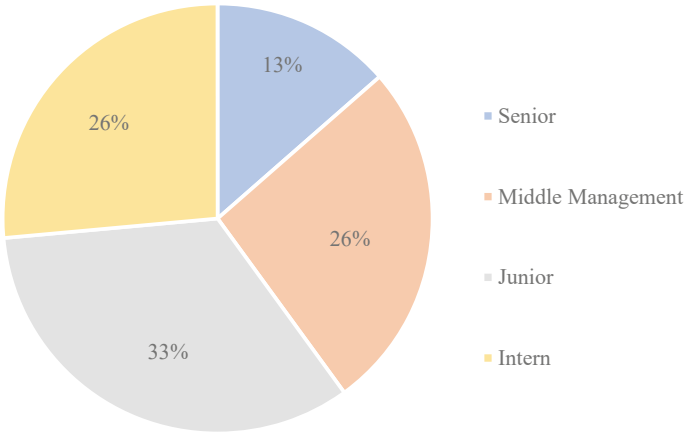

Fig. 3 Skills shortage related to the climate change by considering each organization levels

Table 4 Identified skill and knowledge gaps within built environment professionals

Skill Gaps	Knowledge Gaps
1. Integrated working ability (Teamwork, supervision of the team, decision-making, etc.,) 2. Technical skills (Computer modeling (especially hydraulic modeling), mapping (lack of knowledge based on GIS), programming, supercomputer operating knowledge and.etc.,) 3. Communication skills (Issues of inter-agency collaboration and industry-academic collaboration, conveying decisions, etc.,)	1. Climate change. Mitigation and adaptation knowledge (Sea level rise, global warming, lack of knowledge of the numerical models, greenhouse effect, coastal disaster vulnerability, coastal water quality, heat island effect, alternation of ocean currents/ difference related to climate effect) 2. Research and investigation (Methods of data collection, sample selection, research methodology, data analysis/analytical tools/ data presentation/ academic writing, and so on) 3. Due to a lack of experience, theoretical knowledge and innovative findings reflect the reality 4. Green building concepts 5. Climate change legislation, policies, and national plans

study could help built environment organizations to strengthen the capabilities of the professionals within their organizations to adapt to climate change and make the climate resilient of the built environment.

It was recommended to have a similar study based on the other professional bodies as well.

Acknowledgements The authors wish to acknowledge the EU-funded ERASMUS+ "BEACON" project for the funding provided to conduct this study. Also, the authors thank experts involved in the interview series for the constructive support and the time rendered.

References

1. Abbass K, Qasim MZ, Song H, Murshed M, Mahmood H, Younis I (2022) A review of the global climate change impacts, adaptation, and sustainable mitigation measures. Environ Sci Pollut Res 29(28):42539–42559. Springer Science and Business Media Deutschland GmbH. https://doi.org/10.1007/s11356-022-19718-6
2. Chappin EJL, van der Lei T (2014) Adaptation of interconnected infrastructures to climate change: Asocio-technical systems perspective. Util Policy 31:10–17. https://doi.org/10.1016/j.jup.2014.07.003
3. Cilenti D, Issel M, Wells R, Link S, Lich KH (2019) System dynamics approaches and collective action for community health: an integrative review. In Am J Community Psychol 63(3–4):527–545. Wiley Blackwell. https://doi.org/10.1002/ajcp.12305
4. Grimm NB, Chapin FS, Bierwagen B, Gonzalez P, Groffman PM, Luo Y, Melton F, Nadelhoffer K, Pairis A, Raymond PA, Schimel J, Williamson CE (2013) The impacts of climate change on ecosystem structure and function. Front Ecol Environ 11(9):474–482). https://doi.org/10.1890/120282
5. Hartenberger U, Lorenz D, Lützkendorf T (2013) A shared built environment professional identity through education and training. Build Res Inf 41(1):60–76. https://doi.org/10.1080/09613218.2013.736202
6. Hoffmann R, Muttarak R, Peisker J, Stanig P (2021) Climate change experiences raise environmental concerns and promote green voting. https://doi.org/10.21203/rs.3.rs-738080/v1
7. Hürlimann AC, Warren-Myers G, Nielsen J, Moosavi S, Bush J, March A (2022) Towards the transformation of cities: a built environment process map to identify the role of key sectors and actors in producing the built environment across life stages. Cities 121. https://doi.org/10.1016/j.cities.2021.103454
8. Institute of Policy Studies of Sri Lanka (2016) Climate-Change-Issues-in-Sri-Lanka-January-2016-Volume. 02_E_Book
9. Kwon H-H (2017) Quantile regression analysis: a novel approach to determine distributional changes in rainfall over Sri Lanka. https://crudata.uea.ac.uk/cru/data/hrg/cru_ts_3.22/
10. National Adaptation Plan for Climate Change Impacts in Sri Lanka Climate Change Secretariat Ministry of Mahaweli Development and Environment 2016 (2016)
11. Nianthi KWGR, Shaw R (2015) Climate change and its impact on coastal economy of Sri Lanka. The global challenge, pp 1–21. http://citeseerx.ist.psu.edu/viewdoc/download?doi=10.1.1.455.6242&rep=rep1&type=pdf
12. Nissanka SP, Punyawardena BVR, Premalal KHMS, Thattil RO (2011) Recent trends in annual and growing seasons' rainfall of Sri Lanka. Researchgate Net. https://www.researchgate.net/profile/S-Nissanka-2/publication/315765979_Recent_trends_in_annual_and_growing_seasons_rainfall_of_Sri_Lanka/links/58e32a794585154eb7123ac4/Recent-trends-in-annual-and-growing-seasons-rainfall-of-Sri-Lanka.pdf
13. Rathnayaka B, Siriwardana C, Amaratunga D, Haigh R, Robert D (2023) Climate change impacts on built environment: a systematic review, pp 443–459. https://doi.org/10.1007/978-981-19-2886-4_31
14. Cruz RO, Jafari M, Lal M (2007) Impact of climate change on intensity and frequency of extreme cyclones view project Mostafa Jafari RIFR and TPS for LFCCs. https://www.researchgate.net/publication/284683271
15. Sathischandra HG, Marambe B, Punyawardena R (2014) Seasonal changes in temperature and rainfall and its relationship with the incidence of weeds and insect pests in rice (Oryza sativa L) cultivation in Sri Lanka. ResearchgateNet. https://doi.org/10.5958/2320-642X.2014.00002.7
16. Sri Lanka Climate Risk Country Profile (2020) www.worldbank.org

A Systematic Literature Review on Climate Change Adaptation Measures for Coastal Built Environment

Dilum Rajapaksha, Bawantha Rathnayaka, Chandana Siriwardana, and Lalith Rajapakse

Abstract The built environment has been adversely affected due to the increased impacts of climate change over the past decades. Especially the coastal built environment is more vulnerable to such impacts since the areas are frequently subjected to climate extremes. Adapting to such impacts and functioning during climate extremes are vital for the coastal built environment as they substantially contribute to the economy of the country. However, incorporating adaptation measures only for physical assets of the built environment is inadequate as climate change impacts adversely affect the economy, society, and environment because of the interrelationship with the physical assets. Hence, a Systematic Literature Review (SLR) is employed to explore Climate Change Adaptation (CCA) measures that can be implemented to protect the built environment components. From 2379 suggested articles on the Scopus, Science Direct, and Web of Science scientific databases, 106 most related articles were selected for the study through a structured screening process. Adaptation measures that can be implemented to protect the physical assets of the built environment as well as the economy, society, and environment were retrieved from the selected articles and discussed in this study. Also, identified governance and institutional measures for facilitating the CCA were discussed. The different sectors of physical assets of the built environment, such as transportation infrastructures, residential and commercial buildings, water infrastructures, telecommunication infrastructures, and electricity and energy infrastructures covered by the identified CCA measures. Those measures have been correlated to the applicable life cycle phase to clearly determine the applicable life cycle phase of employing each adaptation measure. The findings provide a comprehensive list of adaptation measures that apply to the built environment components and will help professionals in the built environment adjust to and lessen the effects of climate change.

Keywords Climate change adaptation · Coastal built environment · Systematic literature review · Life cycle phases · BEACON

D. Rajapaksha (✉) · B. Rathnayaka · C. Siriwardana · L. Rajapakse
Department of Civil Engineering, University of Moratuwa, Moratuwa, Sri Lanka
e-mail: rajapaksharadv.22@uom.lk

© The Author(s), under exclusive license to Springer Nature Singapore Pte Ltd. 2023

R. Dissanayake et al. (eds.), *ICSBE 2022*, Lecture Notes in Civil Engineering 362,
https://doi.org/10.1007/978-981-99-3471-3_44

1 Introduction

Climate change has become significant over the recent decades, and now the world is facing its consequences. As evidence of climate change, the nine years from 2013 to 2021 were among the ten warmest years on record, with the last year (2021) being listed as the sixth. Additionally, from 2015 through 2021, the yearly Arctic Sea ice content was among the ten smallest ever recorded. Ninety-four named storms have been recorded in the year 2021, which is also above-average global cyclone activity. Considering global precipitation patterns, in regions of the western contiguous United States, southern South America, northern Africa, the Middle East, and some Pacific Islands, annual precipitation was noticeably below average, whereas significantly above-average precipitation was recorded in the regions of southern Asia, eastern Europe, western and eastern Australia, and northern South America [81]. The coastal region is one of the major affected areas since those areas are frequently subjected to submergence, erosions, and flooding due to extreme events [3].

The coastal built environment, which is situated along the coastline, has become vital due to its substantial contributions to the economies of the countries [29, 76, 126]. For instance, major infrastructures such as ports, airports, and major expressways lie along the coastal line serving the transportation of goods and people in Sri Lanka. The economy of the country is greatly impacted if these transportation systems are significantly disrupted. However, as discussed, the coastal built environment has been subjected to the effects of climate change. As most of the world's population and economic activities are concentrated in built settings, which are more vulnerable to climate change impacts, those who are involved in creating and managing built environments must be prepared for climate change. Many nations have devoted significant attention to CCA in the context of the built environment to cope with the challenges posed by climate change [15, 51, 61, 100].

Even if the nations have implemented multiple steps to control climate change by reducing Green House Gas (GHG) emissions, some further degree of climate change extreme events will be unavoidable, with severe economic, social, and environmental consequences for communities [25, 86, 96]. Therefore, nations will need to adapt to mitigate the negative effects of climate change [100]. The IPCC defines adaptation as an "adjustment in the natural or human system to a novel or shifting environment or in response to actual or expected stimuli or their effects, which moderates harm or utilises beneficial opportunities" [50]. Adaptation focuses on mitigating negative effects while also building resilience and reaping any benefits that may arise. It is all about preventing disasters, dealing with existing hazards or planning for a future threat that is not (yet) recognised as imminent [85, 107, 116]. Adaptation can be reactive, occurring in response to impacts, or proactive, occurring before the impacts of climate change become apparent. Most often, proactive adaptations will be less expensive in the long run and more effective than reactionary adaptations [37, 38].

Adaptation actions include large-scale infrastructure changes, like building coastal defences, heat insulation, revised standards, improved drainage or behavioural shifts like individuals using less water. Such adaptation measures were

suggested, employed, and tested by previous research aiming at different built environment sectors, components, and different types of hazards. This study employs a Systematic Literature Review (SLR) to explore the adaptation measures for climate change impacts, especially focusing on the coastal built environment. Also, other related components of the built environment, such as society, economy, and environment, have been identified, and adaptation measures applicable to those areas are also retrieved. Finally, identified adaptation measures for the built environment were categorised based on their applicability to the different phases of the project life cycle.

2 Components of the Built Environment

The phrase "built environment" refers to man-made environments for human activity, such as buildings, parks and green spaces, as well as neighbourhoods and cities, which may include supporting infrastructures such as water supply and electricity networks [53, 92]. The following sectors of the built environment were taken into study under the phrase "physical assets", and it made the scope of the study more defined. Those are 1. Residential and Commercial buildings, 2. Transport infrastructures, 3. Water supply-related infrastructures, 4. Telecommunication infrastructures, 5. Electricity and Energy sector infrastructures, and 6. Other infrastructure categories.

However, due to the integrated nature of the community, infrastructures are actively interacting with other areas. Previous authors have considered those areas in their studies accordingly. Based on the study conducted by Haigh and Amaratunga [40], the built environment has the ability to contribute to the resilience of the community along with the essential roles of constructing, developing, stimulating, facilitating, protecting, and nurturing. This will strengthen the different areas of physical assets, social assets, economic assets, governance assets, environment assets, and social cohesion. Mottaeva [74] has classified the interactions of construction activities into the areas of social, environmental, natural, economic, and regulatory. Kaklauskas and Gudauskas [55] have shown that the life cycle of the built environment can be assessed in different areas, including economic, social/cultural, environmental, and policy decisions, due to the interaction with those areas. Zhang et al. [127] have highlighted that the benefits of construction land use are directly linked with the social, economic, and eco-environment benefits systems. Also, Liu et al. [63] have identified that most built environment-related studies also focus on sustainable development from a bibliographic study. There are interconnections among the social, environmental, and economic assets. But since the main focus of this study lies on the physical assets, those relations are not considered in this study. Apart from that, previous studies have identified that governance actions can be incorporated to minimise the effects of climate change impacts. Therefore, it is essential to consider different sectors interrelating with the physical assets of the infrastructures. Considering the above discussed points, the classification shown in Fig. 1 will be followed as the components of the built environment in this study.

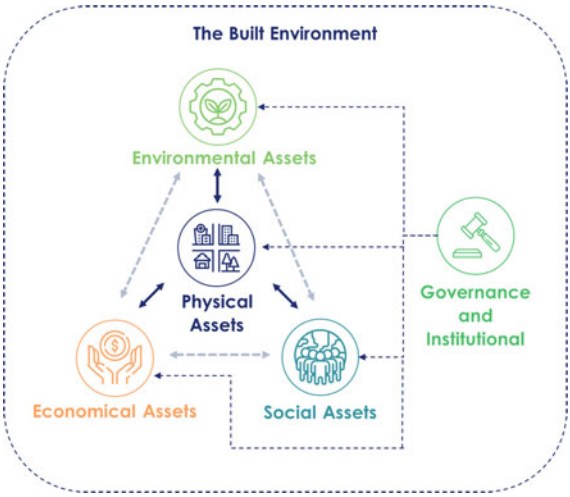

Fig. 1 Scope of the built environment for the study

3 Methodology

A Systematic Literature Review (SLR) has been employed in this study to identify the CCA measures. SLR is a research methodology that gathers, evaluates, and summarises all empirical data that satisfies predetermined eligibility criteria to answer specific research questions [10]. The following research questions were framed under the discussed scope for the literature review:

1. What are the possible CCA measures for physical assets of the built environment?
2. What are the possible CCA measures for mitigating climate change impacts on society, the economy, and the environment?
3. What are the possible governance and institutional measures to facilitate CCA?

The literature was gathered from three scientific databases, namely; Scopus, Web of Science, and Science Direct to identify the CCA measures. These databases were selected due to the availability of a broader range of peer-reviewed journal articles from international publishers. The search query was developed from the combinations of the key terms in Table 1. The included key terms were selected to represent the key thematic areas of the study.

The Preferred Reporting Items for Systematic Reviews and Meta-Analyses (PRISMA) guideline was used in performing the SLR in this study. The PRISMA guidelines contain four steps: identification, screening, eligibility, and inclusion [113]. Only journal articles written in English were included in the study. A summary of the record selection process is shown in Fig. 2.

The proposed CCA measures were extracted from the included articles. Special concern was given to the CCA measures, which can be applied to the coastal infrastructure considering the criticality. As identified in Sect. 2, the proposed CCA measures were extracted under all selected built environment components,

Table 1 Selected key terms to generate the search query

Key thematic area	Key terms
Physical assets of the built environment	Built environment, critical infrastructures, electricity, energy, water, transportation, telecommunication, residential buildings, commercial buildings
Components of the built environment	Social, governance, economy, environment, ecosystem
Climate change adaptation	Climate change adaptation, mitigation

which are physical assets, social assets, economic assets, and environmental assets. The suggested institutional and governance measures to facilitate CCA were also extracted. The importance of categorising the CCA measure under the different phases of the project life cycle is discussed, and the identified adaptation measure for physical assets was conceptually categorised under the different phases of the project life cycle based on mutual agreement among the authors. The findings of the study are presented in the next sections.

4 Results and Discussion

This section contains the results of the SLR. Section 4.1 presents the identified CCA measures for physical assets of the different built environment sectors. Also, it identifies the most appropriate life cycle phase to apply each measure. Sections 4.2, 4.3 and 4.4 discuss the identified CCA measures for social, economic, and environmental assets, respectively. Section 4.5 identifies the possible governance and institutional measures to facilitate CCA.

4.1 Climate Change Adaptation Measures for Physical Assets

This section presents the identified adaptation measures for the physical assets of the built environment. As mentioned above, it includes residential and commercial buildings, transport infrastructures, water infrastructures, telecommunication infrastructures, electricity and energy sector infrastructures, and other infrastructure categories. Figure 3 illustrates the general overview of the focused sectors within the literature. As it depicts, scholars have devoted significant attention to climate change adaptation in the context of transportation infrastructures, water infrastructures, and residential and commercial buildings. A few studies have focused on other major infrastructure categories, such as the electricity and energy and telecommunication sectors.

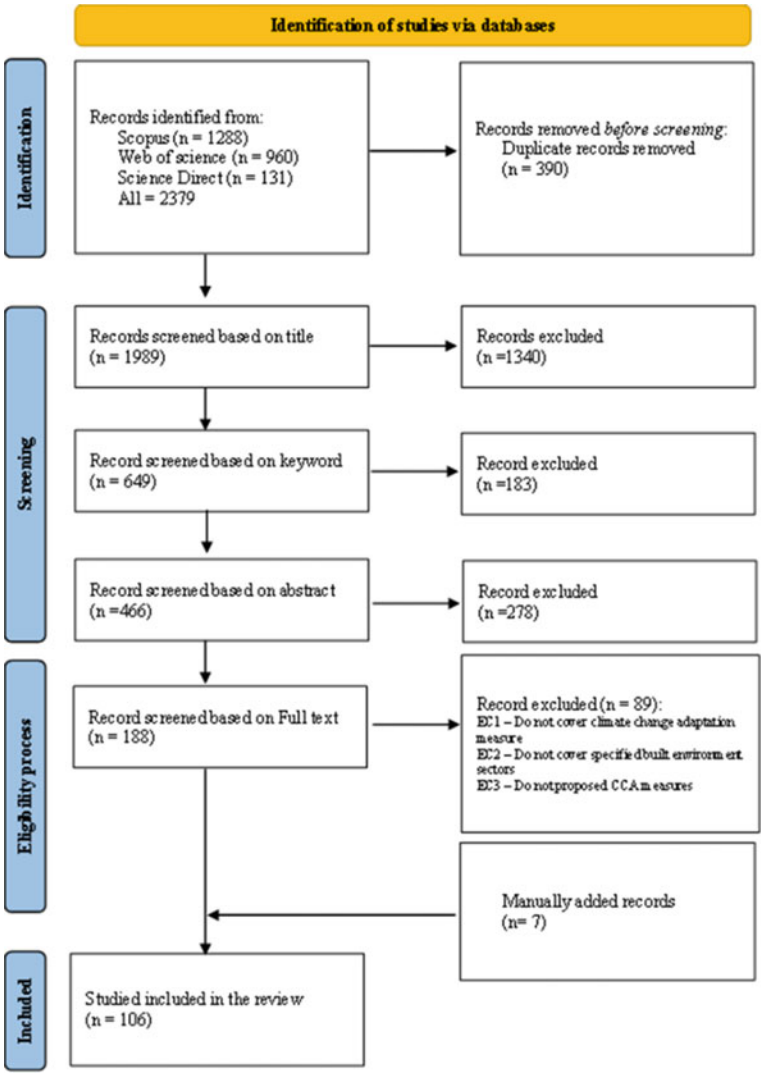

Fig. 2 Screening process of the literature

Considering the alignment of adaptation measures with the different life cycle phases is crucial for effectively functioning physical assets with challenges posed by climate change. This study considers the three main life cycle phases of the built environment project: design and planning, construction, and maintenance and retrofitting. The design and planning stage is an important step of project development. It involves a systematic approach to the installation, operation, and management of the physical assets. Under this stage, built environment professionals consider the material, structural and architectural layouts, energy performance, and structural performance

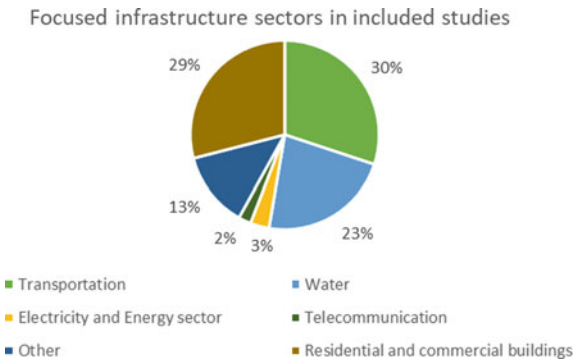

Fig. 3 Infrastructure sectors consider in the past studies

to deliver the best performance for the asset. Within this stage, climate change adaptation can be integrated into several steps. Especially, it can be identified several climate change adaptation measures under the material selection, plans, and energy performance steps. Under the construction stage, following the optimised designs and plans are crucial. Also, during this stage, following effective and efficient construction methods, recycling or reusing material can be adopted. The maintenance and retrofitting stage involves any activity performed to maintain the functionality of the infrastructures. After delivering the project, assets are subjected to maintenance and retrofitting work. Since the physical assets deal with different climate change scenarios over their lifetime, the frequency of maintenance and retrofitting work of infrastructure increases significantly, affecting the life cycle cost of infrastructures unless they acknowledge the climate change adaptation. Hence, the identified adaptation measures were categorised into the design and planning, construction and maintenance, and retrofitting stages which give more understanding of the applicable CCA measures at each phase for different sectors.

Table 2 summarises the identified CCA measures for transportation infrastructures. Table 2 includes measures including the design modifications to the structures and materials, consideration of anticipated loads in the designs, incorporation of additional protection measures, and measures related to the monitoring and maintenance of the transportation infrastructures.

Table 3 summarises the identified CCA measures for residential and commercial buildings. The measures include design modifications aiming at different hazards, changes in building usage patterns, and adopting new materials, and methods for construction.

Table 4 summarises the CCA measures for water-related infrastructures such as dams, tanks, and water pipelines. The CCA measures suggest different approaches such as design modifications to withstand different effects of climate change, innovative monitoring, and maintenance practices.

Table 5 summarises the CCA measures for energy and electricity infrastructures. The measures include design modification, revision of design threshold values based on climate change predictions, optimising the maintenance and monitoring cycle, etc.

Table 2 CCA measures for transportation infrastructure

Adaptation measure	Applicable phase			References
	Design and planning	Construction	Maintenance and retrofitting	
Rising the road level to combat the flooding	●			(Batouli & Mostafavi, 2016; Cervigni et al., 2015; Charlesworth et al., 2016; Cheng et al., 2017; V. Gupta, 2021; Major et al., 2018; Manocha & Babovic, 2017; Markolf et al., 2019; Mauree et al., 2019; Mohebbi et al., 2020; Moura et al., 2016; J. E. Neumann et al., 2015; M. B. Neumann et al., 2015; Oswald Beiler et al., 2016; Picketts et al., 2015; Qiao et al., 2020; Salerno et al., 2018; Scussolini et al., 2017; Seah et al., 2021; Simons et al., 2022; Strauch et al., 2015; van de Ven et al., 2016; World Bank, 2015)
Proper asphalt mix design suits regional climatic conditions	●			
Alternative mix design for the pavement treatment (e.g., Warm mixes, rubberized asphalt, and pervious concrete)	●			
Comprehensive snow and ice control program that includes pre-wetting surfaces to combat ice on roads and using only coarse gravel on roads to minimize air quality and aquatic impacts	●			
Consideration of traffic loads on pavements/load restrictions and Traffic demand prediction and pavement design (With the sea level rise, people move inland, increasing traffic demand)	●			
Improved data (Weather events and crashes, collision data, data sharing)			●	
A method to predict the maintenance of the road in combination with the climate change simulation model (e.g., winter severity index (WSI))	●			
Improved drainage system incorporating the Sustainable drainage system (SUDS) principles in the design	●			
Use of highly reflective coating against the urban heat island		●		
Hydrological and drainage design considering anticipated increment of the precipitation, water levels	●			
Planning for/providing alternative routes in the event of a road/railway closure	●			
Construct roadway over embankments to accept the passage of floodwaters at defined locations (ensuring safe failure)		●		
Proper sizing of the culverts/ Allow undersized culverts to be overtopped by designing for such failures ensuring safety	●			
Use appropriate embankment materials-rock fill at bridge approach, granular materials		●		
Increase longitudinal drains capacities- Ensure Road drainage is routinely shaped by the grader, protect verges and channel side slopes with appropriate vegetation cover, and ensure effective longitudinal drainage capacity in cutting to remove flood water		●		
Provide cutting slope drainage -adequate and effective drainage cut-off drains installed to the top of cutting slopes berms.		●		
Harden river defenses using retaining walls. Gabion baskets, earth dikes, random rubble		●		
Protection of the structural materials against salinity		●		
Robust pavement structures-erosion resistant surfacing	●			
Use of design guidelines for asset design	●			
Adopting tools for evaluating risk, vulnerability, and exposure of the transportation infrastructure	●		●	
Prevent build-up of debris against intermediate supports or under deck soffit through the upstream river and development management			●	
Maintainable back-of-wall drainage			●	
Scour protection around bridge abutment, wing wall, piers, minor culvert, and headwall/toe wall		●		
Deepen foundation, Pilled foundation, Cut-off sheet piling at the foundation	●			
Increase the Vertical clearance of the soffit	●			
Design a bridge to accommodate the permanent raising of the bridge deck	●			
Design the bridge as a floating bridge	●			
Improving material quality with mechanical or chemical material stabilization		●		

Table 3 CCA measures for residential and commercial buildings

Adaptation measure	Applicable phase			References
	Design and planning	Construction	Maintenance and retrofitting	
Elevated building construction in flood-prone areas	●			(Abeysinghe et al., 2020; Ahmad & Afzal, 2020; Al-Faesly et al., 2015; Ardekani & Hosseini, 2012; Bernier et al., 2015; de Ruig et al., 2020; Esteban et al., 2013; R. Gupta & Gregg, 2012; Haddad et al., 2020; Han & Mozumder, 2021; Hinkel et al., 2011; Huang & Hwang, 2016; Hudson, 2020; Hwang et al., 2009; Morin et al., 2008; Mycoo, 2014; Nofal et al., 2020; O'Malley et al., 2014; Porritt et al., 2012; Ross, 2017; Sari, 2021; Shimoda, 2010; Solecki et al., 2011; Storbjörk & Hedrén, 2011; Wu et al., 2019; Zhang et al., 2021)
Building construction on strong pillars and posts	●			
Design for the impact of the tsunami wave and debris flow	●			
Construction of seawalls	●			
Proper detailing of joints to withstand the hydraulic loads	●			
Anchoring the building to the foundation to increase the stability	●			
Increase the weight of the building to increase the stability	●			
Openings on the ground floor in flood and tsunami-prone areas	●			
Wet and dry proofing of buildings in flood-prone areas		●		
Amphibious buildings in flood-prone areas	●			
Use of flood-proof materials		●		
Post-flood drainage system	●			
Better insulation of walls, lofts, and floors for better energy performance		●		
Rainwater harvesting			●	
Solar thermal water heating to reduce energy use			●	
Low energy lighting and more natural lighting			●	
Reused or recycled material		●		
Vegetation cover around the building	●			
Use of material with high albedo rating (cool envelope materials)		●		
Shadings for windows to reduce energy use		●		
Night Ventilation and ventilative cooling			●	
Window rules for reducing energy use			●	
Green roofs, roof pond, and green facades	●			
Optimizing building orientation and placement of openings for better energy performances	●			

Table 6 includes the identified measures for telecommunication infrastructures.

Table 7 summarises identified CCA measures that can be applied generally for any infrastructure sector. Measures suggest considering future effects of climate change, incorporating greener concepts, etc.

Table 4 CCA measures for water infrastructures

Adaptation measure	Applicable phase			References
	Design and planning	Construction	Maintenance and retrofitting	
Safety assessment, reinforcement of discharge facilities in spillways	●			(Cheng et al., 2017; Choi et al., 2017; Emilsson & Ode Sang, 2017; Ghbn, 2016; Hatvani-Kovacs et al., 2018; Herath et al., 2018; Hurlimann & Wilson, 2018; Job et al., 2020; Kohlitz et al., 2020; Lin et al., 2021; Manocha & Babovic, 2017; McPhillips et al., 2020; Mikovits et al., 2017; Moura et al., 2016; M. B. Neumann et al., 2015; Radhakrishnan et al., 2019; Salerno et al., 2018; Salimi & Al-Ghamdi, 2020; Seah et al., 2021; Senosiain, 2020; Shanmugasundaram et al., 2017; Sharifi et al., 2021; Trogrlić et al., 2018; Van Engelenburg et al., 2019; Yerri et al., 2018)
Raising dam level	●			
Adopting dam rehabilitation evaluation techniques			●	
Proper design approaches for drinking water sources (for the local community, Ex: coverage, construction methods to overcome ingress of water)	●			
Increasing storage and pumping capacities/Resilient tank system	●			
Physical barriers such as sea walls to minimize impacts of tidal events and rising elevations of the infrastructure	●			
Design and build floatable critical properties	●			
Relocating vulnerable critical facilities			●	
Adopting green infrastructure	●			
Mapping vulnerable areas and critical facilities	●		●	
Collecting critical data for monitoring purposes			●	
Forecasting model to risk-informed decision making	●		●	
Revision of the codes/policies based on forecasting			●	
Reducing impervious surfaces in land use-Stop the water pollution	●			
Heating systems for water systems hydraulic fracturing at drill sites to prevent frost	●			

4.2 Climate Change Adaptation Measures for Social Assets

Climate change has caused significant disturbances to the community. Food and freshwater insecurity are the major social impact of climate change. Food security is one of the most critical areas that need special attention in climate adaptation among nations. The agriculture sector is the most climate-sensitive sector. Climate-related hazards have significantly affected agricultural production and farm assets recently [8, 57]. Hence, the high climate sensitivity and livelihood dependency of a large population make food security a highly vulnerable sector to climate change impact that needs special attention for climate change adaptation [8]. Also, displacement and

Table 5 CCA measures for energy and electricity infrastructures

Adaptation measure	Applicable phase			References
	Design and planning	Construction	Maintenance and retrofitting	
Review design thresholds and guidelines of structures considering climate change	●		●	(V. Gupta, 2021; Katopodis & Sfetsos, 2019; Varianou Mikellidou et al., 2018)
Upgrading oil platforms, the rigs, and the number of anchors to make it more resilient to hurricanes	●	●		
Offshore drilling companies should invest in lighting protection for offshore drilling	●			
Raising the elevation of infrastructures	●			
Plan and train for the evacuation of personnel			●	
Review of the design of installations located on the coastline.			●	
Relocation of critical facilities and securing of equipment (e.g. Anchoring storage tanks, restraining gas cylinders			●	
Early warning systems	●			
Increasing storage capacities for vital equipment and supplies	●			
Investing and managing drainage systems within critical facilities	●			
Implement a method for risk assessment	●			

Table 6 CCA measures for telecommunication infrastructures

Adaptation measure	Applicable phase			References
	Design and planning	Construction	Maintenance and retrofitting	
Replacing copper wire network with waterproof fiberoptic cables		●	●	(Balcell et al., 2014; V. Gupta, 2021)
Using portable or provisional base stations to provide network continuity and backup power sources	●		●	
Tailoring continuity of service plans based on the needs of localities	●			
Employing network management techniques for addressing congestion			●	

Table 7 CCA measures for other and general infrastructure sectors

Adaptation measure	Applicable phase			References
	Design and planning	Construction	Maintenance and retrofitting	
Planning for future inland movement due to sea level rise	●			(Clark et al., 2018; Gedikli, 2018; Hatvani-Kovacs et al., 2018; Herath et al., 2018; Manocha & Babovic, 2017; Salerno et al., 2018; Scussolini et al., 2017; Shanmugasundaram et al., 2017; Sharifi, 2020; Sharifi et al., 2021; Wang et al., 2019)
Land use incorporating green concepts	●			
Regulating minimum green space ratio	●			
Adopting nature-based solution	●	●		
Networks of parks, urban greenery, and open spaces	●			

loss of livelihoods are other major impacts of climate change on society [56, 80, 89]. Another area where climate change can have a substantial impact is health. Changes in climatic patterns have been linked to increased health risks in studies worldwide. As a result, making major efforts to adapt to potential health risks related to climate change is a top concern [19, 104, 114]. The other social impact of climate change includes the requirement of social protection plans, migration, a threat to human life, causalities, loss of human lives, and risk of conflicts among people. In order to mitigate these impacts on society, different nations have taken several adaptation measures. The present study has identified the following climate change adaptation measures for protecting the community from the literature review [8, 9, 56, 57, 80, 122].

- Preparation in advance for food and medications, availability of safe water, and assurance of accessible public health service during a post-disaster situation
- Increased accessibility to MHEWs facilities
- Conducting safety drills and evacuation plans
- Implementing proper signboards
- Adopting new agricultural technologies to increase the productivity of the agriculture
- Launch awareness programmes on climate change for the public
- Promote climate-resilient building designs and revise building approval systems to increase the climate resilience.

4.3 Climate Change Adaptation Measures for Economic Assets

This section presents the identified adaptation measures for mitigating the adverse impacts of climate change on the economy. As the economic impacts, losses due to infrastructure damages were highlighted as a major impact. As aforementioned, climate change has caused a significant impact on coastal infrastructures. The cost of retrofitting and repairing the damaged infrastructure needs capital. In addition, disruption of infrastructure service will affect the nation's economy as these infrastructures assist in the economic gain of most countries. As aforementioned, coastal built environments are major economic hotspots in most countries. Therefore, any damage to the coastal built environment causes economic depression. On the other hand, most marine-based industries, such as tourism, fisheries, and aquaculture, will be affected due to climate change [13, 76, 109]. One of the major incomes of countries is the marine-based industries. It is evident that climate change has a significant impact on marine-based industries [54, 112]. Hence, the impact of marine-based industries directly affects the economy of the nations. The other identified economic impacts include the cost of adaptation and reconstruction, loss of employment, depletion of resources, and impact on planning economic development. In order to mitigate these impacts on the economy, different nations have taken several adaptation measures. The present study has identified the following climate change adaptation measures for protecting economies of the coastal built environment [15, 29, 53, 76, 107]:

- Introduce innovative risk transfer instruments
- Promote climate-proof infrastructure design practices
- Develop guidelines for economic activities in vulnerable areas
- Identify adaptation actions suitable for respective industries
- Increase the awareness of industrial operators on climate change and its impacts
- Increasing infrastructure protection measures.

4.4 Climate Change Adaptation Measures for Environmental Assets

Environmental assets related to the built environment can identify as natural forests, parks, wetlands, and mangroves. These assets play a pivotal role in climate change mitigation, absorbing CO_2 [32, 33, 60, 117]. Also, they provide shelter for living beings. The identified adaptation measures for protecting environmental assets include the following [6, 23, 24, 32, 33, 36, 107]:

- Conduct research studies on climate change's impact on ecosystems and biodiversity

- Establish a comprehensive programme to monitor climate change impacts on key natural ecosystems and biodiversity
- Prepare and implement adaptive management programmes for climate-sensitive ecosystems
- Prepare and implement recovery plans for highly threatened ecosystems and species
- Develop research institutes' capacity for conducting research on climate change impacts on ecosystems and biodiversity.

4.5 Governance and Institutional Measures to Facilitate Climate Change Adaptation

Governance is the broader term [20, 26]. Generally, in the context of the built environment, it refers to the processes of decision-making involved in the control and management aspect of the built environment [5, 65, 116]. The governance of the infrastructure has a direct impact on other components of the built environment, as presented in Fig. 1. Therefore, strengthening governance is crucial for building climate resilience [5, 28, 121]. The following governance and institutional measures were identified through the present study to facilitate climate change [5, 28, 47, 50, 66]:

- Strengthen the mechanisms for sharing information and data among stakeholders
- Defining clear responsibilities and roles for stakeholders
- Undertake a review of relevant macro and sectoral policies, ordinances, acts, statutes, and procedures to identify options for mainstreaming climate change adaptation activities
- Develop policy recommendations necessary for addressing vulnerability to impacts of climate change in all development/management projects
- Conduct training programmes for government officers and private sector employees on climate change adaptation
- Develop an inventory of international climate donors, funding schemes, training providers, training programmes, research agencies/consortiums, and events (conferences, seminars) for the benefit of local stakeholders of adaptation
- Establish a national network of research agencies and universities that are carrying out research on climate adaptation to promote coordinated research and information dissemination.

5 Conclusion

Due to the increasing impacts of climate change, the research focus on climate change and adaptation related to the built environment has increased. Authors have suggested many adaptation measures for different sectors of the built environment.

Due to the interrelationships of the physical assets of the built environment with other areas such as social, economic, and environmental assets, climate change impacts are affecting not only the physical assets, but also the economy, society, and environment. Through the Systematic Literature Review done in this study, adaptation measures for protecting the built environment components, especially in the coastal regions, were identified. Identified adaptation measures cover the different sectors of physical assets of the built environment, including transportation infrastructures, residential and commercial buildings, water infrastructures, telecommunication infrastructures, and electricity and energy infrastructures. The identified adaptation measures for physical assets of the built environment have been linked with the applicable life cycle phase to identify the related phase of using each adaptation measure. The findings of the study give a comprehensive set of adaptation measures covering the selected built environment components, which will assist the built environment professional to adapt and minimise the impacts of climate change.

Acknowledgements This study was done as a part of the Built Environment Learning for Climate Adaptation (BEACON) project. The authors would like to acknowledge all the partner organisations of the BEACON project and funding agencies.

References

1. Abeysinghe AASE, Bandara CS, Siriwardana CSA, Haigh R, Amarathunga D, Dissanayake PBR (2020) Incorporation of disaster risk reduction mechanisms for flood hazards into the Greensl® rating system for built environment in Sri Lanka. Lect Notes Civil Eng 94:573–587. https://doi.org/10.1007/978-981-15-7222-7_47
2. Ahmad D, Afzal M (2020) Flood hazards and factors influencing household flood perception and mitigation strategies in Pakistan. Environ Sci Pollut Res 27(13):15375–15387. https://doi.org/10.1007/S11356-020-08057-Z
3. Ahmed MA, Sridharan B, Saha N, Sannasiraj SA, Kuiry SN (2022) Assessment of coastal vulnerability for extreme events. Int J Disaster Risk Reduct 82:103341. https://doi.org/10.1016/J.IJDRR.2022.103341
4. Al-Faesly T, Palermo D, Nistor I (2015) Tsunami mitigation measures. In: The 11th Canadian conference on earthquake engineering
5. Amaratunga D, Haigh R, Hettige S (2019) Accountability in the context of disaster risk governance
6. Anjali K, Khuman Y, Sokhi J, Anjali K, Khuman Y, Sokhi J (2020) A review of the interrelations of terrestrial carbon sequestration and urban forests. AIMS Environ Sci 7(6):464–485. https://doi.org/10.3934/ENVIRONSCI.2020030
7. Ardekani A, Hosseini M (2012) Urban and architectural approaches to design against tsunami. In: 15th world conference on earthquake engineering
8. Aryal JP, Sapkota TB, Rahut DB, Marenya P, Stirling CM (2021) Climate risks and adaptation strategies of farmers in East Africa and South Asia. Sci Rep 11(1):1–14. https://doi.org/10.1038/s41598-021-89391-1
9. Aslany M, Brincat S (2021) Class and climate-change adaptation in rural India: beyond community-based adaptation models. Sustain Dev 29(3):571–582. https://doi.org/10.1002/SD.2201
10. Baird R (2018) Systematic reviews and meta-analytic techniques. Semin Pediatr Surg 27(6):338–344. https://doi.org/10.1053/J.SEMPEDSURG.2018.10.009

11. Balcell MP, Fuenfgeld H, McShane I (2014) Telecommunications and disaster management: participatory approaches and climate change adaptation. Aust J Telecommun Digit Econ 2(4):1–14. https://doi.org/10.7790/AJTDE.V2N4.73
12. Batouli M, Mostafavi A (2016) Assessment of sea-level rise adaptations in coastal infrastructure systems: robust decision making under uncertainty. Construct Res Congr 1455–1464. https://doi.org/10.1061/9780784479827.146
13. Becker A, Ng AKY, McEvoy D, Mullett J (2018) Implications of climate change for shipping: ports and supply chains. Wiley Interdiscip Rev: Climate Change 9(2):e508. https://doi.org/10.1002/WCC.508
14. Bernier P, Fenner R, Ainger C (2015) Assessing the sustainability merits of retrofitting existing homes. Proc Inst Civil Eng Eng Sustain 163(E4):197–207. https://doi.org/10.1680/ENSU.2010.163.4.197
15. Busayo ET, Kalumba AM (2020) Coastal climate change adaptation and disaster risk reduction: a review of policy, programme and practice for sustainable planning outcomes. Sustainability 12(16):6450. https://doi.org/10.3390/SU12166450
16. Cervigni R, Liden R, Neumann JE, Strzepek KM (2015) Enhancing the climate resilience of Africa's infrastructure the power and water sectors conference edition
17. Charlesworth S, Warwick F, Lashford C (2016) Decision-making and sustainable drainage: design and scale. Sustainability 8(8):782. https://doi.org/10.3390/SU8080782
18. Cheng C, Yang YCE, Ryan R, Yu Q, Brabec E (2017) Assessing climate change-induced flooding mitigation for adaptation in Boston's Charles River watershed, USA. Landsc Urban Plan 167:25–36. https://doi.org/10.1016/J.LANDURBPLAN.2017.05.019
19. Chersich MF, Wright CY (2019) Climate change adaptation in South Africa: a case study on the role of the health sector. Glob Health 15(1):1–16. https://doi.org/10.1186/S12992-019-0466-X/TABLES/1
20. Chinyere NL, Jacinta OO, Anyim NA (2020) Urban governance: an overview. GNOSI: Interdiscip J Hum Theory Praxis 3(1):85–97. http://www.gnosijournal.com/index.php/gnosi/article/view/86
21. Choi J-H, Yoon T-H, Kim J-S, Moon Y-I (2017) Dam rehabilitation assessment using the Delphi-AHP method for adapting to climate change. J Water Resour Plan Manag 144(2):06017007. https://doi.org/10.1061/(ASCE)WR.1943-5452.0000877
22. Clark SS, Chester MV, Seager TP, Eisenberg DA (2018) The vulnerability of interdependent urban infrastructure systems to climate change: could Phoenix experience a Katrina of extreme heat? Sustain Resil Infrastruct 4(1):21–35. https://doi.org/10.1080/23789689.2018.1448668
23. Climate Change Secretariat (2016) National adaptation plan for climate change impacts in Sri Lanka 2016–2025
24. Collings D (2020) A review of UK greenhouse gas emissions from recent built-environment projects. Proc Inst Civil Eng Civil Eng 173(4):171–176. https://doi.org/10.1680/JCIEN.20.00019
25. Cramer W, Guiot J, Fader M, Garrabou J, Gattuso JP, Iglesias A, Lange MA, Lionello P, Llasat MC, Paz S, Peñuelas J, Snoussi M, Toreti A, Tsimplis MN, Xoplaki E (2018) Climate change and interconnected risks to sustainable development in the mediterranean. Nat Clim Chang 8(11):972–980. https://doi.org/10.1038/s41558-018-0299-2
26. da Cruz NF, Rode P, McQuarrie M (2018) New urban governance: a review of current themes and future priorities. J Urban Aff 41(1):1–19. https://doi.org/10.1080/07352166.2018.1499416
27. de Ruig LT, Haer T, de Moel H, Botzen WJW, Aerts JCJH (2020) A micro-scale cost-benefit analysis of building-level flood risk adaptation measures in Los Angeles. Water Resour Econ 32:100147. https://doi.org/10.1016/J.WRE.2019.100147
28. Dias N, Clegg G, Amaratunga D, Haigh R (2019) A resilient environment through the integration of CCA and DRR: an overview of existing challenges. Int J Adv Sci Eng Inf Technol 9(1):129–135. https://doi.org/10.18517/IJASEIT.9.1.8072
29. Ellena M, Breil M, Soriani S (2020) The heat-health nexus in the urban context: a systematic literature review exploring the socio-economic vulnerabilities and built environment characteristics. Urban Climate 34:100676. https://doi.org/10.1016/J.UCLIM.2020.100676

30. Emilsson T, Ode Sang Å (2017) Impacts of climate change on urban areas and nature-based solutions for adaptation. Theory Pract Urban Sustain Trans 15–27. https://doi.org/10.1007/978-3-319-56091-5_2
31. Esteban M, Tsimopoulou V, Mikami T, Yun NY, Suppasri A, Shibayama T (2013) Recent tsunamis events and preparedness: development of tsunami awareness in Indonesia, Chile and Japan. Int J Disaster Risk Reduct 5:84–97. https://doi.org/10.1016/J.IJDRR.2013.07.002
32. Faivre N, Sgobbi A, Happaerts S, Raynal J, Schmidt L (2018) Translating the sendai framework into action: the EU approach to ecosystem-based disaster risk reduction. Int J Disaster Risk Reduct 32:4–10. https://doi.org/10.1016/J.IJDRR.2017.12.015
33. Fedele G, Donatti CI, Harvey CA, Hannah L, Hole DG (2019) Transformative adaptation to climate change for sustainable social-ecological systems. Environ Sci Policy 101:116–125. https://doi.org/10.1016/J.ENVSCI.2019.07.001
34. Gedikli B (2018) Approaches to climate change in spatial planning and design: international and turkish experiences. METU J Fac Archit 35(1):89–109. https://doi.org/10.4305/METU.JFA.2018.1.9
35. Ghbn N (2016) Dynamic modeling for municipal climate change adaptive measures and integrated watershed management. World Environ Water Resour Congr 642–649. https://doi.org/10.1061/9780784479872.066
36. Grima N, Corcoran W, Hill-James C, Langton B, Sommer H, Fisher B (2020) The importance of urban natural areas and urban ecosystem services during the COVID-19 pandemic. PLoS ONE 15(12):e0243344. https://doi.org/10.1371/JOURNAL.PONE.0243344
37. Gupta R, Gregg M (2012) Climate change: adaptations. Int Encycl Hous Home 164–179. https://doi.org/10.1016/B978-0-08-047163-1.00597-X
38. Gupta V (2021) Mainstreaming climate adaptation for creating resilient infrastructure technical note
39. Haddad S, Barker A, Yang J, Kumar DIM, Garshasbi S, Paolini R, Santamouris M (2020) On the potential of building adaptation measures to counterbalance the impact of climatic change in the tropics. Energy and Build 229:110494. https://doi.org/10.1016/J.ENBUILD.2020.110494
40. Haigh R, Amaratunga D (2010) An integrative review of the built environment discipline's role in the development of society's resilience to disasters. Int J Disaster Resil Built Environ 1(1):11–24. https://doi.org/10.1108/17595901011026454/FULL/XML
41. Han Y, Mozumder P (2021) Building-level adaptation analysis under uncertain sea-level rise. Clim Risk Manag 32:100305. https://doi.org/10.1016/J.CRM.2021.100305
42. Hatvani-Kovacs G, Bush J, Sharifi E, Boland J (2018) Policy recommendations to increase urban heat stress resilience. Urban Climate 25:51–63. https://doi.org/10.1016/J.UCLIM.2018.05.001
43. Herath HMPIK, Halwatura RU, Jayasinghe GY (2018) Evaluation of green infrastructure effects on tropical Sri Lankan urban context as an urban heat island adaptation strategy. Urban Forest Urban Greening 29:212–222. https://doi.org/10.1016/J.UFUG.2017.11.013
44. Hinkel J, Brown S, Exner L, Nicholls RJ, Vafeidis AT, Kebede AS (2011) Sea-level rise impacts on Africa and the effects of mitigation and adaptation: an application of DIVA. Reg Environ Change 2011 12(1):207–224. https://doi.org/10.1007/S10113-011-0249-2
45. Huang KT, Hwang RL (2016) Future trends of residential building cooling energy and passive adaptation measures to counteract climate change: the case of Taiwan. Appl Energy 184:1230–1240. https://doi.org/10.1016/J.APENERGY.2015.11.008
46. Hudson P (2020) The affordability of flood risk property-level adaptation measures. Risk Anal 40(6):1151–1167. https://doi.org/10.1111/RISA.13465
47. Hürlimann AC, Nielsen J, Moosavi S, Bush J, Warren-Myers G, March A (2022) Climate change preparedness across sectors of the built environment—A review of literature. Environ Sci Policy 128:277–289. https://doi.org/10.1016/J.ENVSCI.2021.11.021
48. Hurlimann A, Wilson E (2018) Sustainable urban water management under a changing climate: the role of spatial planning. Water 10(5):546. https://doi.org/10.3390/W10050546

49. Hwang RL, Cheng MJ, Lin TP, Ho MC (2009) Thermal perceptions, general adaptation methods and occupant's idea about the trade-off between thermal comfort and energy saving in hot–humid regions. Build Environ 44(6):1128–1134. https://doi.org/10.1016/J.BUILDENV.2008.08.001
50. IPCC (2014) Climate change 2014 impacts, adaptation, and vulnerability part a: global and sectoral aspects
51. Jetten J, Fielding KS, Crimston CR, Mols F, Haslam SA (2021) Responding to climate change disaster, vol 26, no 3, pp 161–171. https://doi.org/10.1027/1016-9040/A000432
52. Job SC, Harris M, Julius S, Butcher JB, Kennedy JT (2020) Adapting urban best management practices for resilience to long-term environmental changes. Water Environ Res 92(12):2178–2192. https://doi.org/10.1002/WER.1302
53. Joensuu T, Edelman H, Saari A (2020) Circular economy practices in the built environment. J Clean Prod 276:124215. https://doi.org/10.1016/J.JCLEPRO.2020.124215
54. Johnson JE, Allain V, Basel B, Bell JD, Chin A, Dutra LXC, Hooper E, Loubser D, Lough J, Moore BR, Nicol S (2020) Impacts of climate change on marine resources in the Pacific Island region. Springer Climate 359–402. https://doi.org/10.1007/978-3-030-32878-8_10/COVER
55. Kaklauskas A, Gudauskas R (2016) Intelligent decision-support systems and the internet of things for the smart built environment. Start-Up Creat: Smart Eco-Eff Built Environ 413–449. https://doi.org/10.1016/B978-0-08-100546-0.00017-0
56. Kaluarachchi Y (2018) Building community resilience in the re-settlement of displaced communities. Procedia Eng 212:443–450. https://doi.org/10.1016/J.PROENG.2018.01.057
57. Karimi V, Karami E, Keshavarz M (2018) Climate change and agriculture: impacts and adaptive responses in Iran. J Integr Agric 17(1):1–15. https://doi.org/10.1016/S2095-3119(17)61794-5
58. Katopodis T, Sfetsos A (2019) A review of climate change impacts to oil sector critical services and suggested recommendations for industry uptake. Infrastructures 4(4):74. https://doi.org/10.3390/INFRASTRUCTURES4040074
59. Kohlitz J, Chong J, Willetts J (2020) Rural drinking water safety under climate change: the importance of addressing physical, social, and environmental dimensions. Resources 9(6):77. https://doi.org/10.3390/RESOURCES9060077
60. Lau JD, Hicks CC, Gurney GG, Cinner JE (2019) What matters to whom and why? Understanding the importance of coastal ecosystem services in developing coastal communities. Ecosyst Serv 35:219–230. https://doi.org/10.1016/J.ECOSER.2018.12.012
61. Lenzholzer S, Carsjens GJ, Brown RD, Tavares S, Vanos J, Kim YJ, Lee K (2020) Urban climate awareness and urgency to adapt: an international overview. Urban Climate 33:100667. https://doi.org/10.1016/J.UCLIM.2020.100667
62. Lin BB, Ossola A, Alberti M, Andersson E, Bai X, Dobbs C, Elmqvist T, Evans KL, Frantzeskaki N, Fuller RA, Gaston KJ, Haase D, Jim CY, Konijnendijk C, Nagendra H, Niemelä J, McPhearson T, Moomaw WR, Parnell S et al (2021) Integrating solutions to adapt cities for climate change. Lancet Planet Health 5(7):e479–e486. https://doi.org/10.1016/S2542-5196(21)00135-2
63. Liu Z, Yang Z, Osmani M, Van Den Berg P, Dane G, Birenboim A (2021) The relationship between sustainable built environment, art therapy and therapeutic design in promoting health and well-being. Int J Environ Res Publ Health 18(20):10906. https://doi.org/10.3390/IJERPH182010906
64. Major DC, Lehmann M, Fitton J (2018) Linking the management of climate change adaptation in small coastal towns and cities to the sustainable development goals. Ocean Coast Manag 163:205–208. https://doi.org/10.1016/J.OCECOAMAN.2018.06.010
65. Malalgoda C, Amaratunga D, Haigh R (2013) Creating a disaster resilient built environment in urban cities: the role of local governments in Sri Lanka. Int J Disaster Resil Built Environ 4(1):72–94. https://doi.org/10.1108/17595901311299017/FULL/XML
66. Malalgoda C, Amaratunga D, Haigh R (2014) Challenges in creating a disaster resilient built environment. Procedia Econ Financ 18:736–744. https://doi.org/10.1016/S2212-5671(14)00997-6

67. Manocha N, Babovic V (2017) Development and valuation of adaptation pathways for storm water management infrastructure. Environ Sci Policy 77:86–97. https://doi.org/10.1016/J.ENVSCI.2017.08.001
68. Markolf SA, Hoehne C, Fraser A, Chester MV, Underwood BS (2019) Transportation resilience to climate change and extreme weather events—Beyond risk and robustness. Transp Policy 74:174–186. https://doi.org/10.1016/J.TRANPOL.2018.11.003
69. Mauree D, Naboni E, Coccolo S, Perera ATD, Nik VM, Scartezzini JL (2019) A review of assessment methods for the urban environment and its energy sustainability to guarantee climate adaptation of future cities. Renew Sustain Energy Rev 112:733–746. https://doi.org/10.1016/J.RSER.2019.06.005
70. McPhillips LE, Matsler M, Rosenzweig BR, Kim Y (2020) What is the role of green stormwater infrastructure in managing extreme precipitation events? Sustain Resil Infrastruct 6(3–4):133–142. https://doi.org/10.1080/23789689.2020.1754625
71. Mikovits C, Tscheikner-Gratl F, Jasper-Tönnies A, Einfalt T, Huttenlau M, Schöpf M, Kinzel H, Rauch W, Kleidorfer M (2017) Decision support for adaptation planning of urban drainage systems. J Water Resour Plan Manag 143(12):04017069. https://doi.org/10.1061/(ASCE)WR.1943-5452.0000840
72. Mohebbi S, Zhang Q, Christian Wells E, Zhao T, Nguyen H, Li M, Abdel-Mottaleb N, Uddin S, Lu Q, Wakhungu MJ, Wu Z, Zhang Y, Tuladhar A, Ou X (2020) Cyber-physical-social interdependencies and organizational resilience: a review of water, transportation, and cyber infrastructure systems and processes. Sustain Cities Soc 62:102327. https://doi.org/10.1016/J.SCS.2020.102327
73. Morin J, De Coster B, Paris R, Flohic F, Le Floch D, Lavigne F, Wassmer P, Brunstein D, Grancher D, Gomez C, Etienne S, Vautier F, Bernard C, Barthomeuf B, Desgages Geolab UMR, Fournier MNHN, Poizot Intechmer E, Cherbourg C, Leone F et al (2008) Tsunami-resilient communities' development in Indonesia through educative actions lessons from the 26 December 2004 tsunami. Disaster Prevent Manag 17(3):430–446. https://doi.org/10.1108/09653560810887338
74. Mottaeva A (2016) Innovative aspects of ecological and economic management of investment and construction activities for the sustainable development of the region. MATEC Web of Conf 73:07020. https://doi.org/10.1051/MATECCONF/20167307020
75. Moura NCB, Pellegrino PRM, Martins JRS (2016) Best management practices as an alternative for flood and urban storm water control in a changing climate. J Flood Risk Manag 9(3):243–254. https://doi.org/10.1111/JFR3.12194
76. Mouratidis K, Peters S, van Wee B (2021) Transportation technologies, sharing economy, and teleactivities: implications for built environment and travel. Transp Res Part D: Transp Environ 92:102716. https://doi.org/10.1016/J.TRD.2021.102716
77. Mycoo M (2014) Sustainable tourism, climate change and sea level rise adaptation policies in Barbados. Nat Res Forum 38(1):47–57. https://doi.org/10.1111/1477-8947.12033
78. Neumann JE, Price J, Chinowsky P, Wright L, Ludwig L, Streeter R, Jones R, Smith JB, Perkins W, Jantarasami L, Martinich J (2015a) Climate change risks to US infrastructure: impacts on roads, bridges, coastal development, and urban drainage. Clim Change 131(1):97–109. https://doi.org/10.1007/S10584-013-1037-4/TABLES/1
79. Neumann MB, Rieckermann J, Hug T, Gujer W (2015b) Adaptation in hindsight: dynamics and drivers shaping urban wastewater systems. J Environ Manag 151:404–415. https://doi.org/10.1016/J.JENVMAN.2014.12.047
80. Nikuze A, Sliuzas R, Flacke J, van Maarseveen M (2019) Livelihood impacts of displacement and resettlement on informal households—A case study from Kigali, Rwanda. Habitat Int 86:38–47. https://doi.org/10.1016/J.HABITATINT.2019.02.006
81. NOAA National Centers for Environmental Information (2022) Monthly global climate report for annual 2021
82. Nofal OM, van de Lindt JW, Do TQ (2020) Multi-variate and single-variable flood fragility and loss approaches for buildings. Reliab Eng Syst Saf 202:106971. https://doi.org/10.1016/j.ress.2020.106971

83. O'Malley C, Piroozfarb PAE, Farr ERP, Gates J (2014) An investigation into minimizing urban heat Island (UHI) effects: a UK perspective. Energy Procedia 62:72–80. https://doi.org/10.1016/J.EGYPRO.2014.12.368
84. Oswald Beiler M, Marroquin L, McNeil S (2016) State-of-the-practice assessment of climate change adaptation practices across metropolitan planning organizations pre- and post-Hurricane Sandy. Transport Res Part A: Policy Pract 88:163–174. https://doi.org/10.1016/J.TRA.2016.04.003
85. Owen G (2020) What makes climate change adaptation effective? A systematic review of the literature. Glob Environ Chang 62:102071. https://doi.org/10.1016/J.GLOENVCHA.2020.102071
86. Pickering J, McGee JS, Stephens T, Karlsson-Vinkhuyzen SI (2017) The impact of the US retreat from the Paris agreement: Kyoto revisited? Clim Policy 18(7):818–827. https://doi.org/10.1080/14693062.2017.1412934
87. Picketts IM, Andrey J, Matthews L, Déry SJ, Tighe S (2015) Climate change adaptation strategies for transportation infrastructure in Prince George Canada. Reg Environ Change 16(4):1109–1120. https://doi.org/10.1007/S10113-015-0828-8
88. Porritt SM, Cropper PC, Shao L, Goodier CI (2012) Ranking of interventions to reduce dwelling overheating during heat waves. Energy Build 55:16–27. https://doi.org/10.1016/J.ENBUILD.2012.01.043
89. Přívara A, Přívarová M (2019) Nexus between climate change displacement and conflict: afghanistan case. Sustainability 11(20):5586. https://doi.org/10.3390/SU11205586
90. Qiao Y, Dawson AR, Parry T, Flintsch G, Wang W (2020) Flexible pavements and climate change: a comprehensive review and implications. Sustainability 12(3):1057. https://doi.org/10.3390/SU12031057
91. Radhakrishnan M, Löwe R, Ashley RM, Gersonius B, Arnbjerg-Nielsen K, Pathirana A, Zevenbergen C (2019) Flexible adaptation planning process for urban adaptation in Melbourne, Australia. Proc Inst Civil Eng Eng Sustain 172(7):393–403. https://doi.org/10.1680/JENSU.17.00033
92. Rojas-Rueda D, Morales-Zamora E (2021) Built environment, transport, and COVID-19: a review. Curr Environ Health Rep 8(2):138–145. https://doi.org/10.1007/S40572-021-00307-7
93. Ross BE (2017) The learning buildings framework for quantifying building adaptability. In: AEI 2017: resilience of the integrated building—Proceedings of the architectural engineering national conference 2017, pp 1067–1077. https://doi.org/10.1061/9780784480502.089
94. Salerno F, Viviano G, Tartari G (2018) Urbanization and climate change impacts on surface water quality: enhancing the resilience by reducing impervious surfaces. Water Res 144:491–502. https://doi.org/10.1016/J.WATRES.2018.07.058
95. Salimi M, Al-Ghamdi SG (2020) Climate change impacts on critical urban infrastructure and urban resiliency strategies for the middle East. Sustain Cities Soc 54:101948. https://doi.org/10.1016/J.SCS.2019.101948
96. Sanchez Rodriguez R, Ürge-Vorsatz D, Barau AS (2018) Sustainable development goals and climate change adaptation in cities. Nat Clim Chang 8(3):181–183. https://doi.org/10.1038/s41558-018-0098-9
97. Sari DP (2021) A review of how building mitigates the urban heat Island in Indonesia and tropical cities. In: Earth 2021, vol 2, no 3, pp 653–666. https://doi.org/10.3390/EARTH2030038
98. Scussolini P, Van Tran TT, Koks E, Diaz-Loaiza A, Ho PL, Lasage R (2017) Adaptation to sea level rise: a multidisciplinary analysis for Ho Chi Minh City Vietnam. Water Resour Res 53(12):10841–10857. https://doi.org/10.1002/2017WR021344
99. Seah I, Masoud F, Dias F, Barve A, Ojha M, Mazereeuw M (2021) Flux.Land: a data-driven toolkit for urban flood adaptation. J Digit Landsc Archit 381–392. https://doi.org/10.14627/537705034
100. Seidler R, Dietrich K, Schweizer S, Bawa KS, Chopde S, Zaman F, Sharma A, Bhattacharya S, Devkota LP, Khaling S (2018) Progress on integrating climate change adaptation and disaster risk reduction for sustainable development pathways in South Asia: evidence from

six research projects. Int J Disaster Risk Reduct 31:92–101. https://doi.org/10.1016/J.IJDRR.2018.04.023
101. Senosiain JL (2020) Urban regreeneration: Green urban infrastructure as a response to climate change mitigation and adaptation. Int J Des Nat Ecodyn 15(1):33–38. https://doi.org/10.18280/IJDNE.150105
102. Shanmugasundaram J, Gunnell Y, Hessl AE, Lee E (2017) Societal response to monsoon variability in Medieval South India: lessons from the past for adapting to climate change. Anthropocene Rev 4(2):110–135. https://doi.org/10.1177/2053019617695343
103. Sharifi A (2020) Trade-offs and conflicts between urban climate change mitigation and adaptation measures: a literature review. J Clean Prod 276:122813. https://doi.org/10.1016/J.JCLEPRO.2020.122813
104. Sharifi A, Pathak M, Joshi C, He BJ (2021) A systematic review of the health co-benefits of urban climate change adaptation. Sustain Cities Soc 74:103190. https://doi.org/10.1016/J.SCS.2021.103190
105. Shimoda Y (2010) Adaptation measures for climate change and the urban heat island in Japan's built environment. Build Res Inf 31(3–4):222–230. https://doi.org/10.1080/09613210320000097647
106. Simons S, Meek J, Johnson K, Linsenmayer M, Halverson L, Berrens C, Thom K, Webster M (2022) Developing transportation system climate resilience performance measures. In: Technical advisory panel developing transportation system climate resilience performance measures
107. Singh C, Iyer S, New MG, Few R, Kuchimanchi B, Segnon AC, Morchain D (2021) Interrogating 'effectiveness' in climate change adaptation: 11 guiding principles for adaptation research and practice. Clim Dev 14(7):650–664. https://doi.org/10.1080/17565529.2021.1964937
108. Solecki WD, Rosenzweig C, Parshall L, Pope G, Clark M, Cox J, Wiencke M (2011) Mitigation of the heat island effect in urban New Jersey. Glob Environ Change Part B: Environ Hazards 6(1):39–49. https://doi.org/10.1016/J.HAZARDS.2004.12.002
109. Stappers NEH, Van Kann DHH, Ettema D, De Vries NK, Kremers SPJ (2018) The effect of infrastructural changes in the built environment on physical activity, active transportation and sedentary behaviour—A systematic review. Health Place 53:135–149. https://doi.org/10.1016/J.HEALTHPLACE.2018.08.002
110. Storbjörk S, Hedrén J (2011) Institutional capacity-building for targeting sea-level rise in the climate adaptation of Swedish coastal zone management. Lessons from Coastby. Ocean Coastal Manag 54(3):265–273. https://doi.org/10.1016/J.OCECOAMAN.2010.12.007
111. Strauch RL, Raymond CL, Rochefort RM, Hamlet AF, Lauver C (2015) Adapting transportation to climate change on federal lands in Washington State, U.S.A. Clim Change 130(2):185–199. https://doi.org/10.1007/S10584-015-1357-7
112. Tegar D, Gurning ROS (2018) Development of marine and coastal tourism based on blue economy. Int J Marine Eng Innov Res 2(2):2548–1479. https://doi.org/10.12962/J25481479.V2I2.3650
113. Torres-Carrion PV, Gonzalez-Gonzalez CS, Aciar S, Rodriguez-Morales G (2018) Methodology for systematic literature review applied to engineering and education. In: IEEE global engineering education conference, EDUCON, pp 1364–1373. https://doi.org/10.1109/EDUCON.2018.8363388
114. Travert AS, Annerstedt K, Daivadanam M (2019) Built environment and health behaviors: deconstructing the black box of interactions—A review of reviews. Int J Environ Res Publ Health 16(8):1454. https://doi.org/10.3390/IJERPH16081454
115. Trogrlić RŠ, Rijke J, Dolman N, Zevenbergen C (2018) Rebuild by design in hoboken: a design competition as a means for achieving flood resilience of urban areas through the implementation of green infrastructure. Water 10(5):553. https://doi.org/10.3390/W10050553
116. UNDRR (2019) Global assesment report on disaster risk reduction
117. van de Ven FHM, Snep RPH, Koole S, Brolsma R, van der Brugge R, Spijker J, Vergroesen T (2016) Adaptation planning support toolbox: measurable performance information based

tools for co-creation of resilient, ecosystem-based urban plans with urban designers, decision-makers and stakeholders. Environ Sci Policy 66:427–436. https://doi.org/10.1016/J.ENVSCI.2016.06.010

118. Van Engelenburg J, Van Slobbe E, Hellegers P (2019) Towards sustainable drinking water abstraction: an integrated sustainability assessment framework to support local adaptation planning. J Integr Environ Sci 16(1):89–122. https://doi.org/10.1080/1943815X.2019.1636284
119. Varianou Mikellidou C, Shakou LM, Boustras G, Dimopoulos C (2018) Energy critical infrastructures at risk from climate change: a state of the art review. Saf Sci 110:110–120. https://doi.org/10.1016/J.SSCI.2017.12.022
120. Wang T, Qu Z, Yang Z, Nichol T, Dimitriu D, Clarke G, Bowden D (2019) How can the UK road system be adapted to the impacts posed by climate change? By creating a climate adaptation framework. Transp Res Part D: Transp Environ 77:403–424. https://doi.org/10.1016/J.TRD.2019.02.007
121. Wedawatta G, Kulatunga U, Amaratunga D, Parvez A (2016) Disaster risk reduction infrastructure requirements for South-Western Bangladesh: perspectives of local communities. Built Environ Project Asset Manag 6(4):379–390. https://doi.org/10.1108/BEPAM-06-2015-0022/FULL/XML
122. WHO (2019) Regional plan of action for SIDS in the African and South East Asian Regions (Issue March)
123. World Bank (2015) Disaster risk management in the transport sector: a review of concepts and international case studies, Washington, DC. https://openknowledge.worldbank.org/handle/10986/22365
124. Wu J, He X, Li Y, Shi P, Ye T, Li N (2019) How earthquake-induced direct economic losses change with earthquake magnitude, asset value, residential building structural type and physical environment: an elasticity perspective. J Environ Manag 231:321–328. https://doi.org/10.1016/J.JENVMAN.2018.10.050
125. Yerri SR, Piratla KR, Ross BE, Harrison DM (2018) Synthesis of water infrastructure adaptation practices in U.S. coastal regions. In: Construction research congress, pp 516–528. https://doi.org/10.1061/9780784481295.052
126. Yıldız S, Kıvrak S, Gültekin AB, Arslan G (2020) Built environment design—Social sustainability relation in urban renewal. Sustain Cities Soc 60:102173. https://doi.org/10.1016/J.SCS.2020.102173
127. Zhang C, Kazanci OB, Levinson R, Heiselberg P, Olesen BW, Chiesa G, Sodagar B, Ai Z, Selkowitz S, Zinzi M, Mahdavi A, Teufl H, Kolokotroni M, Salvati A, Bozonnet E, Chtioui F, Salagnac P, Rahif R, Attia S et al (2021) Resilient cooling strategies—A critical review and qualitative assessment. Energy Build 251:111312. https://doi.org/10.1016/J.ENBUILD.2021.111312

Tall Buildings

Achieving Net-Zero-Energy Tall Buildings in Sri Lanka

Lu Aye, Amitha Jayalath, and Dan Wu

Abstract Achieving a net-zero-energy tall building with onsite renewables is a challenging task. A low-rise building on a low-density site would have a better chance of being a net-zero-energy building. Some argue that it is more beneficial to work towards net-zero-energy communities rather than net-zero-energy buildings. In general, most of the onsite building electricity generation is done using solar photovoltaic (PV) systems. The prices of solar PV systems have been dropping in most countries. This article investigates the potential of solar PV on the façades of a hypothetical 20 storey building in three selected locations in Sri Lanka. An hourly weather data file is generated for each selected location and the TRNSYS software tool is applied to simulate the performance of the solar PV system. We quantify the electrical output of the solar PV system and compare it with the electricity consumption in each location. The article reports the potential annual electricity generation of rooftop and façade integrated PV in Colombo, Jaffna and Kandy.

Keywords Solar PV · Façade · Colombo · Kandy · Jaffna

1 Introduction

Many countries are trying to establish zero energy building as their future building energy target, even though there is no commonly agreed definition framework. A recent review by Marszal et al. (2011) [1] reported that the zero energy building definitions are expressed with a wide range of terms and no phrases in the literature and no harmonised understanding. For this article grid connected net-zero-energy definition: "Zero Net Energy Buildings are buildings that over a year are neutral,

L. Aye (✉) · A. Jayalath · D. Wu
Renewable Energy and Energy Efficiency Group, Department of Infrastructure Engineering, Faculty of Engineering and Information Technology, The University of Melbourne, Victoria 3010, Australia
e-mail: lua@unimelb.edu.au

D. Wu
School of Architecture, Southwest Jiaotong University, Chengdu 611756, China

© The Author(s), under exclusive license to Springer Nature Singapore Pte Ltd. 2023

R. Dissanayake et al. (eds.), *ICSBE 2022*, Lecture Notes in Civil Engineering 362,
https://doi.org/10.1007/978-981-99-3471-3_45

meaning that they deliver as much energy to the supply grids as they use from the grids" (Laustsen, 2008) [2] is used. The work of the International Energy Agency, Solar Heating and Cooling Programme Task 40: Net Zero Energy Solar Buildings suggests that an appropriate framework for driving net-zero-energy buildings is elaborated in Fig. 1 [3]. The metric for final energy demand and supply, balance boundary for operational energy and balance period for operation year are considered in this article. The basic steps to achieving net-zero targets recommended by IEA-SHC Task 40 are: "make the building as energy efficient as possible through integrated design and energy-saving technologies, add renewable energy onsite and ensure optimal building performance over time" [3].

The construction of tall buildings will continue to grow as a result of rising land prices with respect to urbanisation and population growth. Typical high-rise buildings consume high energy compared to low-rise buildings. Griffith et al. (2007) [4] reported that only about 3% of the buildings with four floors would cater to net-zero-energy by 2025. The site energy use intensity (EUI) for the buildings included in their modelling is about 128 kWh_e m^{-2} of floor area per annum for the maximum energy efficient scenario for the eight major climate zones in the USA.

Chambers (2014) [5] argued that with better technology for building energy performance simulations and advances in onsite energy generation technology, a much higher percentage should be achievable than the predicted amount by Griffith et al. (2007) [4].

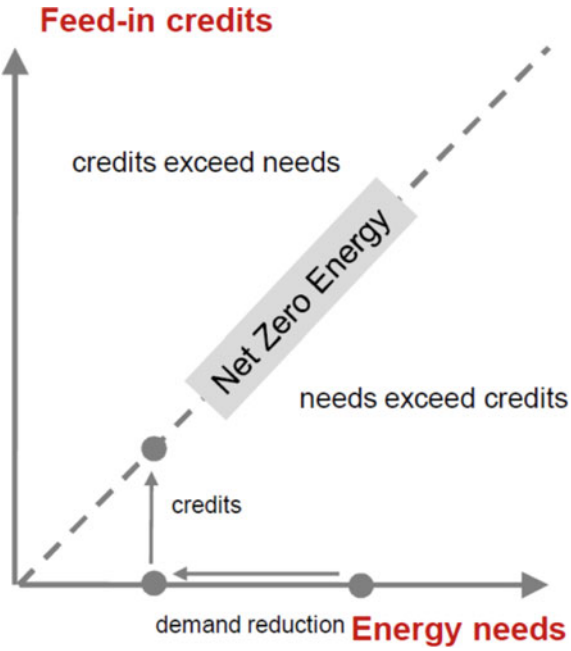

Fig. 1 Net-zero-energy (IEA SHC Task 40, 2015) [3]

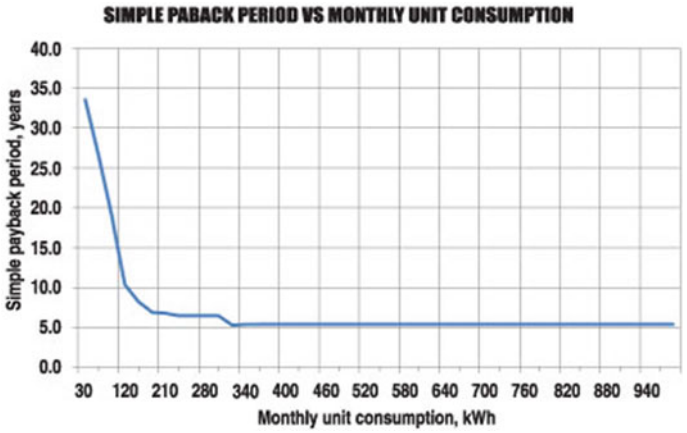

Fig. 2 Domestic solar PV in Colombo [6]

The Zipper Building (91 m, tall) in New York (latitude 39.98° north, longitude 84.90° West) was taken as a case study and was analysed. Thermally active surfaces (i.e., radiant heating and cooling), fully closed-loop geothermal heat exchangers in the ground and solar thermal collectors on the roof were applied. By these technologies alone, the overall energy savings were visible to be more than halfway to net-zero-energy [4].

During the last decade, the prices of solar photovoltaic (PV) modules have decreased in the world market. Miththapala and Karavita (2013) [6] investigated the state of grid-connected domestic solar PV installations in Sri Lanka and presented a ready reckoner feasibility chart (see Fig. 2). It should be noted that the simple payback is approximately 5 years for domestic installations with a monthly electricity consumption of above 340 kWh_e in 2013.

A study by Edirisinghe in 2015 [7] reported that geography and the climate in Sri Lanka justify the capability of harnessing solar energy under the net metering concept. Five parameters (tilt angle, azimuth angle, shadow possibilities, array size, and inverter capacity) which directly affect the performance of the solar PV system, were optimised for rooftop installations.

A framework for assessing progress toward net-zero-energy building through an input-process-output methodology was presented by Hyde et al. (2012) [8]. They investigated a case study in a commercial office building with a 948 m^2 floor area in Colombo. The building has a semi-basement, ground floor and two upper floors. The top floor houses a personal residence. They found the annual average energy intensity of the building to be about 89 $kWh_e\ m^{-2}$. The energy utility indexes for a sample of 20 buildings in Colombo (ten office buildings, five hotels and five mixed development buildings) were reported by Zainudeen et al. in 2008 [9]. The average annual total electricity (the grid, Ceylon Electricity Board, and self-generated onsite electricity) consumption value was found to be 168 $kWh_e\ m^{-2}$.

No study was found on net-zero-energy tall buildings in Sri Lanka in the current literature. The findings on this topic from USA, European countries and Australia are not directly applicable to countries like Sri Lanka which have a tropical rainforest climate.

The main aim of this article is to investigate the potential of solar PV on the façades of a hypothetical 20 storey building in three selected locations (Colombo, Kandy and Jaffna) in Sri Lanka. Colombo was selected based on the current presence and developments of mixed-use skyscrapers [10]. Kandy was selected since it is in the middle of the country. Jaffna was selected because of its greater potential for harvesting solar energy [11]. The optimal orientation of the building to maximise the annual electricity output for each location is identified. The annual electricity output of solar PVs on each façade is quantified. The following section presents the method applied, details of the locations, input parameters used, and the hypothetical building simulated.

2 Method

2.1 Initial Estimate of Rooftop PV Output

A hypothetical 20 storey building, which is likely to be built in Sri Lanka was considered. The footprint of the building is 41 m × 41 m, and the typical floor height is 3.6 m. Approximately, 1680 m2 is the flat roof area. The core dimension was assumed to be 13 m × 13 m. The estimated total area for the air-conditioned zones is 30,240 m^2. The part of the roof area available for solar photovoltaic (PV) system installation was assumed to be about 75% (~660 PV modules of 1.65 m × 0.99 m). The total capacity rooftop solar PV is 198 kW_p. The assumed slope for the rooftop PVs is 10° and they are facing the South.

Typical monocrystalline solar PV modules with a rated efficiency of 18.37% were selected for the rooftop installation. The properties of the modelled rooftop solar PV modules are listed in Table 1.

Wasala (2015) [12] reported that the calculated monthly average global horizontal solar radiation varied between 4.00 to 5.95 kWh m^{-2} per day for Colombo. The initially estimated annual electricity output is about 274 MWh_e based on the annual average global horizontal solar radiation data (Fig. 3) by SWERA (2016) [13] and a conservative PV system annual overall efficiency of 14%.

This value represents 3.63 kWh_e m^{-2} of floor area per annum (~3% of 128 kWh_e m^{-2}), which is about one order of magnitude less than the electricity consumed in a typical building. Installing solar PV modules on the roof alone cannot make net-zero-energy for such a tall building. All surfaces exposed to the sun must be considered for more electricity output.

Semi-transparent PV (STPV) modules were selected for façade integration. The selected STPV modules have opaque monocrystalline solar PV cells with transparent

Table 1 Properties of the rooftop PV modules and inputs to TRNSYS Type94a

Properties	Values
Module power (W_p)	300
Number of cells, 156 × 156 mm (−)	60
Module reference efficiency (%)	18.37
Reference temperature (°C)	25
Reference radiation (Wm^{-2})	1000
Maximum power voltage (V)	31.80
Maximum power current (A)	9.55
Open circuit voltage (V)	38.70
Short circuit current (V)	9.84
Temp. coefficient, short circuit current (C^{-1})	0.0005
Temp. coefficient, open circuit voltage (C^{-1})	−0.0029
Temp. coefficient, maximum power (C^{-1})	−0.0041
Nominal operating cell temperature (°C)	44

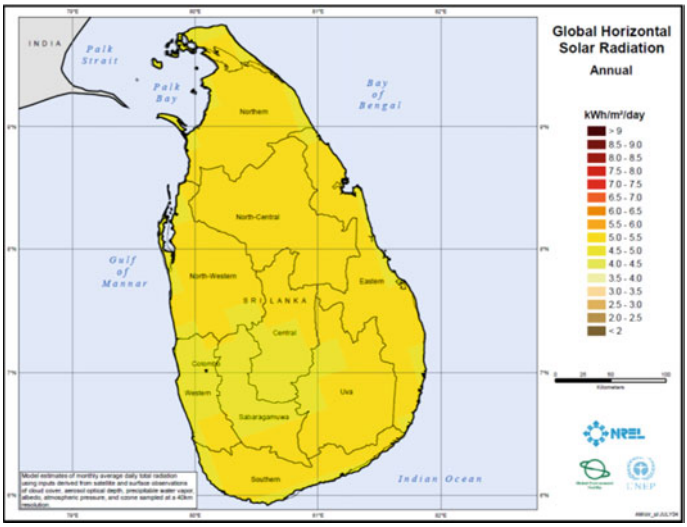

Fig. 3 Annual average global horizontal solar radiation (SWERA 2016) [13]

space in between. The modules have a glass cover and encapsulation material (Ethylene Vinyl Acetate (EVA) sheet). They not only can generate electricity, but also allow light transmission through the transparent part. By blocking incoming solar radiation by PV cells, they reduce solar transmission heat gain and consequently reduce the cooling demand in summer (Fung and Yang, 2008) [14]. The properties of STPV layers are presented in Table 2 and a schematic diagram for a PV cell coverage ratio of 80% (Xu et al., 2014) [13] is presented in Fig. 4 [15]. Table 3 shows the properties

Table 2 Properties of layers for the STPV [14]

Layer	Glass	EVA	Si Cell
Thickness (mm)	6.0	1.8	0.3
Conductivity (Wm^{-1} K^{-1})	0.760	0.116	168
Absorptance (−)	0.108	0.060	0.970
Transmittance (−)	0.81	0.90	0.00
Reflectance (−)	0.082	0.040	0.030

of STPV modules modelled for the simulations. The total capacity of STPV on each side of the building is 432 kW_p. The total solar PV capacity for the four sides of the building is 1728 kW_p.

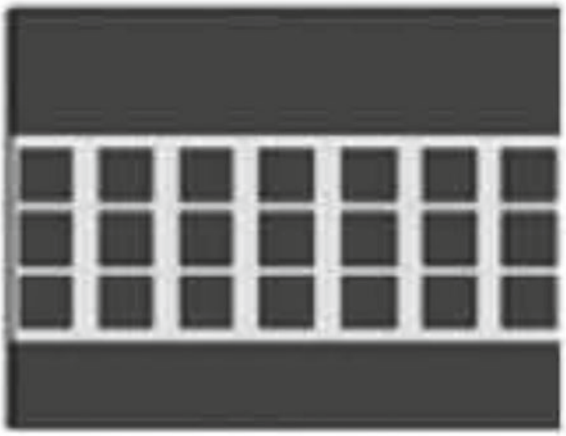

Fig. 4 PV cell coverage ratio = 80% [15]

Table 3 Properties of the STPV modules and inputs to TRNSYS Type652d

Properties	Values
Cell area coverage ratio	0.80
Emittance of glass cover (infra-red)	0.86
Glass cover thickness (mm)	6
Glass cover conductivity (Wm^{-1} K^{-1})	0.76
Refractive index of glass cover	1.5
Solar cell efficiency at reference condition	18%
Reference temperature (°C)	25
Reference radiation (Wm^{-2})	1000
Efficiency modifier for temperature (C^{-1})	−0.0045
Efficiency modifier for radiation (m^2 W^{-1})	0.000009
Internal zone temperature (°C)	24
Back radiant temperature (°C)	24

2.2 Input Data

Three locations in Sri Lanka (details shown in Table 4) were selected for this study. Meteonorm software (Meteotest, 2022) [16] was applied to generate hourly weather data. Historical data from 1991–2010 for irradiation and 2000–2009 for other parameters were selected. Climate Consultant 6.0 software (Milne, 2016) [17] was used to visualise and check the hourly climate data generated.

Colombo and Jaffna have a cooling dominant climate; no space heating is required. As can be seen from Figs. 5 and 6, the best design strategies recommended by Climate Consultant 6.0 for buildings in Colombo and Jaffna are sun shading of windows, cooling and dehumidification. For Kandy, the dehumidification strategy alone could make the indoors thermally comfortable for approximately 60% of the time (Fig. 7).

Table 4 Details of the locations selected

Location	WMO Station No	Latitude (°N)	Longitude (°E)	Elevation (m)
Colombo	43,466	6.90	79.867	7
Kandy	43,444	7.33	80.63	479
Jaffna	43,404	9.65	80.02	3

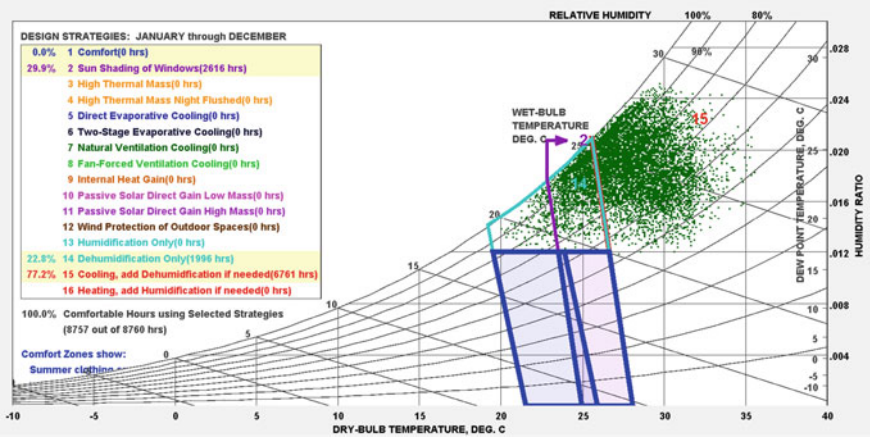

Fig. 5 Design strategies shown on the psychrometric chart, Colombo, WMO No. 43466

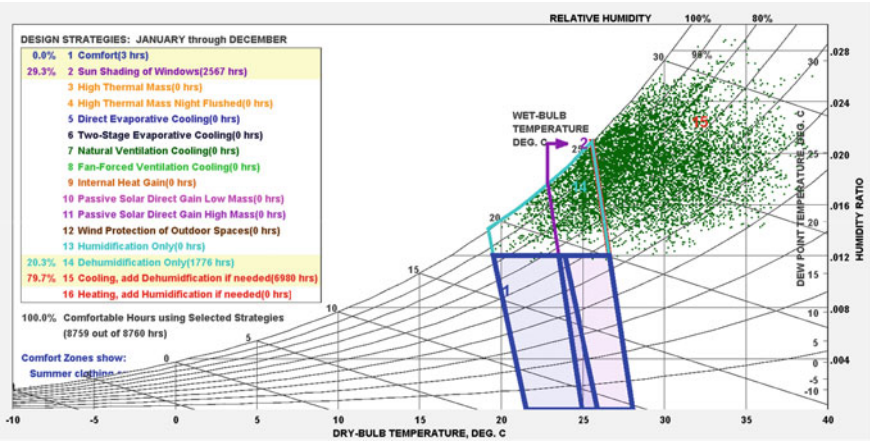

Fig. 6 Design strategies shown on the psychrometric chart, Jaffna, WMO No. 43404

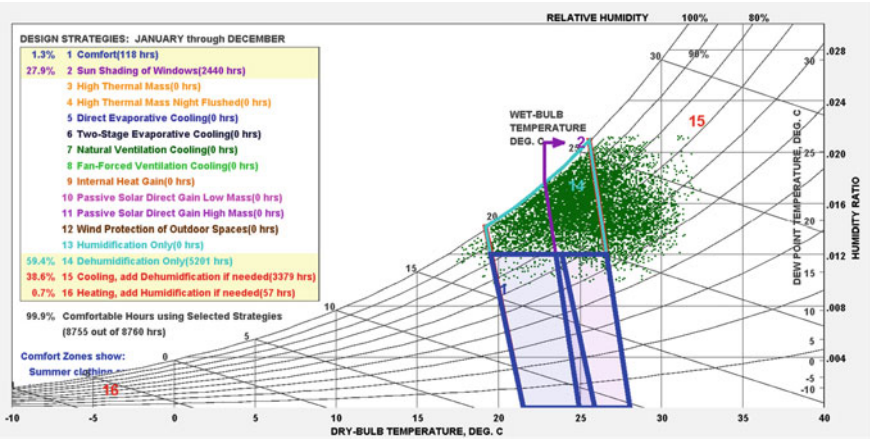

Fig. 7 Design strategies shown on the psychrometric chart, Kandy, WMO No. 43444

2.3 STPV Orientations and TRNSYS Simulations

One of the three key approaches identified by IEA-SHC Task 40 (2015) [3] is that a building design optimises for solar harvesting. Orientation of STPVs is one of the most critical factors that determine electricity output. The highest output orientations for STPV can be found by evaluating yearly total solar radiations on the vertical surfaces in various orientations. The solar radiation received on the vertical surfaces for eight orientations [S (0°), SW (45°), W (90°), NW (135°), N (180°), NE (225°), E

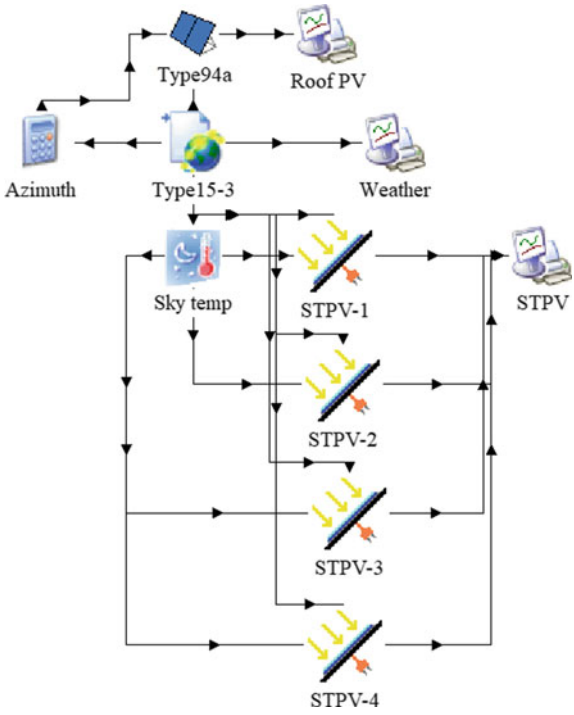

Fig. 8 Project on TRNSYS simulation studio

(270°), SE (315°)] and three locations were estimated based on the hourly climate data generated. As the solar system performance is transient, it was evaluated by computer simulations. TRNSYS software tool (Klein et al. 2020) [18] was employed for this purpose. The orientation of the building was selected to maximise the electricity output from the STPV modules on all four façades of the hypothetical tall building. These were modelled in TRNSYS [18] (see Fig. 8). TRNSYS Type94a [18] and Type562d supplied by TESS [19] were applied for simulations of rooftop PV (Table 1) and STPV (Table 2), respectively.

3 Results and Discussion

The annual solar radiations received on the vertical surfaces of eight orientations for the three locations are shown in Fig. 9. The vertical surface facing the East receives the highest solar radiation (3.72, 3.70, 3.59 GJ m^{-2} in Colombo, Jaffna and Kandy, respectively) and the vertical surface facing the North receives the lowest solar radiation (2.3 GJ m^{-2}).

The hypothetical tall building modelled in this study has a square shape plan (width to length ratio = 1:1). The building façades facing N-E-S-W have an average of 3.11 GJ m^{-2} and those facing NE-SE-SW-NW have an average of 3.14 GJ m^{-2}

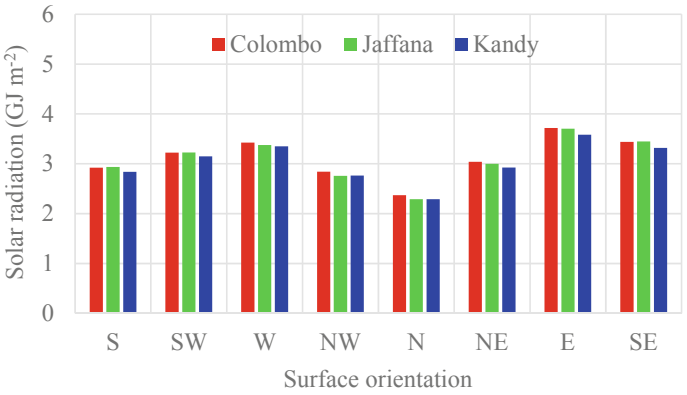

Fig. 9 Annual solar radiations received on vertical surfaces in the three locations in Sri Lanka

Table 5 Solar PV's annual electricity output (MWh_e) (Rooftop 660 × $300W_p$ modules, four wall 2,361 m^2 each)

Location	Colombo	Jaffna	Kandy
Rooftop solar PV	299.5	295.9	287.8
North side STPV	250.8	242.3	240.6
East side STPV	367.6	354.1	354.1
South side STPV	283.8	280.3	272.4
West side STPV	349.7	340.0	337.3
Total	1551.4	1521.6	1492.2
Per floor area ($kWh_e\ m^{-2}$)	51.3	50.3	49.3

in Colombo. The difference is less than 1%. It should be noted that, in Colombo, the horizontal surface receives 6.91 GJ m^{-2} annually.

N-E-S-W building orientation was selected. The surface area of the solar PV cells was estimated for each façade of the building, and it is 2361 m^2 for an 80% cell coverage ratio. The total number of solar PV modules on the flat roof in the simulation study was 660. The annual electricity output from the roof and the four sides of the building are presented in Table 5. The capacity factor for the rooftop PV was found to be 17.3%. The average capacity factor for the façade integrated STPV was found to be 8.4%.

4 Conclusions

The potentials of grid-connected net-zero-energy buildings for three locations in Sri Lanka were investigated. The electricity outputs from the rooftop PV and STPV installed on building façades were quantified for each location.

The façade facing the East received the highest amount of annual solar radiation and the facade facing the North received the lowest amount of annual solar radiation in these locations.

The installed grid-connected PV systems on the 20-story hypothetical tall building in Colombo can accommodate 51.3 kWh_e m^{-2} of building floor area per annum. If this tall building is to be net-zero-energy by using current available PV alone, the electricity consumption of the building must be lower than 51.3 kWh_e m^{-2}.

Credit Authorship Contribution Statement

Lu Aye: Conceptualisation, Methodology, Software, Validation, Formal analysis, Investigation, Resources, Data curation, Writing—original draft, review and editing, Visualisation, Supervision, Project administration, Funding acquisition. **Amitha Jayalath**: Validation, Writing—review and editing, Visualisation, Dan **Wu**: Methodology, Software, Validation, Writing—review and editing.

Declaration of Competing Interest

The authors have no competing interests to declare that are relevant to the content of this article.

Acknowledgements Lu Aye wishes to thank the Council on Tall Buildings and Urban Habitat (CTBUH), Sri Lanka Chapter for the continuing support for my participation in the International Conference on Sustainable Built Environment (ICSBE) series.

Data Availability The datasets generated and analysed for this work are available from the corresponding author upon reasonable request.

References

1. Marszal AJ, Heiselberg P, Bourrelle JS, Musall E, Voss K, Sartori I, Napolitano A (2011) Zero energy building – a review of definitions and calculation methodologies. Energy Build 43(4):971–979
2. Laustsen E (2008) Energy efficiency requirements in building codes. In: Energy efficiency policies for new buildings, OECD/IEA, Paris
3. IEA SHC Task 40 (2015) Position paper: net zero energy solar buildings. http://task40.iea-shc.org/data/sites/1/publications/IEA-SHC-NZEB-Position-Paper.pdf, International energy agency, solar heating and cooling programme task 40 (EBC Annex 52)
4. Griffith B, Long N, Torcellini P, Judkoff R, Crawley D, Ryan J (2007) Assessment of the technical potential for achieving net zero-energy buildings in the commercial sector. Technical Report NREL/TP-550-41957
5. Chambers N (2014) Is net-zero tall possible? CTBUH J (2014)II:18–24
6. Miththapala S, Karavita S (2013) Feasibility of solar electricity in Sri Lanka, MirrorBusiness, 2013-03-28. http://www.dailymirror.lk/27390/feasibility-of-solar-electricity-in-sri-lanka
7. Edirisinghe AJ (2015) Optimum selection of solar systems for net metered consumers a case study: Colombo City. Department of Electrical Engineering, University of Moratuwa, Master of Science

8. Hyde R, Rajapaksha U, Rajapaksha I, Riain MO, Silva F (2012) A design framework for achieving net zero energy commercial buildings. In: Proceedings of the 46th annual conference of the architectural science association, ASA/ANZAScA 2012, Griffith University, Gold Coast, Australia, 14–16 November 2012
9. Zainudeen N, Seneviratne K, Manewa A, Ubesiri N (2008) Contribution of commercial buildings toward GHG emissions: Sri Lankan perspective, the proceedings from international conference on building education and research (BEAR), Salford (United Kingdom) school of the built environment, University of Salford, UK, pp 1417–1429
10. Wickremasinghe HT, Wickramanayake WS, Wickramaarachchi NC (2018) A review of trends in mixed-use skyscrapers in Sri Lanka. In: 2nd international conference on real estate management and valuation
11. Mendis T (2018) The potential of building integrated photovoltaics in Jaffna, Sri Lanka. In: international conference on renewable energy, ICREN 2018, Barcelona
12. Wasala WAML (2015) Global, direct, and diffuse solar insolation analysis on horizontal and tilted surfaces at Colombo, Sri Lanka, master of engineering, department of mechanical engineering, university of Moratuwa
13. SWERA (2016) Solar and wind energy resource assessment (SWERA), facilitated by the united nations environment programme. http://en.openei.org/wiki/Sri_Lanka
14. Fung TYY, Yang H (2008) Study on thermal performance of semi-transparent building-integrated photovoltaic glazings. Energy Build 40(3):341–350
15. Xu S, Liao W, Huang J, Kang J (2014) Optimal PV cell coverage ratio for semi-transparent photovoltaics on office building facades in central China. Energy Build 77:130–138
16. Meteotest (2022) Meteonorm: irradiation data for every place on earth. http://www.meteonorm.com/en/
17. Milne M (2016) Climate consultant. http://www.energy-design-tools.aud.ucla.edu/climate-consultant/
18. Klein S, Beckman W, Mitchell J,Duffie J, Duffie N, Freeman T, Mitchell J, Braun J, Evans B, Kummer J, Urban R, Fiksel A, Thornton J, Blair N, Wiliams P, Bradley D, McDowell T, Kummert M, Arias D, Duffy M (2020) TRNSYS 18: a transient system simulation program, solar energy laboratory, University of Wisconsin-Madison
19. TESS (2016). TESS component library: general descriptions, thermal energy system specialists, LLC, Madison, Wisconsin

Effectiveness of Various Outrigger Systems of Different Structural Materials for Lateral Load Resistance in Reinforced Concrete High-Rise Buildings

N. A. A. C. Nissanka, A. M. Fernando, and J. C. P. H. Gamage

Abstract With the rapid urbanization and fast pace of development in high-strength materials, construction of tall structures has become a go-to option. It is concerned with considerably reducing the weight of buildings while enhancing the slenderness and flexibility of structures. However, as the height increases the structures become more critical under wind and earthquake-induced lateral loads, as it reduces lateral stiffness which is pivotal in maintaining a building's structural efficiency. In such instances, outrigger and belt truss structural systems are often introduced in high-rise structures to provide adequate lateral stiffness to maintain the wind deflection and drift criteria within acceptable limits. According to the Author's knowledge, extensive studies have been done up to date, which only consist of investigations with outrigger systems of a single material, consisting of simple square and rectangular shaped building plan layouts having no consideration for vertical irregularity of the building. Hence, this study aims to bring a broader understanding of both conventional outrigger and virtual outrigger systems by identifying the most efficient lateral load resisting outrigger system for a reinforced concrete high-rise building by analyzing a range of structural materials and alternative arrangements with vertical irregularity. A three-dimensional (3D) numerical model of a high-rise building with lateral load resisting systems was developed and validated theoretically. A parametric study was conducted to determine the applicability of selected alternative outrigger systems. Results indicate that the combination of the outrigger and belt truss structural system in concrete indicated maximum performance while attaining the maximum reduction of 29.7% and 28.5% in lateral displacement and inter-storey drift, respectively. These values tend to vary with each outrigger structural arrangement and the structural material, while all systems seem to significantly enhance the structural performance of the building against wind action, hence resulting in more resilient and sustainable buildings.

N. A. A. C. Nissanka · A. M. Fernando (✉) · J. C. P. H. Gamage
Department of Civil Engineering, University of Moratuwa, Moratuwa 10400, Sri Lanka
e-mail: fernandoam.21@uom.lk

© The Author(s), under exclusive license to Springer Nature Singapore Pte Ltd. 2023

R. Dissanayake et al. (eds.), *ICSBE 2022*, Lecture Notes in Civil Engineering 362,
https://doi.org/10.1007/978-981-99-3471-3_46

Keywords Outriggers · Reinforced concrete building · Composite material · Wind load · Lateral displacement · Inter-storey drift

1 Introduction

Recent advances in the creative design approaches of architects, rapid urbanization and lack of urban lands, excessive cost, and the necessity to prevent disorder in urban expansion have resulted in the growth of high-rise constructions. In the early days, very few structural forms were used in the design of tall buildings. However, due to the rapid technological advancements in modern science along with innovations in material technology, developments in construction techniques and operating systems at present, enables various structural configurations and profiles to be used for tall buildings [1]. In doing so, the buildings become more critical under wind and earthquake-induced lateral loads, as it reduces the structural stiffness of the building. By accommodating a very effective and efficient core wall structural system into a tall building, drift, and displacement parameters due to lateral loads can be reduced remarkably [2]. Nevertheless, in tall buildings, as the structure height increases, the standalone core wall structural system can barely provide sufficient structural stiffness to control the drift and displacement criteria within the acceptable limits. Therefore, in such cases, outrigger structural systems are introduced into tall buildings where deep and stiff elements are connected through the central core wall system and most exterior columns of the building, reducing the sway of the building [3, 4].

The structural performance and efficiency of outrigger systems used in tall buildings to resist lateral loadings depend on several factors such as different forms of structural outrigger configurations, the number of outrigger levels provided in the building, relative locations of outrigger/outriggers along its height of the building, outrigger plan layout, outrigger truss depths, primary structural materials used, etc. [4]. When considering the outrigger plan layout, both conventional outriggers and virtual outriggers are currently used as efficient lateral load resisting mechanisms in tall buildings. The comparison of structural performance of both conventional and virtual outrigger systems to resist lateral loads in tall buildings has been widely investigated and these studies have extensively used various outrigger typologies to determine the optimum number and positions of outriggers to be used at different heights of the building [5]. However, those studies are mostly limited only to concrete outriggers [6–8]. Further, much of the previous work is based on square and rectangular shaped buildings considering simple grids and plans with minor consideration for vertical irregularity in the building structure (Prasad et al. 2016) [9, 10]. Hence, the present study uses both a circular and a rectangular topology having vertical irregularity along its height which represents the actual building topology in modern structures. Moreover, not many studies are based on a single model with distinct forms of outrigger arrangements to identify the most efficient outrigger structural system. Therefore, this study is extended towards analyzing the behaviour of a reinforced concrete high-rise building, for different types of outrigger arrangements

under different structural materials to identify the most efficient outrigger structural system and the optimum primary structural materials to be used in each system when subjected to wind loading.

2 Literature Review

2.1 Structural Systems for Tall Buildings

From a structural engineer's perspective, the selection of the best and the most appropriate structural form for a high-rise building mainly depends on the efficient arrangement of major structural elements to resist the different gravity and horizontal loading combinations. Several other factors such as internal planning, structural material and method of construction, external architectural appearance and perspectives, operation of services, nature and extent of horizontal loading applied on structure, and the height and aspect ratio of the building are also considered crucial [11, 12]. When the structure is taller and slender, it is necessary to select the most appropriate structural form with the required structural stability. Sitapara and Gore [13] have discussed various types of lateral load resisting structural systems including Rigid frame structural systems, Wall-frame structural systems, Braced frame structural systems, Outrigger structural systems, and Tubular structural systems which are employed in high-rise structures to resist lateral forces. Out of those, the outrigger structural system is scientifically proven to be the most effective method to be used for high-rises [14].

2.2 Outrigger Structural System

These systems consist of deep and stiff elements that connect the central core wall system and the most exterior columns of the building, helping in reducing the sway of the building as presented in Fig. 1 [15]. It is recommended that at least one storey deep outriggers are to be accommodated in tall buildings in order to make them sufficiently effective and to increase the flexural and shear rigidity of buildings [9]. This mechanism greatly assists in reducing the moment in the core system of the buildings when compared to a free-standing core wall system without outriggers [14]. As depicted in Fig. 2, the restraint induced by the use of outriggers notably reduces the top storey drift and lateral displacement while improving the structural stiffness of the building by 20–30% [13]. Generally, the insertion of outriggers greatly reduces the available interior space of a building. Therefore, in general, they are placed at mechanical equipment floor levels not to hinder the floor function in the normal floor levels.

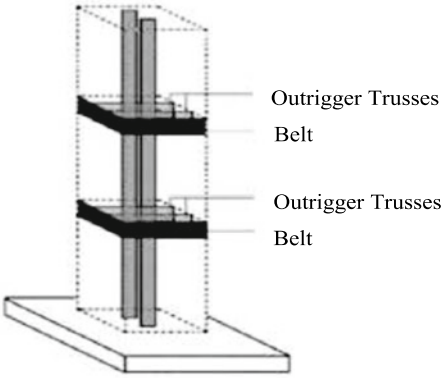

Fig. 1 Multi-level outrigger and belt truss system

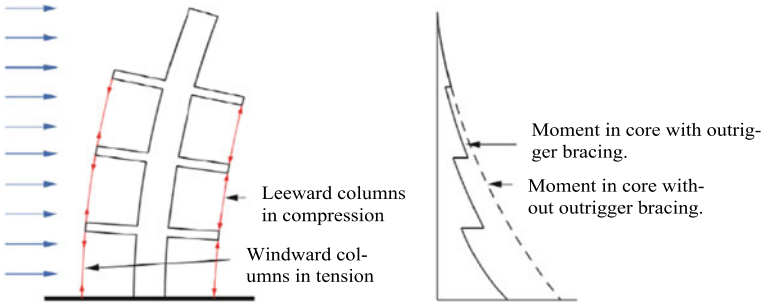

Fig. 2 Outrigger structure displaced under lateral loading and resultant core moments

2.3 Types of Outrigger Systems and Research Trends

Over the past years, outriggers have been extensively utilized in tall building structures [1, 16, 17]. The comparative study by Thejaswini and Rashmi [18] outlines that when accommodating an outrigger at the optimum location of the building, a drift can be fully controlled. Similarly, [14] has studied the progression of the outrigger structural system with time in tall buildings and different applications in terms of optimum topology, design, and construction considerations. Due to the rapid enhancements in technology and science, the choices have widened accordingly with time for the options of structural materials to be used in outriggers as well as for structural forms to be used. Two major forms of outrigger systems can be recognized based on the structural mechanism of connectivity between the outriggers and the core wall system. They are conventional outrigger system and virtual outrigger system. In the conventional outrigger system, outrigger girders are directly tied in between the core walls and exterior columns of the building. In the virtual outrigger concept, the overturning moment is transmitted from the core to the perimeter columns in a

similar pattern, with no direct connection between the outrigger trusses and the core. Due to the curtailment of this direct connection, it mitigates most of the drawbacks which are associated with the conventional outrigger system. However, the study by [6] has resulted in a maximum lateral displacement in virtual outrigger systems. It has also showcased that multi-outrigger systems can reduce structural elements and foundation sizes as well.

The location of the outrigger across the building plan layout is more important for the lateral behaviour of the structure. Several studies have investigated the optimum outrigger locations to be selected during the design stage [19–21, 10]. As per the findings, a general guideline for the location of a single outrigger is to place it at halfway of the building height. For two outriggers, 1/3 and 2/3 height would be the optimum locations. If three outriggers are to be used, 1/4, 1/2, and 3/4 heights are ideal to be used. In case of a three-outrigger system, if one outrigger is to be placed at the top storey, the remaining two outriggers should be located at 1/3 and 2/3 height of the building.

Even though extensive studies have been conducted, several research gaps can be identified after a thorough review of the literature. Primarily, there is a lack of research work on actual architectural plans where the outrigger structural system has been used in the irregular shape of buildings having vertical irregularity since most of the studies are based on square and rectangular shaped buildings having simple layouts. Almost all researchers have investigated the static and dynamic behaviour of structures under elastic limits. Only some have used the non-linear time history analysis method. Moreover, researchers have studied the optimum outrigger position for conventional outrigger systems, but there is a lack of data on the optimum location for the virtual outrigger systems. Hence, a necessity arose to study the multi-outrigger level approach and effects of the two storeys deep and three storeys deep outrigger by adopting two or three numbers of outrigger levels in a tall structure. There exist only a few studies on single models with different outrigger types. Therefore, extensions in identifying the optimum usage of outrigger systems along with different types of truss outriggers are required.

3 Methodology

3.1 Structural Model

The proposed structure is a 55 storey, 197.5 m high RC high-rise building which is assumed to function as an area for retail, offices, and residential space. Single storey deep two outrigger levels have been provided at two mechanical floor levels in fixed positions, to minimize the reduction of usable floor area and any disturbance to aesthetic appearance. Pertaining to the findings of Shivacharan K (2015), the first outrigger is placed on the 18th level (1/3 of the building height) and the second outrigger is placed on the 36th level (2/3 of the building height). Table 1 denotes the

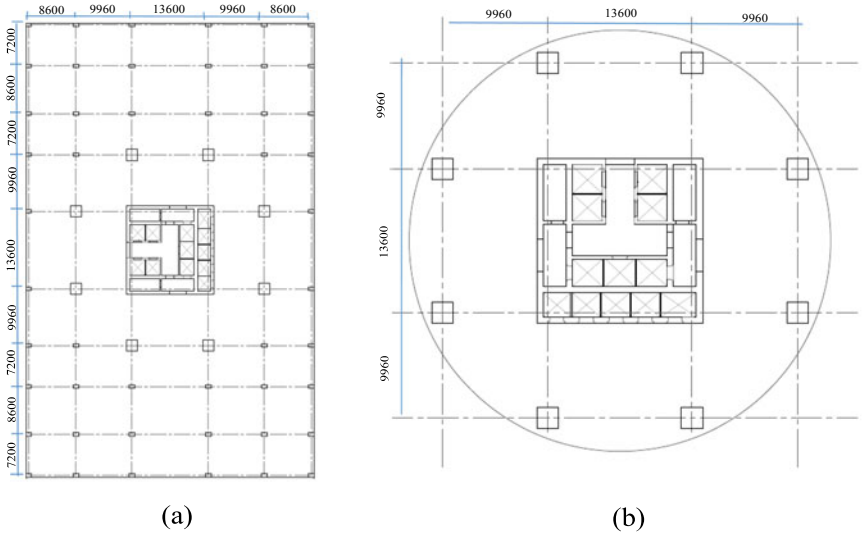

Fig. 3 **a** Layout of the structural floor plan from Level 1–Level 8, **b** Layout of structural floor plan from Level 9–Level 55 (dimensions in mm)

information related to this section. To account for vertical irregularity, the geometry of the building is changed from a rectangular shape to a circular shape beyond level 8 onwards. The bottom floors represent podium floors and the upper floors represent a standalone single tower as in a real structure as presented in Fig. 3. The section properties and material properties of each structural element including outriggers are presented in Table 1.

The primary idea of this study is to identify the effectiveness of conventional and virtual outrigger systems on the structural performance of a RC high-rise building through several combinations of belt truss and outrigger arrangements under each category of different structural materials. Therefore, a total of 10 model types, (as in Table 2) with different outrigger types; only outrigger, only belt truss, and a combination of both belt truss and outrigger under different structural materials; concrete, steel, and composite were modelled.

3.2 Design Loads

Dead loads, super imposed dead loads, live loads, and wind loads are the primary loads considered in structural modelling. The dead load is considered the self-weight of the structure. The self-weight of structural elements is automatically generated by the software based on assigned material properties. Unit weight of concrete and steel was taken as 25 kN/m^3 and 78 kN/m^3, respectively. Superimposed dead loads and live loads were considered as per BS EN 1991–1.1–2001 [22]. The static wind

Table 1 Section properties and material properties

Element		Size (m)		Material properties
Column	Mega columns	1.2 × 1.2		M50
	Podium columns	0.6 × 0.6		
		Width (W)	Depth (D)	
Beam	Perimeter Beams	0.6 × 0.6		M30
		1.2 × 0.6		
	Internal Primary Beams	0.6 × 0.6		
	Internal Secondary Beams	0.6 × 0.4		
Beams at outrigger levels	Perimeter Beams	0.6 × 2		
	Internal Primary Beams	0.6 × 0.6		
	Internal Secondary Beams	0.4 × 0.6		
Slab	At top & bottom of outrigger floors	0.2		M30
	Other levels	0.15		
RC core walls		0.4,0.3		M50
Reinforced concrete wall outriggers		0.4		M50
Steel outriggers	H Iron	1 × 1 × 0.1 × 0.1		S355
Composite outrigger	Concrete Beam	1 × 1		M50
	H Iron	0.6 × 0.6 × 0.06 × 0.06		S355

loads were calculated as per BS EN 1991–1.4–2005 [23], where the wind loads were applied as diaphragm forces for each floor in the building. Basic load combinations were established in accordance with BS EN 1990:2002 [24].

3.3 Method of Analysis

The structure was analysed as a three-dimensional elastic structure, in the CSI ETABS structural analysis software. When modelling, columns and beams were modelled as frame elements and shear walls and slabs were modelled as shell elements. Foundation deformations were neglected in the structural analysis and pin supports were assigned to columns at the base. Auto meshing is done for slab elements while manual meshing was used for wall elements.

Table 2 Model arrangements

Model ID	Model description	Model arrangement
NO	Structural model without outrigger	
Concrete material		
O-CONCTERE	Structural model of concrete outrigger only	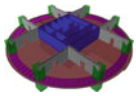
B-CONCRETE	Structural model of concrete belt truss only	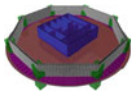
OB-CONCRETE	Structural model of concrete outrigger with belt truss	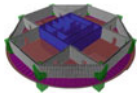
Steel material		
O-STEEL	Structural model of steel outrigger only	
B-STEEL	Structural model of steel belt truss only	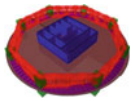
OB-STEEL	Structural model of steel outrigger with belt truss	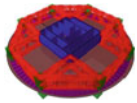
Composite material		
O-COMPOSITE	Structural model of composite outrigger only	
B-COMPOSITE	Structural model of composite belt truss only	

(continued)

Table 2 (continued)

Model ID	Model description	Model arrangement
OB-COMPOSITE	Structural model of composite outrigger with belt truss	

4 Results and Discussion

4.1 Natural Period and Corresponding Frequencies

The results of the natural period and corresponding frequencies for the first two modes of each outrigger structural model of concrete, steel, and composite and for the structural model without outriggers are presented in Table 3.

The frequency of a structure is a characteristic of stiffness. It directly affects the structural performance of a building. The structural model without outriggers has the highest building period for both Mode 1 (Y direction) and Mode 2 (X Direction) when compared with other outrigger structural models. The combination of both outrigger and the belt truss structural system (OB) has the lowest building period for both Mode 1 and Mode 2. The belt truss only (B) outrigger structural system has the highest building period under each material category of concrete, steel, and composite.

Table 3 Natural period and corresponding frequencies for structural models

Model name	Period		Frequency		% Frequency increase	
	Mode 1	Mode 2	Mode 1	Mode 2	Mode 1	Mode 2
	Y direction	X direction	Y direction	X direction	Y direction	X direction
	s	s	Hz	Hz	%	%
NO	7.613	6.989	0.131	0.143	–	–
O-CONCRETE	6.466	5.903	0.155	0.169	18	18
B-CONCRETE	6.576	6.043	0.152	0.165	16	16
OB-CONCRETE	6.425	5.843	0.156	0.171	18	20
O-STEEL	6.614	6.059	0.151	0.165	15	15
B-STEEL	6.749	6.223	0.148	0.161	13	12
OB-STEEL	6.503	5.944	0.154	0.168	17	18
O-COMPOSITE	6.684	6.128	0.150	0.163	14	14
B-COMPOSITE	6.823	6.296	0.147	0.159	12	11
OB-COMPOSITE	6.561	6.003	0.152	0.167	16	16

When comparing different materials, concrete type outrigger systems tend to perform relatively well. The frequency in the structure was increased by a maximum of 18% in the most critical direction of Y for the outrigger systems O and OB compared to the one without outriggers. For outrigger system B, the frequency was increased by a maximum of 16%. For the outrigger types of steel material, a significant difference was observed where the frequency for OB system is increased by 17%, while for systems O and B 15% and 13% increments were obtained. The same pattern of structural performance was observed in different outrigger types of composite material, where the structure frequency was increased by 16%, 14%, and 12% for OB, O, and B systems, respectively.

4.2 Maximum Wind-Induced Lateral Displacement.

The structural model without outriggers has the maximum wind-induced lateral deflection on the top storey in both X and Y directions and those results exceeded the maximum allowable lateral displacement value of H/500. Maximum wind-induced lateral deflection on the top storey values has been reduced in all other outrigger structure models of concrete, steel, and composite in both directions. The values are less than the maximum allowable lateral displacement. Summarized results for the maximum wind-induced lateral deflection in both X and Y directions for each structural model of no outriggers and with outriggers under different structure materials of concrete, steel, and composite are illustrated in Table 4.

When comparing the performance of outrigger structure models of different outrigger arrangements, the pattern of varying the top storey lateral displacement

Table 4 Maximum wind-induced lateral displacement for structural models

Modal name	Displacement at top			% Reduction in displacement	
	X direction	Y direction	Allowable limit	Δx	Δy
	mm	Mm	mm	%	%
NO	397.52	430.562	395		
O-CONCRETE	276.919	309.734	395	30.3	28.1
B-CONCRETE	293.138	321.134		26.3	25.4
OB-CONCRETE	272.072	302.709		31.6	29.7
O-STEEL	292.896	325.108	395	26.3	24.5
B-STEEL	312.624	340.454		21.4	20.9
OB-STEEL	284.691	314.316		28.4	27.0
O-COMPOSITE	299.497	331.555	395	24.7	23.0
B-COMPOSITE	319.377	347.417		19.7	19.3
OB-COMPOSITE	289.792	319.202		27.1	25.9

values is almost unchanged under each material category of concrete, steel, and composite. The minimum deflection in both axes is achieved by the OB outrigger system and the outrigger system B has achieved the maximum deflection in both axes. For different outrigger types of concrete material, the maximum reduction of 29.7%, in the top storey lateral displacement was achieved for OB, O, and B outrigger systems, respectively. Similarly, steel and composite material structures exhibited the same trend, where OB, O, and B outrigger systems in steel have reductions of 27.0%, 24.5%, and 20.9%, with 25.9%, 23.0%, and 19.3% reductions for the composite structure material. The profile of lateral displacement at the top storey for each outrigger building model with varying material options for the most critical direction (Y direction) is presented in Fig. 4.

4.3 Maximum Inter-Storey Drift

The Maximum inter-storey drift values in both X and Y directions for each structural model without outriggers and with outriggers under different structure materials were compared with the maximum allowable inter-storey drift value of 0.25% as demonstrated in Table 5. The structural model without outriggers has the maximum inter-storey drift in both X and Y directions. Those results exceed the maximum allowable inter-storey drift value of 0.25%. Figure 5 illustrates the inter-storey drift of the structure without outriggers in the most critical direction. In contrast, all the other models with different combinations of outrigger structures exhibit values less than the maximum allowable limit. Figure 6 depicts the inter-storey drift for each structural material having different outrigger arrangements [6].

For OB outrigger systems, the maximum reduction in the inter-storey drift of 28.5% was achieved by the concrete type of outrigger with 26.6% and 25.7% for steel and composite types, respectively. The same trend was observed for the other two outrigger systems, where in O type 27.3%, 24.7%, and 23.4%, in B type 25.3%, 21.1%, and 19.6% reductions were obtained for material of concrete, steel, and composite type, respectively.

5 Conclusion and Recommendations

The current study investigated the behaviour and effectiveness of various outrigger systems under different structural materials for a multi-storey reinforced concrete high-rise building when subjected to wind loads. A parametric study was conducted on a numerical model. Different outrigger structure types: only outriggers (O), only belt truss (B), and a combination of both outriggers and belt truss (OB) with varying material categories of concrete, steel, and composite were compared with the structural model without outriggers based on the parameters such as natural frequency,

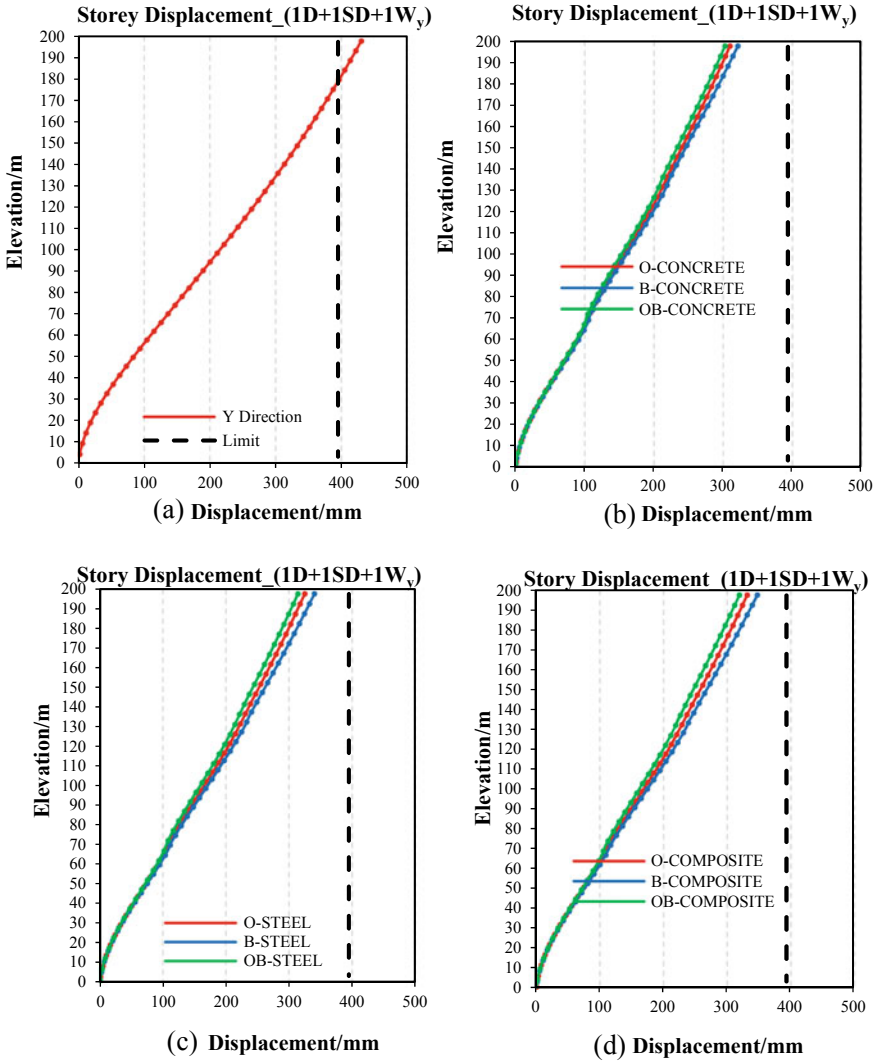

Fig. 4 Maximum storey displacement for structural models, **a** without outriggers, **b** concrete outriggers, **c** steel outriggers, **d** composite outriggers in Y-Direction

maximum lateral displacement of top storey and inter-storey drift. The findings of the investigation can be summarized as follows:

1. The insertion of conventional and virtual outrigger systems has effectively contributed to reduce the natural period of a building by increasing the structural stiffness. It has achieved a decrease in the maximum wind-induced lateral deflection at the top storey and maximum inter-storey drift of the structure by increasing the resistance against the lateral loads.

Table 5 Maximum inter-storey drift for structural models

Modal name	Maximum storey drift			% Reduction in storey drift	
	X direction	Y direction	Allowable limit	Δx	Δy
	%	%	%	%	%
NO	0.2495	0.2648	0.25	-	-
O-CONCRETE	0.1814	0.1925	0.25	27.3	27.3
B-CONCRETE	0.1896	0.1978		24.0	25.3
OB-CONCRETE	0.1778	0.1894		28.7	28.5
O-STEEL	0.1911	0.1993	0.25	23.4	24.7
B-STEEL	0.2013	0.209		19.3	21.1
OB-STEEL	0.1852	0.1943		25.8	26.6
O-COMPOSITE	0.1951	0.2029	0.25	21.8	23.4
B-COMPOSITE	0.2053	0.2129		17.7	19.6
OB-COMPOSITE	0.1882	0.1967		24.6	25.7

2. Concrete-type outriggers exhibit the best structural performance in reducing the building period, top storey lateral displacement, and inter-storey drift. Both OB and O-type concrete outrigger systems have almost similar reduction percentages.
3. For steel outrigger structure types, OB outrigger system is proven to be the best outrigger structure type in reducing all the three parameters of the building compared to the other two outrigger systems. A similar trend was observed for composite material models.

As per the findings, it is clearly depicted how outrigger systems are utilized to obtain a resilient infrastructure. Further, it is seen how different materials and arrangements can result in enhanced structural performance. Following are several recommendations for future studies:

- Outrigger and belt trusses can be placed at different locations of a building along its height and can identify the most optimum location for each outrigger structure type under each category of different structural materials, concrete, steel, and composite.
- The study can be used for different types of truss outriggers and belt trusses under different structural materials of concrete, steel, and composite.
- A similar study can be carried out by increasing the depth of the outriggers into two or three storeys

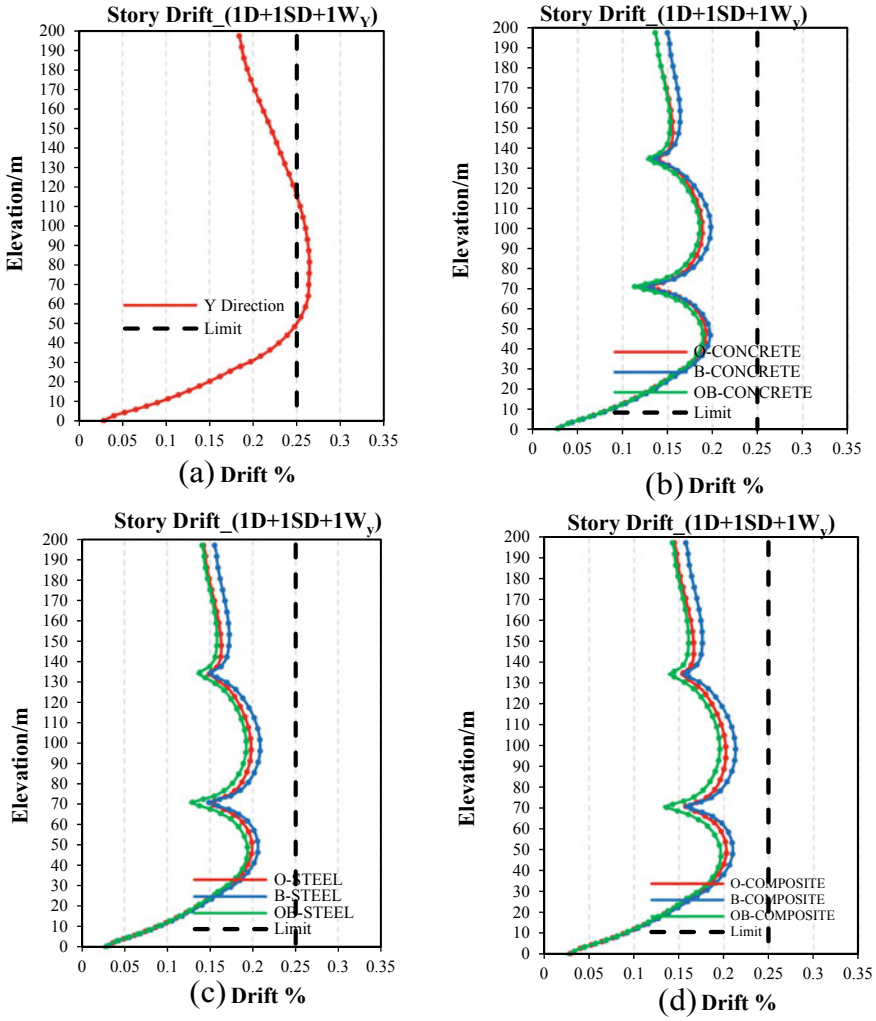

Fig. 5 Maximum inter-storey drift for structural models **a** without outriggers, **b** concrete outriggers, **c** steel outriggers, **d** composite outriggers in Y-Direction

Acknowledgements The author extends gratitude to the staff of the Computer Laboratory, Department of Civil Engineering, University of Moratuwa.

References

1. Choi HS, Joseph L (2012) Outrigger system design considerations high-rise buildings outrigger system design considerations. Int J High-Rise Build 1:237–246

2. Choi HS, Ho G, Joseph L, Mathias N (2017) Outrigger design for high-rise buildings. Outrigger des. High-rise build
3. Mithbhakare NY, Kumbhar (2008) Review on behavior of outrigger system in high rise building. Int Res J Eng Technol 1990–1994
4. Nanduri PMBRK, Suresh B, Hussain MI (2013) Optimum position of outrigger system for high-rise reinforced concrete buildings under wind and earthquake loadings. J Eng Res 2:76–89
5. Kian P (2004) The use of outrigger and belt truss system for high-rise concrete buildings. Civ Eng Dimens 3
6. Bayati Z, Mahdikhani M, Rahaei A (2008) Optimized use of multi-outriggers system to stiffen tall buildings
7. Herath N, Haritos N, Ngo T, Mendis P (2009) Behaviour of outrigger beams in high rise buildings under earthquake loads
8. Nair RS (1998) Belt trusses and basements as "virtual" outriggers for tall buildings. Eng J Am Inst Steel Constr 140–146
9. Gadkari AP, Gore NG (2016) Review on behaviour of outrigger structural system in high-rise building. Int J Eng Dev Res 4:2065
10. Vijay NP, James JS, Kurian N (2017) Optimization of outrigger braced structures using regression analysis. Int Res J Eng Technol 4:1807–1810
11. Vijaya Kumari Gowda MR, Manohar BC (2015) A study on dynamic analysis of tall structure with belt truss systems for different seismic zones. Int J Eng Res 4:158–167
12. Wu J, Li Q (2003) Structural performance of multi-outrigger-braced tall buildings. Struct Des Tall Spec Build - Struct des Tall Spec Build 12:155–176
13. Sitapara KD, Gore G (2016) Review on feasibility of high rise outrigger structural system in seismically active regions. Int Res J Eng Technol 3:1427–1432
14. Ho GWM (2016) The evolution of outrigger system in tall buildings. Int J High-Rise Build 5:21–30
15. Smith BS, Coull A (1991) Tall building structures: analysis and design. Wiley, New York
16. Fawzia S, Fatima T (2016) Optimum position of steel outrigger system for high rise composite buildings subjected to wind loads 12:134–153
17. Hasan RAA (2016) Behavior of beam and wall outrigger in high -rise building and their comparison. Int J Civil Struct Environ Infrastruct Eng Res Dev 19–30
18. Thejaswini RM, Rashmi AR (2015) Analysis and comparison of different lateral load resisting structural forms. Int J Eng Res V4
19. Haghollahi A, Ferdous MB, Kasiri M (2012) Optimization of outrigger locations in steel tall buildings subjected to earthquake loads. in: Proceedings of 15th world conferences on earthquake engineering, lisboa
20. Kamath K, Rao A (2012) A study on static and dynamic behavior of outrigger structural system for tall buildings. Bonfring Int J Ind Eng Manag Sci 2:15–20
21. Kogilgeri SS, Shanthapriya B (2015) A study on behaviour of outrigger system on high rise steel structure by varying outrigger depth. Int J Res Eng Technol 04:434–438
22. British European Standard, London, UK (2001) BS EN 1991–1.1–2001: actions on structures
23. British European Standard, London, UK (2005) BS EN 1991–1.4–2005: wind actions
24. British European Standard, London, U.K. (2002). BS EN 1990:2002: basis of structural design
25. Daril J, Kumar S (2016) Comparison of seismic performance of outrigger and belt truss system in a RCC building with vertical irregularity. Int J Res Eng Technol 05:125–132
26. Shivacharan K, Chandrakala S, Karthik NM (2015) Optimum position of outrigger system for tall vertical irregularity structures. IOSR J Mech Civ Eng (IOSR-JMCE) 12:54–63

Quantification of Degree of Irregularity in Mass Irregular RC Buildings Using Irregularity Index Based on Dynamic Characteristics

H. M. S. C. Rathnasiri, J. A. S. C. Jayasinghe, and C. S. Bandara

Abstract Mass irregular buildings are more vulnerable to seismic loading depending on their degree of irregularity. Therefore, design codes/standards prescribed different irregularity limits to identify the mass irregular buildings. However, design codes/standards are incapable of quantifying the degree of mass irregularity based on its elevation in the building. Furthermore, no effort was made in the past literature to quantify the degree of mass irregularity based on the elevation of the building. Therefore, the present study tried to quantify the degree of mass irregularity in reinforced concrete (RC) buildings based on elevation using a proposed Irregularity Index (μ). Furthermore, a comparison of the degree of mass irregularity was evaluated using the existing irregularity indices which are defined to quantify the geometric irregularities by the past literature. All the selected mass irregular RC buildings are numerically modeled using SAP2000 and modal analysis is performed to compute the degree of mass irregularity using the proposed Irregularity Index (μ). It has been found that the proposed Irregularity Index (μ) can well quantify the degree of mass irregularity depending on its elevation in RC buildings. Furthermore, the comparison of the existing irregularity indices shows that Irregularity Index (λ) proposed by Varadharajan et al. can also be used to quantify the degree of mass irregularity in RC buildings though it has been initially defined for the quantification of the geometric irregularities. The Irregularity Index (μ) can help to identify the different degrees of mass irregularity based on its elevation. Furthermore, it also aids in understanding the seismic vulnerability of mass irregular RC buildings and developing a correlation to study the seismic vulnerability with the degree of mass irregularity.

Keywords Irregularity index · Mass irregularity · Modal analysis · RC buildings

H. M. S. C. Rathnasiri (✉) · J. A. S. C. Jayasinghe · C. S. Bandara
University of Peradeniya, Peradeniya, Sri Lanka
e-mail: saharshac@gmail.com

© The Author(s), under exclusive license to Springer Nature Singapore Pte Ltd. 2023

R. Dissanayake et al. (eds.), *ICSBE 2022*, Lecture Notes in Civil Engineering 362,
https://doi.org/10.1007/978-981-99-3471-3_47

1 Introduction

The demand for housing and infrastructure has grown exponentially over the last decade as people have moved from rural to urban areas in search of better job opportunities, health care, educational institutions, lifestyle options, etc. As a result, cities face challenges in providing affordable housing, water sanitation, transportation, and urban infrastructure services to all their residents. Vertical construction was one of the sustainable innovations in the nineteenth century to overcome these challenges due to the limitation and the cost of land in urban cityscapes [2]. As a result, many city managers and policymakers have turned to multi-story building construction as a means of achieving sustainable urban development [1].

Most multi-story buildings built in the early stages have a regular configuration in both horizontal and vertical planes. However, due to architectural and aesthetic requirements, multi-story buildings are becoming irregular in both horizontal and vertical planes. Therefore, [3] defines two types of structural irregularities that can be encountered in multi-story buildings, namely Plan (horizontal) irregularity and vertical irregularity. The structural irregularities are due to the non-uniform distribution of mass, stiffness, and strength in the horizontal and/or vertical planes of the building [21].

Mass irregularity is a type of vertical irregularity that occurs due to the abrupt changes in the effective mass of any story compared to the adjacent stories. Figure 1 shows a schematic representation of mass irregularity in multi-storied buildings.

The performance of the irregular buildings under earthquake loads depends on the vertical and plan structural irregularities that are recognized as the major causes of failures during a seismic event [15]. Therefore, most of the past researchers studied the structural performance of mass irregular buildings under seismic loading based on different structural configurations, different elevations, and the intensities of the mass irregularity [10, 14-17, 21, 23]. However, no effort has been made in the past literature to quantify the degree of irregularity in mass-irregular buildings. Therefore, the present study aimed to quantify the degree of irregularity in mass-irregular reinforced

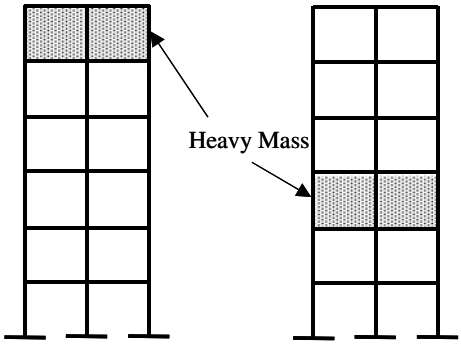

Fig. 1 Mass irregularity in multi-storied buildings

concrete (RC) buildings with mass irregularity at the lower, middle, and upper elevations in the building using a proposed irregularity index. Furthermore, the present study compares the degree of mass irregularity evaluated using the existing irregularity indices which are defined to quantify the geometric irregularities by the past literature. Buildings with specific stories that are allocated for parking spaces, retail shops, swimming pools, etc. make significant changes in the floor mass compared to the adjacent floors. These conditions cause mass irregularities over the height of the buildings. The present study helps to evaluate the degree of irregularity in mass-irregular RC buildings and studies the variation of the degree of mass irregularity based on the elevation of the mass irregularity in the building. Furthermore, quantification of the degree of irregularity can be used to develop the correlation with the seismic vulnerability to study the seismic vulnerability with the degree of mass irregularity of the building.

This paper is organized into five sections. Section 1 provides an overview of the present study and Sect. 2 describes the mass irregularity limits prescribed by the design codes/standards, existing irregularity indices proposed in past literature, and the development of a proposed irregularity index to quantify the degree of mass irregularity. Section 3 describes the numerical modeling of the selected mass-irregular RC buildings with different degrees of mass irregularity. Section 4 describes the computed degree of mass irregularity using the proposed irregularity index and a comparison of the degree of irregularity using the existing irregularity indices. Section 5 draws the conclusions and the future directions of the present study.

2 Quantification of Mass Irregularity

Design codes/standards prescribed different irregularity limits to identify the mass irregularity as shown in Table 1. However, the irregularity limits proposed by the design codes/standards cannot identify the degree of irregularity in mass irregular buildings.

Due to the limitations associated with the irregularity limits prescribed in design codes/standards, past researchers developed irregularity indices to quantify the degree of irregularity in buildings with vertical geometric irregularities. Table 2 summarizes existing irregularity indices defined in the literature for buildings with vertical geometric irregularities.

However, previous research has not attempted to define irregularity indices to quantify the degree of irregularity in mass irregular buildings. Therefore, the present study defines a proposed Irregularity Index (μ) to quantify the degree of irregularity in mass irregular RC buildings with mass irregularity at the lower, middle, and upper elevations in the building. The Irregularity Index (μ) is defined as the ratio of the maximum displacement of the mass irregular RC building in the fundamental mode to that of a reference regular RC building as given in Eq. (1). The Irregularity Index (μ) value of unity represents a building without any mass irregularities and higher or lower values represent the mass irregular RC buildings compared to the

Table 1 Mass irregularity limits prescribed by design codes

Design code	Irregularity limit
Bangladesh	Mass irregularity shall be considered to exist where the effective mass of any story is more than 150% of the effective mass of an adjacent story. A roof that is lighter than the floor below need not be considered [5]
Iran	The distribution of mass over the height of the building shall be approximately uniform such that the mass of no story, except the roof and loft differ more than 50% from the mass of the story located below [11]
America	Weight (mass) irregularity is defined to exist where the effective mass of any story is more than 150% of the effective mass of an adjacent story. A roof that is lighter than the floor below need not be considered [3]
India	Mass irregularity shall be considered to exist where the seismic weight of any story is more than 200% of that of its adjacent stories. The irregularity need not be considered in the case of roofs [12]
Eurocode	Both the lateral stiffness and the mass of the individual stories shall remain constant or reduce gradually, without abrupt changes, from the base to the top of a particular building [9, 18]
New Zealand	**Severe**: Mass of any story <0.7 of mass of adjoining story. **Significant**: Mass of any story <0.9 of mass of adjoining story. **Insignificant**: Mass of any story ≥0.9 of mass of adjoining story [18]

Table 2 Existing irregularity indices proposed by past literature

References	Frame type	Index equation
Karavasilis et al. [13]	Steel moment resisting frames (MRF) with setback	$\varphi_s = \frac{1}{n_s-1}\sum_{1}^{n_s-1}\frac{L_i}{L_i+1}$ $\varphi_b = \frac{1}{n_b-1}\sum_{1}^{n_b-1}\frac{H_i}{H_i+1}$
Roy and Mahato [20]	RC setback MRF	$\varphi_{avg} = \frac{\varphi_s+\varphi_b}{2}$
Sarkar et al. [22]	RC stepped MRF	$\eta = \frac{\Gamma_1}{\Gamma_{1,ref}}$
Varadharajan et al. [24]	RC MRF with setbacks	$\lambda_r = \sum_{1}^{k}\frac{\omega_{ir}}{\omega_r}$
Bhosale et al. [4]	Vertically irregular RC MRF	$\Gamma_i = \frac{\overline{L_i}}{\widehat{m_{ii}}}$ $m_{eff,i} = \frac{(\overline{L_i})^2}{\widehat{m_{ii}}}$
Rathnasiri et al. [19]	Vertically irregular RC MRF	$\psi = \frac{V_{f,\text{regular}}}{V_{f,\text{irregular}}}$

Note n_s is the number of stories; n_b is the number of bays; L_i is bay width; H_i is story height; Γ_1 is the 1st mode participation factor of the stepped frame and $\Gamma_{1,\text{ref}}$ is the 1st mode participation factor for a similar regular frame; ω_{ir} and ω_r are the modal combinations of the frequency of vibration of the irregular and regular building frames from 1st mode to k^{th} mode; $\overline{L_i}$ is the coefficient vector, $\widehat{m_{ii}}$ is the generalized mass matrix; $V_{f,\text{ irregular}}$ is the fundamental mode base shear of the irregular frame, and $V_{f,\text{ regular}}$ is the fundamental mode base shear of a similar regular frame without any irregularities

reference regular building. The reference Regular RC building should consist of the same bay lengths in both X and Y directions, story heights, and the number of stories similar to the plan irregular RC building. The maximum displacement of the fundamental mode is computed for both the irregular and regular RC buildings by performing the modal analysis. The distribution of mass and stiffness in the building determines the maximum displacement of the fundamental mode. Therefore, the proposed Irregularity Index (μ) can account for the degree of irregularity in mass irregular RC buildings with mass irregularity at different elevations in the building.

$$\text{Irregularity Index}(\mu) = \frac{D_{\text{regular}}}{D_{\text{irregular}}} \tag{1}$$

3 Numerical Modeling of Mass Irregular RC Buildings

Mass irregularity is defined to exist where the effective mass of any story is more than 150% of the effective mass of an adjacent story [3]. Therefore, the present study selected single, dual, and triple mass floor RC buildings with mass irregularity at the lower, middle, and upper elevations in the building as shown in Table 3. The effective mass of the mass irregular floor is 200% in the effective mass compared to the adjacent stories in all the selected mass irregular RC buildings.

In the present study, the reference regular RC building is a ten-story building having a story height of 3.0 m and a length of each bay (X and Y directions) of 4 m. The number of bays was taken as 4 in each direction. Live and dead loads are 3.0 kN/m^2 and 2.0 kN/m^2 respectively for all the floors. The beam and column dimensions were taken as 300 mm × 400 mm and 400 mm × 400 mm, respectively. G25 grade concrete having characteristic cylinder strength of 25 MPa is considered for all the structural elements. Further design details of the reference regular RC building can be found in past literature, Satheesh et al. [23]. Mass irregular RC buildings are derived from the reference regular building by introducing mass irregular floors at the lower, middle, and higher elevations in the building as shown in Table 3.

4 Results and Discussion

Table 4 shows the computed degree of mass irregularity for selected mass-irregular RC buildings using the proposed Irregularity Index (μ).

According to Table 4, the Irregularity Index (μ) increases with the elevation of the mass irregular floor. This variation is valid for dual and triple mass floor RC irregular buildings as well. Furthermore, it is noted that the Irregularity Index (μ) increases when comparing the single, dual, and triple mass floor RC buildings with mass irregularity at the same elevation in the building. Therefore, the proposed

Table 3 Selected mass-irregular RC buildings with mass irregularity at different elevations of the building

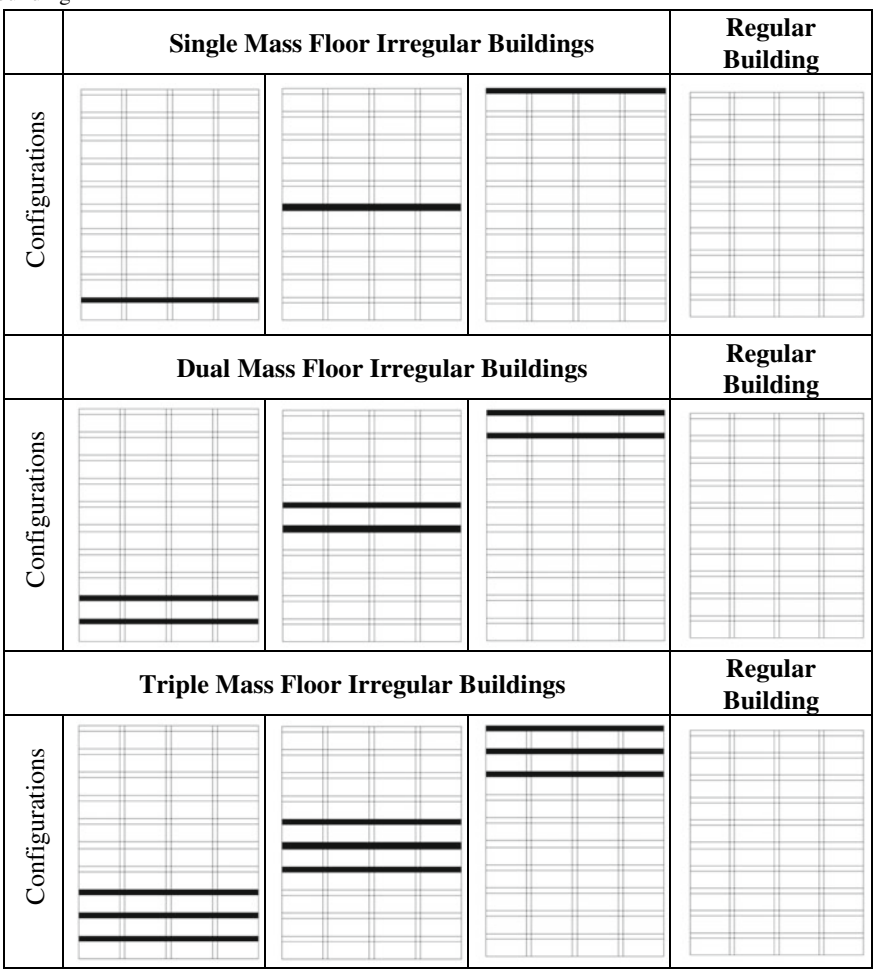

Irregularity Index (μ) can well quantify the different degrees of mass irregular RC buildings based on the number of mass irregular floors and their elevation in the RC buildings.

The present study investigates the applicability of the existing irregularity indices proposed by past literature to quantify the degree of mass irregularity. Table 5 shows a comparison of the evaluated degree of mass irregularity using the existing irregularity indices.

According to the Irregularity Index (ψ) proposed by [19], the degree of irregularity increases with the elevation of the mass irregular floors in triple mass floor irregular RC buildings. However, this variation is not observed for the single- and dual-mass

Table 4 Degree of mass irregularity evaluated by proposed Irregularity Index (μ)

Single Mass Floor Irregular RC Buildings				**Regular**
Fundamental Mode Shape	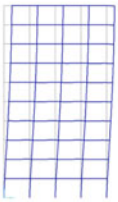	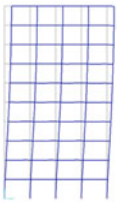	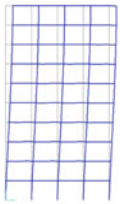	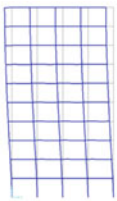
D (mm)	24.85	23.85	23.65	24.85
(μ)	**1.000**	**1.042**	**1.051**	**1.00**
Dual Mass Floor Irregular RC Buildings				**Regular**
Fundamental Mode Shape	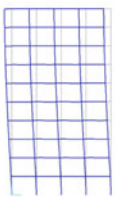	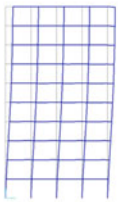	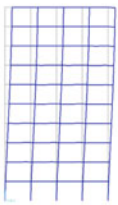	
D (mm)	24.68	22.67	22.37	24.85
(μ)	**1.007**	**1.096**	**1.111**	**1.00**
Triple Mass Floor Irregular RC Buildings				**Regular**
Configuration	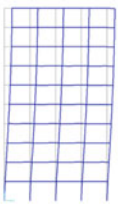	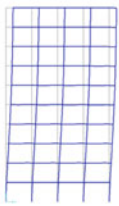	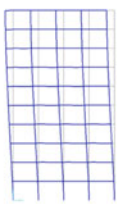	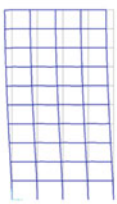
D (mm)	24.27	22.0	21.27	24.85
(μ)	**1.024**	**1.130**	**1.168**	**1.00**

Table 5 Degree of mass irregularity by the existing irregularity indices proposed by past literature

Single mass floor irregular RC buildings					Regular
Fundamental mode shape		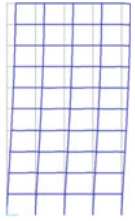	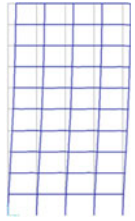	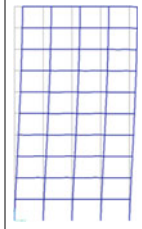	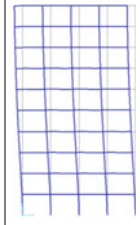
Rathnasiri et al. [19]	V_f kN	660	606	681	741
	(ψ)	**1.12**	**1.22**	**1.09**	**1.00**
Sarkar et al. [22]	Γ_1 kN m	44.1	43.0	52.8	49.5
	(η)	**1.12**	**1.15**	**0.94**	**1.00**
Varadharajan et al. [24]	$\sum_k^1 \omega$	116.2	111.6	108	116.6
	(λ)	**1.00**	**1.04**	**1.08**	**1.00**

(continued)

Table 5 (continued)

Single mass floor irregular RC buildings					Regular
Dual mass floor irregular RC buildings					*Regular*
Fundamental mode shape		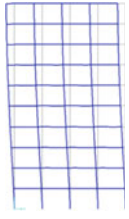	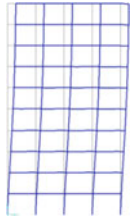	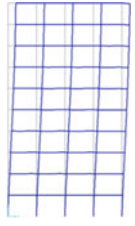	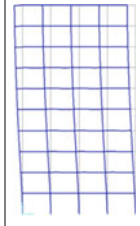
Rathnasiri et al. [19]	V_f (kN)	763	549	635	741
	(ψ)	**0.97**	**1.35**	**1.17**	**1.00**
Sarkar et al. [22]	Γ_1 kN-m	51.4	42.4	55.6	49.5
	(η)	**1.04**	**0.86**	**1.12**	**1.00**
Varadharajan et al. [24]	$\sum_k^1 \omega$	113.2	108	103	116.6
	(λ)	**0.97**	**0.93**	**0.88**	**1.00**

(continued)

Table 5 (continued)

Single mass floor irregular RC buildings					Regular
Triple mass floor irregular RC buildings					*Regular*
Fundamental mode shape		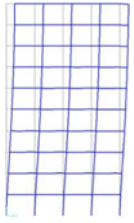	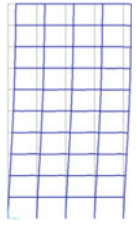	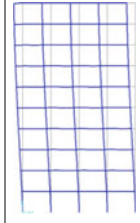	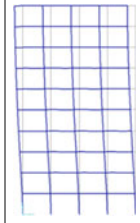
Rathnasiri et al. [19]	V_f (kN)	681	618	595	741
	(ψ)	**1.09**	**1.20**	**1.25**	**1.00**
Sarkar et al. [22]	Γ_1 kN-m	46.9	49.5	57.5	49.5
	(η)	**0.95**	**1.00**	**1.16**	**1.00**
Varadharajan et al. [24]	$\sum_k^1 \omega$	108.6	104.0	100	116.6
	(λ)	**0.93**	**0.89**	**0.86**	**1.00**

floor irregular RC buildings. Therefore, it can be noted that Irregularity Index (ψ) proposed by Rathnasiri et al. [19] cannot well quantify the mass irregularity based on its elevation in the RC buildings.

The degree of irregularity increases with the elevation of the mass irregular floors of the triple mass floor irregular RC buildings, according to the Irregularity Index (η) proposed by [22]. However, this variation is not the same for the single- and dual-mass floor irregular RC buildings shown in Table 5. As a result, the Irregularity Index (η) proposed by Sarkar et al. [22] cannot adequately quantify mass irregularity based on its elevation in the building.

According to the Irregularity Index (λ) proposed by Varadharajan et al. [24], the degree of irregularity increases with the elevation of the mass irregular floors in all the single, dual, and triple mass floor irregular RC buildings. Furthermore, Irregularity Index (λ) decreases with the increasing number of mass irregular floors at the same elevation in the RC building. Therefore, Irregularity Index (λ) proposed by Varadharajan et al. [24] can well quantify the mass irregularity based on its elevation in the RC building.

Varadharajan et al. [24] defined the Irregularity Index (λ) by considering the participation of higher modes to quantify the degree of irregularity in RC buildings with setback irregularity. Therefore, the contribution of the higher modes is incorporated with the Irregularity Index (λ) compared to the irregularity indices proposed by Rathnasiri et al. [19] and Sarkar et al. [22]. The contribution of the higher modes in irregular buildings compared to regular buildings has been confirmed by many past researchers also [4, 6-8, 22]. Therefore, in comparison to the irregularity indices proposed by Rathnasiri et al. [19] and Sarkar et al. [22], the Irregularity Index (λ) proposed by Varadharajan et al. [24] can well quantify the degree of mass irregularity based on the elevation of the mass irregularity in the RC buildings.

5 Conclusions and Future Directions

The structural performance of the mass irregular RC buildings depends on their degree of irregularity. Therefore, the present study made an effort to quantify the degree of irregularity in mass-irregular RC buildings using a proposed irregularity index and existing irregularity indices defined by the past literature.

It has been found that both the proposed Irregularity Index (μ) and Irregularity Index (λ) proposed by Varadharajan et al. [24] can well quantify the degree of irregularity in the mass irregular RC buildings with the mass irregularity at different elevations of the building. Investigation of the irregularity indices proposed by Rathnasiri et al. [19] and Sarkar et al. [22] on the quantification of the degree of mass irregularity shows that such indices cannot be used to quantify the degree of mass irregularity. Since Varadharajan et al. [24] considered the participation of the higher modes in defining the Irregularity Index (λ), it can well quantify the degree of mass irregularity compared to the irregularity.

The present study contributes to evaluating the degree of irregularity in mass-irregular RC buildings. Quantification of the degree of irregularity can be used to develop a correlation with the seismic vulnerability to study the seismic vulnerability of the building with the degree of mass irregularity. The present study can be further extended to study the variation of the degree of mass irregularity with different mass intensities in mass-irregular RC buildings.

References

1. Agyemang FSK, Silva E, Anokye PA (2018) Towards sustainable urban development: the social acceptability of high-rise buildings in a Ghanaian city. GeoJournal 83(6):1317–1329. https://doi.org/10.1007/s10708-017-9837-0
2. Ali MM (2010) Sustainable urban life in skyscraper cities of the 21st century. In: Proceedings of the sustainable city 2010; Brebbia CA, Hernandez S, Tiezzi (eds) WIT Trans Ecol Environ 203–214
3. ASCE/SEI 7-10:2013. Minimum design loads for buildings and other structures, Reston, USA
4. Bhosale AS, Davis R, Sarkar P (2017) Vertical irregularity of buildings: regularity index versus seismic risk. ASCE-ASME J Risk Uncertain Eng Syst Part A: Civil Eng 3(3):04017001-1–04017001-10. https://doi.org/10.1061/AJRUA6.0000900.
5. BNBC (2015) Bangladesh National Building Code, Dhaka. Housing and Building Research Institute (HBRI), Bangladesh
6. Bohlouli Z, Poursha M (2016) Seismic evaluation of geometrically irregular steel moment resisting frames with setbacks considering their dynamic characteristics. Bull Earthq Eng 14(10):2757–2777. https://doi.org/10.1007/s10518-016-9910-y
7. Di Sarno L, Chioccarelli E, Cosenza E (2011) Seismic response analysis of an irregular base-isolated building. Bull Earthq Eng 9(5):1673–1702. https://doi.org/10.1007/s10518-011-9267-1
8. Dutta SC, Das PK, Sengupta P (2017) Seismic behaviour of irregular structures. Struct Eng Int 27(4):526–545. https://doi.org/10.2749/222137917X14881938989765
9. EN1998-1:2004. Eurocode 8: Design of structures for earthquake resistance, Part-1: General rules, seismic actions and rules for buildings. European Committee for Standardization, Brussels, Belgium
10. Georgoussis G, Tsompanos A, Makarios T (2015) Approximate seismic analysis of multi-story buildings with mass and stiffness irregularities. Procedia Eng 125:959–966. https://doi.org/10.1016/j.proeng.2015.11.147
11. INBC:2007. Iranian code of practice for seismic resistant design of buildings (Standard No. 2800), Tehran. Building and Housing Research Center (BHRC), Iran
12. IS 1893-Part 1:2016. Criteria for earthquake resistant design of structures: Part 1 general provisions and buildings. Government of India, Ministry of Earth Sciences, New Delhi, India
13. Karavasilis TL, Bazeos N, Beskos DE (2008) Seismic response of plane steel MRF with setbacks: estimation of inelastic deformation demands. J Constr Steel Res 64(6):644–654. https://doi.org/10.1016/j.jcsr.2007.12.002
14. Manoukas GE (2019) Evaluation of pushover methodology for mass-irregular in elevation RC buildings. J Struct Eng 145(8). https://doi.org/10.1061/(ASCE)ST.1943-541X.0002360
15. Naveen E, S., N. M. Abraham, AK S D (2019) Analysis of irregular structures under earthquake loads. Procedia Struct Integr 14:806–819. https://doi.org/10.1016/j.prostr.2019.07.059
16. Nezhad ME, Poursha M (2015) Seismic evaluation of vertically irregular building frames with stiffness, strength, combined-stiffness-and-strength, and mass irregularities. Earthq Struct 9(2):353–373. https://doi.org/10.12989/eas.2015.9.2.353

17. Ningthoukhongjam SS, Singh KD (2021) Mass irregularity effect on seismic response of moment-resisting steel frame by nonlinear time history analysis using force analogy method. Struct Des Tall Spec Build 30(2). https://doi.org/10.1002/tal.1823
18. NZS 1170-5:2004 Structural design actions—Part 5: earthquake actions. Standards New Zealand, Wellington
19. Rathnasiri H, Jayasinghe J, Bandara C (2020) Development of irregularity index based on dynamic characteristics to quantify the vertical geometric irregularities. Engineer LIII(01):41–51. https://doi.org/10.4038/engineer.v53i1.7398
20. Roy R, Mahato S (2013) Equivalent lateral force method for buildings with a setback: adequacy in the elastic range. Earthq Struct 4(6):685–710. https://doi.org/10.12989/eas.2013.4.6.685
21. Sadashiva VK, MacRae GA, Deam BL (2009) Determination of structural irregularity limits—Mass irregularity example. Bull N Z Soc Earthq Eng 42(4):288–301
22. Sarkar P, Prasad AM, Menon D (2010) Vertical geometric irregularity in stepped building frames. Eng Struct 32(8):2175–2182. https://doi.org/10.1016/j.engstruct.2010.03.020
23. Satheesh AJ, Jayalekshmi BR, Venkataramana K (2019) Effect of in-plan eccentricity in vertically mass irregular RC framed buildings under seismic loads. Asian J Civ Eng 20(5):713–726. https://doi.org/10.1007/s42107-019-00138-w
24. Varadharajan S, Sehgal VK, Saini B (2013) Seismic behaviour of multistorey RC building frames with vertical setback irregularity. Struct Des Tall Spec Build 23(18):1345–1380. https://doi.org/10.1002/tal.1147

Effects of Spandrel Heights on Leapfrog Effect in Tall Buildings

R. A. D. M. Kahatapitiya, T. A. Reckerman, T. G. P. L. Weerasinghe, I. R. A. Weerasekera, W. J. B. S. Fernando, and P. Mendis

Abstract Along with the increasing number of tall buildings, more attention is paid to the façade which has a significant influence on the aesthetic appearance of the building. Therefore, architects are strict in their design to create a unique building. Façade fire is a disastrous hazard that can spread rapidly throughout the building. Leapfrog is a type of fire spread that occurs due to excessive heat from flames projecting from the lower floor to the floor above. Code provisions are available to control leapfrog by changing spandrel heights, but in some cases, it is not feasible due to architectural requirements. A performance-based method was used to study the vertical fire spread issues due to leapfrog using a numerical model. Results have shown that limited ventilation with proper compartmentation under the automatic active fire protection provides considerable fire safety avoiding flames ejecting from the broken glass or glasses in glass curtainwall facades.

Keywords Spandrel · Passive fire protection · Active fire protection · Façade · Performance-based design

1 Introduction

The world's economic development has been influenced by the increasing number of tall buildings and their heights [1, 2]. The growth of population, expansion of technology, scarcity of lands in urban areas, and their prices also contributed to these changes. The land cost can be recovered by increasing the rentable area. The way it

R. A. D. M. Kahatapitiya (✉) · T. A. Reckerman · W. J. B. S. Fernando
Civil and Structural Engineering Consultants (Pvt.) Ltd., Colombo, Sri Lanka
e-mail: dilan.cseci@gmail.com; radmkahatapitiya@gmail.com

T. G. P. L. Weerasinghe · I. R. A. Weerasekera
University of Moratuwa, Katubedda, Moratuwa, Sri Lanka

P. Mendis
University of Melbourne, Melbourne, Australia

© The Author(s), under exclusive license to Springer Nature Singapore Pte Ltd. 2023

R. Dissanayake et al. (eds.), *ICSBE 2022*, Lecture Notes in Civil Engineering 362,
https://doi.org/10.1007/978-981-99-3471-3_48

can be done is by multiplying workspaces vertically to create more rentable spaces. Therefore, an increased number of taller buildings can be expected in the future.

The aesthetic appearance of tall buildings has changed over time [3, 4], and the present architects put more effort into embodying more powerful ideas to develop a unique building design [5]. The nature of the building exterior has more influence on the aesthetic of the building. Thus, architects tend to be more creative concerning the exterior appearance of buildings. The facade is one of the key architectural features of tall buildings that allow architects to showcase their creativity to the world. The facade is an outer envelope of the building, and it is the first feature that decides the building's appearance. The state of the art of tall buildings has been changed with the development of the new material used in the building facade. There are several types of facades used in modern buildings, and the curtain wall facade is most popular among tall buildings, including most of the super tall buildings [6] around the world.

When the height of the building becomes more, lighter materials are used [1]. Due to their slenderness, tall buildings are vulnerable to wind-induced acceleration. Thus, facades are designed to cater to the wind effect [7]. Apart from that, facades are designed considering the thermal comfort and energy consumption of the building [8]. Due to the above-mentioned reasons, most of the building facades are constructed with extensive use of combustible materials and facade geometries without paying much attention to the fire protection of the building [9].

Facade fire can be a disastrous hazard to occupants, building properties, environment, etc. [10]. Fire needs to originate in the façade, or fire needs to get in contact with the facade to cause a facade fire. Once the combustible facades catch fire, limiting its spread becomes harder, and firefighters must put considerable effort into controlling the fire. The most preferred options are to design to minimize fire occurrence. If it can't be achieved, the spreading of the fire along the facades must be limited.

When there is a facade fire, there are several paths it can spread [11]. The vertical fire spread through voids in the facade can be minimized by providing fire barriers as specified in codes. Leapfrog is another critical case where external fire spread can occur in tall buildings. It is a window-to-window mechanism that happens due to excessive heat from flames projected from the lower floor to the floor above. To prevent leapfrog, international building code provisions such as openings shall be separated vertically not less than 914 mm by spandrel girders or by flame barriers that extend horizontally not less than 762 mm can be applied [12] .

The problem is critical as façade fire could occur at the exterior face of the façade, even in façades made with fire-resistant material [13]. In glass curtain wall facades, non-combustibility limits the fire spread along the surface of the facade, fire barriers limit fire spread along the voids, and leapfrog can be controlled by applying code provisions. However, in some cases, code-specified spandrel heights cannot be practically used in the facade due to architectural aspects.

Thus, solutions for this kind of problem have minimal information in the literature. Therefore, the performance-based method was used to provide a solution for this problem regarding curtain wall façades in tall buildings. Based on the fire behaviour of a room, the applicability of using spandrel heights less than the code provisions

were discussed. To save the cost and time of a fire test, a numerical model was used to carry out this study.

2 Methodology

A glass curtain wall facade was selected to study the vertical fire spread issues. The relationship between the spandrel heights of curtain wall facades and the leapfrog effect was studied. Since spandrel heights cannot be changed, possible fire scenarios that can occur inside the building and fire spread under the different ventilation conditions were studied first. A numerical simulation was carried out instead of performing experiments considering practicality, cost, and time. Active and passive fire safety precautions used in the building were counted during the study to predict conditions like actual building conditions. Then the observed results were used to predict the fire severity and fire spread inside the selected compartment. Passive fire safety precautions used in the building were taken into account when selecting the compartment for this study.

2.1 Selection of the Compartment

During the selection of the compartment, the presence of a curtain wall was considered a mandatory requirement. Passive fire protection details used in the site were considered to determine the area of the building in the numerical model, as shown in Figs. 1 and 2.

A bedroom which is located at the edge of the building was selected, based on the details given in the above figures. The idealized dimensions of the selected bedroom were determined by referring to the architectural drawings. The selected length ×

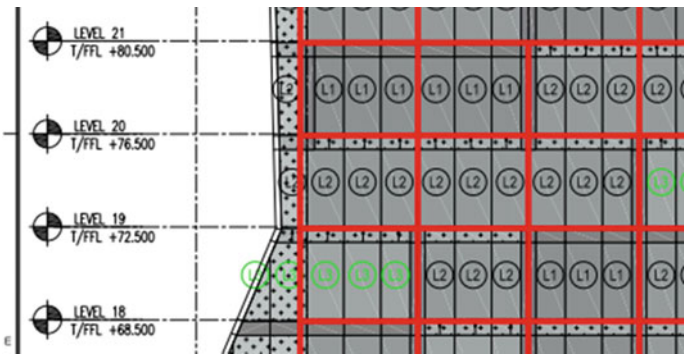

Fig. 1 Fire resistance setting out (vertical and horizontal) used in the building

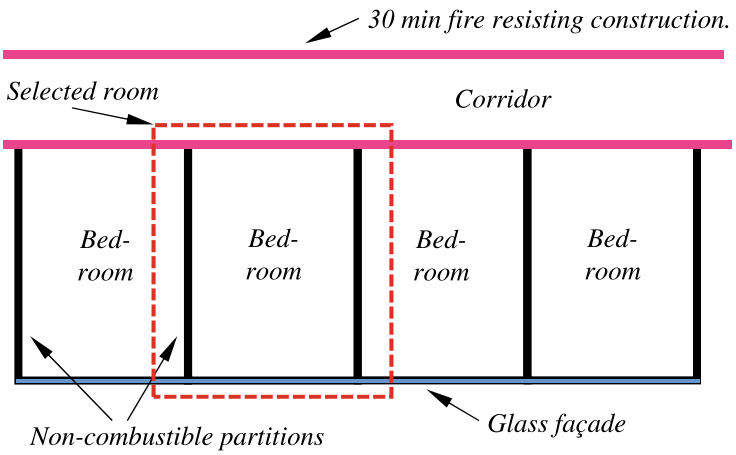

Fig. 2 A sketch of a typical floor plan of the building

width × floor-to-floor height were 6.4 m × 4.5 m × 4 m, respectively, with the ceiling at 3 m from the finished floor level of the room. Other than the dimensions of the compartment, available fuels placed in the room are essential when performing fire modelling. Thus, fuel load in the room was used in the model as given in Fig. 3.

The PyroSim software (version 2021.1.0224) was used to develop 3D numerical models to perform the fire simulation. Considerable care was taken during defining computational meshes to control, considering computational time and the accuracy of the results. Thus, parallel meshes were defined to reduce the computational time based on the capacity of the computer. To achieve optimal accuracy of the results, the size of a primary unit of a mesh was selected through a mesh sensitivity study.

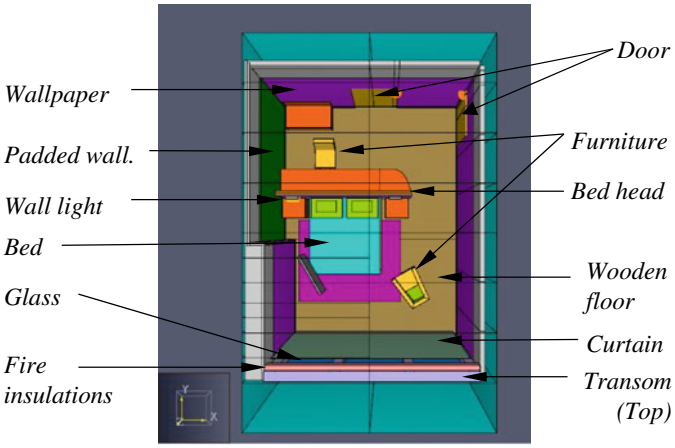

Fig. 3 3D model view from the top (the ceiling is hidden)

Therefore, the dimensions of the cell were selected as 100 mm × 100 mm × 100 mm. Thus, the model consisted of over 150,000 cells. All idealized objects selected to be considered in the model were generated as obstructions, as shown in Figs. 3 and 4. Then the relevant material data were assigned. A summary of the fuels used in the model is given in Table 1.

The bedroom has two doors, and these were considered a source of ventilation to the room. The other source considered was ventilation due to the breakage of glasses at the facade. Therefore, the breaking temperature of the used glass was predicted based on the layers used in the glass site material data as given in Table 2.

Limited ventilation was considered as far as closed doors are concerned while allowing some air leakage through the door gaps [27]. An automatically activating fire suppression system was considered in the model enabling sprinklers to trigger when it reaches the activation temperature. Locations of the sprinklers were based on the fire detection and alarm system drawings. Sprinkler details used in the model are given in Table 3 and Fig. 5.

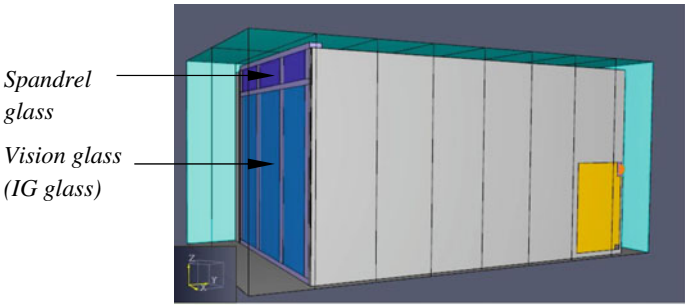

Fig. 4 3D model view from the side

Table 1 Fuels used in the numerical model

Material		Density (kg/m^3)	Specific heat (kJ/kg K)	Conductivity (W/m K)	Ignition temperature (^{o}C)	References
Polyurethane foam		23	1	0.05	190	[14, 15]
Wood	Birch	670	1.96	0.175889	511	[16]
	Eucalyptus	828.1	1.96	0.212995	285	[17]
	Oak	755	1.96	0.195839	450	[18]
	Walnut	680	1.96	0.178236	350	[4]
ABS (Acrylonitrile butadiene styrene)		1050	2.1208	0.18352	416	[20]
Polyester		275	2.01	0.29	360	[19, 21, 20]

Table 2 Glass breakage details

Material	Density (kg/m^3)	Specific heat (kJ/kgK)	Conductivity (W/mK)	Ignition temperature (°C)	References
Spandrel glass (composite panel)—12 mm	2317.917	0.8	0.0569 (minimum PVB layer)	450 (Breaking temperature)	[22, 23, 24]
Laminated glass (composite panel)—40 mm	1378.6	0.76	2.56E-4 (minimum Ar layer)	600 (Breaking temperature)	[22, 25, 26]

Table 3 Sprinkler details

Description	Detail
Sprinkler type	Pendant
Activation temperature	68.33 °C
Flow rate	49.05 L/min
Velocity	5 m/s
Injection duration	60 s

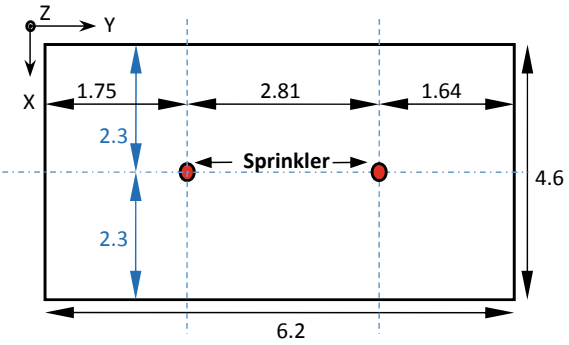

Fig. 5 Locations of the sprinklers in the room (all dimensions in meters)

2.2 Combustion Characteristics

Air in the model was modelled with 21% of Oxygen because only this gas is significant in combustion. The remaining 79% was Nitrogen gas (including other small fractions of gasses). A gas phase balanced equation was defined to govern the combustion in the software. An electric spark in a wall light was selected as the possible cause of the fire in the room to originate a fire. Afterward, the fire was allowed to spread on its own. A considerable number of temperature measuring devices were placed to record the temperature inside the room to extract at the end of the simulation.

2.3 Considered Cases

Two main factors affect fire growth after it breaks out. They are ventilation and fuel load inside the compartment. Thus, a total of eight cases were taken into account changing ventilation and the presence of sprinklers. The fuel load inside the room is constant. Thus, the fuel load was kept constant in all cases. The time to spread over the modern bedrooms is reduced to less than 15 min [28]. Therefore, 30 min was considered in all cases except in case 8, which was considered a real condition in general use. Details of the considered cases are given in Table 4.

3 Results and Discussion

Results generated from the model can be extracted as data sheets or 3D visualizations. Results from both methods are presented below. The fire spread and its severity can be observed clearly by 3D visualization, and the resulting temperature variation can be observed with the help of graphs developed from data sheets as discussed below.

Table 4 Considered cases and their details

Cases	Considered changes		Simulated time (min)
Case 1	Doors open	Without sprinklers	30
Case 2	Doors open	Without sprinklers	30
Case 3	Doors close	Without sprinklers	30
Case 4	Doors close	Without sprinklers	30
Case 5	Doors open	With sprinklers	30
Case 6	Doors open	With sprinklers	30
Case 7	Doors close	With sprinklers	30
Case 8 (Realistic)	Doors close	With sprinklers	120

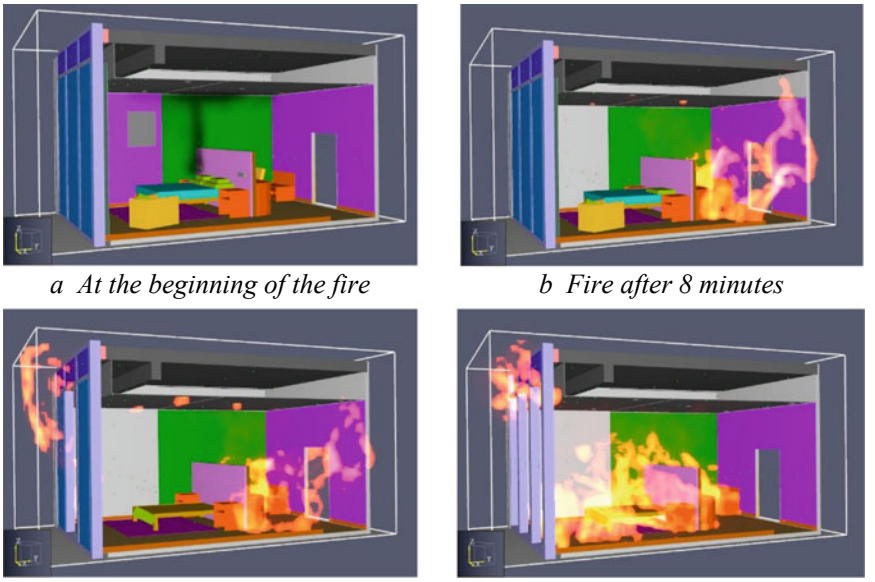

a At the beginning of the fire *b Fire after 8 minutes*

c Glass breakage after 10 minutes *d Well-developed fire after 11 minutes*

Fig. 6 Behaviour of the fire (doors-open case)

3.1 Doors-Open Case

Open doors supply unlimited Oxygen to the originated fire inside the room and enough fuel load is available in the room. Thus, this was a suitable situation for fire to advance into its well-developed stage, as shown in Fig. 6. The spread of fire throughout the room was observed and the temperature was measured. Locations of temperature measuring devices are given in Fig. 7.

Recorded temperatures are graphically illustrated in Fig. 8.

Therefore, all temperature reading devices recorded high-temperature values with the time indicating fire spread pattern throughout the room.

3.2 Doors-Closed Case

During closed-door situations, airflow between the room and outside the room becomes limited. The only possible way of air exchange was through the door gaps under the assumption of properly sealed boundaries. Therefore, not enough Oxygen remains inside the room to sustain the fire. Thus, a self-extinguished fire was observed as given in Fig. 9. Recorded temperatures are given in Fig. 10.

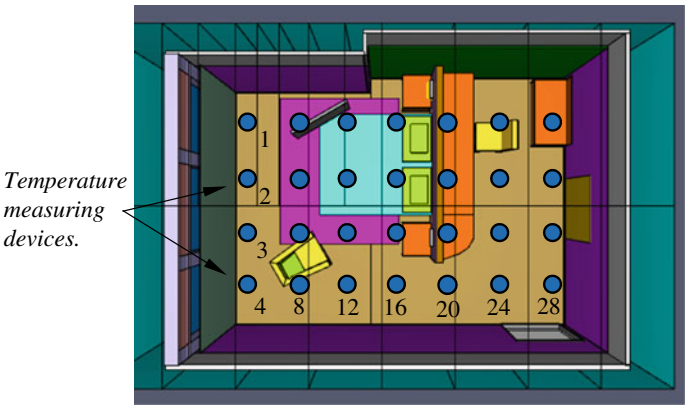

Fig. 7 Location of the temperature measuring devices

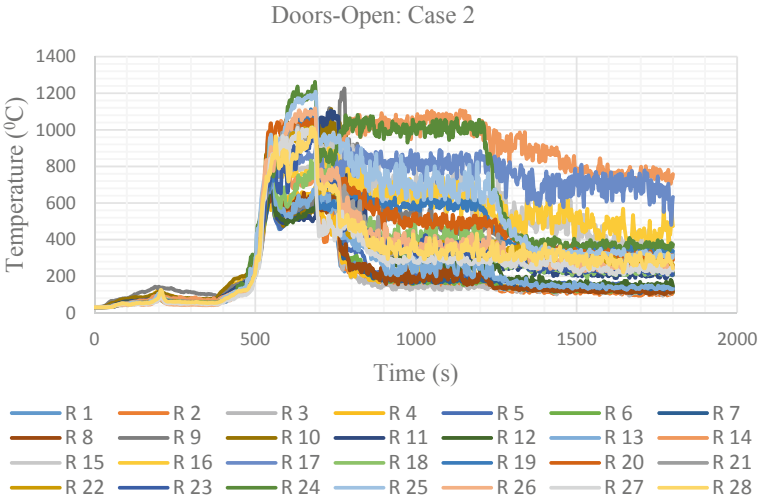

Fig. 8 Recorded temperatures inside the room (doors-open case)

As shown in Fig. 10, a temperature peak is recorded, indicating fire development up to some level, but a sudden drop-down following the temperature peak indicates the extinguishment of fire inside the room.

3.3 Sprinkler-Provided Cases

Recorded temperatures during the simulation are given in Figs. 11 and 12.

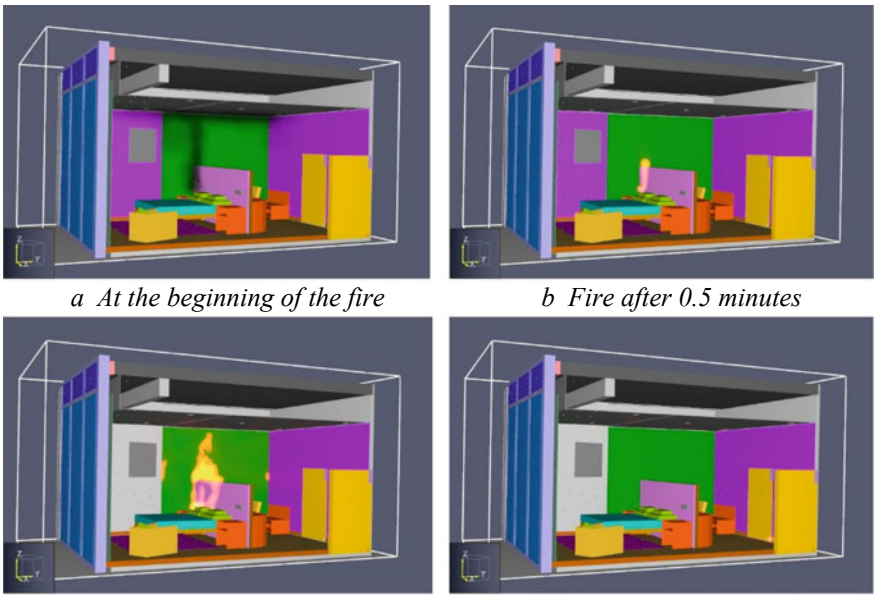

a At the beginning of the fire *b Fire after 0.5 minutes*

c Fire after 2 minutes *d Fire after 3 minutes*

Fig. 9 Behaviour of the fire (doors-closed case)

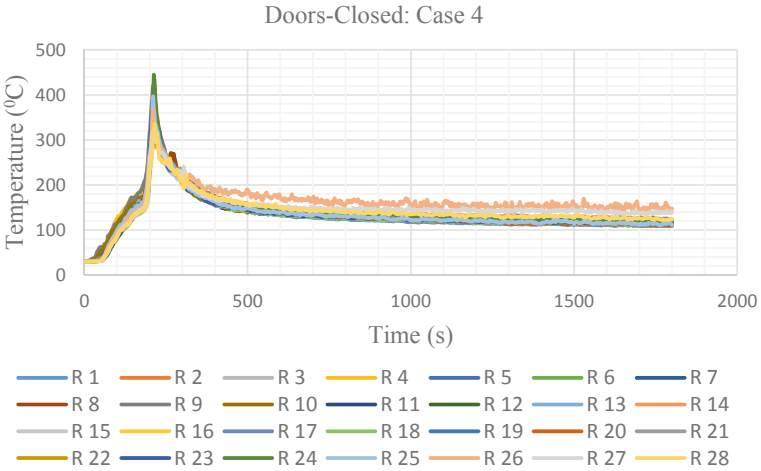

Fig. 10 Recorded temperatures inside the room (doors-closed case)

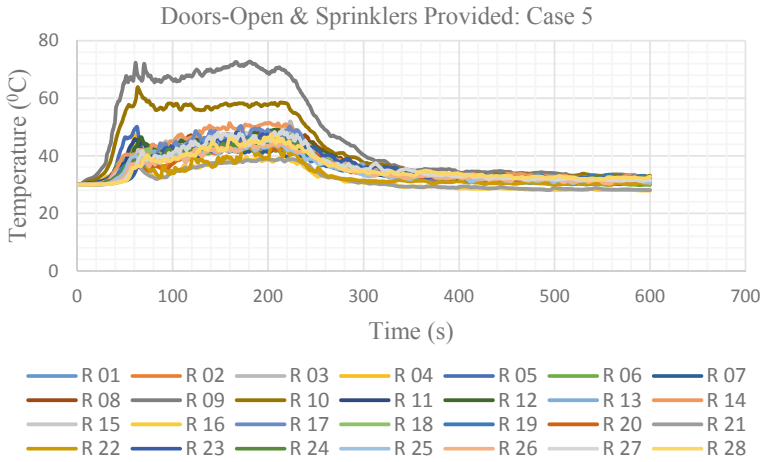

Fig. 11 Recorded temperatures inside the room (doors-open and sprinkler-provided case)

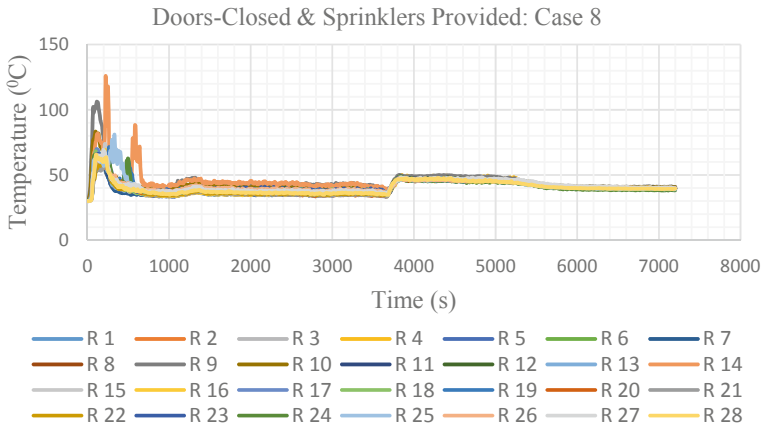

Fig. 12 Recorded temperatures inside the room (doors-closed and sprinkler-provided case)

According to the above graphs, whether doors are opened or closed, sprinklers can control the fire. As per the realistic case, a controlled fire was observed.

4 Conclusions

Results of the models indicated that ventilation plays a significant role in fire development inside the considered room. The fire did not sustain in cases where the doors were closed. Therefore, keeping doors closed is encouraged with the help of door

closers. Furthermore, the automatically activated fire protection system (sprinklers) effectively controlled the fire. Thus, considering the realistic case (doors closed and sprinklers provided), better fire safety can be achieved even though sprinklers are not working. Hence, the fire spread outside of the façade has a very low probability. Thus, based on the fire performance evaluated through the simulations, the leapfrog effect can be neglected. Hence, it is not an issue with the spandrel heights used in the building considered in this study. A future research study covering the spandrel heights effects on leapfrog in well-developed fire situations in buildings is recommended.

Acknowledgements This research was financially supported by Civil and Structural Engineering Consultants (CSEC). We wish to place on record Dr. Shyanaka Dananjaya and Eng. Arthur De Alwis for their keen interest shown throughout the project. Their sharing of resources is gratefully acknowledged and appreciated.

References

1. Ali MM, Moon KS (2007) Structural developments in tall buildings: current trends and future prospects. Archit Sci Rev 50(3):205–223. https://doi.org/10.3763/asre.2007.5027
2. Completions of tall building construction worldwide (2020) Statista. https://www.statista.com/statistics/1069001/number-of-tall-building-completions-worldwide/. Accessed 29 Oct 2022
3. Ali MM, Armstrong PJ (Eds) (1995) Architecture of tall buildings. McGraw-Hill Companies
4. Huxtable AL (June, 1984) The tall building artistically reconsidered: the search for a skyscraper style. Architect Rec (USA) 172(1)63–7, 69, 71, 73, 75, 77, 79. 9 ILLUS (General)
5. Gang J (2008) Wanted: tall buildings less iconic, more specific. In: CTBUH 8th world congress on tall & green: typology for a sustainable urban future, pp 496–502
6. Jacob CM, Tandon PJK (2017) A study on facades of the tall buildings in UAE. Int J Hum Resour Ind Res 4(1):72–82. https://doi.org/10.5281/zenodo.293821
7. Jafari M, Alipour A (2021) Review of approaches, opportunities, and future directions for improving aerodynamics of tall buildings with smart facades. Sustain Cities Soc 72:102979. https://doi.org/10.1016/j.scs.2021.102979
8. Mirrahimi S et al (2016) The effect of building envelope on the thermal comfort and energy saving for high-rise buildings in hot–humid climate. Renew Sustain Energy Rev 53:1508–1519. https://doi.org/10.1016/j.rser.2015.09.055
9. Peng L, Ni Z, Huang X (2013) Review on the fire safety of exterior wall claddings in high-rise buildings in China. Procedia Eng 62:663–670. https://doi.org/10.1016/j.proeng.2013.08.112
10. Delichatsios M (2014) Enclosure and facade fires: physics and applications. Fire Saf Sci 11:3–27. https://doi.org/10.3801/IAFSS.FSS.11-3
11. Jensen G (2013) Fire spread modes and performance of fire stop in vented façade constructions—Overview and standardization of test methods. In: Vallerent S, Florence C (eds) MATEC web of conferences, vol 9, p 02002. https://doi.org/10.1051/matecconf/20130902002
12. 705.8.5 Vertical separation of openings (2018) International building code® 2018. International Code Council Inc., Country Club Hills, IL
13. Nishio Y et al (2016) Fire spread caused by combustible facades in Japan. Fire Technol 52(4):1081–1106. https://doi.org/10.1007/s10694-015-0535-5
14. Eaves DE, Keen CV (1976) Thermally initiated oxidation and ignition of flexible polyurethane foams. Br Polym J 8(2):41–43. https://doi.org/10.1002/pi.4980080202
15. Prasad KR et al (2009) Numerical simulation of fire spread on polyurethane foam slabs, pp 697–708

16. Wood—Densities of Various Species (no date). https://www.engineeringtoolbox.com/wood-density-d_40.html. Accessed 11 Dec 2021
17. ICRAF Database—Wood Density (no date). http://db.worldagroforestry.org/wd/species/Eucalyptus. Accessed 11 Dec 2021
18. Martinka J, Chrebet T (2014) Activation energy of teak and oak wood spontaneous ignition. Adv Mater Res 1001:262–266. https://doi.org/10.4028/www.scientific.net/AMR.1001.262
19. Braun E, Levin BC (1986) Polyesters: a review of the literature on products of combustion and toxicity. Fire Mater 10(3–4):107–123. https://doi.org/10.1002/fam.810100304
20. McGrattan K et al (2021) Fire dynamics simulator technical reference guide volume 3: validation, p 1077
21. Fibres and Flammability | Textiles F.R. Limited (2021). http://textilesfr.co.uk/technical/fibres-and-flammability/. Accessed 11 Dec 2021
22. Babrauskas V (2011) Glass breakage in fires. Fire Science and Technology Inc. https://doctorfire.com/wp-content/uploads/2018/11/GlassBreak.pdf Accessed 19 Oct 2021
23. MORN (2018a) Knowledge about float glass thickness, density, component | MORN glass-best architectural glass supplier. https://www.mornglass.com/knowledge-about-float-glass-thicknessdensitycomponent.html. Accessed 11 Dec 2021
24. Zang M, Chen S (2011) Laminated glass. https://doi.org/10.1002/9781118097298.weoc121
25. Elert G (2021) Density. The Physics Hypertextbook. https://physics.info/density/. Accessed 11 Dec 2021
26. MORN (2018b) Some misunderstanding about glass U value | MORN GLASS-Best architectural glass supplier. https://www.mornglass.com/some-misunderstanding-about-glass-u-value.html. Accessed 11 Dec 2021
27. Gross D (1991) Estimating air leakage through doors for smoke control. Fire Saf J 17(2):171–177
28. Kerber S (2012) Analysis of changing residential fire dynamics and its implications on firefighter operational timeframes. Fire Technol 48(4):865–891. https://doi.org/10.1007/s10694-011-0249-2
29. Burning of wood (no date). http://virtual.vtt.fi/virtual/innofirewood/stateoftheart/database/burning/burning.html. Accessed 11 Dec 2021

Technological Advancement for Safe Water Supply

Advances in Coagulation Technique for COD Removal of Petroleum Wastewater—A Review

Poornima Moremada and Senajith Kalpage

Abstract The COD concentration in petroleum wastewater (PWW) varies widely depending on the type of crude oil and the method used for refining. Coagulation provides a feasible method for removing turbidity, colour, TSS, and TP from wastewater. However, this technique has its own limitations when dealing with highly COD-concentrated PWW above 6000 mg/l. In this paper, the traditional coagulation technique and its limitations are discussed. This review provides insights into the latest developments of coagulation for COD treatment from highly concentrated PWW. The initial pollutant load of PWW was discovered to be one of the main considerations of coagulation treatment efficiency. It was revealed that a modified coagulant known as PFASi is the best approach to treat highly COD-concentrated wastewater (up to 20000 mg/l).

Keywords Coagulation · Flocculation · Petroleum wastewater · COD · Advanced technologies

1 Introduction

The Petroleum industry is regarded as one of the important and largest industries worldwide with respect to its output and demand. Petroleum products, which include not only fuels like gasoline, diesel, kerosene, liquefied petroleum gas (LPG), and lubricant oils but also raw materials for fertilisers, polymers, and pharmaceuticals, play an essential role in a variety of applications like transportation, electricity generation, road construction, and agriculture, among others [26]. Approximately 84 million barrels of crude oil are refined daily to meet the global demand [32]. According to [26], the global petroleum oil demand is expected to increase by 32% from its current

P. Moremada (✉) · S. Kalpage
Faculty of Engineering, University of Peradeniya, Pereira Mawatha, Kandy, Sri Lanka
e-mail: e16240@eng.pdn.ac.lk

S. Kalpage
e-mail: csk@eng.pdn.ac.lk

© The Author(s), under exclusive license to Springer Nature Singapore Pte Ltd. 2023

R. Dissanayake et al. (eds.), *ICSBE 2022*, Lecture Notes in Civil Engineering 362,
https://doi.org/10.1007/978-981-99-3471-3_49

level due to industrial development and population growth. Between 63.6 and 254 l of wastewater can be generated from refining one barrel of crude oil, depending on the type of crude oil and the methods of processing [34]. Globally, $9 \times 10^9 - 14 \times 10^9$ m^3 of oily wastewater was generated in 2012 [22].

PWW contributes to about 70% of pollutants found in the environment [28]. The PWW contains a minor amount of water-soluble compounds but mainly insoluble compounds [6]. When PWW is released into the water sources, a thick layer of oil will be formed on the water surface since most components have densities lower than water [45]. Such oil layers formed will block the access to sunlight and thus cause problems for aquatic life [45]. The soluble pollutants in the PWW can enter the food chains through the consumption of contaminated water sources resulting in harmful effects on health such as kidney failure, blood cancers, and even death [48]. Therefore, the disposal of polluted PWW should be done carefully to avoid environmental pollution and the resulting adverse health consequences.

A typical PWW treatment process consists of three main stages; primary, secondary, and tertiary treatments [53]. The coagulation/flocculation treatment method that belongs to the secondary treatment stage has gained increased attention among water industrialists in recent years due to its environmental friendliness and economic effectiveness [57]. However, the coagulation process has some limitations in treating PWW on account of less efficiency in treating organic content [1, 2, 53]. Consequently, many researchers have placed great emphasis on novel coagulation methods to overcome this problem. Therefore, in this literature review, drawbacks in conventional coagulation methods and the latest developments will be discussed. In the beginning of this literature review, the ability of the coagulation/flocculation process and biological treatments for COD removal in PWW will be discussed. Ultimately, the novel coagulation methods and the potential of substituting these novel methods for removing COD in PWW are going to be discussed.

2 Conventional Methods Used in the PWW Industry

A variety of treatment units are used in the petrochemical industry to achieve the desired water quality. The most common units include dissolved air floatation (DAF), membrane filtration, coagulation/flocculation, and numerous biological treatment systems. For setting up a wastewater treatment plant, various treatment units are combined upon the characteristics of wastewater, environmental considerations, and economic factors. Figure 1 shows a classification of PWW treatment units.

2.1 Primary Treatment

The first part of the primary stage focuses on the physical separation of impurities without using any chemicals. The principal treatment processes are screening,

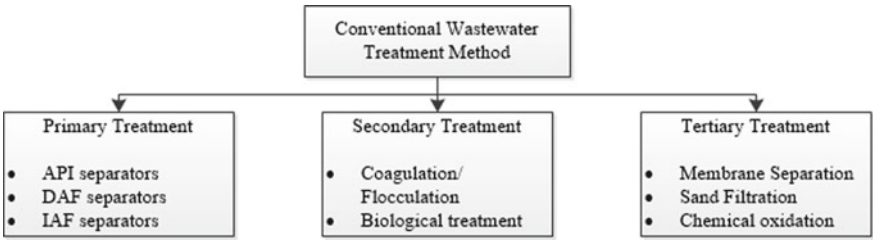

Fig. 1 Main stages in conventional treatment process

floatation, and gravity separation [2, 26, 53]. This stage is capable of removing immiscible particles with diameters greater than 50 μm effectively [10]. Further, the primary treatment eliminates insoluble particles in wastewater and plays an essential role in preparing feed for the subsequent treatment stages (Yu et al. 2017). Furthermore, with low operating costs and good removal effectiveness of suspended and immiscible particles, the primary stage plays a vital role in the treatment process [2].

2.2 Secondary Treatment

The secondary treatment stage is responsible for removing particles such as organic substances and sulphides from the wastewater and immobilizing the microorganisms present [35]. The Secondary stage includes biological treatment methods and coagulation/flocculation [53]. However, depending on the application, the coagulation process can also be applied to either primary, secondary, or tertiary treatment [38].

In biological treatments, specialized microorganisms are utilized to convert organic impurities into simpler molecular compounds such as CO_2, H_2O, and CH_4. The effectiveness of biological treatment is highly reliant on the biodegradability of the wastewater [2]. The ratio between chemical oxygen demand (COD) to biochemical oxygen demand (BOD) of the wastewater can be used to determine the biodegradability of wastewater, wastewater with lower biodegradability has a higher COD/BOD ratio than 2 [44]. Based on the information given in Table 1, it can be noted that petroleum water has a relatively lower biodegradability. Because of this fact, the biological treatment necessitates a long retention time, resulting in bigger tank sizes. A higher sludge production rate and lower treatment efficiencies are also identified as negative effects of biological treatment [26, 37].

Coagulation is a physicochemical process that destabilizes fine-charged colloidal particles in the wastewater by neutralizing and agglomeration. Coagulation can efficiently reduce the total suspended solid (TSS) content, total phosphorus (TP), turbidity, and colour in PWW [2, 19]. Coagulation is more effective in treating suspended organic matter than in the treatment of dissolved organic matter [38]. The dissolved solids in wastewater typically have a diameter of less than 1 μm [10], yet the traditional coagulation process is more successful in treating compounds with a

Table 1 COD, BOD, and COD/BOD ratio of PWW

Parameter	[40]	[24]	[54]	[21]	[14]	[12]	[25]
COD (mg/l)	450	1250	15,000–60,000	7896	21,000	800	1209
BOD (mg/l)	174	625	8000–32,000	3378	8000	350	327
COD/BOD ratio	2.6	2	1.9	2.3	2.6	2.3	3.7

Table 2 Comparison of biological and coagulation treatments [1]

Process	COD removal (%)	TSS removal (%)	Processing time (min)
Biological	83	93	240
Coagulation	78	90	45

diameter greater than 2 μm [6]. Soluble contaminants make up a significant fraction when at the higher oil concentration in PWW [6]. As a result, the effectiveness of COD removal by coagulation is lower in highly concentrated oil water. Treating highly concentrated PWW is thus a major handicap of traditional coagulation, despite its suitability for treating moderately concentrated PWW.

Ahmad et al. [1] studied the efficiency of biological and coagulation processes for PWW. Their findings are given in Table 2.

When comparing the results in Table 2, it can be suggested that, except for COD elimination, the coagulation approach is more effective than the biological treatment because the biological process' retention time is around five times longer than the coagulation, resulting in higher overall operating costs and a more extensive treatment area.

2.3 Tertiary Treatment

The tertiary treatment stage is the ultimate polishing process to remove any remaining metal ions, fine particles, and organic compounds that primary and tertiary treatments failed to remove, and this stage includes sand filtration, chemical oxidation, and membrane technologies [53]. Fouling is a significant challenge with both sand filtration and membrane filtration [2, 53]. If the fouling rate is high, frequent filter renewal will be a critical challenge.

3 Coagulation/Flocculation as a PWW Treatment Method

Fine colloidal particles present in PWW have very high negative surface charges [4, 19, 58]. The positive charge ions present in the water are attracted to the colloidal particle due to the high negative surface charge, and a small number of negative

charge ions are trapped in between attracted ions due to the kinetic motion, resulting in the formation of a thin layer known as an "electrical double layer" [7]. A term called zeta potential is proposed to quantify the stability of colloidal particles distributed through wastewater because the stability of the colloidal particle changes with the thickness of the electrical double layer [9]. Untreated surface wastewater typically has a higher zeta potential value of −15 to −25 mV and when the magnitude of the zeta potential decreases below 5 mV, the particles tend to aggregate and these aggregated particles can be separated by sedimentation [5]. The coagulation treatment procedure is based on this principle, in which charged particles are linked together and form microflocs by lowering the water's zeta potential value. Flocculation is a continuous mixing phase that aggregates all microflocs into huge agglomerates known as pinflocs that may be removed from water by sedimentation. In some treatment processes, flocculants, also known as coagulant aids, are used to speed up the flocculation process by increasing the size of pinflocs and adding toughness to the flocs so that they do not break up during the mixing and settling process. Flocculants are high-molecular-weight chemicals with long chains that form a long bridge to attract more microflocs and form stabilized pinflocs [61].

The effectiveness of the coagulation process in removing suspended solids in wastewater depends on various factors, including the type of coagulant used, coagulant dose, pH value of the water, temperature of the water, and concentration of the water [19, 57].

4 Advanced Coagulation Technologies for PWW Treatment

4.1 Electrocoagulation

Electrocoagulation is based on anodic metal dissolution theory, where the coagulant is formed via direct electric current running through the electrode, causing the production of hydroxyl ions through anodic and cathodic reactions. The anode decays, releasing hydroxyl irons; consequently, the anode must be replaced on a regular basis. Unlike in conventional coagulation, there is no need to add chemicals as coagulants because the metal electrode provides the cations for neutralization by an electrochemical reaction [3, 47]. Although many materials can be used as electrodes, Al and Fe are commonly used as anode materials because they are relatively inexpensive, non-toxic, and readily available [42]. Al and Fe hydrolysis produce cations (Al^{3+}, Fe^{3+}, etc.) with strong adsorption properties, allowing them to bind more colloidal particles distributed in wastewater than conventional coagulation [4].

Electrocoagulation efficiency is influenced by several parameters, including electrode material, pH, current density, electrolysis time, conductivity, electrode distance, electrode configurations, temperature, etc. [42]. Table 3 shows the treatment efficiencies and operating conditions for oily wastewater. The Fe electrode removes more COD than the Al electrode, as can be seen in Table 3. In addition, increasing the

number of metal electrodes can enhance COD removal efficiency [46]. The most important parameters in electrocoagulation are current density and electrolysis time, as they determine not only the removal efficiency but also the overall cost of the operation [27].

In Sri Lanka, the maximum COD concentration of treated wastewater that can be discharged into surface waters is 250 mg/l [33]. As demonstrated in Table 3, raw wastewater with a low concentration (less than 2000 mg/l of COD) achieved the wastewater COD's dischargeable limit. However, when the initial COD concentration is very high, the electrocoagulation could not achieve the desired COD concentration in the treated water. Therefore, the treated water from electrocoagulation must be treated further in order to attain the permissible discharge wastewater concentrations.

Despite the fact that all the above-mentioned parameters do influence the removal effectiveness, the cost of electrocoagulation is mostly controlled by the current density, electrolysis time, and electrode material [23, 24]. The results in Table 4 show that the initial COD concentration of the wastewater has a considerable impact on the cost and final COD concentration (Table 5).

The following general conclusion concerning electrocoagulation can be drawn from the findings of numerous past studies. The electrocoagulation's COD removal efficiency is strongly reliant on the wastewater's initial COD concentration, as lower COD concentrated water around 2000 mg/l has reached the wastewater's dischargeable limit of COD and has a lower operating cost.

4.2 Coagulation with Novel Coagulants/Flocculants

Due to the low effectiveness in COD level reduction, traditional coagulation treatments are typically utilized for wastewater with low organic content or as the final treatment effort [2]. As a result, various approaches to novel coagulants and flocculants (coagulant aids) have been done over the years in order to improve coagulation treatment efficiency as indicated in Table 5.

Zeng et al. [61] used some traditional and a novel coagulant such as Poly-Zinc Silicate Sulphate (PZSS) to compare the treatment efficiency of a heavy oil wastewater sample. PZSS gave higher removal efficiency, and it was stated that PZSS has a higher charge density in the presence of zinc ions, which helps it grab more colloidal substances and form strong microflocs, resulting in a higher removal efficiency with lower coagulant dosage [60].

For the treatment of highly concentrated oily wastewater with a very high initial COD content of 20,000 mg/l, [52] employed Polymeric Aluminium Ferric Silicate (PAFSi) as a new coagulant in an acidic medium. The final concentration was 360 mg/l which was slightly higher than the permissible dischargeable COD concentration for COD. However, this new coagulant is feasible in treating highly concentrated wastewater when compared with electrocoagulation. The increased removal rate is due to the proportion of Al, Fe, and Si in the coagulant, which results in a higher degree

Table 3 Summary of removal efficiency of oily pollutants from electrocoagulation

Electrode		No. of electrodes	Operating conditions				Initial COD concentration (mg/l)	COD removal efficiency (%)	Final COD concentration (mg/l)	References
Anode	*Cathode*		*Temperature* (°C)	*pH*	*Electrolysis time* (min)	*Current density* (mA/cm^2)				
Al	Al	2	25	8	60	13	596	63	220.5	[17]
Al	Al	2	40	–	30	30	–	–	–	[18]
Mild steel	Stainless steel	2	30	8	40	9	1250	87	162.5	[24]
Fe	Fe	10	–	6	90	–	17,000	92.8	1224	[47]
Al	Fe	2	–		10	150	–	–	–	[13]
Al	Al	4	25	9	18	9.9	130	78.8	27.56	[23]
Al	Al	6	25	7	40	–	–	99.1	–	[41]
Al	Stainless steel	5	30	7	60	12	250	96.8	8	[3]
Fe	Fe	2	–	4.5	45	1.9 A	1280	98.6	17.9	[15]
Fe	Fe	2	32	–	15	20	21,000–25,000	89.7	2163–2575	[31]
Al	Al	2	25	7.8	5 ml/min	33	5064	57	2177.52	[16]

Table 4 Cost comparison on electrocoagulation

References	Initial COD level (mg/l)	COD Removal efficiency (%)	Final COD level (mg/l)	Cost (US$/m^3)
[23]	130	78.8	27.56	0.654
[15]	1280	98.6	17.92	0.270
[31]	21,000–25,000	89.7	2160–2575	6.280

Table 5 Summary of the removal of oil/COD by using novel coagulant/flocculant systems

Coagulant/flocculant	Target parameter	Initial concentration (mg/l)	Removal efficiency (%)	Final concentration (mg/l)	References
Coagulant-PZSS Flocculant-A-PAM	Oil	400–1000	99	10	[61]
Coagulant-PAFSi	COD	20,000	98.4	360	[52]
Coagulant-PSAFS Flocculant-Mn salt	Oil	5000	99.78	11	[59]
Coagulant-mixture of traditional coagulant (ferric chloride and copper sulphate)	COD	8100	81	1539	[51]

of polymerization and charge neutralization ability, allowing almost all charged particles to be removed [63]. As a result, PAFSi is ideal for treating highly concentrated wastewater with a concentration of around 20,000 mg/l.

You et al. [59] evaluated the performance of Polysilicate Aluminium Ferric Sulphate (PSAFS), which is a new inorganic polymer coagulant to treat emulsified oily wastewater with a concentration of 5000 mg/l. The final resulting oil concentration was 11 mg/l. The reason behind this higher removal is the good demulsification and turbidity-removal effect of the Mn-PSAFS mixture.

Singh and Kumar [51] analysed the effects of utilizing mixed coagulants (ferric chloride and copper sulphate mixture) to remove petroleum effluent with an initial COD concentration of 8100 mg/l. The mixed copper sulphate and ferric chloride mixture performed better When compared to utilizing coagulant separately. The main reason for this lower performance of traditional coagulants is due to the higher initial COD concentration of the effluent (>6000 mg/l) [52]. The ability of the blended mixture to create larger and stable flocs is the cause for the increased COD removal with a mixed coagulant, according to the study. Despite the fact that the blended mixture increases COD removal efficiency, the final COD concentration could not approach the dischargeable limit of COD. However, blending two or more traditional coagulants results in a better COD removal than applying only one. This mixed coagulant approach is ideal for removing moderately concentrated wastewater samples.

Based on the above findings, several conclusions can be made on modifications of coagulation/flocculation systems. The PAFSi system is the best for the treatment of highly concentrated wastewater with COD levels of up to 20,000 mg/l. Applying mixed coagulants is a good approach since the traditional coagulant capabilities are boosted by the presence of several coagulants in a single system. This combined coagulant approach is suitable for eliminating COD in moderately concentrated water. To accelerate the flocculation, A-PAM can be used as a flocculant because it has a 99% overall efficiency at a very low dosage (1 mg/l) [61].

4.3 Combined Technologies

4.3.1 Coagulation Flocculation-Floatation Treatment

As mentioned in Chap. 2, the floatation method is a primary separation process used to remove large and immiscible particles with a diameter greater than 50 μm. However, some research has discovered that the flocculation effect can be improved by combining the floatation technique with the coagulation process [10].

Rathilal [37] evaluated the feasibility of three different types of coagulants in treating concentrated petrochemical wastewater using a DAF separator and a coagulation/flocculation technology. A novel coagulant which is called Polyaluminium silicate sulphate (PASS) was used as the coagulant and was able to remove 89.9% of COD from concentrated water, resulting in a final concentration of 1211.5 mg/l. The floc-air bubble attachment, which allows flocs to float on the water surface, is the reason for greater COD removal efficiency in this technology. As a result, more flocs were able to float on the water surface compared to coagulation without applying DAF [11]. Santo et al. [43] followed the same procedure to compare efficiencies with and without applying DAF separator in the coagulation process. When the initial COD level was 6880 mg/l, the resulting final COD concentration was 150 mg/l. This treatment process is therefore suitable for treating moderately contaminated wastewater.

Using the standard floating technique and microbubble flotation approaches, You et al. [59] compared the overall efficiency of the coagulation process. The mass reduction in flocs when absorbing higher content of microbubbles resulted in a significant buoyancy force on the flocs, which helped a steady floc flotation on the water surface. It was observed that the flocculation efficiency is higher when using the microbubble floatation over the standard floatation. To improve the separation efficiency, experiments were performed with polyacrylamide (PAM) as a flocculant. The results revealed that the addition of a flocculant improves the binding ability of flocs.

4.3.2 Coagulation Flocculation-Adsorption Treatment

Generally, adsorption is used for removing a wide range of contaminants from industrial wastewater, especially for the removal of various micropollutants, non-degradable organic compounds, and metal ions [29]. The mainly used adsorbent is activated carbon because it has a larger surface area for adhering to different types of contaminants in water [20]. According to [30], adsorption can remove dissolved organic compounds more efficiently which is attributed to the high microporosity and selective for the adsorption of low-molecular-weight hydrocarbon compounds.

Wang et al. [55] studied the possibility of combining coagulation with adsorption to treat PWW. It was reported that, when the adsorption procedure was applied before the coagulation, the COD concentration reduced from 1458.4 to 156.4 mg/l (removal efficiency of 89.27%). When the adsorption procedure was used after the coagulation, only 75.65% of COD was removed. The reason for the poorer removal effectiveness when applying adsorption after coagulation is attributed to the increase in colloidal fine particle size during coagulation, which could not penetrate the pores in activated carbon. Hence, they have concluded that the order of the operations is important when treatment processes are combined.

Because the organic and suspended solid loading for the tertiary treatment can be minimized, the combined coagulation and adsorption approach is preferred [49]. Rasouli et al. [36] investigated the efficacy of lowering the membrane fouling rate when coagulation/floatation combined with adsorption for oily wastewater and identified that the fouling rate of the membrane can be significantly reduced.

Based on the findings of numerous research works, it can be concluded that the advection-coagulation technique is better suited for treating low COD concentrated water (in the range of 1400 mg/l).

4.3.3 Coagulation/Flocculation with Photo-Fenton Oxidization

Fenton process is extensively using novel technology to treat organic content wastewater [56]. The Fenton process degrades organic compounds to simple compounds such as CO_2 and H_2O by using hydroxyl radicals (•OH) generated by an oxidation reaction between Fe and H_2O_2. However, the traditional Fenton method has limitations in terms of sludge production and operating pH range. The photo-Fenton technique has gotten a lot of interest due to its low sludge output [62]. In the presence of UV light, the yield of producing •OH free radical is increased, resulting in more CO_2 and H_2O and less sludge generation [50].

Using this photo-Fenton oxidization technique, [40] evaluated the effectiveness of coagulation in removing COD from petroleum effluent. The photo-Fenton process was introduced before and after the coagulation process in this experiment, and it was discovered that using the photo-Fenton process before the coagulation process has more benefits than using it after the coagulation process. When the photo-Fenton technique is used before the coagulation process, oxidized Fe^{3+} can be used as coagulants, resulting in cost savings. This combination method is promising in reducing

sludge production and treatment time, but the higher operating cost was the main disadvantage.

4.3.4 Coagulation with Bioreactions

The moving bed biofilm reactor (MBBR) is an advanced biological process that has drawn interest in municipal wastewater and drinking water treatment plants. The MBBR's main component is a moving carrier that serves as a habitat for biomass. The biomass attached to the carriers moves around the bioreactor and causes the degradation of dissolved solids into simple compounds like CO_2 and H_2O. MBBR is a potential treatment technology for treating highly concentrated wastewater [8].

The removal efficiencies of a hybrid coagulation and MBBR system were investigated by [39]. In their experiments, MBBR was introduced before the coagulation process and was able to eliminate more than 95% of organic compounds (including Aromatics, Phenol, Acetone, Toluene, and Benzene). The effectiveness of the post-coagulation process is attributed to the reduction of the COD load by the MBBR process. The significantly overlong retention period, roughly around 55 days, is the major drawback of this technique.

5 Conclusion

Due to the simple technology and cost-effectiveness, coagulation has gained a renewed attraction in the wastewater industry. Conventional coagulation has been demonstrated to have great potential in treating turbidity, colour, TSS, and TP. Coagulation is a salient step in wastewater treatment; removing microscale and suspended particles, which are larger than around 2 μm. Due to the poor performance of coagulation in treating dissolved contaminants in the wastewater, coagulation is not applicable in treating higher initial COD concentrated wastewater. That is because the highly concentrated wastewater contains a higher fraction of dissolved solids. Due to the limitation in treating highly concentrated wastewater, particularly in PWW, expertise is implementing new strategies for improving coagulation. The current review summarizes novel research and studies on PWW treatment by the coagulation method.

In electrocoagulation, coagulants are generated by electrolytic reactions. The cations generated from electrocoagulation (Al^{3+}, Fe^{3+}, etc.) exhibit beneficial adsorption properties, allowing them to bind more colloidal particles distributed in wastewater than conventional coagulation. Novel coagulants (such as PZSS, PAFSi, and PSAFS) are formed through polymerization and have higher charge densities than traditional coagulants. Flocculants (coagulant aids) have a long-chained structure which gives them the ability to grab more microflocs. As a result, adding flocculants boosted the flocculation process by aggregating more microflocs into bigger pinflocs. And these pinflocs can be separated easily by sedimentation.

The coagulation-microbubble floatation technique showed higher performance in treating oily wastewater than applying the traditional floatation technique to the coagulation. Since adsorption is applicable in treating dissolved organic compounds, the coagulation-adsorption process shows promising results in COD removal. When considering combined technique strategies, the order in which the method is applied is influential for coagulation-floating, coagulation-adsorption, and coagulation-photo-Fenton technologies.

The selection of appropriate treatment methods depends on wastewater composition, efficiency, regulatory limitation, operating cost, etc. For higher COD concentrated water with COD levels of up to 20,000 mg/l, polymeric aluminium ferric silicate (PAFSi) is an excellent novel coagulant. The combined Coagulation-Floatation technique is more suitable to treat moderately concentrated water up to 7000 mg/l in this technique, and PASS is the novel coagulant used in coagulation. For moderately low concentrated water, up to around 2000 mg/l electrocoagulation and Coagulation-Adsorption techniques were feasible.

References

1. Ahmad H, Lafi WK, Abushgair K, Assbeihat JM (2016) Comparison of coagulation, electrocoagulation and biological techniques for the municipal wastewater treatment. Int J Appl Eng Res 11(22):11014–11024
2. Aljuboury DA, Palaniandy P, Abdul Aziz HB, Feroz S (2017) Treatment of petroleum wastewater by conventional and new technologies—A review. Glob Nest J 19(3):439–452. https://doi.org/10.30955/gnj.002239
3. Alkurdi SS, Abbar AH (2020) Removal of COD from petroleum refinery wastewater by electro-coagulation process using SS/Al electrodes. IOP Conf Ser: Mater Sci Eng 870(1). https://doi.org/10.1088/1757-899X/870/1/012052
4. An C, Huang G, Yao Y, Zhao S (2017) Emerging usage of electrocoagulation technology for oil removal from wastewater: a review. Sci Total Environ 579:537–556. https://doi.org/10.1016/j.scitotenv.2016.11.062
5. Bean EL, Campbell SJ, Anspach FR (1964) Zeta potential measurements in the control of coagulation chemical doses. J Am Water Works Assoc 56(2):214–227. https://doi.org/10.1002/j.1551-8833.1964.tb01202.x
6. Bobra M (1992) Solubility behaviour of petroleum oils in water
7. Bratby J (2016) Colloids and interfaces. In: Coagulation and flocculation in water and wastewater treatment, 3rd edn. IWA Publishing, pp 9–26
8. Cao CY, Zhao YH (2012) The comparison of MBBR and ASP for treatment on petrochemical wastewater. Pet Sci Technol 30(14):1461–1467. https://doi.org/10.1080/10916466.2010.506458
9. O'Melia CR (1978) Coagulation in wastewater treatment 24(3):247–256
10. Coca J, Gutierrez G, Benito JM (2011) Treatment of oily wastewater 1–55. https://doi.org/10.1007/978-90-481-9775-0
11. Crossley IA, Valade MT (2006) A review of the technological developments of dissolved air flotation, 479–491. https://doi.org/10.2166/aqua.2006.057
12. Demirci Ş, Erdogan B, Ozcimder R (1998) Wastewater treatment at the petroleum refinery, Kirikkale, Turkey using some coagulants and Turkish clays as coagulant aids. Water Res 32(11):3495–3499. https://doi.org/10.1016/S0043-1354(98)00111-0

13. Dimoglo A, Akbulut HY, Cihan F, Karpuzcu M (2004) Petrochemical wastewater treatment by means of clean electrochemical technologies. Clean Technol Environ Policy 6(4):288–295. https://doi.org/10.1007/s10098-004-0248-9
14. Dincer AR, Karakaya N, Gunes E, Gunes Y (2008) Removal of COD from oil recovery industry wastewater by the advanced oxidation processes (AOP) based on H2O2. Glob Nest J 10(1):31–38. https://doi.org/10.30955/gnj.000479
15. El-Etriby H, Radwan K, Taha K (2020) Electrocoagulation for oil and grease wastewater treatment using aluminum electrodes. (Dept. C). Bull Fac Eng (Mansoura University) 40(5):53–63. https://doi.org/10.21608/bfemu.2020.104936
16. El-Naas MH, Al-Zuhair S, Al-Lobaney A (2013) Treatment of petroleum refinery wastewater by continuous electrocoagulation. Desalination 2(10):201–205. https://doi.org/10.1016/j.desal.2010.03.013
17. El-Naas MH, Al-Zuhair S, Al-Lobaney A, Makhlouf S (2009) Assessment of electrocoagulation for the treatment of petroleum refinery wastewater. J Environ Manag 91(1):180–185. https://doi.org/10.1016/j.jenvman.2009.08.003
18. Fadali OA, Ebrahiem EE, El-Gamil A, Altaher H (2016) Investigation of the electrocoagulation treatment technique for the separation of oil from wastewater. J Environ Sci Technol 9(1):62–74. https://doi.org/10.3923/jest.2016.62.74
19. Farajnezhad H, Gharbani P, Branch A (2012) Coagulation treatment of wastewater in petroleum industry using poly aluminium chloride and ferric. Ijrras 13(October):306–310
20. García-Araya JF, Beltrán FJ, Álvarez P, Masa FJ (2003) Activated carbon adsorption of some phenolic compounds present in agroindustrial wastewater. Adsorption 9(2):107–115. https://doi.org/10.1023/A:1024228708675
21. Gasim HA, Kutty SRM, Isa MH, Alemu LT (2013) Optimization of anaerobic treatment of petroleum refinery wastewater using artificial neural networks. Res J Appl Sci Eng Technol 6(11):2077–2082. https://doi.org/10.19026/rjaset.6.3827
22. Gitis V, Rothenberg G (2016) Ceramic membranes new opportunities and practical applications
23. Giwa S, Zeybek Z, Hapoglu H (2013) Electrocoagulation treatment of petroleum refinery wastewater: optimization through RSM. Int J Eng Res Technol 2(8):606–615
24. Ibrahim DS, Lathalakshmi M, Muthukrishnaraj A, Balasubramanian N (2013) An alternative treatment process for upgrade of petroleum refinery wastewater using electrocoagulation. Pet Sci 10(3):421–430. https://doi.org/10.1007/s12182-013-0291-4
25. Ishak S, Malakahmad A (2013) Optimization of Fenton process for refinery wastewater biodegradability augmentation. Korean J Chem Eng 30(5):1083–1090. https://doi.org/10.1007/s11814-013-0002-2
26. Jain M, Majumder A, Sarathi P, Kumar A (2020) A review on treatment of petroleum refinery and petrochemical plant wastewater: a special emphasis on constructed wetlands. J Environ Manag 272(July):111057. https://doi.org/10.1016/j.jenvman.2020.111057
27. Kabdaşlı I, Arslan-Alaton I, Ölmez-Hancı T, Tünay OJ (2012) Electrocoagulation applications for industrial wastewaters: a critical review, 37–41
28. Kwon TS, Lee JY (2015) Options for reducing oil content of sludge from a petroleum wastewater treatment plant. Waste Manag Res 33(10):937–940. https://doi.org/10.1177/0734242X15597776
29. Li L, Ai J, Zhang W, Peng S, Dong T, Deng Y, Cui Y, Wang D (2020) Relationship between the physicochemical properties of sludge-based carbons and the adsorption capacity of dissolved organic matter in advanced wastewater treatment: effects of chemical conditioning. Chemosphere 243:125333. https://doi.org/10.1016/j.chemosphere.2019.125333
30. Lorenc-Grabowska E, Gryglewicz G (2007) Adsorption characteristics of Congo Red on coal-based mesoporous activated carbon. Dyes Pigm 74(1):34–40. https://doi.org/10.1016/j.dyepig.2006.01.027
31. Maha Lakshmi P, Sivashanmugam P (2013) Treatment of oil tanning effluent by electrocoagulation: influence of ultrasound and hybrid electrode on COD removal. Sep Purif Technol 116:378–384. https://doi.org/10.1016/j.seppur.2013.05.026

32. Martínez-Huitle CA, De Moura DC, Da Silva DR (2014) Applicability of electrochemical oxidation process to the treatment of petrochemical effluents. Chem Eng Trans 41(Special Issue):373–378. https://doi.org/10.3303/CET1441063
33. National Environmental (Ambient Water Quality) Regulations, No. 01 of (2019) Act, No. 47 of 1980: Ambient Water Quality Standards. Government Gazette, PG 4738—2017, 05 November
34. Oves M, Ansari MO, Khan MZ, Shahadat M, Ismail IMI (2020) Modern age waste water problems. In: Modern age waste water problems. https://doi.org/10.1007/978-3-030-08283-3
35. Quach-Cu J, Herrera-Lynch B, Marciniak C, Adams S, Simmerman A, Reinke RA (2018) The effect of primary, secondary, and tertiary wastewater treatment processes on antibiotic resistance gene (ARG) concentrations in solid and dissolved wastewater fractions. Water (Switzerland) 10(1):13–18. https://doi.org/10.3390/w10010037
36. Rasouli Y, Abbasi M, Hashemifard SA (2019) A new combination of microfiltration, powdered activated carbon and coagulation for treatment of oily wastewater. Int J Environ Sci Technol 16(10):5595–5610. https://doi.org/10.1007/s13762-018-1906-5
37. Tetteh EK, Rathilal S (2020) Evaluation of different polymeric coagulants for the treatment of oil refinery wastewater7:1785756. https://doi.org/10.1080/23311916.2020.1785756
38. Renault F, Sancey B, Badot PM, Crini G (2009) Chitosan for coagulation/flocculation processes—An eco-friendly approach. Eur Polymer J 45(5):1337–1348. https://doi.org/10.1016/j.eurpolymj.2008.12.027
39. Ribera-Pi J, Badia-Fabregat M, Arias D, Gómez V, Taberna E, Sanz J, Martínez-Lladó X, Jubany I (2020) Coagulation-flocculation and moving bed biofilm reactor as pre-treatment for water recycling in the petrochemical industry. Sci Total Environ 715. https://doi.org/10.1016/j.scitotenv.2020.136800
40. Saber A, Hasheminejad H, Taebi A, Ghaffari G (2014) Optimization of Fenton-based treatment of petroleum refinery wastewater with scrap iron using response surface methodology. Appl Water Sci 4(3):283–290. https://doi.org/10.1007/s13201-013-0144-8
41. Safari S, Azadi Aghdam M, Kariminia HR (2016) Electrocoagulation for COD and diesel removal from oily wastewater. Int J Environ Sci Technol 13(1):231–242. https://doi.org/10.1007/s13762-015-0863-5
42. Sahu O, Mazumdar B, Chaudhari PK (2014) Treatment of wastewater by electrocoagulation: a review. Environ Sci Pollut Res 21(4):2397–2413. https://doi.org/10.1007/s11356-013-2208-6
43. Santo CE, Vilar VJP, Botelho CMS, Bhatnagar A, Kumar E, Boaventura RAR (2012) Optimization of coagulation-flocculation and flotation parameters for the treatment of a petroleum refinery effluent from a Portuguese plant. Chem Eng J 183:117–123. https://doi.org/10.1016/j.cej.2011.12.041
44. Santos A, Bernardo M, Vespeira C, Cantinho P, Minhalma M (2012) Cork industry wastewater characterization: assessment of the biodegradability, reuse and of the relationship between BOD, COD and tannins with TOC. J Water Reuse Desalin 2(1):33–39. https://doi.org/10.2166/wrd.2012.047
45. Schweitzer L, Noblet J (2018) Water contamination and pollution. In: Green chemistry, pp 261–290. https://doi.org/10.1016/b978-0-12-809270-5.01001-3
46. Shahriari T, Karbassi AR, Reyhani M (2019) Treatment of oil refinery wastewater by electrocoagulation–flocculation (Case Study: Shazand Oil Refinery of Arak). Int J Environ Sci Technol 16(8):4159–4166. https://doi.org/10.1007/s13762-018-1810-z
47. Shahriari T, Reyhani ARKM (2018) Treatment of oil refinery wastewater by electrocoagulation—flocculation (Case Study: Shazand Oil Refinery of Arak). Int J Environ Sci Technol 0123456789. https://doi.org/10.1007/s13762-018-1810-z
48. Sharma S, Chatterjee S (2017) Microplastic pollution, a threat to marine ecosystem and human health: a short review. Environ Sci Pollut Res 24(27):21530–21547. https://doi.org/10.1007/s11356-017-9910-8
49. Shirasaki N, Matsushita T, Matsui Y, Urasaki T, Kimura M, Ohno K (2014) Virus removal by an in-line coagulation—Ceramic micro fi ltration process with high-basicity polyaluminum coagulation pretreatment, 429–437. https://doi.org/10.2166/ws.2013.218

50. Singa PK, Isa MH, Lim JW, Ho YC, Krishnan S (2020) Photo-Fenton process for removal of polycyclic aromatic hydrocarbons from hazardous waste landfill leachate. Int J Environ Sci Technol 0123456789. https://doi.org/10.1007/s13762-020-03010-6
51. Singh B, Kumar P (2020) Pre-treatment of petroleum refinery wastewater by coagulation and flocculation using mixed coagulant : optimization of process parameters using response surface methodology (RSM). J Water Process Eng 36(April):101317. https://doi.org/10.1016/j.jwpe.2020.101317
52. Sun Y, Zhu C, Zheng H, Sun W, Xu Y, Xiao X, You Z, Liu C (2017) Characterization and coagulation behavior of polymeric aluminum ferric silicate for high-concentration oily wastewater treatment. Chem Eng Res Des 119(17):23–32. https://doi.org/10.1016/j.cherd.2017.01.009
53. Varjani S, Joshi R, Srivastava VK, Ngo HH, Guo W (2020) Treatment of wastewater from petroleum industry: current practices and perspectives. Environ Sci Pollut Res 27(22):27172–27180. https://doi.org/10.1007/s11356-019-04725-x
54. Wahid ZA (2012) Application of chemical and biological coupled treatment technology in POME and petroleum waste water as biodegradation alternative. https://doi.org/10.3923/jest.2012.155.167
55. Wang B, Shui Y, Ren H, He M (2017) Research of combined adsorption-coagulation process in treating petroleum refinery effluent. Environ Technol (United Kingdom) 38(4):456–466. https://doi.org/10.1080/09593330.2016.1197319
56. Wang N, Zheng T, Zhang G, Wang P (2016) A review on Fenton-like processes for organic wastewater treatment. J Environ Chem Eng 4(1):762–787. https://doi.org/10.1016/j.jece.2015.12.016
57. Wei H, Gao B, Ren J, Li A, Yang H (2018) Coagulation/flocculation in dewatering of sludge: a review. Water Res 143(2015):608–631. https://doi.org/10.1016/j.watres.2018.07.029
58. You Z, Xu H, Sun Y, Zhang S, Zhang L (2018) Effective treatment of emulsified oil wastewater by the coagulation-flotation process, 40639–40646. https://doi.org/10.1039/c8ra06565a
59. You Z, Zhang L, Zhang S, Sun Y, Shah KJ (2018) Treatment of oil-contaminated water by modified polysilicate aluminum ferric sulfate 6(7):1–14. https://doi.org/10.3390/PR6070095
60. Zeng Y, Park J (2009) Characterization and coagulation performance of a novel inorganic polymer coagulant-Poly-zinc-silicate-sulfate. Colloids Surf A 334(1–3):147–154. https://doi.org/10.1016/j.colsurfa.2008.10.009
61. Zeng Y, Yang C, Zhang J, Pu W (2007) Feasibility investigation of oily wastewater treatment by combination of zinc and PAM in coagulation/flocculation 147:991–996. https://doi.org/10.1016/j.jhazmat.2007.01.129
62. Zhang MH, Dong H, Zhao L, Wang DX, Meng D (2019) A review on Fenton process for organic wastewater treatment based on optimization perspective. Sci Total Environ 670:110–121. https://doi.org/10.1016/j.scitotenv.2019.03.18
63. Zouboulis AI, Moussas PA (2008) Polyferric silicate sulphate (PFSiS): preparation characterisation and coagulation behaviour. Desalination 224(1–3) 307–316. https://doi.org/10.1016/j.desal.2007.06.012

Efficiency of Emerging Low-Cost Adsorbent Materials in Removal of Colour from Stabilized Landfill Leachate

W. S. M. S. K. Wijerathna, L. M. L. K. B. Lindamulla, R. M. L. D. Rathnayake, K. G. N. Nanayakkara, and K. B. S. N. Jinadasa

Abstract Municipal Solid Waste management is becoming an increasing and complex global threat. Leachate generated in landfills contains toxic contaminants that adversely affects the ecosystem if it is not properly treated before discharge. The present study investigates the efficiency of low-cost adsorbents; derivatives of sawdust (SD), rice husk (RH), and chitosan, while focusing on the removal of colour-causing contaminants from a permeate of an Anoxic/Oxic Membrane bioreactor system (A/O MBR) used for stabilized landfill leachate treatment. The results showed that biochar derived using SD (SDBC) and RH (RHBC) could be used as efficient adsorbents with colour removal efficiencies of 38.2% and 36.2% at optimum conditions which were found for pH, contact time, adsorbent dosage, and rotating speed as 2, 24 h, 10 g/l, and 200 rpm respectively. Unexpectedly, no significant enhancement was observed in colour removal after chemical modifications were done to biochars using H_3PO_4 and KOH, which were contradicting previous studies. However, composites made with biochars and chitosan showed increased removal efficiencies of 51.4% and 53.2% for Chitosan + SDBC and Chitosan + RHBC composites respectively, when the materials were chemically modified into a crosslinked protonated material with Glutaraldehyde ($C_5H_8O_2$) and Hydrochloric acid (HCl). As an ongoing study, further recommendations are made to use different analytical techniques for characterization of the materials. Nonetheless, the results indicate that the use of low-cost adsorbents composited with biosorbents is much more effective in colour-causing contaminant removal from stabilized landfill leachate compared to the use of raw materials itself.

Keywords Landfill leachate · Colour removal · Sawdust · Rice husk · Biochar · Chitosan

W. S. M. S. K. Wijerathna (✉) · L. M. L. K. B. Lindamulla · R. M. L. D. Rathnayake · K. G. N. Nanayakkara · K. B. S. N. Jinadasa
Department of Civil Engineering, Faculty of Engineering, University of Peradeniya, Peradeniya 20400, Sri Lanka
e-mail: wsmsamanthi94@eng.pdn.ac.lk

L. M. L. K. B. Lindamulla
School of Engineering, RMIT University, GPO Box 2476, Melbourne 3001, Australia

© The Author(s), under exclusive license to Springer Nature Singapore Pte Ltd. 2023

R. Dissanayake et al. (eds.), *ICSBE 2022*, Lecture Notes in Civil Engineering 362,
https://doi.org/10.1007/978-981-99-3471-3_50

1 Introduction

In most developing countries, Municipal Solid Wastes (MSW) are still being managed by disposing of them in landfills which may be open dumpsites, sanitary landfills, or engineered landfills. When the rainwater percolates through these landfill dumps, contaminants such as organic and inorganic matter, heavy metals, and xenobiotic compounds will leach out forming landfill leachate [15]. Landfill leachate contains many toxic compounds and hence needs to be treated using a suitable treatment technique before discharging it into a receiving body, which in most cases is a surface water body. Leachate treatment usually requires a combined treatment system including biological and physicochemical methods [5].

Anoxic-Oxic Membrane Bioreactor (A/O MBR) is one such system which can be used in the treatment of landfill leachate. However, as part of our previous study, it was identified that adequate colour removal cannot be achieved using this system. As adsorption is one the most effective, economical, and widely used treatment methods for contaminant removal, it was identified to be used as a tertiary unit to be integrated into the A/O MBR [4]. The outline of this study is illustrated in Fig. 1.

Colour in matured leachate is formed mainly due to the decomposition of organic matter such as humic and fulvic compounds. This can result in a yellow, brown, or black colour liquid [1]. However, colour formation further depends on the type of waste being deposited in the landfill. For instance, paints, pigments, colour compounds, and iron-based materials which are used in construction can cause the colour in landfill leachate [2].

Biochar, derived from pyrolysing various biomasses (sawdust, rice husk, tamarind fruit seed, oat hull, etc.) is becoming a popular adsorbent for contaminant removal which could replace activated carbon. This adsorbent can be activated using physical (steam, gas) or chemical (acid, alkali, and oxidation) activation methods or can be made into a composite to enhance the adsorption capacity [7, 10].

There are several functional groups such as carboxyl, hydroxyl, and phenolic in biochar surface that can bond with contaminants thus removing them from the solution. Acid modifications provide more oxygenated functional groups and carboxylic groups on the surface, and it enhances the micropore structure of biochar leading to an increase in the surface area. Similarly, base modifications also provide more oxygenated functional groups resulting in proton-donating exchange sites and further supporting the increase of the porosity and the surface area [8]. Furthermore, in

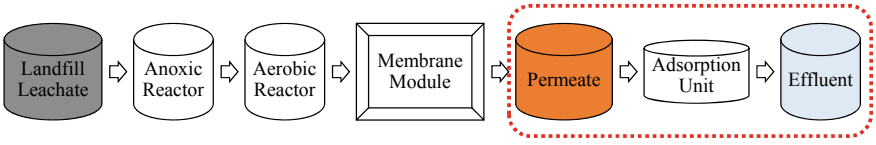

Fig. 1 Outline of the study

biochar modification processes, different materials are used for impregnating biochar to produce biochar-based composites. In this regard, biochar is used as a high surface area scaffold and acts as a support to the materials being deposited. The compositing process involve the creation of new functional groups on surfaces which did not exist on the feedstock or biochar surface before modification [8, 12]. On the other hand, chitosan, which is a linear polysaccharide, possesses high amino and hydroxyl functional groups making it capable of removing a wide range of pollutants. However, due to the poor chemical stability and mechanical strength, its use as an adsorbent is limited. Chitosan + biochar composite involves in strong complexation of pollutants with the amino moieties, hence enhancing the sorption capacity by combining the advantageous properties of chitosan with a reinforcing effect and high specific surface area of biochar [9].

Hence, in this study, biochar derived from sawdust and rice husk were used as base materials, and different modification methods were used to study the colour removal of a permeate obtained as the effluent from an A/O MBR which was used in landfill leachate treatment.

2 Materials and Methods

Raw leachate was obtained from the Gohagoda landfill (7.313585N, 80.621934E) located in Kandy District, Sri Lanka. Sample collection was carried out during the daytime at the leachate outlet of the landfill and used as the influent to the A/O MBR unit. The permeate from the A/O MBR was collected.

2.1 Preparation of Chemically Modified Biochar

2 g of rice husk biochar (RHBC) was mixed with 500 ml of 2.0M NaOH solution and then stirred for 1 h with a magnetic stirrer. Thereafter, the biochar suspension was left for 2 h and then filtered, and rinsed with distilled water to remove excess NaOH on the biochar surface after which the material was oven dried at 34 °C (RHBC-NaOH). A similar process was followed to modify sawdust biochar (SDBC) as well (SDBC-NaOH).

For the acid modification, 2 g of RHBC was activated with H_3PO_4 (10%) by mixing and stirring for 6 h and then filtered and rinsed with distilled water until the pH was constant. Then, the material was dried at 34 °C (RHBC-H_3PO_4). A similar process was followed in making SDBC-H_3PO_4 in acid modification.

2.2 Preparation of Composite Material

SDBC and RHBC were obtained after pyrolysing the raw materials. The raw chitosan (3 g) was dissolved into 100 ml of 1% (v/v) acetic acid solution by stirring it for 5 h at room temperature. Then SDBC, RHBC, and activated carbon (AC) were added 1 g from each to separate beakers. The obtained gel was added dropwise to 1.0 M NaOH solution at a constant rate to prepare beads and they were kept for 2 days in room temperature conditions. The formed beads (CHT + SDBC, CHT + RHBC, CHT + AC) were washed with distilled water until a constant pH reading was obtained. The wet chitosan composite beads were cross-linked with 2.5 wt% glutaraldehyde solution (glutaraldehyde solution: wet chitosan composite beads = 10 ml:1 g). The mixtures were kept in a refrigerator at 20 °C for 48 h to facilitate the cross-linking reaction. The cross-linked beads (CHT + SDBC-CL, CHT + RHBC-CL, CHT + AC-CL) were washed with distilled water to remove any free glutaraldehyde. Thereafter, the beads were treated with concentrated HCl for about 30 min for the protonation of amine groups in chitosan. The resulting Protonated Cross-linked Chitosan Beads (CHT + SDBC-CLP, CHT + RHBC-CLP, CHT + AC-CLP) were then washed with distilled water to a constant pH, dried at room temperature, and were used for adsorption studies [7].

2.3 Batch Experiments

Batch experiments using different adsorbent materials were conducted to study the effect of various influencing parameters. Adsorption experiments were performed using 100 ml HDPE sampling bottles where 50 ml of sample was mixed with appropriate amounts of adsorbent dosages and then shaken for a period of 24 h at 200 rpm. The temperature of the adsorption was maintained at room temperature. Sorption experiments conducted with adsorbent materials were filtered using Whatman No. 42 filter paper and were analysed for colour using the colorimeter, after which the removal efficiencies were calculated using Eq. (1):

$$\text{Removal Efficiency}\,(\%) = (C_i - C_f)/C_i \times 100\% \tag{1}$$

where C_i and C_f are the initial and final colour concentrations of leachate pollutant/permeate, respectively. The measurement of colour levels was done using HACH DR 900 colorimeter.

3 Results and Discussion

3.1 Effect of Biochar Particle Size on Colour Removal

As illustrated in Fig. 2, the highest removal efficiency was observed as 12.8% when RHBC was used in particle size 0.85–0.425 mm range. SDBC did not reach more than 5% removal efficiency in any particle size range showing a low affinity towards the colour-causing contaminants in the permeate.

Typically, the adsorption capacity increases with a decrease in the particle size of the adsorbent. This is due to several reasons such as the increase in surface area and the transfer of contaminants through shorter pathways inside the adsorbent particle pores [14]. However, when the pore sizes of the material are large, the contaminants may be unable to penetrate some interior pores which could cause a reduction in adsorption capacity [6].

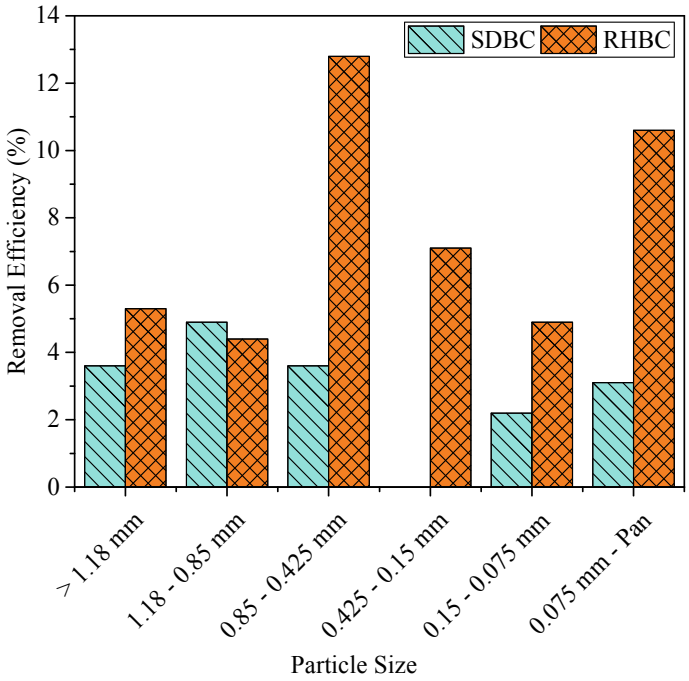

Fig. 2 Effect of biochar particle size on colour removal (pH = 7, Contact time = 24 h, Adsorbent dosage = 10 g/L)

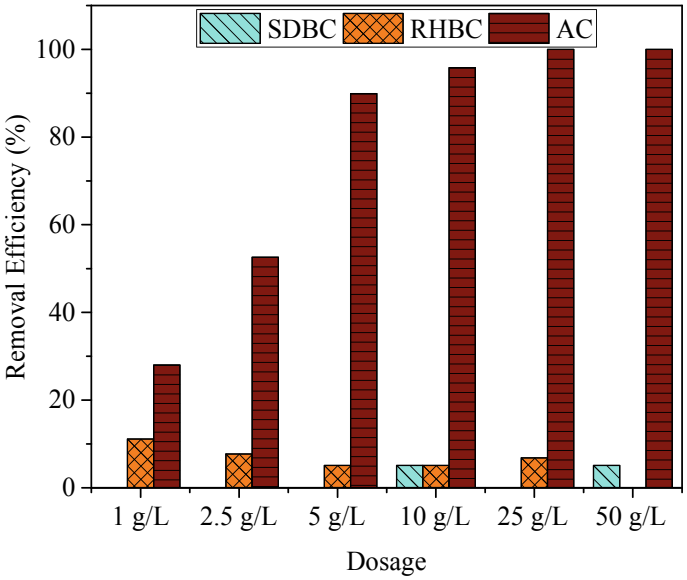

Fig. 3 Effect of biochar dosage on colour removal (pH = 7, Contact time = 24 h)

3.2 Effect of Biochar Dosage on Colour Removal

When considering the AC dosage variation, the amount of adsorbent significantly influenced the colour removal reaching 95.8% at 10 g/L dosages and 100% at 25 g/L (Fig. 3). When the dosage is low, adsorbent sites are exposed and saturate faster but at higher dosages, the availability of a larger fraction of lower energy sites results in low adsorption capacities [6].

However, SDBC and RHBC were unable to show adequate colour removal even when the dosage was increased. RHBC showed a decrease in removal efficiency which could have happened due to the particle collision during adsorption caused by increased dosage. In addition, when the biochar dosage increases, it may induce pH variation affecting the adsorption of contaminants in the aqueous system by altering the adsorbent surface charge and degree of ionization of adsorbates that can ultimately result in creating repulsive forces between the contaminants and adsorbent, thus reducing the removal efficiency [13].

3.3 Effect of Chemical Modification on Colour Removal

NaOH-modified biochar has more negative surface charges compared to pristine biochar. Hence, it encourages more positively charged ion attraction [3]. The highest

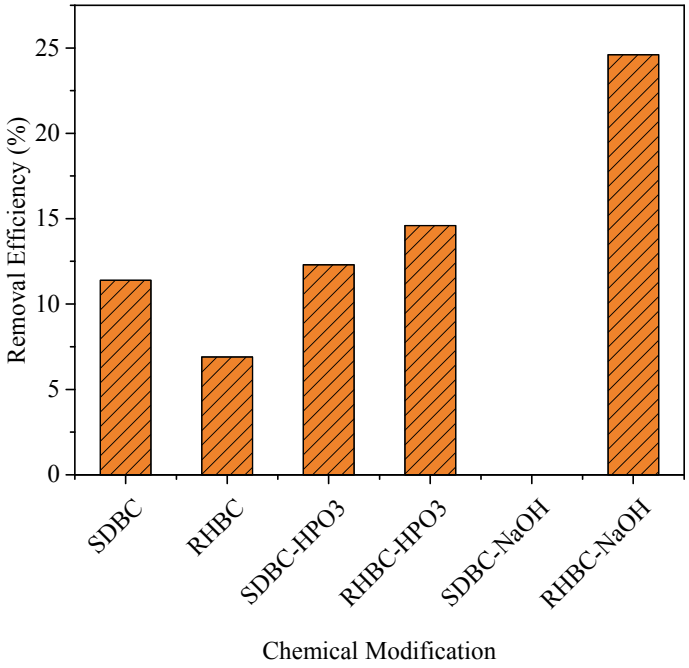

Fig. 4 Effect of chemical modification on colour removal (pH = 7, Contact time = 24 h, Adsorbent dosage = 10 g/L)

colour removal was observed when RHBC-NaOH was used which was 24.6% and SDBC-NaOH showed no improvement by alkali modifications (Fig. 4).

However, considering RHBC, acid and alkali modifications have increased the removal efficiency while for SDBC only a slight improvement after acid modifications has been observed. Nevertheless, though these chemical modifications could have removed colour caused by Fe(III) complexes since the colour of leachate is mostly due to humic and fulvic fractions, these chemical modifications cannot adequately remove the colour from the permeate [1].

3.4 Effect of Composite Adsorbents on Colour Removal

According to Fig. 5, it was observed that the removal efficiency increased with each step of modification performed for the composite. Crosslinking of the material with glutaraldehyde has given mechanical stability to the material, and the protonation has provided the material with $–NH_3^+$ functional groups which are favourable towards adsorbing colour through various types of interaction mechanisms such as electrostatic attractions and chelation [11]. All protonated composites have reached colour

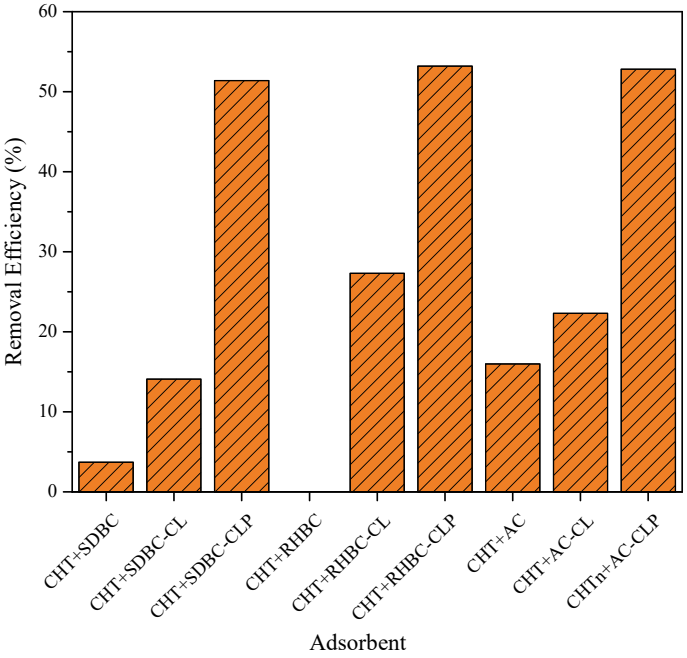

Fig. 5 Effect of composite adsorbents on colour removal (pH = 7, Contact time = 24 h, Adsorbent dosage = 10 g/L)

removal greater than 50%, and the highest removal of 53.2% was achieved at given conditions when CHT + RHBC-CLP was used as the adsorbent.

4 Conclusion

The batch experiments conducted in this study provide information regarding the colour removal from permeate collected from an A/O MBR. Composites made with biochar and chitosan are becoming promising alternatives to replace conventional adsorbents. In this regard, CHT + SDBC-CLP and CHT + RHBC-CLP showed increased removal efficiencies of 51.4% and 53.2%, respectively. Results show that compositing low-cost adsorbents with biosorbents such as chitosan is much more effective to remove colour-causing contaminants which could be integrated as a tertiary polishing unit for an A/O MBR used in the treatment of stabilized landfill leachate.

However, each adsorbent has its advantages and disadvantages making it difficult to compare them. Since there is a variety of adsorbents (biochar, chemically modified biochar, biochar composites, etc.), further in-depth studies (to study the effect of varying operational parameters such as pH, adsorbent dosage, contact time,

initial concentration, temperature, and rotating speed) are recommended to study the adsorption capacities to identify which adsorbent performs better in given conditions. In addition, materials need characterization using different techniques such as Fourier Transform Infrared Spectroscopy (FTIR), Scanning Electron Microscopy (SEM), X-Ray Diffraction (XRD), and Brunauer-Emmet-Teller (BET) specific surface area to identify the surface, micro and macro characteristics of each material which would be beneficial to deduce the adsorption mechanisms.

Acknowledgements The authors gratefully acknowledge the scholarship provided by the Post-graduate Programme in Civil Engineering, University of Peradeniya, Sri Lanka, to the first author and the chitosan material received from the Norwegian University of Life Sciences.

References

1. Aziz HA et al (2007) Colour removal from landfill leachate by coagulation and flocculation processes. Biores Technol 98(1):218–220. https://doi.org/10.1016/j.biortech.2005.11.013
2. Aziz HA et al (2011) Removal of high-strength colour from semi-aerobic stabilized landfill leachate via adsorption on limestone and activated carbon mixture. Res J Chem Sci 1(6):1–7
3. Bashir S et al (2018) Comparing the adsorption mechanism of Cd by rice straw pristine and KOH-modified biochar. Environ Sci Pollut Res 25(12):11875–11883. https://doi.org/10.1007/s11356-018-1292-z
4. Braghiroli FL et al (2018) Activated biochar as an effective sorbent for organic and inorganic contaminants in water. Water Air Soil Pollut 229(7):1–37. https://doi.org/10.1007/s11270-018-3889-8
5. Gotvajn AŽ, Tišler T, Zagorc-Končan J (2009) Comparison of different treatment strategies for industrial landfill leachate. J Hazard Mater 162(2–3):1446–1456. https://doi.org/10.1016/j.jhazmat.2008.06.037
6. Gupta VK, Rastogi A, Nayak A (2010) Adsorption studies on the removal of hexavalent chromium from aqueous solution using a low-cost fertilizer industry waste material. J Colloid Interface Sci 342(1):135–141. https://doi.org/10.1016/j.jcis.2009.09.065
7. Rupasinghe NKLC, Senanayake SAME, Nanayakkara KGN (2022) Development, characterization and mechanisms study of protonated sawdust biochar-chitosan composite bead biosorbent for defluoridation of contaminated groundwater. Bioresour Technol Rep 17(100946). https://doi.org/10.1016/j.biteb.2022.100946
8. Sizmur T et al (2017) Biochar modification to enhance sorption of inorganics from water. Biores Technol 246:34–47. https://doi.org/10.1016/j.biortech.2017.07.082
9. Tabrizi NS, Yavari M (2020) Fixed bed study of nitrate removal from water by protonated cross-linked chitosan supported by biomass-derived carbon particles. J Environ Sci Health—Part A Toxic/Hazard Subst Environ Eng 55(7):777–787. https://doi.org/10.1080/10934529.2020.1741998
10. Tan XF et al (2017) Biochar as potential sustainable precursors for activated carbon production: multiple applications in environmental protection and energy storage. Bioresour Technol 227:359–372. https://doi.org/10.1016/j.biortech.2016.12.083
11. Wan Ngah WS, Teong LC, Hanafiah MAKM (2011) Adsorption of dyes and heavy metal ions by chitosan composites: a review. Carbohyd Polym 83(4):1446–1456. https://doi.org/10.1016/j.carbpol.2010.11.004
12. Xiang W et al (2020) Biochar technology in wastewater treatment: a critical review. Chemosphere 252:126539. https://doi.org/10.1016/j.chemosphere.2020.126539

13. Zand AD, Abyaneh MR (2020) Adsorption of cadmium from landfill leachate on wood-derived biochar: non-linear regression analysis. Environ Process 7(4):1129–1150. https://doi.org/10.1007/s40710-020-00461-4
14. Zand AD, Abyaneh MR (2020b) Adsorption of Lead, manganese, and copper onto biochar in landfill leachate: implication of non-linear regression analysis. Sustain Environ Res 30(1). https://doi.org/10.1186/s42834-020-00061-9
15. Zhang D et al (2016) Microbes in biological processes for municipal landfill leachate treatment: community, function and interaction. Int Biodeterior Biodegrad 113:88–96. https://doi.org/10.1016/j.ibiod.2016.02.013

Simulation of the Dynamic Behaviour of Pollutants Releasing from a Long Sea Outfall

D. P. C. Laknath, R. N. Udarika, and I. L. Abeygoonasekera

Abstract The present study was carried out to identify the dynamic behaviour of pollutants released from the Wellawatta long sea outfall. Accordingly, dispersive and assimilative capacities of the pollutants, plume directions, plume areas, and critical areas of selected pollutants were identified. Faecal Coliform, BOD5, and Total Suspended Solids (TSS) were selected as the main pollutants. Near-field and far-field simulations were carried out using CORMIX and MIKE 21 modelling systems for the defined scenarios. As the outcome of the near-field simulation, a low concentration of pollutants was identified at the discharge location during the southwest (SW) monsoon with high dilution. From the far-field simulation, the plume dispersion direction for SW monsoon was identified as directed to the north direction, and it was to the south direction for northeast (NE) and inter-monsoon (IM) seasons. Based on the identified critical zones, it was observed that primary and secondary recreational activities are limited during the SW monsoon season due to the presence of larger critical areas off the shoreline. However, recreational activities are desirable during the SW monsoon near the shoreline as isolines of critical zones are not close to the shoreline.

Keywords MIKE 21 · CORMIX · Dispersion · Plume · Critical areas

1 Introduction

Sri Lanka's largest metropolis and commercial capital is Colombo. Being a coastal city, coastal-water-associated recreational activities are popular among tourists in Colombo City. In addition, the fishing industry is an important economic activity in the local community [5]. Therefore, it is crucial to safeguard public health and

D. P. C. Laknath (✉) · I. L. Abeygoonasekera
Lanka Hydraulic Institute Ltd, Katubedda, Sri Lanka
e-mail: chanaka.laknath@gmail.com

R. N. Udarika
Saitama University, Sakura Ward, Saitama 338-8570, Japan

© The Author(s), under exclusive license to Springer Nature Singapore Pte Ltd. 2023

R. Dissanayake et al. (eds.), *ICSBE 2022*, Lecture Notes in Civil Engineering 362,
https://doi.org/10.1007/978-981-99-3471-3_51

environmental well-being in the surrounding areas, beaches, and near-shore waters of Colombo City by maintaining seawater quality at a recommended level. Colombo City's collected wastewater is released into the Indian Ocean through two long, deep-sea outfalls, namely Wellawatta and the Mutwal Outfall. The Mutwal Outfall could be modified, and a new long sea outfall added upon completion of the existing Colombo Port City Development Project and the planned North Port Development Project. As the locations and designs of these outfalls are not finalized yet, the present study examined only the dynamic behaviour of pollutants released from the Wellawatta Sea outfall in terms of health and the environment. Several models are already available to examine how wastewater discharge from point sources affects the environment along the coast [2]. Accordingly, the present study was carried out to simulate the dynamic behaviour of representative pollutants from Wellawatta Sea Outfall and its surrounding areas for representative monsoon climatic conditions using numerical model simulation for the predicted pollution loading in 2030. The main objective was fulfilled by accomplishing the following three sub-objectives: (a) to identify dispersive and assimilative capacities of the discharge location; (b) to identify plume directions and plume area of each representative pollutant; (c) to determine critical areas of the pollutants.

2 Study Area

The existing piped sewer network of Colombo City was constructed between 1906 and 1920. The sewerage system in Colombo City is divided into North and South Catchments and comprises about 320 km long sewers and 18 pumping stations. A large quantity of wastewater in Colombo City is collected through mixed gravity and pump collection and conveyance network system into two main pumping stations, which are located at Madampitiya and Wellawatte. Finally, collected wastewater is discharged to the Indian Ocean through two long and deep-sea outfalls, namely Mutwal (Northern) Outfall and Wellawatte (Southern) Outfall (Fig. 1).

The location of the Mutwal Outfall would change in the future because of the present and anticipated development near the Colombo Port (namely, the existing Colombo Port City Development Project and the proposed North Port Development Project). Therefore, only the impact of the Wellawatte Outfall is taken into account in this analysis. The southwest monsoon primarily controls the wave climate on the west coast (SW). The northeast (NE) monsoon is dominated by northeast winds from December to February, whereas the southwest (SW) monsoon is dominated by southwest winds from May to September in Sri Lanka. The wind pattern changes between the monsoons; inter-monsoon 1 (IM1) (October–November) and inter-monsoon 2 (IM2) (March–April). In this study, the simulations taken into account are the southwest (SW), northeast (NE), and inter-monsoon (IM) seasons.

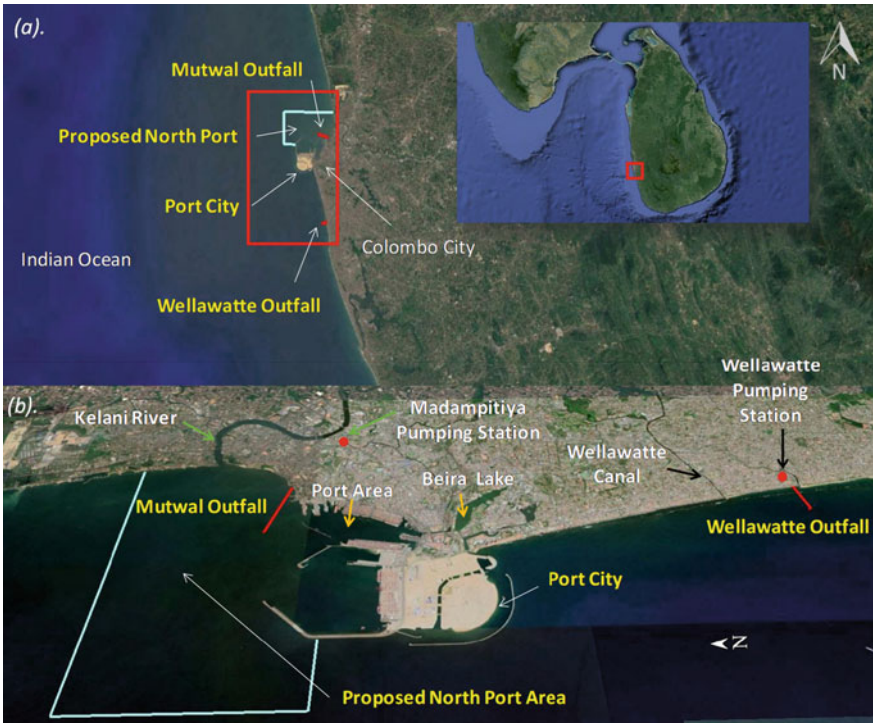

Fig. 1 Study area: **a** Location of outfalls, ongoing/proposed developments in Colombo; **b** Mutwal, Wellawatte Outfalls, and other main pollutant sources

3 Methodology

3.1 Near-Field and Far-Field Models

The hydrodynamics of continuously discharging effluent can be conceptualized as a mixing process occurring in two separate regions. In the first region ("Near-field"), the initial jet characteristics of momentum flux, buoyancy flux, and outfall geometry influence the jet trajectory and mixing. After the effluent flow has interacted with the water surface, bottom, and pycnocline, far-field mixing begins. To understand the dynamic behaviour of pollutants, numerical simulations were carried out for the "Near-Field" and "Far-Field" regions at the diffusers of the Wellawatte Outfall. For the simulation in the near-field region, CORMIX (Version 9.0) the mixing zone model was used. The simulation for the far-field region was carried out by using MIKE 21 modelling system. Subsequent dilutions in the mass uniform body of water in the "far-field" region were simulated by using Hydrodynamic (HD) and Advection-Dispersion (AD) modules of the MIKE 21 modelling system, respectively.

3.1.1 CORMIX Modelling System

CORMIX is a Mixing Zone Model and decision support system for environmental impact assessment of regulatory mixing zones resulting from continuous point source discharges. The system emphasizes the role of boundary interaction to predict steady-state mixing behaviour and plume geometry. In the present study, we used CORMIX2, which contains a system to simulate multiport diffuser discharges. To study the dynamic behaviour of pollutants, Faecal Coliform, 5-day Biochemical Oxygen Demand (BOD5), and Total Suspended Solids (TSS) were selected as the main pollutants. For calculation purposes, sewage is classified as a conservative and nonconservative matter in the present study. Thus, Faecal Coliform was taken as a non-conservative pollutant and BOD5 and TSS were taken as conservative pollutants. In CORMIX simulation, the description of discharge and ambient conditions are specified as input data. The concentration and dilution factors of each pollutant under different climatic conditions in the near-field are calculated as the outcome of the model.

3.1.2 MIKE 21 Modelling System

MIKE 21 HD (Hydrodynamic) module is used to simulate water levels and flow currents. MIKE 21 HD is the hydrodynamic module within the MIKE 21 modelling system. It is based on the numerical solution of total non-linear equations of conservation of mass and momentum integrated vertically.

It is based on the numerical solution of full non-linear equations of conservation of mass and momentum integrated vertically to describe flow and water level variations. MIKE 21 HD setup requires bathymetry, boundary conditions (water level or flow data), initial conditions (water-surface elevations of flux densities), meteorological data, and initial values for the calibration coefficients. In the MIKE 21 HD model setup of the present study, computations were performed on a nested grid setup, starting from a larger regional model and gradually reducing to smaller models while moving towards the area of interest. MIKE 21 AD is the Advection-Dispersion module of the MIKE 21 modelling system for the assessment of the spreading of excess pollutants, subject to advection and dispersion processes due to current or combined wave-current flow. In the present study, the interface discharge boundary conditions for the far-field simulation (MIKE 21 AD) were established using the CORMIX near-field model. Since MIKE 21 AD is a depth-averaged model, appropriate concentration is selected from CORMIX simulation at the mid-depth of the near-field boundary. MIKE 21 AD calculates the dispersion of the dissolved substance on a rectangular grid covering the area of interest based on the hydrodynamic data obtained from a simulation with MIKE 21 HD and the wave parameters calculated by MIKE 21 PMS, together with information about the characteristics of the source and sink. The Advection-Dispersion module solves the so-called Advection-Dispersion equation for dissolved or suspended substances (i.e., mass-conservation equation). The concentration of pollutants, plume areas, directions,

Table 1 Design parameters of wellawatte outfall

Design parameters	Wellawatte
Main pipe (length and diameter) (m)	1243 and 1.5
Diffuser (length and diameter) (m)	122 and 1.5
Ports (No. and diameter) (m)	50 and 75
Water depth at diffuser (m)	15
2030 projected flow (m^3/s)	2.80

and sizes of pollutants in the far field are the main outcomes of the MIKE AD simulation. The same "Bathymetry and Grid Details", "Wind and Wave Boundaries", and "Tidal Boundaries" of the MIKE 21 HD model setup were used in MIKE 21 AD simulation. Details of the grids, bathymetries, and boundary conditions of the MIKE 21 HD and AD models are explained in detail in [4]. In this study, four sources of freshwater/wastewater discharges were incorporated into the local HD/AD model (Table 4). Discharges from Kelani River, Colombo Port Outfalls, Beira Lake, and Wellawatte Canal have been considered as time series and point source discharges as appropriate, and the same conditions in Table 4 were assumed for all seasons due to the data unavailability.

3.2 Design Parameters of the Wellawatte Outfall

For the CORMIX model simulation, the design parameters given in Table 1 were used for the Wellawatte Outfall. The simulation was carried out for the 2.8 m^3/s wastewater loading in 2030 which was assumed based on the projected population in the year 2040.

3.3 Model Scenarios

Based on the "high" and "average" wave conditions of each monsoon, CORMIX, MIKE 21 HD, and AD simulation were carried out for 5 scenarios, representing different combinations of the tide, wind, and wave conditions (Table 2). IM season was selected representing IM-1 and IM-2 seasons. In Table 2, west-south-west, north-west and west directions are denoted by WSW, NW, and W, respectively.

Table 2 Model scenarios

Scenario no	Climatic condition	Tide condition	Wind condition		Wave condition		
			Speed (m/s)	Dir.	Height (m)	Period (s)	Dir.
S1	SW-average	Spring	5	SW	1.4	10.5	WSW
S2	SW-high	Spring	10	SW	2.3	10.5	WSW
S3	NE-average	Spring	4	NW	0.6	10.5	W
S4	NE-high	Spring	8	NW	1.3	10.5	W
S5	IM-high	Spring	8	W	1.7	10.5	WSW

3.4 Concentration of the Pollutants and Other Pollutant Sources

Following the "Sri Lankan standard for tolerance limit values for the discharge of wastewater or effluent into marine waters", treated concentrations of Faecal Coliform were selected [3]. Concentrations of BOD5 and TSS were selected as per Metcalf and Eddy [6]. Thus, assigned discharging concentrations of the selected pollutants are given in Table 3.

In addition to the discharge of the Welllawatte Outfall, the effect of other pollutant sources was considered in the MIKE 21 HD/AD simulation. Accordingly, discharges and pollutant concentrations at 4 locations (i.e., Kelani River, Colombo Port Outfalls, Beira Lake, and Wellawatte Canal) were input to HD/AD models (Table 4). Discharge locations are given in Fig. 1.

Table 3 Concentration of the discharging pollutants

Parameter	Value
Faecal coliform (MPN/100 ml)	10^7
BOD (mg/l)	190
TSS (mg/l)	210

Table 4 Flow rates and concentration of the other pollutant sources

Discharge location	Flow rate (m^3/s)	Faecal coliform (MPN/100 ml)	BOD (mg/l)	TSS (mg/l)
Kelani river	MIKE11 HD Result	6,000	5	14
Port area	0.47	603,750	5	14
Beira	0.23	4,350,000	7	15
Wellawatte canal	4.79	8,000	10	15

4 Results and Discussion

4.1 Dispersive and Assimilative Capacities of the Discharge Location

During the defined scenarios, the dispersive and assimilative capacities of each pollutant were identified based on the outcome of the CORMIX simulations. Mainly, simulated concentration and dilution factor of pollutants at the near field were considered for the analysis. Figure 2 shows the typical output of the CORMIX simulation of Faecal Coliform for the SW-Average condition (S1). As the outcome of the simulation, the excess pollutant concentration distribution of the outfall (diffuser) in the near-field, near-field limit, excess pollutant concentration, and dilution factor at the limit of near-field boundaries were identified. X and Z lines represent the plume centerline and depth, respectively.

Excess concentration and dilution factors of Faecal Coliform, BOD, and TSS after the initial dilutions at mid-depth of the diffusers at Wellawatte Outfalls for SW, NE, and IM seasons are given in Table 5. Compared to the SW-Average case, the concentration of each pollutant for the SW-High case is lower than "average" conditions as dilution is high during the "high" wave and wind conditions. However, for the NE High and Average cases, a high dilution is observed in the NE-Average case. For the IM-High case, the expected dilution factor is between SW and NE high cases, following the wind and wave conditions. Overall, a low concentration of pollutants is identified during the SW monsoon due to the high dispersive capacity resulting from the high wind and wave effects. A high concentration of pollutants was identified during the NE monsoon due to the low wind and wave effects. The

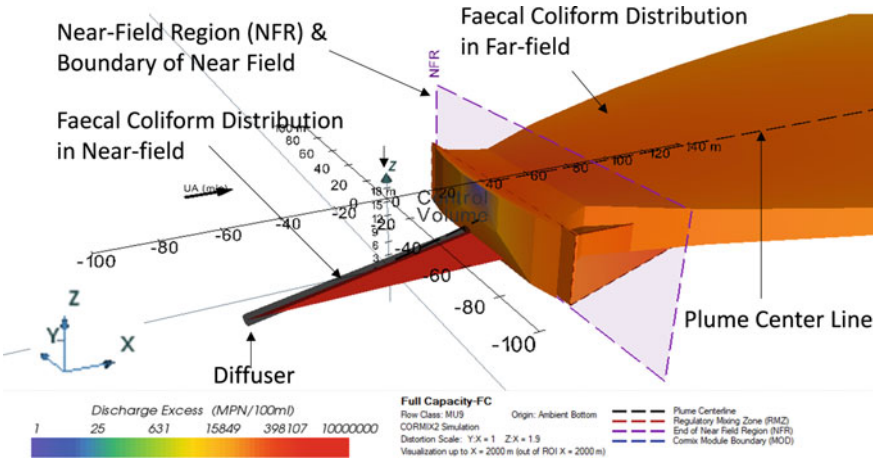

Fig. 2 CORMIX results for SW-average Case (S1): near field region (NFR), and distribution of pollutant (Faecal Coliform) in the near field

Table 5 Excess concentration* and dilution factors** of the pollutants at mid-depth of the diffuser

WQ parameter	SW-high	SW-average	NE-high	NE-average	IM-high
Faecal coliform (MPN/100 ml)	126,328.4* [78.2]**	142,768.6 [68.4]	147,022.2 [66.1]	140,454.9 [66.9]	119,122.3 [71.6]
BOD_5 (mg/l)	2.43 [78.2]	2.78 [68.4]	2.88 [66.1]	2.84 [66.9]	2.65 [71.6]
TSS (mg/l)	2.69 [78.2]	3.07 [68.4]	3.18 [66.1]	3.18 [66.9]	2.93 [71.6]

identified excess pollutant concentrations at the edge near-field boundary are used as input to the MIKE 21 AD model.

4.2 Plume Directions and Plume Area of Pollutant

The secondary dilution after the initial dilution in the near field and the plume behaviour were assessed from the outcome of the MIKE 21 AD results. The concentration of Faecal Coliform, BOD5, and TSS for a selected scenario (SW-High Scenario (S2)) is shown in Fig. 3.

It is clear that the plume has developed only for Faecal Coliform for the Wellawatte Outfall even for the SW-High (S2) scenario which has high wind and wave effects. In the case of BOD and TSS, both pollutants have been diluted instantly, without making a plume. Hence, plume dispersion after the secondary dilution is not significant for BOD5 and TSS. The concentrations of the outside isolines of the plume of Faecal Coliform, BOD5, and TSS are approximately 150 MPN/100 ml, 2 mg/l, and 3 mg/l, respectively. Since the effect of BOD5 and TSS is not dominant at Wellawatte

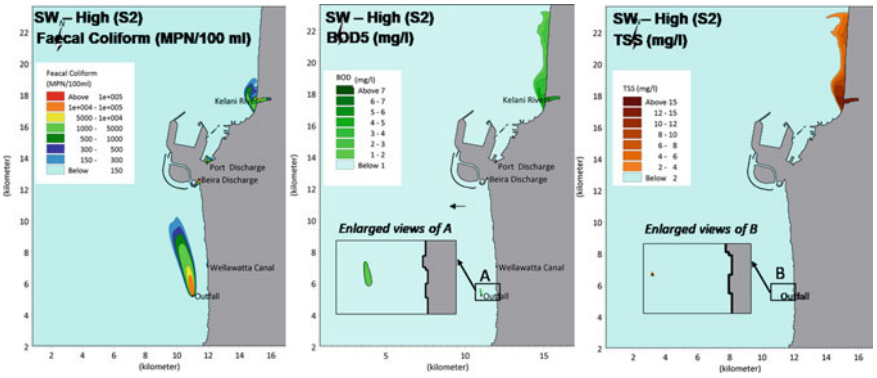

Fig. 3 Concentration of Faecal Coliform, BOD5, and TSS for SW-high case (S2) with other pollutant sources in Table 4 (A and B—Enlarged views of the plume at diffusers of the outfall)

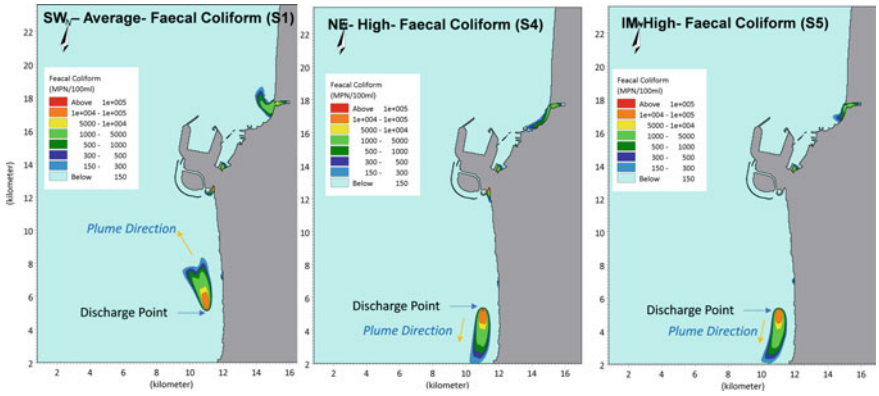

Fig. 4 Concentration of Faecal Coliform for Selected scenarios (S1, S4, and S5)

Outfall, the remaining analysis will be carried out based on the concentration of Faecal Coliform for the defined scenarios in Table 2. Further, with the high value of Faecal Coliform, BOD5, and TSS, a significant effect of pollutant load from the Kelani River is identified.

Concentration and plume behaviours of Faecal Coliform in the selected scenarios (S1, S4, and S5) are shown in Fig. 4. S2 has already been presented in Fig. 3. Further S4 represents S3. Therefore S2 and S3 were not included in Fig. 4. Generally, the plume dispersion direction for all scenarios of SW monsoon is directed in the north direction from the south. In the case of NE and IM seasons, the plume dispersion direction is directed to the south direction. Even though Kelani River is identified as a significant pollutant source, the effect on the plume of Wellawatte Outfall is not affected by Kelani River and other pollutant sources. It is observed that 150 MPN/100 ml isoline of Faecal Coliform does not reach the shoreline in all scenarios, indicating safety for the primary contacts. However, with the considered pollutant sources (i.e., Kelani River, Colombo Port, Beira Lake, and Wellawatte Canal), Faecal Coliform concentration has increased in the neighbouring shoreline areas.

Further, in the S2 Case, 150 MPN/100 ml isoline of Faecal Coliform reached near Colombo Port City (Fig. 3). Moreover, the plume area is significantly larger for the "high" condition of SW monsoon (S2), compared to the "average" case (S1), limiting the recreational activities. Comparing all monsoons, the SW monsoon would have an adverse effect since the duration and plume lengths are longer than NE and IM seasons.

4.3 Critical Areas of the Faecal Coliform

Ambient water quality standards at marine water for "primary contacts" (e.g., swimming) and "secondary contacts" (e.g., boat ride/fishing) tolerance limits were used

to identify the critical areas for safe recreational activities. Accordingly, isolines of Faecal Coliform concentration relevant to 150 and 1000 MPN/100 ml were selected relevant to primary contacts (i.e., frequent direct contact with water) and secondary contact (i.e., less-frequent direct contact with water) limits, respectively [1].

It is desirable to not exceed Faecal Coliform concentration (i) 150 MPN/100 ml for primary contacts (i.e., the suitable area is A) and (ii) 1000 MPN/100 ml (i.e., suitable area is A + B) for secondary contacts respectively for safe recreational activities.

In Table 6, areas of B and C zones for all scenarios (S1–S5) are presented. These areas A, B, and C are illustrated in Fig. 5. With the high areas (7.9 and 1.9 km^2) of zone B and C, it can be observed that primary and secondary recreational activities are limited during the SW monsoon season (S1 and S2) off the shoreline. On the other hand, low areas are identified for NE monsoon, demonstrating safe and desirable conditions for primary and secondary contract activities. Based on generated isolines for Faecal Coliform concentrations, the nearest distances to the shoreline for defined scenarios were measured and tabulated in Table 7.

As seen in Table 7, all isolines are within 1 km of all scenarios. Even though recreational activities are limited due to the larger plume sizes in the SW monsoon, isolines for the SW monsoon are not closer to the shoreline than in other seasons, indicating desirable conditions to carry out recreational activities near the shoreline.

Table 6 Area of Faecal Coliform concentration for selected regions

Regions correspond to Isolines	Area (km^2)				
	SW-high	SW-avg	NE-high	NE-avg	IM-high
Area B (150–1000 MPN/100 ml Isolines)	7.9	5.7	5.5	3.9	5.3
Area C (>1000 MPN/100 ml Isolines)	1.9	1.6	1.5	1.0	1.4

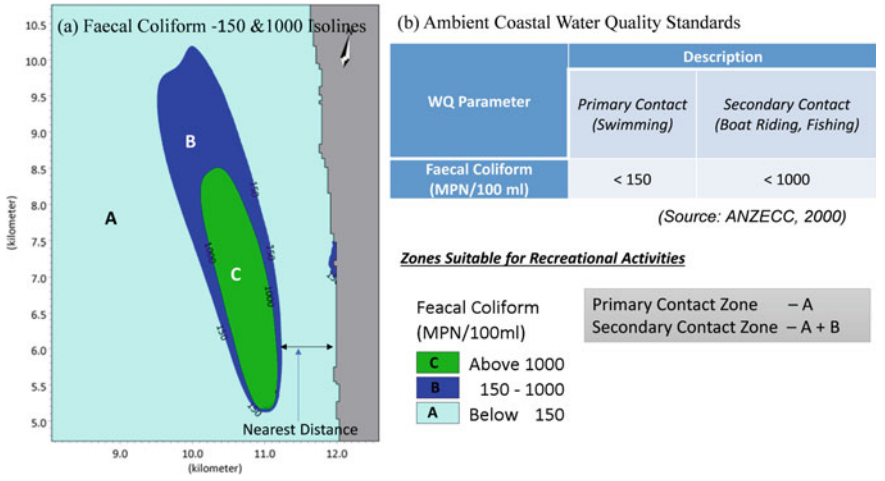

Fig. 5 Critical areas correspond to the isolines of Faecal Coliform and water quality standards

Table 7 Nearest distance from Isolines to the shoreline from 150 and 1000 isolines for Faecal Coliform

Isoline (MPN/100 ml) and recreational purpose	Distance (km)				
	SW-high	SW-avg	NE-high	NE-avg	IM-high
150-primary contact (Swimming)	0.76	0.69	0.55	0.33	0.51
1000-secondary contact—(Boat riding/ fishing)	0.83	0.75	0.65	0.47	0.62

5 Conclusions

The present study was carried out to identify the behaviour of pollutants, released from the Wellawatte long sea outfall. The main objective was accomplished by identifying (a) the dispersive and assimilative capacities of the pollutants at the discharge location, (b) plume directions and plume areas of pollutants, and (c) critical areas of the pollutants. To study the dynamic behaviour of pollutants, Faecal Coliform, 5-day Biochemical Oxygen Demand (BOD5), and Total Suspended Solids (TSS) were selected as the main pollutants. Model simulations were carried out for representative scenarios defined for SW, NE, and IM seasons. Near-field and far-field simulations were carried out using CORMIX and MIKE 21 modelling systems. Mainly, the concentration and dilution factors of pollutants at the near-field were used to identify the dispersive and assimilative capacities of the pollutants at the discharge location. Thus, a low concentration of pollutants was identified at the discharge location during the SW monsoon due to the high dispersive capacity resulting from the high wind and wave effects. A high concentration of pollutants was identified during the NE monsoon due to the low wind and wave effects. From the far-field simulation, it was identified that a plume was developed only for Faecal Coliform and BOD and TSS were diluted instantly, without making a plume. The plume dispersion direction for the SW monsoon is directed to the north direction from the south, and plumes were directed to the south from the north direction for NE and IM seasons. Further, a significant effect of the pollutant load from the Kelani River is identified from the far-field simulation. Based on the identified critical zones for "primary contacts" and "secondary contacts", it can be observed that safe primary and secondary recreational activities are limited during SW monsoon season due to the presence of larger critical areas off the shoreline. However, as 150 MPN/100 ml isolines of Faecal Coliform are not closer to the shoreline than in other seasons for the SW monsoon, desirable and safe conditions in terms of health aspects were identified to carry out recreational activities near the shoreline during the SW monsoon. Since the location is not finalized yet, the impact of Mutwal Outfall in the vicinity of the proposed North Port Development Project and possible discharge from the ongoing Colombo Port City Development Project were not considered for the simulation. Hence, it is recommended to incorporate their impact for future studies for a better understanding of the combined plume effects of the discharge of outfalls.

Acknowledgements The authors wish to acknowledge the "Greater Colombo Wastewater Management Project (GCWMP)" in Sri Lanka.

References

1. ANZECC and ARMCANZ (2000) Australian and New Zealand guidelines for fresh and marine water quality volume 1 the guidelines (Chapters 1–7), ANZECC, Canberra
2. Cebe K, Balas L (2016) W*ater quality modelling in kaş bay*. Appl Math Model 40(3):1887–1913. https://doi.org/10.1016/j.apm.2015.09.037
3. CEA (2004) Proposed ambient water quality standards, central environmental authority, Sri Lanka
4. LHI (2013) Greater Colombo Wastewater management project-design & numerical modeling of Mutwal Sea Outfall, Katubedda
5. Manage PM, Liyanage GY, Abinaiyan I, Madusanka DAT, Bandara KRV (2022) Pollution levels in Sri Lanka's west-south coastal waters: making progress toward a cleaner environment. Region Stud Marine Sci 51:102193. https://doi.org/10.1016/j.rsma.2022.102193
6. Metcalf and Eddy (2004) Wastewater engineering, 3rd edn. McGraw-Hill, New York

Coastal Pollution in Sri Lanka: Perspectives on the Current Status, Policy Implementation, and Institutional Mechanism

D. P. C. Laknath, I. G. I. K. Kumara, and T. U. S. Manamperi

Abstract Coastal Pollution in Sri Lanka was assessed from the perspective of the current status of water quality, policy implementation, and legal/institutional mechanisms. Identification of the status of coastal water pollution is one of the main objectives of this study. Further, the evaluation of the effectiveness of past management policies, strategies, and actions proposed through Coastal Zone Management Plans (CZMPs) and making effective policy recommendations related to coastal water pollution are the other focus areas of this study. The assessment was carried out by analysing the secondary data obtained from different agencies and sources. Thus, the causes and sources of coastal pollution and the current status of coastal pollution in Sri Lanka were assessed. After reviewing the current legal and institutional mechanism, and mitigation measures of coastal pollution, proposals to make effective policies related to coastal water pollution were recommended. Moreover, based on the availability of water quality data, Coastal Zoning for designated uses was preliminary developed for Sri Lanka through this study.

Keywords Water quality · Solid waste · Institutional strengthening · Water zoning

1 Introduction

Sri Lanka is an island country, situated off the southern coast of the Indian subcontinent in the Indian Ocean. Sri Lanka has 1,620 km of coastline, and is abundant with natural resources. The country has 103 rivers and most of the rivers radiate from the central hill's massif and flow into the sea. The coastline is characterized by numerous lagoons and estuaries which are structurally diverse and support multiple uses. The coastal zone of Sri Lanka is a highly productive but fragile ecosystem. The diverse natural ecosystem found within the coastal zone plays an important role in

D. P. C. Laknath (✉) · I. G. I. K. Kumara · T. U. S. Manamperi
Lanka Hydraulic Institute Ltd, Katubedda, Sri Lanka
e-mail: chanaka.laknath@gmail.com

© The Author(s), under exclusive license to Springer Nature Singapore Pte Ltd. 2023

R. Dissanayake et al. (eds.), *ICSBE 2022*, Lecture Notes in Civil Engineering 362,
https://doi.org/10.1007/978-981-99-3471-3_52

the daily lives of people in terms of livelihood, economic output, and food production. However, due to human activity as well as natural processes that take place on land and in the sea, coastlines are extremely vulnerable to degradation. The coastal ecosystem is being degraded due to several causes, including coastal pollution from various sources, such as tourism, one of the country's main revenue earners [3]. Most of the world's coastlines have been found to be polluted, which has a negative impact on marine and coastal fisheries. There can be many reasons for coastal pollution, and it varies depending on the place where it takes place [7]. Coastal water pollution had been identified as one of the major issues in the coastal zones in Sri Lanka and has been addressed respectively through 1997 and 2004 Coastal Zone Management Plans (CZMPs). The basis for addressing the water pollution issues in the coastal regions through previous CZMPs has mainly relied on primary and secondary information gathered from the Southern and Western coastal regions only due to the civil conflicts that predominated in the Northern and Eastern coastal regions over the last four decades. In the areas of the country affected by the conflicts, rapid rehabilitation and other economic development plans have been put in place and are currently being carried out. To identify current and future problems, it is crucial to examine both direct and indirect impacts on the environment and the consequent coastal water pollution issues across the entire country. This new knowledge would be useful for the formulation of effective management policies, strategies, and actions to enable effective coastal zone management. Accordingly, one of the main goals of the current study is to identify the level of coastal water pollution and solid waste issues that are prevalent in the coastal zone. The other primary target areas of this study include evaluating the efficacy of previous management policies, strategies, and actions suggested by CZMPs as well as making sensible policy suggestions about coastal water pollution.

2 Methodology

In compliance with the Coast Conservation Act, this section describes the study area, which is Sri Lanka's coastal zone (Fig. 1). There are also descriptions of data collection and analysis procedures.

2.1 Study Area

The Coast Conservation Act No. 57 of 1981 defines the coastal zone in Sri Lanka for the purposes of coastal resource management (Fig. 2). The region falls within a limit of 300 m landward of the Mean High-Water Line (MHWL) and a limit of 2 km seaward of the Mean Low Water Line, which are the legal boundaries of the coastal area (MLWL).

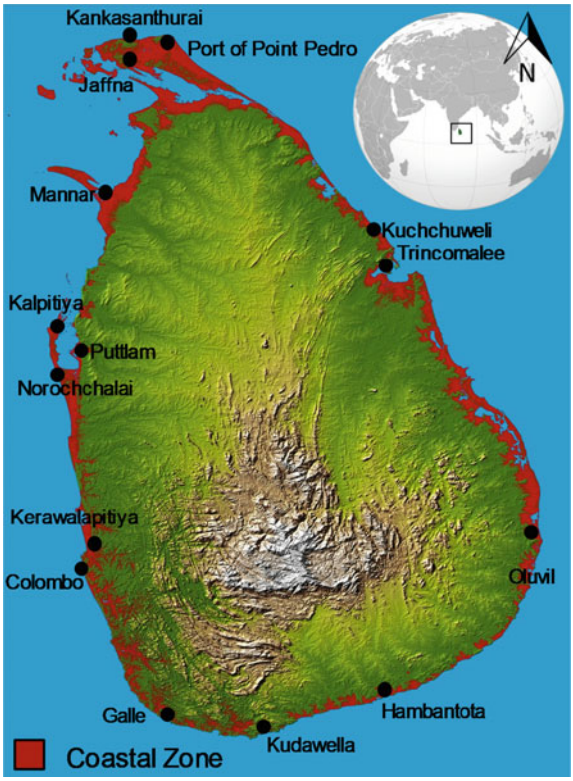

Fig. 1 Coastal zone of Sri Lanka

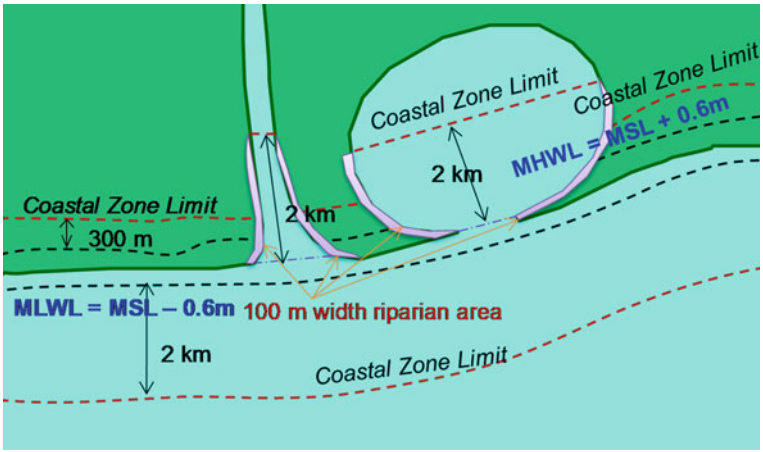

Fig. 2 Definition of the boundaries of the coastal zone

Fig. 3 Sources of coastal pollution: **a** Hikkaduwa beach; **b** Solid waste dumping sites in Mannar; **c** Kudawella Harbour Basin (*Sources* Field Visit, 2014; [2])

The landward border for the water bodies that are periodically or permanently connected to the sea is 2 km long, measured perpendicular to a line drawn through the natural entrance point of the water body to the sea.

2.2 Data Collection and Analysis

Data was gathered from secondary sources and analysed using both quantitative and qualitative techniques to meet the objectives of the study. Wastewater discharges and the disposal of solid waste in or near the coastal zone were taken into consideration as the main sources of coastal water pollution. Further, possible waste generation from recent development plans of the Government of Sri Lanka (GOSL) such as tourism, maritime, and energy hubs, and waste from fishery harbours and anchorages were also considered. In order to gather expected information, all relevant agencies and institutions were identified. Secondary data collection comprised the collection of currently available data and literature relevant to coastal water pollution along the coastal area and general policies and standards implemented under environmental laws. Current CZMP (2004 CZMP was only considered in the present study and 2018 CZMP was not considered in this analysis) in the country and present and past management policies, strategies, and proposed actions were collected for the purpose of evaluating the effectiveness and applicability of the current CZMP in

future developments. In line with research objectives, all available data and gathered information were qualitatively and quantitatively analysed.

3 Results

This section has explored the causes and sources of coastal pollution and how to control coastal pollution in Sri Lanka using the current legislative and institutional framework.

3.1 Causes and Sources of Coastal Pollution

As the main causes of coastal pollution, population growth, urbanization, industrialization, agriculture, aquaculture activities, tourism, oil exploration, development of ports, fishery harbours and anchorages, and thermal power plants were identified. Based on the identified causes of pollution, sources of pollution (i.e. point and non-point sources) such as sewerage, solid waste, and industrial effluent are described in this section. After assessing the growth of the population and urbanization, it was identified that population density has been weighed towards the coastal regions.

Sri Lanka's population has concentrated in large numbers around its coast. Increasing urbanization has caused the density to concentrate in the Western Province [4]. In comparison to the Western and Southern Provinces of Sri Lanka, the population and population densities in the Northern and Eastern Provinces are not as high. With the rapid reconstruction, and other ongoing and proposed economic development programs in the Northern and Eastern Provinces, the population could increase rapidly in both provinces in the future. According to the Sri Lankan 2030 National Physical Plan, 5 metro regions are proposed in the Northern, North Central, Eastern, Southern, and Western regions [5]. Except for the North Central region, the other metro regions are in the coastal region. Therefore, there is a higher tendency for the occurrence of coastal pollution due to future development activities and human activities in these regions. Effluent discharge from factories is one of the major causes of coastal pollution. In general, industrial effluents are discharged to near-shore water that has undergone little or no treatment. Out of all industries of the country, including small, medium, and large-scale industries, it is estimated that 61.6% of industrial units are in the coastal zone. In Sri Lanka, there are 9 Export Processing Zones (EPZ), 3 Industrial Parks (IP), and 1 Export Processing Park (EPP) operated under the purview of the Board of Investment (BOI). Further, according to Sri Lanka 2030 National Physical Plan, 7 EPZs are proposed to be constructed in Northern, Eastern, and Southern Provinces. In the case of the tourism industry, the growth of the tourism industry stagnated as a result of the 30-year-long civil war in Sri Lanka. However, after the end of the civil war in 2009, there is robust growth in the number of tourist arrivals in the country. According to [6], approximately 172

tourist hotels within the coastal zone are registered with the Sri Lanka Tourist Board. As a result of the development of the tourism industry in the coastal zone, there is a high possibility of an occurrence of coastal pollution and degradation of the coastal water quality. This could be a result of untreated sewage, sullage in the form of kitchen and laundry wastewater, and solid waste including plastics. According to the tourism development plan of GOSL, there are new tourism development areas along the coastal zone of the country. Thus, Mannar, Jaffna, Kuchchuweli, and Kalpitiya areas will be developed as new tourism development areas. Further, several locations were identified as Beach-Ocean-based tourism development areas. Presently, Sri Lanka has 7 commercial ports around the Island (Colombo Port, Galle Port, Hambantota Port, Oluvil Harbour, Trincomalee Harbour, Port of Point Pedro, and Kankasanthurai Harbour). All harbours are possible sources of coastal pollution. Oil pollution is the most common mode of pollution identified in these ports. Sewage, wastewater, and ballast water are other pollutant sources related to water pollution in harbour areas. In the case of fishery harbours, at present, there are 22 fishery harbours in operation along the coastal zone of Sri Lanka. Additionally, some fishery harbours (Gandara) and anchorage sites are being developed in the Southern, Northwestern, Northern, and Northeastern parts of the country. Expansion of fishery harbours and fish landing sites contributes to pollution of coastal water (e.g. improper disposal of used oil, waste disposal, improper sewage systems, and fish waste).

Sri Lanka is an agricultural country and uses a larger amount of synthetic fertiliser and chemical pesticides compared to other Asian countries (i.e. 2–8 times more than other Asian countries). Sri Lanka has a river network of 103 rivers. Most rivers spring from the central hills' mountain range and flow out to the coastal areas. Thus, surface runoff of agricultural land carries fertiliser and pesticides to rivers, streams, and lagoons which are connected to the ocean. Synthetic fertilisers and pesticides have non-conservative materials such as Nitrogen (N), Phosphorus (P), and conservative materials (e.g. Persistent Organic Pollutants (POP)). These materials are carried by rivers to the coast. Further, shrimp farming is one of the main areas of the aquaculture industry in Sri Lanka. On the other hand, shrimp farming is the highest threat to the pollution of coastal water in the aquaculture industry. According to Food and Agriculture Organization (FAO) records, Sri Lanka has 1344 shrimp farms. However, 47.7% of shrimp farms are reported to be operating without a proper license. Effluents from shrimp farms have a large content of BOD, Suspended Solids (SS), and nutrients. Shrimp farmers use artificial shrimp food with an additive that contains Chlorine. Chlorine decreases its pH value when a shrimp farm is located in a stagnant water body like a lagoon.

Moreover, farmers use pesticides to prevent the microbial diseases of shrimp. This causes contamination of Persistent Organic Pollutants (POP) in coastal water. Currently, Sri Lanka has three thermal power plants located in the coastal zone (Kerawalapitiya, Puttlam, and Norochchalai). Power Plant uses coal as an energy source. Adverse consequences on the coastal water are anticipated from oil contamination and hot water discharge from the cooling system throughout the development and operation phases.

Sewage can result from point and non-point sources. Out of a population of 20,263,723 people in Sri Lanka, the majority lives in coastal areas. In the year 2012, the population in coastal districts was estimated to be 11,392,903. The generated wastewater in the coastal areas was approximated as 1,822,864 m^3 per day. Domestic generated wastewater quantity in the coastal area is a significant amount, and it is discharged into the coastal zone through canals, drains, and pipes. Among all cities of Sri Lanka, only Colombo has a sewage system. According to the 2004 CZMP, many other cities don't have a proper sewage system. Even though Colombo City has a sewage system, its capacity is inadequate since it has been designed about 100 years ago. Out of a total of 370,000 m^3 of daily wastewater generated in the greater Colombo area, only 90,000 m^3 is discharged through ocean outfalls. The remaining amount of 280,000 m^3 re-enters the environment as wastewater. In the case of rural areas of Sri Lanka, in 2012, it was identified that 3% of the population in rural areas doesn't have sufficient sanitation facilities. Through the radial river system of Sri Lanka, untreated sewage could be carried into the coastal areas. Tourist hotels located in the coastal belt of Sri Lanka discharge wastewater into the coastal zone. In the year 2013, tourist arrivals in Sri Lanka were approximately 100,000 per month and the generated wastewater volume per month was estimated at 19,000 m^3.

Moreover, solid waste is another major source of coastal pollution. Solid waste includes non-liquid garbage and refuse from domestic, institutional, market, medical, commercial, and industrial sources. Discarded organic waste such as food, vegetation, paper, and rubber are also included in this category.

3.2 Current Status of Coastal Pollution

To assess the current status of water quality along the coastal zone of Sri Lanka, the data gathered from 2000 to 2013, from 31 sampling locations, and a study done by the Central Environmental Authority (CEA) on 46 solid waste dumping sites were used. On the basis of the availability of water quality and solid waste data, it was attempted to assess the status and magnitude of the level of coastal pollution. According to the outcome of the water quality analysis data, it was identified that "microbiological" and "oil content" water quality parameters in areas famous for tourism (e.g. Mount Lavinia, Kalutara, Wadduwa, Bentota, Hikkaduwa, Unawatuna, Polhena, and Tangalle) have not met the required standard value for "primary contact" purpose in some seasons. Except for Tangalle, Bentota, and Wadduwa, other sites were identified as suitable for "secondary contact" activities. At several locations, Faecal pollution and oil pollution have mainly resulted from wastewater discharge from tourist hotels. Hence, relevant authorities are required to take immediate action to avoid the release of untreated wastewater into coastal water by tourist hotels. However, except in places like Panama, Arugam Bay, Batticaloa, Passikuda, Vakarai North, Nilaweli, Pigeon Island, and Mandathivu, there are no sufficient water quality data in the Northern and Eastern Provinces to identify the present status of the water quality completely. Out of 46 solid waste dumping sites, more than 80% are

located in the Northern and Eastern Provinces. A higher number of these sites are owned by local authorities. Approximately, 95% of the dumping sites operate without having environmental approval. Most dumping sites are open dumping sites and operate freely without undergoing any solid waste management system. Out of all dumping sites, only 4% of sites use bare land as dumping sites. Other sites are located in wetlands and marshy lands, leading to the destruction of these wetlands and increasing the leachate contamination with coastal water.

3.3 Legal and Institutional Mechanisms

The relevant existing laws for Sri Lankan coastal pollution control include the National Environment Act, No. 47 of 1980, National Environmental (Amendment) Act, No. 56 of 1988, National Environmental (Amendment) Act, No. 53 of 2000, Marine pollution prevention Act, No. 59 of 1981 and its amendment No. 35 of 2008, Coast Conservation Act No. 57 of 1981 and amendment of 1988 and Coast Conservation (Amendment) Act, No. 49 of 2011. There are over 40 laws relating to water resources in Sri Lanka in different aspects. The Coast Conservation Act, No. 57 of 1981, which came into operation in 1983, defines the Coastal Zone as 300 m landwards from the high waterline and 2 km seawards from the low water line, where it also states that any development activity within the coastal zone, e.g. buildings, hotels, and houses, has to be constructed after obtaining a permit from the Coast Conservation Department (CCD) (currently CC and CRMD). The Coast Conservation Act, No. 57 of 1981, specifies that a permit has to be obtained from the CCD for any development activity in the coastal zone. There is no necessity to pass any laws or gazette notifications if one abides by this Act. The Coast Conservation Department should take a leading role in this matter and inform all concerned parties and take immediate action. This act was amended in 2011 as Act, No. 49 of 2011. The requirement of the amendment is due to the inadequacy of previous regulations and to take preventive actions in order to stop any repetitions or to control offenders of the right.

The control of coastal pollution is not a responsibility of a single institution or an individual. Many people contribute to protecting the coastal environment of Sri Lanka. Mainly Central environmental authority (CEA) and Coast Conservation and Coastal Resource Management Department (CC & CRMD) are involved in these activities. There are a number of institutions at national and local levels responsible for coastal and marine resource management. At the national level, there are policy-making bodies such as the Ministry of Fisheries and Aquatic Resources Development (MF & AR) and Ministry of Environment and Renewable Energy (ME & RE), implementing agencies such as the CC & CRMD, CEA, Marine Environment Protection Agency (MEPA), National Aquatic Resources Research and Development Agency (NARA), The Department of Wildlife Conservation (DWLC), and Forest Department (FD). At the provincial level, there are Provincial Councils and at the local level, there are Divisional Secretariates and Local Authorities. The overall responsibility is the

management and protection of resources within the coastal zone except for fisheries and aquatic which is lying within the CC & CRMD, coming under the purview of the Ministry of Defence (MOD) and Urban Development Authority (UDA). This responsibility of the CC & CRMD is a centralized function and therefore encompasses the entire Sri Lankan coastline.

Policies, regulations, standards, and implementation procedures have been formulated for controlling coastal pollution in Sri Lanka. There are several policies (e.g. National Environment Policy, Cleaner Production Policy, National Watershed Management Policy, National Policy on Wetlands, National Biosafety Policy, National Land Use Policy, and National Policy on Solid Waste Management) that relate to coastal pollution control. These policies are controlled by several institutions.

4 Discussion

Controlling and mitigation measures and proposals for coastal pollution, institutional strengthening, and review of previous CZMPs have been discussed in the discussion. Further, preliminary developed coastal water zoning for designated uses is presented in this section.

4.1 Controlling and Mitigation of Coastal Pollution

The impact of land-based pollution was found to be significant when compared to marine-based pollution. Development and human activity in both coastal and non-coastal locations are the main cause of this. There is a chance that the proposed development activities could worsen the coastal pollution in coastal zones. Therefore, during the implementation and operational phases, appropriate mitigating and preventive measures must be taken. Even while numerous coastal water bodies have been contaminated by organic and inorganic pollutants, corrective measures have been implemented at a limited number of locations. Hence, mitigation and restoration actions must be taken at the national, provincial, and local levels. It was determined that in the Northern and Eastern Provinces, there are insufficient water quality data to determine the current status of the water quality. Therefore, it is advised to implement ongoing programs for measuring and monitoring the quality of the water in these areas to ascertain and track the pollution levels brought on by nutrients, agrochemicals, industrial effluents, and organic and inorganic waste. Additionally, water quality mapping is advised, particularly in existing or future tourist areas. It is proposed that SEA be conducted for the identified industrial areas. Further, mineral extraction sites such as Pulmudai are required to monitor for mitigating possible coastal pollution. Especially, for the Northern and Eastern provinces of Sri Lanka, proper solid waste management systems and sanitation facilities are essential to reduce coastal pollution with new human settlements and proposed development activities. As there is water

pollution (e.g. eutrophication due to high nutrient levels) identified in main lagoons in Sri Lanka, it is recommended to carry out immediate water quality restoration programs to improve water quality in affected coastal lagoons and river estuaries. Further, proper water quality indices should be developed to enable the ranking of coastal water resources. Since existing water quality data is not sufficient to evaluate the status of coastal pollution in all coastal areas of the country, water quality measurement and monitoring programs are required to carry out at the national level by relevant parties to evaluate the current water quality situation of the coastal water in Sri Lanka.

4.2 Institutional Strengthening and Review on Previous CZMPs

Controlling coastal pollution requires institutional strengthening at the organizational and legal levels. To combat pollution from both point and non-point sources, efficient policies and implementation strategies are also required. Sri Lanka, one of the island states with a CZMP in place at the national level, had a number of issues with its existing coastal policies and regulations. This failure is due to a number of reasons, including poor communication, lack of understanding of regulations among many stakeholders, and lack of clarity over responsibilities shared among different levels of the government. The application of some rules pertaining to new construction in the coastal zone, as per the regulations of the CC & CRMD, former CCD, is still up for debate. Therefore, introducing zoning regulations based on a coastal vulnerability index that takes into consideration the size and density of human settlements as well as the varied coastal geomorphology may be a better alternative. Another consideration is whether the implementation of more place-specific coastal regulations (e.g. Special Area Management (SAM)) could be devolved to local governments. Thus, the existing CZMP requires more improvements in their lacking areas such as

- Promoting formulation of effluent discharge standards for development activities that have not been addressed in the environment protection act.
- Water quality monitoring is essential in the near-shore coastal region, because there is no single institution mandated with legal responsibility for regular water quality monitoring in the near-shore coastal water yet.
- Participation by local officials and coastal communities must be strengthened.

4.3 Coastal Water Zoning for Designated Uses

Zoning techniques can be applied to coastal areas for several objectives, including preserving natural habitats, ensuring public access to the shore, and boosting tourism. Zones are a useful tool for separating various conflicting uses and reducing user

problems. To prevent pollution in sensitive parts of the coastal system, it is necessary to divide it into different zones, each with its own designated use and related quality standards [1].

Based on available water quality data, preliminary coastal zoning for designated uses was developed in the current study. These beneficial uses are identified in response to present prevailing practices and anticipated practices in the near future. Defined coastal zones and slightly identified varied uses of coastal water, including tourist, nature conservation, fisheries for shellfish, fisheries for finfish, and non-consumption uses are shown in Fig. 4. At other remaining significant areas along the coastline, the developed zoning has to be further extended with more water quality parameters.

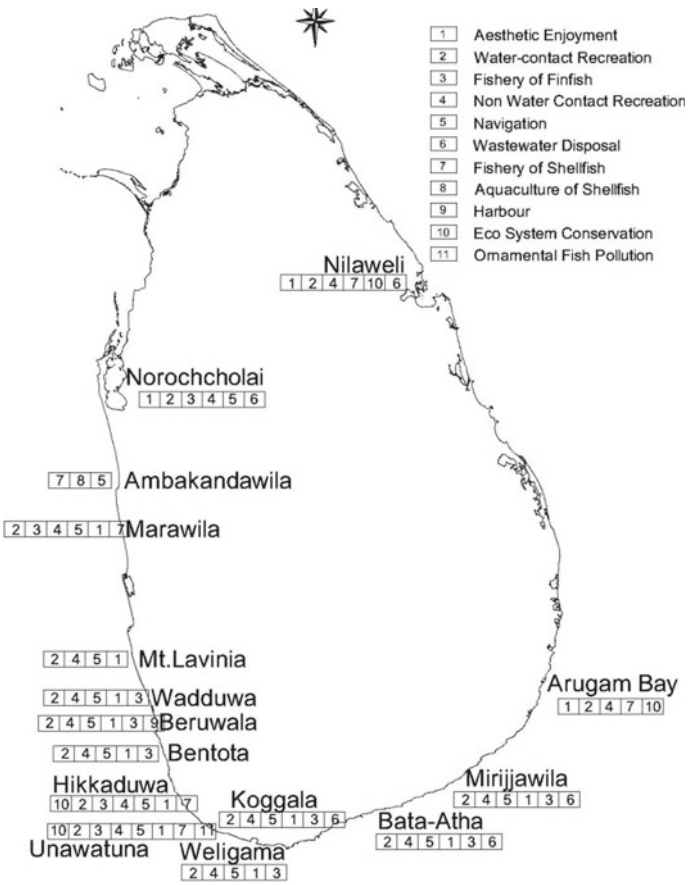

Fig. 4 Coastal zones in Sri Lanka for designated uses

5 Conclusions

In this study, coastal pollution in Sri Lanka has been evaluated from the perspectives of the existing water pollution status, policy implementation, and legal and institutional procedures. Accordingly, the status of coastal water pollution and solid waste problems confronted within the coastal zone together with different sources and causes of coastal pollution was identified. As main causes of coastal pollution, population growth, urbanization, industrialization, agriculture and aquaculture activities, tourism, oil exploration, development of ports, fishery harbours and anchorages, and thermal power plants were identified. As the sources of pollution (i.e. point and non-point sources), sewerage, solid waste, and industrial effluent were identified. With the proposed development activities of the Government of Sri Lanka (GOSL), there is a possibility to intensify the coastal pollution in coastal zones of the country. Therefore, suitable mitigation and preventive actions must be taken during the implementation and operational stages. It was identified that remedial actions for coastal pollution have been taken only in a few places in Sri Lanka. Hence, mitigation and restorative measures must be implemented at the national, provincial, and local levels.

On the basis of available water quality and solid waste data along the coastal zone of Sri Lanka, the status and magnitude of the level of coastal pollution were assessed. However, except in places like Panama, Arugam Bay, Batticaloa, Passikuda, Vakarai North, Nilaweli, Pigeon Island, and Mandathivu, there are no sufficient water quality data in Northern and Eastern Provinces of the country to identify the present status of the water quality. Therefore, it is recommended to carry out continuous water quality measurements and monitoring programs in these areas to determine and monitor the levels of pollution. It was identified that "microbiological" and "oil content" water quality parameters in famous tourist areas (e.g. Mount Lavinia, Kalutara, Wadduwa, Bentota, Hikkaduwa, Unawatuna, Polhena, and Tangalle) have not met the required standard value for "primary contact" purpose. For the identified industrial areas, it is proposed to carry out Strategic Environmental Assessment (SEA). Further, mineral extraction sites such as Pulmudai are required to monitor to mitigate possible coastal pollution. Moreover, for the North and East provinces of Sri Lanka, proper solid waste management systems and sanitation facilities are essential to reduce coastal pollution with new human settlements and proposed development activities.

After reviewing the existing institutional and legal framework, it was recognized that many agencies and authorities contribute to protecting the coastal environment in Sri Lanka. Mainly Central Environmental Authority (CEA) and Coast Conservation and Coastal Resource Management Department (CC & CRMD) involve in these activities. Further, there are a number of institutions at national and local levels responsible for coastal and marine resource management. At the national level, there are policy-making bodies, and implementing agencies. At the provincial level, there are Provincial Councils and at the local level, there are Divisional Secretaries and Local Authorities. The overall responsibility for the management and protection of resources within the coastal zone except for fisheries and aquatic lies within the CC &

CRMD, coming under the purview of the Ministry of Defence (MOD) and Urban Development Authority (UDA).

Additionally, the effectiveness of previous management policies, strategies, and actions related to coastal water pollution proposed through CZMPs was assessed. It was identified that existing coastal policies and regulations suffered from numerous shortcomings, resulting due to communication problems, unawareness of regulations by many stakeholders, and a lack of clarity over responsibilities shared among different levels of government. After examining the current institutional and legislative framework, it was identified that institutional strengthening in both terms of organization and law is required to control coastal pollution. Accordingly, effective policies and implementation mechanisms are needed to address pollution from both point and non-point sources. Thus, implementation of more place-specific coastal regulations (e.g. Special Area Management (SAM)) can be devolved to local governments. Further, the importance of maintaining collaborative efforts on the part of government agencies, NGOs, and local communities is identified to address the root causes of environmental degradation in the coastal zone. Moreover, coastal zoning for designated uses was preliminary developed for Sri Lanka in this study to prevent pollution in sensitive parts of the coastal system.

Acknowledgements The Department of Coast Conservation and Coastal Resource Management (DCC & CRM) is gratefully acknowledged by the authors for their various support.

References

1. GOSL-G-9120 (2008. Government of Sri Lanka. The gazette of the democratic socialist republic of Sri Lanka G-9120 I – I, environmental protection licensing scheme, national environmental act no.47 of 1980, Government Press, Colombo.
2. Laknath DPC, Sasaki J (2011) Assessment of the tsunami rehabilitated fishery harbors in Sri Lanka. J Coast Res 64:1245–1249
3. Lowry K, Wickremeratne HJM (1988) Coastal area management in Sri Lanka, Ocean Year Book 7, University of Chicago, pp 263–293
4. Manage PM, Liyanage GY, Abinaiyan I, Madusanka DAT, Bandara KRV (2022) Pollution levels in Sri Lanka's west-south coastal waters: Making progress toward a cleaner environment. J Coast Res 51:102193. https://doi.org/10.1016/j.rsma.2022.102193
5. National Physical Planning Department Staff (2011) "Sri Lanka 2011–2030 national physical plan and project proposals"., National physical planning department, Battaramulla
6. SLTDA (2014) Annual statistical report, research & international relations division, Sri Lanka tourism development authority, Colombo
7. Vikas M, Dwarakish G (2015) Coastal pollution: a review. Aquat Procedia 4:381–388

Experimental Investigation of Debris Transport Due to Extreme Hydrodynamic Flows Induced by Tsunami

N. R. Josiah, S. Araki, and D. P. C. Laknath

Abstract Entrainment of floating objects and their impacts in disaster-prone coastal areas were well-observed phenomena during the forensic surveys of the aftermath of extreme coastal disasters such as tsunamis. The impacts of floating objects have not been very well understood recently. This paper presents a series of hydraulic experiments conducted with the various arrangements of cuboid elements subjected to disparate dam break waves to identify the behaviour of the movements and resultant dispersion over a mildly sloped bed. The motion of the cuboids was tracked through a high-speed camera to estimate the moving velocity of the debris and to identify the trajectories. Results indicated that the velocity of the debris was predicted with reasonable accuracy compared with the empirical formulation. Also, debris transport could be expressed as a normal distribution, symmetrically dispersed over the plane. Furthermore, it was observed that the initial configuration parameter and flow characteristics played a crucial role in debris transport modes.

Keywords Tsunami · Debris transport · Dam break · Hydraulic experiment

1 Introduction

As witnessed in the recent past, residential and building facilities are frequently vulnerable to severe natural hazards like tsunamis and typhoons in disaster-prone coastal regions around the world. Forensic surveys of aftermath disasters such as the 2004 Indian Ocean tsunami, the 2011 Tohoku tsunami and the 2018 Indonesian tsunami [1, 2] have shown that waterborne objects hindered the public's escape during the evacuation. Further, their interactions with onshore structures led to partial or complete damage. Therefore, an investigation of the dynamics of entrained objects

N. R. Josiah (✉) · S. Araki
Department of Civil Engineering, Osaka University, Osaka, Japan
e-mail: renee_josiah@civil.eng.osaka-u.ac.jp

D. P. C. Laknath
Lanka Hydraulic Institute Ltd, Moratuwa, Sri Lanka

© The Author(s), under exclusive license to Springer Nature Singapore Pte Ltd. 2023

R. Dissanayake et al. (eds.), *ICSBE 2022*, Lecture Notes in Civil Engineering 362,
https://doi.org/10.1007/978-981-99-3471-3_53

and their consequent mechanisms is essential to propose proper disaster management plans during the devising stage of construction projects in coastal areas.

Naito et al. [3] provided basic guidelines to categorise and analyse the availability of debris in a coastal area and the possible modes of damage based on the 2011 great east Japan tsunami survey data. The same study also determined conservative estimations of maximum dispersion angles (i.e. $\pm 22.5°$) based on the initial and final locations of the objects. However, the suggested formula by [4] indicates that the dispersion angle is significantly lower in laboratory settings compared to [3]. Shafiei et al. [5] studied the characteristics of floating debris by embedding accelerometers and came up with an empirical formula for debris velocity. Furthermore, Stolle et al. [6] conducted hydraulic experiments and expressed that debris transport depended on hydraulic characteristics, properties of the fluid, material properties of debris and their configurations. Moreover, the hydraulic experiments of [7], with varying dimensions of debris under a fixed trajectory, proposed combinations of mass and flow conditions for the movement of debris to make an impact with an obstacle. However, the stochastic nature of debris entrainment was not examined by [7]. Similarly, previous literature suggested that assessment of debris transport in the lower hydraulic scale models for various tsunami-like boundary conditions is almost non-existent. At the same time, there is a need for rigorous experimental data sets to calibrate and validate future numerical models.

Therefore, this study focused on analysing the debris transport in an idealised laboratory setting to divulge the debris transport patterns of cuboid objects subjected to various hydrodynamic boundary conditions to identify their driftage path and moving velocity. Further, the lateral dispersion of debris was tracked to estimate dispersion angles and standard deviations to propose a suitable data distribution function.

2 Methodology

2.1 Experiment Setup

Experiments were performed at the two-dimensional wave flume facility of the Department of Civil Engineering, Osaka University, Japan (Fig. 1). The wave tank is 44 m long, 0.7 m wide and 1.2 m high. In order to aid wave propagation and the experimental plane, parts of the flume with slopes of 1/40 and 1/100 were included. A gate was installed at a distance of 7.9 m to create a reservoir to impound different volumes of water to generate dam-break waves by swiftly lifting it.

This experimental setup was employed with wave gauges placed along the centre-line to measure the variations of water surface elevations in the pre-determined locations. Further, a digital camera (C_1) having high-speed video mode was installed to track the debris motion over the flume bed. Video mode has a frame size of 640×480

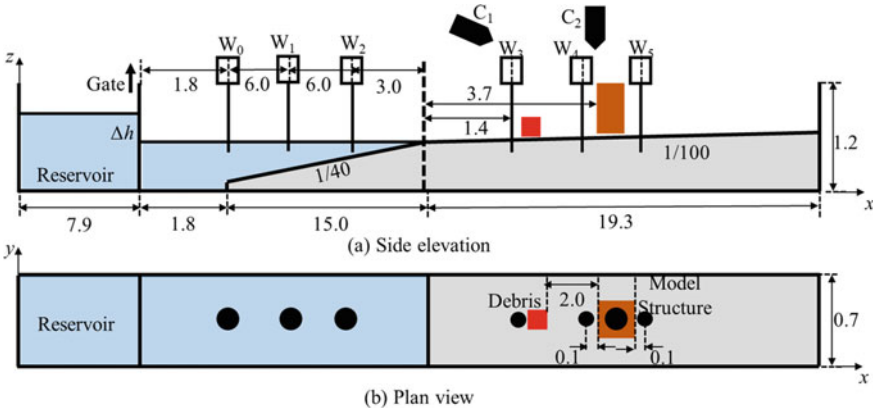

Fig. 1 Schematic diagram of the experimental setup (All dimensions are in meters; not to scale)

pixels with a sensor output of 200 *fps*. Grids of 0.05 m × 0.05 m were delineated in the flume bed to quickly reference the coordinates and point out the debris locations during the analysis.

A scale of 1:100 was decided upon for the experiments based on the measured hydrodynamic parameters during preliminary tests and the available geometries. To study the transport of debris, a scaled-down version of 3.0 m (20 *ft.*) shipping containers made of solid smooth wood was used. Each object is 0.06 m in length and has an equivalent width and height of 0.024 m. Every object has a density of 462 kg/m^3 with a draught of 0.012 m. Water-resistive paint was applied on the surface of the objects to minimise water absorption during the experimental runs. After each run, the surface of the debris was adequately wiped and dried before commencing the next run. In all cases, the cuboid was placed along the centreline, where the length was normal to the flow direction (Fig. 2). Moreover, a square-prism-shaped obstacle (0.1 m length × 0.1 m width × 0.25 m height) was installed at a distance of 2 m to observe the debris-structure interaction.

Figure 2 shows the configurations considered in this study to evaluate the debris entrainment. In this study, the characteristics of Fig. 2a are analysed in detail. Further, comparisons were made for other configurations Fig. 2b–e, with respect to Fig. 2a in terms of dispersion.

2.2 Experimental Procedure

First, water was filled to an initial water level of 0.440 m, and the gate was closed. Then, subsequently, water levels listed in Table 1 were regulated at the reservoir to generate dam break waves by quickly lifting the gate. Dam break wave is considered one of the better representations of a generation of tsunami-like waves in laboratory

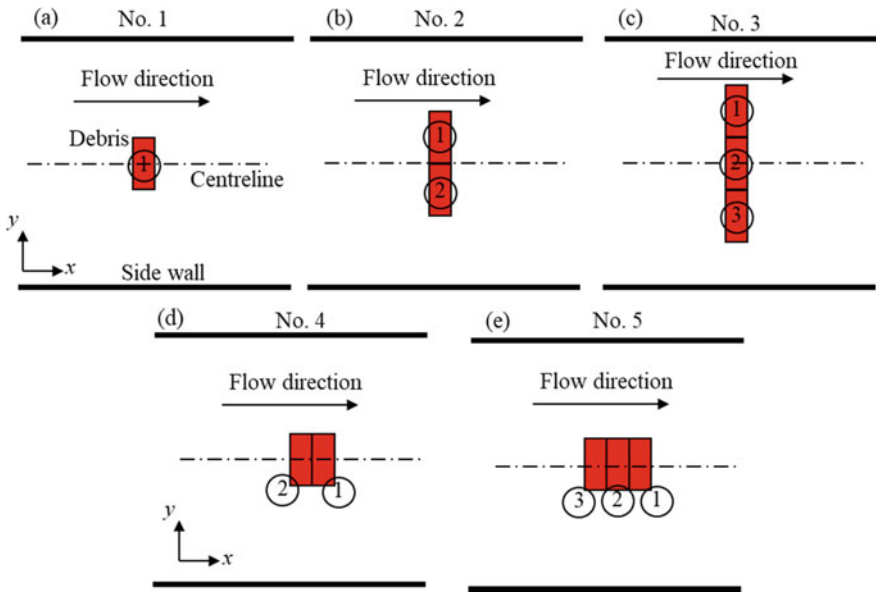

Fig. 2 Arrangements of debris over the flume bed

Table 1 Characteristics of boundary conditions

Case No	Dh (*m*)	Reservoir WL (*m*)
I	0.100	0.540
II	0.120	0.560
III	0.150	0.590
IV	0.170	0.610

conditions [8]. This procedure is reiterated for all test cases by removing and refilling the determined water depths. Each experimental case was repeated five times to maintain the accuracy of the hydrodynamic environment and to observe various patterns of debris transport.

2.3 Analysis

2.3.1 Flow Velocity

Due to the varying local velocity around the vicinity of the debris, the concept of the velocity of the moving bore (1) was established as outlined in [7] to surrogate the variations of local velocity. This was estimated using the gauges in front of the debris (W_3) and in front of the obstacle (W_4). From that, the relationship between

the velocity of the moving bore (c) and inundation depth (d) was found. This was employed to determine the Froude, Reynolds and Weber numbers to distinguish the flow type around the debris and near the obstacle.

$$c = \alpha.\sqrt{gd} \tag{1}$$

herein, g is the gravitational acceleration and α is a constant.

2.3.2 Debris Movement

An open-source object tracking algorithm based on the OpenCV library [9] was utilised to determine the locations of the centroid of the moving cuboid. Video data was manually processed frame by frame by geo-referencing the coordinates of delineated grids on the flume bed. Displacement along the x and y directions and the time series of the velocity of the debris along the x-direction were obtained. Using this data, the correlation of lateral and longitudinal displacements was investigated.

3 Results and Discussion

3.1 Hydrodynamic Environment

Figure 3 a and b shows the variation of water depths in front of the debris (W_3) and the obstacle (W_4) respectively. Maximum water surface elevations varied between 0.022 m and 0.050 m in front of the initial location of the debris. Similarly, the highest water depth in front of the structure was between 0.032 m and 0.095 m.

The measured maximum inundation depths at W_4 and the estimated moving bore velocities (1) were correlated. From that, it was found that α of Eq. (1) was 1.68. Based on this, Froude, Reynolds and Weber numbers were calculated for each experimental case. By considering the maximum water depths and the calculated moving bore velocities, flow characteristics were identified as supercritical turbulent flows. Further, Weber numbers significantly exceeded the critical value specified for the smaller-scale experiments, indicating that the effects of surface tension generated around the debris and around the obstacle could be negligible [10].

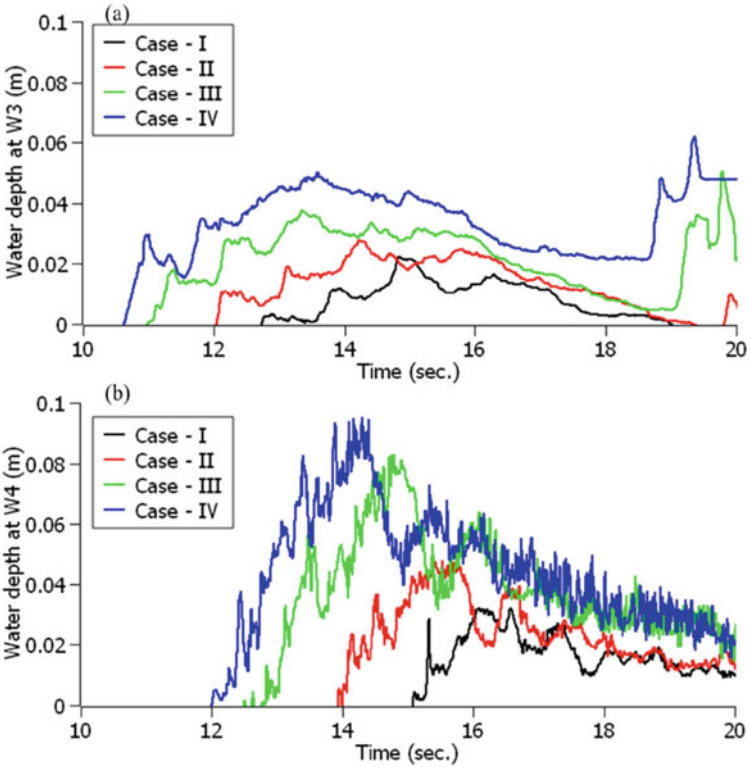

Fig. 3 Variations of water depths. **a** at W_3 and **b** at W_4

3.2 Transport of Single Debris

3.2.1 Velocity of the Debris

The velocity of the debris was estimated using the object tracking algorithm. Figure 4 shows the estimated velocity for each flow condition for debris configuration No.1 (Fig. 2a) using the detection algorithm. Detected velocities were compared with the empirical formula (2) of [5].

$$u_d(t) = c - \left(\frac{C_d \rho A}{2m}.t + \frac{1}{c}\right)^{-1} \tag{2}$$

where c is the velocity of the moving bore, C_d is the drag coefficient, ρ is the density of water, A is the area of debris in the flow direction, m is the mass of the debris and t is the debris travel time.

Equation (2) was derived based on the assumptions such as debris transport begins after the leading bore wave passes the debris and the velocity behind the wave is

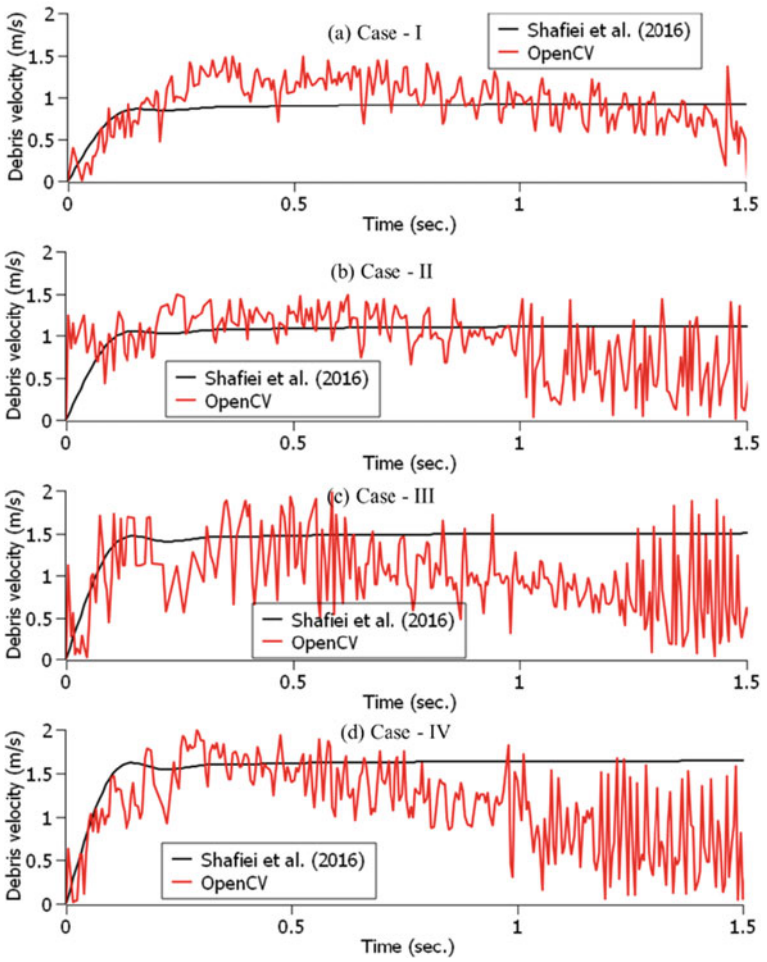

Fig. 4 Comparisons of the velocity of the single debris

constant. Therefore, the maximum debris velocity attained the equivalent value of c (1) by giving adequate time for the surge to proceed.

However, detected velocities of the moving debris showed fluctuating velocities. Even though it was adapting a similar profile of Eq. (2) at the beginning of the entrainment process, the fluctuations began to occur with the longitudinal displacement of debris. In general, the low flow conditions (i.e. Cases *I* and *II*) showed a lower discrepancy with the empirical formula (2). But, the high flows (i.e. Cases *III* and *IV*) indicated a series of significant undulations with time. This might be caused due to the increment in moving surge-induced drag and rotation on the debris. Further, the splashing surge on the surface of the debris and the lag between the surge tip and the debris might also have caused the inconsistency. Overall, it can be said that the

detection algorithm captured the debris velocity with reasonable accuracy compared to Eq. (2). However, a numerical investigation is needed to evaluate the outcomes of both the empirical formula (2) and the capabilities of the detection algorithm of this study.

3.2.2 Displacement of the Debris

The variation of displacement of single debris (Fig. 2a) is shown in Fig. 5. As can be seen, a higher deviation occurred with the increment in the travelling distance. The dispersion angle (±22.5°) of [3] and the proposed formula (3) of [4] were enclosed in Fig. 5 to get the qualitative comparison. Observations indicated that experimentally obtained displacements were well agreed with Eq. (3)

$$\pm\theta = \pm 3.69 \pm 0.80N \tag{3}$$

where θ is the dispersion angle in the lateral direction and N is the number of debris.

Further, the standard deviations (4) of lateral displacement (in the y-direction) were calculated. Figure 6 shows the estimated standard deviations over the travel distance of 2.0 m in the longitudinal (x) direction in steps of 0.5 m. As indicated in Fig. 6, a monotonic increase of standard deviation with the increment in the longitudinal direction was observed.

The lowest flow condition (i.e. Case *I*) indicated a lower standard deviation among all cases. Case *II* showed that the standard deviations were lower for a considerable distance along the longitudinal direction ($x < 1.5$ m). However, towards nearing the obstacle higher deviations were observed. Compared to Case *I*, Case *II* showed quite an increase in standard deviations. However, the largest flow conditions (i.e. Cases *III* and *IV*) indicated higher standard deviations compared to the other two flow conditions.

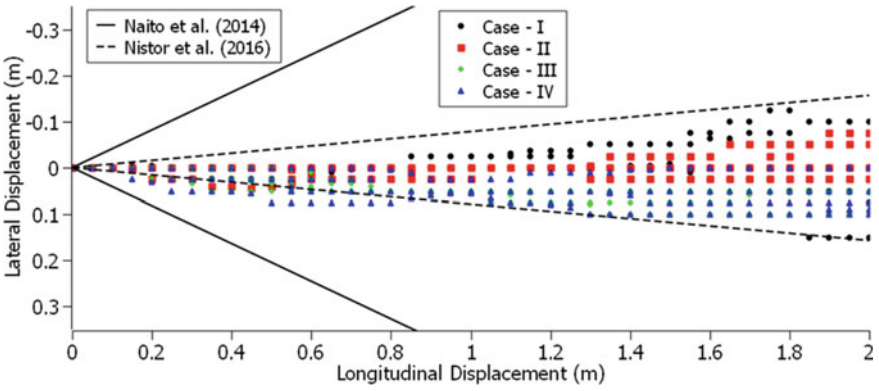

Fig. 5 Displacements of centroid of the cuboid

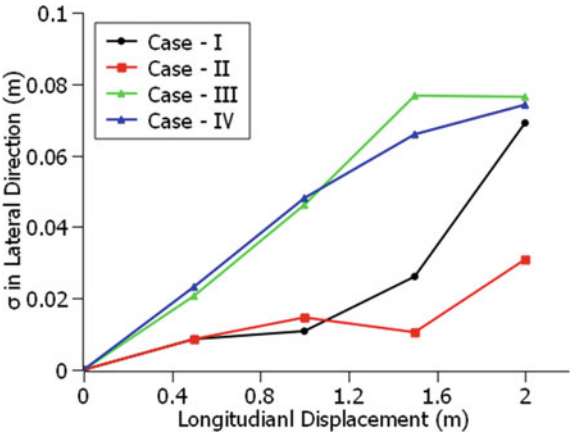

Fig. 6 Standard deviation along the lateral direction

According to the experimental observations, the contact between the flume bed and the debris surface tended to generate wakes around the debris rotate and deviate from the intended trajectory (i.e. $\overline{\delta y} = 0$). Nevertheless, the increment in the turbulent behaviour of fluid due to the interaction with the placed structure also caused the higher deviation that occurred in the region $x > 1.5$ m.

$$\sigma = \sqrt{\frac{1}{n}\sum \left(\delta y - \overline{\delta y}\right)^2} \tag{4}$$

$$P(x, y) = \frac{1}{\sigma\sqrt{2\pi}}.e^{\left[-\frac{(\delta y - \overline{y})^2}{2\sigma^2}\right]} \tag{5}$$

$$CI_{95\%} = \overline{\delta y} \pm z_{95\%}\left(\frac{\sigma}{\sqrt{n}}\right) \tag{6}$$

here, δy is the displacement in the y-direction, $\overline{\delta y}$ is the mean displacement, $P(x,y)$ is the probability distribution of lateral displacement along the longitudinal displacement, CI is the confidence interval and z is the standard value from the z-table.

The lateral displacements from the initial location were counted from all experimental runs and the plotted frequency histogram is shown in Fig. 7. The same histogram is also enclosed with the curve of theoretical probability distribution (5). As calculations indicate, the lower flow conditions (i.e. Cases *I* and *II*) showed the best fit with a very good match with the experimental values for all longitudinal (x) distances. However, the higher deviation occurred for, the larger flow conditions (i.e. Cases *III* and *IV*), causing debris to deviate from the intended trajectory after $x >$ 1. 0 m, not given an exact match with the theoretical distribution. Nevertheless, it can be said that the theoretical distribution (5) could be applied to predict the lateral dispersion of the debris.

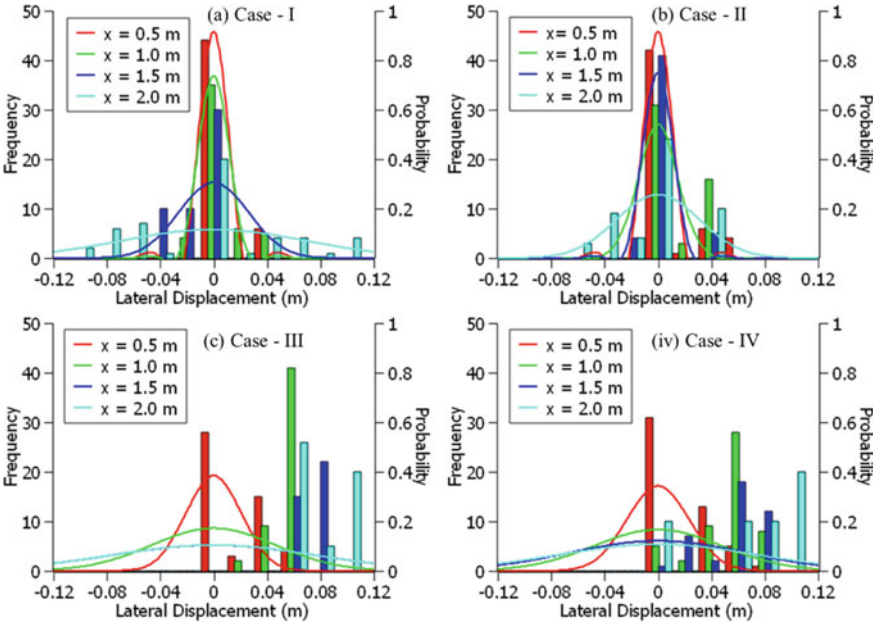

Fig. 7 Histograms of lateral displacement of debris

Moreover, Fig. 8 shows the mean trajectory of the centroid of the debris for each experimental case bounded with the 95% confidence interval (6) of the debris spread. For Cases *I* and *II*, the mean debris trajectory was nearly along the $y = 0$; however, for other cases, it was skewed from the initial location. This behaviour can also be seen in the histogram (Fig. 7).

3.3 Comparative Analysis with the Transportation of Multiple Debris

This section explains the spread of multiple debris (Fig. 2b–e) as a comparison made to the transport of a single object (Fig. 2a).

3.3.1 Configurations No. 2 and No. 3

Configurations No. 2 (Fig. 2b) and No. 3 (Fig. 2c) consist of the numbers of debris (*N)* 2 and 3, respectively. Debris arrangements were made in serial, where the length is perpendicular to the flow direction. As shown in Fig. 9b–c, the objects were diffused independently regardless of their initial location. Further, tracking the initial and final coordinates of the centroid of the objects indicated the dispersion angles of

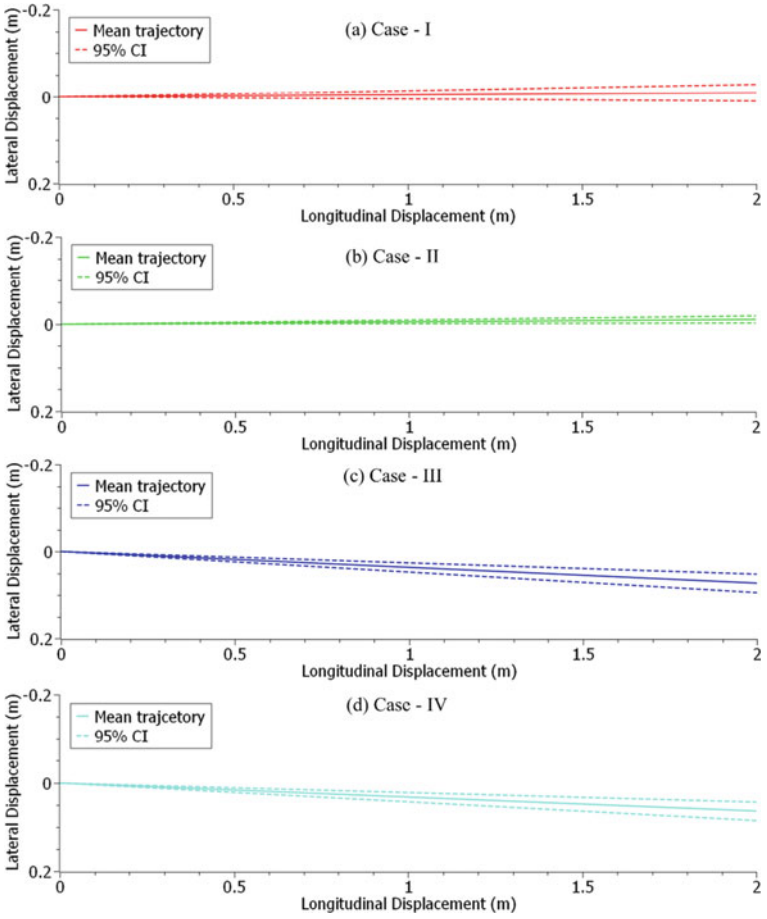

Fig. 8 Confidence intervals of lateral displacement of the debris

$\pm 7°$ and $\pm 10°$ for No.2 and No.3, respectively. Comparison with Eq. (3) hinted that the experimental observations yielded larger dispersion due to their independent diffusion.

3.3.2 Configurations No. 4 and No. 5

Debris was arranged in configurations No. 4 (Fig. 2d) and No. 5 (Fig. 2e) parallel to each other and with lengths normal to the flow direction. In contrast to the serial arrangement discussed in Sect. 3.3.1, this type showed debris travelled as a cluster for a longer distance, which can be treated as an extended single debris problem (debris with a larger length and width) in terms of lateral spread as observations indicated a depended diffusion (Fig. 9d,e) from each other. Similar to Sect. 3.3.1, maximum

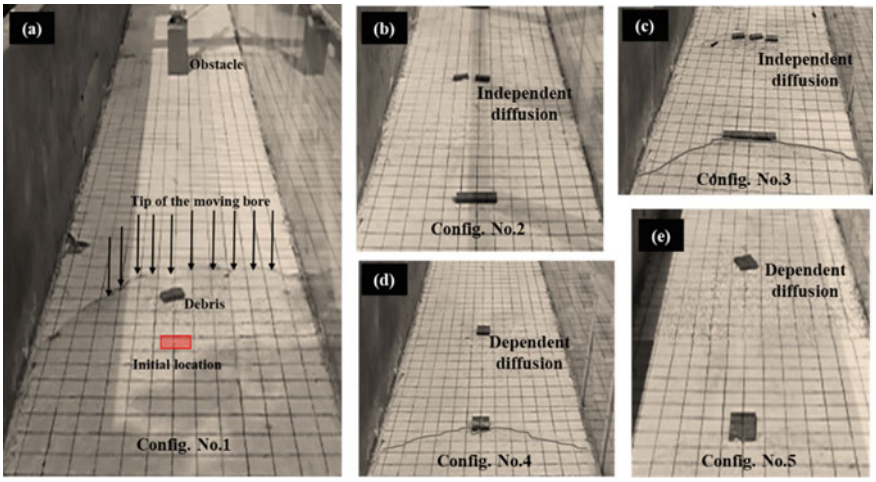

Fig. 9 Debris driftage during the experiments

dispersion angles were noted as ±5.7° and ±8.5° for arrangements No. 4 and No. 5, namely.

3.4 Other Remarks

The experiment environment was designed by considering the characteristics of the tsunami wave obtained in the post-field tsunami survey (e.g. [1]).

Certain assumptions were made in this study, such as neglecting the friction between inter-objects and with objects and flume bed, as the scope of this study was to evaluate the transport in an extreme hydrodynamic event with no dominance over such parameters. In addition, by imposing the velocity of the moving bore in the analysis, it was presumed that all debris at the initial locations received the same interaction with the wave.

Even though the object detection algorithm estimated the velocities of the moving object, the detection capability of the algorithm needs to be improved to capture the debris under highly turbulent environments. It also depends on the capabilities of the camera in place. This needed to be evaluated under the numerical model further.

4 Conclusions

This study conducted hydraulic experiments to understand the basics of the debris transport phenomenon during tsunami-like wave events in a smaller scale environment. The initial configurations and hydraulic boundary conditions were taken as variables, and the debris motion and spread were studied.

It was found that velocity variation single moving debris could be reasonably predicted by analysing the debris motion using an open-source object detection algorithm. It was observed that debris spread occurred symmetrically over the experiment plane. The increment in flow conditions (velocity and inundation depths) resulted in a higher deviation from the mean lateral displacement of zero. In contrast, small flow conditions yielded a lower deviation from the initial location. In general, the lateral spread can be expressed as a normal distribution for low-flow conditions. The high-flow conditions could be expressed as a skewed normal distribution. Moreover, the initial arrangement of the objects and the placement of the obstacle likely influenced the entire transport process.

Acknowledgements This work was supported by the grant of JSPS KAKENHI (JP19H00809), for which the authors express their gratitude.

References

1. Murata S, Imamura F, Katoh K, Kawata Y, Takahashi S, Takayama T (2016) Tsunami: to survive from tsunami. World Scientific Publications, Singapore
2. Stolle J, Krautwald C, Robertson I, Achiari H, Mikami T, Nakamura R, Takabatake T, Nishida Y, Shibayama T, Esteban M, Nistor I, Goseberg N (2020) Engineering lessons from the 28 September 2018 Indonesian tsunami: debris loading. Can J Civ Eng 47:1–12
3. Naito C, Cercone C, Riggs H, Cox D (2014) Procedure for site assessment of the potential for tsunami debris impact. J Waterw Port Coast Ocean Eng 140:223–232
4. Nistor I, Goseberg N, Stolle J, Mikami T, Shibayama T, Nakamura R, Matsuba S (2016) Experimental investigations of debris dynamics over a horizontal plane. J Waterw Port Coast Ocean Eng 143(3):04016022
5. Shafiei S, Melville BW, Shamseldin AY, Beskhyroun S, Adams KN (2016) Measurements of tsunami-borne debris impact on structures using an embedded accelerometer. J Hydraul Res 54:435–449
6. Stolle J, Nistor I, Goseberg N, Petriu E (2020) Development of a probabilistic framework for debris transport and hazard assessment in tsunami-like flow conditions. J Waterw Port Coast Ocean Eng 146(5):04020026
7. Josiah NR, Araki S, Laknath DPC (2022) Understanding the collision of debris carried by tsunami-like flows on a residential structure. In: Proceedings of the 41st international conference on ocean, offshore and arctic engineering, Hamburg, Germany, vol 4. Ocean Space Utilization, pp V004T05A024:1–9
8. Nistor I, Goseberg N, Stolle J (2017) Tsunami-driven debris motion and loads: a critical review. Front Built Environ 3
9. Bradski G (2000) The OpenCV library. Dr Dobb's J Softw Tools 4:2236121
10. Peakall J, Warburton J (1996) Surface tension in small hydraulic river models – the significance of weber number. J Hydrol 35:199–212

Waste in the Construction Industry

Manufacturing of Paving Blocks Using Tile Waste

D. L. C. P. Chandrasekara and M. L. C. Surangi

Abstract Huge amounts of tile waste are daily generated by ceramic companies and construction sites. As a result, they are piled up on empty lands or dumped in land fillings. This type of waste causes environmental pollution and groundwater pollution. This study was accomplished to provide a solution to reduce large quantities of tile waste to some extent. This study is a good reference to identify the benefits of these waste ceramic tile particles as an alternative material for fine and coarse aggregate in the paving block manufacturing industry. Concrete mixture proportions were suggested according to the Grade 25 concrete mix design. Further, blocks were prepared according to different (0, 25, 50, 75, and 100%) replacements of both aggregate types from tile waste. The paving blocks were characterized using a flexural strength test, compressive strength test, and water absorption test. Compressive strength results were collated with standard strength values in Indian standards for paving blocks. It was observed that with the increase of tile waste particles, the slump was reduced. All blocks (including the control sample) met 30 MPa strength after 28 days of curing for lightweight traffic. The strength of the blocks was increased with the rise of tile waste percentage from 0 to 100%. Results revealed that 50% of both aggregate replacements with tile waste are practicable in the paving block manufacturing process. It is suitable for use on roads and parking slots. This study shows that the use of tile waste in the paving block industry, as an alternative material for manufacturing paving blocks, is technically a feasible solution.

Keywords Paving block · Tile waste · Stone powder · Compressive strength · Water absorption

D. L. C. P. Chandrasekara · M. L. C. Surangi (✉)
General Sir John Kotelawala Defence University, Kandawala Rd, Ratmalana 10390, Sri Lanka
e-mail: chaminisliyanage@gmail.com

© The Author(s), under exclusive license to Springer Nature Singapore Pte Ltd. 2023

R. Dissanayake et al. (eds.), *ICSBE 2022*, Lecture Notes in Civil Engineering 362,
https://doi.org/10.1007/978-981-99-3471-3_54

1 Introduction

Ceramic tiles are a very important construction material used in the construction of walls, floors, balconies, etc. Therefore, tile wastes are generated during the demolition of structures and as remains from tile paving works. According to daily construction waste generation in Sri Lanka, 10% of the daily generated waste is categorized as ceramic tile waste.

Daily generated tile wastes are piled on sanitary land fillings, hence, groundwater can get polluted. These ceramic wastes can pose a threat to human and animal health because manufacturers use clay, feldspar, silica, sand, and some chemicals when making and fixing these tiles. Some of these materials are hazardous and can cause serious injuries.

This study provides a solution for the tile waste generated on construction sites. The research was carried out to find a solution for the discarding of tile waste up to some extent. Considering R3 principles (reuse, reduce, recycle), the reuse process was used to provide a solution to tile waste from this new manufacturing process. Paving blocks are made from remaining natural recourse (sand, aggregate,) and they are limited to some extent. Paving blocks made from natural waste provide a sustainable solution for the shortage of current blocks made by sand and aggregate.

This study is focused on constructing a new paving block using tile waste as a replacement material for natural aggregate to provide a better solution for aggregate shortage and tile waste generation. Normal blocks were rectangular-shaped in the beginning. However, presently paving blocks are coming to the market in different shapes. A well-designed block gives an excellent performance as far as strength and durability are concerned. Paving blocks can be applied outside paving areas. The service life of paving blocks possibly reduces due to geological, traffic, environmental, and operational constraints.

The quality of paver blocks will depend on various parameters like the compaction capacity and vibration of the machine, cement grade, water content, aggregate quality, mix design, additives used, managing equipment employed, methods of curing, level of supervision, workmanship, and achieving quality.

These blocks will reduce environmental impact, waste disposal at landfills, and natural aggregate consumption. In addition, this block is cheaper than the paving blocks available in the market because this was constructed using 50% replacement of natural aggregate of tile wastes.

The importance of using wastes in concrete production implies the improvement of concrete performance according to [6]. The strength of the concrete mixture, durability performance, water absorption properties, oxygen permeability, and chloride diffusion were in a suitable range compared to the control mixture properties when fine aggregate was replaced by 20% tile waste. References [5, 8], also studied concrete mixture property variation with different types of wastes and they observed that ceramic wastes increase the properties of the concrete mixture. Concrete made with precast waste also gives better performance in porosity, durability, and strength according to Thomas et al. [13]. Glass waste also gives better strength performance

in 10% aggregate replacement from glass waste in concrete manufacturing by [2, 11] designed a concrete using agricultural wastes. This concrete can be used as sustainable concretes due to its low strength and other properties. According to [12] study, polythene and rubber wastes can be used for manufacturing an eco-friendly concrete mixture with better strength and durability performance.

Due to the growth of paving block usage, natural resource requirement for the manufacturing process is increasing day by day. As a result, researchers moved into finding substitute materials to reduce natural resource consumption in the paving block manufacturing process. They have used waste materials as substitute materials and these wastes increase different properties of these paving blocks. Paving blocks made with crusher dust and fly ash give better performance in flexural strength and compressive strength. Santhosh and Talluri [10] studied paving blocks made with recycled aggregate and crushed clay bricks. Due to the higher water absorption of clay brick particles, water absorption was increased. Hence, they used 25% weighted clay bricks as aggregate and obtained the desired strength. This brick waste can be used for constructing sustainable paving blocks. Research papers by [4] and [9] also evince the strength reduction of paving blocks due to the usage of brick waste as substituting material. Penteado et al. [7] and Wattanasiriwech et al. [15] studied ceramic waste usage in the paving block industry and they proved that the substituting of aggregate with ceramic waste will increase the strength properties of paving blocks. Turgut and Yahlizade [14] studied paving blocks made by substituting aggregate with glass waste. They proved that the compressive strength, flexural strength, splitting tensile strength, and abrasion resistance of the 20% waste replaced sample is at a significant level compared to the control sample. Bakis [1] studied marble waste substitution with aggregate and he observed that it increases the strength of the paving block.

The main purpose of my research is to find the possibility of using tile waste as a substitute material for natural aggregate.

2 Experimental Procedure

2.1 Materials

Indian-type Ultratech cement made in Sri Lanka was used in constructing these paving blocks. Natural aggregate and tile waste were used as coarse aggregate; stone dust and tile waste dust were used as fine aggregates. The density of gravel was measured according to (BS 1377 Part 2), and the densities of tile waste and stone dust were measured according to (BS 1377 Part 2). Ceramic tile wastes used in this study came from construction sites. The tile waste sample density is 2.48 g/cm^3. The particle size distribution of course and fine aggregates, obtained by sieving, according to (ASTM 422).

Physical properties of coarse and fine aggregate used in concrete paving blocks were obtained after laboratory testing.

Table 1 Material properties

Material	Specific gravity	Water absorption %
Chip aggregate	2.69	0.899
Quarry dust	1.91	2.774
Tile waste	2.31	2.57

2.2 Specific Gravity and Water Absorption

The Specific Gravity of Material Greater than 15 mm Particle Size

Specific gravity and water absorption of chip aggregate and tile waste were calculated using the equation below:

$$Specific\ Gravity = \frac{C}{B - A} \tag{1}$$

weight in grams saturated aggregate in water (A_2-A_1)

B = Weight of saturated surface dry aggregate in air

C = Weight of Oven dried aggregate in air.

The Specific Gravity of Material Less than 10 mm Particle Size

The specific gravity of quarry dust was measured using a psychometric flask, using the below equations (Table 1):

$$Specific\ Gravity = \frac{D}{C - (A - B)} \tag{2}$$

Weight of (vessel + Sample + Distill water)

B = Weight of vessel + Distil water g

C = Weight of saturated surface dry sample g

D = Weight of Oven dry sample g.

2.3 Grading of Materials (Sieve Analysis)

Material samples were weighed before starting the test. Then the sieves were cleaned, and the initial weights were measured. After grading using the sieve analysis apparatus weights of the sieves (with the materials) were measured. Then the percentage retained and passed was determined.

Grading results reveal that the particle sizes of tile wastes are ranging from 14 μm to 63 μm. Most of them are passing through 5–10 micro-meter range sieves and chip aggregate particles are also in the same range according to results. Then according to the results, quarry dust particle size variation was identified as 3.35 micro-meters to 63 μm.

After finishing the material testing, paving blocks were manufactured using a Grade 25 mix design (1:1:2) by replacing fine and coarse aggregates with 50% tile waste. Then finally, paving blocks were cured for 7 and 28 days to obtain strength.

2.4 Testing of Specimens

Compressive Strength

Compressive strength tests were carried out according to Indian standards (IS:15,658–2006, 2006). In 7 and 28 days, compressive strength was checked by Universal Testing Machine. First, the block specimens were placed in water maintained at a temperature of 20 °C, for 24 h. Then the dimensions of the paving blocks were measured. Finally, the load was applied without shock and was continuously increased at a rate of 15 + 3 N/mm^2/min.

Water Absorption

Water absorption was then carried out for paving block samples. First, the wet weight of the samples was measured after 24 h of submerging them in water, then finally the specimens were oven-dried at 107 °C and the weight of the specimens was calculated. Then water absorption of individual concrete paving blocks was calculated using the equation below, according to [3] IS 15658: 2006.

t weight of the sample

B = Dry weight of the sample.

Flexural Strength

Finally, the flexural strength test was carried out for each sample to identify the three-point bending resistance of the paving block. The first two specified steel plates were placed on top and bottom of the block and then the specimen was subjected to vertical load from the top surface of the block like simple beam loading through a roller placed in the middle and between the supporting rollers. The load was applied continuously at a uniform rate of 6 kN/min (IS:15,658–2006, 2006). Then the load was increased until the specimen cracked (Failed).

$$F_b = \frac{3Pl}{2b\mathrm{d.d}} \tag{3}$$

F_b = Flexural Strength, in N/mm^2

p = Maximum Load, in N

l = Distance between central lines of supporting rollers.

b = Average Width of blocks, measured from both faces of specimen in mm.

d = average thickness, measured from both ends of the fracture line, -in mm.

The maximum load P shall be reported as the breaking load, nearest to 1 N.

The test results of compressive strength, flexural strength, and water absorption were used to identify the best percentages of waste in the concrete mixture design for the paving block manufacturing process.

Results and Discussion

Materials and block specimen tests were done according to Indian standards and British standards. Specific gravity, water absorption, and grading tests were conducted under material testing. Finally, the paving blocks were tested for compressive strength, bending, and water absorption to select the best sample out of five different samples prepared using 5 different waste proportions.

Altogether 25 blocks were constructed for compression, water absorption, and flexural strength tastings. Each sample contains 5 blocks constructed by replacing 0, 25, 50, 75, and 100% chip aggregate and quarry dust with fine and coarse tile waste particles, which were referred to as T0, T25, T50, T75, and T100, respectively. Here, a grade 25 concrete mix design (1:1:2; Cement 1: Sand 1: aggregate 2) was used to prepare the concrete mixture. After completing the block preparation, blocks were cured for 7 and 28 days before testing.

After curing 5 samples for 7 days and 5 samples for 28 days, compressive strength testing was done for each sample according to Indian standards. Compressive strength results are given in Fig. 1.

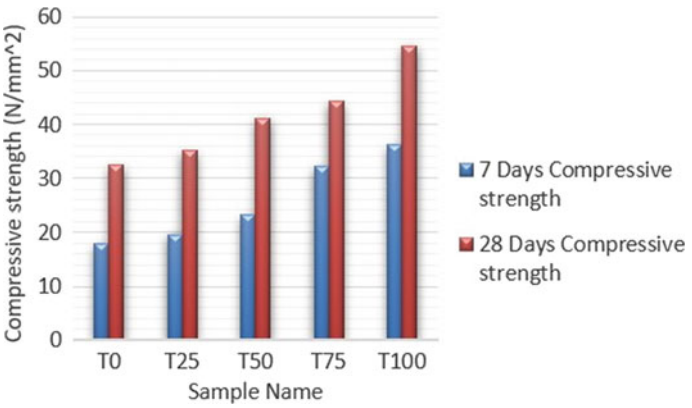

Fig. 1 Compressive strength properties

Considering the strength of the 5 samples, a 100%-replaced sample is the best one, and 50 and 75% tile waste-replaced samples also evince the best compressive strength compared to the control sample.

The water absorption test was then conducted according to Indian Standards (IS:15,658–2006, 2006). After curing for 28 days, the blocks were submerged in the water for one day and the wet weight of the paving blocks was calculated. Then, the sample was oven dried. Finally using these results, water absorption values were calculated. Figure 2 shows the results of the water absorption test.

Samples T50, T75, and T100 show the best performance in durability concerns which means that their water absorption is lower compared to the control sample. Finally, paving blocks were tested for flexural strength to identify the maximum withstanding load for bending and the results are shown in Fig. 3.

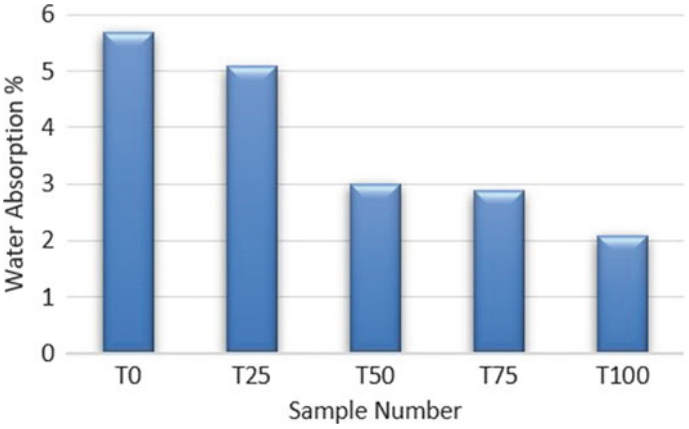

Fig. 2 Water absorption

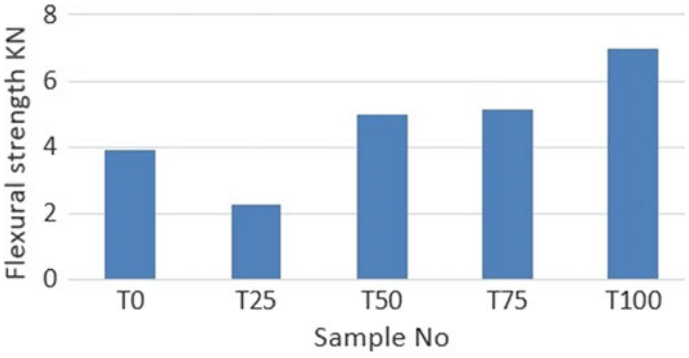

Fig. 3 Flexural strength

T100%, T75%, and T50% tile waste replaced samples are suitable for residential driveways according to Indian standards and these blocks give a higher performance in three points bending compared to the control sample.

3 Conclusion

In the construction industry, ceramic tile waste is daily generated from the construction, demolition, and maintenance work. Usually, these types of waste are disposed of on sanitary land fillings all over the world. This study focuses on using tile waste as a replacement material for concrete for the paving block manufacturing process. The followings are the important findings of the study.

1. Water absorption of paving blocks decreased with the increase of ceramic waste particles.
2. Paving blocks made with all percentages of natural aggregate replaced samples meet the Indian standard compressive strength requirement for paving blocks (30 MPA).
3. Manufacturing cost for these paving blocks increased with the increase of waste percentage due to the lack of available grinding methods, hence, 50% of the waste replaced sample can be decided as an economically and environmentally feasible block sample.

From these findings, it can be observed that tile wastes can be used as an alternative material for chip aggregate and quarry dust in the paving block manufacturing industry. This study will help to reduce a significant amount of tile waste dumping.

References

1. Bakis A (2019) Increasing the durability and freeze-thaw strength of concrete paving stones produced from ahlat stone powder and marble powder by special curing method. Adv Mater Sci Eng. https://doi.org/10.1155/2019/3593710
2. Gautam SP, Srivastava V, Agarwal VC (2012) Use of glass wastes as fine aggregate in Concrete. J Acad Ind Res 1(6):320
3. IS:15658–2006 (2006) Indian standard precast concrete block for paving-specification. In: Bureau of Indian standards, pp 1–27
4. Jankovic K, Nikolic D, Bojovic D (2012) Concrete paving blocks and flags made with crushed brick as aggregate. Constr Build Mater 28(1):659–663. https://doi.org/10.1016/j.conbuildmat.2011.10.036
5. López V et al (2007) Eco-efficient concretes: impact of the use of white ceramic powder on the mechanical properties of concrete. Biosys Eng 96(4):559–564. https://doi.org/10.1016/j.biosystemseng.2007.01.004
6. Pacheco-Torgal F, Jalali S (2010) Reusing ceramic wastes in concrete. Constr Build Mater 24(5):832–838. https://doi.org/10.1016/j.conbuildmat.2009.10.023

7. Penteado CSG, Viviani De Carvalho E, Lintz RCC (2016) Reusing ceramic tile polishing waste in paving block manufacturing. J Clean Prod 112:514–520. https://doi.org/10.1016/j.jclepro.2015.06.142
8. Poon CS, Chan D (2006) Feasible use of recycled concrete aggregates and crushed clay brick as unbound road sub-base. Constr Build Mater 20(8):578–585. https://doi.org/10.1016/j.conbuildmat.2005.01.045
9. Poon CS, Chan D (2007) The use of recycled aggregate in concrete in Hong Kong. Resour Conserv Recycl 50(3):293–305. https://doi.org/10.1016/j.resconrec.2006.06.005
10. Santhosh J, Talluri R (2015) Manufacture of interlocking concrete paving blocks with fly ash and glass powder. Int J Civil Eng Technol (IJCIET) 0976(4):46–54. www.jifactor.com
11. Shafigh P et al (2014) Agricultural wastes as aggregate in concrete mixtures - a review. Constr Build Mater 53:110–117. https://doi.org/10.1016/j.conbuildmat.2013.11.074
12. Tawfik ME, Eskander SB (2006) Polymer concrete from marble wastes and recycled poly(ethylene terephthalate). J Elastomers Plast 38(1):65–79. https://doi.org/10.1177/0095244306055569
13. Thomas C, Setién J, Polanco JA (2016) Structural recycled aggregate concrete made with precast wastes. Constr Build Mater 114:536–546. https://doi.org/10.1016/j.conbuildmat.2016.03.203
14. Turgut P, Yahlizade ES (2009) Research into concrete blocks with waste glass. Int J Civil Environ Eng 1(4):203–209
15. Wattanasiriwech D, Saiton A, Wattanasiriwech S (2009) Paving blocks from ceramic tile production waste. J Clean Prod 17(18):1663–1668. https://doi.org/10.1016/j.jclepro.2009.08.008

Use of Waste Materials for Sustainable Pavement Industry in Australia: A Review

C. Gallage and S. Jayakody

Abstract The demand for fresh materials for the construction and maintenance of pavements is increasing daily with the rapid development of infrastructures. The continuous extraction of natural resources to meet this demand causes environmental, social, and economic dissatisfaction. Recycled materials are the best alternative to replace fresh pavement materials, conversely, to align with the sustainability of the pavement industry. Crumb rubber, reclaimed asphalt pavement, recycled concrete aggregates, crushed bricks, and glass, fly ash, and recycled plastics are viable recycled materials. A progressive trend toward recycled materials is recorded worldwide. However, it needs continuous enforcement to standardize specific criteria to retain a steady demand for their applications in every part of the world. Australia has made significant strides in utilizing recycled materials in the pavement industry under various circumstances. This paper presents an overview of recycled materials, their properties and applications in different layers of flexible pavements in Australia.

Keywords Recycled materials · Flexible pavements · Reclaimed asphalt pavement · Recycled concrete aggregates · Recycled plastic · Crush glass · Fly ash

1 Introduction

The interest in aggregates from waste sources is becoming more popular in the construction industry. Natural resource depletion, economic and environmental benefits, and government legislation are motivated to recycle and reuse the waste. In particular, looking for recycled materials in pavement construction is most significant since it demands more materials than other constructions. A progressive trend toward recycled materials for pavements is recorded worldwide. The possible recycled materials: crumb rubber, reclaimed asphalt pavement, recycled concrete aggregates, crushed bricks and glass, fly ash and recycled plastics have been considered

C. Gallage · S. Jayakody (✉)
Queensland University of Technology, Brisbane, Australia
e-mail: s.jayakodyarachchige@qut.edu.au

© The Author(s), under exclusive license to Springer Nature Singapore Pte Ltd. 2023

R. Dissanayake et al. (eds.), *ICSBE 2022*, Lecture Notes in Civil Engineering 362,
https://doi.org/10.1007/978-981-99-3471-3_55

in this study which are being currently used in pavement constructions in Australia [5].

Crumb rubber is derived from end-of-life tires and mitigates the environmental and health challenges of disposed tires. Numerous investigations on crumb rubber have been conducted in many countries aiming to modify the bitumen and replace the aggregates in asphalt mixtures [10, 45]. Reclaimed asphalt pavement (RAP) is widely used in road applications that are reprocessed by crushing and screening of removed asphalt wearing or intermediate courses. Many successful investigations have been conducted to explore the reuse of RAP in new asphalt due to the oxidized binding property [13] and to replace the aggregates partially and completely in base and subbase courses [21, 42].

Recycled concrete aggregate (RCA) is produced from demolished concrete structures and is considered the most promising recycled material for replacing the fresh quarry aggregates in base and subbase courses. Many research studies have revealed the high strength and stiffness of RCA as a pavement material due to self-cementing properties [1, 19]. Further studies have compiled the quality requirements of RCA for use as aggregates in asphalt concrete [24]. Therefore, as a durable recycled material, RCA is currently being employed in many road projects across various regions.

Crushed brick is derived from construction and demolition waste and many investigations have recommended employing it as a subbase material to partially replace the fresh aggregates [36]. Furthermore, studies have revealed the potential use of hardened crushed clay bricks to partially mixed with aggregates in asphalt layers [47]. Recycled crushed glass is produced from food and beverage containers and has been subjected to many research studies to determine the feasibility of using as pavement aggregates. Successful outcomes revealed blending the crushed glass with other typical recycled materials such as RCA, crumb rubber, and bricks in achieving the required characteristics of pavement materials [9, 40]. Further studies have recommended using the crushed glass to replace the fresh aggregates in asphalt [11] and for mixing with fly ash for the stabilization of weak subgrade [28]. Fly ash (FA) is a by-product of coal combustion and a feasible alternative to improve weak subgrade soil [49]. Investigations on fly ash have recommended its use as an asphalt filler [8] and a secondary stabilizing agent to modify bitumen [39]. Recycled plastic is an emerging material to be used in pavement construction. The elastomeric and plastomeric properties of plastic have been investigated to apply as a bitumen modifier [34] and partially replace the bitumen in asphalt concrete [30]. Comprehensive investigations are needed to reveal the potential use of recycled plastic in manufacturing the geosynthetic that is significant to reinforce weak subgrade soil [29].

Australia is far ahead in employing recycled materials in the pavement industry under different circumstances. This paper presents an overview of recycled materials, their properties, and applications in different layers of flexible pavements, in Australia.

2 Waste Generation and Recycling

Recycling is one of the best solutions in waste management that would otherwise be disposed of as waste. The use of recycled waste materials addresses the current issues related to mining natural resources and waste generation. In contrast, it creates more benefits in waste prevention, energy saving, saving primary sources, and avoiding landfilling.

Figure 1 compares Australia's rates of waste generation, disposal, recycling, and resource recovery with selected other countries. Australia records a progressive improvement in waste management and recycling and the government's target is to increase Australia's resource recovery rate to 80% by 2030 through recycling and recovering energy or other resources from waste [4]. Therefore, the use of recycled materials for construction particularly for pavement constructions, would assure the aspects of sustainability in the pavement industry. Figure 2 shows the generated and recycled waste in Australia in 2018–2019 which are applicable as pavement materials. A total of 65% of waste has been recycled and which is a significant achievement in waste management. The masonry which represents concrete, bricks, asphalt, steel, etc., records the highest recovery (over 80%) however, ash and plastic need to be paid more attention due to the low rate of recycling (less than 50% recorded).

All recycled materials are not being suitable as pavement materials, and they must possess the necessary properties to meet the required service life of the pavement. Readily available recycled materials for pavements in Australia are crumb rubber, RAP, RAC, crushed bricks, and glass, fly ash. There is a significant improvement in the research sector on these materials in the recent past and successful outcomes are currently being practiced in real world applications in all states in Australia.

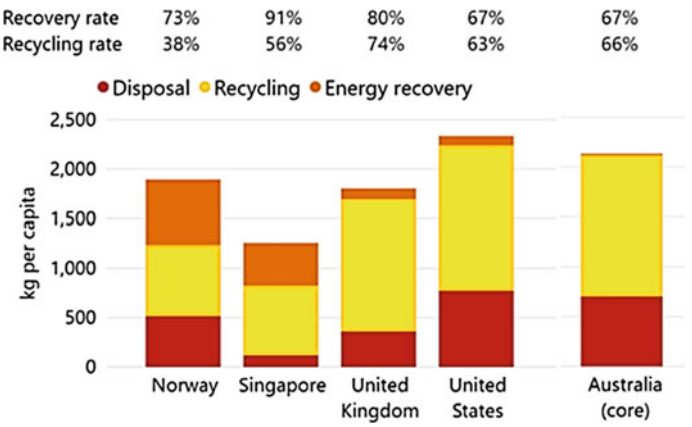

Fig. 1 Comparison of annual waste generation and fate per capita, Australia and selected countries [35]

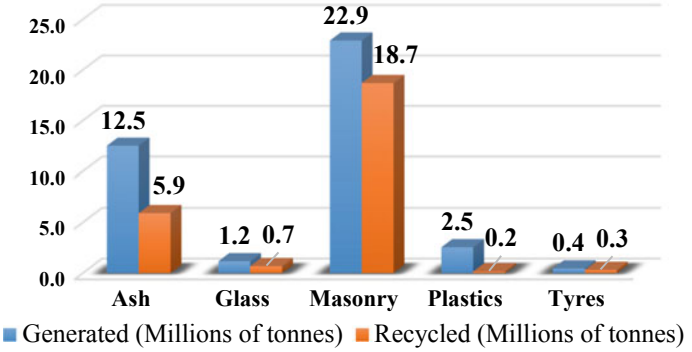

Fig. 2 Waste generation and recycling by material category in Australia 2018–2019 [35]

3 Applications of Waste Materials in Pavements

Applications of recycled waste materials in pavements are being pursued in Australia either as alternatives to replace conventional materials or as supplementary to enhance the properties of conventional materials. Recent research outcomes in applications of recycled materials for subgrade stabilization, subbase and base courses, bitumen modification, and asphalt layers in Australia are discussed in this section.

3.1 Subgrade Stabilization

Subgrade soils are very problematic in Australia due to weak soft soil such as expansive clay soils. It covers more than 20% of Australia, and they are frequently found in populated regions as shown in Fig. 3a. Cement and lime are commonly used as chemical stabilizers to stabilize expansive clays while geosynthetics are used to provide structural reinforcement on the weak subgrades [22, 23]. However, high cost and scarcity are major constraints of these methods.

Fly ash is the best alternative subgrade stabilizer to replace lime when expansive clay soil presents itself. Pozzolanic reactions take place when FA blends with expansive soil consequently, strength and stiffness increase. Figure 3b shows recent research outcomes of subgrade improvement with FA in Australia. According to Karami et al. [25], the strength of the weak subgrade soil was improved and reflected by 26% of the California bearing ratio (CBR) with 15% of FA in Melbourne. However, it was required to add 3% of lime in FA as an activator to take place pozzolanic reactions and enhance the strength. Zimar et al. [49] studied soft soil in Victoria and applied Municipal solid waste incineration (MSWI) FA for subgrade improvement. CBR value of the subgrade soils was recorded over 60 with 20% of MSWI FA and observed a 46% reduction of shrinkage than the control sample. Renjith

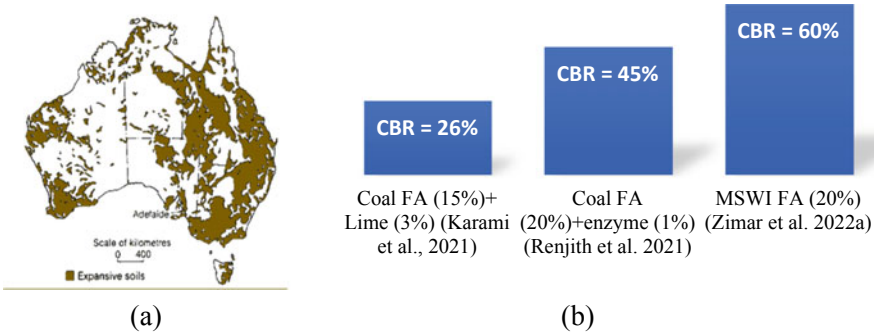

Fig. 3 **a** Distribution of expansive soils in Australia [38] **b** Improvement of subgrade with Fly ash

et al. [37] introduced a little quantity (1%) of commercially available enzyme as a secondary stabilizer with FA to initiate the pozzolanic reaction. These results revealed an increase of CBR up to 45% with 20% fly ash compared to the control soil.

Yaghoubi et al. [46] introduced recycled glass as a non-chemical soil treatment to improve natural expansive clay in the western metropolitan area of Melbourne, Australia. Sand-size recycled glass has been used to mix with clay subgrade soil, and the experimental results showed over 100 MPa of resilient modulus which is a 113% increase compared to the untreated soil, achieved by adding 30% of recycled glass.

Recent research outcomes have emphasized the potential use of FA to stabilize weak and expansive subgrade and, it is the best alternative to replace lime. Therefore, benefits can be gained by reducing the mining of lime for subgrade stabilization.

3.2 Subbase Course

The subbase course of the unbound pavement structures provides adequate stiffness to avoid excessive deformation of the subgrade. Subbase would be the thickest layer in a pavement structure which is built with low-quality materials comparatively base course. Therefore, the subbase demands more materials to facilitate a strong working platform on top of the subgrade as per the designed traffic volume. Alternatives are widely available to replace the quarry aggregates in subbase courses and several types of waste materials are currently employed in Australian roads.

Recycled concrete aggregate (RCA) has been paid more attention by researchers in the recent past and revealed significant outcomes on the strength and performance characteristics as a subbase material [16, 17]. Arulrajah et al. [3] recommended RCA with 25% of crushed bricks for subbase applications. Their research indicated high resilient modulus over 400 MPa at low moisture contents (70% of OMC) and gradually decreased below 200 MPa with high moisture values (87% of OMC). Mohammadinia et al. [32] recommended RCA with 2% of cement to meet the local authority requirements for subbase materials in Australia. Their conclusion was based

on the unconfined compressive strength (UCS) values of 3 MPa and secant modulus over 2000 kPa of cement treated RCA sample. Jayakody et al. [18] also studied the UCS of RCA without binding agents and revealed around 0.4 MPa with the presence of 20% RAP materials in RCA. The strength of the same samples was observed as 75–80% of CBR and recommended to add 20% of RAP to mix with RCA to apply in sub-base layers in high-volume roads in Australia.

Li et al. [27] introduced crumb rubber to mix with RCA and recommended 1.5% to meet the minimum required value of CBR of 80%. Tire-derived aggregate was tested with RCA by Arulrajah et al. [2] and achieved around 80% of CBR with 3% of tire-derived aggregates. Saberian et al. [41] introduced crumb rubber and crushed glass to blend with RCA and observed a significant increase in resilient modulus from 42 to 228 MPa when 1% of crumb rubber and 5% of crushed glass were blended with RCA. According to the permanent deformation results, they exhibited plastic shakedown which underwent hardening of the compacted materials with an increase in load repetitions.

The research outcomes reflect a significant role of RCA as a recycled material in subbase courses. It further emphasizes the potential use of other recycled materials with RCA which creates more opportunities to use recycled materials in pavements.

3.3 Base Course

High-quality materials are employed in the base course to provide high strength and stiffness that control the intensity of stress in the below layers of the pavement structures. Therefore, comprehensive investigations are required when nonconventional materials are introduced in the base course.

RCA has been subjected to comprehensive research studies in many countries and revealed significant outcomes to be used as base material even with other recycled materials such as RAP, crushed bricks, and glass [12].

Mohammadinia et al. [33] studied the response of resilient modulus on axial and confining stresses and observed a significant increase from around 250 to 700 MPa for the range of the axial stress 20 to 275 kPa and the confining pressure 20.7 to 137.9 kPa. Further testing on secant modulus and unconfined compressive strength revealed the high stiffness with curing time and the presence of cement in RCA. They observed a substantial gain of stiffness with 4% cement in RCA from 1.2 MPa to 6 MPa from no-curing to 28 days of curing [32].

Arulrajah et al. [2] observed high CBR values of RCA which was 180% and recommended as base course materials. Further, RLT test results revealed a resilient modulus over 350 MPa and less than 0.5% of strain in RCA with a moisture content of 90% of OMC. The strain gained experienced plastic shakedown which reflects the hardening of the compacted samples with load repetitions.

Jayakody et al. [18] observed a high strength of RCA at their respective optimum moisture contents (OMCs) and maximum dry densities (MDDs). The soaked CBR value was recorded as 150% when RCA had no constituents. However,

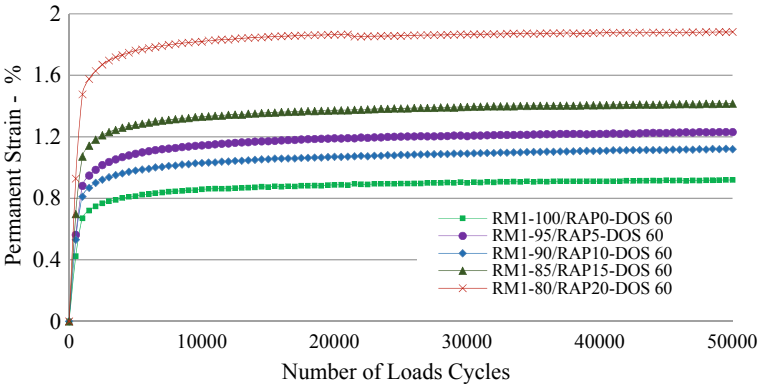

Fig. 4 Permanent strains of RAP mixed RCA samples at 60% of DoS within 50,000 load cycles

they observed a decrease in soaked CBR with the presence of RAP exceeding 15% in RCA. Therefore, adding RAP was recommended only up to 15% for base course applications.

Figure 4 shows the accumulation of plastic deformation of RCA with and without RAP which approach in the range of "plastic shakedown limit" due to the hardening of the plastic strain with the increase of the load cycles. The resilient modulus also gradually decreased from 247 to 233 MPa with the Presence of RAP in RCA, ranging from 0 to 20% at the 60% of the degree of saturation [20].

Saberian et al. [40] introduced rubber with RCA as base layer material and a very low permanent axial strain of around 0.025 was recorded with 0.5% of fine rubber. Further noticed that the increase in particle size of rubber and rubber content adversely affected the permanent deformation of RCA. The presence of coarse rubber of more than 0.5% in RCA caused plastic creep in gaining of permanent strain and eventually collapsed with the increase of load intensity. Therefore, based on the results, 0.5% of rubber with RCA was recommended as a base material in the pavement in terms of long-term permanent deformation.

Mohammadinia et al. [31] recorded a higher resilient modulus in RAP than in RCA under the same stress conditions. The results showed that RAP yielded a resilient modulus of about 1350 MPa whereas the RCA had around 700 MPa at the same confining pressure and axial stress. Mohammadinia et al. [31] introduced FA to be mixed with RAP as a viable binder to increase UCS and resilient modulus. The results recommended 15% of FA to obtain the optimum performance of RAP for pavement base applications.

RCA is the well-recognized recycled material to replace the fresh aggregates in the base course. However, quality control aspects should be applied prior to their applications to ensure consistent characteristics [19]. RAP also has revealed comparable strength and performance characteristics however, no more significant concern regarding its applications in the base course.

3.4 Asphalt Course

Asphalt course plays the role of the structural layer in pavement as a mixture of bituminous binder and aggregates. Asphalt courses are usually struggling to achieve their design life with conventional bitumen under increased traffic volumes and heavy loadings. Therefore, there is a growing trend of investigating the asphalt modification methods that involve modifying conventional bitumen with recycled materials in such a way that it can resist rutting, fatigue, and other road distresses while addressing waste management.

Jamal et al. [14] showed significant improvement in the rutting resistance of the asphalt with modified bitumen with crumb rubber on local Australian roads. Their study introduced crumb rubber 7.5% to modify the bitumen and the strain was reduced to half of the original asphalt. Their further study revealed the reduction of damage by UV radiations and thermal aging with modified bitumen with crumb rubber. The results showed that when 22.5% of crumb rubber was used in modified bitumen, the asphalt layer was almost 60 kPa away from the damage zone and it was a 50% reduction of the damage on the asphalt layer [15].

Kidd et al. [26] also studied the performance of asphalt with crumb rubber-modified bitumen. High stiffness was observed under the wheel tracker test, the rutting depth of asphalt decreased from 7.6 mm to 5.6 mm when the bitumen was modified with 5% of crumb rubber.

Several investigations on recycled materials to replace fresh aggregates in asphalt layers are recorded and RAP is in the top priorities. White [43] applied RAP and did not observe detrimental effects with 5–10% of RAP in asphalt. The resilient modulus was recorded over 6700 MPa with 10% of RAP which was recorded at around 5000 MPa without RAP in asphalt. Wheel tracker test results further emphasized the previous conclusion that rutting was reduced by 0.7 mm with 10% of RAP in asphalt.

Fatigue behavior and thermal characteristic properties of asphalt with RAP were studied by Clark et al. [5]. The inclusion of RAP 15% in asphalt increased the material's fatigue properties at high temperatures ($30\ ^{0}$C). Fatigue failure was recorded at over 1,500,000 number of load repetitions, however, it was less than 500,000 without RAP in asphalt. Conversely, it was observed that the mixture without RAP performed significantly better than the mixture with RAP at a low temperature (10 °C) [7].

White et al. [43] studied the effect of plastic on asphalt and observed an increase in workability and resistance to deformation. Comprehensive test results were analyzed to introduce 10% of plastic which increased the resilient modulus from 4100 to 4300 MPa and fatigue life from 115,000 to 130,000 of load repetitions. Further, noticed a significant reduction of rutting with 6% of plastic as an aggregate in asphalt in wheel track tests as it recorded 1 mm and 1.75 mm with and without plastic aggregate respectively.

According to past studies, RAP had significantly performed in asphalt concrete, and, crumb rubber is the best to modify the bitumen. In addition, recycled plastic has been recognized as a potential bitumen modifier and a substitution for aggregate in asphalt concrete.

4 Standards Specifications

All recycled materials are not suitable as pavement materials hence, they should be applied in accordance with the required specifications. Australian standards and specifications for the use of recycled waste materials in pavements have been developed by considering constructability, performance, and sustainability. Constructability implies the support of the materials on robust pavement design methods, workability, safety, and health to humans and the environment. Availability of the materials at low cost is also an important factor together to effectively transport with minimum effort and time. Mechanical characteristics of the waste materials which are caused by high durability, low maintenance, and high resistance to distress should be assessed to ensure better performance of the pavements during the design life. Deformation modes, cracking, and degradation of the materials need to be investigated by strength and performance tests to predict the service life failure. The most significant concern is the designing and planning of the methods and/or system to reuse and recycle the used recycled materials at the end of service life. That would promote sustainability to the next level in the use of waste materials for pavement construction.

Australia has developed national standards and specifications for the use of recycled content in a broad range of road projects. Pavement authorities of all states in Australia are currently being practiced specifications and standards for selected recycled materials for pavement applications and the government expects to address the followings through the standards and specifications:

- to ensure that the performances of recycled materials are better or equal to standard materials;
- to estimate the potential cost saving;
- to ensure the consistent quality of practicing recycled materials by both government and private sectors;
- to maintain consistent demand for recycled materials to encourage and develop the recycling waste industry;
- to identify the deficiencies for further research and investigations.

5 Conclusion

This review study was based on recent investigations on recycled materials for pavement applications in Australia and the following conclusions are drawn.

- Fly ash is the best alternative to replace lime in improving weak and expansive subgrade soil. However, significant performances have been recorded with an activator to initiate pozzolanic reactions.
- RCA has been recognized as the best alternative to replace fresh aggregates in base and subbase courses. The high strength of RCA has been measured by CBR and UCS while significant performance has been recorded in resilient modulus and permanent strain due to self-cementing properties.

- RCA has revealed satisfactory performance as base and subbase materials when other recycled materials are blended such as RAP, crushed bricks, and glass.
- RAP has performed as the best-recycled material in asphalt that revealed high stiffness and, crumb rubber has been recognized as the best-recycled material for modification of bitumen binder.

6 Future Research and Directions

The authors suggest the following future research directions in recycled materials in the pavement industry:

- Trial and demonstration projects for closely monitoring the field performance and distress modes of pavements with recycled materials.
- Develop and design the methods to reuse and/or recycle the used recycled materials.
- Health and environmental risk assessment with time and degradation of each recycled material in pavements.
- Cost estimation for all recycled materials based on their specific applications to cover all the aspects for the best use.

References

1. Ahmed EAE-MB (2013) Utilization of cement treated recycled concrete aggregates as base or subbase layer in Egypt. Ain Shams Eng J 4:661-673
2. Arulrajah A, Mohammadinia A, Maghool F, Horpibulsuk S (2019) Tire derived aggregates as a supplementary material with recycled demolition concrete for pavement applications. J Clean Prod 230:129–136
3. Arulrajah A, Piratheepan J, Bo MW, Sivakugan N (2012) Geotechnical characteristics of recycled crushed brick blends for pavement sub-base applications. Can Geotech J 49:796–811
4. Australian Government SaTGaTaLGA (2019). National Waste Policy Action Plan 2019
5. Clark B, Johnson M, Wu J, Herrington P, Parker B, Clift Z (2022) Guide to pavement technology Part 4E: Recycled Materials. Level 9:287. Elizabeth Street Sydney NSW 2000 Australia
6. Clark BR, Gallage C (2020) Superior performance benefits of multigrade bitumen asphalt with recycled asphalt pavement additive. Constr Build Mater 230:116963
7. Clark BR, Piacere L, Gallage C (2018) Effects of recycled asphalt pavement on the stiffness and fatigue performance of multigrade bitumen Asphalt. J Mater Civ Eng 30:04017278
8. De Oliveira LS, Lucas Júnior JLO, Babadopulos LFAL, Soares JB (2022) Stiffness and fatigue evaluation in cyclic tests with rest periods for asphalt mixtures with or without fly ash. Constr Build Mater 322:126426
9. Disfani MM, Arulrajah A, Bo MW, Hankour R (2011) Recycled crushed glass in road work applications. Waste Manage 31:2341–2351
10. Duan H, Zhu C, Li Y, Zhang H, Zhang S, Xiao F, Amirkhanian S (2021) Effect of crumb rubber percentages and bitumen sources on high-temperature rheological properties of less smell crumb rubber modified bitumen. Constr Build Mater 277:122248
11. Gedik A (2021) An exploration into the utilization of recycled waste glass as a surrogate powder to crushed stone dust in asphalt pavement construction. Constr Build Mater 300:123980

12. Gobieanandh V, Jayakody S (2016) Evaluate the strength of cement treated recycled construction and demolition aggregates as a pavement material. In: Proceedings of the 7th International Conference on Sustainable Built Environment. Kandy, Sri Lanka
13. Guo M, Liu H, Jiao Y, Mo L, Tan Y, Wang D, Liang M (2020) Effect of WMA-RAP technology on pavement performance of asphalt mixture: A state-of-the-art review. J Clean Prod 266:121704
14. Jamal M, Giustozzi F (2020) Low-content crumb rubber modified bitumen for improving Australian local roads condition. J Clean Prod 271:122484
15. Jamal M, Lanotte M, Giustozzi F (2022) Exposure of crumb rubber modified bitumen to UV radiation: A waste-based sunscreen for roads. J Clean Prod 348:131372
16. Jayakody S, Gallage C, Kumar A (2012) Assessment of recycled concrete aggregates for road base and sub-base. In: Proceedings of the 2nd International Conference GEOMATE. Malaysia
17. Jayakody S, Gallage C, Kumar A (2014) Assessment of recycled concrete aggregates as a pavement material. Geomech Eng 6:235–248
18. Jayakody S, Gallage C, Ramanujam J (2019) Effects of reclaimed asphalt materials on geotechnical characteristics of recycled concrete aggregates as a pavement material. Road Mater Pavement Des 20:754–772
19. Jayakody S, Gallage C, Ramanujam J (2019) Performance characteristics of recycled concrete aggregate as an unbound pavement material. Heliyon 5:e02494
20. Jayakody S, Gallage C, Ramanujam J (2021) Assessment of RCA with RAP materials for pavement applications. IOP Conf Ser: Mater Sci Eng 1075:012020
21. Jayakody S, Gallage C, Ramanujam J, Kumar A (2013) Laboratory study on the performance of recycled concrete aggregates blended with reclaimed asphalt pavement as pavement granular material. In: Proceedings of the Third International Conference—GEOMATE 2013. Japan.
22. Jayalath C, Gallage C, Wimalasena K, Lee J, Ramanujam J (2021) Performance of composite geogrid reinforced unpaved pavements under cyclic loading. Constr Build Mater 304:124570
23. Jayalath CPG, Gallage C, Wimalasena K (2022) Development of design guidelines for composite-geogrid reinforced unpaved pavements. Road and airfield pavement technology. Springer International Publishing, pp 375–387
24. Juan Gabriel B-M, Reyes-Lizcano FA, Rondón-Quintana HA (2022) Use of recycled concrete aggregates in asphalt mixtures for pavements: A review. J Traffic Transp Eng (Engl Ed)
25. Karami H, Pooni J, Robert D, Costa S, Li J, Setunge S (2021) Use of secondary additives in fly ash based soil stabilization for soft subgrades. Transportation Geotechnics 29:100585
26. Kidd A, Stephenson G, White G (2021) Towards the use of crumb rubber modified asphalt for local government roads
27. Li J, Saberian M, Nguyen BT (2018) Effect of crumb rubber on the mechanical properties of crushed recycled pavement materials. J Environ Manage 218:291–299
28. Perera STAM, Saberian M, Zhu J, Roychand R, Li J (2022) Effect of crushed glass on the mechanical and microstructural behavior of highly expansive clay subgrade. Case Stud Constr Mater 17:e01244
29. Mainroads DOTA (2020) Technical Note TN193 Use of recycled materials in road construction. Department of Transport and Main Roads
30. Marta V-C, Pedro L-G, Miguel Ángel C-P, Indacoechea-Vega I (2019) 15—The use of recycled plastic as partial replacement of bitumen in asphalt concrete. In: Pacheco-Torgal F, Khatib J, Colangelo F, Tuladhar R (eds.) Use of recycled plastics in eco-efficient concrete. Woodhead Publishing
31. Mohammadinia A, Arulrajah A, Horpibulsuk S, Chinkulkijniwat A (2017) Effect of fly ash on properties of crushed brick and reclaimed asphalt in pavement base/subbase applications. J Hazard Mater 321:547–556
32. Mohammadinia A, Arulrajah A, Sanjayan J, Disfani M, Bo M, Darmawan S (2015a) Geotechnical characteristics of cement-treated recycled materials in base and sub-base applications
33. Mohammadinia A, Arulrajah A, Sanjayan J, Disfani MM, Bo MW, Darmawan S (2015b) Geotechnical properties of lightly stabilized recycled demolition materials in base/Sub-base applications. IFCEE 2015

34. Nizamuddin S, Jamal M, Gravina R, Giustozzi F (2020) Recycled plastic as bitumen modifier: The role of recycled linear low-density polyethylene in the modification of physical, chemical and rheological properties of bitumen. J Clean Prod 266:121988
35. Pickin J, Wardle C, O'farrell K, Nyunt P, Donovan S (2020) National Waste Report 2020. Department of Agriculture, Water and the Environment. Blue Environment
36. Poon CS, Chan D (2006) Feasible use of recycled concrete aggregates and crushed clay brick as unbound road sub-base. Constr Build Mater 20:578–585
37. Renjith R, Robert D, Setunge S, Costa S, Mohajerani A (2021) Optimization of fly ash based soil stabilization using secondary admixtures for sustainable road construction. J Clean Prod 294:126264
38. Richards BG, Peter P, Emerson WW (1983) The effects of vegetation on the swelling and shrinking of soils in Australia. Géotechnique 33:127–139
39. Rosyidi SAP, Rahmad S, Yusoff NIM, Shahrir AH, Ibrahim ANH, Ismail NFN, Badri KH (2020) Investigation of the chemical, strength, adhesion and morphological properties of fly ash based geopolymer-modified bitumen. Constr Build Mater 255:119364
40. Saberian M, Li J (2019) Long-term permanent deformation behaviour of recycled concrete aggregate with addition of crumb rubber in base and sub-base applications. Soil Dyn Earthq Eng 121:436–441
41. Saberian M, Li J, Boroujeni M, Law D, Li C-Q (2020) Application of demolition wastes mixed with crushed glass and crumb rubber in pavement base/subbase. Resour Conserv Recycl 156:104722
42. Ullah S, Tanyu BF, Dawson A (2022) Reclaimed asphalt pavement (rap) as an unbound base course material: a mechanistic design approach based on multi-stage repeated load triaxial tests. Transportation Geotechnics 33:100729
43. White G (2019) Quantifying the impact of reclaimed asphalt pavement on airport asphalt surfaces. Constr Build Mater 197:757–765
44. White G, Magee C (2019) Laboratory evaluation of asphalt containing recycled plastic as a bitumen extender and modifier. J Traffic Transp Eng 7:218–235
45. Wulandari PS, Tjandra D (2017) Use of crumb rubber as an additive in asphalt concrete mixture. Procedia Engineering 171:1384–1389
46. Yaghoubi E, Yaghoubi M, Guerrieri M, Sudarsanan N (2021) Improving expansive clay subgrades using recycled glass: Resilient modulus characteristics and pavement performance. Constr Build Mater 302:124384
47. Zachariah JP, Sarkar PP, Pal M (2021) A study on the moisture damage and rutting resistance of polypropylene modified bituminous mixes with crushed brick aggregate wastes. Constr Build Mater 269:121357
48. Zimar Z, Robert D, Sidiq A, Zhou A, Giustozzi F, Setunge S, Kodikara J (2022) Waste-to-energy ash for treating highly expansive clays in road pavements. J Clean Prod 374:133854
49. Zimar Z, Robert D, Zhou A, Giustozzi F, Setunge S, Kodikara J (2022) Application of coal fly ash in pavement subgrade stabilisation: A review. J Environ Manage 312:114926

Evaluation of Elemental and Chemical Compositions of Recycled Concrete Aggregates Produced from the Cowam Center, Sri Lanka

K. P. Arandara, S. T. Priyadarshana, G. N. Paranavithana, R. B. Mallick, and R. Dissanayake

Abstract Recycled Concrete Aggregate (RCA) is produced from demolished concrete waste generated in the construction industry. RCA is a sustainable construction material that contributes to minimize land pollution. Because of the adhered mortar on the surface of RCA, it has distinct characteristics, which affect the quality of the green materials made by RCA. To study them more effectively and scientifically, reviewing the elemental and chemical compositions of RCA is essential. This paper presents the findings of X-Ray Florescence (XRF) and X-Ray Diffractometry (XRD) analyses of RCA in the Sri Lankan context. For this study, the RCA samples were collected from the Construction Waste Management (COWAM) center in Galle. The control samples of Natural Concrete Aggregate (NCA) were obtained from a quarry in Avissawella. The test samples in powder form were examined using the XRF test to identify the chemical oxides and using the XRD test to classify the nature of materials consisting in RCA. It concludes that there are higher amounts of CaO and Loss of Ignition (LOI) in RCA than in NCA. And also, there are minor portions of chemical oxides, namely, SiO_2, Al_2O_3, K_2O, Fe_2O_3, and MgO available in RCA against NCA. Finally, the authors recommend further research, especially on the findings of loss of ignition (LOI) that could be associated with the release of volatiles.

Keywords Recycled concrete aggregates · Elemental compositions · Chemical compositions · X-Ray florescence · X-Ray diffractometry

K. P. Arandara (✉) · S. T. Priyadarshana · G. N. Paranavithana
Department of Civil Engineering, Open University of Sri Lanka, Nawala, Sri Lanka
e-mail: kokila@leanandgreensolusions.com

R. B. Mallick
Indian Institute of Technology, Delhi, India

R. Dissanayake
Department of Civil Engineering, University of Peradeniya, Peradeniya, Sri Lanka

© The Author(s), under exclusive license to Springer Nature Singapore Pte Ltd. 2023

R. Dissanayake et al. (eds.), *ICSBE 2022*, Lecture Notes in Civil Engineering 362,
https://doi.org/10.1007/978-981-99-3471-3_56

1 Introduction

There are several definitions and explanations for the word "Sustainability". According to the World Commission on Environment and Development (WCED), one explanation is "meeting needs of the present without compromising the ability of the future generations to meet their own needs" [12]. The demand for sustainable construction and materials is increasing in global and local contexts. Recycled Concrete Aggregate (RCA) is a sustainable construction material produced from demolished concrete waste generated in the construction industry.

Recycled Concrete Aggregates are identified and described in several forms by different researchers with unique abbreviations. For example, Recycled Aggregate (RA) [14], Recycled Concrete Fine Aggregate (RCFA) [19], and Recycled Concrete Coarse Aggregate (RCCA) [6]. There are plenty of Construction and Demolition Waste (CDW) recycling plants in different parts of the world.

Similarly, there are numerous numbers of International Scientific Journals that are cited and utilized by different researchers who are in the industry of RCA from academia as well as from industries across the world. Some of them are the Journal of Cleaner Production, Waste Management, and Industrial Ecology and as per Clarivate Analysis (2017), those journals have average Impact Factors of 5.715, 4.030, and 4.123, respectively [5].

2 Background

In general, RCA is a combination of Natural Concrete Aggregate (NCA) and adhered mortar. As a result, the performance of RCA differs from NCA, particularly in regard to its inertness. As a result, it leads to quite a number of challenges to utilize as an alternative material. RCA shows high porosity & water absorption, low density, weak adhesion between the interfacial transmission zone (ITZ) [8], but adversely, low mechanical strength [14] compared to NCA. Further, it is difficult to predict the behaviour of RCA with respect to cement hydration and alkali-silica reactivity (ASR), due to the lack of knowledge of its chemical constituents.

There are various studies that are performed on the utilization of RCA. By knowing the chemical compositions of RCA, related research could be driven more effectively.

X-Ray Florescence (XRF) analysis and X-Ray Diffractometry analysis (XRD) are two types of useful non-destructive techniques that are available for analyzing the structure of materials, primarily at the atomic and molecular level. Accordingly, those two techniques are used to carry out elemental and chemical composition analysis in material science.

This paper presents findings of XRF and XRD analyses on RCA obtained from the Construction Waste Management (COWAM) center, Galle, Sri Lanka.

3 Aim and Objectives

The study was proceeded to achieve the following aim and objectives.

3.1 Aim

The aim is to review the elemental and chemical compositions of recycled concrete aggregates obtained from the COWAM center.

3.2 Objectives

i. To identify the potential oxide components and their percentage existing in the RCA by XRF analysis;
ii. To recognize the nature (phase) of the selected RCA samples by using XRD analysis;
iii. To compare the results of RCA against NCA and similar findings related to RCA obtained from a literature review.

4 Methodology

In order to achieve the above aim and objectives, the methodology in the flow chart shown in Fig. 1 was adopted.

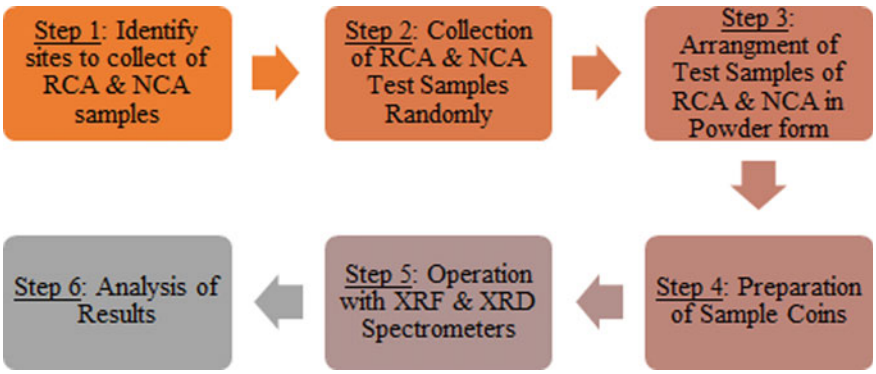

Fig. 1 Steps of the methodology

4.1 Identify Sites and Collection of RCA & NCA Test Samples

For this study, RCA and NCA materials were collected from COWAM center, Galle, and from a well-established quarry in Avissawella. Those were processed manually and maintained to have size number 6 (nominal size 19.0–9.5 mm) as per ASTM C 33. Three sets of samples of RCA were picked randomly as test samples from graded materials. Then, all the RCA and NCA samples were presented in step 3.

4.2 Test Samples in Powder Form

Both RCA and NCA aggregate samples were manually ground to produce finer particles (in powder form) that have a nominal size of less than 100 μm. For this, the service of the National Building Research Organization (NBRO) was taken. Finally, respective test samples were directed to the laboratory to proceed with XRF and XRD analyses.

4.3 Preparation of Coin Samples

Each sample in powder form was mixed with a binding agent (gridding aid) and then homogeneous coins (pallets) were prepared by pressing the mixture in a die. Figure 2 shows the preparation of coin samples.

Fig. 2 Test coin samples preparation in progress

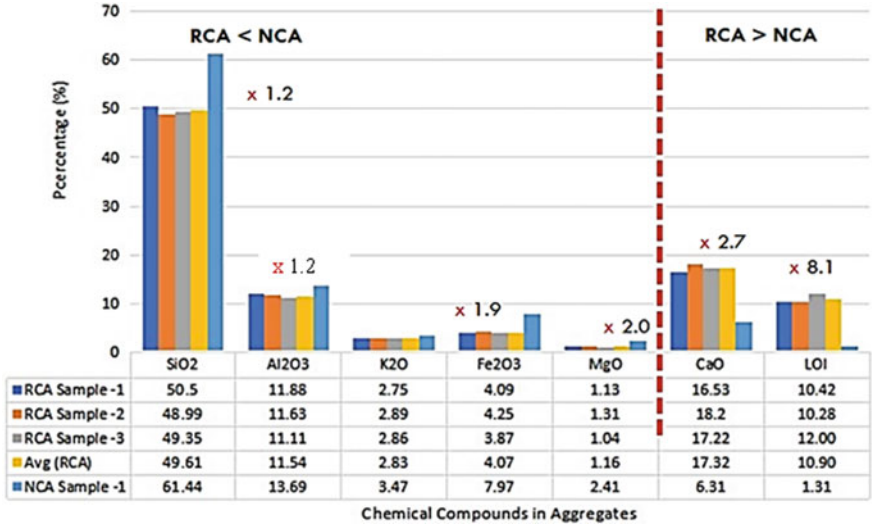

	SiO2	Al2O3	K2O	Fe2O3	MgO	CaO	LOI
RCA Sample -1	50.5	11.88	2.75	4.09	1.13	16.53	10.42
RCA Sample -2	48.99	11.63	2.89	4.25	1.31	18.2	10.28
RCA Sample -3	49.35	11.11	2.86	3.87	1.04	17.22	12.00
Avg (RCA)	49.61	11.54	2.83	4.07	1.16	17.32	10.90
NCA Sample -1	61.44	13.69	3.47	7.97	2.41	6.31	1.31

Graph 1 Analysis of results of XRF of RCA and NCA

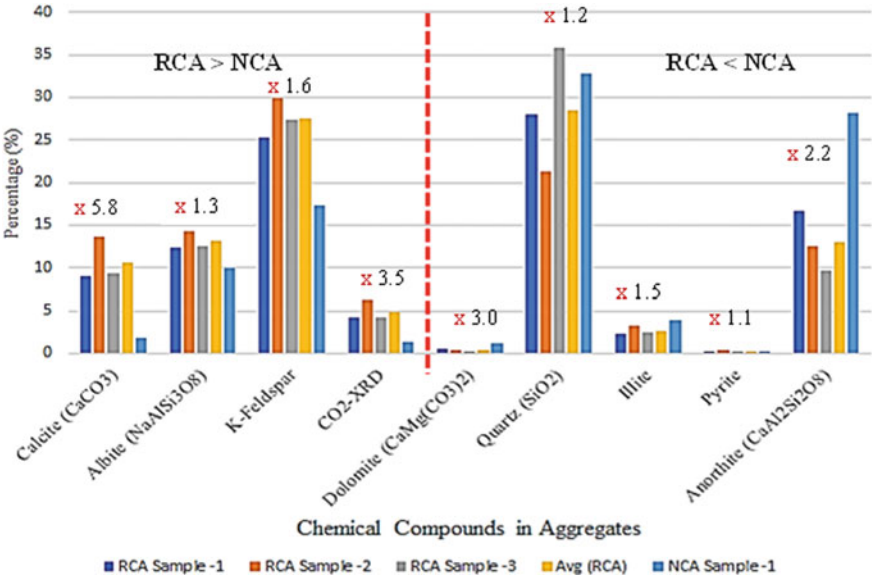

Graph 2 Analysis of results of XRD of RCA and NCA

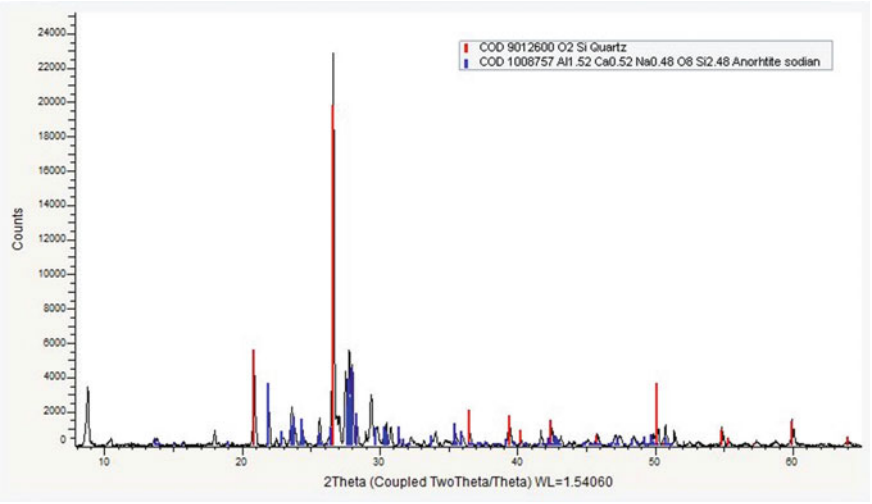

Graph 3 XRD graph–RCA sample 1

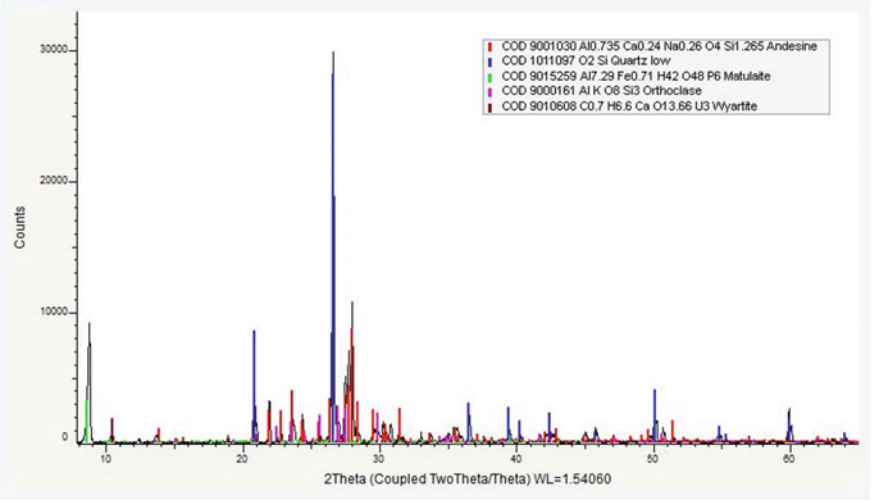

Graph 4 XRD Graph – NCA Sample 1

4.4 Operation with Spectrometers

For this study, timely calibrated XRF and XRD spectrometers and relevant laboratory facilities were utilized. In case of XRF analysis, the brand and the model number are, respectively, "*Thermo ARL*" and "*ARL 9800 OASIS*". Similarly, for the XRD analysis, the "BRUKER" and "*D2 Phaser-2nd Gen*" spectrometers were used.

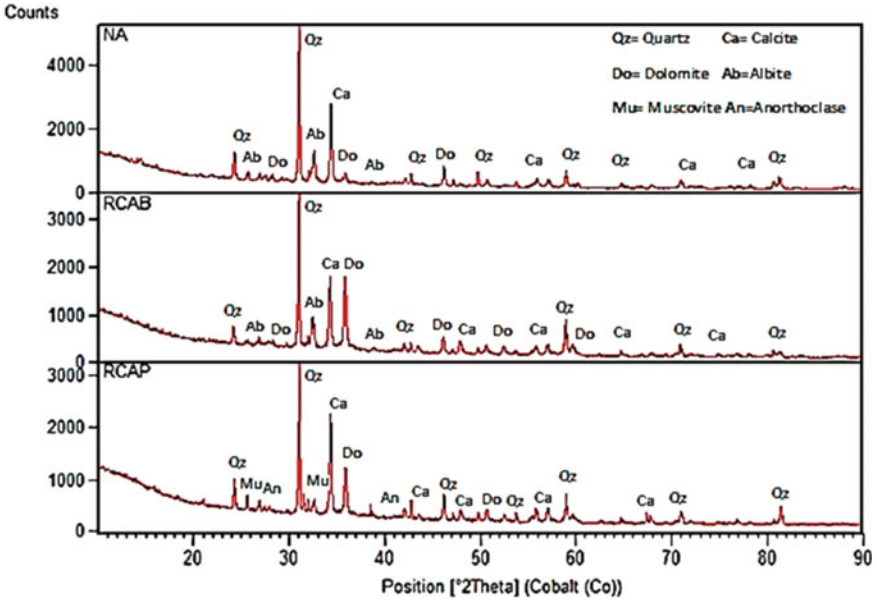

Graph 5 XRD Patterns of Natural Aggregate (NA), RCAP, and RCAB abstracted from the literature [16]

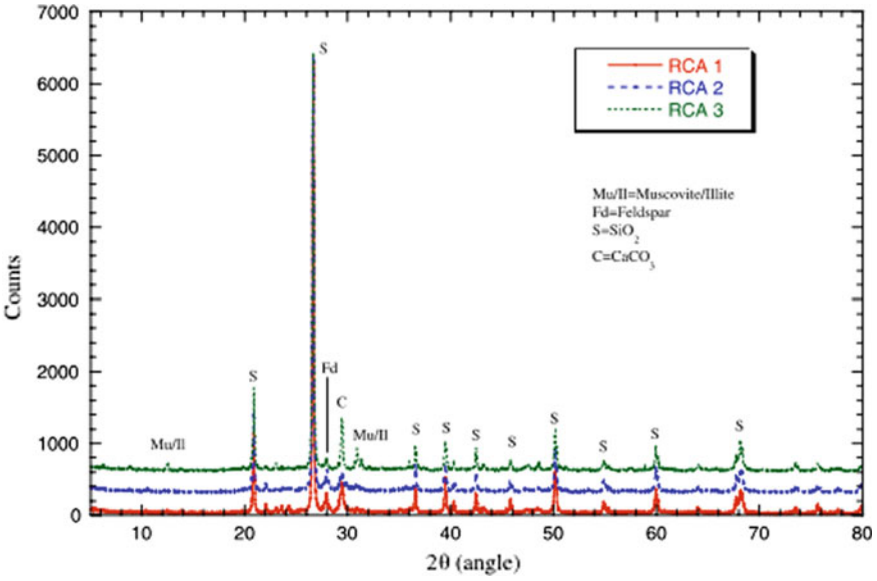

Graph 6 XRD Patterns of RCA Samples (RCA1, RCA2, and RCA3) abstracted from the literature [9]

XRF analysis was proceeded to review the chemical oxides, namely, SiO_2, Al_2O_3, K_2O, Fe_2O_3, MgO, CaO, and loss of ignition (LOI) that are suspected to be available in subjected material samples while following ISO/TR 12,389 standard.

XRD analysis was carried out based on ASTM C 1365 standard and the undermentioned chemical compounds pertaining to selected samples were focused and reviewed. Those compounds are Calcite ($CaCO_3$), Albite ($NaAlSi_3O_8$), K-Feldspar, Dolomite ($CaMg(CO_3)_2$), Quartz (SiO_2), Illite, Pyrite, Anorthite ($CaAl2Si_2O_8$), and CO_2-XRD.

5 Results and Discussion

The chemical oxides' percentages (in weight) produced by the XRF spectrometer are presented in Table 1 and Graph 1.

The above findings are compared with the results abstracted from previous studies pertaining to similar research [16, 3, 2, 13, 4] and presented in Table 2. As per Sanchez-Cotte [16], RCAB and RCAP refer to Recycled Concrete Aggregates of a Building and a Pavement, respectively.

The summary of the literature reveals that there are lower portions of SiO_2, Al_2O_3, and Fe_2O_3 chemical oxides are contained in RCA with respect to NCA. Then the XRF test results of this study are fitted with the comparison presented by Sanchez-Cotte [16]. Also, the amounts of K_2O and MgO are comparatively matched with the summarized results given in Table 2. Further, the XRF results of RCA and NCA pertaining to CaO indicate similar combinations and patterns in the aforementioned comparison.

It could be further investigated to find out whether the respective components resulting in this study as LOI (volatile compounds) are reactive or inactive at ambient

Table 1 Results from XRF Analysis: Percentages of chemical oxides

No	Chemical component	Portions of components (%)				
		RCA sample−1	RCA sample−2	RCA sample−3	Avg (RCA)	NCA sample−1
1	SiO_2	50.5	48.99	49.35	49.61	61.44
2	Al_2O_3	11.88	11.63	11.11	11.54	13.69
3	K_2O	2.75	2.89	2.86	2.83	3.47
4	Fe_2O_3	4.09	4.25	3.87	4.07	7.97
5	MgO	1.13	1.31	1.04	1.16	2.41
6	CaO	16.53	18.2	17.22	17.32	6.31
7	LOI	10.42	10.28	12.00	10.90	1.31
	Total	97.30	97.55	97.45	97.43	96.60

Table 2 Summary of results of XRF test of RCA abstracted from the literature

No	Chemical Oxide	XRF values from literature Sánchez-Cotte et al. [16]						
		RCA				RCAB	RCAP	NCA
		Bianchini et al. [3]	Angulo et al. [2]	Medina et al. [13]	Bui [4]	Sánchez-Cotte et al. [16]		
1	SiO_2	38.65–42.95	68.6	58.29	62.56	34.43	32.13	49.88
2	CaO	19.24–22.8	6.5	13.27	12.01	39.08	43.1	20.85
3	Al_2O_3	7.26–8.85	10.2	7.69	12.52	8.65	7.85	12.0
4	Fe_2O_3	3.09–3.36	3.3	6.12	5.82	3.06	3.01	5.85
5	Na_2O	0.94–1.06	1.6	1.45	2.69	7.1	7.1	5.45
6	MgO	4.36–5.11	1.2	2.28	1.83	5.73	4.85	2.73
7	K_2O	1.31–1.60	2.8	0.8	1.3	1.03	1.05	0.99
8	Ti_2O	0.29–0.39	–	0	0.62	0.16	0.13	0.33
9	MnO	0.12–0.15	–	0.16	0.12	0.05	0.5	0.17

temperature and under normal conditions. These components could be mainly associated with the release of volatiles; the liberation of water from hydrated lime and hydrated calcium silicates; the emission of carbon dioxide from carbonates; and the loss of water from phyllosilicates and other minor minerals present in CDW [10, 17, 21].

The results related to XRD analysis are given in Table 3 and further analysis is offered based on Graph 2. Here, the percentages are expressed in weight.

Table 3 XRD results and analysis: Percentages of chemical compounds

No	Chemical component	Portion (%)				
		RCA sample−1	RCA sample−2	RCA sample−3	Avg (RCA)	NCA sample−1
1	Calcite ($CaCO_3$)	8.95	13.67	9.4	10.67	1.83
2	Albite ($NaAlSi_3O_8$)	12.41	14.33	12.58	13.11	9.94
3	K-Feldspar	25.25	29.91	27.28	27.48	17.34
4	CO_2-XRD	4.22	6.22	4.23	4.89	1.39
5	Dolomite ($CaMg(CO_3)_2$)	0.6	0.43	0.2	0.41	1.23
6	Quartz (SiO_2)	28.03	21.36	35.77	28.39	32.69
7	Illite	2.26	3.23	2.53	2.67	3.93
8	Pyrite	0.23	0.42	0.07	0.24	0.25
9	Anorthite ($CaAl_2Si_2O_8$)	16.69	12.57	9.57	12.94	28.1

Graph 2 shows that there are significantly higher portions of Calcite, Albite, and K-Feldspar available in RCA than in NCA. Also, considerably, less amount of dolomite, quartz, and anorthite are counted in RCA with respect to NCA.

Further, Graphs 3 and 4 obtained from the XRD spectrometer elaborate on the nature of the materials related to RCA sample 1 and NCA sample 1, respectively. In case of a sharp peak, the material may be taken as crystalline. Also, for a broader peak, it may be poly-crystalline, while in case where there is no peak, but some noisy pattern, then it may be amorphous nature.

The XRD outcomes of this study also are likened to previous findings of previous research. It is found that Graphs 3 and 4 present similar patterns with respect to Graphs 5 and 6 which were reported by Sanchez-Cotte [16] and Limbachiya [9], respectively. Here, RCA1, RCA2, and RCA3 given in Graph 6 refer to recycled concrete aggregate samples obtained from sources 1, 2, and 3, respectively [9].

It is found that XRD patterns for natural concrete aggregates and recycled concrete aggregates samples present predominant peaks of quartz mineral (SiO_2) and Calcite ($CaCO_3$) except for the NCA examined in this study. Also, K-feldspars and sodium silico-aluminates ($NaAlSi_3O_8$) called albite, belonging to the family of feldspar shows comparatively lower peaks with respect to SiO_2 and $CaCO_3$. Also, authors argue that significant mineralogical distinctions were identified in both 3 RCA samples obtained from the COWAM center, Galle as rather minor peaks of illite, indicating the presence of low content in bricks/ceramics bearing phyllosilicate phases. As per Limbachiya [9], this is related to the recycling process at the stage of removal of bricks and other ceramics present in the Construction & Demolition (C&D) waste.

In general, NCA is chemically inactive and in the case of reactive aggregates, those are defined as aggregate-containing substances capable of reacting chemically with the products of solutions or hydration of the Portland cement in concrete or mortar under ordinary conditions of exposure, resulting in some cases in harmful expansion, cracking and staining (ACI 116R-00, 2000). Naturally occurring concrete aggregates are a mixture of rocks and minerals such as granite containing quartz, feldspar, mica, and limestones consisting of calcite and dolomite. Generally, 60% to 70% of the concrete volume is occupied by fine and coarse aggregates and the rest of the volume is mainly decided by the hydrated cement paste. When RCA is produced by crushing such concrete, by default, similar chemical components and chemical oxides could be observed in RCA also. Accordingly, the aforementioned XRF and XRD test results of NCA of RCA validate the same facts by presenting related chemical oxides and compositions in different phases.

Further, in the case of NCA that would consist of certain dolomitic limestones which are alkali reactive and the resulting NCA could be chemically reactive. Such reactive aggregates could react with alkali hydroxides in concrete (Alkali Silica-Reaction (ASR)) and it could be harmful when it produces significant expansion [11]. The phenonium of ASR has been recognized as a potential destress in concrete since the late 1930s (PCA, 1940). The fundamental processes in ASR are swelling and/or dissolution of soluble silica and the formation of alkali silicate gel by their reaction with calcium ions (Ca^+) supplied by cement hydration reactions (SHRP-C-342, 1993). Also, RCA could lead to ASR when the particular RCA is produced

from concrete that has been subjected to an alkali-silica reaction or consisted of silica-reactive aggregates (fine and/or coarse).

Consequently, the types and amounts of chemical oxides of NCA and RCA derived from XRF test could explain the potentials of alkali-silica reaction. For example, Na_2O, K_2O, and CaO of NCA and RCA could encourage alkali-silica reaction by providing Na^+, K^+, and Ca^+ cations respectively to the pore solution in concrete. Also, ASR could be performed in concrete when there are required amounts of reactive-silica (SiO_2) available in particular NCA and/or RCA used for the same concrete. The said scenario is supported by the equation (Eq. 1) presented by Fanijo et al. [7]. Equation 1 explains that Alkali-silicate solution and gel (depending on the level of moisture) are preliminary products of the reaction between siloxane groups ($\equiv Si - O - Si \equiv$) and hydroxyl ions, while R^+ denotes Na^+ and K^+ cations [7].

$$\equiv Si - O - Si \equiv + OH^- + R^+(Naor K) = \equiv Si - O - Na + H - O - Si \equiv \quad (1)$$

6 Conclusions

Based on the above results and discussion, the following conclusions are made.

a. RCA and NCA consist of different chemical oxides and key oxides are SiO_2, Al_2O_3, K_2O, Fe_2O_3, MgO, and CaO.
b. In itself, RCA has a significantly higher percentage in weight of SiO_2, Al_2O_3, and CaO with respect to other types of oxides.
c. XRF analysis indicates that there could be volatile components that are denoted by loss of ignition (LOI).
d. Comparatively, there are fewer portions of SiO_2, Al_2O_3, K_2O, Fe_2O_3, and MgO chemical oxides consisted in RCA with respect to NCA. At the same time, a higher amount of CaO counted in RCA against NCA.
e. RCA has a comparatively higher percentage in weight of $CaCO_3$ than NCA.
f. RCA and/or NCA materials could encourage function ASR in concrete in the event of availability of reactive-silica and other supportive backgrounds.

Also, the authors recommend to have further research on the findings especially, on LOI that could be associated with the release of volatiles.

Acknowledgements The authors express their sincere thanks to those who extended their support to carry out this study. A special thank goes to the COWAM center, Galle, Quarry in Avissawella, and the respective management teams who provided the RCA material samples. Also, the authors convey their regards to the laboratory and its team of Siam City Cement (Lanka) Limited for providing laboratory facilities to carry out the experiments timely.

References

1. ACI 116R-00 (2000) Cement and Concrete Terminology. American Concrete Institute, s.l
2. Angulo SC et al (2008) Chemical-mineralogical characterization of C&D waste recycled aggregates from Sao Paulo Brazil. Waste Manage 29(2):721–730
3. Bianchini G, Marrocchino E, Tassinari R, Vaccaro C (2005) Recycling of construction and demolition waste materials: a chemical-mineralogical appraisal. Waste Manage 25(2):149–159
4. Bui NK (2018) Enhancement of recycled aggregate concrete by a new treatment method. Int J Geomate 14:68–76
5. Chen J, Su Y, Si H, Chen J (2018) Managerial areas of construction and demolition waste: A scientometric review. Internaitonal J Environ Res Public Health 15(2350)
6. Courard L, Rondeux M, Zhao Z, Michel F (2020) Use of recycled fine aggregates from C&DW for unbound road sub-base. Materials-MDPI 13
7. Fanijo EO, Kolawole JT, Almakrab A (2021) Alkali-silica reaction (ASR) in concrete structure: Mechanism, effects, and evaluation test methods adopted in the United States. Case Stud Constr Mater 15
8. Forero JA, Brito JD, Evangelista L, Pereira C (2022) Improvement of the quality of recycled concrete aggregate improvement of the quality of recycled concrete aggregate. Materials 15(2740)
9. Limbachiya MC, Marrocchino E, Koulouris A (2007) Chemical-mineralogical chararaterization of coarse recyled concrete aggregate. Waste Manage 27:201–208
10. Llanes CM (2022) Construction and demolition waste as recycled aggregate for environmentally friendly concrete paving. Environ Sci Pollut Res 29:9826–9840
11. Mather B (1975) New Concern over Alskil-Aggregate Reaction. National Aggregates Association (NAA) and National Ready Mixed Concrete Association (NRMCA), Maryland
12. McDonough W, Partner 1, Partner 2 (1992) The Hannover Principles: Design for Sustainability. Hannover, Germany, Expo 2000 World's Fair
13. Medina C et al (2015) Effect of the constituents (asphalt, clay materials, floating particles and fines) of construction and demolition waste on the propeties of recycled concretes. Constr Build Mater 79:22–22
14. Naik TR, Moriconi G (2005) Environmental-friendly durable concrete made with recycled materials for sustainable conrete construction. J Struct Eng 61(01):237–244
15. PCA (1940) Tests of concrete road materials from California, Major Series 285. Portland Cement Association, s.l
16. Sánchez-Cotte, E. H. et al., 2020. The Chemical-Mineralogical Characterization of Recycled Concrete Aggregates from Different Sources and Their Potential Reactions in Asphalt Mixtures. *International Journal of Materials* , 13(5592).
17. Sharma D, Goyal S (2020) Effect of accelerated carbonation curing on near surface properties of concrete. Eur J Environ Civ Eng: 1300–1321
18. SHRP-C-342 (1993) Alkali-Silica Reactivity: An Overview of Research. Strategic Highway Research Program, National Research Council, Washington, DC
19. Wagih AM, Karmoty HZE, Ebid M, Okba SH (2012) Recycled construction and demolition concrete waste as aggregate for structural concrete. HBRC J, Hous Build Natl Res Cent 9:193–200
20. Yunusa M, Zhang X, Cui P, Tian X (2022) Durability of Recycled Concrete Aggregates Prepared with Mechanochemical and Thermal Treatment. Materials, 15(5792)
21. Zhang D, Ghouleh Z, Shao Y (2017) Review on carbonation curing of cement-based materials. J CO2 Util 21:119–131

Water Resources Planning and Pollution Control

Greywater Treatment by Vertical Subsurface Flow Constructed Wetlands Planted with *Cyperus Involucratus*

M. N. S. Dayarathna, G. M. P. R. Weerakoon, and M. I. M. Mowjood

Abstract In recent decades, constructed wetlands (CWs) have been identified as a cost-effective technique that mimics natural processes in treating wastewater. Reduction of land area requirement while achieving high treatment capabilities is one of the major concerns currently. Therefore, this study evaluated the impact of greenhouse technology on greywater treatment. The experimental setup consists of eight vertical subsurface flow (VSSF) constructed wetland (CW) units planted with emergent macrophyte; *Cyperus involucratus* (umbrella palm). Each wetland unit is sized 45 × 65 cm (diameter x height), prepared using 8–10 mm gravel as the bed media, and planted with four shoots of umbrella palm, approximately 30 cm high. Then, four wetland units were kept inside a greenhouse, while the remaining four were kept outside the greenhouse. Each wetland unit had been fed with synthetic greywater at a 30 cm/day hydraulic loading rate (HLR). Water quality parameters such as pH, electrical conductivity (EC), five-day biochemical oxygen demand (BOD_5), total suspended solids (TSS), total nitrogen (TN), ammonium nitrogen (NH_4–N), nitrate nitrogen (NO_3–N), total organic carbon (TOC) and Copper (Cu) were measured in water samples that were collected from the influent and effluents of each wetland unit. Further, TN and Cu uptake by umbrella palm with respect to plant growth were monitored throughout the study period. Results showed that VSSF CWs planted with locally available emergent macrophyte; *Cyperus involucratus* (umbrella palm) found to be efficient in removing BOD_5, TSS, Cu and NO_3–N from greywater, while NH_4–N, TN and TOC, had a considerable removal in both inside the greenhouse (82, 87, 97, 76, 32, 51 and 45%, respectively) and outside greenhouse (82, 85, 97, 60, 48, 53 and 60%, respectively) wetland systems. No significant difference between the two wetland systems was obtained except for NO_3–N removal, which showed a higher

M. N. S. Dayarathna (✉) · M. I. M. Mowjood
Postgraduate Institute of Agriculture, University of Peradeniya, Peradeniya, Sri Lanka
e-mail: sepalidayarathna@gmail.com

M. I. M. Mowjood
e-mail: mowjood@agri.pdn.ac.lk

G. M. P. R. Weerakoon
Department of Civil Engineering, Faculty of Engineering, University of Peradeniya, Peradeniya, Sri Lanka
e-mail: prabhaw@eng.pdn.ac.lk

© The Author(s), under exclusive license to Springer Nature Singapore Pte Ltd. 2023

R. Dissanayake et al. (eds.), *ICSBE 2022*, Lecture Notes in Civil Engineering 362,
https://doi.org/10.1007/978-981-99-3471-3_57

removal inside the greenhouse wetland system. Similarly, no significant difference in Cu and TN uptake by umbrella palms was observed in VSSF CWs kept inside and outside the greenhouse throughout the study period.

Keywords Greenhouse conditions · *Cyperus involucratus* · Synthetic greywater · Vertical subsurface flow constructed wetlands

1 Introduction

Among the varieties of wastewater, greywater holds a significant proportion of domestic wastewater generated from household activities, except toilet discharge. It is considered a high-volume and low-strength wastewater with a potential for reuse in various purposes such as irrigation, car washing, laundry and toilet flushing [11]. Hence, using high energy utilization techniques to treat greywater will not be cost-effective as it will experience high construction, operation and maintenance costs. Over the conventional wastewater treatment technologies, constructed wetlands (CWs) appeared to be a successful technique for treating greywater as it utilizes natural functions and processes to remove impurities, such as nitrogen, phosphorous, organic compounds and heavy metals from wastewater, by interacting with wetland vegetation, medium and microorganisms [6].

Generally, CWs are classified considering three main factors; the water level in the system, dividing as free water surface and subsurface flow systems; vegetation type, categorizing as emergent, submerged, floating leaves and free-floating type systems; and flow direction, dividing the subsurface systems as horizontal subsurface flow and vertical subsurface flow systems [6]. Among different types of CWs, vertical sub-surface flow (VSSF) CWs have been recognized as a promising technology for treating domestic wastewater due to their unique qualities, such as discontinuous loading of wastewater, higher oxygen transferring capability and efficient removal of organics and other nutrients [18]. However, CWs are engaged with some constraints during the practical application, such as the design requirement of large land area and vulnerability to extreme weather conditions. Greenhouses have become increasingly important when climatic conditions are at extremes, and it utilizes the area efficiently while maintaining controlled environmental conditions for agricultural production. Since wetland plants are crucial for removing pollutants, establishing greenhouse conditions with the help of suitable macrophytes could be sustainable to overcome some of the limitations in CWs.

2 Materials and Methods

2.1 Description of the Experimental Setup

This experiment was conducted at Meewathura Farm of the Department of Agricultural Engineering, Faculty of Agriculture, University of Peradeniya (80° 35′ 32″ E, 70° 15′ 16″ N). The experimental setup consisted of eight VSSF CWs units of size 45 × 64 cm (average diameter x height), prepared using 8–10 mm gravel as the wetland media and gravel (10–12 mm) as the drain field. Each wetland unit was planted with four shoots of locally available emergent macrophyte *Cyperus involucratus* (umbrella palm) at approximately 25 cm height (Fig. 1). Four of these VSSF CWs units were kept inside a greenhouse, while the remaining four were kept outside the greenhouse in an open environment as control units. Figure 1 presents the layout plan of the experimental setup and the schematic view of a VSSF CW unit planted with umbrella palms, respectively.

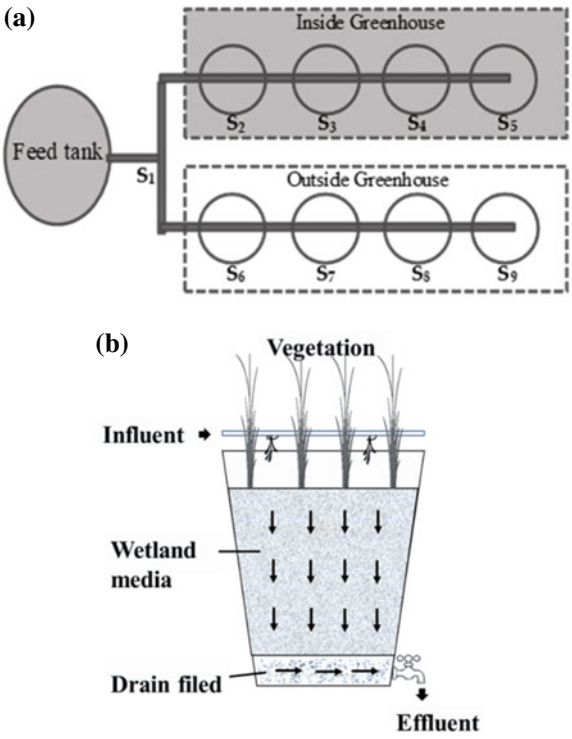

Fig. 1 **a** Layout plan of experimental units (S1–S9: Sample points) **b** Schematic diagram of a wetland unit

2.2 Synthetic Greywater Preparation

Greywater was produced synthetically, according to [1], using 100 g of granular sugar, 20 g of urea, 120 g of sodium chloride, 85 g of sodium hydrogen carbonate, 55 g of calcium chloride, 120 g of magnesium sulphate, 85 g of monopotassium phosphate, 3 g of boric acid, 0.35 g of ammonium molybdate tetrahydrate, 25 g of sodium sulphate, 20 g of potassium nitrate, 30 g of calcium nitrate, 75 g of ammonium chloride and 7 g of copper (II) sulphate in 1000 L tap water and all eight wetland units were fed at 30 cm/day hydraulic loading rate (HLR) intermittently in 12 batches using a pressure pump and a GRÄSSLIN programmable digital timer. Before applying synthetic greywater, all the units were kept under submerged conditions for four weeks and two weeks under intermittent feeding with tap water to facilitate plant growth and wash off the remaining impurities in wetland units.

2.3 Wastewater Analysis

Once the synthetic greywater was introduced to wetland systems, after an acclimatizing period of two weeks, samples were collected from the influent and effluents of each wetland unit at the one-week interval and immediately sent to the Environmental Engineering laboratory at the University of Peradeniya for analysis. Water quality parameters such as pH, electrical conductivity (EC), five-day biochemical oxygen demand (BOD_5), total suspended solids (TSS), total nitrogen (TN), total organic carbon (TOC), ammonium nitrogen (NH_4–N), nitrate nitrogen (NO_3–N) and copper (Cu) were measured in each sample, following the Standard Methods for Water and Wastewater Analysis [5]. Then, the removal efficiencies (*RE*) of each water quality parameter for each wetland unit were estimated using Eq. 1.

where *Ci*–Influent concentration; *Ce*–Effluent concentration.

$$RE = \frac{Ci - Ce}{Ci} \times 100 \tag{1}$$

The BOD_5 concentration was determined using a standard 5-day BOD test, using a membrane electrode DO meter (HI 2400 of HANNA Instruments) for DO measurements. The common filtration technique was followed to analyse TSS, and pH and EC were measured using portable pH and EC probes. TN and TOC were determined by using SHIMADZU TOC-L total organic carbon analyser. NH_4–N and NO_3–N were measured using a UV/VIS spectrophotometer (UV-T600S and SHIMADZU UV-2700, respectively), while Cu concentration was measured using SHIMADZU AA-7000 atomic absorption spectrophotometer.

2.4 Plant Growth Measurements

Plant growth parameters such as plant height and the number of shoots were measured throughout the study period at a 1 week's interval. Further Cu and TN uptake by leaves also were measured.

2.5 Statistical Analysis

All statistical analysis was performed using "MINITAB 17" statistical software. The Anderson–Darling test determined the normality of measured wastewater parameters. The two-sample t-test was used to determine the significant treatment differences of means between wetland systems under the probability of 0.05.

3 Results and Discussion

3.1 Wastewater Characteristics

The average influent and effluent wastewater concentrations in VSSF CWs kept inside and outside the greenhouse during the study period are presented in Table 1. The corresponding average removal efficiencies of each parameter are shown in Table 2.

Table 1 Average influent and effluent characteristics in VSSF CWs units kept inside and outside the greenhouse

Parameter	Influent	Effluents	
		Inside the GH	*Outside the GH*
pH	6.77 ± 0.2	6.80 ± 0.3	6.73 ± 0.2
EC (μS/cm)	938.69 ± 75.3	956.27 ± 66.8	953.00 ± 74.2
BOD_5 (mg/l)	41.99 ± 11.6	6.71 ± 1.8	7.25 ± 3.6
TSS (mg/l)	26.23 ± 3.3	3.44 ± 1.7	3.86 ± 1.4
TN (mg/l)	70.54 ± 15.1	34.56 ± 3.1	33.35 ± 3.8
TOC (mg/l)	31.89 ± 6.2	17.39 ± 11.5	12.74 ± 0.8
NH_4–N (mg/l)	13.88 ± 5.3	10.31 ± 2.9	8.74 ± 4.9
NO_3–N (mg/l)	4.36 ± 1.6	1.02 ± 0.3	2.13 ± 1.3
Cu (mg/l)	0.22 ± 0.101	0.008 ± 0.010	0.006 ± 0.005

Table 2 Average removal efficiencies of BOD_5, TSS, TN, TOC, NH_4–N, NO_3–N and Cu in VSSF CWs kept inside and outside the greenhouse

Parameter	Removal efficiency (%)		*P value*
	Inside the GH	Outside the GH	
BOD_5	82	82	0.921
TSS	87	85	0.454
TN	51	53	0.712
TOC	45	60	0.670
NH_4–N	32	48	0.436
NO_3–N	76	60	0.030
Cu	97	97	0.743

3.2 Five-Day Biochemical Oxygen Demand (BOD_5) Removal

The variation of BOD_5 concentrations and BOD_5 removal efficiencies for VSSF wetland units kept inside and outside the greenhouse are shown in Fig. 2a and b, respectively.

Accordingly, it was noted that there is a higher reduction of BOD_5 in both inside and outside wetland systems with the same average removal efficiency of 82%, obtaining no significant difference between them, proving both systems are capable of removing BOD_5 effectively.

BOD_5 evaluates the degradation of organic matter, where microbial metabolism and physical mechanisms such as sedimentation and adsorption are the main routes for removing BOD_5 in the presence of dissolved O_2 [8]. The VSSF CWs can remove higher BOD_5 under better O_2 transfer capability, and biological degradation is mostly aerobic [9, 17]. Moreover, [8] and [13] mentioned that the rhizosphere of plants provides sufficient habitat for the growth of decomposing bacteria while releasing O_2 for better aeration within the wetland system to remove the BOD_5 effectively.

3.3 Total Suspended Solid (TSS) Removal

The variation of TSS concentrations and TSS removal efficiencies for VSSF wetland units kept inside and outside the greenhouse are shown in Fig. 3a and b, respectively.

Accordingly, both inside and outside CWs showed a substantial reduction of TSS, 87% for the inside system and 85% for the outside system, even though no significant difference could be observed between them ($P > 0.05$), showing both systems are capable of effective removal of TSS.

Physical mechanisms, including sedimentation and filtration, are responsible for removing suspended solids, while non-settleable solids are mostly removed through bacterial digestion and adsorption [15]. According to [3] and [13], the availability of suitable macrophytes with extensive root systems in CWs could develop a higher

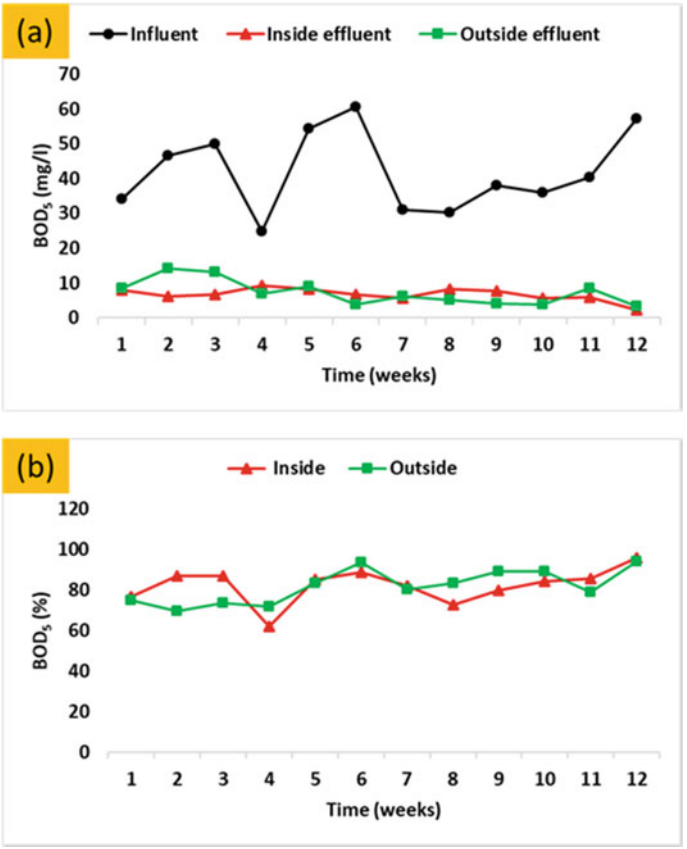

Fig. 2 Variation of **a** BOD_5 concentrations at the influent and effluents and **b** BOD_5 removal efficiencies in VSSF wetland units kept inside and outside the greenhouse

removal of TSS by increasing the surface area for microbial attachment while settling and filtering of solids by reducing the velocity.

3.4 Nitrogen Removal

Physicochemical and biological processes are the commonly involved two key processes in nitrogen removal in CWs. Major biological mechanisms include ammonification, nitrification, denitrification, anaerobic ammonia oxidation, plant uptake and absorption, microbial uptake and nitrogen fixation, while major physico-chemical mechanisms include volatilization, adsorption and sedimentation [10, 16].

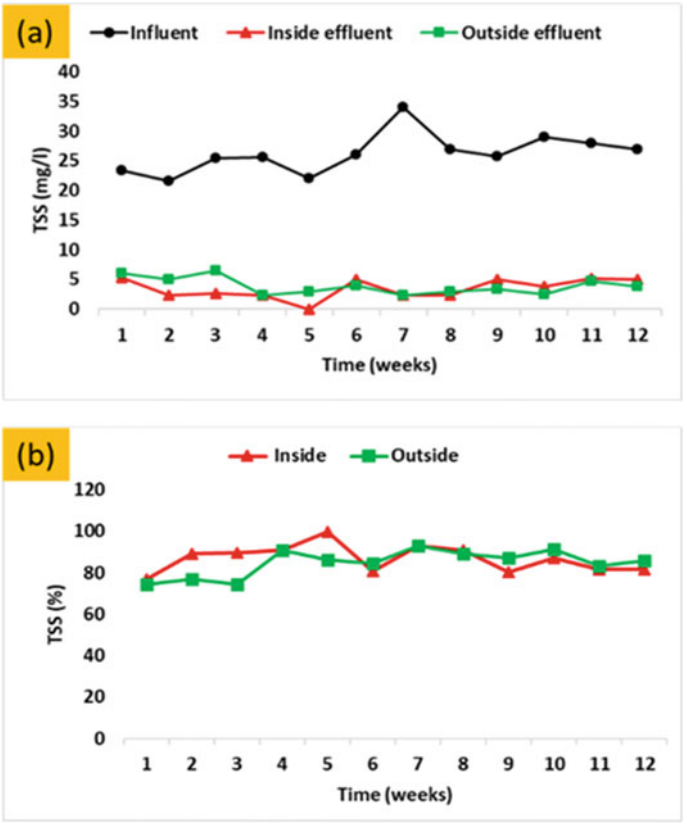

Fig. 3 Variation of **a** TSS concentrations at the influent and effluents and **b** TSS removal efficiencies in VSSF wetland units kept inside and outside the greenhouse

3.4.1 Ammonium Nitrogen (NH_4–N) Removal

Variations of NH_4–N concentration and NH_4–N removal efficiencies for VSSF wetland units kept inside and outside the greenhouse are shown in Fig. 4a and b, respectively.

Accordingly, wetland systems kept inside the greenhouse removed only NH_4–N 32% while outside systems removed 48%, respectively. However, the statistical analysis showed no significant difference between wetland systems.

Although a significant reduction in NH_4–N was expected in VSSF wetlands due to the higher O_2 transferring capacity, both systems could not considerably reduce NH_4–N in this study. This could be due to the complexity of nitrogen removal processes in CWs. As [10] and [18] explain, nitrification and denitrification processes are central for removing nitrogen in CWs compared to other nitrogen removal mechanisms. In the nitrification process, NH_4^+ is biologically converted to NO_2^- and NO_3^- by nitrifying bacteria such as *Nitrosomonas* and *Nitrobacter* in the presence of O_2

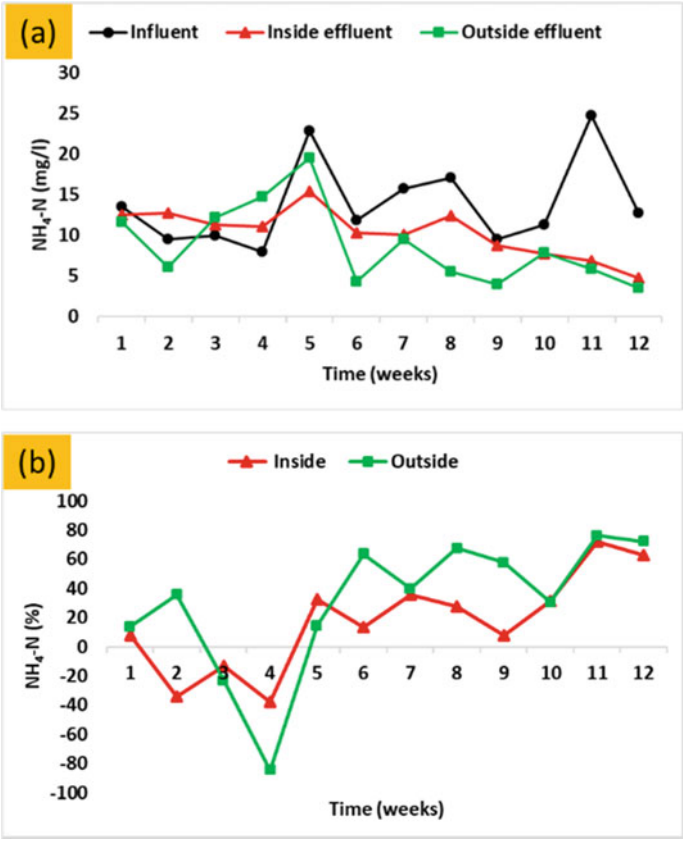

Fig. 4 Variation of **a** NH_4–N concentrations at the influent and effluents and **b** NH_4–N removal efficiencies in VSSF wetland units kept inside and outside the greenhouse

[10]. However, the less successful nitrification observed in the two systems in this study could have been caused by several different factors. According to [16] and [10], temperature, pH, inorganic C, moisture content, microbial population, NH_4–N concentration and dissolved O_2 are the key determinants that affect the rate of nitrification. In addition, [16] noted that the potential magnitude for ammonification is high, while adsorption, plant uptake and microbial uptake are low in VSSF CWs compared to the other types of nitrogen removal mechanisms.

3.4.2 Nitrate Nitrogen (NO_3–N) Removal

Variations of NO_3–N concentration and NO_3–N removal efficiencies of VSSF wetland units kept inside and outside the greenhouse are shown in Fig. 5a and b, respectively.

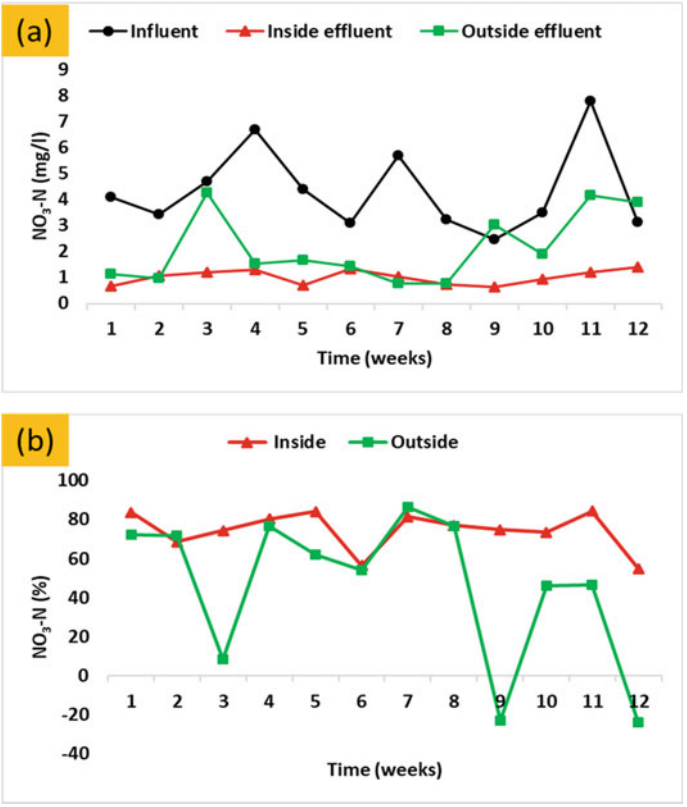

Fig. 5 Variation of **a** NO_3–N concentrations at the influent and effluents and **b** NO_3–N removal efficiencies of VSSF wetland units kept inside and outside the greenhouse

Accordingly, there is a considerable reduction of NO_3–N in both inside and outside VSSF wetland systems (76% and 60% REs, respectively), whereas the inside system showed a significantly higher removal compared to the outside system. Besides, these results contradicted the common point of accumulation or increment of NO_3–N at the effluent of VSSF CWs in the presence of greater O_2 availability.

Denitrification, which is carried out by denitrifying bacteria like *Pseudomonas* under anoxic or anaerobic conditions, is the most common mechanism of removing NO_3–N in CWs, and the rate of denitrification process is influenced by the availability of denitrifying bacteria, sufficient organic carbon, NO_3^- concentration, pH value, temperature and anoxic conditions [16]. In addition, it is mentioned that the potential rate of N uptake by different plant species could be varied depending on their preferred form of N and environmental factors such as temperature [14]. Therefore, favourable conditions such as high temperature and high humidity appeared good for higher removal of NO_3–N in the VSSF wetland systems kept inside the greenhouse.

3.4.3 Total Nitrogen (TN) Removal

Variations of TN concentration and TN removal efficiencies for VSSF wetland units kept inside and outside the greenhouse are shown in Fig. 6a and b, respectively. Both inside and outside wetland systems achieved 51 and 53% of average REs, respectively. But the statistical analysis showed no significant treatment difference ($P > 0.05$) for TN removal between the two systems.

According to [16], only a few processes, such as denitrification, plant uptake, nitrogen fixation and volatilization, are governed by removing total nitrogen (TN) from wastewater, while many other processes convert nitrogen into nitrogen in various other forms. Further, it was noted that these results agree with [16], who mentioned that removal of TN in different CWs could be varied between 40 and 55%.

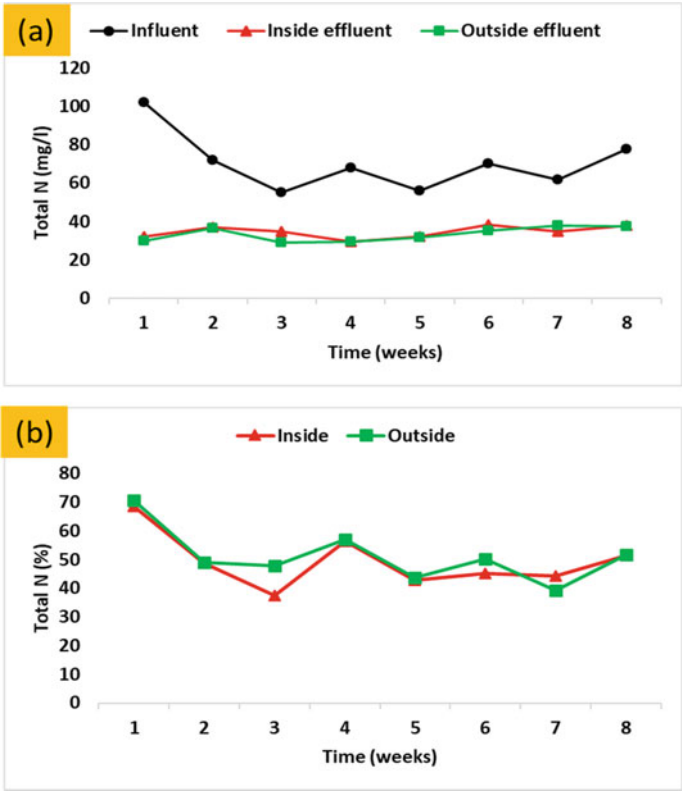

Fig. 6 Variation of **a** TN concentrations at the influent and effluent and **b** TN removal efficiencies in VSSF wetland units kept inside and outside the greenhouses

3.5 Total Organic Carbon (TOC) Removal

In this study, the average TOC removal efficiency in VSSF CWs kept outside the greenhouse was significantly higher (60%) than in the VSSF CWs kept inside the greenhouse (45%).

The main mechanisms for removing organics in subsurface flow CWs include aerobic and anaerobic degradation. In aerobic degradation, organic carbon digestion is perfomed by aerobic heterotrophs, while the anaerobic heterotrophs help in the anaerobic digestion of organic carbon. Among these two types of microbes, aerobic bacteria extensively depend on providing organic material and oxygen for their metabolization.

Since VSSF CWs can intermittently transmit O_2 to the system, aerobic organics removal is highlighted in such systems [12]. Moreover, suitable macrophytes could enhance a better O_2 transfer to the aerobes through their root systems. However, the strength of removing organic carbon could be changed due to the properties of available carbon sources in wastewater concerning the easiness of biodegradability. Additionally, depending on the type of plant, the carbon exudates released from plant roots could increase the effluent's carbon content [7]. This statement could be supported by the significant root development of umbrella palm systems in the inside system, compared to the outside system, which causes a lower removal of organic carbon.

Moreover, [12] reported that organic C removal mechanisms in CWs strongly depend on environmental factors such as pH, temperature and oxygen level, and operational aspects such as organic load, feeding mode and hydraulic retention time (HRT).

3.6 Copper (Cu) Removal

Variations of Cu concentration and Cu removal efficiencies in VSSF wetland units kept inside and outside the greenhouse are shown in Fig. 7a and b, respectively.

In the present study, VSSF wetland systems planted with umbrella palms showed a greater removal efficiency of Cu (inside: 97% and outside: 97% REs, respectively) with no significant treatment difference while establishing capability in effective removal of Cu.

The main mechanisms for heavy metal removal in CWs contain adsorption, precipitation, deposition and absorption or biochemically induced changes by plants and microorganisms [6]. It has been reported that heavy metal accumulation in plants differs depending on the species. Also, it has been reported that the accumulation initially retains by roots and rhizomes, followed by aerial parts [2]. Moreover, [4] determined that heavy metal removal in VSSF CWs planted with *Cyperus alternifolius,* which belongs to the family Cyperaceae, was highly successful.

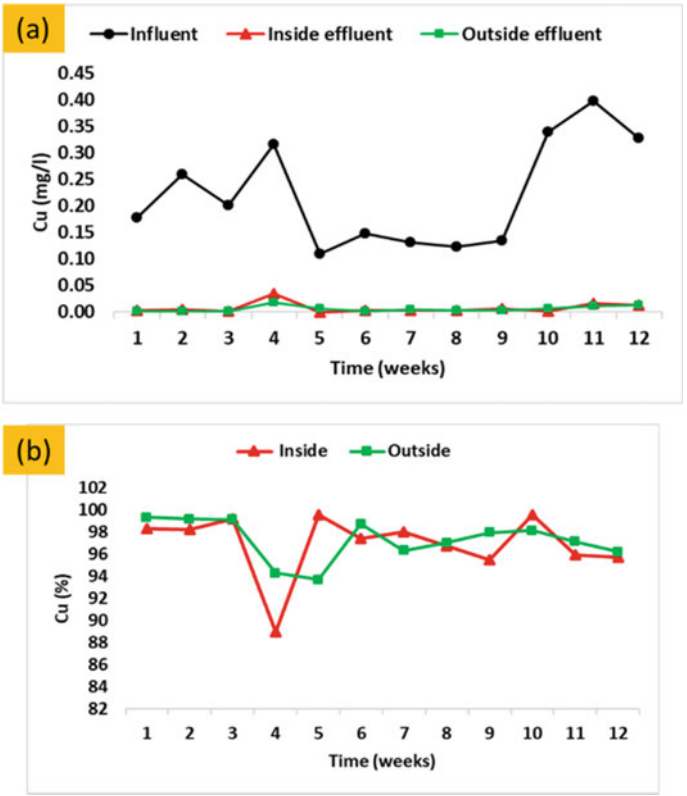

Fig. 7 Variation of **a** Cu concentrations at the influent and effluents and **b** Cu removal efficiencies in VSSF wetland units kept inside and outside the greenhouse

3.7 Plant Growth and TN and Cu Uptake

Changes in plant growth concerning the plant height and the number of shoots in VSSF CWs planted with umbrella palms during the study period are shown in Fig. 8a and b, respectively.

It was observed that average plant growth with respect to plant height was higher in the inside GH system (68 cm) than the outside GH system (61 cm), while the average number of shoots was the slightly opposite way (22 and 25, respectively).

Variations of Total Nitrogen (TN) and copper (Cu) concentrations in leaves of umbrella palms in VSSF wetland units kept inside and outside the greenhouse are shown in Fig. 8c and d, respectively. It was noted that there is no significant difference in Cu and TN uptake by leaves of umbrella palms in VSSF CWs kept inside and outside the greenhouse throughout the study period.

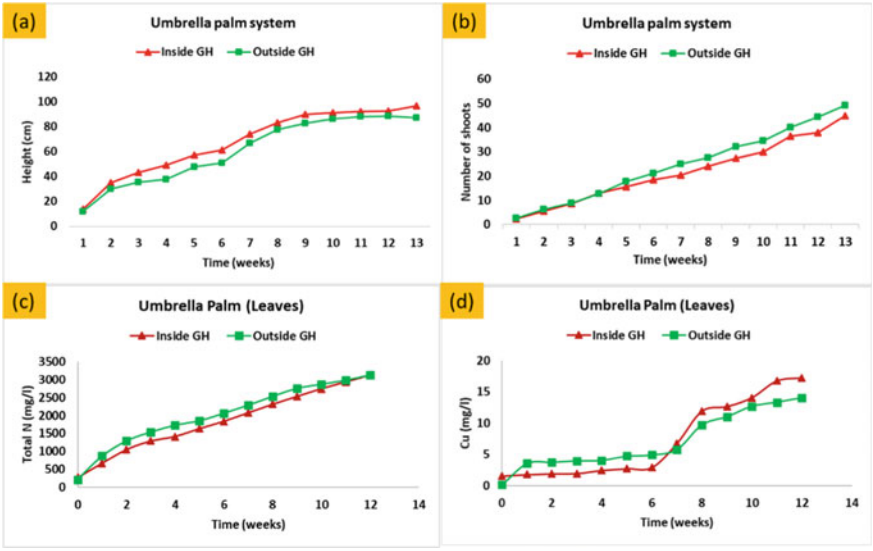

Fig. 8 Variation of **a** average height, **b** an average number of shoots, **c** TN concentration in leaves and **d** Cu concentration in leaves of VSSF wetland units planted with umbrella palms, kept inside and outside the greenhouse

4 Conclusion

Observed results revealed that VSSF CWs planted with locally available emergent macrophyte; *Cyperus involucratus* (umbrella palm) were found to be efficient in removing BOD_5, TSS, Cu and NO_3–N from greywater, while NH_4–N, TN and TOC had a considerable removal in both inside the greenhouse (82, 87, 97, 76, 32, 51 and 45%, respectively) and outside greenhouse (82, 85, 97, 60, 48, 53 and 60%, respectively) wetland systems. No significant difference was obtained between the two wetland systems except for NO_3–N removal, which showed a higher reduction inside the greenhouse wetland system. This suggests that the emergent macrophyte *Cyperus involucratus* plant can be used as a viable vegetation for VSSF CWs to treat greywater, though there is no significant impact from the greenhouse condition in this study.

Acknowledgements The authors would like to acknowledge the Norad WaSo Asia project of the University of Peradeniya for providing funds for this research.

References

1. Abed SN, Scholz M (2016) Chemical simulation of greywater. Environ Technol 37(13):1631–1646
2. Arivoli A, Mohanraj R, Seenivasan R (2015) Application of vertical flow constructed wetland in treatment of heavy metals from pulp and paper industry wastewater. Environ Sci Pollut Res 22(17):13336–13343. https://doi.org/10.1007/s11356-015-4594-4
3. Brix H (1997) Do macrophytes play a role in constructed treatment wetlands? Water Sci Technol 35(5):11–17. https://doi.org/10.2166/wst.1997.0154
4. Cheng S, Grosse W, Karrenbrock F, Thoennessen M (2002) Efficiency of constructed wetlands in decontamination of water polluted by heavy metals. Ecol Eng 18(3):317–325. https://doi.org/10.1016/s0925-8574(01)00091-x
5. Eaton, A.D., Clesceri, L.S., Rice, E.W., Greenberg, A.E. and Franson, M.A.H.A. (2005). APHA: standard methods for the examination of water and wastewater. *Centennial Edition., APHA, AWWA, WEF, Washington, DC*.
6. Herath, I. and Vithanage, M. (2015). Phytoremediation in constructed wetlands. In *Phytoremediation* (pp. 243–263). Springer, Cham.
7. Hunter RG, Combs DL, George DB (2001) Nitrogen, phosphorous, and organic carbon removal in simulated wetland treatment systems. Arch Environ Contam Toxicol 41(3):274–281
8. Karathanasis AD, Potter CL, Coyne MS (2003) Vegetation affects fecal bacteria, BOD, and suspended solid removal in constructed wetlands treating domestic wastewater. Ecol Eng 20(2):157–169. https://doi.org/10.1016/s0925-8574(03)00011-9
9. Kurniadie, (2011) Wastewater Treatment Using Vertical Subsurface Flow Constructed Wetland in Indonesia. Am J Environ Sci 7(1):15–19. https://doi.org/10.3844/ajessp.2011.15.19
10. Lee C, Fletcher TD, Sun G (2009) Nitrogen removal in constructed wetland systems. Eng Life Sci 9(1):11–22. https://doi.org/10.1002/elsc.200800049
11. Oteng-Peprah, M., Acheampong, M.A. and deVries, N.K. (2018). Greywater Characteristics, Treatment Systems, Reuse Strategies and User Perception—a Review. *Water, Air, & Soil Pollution*, [online] 229(8). doi:https://doi.org/10.1007/s11270-018-3909-8.
12. Saeed T, Sun G (2012) A review on nitrogen and organics removal mechanisms in subsurface flow constructed wetlands: Dependency on environmental parameters, operating conditions and supporting media. J Environ Manage 112:429–448. https://doi.org/10.1016/j.jenvman.2012.08.011
13. Sehar S, Sumera N, S., Perveen, I., Ali, N. and Ahmed, S. (2015) A comparative study of macrophytes influence on wastewater treatment through subsurface flow hybrid constructed wetland. Ecol Eng 81:62–69. https://doi.org/10.1016/j.ecoleng.2015.04.009
14. Vymazal, J. (1995). Algae and element cycling in wetlands. *Lewis Publishers Inc.*
15. Vymazal, J. (1998). Removal mechanisms and types of constructed wetlands. *Constructed wetlands for wastewater treatment in Europe*, pp.17–66.
16. Vymazal J (2007) Removal of nutrients in various types of constructed wetlands. Sci Total Environ 380(1–3):48–65. https://doi.org/10.1016/j.scitotenv.2006.09.014
17. Vymazal J (2010) Constructed Wetlands for Wastewater Treatment. Water 2(3):530–549. https://doi.org/10.3390/w2030530
18. Weerakoon GMPR, Jinadasa KBSN, Herath GBB, Mowjood MIM, Zhang D, Tan SK, Jern NW (2016) Performance of Tropical Vertical Subsurface Flow Constructed Wetlands at Different Hydraulic Loading Rates. CLEAN - Soil, Air, Water 44(8):938–948. https://doi.org/10.1002/clen.201500101

Reuse Potential of Drinking Water Treatment Plant Sludge for the Manufacture of Concrete Paving Blocks

S. Sajitthan, E. P. Rajapakshe, I. M. W. K. Illangasinghe, and J. M. A. Manatunge

Abstract This research intends to identify the reuse potential of drinking water treatment plant (DWTP) sludge in concrete paving blocks (CPB). In the current market, the traditional fine aggregate (sand) is completely replaced by quarry dust (QD) due to the increased price and sand mining issues. This study will discuss the suitability of DWTP sludge as an alternative to fine aggregate for the manufacturing of CPB considering the seasonal variation of DWTP sludge. CPBs were cast with the dried WTPS from the Ulapone water treatment plant. The fine aggregate was replaced with WTPS in 30, 40, and 50% by mass (w/w). In addition, Sika Plast®-208 PC (Sika), a high-range water-reducing admixture for early strength concrete was added to every 100 g of cement in the range of 1.0–2.0 ml as per the manufacturer's recommendation. The control sample was cast with the mass mix ratio of 1:2:4 (cement: QD: coarse aggregate). The water/cement (w/c) ratio was varied within the range of 0.5–1.0 in every mix. Compressive strength tests were conducted on the cast samples after 7 days of curing. The 30, 40 and 50% DWTP sludge replaced mix attained 14.08 MPa at 0.6w/c, 14.26 MPa at 0.8w/c and 11 MPa at 0.75w/c, respectively, where the required compressive strength for Class-4 CPB is 15 MPa as per the SLS 1425 Part 2:2011. In the future, the possibility of replacing 50% DWTP sludge with quarry dust can be investigated along with compressive strength tests and durability checks.

Keywords Compressive strength · Concrete paving block · Reuse of sludge · Water/cement ratio · Water reducing admixture · Water treatment plant sludge

S. Sajitthan (✉) · E. P. Rajapakshe · I. M. W. K. Illangasinghe
National Water Supply and Drainage Board, JRDC Building, EOE Pereira Mawatha, Peradeniya, Sri Lanka
e-mail: sajitthan95@gmail.com

J. M. A. Manatunge
University of Moratuwa, Katubedda, Sri Lanka

© The Author(s), under exclusive license to Springer Nature Singapore Pte Ltd. 2023

R. Dissanayake et al. (eds.), *ICSBE 2022*, Lecture Notes in Civil Engineering 362,
https://doi.org/10.1007/978-981-99-3471-3_58

1 Introduction

The circular economy is considered the most suitable sustainable economic system where economic growth is interconnected with the efficient use of resources by reduction and recycling. Drinking water treatment plants (DWTP) in a country can be deemed as an important industrial sector, having the responsibility of solving the basic needs of diverse people and subsequently taking the main role in the economy. The conventional water treatment process is generally consisting of six basic steps of processing: screening, aeration, coagulation and flocculation, sedimentation, filtration, and disinfection. Additionally, some DWTPs include other water treatment processes such as adsorption, air stripping, and ion exchange based on raw water quality and targeting chemical or pollutant removal and for any ascertained purposes [5]. The major sources of residuals (byproducts) from conventional DWTPs are alum or iron coagulation sludges, softening sludge, and filter backwash. These residuals contain organic and inorganic turbidity-causing solids, algae, bacteria, viruses, silt, and clay and precipitated chemicals that are produced during treatment [15]. Figure 1 illustrates the process flow diagram for sludge management in a water treatment plant [4]. In general, the dewatered sludge is dumped into nearby water bodies or in landfills in several countries since it is less expensive but is not an attractive solution due to the possibility of chemical contamination [1]. The relevant environmental protection authorities in each country have set strict guidelines for disposing of waste from DWTPs in open landfills and any water bodies. Thus, DWTP sludge has become a huge burden to the water industries in economic and environmental aspects.

The unsafe way of waste sludge disposal encouraged professionals to reuse it in building and construction material, geotechnics, agricultural application, and pottery making without exposing it to the environment [12]. Also, the unsustainable concrete construction practice due to the high consumption of natural raw resources and the release of greenhouse gases of Portland cement production, leads to the use of many

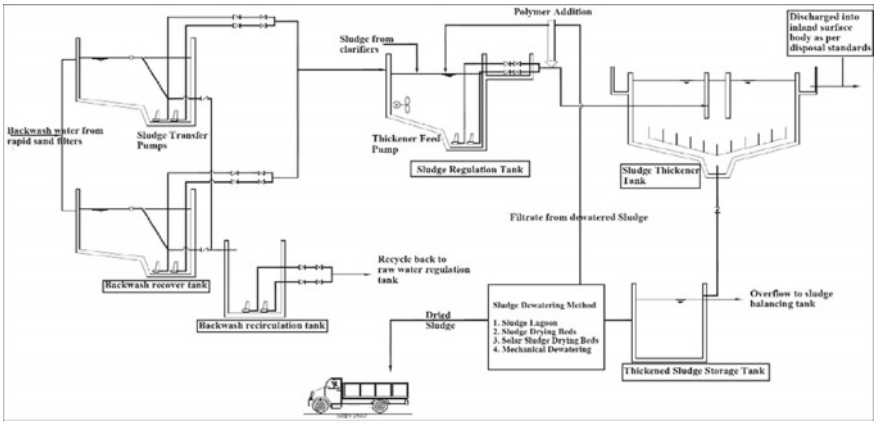

Fig. 1 Process flow diagram for sludge management in water treatment plant

by-products and solid recyclable materials in concrete mixtures for the replacement of cement and aggregates depending on their physical and chemical properties [10].

Further, replacing sludge with fine aggregate will reduce the over-extraction and depletion of river sand [6]. The DWTP sludge particles are generally smaller than fine aggregates, thus enhancing to absorb high amount of water and act as an internal curing resource [14].

Most recent years concrete paving blocks (CPB) usage has increased in low-strength asphalt pavements since bitumen (the primary material of asphalt) is the byproduct of purified crude oil which has an escalating price tendency. As a result, CPB is used in rural roads instead of bitumen roads considering the benefits of low construction and maintenance costs, aesthetic appearance, and durability [9]. A few studies were conducted to utilize the DWTP sludge in CPB. Liu et al. [8] incorporated the application of DWTP sludge as a replacement for sand in the CPB production and tested the prepared CPB with sludge for compressive strength, water absorption, abrasion resistance, sulfate attack and metal leachability. Further, the study illustrates that 10% of DWTP sludge replacement can be replaced for sand in CPB from the test results.

Generally, air-entraining admixtures, polymer-based admixtures, retarders, accelerators, superplasticizers and other several special admixtures are added to cement-based materials to increase the performance of concrete by changing its properties [3]. This research intends to find the suitability of selected air-dry DWTP sludge considering the seasonal variation in CPB production with the addition of high range water reducing admixture (i.e., SikaPlast®-208 PC). The uniaxial compressive strength (UCS) was evaluated for the CPBs with different replacement ratios of DWTP sludge to quarry dust. Further, it discusses the highly variable properties of sludge regarding the seasonal variations in DWTP.

2 Methodology

Initially, a questionnaire survey was carried out for the DWTPs operated by the National Water Supply and Drainage Board, Sri Lanka, the major drinking water utility provider. Based on the survey and the ease of accessibility, six numbers of DWTP as given in Table 1 were selected for the study and sludge samples were collected. The dosage of coagulant and lime given in the Table 1 were the average values used during the particular month when the sludge was collected. All the collected sludge samples were air dried and tested for particle sieve analysis and Atterberg limit according to the test method mentioned in BS 1377: 1990 (Part 2) to identify the soil composition (sand, silt and clay) and plasticity index, respectively. The mass loss on ignition and specific gravity were measured for sludge samples in accordance with BS 1377: 1990 (Part 3) and BS 1377: 1990 (Part 6), respectively.

After considering all the test results, it was decided to use Ulapone sludge which originated in a wet zone of mid-country in Sri Lanka for casting CPB. To find the effect of seasonal variation in raw water, the sludge was collected in both wet and

Table 1 Selected DWTP details from survey (*Note* SL–Sludge Lagoon)

Region	Name of water supply scheme	Type of water sources	Amount of coagulant (mg/l)	Amount of Lime used for PH correction (mg/l)	Average water production (m^3/month)	Average sludge dry production (m^3/month)	Sludge drying process	Treatment for algae
Central East	Balagolla WSS	Reservoir	100	–	370,000	N/A	N/A	No
Central South	Meewathura	River	6	1	1,050,000	42	SL	No
Central South	Ulapone	River	6	–	250,000	10	SL	No
Western	Kethhena WTP	River	7.5	7	1,500,000	80	Decanter	No
Western	Kalatuwawa	Lake	15	12	2,745,000	70	Decanter	DAF
Western	Biyagama I & II	River	10	2	10,800,000	1,200	Decanter	No

dry seasons. Quarry dust is widely used in Sri Lanka's CPB block market since river sand costs are high due to resource scarcity and stringent mining restrictions. In order to find the variation in clay, silt, and sand contents of Ulapone DWTP sludge, particle sieve analysis was carried out using Fritsch-Analysette 22 Nano Tec particle size analyzer. The average turbidity of Ulapone Oya at the DWTP raw water intake point was collected from the central south region laboratory of NWSDB and actual monthly rainfall data was collected from the Kandy rainfall station of the Center for Urban Water, Sri Lanka for the period from June 2021 to July 2022.

CPB samples casting were carried out at the Structural Testing Laboratory at University of Moratuwa, Sri Lanka. The control sample was mixed in the mass ratio of 1:2:4 (cement: quarry dust: coarse aggregate (20 mm)) in 200 * 100 * 65 mm molds. The quantity of sludge as a replacement for quarry dust was varied with 30, 40 and 50% in CPB mix. In addition, SikaPlast®-208 PC (water-reducing admixture) was added within the range of 1.0–2.0 ml to every 100 g of cement as per the manufacturer's recommendation. The composition of CPB mixes cast in the laboratory is summarized in Tables 2 and 3. The CPB samples were cast using the concrete mixer which operates at 15 rpm for 8–10 min. Later, the concrete slump test was measured to check the consistency of each concrete mix and compacted on a vibrating machine table for 2–3 min. The CPB samples were checked for uniaxial compressive strength test after 7 days of curing according to the SLS 1425 Part 2:2011. All the compressive strengths for cast CPB were compared with the required compressive strength of 15 MPa for Class-4 CPBs as per the mentioned standard.

3 Results and Discussion

Particle Sieve Analysis

Table 4 reveals that the sludge produced from reservoir raw water sources (i.e., Kalatuwewa and Balagolla) has higher sand content and loss of ignition (which represents organic content) than the sludge produced from river raw water sources. The specific gravity was less in the sludge from reservoir raw water sources. Specific gravity of the sludge produced from river water sources attained in the range of 2.21–2.35. The plastic limit of sludge depends on the chemicals and their dosages used for the coagulation and flocculation process as well. At the Meewathura, Ulpone, and Biyagama DWTP sludges had non-plastic phenomenon due to the combined effects of raw water source, coagulant type, sludge thickening, sludge dewatering/ drying process and seasonal variation.

Seasonal Variation of Sludge Characteristics

The sludge was collected in the wet and dry seasons from Ulapone DWTP and analyzed. Figure 2 shows that the sludge collected in the dry period consists of clay (11.9%), silt (72.7%), and fine sand (15.4%) while the sludge collected in the wet period consists of clay (6.6%), silt (49.5%), fine sand (38.5%), and medium sand

Table 2 CPB mix material composition in Laboratory with sludge collected on wet season

Sample no	Cement (g)	Quarry Dust (g)	Sludge (g) (g)	%	Coarse aggregate (g)	Water/ cement Ratio	Admixture (ml)	(Sika Plast®-208 PC) every 100gm of ce	Slump (mm)	Length (mm)	Width (mm)	(mm)
LCPBS40-N1	1500	1800	1200	40	6000	0.5	22.5	1.5	16	201	101	62
LCPBS40-N2	1500	1800	1200	40	6000	0.6	22.5	1.5	25	199	98	63
LCPBS40-N3h	1500	1800	1200	40	6000	0.8	22.5	1.5	35	201	100	62
LCPBS50-N1	1500	1500	1500	50	6000	0.6	30	2	20	199	98	63
LCPBS30-N1	2000	1200	2800	30	8000	0.6	20	1	15	199	98	60
LCPBS40-N4	2000	1600	2400	40	8000	0.8	25	1.25	12	200	100	62
LCPBS50-N2	2000	2000	2000	50	8000	0.75	30	1.5	17	199	98	65

Table 3 CPB mix material composition in Laboratory with Ulapone sludge collected on dry season

Sample no	Cement (g)	Quarry dust (g)	Sludge		Coarse aggregate (g)	Water/ Cement ratio	Admixture (Sika Plast®-208 PC)		Slump (mm)	Length (mm)	Width (mm)	Depth (mm)
			(g)	(%)			**(ml)**	every 100 g of cement (%)				
LCPBS0-1	2000	4000	0	0	8000	0.5	0	0	40	199	98	63
LCPBS0-2	2000	4000	0	0	8000	0.6	0	0	155	200	98	64
LCPBS0-3	2000	4000	0	0	8000	0.6	20	1	175	200	98	65
LCPBS30-1	2000	2800	1200	30	8000	0.9	0	0	20	199	98	65
LCPBS30-2	2000	2800	1200	30	8000	0.6	20	1	0	199	97	66
LCPBS30-3	2000	2800	1200	30	8000	0.7	20	1	12	200	99	66
LCPBS30-4	2000	2800	1200	30	8000	0.8	20	1	45	199	98	65
LCPBS30-5	2000	2800	1200	30	8000	0.9	20	1	55	199	98	63
LCPBS40-1	2000	2400	1600	40	8000	0.6	25	1.25	0	199	98	67
LCPBS40-2	2000	2400	1600	40	8000	0.7	25	1.25	0	200	99	64
LCPBS40-3	2000	2400	1600	40	8000	0.8	25	1.25	0	201	99	64
LCPBS40-4	2000	2400	1600	40	8000	0.9	25	1.25	15	200	98	64
LCPBS50-1	1000	1000	1000	50	4000	0.6	30	1.5	0	199	98	67
LCPBS50-2	2000	2000	2000	50	8000	0.7	30	1.5	0	200	98	63
LCPBS50-3	2000	2000	2000	50	8000	0.75	30	1.5	0	199	98	65
LCPBS50-4	2000	2000	2000	50	8000	0.8	30	1.5	0	200	98	63
LCPBS50-5	2000	2000	2000	50	8000	0.9	30	1.5	5	199	98	64
LCPBS50-6	1500	1500	1500	50	6000	0.7	30	2	10	202	100	62

(continued)

Table 3 (continued)

Sample no	Cement (g)	Quarry dust (g)	Sludge		Coarse aggregate (g)	Water/ Cement ratio	Admixture (Sika Plast®-208 PC)		Slump (mm)	Length (mm)	Width (mm)	Depth (mm)
			(g)	(%)			**(ml)**	every 100 g of cement (%)				
LCPBS50-7	1500	1500	1500	50	6000	0.75	30	2	15	201	101	62

Table 4 Particle size distribution, loss of ignition, plasticity index and specific gravity of DWTP sludge collected in the dry season

DWTP	Particle size distribution (%)					LoI (%)	PI (%)	Specific gravity
	Clay	Silt	Sand					
			Fine	Medium	Coarse			
Meewathura	13	74	13	0	0	8	Non-plastic	2.21
Ulapone (Dry season)	12	73	15	0	0	9.8	Non-Plastic	2.31
Kethhena	11	60	29	0	0	8.3	30	2.25
Kalatuwewa	0	36	2	8	54	13.5	19	1.75
Balagolla	5	30	35	30	0	17.1	N/A	1.95
Biyagama	0	100	0	0	0	7.9	Non-Plastic	2.35

(5.4%). Figure 3 illustrates that the raw water extract from Ulapone Oya has low turbidity water in the dry season (January–June) and considerably high turbidity water in the wet season (July–December). Further, it was noted that TDS in the raw water is apparently higher in the dry season. The river Ganga had the same scenario where the silt content decreased by almost 20% and fine sand increased by almost 20% in the wet season compared to the dry season [2].

Compressive Strength

The laboratory tests using the sludge from Ulapone DWTP were made by mix ratios of 30, 40, and 50% as the replacement for quarry dust by mass as in Table 3. Figure 4 shows the compressive strength of three control samples which have the same material composition but different water/cement ratio (w/c) and admixture content. The

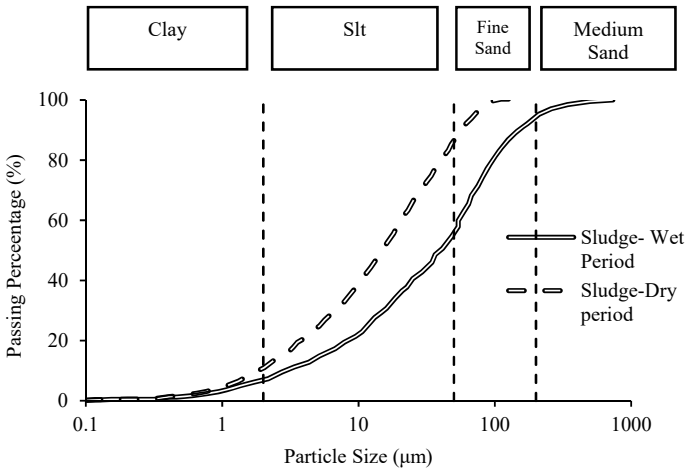

Fig. 2 Particle sieve analysis of Ulapone DWTP sludge collected on Wet and dry periods

compressive strength of LCPBS0-3 (with 1% admixture) was 23.89 MPa, slightly higher than LCPBS0-1 and LCPBS0-2 (without admixture) which achieved the compressive strengths of 20.97 MPa and 19.57 MPa, respectively. All the control samples were satisfied the required compressive strength of 15 MPa for Class-4 CPBs mentioned in SLS 1425 Part 2:2011.

The effect of incorporating Ulapone DWTP sludge in CPB samples can be explained by the compressive strength performance as shown in Figure. The LCPBS30-1 sample (without admixture) which was prepared with an increased w/c has a lower compressive strength of 9.15 MPa compared to the other samples due to the higher water absorption of DWTP sludge. The addition of DWTP sludge causes a lack of water for cement hydration. In addition, the presence of organic matter in

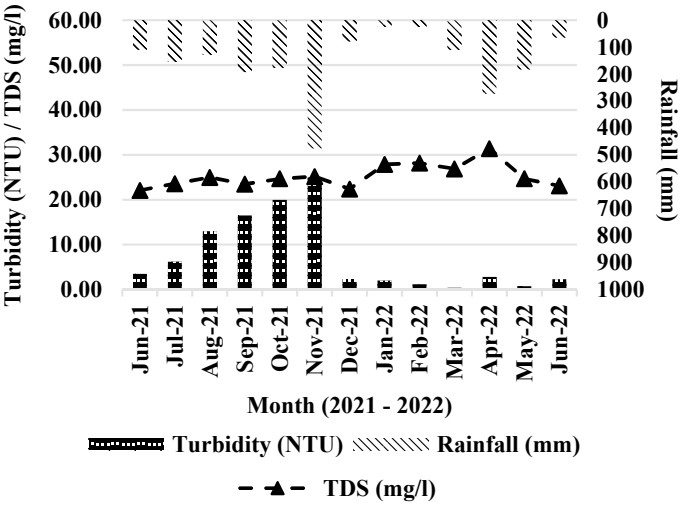

Fig. 3 Rainfall data at Kandy and Turbidity and TDS of raw water at Ulapone intake point

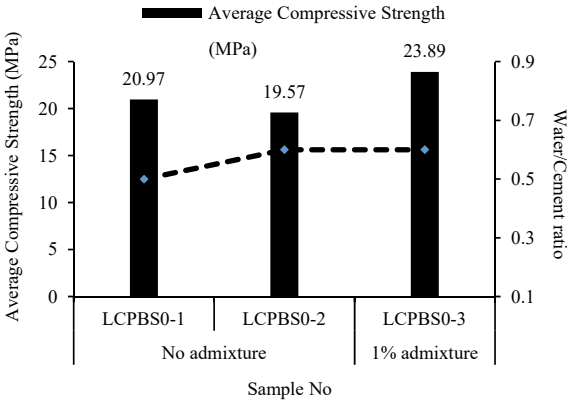

Fig. 4 Control sample for laboratory analysis

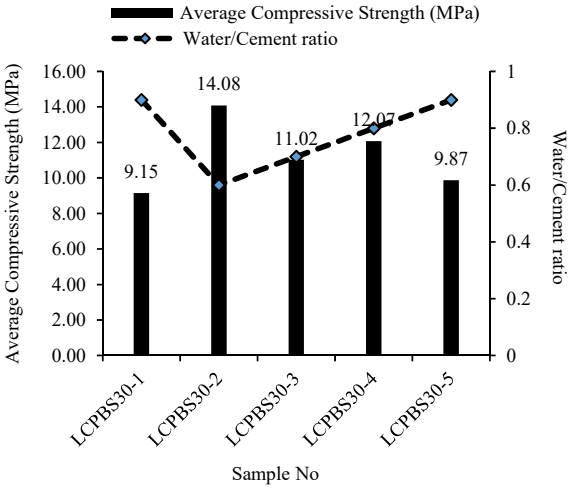

Fig. 5 30% sludge + 1% admixture for laboratory

DWTP sludge may also hinder cement hydration [7, 8]. The inclusion of admixture led the mixes to gain increased compressive strength. The adsorption between the fine particles in DWTP sludge and admixture reduces occurrences of water absorption while the hydration is in progress. Hence, the amount of free water increases and is incorporated for cement hydration. Thus, the slump value was observed higher in LCPBS30-5 (55 mm) than in LCPBS30-1 (20 mm) where both were prepared with the same mix proportions and w/c. Higher strength could be achievable by decreasing the w/c ratio and at the same time increasing the slump of the concrete [11]. However, in the market, CPBs used to be manufactured using hydraulic or electrical machineries where the molds were removed from the fresh blocks instantly. Thus, it is recommendable to produce zero-slump concrete to fulfill the requirement [9]. The LCPBS30-2 sample has a higher value of compressive strength of 14.08 MPa having 0.6 w/c and 0 mm slump. Accordingly, the compressive strengths of LCPBS30-3, LCPBS30-4, and LCPBS30-5 were 11.02, 12.07, and 9.87 MPa, respectively, caused by the rise of w/c.

The higher the water reduction capacity of superplasticizer/ admixture greater the compressive strength gain [13]. In order to find the influences of admixtures, the amount was increased as 1, 1.25, 1.5, and 2% while the DWTP sludge replacement increases as 30, 40, and 50% for quarry dust. Figure 6 illustrates that the optimum compressive strength of 14.26 MPa for the LCPBS40-3 sample was achieved for 40% sludge replacement for quarry dust at 0.8 w/c and in the presence of 1.25% admixture while LCPBS40-1, LCPBS40-2, and LCPBS40-4 were attained 3.69 MPa at 0.6 w/c, 10.37 MPa at 0.7 w/c, and 8.53 MPa at 0.9 w/c, respectively. Likewise, Fig. 7 shows the optimum compressive strength of 11.00 MPa for the LCPBS50-3 sample was achieved for 50% sludge replacement for quarry dust at 0.75 w/c and in the presence of 1.5% admixture while LCPBS50-1, LCPBS50-2, LCPBS50-4, and LCPBS50-5 were attained 3.14 MPa at 0.6 w/c, 7.83 MPa at 0.7 w/c, 7.61 MPa at 0.8 w/c,

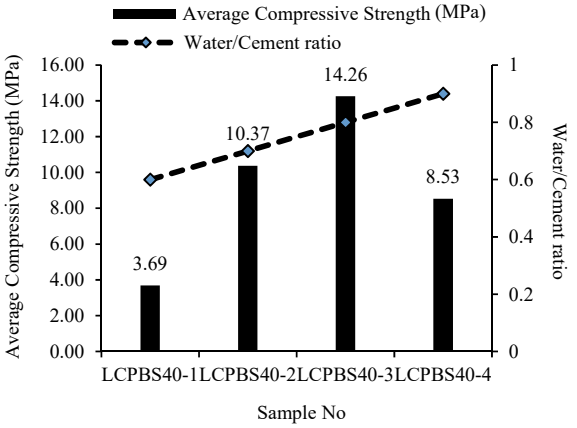

Fig. 6 40% sludge + 1.25% admixture for laboratory analysis

and 7.49 MPa at 0.9 w/c, respectively. Later, the addition of admixture was slightly increased to 2% from 1.5% for the 50% replacement of sludge as shown in Fig. 8. Both the samples (LCPBS50-6 and LCPBS50-7) attained the required strength of 15 MPa at 0.7 and 0.75 w/c.

Figure 9 shows the comparison of the compressive strength of CPBs with sludge collected from dry and wet periods. The CPBs with 30% sludge replacement (wet period), have slightly higher compressive strength in the mix. Likewise, the 40% and 50% sludge replacement with the relevant mix in Fig. 10 shows significant improvement in compressive strength. Lesser the particle size higher the water absorption. Thus, the CPB mix incorporated with the sludge collected from the wet season has better result than the CPB mix incorporated with the sludge collected from the dry season which is illustrated in Fig. 10. CPB mixes LCPBS40-N1, LCPBS40-N2, and LCPBS50-N1 have the compressive strength value of 20.94 , 16.68 , and 18.91 MPa which have exceeded the required value of 15 MPa in SLS 1425 Part 2:2011 by incorporating the sludge collected from the wet season. The CPB mix of LCPBS40-N3 attained 12.35 MPa, less compared to the other mixes which have included the sludge from the wet season due to the increase of w/c.

4 Conclusion and Recommendations

Management of the by-product of the water treatment process, sludge has become critical due to environmental restrictions. However, it has the potential to reuse/recycle and incorporate into the circular economy. This study investigated the reuse potential of DWTP sludge in concrete paving block manufacturing for Class-4 as per the SLS 1425 Part 2:2011. The experimental result of this study determines that the sludge mixed in 40% as a replacement for quarry dust has attained the maximum

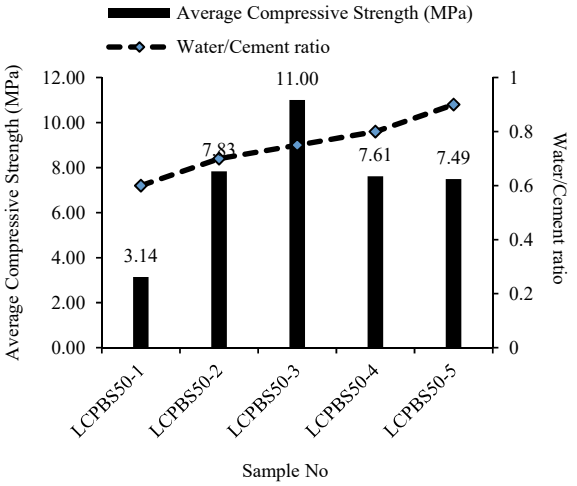

Fig. 7 50% sludge + 1.5% admixture for laboratory analysis

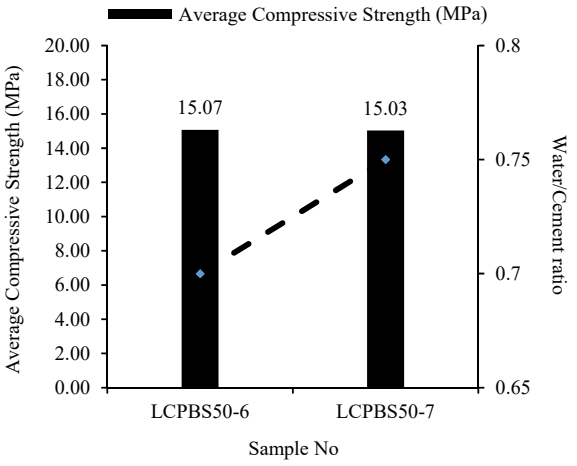

Fig. 8 50% sludge + 2% admixture for laboratory analysis

compressive strength of 20.94 MPa at 0.5 w/c and 1.5% admixture. In addition, some other conclusions can be drawn as follows:

1. Physical properties of the DWTP sludge vary depending on the type of intake water source, seasonal variations, chemicals used during the treatment process, sludge treatment techniques. It is observed that the sludge collected from the wet season contains high sand content than the sludge collected from the dry season due to the higher turbidity in the wet season.
2. When the raw water intake is located at reservoirs, the sludge contains higher sand contents and less clay and silt contents.

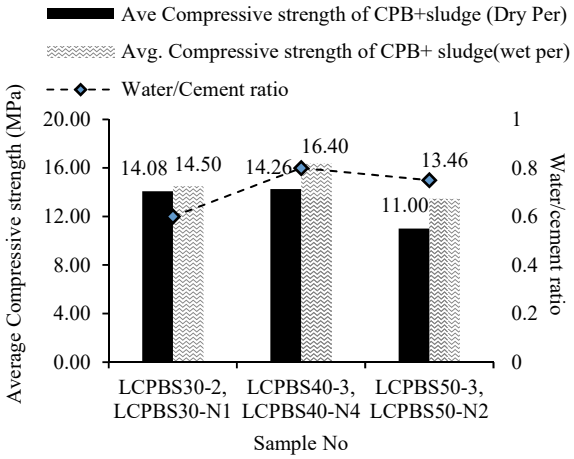

Fig. 9 Comparison of compressive strength due to sludge seasonal variation

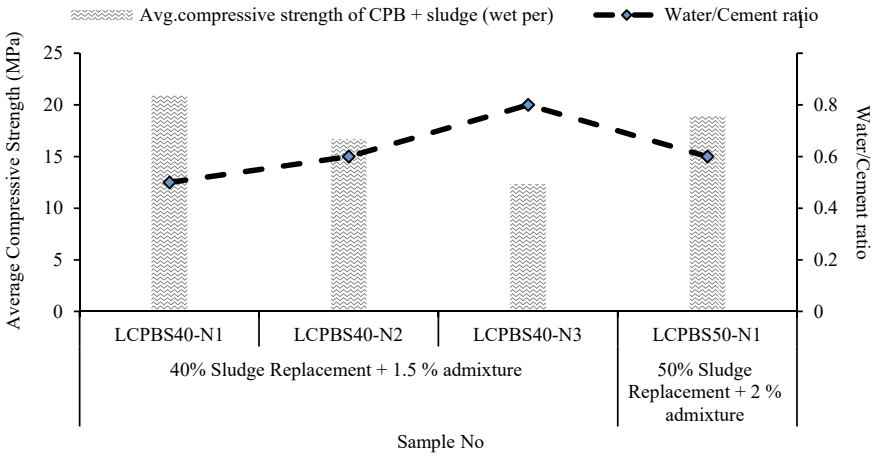

Fig. 10 Compressive strength of CPB with Ulapone sludge collected at wet season

3. The compressive strength of CPB mixed with DWTP sludge has increased after the addition of high range water reducing admixture (i.e., SikaPlast®-208 PC) with optimum w/c since, adsorption between the fine sludge particles and admixture reduces the water absorption capacity of sludge fine particles while the hydration is in progress
4. The CPBs cast with sludge collected in the wet season have higher compressive strength than the CPB cast with the sludge collected in the dry season.

The possibility of sludge replacement for quarry dust by more than 50% can be investigated in the future by increasing admixture and reducing w/c. In addition, to

compressive strength, it is recommended to study the durability of CPB manufactured with DWTP sludge.

Acknowledgements The authors are grateful for the support of the National Water Supply and Drainage Board and Structural Laboratory Testing Laboratory of the University of Moratuwa.

References

1. Ahmad T, Ahmad K, Alam M (2016) Characterization of water treatment plant's sludge and its safe disposal options. Procedia Environ Sci 35:950–955. https://doi.org/10.1016/j.proenv.2016.07.088
2. Ahmad T, Ahmad K, Alam M (2017) Sludge quantification at water treatment plant and its management scenario. Environ Moni Assess 189(9). https://doi.org/10.1007/s10661-017-6166-1
3. Ahmed, A. R. M. A. R., & Mahjoub, M. O. (2001). *The Effect of Admixtures on Concrete Properties. 2001*.
4. Design Manual-D3 Water Quality and Treatment (2020). National Water Supply and Drainage Board
5. Jain R, Camarillo MK, Stringfellow WT (2014) Threats.Drink Water Secur Eng, Plan, Manag:45–67. https://doi.org/10.1016/B978-0-12-411466-1.00003-3
6. Kaish ABMA, Odimegwu TC, Zakaria I, Abood MM, Nahar L (2021) Properties of concrete incorporating alum sludge in different conditions as partial replacement of fine aggregate. Constr Build Mater 284:122669. https://doi.org/10.1016/j.conbuildmat.2021.122669
7. Liu Y, Zhuge Y, Chow CWK, Keegan A, Li D, Pham PN, Huang J, Siddique R (2020a) Utilization of drinking water treatment sludge in concrete paving blocks: Microstructural analysis, durability and leaching properties. J Environ Manag 262(November 2019):110352. https://doi.org/10.1016/j.jenvman.2020.110352
8. Liu Y, Zhuge Y, Chow CWK, Keegan A, Li D, Pham PN, Huang J, Siddique R (2020) Properties and microstructure of concrete blocks incorporating drinking water treatment sludge exposed to early-age carbonation curing. J Clean Prod 261:121257. https://doi.org/10.1016/J.JCLEPRO.2020.121257
9. Mampearachchi W (2019) Handbook on concrete block paving. In: Handbook on Concrete Block Paving. https://doi.org/10.1007/978-981-13-8417-2
10. Moriconi G (2007) Recyclable materials in concrete technology: sustainability and durability. In: Proc Special sessions of first inter. conf. on sustainable construction materials and technologies, pp 11–13
11. Nkinamubanzi PC, Mantellato S, Flatt RJ (2016) Superplasticizers in practice. Sci Technol Concr Admix:353–377. https://doi.org/10.1016/B978-0-08-100693-1.00016-3
12. Odimegwu TC, Zakaria I, Abood MM, Nketsiah CBK, Ahmad M (2018) Review on different beneficial ways of applying alum sludge in a sustainable disposal manner. Civil Eng J 4(9):2230. https://doi.org/10.28991/cej-03091153
13. Pereira P, Evangelista L, De Brito J (2012) The effect of superplasticisers on the workability and compressive strength of concrete made with fine recycled concrete aggregates. Constr Build Mater 28(1):722–729. https://doi.org/10.1016/j.conbuildmat.2011.10.050
14. Pham PN, Duan W, Zhuge Y, Liu Y, Tormo IES (2021) Properties of mortar incorporating untreated and treated drinking water treatment sludge. Constr Build Mater 280:122558. https://doi.org/10.1016/J.CONBUILDMAT.2021.122558
15. Qasim SR, Motley EM, Zhu G (2000) Water works engineering : planning, design, and operation. p 844

Effect of Available Topographic Maps on Flood Modeling Studies in Sri Lanka

P. D. P. O. Peramuna, N. G. P. B. Neluwala, K. K. Wijesundara, P. B. R. Dissanayake, S. DeSilva, and S. Venkatesan

Abstract The topography of a model will highly influence the uncertainty of hydraulic model predictions, thus making it a critical factor in urban flood modeling studies. Therefore, features of topographic maps, associated budget requirements, intended accuracy, and purpose of the flood modeling study have to be considered when selecting a dataset. In the Sri Lankan context, Digital Elevation Models (DEM) from topographic maps from the Survey Department of Sri Lanka and remote sensing methods such as Light Detection And Ranging (LiDAR) and Shuttle Radar Topographic Mission (SRTM) have been used for flood modeling. All these datasets possess distinct characteristics and an associated budget. This research is focused on the datasets of LiDAR, SRTM, and topographical maps from the Survey Department and measured the cross sections from a geographic survey. A methodology has been conducted to identify the effect of these datasets to identify relevant information. The study found that datasets are having mismatches in coordinates and could not capture some land features which were eventually rectified according to the study requirements. Furthermore, an accurate depiction of river bathymetry for a flood modeling study is essential. Hence, this paper provides knowledge on the available datasets and their depictions of river bathymetry following insights on selecting the most effective depending on the purpose and resources available. Hence, the findings would be beneficial for terrain map users to accomplish their tasks effectively.

Keywords LiDAR · SRTM · DEM · Terrain

P. D. P. O. Peramuna (✉) · N. G. P. B. Neluwala · K. K. Wijesundara · P. B. R. Dissanayake
Department of Civil Engineering, University of Peradeniya, Peradeniya, Sri Lanka
e-mail: oshini.peramuna@eng.pdn.ac.lk

P. D. P. O. Peramuna · S. DeSilva · S. Venkatesan
Department of Civil Engineering, Royal Melbourne Institute of Technology, Melbourne, Australia

© The Author(s), under exclusive license to Springer Nature Singapore Pte Ltd. 2023

R. Dissanayake et al. (eds.), *ICSBE 2022*, Lecture Notes in Civil Engineering 362,
https://doi.org/10.1007/978-981-99-3471-3_59

1 Introduction

Digital Elevation Models (DEM) developed from topographic maps are at the core of parameters for accurate predictions in runoff flood modeling in a basin. Several topographic maps are available and used for flood modeling studies and those exhibit different characteristics depending on the region. Moreover, some datasets are freely available on the Internet and some have to be acquired from relevant government authorities. Nevertheless, most of the modeling has been done without focusing on the accuracy of the datasets. Therefore, it is essential to analyze the behavior of these datasets before using them for flood modeling concerning the budgetary requirements and the intended accuracy. This paper is intended to describe the differences between such existing spatial datasets, especially in the Sri Lankan context, their behaviors in specific regions, and the depiction of river bathymetry in the final terrain.

Shuttle Radar Topographic Mission (SRTM), Advanced Spaceborne Thermal Emission (ASTER), Light Detection And Ranging (LiDAR), and the topographic maps from the Survey Department of Sri Lanka are the main sources to develop a DEM in Sri Lanka. In a few studies, HydroSHEDS data with 30 s (approximately 900 m) resolution has been used [1]. The topographic maps from the Survey Department are the traditional source for studies which are either 1:10,000 or 1:50,000 maps. In recent times, DEMs have been developed by integrating both 1:10,000 and aerial images for a limited area of the Island. Furthermore, LiDAR data are also available for a specific region such as in parts of the Kelani and Mahaweli basins which can be purchased from the Survey Department of Sri Lanka. Both SRTM and ASTER DEM can be obtained via the official websites for free. One other important aspect of the datasets which must be highlighted is the projection systems which are normally unnoticed. The global datasets of SRTM and ASTER DEM have only a geographic coordinate system with the measurements in angular units. Nevertheless, other datasets possess a projected coordinate system that shows measurements in lengths. Therefore, all the datasets must be projected to a projected coordinate system that is more suitable to Sri Lanka. SLD99_SriLanka_Grid_1999 is the coordinate system commonly used for flood modeling studies in Sri Lanka [2].

In most instances, DEM can be derived directly from spatial datasets such as SRTM, ASTER, and LiDAR. Otherwise, software such as ArcGIS or QGIS is used to develop DEM in most flood modeling studies. However, with the advent of new versions of flood modeling software such as HEC RAS, the DEM can be developed using these new features. This paper contributes to the literature by describing a successful methodology to develop a high-accuracy symmetry map using both software ArcGIS and HEC-RAS (version 6.3) in a Sri Lankan context, which has not been done according to the best of the author's knowledge.

2 Literature Review

Studying the effect of topographic maps in flood modeling in the Sri Lankan context has become an intense topic due to its utmost importance. This literature review mainly focuses on SRTM, LiDAR, and topographical maps of basins commonly used in Sri Lanka.

The usage of LiDAR data is still an emerging practice in Sri Lanka due to its excessive cost in purchasing and acquiring data, thus making it unavailable for the entire island. In Sri Lanka, LiDAR datasets have different resolutions in different regions. [3] has used a LiDAR dataset of 10 m resolution which is available for the lower Kelani basin. In the study of [4], the availability of LiDAR datasets of 1 m and 2 m resolutions in the parts of Western, Central, and Uva provinces can be observed. However, in the latter study, the inability of LiDAR and SRTM data to obtain the river bathymetry elevation is also highlighted.

Nevertheless, to acquire lower elevations in the coastal areas, LiDAR data is used, according to the study of [5]. It mentions the requirement of high-resolution data to assess the future sea level inundation.

The study of Wickramagamage et al. [6], which compared the elevation data of SRTM and LiDAR with a 1:10,000 agricultural-based mapping project (reference dataset), shows that the LiDAR dataset showed the best match with the reference dataset. Furthermore, in that study, SRTM has shown quite an impressive match at higher elevations compared to the lower elevation regions. Nevertheless, as LiDAR is confined to a small region, it concluded that SRTM of 30 m resolution has the most acceptable elevation data for the entire island.

SRTM DEM has been used for many studies in modeling due to its easy access to the datasets and it is free of charge [7]. In some studies, both 1:10,000 maps with 1 m contours and SRTM of 90 m resolution have been used to prepare DEM for the flood modeling study [8, 9].

In the [10], several datasets have been used for the entire Mahaweli basin. However, a detailed investigation of the elevation of the individual datasets that are been used to develop the final DEM has not been discussed. On that account, this paper focuses on different datasets and their accuracy in representing the terrain with special consideration to river bathymetry.

3 Study Area and Datasets

This study uses topographic maps representing a part of the Mahaweli River Basin in the analysis (Fig. 1a). Mahaweli river basin is the largest basin that benefits from both the Southwest and the Northeast monsoons. The basin is subdivided into the Upper Mahaweli Basin, which represents a hilly terrain, and the Lower Mahaweli Basin,

which has a flat topography [10]. In this study, a 46 km long stretch of the Mahaweli River, starting from the Kothmale reservoir up to the Polgolla barrage belonging to the Upper Mahaweli Basin, is considered.

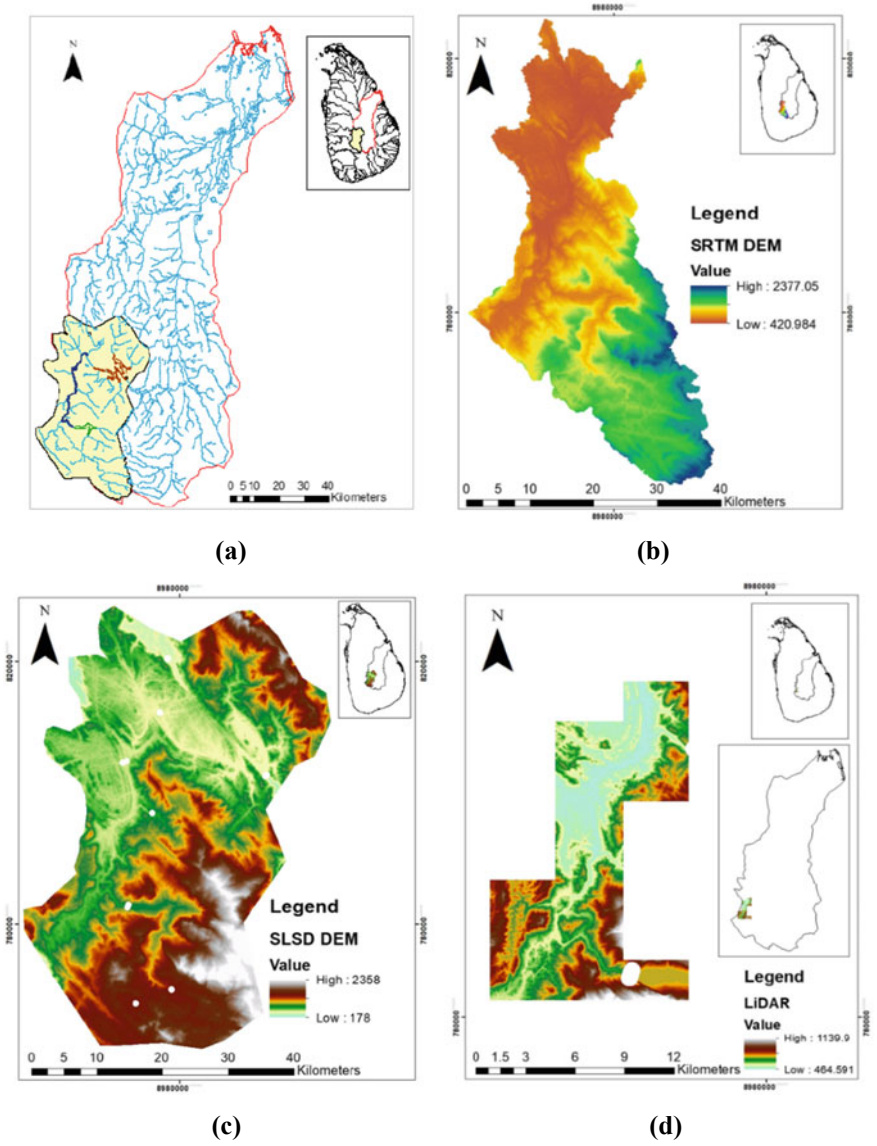

Fig. 1 Study area (**a**), SRTM DEM confined to the study area (**b**), DEM from topographic maps purchased from Sri Lanka Survey Department (SLSD DEM) (**c**) and LiDAR DEM purchased from Sri Lanka Survey Department (**d**)

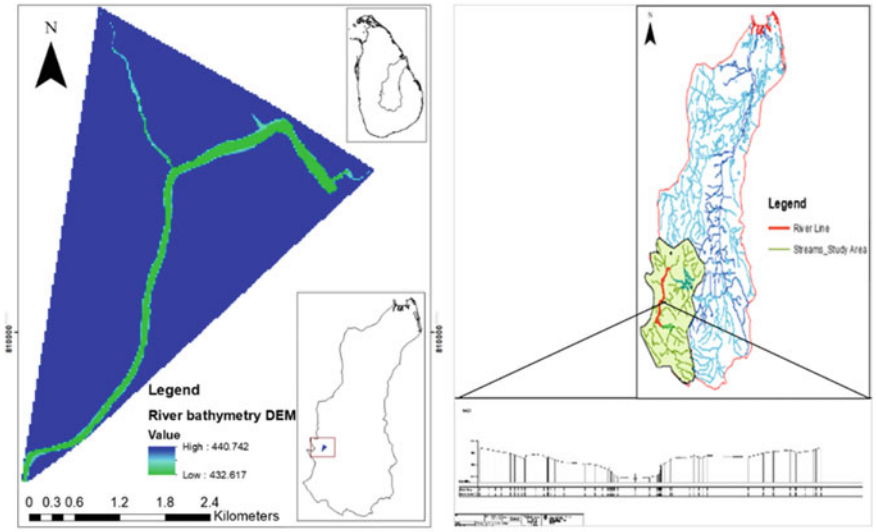

Fig. 2 River bathymetry DEM derived from the study of Lindamulla et al. [12] (**a**) and one of the River cross sections for the 46 km stretch of Mahaweli River (**b**)

The datasets used in this study include modified SRTM DEM confined to the study area, DEM from topographic maps (SLSD DEM) and LiDAR DEM purchased from the Survey Department of Sri Lanka (*Survey Department of Sri Lanka.* (n.d.)). The river bathymetry DEM obtained from the study of Lindamulla et al. [12] and the measured cross sections are shown in Figs. 2a and 2b respectively. Table 1 depicts the sources of the datasets used in the study along with the projection systems, cost per square km and accuracy in both vertical and horizontal directions.

4 Methodology

For a flood modeling study, the topography of the flood plain and watercourse are essential. This section represents the methodology adapted to distinguish the differences between the datasets, representing the topographic features of the study area by bringing all datasets to a common platform where the identification of differences can be easily compared.

The topographic features of the flood plain are mainly represented by LiDAR DEM, SLSD DEM, and SRTM DEM. LiDAR DEM was in the projection system of SLD99_SriLanka_Grid_1999 and thus, used as the common projection system. Hence, both SLSD DEM and SRTM DEM were projected to the same coordinate system using the project raster tool available in ArcGIS software (10.7.1. version).

Table 1 Characteristics of datasets

Dataset	Source	Projection system	Cost per 1 km^2	Accuracy	
				Horizontal	Vertical
LIDAR	Survey department, Sri Lanka	SLD99_ SriLanka_ Grid_1999	Rs. 100	1 m	1–3 m
DEM from SRTM 1 ArcSeond	USGS (*EarthExplorer*. (n.d.))	GCS_WGS_ 1984	Free of charge	30.95 m	10–15 m
DEM from topographical maps	Survey department, Sri Lanka	WGS_1984_ Transverse Mercator	Rs. 5	5.04 m	5–10 m
River bathymetry DEM	Lindamulla et al. [12]	Kandawala_ SriLanka_ Grid	Upon permission from the researcher	25 m	3–5 m
Measured cross sections	Mahaweli authority, Polgolla	No projection system	Free of charge	Cross sections survey with a spacing of 200 m	

However, the elevation of the river bathymetry is not represented extensively by either of these datasets. On the other hand, other datasets on river bathymetry are being focused on. Therefore, the methodology used to develop and modify DEM from the river cross sections and the river bathymetry DEM is discussed here.

4.1 Development of River Bathymetry Digital Elevation Model from Measured Cross-Sections

Measured cross sections were available from the Kothmale reservoir to the Polgolla reservoir, which were obtained from the Mahaweli Authority, Polgolla. In general, the development of a river bathymetry DEM using ArcGIS software is a tedious task. However, generating a river bathymetry DEM in HEC RAS software is quite efficient and it can be used later for flood modeling in the same software.

When the terrain with the selected projection system is input to HEC RAS software, the river profile and the cross sections can be identified very easily at measured distances. Therefore, using the tools in HEC-RAS, the elevations of the cross sections can be edited to form a river bathymetry file. The river bathymetry DEM layer which is in GeoTIFF format was formed by following the methodology shown in Fig. 3.

The cross-section data were in the format of AutoCAD drawings. Therefore, all the elevation data with the longitudinal profile of the cross sections were extracted to an Excel file to make the work easier. Thereafter, google maps were overlaid on the terrain developed from SLSD DEM to draw the river profile and the cross sections on

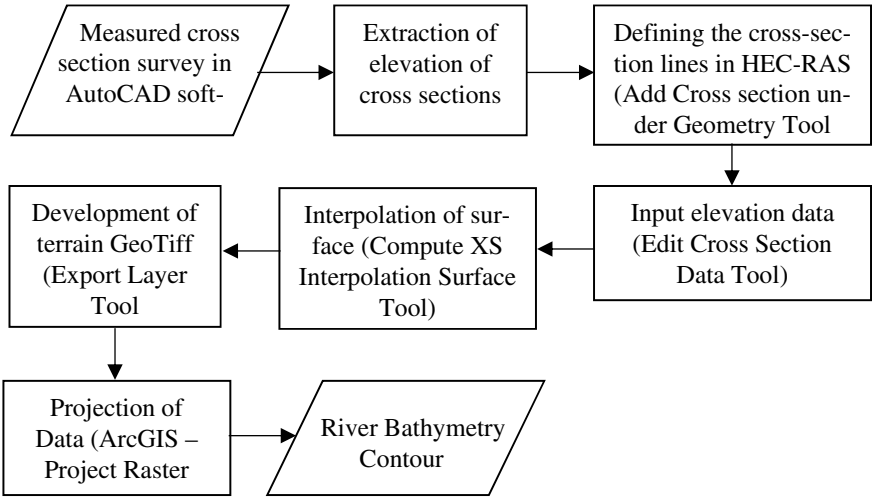

Fig. 3 Flowchart for development of river bathymetry DEM

the HEC RAS software. After that, the elevations extracted from the Excel file were arranged using the cross-section editor in the geometric editor panel. Following the interpolation of the surface, river bathymetry DEM in GeoTIFF format was obtained. This will be named River DEM hereafter. This River DEM was projected to the same projection system; SLD99_SriLanka_Grid_1999 and used for analysis. In addition, this dataset was also analyzed to observe a shift. But none was found. The importance of the projection system and the methodology to observe the shift will be discussed in the latter sections.

4.2 Modification of River Bathymetry DEM from the Study of Lindamulla et al. [12]

The river bathymetry DEM obtained from the study of Lindamulla et al. [12], basically consists of elevations of the flood plain and the bathymetry near the Polgolla barrage. However, there was a constant elevation of 440.74 m in the floodplain area. In addition, although the DEM is projected to the SLD99_SriLanka_Grid_1999 coordinate system, there was a slight shift of the DEM. Therefore, a methodology was formulated to extract only the river bathymetry elevations and to rectify the shift of the DEM (Fig. 4).

Using the identification tool in the ArcGIS software, the elevation of the dataset was measured. A constant elevation was identified in the flood plain while the elevations in the river section varied. Thereafter, the elevation of the river bathymetry data was extracted using an extraction tool and then a terrain was projected and exported in ArcGIS software. Following the methodology, all the datasets; the exported river

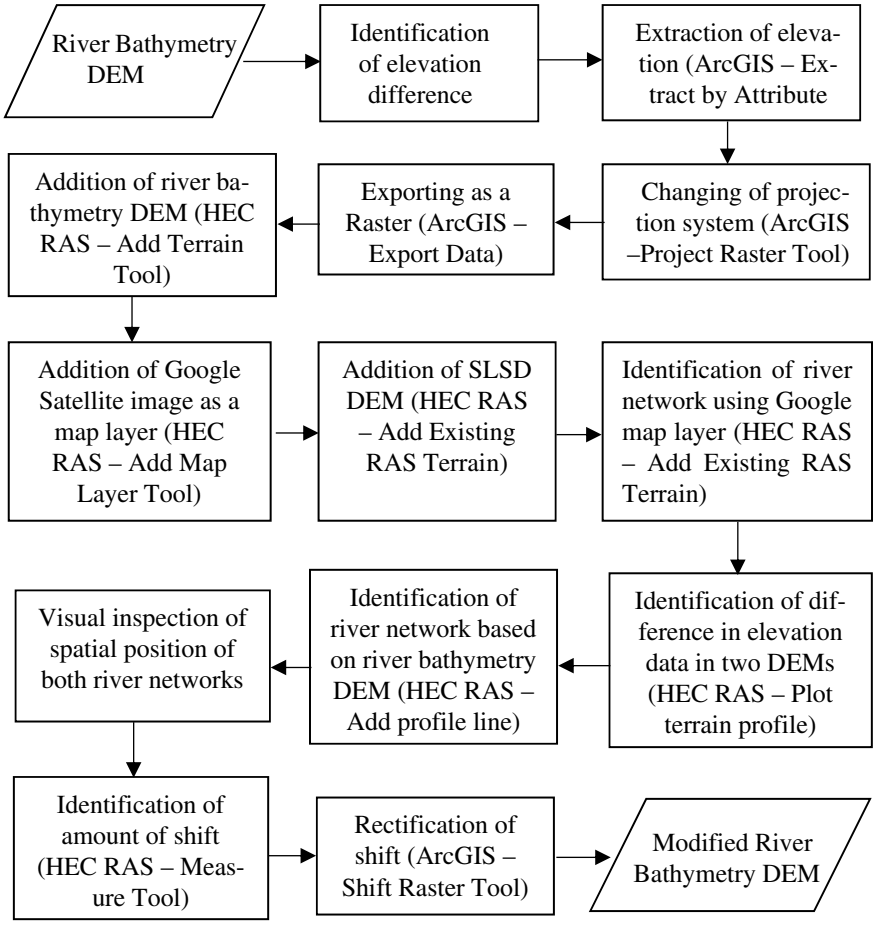

Fig. 4 Flowchart for the modification of river bathymetry DEM

bathymetry DEM, SLSD DEM, and the Google satellite image were added to HEC-RAS software. Then the river network was drawn using the Google satellite image and the elevations along the drawn line were observed. As there was an unusual change in the elevation, the river network was drawn as another profile line based on the river bathymetry DEM. Then a shift was identified, and it was measured using a measuring tool. The shift that was identified in this DEM is 250 m to the positive x direction and 40 m to the positive y direction.

Thereafter, the river bathymetry DEM developed in the ArcGIS software was rectified and a modified river bathymetry DEM was obtained.

The obtained river bathymetry DEM and the river DEM were compared with the other datasets to find the discrepancy between each dataset.

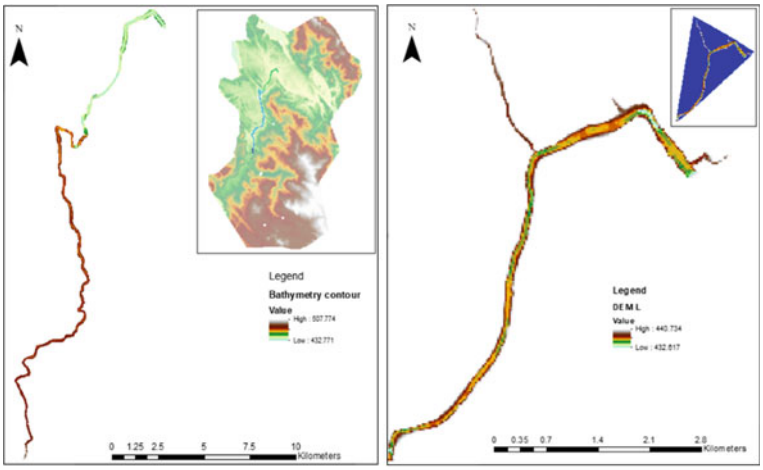

Fig. 5 Developed river DEM from cross sections (**a**) and modified river bathymetry DEM (**b**)

5 Results

5.1 Developed River DEM Using Measured Cross-Sections

Figure 5a depicts the river bathymetry DEM developed in HEC-RAS following the methodology in Fig. 3 and the DEM when overlaid on the study area. DEM is in the GeoTIFF format and GeoTIFF is a georeferenced tag image file format that is used worldwide as a distributed format for aerial photography, DEM, and other data.

In HEC RAS, the DEM can be developed to represent the river bathymetry as well as the overbank areas by interpolating the surface. However, this DEM only represents the river bathymetry. Furthermore, DEM is automatically projected to the SLD99_SriLanka_Grid_1999 coordinate system in the HEC-RAS software. It shows no shift with the other datasets. This developed dataset can be used as a reference when detecting the elevation of the river bathymetry.

5.2 Modified River Bathymetry DEM from the Study

Only the elevation of the river bathymetry was extracted from the DEM by following the methodology in Fig. 4. Figure 5b depicts the river stretch of 7 km ending at the Polgolla barrage. The river bathymetry obtained has a spatial resolution of 25 m and is projected to the SLD99_SriLanka_Grid_1999 coordinate system. The river bathymetry DEM depicts the tributaries joining the Mahaweli River which was not

given in the other datasets. In the latter sections, the elevations of the river bathymetry of Fig. 5a and b along with the other datasets are analyzed and presented.

5.3 *Comparison of Features of Datasets in the Floodplain by Visual Inspection*

When all the datasets representing the floodplain are overlaid in either ArcGIS or HEC RAS software, the datasets can be visually inspected. The continuation of a mountain ridge can be observed clearly in Fig. 6a in which there is no shift between the LiDAR and SLSD DEM.

When the datasets are compared visually for a specific river stretch with bank lines and small islands in the river course, the following conclusions can be drawn.

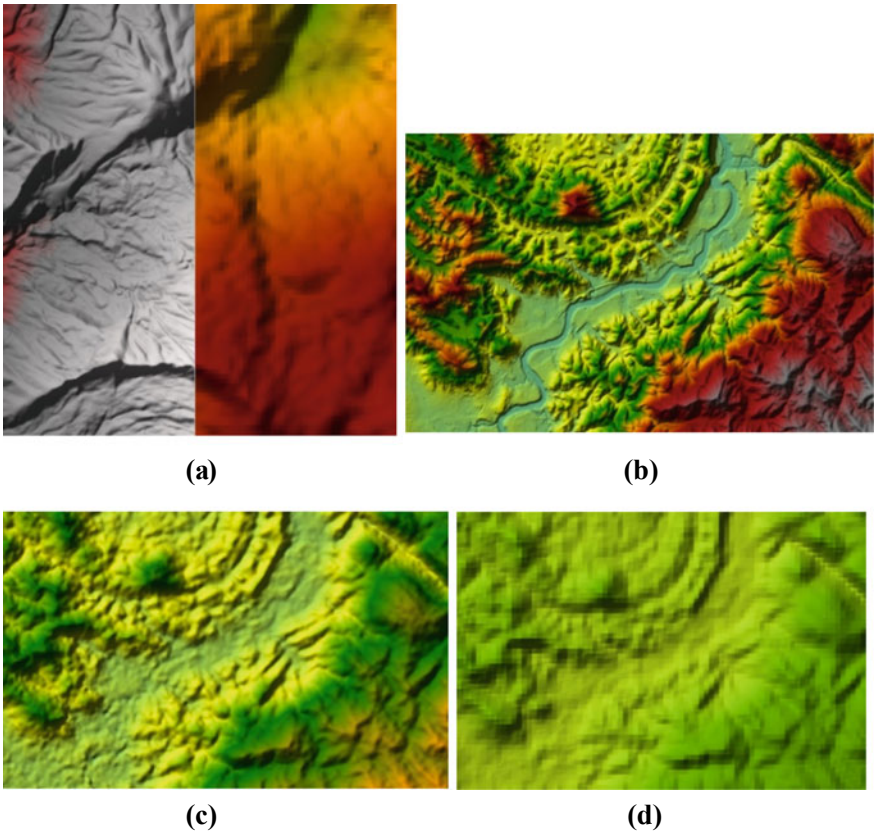

Fig. 6 LiDAR and DEM of the same area (**a**) and representation of river in LiDAR data (**b**), SRTM DEM (**c**), and SLSD DEM (**d**)

Due to the high resolution of the LiDAR dataset, it depicts the delicate details of the terrain very clearly in comparison to other datasets Fig. 6b. Furthermore, SRTM DEM (Fig. 6c) shows a better representation of the terrain visually than the SLSD DEM. The spatial resolution of SLSD DEM is quite smaller than SRTM DEM. SRTM DEM might represent the terrain features with the ability to interpolate the elevations which is a better guess than the correct elevation of the area done with good intention (*SRTM 90 m Digital Elevation Database v4.1—CGIAR-CSI. (n.d.).* In addition, upon the limited use of LiDAR DEM, the SLSD DEM can also be used and it also shows quite a better representation as shown in Fig. 6d. Nevertheless, all the datasets have captured the low-lying and high-ground areas quite accurately. This topic will be further discussed in the next section by comparing the specific land features.

5.4 Comparison of Elevation of Datasets

This section compares the elevation of the DEM derived from each dataset and their differences in various terrains. The extent of the datasets is shown in Figs. 1 and 2. LiDAR DEM covers only 28 m of the 46 km stretch of the Mahaweli River from Kothmale to Polgolla. Both SLSD DEM and SRTM DEM cover the entire region. The river bathymetry DEM covers the river stretch from 39 to 46 km of the Mahaweli River segment. Therefore, when comparing the elevations, the elevation of the measured cross sections covering the entire 46 km stretch is considered as the reference dataset.

LiDAR DEM, which only covers the river up to GeliOya from the Kothmale reservoir shows distinct differences in hilly slope and mild slope areas. This difference is evident in both Fig. 7a and b. Figure 7a, which denotes the cross-section profile of a steep region is in good agreement with the measured cross-sections whereas, in Fig. 7b, the LiDAR DEM shows a higher elevation than the measured one.

This phenomenon happens because the traditional laser system that develops LiDAR DEM cannot capture elevations of the bottom of the river as it cannot penetrate the water column. In the steep regions, the water flows comparatively faster, and the water will not get stagnated in one place. Furthermore, the water volume at the beginning of the river course is comparatively lower as the Kothmale reservoir has blocked the natural stream making it a dead stream. However, in mild slope regions that hold more water and the water velocity is quite low, the elevation difference is high. In addition, sub-basins will bring more water to the downstream region as the river progresses down. However, this difference can be rectified by introducing the river DEM to the terrain which is developed from measured cross sections. Moreover, when the number of data points in datasets are compared, the resolution of the datasets can be determined. LiDAR DEM which has the lowest resolution has many data points to represent the terrain. As the resolution increases, the number of data points representing elevation is also getting lower.

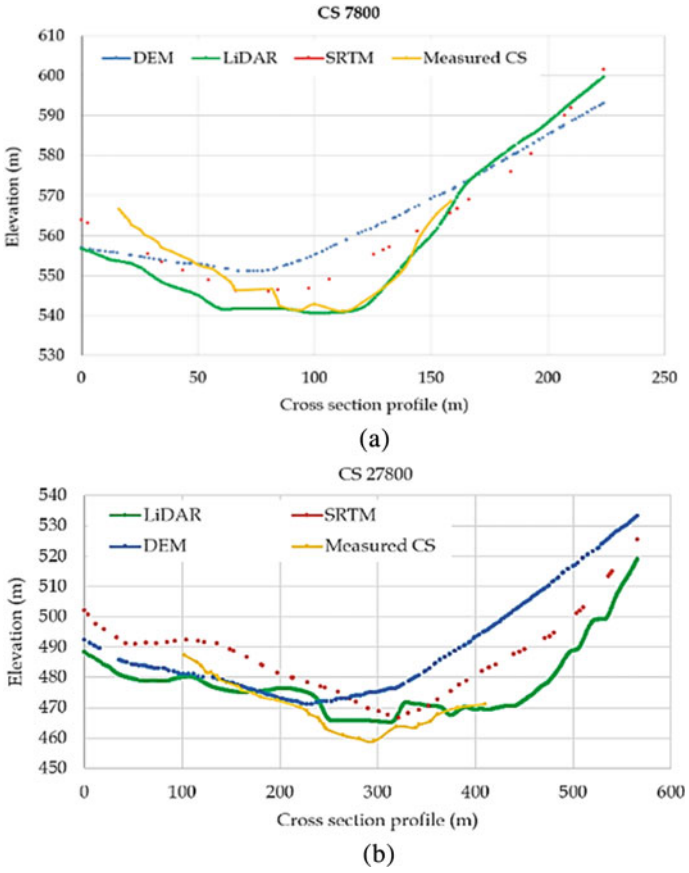

Fig. 7 Cross-section profile of a steep region (**a**) and mild slope region (**b**) with LiDAR data, SLSD DEM, SRTM DEM, and measured cross-sections

Nevertheless, the elevations shown by measured cross sections are quite consistent with the river bathymetry DEM (Fig. 8) proving that the measured cross sections are accurate. However, as the river bathymetry DEM has a spatial resolution of 25 m, using that in the specific region can also be considered as a possible option.

In addition, as shown clearly in Figs. 7 and 8, it can be stated that all the datasets show the same trend in elevations. SRTM DEM shows the highest elevation which will be useful for hydrological modeling studies as the dataset is issued for free. As the radar waves are used in SRTM DEM, those waves cannot penetrate the water column to retrieve bathymetry data. In addition, SLSD DEM shows a relatively higher elevation in the course of the river. Therefore, it proves the necessity of river bathymetry to accurately represent the flow path.

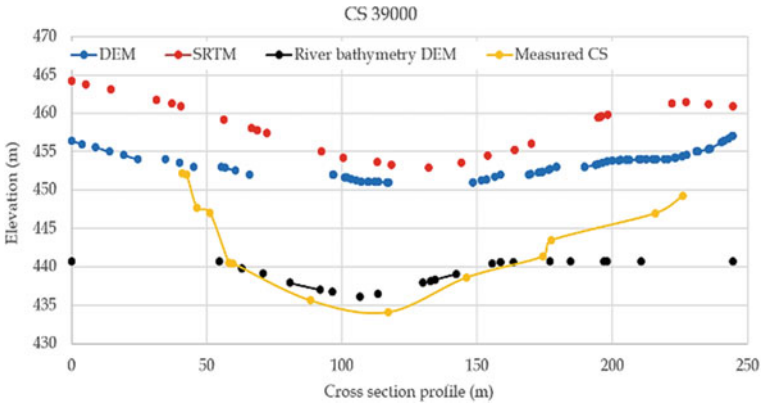

Fig. 8 Cross-section profile of a steep region with SLSD DEM, SRTM DEM, river bathymetry DEM, and measured cross-sections

5.5 Comparison of Features by the Elevation of Datasets

The resolution of datasets would affect the fine representation of details. For example, when representing paddy fields and roads near the course of the river, which can be detected from google maps, the capability of datasets to capture that specific land feature depends on the extent of the land feature or in other terms, the resolution of the dataset. This can be seen when google maps are overlaid onto the terrain maps in HEC-RAS software. Furthermore, attention must be paid when drawing the profile lines in the HEC-RAS software as the line drawn from left to right will denote the elevations from left to right. If a common practice is not used throughout the flood modeling process when using the software, data might be misinterpreted.

The purple line in Fig. 9a denotes the cross-section line that cuts through paddy fields and a road section. The red circle denotes the position of the paddy fields while the green box denotes the position of a narrow road. However, as depicted in Fig. 9b, SRTM DEM could not capture the paddy fields. But the elevation shows a depression in the region. Due to the small width of the road section, it could not be captured by SRTM DEM at all. SLSD DEM also shows a lower elevation in the red color region showing depression in the area. But the trend in elevation seems quite suspicious. Even though it has a spatial resolution of 5 m, the narrow road section details are not represented. A possible reason might be that the SLSD DEM has been developed using both 1:10,000 maps and aerial images. Thus, the unavailability of fine-resolution data in that area might have caused this. However, LiDAR DEM shows the paddy fields quite accurately with a constant elevation. Furthermore, the road section details have been captured by the LiDAR DEM as the resolution is between 1 to 3 m. Overall, all the datasets have shown a depression in the paddy field region which has a greater extent. Narrow section details are not represented other than in the LiDAR DEM (Fig. 9a).

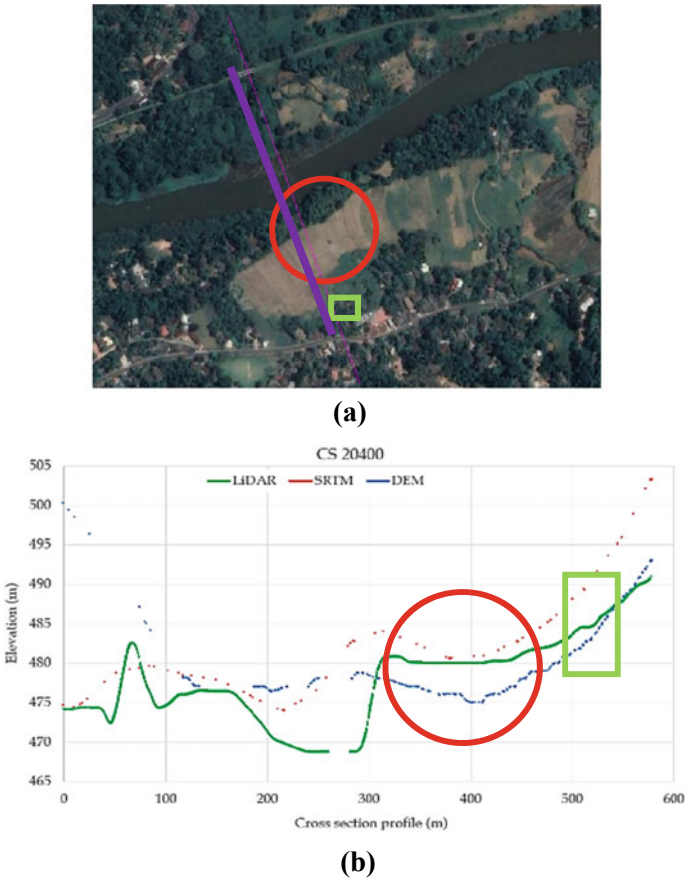

Fig. 9 Representation of the paddy fields and road in Google Maps (**a**) and the elevation along the purple color line (**b**)

Nonetheless, it is better to be mindful of the accuracy required for modeling purposes. If the purpose is not to represent more fine details of the terrain, acquiring a costly dataset like LiDAR DEM would not be essential.

Moreover, SRTM data acquisition is comparatively easy as this is available on the Internet. Therefore, for urgent flood modeling studies, the use of SRTM DEM will be more helpful.

SLSD DEM is not costly compared to LiDAR DEM. It can also be used for flood modeling studies. Therefore, when selecting a suitable topographic map for a study, knowledge ‘of the effect of these topographic features is beneficial for effective modeling.

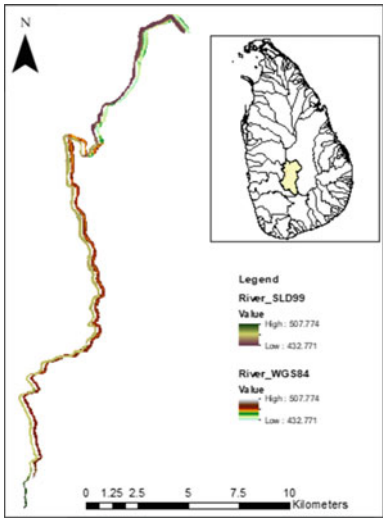

Fig. 10 Representation of the difference in the coordinate system

5.6 Importance of Projection System in Flood Modeling Studies

As discussed previously, the coordinate system is a crucial parameter in identifying the differences in elevation. Figure 10 depicts the difference between the same dataset belonging to two different coordinate systems. There is a slight shift between the datasets, which in turn would affect the result. Therefore, it is advisable to project all the datasets into one projection system and to identify the discrepancy between the elevations beforehand.

However, there can be slight shifts even when projected to the same coordinate system. Therefore, a special concern must be kept in retrieving elevation from the DEMs.

6 Conclusions

This paper concludes the differences in elevations and representation of land features of datasets by forming a common platform using a common projection system for easy comparison. A methodology was adopted to modify the datasets and the modification process was carried out using only ArcGIS and HEC RAS software. The results show that to create an accurate terrain, the characteristics of the datasets have to be identified beforehand. Furthermore, upon the identification of the characteristics of the datasets, decisions on the use of datasets for flood modeling can be determined. More attention must be focused on minor details such as river bathymetry and projection systems which would affect the results in a great way.

In conclusion, the methodology discussed in the paper will guide practicing engineers to select suitable topographic maps for their studies balancing the budgetary and accuracy requirements. In addition, for future studies, comparisons between other datasets such as MERIT DEM, ASTER DEM, and other novel datasets concerning Sri Lankan studies are recommended. Moreover, open-source software such as QGIS can also be incorporated to perform the methodology.

Acknowledgements The authors would like to acknowledge the Department of Civil Engineering, Faculty of Engineering, University of Peradeniya, Sri Lanka, Sri Lanka Survey Department, and Mahaweli Authority of Sri Lanka for their assistance and information. Furthermore, the authors would acknowledge the financial support given by RMIT University and the computational resources funded by Erasmus CCWater Project.

References

1. Yoshimoto S, Amarnath G (2017) Applications of -based rainfall estimates in flood inundation satellite modeling—a case study in Mundeni Aru River Basin, Sri Lanka. Remote Sensing 9(998):1–16. https://doi.org/10.3390/rs9100998
2. Edirisinghe EAKR, Pussella PGRNI, Vidarshana WDM (2021) GIS based approach for planning the evacuation process during flash floods : Case study for gampaha divisional secretariat division, Sri Lanka. J Geospatial Surv 1(1)
3. Edirisooriya EMNT (2019) Two-dimensional flood inundation modeling in lower Kelani basin. Thesis, University of Peradeniya, MSc
4. Suja ACA, Rajapakse RLHL (2020) Evaluation of topographic data sources for 2D flood modeling : case study of Kelani basin, Sri Lanka Evaluation of topographic data sources for 2D flood modelling : case study of Kelani basin, Sri Lanka. IOP Conference Series: Earth and Environmental Science. https://doi.org/10.1088/1755-1315/612/1/012043
5. Palamakumbure L, Ratnayake AS, Premasiri HMR (2020) Sea-level inundation and risk assessment along the south and southwest coasts of Sri Lanka. Geoenvironmental Disasters 7(1):1–9
6. Wickramagamage P, Wickramanayake N, Kumarihamy K, Vidanapathirana E (2012) A comparative study of elevation data from different sources for mapping the coastal inlets and their catchment boundaries
7. Nandalal HK, Ratnayake UR (2010) Event based modeling of a watershed using HEC-HMS. Eng: J Inst Eng, Sri Lanka 43(02): 28–37
8. Josiah NR (2018) Two-dimensional flood inundation modeling from gampola to. University of Peradeniya
9. Jayasena HAH, Chandrajith R, Gangadhara KR (2011) Water management in ancient tank cascade systems (TCS) in Sri Lanka : Evidence for systematic tank distribution. J Geol Soc Sri Lanka 14:29–34
10. CRIP—DBIP project (2018) Climate resilience improvement project (CRIP) Volume 6 : Computational framework specific to Mahaweli Ganga Basin
11. Survey Department of Sri Lanka (n.d.). Available at https://www.survey.gov.lk/sdweb/home.php?l=h. Accessed 18 Oct 2021
12. Lindamulla LMLKB, Dissawa DMSB, Weerakoon SB (2017) Two dimensional computational modelling of flow in Polgolla reservoir. In: The 28th International Symposium on Transport Phenomena, pp 1–3

13. Earth Explorer (n.d.). Available at: https://earthexplorer.usgs.gov/. Accessed 17 Oct 2021
14. SRTM 90m Digital Elevation Database v4.1—CGIAR-CSI (n.d.). Available at: https://cgiarcsi.community/data/srtm-90m-digital-elevation-database-v4-1/. Accessed 05 Nov 2021

Importance of Leaving Intermittent Rivers and Ephemeral Streams (Ires) Untouched in a Sustainably Built Environment

M. D. D. Perera, T. M. C. I. Madhushani, and P. I. A. Gomes

Abstract Intermittent rivers and ephemeral streams (IRES) are temporary waterways that flow only at certain periods of the year and consist of more than half of the world's total stream/river length. They have essential hydro-ecological functions and provide many ecosystem services but are widely ignored and considered as mere surface flow or trenches, and Sri Lanka is no exception. That is why we do not see such streams even in semi-urban townships, an indication that those have been either reclaimed or replaced with man-made (e.g., concrete-lined) drainages. In this study, we discuss the importance and sustainable management of IRES in the dry and intermediate climatic zone of Sri Lanka which has townships, extensive agriculture, tourism infrastructure, and where the built environment shows signs of expansion. A unique characteristic observed in IRES of the study area was their signature high infiltration at the stream bed (about 40 times that of the catchment), and somewhat high infiltrations in the low-flow areas. High infiltration of the beds contributes to groundwater recharge, where all rainfall received during the dry season (including runoff from the catchment) is infiltrated (therefore, no flow in the stream). To control flooding in the wet season, a large portion of the runoff is infiltrated as well. However high percolation rates (more than 10 times that of the catchment) indicated that water draining into the soil does not undergo any type of natural filtration process. Therefore, groundwater contamination is potentially high. These findings indicate the importance of the consideration of IRES in city planning during urbanization, in the context of groundwater recharge, flood control, and siltation of reservoirs. In this regard, we emphasize that even treated wastewater should not be released into such dry stream beds to avoid groundwater contamination and no lining should be done to control floods and to avoid silting reservoirs. Alteration of the natural status quo of IRES in any manner would have adverse effects on the natural and built environment, and it is important that awareness and understanding of these streams are improved.

Keywords Intermittent rivers and ephemeral streams · Infiltration; percolation · Groundwater recharge · Flood control

M. D. D. Perera (✉) · T. M. C. I. Madhushani · P. I. A. Gomes
Sri Lanka Institute of Information Technology, Malabe, Sri Lanka
e-mail: devki.d.perera@gmail.com

© The Author(s), under exclusive license to Springer Nature Singapore Pte Ltd. 2023

R. Dissanayake et al. (eds.), *ICSBE 2022*, Lecture Notes in Civil Engineering 362,
https://doi.org/10.1007/978-981-99-3471-3_60

1 Introduction

Streams and rivers are water bodies that flow in one direction (i.e., upstream to downstream) within a channel or conduit. Those that we are most familiar with, flow continuously and are known as perennials. However, non-perennial streams can completely dry for a certain period/s of a year and are commonly referred to as Intermittent rivers and Ephemeral streams (IRES). The name is derived from the fact that ephemeral streams have a shorter flow duration and less predictability in comparison to intermittent rivers. A stream is therefore, more probable to be ephemeral, and rivers to be intermittent when considering the general link between channel size and flow duration [1]. IRES is a common feature of watersheds that play a critical role in the preservation and protection of water resources, human health, and the environment [2]. Dry riverbeds, which are frequently observed as harsh environments, are susceptible to flow disturbances that mobilize, deposit, and scour bed sediments. They may also be subjected to intense winds, scorching temperatures, and solar radiance. Although they are sometimes associated with negative connotations, dry riverbeds have several significant societal and ecological values [3]; things that are not given due prominence. This is the situation in Sri Lanka, where the public sees these streams as mere surface drainage paths. These streams serve a variety of functions such as the exchange of surface and subsurface water, groundwater recharge and discharge, transport, storage and deposition of sediment to help maintain and develop floodplains, the provision of wildlife habitat and migration routes, the support of vegetation communities that help stabilize stream banks and provide wildlife services, water supply and hydrological connectivity, and nutrient processing [2]. These streams also have a unique set of flora in their riparian zone that is different from perennials within the same region [4]. This may extend to fauna as well.

There are many threats to IRES, and most are human-originated [1]. These include reclamation, burial, regulation works such as straightening and concrete lining of the channel, sand mining, etc. The majority of IRES, however, are not as legally protected as their perennial equivalents, which reflects how seldom society values their ecological characteristics and ecosystem services [5], and Sri Lanka is no exception. There are no specific rules related to IRES in Sri Lanka, other than indirect protection under certain rules such as the own lands ordinance (1949) and recently, the Agrarian development act (2000, amended in 2011). It is evident that the lack of legal protection of IRES could be due to the lack of sufficient knowledge of them by decision-making. Interestingly, this is the stance when it comes to voluntary compliance tools such as green (sustainable) ratings. Many tools, including the manuals developed by the Green Building Council of Sri Lanka, target well-defined buildings and lands, and therefore, landscape features like streams may be overlooked. Also, marking schemes only indirectly account for the sustainable use of streams. In this study, we stress the importance of considering IRES in rating manuals as well as environmental policies. This study aims to discuss the importance of intermittent rivers and ephemeral streams (IRES) and their sustainable management in the built environment of Sri

Lanka's dry and intermediate climatic zones. This study intends to emphasize the negligence of roles played by small streams in development planning (this is the case for IRES) and inappropriate application of engineering principles in the regulation of these streams in cases where regulation is unavoidable (e.g., straightening, and concrete-lined channel sections to increase the discharge and to reclaim the land). The objective of the study is to evaluate the unique characteristics of IRES in terms of their infiltration and percolation capacities and discuss the effects of stream regulation and wastewater discharge into them. A comparison of IRES and perennial streams was done to highlight the importance of IRES in order to devise a way forward by including IRES as equally as perennial streams in policies for a sustainably built environment.

2 Methodology

2.1 Study Area

IRES of the dry climatic zone and intermediate climatic zone were considered (Fig. 1), and fieldwork was done in Habarana (8° 01′ 56″ N 80° 45′ 00″ E) and Meegahakivula (7° 08′ 17″ N 81° 02′ 54″ E) areas. Habarana (Fig. 1a, b) is in the Anuradhapura district in the North Central province and falls under the dry climatic zone of Sri Lanka with an average annual rainfall of 1085 mm. The wet season generally occurs during the months of October and December, during the North-East monsoons. The dry season generally occurs from May to July. The IRES that were observed in Habarana is a component of a lotic water network that gradually drains into the Minneriya tank.

Meegahakivula (Fig. 1a and c) belongs to the Badulla District which belongs to the Uva Province, and is in the intermediate zone with an average annual precipitation of 2082 mm. This area experiences heavy rainfall during the month of November. The least rainfall is recorded around the month of July [6]. The streams that were considered for this study in Meegahakivula are tributaries that flow to Loggal Oya. Some large IRES are marked on 1:10,000 topographical maps, especially in the Habarana area, and some are also named and identified as significant features by locals (e.g. Heen Ela, Batu oya). However, over 90% of the IRES are unmarked on maps and had to be identified via field visits referring to the drainage network developed using a digital elevation model.

2.2 Investigation of the Infiltration Capacity

Infiltration is the ability of water absorbance into a soil profile [7], and the infiltration rate is a measure of the velocity at which water flows vertically down through

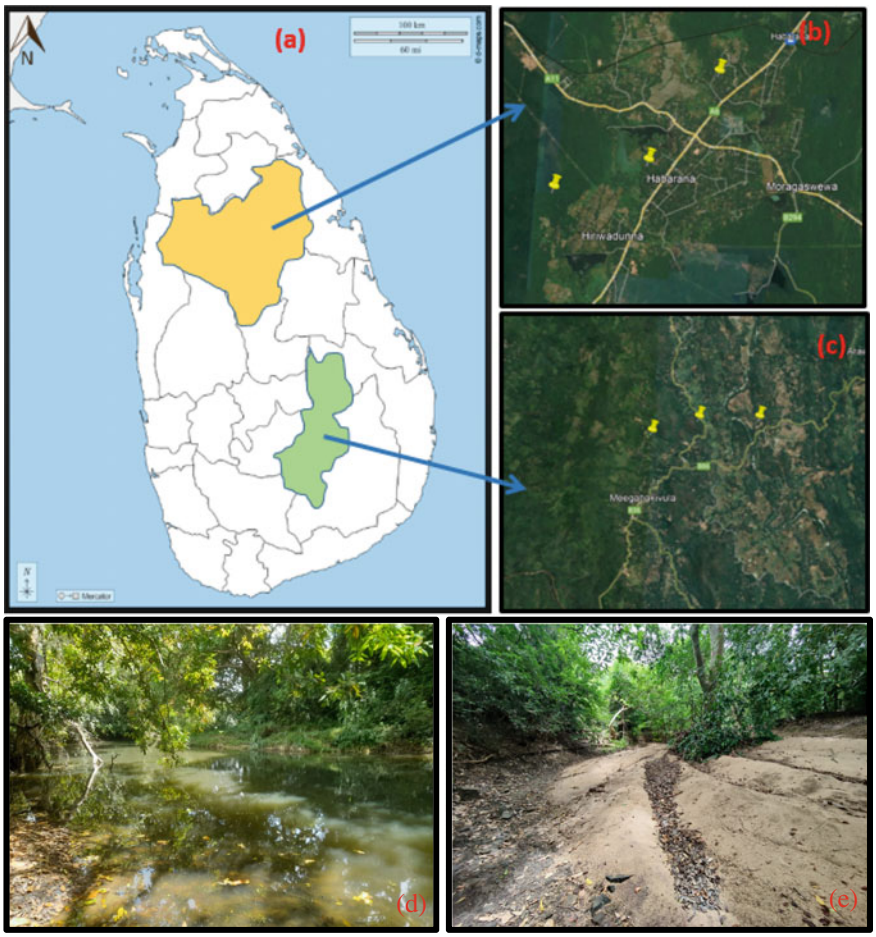

Fig. 1 **a** District location on a Sri Lankan map **b** Study areas in Habarana c Study areas in Meegahakivula **d** flowing ephemeral stream **e** dry ephemeral stream

the soil. There are many major factors affecting infiltration rates, such as the soil texture and structure, the condition of the sediment surface, the distribution of soil moisture, the chemical and physical nature of the water, the head of the applied water, the depth to groundwater, the length of time of application of water, biological activity, the percentage of entrapped air in the sediments, and the type of equipment or method used for measuring the rate [8]. The standard test method D3385-18 by ASTM (American Society for Testing and Materials) standards were used for this study. Evaluations of the infiltration capacity were done at various transverse (active channel, low flow, high flow, and terrestrial zones) and longitudinal locations for wet and dry seasons in both IRES and perennial streams. Infiltration was done for 2 streams per study area, 3 reaches per stream (each more than 50 m apart) and 2

stable cross sections per reach. 2 points per each transverse zone were tested for the stream bed, low flow, high flow, and terrestrial zones at each cross section.

Equations 1, 2 and 3 were used in calculating the infiltration rate from continuous measurements taken of the heights of the water column in the infiltrometer and the duration for water to infiltrate into the soil. Where H is infiltration depth and t is the time period.

$$(\mathrm{H}) = \text{Height (previous)} - \text{Height (current)} \tag{1}$$

$$\text{Cumulative infiltration rate} = \sum_{1}^{i} Hi \tag{2}$$

$$\text{Infiltration capacity} = \frac{\mathrm{H}}{\mathrm{t}} \tag{3}$$

2.3 Investigation of the Percolation Rate

Soil percolation can be defined as the movement of water through the soil until it meets the groundwater aquifer. The percolation test procedure measures the time taken for a certain amount of water to travel into the soil from a saturated hole dug into the ground. Performing a percolation test provides an accurate measure of how quickly the soil drains and how much surface area is required for water to infiltrate properly ([9]. The rate at which water percolates varies from one soil type to another; clayey soil takes more time, whereas sandy soil takes less time. The BS 6297: 2007 code of practice prescribes how drainage fields for wastewater treatment should be designed and installed. It incorporates recommendations for preliminary planning, the site investigation to identify the appropriate drainage field location, and the evaluation of site characteristics. Percolation tests followed the same spatiotemporal schedule of infiltration. Percolation rate refers to the inverse definition of the percolation value, which represents the time required for a particular water depth to drain into the ground. Percolation was done for 2 streams per study area, 3 reaches per stream (each more than 50 m apart) and 2 stable cross sections per reach. 2 points per each transverse zone were tested for the stream bed and terrestrial zones.

Percolation value (Vp) was calculated using Eq. 4. Where T1 is the time when the water level is at 225 cm and T2 is the time when the water level is at 75 cm.

$$\text{Time elapsed} = \mathrm{T2} - \mathrm{T1} \tag{4}$$

$$\mathrm{Vp}\left(\frac{\mathrm{min}}{\mathrm{mm}}\right) = (Time\ elapsed)/150$$

3 Data Analysis

The t-test and one-way ANOVA methods were used to investigate significant differences by the IBM SPSS statistics software. A t-test is a statistical hypothesis test in which the means of two groups are compared to determine if one influences the other or if they are significantly different. One-way ANOVA is used to compare the means for three or more samples.

4 Results and Discussion

4.1 Infiltration Capacity of IRES and Perennial Streams

Figure 2 shows the infiltration capacity of both IRES and perennial streams in Meegahakivula and IRES in Habarana during dry and wet seasons. The perennial stream experiments were done at high-flow and terrestrial zone only as the stream beds and low-flow areas were subjected to stream flows during both dry and wet seasons. The infiltration capacity during the dry season was significantly (t-test; $P < 0.05$) higher, especially in IRES. During the dry season, the IRES was fully dried and the soil was unsaturated as there was no connection to the groundwater table and therefore no input of water. This lead to significantly higher (t-test; $P < 0.05$) infiltration rates in the IRES streambed in the dry season, in comparison to all other zones and seasons. It was also noted that the infiltration capacities of the dry perennial streams were higher than the wet IRES, but the difference was not significant (t-test; $P > 0.05$). High flow zone infiltration capacity had a higher value than the terrestrial zone. However, it was not significant (t-test; $P > 0.05$). A large variation of infiltration rates was observed in IRES in Habarana. Landscape and geographical features, such as the presence of bedrock causing lateral flow, and sandy soil that was completely dry, was attributed to this variation. Overall, the infiltration capacity of IRES remained higher than that of perennials at any given season and location, indicating that they play a more significant role in groundwater recharge and flood control.

4.2 Percolation Rate of IRES and Perennial Streams

Figure 3 represents the percolation values of both IRES and perennial streams during dry and wet seasons. The percolation value was lower in the stream bed than in the terrestrial zone, due to the differences in soil type. The stream bed was noted to have sandier soil, which has a higher water absorbance capacity (as the absorbance rate increases and water moves faster through the soil, the percolation value decreases). The percolation value of the IRES stream bed during the dry season was noted to be half of that of the terrestrial zone and this difference was significant (t-test; P

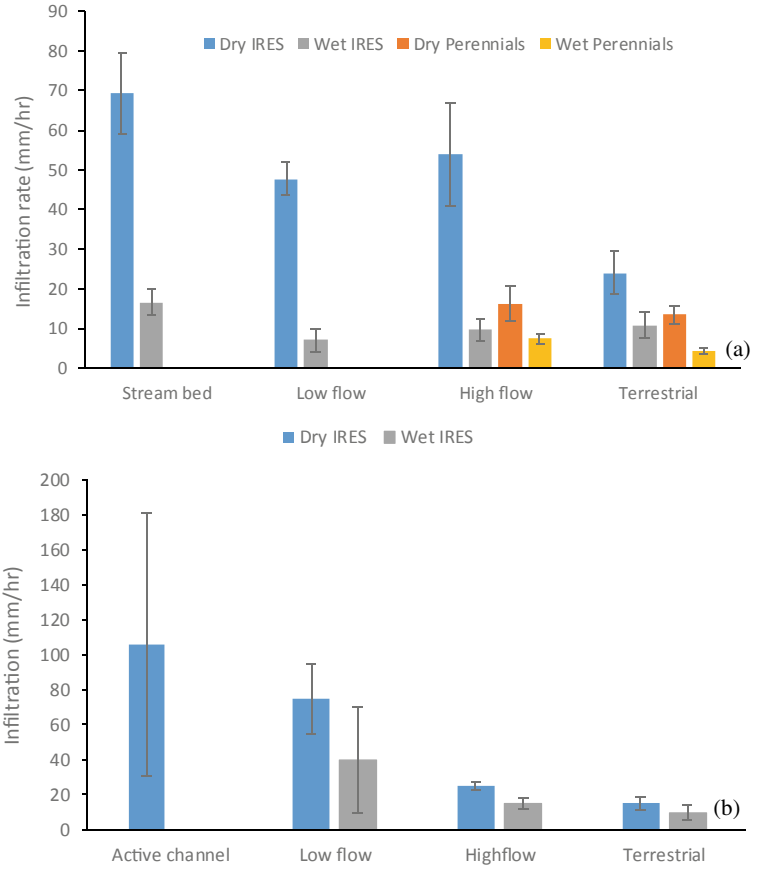

Fig. 2 Infiltration rates of IRES and perennial streams during wet and dry seasons **a** Meegahakivula **b** Habarana

< 0.05). This difference was noted even more prominently during the wet season. The percolation values of IRES also showed significant differences (t-test; $P < 0.05$) between seasons only at the terrestrial zone. It was noted that the percolation values of IRES and perennial stream terrestrial zone were significantly different (t-test; $P > 0.05$) only during the dry season. In perennial streams, the water table already lies at a closer elevation to the stream bed and the water penetration rate may be less due to the partial saturation of the contributing catchment. When the percolation value is high, the percolation rate is less. Overall, the percolation rate remains higher in IRES than in perennials, and during the dry season in comparison to the wet season. Therefore, any discharges into IRES must be done carefully, even more so than into perennials.

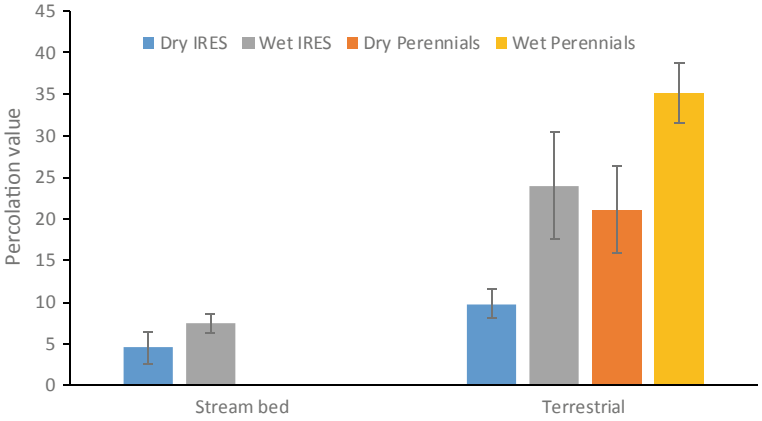

Fig. 3 Percolation values of IRES and perennial streams during the wet and dry seasons

4.3 Impacts of the Negligence of IRES

The majority of IRES can be found in the North Central Province, Uva Province, and a part of Sabaragamuwa Province in Sri Lanka, which are in the dry and intermediate zones. It is important to take these rivers and streams into account when considering extreme flood events. But somehow, it is difficult to find these waterways in built areas. This indicates the disappearance of IRES in tandem with urbanization, similar to that observed by Elmore and Kaushal [10] in a study done in Baltimore City, USA. The other common regulations, perhaps, deemed less harmful by Engineers include replacing streams with a straightened canal with or without hardline material such as concrete or even using a hume pipe. The high infiltration rates of IRES make it ideal grounds for groundwater recharge and a natural flood control solution as runoff ceases when water moves into the soil. In some areas, IRES remain the major source of aquifer recharge. Due to some of the stream regulations such as the concrete lining of streams, infiltration and percolation have been reduced or completely stopped, causing a major effect on groundwater recharge and increasing the potential for flooding of the catchment, especially in downstream areas.

IRES are major contributors in hydraulic connectivity and direct water to perennials and water bodies during their flowing phase. One important area of evaluation is the impact of wastewater flow and inputs on channel bed morphology and the status quo of IRES. Treated and untreated wastewater is commonly released into these streams as they are widely ignored as a water resource and a productive ecosystem. This has severe consequences as with a high percolation rate, contaminants can reach the groundwater table with minimum filtering causing complex pollution effects [9]. Changes in physicochemical characteristics between both upstream and downstream reaches are caused by contaminant infiltration into gravel and then into groundwater aquifers. This has a significant impact on the water quality parameters of downstream perennials as well. The flow of wastewater causes the transition from a dry, IRES

channel with periodic floods to a continual flow pattern similar to humid environments. Domestic sewage flow into the lower part of streams leads to the establishment of dense vegetation along the channel, consequently resulting in the channel becoming stable and very narrow. One of the main purposes of open channels is the transfer of sediment. Streams act as conduits for sediment from the watershed and assist in maintaining a delicate balance between elements, such as friction from the wetted perimeter, channel slope, and other factors; burial of IRES disrupts this balance. Furthermore, the texture of the bed changes as fine sediment from domestic and industrial wastewater infiltrates and cements the gravel bed, effectively increasing the bed's stability.

4.4 A Way Forward to Protect and Incorporate IRES into a Sustainable Built Environment

With urbanization and increasing water demand, the consequences of the impacts on IRES and the lack of protection will be evident in the foreseeable future. Vulnerabilities in IRES ecological services such as carbon storage or release and their biodiversity are insufficiently characterized. As a result, the successful preservation of IRES requires knowledge and further investigation of the cumulative effects of the various threats that they experience. In addition to being valuable ecosystems, their contribution to groundwater recharge needs further investigation to ensure the legal protection of these streams as potential water resources. The formation of standards, rules, and regulations for protection can be done with the contribution of experts and other various stakeholders if the importance of these streams is emphasized and understood. Also, the rating tools such as green building council manuals should consider the sustainable development aspects of IRES as well.

Recognizing IRES as crucial parts of natural river networks rather than 'stressed' or damaged variations of perennial streams is one step towards embracing systems with flexible water governance [11]. As an agricultural nation, Sri Lanka has always benefited significantly from irrigation in terms of its industry of cultivation. Water has emerged as a key resource for industry, the provision of services, consumption (drinking), as well as recreational and leisure activities, and the generation of hydropower (Land and Development, 2014). The fundamental goal is to preserve Sri Lanka's water sources by protecting and conserving all of its reservations, conservation areas, and nearby catchment regions (Land and Development, 2014). The government of Sri Lanka has implemented a variety of laws and policies intended to safeguard the country's water resources. Some of these well-known policies include the National Environment Policy, National Forest Policy, National Land Use Policy, and National Policy on Watershed Management (Land and Development 2014), and IRES must be considered and included in these policies as well. The fact that most of these streams are not even included in maps implies the requirement for further study of these streams and incorporation into literature and reference maps.

5 Conclusion

When considering the hydrological aspects of a sustainable built environment, it is critical to address IRES, which are important in flood control and groundwater recharge. River regulations such as concrete lining and burying are common during the urbanization process, and this results in the destruction of beneficial characteristics of these streams and their stream beds. Since the infiltration and percolation rates are higher in IRES, wastewater discharge must be done sustainably to prevent the risk of groundwater contamination. The negligence of these streams during urbanization and environmental modification can have complex and long-term ecological and hydrological effects that may be irreversible. This study provides a sufficient emphasis on the importance of the protection of these streams, and the first step in doing so is to further understand these streams and their inclusion in legislation and stream preservation policies.

Acknowledgements This study was funded by a research grant from the Faculty of Graduate Studies and Research (No: FGSR/RG/FE/2022/03) of the Sri Lanka Institute of Information Technology.

References

1. Datry, T., Bonada, N. and Boulton, A.J. (2017) *General introduction, Intermittent Rivers, and Ephemeral Streams: Ecology and Management*. Elsevier Inc. Available at: https://doi.org/10.1016/B978-0-12-803835-2.00001-2.
2. Levick, L.R. et al. (2008) *The Ecological and Hydrological Significance of Ephemeral and Intermittent Streams in the Arid and Semi-arid American Southwest*, US Environmental Protection Agency, Office of Research and Development., pp. 1–116. Available at: https://doi.org/US Environmental Protection Agency and USDA/ARS Southwest Watershed Research Center, EPA/600/R-08/134,ARD/233046.
3. Steward, A.L. et al. (2012) *When the river runs dry: Human and ecological values of dry riverbeds*, Frontiers in Ecology and the Environment, 10(4), pp. 202–209. Available at: https://doi.org/10.1890/110136.
4. Gomes, P.I.A., Wai, O.W.H. and Dehini, G.K. (2020) *Vegetation dynamics of ephemeral and perennial streams in mountainous headwater catchments*, Journal of Mountain Science, 17(7), pp. 1684–1695. Available at: https://doi.org/10.1007/s11629-017-4640-4.
5. Chiu, M. C., Leigh, C., Mazor, R., Cid, N. and Resh, V. (2017) Anthropogenic threats to intermittent rivers and ephemeral streams. In Intermittent rivers and ephemeral streams pp. 433–454. Academic Press.
6. Alahacoon N, Edirisinghe M (2021) *Spatial variability of rainfall trends in sri lanka from 1989 to 2019 as an indication of climate change*, ISPRS International Journal of Geo-Information, 10(2). Available at: https://doi.org/10.3390/ijgi10020084
7. Coes, A. and Pool, D. (2005) *Ephemeral-stream channel and basin-floor infiltration and recharge in the Sierra Vista subwatershed of the Upper San Pedro Basin, southeastern Arizona*, USGS Open-File Report 2005–1023, pp. 1–67. Available at: http://oai.dtic.mil/oai/oai?verb=getRecord&metadataPrefix=html&identifier=ADA439921.
8. Johnson, A.I. (1963) *A Field Method for Measurement of Infiltration*, Geological Survey Water-Supply Paper, 1544-F, p. 27.

9. Brian G. Bearden, P.E. (2007) *Percolation Testing Manual*. Available at: http://www.deq.gov.mp/resources/files/CNMI Percolation Testing Manual.pdf.
10. Elmore, A. J. and Kaushal, S. S. (2008) Disappearing headwaters: patterns of stream burial due to urbanization. *Frontiers in Ecology and the Environment, 6*(6), 308–312.
11. Fritz, K., Cid, N. and Autrey, B. (2017) Governance, legislation, and protection of intermittent rivers and ephemeral streams. In Intermittent rivers and ephemeral streams pp. 477–507. Academic Press.
12. Hassan, M.A. and Egozi, R. (2001) *Impact of wastewater discharge on the channel morphology of ephemeral streams*, Earth Surface Processes, and Landforms, 26(12), pp. 1285–1302. Available at: https://doi.org/10.1002/esp.273.
13. Jin (no date) *Difference between T-Test, One Way ANOVA, And Two Way ANOVA*. Available at: https://researchpedia.info/difference-between-t-test-one-way-anova-and-two-way-anova/ (Accessed: 4 December 2022).
14. *Percolation Test Method - Free Calculation -Drainstore* (no date). Available at: https://drainstore.com/percolation-test-method/ (Accessed: 14 November 2022).